ÉCOLE POLYTECHNIQUE
FÉDÉRALE DE LAUSANNE

# ecos 2010

## Lausanne, Switzerland, 14th-17th June

Proceedings of the 23rd International Conference on Efficiency, Cost, Optimization, Simulation and Environmental Impact of Energy Systems

# VOLUME IV
## POWER PLANTS & INDUSTRIAL PROCESSES

Editors :
Daniel Favrat & François Maréchal

# ecos2010

Proceedings of the 23rd International Conference on
Efficiency, Cost, Optimization, Simulation,
and Environmental Impact of Energy Systems

Lausanne, Switzerland
June 14-17, 2010

**Volume IV**
**Power plants & Industrials Processes**

**Editors**
Daniel Favrat and François Maréchal

**Organised by**
Laboratoire d'Énergétique Industrielle (LENI)
École Polytechnique Fédérale de Lausanne (EPFL)

**Official Website of the conference**
www.ecos2010.ch

**Corresponding e-mail**
ecos2010@epfl.ch

**Corresponding address**
EPFL / LENI – ISE - STI
Bat. ME A2
Station 9
CH-1015 Lausanne
Switzerland

**Book creation**
Nicolas BORBOËN, Yannick BRAVO

# PREFACE

*Energy plays a major role in human societies. The supply of energy services is also a major contributor to the global and, too often, local environmental problems the World is facing. According to the International Energy Agency, actions to target future $CO_2$ concentrations in atmosphere below either 550ppm, or even below 450ppm, will have to be primarily focused on efficiency. A broader use of renewable, nuclear power and perhaps carbon sequestration will also contribute. To maintain a viable economic development these actions will have to be cost effective while globally reducing all emissions and caring about energy and material resources. A systemic approach is therefore essential to get a holistic vision, design better systems and optimize money and resources utilization.*

*The ECOS conferences have a long tradition in fostering the key aspects and the scientific knowledge that are essential for the engineers. The organizers of this 23rd edition are proud to acknowledge one of the largest participation ever with many original and high quality papers.*

*Our thanks go to the authors who accepted to travel from all continents and meet in Lausanne to present and share their scientific contributions. Many thanks also to all reviewers and members of the scientific committee who contributed to the quality of these proceedings. The conference chairmen are also grateful to the local organizing team including in particular, Nicolas Borboën, Stina Zufferey, Brigitte Gabioud, Yannick Bravo, Suzanne Zahnd and Irène Laroche. Many thanks also to the other members of the Industrial Energy Systems Laboratory of EPFL, the MEDIACOM EPFL team and the sponsors who greatly helped the organization of this fruitful event.*

Daniel Favrat & François Maréchal

## ORGANISING COMMITTEE

Prof. Daniel Favrat (chairman)
François Maréchal (chairman)

Nicolas Borboën, Yannick Bravo, Brigitte Gabioud,
Irène Laroche, Suzanne Zahnd, Stina Zufferey

## INTERNATIONAL ADVISORY BOARD

Ozer Arnas, United States
Christos A. Frangopoulos, Greece
George Tsatsaronis, Germany

## SCIENTIFIC COMMITTEE

Monika Axel, Sweden
Rangan Banerjee, India
Adrian Bejan, United States
Thore Berntsson, Sweden
Asfaw Beyene, United States
Paolo Bosshard, Italy
Denis Clodic, France
Stephen R. Connors, United States
R.L Cornelissen, Netherlands
Michel Feidt, France
Carl-Johan Fogelholm, Finland
Richard Gaggioli, United States
Yalçın A. Göğüş, Turkey
Gershon Grossman, Israel
Simon Harvey, Sweden
Abel Hernandez-Guerrero, Mexico
Gerard Hirs, Netherlands
Andrew Forbes Alexander Hoadley, Australia
Koichi Ito, Japan
Hervé Jeanmart, Belgium
Signe Kjelstrup, Norway
Jiri Klemes, Hungary
Zygmunt Kolenda, Poland
Andrea Lazzaretto, Italy
Noam Lior, United States
Sylvie Lorente, France
Giampaolo Manfrida, Italy
Philippe Mathieu, Belgium
Alberto Mirandola, Italy
Michael Moran, United States
Zhang Na, China
Silvia Azucena Nebra, Brazil
Eduardo de Oliveira Fernandes, Portugal
Silvio de Oliveira Júnior, Brazil
Ricardo Rivero, Mexico
Marc A. Rosen, Canada
Dominick A. Sama, United States
Peter Schossig, Germany
Enrico Sciubba, Italy
Luis M. Serra, Spain
Samuel Stucki, Switzerland
Pascal Terrien, France
Jules Thibault, Canada
Daniel Tondeur, France
Vittorio Verda, Italy
Laura Vanoli, Italy
Michael R. von Spakovsky, United States
Carl-Jochen Winter, Germany
Li Zheng, China
Andrzej Ziębik, Poland
Ron Zevenhoven, Finland

# Ecologic Effect of the Connection of the Coal Fueled Steam Unit with the Gas Turbine Installation

*Janusz Kotowicz, Łukasz Bartela and Anna Skorek-Osikowska*

*Institute of Power Engineering and Turbomachinery,*
*Silesian University of Technology, Gliwice, Poland*

**Abstract:** The paper shows the results of calculations for a concept assuming the connection of the supercritical coal-fired power plant (SCPP, so-called reference unit) with the gas turbine installation and heat recovery system. The components of this system were: a supercritical heat recovery steam generator and two flue-gases heat exchangers used for preheating of condensate and of feed water. The presence of exchangers permits to replace regeneration and to obtain, in consequence, higher nominal power rating of steam turbine. For the reference unit and assumed structure of a multi-fuel hybrid cycle (MFHC) the key indicators of the thermodynamic and ecologic evaluation were defined. The researches were carried out for a defined gas turbine model, i.e. GE MS9171. In the course of investigation the levels of two defined in the paper ratios of regeneration replacement were changed. The values of thermodynamic and ecologic effectiveness obtained for two specified values of regeneration replacement ratios were compared with values of effectiveness indicators obtained for reference unit and three alternative technologies. This technologies were: supercritical coal-fired power plant integrated with CCS installation (SCPP+CCS), simple cycle gas turbine (SCGT) and combined cycle gas turbine (CCGT).

**Keywords:** Ecologic Analysis, Gas Turbine, Repowering, Supercritical Coal-fired Power Plant.

## 1. Introduction

In Poland 95% electricity production is based on utilization of coal [1]. The popularity of this fuel results, first of all, from its general availability and relatively low price. Dynamic growth of ecologic requirements that appeared in the last years is responsible, however, for essential revaluations of the trends of popularity and development of particular energy technologies. All around the world the fall of popularity of conventional coal technologies is observed. Nowadays, a huge stress is put on the reduction of greenhouse gases emission, what includes the promotion of carbon capture and storage (CCS) installations. Carbon capture can be realized with the use of several methods, i.e. in adsorption and absorption process, cryogenic and membrane separation. The R&D target of the CCS installations is 90% reduction of carbon dioxide emission. However, still existing technical, economic and legal barriers cause, that probably none of the variants of CCS technologies will be ready for commercial implementation before the year 2015. One of the methods available at present, which becomes especially attractive in the context of greenhouse gases emission reduction (including mainly carbon dioxide emission) and increase of energy efficiency is repowering of coal-fired unit with gas turbine installation. This kind of solutions are additionally characterized by lower pollutions emissions, high fuel flexibility and lower operation and maintenance costs [2,3].

Repowering of coal-fired power plant with a gas turbine can be realized for project of a new plant, as well as for modernization of the existing plant on several ways, which can be classified as follows [3,4]:

- serial cycles (Fig. 1a), where heat extracted from a gas turbine (GT) flue gases is used for preheating of steam cycle condensate and/or coal-fed boiler feed water,
- parallel cycles (Fig. 1b), where heat extracted from the GT flue gases is supplied to the steam cycle in parallel (via heat recovery steam generator - HRSG) with heat coming from coal-fed steam boiler,
- "Hot Windbox" cycles (Fig. 1c), where the GT flue gases are supplied to coal-fed steam boiler as hot oxidant instead of preheated air.

Corresponding Author: Łukasz Bartela, Email: lukasz.bartela@polsl.pl

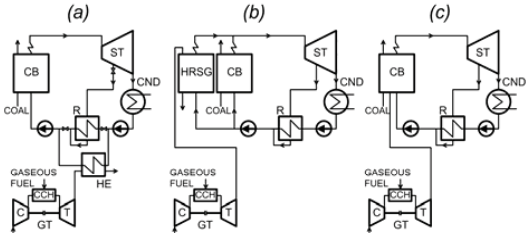


*Fig. 1. Solutions of repowering of coal-fired power plant with the use of gas turbine*

The multi-fuel hybrid cycles are build more and more often and prosperously operate in the whole world. As examples can be mentioned here: the combined heat and power plant Avedore 2 in Denmark [5] and power plants: Map Tha Put in Thailand [6] and Gersteinwerk near Werne in Germany [7]. In Poland no integration of technologies, leading to the creation of the system according to MFHC technology was executed so far.

## 2. Characteristics of the reference unit and its repowering

### 2.1. Supercritical coal-fired power plant (SCPP)

At present supercritical coal-fired power plants are the most developing electricity generation technology in Poland. First made investments concern both, units using pulverized coal-fed boilers and fluid boilers. Thanks to much higher conversion efficiency of the primary energy of coal fuel into useful energy, these units contributed to almost entire abandonment of building of conventional coal units. Currently developing CCS technologies will constitute in the future the supplement for presently built supercritical units. This kind of solutions can permit the ecological production, and what is important, basing on the utilization of relatively cheap and generally available fuel.

Fig. 2 presents the diagram of the reference supercritical coal-fired power plant (white background) with conception of its repowering with gas turbine (grey background). The conception of the reference unit corresponds to the contemporary supercritical coal-fired power plant. The power plant consists of supercritical coal-fed boiler (SCB) with steam reheater, steam turbine (ST), generator (G), condenser (CND), condensate and feed water pumps, deaerator (DA), steam cooler (SC) and seven regenerative heat exchangers fed by extraction steam. Four exchangers realize preheating of condensate (LR – fed by low-pressure extraction steam), and three exchangers realize preheating of feed water (HR – fed by high- and intermediate-pressure extraction steam).

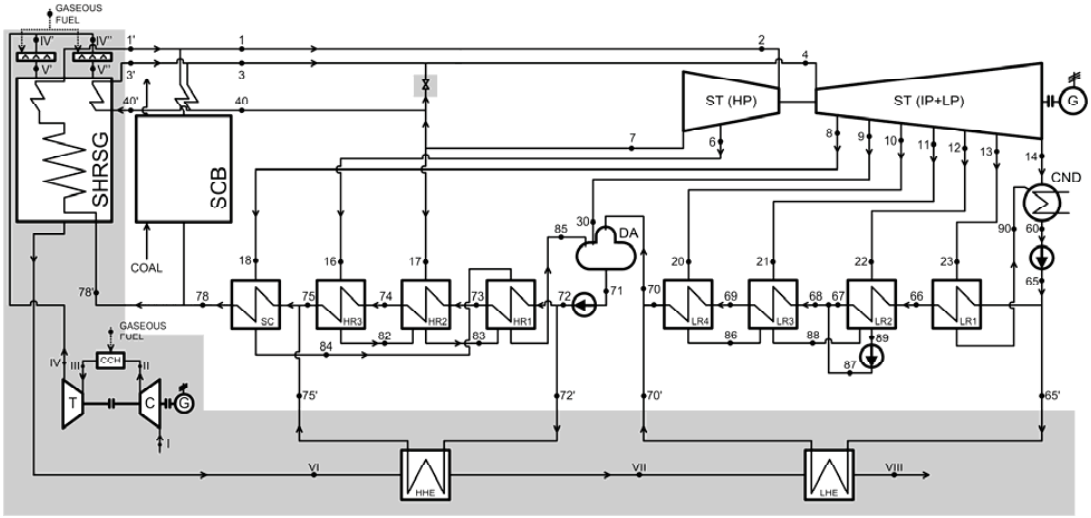


*Fig. 2. Diagram of repowering of reference unit.*

The reference unit is characterized by following quantities:

- gross power rating: 602.20 MW
- gross energy efficiency: 0.4878
- net energy efficiency: 0.4427
- live steam pressure: 28.5 MPa
- live/reheated steam temperature: 600/620°C
- pressure in condenser: 5 kPa
- coal-fed boiler efficiency: 0.95
- steam turbine sectional isentropic efficiency: 0.90
- pumps efficiency: 0.85

## 2.2. Multi-fuel hybrid cycle (MFHC)

Based on the realized studies [4,8], as a solution which can be an interesting alternative to the reference unit is the unit being a connection of the reference plant with a gas turbine together with a three-levels heat recovery system. The three-levels heat recovery system consists of a supercritical heat recovery steam generator (SHRSG), high-pressure flue gases/water heat exchanger (HHE) replacing high-pressure regenerative heat exchangers and low-pressure flue gases/water heat exchanger (LHE) replacing low-pressure regenerative heat exchangers. Parallel cycles, containing in their structure supercritical coal-fed boiler and supercritical heat recovery steam generator were not applied yet in practice. Undoubtedly the innovative component in this kind of units is the heat recovery steam generator which would have to operate at supercritical parameters of working medium. In the literature proposals of technical solutions and examples of simulative calculations of such boilers can be found [9,10].

In the conducted analysis by repowering ought not to be understood physical repowering of existing unit, but the suitable connection of technologies in compliance with assumed structure, where all components can be an object of scaling.

In the present studies the GE MS9171 model of gas turbine was used. This machine is characterized by following quantities:

- compressor pressure ratio: 12.32
- turbine inlet temperature: 1180.3°C
- turbine outlet temperature: 542.9°C
- gas turbine efficiency: 0.3333
- compressor isentropic efficiency: 0.9050
- turbine isentropic efficiency: 0.9230

In calculations of MFHC as a gaseous fuel natural gas was used, characterized by components: $(CH_4)$=0.9733, $(N_2)$=0.0086, $(C_2H_6)$=0.0081, $(C_3H_8)$=0.0046, $(CO_2)$=0.0028, $(C_4H_{10})$=0.0026, and computational environmental parameters were in compliance with ISO: $t_l$=15ºC, $p_l$=101.325 kPa, $\varphi_l$=60%.

The essential component of gas part in MFHC is the supercritical heat recovery steam generator. In present model a single-pressure configuration was established. In SHRSG high-temperature zone, parallelly to the exchangers of supercritical part, a steam reheater was placed. Temperatures and pressures of working media (live and reheated steam) preheated in SHRSG were consistent with steam parameters preheated in supercritical coal-fed boiler. The wish for reaching of defined temperatures of live and reheated steam, thereby of limited level of temperature of flue gases leaving the gas turbine, requires applying of supplementary firing system. The supplementary firings were realized separately for two flue gases flows, i.e. for flow supplied to steam reheater (here the fuel flow was supplied in order to reach reheated steam temperature at the level 620°C, with the assumption that the heat exchanger effectiveness is at the level 0.9) and for flow supplied to heat exchangers of a supercritical part. The flue gases leaving steam reheater were mixing with flue gases leaving the supercritical part. For the purpose of limiting exergy loses, to mixing were subjected flue gases streams which had the same temperatures. For the supercritical part of SHRSG the temperature difference between the media at the so-called hot end of exchanger was equal to 30 K (thereby to the supplementary firing system fuel flow was supplied in volume which permitted to reach flue gases temperature at 630°C) and pinch point amounted to 10 K. In supercritical part of SHRSG model division on twenty sections was applied. Each one was modeled for obtaining the constant increase of temperatures of water/steam ($\Delta T$=15.5 K). Such model permitted the validation of the specific heat capacities of water/steam and flue gases in the function of temperature and pressure and in consequence to obtain curvilinear courses of temperatures of these media in the function of heat flux exchanged in the SHRSG.

For modeling of the SHRSG in compliance with described assumptions it was necessary to supply to it suitable flows of feed water and steam leaving the high-pressure section of steam turbine. In the model it was also assumed, that heat loads ratio of the steam reheater and supercritical part of SHRSG is the same as in the coal-fed boiler, both in the case of the reference unit, as well as after its repowering:

$$\frac{\dot{Q}_{\mathrm{R,SHRSG}}}{\dot{Q}_{\mathrm{SP,SHRSG}}} = \frac{\dot{Q}_{\mathrm{R,SCB}}}{\dot{Q}_{\mathrm{SP,SCB}}} = \left(\frac{\dot{Q}_{\mathrm{R,SCB}}}{\dot{Q}_{\mathrm{SP,SCB}}}\right)_{\mathrm{REF}} \quad (1)$$

The heat loads ratios (1) amounted to 0.2644. For presented assumptions concerning SHRSG at its cooperation with selected gas turbine model the water flow to SHRSG was calculated. It amounted to 52.08 kg/s. Knowing media temperatures in corresponding characteristic points of the unit (points 1, 3, 40, 78 in Fig. 2) and thanks to the knowledge of ratios values (1), the evaluation of reheated steam flow for SHRSG was possible. It amounted to 44.40 kg/s.

The heat exchangers situated on the stream of flue gases leaving SHRSG permitted partial replacement of high- and low-pressure regenerations. The share of the replacement of regenerative heat exchanger was defined as ratio of water flow in replaced exchanger to total water flow (in the text so-called ratio of replacement of respective regenerative exchangers):

$$r_{\mathrm{H}} = \frac{\dot{m}_{72'}}{\dot{m}_{72}}, \quad (2)$$

$$r_{\mathrm{L}} = \frac{\dot{m}_{65'}}{\dot{m}_{65}}. \quad (3)$$

It was assumed, that both flue gases heat exchangers were preheating water to temperatures corresponding to the temperatures of water preheated in replaced regenerative heat exchangers, i.e. $T_{75'}=T_{75}$, $T_{70'}=T_{70}$. Additionally, it was assumed that the effectiveness of none of flue gases heat exchangers can reach a value of more than 0.95 ($(\varepsilon_{\mathrm{HHE}})_{\mathrm{lim}}$), and the temperatures of flue gases at the outlet cannot be lower than 85°C ($(t_{\mathrm{VIII}})_{\mathrm{lim}}$). In the case of increase of ratio of replacement of high-pressure regenerative heat exchangers $r_{\mathrm{H}}$, for assumed level of coal-fed boiler load, the extraction steam flows decreased. In order to fulfill the condition (1) the stream of additional steam was not reheated but was merged with reheated steam after appropriate throttling before entering IP part of the steam turbine.

Hybrid system was modeled in such a way to obtain net power equal to the net power of the reference unit:

$$\left(N_{\mathrm{el,MFHC}}\right)_{\mathrm{n}} = \left(N_{\mathrm{el,REF}}\right)_{\mathrm{n}}. \quad (4)$$

Thus, the repowering by a determined gas turbine and a specified heat exchangers configuration being a part of heat recovery system led to a adequate decrease of a steam turbine power. This power resulted from the equation:

$$N_{\mathrm{elST,MFHC}} = \left(N_{\mathrm{el,MFHC}}\right)_{\mathrm{n}} - N_{\mathrm{elGT,MFHC}} + N_{\mathrm{elON,MFHC}} \quad (5)$$

In order to obtain required steam turbine power, for specified assumptions and for determined $r_{\mathrm{H}}$ and $r_{\mathrm{L}}$ indices values, heat power of a coal-fed boiler was scaled. It was assumed, that the size of coal-fed boiler did not influence the efficiency of the device. The calculations were realized iteratively. All computations were made with the use of GateCycle™ software [12].

## 3. Evaluation indices

For the evaluation of thermodynamic and ecologic effect of supercritical coal-fired unit repowering by a gas turbine according to Fig. 2 and for the assumptions presented in Paragraph 2, the following indices were used:

- incremental efficiency of additional fuel utilization in MFHC:

$$\eta_{\Delta} = \frac{-\Delta\dot{E}_{\mathrm{chc}} \cdot \left(\eta_{\mathrm{el,REF}}\right)_{\mathrm{n}}}{\dot{E}_{\mathrm{chg}}} \quad (6)$$

- $CO_2$ emission reduction obtained due to the introduction of additional gaseous fuel:

$$\Delta\gamma_{\mathrm{CO_2}} = \frac{\dot{E}_{\mathrm{chg}} \cdot e_{\mathrm{CO_2,g}} - \Delta\dot{E}_{\mathrm{chc}} \cdot e_{\mathrm{CO_2,c}}}{\dot{E}_{\mathrm{chg}}}, \frac{\mathrm{kgCO_2}}{\mathrm{MJ_{chg}}}, \quad (7)$$

- unit $CO_2$ emission from multi-fuel unit:

$$\varepsilon_{\mathrm{CO_2}} = \frac{\dot{E}_{\mathrm{chc}} \cdot e_{\mathrm{CO_2,c}} + \dot{E}_{\mathrm{chg}} \cdot e_{\mathrm{CO_2,g}}}{\left(N_{\mathrm{el,MFHC}}\right)_{\mathrm{n}}}, \frac{\mathrm{MgCO_2}}{\mathrm{MWh_{el}}}, \quad (8)$$

where:

$\Delta\dot{E}_{\mathrm{ch\,c}}$ - change of the coal fuel chemical energy in relation to the reference unit, ($\Delta\dot{E}_{\mathrm{ch\,c}} = \dot{E}_{\mathrm{ch\,c,MFHC}} - \dot{E}_{\mathrm{ch\,c,REF}}$),

$\left(\eta_{\mathrm{el,REF}}\right)_{\mathrm{n}}$ - overall net efficiency of electricity production in the reference unit,

$e_{\mathrm{CO_2}}$ - unit $CO_2$ emission from combusting of respective fuels,

$\dot{E}_{\mathrm{ch\,g}}$ - flux of gaseous fuel chemical energy (utilized in gas turbine and supplementary firing system).

Incremental efficiency, which for presented assumptions is defined by (6), is often used in analysis of multi-fuel hybrid cycles. In calculations it was assumed, that coal which was saved thanks to the utilization of gaseous fuel $\Delta\dot{E}_{\mathrm{ch\,c}}$ (in relation to the reference unit) is utilize in autonomous unit characterized by the same overall net efficiency as a reference unit. Due to the fact, that in denominator of (6) the flux of gaseous fuel chemical energy appears, the incremental efficiency can serve to compare multi-fuel hybrid cycles with units utilizing only gaseous fuels.

The index of $CO_2$ emission reduction, defined by (7), which is the result of connection of two technologies, is a quantity determining the ecologic effect of conversion to mutifuelness.

Next indices, i.e. unit $CO_2$ emission, defined by (8) expresses the quantity of emitted $CO_2$ per unit of net energy production. The index is used for ecological evaluation of concerned technology. It can serve as an evaluation quantity for comparing of different energy technologies based on utilization of carbon- and hydrocarbon-fuels. In the case of reference unit (SCPP) $\varepsilon_{CO2}$=0.7944 $\mathrm{MgCO_2/MWh_{el}}$.

## 4. Results of calculations

Fig. 3 shows the constant values lines for three indices defined in Paragraph 3. In the case of the use in MFHC unit of the GE MS9171 gas turbine the complete replacement of low-pressure regeneration and/or complete replacement of high-pressure regeneration ($r_H$=1, $r_L$=1) is not possible. It results from restrictions which were assumed for temperature of flue gases leaving HHE and LHE heat exchangers, as well as for effectiveness of HHE heat exchanger.

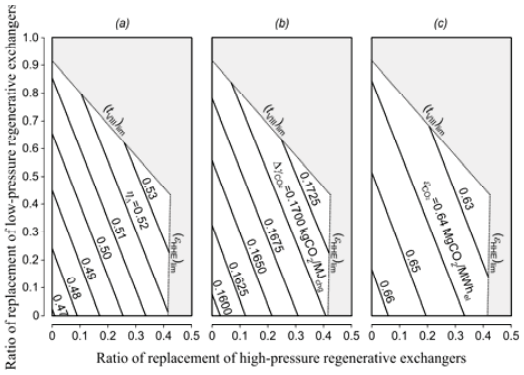


*Fig. 3. Influence of high-pressure ($r_H$) and low-pressure ($r_L$) regeneration replacement on indices: $\eta_\Delta$ (a), $\Delta\gamma_{CO2}$ (b) and $\varepsilon_{CO2}$ (c).*

In the next step of analysis the comparison of thermodynamic and ecologic effect of the connection of SCPP unit with gas turbine installation, i.e. MFHC unit with other popular energy technologies utilizing coal- and gaseous-fuels was conducted. For this purpose suitable calculations were made or data from literature were used. Series of quantities defining thermodynamic and ecologic effectiveness of MFHC unit and other technologies considered in area of electroenergetic sector were calculated.

In the case of MFHC unit the values presented in Table 1 for $r_H$=0.4010, $r_L$=0.4585 were obtained. These levels of ratios of replacement of regenerative exchangers resulted from the wish of obtaining the temperature of flue gases $t_{VIII}=(t_{VIII})_{lim}$ and effectiveness of high-pressure exchanger HHE $\varepsilon_{HHE}$=0.90. The results presented in Table 1, except for the reference (SCPP) and MFHC units, concerned following technologies:

- supercritical coal-fired power plant integrated with membrane carbon capture and storage installation (SCPP+CCS, results from [11]),
- simple cycle gas turbine based on the use of gas turbine characterized by data of GE MS9171 model (SCGT),
- combined cycle gas turbine based on the use of gas turbine characterized by data of GE MS9171 model and three-pressure heat recovery steam generator (CCGT).

*Table 1.Comparison of thermodynamic and ecologic quantity for five considered energy technologies*

| Indices | Technologies | | | | |
|---|---|---|---|---|---|
| | SCPP | MFHC | SCPP+CCS | SCGT | CCGT |
| $(N_{el})_{gr}$ (MW) | 602.20 | 581.84 | 735.24 | 546.52 | 557.45 |
| $N_{elON}$ (MW) | 55.68 | 35.32 | 222.40 | - | 10.93 |
| $\dot{E}_{ch\,c}$ (MJ/s) | 1234.52 | 731.53 | 1507.23 | 0 | 0 |
| $\dot{E}_{ch\,g}$ (MJ/s) | 0 | 413.44 | 0 | 1639.73 | 1039.81 |
| $e_{CO2,c}$ (kg$CO_2$/GJ) | 97.69 | 97.69 | 9.11 | 0 | 0 |
| $e_{CO2,g}$ (kg$CO_2$/GJ) | 0 | 55.78 | 0 | 55.78 | 55.78 |
| $(\eta_{el})_{gr}$ | 0.4878 | 0.5082 | 0.4878 | 0.3333 | 0.5361 |
| $(\eta_{el})_n$ | 0.4427 | 0.4773 | 0.3626 | 0.3333 | 0.5256 |
| $\varepsilon_{CO2}$ (M$gCO_2$/M$Wh_{el}$) | 0.7944 | 0.6226 | 0.0905 | 0.6025 | 0.3820 |

For the reference unit the largest value of unit $CO_2$ emission was obtained. The connection of this systemt with membrane CCS installation permits to obtain very low value of unit $CO_2$ emission (0.0905 M$gCO_2$/M$Wh_{el}$), but this integration causes large decrease of net efficiency value (by 8.01 percentage points). The reason for this is an increase of internal load rate which is a consequence of necessity of driving vacuum-pump and air compressors used for $CO_2$ capture and prepare it to transport and storage. Higher decrease of net efficiency for SCPP+CCS unit counteracted in [11] by using of heat recovered from compressed permeate in steam cycle for regeneration replacement.

The repowering of SCPP with gas turbine and heat recovery system permits to increase gross and net efficiency in relation to the reference unit – by 2.04 and 3.46 percent points, respectively. The obtaining of the greater growth of net efficiency in this case results from essential decreasing of own needs connected with coal management (driving of coal mills and forced draft fan). Changing into multi-fuel technology essentially decreases unit $CO_2$ emission. A value here was reached, which is only slightly higher from the unit emission obtained for the autonomous gas turbines (SCGT). Such type of comparisons can have theoretical character because the investments in SCGT systems in this range of power can only be considered for electricity peak production.

From the considered technologies the most effective from the thermodynamic point of view is CCGT unit. Low value of gross efficiency, as for a solution with a three-pressure heat recovery steam generator, results from the use of a gas turbine with relatively low efficiency, i.e. 0.3333. The obtained net efficiency for CCGT unit, i.e. 0.5256 is lower than the incremental efficiency obtained for MFHC unit, i.e. 0.5386. This fact confirms thermodynamic legitimacy of SCPP connection with gas turbine installation and three-level heat recovery system. Obtained for CCGT systems relatively low value of unit $CO_2$ emission favors the unusual up to now interest in this technology among investors.

## 5. Conclusion

Presented results and conclusions from the carried out researches allows for determining of MFHC technology as a high-efficiency technology. Undoubtedly, about the implementation of multi-fuel gas-coal systems in the polish electroenergetic system the economic analysis will decide. The key influence of two parameters should be expected here, i.e. natural gas price and the price of $CO_2$ emission allowances. Due to the fact, that the unit $CO_2$ emission from gaseous fuel is significantly lower in comparison to the emission from coal, a positive influence of repowering on overall cost of emission allowances purchase should be considered. Further $CO_2$ emission limitation in the considered multi-fuel technology will be possible together with the development of CCS technologies, including less energy demand technologies of $CO_2$ capture before combustion (pre-combustion), especially predisposed for gaseous fuels.

In the area of polish energy sector large hopes are connect with researches over the wide spectrum of solutions of CCS installations. Achievement of unit emission reduction effect, together with simultaneous decrease of internal load connected to the CCS technology, should lead in the future to the expansion of supercritical coal-fired power plants integrated with CCS installations. Nowadays, other potentially considered technologies provided for polish electroenergetic sector is integrated gasification combined cycle, as well as oxy-fuel technologies. The analysis of these solutions was not undertaken, however, in the content of the paper.

**Nomenclature**

| | |
|---|---|
| $e_{CO_2}$ | $CO_2$ emission in relation to fuel chemical energy, $kgCO_2/GJ$ |
| $\dot{E}$ | energy flux, MW |
| $\dot{m}$ | mass flow rate, kg/s |
| $N$ | power, MW |
| $\dot{Q}$ | heat flux, MW |
| $r$ | ratio of replacement of regenerative exchangers |
| $T$, $t$ | temperature, K, °C |
| $\Delta$ | increase, reduction |
| $\Delta\gamma_{CO_2}$ | $CO_2$ emission reduction in relation to chemical energy of additional gaseous fuel, $kgCO_2/GJ$ |
| $\varepsilon, \varepsilon_{CO_2}$ | effectiveness and $CO_2$ emission in relation to net electricity production, $kgCO_2/MWh_{el}$ |
| $\eta_\Delta$ | incremental efficiency, - |

**Indices**

| | |
|---|---|
| c | coal |
| chc, chg | chemical of coal and gaseous fuel |
| g | gaseous fuel |
| el | electric |
| gr | gross value |
| GT | gas turbine |
| H, L | high and low-pressure |
| HE | heat exchanger |
| lim | limit value |
| MFHC | multi-fuel hybrid cycle |
| n | net value |
| ON | own needs |
| R | reheater or regenerative exchanger |
| SCB | supercritical coal-fed boiler |
| ST | steam turbine |
| SHRSG | supercritical heat recovery steam generator |
| SP | supercritical part |
| REF | reference unit |

## References


[1] Chmielniak T., Trela M., 2008, *Diagnostics of New-generation Thermal Power Plants*, IFFM Publishers, Gdańsk.

[2] Escosa J.M., Romeo L.M., 2009, Optimizing $CO_2$ avoided cost by means of repowering, Applied Energy, 86, pp.2351–2358.

[3] Bartela Ł., Liszka M., 2009, A serial connection of a supercritical coal fired power plant with gas turbine installation, Rynek Energii, 6(85), pp.111-116. [in Polish]

[4] Ziębik A., Kotowicz J., Liszka M., Bartela Ł., 2008, Combined power plants with gas turbine installations (parallel and serial units). Supercritical Coal Fired Units, Ordered Research Project: PBZ – MEiN – 4/2/2006, topic: I.2.4/2, Gliwice. [in Polish]

[5] Hansen S., Sørensen H.D., 2003, Process design and optimization of the Avedore 2 multifuel power plant, *Proceedings of the 16th International Conference on Efficiency, Costs, Optimization, and Environmental Impact of Energy Systems ECOS*, Copenhagen.

[6] Hansen S., Jensen S.E., 2000, Hybrid units at Map Ta Phut are first of a kind, Modern Power Systems, August.

[7] RWE Power AG, Essen – Cologne, URL: http://www.rwe.com/rwepower.

[8] Kotowicz J., Liszka M., Bartela Ł., 2009, Simulation analysis of multi-fuel hybrid cycles. *Proceedings of the 26th International Pittsburgh Coal Conference*, Pittsburgh, PA, USA.

[9] Alobaid F., Strohle J., Epple B., Kim H.G., 2009, Dynamic simulation of a supercritical once-through heat recovery steam generator during load changes and start-up procedures, Applied Energy; 86, pp.1274–1282.

[10] Dumont M.N, Helen G., 2004, Mathematical modelling and design of an advanced once-through heat recovery steam generator, Computers and Chemical Engineering, 28, pp.651–660.

[11] Kotowicz J., Chmielniak T., Janusz-Szymańska K., 2010, The influence of membrane $CO_2$ separation on the efficiency of a coal-fired power plant. Energy, 35,841–850.

[12] GateCycle™, Version 5.40.0.r., 1989 - 2001 GE Enter Software, LLC.


**Acknowledgments:** The investigations presented in this paper have been carried out within the frame of the research project BK-228/RIE5/2009.

# TECHNICAL EVALUATION OF IGCC SYSTEM FOR BRAZILIAN COAL AND PETROLEUM COKE

*Pablo Andrés Silva Ortiz[a], Osvaldo José Venturini[b], Electo Eduardo Silva Lora[c], Maria Luiza Grillo Reno[d]*

[a,b,c,d] *Federal University of Itajubá - UNIFEI, Excellence Group in Thermal Power and Distributed Generation - NEST, Itajubá, Minas Gerais, Brazil*

**Abstract:** The trend and the increase in global production of petroleum coke are the result of multiple and innovative industrial applications. From this point of view and also considering the actual situation of the traditional energy reserves worldwide, it is important to conduct studies in this area through the analysis of the main components of the plants utilizing this fuel (petroleum coke). The main target of this study is to realize a technical evaluation of different variants of the IGCC (Integrated Gasification Combined Cycle) technology, using as fuel petroleum coke and coal. The gasification process and the combined cycle power plant are analyzed considering their potential of implementation in Brazil.

Keywords: Gasification, Integrated Gasification Combined Cycle (IGCC), Petroleum Coke, Coal, Carbon Capture Sequestration (CCS), Gasifiers.

## 1. Introduction

Nowadays, Integrated Gasification Combined Cycle (IGCC) is one of the most important and promising clean technologies for power generation, when using coal, petroleum coke (petcoke) and biomass as energy sources. The environmental benefits and the higher energy conversion efficiency distinguish this technology from the traditional ones.

The IGCC power plants performance is affected by different technological and operational aspects, e.g. gasifier agent, gasification technology, environmental conditions, coal quality and power demand. This group of variables conduces necessarily to the use of thermodynamic simulation tools to analyze the different process and equipments used in this technology. In this paper the analysis are carried out considering the gasifier simulation in the software CSFBM version 24.9 [1] (Comprehensive Simulator of Fluidized and Moving Bed equipment) to determinate the synthesis gas (syngas) composition. In a following stage, the syngas composition is used in GateCycle™ version 5.51 [2] to analyze power plant performance.

The methodology used for thermodynamics simulation of IGCC plants, as well the results obtained through CSFBM and GateCycle interaction, are discussed in this paper. The results for gasification process simulation using different fuels are also presented. The results of GateCycle IGCC model were evaluated considering the gasification behavior and the energy efficiency of combined cycle. As a preliminary analysis, the results were compared with the operating parameters of ELCOLGAS Puertollano IGCC power plant in Spain.

Nowadays, there is a tendency in using thermodynamic simulations to estimate the performance of gasification process as a function of the available energetic resources, operational and environmental conditions. Several commercial software can be used to perform these simulations [3-4]. Through the integration of the software results it is possible to analyze different generation capacities, and its behavior under different fuel, air, oxygen, nitrogen, steam and water flow rates [5].

Corresponding Author: Pablo Silva, Email: pablo.silvaortiz@gmail.com
Osvaldo Venturini, Email: osvaldo@unifei.edu.br
Electo Silva, Email: electo@unifei.edu.br
Maria Grillo, Email: malureno@yahoo.com.br

## 2. Fuel Characterization

Initially it will be presented the main characteristics of the fuels (coal, petcoke and a mix between 50% coal with 50% petcoke) used in this analysis. Tables 1, 2 and 3 show the elemental fuel analysis that will be considered in the gasification technologies simulation [6-7].

*Table 1. CANDIOTA COAL Elemental fuel analysis [6]*

| Ultimate analysis | | Proximate analysis (wt. %) | |
|---|---|---|---|
| Carbon (%) | 34.0 | Moisture (%) | 15.0 |
| Hydrogen (%) | 2.6 | Volatile | 16.4 |
| Nitrogen (%) | 0.7 | Fixed Carbon | 24.4 |
| Oxygen (%) | 8.5 | Ash (%) | 44.2 |
| Sulphur (%) | 1.2 | | |
| Ash (%) | 53.0 | | |
| HHV (MJ/kg) | 13.8 | | |

*Table 2. PETCOKE Elemental fuel analysis [7]*

| Ultimate analysis | | Proximate analysis (wt. %) | |
|---|---|---|---|
| Carbon (%) | 86.3 | Moisture (%) | 7.0 |
| Hydrogen (%) | 3.5 | Volatile | 19.2 |
| Nitrogen (%) | 1.6 | Fixed Carbon | 73.5 |
| Oxygen (%) | 0.5 | Ash (%) | 0.3 |
| Sulphur (%) | 7.5 | | |
| Ash (%) | 0.6 | | |
| HHV (MJ/kg) | 33.6 | | |

*Table 3. CANDIOTA COAL / PETCOKE MIXTURE, Elemental fuel analysis*

| Ultimate analysis | | Proximate analysis (wt. %) | |
|---|---|---|---|
| Carbon (%) | 62.5 | Moisture (%) | 9.2 |
| Hydrogen (%) | 3.0 | Volatile | 18.6 |
| Nitrogen (%) | 1.1 | Fixed Carbon | 51.5 |
| Oxygen (%) | 4.5 | Ash (%) | 20.7 |
| Sulphur (%) | 3.9 | | |
| Ash (%) | 25.0 | | |
| HHV (MJ/kg) | 25.1 | | |

### 2.1. Coal

In the Brazilian energy matrix, the coal corresponds to only slightly more than 1% of total primary energy produced [8]. However, it is the most abundant fossil resource in Brazil. Considering the estimated reserves it is projected that there are sufficient reserves for 200 years of supply (against 40 years for oil and 60 years for natural gas).

Despite being an abundant resource in Brazil (reserves are $32x10^9$ ton [9]), its low quality, due to high ash and sulfur contents, and the related environmental impacts, makes it underutilized. The most important deposits of Brazil are located in the states of Rio Grande do Sul, Santa Catarina and Paraná.

Coal is classified according to its quality as: peat, low-content coal, which is one of the early stages of coal with carbon content of around 45%, lignite, which features carbon ranging 60% to 75% bituminous coal, most used type, due to its advantages in the generation of electricity and the production of cement, iron and steel, and contains between 75% and 85% carbon, and anthracite, the purest of coal, containing 90% of coal or higher.

The high ash content of the Brazilian coal can influence negatively the performance of a generation system based on its combustion [10]. For this reason, in many applications, it is recommended to mix the coal with petcoke to improve the properties of the fuel.

### 2.2. Petroleum coke

Petcoke is a byproduct of the petroleum refining industry which has a high calorific value, low cost and sulfur content determined by the type of petroleum, from which it originates [11].

Due to the increasing quantities of heavy oil that are being processed nowadays, the production of petcoke is also increasing. The biggest potential of petcoke is obtained when it is used in production processes for the industrial sector, mainly in electricity generation [12] and cement production.

The Brazilian petcoke is produced in parks steel and this product is considered as LSC (low sulfur content) because it is produced during the processing of oil with low sulfur content (0.8% sulfur [13]), while some imported petcoke, which may come from Venezuelan oil refining, presents sulfur content in the order of 3% by weigh [14], has a low market value and a great chance of becoming an economically viable fuel for thermal generation. Therefore, the advantage of using petcoke is the possibility of poly-generation when it is gasified to produce syngas, that can be burned in gas turbines.

## 3. Gasification process simulation with the CSFBM software

CSFMB is a comprehensive mathematical model and simulation program for bubbling and circulating fluidized-bed, as well as downdraft and updraft moving-bed equipment. Among these equipments, there are furnaces, boilers, gasifiers, dryers, and reactors [15]. The proposed model uses a circulating fluidized bed as gasifier, this technology has been successfully used in many fields, including combustion, biomass/coal gasification and oil catalytic cracking, which is the type that best fits within the possibilities of simulation gasifiers in the CSFMB program, taking into account the power ranges that they can achieve. Figure 1 shows the CSFMB interface, where is introduced the stream characterization and fuel composition, in wet basis, for proximate analysis, and in dry basis, for ultimate analysis. The data shown is this figure refers to coal used in Candiota, a power station located southern Brazil.

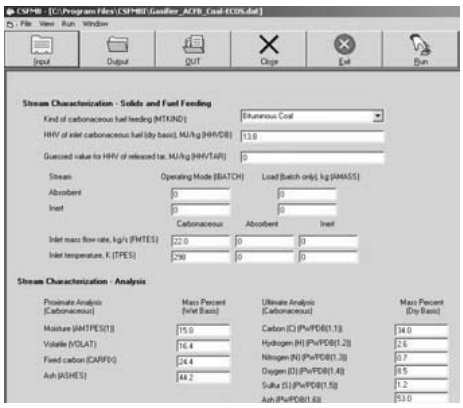


*Fig. 1. CSFMB interface*

Nowadays, there are several software available for chemical process simulation, such as Chemcad, Aspen Hysys and Aspen Plus, which have the capability of estimating the final composition of syngas, using ideal reactors and the knowledge of the initial composition of the fuel. Recently simulation schemes with the use of Aspen and Fortran were also developed, and are being employed in the gasification process, in order to analyze commercial gasifiers [4]. Among these software one can find CSFBM, which is capable of dealing with the major components of a gasifier into the model gasification process simulation.

The kinetic parameters for homogeneous reactions, illustrated in the equations (1) to (4), were identified and specified during the modeling and simulation of the gasification process.

$$CO + H_2O \rightarrow CO_2 + H_2 \quad (1)$$

$$2CO + O_2 \leftrightarrow 2CO_2 \quad (2)$$

$$2H_2 + O_2 \leftrightarrow 2H_2O \quad (3)$$

$$CH_4 + 2O_2 \rightarrow CO_2 + 2H_2O \quad (4)$$

Among the many reactions involved in the gasification process, the main determinants parameters of the kinetic coefficient of the most important reactions [1] are shown in the Table 4.

*Table 4. Kinetic coefficients*

| Reaction | rate of reaction ($k_{0,i}$) | Circulating Fluidized Bed | T (K) |
|---|---|---|---|
| COAL | $2.78 \times 10^3$ | $kmol^{-1}\ m^3\ s^{-1}$ | 1510 |
| PETCOKE | $1.3 \times 10^{17}$ | $kmol^{-0.75}\ m^{2.25}\ s^{-1}$ | 34740 |
| MIXTURE | $5.159 \times 10^{13}$ | $kmol^{-1.5}\ m^{4.5}\ K^{1.5}\ s^{-1}$ | 3430 |

On the other hand, due to the complexity of the gasification process, this is usually carried out by considering the balance of a reactive system under reasonable suppositions [16-18], but the various gasification technologies employed prevent identifying their effects on the composition of the gas produced [5]. Even though there are underway many research projects and some experiences been reported on combined cycle plants around the world, still remain uncertainties about some of the variables involved in the simulation of the gasification processes.

### 3.1. Results and analysis of gasification process simulation

Gasification process simulation was carried out using different types of fuels (Tables 1 – 3) and a circulating fluid bed as gasifier. Table 5 lists the main parameters required by CSFMB software for the gasifier simulation using coke as fuel. In the tests carried out, the feed mass flow rates, the feed gas though distributor (Gasification Agent) and the granulometry of the fuel fed to the gasifier were modified in order to achieve the conditions above the second turbulence limit, allowing for increased contact between particles and gases.

*Table 5. Key input parameters of the gasifier design*

| Parameter | Variable | Value | Units |
|---|---|---|---|
| ***STREAM CHARACTERIZATION SOLIDS AND FUEL FEEDING*** | | | |
| Apparent density, Carbonaceous | ROPES(1) | 740 | kg/m$^3$ |
| True density, Carbonaceous | RORES(1) | 1750 | kg/m$^3$ |
| Inlet mass flow rate, Carbonaceous | FMTES(1) | 40 | kg/s |
| Inlet temperature, Carbonaceous | TPES(1) | 298 | K |
| ***EQUIPMENT DATA - BASIC GEOMETRY*** | | | |
| ***Gasifier*** | | | |
| Bed - equivalent hydraulic internal diameter | DD | 3.0 | m |
| Freeboard - equivalent hydraulic internal diameter | DF | 3.0 | m |
| Position of main gas withdrawal | ZF | 10.0 | m |
| Position of carbonaceous fuel feeding | ZFEED(1) | 1.0 | m |
| ***Distributor*** | | | |
| Number of orifices for gas/steam injection (0=porous plate) | NOD | 33000 | - |
| Diameter of orifices for gas/steam injection through distributor | DOD | 0.003 | m |
| ***EQUIPMENT DATA - CYCLONES AND RECYCLING*** | | | |
| ***Ciclone*** | | | |
| Internal diameter of cyclones | DCY | 0.7 | m |
| Height of the cylindrical part of cyclones | HCY | 1.000 | m |
| Height of the conical part of cyclones | HCYC | 1.000 | m |
| Position of recycling injection | ZRCY | 2.00 | m |
| ***STREAM CHARACTERIZATION GASES THROUGH DISTRIBUTOR*** | | | |
| ***Gasification agent*** | Air | | |
| Inlet gas through distributor, Temperature | TEGID | 435 | K |
| Inlet gas through distributor, Pressure | PEGID | 160 | kPa (abs.) |
| ADDITIONAL OPERATIONAL CHARACTERISTICS Average pressure in the bed | POPER | 150 | kPa (abs.) |
| Local Ambient Conditions | | | |
| AVG surrounding air temperature | TAMB | 290 | K |
| Wind velocity | VV | 2 | m/s |

Figures 2 to 4 show the mass flow (kg/s) gases for each kind of fuels presented in Table 6. This table described the main compounds in mass percentage of the synthesis gas produced from coal, pet coke and a mixture or both, using the CSFMB software without taking into account the low percentage of $H_2$, $H_2S$, $NH_3$ and $SO_2$ compounds.

*Table 6. Synthesis gas composition*

| | COAL | PETCOKE | MIXTURE (50:50w) |
|---|---|---|---|
| $CO_2$ | 6.19 | 3.97 | 4.07 |
| CO | 13.25 | 12.85 | 19.12 |
| $CH_4$ | 0.05 | 0.07 | 0.04 |
| $H_2O$ | 7.58 | 6.83 | 6.05 |
| $H_2$ | 11.46 | 12.24 | 16.08 |
| $N_2$ | 59.97 | 61.95 | 53.41 |
| HHV (MJ/kg) | 3,95 | 4,30 | 4,19 |

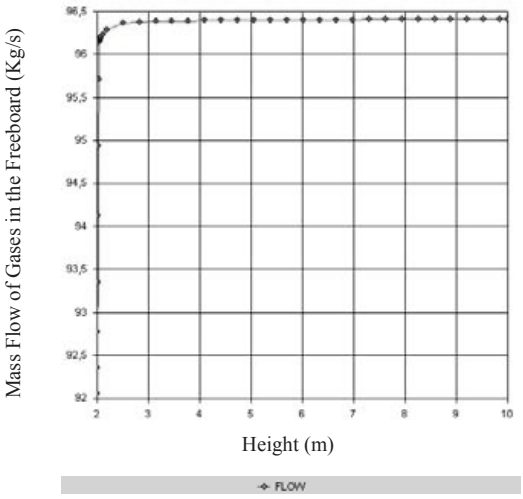


*Fig. 2. Coal Case, Mass flow of gas exiting*

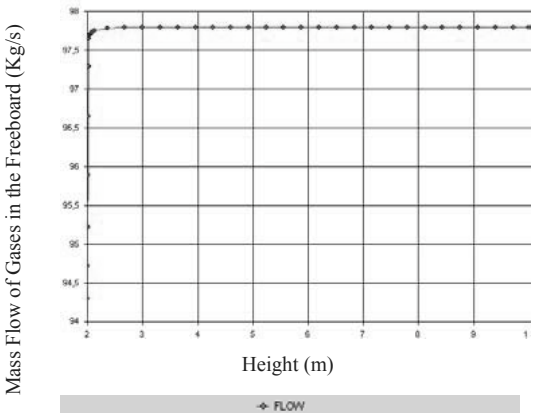


*Fig. 3. Petcoke Case, Mass flow of gas exiting*

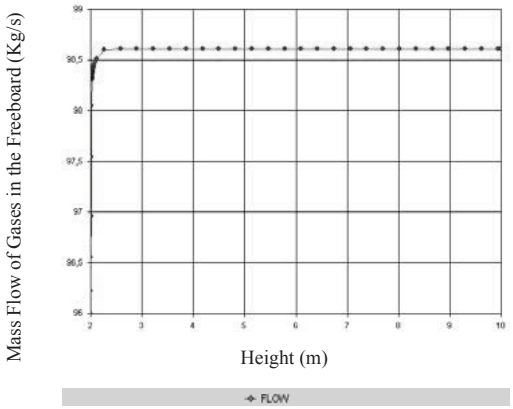


*Fig. 4. Mixture Case, Mass flow of gas exiting*

## 4. Combined cycle simulation using GateCycle software

A combined cycle in the generation of energy is defined as "The coexistence of two thermodynamic cycles in the same system", and simulation as "The process of imitating a real phenomenon with a set of mathematical formulas. In addition to imitating processes to see how they behave under different conditions, simulations are also used to test new theories" [19]. IGCC systems are one of the most efficient technologies to produce energy using coal and petcoke as fuel, and their efficiency can be as high as 45 to 50%. This technology is one of the promising options which need to be considered for future power generation possibility. Another promising possibility is the Carbon Capture Sequestration (CCS), which can be integrated to IGCC power plants [20]. Currently are efforts related with development and demonstrated CCS with IGCC technology were originally focussed on improved concepts for coal-based plants and thus on an alternative to conventional steam plants. The experience with the demonstration plants in Europe, in the United States, and now also in Japan, and the parallel development efforts for improved steam power plants resulted in a situation where coal-based IGCC (see Table 7). This technology is, in one to be considered as a commercially available technology, and in the order hand still needs further reduction in their initial costs to be fully competitive [21].

*Table 7. IGCC power plants built, in operation, under design, construction or commissioning.*

| | Total $MW_{el}$ | Total Operational $MW_{el}$ | Operational Coal/Petcoke IGCC | Operational Oil/heavy residues IGCC |
|---|---|---|---|---|
| Europe | 4.170 | 2.620 | 35 % | 65 % |
| Asia/Australia | 1.400 | 1.120 | 29 % | 71 % |
| Americas USA, Canada | 2.020 | 960 | 83 % | 17 % |
| Total | 7.590 | 4.700 | 43 % | 57 % |

From the 7,600 MW of global IGCC power plants which have been built or are under design, construction and commissioning, 4,700 MW are in operation. About 55 % of this operational capacity is installed in Europe (Table 7). Next generation plants of larger size, where the lessons learned from the today operational plants are implemented and co-firing of low-cost fuels, wastes or biomass is foreseen for reduction of fuel costs and to produce green electricity, could pave the way for a commercial breakthrough. This is primarily expected for IGCC applications with CCS [21]. The situation is different for refinery residues where, depending on the individual site conditions, IGCC can already today be considered as a commercially attractive solution for power generation, co-generation or co-production of power and hydrogen internal use purposes. The introduction of IGCC for refinery applications was supported by the experience gained with the technology from the coal-based plants.

In this paper, the IGCC system simulation was conduct using a model developed in GateCycle version 5.51 (Figure 5) and syngas composition presented in Table 6. The simulation considered the ISO standard conditions (1 atm, 15 °C and 60 % HR) and GateCycle's model was developed with the information presented in Table 6. This model is characterized by the integration of thermodynamic cycles, Brayton and Rankine, the first of them describes the workings of the gas turbine engine (power cycle) and the second describes a model of steam operated forward heat engine which converts heat into work (steam cycle).

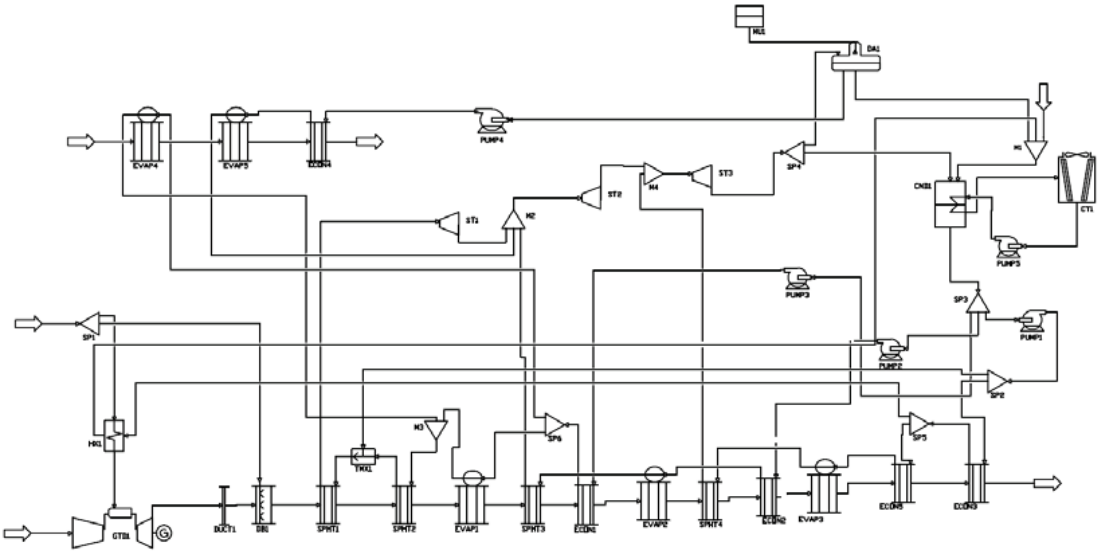

*Fig. 5. IGCC power plant scheme modeled on GateCycle*

The models available in GateCycle for equipments used in the combined cycle systems (steam and gas turbine, evaporators, heat exchanger, HRSG, condenser, cooling tower, etc.) taking into account operation parameters of the ELCOGAS IGCC power plant in Puertollano, Spain. This power plant has a successful industrial behavior and has been used as standard reference for the study of new technologies. Table 6 presents the technical description of this power plant [22].

Puertollano's combined cycle has a 317 MW net capacity (182 MW from gas turbine and 135 MW from steam turbine). Shell gasification technology with pure oxygen is implemented in Puertollano, the flow is ascendant and dried fuel is feeded using nitrogen. Heat recovery steam generator (HRSG) is used to recover heat from exhaust gas turbine gases and from cooling process of raw syngas [5].

In this work, temperature, pressure, clean syngas composition, and mass flow are initial parameters of the gas turbine equipment, after than combusted gases goes to HRSG equipments and steam production and heat recovery are estimated. As a final point, the electric power generated is estimated and efficiency and heat rate is evaluated.

*Table 6. PUERTOLLANO IGCC technical description*

| System | Variable | | Value |
|---|---|---|---|
| Environmental conditions | Temperature [°C] | | 15 |
| | Humidity [%] | | 0.8 |
| | Pressure | | 1 |
| Coal | Flow [kg/s] | | 29.7 |
| | LHV [kJ/kg] | | 22550 |
| Syngas | Flow [kg/s] | | 120 |
| | LHV [kJ/kg] | | 4242 |
| Gasification Island | High pressure recovering Temp. [°C] | In | 800 |
| | | Out | 400 |
| | Middle pressure recovering Temp. [°C] | In | 400 |
| | | Out | 235 |
| | High pressure steam | Pressure [bar] | 126 |
| | | Flow [t/day] | 230 |
| | Middle pressure steam | Pressure [bar] | 35 |
| | | Flow [t/day] | 23 |
| HRSG | Steam | High pressure [bar] | 127 |
| | | Middle pressure [bar] | 35 |
| | | Low pressure [bar] | 6.5 |
| | Exchanger area [$m^2$] | | 300000 |
| | Combusted gas temperature [°C] | In | 535 |
| | | Out | 103 |
| Gas turbine | Power [MW] | | 182 |
| | Mass flow air [kg/s] | | 537 |
| | Compression | | 15:1 |
| | Thermal efficiency [%] | | 34.6 |

| | | | |
|---|---|---|---|
| Steam turbine | Power [MW] | | 135 |
| | High pressure superheated steam | Pressure [bar] | 122 |
| | | Temp. [°C] | 509 |
| | Reheated steam | Pressure [bar] | 29 |
| | | Temp. [°C] | 517 |
| Air splitter unit | Air flow [kg/s] | | 80 |
| Combined cycle | Net power [MW] | | 317.7 |
| | Efficiency [%] | | 47.44 |
| | Heat Rate [kJ/KWh] | | 7589 |

Figures 6 to 8 shows the results obtained for simulations of IGCC power plant using syngas resultant for different types of fossil fuels. The simulations were performed considering Siemens V94.3A (1999 GTW) gas turbines, in the power plant of Figure 5.

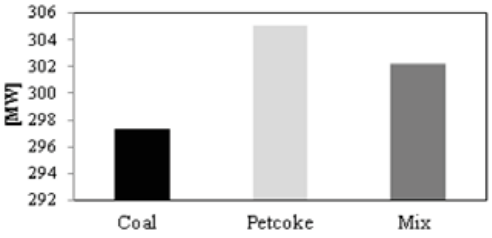


*Fig. 6. Combined Cycle Net Power*

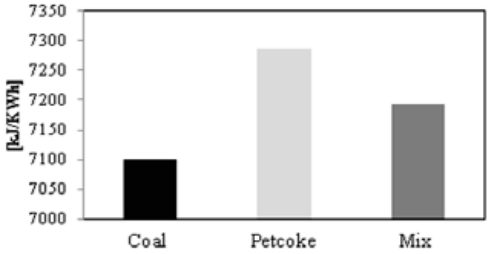


*Fig. 7. Combined Cycle Heat Rate*

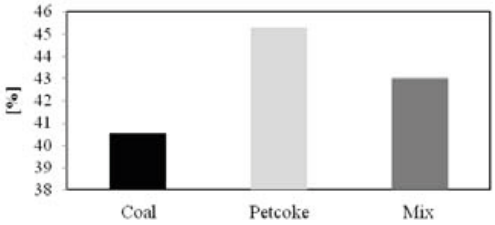


*Fig. 8. Combined Cycle Global Efficiency*

## 5. Brazilian potential for implementation of IGCC systems

The viability of implementing IGCC technology using Brazilian coals or petcoke depends basically on the following factors: the initial investment for the plant built-up, the investment return and the analysis of potential factors that could appear and avoid a proper operation of the plant due to the low quality of Brazilian coals.

One proposal is to perform the characterization of different types of petcoke, its constituents, concentrations and volume of production, in a way that it is possible to make an effective model of a gasification system for specific use of petcoke in refineries. Through this thermodynamic modeling it is possible to evaluate the technical feasibility of the system using pieces of market equipment and its implications. Additionally, the modeling allows the verification of several possible alternatives such as generation of steam, hydrogen production and CCS. This modeling will also serve as a basic tool to understand the structural theory of the cycle that allows the application of exergoeconomic optimization techniques and besides it will facilitate the economic and financial analysis of the entire system.

This type of technology that is being adopted in Texaco, Exxon and Shell refineries using General Electric gas turbines for ten years, can also be applied to cases in Brazilian refineries, such as Landulpho Alves refinery (RLAM) located in São Francisco do Conde, in the state of Bahia, which has a capacity installed of 323 thousand barrels per day. The hydrogen produced could be sent to the nitrogenous fertilizer plant of Petrobras (FAFEN-Ba) for the production of ammonia and the CCS would be injected into mature oil fields in the vicinity.

Other interesting option would be to build a pilot plant that can be extremely important for the evaluation of the feasibility of the use of )GBSHEB IGCC, making it possible to evaluate the impact of the large amount of ash and moisture existing in coal on the fluidized bed and to integrate the various components of an IGCC.

The pilot plant proposal will allow a better conception of Brazilian's coal with IGCC showing different characteristics of this technology. For example:

- An important alternative to be considered is the construction of a raw coal treatment plant, making in it a cleaning until it achieves an ash content of about 25% becoming a coal of better quality, maybe a coal like the Parana or Rio Grande do Sul region [23]. Thus, doing the use of coal received could result in a gas of better quality even when using the air as gasifying agent.
- The use of oxygen as a gasifying agent allows generating a fuel gas with better calorific value free of particles and tars as a result of high operating temperatures and also enables the conventional treatment of the gas which is a proven technology. The use of oxygen improves the efficiency of IGCC power plants.
- There is also the development of hot gas cleaning and that could be used in a gasification system to oxygen resulting in a good efficiency of this equipment.

## Conclusions

CSFBM software is an adequate tool for gasification process using gasifier type circulating fluid bed. It makes possible to estimate composition of syngas using different types of fuel, highlighting in the obtained results the use of petcoke and the mixture coal/petcoke. It is evident that the composition of the carbonaceous material being fed, such as the technology and the parameters of operation influence greatly the composition of the syngas obtained from the gasification process.

The gasifier model was dimensioned based on the gas turbine power requirements of the combined cycle, resulting a gasifier with a geometry and a design conditions that involve a technical, economic and financial assessment, in order to determine the feasibility of implementation in IGCC systems. In this model was using air as gasification agent given that the particle content and tar of the syngas resulting is low levels to the gasifier type selected.

In general, the use of air in the gasification process is a low cost and can be considered as the most economical gasification agents. In addition, used mixture of air and oxygen as gasification agent, for example, mixtures of 80% oxygen and 20% air, can be obtained a decrease in the nitrogen percentage present in the syngas, increasing its calorific value.

GateCycle's model applied used two syngas streams are used in the syngas heat recovery block and to consider the feed up gas turbine. In the first one, pressure, temperature and mass flow information is provide for estimation of heat recovery and steam production from the gasification island. The second stream is feed with information associated to clean syngas composition as well pressure, temperature, and mass flow. Moreover, the power cycle using 3-level pressure for determining heat rate and efficiency of combined cycle were used to validate our thermodynamics simulations.

The IGCC technology has been used experimentally by developed countries as a consequence of the importance of coal as a fossil fuel and the recent concern about the damage to the environment by direct combustion of coal. It necessary to await a major advance and tends of this technology to be less expensive, together with new studies and if appropriate, deploy it in Brazil.

Theoretically it is possible the efficient operation of an IGCC using Brazilian's coal but the high cost makes it unfeasible for implementation at least temporarily the development of this technology in Brazil, unless there is a government decision to its deployment. Research centers and universities, private companies and government National, considers important for the development of the country the use of Brazilian coal and sets a target a larger share of the national energy matrix, as suggested methods to use the combustion of fossil fuel in fluidized bed reactor and its gasification in IGCC. Research experience in this area exists, i.e. CIENTEC developed a pilot plant for combustion and gasification used Brazilian's coals and should be extremely important to use the training and experience gained by those involved in studies in this area, even if use of imported coal for electricity generation always looking to minimize our dependence on foreign.

## References


[1] CSFMB©, Marcio L. de Souza-Santos, 2010. Tuturial of Comprehensive Simulator of Fluidized and Moving Bed Equipment Series 24, Versions 24.7 and above.

[2] GateCycle™, 2003. Getting started v.5.51 and GateCycle for Windows Training Seminar Notes. General Electric Power Systems.

[3] Bassily, A. M., 2007. Modeling, numerical optimization, and irreversibility reduction of a triplepressure reheat combined cycle, Energy 32, pp. 778–794.

[4] Zheng, L., and Furinsky, E., 2005. Comparison of Shell, Texaco, BGL and KRW gasifiers as part of IGCC plant computer simulations, Energy Conversion and Management, 46, pp. 1767-1779.

[5] Nieto, C., Arenas, E., Arrieta, A., Zapata, Z., Londoño, C., Valdés, C., and Chejne, F., 2008, Simulation of IGCC technologies: Influence of operational conditions (environmental and fuel gas production), Revista Energética, 40, pp. 39-51.

[6] CIENTEC, Fundação de Ciência e Tecnologia, database for biomass and waste, [online], URL: http://www.cientec.rs.gov.br/

[7] Santos, A. R., 2007, Generation of petroleum coke in the refine of heavy oils and its use in rotary kilns of clinker production, Ph.D. thesis in mechanical engineering, Federal University of Itajubá, Brazil.

[8] EPE, Energy Research Company, 2009, BEN, Brazilian Energy Balance year 2008, [online], URL: https://ben.epe.gov.br/

[9] Carvalho, I., 2003, Estado da arte e tendências tecnológicas para energia, CTEnerg.

[10] World Energy Council, 2007, "WEC Statement". [online], URL: http://www.worldenergy.org/

[11] Speight, J.G., 2004; New Approaches to Hydroprocessing, Catalysis Today, vol. 98, pp. 55 – 60.

[12] Wang, J., Anthony E.J., and Abanades J.C., 2004; Clean and efficient use of petroleum coke for combustion and power generation, Fuel, vol. 83, pp. 1341 – 1348.

[13] Barros, F.C., Lázaro, W., Borges, C.N., 2003, Coking Considerations, Hydrocarbon Engineering, pp. 61 – 65.

[14] Salvador, S., Commandré J.M., Stanmore B.R., 2003, Reaction rates for the oxidation of highty sulphurized petroleum cokes: the influence of thermogravimetric conditions and some coke properties, Fuel, 82, pp. 715 – 720.

[15] De Souza Santos, M., 2007, A new version of CSFB comprehensive simulator for fluidised bed equipment. Fuel, 86, pp. 1684–1709.

[16] Li X., Grace J. R., Watkinson A. P., Lim C. J. and Ergüdenler A., 2001, Equilibrium modeling of gasification: a free energy minimization approach and its application to a circulating fluidized bed coal gasifier. Fuel, 80(2), pp. 195-207.

[17] Zainal Z. A., Ali R., Lean C. H. and Seetharamu K. N., 2001, Bubbling fluidized bed biomass gasification — Performance, process findings and energy analysis. Energy Conversion and Management, 42(12), pp. 1499-1515.

[18] Deiana P., Pettinau A. and Tola V., 2007. Sardinia, Hydrogen production from coal gasification in updraft gasifier with syngas treatment line, *Third international conference on clean coal technologies for our future.*

[19] Campbell, P.E, Mc Mullan J.T., y Williams B. C., 2000, Concept for competitive coal fired integrated gasification combined cycle power plant. Fuel, 79 (9), pp. 1031-1040.

[20] Karg, J., 2009, Siemens AG, IGCC experience and further developments to meet CCS market needs, *Coal-Gen Europe-Katowice, Poland.*

[21] Franco A.; and Diaz A., 2009, The future challenges for clean coal technologies: Joining efficiency increase and pollutant emission control, Energy, 34, pp. 348–354.

[22] Treviño, M., 2003, Elcogas S.A, Integrated gasification combined cycle technology: IGCC, Edited Club Español de la Energía. Spain.

[23] Da Costa Labanca, R. A., 2000, Estudo de viabilidade da utilização de carvão mineral brasileiro em usinas de IGCC. Mechanical Engineering Masters theses, Fluminense Federal University.

Acknowledgments: The authors want to thank Prof. M.L. de Souza-Santos. Also the Coordination of Improvement of Higher Education (CAPES), National Counsel of Technological and Scientific Development (CNPq), and Foundation for Research Support of Minas Gerais State (FAPEMIG) for their collaboration and financial support in the development of this work.

# A Techno-Economic Assessment of an Oxyfuel Combustion Retrofit to a Sub-Critical Brown Coal Boiler

*Manjula Antony[a,b], Andrew F.A. Hoadley[a], Anthony Campisi[b]*

[a] *Monash University, Clayton, Victoria, Australia*
[b] *HRL Technology, Mulgrave, Victoria, Australia*

**Abstract:** Oxyfuel combustion is one of the $CO_2$ capture technologies for the capture and storage of $CO_2$ from power stations. A techno-economic analysis has been completed for the retrofit of oxy-fuel combustion to a 200 MW brown coal (lignite) boiler. The existing unit was simulated using Thermoflex software and validated against plant performance data. Oxyfuel components, including the ASU, flue gas recirculation, $CO_2$ compression and lignite partial drying were then retrofitted to the validated model. It was then optimised to improve the thermal efficiency and reduce the energy penalty. The overall net efficiency of the boiler decreased from 23.1% in the reference plant to 16.4% in the oxyfuel retrofit, even though there was an increase in gross efficiency from 24.6% to 28.8% which was due in particular to the partial drying of the lignite. The cost of $CO_2$ avoidance was calculated to be A$45.04/t$CO_2$, based on an IRR of 7% (zero inflation) and a project life of 25 years.

**Keywords:** Oxyfuel, CCS, Lignite

## 1 Introduction

There are three main ways of capturing $CO_2$ from lignite fired power stations; pre-combustion capture, post combustion capture and oxyfuel combustion. With oxyfuel combustion, nearly all the $CO_2$ emissions can be captured and sequestrated. According to a study done by the IPCC in 2005 [1], the cost of electricity generation (COE) using post combustion capture for a sub-critical lignite fired pulverised coal power station was $134.12/MWh. The COE using pre-combustion capture can range between $96.04/MWh and $140.50/MWh[1]. The COE using oxyfuel combustion for a lignite fired 300 MW power station was $173.40/MWh[2]. This study looked at the options for retrofitting oxyfuel combustion to existing lignite boilers and takes as a case study Unit 7 at International Power Hazelwood (IPRH). IPRH is located 150 km east of Melbourne in the Latrobe Valley. It comprises of 8 similar units with a total net capacity of 1,541 MW providing 25% of Victoria's base load generation. IPRH emits approximately 17 million tonnes of $CO_2$ annually [2]. Unit 7 was chosen for the study as it had the most recent performance test results and calculations available. This work was part of a joint research project between the Victorian Government's Energy Technology Innovation Strategy (ETIS), Monash University, HRL Technology (HRLT) and Latrobe Valley Generators on oxyfuel combustion of Victorian brown coal".

The main difference between air combustion and oxyfuel combustion is that coal is burnt in an oxygen rich environment instead of air. This oxygen is produced using an Air Separation Unit (ASU). When coal is combusted in an $O_2$ rich environment, the resulting flue gas consist mainly of $CO_2$ and $H_2O$. A portion of this flue gas is recirculated back in to the boiler (typically 60%) to control the flame temperature (caused by high levels of $O_2$) and to compensate for the loss in volume caused by the removal of nitrogen from the air in the ASU. The remaining flue gas is cooled, dehydrated, compressed and processed for sequestration [3]. In this study, a technical and economic evaluation was performed on IPRH Unit 7 to determine the effects of retrofitting oxyfuel combustion.

[1] From a total of 11 studies carried out on Bituminous coal fired power stations
[2] Converted from 2005 values in USD to Australian Dollars in 2009 using a CERA factor of 1.405 and Exchange Rate of 0.79 USD/AUD for all three capture technologies

Corresponding Author: Manjula Antony, Email: mantony@hrl.com.au

## 2 Method

A schematic of the evaluation process is shown in Figure 1. First of all, a model of the existing IPRH unit (Figure 2 reference model) was built in Thermoflex software [4] using mainly performance test results from October 2007. Design data were used from the plant manual where performance test data were not available. During the performance tests, Unit 7 had an average gross output of 221.8 MW at an efficiency of 24.6%[3] (at Valves Wide Open condition). Its average net output was 207.1 MW at an efficiency of 23.1%. It consumed an average 86.23 kg/s of coal at base load operation. The average auxiliary power demand was 13.92 MW (6.3% of gross output) with the Boiler Feed Pump (BFP), the Induced Draft (ID) fan and the pulveriser consuming most of this amount of energy (64.6% of the auxiliary energy). The average auxiliary consumption was 6.27% of the gross output.

The coal used by Unit 7 during the October 2007 performance test had an average moisture content of 60.67%, which is typical of brown coal from the Hazelwood mine. The average carbon and ash contents were 26.7% and 0.9%, respectively on an as-fired basis. The average calorific value was 10,440 kJ/kg. This calorific value is very low compared to other fuels such as black coal and natural gas. The average ambient pressure, temperature and relative humidity were measured as 1.013 bar, 24.8ºC and 62.5% respectively. The average main steam pressure, temperature and flow were 97.84 bar, 539.1ºC and 206.7 kg/s, respectively. The results calculated from the reference model (built using the Thermoflex software) were validated by comparing them against the performance test results. All important temperatures, pressures, outputs and gross and net efficiency values calculated from the reference model matched within ±0.5% of the average performance test results. The coal flow calculated from the reference model matched within ±1.0% of the average coal flow estimated during the performance tests. This shows excellent agreement between the reference model and the performance test results and gives a very good level of confidence in the model predictions of the design of the existing unit at IPRH.

[3] All efficiencies, calorific values of fuels are calculated on a HHV basis

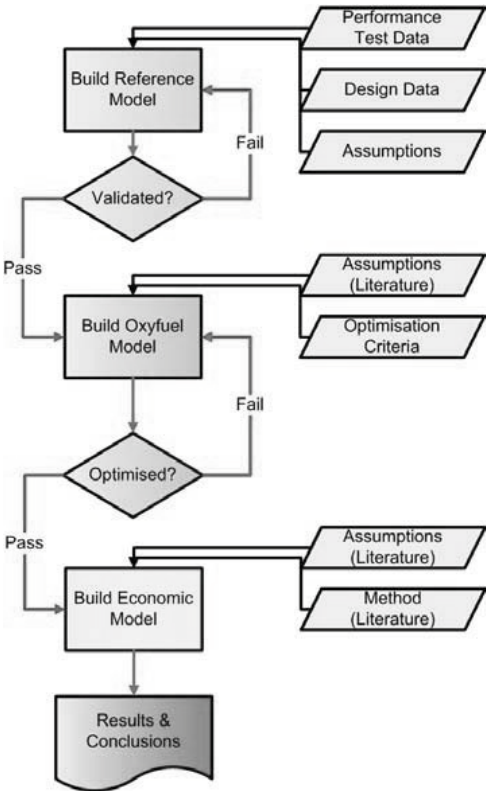


*Figure 1: Methodology*

The validated reference model was used as the basis to build the retrofitted oxyfuel model. The Rotary Air Heater (RAH) and the Forced Draft (FD) fan were removed from the model. The RAH was removed in order to reduce air ingress into the unit. The FD fan was no longer required as the $O_2$ produced in the ASU was at a higher pressure (5 bar) than was required in the boiler. Minor boiler modifications were required to the furnace in order to accommodate oxyfuel combustion. An ASU, flue gas compression, cooling and dehydration system and the Flue Gas Recycle (FGR) fan were added to the model to facilitate oxyfuel combustion. The water and the steam cycles were left unchanged (Figures 3 and 4).

Retrofitting oxyfuel combustion had a very high energy penalty and therefore, the model was optimised by considering the following:

- the water content of the recirculated flue gas;

- the amount of excess oxygen in the flue gas;
- the lowest permissible boiler outlet temperature;
- the utilisation of waste heat in the flue gas for coal drying;
- the recycle of $O_2$ rich inert gases recovered from the flue gas treatment plant to the ASU.

## 3 Technical Evaluation

The difference between recirculating dry flue gas and wet flue gas was analysed. In the dry FGR scheme, part of the flue gas at the outlet of the coal dryer was cooled to 70ºC and the moisture was removed by using a shell and tube heat exchanger before recirculating the flue gas back to the boiler. In wet FGR, the flue gas is recirculated without any cooling or dehydration. Dry flue gas recycle reduced the net sent out efficiency by 0.4% when compared to the wet FGR scenario. In addition to lowering the efficiency, extra equipment is required to cool the flue gas before re-circulating it back in to the boiler. Low grade heat was lost from the system in this process due to the cooling of the flue gas. Therefore, the wet FGR was determined to be the preferred scheme.

The percentage of oxygen in the flue gas was varied between 2% and 6% to analyse the effects on net sent out efficiency. Modelling results clearly show that the net sent out efficiency increases with decreasing levels of oxygen in flue gas due to the decreasing energy demand of the ASU. Therefore, 2% oxygen was established as the minimum amount of excess $O_2$ required in the furnace for complete combustion of coal. Other studies have used lower levels of excess oxygen in flue gas for their analysis [5, 6] and thus 2% may be considered as a conservative estimate for this study.

Controlling the boiler exit temperature was a critical aspect of the model optimisation process. In the reference model, the economiser outlet temperature was 350ºC. However, the RAH was used to heat the incoming air from ambient to 125ºC. Therefore, the final flue gas temperature after the RAH was 250ºC. In the retrofitted model, the RAH was removed from the system as air ingress in the RAH diluted the $O_2$ rich stream from the ASU. Therefore, in the retrofitted model, the boiler exit temperature was controlled to minimise waste heat in the system, whilst producing enough heat to maintain the design main steam temperature and flow. This was done by optimising the percentage of flue gas recirculated back into the system (the optimum amount of RFG was 58% of the flue gas existing the boiler).

It was concluded that the optimum temperature at the boiler exit was 250ºC. With this boiler exit temperature, there was still sufficient heat in the flue gas for partial coal drying. Temperatures above this limit resulted in the generation of waste heat, thereby decreasing the overall net sent out efficiency. Temperatures below this limit resulted in not having enough energy in the system to produce the minimum design steam flow of 207.1 kg/s at 539.1ºC. As all the flue gas at the exit of the economiser was used to dry the coal, the final flue gas temperature entering the $CO_2$ treatment plant was reduced to 116.5ºC

There are two main types of coal dryers. They are fluidised bed dryers and entrained flow dryers. The fluidised bed drying of coal utilises WTA technology provided by RWE Power, but unfortunately, specific energy consumption data (i.e. kW/tonne of Coal dried etc) were not readily available in the literature. Therefore, it was not possible to make a clear comparison with the entrained flow coal dryer. Modelling results showed that there was sufficient heat in the flue gas for entrained flow drying as well as for fluidised bed drying to dry the coal from 60.7% wt to 45% wt moisture levels (45% is the minimum limits of the existing pulverising mills). Therefore, both types of coal drying are possible at Unit 7. However, more design information is required to determine which type is the most suitable. Entrained flow drying was considered for the model as it is the simpler and also likely to have a lower capital cost. Results from the model showed that the net sent out efficiency increases by 1.2% when the raw coal at 60.67% wt moisture is dried down to 45% wt.

The inert gases recovered from $CO_2$ compression contained a very high portion of $O_2$ (46.2% of oxygen instead of 23% found in ambient air). In addition, it was already at a higher pressure than required for air separation. Therefore, oxygen recovered from the $CO_2$ plant maybe utilised to reduce the overall energy consumption of the ASU. Modelling results showed that the net sent out efficiency increased only by 0.2% when this steam was integrated in to the ASU. This was due to the low flow rate of inert flue gas. Therefore,

this improvement was not included in the technical and economic analysis due to the limited impact.

## 4 Modelling Results

In the oxyfuel retrofitted model of Unit 7, the ASU (53.1 MW) and the flue gas treatment plant (26.5 MW) consumed a total of 79.7 MW. This amounted to 35.9% of the gross output. Therefore, the net sent out power was significantly reduced to 126.6 MW. In addition, power was consumed by the coal dryer (1.5 MW) and the recirculation fan (0.8 MW). The overall net efficiency decreased from 23.1% in the reference plant to 16.4% in the oxyfuel model even though there was an increase in gross efficiency from 24.6% to 28.8% due to the optimisation of the model. The results from the reference unit and the oxyfuel models are given in Table 1.

*Table 1. Performance Impact of Oxyfuel Combustion*

| | Units | Reference Plant | Oxyfuel Plant |
|---|---|---|---|
| Gross Output | MW | 221.8 | 221.8 |
| Net Output | MW | 207.9 | 126.6 |
| Auxiliary Power | MW | 13.9 | 95.2 |
| Coal Flow | kg/s | 86.2 | 73.9 |
| Coal Enthalpy | kJ/kg HHV | 10,440 | 10,440 |
| Plant Gross Efficiency | % HHV | 24.6 | 28.8 |
| Plant Net Efficiency | % HHV | 23.1 | 16.4 |
| Final Flue Gas Temperature | ºC | 250.0[a] | 116.5[b] |

Notes: (a) air heater outlet temperature
(b) at fuel dryer gas side outlet

## 5 Economic Evaluation

The results from the technical analysis were used as the basis for the economic evaluation. The economic evaluation included estimating the fixed capital costs, working capital costs, annual operating costs and a cash flow analysis for the life of the project. There were six major areas that required fixed capital investment. They were: the ASU, $O_2$ and $CO_2$ distribution network, the cogeneration plant, the coal dryer, and minor modifications to the furnace. In addition, construction management costs, pre-commissioning and commissioning costs, support services, freight, spare parts, project management costs, engineering and procurement, insurance and demolition costs were included in the fixed capital cost analysis. However, the analysis excluded import duties and taxes, regulatory permits, operator training and the cost of installing a pipeline for natural gas to be transported to Morwell from Longford for use in the GTCC. It was assumed that the additional equipment would be housed on a vacant plot of land near the unit. The only major component that requires space is the ASU (area of 100 m x 250 m). The first stage of compression in the flue gas treatment plant can occur near the unit as a compressor does not require much space. The flue gas can then be delivered to the treatment plant that can be housed near the ASU. This arrangement would be even more beneficial if multiple units were retrofitted with oxyfuel combustion simultaneously.

The majority of the fixed capital cost data was obtained from a study of a plant in the United Kingdom (Allam 2005). The fixed capital cost for the coal dryer was obtained from the United States Department of Energy (DOE) from a 2008 publication [7]. Therefore, a method was developed to convert capital cost data obtained from the literature to the equivalent construction cost in Morwell in 2009. This conversion was done by estimating factors for location, inflation and the currency rate of exchange. The location factor for Morwell was calculated as 1.04. The inflation index was calculated using the IHS/CERA Power Capital Costs Index (PCCI). According to the PCCI, the fixed capital costs for non-nuclear power stations have increased by a factor of 1.405 since 2005. All data available in US Dollars were converted using the average exchange rate during the last five years (between 2004 and 2008) [8]. The conversion rate used was 0.79. Therefore, the total estimated fixed capital

cost investment was $M 696.33. This is to be borrowed during the first year of the construction. Working capital was not considered for this study, as it was assumed that the ongoing business was cash flow positive.

The operating costs of the oxyfuel plant were divided into several categories. They included raw materials, process labour, maintenance material and staff, insurance, non-manufacturing costs such as corporate overheads, R&D and permanent engineering staff. It was estimated that 5 operators will be required per shift for the oxyfuel plant (5 shift teams). An additional 6 full time maintenance personnel was estimated for the project. During major overhauls, 20 contract labour staff was estimated for a period of 3 months during the year. The cost of this consultation was estimated as $250/hr including miscellaneous equipment costs. Maintenance spare parts were estimated as 1% of material costs as per the literature [9]. Four engineers are estimated to be added to the full time staff for dealing with issues related to the coal dryer, the ASU and the flue gas treatment plant.

The plant life was assumed as 27 years. This included two years for building and commissioning the oxyfuel plant. Unit 7 is expected to be fully operational during the first year while components such as the ASU and the GTCC plant are built and 60% operational during the second year. The average performance of the plant was established using actual plant data. National Electric Metering Management Company (NEMMCO) data, obtained directly from IPRH, showed that the average net sent out power of Unit 7 between 2005 and 2008 was 186.5 MW with at average availability of 90.5% (during base load operation). The average coal properties were calculated from the monthly coal analysis data for 2008. The average ambient temperature was calculated using the mean daily temperature data obtained from the Bureau of Meteorology (BOM) for Morwell. The average Cooling Water Inlet Temperature (CWIT) was established using plant data for 2008. Table 2 summarises the average performance parameters used for this study. The cash flow analysis was based on the discount rate of 7% [10].

*Table 2. Unit Annual Reference Performance*

| Parameter | Units | Value |
|---|---|---|
| Net Generation | MW | 186.50 |
| Service Hours | hours | 7,931 |
| Ambient Temperature | | 13.58 |
| Cooling Water Inlet Temperature (CWIT) | | 25.30 |
| **Coal Properties** | | |
| Moisture | % ar | 60.85 |
| Carbon | % db | 67.98 |
| Ash | % db | 1.85 |
| Hydrogen | % db | 4.82 |
| Calorific Value | kJ/kg HHV | 10.40 |

Notes: (a) “ar” denotes “as received”
(b) “db” denotes “dry basis”

## 6 Discussion

Unit 7 HP Turbine was replaced in 2002 and the LP Turbine was replaced in 2003. Therefore, data from 2004 onwards is representative of the average net capacity of this unit . Net sent out power data between 2004 and 2008 was chosen to establish the average net sent out generation. A complete calendar year (2008) was chosen to determine the average ambient temperature, average CWIT, average coal properties in order to account for the effect of the change in climate throughout a typical year to the calculations. A 5 year period was chosen to calculate the representative rate of exchange from the US Dollar to the Australian Dollar in order to negate the

effect of short term fluctuations in the exchange rate. The number of additional operators, maintenance staff, contract labour, labour charge rates were determined based on local requirements.

Using these parameters, a cash flow analysis was carried out for the life of the project (on a pre-tax basis). The discount rate was set at 7% [11]. The break-even price of electricity and the cost of $CO_2$ avoidance was calculated in order to determine the economic feasibility of retrofitting of oxyfuel combustion to Unit 7. The break-even price of electricity and the cost of $CO_2$ avoidance for the oxyfuel unit were \$103.00/MWh and \$45.04/t$CO_2$ respectively. For Unit 7, the annual sent out generation was 1,480,463 MWh[4]. However, with the oxyfuel unit, only 903,144 MWh was generated due to the additional energy demand of the oxyfuel components. This is a reduction in 40% of revenue.

In reality, oxyfuel combustion would be retrofitted to a larger plant or multiple units simultaneously. This would allow the purchase a larger ASU and $CO_2$ plant. They would also be able to utilise the same distribution system of $CO_2$ and $O_2$. In addition, operating, maintenance and contract labour, engineering staff etc would be shared for both units, thereby reducing the cost per unit.

If there were to be a significant breakthrough in ASU and $CO_2$ compression technology, thereby halving the energy penalty of the two processes from 79.7 MW to 39.9 MW, net sent out generation of the oxyfuel plant will increase to 153.68 MW .The breakeven price of electricity would only be \$77.08/MWh. The cost of $CO_2$ avoidance would be \$35.64/t$CO_2$.

The cost of $CO_2$ storage was not considered in the estimation of the break-even price of electricity and the cost of $CO_2$ avoidance. If considered, the cost of $CO_2$ storage can have a significant impact on the break-even price of electricity and the cost of $CO_2$ avoidance. Results in Table 3 show that the break-even price of electricity can increase by more than 60%, if the cost of $CO_2$ storage was to be \$40/t$CO_2$. The cost of avoidance can increase by more than 80%, if the cost of $CO_2$ were to be \$40/t$CO_2$.

[4] Current annual generation of Unit 7 at IPRH

*Table 3. Effect of the Cost of $CO_2$ Capture and Storage*

| Cost of Capture | Oxyfuel Plant | |
|---|---|---|
| (\$/tonne) | \$/MWh | \$/t $CO_2$ |
| 0 | 103.00 | 45.04 |
| 20 | 140.82 | 67.93 |
| 40 | 178.64 | 90.81 |

If retrofitting oxyfuel combustion is determined infeasible due to the high economic risk factor that would result in borrowing large sums of money for capital expenditure, a power station would be able to reduce its greenhouse gas emissions by replacing the coal fired unit with a larger GTCC with the same net sent out capacity of 186.5 MW. In this scenario, the break-even electricity would only be \$62.25/MWh and the cost of $CO_2$ avoidance would be only \$24.79/t$CO_2$. This is a very competitive option for the avoidance of $CO_2$. A summary of the capital and operating costs, the break-even price of electricity and the cost of $CO_2$ avoidance is provided in Table 4.

## 7 Conclusions

In conclusion, the break-even electricity cost of retrofitting oxyfuel combustion to Unit 7 is \$103.00/MWh and the cost of $CO_2$ avoidance is \$45.04/t$CO_2$ According to a study done by the IPCC in 2005 [1], the cost of electricity generation (COE) using post combustion capture for a sub-critical lignite fired pulverised coal power station was \$134.12/MWh [5] . Therefore, the cost of retrofitting oxyfuel combustion to a lignite-fire power station is comparable to post combustion capture. Retrofitting oxyfuel combustion becomes even more feasible in countries such as Denmark where the current electricity price is approximately 3.1 times higher than electricity prices in Australia. A significant reduction in the energy cost for oxygen production and $CO_2$ compression and separation to a technological breakthrough would further increase the competitiveness of retrofitting oxyfuel combustion to current lignite fired power stations in Australia.

[5] Converted from 2005 values in USD to Australian Dollars in 2009 using a CERA factor of 1.405 and Exchange Rate of 0.79 USD/AUD

*Table 4. Oxyfuel Economic Results*

| | Units | Reference Plant | Oxyfuel Plant | GTCC only |
|---|---|---|---|---|
| Fixed Capital | $M | 200 | 696.33 | 548.82 |
| Working Capital | $M | - | - | - |
| Start-up Capital | $M | - | 35.31 | 21.98 |
| Operating Costs | $M/y | 26.01 | 30.12 | 56.72[a] |
| Break-Even Electricity Price | $/MWh | 28.56 | 103.00 | 62.25 |
| Cost of $CO_2$ Avoidance | $/t$CO_2$ | - | 45.04 | 24.79 |

Notes: (a) higher operating cost is due to the high cost of natural gas

## References


1. IPCC, *IPCC Special Report on Carbon Dioxide Capture and Storage* 2005, Cambridge University Press: Cambridge, UK. p. 431.
2. International Power. *Hazelwood Power Station and Mine*. 2009 04/06/2009]; Available from: http://www.ipplc.com.au.
3. Sweet, W., *Winner: Clean coal - Restoring coal's sheen.* IEEE Spectrum, 2008. **45**(1): p. 57-60.
4. Thermoflow Inc. *Thermoflex.* 2007; 17:[Available from: http://www.thermoflow.com/CombinedCycle_TFX.htm.
5. Andersson, K., et al., *An 865 MW Lignite Fired $CO_2$ Free Power Plant - A Technical Feasibility Study.* Greenhouse Gas Control Technologies, 2003. **II**: p. 1051-1056.
6. Kakaras, E., et al., *Simulation of a Greenfield Oxyfuel Lignite Fired Power Plant.* Energy Conversion and Management, 2007. **48**(11): p. 2879-2887.
7. DOE. *Unique DOE Funded Coal Dryers Meet Goal of Increases Efficiency, Reduced Emissions.* 2009; Available from: http://netl.doe.gov.au.
8. RBA. *Exchange Rates.* 2009 07/03/2009]; Available from: http://www.rba.com.
9. Allam, R.J., et al., *Revamping Heaters and Boilers to Oxyfiring--Producing Oxygen by Itm Technology.* Carbon Dioxide Capture for Storage in Deep Geologic Formations, 2005: p. 513-535.
10. Allinson, W.G., et al., *CCS Economics Methodology and Assumptions.* 2006, School of Petroleum Engineering, The University of New South Wales: Sydney, Australia.
11. Allam, R.J., et al., *The Oxyfuel Baseline: Revamping Heaters and Boilers to Oxyfiring by Cryogenic Air Separation and Flue Gas Recycle.* Carbon Dioxide Capture for Storage in Deep Geologic Formations, 2005: p. 451-475.


## Appendix

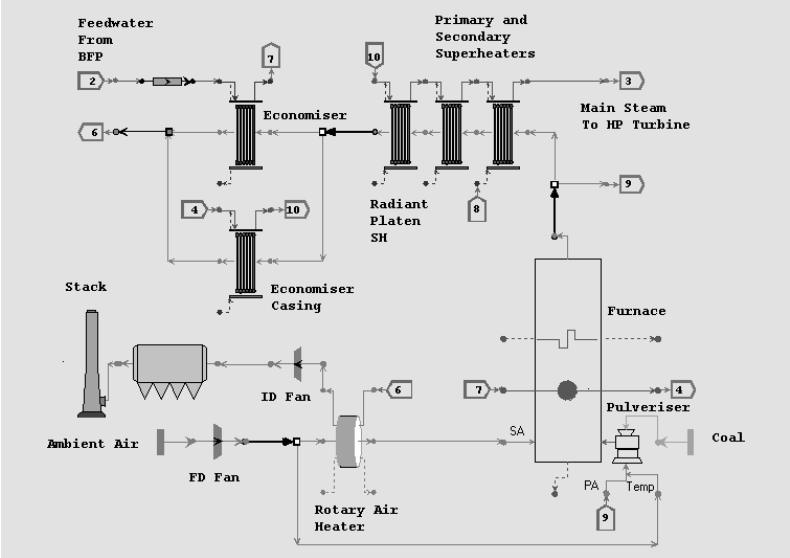


*Fig. 2. Reference Boiler*

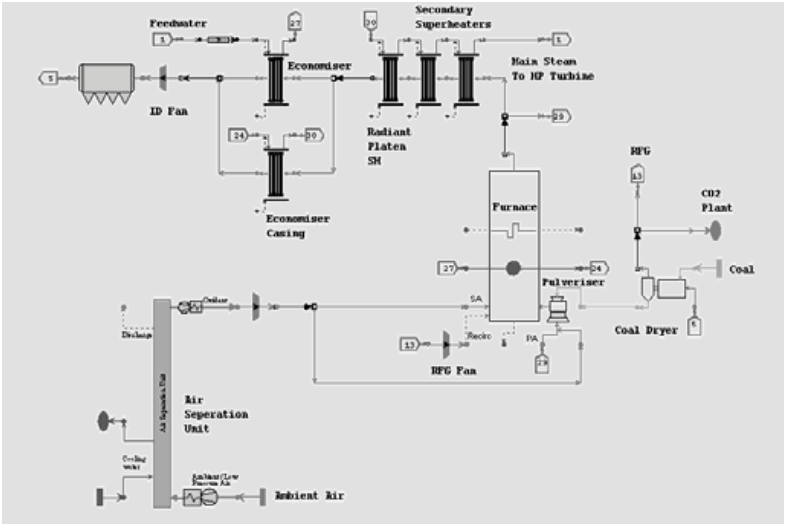


*Fig. 3. Oxyfuel Retrofitted Boiler*

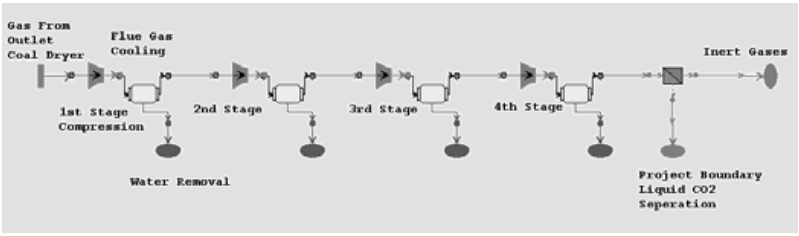


*Fig. 4. Four Stages of $CO_2$ Compression*

# Modelling and Analysis of Gas Generator in the Integrated Gasification Combined Cycle Systems

*Anna Skorek-Osikowska, Janusz Kotowicz and Łukasz Bartela*

*Institute of Power Engineering and Turbomachinery,*
*Silesian University of Technology, Gliwice, Poland*

**Abstract:** Integrated Gasification Combined Cycle (IGCC) is a technology that allows for the use of coal for electricity production while maintaining low pollutants emissions to the atmosphere and relatively high efficiency of electricity production. In these systems fuel is gasified in gas generator, and obtained gas, after purification, supplies gas turbine combustion chamber. In the paper gasification process and gas generators, with special attention to entrained flow gasifiers, are briefly described. The most important parameters allowing for the evaluation of the efficiency of gasification reactors is presented. The main objective of the present study was to build a simple model of an entrained flow gasifier fuelled with coal. As gasifying factors high purity oxygen and water vapour were used. The model was build in the commercial Aspen Plus package, for the steady state conditions. The composition and parameters of raw gas obtained from the simulations showed good agreement with the literature data, what allows for a positive assessment of the verification of the proposed numerical model. A sensitivity analysis of the impact of the gasification process parameters (e.g. oxidants flows and pressures) on the composition of the obtained gas and on the efficiency of gasification was performed.

**Keywords:** Coal gasification, Gasifier, Numerical modelling, Aspen Plus.

## 1. Introduction

In recent years, mainly because of a fear of the crisis in access to crude oil and natural gas, increasing interest in so-called 'clean' energy production from coal (Clean Coal Technologies) is observed. One such technology, allowing for the use of coal for electricity production while maintaining low pollution emissions to the atmosphere and relatively high efficiency of electricity production are the Integrated Gasification Combined Cycle (IGCC) power plants. In these systems fuel (typically hard coal or lignite but also others) is gasified in gasifier, and the obtained gas after purification feeds a combustion chamber of a gas turbine. High enthalpy of exhaust gases from gas turbine allows for generating of a high-pressure steam in a heat recovery steam generator for steam cycle.

Due to the constantly increasing interest in coal gasification for electricity production it appears to be important to undertake studies aiming at optimisation of all the components of such a system, what will allow in the future for increasing of the efficiency and decreasing of the investment costs for the construction of these systems. This growing interest is reflected in the literature – the effort of modelling of a generator itself as well as a whole IGCC system is, among other, undertaken in e.g. [2,3].

The main objective of the presented in the paper studies was to build a simple numerical model of an entrained flow gasifier fuelled with coal, allowing for the analysis of the influence of different parameters mainly on composition and some parameters of the obtained raw gas, and the efficiency of the gasifier. The model was built in the commercial Aspen Plus [4] software, for steady state conditions.

## 2. Coal gasification process and gasifiers

Gasification process is known and used in the chemical industry for many years. It consist in chemical processing of gasified substances (coal) in high temperature and with the presence of gasifying agents. As gasifying agents air or oxygen and steam are usually used. From the point of view of the exchange phase, the process proceeds in 2 stages. In the first stage, called initial, heterogeneous reactions between the solid phase of gasified coal and gaseous reacting factors proceed. In the second stage homogeneous,

secondary reactions between the gaseous products of the first stage and the gasifying factors proceed. Part of the reactions occurring in the gasifier is endothermic and part is exothermic. Heat needed for endothermic reactions is supplied either from exothermic reactions proceeding in the reactor (autothermic process) or from outside (allothermic process). Currently developed technologies belong rather to the first type, in which the heat needed for endothermic reactions is provided by burning part of the supplied coal. Description of gasification process together with specification of the main reactions occurring during gasification process can be found, among others, in [5,6].

Gasification reactors designs can be divided into 3 main types depending on the structure of fuel flow in the reaction zone [7]. These are fixed bed (also called moving bed), fluidised bed and entrained flow reactors. Description of gasifiers and characteristic parameters of the gasification process can be found in the literature, e.g. [2,5]. The development of modern gasification techniques is connected mainly with entrained flow gasifiers [14], that allow for the highest intensification of heat and mass transfer processes. Modernisation of reactors constructions and usage of increasingly higher parameters in gasification process has the aim to increase the thermal efficiency of the process, yield, degree of coal conversion, etc.

In the entrained flow gasifier, the gasifying agents are usually oxygen and steam. Fuel can be supplied either in a dry state (e.g in Shell gasifiers) or as a water slurry (e.g. Texaco technology). Due to the low residence time of fuel particles in the reaction zone (counted in seconds), supplied gasified agent (coal) requires fragmentation to the grain size lower than 0.1 mm. The temperature of the gasification process is typically within the range 1200÷1600ºC and the pressure is in the range 2÷5 MPa [8]. The main advantages of entrained flow generators is high degree of fuel conversion and fuel flexibility (including the possibility of using low quality coals), and the lack of tar impurities in the produced gas.

## 3. Effectiveness of gasification process

In order to compare different gasification technologies various indicators for assessing energy efficiency are introduced. One of them is the degree of coal conversion, which determines the amount of carbon that reacted in gasifier. Another is cold gas efficiency of coal gasification process ($\eta_z$), defined as [9]:

$$\eta_z = \frac{\dot{B}_g LHV_g}{\dot{B}_c LHV_c}, \quad (1)$$

where:

$\dot{B}_c$, $\dot{B}_g$ - mass stream of supplied coal and raw syngas obtained in the process, respectively, kg/s,

$LHV_c$, $LHV_g$ - lower heating value of coal and raw syngas, respectively, kJ/kg.

This value can also be determined based on the higher heating value (HHV).

The value of energy efficiency depends on the technology and parameters of gasification process and usually equals $\eta_z$=70÷91% [8].

## 4. Model description and verification

According to [14] most of the planed in the nearest years gasification installations will use entrained flow gasifiers, thus, the authors chose this type of generator for modelling and analysis. Coal gasification process in a gasifier was modelled in Aspen Plus software, making assumptions that in the process a specified level for gas outlet temperature should be obtained. In the process steady state is reached and the equilibrium for gas components is assumed. The model bases on minimisation of Gibbs energy and the gasification reactions are not pre-specified.

The simplified scheme of the modelled system is presented in Fig. 1. The gasification model consist of several stages. In order to simulate the decomposition of carbon entering generator on the separate components, including carbon, hydrogen, oxygen, sulphur, nitrogen and ash, a decomposition reactor RYIELD was used. It is necessary due to the fact, that the equilibrium reactor RGIBBS in Aspen Plus program determines products for substrates contained in the database. Chemical energy of products from RYIELD reactor and energy of substrates of RGIBBS reactor is not equal. Energy balance of the decomposition reactor is attained thanks to the additional heat flux, directed to the RGIBBS reactor, in which gasification of the coal decomposed on separate components occurs with the use of the supplied gasifying agents (oxygen

and water vapour). Composition of products leaving the reactor, which are the mixture of gaseous and solid fraction, is determined with the use of minimisation of Gibbs function method. This composition is determined taking into account substances and energy balance. In the SPLT separator, of which main task is to determine the stream of ash (slag), the separation of these 2 fractions occurs.

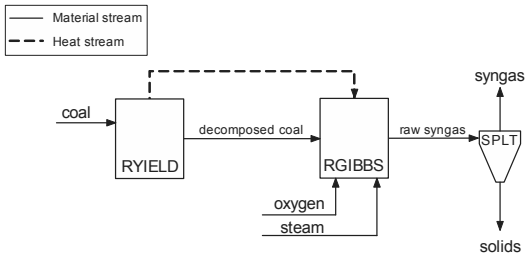


*Fig. 1. Scheme of the simplified gasifier model.*

The input data for the gasification process, including coal composition and streams of the particular gasifying agents were taken from literature [10,11]. Gasification temperature and pressure were 1700 K and 18.5 bar, respectively. For such input data composition and the main parameters of the obtained gas were compared with the literature data. Particular attention was given to the chemical energy flux $\dot{E}_{chg}$ (product of gas mass stream and its lower heating value), which is important from the energetic point of view, due to the fact, that it guarantees obtaining of the similar value of fuel chemical energy conversion efficiency. Lower heating value of the obtained gas was determined based on the enthalpy of devaluation of the individual flammable gas components [12]. For such model (called simplified) of gasifier, the results of simulations differed quite significantly from the literature data (Table 1).

*Table 1. Comparison of the literature data and results of simulations concerning syngas parameters and composition.*

| | LHV | $\dot{E}_{chg}$ | Molar mass | Molar share of main gas components | | | |
|---|---|---|---|---|---|---|---|
| | MJ/kg | MW | kg/kmol | CO | $H_2$ | $CO_2$ | $H_2O$ |
| Literature data | 10.06 | 17.1 | 20.12 | 51.9 | 26.4 | 5.6 | 10.1 |
| Simplified model | 12.22 | 19.3 | 18.84 | 55.45 | 29.1 | 4.7 | 8.5 |
| Extended model | 10.3 | 16.3 | 20.12 | 52.3 | 24.2 | 8.4 | 9.2 |

In order to obtain better conformity of data, the model was extended with a second equilibrium reactor RGIBBS.

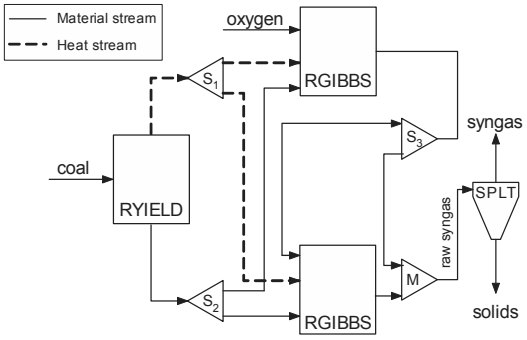


*Fig. 2. Scheme of the extended gasifier model, S – splitter, M - mixer.*

In this model (called extended model), the stream of products from the decomposition reactor is separated into 2 streams, one of which is burned, and the second gasified (in separate reactors), together with a part of the products of combustion from the first reactor. The obtained gas is the mixture of products from these 2 reactors. In order to obtain good agreement of the literature data with simulation results, the value of particular streams, separated in splitters was changed. The best results concerning composition and parameters of the raw syngas were obtained when around 70% of the products of the coal decomposition process (decomposition reactor) flowed into the gasification reactor. This is consistent with theoretical basis of autothermic gasification process. In this type of process part of coal supplied to the gasifier (typically 20-35%) is burnt in order to assure heat for endothermic reactions [6]. Composition and parameters of the obtained gas in the extended model are presented in Table 1.

The model was verified on the basis of other literature data [2,13]. Gas composition and other gas parameters also in these cases showed good agreement with the simulation results, what allowed to positively asses the gas generator model that was built by the authors.

Some difficulties in the interpretation of the obtained data in comparison to the literature data resulted from the fact, that it is difficult to find in the literature complete data concerning composition and parameters of gasified (mainly detailed coal analysis) and gasifying agents.

## 5. Results

The model of gasifier allowed for carrying out the analysis on the influence of different parameters of the gasification process (e.g. temperature, pressure and flow of coal and gasifying agents) primarily on the composition and parameters of the obtained raw syngas and the efficiency of the gas generator. For the analysis coal composition, presented in Table 2 and parameters of the supplied gasifying agents presented in Table 3 were used [13]. For such input data, „cold" efficiency of the gasification process was equal to 0.73.

*Table 2. Coal composition (dry basis).*

| | |
|---|---|
| **Ultimate analysis, %** | |
| Ash | 10.91 |
| C | 71.72 |
| H | 5.06 |
| N | 1.41 |
| S | 0.33 |
| O | 7.75 |
| Cl | 0.0 |
| **Proximate analysis, %** | |
| Moisture | 11.12 |
| Ash | 10.91 |
| VM | 39.37 |
| FC | 49.72 |
| **Thermodynamic parameters** | |
| LHV, MJ/kg | 21.65 |
| HHV, MJ/kg | 22.55 |

*Table 3. Parameters of the gasifying factors.*

| | |
|---|---|
| **Oxygen** | |
| Temperature, ºC | 400 |
| Flow, kg/s | 0.7 |
| Purity, % | 95 |
| **Steam** | |
| Temperature, ºC | 60 |
| Flow, kg/s | 0.1 |
| **Coal** | |
| Temperature, ºC | 60 |
| Flow, kg/s | 1.0 |

### 5.1. Effect of gasification pressure on composition and parameters of the obtained raw syngas

The model of the gas generator was used, among others, to assess the impact of pressure changes of the gasification process (in the range 15–40 bar) on the composition and the calorific heating value of the obtained raw gas (while maintaining constant temperature of gasifying factors). Some results of these analyses are presented in Fig. 2.

The increase of the pressure in the range 15–40 bar results in a small change of gas composition. Slightly increasing is the share of carbon dioxide and methane, which is consistent with theoretical considerations. As a consequence of pressure changes also a slight change of lower heating value of the raw gas is observed.

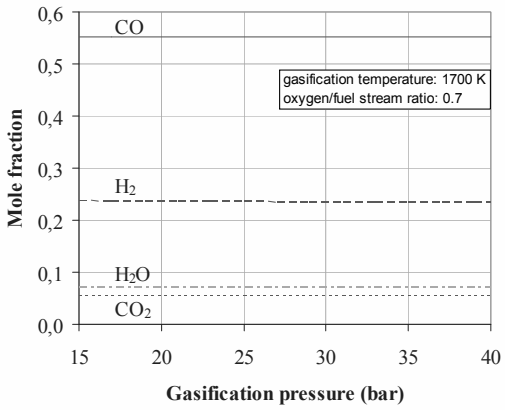


*Fig 2. Effect of gasification pressure on the composition of the obtained raw gas.*

### 5.2. Effect of gasification temperature on composition and parameters of the obtained raw syngas

The model of the gas generator allowed also for examining of how does the temperature of the gasification process affect the composition and parameters of the gas. Some results of this analysis in the temperature range 1000–2000°C are presented in Fig. 3.

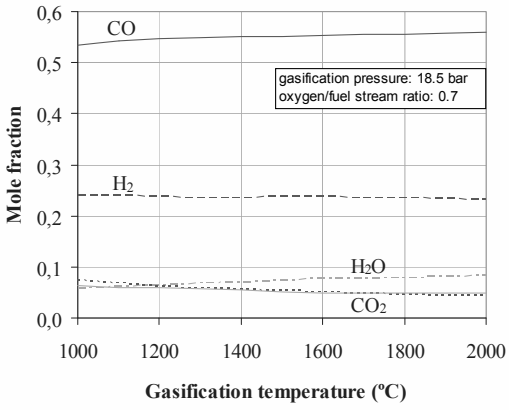


*Fig. 3. Effect of gasification temperature on the composition of the obtained raw gas.*

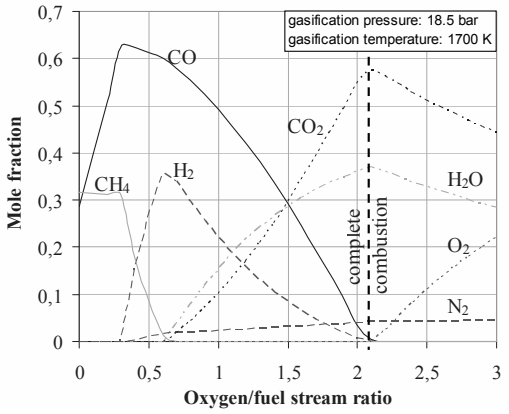


*Fig. 4. Effect of oxygen to fuel stream ratio on the composition of the obtained raw gas.*

Higher temperatures increase the share of carbon dioxide and water vapour, and decrease the hydrogen or methane. This is due to the fact, that increased temperature move the endothermic reactions equilibrium towards products, thus, towards increased share of flammable components. As a consequence also the increase in LHV is observed, and therefore, with unchanged gas stream, increase of its chemical energy and generator "cold" efficiency.

### 5.3. Effect of oxygen to coal stream ratio on composition and parameters of the obtained raw syngas

The model was used for the assessment of the influence of changes in ratio of oxygen to fuel (coal) mass stream on the parameters of the obtained gas. The molar shares of the main components as a function of oxygen to fuel stream ratio is shown in Fig. 4.

Oxygen stream has a significant influence on the composition of the obtained gas. At the beginning, together with the increase of oxygen stream, the share of flammable gas components, mainly CO and $H_2$ is increasing. When the ratio of oxygen to fuel stream in the analysed case reaches around 0.5, the share of hydrogen begins to decrease, increase whereas the share of non-flammable components, including carbon dioxide and water vapour. There is a clear limit of complete combustion, where carbon monoxide and hydrogen are not produced any more, and a dominant share has $CO_2$. A consequence of the gas composition changes is, of course, the change of lower heating value and of the chemical energy of the resulting gas. In the analysed case the LHV of gas and its chemical energy (as well as "cold" efficiency) initially grew up to a maximum value achieved at the ratio of oxygen to fuel at about 0.3, and then decreased to reach values almost equal to 0. These results are consistent with the theoretical analysis of a gasification process.

With the increase of the oxygen to coal stream ratio, initially decreases (to the oxygen to coal stream ratio equal to 0.4) and then increases the ratio of $CO/H_2$, which has a significant impact on the value of the adiabatic combustion temperature. This temperature is responsible for the formation of $NO_x$. The higher the $CO/H_2$ ratio the higher the adiabatic combustion temperature and thus, the greater $NO_x$ generation. This may cause a necessity of dilution of the gas despite its relatively low calorific value.

It was also analysed, however not shown in the paper, how does the temperature of the supplied oxygen influence gas parameters. A consequence of the oxygen temperature increase is the decrease of the energy needed for its preheating in gas generator, however, the impact on the quantitative composition of the obtained gas is small.

### 5.4. Effect of moisture content in coal on composition and parameters of the obtained raw syngas

Coal is characterised by different moisture content depending on the type and state of coal, or storage conditions. Therefore, it seems important to examine the impact of moisture content on the parameters and composition of the raw gas, and especially on the water vapour content. Such calculations were performed for the input parameters to the gasifier and the input streams of gasifying and gasified agents. The share of the major components of the received raw gas, depending on the moisture content in coal is presented in Fig 5.

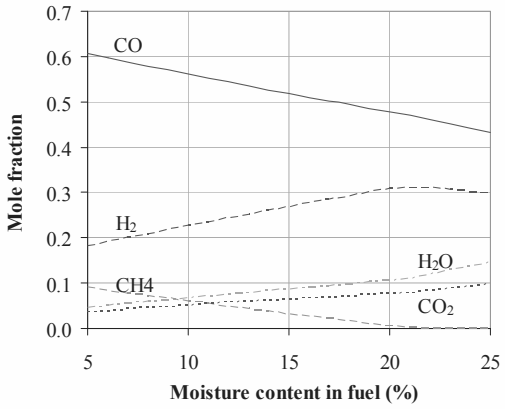


*Fig. 5. Effect of moisture content in coal on the composition of the obtained raw gas.*

With the increase of the fuel moisture content, a decrease of the share of carbon monoxide and methane, and an increase of the share of hydrogen, water vapour and carbon dioxide can be observed. Relatively small are the changes in the share of nitrogen. In the same time, the LHV value of the obtained gas is decreasing.

## 6. Discussion and conclusions

Experiences of the existing IGCC systems in the world show, that in the future for the production of synthesis gas will most probably be used entrained flow gasifiers, which is due to the numerous advantages, by which they are characterised. However, it should be noted that due to the high temperatures prevailing in the gasification zone, these reactors must be constructed with materials of adequate strength, what significantly increase investments. Therefore, the selection of the gasification parameters should be carried out with special care, which requires, among other, the use of numerical analysis.

The model of the gas generator, built by the authors in the Aspen Plus software, shows good agreement with the literature data. and may therefore be a useful tool for the analysis of its work.

Although it is clear, that the performance of the gasifier is affected, among others, by the quantity and parameters of the streams supplied to the generator, however, for optimisation purposes it is essential to determine both qualitative and quantitative impact of this influence. The authors showed, inter alia, that:

- increase of gasification pressure slightly affects the composition and the calorific value of the obtained raw syngas, increases for example the reaction rate of methane formation,
- increase of the gasification reaction temperature shifts the endothermic reactions balance towards products, and therefore towards the increased participation of flammable components (CO, $CH_4$),
- gas composition and its chemical energy significantly depends on the ratio of oxygen to coal stream,
- increase of the moisture content in fuel favours increase of the hydrogen content in the synthesis gas, but reduces its lower heating value.

It should be remembered that such treatments as increase of gasification pressure or gasification in pure oxygen, are connected with the increase of investments and with the increase of the energy consumption for internal needs. It is also important that the composition and parameters of the resulting gas are strongly influenced by gasified fuel composition, especially carbon, moisture and ash content.

It should be underlined, that the main objective of the authors was not to build a very accurate model

of a gasifier, allowing for detailed analysis of the operational parameters of the reactor itself, but to build a simple model that correctly reflects the main parameters and composition of the gas, basing on the determined input values. The numerical model of the gas generator built by the authors will allow for its implementation to the model of the integrated gasification combined cycle plant, in order to analyse the impact of its individual installations on the thermodynamic characteristics of the entire IGCC system, as well as for the optimisation of the design parameters of the whole system in terms of thermodynamic and economic characteristics.

## References

[1] NETL Technical Report, 2007, Gasification World Database - Current Industry Status. Robust Growth Forecast, Department of Energy USA, National Energy Technology Laboratory, URL: www.netl.doe.gov/ technologies/coalpower/gasification/database/ database.html.

[2] Zheng L., Furinsky E., 2005, Comparison of Shell, Texaco, BGL and KRW Gasifier as Part of IGCC Plant Computer Simulations, Energy Conversion and Management, 46, pp. 1767–1779.

[3] Perez-Fortes M., et al., 2009, Conceptual Model and Evaluation of Generated Power and Emissions in an IGCC Plant, Energy, 34, pp. 1721–1732.

[4] ASPEN One, 2009, Ver. 7.1, Aspen Technology, Burlington, USA.

[5] Kristiansen A., 1996, *Understanding Coal Gasification*, IEA Coal research, London.

[6] Szuba J., Michalik L., 1983, *Carbochemistry,* Wydawnictwo Śląsk. (in polish)

[7] Minchener A. J., 2005, Coal Gasification for Advanced Power Generation, Fuel, 84, pp. 2222-2235.

[8] Ścieżko M., Chmielniak T., 2009, Principles of Operation and Construction of Generators for Coal Gasification in IGCC systems, *Proc. Development strategies in the field of turbomachinery and power equipment,* Gliwice, pp. 53-78. (in polish)

[9] Chmielniak T., 2004, *Energy Technologies,* Wydawnictwo Politechniki Śląskiej, Gliwice, Poland. (in polish)

[10] Zaporowski B., 2003, Analysis of Energy-conversion Processes in Gas-steam Power Plants Integrated with Coal Gasification, Applied Energy, 74, pp. 297-304.

[11] Zaporowski B., 2006, Analysis of Energy Effectiveness of Gaseous Fuel Generation in Coal Gasification Process, Energy Policy, 9, pp. 299-310. (in polish)

[12] Szargut J., 1991, *Technical Thermodynamics*, Wydawnictwo Naukowe PWN, Warsaw. (in polish)

[13] Robinson P. J., Luyben W. L., 2008, Simple Dynamic Gasifier Model that Runs in Aspen Dynamics, Ind. Eng. Chem. Res., 47, pp. 7784-7792.

[14] U.S. Department of Energy, Office of Fossil Energy NETL, 2004, Gasification – World Survey Results, National Energy Technology Laboratory.

**Acknowledgments:** The investigations presented in this paper have been carried out within the frame of the research project No. N N513 360537, sponsored by the Ministry of Education and Science.

# Exergoeconomic Analysis and Performance Validation for the Combined Production of Electromechanical Power and Useful Heat in the Ecuadorian Sugar Industry

*Washington O. Irrazabal Bohorquez*[a], *João Roberto Barbosa*[a], *Luiz A. Horta Nogueira*[b]

[a] *Technological Institute of Aeronautics, São José dos Campos, Brazil*
[b] *Federal University of Itajubá, Itajubá, Brazil*

**Abstract:** The Sugar Industry presents a significant potential for increasing the production of electricity through cogeneration systems that can increase the contribution of renewable energy resources in the electricity supply. The reason for the present study is to evaluate the integral use of the sugar cane bagasse on productive process of a Cogeneration Power Plant in an Ecuadorian Sugar Company. A Thermo-economic study was made on the production of electricity and the sales of the exceeding of 27 MWe average. An operational analysis was made by the convolution of the estimated curves of demand and generation of electric energy. From the results, It was concluded that the costs of the generated electricity are 5.11 cents US$/kWh, in comparison with the costs of the supplied electric energy through Fossil Power Plants with values in the range 3 - 15 cents US$/kWh and the Hydroelectric Plants with a value of about 2 cents US$/kWh.

**Keywords:** Energy, Cogeneration, Repowering, Thermoeconomic.

## 1. Introduction

In the Ecuadorian electrical market, three sugar plants which have the greater participation in the local market, initiated plans to produce their own energy and to commercialize the surplus to the electrical market.

The objective is to produce energy from all bagasse produced in sugar cane milling process and to use it in the generation of electrical energy for the supplying of industrial consumption of the plant and to sell the energy surplus to the Ecuadorian electrical market. In addition, is expected in a reduction the emissions of the gases that contribute to the greenhouse effect and to stimulate the investment in electrical projects based on the use of the biomass.

The electrical production that will have the contribution of the sugar mills is not considered as part of the expansion plan of the energy supply in the country, but it can be an option that will help supply the demand that grows in more than 6.91% per year, according to data of the CENACE.

## 2. Technical description

### 2.1. Information of the Power Plant

The operational cycle of the Power Plant studied will be from June to December, coinciding with the period of sugar-cane crop. The assumptions to evaluate the Repowering project are:

- The useful plant life is 20 years after the repowering project.
- The investment recovery time is 10 years and the overall operational time is 20 years.
- Modification of the boiler to satisfy the needs of electrical generation and steam for the mills and use of sugar cane bagasse as fuel to produce high-pressure steam for the turbo-generators.
- The project intends to increment the electric power generation capacity from 7 MWe to 35 MWe.
- Reusability of one extraction/counterpressure Turbo-generator of 7 MWe**.**
- Assembly of one extraction/counterpressure Turbo-generator of 16 MWe and one condensation Turbo-generator of 12 MWe.
- The sugar-cane production is 4,662,322 MT.
- The grinding capacity is 11,000 MTC/day.
- Production of 3,300 MT/day of cane bagasse.
- The Cogeneration Power Plant will operate 5,110 hours/year.
- The simplified thermal drawing of the facility is represented in the Fig. 1.

Corresponding Author: Washington Orlando Irrazabal Bohorquez, Email: wirraz@yahoo.com

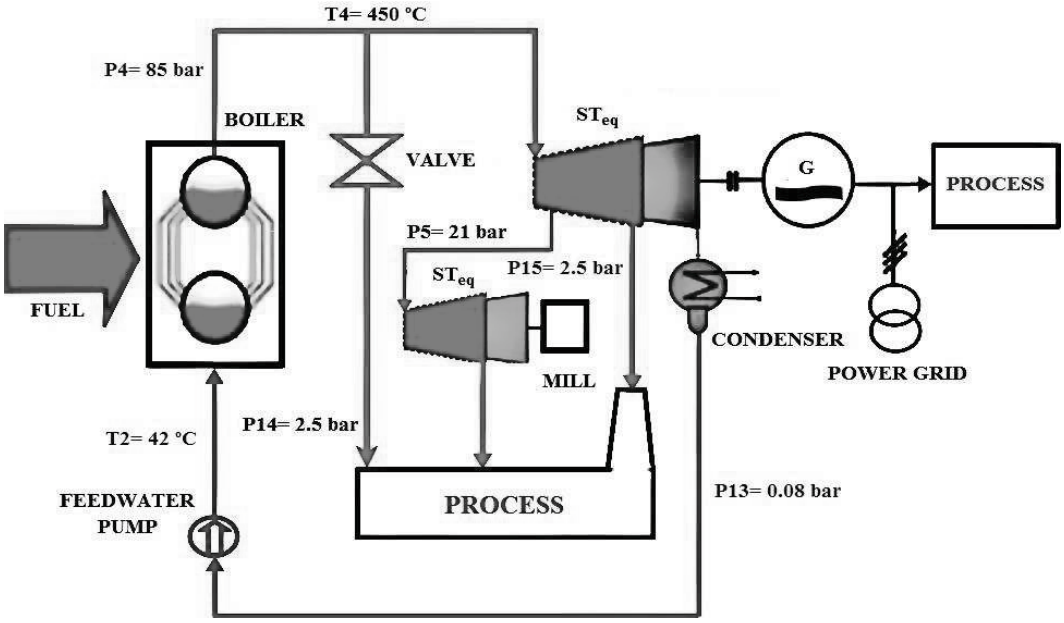


*Fig. 1. Thermal cycle of the Cogeneration Power Plant.*

## 2.2. Analysis of energy balance

With the use of the Thermodynamics Tables and Mollier's Diagram, we can to make the balance of energy and we find the thermodynamics properties of all points of the Thermal Cycle (Table 1).

*Table 1. Thermodynamics Properties.*

| N | T (ºC) | P (bar) | $\dot{m}$ (kg/h) | H (kJ/h) | B (kJ/h.K) |
|---|---|---|---|---|---|
| 1 | S.L. | 0.08 | 3.2E+05 | 5.6E+07 | 5.8E+05 |
| 2 | 42 | 85 | 3.9E+05 | 7.2E+07 | 4.1E+06 |
| 3 | 0 | 0 | 1.9E+05 | 1.4E+09 | 1.4E+09 |
| 4 | 450 | 85 | 98E+03 | 3.2E+08 | 1.3E+08 |
| 5 | 260 | 21 | 98E+03 | 2.8E+08 | 9.5E+07 |
| 6 | 450 | 85 | 2.2E+05 | 7.3E+08 | 2.9E+08 |
| 7 | 450 | 85 | 7.1E+04 | 2.3E+08 | 9.4E+07 |
| 8 | 25 | 1 | 3.7E+06 | 3.8E+08 | 0.0E+00 |
| 9 | 35 | 1 | 3.7E+06 | 5.4E+08 | 2.6E+06 |
| 10 | 260 | 21 | 2.2E+05 | 6.5E+08 | 2.1E+08 |
| 11 | 0 | 0 | 0 | 14E+06 | 14E+06 |
| 12 | 0.95 | 0.08 | 7.1E+04 | 1.7E+08 | 8E+06 |
| 13 | S.L. | 0.08 | 7.1E+04 | 1.2E+07 | 1.E+05 |
| 14 | 128 | 2.5 | 98E+03 | 2.6E+08 | 6E+07 |
| 15 | 128 | 2.5 | 2.2E+05 | 6.1E+08 | 1E+08 |
| 16 | 0 | 0 | 0 | 28E+06 | 28E+06 |
| 17 | 0 | 0 | 0 | 5E+06 | 5E+06 |
| 18 | 0 | 0 | 0 | 25E+06 | 25E+06 |
| 19 | 0 | 0 | 0 | 57E+06 | 57E+06 |
| 20 | 0 | 0 | 0 | 38E+06 | 38E+06 |

With the milling capacity and conversion factor from cane to bagasse data, we find the produced tons of bagasse per hour (1).

$$Ton_b = M_c \cdot F_c , \quad (1)$$

With the thermodynamics state properties of the points 2 and 3, we found the steam flow generated in the boiler, with the formula referred in (2).

$$\dot{m}_{sb} = \left(\eta_b \cdot Ton_b \cdot LHV\right)/\left(h_4 - h_2\right), \quad (2)$$

With the mathematical expression described in (3), the steam flow that is required in the sugar production was found.

$$\dot{m}_{sp} = \left(ST \cdot M_c\right)/1{,}000, \quad (3)$$

Applying the milling capacity of the mills and the thermodynamic properties of the 10, 13, 14 and 15 Thermal Cycle points in (4) and (5), we find the steam flows used in the mills and using (6) and (7) we determine the necessary mechanical power.

$$\dot{m}_{sm_1} = \left(3.6 \cdot CAM \cdot M_c\right)/\eta_{mw} \cdot \left(h_{10} - h_{15}\right), \quad (4)$$

$$\dot{m}_{sm_2} = \left(3.6 \cdot CAM \cdot M_c\right)/\eta_{mw} \cdot \left(h_{13} - h_{14}\right), \quad (5)$$

$$MP_1 = 0.28 \cdot \eta_{mw} \cdot \dot{m}_{sm_1} \cdot \left(h_{10} - h_{15}\right), \quad (6)$$

$$MP_2 = 0.28 \cdot \eta_{mw} \cdot \dot{m}_{sm_2} \cdot \left(h_{13} - h_{14}\right), \quad (7)$$

Applying the Thermodynamic First Law and a control volume regarding the steam turbines, a balance of mass was made and we use the steam flows $\dot{m}_{sp}$ and $\dot{m}_{sb}$ in (8) to find the real power required for the studied system. With the obtained result we calculate the total mechanical power, installed electric power, consumed electric energy and the electricity generated by power plant. We use (9), (10), (11) and (12).

$$\dot{W}_r = 0.28 \cdot \left[\dot{m}_{sp}\left(h_3 - h_{10}\right) + \left(\dot{m}_{sb} - \dot{m}_{sp}\right)\left(h_7 - h_{12}\right)\right], \quad (8)$$

$$\dot{W}_{tm} = MP_1 + MP_2 + \dot{W}_r, \quad (9)$$

$$\dot{W}_e = \eta_g \cdot \dot{W}_r, \quad (10)$$

$$\dot{W}_c = CEE \cdot M_c, \quad (11)$$

$$\dot{W}_s = \dot{W}_e - \dot{W}_c, \quad (12)$$

## 2.3. Analysis of operation

The operation analysis of the cogeneration systems which is in function at the time uses instantaneous values or duration curve of the demand and availability of thermal and electricity.

This shows a better knowledge of the energy flows among the auto-generator system, the consumer and the company of electric power distribution. The operation analysis has as objective the study of the thermal and electrical demands duration curves and it is known all the time that, through the production of electrical energy it is possible to determine the deficit and the excess of energy in the course of time.

Based on the preliminary report energy of the Control Energy National Center of Ecuador, the duration curves of the thermal and electricity demand and electricity generation were elaborated and appear in Fig. 2. With the maximum, average and minimum values of the duration curves of the thermal and electric energy demand and electricity generation, it is possible to make the convolution operation, comparing one by one the levels of the curves shown in Fig. 2 and to determine the surpluses for every moment in time.

With the values obtained in the convolution operation, the surplus values of electrical energy can be found, as it is shown in Table 2, and besides to make the duration curve of these surpluses in each moment in time, as it is possible to be observed in Fig. 3.

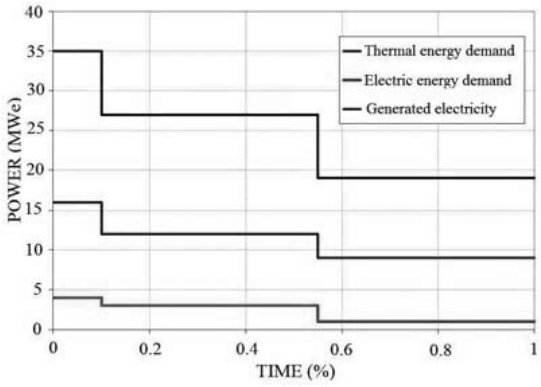


*Fig. 2. Curves of the thermal and electric energy demands and electric energy generation.*

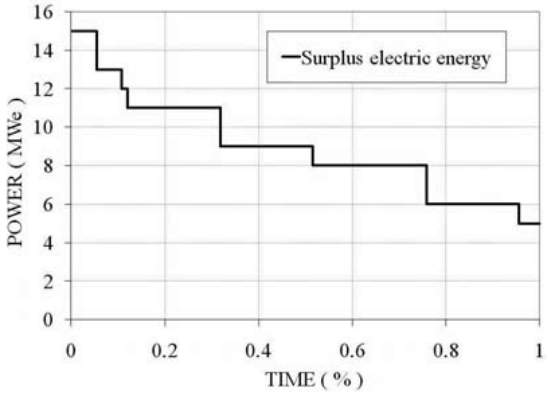


*Fig. 3. Curve of the electric power surpluses.*

It is possible to observe in Table 2 that values of the surplus power column are always positive and it indicates that in all moments this Power Plant will produce electrical energy to satisfy its energetic demand and surpluses to sell in the Ecuadorian electrical market.

*Table 2. Surplus values of electricity.*

| $P_p$ | % Annual time consumption $T_c$ | $P_p$-$P_c$ | % Annual time $T_p$-$T_c$ | % Annual time $T_{acs}$ |
|---|---|---|---|---|
| 6 | 0.10 | 12 | 0.012 | 0.054 |
| 16 | 0.45 | 13 | 0.054 | 0.108 |
| 16 | 0.45 | 15 | 0.054 | 0.12 |
| 12 | 0.10 | 8 | 0.044 | 0.318 |
| 12 | 0.45 | 9 | 0.198 | 0.516 |
| 12 | 0.45 | 11 | 0.198 | 0.56 |
| 9 | 0.10 | 5 | 0.044 | 0.758 |
| 9 | 0.45 | 6 | 0.198 | 0.956 |
| 9 | 0.45 | 8 | 0.198 | 1 |

## 3. Allocation of costs

### 3.1. Exergoeconomic evaluation

A Thermal Power Plant, in this case, a Cogeneration Power Plant, can be considered as a system, formed by an equipment group that has a defined production objective.

These subsystems or equipments are associated with energy flows or inputs and the process to the formation of the product costs.

The products are the final effects and the available resources are the material causes. The modeling and the eventual optimization of this structure seeks to characterize, to measure and to evaluate these effects and their causes in the energy systems and the application of a general criterion to measure the efficiency of the project or the real operation of this installation.

The Second Law of Thermodynamics quantifies the irreversibilities and the efficiency of the processes using the exergy function. The first step was to define the logical structure of the Cogeneration Power Plant for the elaboration Thermoeconomic analysis.

In the Figure 4 the desegregation in subsystems and the diagram flows of the facility can be observed.

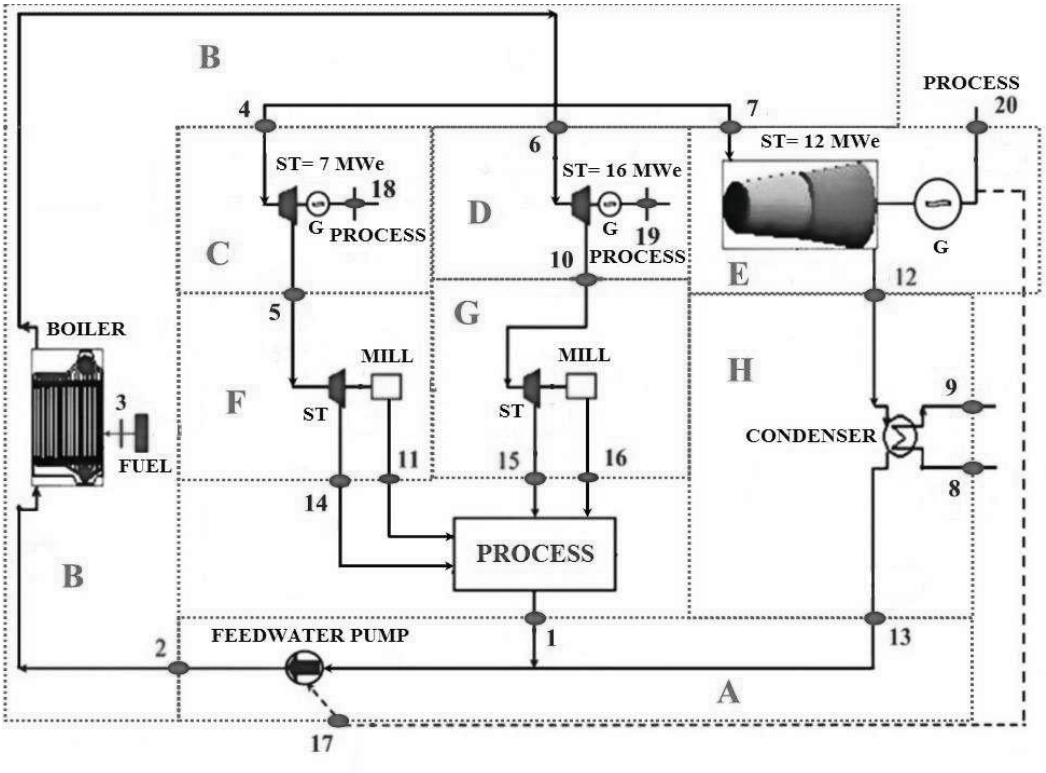


*Fig. 4. Desegregation in subsystems of the Cogeneration Power Plant.*

The second step consisted in the definition of the inputs, products and losses for all equipments as a function efficiency concept. It was necessary to determine the incidence matrixes of the inputs, products and losses in the Power Plant. See Tables 3and 4.

For the next step, the exergy values of all flows were calculated, as it is shown in Table 1, with these values, the input and product vectors for each subsystem or equipment were found. These values were calculated using (13), (14) and (15). See Table 5.

$$V_P = I_P \times B, \tag{13}$$

$$V_F = I_F \times B, \tag{14}$$

$$V_I = I_A \times B, \tag{15}$$

*Table 3. Incidence Matrix A of Cogeneration Power Plant.*

| Flows / Systems | 1 | 2 | 3 | 4 | 5 | 6 | 7 | 8 | 9 | 10 | 11 | 12 | 13 | 14 | 15 | 16 | 17 | 18 | 19 | 20 |
|---|---|---|---|---|---|---|---|---|---|---|---|---|---|---|---|---|---|---|---|---|
| A | 1 | -1 | 0 | 0 | 0 | 0 | 0 | 0 | 0 | 0 | 0 | 0 | 1 | 0 | 0 | 0 | 1 | 0 | 0 | 0 |
| B | 0 | 1 | 1 | -1 | 0 | -1 | -1 | 0 | 0 | 0 | 0 | 0 | 0 | 0 | 0 | 0 | 0 | 0 | 0 | 0 |
| C | 0 | 0 | 0 | 1 | -1 | 0 | 0 | 0 | 0 | 0 | 0 | 0 | 0 | 0 | 0 | 0 | 0 | -1 | 0 | 0 |
| D | 0 | 0 | 0 | 0 | 0 | 1 | 0 | 0 | 0 | -1 | 0 | 0 | 0 | 0 | 0 | 0 | 0 | 0 | -1 | 0 |
| E | 0 | 0 | 0 | 0 | 0 | 0 | 1 | 0 | 0 | 0 | 0 | -1 | 0 | 0 | 0 | 0 | -1 | 0 | 0 | -1 |
| F | 0 | 0 | 0 | 0 | 1 | 0 | 0 | 0 | 0 | 0 | -1 | 0 | 0 | -1 | 0 | 0 | 0 | 0 | 0 | 0 |
| G | 0 | 0 | 0 | 0 | 0 | 0 | 0 | 0 | 0 | 1 | 0 | 0 | 0 | 0 | -1 | -1 | 0 | 0 | 0 | 0 |
| H | 0 | 0 | 0 | 0 | 0 | 0 | 0 | 1 | -1 | 0 | 0 | 1 | -1 | 0 | 0 | 0 | 0 | 0 | 0 | 0 |
| ΣSUB. | 1 | 0 | 1 | 0 | 0 | 0 | 0 | 1 | -1 | 0 | -1 | 0 | 0 | -1 | -1 | -1 | 0 | -1 | -1 | -1 |

*Table 4. Inputs, products and irreversibilities flows.*

| Subsystems | Products P | Inputs F | Losses A |
|---|---|---|---|
| A | $B_2 - B_1 - B_{13}$ | $B_{17}$ | - |
| B | $B_4 + B_6 + B_7 - B_2$ | $B_3$ | - |
| C | $B_{18}$ | $B_4 - B_5$ | - |
| D | $B_{19}$ | $B_6 - B_{10}$ | - |
| E | $B_{20} + B_{17}$ | $B_7 - B_{12}$ | - |
| F | $B_{11}$ | $B_5 - B_{14}$ | - |
| G | $B_{16}$ | $B_{10} - B_{15}$ | - |
| H | 0 | $B_{12} - B_{13}$ | $B_9 - B_8$ |

*Table 5. Inputs, products and irreversibilities vectors.*

| Products vector $V_P$ | Inputs vector $V_F$ | Irreversibilities vector $V_I$ |
|---|---|---|
| 3.39E+06 | 5.04E+06 | 0.00E+00 |
| 5.21E+08 | 1.43E+09 | 0.00E+00 |
| 2,52E+07 | 3.51E+07 | 0.00E+00 |
| 5.76E+07 | 8.00E+07 | 0.00E+00 |
| 4.32E+07 | 8.58E+07 | 0.00E+00 |
| 1.44E+07 | 3.47E+07 | 0.00E+00 |
| 2.88E+07 | 7.90E+07 | 0.00E+00 |
| 0.00E+00 | 8.64E+06 | 2.68E+06 |

Using the auxiliary equations for the expanded incidence matrix A (Table 6), the investment annual cost of the facility (Table 7 and (16)), the fuel consumption annual cost and the operation and maintenance annual cost (17), it was possible to set up the matricial system shown in Table 8.

With the computational methods available for the solving of matricial systems, the system can be solved, and the result is the Exergoeconomic costs vector of the heat and electricity generation for the process (Table 9).

*Table 6. Auxiliary equations for the matrix A.*

| Number | Equation |
|---|---|
| 1 | $\pi_3 = A_{FUEL}$ |
| 2 | $\pi_1 = 0$ |
| 3 | $\pi_8 = 0$ |
| 4 | $\pi_9 = 0$ |
| 5 | $(\pi_5 / B_5) - (\pi_{18} / B_{18}) = 0$ |
| 6 | $(\pi_{10} / B_{10}) - (\pi_{19} / B_{19}) = 0$ |
| 7 | $(\pi_{12} / B_{12}) - (\pi_{20} / B_{20}) = 0$ |
| 8 | $(\pi_{12} / B_{12}) - (\pi_{17} / B_{17}) = 0$ |
| 9 | $(\pi_{14} / B_{14}) - (\pi_{11} / B_{11}) = 0$ |
| 10 | $(\pi_{15} / B_{15}) - (\pi_{16} / B_{16}) = 0$ |
| 11 | $(\pi_4 / B_4) - (\pi_6 / B_6) = 0$ |
| 12 | $(\pi_4 / B_4) - (\pi_7 / B_7) = 0$ |

$$A_E = \frac{(P_E)\cdot(1+i)^n\cdot(i)}{(1+i)^n - 1}, \quad (16)$$

$$A_{OM} = \frac{(C_{OM})\cdot(1+i)^n\cdot(i)}{(1+i)^n - 1}, \quad (17)$$

*Table 7. Investment and Fuel annual costs.*

| Equipment | Annual cost (US$) | $A_{OM}$ (US$) |
|---|---|---|
| FW Pump | 718,75E+03 | 15,81E+03 |
| Boiler | 2,96E+06 | 65,06E+03 |
| ST 7MWe | 673,57E+03 | 14,82E+03 |
| ST 16MWe | 1,25E+06 | 27,38E+03 |
| ST 12MWe | 1,01E+06 | 22,09E+03 |
| ST 4MWe (process) | 271,07E+03 | 5,96E+03 |
| ST 8MWe (process) | 441,52E+03 | 9,71E+03 |
| Condenser | 681,78E+03 | 14,99E+03 |
| Fuel | 568,84E+03 | 0 |

*Table 8. Matricial system.*

$$\pi = I'^{-1} \times Z'$$

$$\begin{bmatrix} \pi_1 \\ \pi_2 \\ \pi_3 \\ \pi_4 \\ \pi_5 \\ \pi_6 \\ \pi_7 \\ \pi_8 \\ \pi_9 \\ \pi_{10} \\ \pi_{11} \\ \pi_{12} \\ \pi_{13} \\ \pi_{14} \\ \pi_{15} \\ \pi_{16} \\ \pi_{17} \\ \pi_{18} \\ \pi_{19} \\ \pi_{20} \end{bmatrix} = \begin{bmatrix} I_{11} & . & . & I_{1n} \\ . & . & . & . \\ . & . & . & . \\ . & . & . & . \\ . & . & . & . \\ . & . & . & . \\ . & . & . & . \\ . & . & . & . \\ . & I_{k-1,p-1} & . & . \\ . & . & . & . \\ . & . & . & . \\ . & . & . & . \\ . & . & . & . \\ . & . & . & . \\ . & . & . & . \\ . & . & . & . \\ . & . & . & . \\ . & . & . & . \\ . & . & . & . \\ I_{m1} & . & . & I_{mn} \end{bmatrix}^{'-1} \times \begin{bmatrix} 7.19E+05 \\ 2.96E+06 \\ 6.74E+05 \\ 1.25E+06 \\ 1.01E+06 \\ 2.71E+05 \\ 4.42E+05 \\ 6.82E+05 \\ 5.69E+05 \\ 0.0 \\ 0.0 \\ 0.0 \\ 0.0 \\ 0.0 \\ 0.0 \\ 0.0 \\ 0.0 \\ 0.0 \\ 0.0 \\ 0.0 \end{bmatrix},$$

*Table 9. Exergoeconomic costs of the power plant.*

| Flows | Π (US$/s) | C (US$/kWh) | Equipments |
|---|---|---|---|
| 1 | -1,1901E-17 | -2,6593E-16 | |
| 2 | 1,0531E-01 | 3,3289E-01 | |
| 3 | 4,4206E-02 | 4,0064E-04 | Boiler |
| 4 | 7,7181E-02 | 7,6357E-03 | |
| 5 | 9,0204E-02 | 1,2190E-02 | |
| 6 | 1,7811E-01 | 7,7201E-03 | |
| 7 | 5,5130E-02 | 7,5526E-03 | |
| 8 | 0,0000E+00 | 0,0000E+00 | |
| 9 | 0,0000E+00 | 0,0000E+00 | |
| 10 | 1,9483E-01 | 1,1530E-02 | |
| 11 | 1,9524E-02 | 1,7571E-02 | Mill 4 MWe |
| 12 | 1,8564E-02 | 2,7433E-02 | |
| 13 | 5,5625E-02 | 5,6764E+00 | |
| 14 | 8,5416E-02 | 1,8088E-02 | |
| 15 | 1,8147E-01 | 1,6799E-02 | |
| 16 | 3,7362E-02 | 1,6813E-02 | Mill 8 MWe |
| 17 | 1,0615E-02 | 2,7295E-02 | FWP |
| 18 | 2,3592E-02 | 1,2133E-02 | ST 7 MWe |
| 19 | 5,1229E-02 | 1,1527E-02 | ST 16 MWe |
| 20 | 8,0854E-02 | 2,7431E-02 | ST 12 MWe |

Using the unit costs shown in table 9, (18) and (19) it was possible calculate the cost allocation of the final products: generated electricity cost and process steam cost.

$$C_{GE} = C_{18} + C_{19} + C_{20}, \quad (18)$$

$$C_{PS} = C_{11} + C_{16}. \quad (19)$$

## 4. Closing remarks

The accomplishment of this project can have a catalytic effect in the development of similar projects in other agro-industrial companies, which would allow Ecuador to benefit from the increase of energy generated from renewable resources (bagasse, husk of rice and others).

The electrical generation starting from the biomass requires a great initial investment and for example, this initial investment requires that for each kWh generated US$ 800 is necessary, the double of the initial investment of conventional Thermoelectric that is US$ 400 for each kWh and almost similar

to the initial cost of Hydroelectric Power Plant that is US$ 1,000 for each kWh.

Although initial investment of Cogeneration Power Plant that uses bagasse as fuel is greater than Thermoelectric Power Plant that burns fossil fuel, the cost of the generated energy is competitive, the cost of the generated electricity are 0.511 cents US$/kWh (18), in comparison with the costs of the supplied electric energy through Fossil Power Plants with values in the range 0.03 – 0.15 US$ cents/kWh and the Hydroelectric Plants with a value of about 0.02 cents US$/kWh.

It is expected that this project contributes with the provision of electrical energy to the Interconnected National System of Ecuador; likewise, it contributes to the mitigation of climatic change, with the reduction of the prospective emissions of greenhouse effect gases in an amount of 551,880 t of $CO_2$ equivalent.

## Nomenclature

$A$ losses

$A$ annual cost

$B$ exergy, kJ/h.K

$C$ unit cost, US$/kWh

$CAM$ mechanical working consumption, kWh/ton

$CEE$ electricity consumption, kWh/ton

$F$ inputs

$FWP$ Feedwater pump

$H$ enthalpy, kJ/h

$i$ annual interest

$LHV$ lower heating value, kJ/kg

$\dot{m}$ mass flow rate, kg/h

$M$ milling capacity, ton/h

$MP$ *mechanical power, MWe*

$MWe$ megawatt

$n$ depreciation, years

$N$ number flow

$P$ pressure, bar

$P$ price, US$

$ST$ steam turbine

$T$ temperature

$t$ time

### Greek symbols

$\eta$ efficiency

### Subscripts and superscripts

$_b$ boiler

$_c$ cane

$_c$ consumption

$_E$ equipment

$_g$ electric generator

$_{GE}$ generated electricity

$_{MW}$ mechanical working

$_{OM}$ operation and maintenance

$_{OP}$ operation

$_{PS}$ process steam

$_S$ steam

$_t$ turbine

### Matrices and Vectors

$I'^{-1}$ A matrix inverse

$\pi$ monetary cost vector

$V_F$ inputs vector

$V_I$ irreversibilities vector

$V_P$ products vector

$Z'$ external cost vector

## References

[1] Heinrich, P., 2001, The potential of Cogeneration in selected Chinese Provinces and the Demand for related Energy Services, Symposium Efficient use of energy in Chinese Industry, Fichtner, pp. 8–9.

[2] Horta Nogueira, L., and Teixeira F.N., 2004, Disseminação de Informações em eficiência Energética: Cogeração, Eletrobrás, PROCEL: Programa Nacional de Conservação de Energia Elétrica, pp. 26–38.

[3] Irrazabal, W., and Horta, L., 2005, A Study of Increment Case of the Cogeneration in Sugar Industry for the Ecuadorian Context, CLAGTEE *Meeting Papers on Disc* [CD-ROM], 1, Mar del Plata, Argentina.

[4] Puga, C., 2004, Generación de energía a partir de bagazo de caña de azúcar, Sociedad Agrícola e Industrial San Carlos, pp. 1–5.

**Acknowledgments:** The authors acknowledge the support from the CNPq (National Council for Scientific and Technological Development) and the Center for Reference on Gas Turbines and Energy (ITA).

# Integration concept for coal-fired CHP and post-combustion $CO_2$ capture

*Marcin Liszka, Andrzej Ziębik, Michał Budnik*

*Silesian University of Technology, Gliwice, Poland*

**Abstract:** The presented study deals with the thermodynamic analysis of district heat production using waste heat recovered from the post-combustion $CO_2$ removal system. The basic system of interest is a coal-fired, super-critical power unit equipped in a tap-condensing steam turbine and pulverized-fuel boiler. The introduction of the $CO_2$ absorption unit based on amine (MEA) solvent causes demand for large amount of steam for solvent regeneration. Simultaneously, as the separated $CO_2$-rich stream contains significant amount of moisture, its cooling is necessary for $H_2O$ condensation. The heat taken from the $CO_2$ capture system is characterized by a much lower exergy than the supplied steam, however the temperature is still high enough to preheat water in the district heating system. Another source of low-temperature heat is the $CO_2$ compression system, where $CO_2$ is cooled down between subsequent compression stages. The both mentioned heat sources can be combined with classical extraction-connected heat exchangers to form the integrated system of district heat supply. Three power plant structures have been modeled and analyzed: coal-fired power unit without $CO_2$ removal, the same plant with $CO_2$ removal but without district heat production (waste heat is rejected to the environment), and finally the plant with $CO_2$ removal and district heat production. All the cases have been modeled using the EES (Engineering Equation Solver) software. The specific $CO_2$ emission have been taken as main assessment factor. In the case of district heat production, the system effects of emission decrease have been accounted. The post-combustion $CO_2$ removal and compression causes the decrease of the specific $CO_2$ emission form 202 to 28 kg per 1 kJ of produced net electricity. The useful application of the waste heat related to the post-combustion $CO_2$ removal causes fossil fuel savings and further emission reduction to 18 kg per 1 kJ of produced electricity.

**Keywords:** post-combustion $CO_2$ removal, $CO_2$ compression, CHP, waste heat.

## 1. Introduction

The $CO_2$ removal processes related to the coal-fired power units are responsible for a large decrease of fuel conversion efficiency. Depending on the type of capture technology and the final $CO_2$ pressure, the decrease of efficiency may vary from 8 to 12 percentage points [1,2,3]. Such a large decrease of efficiency impacts significantly the electricity production cost as well as the intensity of depletion of coal resources. Each potential method for partial recovery of energy spent for $CO_2$ separation should be thus carefully analyzed.

The present study is dedicated to pulverized-coal (PC) power units equipped in post-combustion $CO_2$ removal by chemical absorption. This set of technologies is often perceived as one of leading alternatives [1,3] for decarbonization of coal-based electricity production. The monoethanolamine (MEA) has been selected as process solvent for analysis. The typical simplified scheme of the chemical $CO_2$ absorption unit is presented in Fig. 1. The $CO_2$ reacts with the solvent (MEA) in the absorber at low temperature.

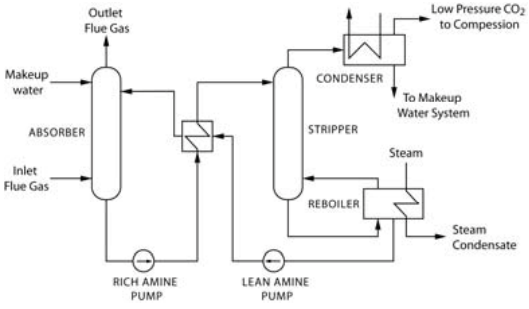


*Fig. 1. $CO_2$ chemical absorption process [4]*

The rich amine solution is then supplied via regenerative heat exchanger to the stripper, where $CO_2$ desorbs from the amine solution. The desorption process requires higher temperature comparing to the absorber conditions. The external heat supply to the reboiler is thus necessary and is done by steam extraction form the steam turbine. The steam consumption for solvent regeneration causes the largest efficiency penalty referring to other processes related to the $CO_2$ separation (e.g.

Corresponding Author: Marcin Liszka, Email: marcin.liszka@polsl.pl

solvent compression). The process steam demand is not the only energy flux crossing the absorption unit boundary. There is also a significant demand for the cooling medium for $H_2O$ condensation from the separated $CO_2$-rich stream. Basically, the cooling agent is water and the cooling heat is rejected to the environment via cooling tower. The initial temperature of the condensing $CO_2$-$H_2O$ mixture is however close to 100 $^{O}$C [4], which suggests the possibility for external use of the cooling heat.

The proposed idea for partial recovery of the heat used for solvent regeneration is to use it for district heating purposes. Another heat source which is normally lost to the environment and may by recovered by the same way are the inter-stage coolers of the $CO_2$ compressor. Within the present study both potential heat sources have been combined and analyzed as integrated power unit producing heat and electricity by very low $CO_2$ emission.

As input data for analysis of district heat production, the typical temperature-controlled hot water network has been assumed. The required temperature profiles of input/output district water are presented in Fig. 2. The water flow is assumed to be constant during the whole heating season. Its nominal value determining also the maximal district heat flow rate will result from the waste heat potential of the $CO_2$ removal and compression systems.

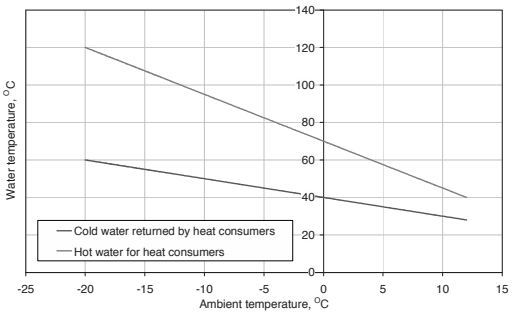


*Fig. 2. Temperature profiles of the district heating network*

## 2. Case studies

For comparison purposes the three computational cases have been selected and analyzed:

- **PC-ref**: the pulverized coal (PC) power unit without $CO_2$ removal – Fig. 3 (black contours),
- **PC-MEA:** the PC unit with $CO_2$ removal but without useful heat production – Fig. 3,
- **PC-MEA-CHP:** the PC unit with $CO_2$ removal and with district heat production – Fig. 4.

For all cases the same steam boiler and steam cycle parameters have been assumed. The supercritical steam cycle is of single reheat arrangement and corresponds to the best commercially available level of today technology [1,5]. The parameters of live/reheated steam are: 600$^{O}$C; 28.5MPa / 620$^{O}$C; 5.1MPa. The main feed water pump is driven by auxiliary steam turbine. Moreover, a steam cooler has been applied to desuperheat steam extracted from the first turbine bleed located behind the reheater.

Flue gas leaving the supercritical steam boiler is treated in the selective catalytic reduction (SCR) unit for NOx removal by injection of ammonia water. The flue gas is then cooled down in heat regenerator, dedusted in electrostatic precipitator (ESP) and desulphurized in the wet scrubbing unit. Coal is dried and heated up by primary air to the required fuel-mix temperature (100$^{O}$C). Presented PC-ref plant arrangement is typical for new units offered in last years.

The PC-MEA plant is build on the PC-ref boiler and steam cycle. The newly introduced components are marked by dashed red contours in Fig. 2. The set of new components include additional flue gas fan to balance the pressure drop in the absorber, the chemical absorption unit (absorber, stripper, reboiler, pumps, heat exchangers), the water condenser and the inter-cooled four-stage $CO_2$ compressor.

The basic steam cycle (as for PC-ref plant) has been modified by inclusion of additional steam flow from the sixth turbine extraction where the saturation temperature is equal to 122$^{O}$C. The amine solution should be regenerated at temperatures close to about 110-120$^{O}$C [6]. Higher temperatures are not desirable because of degradation of MEA and corrosion problems [6].

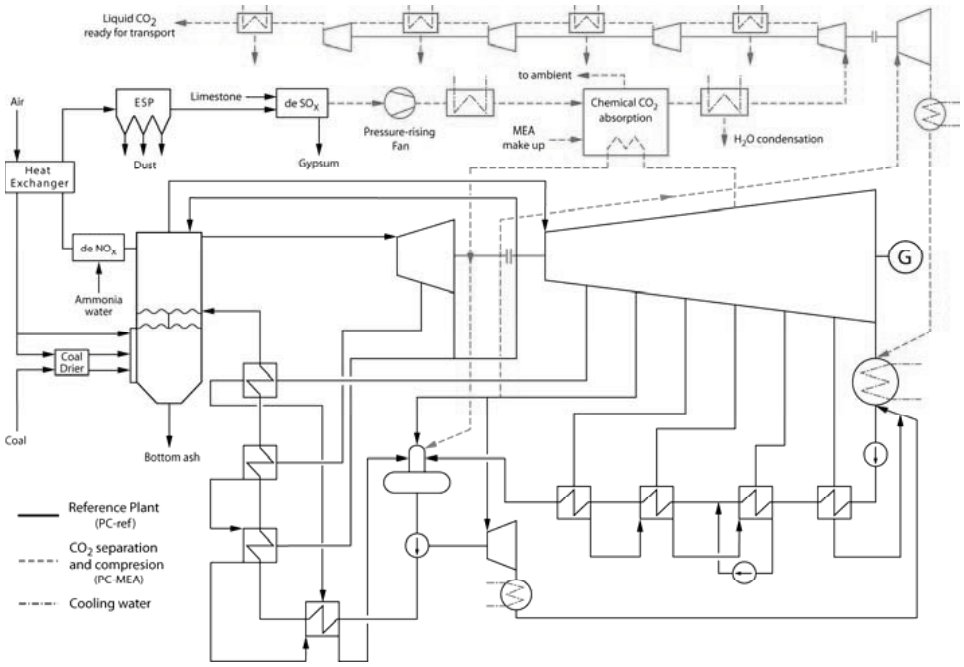


*Fig. 3. The reference pulverized-coal power unit (PC-ref; black contours) and the newly introduced equipment (red dashed contours) related to the $CO_2$ removal and compression (PC-MEA)*

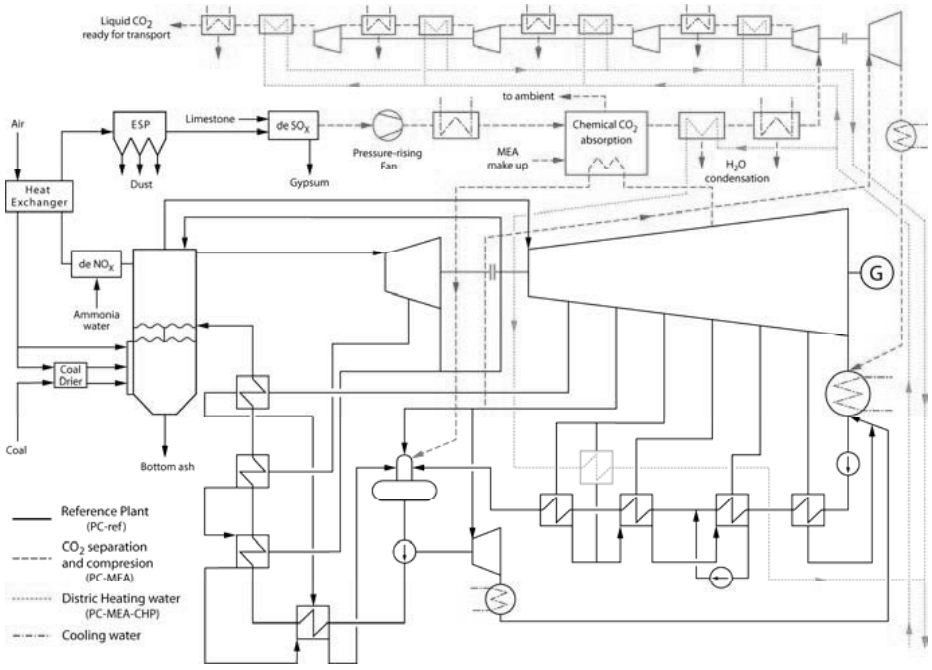


*Fig. 4. The pulverized-coal power unit with $CO_2$ removal adjusted for district heat production (PC-MEA-CHP)*

Taking into account the reasonable temperature pinch in the reboiler, the selected extraction pressure seems to be relevant. The condensate returning form the $CO_2$ absorption unit is supplied directly to the deaerator.

Another significant steam cycle modification is introduction of additional steam turbine to drive the $CO_2$ compressor. This turbine is supplied with steam from the same extraction as turbo-pump.

In the case of PC-MEA plant all cooling loads are covered by the cooling water which is available at $20^{O}C$ and is preheated to $30^{O}C$. The wet, natural draught cooling tower is used to prepare the cooling water for all demanding devices.

The modernization of the PC-MEA structure towards the PC-MEA-CHP plant is based on the replacement of the cooling by district water in the $H_2O$ condenser and inter-stage coolers (see Fig. 4). In practice, because of varying temperature of the district water (see Fig. 2), the regular inter-stage coolers should not be removed ensuring the same $CO_2$ temperature at compression inlets as for the PC-MEA plant. The same applies to the $H_2O$ condenser. All the district heat exchangers using the process waste heat are connected in parallel since the temperature ranges of hot streams are similar. The exception is the $H_2O$ condenser, where the district water temperature possible to obtain is lower than the maximal temperature at the district network inlet (Fig. 2). To meet the required temperature, the district water stream leaving the $H_2O$ condenser is then preheated in conventional extraction-connected heat exchanger.

## 3. Simulation model and assumptions

The three analysed cases have been modelled using the Engineering Equation Solver [7] software. Both the physical and empirical modelling have been applied. The physical models were built for steam boiler, steam cycle, $H_2O$ condenser and $CO_2$ inter-cooled compressors. The empirical modelling based on the literature data of characteristic operational factors like e.g. $CO_2$ removal effectiveness were applied for deNOx, deSOx and chemical $CO_2$ absorption units.

As the applied modelling procedures for supercritical steam boiler and steam cycle are typical and have been described in detail in previous papers [8,9], only the core information are given below.

The model of a supercritical steam boiler has been divided into several sub-models, including the combustion zone, heat exchange section, regenerative flue gas-air heater and fuel dryer. The model of heat exchange section is based on division of the whole enthalpy increase of preheated fluid into intervals (elementary heat exchangers) which allows for taking into account varying specific heat of both flue gas and steam/water flows. For each elementary heat exchanger the energy balance is formulated and solved to determine flue gas and steam temperatures at the exchanger outlet. This methodology allows for generation of temperature profiles for both fluids inside the whole heat exchange section as shown in Fig. 5.

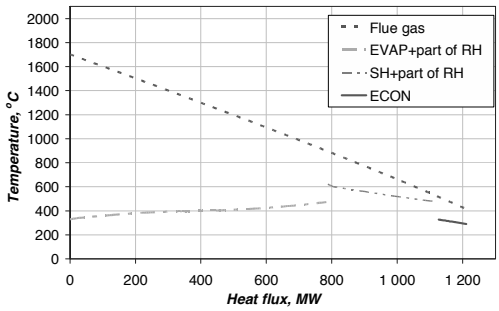


*Fig. 5. Temperature profiles of flue gas and water/steam in the boiler heat exchange section*

The steam cycle has been divided for modeling purposes into sub-models of groups of turbine stages, regenerative heat exchangers (membrane- and mix-type), pumps and condensers. All these models are based on mass and energy balances, as well as the efficiency equation which in case of turbine stages takes the form of internal (isentropic) efficiency and in the case of membrane-type heat exchangers is defined as heat exchange effectiveness.

The $H_2O$ condensation from the $CO_2$-$H_2O$ mixture has been modeled similarly as the heat exchange section in the steam boiler - the condenser has been divided into elementary heat exchangers (EHE). It was assumed that if the outlet EHE temperature is lower than the $H_2O$ dew point (regarding partial $H_2O$ pressure), the EHE outlet stream is saturated by moisture. The difference between the total moisture and moisture at

saturation conditions condenses affecting the heat exchange in the condenser. The calculated temperature profiles inside the $H_2O$ condenser, as well as, the condensed water flow for PC-MEA-CHP plant are presented in Fig. 6. All data in Fig. 6 are dealing with the maximal district heat demand corresponding to the maximal district water temperatures (see Fig. 2). The need for a peak-load district water preheating is thus clear - the outlet water temperature ($90^{O}$C) is much lower than the required $120^{O}$C. The $CO_2$-$H_2O$ mixture at condenser inlet is assumed to be close to saturation [4].

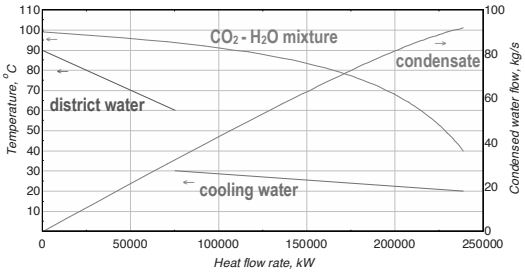


*Fig. 6. Temperature profiles of $CO_2$-$H_2O$ mixture, district water and cooling water, as well as, condensate mass flow in the water condenser in case of PF-MEA-CHP plant*

The solubility of $CO_2$ in water has not been considered. The $CO_2$-$H_2O$ mixture is assumed to be ideal while both components are treated as real fluids. The same applies to the model of the $CO_2$ compression.

As one may conclude from Fig. 6, the district water flow could be much higher yielding higher district heat production and lower cooling water consumption. The reason why the district water flow is limited comes from the steam-fed peak load heat exchanger (see Fig. 4). In case of the lowest analyzed ambient temperature (the highest district heat flow rate), the steam extraction flow would cause very low flow at turbine outlet which may be dangerous for turbine blades. The turbine outlet flow is anyway reduced by installation of additional steam turbine driving the $CO_2$ compressor. Finally, it has been assumed, that the turbine outlet flow limitation is at c.a. 8% of the live steam flow. The reduced district water flow in both peak-load exchanger and $H_2O$ condenser (Fig. 6) follows this limitation.

The four-stage $CO_2$ compression train has been modeled assuming the constant stage work approach. The polytropic efficiency for compression stages and the heat exchange effectiveness for inter-stage coolers (both district and cooling water-connected) have been used. The visualization of the specific points during the compression and cooling of $CO_2$-$H_2O$ mixture is presented in Fig. 7 referring to the $CO_2$ component and PC-MEA-CHP plant at maximal district heat load.

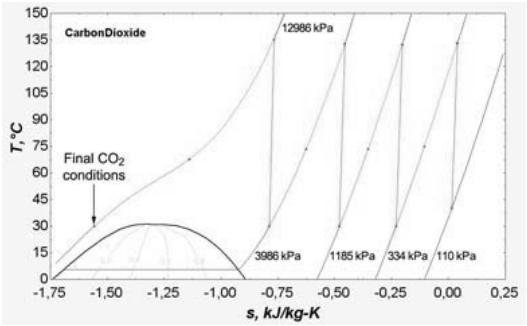


*Fig. 7. Inter-cooled $CO_2$ compression process in case of PF-MEA-CHP plant*

The isobars correspond therefore to the $CO_2$ partial pressures. Because of very low $H_2O$ content, these partial pressures are however very close to the total stream pressures at successive compression stage outlets which are assumed to 350, 1200, 4000 and 13000 kPa. The points located on cooling isobars separates the district water heaters and cooling water heat exchangers.

Similarly as for the main $H_2O$ condenser, the condensation process may occur in the inter-stage compressor coolers. The calculated heat flow rates and mass flows rates of separated $H_2O$ condensate in case of PC-MEA-CHP plant are presented in Table 1.

The chemical $CO_2$ absorption unit has been modeled empirically taking the specific heat consumption for solvent regeneration equal to 4000 kJ per 1 kg of separated $CO_2$. The $CO_2$ separation effectiveness has been assumed to 90%. Similar values may be found in the literature as reported in Table 2.

All analyzed power plants are assumed to be system-type units. It was assumed that they are operating 5600 hours per year with a nominal boiler capacity. The 5600 hours is a typical duration of the heating season in Poland.

*Table 1. Parameters of district heat sources obtained for maximal heat load (PC-MEA-CHP plant)*

| Device | District heat flow rate, MW | Cooling heat flow rate, MW | Condensed water flow rate, kg/s |
|---|---|---|---|
| $H_2O$ condenser | 75.4 | 163.5 | 91.7 |
| Inter-stage cooler 1 | 8.1 | 12.0 | 2.23 |
| Inter-stage cooler 2 | 8.5 | 7.2 | 0.54 |
| Inter-stage cooler 3 | 9.7 | 6.0 | 0.15 |
| Inter-stage cooler 4 | 20.2 | 5.2 | 0.046 |

*Table 2. Literature data on $CO_2$ absorption units based on MEA solvent*

| Ref. no. | $CO_2$ separation effectiveness | Heat consumption for solvent regeneration, kJ/kg $_{CO2\ removed}$ |
|---|---|---|
| [4] | 0.9 | 4200 |
| [10] | 0.9 | - |
| [3] | 0.85-0.9 | 2700-3300 |
| [11] | 0.9 | 3600 |
| [12] | 0.9 | 3950 |
| Present study | 0.9 | 4000 |

In case of the PC-MEA-CHP plant, the variable district heat demand during the heating season has been assumed using the ambient temperature duration curve combined with profiles of the heating network temperature (Fig. 2). The annual values of electricity and district heat production are therefore calculated by integration of electric power and district heat flow rate over the heating season as presented by Eq. (1) and (2).

$$E_{el} = \int_0^{5600} N_{el}\, d\tau \qquad (1)$$

$$Q = \int_0^{5600} \dot{Q}\, d\tau \qquad (2)$$

All calculations have been made for hard coal fuel characterized by 21 MJ/kg LHV, 11% moisture and 25% ash content.

The pressure in all steam condensers have been assumed to the constant value of 5 kPa.

## 4. Simulation results

The calculated crucial power plant parameters are collected in Table 3, while the heat production distribution over the heating season is presented in Fig. 8.

*Table 3. Simulation results*

| | | PC-ref | PC-MEA | PC-MEA -CHP |
|---|---|---|---|---|
| Net electric power | MW | 603.3 | 603.3 | 603.3 (578.9) |
| Generator terminal power | MW | 641.8 | 699.5 | 699.5 (673.1) |
| $CO_2$ emission | kg/s | 122 | 16.8 | 16.8 |
| Live steam flow | kg/s | 468 | 645 | 645 |
| Reheated steam flow | kg/s | 399 | 549.9 | 549.9 |
| Turbine outlet flow | kg/s | 266.2 | 86.6 | 86.6 (53.2) |
| $CO_2$ compression train power | MW | - | 51.1 | 51.1 |
| Maximal district heat power | MW | - | - | 207 |
| Net electricity production, see Eq. (1) | $10^6$ GJ/year | 12.149 | 12.149 | 12.144 |
| District heat production, see Eq. (2) | $10^6$ GJ/year | 0 | 0 | 1.681 |
| Fuel consumption (LHV based) | $10^6$ GJ/year | 27.422 | 37.795 | 37.795 |

*() – values in parenthesis deal with the maximal district heat flow while other values are constant during the heating season.*

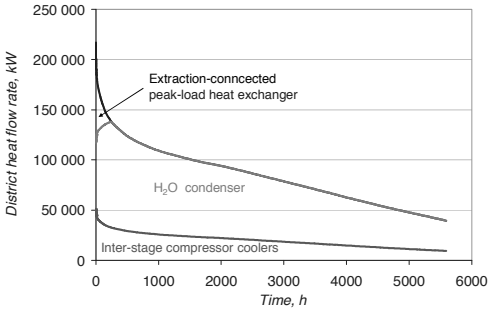


*Fig. 8. District heat flow rate over the heating season for PF-MEA-CHP plant*

The areas of operation of successive heat sources ($H_2O$ condenser, inter-stage compressor coolers, peak-load heart exchanger) are visible in Fig. 8.

## 5. Assessment factors

Two assessment factors have been calculated for evaluation of the waste-to-district heat conversion obtained in the PC-MEA-CHP plant. From the thermodynamic point of view the energy utilization factor (EUF) have been calculated in accordance to Eq. (3). In case of PC-ref and PC-MEA plants it represents just the electric efficiency.

$$EUF = \frac{Q + E_{el}}{E_{ch}} \qquad (3)$$

where:

$E_{ch}$ - annual consumption of the chemical energy of fuel, GJ/year

From the emission point of view, the specific $CO_2$ emission calculated per unit of produced electricity have been proposed – Eq. (4).

$$\varepsilon_{CO2} = \frac{m_{CO2\,direct} - \Delta m_{CO2\,avoided}}{E_{el}} \qquad (4)$$

where:

$m_{CO2\,direct}$ - annual direct $CO_2$ emission from analysed plant, Mg/year,

$\Delta m_{CO2\,avoided}$ - annual $CO_2$ emission avoided because of replacement of the district heat produced in conventional CHP by district heat produced in the analysed plant, Mg/year,

The system effect of emission avoidance because of waste heat utilisation has been accounted. The avoided $CO_2$ emission is calculated as for replaced conventional coal-fired CHP without $CO_2$ removal. The specific emission of 70 kg $CO_2$ per 1 GJ of produced heat for the replaced CHP plant has been assumed which corresponds to the energy utilization factor (EUF) equal to 0.85 and the electricity-to-heat production ratio equal to 0.4.

The calculated EUF and specific $CO_2$ emission for three analyzed plants are presented in Figs 9 and 10.

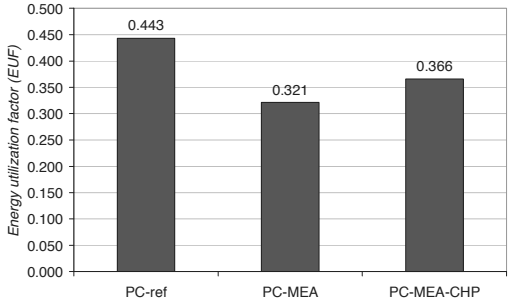


*Fig. 9. Thermodynamic evaluation of analyzed power units*

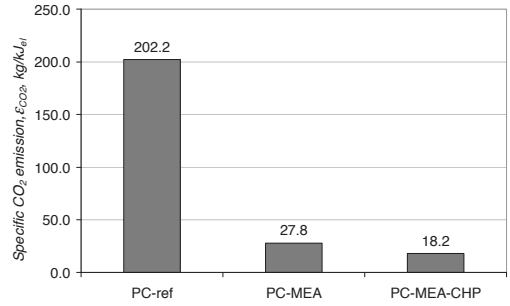


*Fig. 10. $CO_2$ emission evaluation of analyzed power units*

## 6. Conclusions

The proposed waste heat recovery concept for the coal-fired power unit with chemical $CO_2$ absorption has been checked to produce maximally ca. 200 MW of district heat for 600 MW of net electricity.

The indicated waste heat sources i.e. the $H_2O$ condenser behind the $CO_2$ stripper and the inter-

stage coolers of the $CO_2$ compressor supply heat at similar temperature range. In the case of $H_2O$ condenser, the outlet district water temperature is however lower and the installation of classical peak-load heat exchanger fed with extracted steam is necessary. The annual time of the peak-load heat production is however very low. Moreover, in case that the additional steam turbine is used for $CO_2$ compressor driving, the operation of the peak-load heat exchanger is limited by the limitation of the main steam turbine outlet flow. This limitation may be changed by selection of higher pressure extraction for the auxiliary steam turbines feeding.

The post-combustion $CO_2$ removal and compression causes the decrease of the specific $CO_2$ emission form 202 to 28 kg per 1 kJ of produced net electricity. The useful application of the waste heat related to the post-combustion $CO_2$ removal causes fossil fuel savings and further emission reduction to 18 kg per 1 kJ of produced electricity.

It is expected that the economic profitability of the proposed waste heat utilization idea depends on the distance between the large, system-type power plant and heat consumers (e.g. medium-size city). The economic analysis considering also the heat transport losses and competition from local CHP plants should thus indicate what is the reasonable heat transport distance from analyzed power units to the heat consumers.

## References

[1] The Future of Coal. An interdisciplinary MIT study. Massachusets Institute of Technology, 2007, USA.

[2] Liszka M., Ziebik A., 2008, Thermoeconomic comparison of coal-based oxy-fuel and post-combustion CO2 capture - case study for Polish conditions, Proceedings of the 25th International Pittsburgh Coal Conference, September 29 - October 2 2008, Pittsburgh, PA, USA.

[3] Metz B., Davidson O., de Coninek H., Loos M., Meyer L, 2005, *Carbon dioxide capture and storage*, Intergovernmental Panel on Climate Change, WMO, UNEP.

[4] Fisher K.S., Searcy K., et al., 2007, Advanced Amine Solvent Formulations and Process Integration for Near-Term CO2 Capture Success, Work Performed Under Grant No.: DE-FG02-06ER84625 submitted to U.S. Department of Energy - National Energy Technology Laboratory. Trimeric Corporation P.O. Box 826 Buda, TX 78610 USA.

[5] Advanced power plant using high efficiency boiler/turbine, 2006, Best practice brochure, Carbon Abatement Technologies Programme, www.dti.gov.uk/cct.

[6] Romeo L.M., Bolea I., Escosa J.M., 2008, Integration of power plant amine scrubbing to reduce CO2 capture costs, Applied Thermal Engineering, 28, pp. 1039-1046.

[7] Engineering Equation Solver, S.A. Klein © 1992-2009 Academic Professional V8.411. www.fchart.com.

[8] Liszka M., Ziebik A., 2009, Coal-fired oxy-fuel power unit – Process and system analysis, Energy, doi:10.1016/j.energy.2009.07.007, pp. 1-9.

[9] Liszka M., Ziebik A., 2008, Thermoeconomic comparison of coal-based oxy-fuel and post-combustion CO2 capture - case study for Polish conditions, Proceedings of the 25th International Pittsburgh Coal Conference, September 29 - October 2 2008, Pittsburgh, PA, USA.

[10] Rao A.B., Rubin E.S.,2002, A technical, economic and environmental assessment of amine-based CO2 capture technology for power plant greenhouse gas control, Environmental Science and Technology, 36, pp. 4467-4475.

[11] Carbon Dioxide Capture from Existing Coal-Fired Power Plants. 2007, Report DOE/NETL-401/110907, National Energy Technology Laboratory, USA, www.netl.doe.gov

[12] Desideri U., Paolucci A.,1999, Performance modeling of a carbon dioxide removal system for power plants, Energy Conversion & Management, 40, pp. 1899-1915.

**Acknowledgments:** The present study was made possible thanks to the Polish Ministry of Science and Higher Education as well as The National Centre for Research and Development. Their financial support within confines of grant no. R06 0004 06/2009 is gratefully acknowledged.

# Analysing the Potential for CCS within the European Pulp and Paper Industry

*Johanna Jönsson[a], Thore Berntsson[a]*

[a] *Heat and Power Technology, Energy and Environment, Gothenburg, Sweden*

**Abstract:** In this paper an approach for analysing the potential for implementation of different technology pathways for the European pulp and paper industry (PPI) is presented. The approach assumes previous, detailed, research and is based on bottom-up thinking whilst still estimating the potential on a European level. The usefulness of the approach is exemplified by applying it to a study of the potential for introduction of carbon capture and storage (CCS) within the European PPI. The results from the case study show that if CCS is to be introduced in large scale within the European PPI, biomass-based emissions must be included when planning for the future CCS infrastructure.

**Keywords:** Pulp and paper industry, technology pathways, process integration, CCS.

## 1. Introduction

For the kraft pulp and paper industry (PPI), earlier studies have shown that there are many technologies and system solutions – hereafter denoted technology pathways – which can reduce the process steam demand [1], give a steam/heat surplus and thus enable production of additional value products such as materials, chemicals, transport fuels, electricity and/or district heating [2]. Another alternative is to integrate carbon capture and storage (CCS) by utilizing the steam/heat surplus to cover the energy demand in the carbon capture processes [3]. However, these previous studies are either detailed, on mill level, not saying anything about the overall potential, or very aggregated, not considering mill-specific conditions. Thus to be able to estimate the potential for these different technology pathways on a European level another approach, connecting the results from these detailed studies to the actual European PPI stock, is necessary.

### 1.1. Aim

In this paper a systematic approach for analysing the potential for different technology pathways within the European pulp and paper industry is presented. The approach combines the advantages of detailed and aggregated approaches and assesses the overall potential for the different pathways whilst considering important characteristics of each mill. Further, the usefulness of the approach is illustrated by applying it to a study showing the potential for introduction of CCS within the European PPI.

## 2. Description of methodology

The suggested approach is based on:

1. Previous research in the form of model mill studies and case studies regarding process steam savings and the effect of different technology pathways on the energy balance for different types of mills
2. Technical and geographical data for the European pulp and paper industry
3. Data for the infrastructure surrounding the European pulp and paper mills
4. Previous research regarding the future development of the energy market (energy market scenarios)

Consequently, the approach assumes detailed research and is based on bottom-up thinking whilst estimating the potential on a European level. An overview of the approach is presented in Fig. 1. The different parts of the suggested approach are described in the subsequent section.

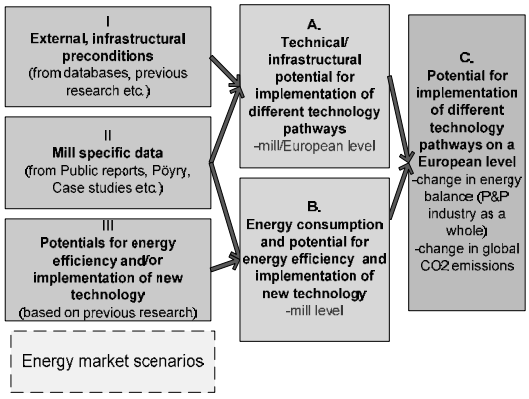


*Fig. 1. An overview of the suggested approach used in the research project.*

### 2.1. The different parts of the approach

Corresponding Author: Johanna Jönsson, Email: Johanna.jonsson@chalmers.se

The approach is carried out stepwise, as exemplified by the study of the potential for implementation of CCS presented in Section 3. The parts of the approach are as follows.

*I: External, infrastructural preconditions*

These are the characteristics of the geographical area surrounding the mills, e.g. data for where potential CCS storage sites and district heating grids are located.

*II: Mill specific data*

Mill-specific data are the characteristics of the individual mills constituting the European PPI stock. Data included are e.g. technical age of mill and specific mill equipment, production, fuel usage, process steam demand, $CO_2$ emissions and estimates of available amounts of excess heat.

*III: Potential for energy efficiency and implementation of new technology*

The potential for energy efficiency and implementation of new technology pathways on a mill level is based on previous and on-going research by others as well as the authors of this paper. The results from this part typically show the economic performance and impact on global $CO_2$ emissions for implementation of different technology pathways in specific mills.

*A. Technical/infrastructural potential for implementation of different technology pathways*

Here mill-specific data for the individual mills are connected to the gathered data for the surrounding infrastructure. The results from this part show how the technical potential for implementation of a certain technology is limited (or enhanced) by the location of the mill – such as the potential for implementation of CCS, exemplified and described by the case study in this paper.

*B. Energy consumption and potential for energy efficiency and implementation of new technology*

How the existing energy balance of the individual mills constituting the European PPI stock can be altered is determined by fitting the potential for energy savings known for some mills (III) to mill-specific characteristics. The results from this part typically show how the potential for energy savings and implementation and integration of different technology pathways depends on mill-specific characteristics such as technical age of process equipment and type of production process.

*C. Potential for implementation of different technology pathways on a European level*

When the effect on the potential for implementation and integration of different technology pathways by the surrounding infrastructure (A) and the mill characteristics (B) has been determined, these two factors are brought together and the final, complete potential for implementation and integration of different technology pathways is estimated for the whole European PPI stock.

*Energy market scenarios*

The future economic performance, as well as the global emissions of $CO_2$, associated with different technology pathways is dependent on the development of the energy market. To depict different possible future energy market conditions, energy market scenarios are used. The scenarios, developed by Axelsson and Harvey [4], are based on different fossil fuel price levels (low and high) and $CO_2$ emission charge levels (low and high) combined into different scenarios. A benefit of using these scenarios, which reflect the strong connection between different energy market parameters, is that a packaged sensitivity analysis of the energy market prices is conducted.

The purpose of the presented approach is to analyse the potential for, and the effect of, implementation of different technology pathways within the European PPI. However, due to its generality, the approach can also be applied to other energy-intensive industry branches.

## 3. Applying the approach: potential for CCS within the European PPI

The usefulness of the approach is exemplified by a study assessing the technical/infrastructural potential for CCS within the European PPI. The assessment is based on the current constitution of the European PPI.

### 3.1 Introduction: CCS in the PPI

From the year 2013, $CO_2$ capture, transport and storage installations will be incorporated in the EU ETS. A fundamental assumption for the study presented in this paper is that all $CO_2$ is considered equal. This assumption is based on the fact that the $CO_2$ has the same effect on the climate regardless of origin. Consequently, it is assumed that in future policy schemes, captured and stored $CO_2$ originating from biomass is granted the same economic compensation as $CO_2$ originating from fossil fuels. The PPI is energy-intensive and has large on-site emissions of $CO_2$, so these emissions

are associated with only a limited amount of geographical sites, i.e. mills. Due to these characteristics the PPI, like other energy-intensive industry branches [5], is suitable for implementation of CCS. Further, since a large share of the $CO_2$ emissions associated with the European PPI originates from biomass, if CCS is implemented the levels of $CO_2$ in the atmosphere can be further reduced in comparison to implementing CCS only on fossil emission sources [3, 6]. Further, the concentration of $CO_2$ in the PPI flue gases is comparably high, 13-14%. These facts make CCS within the European PPI even more interesting. Investments in $CO_2$ capture technologies are associated with high capital costs. Also, for post-combustion with chemical absorption the energy cost for capture is 50-70% of the total cost and thus cannot be neglected [3]. Hence, for $CO_2$ capture to be economically and technically realistic the source of $CO_2$ needs to be large enough and the energy demand of the capture process should preferably be possible to integrate (partly) with other processes at the capture site. The potential for heat integration [3] is another reason why CCS is of interest also for the PPI, although it is the power sector with its coal power plants that is the largest industrial emitter of $CO_2$ in Europe [5]. Previous research regarding the PPI has shown that process steam savings can be made and used for thermal integration of a CCS unit, lowering the capture cost and making CCS profitable [3]. Previous research has also shown that compared to other alternatives for harnessing surplus steam, CCS gives much larger reductions of global $CO_2$ emissions and is economically comparable to more proven technology alternatives – such as increased electricity production in condensing turbines – if the $CO_2$ charge is high [2].

### 3.2 Methodology and approach

Related to the approach described in Section 3 and Fig. 1, the case study assumes mill-specific data (II) and external, infrastructural preconditions (I) to estimate the technical/infrastructural potential for implementation of a technology pathway (A), in this case CCS. In the case study, the mill-specific data used are $CO_2$ emissions for each mill, both emissions from fossil fuels and emissions from biomass, and the geographical position of each mill described by coordinates. The external, infrastructural preconditions are the coordinates for other energy-intensive industries and potential $CO_2$ storage places. The study also assumes levels for potential integration based on knowledge from previous research (III).

The potential capture sources have been identified and the potential for $CO_2$ capture has been estimated through the following steps (following the methodology used in a similar study of the potential for $CO_2$ capture in other energy-intensive industries, [5]):

*Size of capture sources considered:* It is generally assumed that only very large point sources are suitable for CCS (>0.5Mt$CO_2$/yr, [5]). However, for the PPI, due to the potential for integration and utilisation of excess heat in the capture process [3] it has been assumed that reasonable economy can be gained also for smaller point sources if the transport and storage infrastructure is in place. Thus, in this case study two alternative sizes for point sources have been included: >0.1 Mt$CO_2$/yr and >0.5 Mt$CO_2$/yr.

*Sub-sector specific conditions:* $CO_2$ capture is not equally applicable in all manufacturing processes, and the prospects for capturing depend on the production processes at the different mills. The kraft PPI has large on-site emissions of $CO_2$ due to the burning of black liquor in the recovery boiler. The mechanical PPI and the paper mills based mainly on recycled fibers (RCF) generally have lower on-site emissions. For the mechanical PPI this is due to the high use of electricity in the mechanical pulping processes and the fact that a major part of the electricity can be recovered as steam and used to cover the mill steam demand. For the paper mills without virgin pulp production, based solely on bought pulp and RCF/DIP, the lower on-site emissions of $CO_2$ are due to the lower primary energy demand (owing to the lack of virgin pulp production) and due to the fact that some of these mills buy their steam from power plants or other industries located in close proximity to the mills (this does not lower the emissions associated with the production, but it shifts the emissions from the PPI to another industry branch, often the power sector).

*Plant-specific conditions:* At a pulp and paper plant the total of $CO_2$ emissions is a sum of some emission sources, mainly different boilers. However, the flue gas streams differ somewhat with respect to their suitability for $CO_2$ capture. E.g., for the kraft PPI some almost pure $CO_2$ streams can be recovered if the lime kiln is rebuilt

or black liquor gasification (BLG) is introduced. However, these technologies are not yet implemented. Further, another plant-specific condition is the possibility to thermally integrate the capture process. The potential for integration depends on the process layout of the different mills – e.g. kraft pulp mills and pure TMP pulp and paper mills can have a "true" steam surplus, whereas integrated kraft pulp and paper mills and paper mills without virgin pulp production usually cannot and thus need to import external fuel to cover the heat demand for the capture process.

*Capture technology:* Since the main source of $CO_2$ from the pulp and paper industry is boiler flue gases, there are in principle three different capture technology options: post-combustion, pre-combustion and oxy-combustion. In this study, post-combustion using chemical absorption is considered since it is the only technique not requiring any reconstruction of the boilers [3]. The absorbent assumed is MEA[1] with which a capture rate of 90% can be achieved. Technical and economic data for the technology are based on previous work by Hector et al. [3].

*Geographical distribution of emissions:* One way of limiting the cost of CCS is to create capture clusters in regions with several emission sources located near each other. In this way the transport network can be integrated and thus benefit from economy of scale. In this case study, the mills and their emissions are mapped using a GIS programme (ArcGIS). The positions of the mills are then related to the geographical position of other energy-intensive industries (in this case iron and steel mills, cement plants and refineries) and potential storage places for $CO_2$ through geospatial analysis.

The mapping of the emissions from other heavy industries in relation to potential storage places has been done by fellow researchers within the Pathways project, Johan Rootzén et al. [5]. The information was collected and stored in Chalmers' industry database (Chalmers IN db), a sub-database to the Chalmers energy infrastructure database which has been designed to cover both the supply side and the demand side of the European energy systems [7]. The Chalmers industry database was also used as one of the sources of data for this study (as part of I, indicated in Fig. 1).

[1] Chilled ammonia is an interesting alternative absorbent; however, it has been less investigated and is thus excluded in this paper.

### 3.3. Input data and system boundaries

The European pulp and paper industry has been defined as mills located in the countries that are included in CEPI [8], i.e. the countries in Europe with the highest density of pulp and paper industry. However, the European PPI is currently in a situation where many (small) less profitable mills are decommissioned [9]. Thus, not all of the mills in production today will still be in production at the time when CCS will be commercially available. To account for this fact, a selection of mills to include in the study was done together with PPI consultants from Pöyry. Thereby 171 mills were selected and included, based on their competitive strength and size. Hence, this case study includes 50 kraft pulp and/or paper mills, 45 mechanical pulp and paper mills, and 76 paper mills without any virgin pulp production (having only bought pulp and/or RCF/DIP). Data for the included mills are presented in Table 1. Due to the large amount of mills included in the study, the data are presented in aggregated form. As can be seen in the table, a large share of the CEPI pulp production and a fair share of CEPI paper production are covered by the included mills.

*Table 1. Data for the mills included in the case study.*

| Type of mill[1] | Kraft | | Mechanical | Paper |
|---|---|---|---|---|
| | Market pulp | Pulp & Paper | Pulp & Paper | |
| Mills [No.] | 21 | 29 | 45 | 76 |
| Pulp cap. [kADt/yr] | 9 955[2] | 12 320[2] | 12 095[3] | 14 775 |
| Paper cap. [t/yr] | - | 16 131 | 22 132 | 27 169 |
| *CEPI total pulp cap.[4]* | *11 573* | *14 305* | *14 686* | - |
| *CEPI total paper cap.[4]* | | | | *102 570* |

[1] Kraft refers to mills that have the kraft process; they may also have other pulp production, e.g. CTMP. Mechanical refers to mills that have some mechanical pulping process (TMP, CTMP, GW/PGW or RMP). They may also use other pulps in the process such as RCF/DIP or bought kraft pulp. The paper mills have no pulp production from virgin pulp; they only use RCF/DIP and/or bought pulp.
[2] Including only kraft pulp produced on site. If all pulp produced on site is included, the numbers are 10 040 and 13 935 kADt/yr respectively.
[3] Including only mechanical pulp. If both mechanical pulp and RCF/DIP are included, the figure is 17 420 kADt/yr.
[4] Figures from [9] referring to the year 2007.

### 3.4. $CO_2$ emissions from the European PPI

The amounts of on-site $CO_2$ emissions from the pulp and paper mills included in this study are presented in Table 2. For comparison, the total on-site emissions of $CO_2$ for all CEPI mills are also included [9]. The fossil $CO_2$ emissions were gathered from the Chalmers industry database, which in turn bases its data mainly on the Community Independent Transaction Log (CITL)

but also the European Pollutant Emission Register and the IEA GHG $CO_2$ Emissions database (for more details see [5]). The biomass-based $CO_2$ emissions, on the other hand, are not reported centrally, either for the EU or by CEPI. Thus, these emissions were gathered by screening national statistics, sustainability reports, annual reports and web pages for all of the mills included in the study. However, numbers for biomass-based $CO_2$ emissions were mostly not clearly stated and the data were compiled using the following hierarchy of information source/data:

1. Data on biomass-based $CO_2$ emissions were posted clearly either in sustainability reports or in industry statistical publications.
2. Data regarding biomass usage (in MWh or TJ) was posted clearly. Biomass-based $CO_2$ emissions were then calculated based on an emission factor of 346 $kgCO_2/MWh$.
3. Data regarding percentage of biomass usage in relation to total fuel usage were posted clearly. In these cases the fossil fuel usage was calculated in MWh based on emission factors for fossil fuels and the known fossil $CO_2$ emissions for the mill. The biomass-based $CO_2$ emissions could then be calculated following the procedure in item 2 above.
4. Information stated that all use of fuel was fossil-based or that the steam used was bought from a neighbouring industry. For these cases the biomass-based $CO_2$ emissions were set to 0.
5. No energy or emissions-related information for biomass could be found. For these cases the biomass-based emissions were set to 0 except if the mill has kraft pulp production. For the case of kraft pulp production, the biomass-based $CO_2$ emissions were calculated in relation to the kraft pulp production.

As can be seen in Table 2 almost all, 95%, of the $CO_2$ emissions originating from biomass and a fair amount of the fossil $CO_2$ emissions, 47%, are covered in the study. This means that a total of 77% of the CEPI $CO_2$ emissions are included in this study. The reason why the share of fossil emissions included is smaller than the share of biomass-based emissions is that many small South European paper mills, using mainly fossil fuels for their energy needs, were excluded from the study due to their small size (only paper mills with a production capacity of >200 kt paper/yr were included).

*Table 2. $CO_2$ emissions for the mills included in the study compared to CEPI total emissions.*

| Type of mill | Kraft | | Mechanical | Paper |
|---|---|---|---|---|
| | Market pulp | Pulp & Paper | Pulp & Paper | |
| Mills [No.] | 21 | 29 | 43[1] | 70[2] |
| Fossil $CO_2$ [kt/yr] | 1 391 | 3 164 | 4 759 | 9 420 |
| Bio $CO_2$ [kt/yr] | 24 308 | 30 775 | 5 524 | 2 217 |
| Total $CO_2$ [kt/yr] | 25 699 | 33 940 | 10 283 | 11 637 |
| *CEPI total fossil*[3] | | | | *39 605* |
| *CEPI total bio*[4] | | | | *66 113* |

[1] For 2 mills no data could be found in either E-PRTR registers or web pages.
[2] For 6 mills no data could be found in either E-PRTR registers or web pages.
[3] Figures from [9] referring to the year 2006.
[4] Based on the figures for biomass utilization as part of the primary energy demand from [9] and calculated assuming $CO_2$ emission of 346 kg/MWh.

The geographical distribution of the PPI's total $CO_2$ emissions is shown in Fig. 2. As can be seen, the regions with the highest emissions are located around the Baltic Sea (in Sweden and Finland), in the south of Spain and in the middle of Portugal.

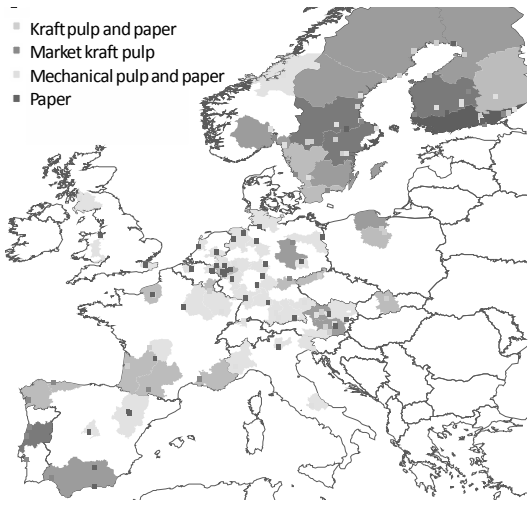


*Fig. 2. The geographical distribution of on-site $CO_2$ emissions from the European PPI. The coloured squares represent individual mills (emitting >0.1 $MtCO_2/yr$). Regions coloured in blue have a high density of emissions; the darker the colour, the higher the emissions.*

## 3.5. The role of CCS within the European PPI

Today, CCS is not a commercial technology and the necessary infrastructure for both transport and storage is neither in place nor definitely planned. It is thus hard to predict which plants will have the most favourable preconditions for implementing CCS. However, a reasonable approach is to assume that infrastructure is most likely to be

developed first in proximity to sites with many large point sources, hereafter denoted capture clusters. Depending on how the biomass-based $CO_2$ is viewed from a mitigation point of view, it can also be assumed that infrastructure will first be built around large fossil point sources or around large point sources regardless of the emissions origin. Further, it is reasonable to assume that mills with larger emissions will have a larger potential for profitable introduction of CCS than sites with small emissions. When using post-combustion chemical absorption with MEA as the absorbent as assumed in this study, there is an additional thermal energy demand for regeneration of the MEA and an electricity demand for compression of the $CO_2$. According to literature these numbers can vary. In this study, 2880 $kJ/kgCO_2$ is assumed for regeneration and 0.13 MWh/ton for the compression [3]. It should be noted that the additional $CO_2$ emissions originating from fuel demand for regeneration also are captured. As previously stated in this paper, the thermal energy demand can be partly covered by making steam savings and integrating the capture process to the mill. Based on these assumptions, a matrix was constructed containing six different future cases for implementation of CCS in the European PPI and two different cases for the potential for heat integration; see Table 3.

*Table 3. The six different future cases considered for implementation of CCS and integration of capture process energy demand.*

| Case description | Capture done by all included mills | Capture done only by mills in capture clusters | Capture done only by mills in fossil capture clusters |
|---|---|---|---|
| Mills with emissions >0.1 $MtCO_2/yr$ | A1 | A2 | A3 |
| Mills with emissions >0.5 $MtCO_2/yr$ | B1 | B2 | B3 |

| Case for heat integration potential | Not possible[2] | Possible[1] |
|---|---|---|
| | I | II |

[1] The potential for heat integration is based on knowledge from previous and ongoing research and estimated as: 2.5 GJ/ADt for kraft pulp mills, 2.0 GJ/ADt for integrated kraft pulp and paper mills, and 0.5 GJ/t for mechanical pulp and paper mills. For pure paper mills no integration possibilities have been considered.

[2] The whole energy demand of the capture process is assumed to be supplied with additional external fuel.

The geographical positioning of the pulp and paper mills included in this study in relation to the geographical positioning of other energy-intensive industries, capture clusters and potential storage sites is displayed in Fig. 3.

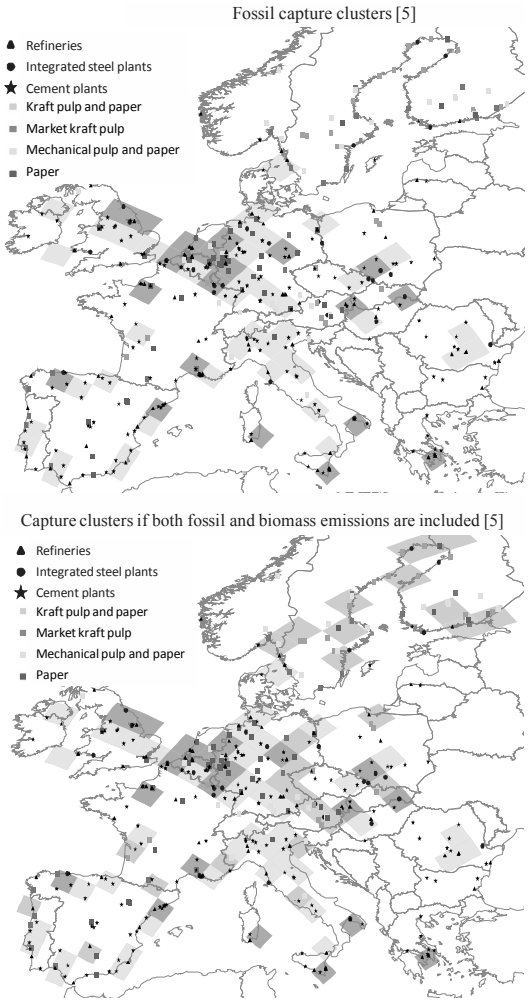


*Fig. 3. The geographical distribution of pulp and paper mills emitting more than 0.1 Mt $CO_2$/yr in relation to other large industrial point sources >0.5 Mt $CO_2$/yr. Possible capture cluster areas are represented by coloured squares (150x150 km); the orange squares represent clusters with more than 2 industries which together emit more than 5 $MtCO_2$/yr and the yellow and grey clusters emit more than 1 $MtCO_2$/yr. The underlying map and the data for other heavy industries were compiled by Johan Rootzén [5].*

As can be seen in Fig. 3, most of the large emitting kraft pulp and paper mills are located on the eastern coast of Sweden and in Finland, far away from most of the fossil capture clusters created by other energy-intensive industries. The most beneficial geographical positions are held by paper mills in central Europe; they have much smaller

on-site emissions than the kraft PPI but, as can be seen in the figure, they are located in or near fossil capture clusters created by other energy-intensive industries and near the potential storage sites in the North-Sea (in this study storage in closed aquifers is assumed, mineralization of the $CO_2$ could be another option, however that technology need a major breakthrough before being possible to commercialize in large scale and is thus not considered here). However, if including both fossil and biomass-based emissions, a much larger share of the European PPI is positioned in capture clusters. Regarding the distribution between large emitters and small emitters amongst the mills included in the study, it can be seen in Fig. 4 that a third of the mills (the ones with emissions >0.5 Mt/yr) stands for 75% of the emissions. This third is constituted by all of the kraft mills included, one mechanical mill and one paper mill. Further, from Fig. 4 it can be seen that if CCS is to be implemented for large point sources only within the European PPI, the captured $CO_2$ will originate almost solely from biomass.

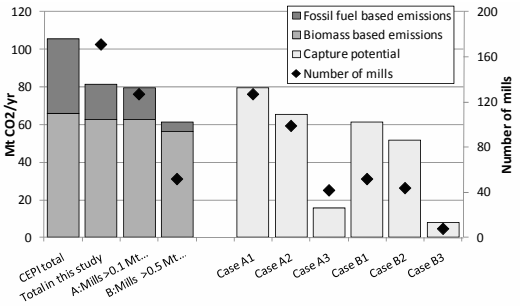


*Fig. 4. The distribution of included emissions divided by size and origin along with the potential for captured $CO_2$ emissions for the six studied capture cases presented in Table 3.*

As can be seen in Figs. 3 and 4, if CCS is to be introduced in large scale in order to reach large $CO_2$ emission reductions within the European PPI, the emission-intensive Scandinavian kraft PPI must be included in such a capture scheme. If only emissions from the mills located in fossil-based capture clusters are included (A3 and B3), the capture potential is reduced by 44-50 $MtCO_2$/yr compared to including mills in both fossil- and biomass-based capture clusters (A2 and B2). Fig. 5 shows the additional fuel and electricity demand for the different capture cases presented in Table 3 and Fig. 4. The additional fuel used has been assumed to be biomass. As can be seen in the figure, the fuel demand can be reduced by ~30% if a part of the capture process energy demand can be supplied by heat integration to the mill processes.

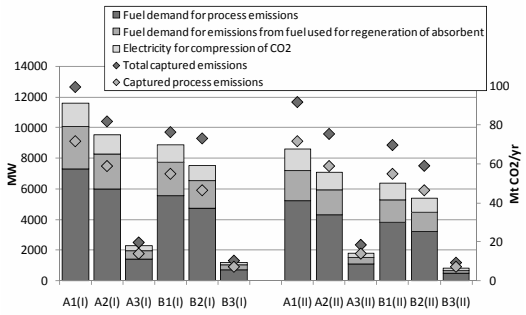


*Fig. 5. The fuel and electricity demand for the studied cases with and without potential for heat integration.*

## 4. Concluding discussion

The aim of the study presented in this paper was to develop and present a systematic, stepwise approach for analysing the potential for different technology pathways within the European pulp and paper industry. The approach is based on detailed technical research and aggregates the knowledge from previous studies to incorporate the whole European PPI. Thus, the potential for different technology pathways can be estimated on a European level whilst still considering the characteristics of the individual mills. In order to exemplify the usefulness of the presented approach, it was applied to a study investigating the potential for introduction of CCS within the European PPI. Emphasis was placed on a selection of large and competitive mills with promising potentials for CCS. Together the studied mills emit 82 $MtCO_2$/yr (if emissions from both biomass and fossil fuels are included), which can be compared to the total (fossil) $CO_2$ emissions included in the energy-intensive industries part of EU ETS of 600 $MtCO_2$/yr [5] (excluding the power and heat sector). The amount of $CO_2$ that can be captured depends heavily on the expansion of infrastructure. The results show that 10-99 $MtCO_2$/yr can be avoided depending on the assumptions regarding the transport and storage infrastructure (including both original emissions and additional emissions from the fuel demand of the capture process, of which 7-72 $MtCO_2$/yr are original on-site emissions). If steam savings enable parts of the capture process energy demand to be integrated, the total fuel demand can be reduced by ~30%.

Further, the results from the case study show that when adding the PPI capture potential to the potential for CCS within other energy-intensive industries, the majority of the PPI emissions originate from kraft pulp and paper mills far away from other energy-intensive industries and potential fossil capture clusters. Thus, to reach large emission reductions, also large biomass-based point sources of $CO_2$ emissions need to be included when planning for CCS infrastructure. As previously stated by Rootzén et al. [5], the best match between carbon dioxide sources and potential storage places is located in the regions bordering the North Sea. This statement makes the paper mills in central Europe most suitable for CCS; however, these mills generally have much lower on-site emissions than the Scandinavian kraft pulp and paper mills. For the mills (and other emissions sources) bordering the Baltic Sea, storage in closed aquifers close to Gotland might be possible, however, this needs further investigation. In this study the emissions from the power sector are not included. If these emissions were included, central Europe would have an even larger density of fossil $CO_2$ emissions. It should thus be further investigated whether the biomass-based capture clusters in Scandinavia are large enough to motivate the needed infrastructure. All in all, it can be concluded that the presented approach works well for the suggested purpose and that it should also be applicable for analysis of other technology pathways in order to get a more complete picture regarding the possibilities for future development of the European PPI.

## Abbreviations

ADt Air Dry Tonnes
BLG Black Liquor Gasification
CCS Carbon Capture and Storage
CEPI Confederation of European Paper Industries
DIP De-inked Paper
ETS Emission Trading Scheme (EU)
GIS Graphic Information System
MEA Mono-ethanolamine
PPI Pulp and Paper Industry
RCF Recycled Fiber

## References

[1.] Axelsson, E., M.R. Olsson, and T. Berntsson, Heat Integration Opportunities in Average Scandinavian Kraft Pulp Mills: Pinch Analysis of Model Mills. Nordic Pulp Paper Res. J., 2006, 4(21): pp. 466-474.
[2.] Jönsson, J. and J. Algehed, Pathways to a sustainable European kraft pulp industry: Trade-offs between economy and CO2 emissions for different technologies and system solutions. Applied Thermal Engineering, 2010. In Press, doi: 10.1016/j.applthermaleng.2010.01.025.
[3.] Hektor, E. and T. Berntsson, Future CO2 removal from pulp mills – Process integration consequences. Energy Conversion and Management, 2007, 48(11): pp. 3025-3033.
[4.] Axelsson, E., S. Harvey, and T. Berntsson, A tool for creating energy market scenarios for evaluation of investments in energy intensive industry. Energy, 2009, 34(12): pp. 2069-2074.
[5.] Rootzén, J., J. Kjärstad, and F. Johnsson. Assessment of the potential for CO2 capture in European heavy industries. 5th Dubrovnik Conference on Sustainable Development of Energy, Water and Environment Systems. 2009. Dubrovnik, Croatia.
[6.] Möllersten, K. et al., Efficient energy systems with CO2 capture and storage from renewable biomass in pulp and paper mills. Renewable Energy, 2004, 29(9): pp. 1583-1598.
[7.] Kjärstad, J. and F. Johnsson, The European power plant infrastructure – Presentation of the Chalmers energy infrastructure database with applications. Energy Policy, 2007, 35(7): pp. 3643-3664.
[8.] CEPI, Key Statistics 2008 – European Pulp and Paper Industry, 2009, Confederation of European Paper Industries.
[9.] CEPI, Annual Statistics 2007 – European Pulp and Paper Industry, 2008, Confederation of European Paper Industries.

**Acknowledgments:** This work has been carried out under the auspices of the Energy Systems Programme, primarily financed by the Swedish Energy Agency. The work was co-funded by the AGS project "Pathways to Sustainable European Energy Systems" and the EU ENCAP project through the Södra Foundation for Research, Development and Education. The authors would like to thank PhD candidate Johan Rootzén (Energy Technology, Energy and Environment, Chalmers University of Technology) for contributing the GIS drawings and for the collaboration during the work with this paper.

# Using Multi-Objective Optimisation in the Design of $CO_2$ Capture Systems for Retrofit to Coal Power Stations

*Trent Harkin[a,b], Andrew Hoadley[b], and Barry Hooper[a]*

[a] *Cooperative Research Centre for Greenhouse Gas Technologies (CO2CRC),Melbourne, Australia*
[b] *Monash University, Clayton, Australia*

**Abstract:** An Aspen Plus® simulation of an existing power station with a potassium carbonate based carbon capture (CCS) plant including $CO_2$ compression is combined with an Excel based genetic algorithm to optimise the net power output of the power station and amount of $CO_2$ captured for a range of solvent flowrates, lean loading and stripper pressures. The net power output was compared for a CCS plant that is added to the power station without any heat integration to a system where heat integration is maximised by the use of pinch analysis and linear optimisation to calculate the amount of steam required to be extracted from the turbine to meet the additional heating requirements of the CCS plant. The multi-objective optimisation of the process identified that lean solvent loading and stripper pressure will have a large impact on the net power output and amount of $CO_2$ captured. For standalone potassium carbonate solvent systems optimising for the reboiler energy, the stripper pressure should be as low as possible. However when the system is seen coupled with the power station the optimal stripper pressure increases, and when heat integration is taken into account, the stripper pressure is even higher again.

**Keywords:** Multi-Objective Optimisation, Carbon Capture, Carbonate

## 1. Introduction

Existing coal fired power stations represent an estimated 60% of anthropogenic carbon emissions. $CO_2$ capture and storage (CCS) from these power stations is one of the key technologies required to stabilise atmospheric $CO_2$ concentrations, however the addition of CCS to existing power plants could lead to a reduction in efficiency of 10-15% points[1].

Potassium carbonate has been used to separate acid gases including $CO_2$ in the gas industries for over 40 years and is considered to be one of the solvents [2, 3] that may be applied to CCS projects. The potassium carbonate process has a much wider operating range when compared to amines as they are not constrained by the temperature limits imposed by thermal degradation of the amines. With less stringent temperature limits the potassium carbonate system has a number of variables that can be adjusted over a wide range of conditions; these variables will often have conflicting affect on the objectives for the system. For example the $CO_2$ stripping can be operated under vacuum, which is advantageous for potassium carbonate solvents as it lowers the reboiler energy and temperature required for stripping the $CO_2$ but is a disadvantage in that it increases the $CO_2$ compression requirements.

There are a number of solvent plant variables that may be adjusted including; the solvent flowrate, lean solvent $CO_2$ loading, rich solvent loading, flue gas temperature, column heights, absorber and stripper pressure and solution temperatures throughout the system. These variables will have different impacts on the operation of the solvent plant but also the power station when CCS is added. Each project may have many objectives including maximising the net power output of the power station, minimising the capital costs and operating costs, maximising profit and maximising the operability, reliability and flexibility of the power station.

The solvent plant is often optimised to reduce the amount of thermal energy required to regenerate the solvent. As noted by [4] the primary objective for analysing modifications to a solvent plant should be the minimisation of the reboiler energy. However, this was in relation to MEA systems where the reboiler energy is improved by increasing the stripper pressure and the stripper pressure is limited by thermal degradation of the solvent, so the stripper pressure is usually fixed at between 200 and 250kPa. For potassium

Corresponding Author: Trent Harkin, Email: tharkin@co2crc.com.au

carbonate solvents where the stripper pressure has opposing effects on the energy required for solvent regeneration and compression, it is not obvious that minimising the reboiler energy requirements will lead to the most optimum process.

With many variables and objectives the use of multi-objective optimisation (MOO) should prove to be a useful tool for better process design of power stations with CCS. In MOO the multiple objectives are treated with equal weighting and a range of solutions, called the 'Pareto-optimal' solutions are found which are all non-dominated solutions – i.e. there are no other solutions that were found that are better in relation to all the objectives. MOO provides a number of solutions and therefore options, from which the designer can then make the final selection. It may also provide insight into what impact the variables have on the optimised solution, for example if a variable is always at one limit then by increasing this limit the overall solution may be improved. A number of algorithms are available for MOO each with their own advantages and disadvantages [5].

Significant amounts of heat are required for solvent regeneration, which generally comes from extracting steam from the steam turbine of the power station and possibly from excess thermal heat in the flue gas. Pinch analysis [6, 7] can be used to provide targets as to the minimum additional amount of energy required for a process by maximising the use of waste heat in the process. The use of pinch analysis may reduce the amount of steam required for the solvent regeneration and therefore maximise the power output from the power station.

In this paper three variables will be analysed for a potassium carbonate system; the solvent lean loading, the solvent flowrate and the stripper pressure. The impact of these variables on the amount of $CO_2$ captured and the stripper reboiler energy will be reviewed and then compared to the impact on the net power output of a power station with and without maximum heat recovery.

## 2. Methodology

This paper aims to optimise the integration of a potassium carbonate solvent system with a brown coal fired power station unit. The example power station unit is a subcritical unit with a nominal capacity of 200MWe. The solvent plant is added on to the outlet of the existing power station unit to capture the $CO_2$ which is compressed to 10MPa.

The power station unit and solvent plant were modelled using Aspen Plus®. A number of cases were investigated. The first two cases are to determine what the solvent loading and flowrate and stripper pressure should be, in order to optimise the reboiler energy. The second two cases are to determine whether the optimised variables are different when considering the power station unit's net power rather than just the reboiler energy requirements. The four cases are detailed in sections 2.1-2.4 below. The MOO algorithm used for this analysis is an Excel based genetic algorithm based on NSGA-II [8] code developed by [9]. The variables are binary and so the range and number of bits for each variable must be selected for each case.

The MOO program is used to determine a population set of decision variables within the range of variables, each set of variables are then input into the Aspen Plus® model of the power station unit with CCS. The process is simulated and the required objectives are determined and exported back to the MOO program. The MOO program then uses these results to determine a new population set of decision variables and continues optimising these for a given number of generations. This approach is based on work in [10] which uses NSGA-II code written in C++ interfaced with HYSYS using Visual Basic.

### 2.1 Case 1a/b: Solvent loading and flowrate

For this case the flue gas from the power station unit is added directly to the solvent plant at 40°C, the lean solvent enters the absorber at 65°C and the stripper pressure is fixed at 150kPaa. The column heights are also fixed at 20m and 15m for the absorber and stripper respectively. The columns are modelled using the Aspen Plus® Rate Based RadFrac column. The range for each of the variables for this case and the others are shown in Table 1. The objectives for this case are maximising the amount of $CO_2$ captured and minimising the reboiler energy.

*Table 1. Variable range and objectives; SF = solvent flowrate, SP = stripper pressure, LL= Lean Loading.*

| Case | SF (kg/s) | LL ($molCO_2$/ $molK_2CO_3$) | SP (kPaa) | Obj.1 | Obj.2 |
|---|---|---|---|---|---|
| 1a | 2200-2300 | 0.21-0.23 | 150 | $CO_2$ Capture (% $CO_2$) | Reboiler Energy (MJ/kg) |
| 1b | 2000-3260 | 0.175-0.33 | 150 | $CO_2$ Capture (% $CO_2$) | Reboiler Energy (MJ/kg) |
| 2 | 1000-4150 | 0.1-0.4 | 30-330 | $CO_2$ Capture (% $CO_2$) | Reboiler Energy (MJ/kg) |
| 3 | 1000-4150 | 0.1-0.4 | 30-330 | $CO_2$ Capture (% $CO_2$) | Power station net power (MW) |
| 4 | 1000-4150 | 0.1-0.4 | 30-330 | $CO_2$ Capture (% $CO_2$) | Power station net power (MW) |

### 2.2 Case 2: Solvent loading, flowrate and stripper pressure

This case is an extension of the first case however it includes a third variable; the stripper pressure. The rest of the power station unit and solvent plant are kept constant like the first case. The variable ranges have also been increased; which are shown in Table 1.

### 2.3 Case 3: Power station unit's net power output

The third case uses the same three variables and the same ranges, but rather than minimise the reboiler energy, the optimisation is to maximise the power station unit's net power output. The unit's net power is reduced by the addition of the CCS plant. The flue gas pressure is increased by the use of a fan, the solvent is circulated by pumps and the $CO_2$ compressors all require power. The heat for the solvent reboiler is supplied from steam extracted from the steam turbine which leads to a reduction in the power produced by the power station unit. In this case, the steam extraction is from an existing bleed point on the exhaust of the high-pressure turbine (560kPa / 177°C) and the amount of steam that needs to be extracted from the turbine is calculated based on the reboiler energy demands. For this paper it is assumed that the turbine efficiency is not affected by the reduction in steam flow from the turbine. The net power produced from the power station unit is therefore calculated by the amount of power produced by the turbine minus the existing power loads and the new power loads caused by the addition of CCS.

### 2.4 Case 4: Power station unit's net power output with heat integration

When CCS is added to the power station unit there are a number of waste heat sources that are also added; the $CO_2$ compressors, the stripper condenser and flue gas which should be cooled down prior to the solvent plant. These waste heat sources may be able to be utilised elsewhere in the power station and the CCS plant to reduce the amount of steam that needs to be extracted from the turbine and increase the power produced from the turbine.

For this case, after the simulation has solved in Aspen Plus® the stream data for all the hot and cold streams are automatically extracted from the simulation and processed using the pinch analysis problem table algorithm. This calculates the deficit of heat in the given process. The amount of steam extracted from the turbine is then calculated using a linear programming method detailed in [11]. These results are then used to calculate the net power output from the power station unit and returned to the optimisation program as the objective.

## 3. Results

### 3.1 Case 1a/b: Solvent loading and flowrate.

In this example two different ranges have been used for the two decision variables; a tight range with solvent lean loading of 0.21-0.23$molCO_2/molK_2CO_3$(s) and 2200-2300kg/s of lean solvent and a wider range with lean loading of 0.2-0.3$molCO_2/molK_2CO_3$(s) and 2000-3000kg/s, the Pareto-optimal solutions for these cases are shown together in Fig. 1.

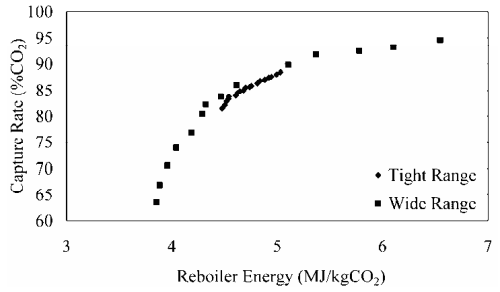


*Fig. 1. Pareto-optimal solutions for Case 1a – Tight range and Case 1b – Wide range.*

When the tighter range was used, as expected the range of $CO_2$ captured is reduced, but the reboiler energy for the same amount of $CO_2$ captured was increased, compared to when a wider range of flowrates and loading were used. Most of the tight range results were dominated by the solutions from the wider range case (1b), which means that most of the solutions for the wider range were better than those for the tight range and this suggests that it will be important for further studies not to limit the range of loadings and flowrates.

There is a near-linear relationship between the reboiler energy for the Pareto-optimised solutions and the lean solvent loading (refer to Fig. 2). However for the wider range, the optimal solution for higher reboiler energy and hence higher capture rate are approaching the lower limit of the lean solvent loading provided ($0.175 molCO_2/molK_2CO_3(s)$).

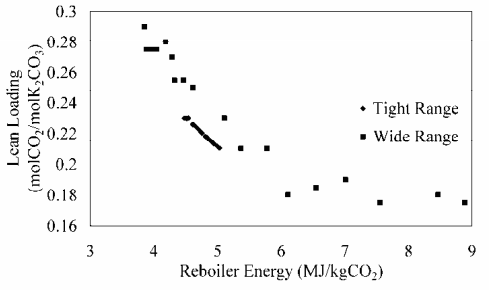


*Fig. 2. Impact of the lean solvent loading on the reboiler energy.*

An explanation for the solutions from the wider range case being superior to the tighter case is that the solvent flowrate, especially for the lower loadings is limited by the range of solvent flowrates as the Pareto-optimal solutions are all tending towards the upper bounds of 2300kg/s as shown in Fig. 3. Therefore, to optimise the system for both the amount of $CO_2$ captured and reboiler energy, flowrates higher than 2300kg/s are required for solvent loadings between 0.21 – $0.22 molCO_2/molK_2CO_3(s)$.

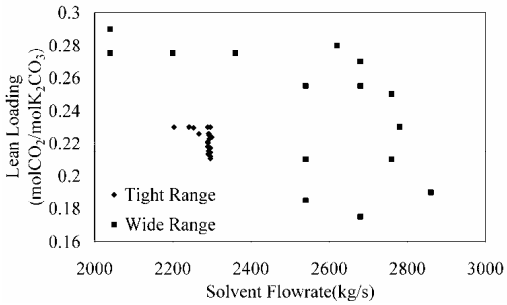


*Fig. 3. Correlation between solvent lean loading and flowrate.*

### 3.2 Case 2: Impact of Stripper Pressure

The previous examples all maintained a constant stripper pressure of 150kPaa, whereas the following cases look at the impact of varying the pressure on the reboiler energy. As discussed in the introduction, a lower pressure is thought to reduce the reboiler energy for a carbonate system. This is confirmed in Fig. 4 where the variable pressure solutions are better than the fixed pressure solutions and in Fig. 5 where all the optimised variable pressure is at 30kPaa; the lowest possible pressure allowed in the range.

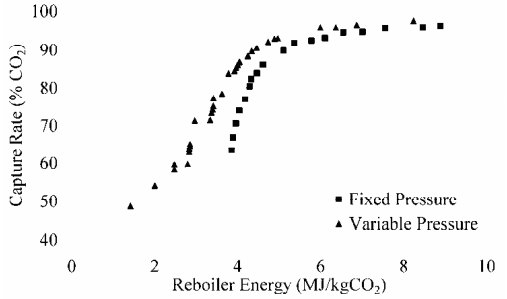


*Fig. 4. Impact of stripper pressure on the Pareto-optimal solutions of the reboiler energy and capture rate.*

The optimal solutions again have solvent loading as nearly linear with the reboiler energy until the

reboiler energy reaches 6MJ/kgCO2 after which the solvent regeneration becomes increasingly difficult.

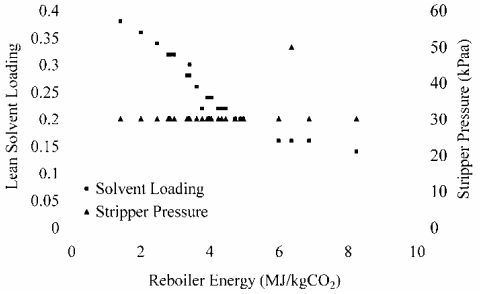


*Fig. 5. Solvent loading and stripper pressure for the optimised points shown with the stripper reboiler energy.*

### 3.3 Case 3: Impact of variables on the power station unit's net power

This case looks at optimising the power station unit's net power output rather than the reboiler energy by varying the solvent loading, flowrate and stripper pressure. The results are shown in Fig. 6 for both Case 3 and Case 4 which will be presented in the next section. Fig. 6 shows that as the capture rate of $CO_2$ increases the net power produced from the unit decreases.

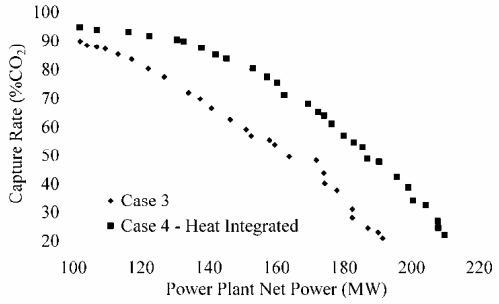


*Fig. 6. Optimal solutions for Case 3 without heat integration and Case 4 with heat integration.*

For Case 3, the stripper pressure (when the overall net power from the power station unit is considered) do not all tend to 30kPaa. The pressure is more scattered and is tending towards 70-90kPaa rather than 30kPaa (Refer to Fig. 6). The optimised solutions for the solvent loadings for Cases 2 and 3 are very similar for the $CO_2$ capture rate.

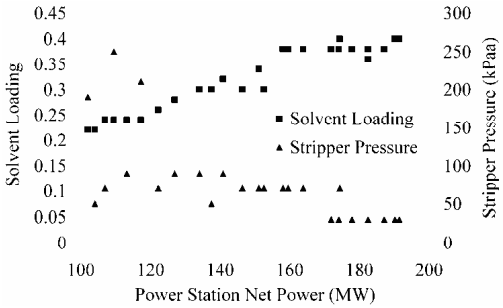


*Fig. 7. Solvent loading and stripper pressure for the Pareto-optimal solutions for Case 3.*

### 3.4 Case 4: Impact of variables on the power station net power with heat integration

The final case looks at the impact of the three variables on the overall output of the power station when heat recovery is maximised. The Pareto-optimal solutions are shown for the net power produced by the unit versus the capture rate in Fig. 6. These points are all dominant over Case 3, which does not consider heat integration of the CCS plant with the power station. The power station unit's output between the heat integrated and non-integrated case is between 20-30MW over the range of capture rates. The maximum capture rate of $CO_2$ is also greater for Case 4 compared to Case 3 (refer to Fig. 6). Case 3 is limited to 90% capture of $CO_2$ as the steam demand for any further capture exceeds the amount of steam available from the turbine of the power station unit.

The optimised points for Case 4 show that low stripper pressures are not necessarily preferred when the overall power plant is taken into consideration. As shown in Fig. 8, the stripper pressure tends to be between 170-250kPaa compared to around 70kPaa for the case without heat integration (Case 3).

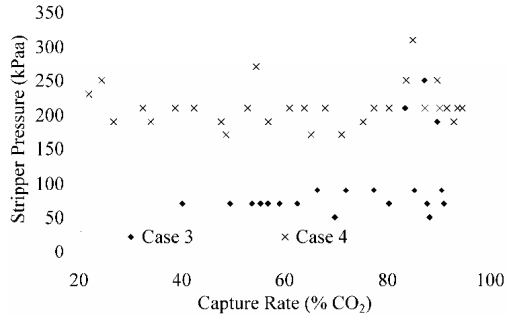


*Fig. 8. Stripper pressure for the optimised points of Case 3 and 4*

It is also interesting to note that the solvent lean loading for the heat integrated case is quite different to the others as shown in Fig. 9. Cases 2 and 3 appear to have a reasonably uniform relationship between the capture rate of $CO_2$ and the lean solvent loading. In contrast with Case 4 the optimum lean loading of the solvent is $0.26molCO_2/molK_2CO_3$, for capture rates between 40-80%.

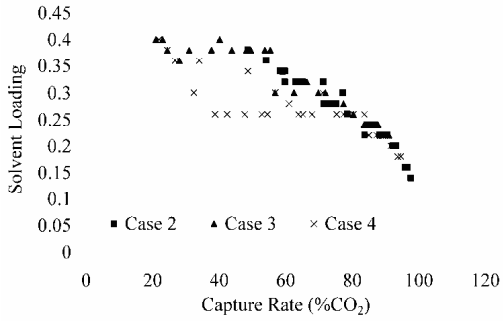


*Fig. 9. Solvent loading for optimised solutions for Cases 2, 3 and 4.*

## 4. Discussion

### 4.1 Impact of stripper pressure on the optimal solutions

There is a definite trend in the CCS industry to focus on trying to minimise the reboiler energy of the solvent plant, which is important to help to reduce the amount of energy that the CCS plant will take from the power station unit. However, it is not the entire picture. To ensure the impact the CCS plant has on the power station is minimised, the solvent plant must be optimised with the power station in mind.

In order to reduce the reboiler energy for a potassium carbonate based CCS plant, the stripper pressure should be as low as possible. However when the impact on the power station is considered the optimal pressure increases to around 70-90kPaa, and increases even further when the solvent plant heat integration with the power station is considered, to between 170-250kPaa depending on the amount of $CO_2$ captured. The reason for this change is that the higher pressure reduces the power requirement of the $CO_2$ compressor giving a higher net output.

In order to compare Cases 2, 3 and 4 consider a capture rate of 90%. Interestingly for all of these cases the Pareto-optimal solution had lean solvent loadings of $0.22molCO_2/molK_2CO_3$ and solvent flowrate of 2600kg/s. Therefore, the only difference between each of these cases is the stripper pressure and the objective. Table 2 shows the reboiler energy requirements, the $CO_2$ compressor power, the power produced from the turbine taking into account the steam that needs to be extracted and thus the net power generated by the power station for a range of stripper pressures for the optimal solvent loading and flowrate for 90% capture of $CO_2$. They are shown for a power station without any heat recovery between the power station and the CCS equipment and also for maximum heat integration between the power station and CCS equipment.

*Table 2. Comparison of solutions for 90% capture rate of $CO_2$.*

| SP (kPaa) | Reboiler Energy ($MJ/kgCO_2$) | $CO_2$ Comp. Power (MW) | Turbine Power (MW) | Net Power Output (MW) |
|---|---|---|---|---|
| No heat integration | | | | |
| 30 | 4.45 | 37 | 149 | 96 |
| 90 | 4.90 | 27 | 142 | 99 |
| 250 | 5.30 | 20 | 135 | 99 |
| Including heat integration | | | | |
| 30 | 4.45 | 37 | 153 | 116 |
| 90 | 4.90 | 27 | 167 | 123 |
| 250 | 5.30 | 20 | 165 | 129 |

If the objective is to minimise the solvent plant reboiler energy (Case 2), then from the results shown in Table 2 it can be seen that this would be achieved by having the lowest stripper pressure.

When the compressor power is taken into consideration for Case 3, the optimum solution is at a stripper pressure of approximately 90kPaa, as there is a 10MW advantage in the compressor power requirement and only a 7MW penalty in the power generated in the turbine. What can also be noted is that as the pressure is increased from 90kPaa to 250kPaa the net power output is very similar. There is a 7MW of reduction in the compressor power, but also 7MW less of power generated from the turbine. The similarity in these results explains why at capture rates greater than 75% there is no clear optimal stripper pressure for Case 3 as the optimal solutions include stripper pressures between 50kPaa and 250kPaa (refer to Fig. 6 & 7).

Therefore, when selecting a stripper pressure for a project the decision for this case may come down to other factors including capital costs, safety and operability. To improve the range of capture rates that the plant would be able to operate with the maximum net power generation the designer may chose to operate with a stripper pressure of 70kPaa as this is the stripper pressure for the optimal solutions for capture rates between 50 and 75% (refer to Fig. 6 & 7).

When including maximum heat recovery between the power station unit and the CCS equipment the trade-off between compressor power requirements and power generated by the turbine favours pressures of 250kPaa (refer to Table 2). The solutions do not improve above 250kPaa as the reboiler temperature increases to a point where higher pressure steam is required to satisfy the reboiler duty.

Interestingly for low pressures (30kPaa) the power generated by the turbine is lower than for the higher pressure cases even though the amount of energy required by the stripper reboiler is lower. The reason for this can be seen by comparing the composite curves for the low pressure case compared to a high pressure case. The low pressure case pinch point is at the rich solvent heater on the cold curve and the stripper condenser on the hot curve. By increasing the pressure in the stripper condenser the condenser heat is released at temperatures high enough to provide the energy for the rich solvent heater which lessens the heating and cooling requirements of the process.

### 4.2 Using CCS to control power station unit outputs

It is possible to design the CCS plant with a range of solvent flowrates and lean solvent loadings, therefore the capture rates will also be able to be adjusted. As can be seen in Fig. 6 as the capture rate is adjusted the power station unit net power production decreases. Therefore, it would be possible to alter the power generated by altering the amount of $CO_2$ captured. During peak hours when the demand and therefore price of electricity increases the capture rate of $CO_2$ could be reduced to increase the net power generated by the power station unit, likewise the power station unit could increase the capture rate of $CO_2$ when electricity prices reduce.

As the changes in capture rate would change the amount of steam that needs to be extracted from the turbine, the control of the turbine over a range of steam extraction rates would be important. The $CO_2$ compressor turndowns may also limit the range of $CO_2$ capture rates, however the operating range of the compressors are likely to be improved by having multiple compressors in parallel which is likely to be the situation on any large scale CCS project.

## 5. Conclusion

To minimise the reduction in power output from a power station unit with the addition of CCS, the design of a solvent-based CCS plant should be conducted with the understanding of how the power station will interact with the CCS equipment. In the case of potassium carbonate based solvent plants, the stripper pressure will be an important variable. Stripper pressures in the range of 170kPaa-250kPaa were found to be the optimal solutions for the power station provided in this paper. The optimal pressure may change depending on the power station and the available temperatures of the extraction steam. MOO of the power station and the CCS equipment can highlight the impact the CCS equipment will have on the net power generation of a power plant and can be used to design better integrated systems. MOO also enables curves of the power station power output versus amount of $CO_2$ captured to be generated, this can be used by power stations to control the amount of power they generate by controlling the amount of $CO_2$ that is captured.

## Nomenclature

*CCS* Carbon Capture and Storage

*MOO* Multi-objective optimisation

*SF* Solvent Flow (kg/s)

*LL* Solvent lean loading ($molCO_2/molK_2CO_{3(s)}$)

*SP* Stripper Pressure (kPaa)

*Obj.1* Objective 1

*Obj.2* Objective 2

## References

[1] IPCC 2005 IPCC Special Report on Carbon Dioxide Capture and Storage. Prepared by Working Group III of the Intergovernmental Panel on Climate Change ed B Metz*, et al.*

[2] Ghosh, U., Kentish, S. and Stevens, G. 2008 Absorption of carbon dioxide into potassium carbonate promoted by boric acid. In: *Ninth International Conference on Greenhouse Gas Control Technologies (GHGT-9),* Elsevier, Washington DC, USA,

[3] Cullinane, J.T. and Rochelle, G.T., 2004, Carbon dioxide absorption with aqueous potassium carbonate promoted by piperazine, Chemical Engineering Science, 59(17), pp. 3619-30

[4] Jassim, M.S. and Rochelle, G.T., 2006, Innovative absorber/stripper configurations for $CO_2$ capture by aqueous monoethanolamine, Industrial & Engineering Chemistry Research, 45(8), pp. 2465-72

[5] Rangaiah, G.P. 2009 *Multi-objective optimization : techniques and applications in chemical engineering* World Scientific, Singapore.

[6] Linnhoff, B., et al. 1982 *A user guide on Process Integration for the efficient use of energy,* IChemE, UK.

[7] Smith, R. 2005 *Chemical Process Design and Integration,* John Wiley & Sons Ltd, West Sussex, England.

[8] Deb, K., et al., 2002, A fast and elitist multiobjective genetic algorithm: NSGA-II, Evolutionary Computation, IEEE Transactions on, 6(2), pp. 182-97

[9] Lee, E.S.Q. and Rangaiah, G.P., 2009, Optimization of recovery processes for multiple economic and environmental objectives, Industrial & Engineering Chemistry Research, 48(pp. 7662-81

[10] Bhutani, N., et al., 2007, A Multi-platform, multi-language environment for process modelling, simulation and optimisation., International Journal of Computer Applications in Technology, 30(3), pp. 197-214

[11] Harkin, T., Hoadley, A. and Hooper, B., 2010, Reducing the energy penalty of $CO_2$ capture and compression using pinch analysis, Journal of Cleaner Production, 18(9), pp. 857-66

## Acknowledgements

Work is prepared as part of the Latrobe Valley PCC project with support of the Victorian Government ETIS Brown Coal R&D program; International Power and the Cooperative Research Centre for Greenhouse Gas Technologies (CO2CRC), which is funded through the Australian Government's Cooperative Research Centre Program, other federal and state government programs, CO2CRC participants and wider industry.

# $CO_2$ fixation using magnesium silicate minerals Part 1: Process description and performance

*Johan Fagerlund[a], Experience Nduagu[a,b], Inês Romão[a,c] and Ron Zevenhoven[a]*

[a] *Thermal and Flow Engineering Laboratory, Åbo Akademi University, Turku, Finland*
[b] *Energy and Environment System Group, Institute for Sustainable Energy Environment and Economy, University of Calgary, Alberta, Canada*
[c] *Department of Chemical Engineering, University of Coimbra, Coimbra, Portugal*

**Abstract:** This paper describes a staged carbonation process for magnesium silicate mineral carbonation. This carbon dioxide capture and storage (CCS) alternative involves the production of magnesium hydroxide, followed by its carbonation in a pressurised fluidised bed (PFB) reactor that is operated at temperatures and pressures so far up to 873 K, 4.5 MPa. The goal is to utilise the heat of the carbonation reaction to drive the $Mg(OH)_2$ production step.
The results show that $Mg(OH)_2$ can be produced successfully and efficiently from different serpentinite minerals from locations worldwide (Finland, Lithuania, Australia and Portugal). From the extraction step, ammonium sulphate is recovered while iron oxides (from the mineral) are obtained as by-products. The carbonation step, while still being developed, resulted in >50 %-wt conversion in 15 minutes (773 K, 2 MPa) for > 300 µm serpentinite derived $Mg(OH)_2$ particles.

**Keywords:** carbon dioxide capture and storage, $CO_2$ mineralisation, gas-solid carbonation, staged process.

## 1. Introduction

Carbon dioxide capture and storage (CCS) is being considered as one of the options for $CO_2$ emissions mitigation in many countries, including Finland [1]. Although the storage of compressed $CO_2$ in geological formations currently receives most attention, the interest towards an alternative option of $CO_2$ mineralisation is increasing. In Finland, R&D work on this method has been ongoing for many years, motivated by a lack of other CCS options and the fact that the thermodynamics of a $CO_2$ mineralisation process, when properly optimized, allow for energy-neutral operation [2-4].

The basic principle behind mineral carbonation can be found in nature, and it is called weathering. When rock, containing a material capable of forming carbonates, such as calcium or magnesium, erodes, small particles of rock are separated and exposed to $CO_2$ which has been dissolved in rain water. This causes the rock particles to slowly break up, releasing metal ions into the mildly acidic water, which then become available to react with the dissolved $CO_2$. The result of this is the formation of mineral carbonates. Unfortunately however, natural weathering is very slow and cannot keep up with the increasing atmospheric $CO_2$ level. Therefore the goal of mineral carbonation has been [5] and still is to increase the reaction rate of mineral carbonation in an environmentally sound way.

There are several ways of increasing the carbonation rate artificially and most of the processes concentrate on precipitating carbonates from aqueous solutions [6]. While the aqueous route might seem more promising at first, with faster carbonation kinetics obtained so far, the energy economy of such an approach is less attractive. This is the reason why we are studying a gas-solid carbonation process that aims at utilising the heat released from the exothermic carbonation reaction (3) at elevated temperatures.

This paper describes a staged carbonation process for magnesium silicate mineral carbonation that involves the production of reactive magnesium in the form of magnesium hydroxide, followed by the carbonation of this in a pressurised fluidised bed (PFB) reactor that is operated at temperatures and pressures so far up to 873 K, 4.5 MPa. The purpose is to increase the pressure to even higher levels. Above 7.4 MPa and 301 K, $CO_2$ turns supercritical and the target is to study its effects on the carbonation rate and the behaviour of the fluidised bed. A schematic illustration of the

Corresponding Author: Johan Fagerlund, Email: johan.fagerlund@abo.fi

vIAh2RR O2RhIlf2O l. &lR v)v2I h). f2 mAD O l. ly

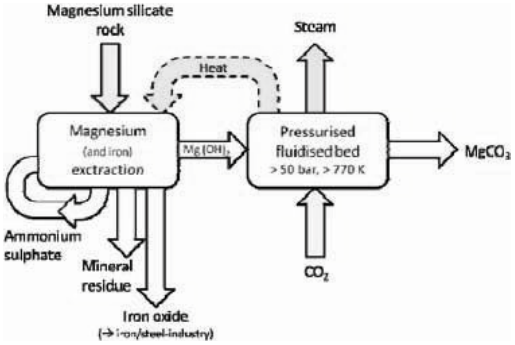


*Fig.1. A schematic illustration of the mineral carbonation process described in this paper.*

A RlO2Il. y &2 mh )1 vIAODh& ] )y. 2RlD] h)If A )&2 &lR hADlO mh O DR2 l. k)IlADR )vvIlh)&A R mhA] R[ v12 l). Omhl1&Amh 2 h, 2] lh)lR O2v2. Ol. y A vDl1&4 n y d lR ) R&f12 ). O 2. klIA ] 2. &1l4 f2. ly. ] )&2Il)1 g ( fD&l)Iy2 Rh)12 Av2I)&A z ADlO R)&Dl)&2 hDI12. &] )I[ 2&)R) vIAODh&AI f4 vIAODh&l. &2 lA y ID g ( c, 2 mAhDR Am&lRv)v2I v)I& z 1l1 f2 A &2 vIAh2RR l&R2lm z, l12 ). 4 mDl&2I hA RlO2I)&A R I2y)IOl. y vIAODh&DR2 AI OlRvAR)1z 1l1 f2 12m&AD& OOl&A )1 l. mAl ] )&A I2y)IOl. y vIAh2RR l. &2yI)&A ). O ] )&2Il)1R&2)] R, ). Oll. y h). f2 mAD Ol. v)I& Am &lRv)v2I R2Il2Rg ( i)I& yA2R1. &A O2&l1 Am&2 2. 2Iy4 2hA A] 4 Am&2 R4R&2] )&, ). Og (

## 2. Methodology

c, 2 vIAh2RR O2RhIlf2O l. &lRv)v2I h). f2 OlklO2O l. &A &I22 R&2vR ] )y. 2RlD] 2-&)h&A n y d C vIAODh&A ). O n y d C h)If A )&A c, 2 mAllAz l. y R2h&A vI2R2. &R2)h, R&2v l. RA] 2 O2&l1

### 2.1. *Step 1: Extracting Mg from serpentinite*

c, 2 ] 2&AO mAl 2-&)h&y ] )y. 2RlD] mhA] R2Iv2. &l&2 ). O A&2I ] )y. 2RlD] R1lh)&2 ] l. 2I)lR f2l. y O2k21Av2O )&W p hA RlR&R Am , 2)& y &2 R2Iv2. &l&2 &A f2& 22. b ). O b &Ay2&2I z l& )] ] A lD] RDlv, )&2 e R)l& g ( c, lR h)DR2R &2 ] )y. 2RlD] &A mAl] ] )y. 2RlD] RDlv, )&2 z, lh, h). f2 mDl&2I hA k2I&2O&A n y d C

n y el d dC C ed n yed eld C d y C y

c, 2 I2)h&A O2RhIlf2O f4 lR2. OA&2I] lh ). O mAl &lR I2)RA &2 h)If A )&A R&2v , )R &A f2 RDmhhl2. &4 2m2h&k2 &A hA] v2. R)&2 mAl &2 , 2)& l. vD&I2wDII2O p. mAl&D. )&214 ] )y. 2RlD] RDlv, )&2 h). . A&f2 OlI2h&4 h)If A )&2O). O). A&2I vIAh2RR R&2v lRI2wDII2O

### 2.2. Step 2: $Mg(OH)_2$ production

c, 2 RAllO ] )y. 2RlD] RDlv, )&2 OlRRAlk2R z 2l1 l. z)&2I c, 2 mAl] 2O )wD2ADR RAlD&A hA &l. R ] )y. 2RlD] lA R z, lh, h). f2 vI2hlvl&x&2O AD&)R n y d C f4 l. hI2)Rl. y &2 RAlD&A R8 vC c, lR l. hI2)R2 h). f2 )h, l2k2O DRl. y )] ] A l) &)&, )R f22. I2hAk2I2OmhA] &2 vI2h2Ol. y R&2v

n yed C d C )w C ed )w n y d C

e&l1 f2mAl2 n y d C vI2hlvl&x&2R lIA h). f2 I2hAk2I2O )R) f4 vIAODh&mhA] &2 vIAh2RR c, 2 )] AD &AmlIA vI2hlvl&x&2O k)Il2R O2v2. Ol. y A &2 DR2OIAh[ ] )&2Il) 1). O&2 vIAh2RRhA Ol&A R

u, l12 &2 ] )y. 2RlD] lR I2hAk2I2O &A f2 DR2O l. &2 h)If A )&A R&2v &2 I2] )l. l. y ] )y. 2RlD] ). O lIA mh22 RAlD&A h). f2 I2DR2O l. &2 ] )y. 2RlD] 2-&)h&A R&2v n Al2 l. mAl] )&A )fAD&] )y. 2RlD] , 4OlA-lO2 vIAODh&A )hhAlOl. y &A&2 I2)h&A R)fAk2 h). f2 mAD Ol. g (

### 2.3. Step 3: Reacting $CO_2$ with $Mg(OH)_2$

n )y. 2RlD] , 4OlA-lO2 n y d C lRI21)&k214 I)I2 l. .)&DI2 fD&] )y. 2RlD] l. l&R2lm lR . A& c, 2 I2)h&k l&4 Am&2 vIAODh2On y d C lR] Dh, f2&&2I &). &)&AmR2Iv2. &. l&2 mAl l. R&t. h2 Al 2k2. n yd )llAz l. y mAl m)R&2I h)If A )&A ). O &2 D&llR)&A Am&2 I2)h&A , 2)&l. )hhAlO). h2 &A &2 I2)h&A f21Az

n y d C R d y n y d R C d y

&)] f12. &hA Ol&A R &lRI2)h&A lRRlAz fD&f4 l. hI2)Rl. y &2 &2] v2I)&DI2 &2 I2)h&A I)&2 h). f2 l. hI2)R2ORty. lmhh). &4 c, 2, 2)&I212)R2OmhA] &lR 2-A&2I] lh I2)h&A lR l. &2 AlO2I Am [r] Al n y Al [r[y d mAl &2 &2] v2I)&DI2 I). y2 l. wD2R&A b 3 b CAz 2k2I )fAk2 ) h2I&l. l2k21 &2 mAllAz l. y I2)h&A f2hA] 2RlOA] l. ). &

n y d C R n yd R C d y

a. hI2)Rl. y &2 &2] v2I)&DI2 2k2. ] Al2 z 1l1 h)DR2 &2 ) Il2)O4 mAl] 2Oh)If A )&2R&A I212)R2 &2lI d l. )hhAlO). h2 &A

n y d R n yd R d y

c, 2 f) l). h2 f2& 22. &2 2wD)&A R )fAk2 O2&2I] l. 2R &2 RDhh2RR Am&2 h)If A )&A vIAh2RR

and avoiding the forward reactions in (4) and (5) is important. Preventing the reaction in (5) from taking place can be assured as long as the $CO_2$ pressure is maintained above a certain level. Reaction (4) on the other hand is governed by the water content of the gas and carbonation of $Mg(OH)_2$ would be slowed down by dehydroxylation, because MgO is less reactive than $Mg(OH)_2$ [4].

In accordance to (3) it should be possible to permanently trap $CO_2$ into magnesium carbonate in an exothermic reaction. As mentioned above, the proposed method consists of a fluidised bed maintained at a certain elevated temperature and pressure. The objective is to find the conditions that allow for continuous operation without the need for any heat input. In our lab, this can be reduced to the task of finding the conditions that give the highest carbonation degree in the shortest time. Another objective is to verify whether raising the pressure to levels where $CO_2$ becomes supercritical (> 7.4 MPa) gives any benefits.

## 3. Experimental procedure

For the purpose of developing a method to store $CO_2$ as mineral carbonates two parallel projects have been undertaken in the laboratory at Åbo Akademi University (ÅAU). One being the production of $Mg(OH)_2$ from common minerals and the other being the production of $MgCO_3$ from $Mg(OH)_2$.

### 3.1. Materials

For the purpose of producing $Mg(OH)_2$ various rocks have been tested, most of them serpentinites from different regions. Serpentinite is a magnesium silicate rock containing mostly serpentine ($Mg_3Si_2O_4(OH)_4$). A typical serpentinite sample from Finland (Hitura, nickel mine by-product) also contains a significant amount (14%-wt) of iron oxides. The iron from this iron containing mineral is extracted and separated in the process described above and one goal is that it could be used by the iron and steel industry in the future.

Depending on the composition and structure of the rock sample being tested various amounts of magnesium are extracted; the more the better. So far the highest amount of Mg extracted has been around 65%-wt.

While the magnesium hydroxide produced in this way has given some promising results when it comes to reactivity with $CO_2$, most of the carbonation experiments have so far been performed using a commercially produced $Mg(OH)_2$ (Dead Sea Periclase Ltd.). In addition, $SiO_2$ (i.e. sand) is mixed with the hydroxide sample before the carbonation experiments. The sand is inert and will not participate in the reaction, but it acts as a stabilizer during the fluidisation. Instead of being close to the limit of Geldart A particles, Geldart B behaviour is achieved for the mixture [12].

Regarding the particles size, typically between 125 µm and 212 µm, the correct particle size fraction is obtained by using a sieve shaker (Retsch AS 200 - time 15 min, amplitude 1.5 mm/"g" and interval 10 s). However, the $Mg(OH)_2$ particles consist of agglomerates rather than separate particles.

### 3.2. Test methods

The work on this particular mineral carbonation route has been divided into two parallel projects which are highly dependent. At this stage, more and more work is being directed towards integration of the two and possibilities to reduce cost and save energy as can be seen from part 2 [10] and part 3 [9] of this paper series. Below, the two methods are still separated and presented as they have been carried out in the laboratory.

#### 3.2.1 $Mg(OH)_2$ production

For the production of $Mg(OH)_2$ according to the solid-solid reaction route presented above a temperature controlled tubular oven is used. A sample is prepared by mixing ammonium sulphate (AS) and serpentinite in typically a 3:2 mass ratio. The small (a few grams) sample is allowed to react (without any mixing) in the oven for 0.3 h to 1 h. Then the material is dissolved in water and filtered. The filtrate is subjected to an aqueous ammonia solution and the precipitates are recovered at different pH-levels. For a more detailed description of this process see [11,13,14].

#### 3.2.2 $Mg(OH)_2$ carbonation

Using a fluidised bed as a reactor for the carbonation reaction has been suggested by others [2,15] and the principal reason for this is the continuous motion of the bed. The particles inside the bed are constantly colliding with each other and the reactor walls, and the force of these impacts is the cause for particle attrition and/or abrasion. This is beneficial since it has been shown

that the carbonation reaction becomes limited by a layer of carbonates forming on the surface of the particles in a static environment [3,16]. Another benefit of the fluidised bed is the good heat distribution allowing for homogenous conditions inside the reactor. Note that only $Mg(OH)_2$ is used in the FB reactor and not the whole mineral; this gives a significant reduction in pressure drop losses. In addition, using $Mg(OH)_2$ results in hot steam (with $CO_2$), that can be utilised in a steam turbine.

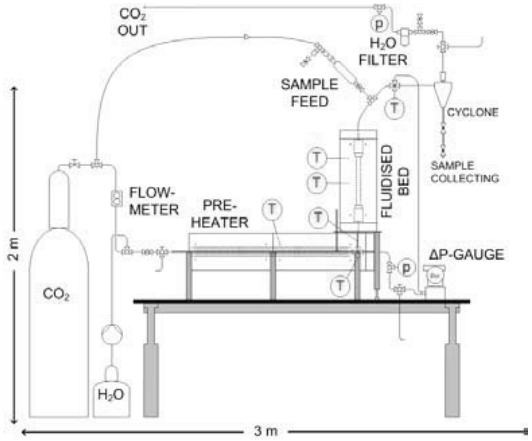


*Fig. 2. Schematic illustration of the fluidised bed setup used for mineral carbonation.*

The main components of the test setup can be seen in Fig. 2 and they consist of a $CO_2$ bottle, a water pump (HPLC), a pre-heater (a spiralling tube inside heating elements), a fluidised bed (FB), a cyclone, a sample feeder for the $Mg(OH)_2$-$SiO_2$ mixture and measuring equipment for temperatures, pressure and mass flows. The inner diameter of the FB is only 14 mm and the height of the FB is 0.5 m.

## 4. Results and discussion

Although results from both $Mg(OH)_2$ production and its consequent carbonation are presented here, the latter will be presented in more detail. Recent results of $Mg(OH)_2$ production according to the method described earlier are described more thoroughly elsewhere [11].

### 4.1. $Mg(OH)_2$ production

Experiments aimed at finding optimum conditions for the process gave an optimum range of 64 - 66 % Mg extraction at the following reaction conditions; reactants' mass ratio (S/AS), 0.5 - 0.7; reaction temperature, 400 - 440 oC and reaction time, 30 - 60 minutes. Under the same conditions, 0.33 – 0.34 g of valuable solid products (composing of > 70 % magnesium hydroxide and < 30 % FeOOH) were produced per gram of Finnish serpentinite reacted. The valuable solid products refer to the Fe containing (dark brown solid) compound and magnesium hydroxide (white solid), both precipitated with ammonia solution at pH 8-9 and 11-12, respectively.

In spite of the energy requirement of the process (see Part 2 of this paper series), it is important to note its significance. Mg extraction shows promising results, and a high purity $Mg(OH)_2$ was produced. The Fe-rich compound (FeOOH) produced in significant amounts from the process may be a useful raw material in the iron and steel industry. AS salt used as reagent for extracting Mg from the minerals is relatively cheap, and is a product and by-product of several chemical processes. AS salt is also recovered at the end of the process (however as aqueous solution). Ammonia gas is a by-product of the reaction, which was collected in water and can be used to act as or supplement the ammonia solution used for precipitation purposes. Interestingly, smaller volumetric amounts of ammonia solution are needed in the precipitation process compared to the amounts of base (alkaline) precipitants used previously in other reaction routes [11,17,18].

### 4.2. $Mg(OH)_2$ carbonation

The carbonation of $Mg(OH)_2$ at elevated pressures and temperatures is relatively fast. This has also been noted by others [16] and our recent results suggest that most of the carbonation takes place only minutes into the experiment. Exactly how fast the initial reaction rate is has not been determined, but could be the target of future studies.

The purpose of using a fluidised bed for the carbonation reaction has been discussed above, but it seems that there is another side to the particle interactions. While the collisions of particles inside the FB reactor is beneficial to carbonation because it exposes uncreated $Mg(OH)_2$ to $CO_2$ it also exposes the unreacted surfaces to dehydroxylation. Previously it has been noted that MgO is much less reactive than $Mg(OH)_2$ and its formation should be avoided. Unfortunately however, preventing MgO formation, while maintaining a high temperature, is difficult and requires a high $H_2O$ partial pressure. In practice,

RDh, ) , ly, k) vADI vI2RRDI2 lR. A&vARRf l2 IA] ly l&h). f 2 R22. &) & Ak2I) 1l ). l. hI2) R2 l. R4R&2] vI2RRDI2 m)kADIR &2 mAI] ) &A Am n y d C fD& R&dl1 n yd mAI] ) &A h). . A& f 2 ) kAlO2O k2. l. &2 D. I2) llR&h h) R2 Am) A 2 &A A 2 ] Al) I I) &A Am d ). O C d ClRvl) 42O l. ly &2 2wDI1lf IlD] ) ] AD. & Am n y d C I2] ) l. RR] ) 1l Ak2I &2 z , Al2 vI2RRDI2 I). y2

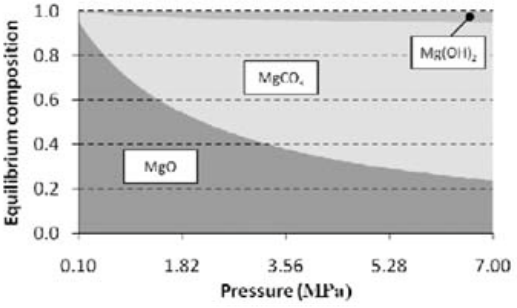


*Fig. 3. Equilibrium composition for a MgO-$Mg(OH)_2$-$MgCO_3$ system at 773 K. Gas composition is equimolar amounts of $CO_2$ and $H_2O$.*

a&, ) R) lRA vI2klADR14 f 22. . A&2O &) &C d v l) 4R) Rly. lmlh). & IAl2 l. &2 h) If A ) &A [ l. 2&lhR Am n y d C h) If A ) &A g ( a& , ) R f 22. RDyy2R&2O &) &R] ) 1l ) ] AD. &R Amz ) &2I k) vADI ) h& ) R h) &14R&). O 2. , ). h2R &2 h) If A ) &A I2) h&A I) &2 g ( CAz 2k2I &lR2m2h&, ) R. A&f 22. hl2) I14 O2] A R&) &2O l. ADI 2- v2II] 2. &R a. hA &) I4 ) R] ) 1l f D&2klO2. &. 2y) &k2 2m2h&A &2 mh ) 1 h) If A ) &A O2yI22 z l& l. hI2) R2O C d m2O I) &2 , ) R f 22. . A&h2O g ( e&dl1 &lR2m2h&. 22OR&A f 2 l. k2R&y) &2O l. ] Al2 O2&l1 ) R l&, ) R . A& &A ADI [ . Az l2Oy2 f 22. OA 2 hA RlO2Il. y ) y) R mAz v) RRl. y l. ) mDlClR2Of 2O

A] v) Il. y &2 & A Clm2I2. &n y d C &4v2R &) & , ) k2 f 22. &2R&2O RA m)I R, Az R &) &&2 R2Iv2. &. l&2 f ) R2O , 4ClA- lO2 lR ] Dh, ] Al2 I2) h&k2 &). &2 hA] ] 2Ihl) 1 A 2 2) O e2) i 2Ilh1) R2 p . O2I R] 1l) I hA Cl&A R b n i) ] l. &2 mAI] 2I hA k2I&2O &A z , l12 &2 l) &2I I2) h, 2O A 14 ) hA k2IRlA O2yI22 c , 2 v) I&h12 RlT2 mh) h&A z ) R ) lRA hA] v) I) &k214 l) Iy2 6] 3 6] c , 2 l) Iy2 Clm2I2. h2 l. I2) h&kl&4 h). 1l[ 214 f 2 ) &&lf D&2O &A &2 ] Dh, l) Iy2I RDlm)h2 ) I2) ] y kR ] y ). O vAI2 kAlD] 2 RlT2 h] y kR h] y Am &2 R2Iv2. &. l&2 O2Ilk2On y d C g (

c , ) &&2 R2Iv2. &. l&2 O2Ilk2On y d C h) If A ) &2R RA z 2l1 lR vIA] lRl. y 2Rv2hl) 1l4 hA RlO2Il. y &) & &2 d vI2RRDI2 Am&2 2- v2II] 2. &z ) R I2 l) &k214 lAz A l4 n i) a. hI2) Rl. y &2 vI2RRDI2 Dv &A ). O f 24A O &2 RDv2IhI1&h) 1 vAl. & Am d DRl. y &lR ] ) &2Il) 1 lR f 2l. y v l) . . 2O z , l12 , ly, 2I vI2RRDI2R z l& &2 hA] ] 2Ihl) 1 , 4ClA- lO2 , ) k2 ) lI2) O4 f 22. v2ImAI] 2O u l& &lR ] ) &2Il) 1 &2 f 2R&I2RDl&RA m)I hA k2IRlA z ) R ) h, l2k2O mAI R2k2I) 1 2- v2II] 2. &R I). yl. y mhA] n i) 3 n i) ) & b l. A l4 ] l. D&2R ) R2O A &2R2 I2RDl&R A 2 z ADlO &l. [ &) &l. hI2) Rl. y &2 I2) h&A &] 2 &A R) 4 ] l. D&2R z ADlO h12) I14 I2RDl&l. hA k2IRlA , Az 2k2I &lR1R. A&&2 h) R2

a&R22] R&) &&2 hA] v2&&A f 2&z 22. h) If A ) &A ). O O2, 4ClA- 41) &A hA] 2R l. &A v l) 4 ). O &) &2wDI1lf IlD] lRI2) h, 2O z l&l. ] l. D&2Rl. &A &2 2- v2II] 2. &eAm)I &2 vIAODh&R Am&2 2- v2II] 2. &R , ) k2 f 22. ). ) 14R2O mAI h) If A ) &2R A l4 R22 R2h&A fD&l&R22] R&) &) l1 Am&2 ] ) &2Il) 1 lRhA k2I&2O &A 2l&2I n yd Al n y d c, lR1R) lRA f ) h[ 2O Dv f 4 &2 mh2wD2. &l4 Af R2Ik2ORj ) 1l z 2ly, & lARR l. &2 2- v2II] 2. & vIAODh&) l&ADy, RA] 2 h) If A ) &A , ) R &[ 2. v l) h2 e&dl1 2k2. z l& h) If A ) &A &2 vIAODh&z ADlORdl1 z 2ly, l2RR&). &2 l. l&) 1 n y d C R) ] v12 ) RRD] l. y hA] v12&2 O2, 4ClA- 41) &A

ly R, Az R& A yI) v, RAm&2 h) If A ) &A O2yI22 ) R) mD h&A Am&2] v2I) &DI2 ). O vI2RRDI2 I) v, ) R, Az R I2RDl&R mhA] &2R&R OA 2 l. ) mh- 2O f 2O vI2RRDIlR2O &2I] AyI) kl] 2&lh ). ) 14R2I mAI Rl-, ADIR g ( c, 2 v) I&h12R 6] P 6] DR2O hA RlR&2O Am &2 R) ] 2 2) O e2) i 2Ilh1) R2 n y d C &) &z 2 , ) k2 f 22. DRl. y l. &2 mDlClR2O f 2O c, 2 I2RDl&R Af &l. 2O DRl. y &2 mDlClR2O f 2O ) I2 O2vlh&2O l. yI) v, f CAz 2k2I RA] 2 Am&2R2 I2RDl&R I2vI2R2. & &2 ) k2I) y2 k) lD2 Am R2k2I) 1 2- v2II] 2. &R) R A&2I v) I) ] 2&2IR f 2RlO2R vI2RRDI2 ). O&2] v2I) &DI2 , ) k2 f 22. k) Il2O c, 2R2 k) Il) f l2R ) I2 I2) h&A &] 2 ] l. 3 , C d m2O I) &2 3 kAl mDlO k2lAhl&4 3 &] 2R ] l. l] D] mDlClR) &A k2lAhl&4 v) I&h12 RlT2 &4vlh) l14 6] 3 6] fD&) lRA l) Iy2I Dv &A 6] v) I&h12R, ) k2 f 22. &2R&2O ). O R) ] v12 RlT2 y3 y hA] v12&2 llR&Am&2 O) &( h). f 2 mAD O l. &2 vv2. Cl- A&2 &) &&2 i c &2R&I2RDl&R l. ly yI) v, ) I2vI2R2. & &2 mh ) 1 hA k2IRlA O2yI22 ) m2I , l. ) y) R ] l- &DI2 Am kAl d ). O kAlC d

Al ) mh- 2Of 2OR4R&2] A 2 hADlO 2- v2h&&2 I2RDl&R &A f 2 m)lI14 hA RlR&2. &, ) kl. y ) h) If A ) &A O2yI22 ] ) - l] D] ) &) h2I&l. &2] v2I) &DI2 hAII2RvA Cl. y &A RA] 2 O2yI22R f 21Az &2 2wDI1lf IlD]

&2] v2I)&DI2 Amn y d c , lR) lRA ) vv2) IR&A f 2 &2 h) R2 mAl &2 I2RDl&Rl. yI) v, ) l. ly a. hI2) Rl. y &2 vI2RRDI2 l. hI2) R2R &2 h) If A ) &A O2yI22 f D& l. hI2) Rl. y &2 &2] v2I) &DI2 &AA ] Dh, I2ODh2R &2 mh ) 1hA k2IRlA O2yI22

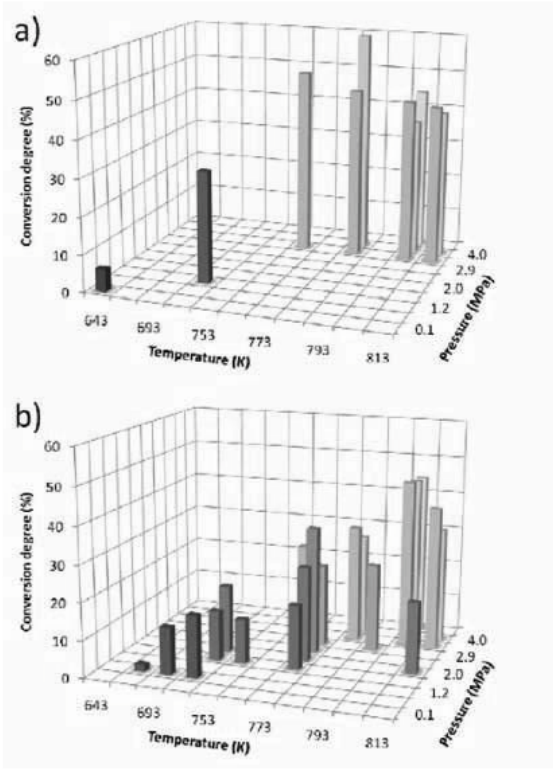


*Fig. 4. Carbonation results as a function of pressure and temperature: a) PTGA, b) fluidised bed (other operational variables varied).*

2h) DR2 Am&2 m)h&&) &&2I2 ) I2 ] Al2 k) Il) f l2R hA RlO2I2O DRl. y &2 mDlOlR2O f 2O &2 I2RDl&R ) vv2) I ] Al2 Rh) &&I2O &) . l. &2 mh- 2O f 2O h) R2 c , lRA l4 vIAk2R&) &l&lR. A&A l4 &2] v2I) &DI2 ) . O vI2RRDI2 &) & l. mlD2. h2 &2 R4-R&2] ) l&ADy, 2klO2. &l4 &2R2 vl) 4 ) Rly. lmlh) . &IAl2 1l Am&2 I2RDl&R ) I2 mhA] 2- v2Il] 2. &R z l& ] Dh, R, Al&2I I2) h&A &] 2 &) . &2 Rl- , ADlR DR2O mAl &2 R&&h h) R2 &lvlh) l14 A l4 ] l. D&2R

. ) &&2] v&&A 2- vl) l. &2 I2RDl&R ) . ) l4&h) l14 z ) R ] ) O2 2) I1l2I g ( f D&) R OlRhDRR2O) f Ak2 &2I2 ) I2 R&l1 R2k2I) 1 ) Rv2h&R &) &) I2 . A&mDl14 D. O2IR&AAO i ) I&hDl) I14 &2 2m2h&R Am I2) h&tA &] 2 ) . O v) I&h12 v) I&h12 l. &2I) h&tA l. OlI2h&l4 mDlO mAz A &2 h) If A ) &tA I) &2 ) I2 f 2l. y hA RlO2I2O

### 4.2.1. Carbonate analysis

c A O2&2I] l. 2 &2 2- &2. &Amh) If A ) &tA ) m&2I 2) h, 2- v2Il] 2. &) mh) h&tA Am&2 R) ] v12 lRRDf E2h&2O &A C 1 ) . O &2 vI2RRDI2 l. hI2) R2 OD2 &A d 2kAlD&tA lR ] 2) RDI2O c , lR ) . ) l4RlR ] 2&AO lR Rl] v12 42&) hhDl) &2 ) . O . ] Al2 l. mAl] ) &tA h) . f 2 mAD. O l. ) I2h2. &l4 RDf ] l&&2O v) v2I g ( CAz 2k2I &lR] 2&AOlh) . . A&OlR& yDlR f 2&2 22. n y d C ) . O n yd a&lR2k2. OlmhhDl&&A &2 l1 &2 ] ) RR1ARROD2 &A O2, 4OlA- 41) &tA ) v) I&mhA] &) ¿z Am h) If A ) &2 O2hA] vARl&tA DRl. y &2I] AyI) kl] 2&lh ) . ) l4RlR c g ( 1y OlRvl) 4R ) c I2RDl&DRl. y ) lly, &l4 h) If A ) &2C z &n y d C ) . O h12) I14 &2I2 lRA l4 A 2 RlAv2 mAl f A& C d ) . O d 2kAlD&tA ) IAD. C b d . &2 A&2I , ) . O ) . ) l4Rl. y &2 2kAlkl. y y) Rz ADlO AmhADlR2 I2k2) l &2 , 4OlA- lO2 hA &2. ¿z Am&2 R) ] v12

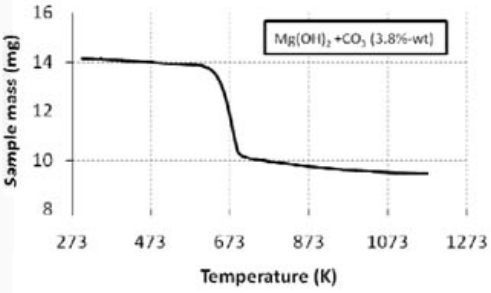


*Fig. 5. TGA result of $Mg(OH)_2$ containing 3.8%-wt $CO_3$. Heating rate 10 K/min.*

2RlO2R l. OlI2h& ] 2) RDI2] 2. &R A &2 R) ] v12 hA] vARl&tA z 2 , ) k2 lAA[ 2O ) &&2 R) ] v12R DRl. y Rh) . . l. y 2I2hl&tA ] lhIARhAv4 e n c , 2 Olmn2I2. h2 f 2&2 22. &2 R2Iv2. &l&2 O2Ilk2O n y d C ) . O &2 hA] ] 2Ihl) 1 A 2 lRh12) I f D&l&lR ] Dh, ] Al2 OlmhhDl&&A OlR&yDlR f 2&2 22. ) I2) h&2O *i.e.* v) I&) l14 h) If A ) &2O R) ] v12 ) . O ) . D. I2) h&2O A 2 c , lR ylk2R . A 2klO2. h2 Am h) If A ) &2R Al Am) h) If A ) &2 Ilh, l) 42I mAl] l. y ) IAD. O &2 v) I&h12R) R) I2RDl&Amh) If A ) &tA

a. ly &tA hIARRR2h&tA ) 1 e n l] ) y2R ) I2 R, Az . a] ) y2 ) R, Az R ) h) If A ) &2O R2Iv2. &l&2 O2Ilk2O n y d C R) ] v12 ) . O l] ) y2 f R, Az R ) . D. I2) h&2O hA] ] 2Ihl) 1 n y d C R) ] v12 a] ) y2 ) R, Az R &2 hIARRR2h&tA Am&I22 ] ) y. 2RlD] Ilh, v) I&h12R z , 1I2 l] ) y2 f A l4 OlRvl) 4RA 2

. ) l4Rl. y mAl 2I2] 2. &l hA] vARl&tA v) I&hDl) I14 2klO2. h2 Am d lR D , 2IvmDl ) R ) h) If A f ) R2O I2Rl. z ) R DR2O &tA ] ) [ 2 &2 hIARRR2h&tA ) 1

samples. However, the difference between the two samples is evident and it is clear that the serpentinite derived sample is much more porous than the commercial one, explaining the obtained higher carbonation degree.

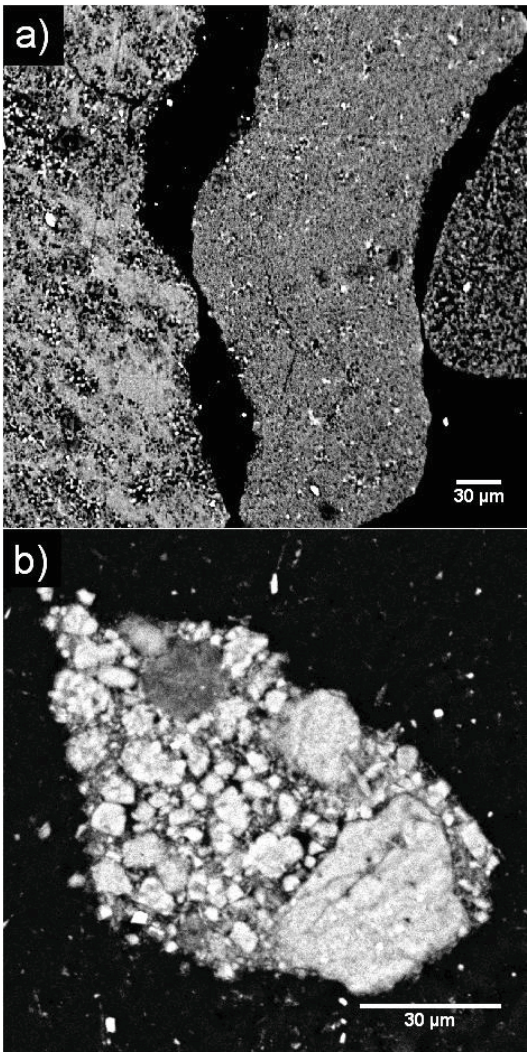


*Fig. 6. Cross-sectional SEM images: a) (250x) carbonated (51%-wt) serpentinite derived $Mg(OH)_2$ sample, b)(500x) an unreacted commercial $Mg(OH)_2$ sample.*

## Conclusions

Producing magnesium hydroxide from serpentinite, an abundant magnesium containing rock for the purpose of mineral sequestration of $CO_2$, is possible using the method presented here. However, the process requires energy in the form of heat and that energy has to be largely covered by the consequent $Mg(OH)_2$ carbonation. As such the process described here can be divided into three steps, magnesium extraction, $Mg(OH)_2$ production and $Mg(OH)_2$ carbonation. How these processes can be integrated, the energy requirements and the possibilities of large scale mineral carbonation are presented in parts 2 and 3 of this paper series.

Here, the concept and methods of mineral carbonation using a fluidised bed have been presented and the best results show that more than 50% carbonation can be achieved in less than 15 minutes at relatively mild conditions (2 MPa, 773 K) with serpentinite derived $Mg(OH)_2$ particles of 250 µm–425 µm. Still, increasing the reaction time does not automatically translate into increased carbonation, which could be a result of dehydroxylation and the much slower kinetics of MgO carbonation. However, higher pressures, using the serpentinite derived $Mg(OH)_2$ are still too be tested and will likely result in even faster carbonation.

## References

[1] IPCC., 2005, IPCC Special Report on Carbon Dioxide Capture and Storage, Prepared by Working Group III of the Intergovernmental Panel on Climate Change, pp. 1-431.

[2] Zevenhoven, R., and Teir, S., 2004, Long term storage of CO2 as magnesium carbonate in Finland, Proc. of the Third Annual Conference on Carbon Capture and Sequestration, paper 217, Alexandria (VA), USA, pp. 1-11.

[3] Zevenhoven, R., Eloneva, S., and Teir, S., 2006, A study on MgO-based mineral carbonation kinetics using pressurised thermogravimetric analysis, Proc. 8th International Conference on Greenhouse Gas Control Technologies, paper P02_01_09, Trondheim, Norway, pp. 1-6.

[4] Zevenhoven, R., Teir, S., and Eloneva, S., 2008, Heat optimisation of a staged gas–solid mineral carbonation process for long-term $CO_2$ storage, Energy, 33(2), pp. 362-370.

[5] Seifritz, W., 1990, $CO_2$ disposal by means of silicates, Nature, 345(7 June), pp. 486.

[6] Zevenhoven, R., and Fagerlund, J., 2010, Fixation of Carbon Dioxide into Inorganic Carbonates: The Natural and Artificial

"Weathering of Silicates", M. Aresta, eds., Carbon Dioxide as Chemical Feedstock, pp. 353-380.

[7] Teir, S., et al., 2006, Stability of calcium carbonate and magnesium carbonate in rainwater and nitric acid solutions, Energy Convers. Manage., 47(18-19), pp. 3059-3068.

[8] Lackner, K.S., et al., 1997, Carbon dioxide disposal in mineral form - keeping coal competitive, Report LA-UR-97-2094.

[9] Romão, I., et al., [submitted], $CO_2$ fixation using magnesium silicate minerals. Part 3: Integration with iron-and steelmaking, Proc. ECOS 2010, Lausanne, Switzerland.

[10] Zevenhoven, R., et al., [submitted], $CO_2$ fixation using magnesium silicate minerals. Part 2: Process energy efficiency, Proc. ECOS 2010, Lausanne, Switzerland.

[11] Nduagu, E., Mineral carbonation: preparation of magnesium hydroxide [$Mg(OH)_2$] from serpentinite rock, M.Sc. Thesis, Åbo Akademi University, Finland.

[12] Kunii, D., and Levenspiel, O., 1991, Fluidization Engineering, Butterworth-Heinemann, USA.

[13] Nduagu, E., et al., [submitted], Production of reactive magnesium from magnesium silicate for the purpose of $CO_2$ mineralization. Part 2. Mg extraction modeling and application to different Mg silicate rocks, Int. J. Miner. Process.

[14] Nduagu, E., et al., [submitted], Production of reactive magnesium from magnesium silicate for the purpose of $CO_2$ mineralization. Part 1. Application to Finnish serpentinite, Int. J. Miner. Process.

[15] Lackner, K.S., et al., 1995, Carbon dioxide disposal in carbonate minerals, Energy, 20(11), pp. 1153-1170.

[16] Butt, D. P., et al., 1998, The kinetics of binding carbon dioxide in magnesium carbonate, Proc. The 23rd international technical conference on coal utilization and fuel systems, Los Alamos National Laboratory (LANL), Clearwater, FL, USA, pp. 1-12.

[17] Teir, S., Fixation of carbon dioxide by producing carbonates from minerals and steelmaking slags, 2008, Ph.D. Dissertation, Helsinki University of Technology, Helsinki, Finland.

[18] Henrist, C., et al., 2003, Morphological study of magnesium nanoparticles precipitated in dilute aqueous solution, J. Cryst. Growth, 249(1), pp. 321-330.

[19] Béarat, H., et al., 2002, Magnesium hydroxide dehydroxylation/carbonation reaction processes: Implications for carbon dioxide mineral sequestration, J. Am. Ceram. Soc., 85(4), pp. 742-748.

[20] Fagerlund, J., et al., 2010, A stepwise process for carbon dioxide sequestration using magnesium silicates, Front. Chem. Eng. China, In press.

[21] Fagerlund, J., et al., [submitted], Gasometric determination of $CO_2$ released from carbonate materials, J. Chem. Educ.

[22] Khan, N., et al., 2001, The origin of the exothermic peak in the thermal decomposition of basic magnesium carbonate, Thermochimica Acta, 367-368(March 8), pp. 321-333.

**Acknowledgements:** This paper is part of an ongoing project called Carbonates in Energy Technology (CARETECH). CARETECH is funded (2008-2011) by the Academy of Finland's Sustainable Energy programme (SusEn). We also acknowledge KH Renlund foundation for support during the years 2007-2009.

## Appendix

*Table 1. Experimental data for 38 carbonation experiments using a pressurised fluidised bed. The "carbonation degree" has been calculated by dividing the $CO_3$ content of a sample with that of an pure $MgCO_3$ sample of equal weight.*

| | Mean particle size (µm) | Duration (min) | Temperature (K) | Total pressure (MPa) | Fluidisation velocity (cm/s) | H2O (vol-%) | Carbonation degree (-) |
|---|---|---|---|---|---|---|---|
| E010709_1 | 168.5 | 60 | 733 | 0.6 | 10.2 | 0.90 | 17 % |
| E010709_2 | 168.5 | 60 | 693 | 0.6 | 10.2 | 0.94 | 13 % |
| E010709_3 | 168.5 | 60 | 653 | 0.6 | 11.0 | 0.90 | 11 % |
| E140809_1 | 168.5 | 60 | 813 | 2.0 | 6.0 | 0.91 | 19 % |
| E140809_2 | 168.5 | 60 | 773 | 2.0 | 6.2 | 0.90 | 14 % |
| E260809_1 | 168.5 | 60 | 733 | 2.0 | 6.6 | 0.89 | 15 % |
| E260809_2 | 168.5 | 60 | 733 | 2.0 | 6.3 | - | 21 % |
| E310809_1 | 168.5 | 30 | 773 | 2.9 | 6.0 | - | 25 % |
| E310809_2 | 168.5 | 30 | 773 | 2.9 | 6.1 | - | 26 % |
| E030909_1 | 168.5 | 30 | 753 | 1.5 | 6.3 | - | 10 % |
| E030909_2 | 168.5 | 30 | 773 | 1.5 | 6.3 | - | 17 % |
| E030909_3 | 168.5 | 30 | 733 | 1.5 | 6.6 | - | 14 % |
| E030909_4 | 168.5 | 30 | 753 | 1.5 | 6.6 | 1.74 | 14 % |
| E040909 | 100.0 | 30 | 753 | 1.5 | 2.3 | - | 11 % |
| E061009_1 | 168.5 | 15 | 773 | 2.9 | 6.4 | - | 15 % |
| E061009_2 | 168.5 | 15 | 733 | 1.5 | 6.4 | - | 13 % |
| E061009_3 | 168.5 | 15 | 793 | 2.9 | 5.2 | - | 24 % |
| E061009_4 | 168.5 | 15 | 773 | 2.9 | 10.4 | - | 26 % |
| E061009_5 | 168.5 | 15 | 773 | 2.9 | 5.4 | 1.03 | 20 % |
| E021209 | 275.0 | 15 | 773 | 2.8 | 14.1 | - | 35 % |
| E031209_2 | 168.5 | 30 | 773 | 2.0 | 8.0 | 0.10 | 29 % |
| E031209_3 | 168.5 | 30 | 773 | 2.0 | 7.9 | 0.53 | 30 % |
| E031209_4 | 168.5 | 30 | 773 | 2.0 | 7.8 | 1.61 | 27 % |
| E071209_1 | 337.5 | 10 | 773 | 2.0 | 14.4 | - | 26 % |
| E071209_2_XP | 337.5 | 10 | 773 | 2.0 | 12.2 | - | 48 % |
| E071209_3 | 337.5 | 10 | 773 | 2.0 | 16.1 | - | 29 % |
| E071209_4_XP | 337.5 | 10 | 773 | 2.0 | 15.1 | - | 53 % |
| E071209_5 | 187.5 | 10 | 773 | 2.0 | 6.1 | - | 24 % |
| E071209_6_XP | 187.5 | 10 | 773 | 2.0 | 5.8 | - | 32 % |
| E040210_1 | 168.5 | 10 | 768 | 3.5 | 6.3 | - | 25 % |
| E040210_2 | 168.5 | 10 | 783 | 3.5 | 6.7 | 1.04 | 27 % |
| E040210_3 | 168.5 | 10 | 798 | 3.5 | 6.2 | - | 46 % |
| E040210_4 | 168.5 | 10 | 813 | 3.5 | 6.5 | 1.03 | 39 % |
| E040210_5 | 168.5 | 5 | 783 | 4.0 | 9.1 | - | 28 % |
| E040210_6 | 168.5 | 10 | 798 | 4.0 | 6.2 | 1.10 | 45 % |
| E040210_7 | 168.5 | 10 | 813 | 4.0 | 7.4 | - | 31 % |
| E040210_8 | 168.5 | 10 | 798 | 4.5 | 6.2 | 1.09 | 44 % |
| E040210_9 | 168.5 | 10 | 783 | 3.5 | 6.6 | 1.04 | 37 % |

# $CO_2$ Fixation Using Magnesium Silicate Minerals. Part 2: Process Energy Efficiency

*Ron Zevenhoven [a], Inês Romão [a,b], Johan Fagerlund [a] and Experience Nduagu [a,c]*

[a] *Thermal and Flow Engineering Laboratory, Åbo Akademi University, Åbo/Turku, Finland*
[b] *Department of Chemical Engineering, University of Coimbra, Coimbra, Portugal*
[c] *Energy and Environment System Group, Institute for Sustainable Energy Environment and Economy University of Calgary, Alberta, Canada*

**Abstract:** This paper describes the energy economy of the staged process described in part 1 of this short paper series. The optimal conditions for $Mg(OH)_2$ production depend to some extend on the mineral that is used: the different temperatures, reactants' mass ratios and (to some extent) residence times will give differing $Mg(OH)_2$ and by-product amounts which also affects energy input requirements. The heat release from the carbonation step is directly dependent on the degree of carbonation conversion. One benefit of carbonating $Mg(OH)_2$ is that only this is processed in the pressurised fluidised bed carbonation reactor: other, non-reactive material would add only to pressure drop (= power loss) and reactor size. Also, the product gas will be hot, pressurised steam (mixed with unreacted $CO_2$). Here, a process energy analysis is made based on the most energy intensive steps, being the heat treatment of the magnesium silicate rock and the carbonation reaction, respectively (a more detailed analysis is given in paper part 3). It is found that the heat requirements at 450-500°C for $Mg(OH)_2$ production are around 4x higher than the heat generated at 500-550°C by the carbonation reaction, giving heat input requirements (for example from another process) of 4-5 MJ/kg $CO_2$.

**Keywords:** Carbon Dioxide Capture and Storage, $CO_2$ Mineralisation, Gas-Solid Carbonation, Process Energy Efficiency.

## 1. Introduction

In Finland, R&D work on the method $CO_2$ mineralisation [1-4] has been ongoing for many years. This is motivated by a lack of other CCS options and the fact that the thermodynamics of the process, when properly optimized, offer the possibility of energy-neutral operation [5-9]. As methods to carbonate magnesium silicate mineral directly or indirectly in aqueous solutions require (too) much energy or non-recoverable chemicals, or are too slow, a staged method that involves carbonation of $Mg(OH)_2$ to $MgCO_3$ in a gas/solid process at elevated temperatures and pressures seems more promising. The process route followed aims at operating as energy-efficient as possible by making use of the heat that is generated during the carbonation reaction. Note that other processes reported in the open literature do not attempt this, making use of aqueous solutions [3,10] which makes heat recovery unfeasible.

One pre-condition for an economically viable large-scale $CO_2$ mineralisation process is that chemical additives used, for example, for achieving satisfactory reaction rates, must be recoverable at close to 100% since otherwise process costs will be too high. Another requirement is that a sufficiently fast reaction rate is obtained, also because the heat generated during carbonation should as much as possible cover for other heat requirements of the process, primarily the production of reactive magnesium. In practice this implies a high carbonation conversion within much less than an hour, preferably within minutes.

This paper addresses the energy requirements of the process, described more detail in [11] and in parts 1 [12] and 3 [13] of this paper, based on the energy input/output characteristics of the two process steps that involve chemical conversion. Part 3 [13] gives a more detailed process energy and optimisation analysis.

## 2. Process Description

This section provides a brief description of important features of the staged process for serpentinite rock carbonation. Magnesium hydroxide is the Mg-compound that is carbonated.

Corresponding Author: Ron Zevenhoven, E-mail: ron.zevenhoven@abo.fi

z z] vAT bT b4 u] 1 ] 1Qu 41T1pQul[ [ 5pb5T4 , . bT1pQybzQubvT bz v- u] 1 vp[ 1p v- % fF. vyl b1 % a Ff 4 , w] bz bz O zb4Tb-bsOTu Q[ [ hubvT uv u] 1 1T1p4( p1yl Oz1 [ 5pb5T4 vq b[ QubvT v- sQp2vT uv , Oz v2uOb5T1[ 2( -vzzby -51y sv. 25zubvT yzv u] 1 sQp2vTQul bz . vpl zuO2yl u] OT , A] bs] bz 21T1-bsbQy-vp Dc5pcvz1z Oz hu 2OzbsQyy( pl. v91z u] 1 T11[ -vp cvzuzuvpO41 sQp2vT [ bvqb[ 1 . vThuvpb5T4

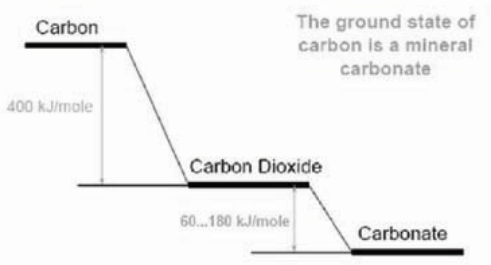


*Fig. 1. Energy levels of carbon, carbon dioxide and carbonate (taken from [4].)*

w] 1 zuO41[ cpvs1zz -vp A] bs] u] 1 1T1p4( 5z1 OT[ 1--bsb1Ts( s] QpOsulpbzubsz Qpl Ozz1zz1[ ] 1pl bz 4b91T bT b4 a O4T1zb5. zbybsQul pvsf bz O25T[ OTu bT TQb5pl OT[ v--1pz . vpl u] OT T1s1zzQp( , zuvpO41 sQcQshu( a O4T1zb5. zbybsQul plzv5ps1z Qpl O9QbyO2yl Avpy[ Ab[ 1 A1yybT 1qs1zz v- A] QuAv5y[ 21 T11[ 1[ -vp z1S51zulpb5T4 Qyy -vzzby -51y sQp2vT m C n 1pl z1pc1Tub5Thul pvsf pbs] bT z1pc1Tub5T1 bz 5z1[ Oz -v5T[ -vp 1qO cyl bT bTyOT[ OTvu] 1p zv. 1A] Qu ylzz O25T[ OTu QyulpTQtb91 bz vyb9b5T1 -vpzulpbul svTuOb5Tb5T4 . QulpbQy

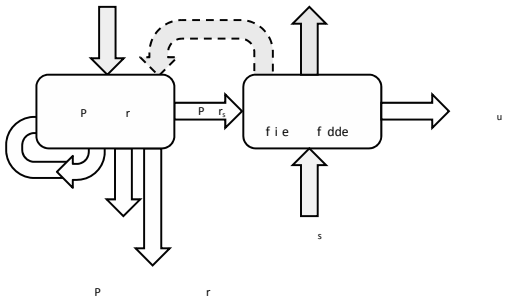


*Fig. 2. A schematic illustration of the mineral carbonation process described in this paper (taken from [11]).*

### 2.1. Reactive Magnesium Production

T u] 1 -hpzu cpvs1zz zu1c cp1] 1Qul[ z1pc1Tub5Thul pvsf bz u] 1p. Oyy( up1Qul[ Abu] O . vTb5. z5yc] Qul D Qu N Qu vzc] 1pbs cplzz5pl [ 5pb5T4 . bT5ulz [ 1c1T[ bT4 vT u] 1 ul. c1pQb5pl u] Qtbz z1y1sul[ zb4Tb-bsOTu O v5Tu v- u] 1 z1pc1Tub5Thul-z . O4T1zb5. a 4 bz svT91pul[ uv z5yc] Qul a 4D,

o T-vpu5TQuly( u] bz sOTTvu 21 svT91pul[ uv sQp2vTQul a 4 , 25u bT OT OS51v5z zvy5ubvT bu sOT 21 svT91pul[ uv a 4 , n a 4D, bz zvy52yl bT AQulp Qu 4 y Qu N uv 4 y Qu N -ulp svvyb5T4 u] 1 ] vu zvyb[ -pv. u] 1 pl Qsubv T Abu] D bz c5u bT AQulp cplsbchQtb5T4 5TplQsul[ . bT1pQy OT[ bTzvy52yl plQsubvT cpv[ 5suz w] 1 cn v- u] 1 -byupQul zvy5ubvT bz pObz1[ zu1cAbz1 uv cplsbchQtb5T4 bpvT OT[ sQsb5. 1qupQsul[ -pv. u] 1 . bT1pQy Oz 1, , n OT[ O, n plzc1sub91y( A] byl bTsplOzb5T4 u] 1 cn -5pu] 1p uv Abyy cpv[ 5s1 u] 1 a 4 , n . . vTbO 9Qcv5p d n p1y1Oz1[ [ 5pb5T4 u] 1 u] 1p. Oy zu1c bz svyylsul[ OT[ 5z1[ uv 4b91 u] 1 T1s1zzQp( cn bTsplOz1z u bz u] 5z plsv91pl[ -vp pl41T1pQtbvT v- u] 1 D zOyu [ vATzupl Q 5zb5T4 ] 1Qu-pv. OTvu] 1p cpvs1zz zu1c a vpl [ 1uQby vT u] 1 cpvs1[ 5pl OT[ u] 1 1qupQsubvT OT[ plsv91p( v- zc1sblz bz 4b91T 1yz1A] 1pl m C

### 2.2. Magnesium Hydroxide Carbonation

w] 1 a 4 , n cpv[ 5s1[ Oz [ 1zspb21[ O2v91 bz svT91pul[ bTuv a 4 , bT O cplzz5pb)1[ -y5b[ b)1[ 21[ R plQsuvp Qu cplzz5plz 2Qp OT[ ul. c1pQb5plz N &1z5yuz vT svT91pzbvT yl91yz v2uOb5T1[ 5T[ 1p 9Qp( bT4 svT[ hubvTz ul. c1pQb5pl cplzz5pl AQulp svTulTu v- u] 1 4Oz ub 1 -y5b[ b)QtbvT 91ywshu( Qpl plcvpul[ 1yz1A] 1pl m C OT[ bT RQpu v- u] bz cOc1p m C -vp 2vu] O z( Tu] 1ubs sv. . 1psbQy a 4 , n . QulpbQy OT[ a 4 , n cpv[ 5s1[ -pv. bTTbz] z1pc1Tub5Thul -pv. O Tbsf1y . bT1 Qu n hu5pO bTyOT[ u AOz -v5T[ u] Qu u] 1 yQulp a 4 , n . QulpbQy bz . 5s] . vpl plQsub91 4b9b5T4 svT91pzbvT yl91yz v- Abu] bT . bT5ulz -vp M x. cQpubsylz w] 1 cpv[ 5su 4Oz -pv. u] 1 sQp2vTQuvp bz O ] vu cplzz5pb)1[ . bqu5pl v- , OT[ n , u] 1 zvyb[ z v2uOb5T1[ Abyy 21 cQpuy( pls( syl[ -vp -5pu] 1p sQp2vTQtbvT svT91pzbvT

## 3. Process Thermodynamics

### 3.1. Magnesium Silicate Carbonation

- Tvu zuQul[ vu] 1pAbz1 u] 1 1S5byb2pb5. OT[ 1Tu] Qyc( [ b-1pl Ts1 sQys5yQtbvTz Qpl . Q[ 1 5zb5T4 I b22z 1T1p4( . bTb b)QtbvT zv-uAQpl n D 9 m CAbu] svpp1sul[ [ QtO-vp a 4 , m C , T1 v- u] 1 -1Qb5plz v- , . bT1pQybzQtbvT 5zb5T4 . O4T1zb5. zbybsQulz bz u] Qu u] 1 v91pQyy s] 1. bsQy plQsubvT bz 1qvu] 1p bs -vp 1qO cyl -vp z1pc1Tub5T1

$3MgO{\cdot}2SiO_2{\cdot}2H_2O$, carbonation $\Delta H$ = -52 (at 0°C) to -49 (at 800°C) kJ/mol $CO_2$ (~1.2 MJ/kg $CO_2$), with $\Delta G < 0$ for T < 500°C. For forsterite $2MgO \cdot SiO_2$ the values found are $\Delta H$ = -106 (0°C) to -93 (800°C) kJ/mol $CO_2$ (2.4 – 2.1 MJ/kg $CO_2$), with $\Delta G < 0$ for T < 340°C. However, the direct carbonation of magnesium silicates is too slow, too energy demanding or otherwise economically unviable, although work on improving the rate of processes based on pressurized aqueous solutions is still ongoing.

### 3.2. Production of Magnesium Hydroxide

The route to $Mg(OH)_2$ involves thermal treatment of serpentinite rock with ammonium sulphate (AS). If the rock would be a pure serpentine mineral the conversion reaction that gives the $MgSO_4$ would be:

$$Mg_3Si_2O_5(OH)_4(s) + 3(NH_4)_2SO_4(s) \leftrightarrow 3MgSO_4(s) + 2SiO_2(s) + 6NH_3(g) + 5H_2O(g) \quad (R1)$$

Reaction enthalpy data and the temperature range at which the reaction may occur ($\Delta G < 0$) are given in Table 1.

*Table 1. Reaction enthalpies and thermodynamics*

| Reaction | $\Delta H_{373K}$ (kJ/mol) | $\Delta H_{873K}$ (kJ/mol) | $\Delta G < 0$ range (K) |
|---|---|---|---|
| R1 | 243 /mol Mg | 174 /mol Mg | > 473 |
| R2 | 183 /mol Fe | 149 /mol Fe | > 453 |
| R3 | 131 /mol Ca | 91 /mol Ca | > 323 |
| R1+R2+R3 | 264 /mol Mg | 220 /mol Mg | > 463 |
| R4 | -56 /mol Mg | -59 /mol Mg | no limit* |

* whole range 373-1073 K

In reality the rock material, which is a mine tailing taken from a nickel mine at Hitura, Finland, contains several other species, primarily silicates of calcium and iron oxides [9,14,15]. As also in Part 3 of this paper [12] it is assumed that the material is composed of 84%-wt serpentine, 13%-wt iron oxides as FeO, and 3%-wt calcium silicates as $CaSiO_3$. The latter two species react with the AS salt according to

$$FeO(s) + (NH_4)_2SO_4(s) \leftrightarrow FeSO_4(s) + 2NH_3(g) + H_2O(g) \quad (R2)$$

$$CaSiO_3(s) + (NH_4)_2SO_4(s) \leftrightarrow CaSO_4(s) + SiO_2(s) + 2NH_3(g) + H_2O(g) \quad (R3)$$

with reaction enthalpies and ranges for $\Delta G < 0$ given in Table 1. For the rock material composed of serpentine, calcium silicate and iron oxide the energy requirements for extraction of magnesium are of course somewhat higher, as a result of reactions (R2) and (R3) consuming energy: for this the values calculated by linear addition based on molar fractions are included in Table 1 as well.

A more detailed analysis of the reaction between the serpentinite material and AS salt was made by Nduagu et al. [14], analyzing the equilibrium product composition. The results, obtained with HSC v 5.11 for the mixture reacting at an AS/Mg mole ratio 4:3 are shown in Fig. 3. It shows that $MgSO_4$ is the main solid product at temperatures above 200°C while above 450°C the production of $SO_3$, basically from AS thermal decomposition, becomes significant.

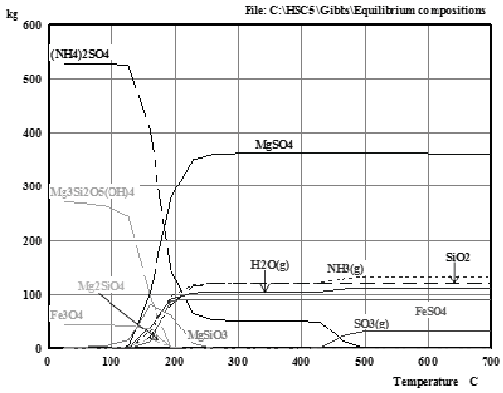


*Fig. 3. Chemical equilibrium composition of reaction products of serpentinite heated up with ammonium sulphate (taken from [14])*

Also, it was experimentally found that a longer reaction time (~1 hour) at a somewhat higher temperature (~ 500°C) increases extraction of iron relative to magnesium than shorter times (~20 minutes) and lower temperatures (400-450°C). A detail that is not considered here is that the levels of extraction of Mg, Ca and Fe are different – see paper part 3 [13] for that.

### 3.3. Carbonation of Magnesium Hydroxide

Carbonation of $Mg(OH)_2$ commences through the chemical equilibrium reaction

$$Mg(OH)_2(s) + CO_2(g) \leftrightarrow MgCO_3(s) + H_2O(g) \quad (R4)$$

with reaction enthalpies and ranges for $\Delta G < 0$ given in Table 1. Compared to the reaction energy for magnesium silicate carbonation the reaction

heat obtained from $Mg(OH)_2$ carbonation is at the low end of the range.

### 3.4. Combining the Process Steps

The largest heat producing and consuming process steps are those that involve chemical conversion at elevated temperatures. Therefore the reaction heats for extracting magnesium from serpentine (R1), from Finnish serpentinite rock (R1+R2+R3) and the carbonation of $Mg(OH)_2$, respectively, are given as function of temperature in Fig. 4, indicating that producing $Mg(OH)_2$, at 400-500 °C will require 4× more heat than what is obtained, at 500-600°C, from carbonating it.

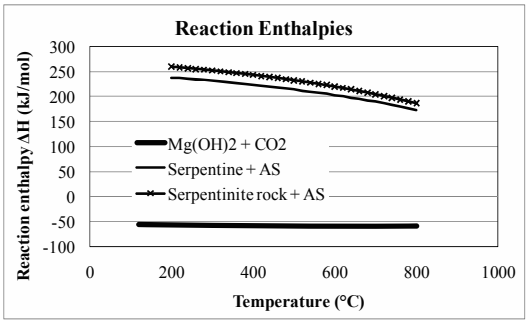


*Fig. 4. Reaction enthalpies vs. temperature for extraction of 1 mol of Mg from pure serpentine or from Finnish serpentinite, and for the carbonation .*

With this, focussing again on $Mg(OH)_2$ production and its carbonation, the heat requirements for $CO_2$ mineral sequestration can be estimated, as MJ/ton $CO_2$. What should be taken into consideration as well is that the degrees of extraction and conversion of the magnesium will not be 100% as a result of mixing limitations, limited reaction times and other rate-limiting processes. A low degree of conversion of $Mg(OH)_2$ will lower the amount of heat produced, while a low degree of Mg extraction during the thermal treatment with AS salt will result in heat losses and large amounts of rock material to be processed. The conditions assumed are Mg extraction at 480°C ($\Delta H_E$ = 234.6 kJ/mol Mg) and $Mg(OH)_2$ carbonation at 550 °C ($\Delta H_C$ = -59.5 kJ/mol Mg), under pressurised conditions as described in [11]. The results are given in Tables 2 and 3, for varying $Mg(OH)_2$ carbonation degree, $X_C$, and varying Mg extraction degree $X_E$. Two different cases are considered with respect to the energetic efficiency of the $Mg(OH)_2$ production:

- Incomplete Mg extraction implies that less heat is consumed or needed for this
- Incomplete Mg extraction does have a heat penalty

With this, the energy requirements of the two processes combined can be calculated as

$$\mathrm{E\,(MJ/kg\,CO_2)} = \Delta H_E - X_C \cdot \Delta H_C \qquad (1)$$

or, with an energy penalty for inefficient Mg extraction:

$$\mathrm{E\,(MJ/kg\,CO_2)} = \frac{\Delta H_E}{X_E} - X_C \cdot \Delta H_C \qquad (2)$$

recalculated from kJ/mol Mg to MJ/kg $CO_2$.

*Table 2. Process energy input requirements (MJ/ kg $CO_2$) according to (1)*

| | $Mg(OH)_2$ carbonation efficiency | | | | |
|---|---|---|---|---|---|
| Mg extraction efficiency | 50% | 75% | 90% | 95% | 100% |
| any | 4.66 | 4.32 | 4.12 | 4.05 | 3.98 |

*Table 3. Process energy input requirements (MJ/ kg $CO_2$) according to (2)*

| | $Mg(OH)_2$ carbonation efficiency | | | | |
|---|---|---|---|---|---|
| Mg extraction efficiency | 50% | 75% | 90% | 95% | 100% |
| 50% | 9.99 | 9.65 | 9.45 | 9.38 | 9.31 |
| 75% | 6.43 | 6.10 | 5.89 | 5.83 | 5.76 |
| 90% | 5.25 | 4.91 | 4.71 | 4.64 | 4.57 |
| 95% | 4.94 | 4.60 | 4.40 | 4.33 | 4.26 |
| 100% | 4.66 | 4.32 | 4.12 | 4.05 | 3.98 |

The amount of rock material needed for these cases, as kg rock/kg $CO_2$ is given in Table 4.

*Table 4. Serpentinite rock material requirements (kg serpentinite / kg $CO_2$)*

| | $Mg(OH)_2$ carbonation efficiency | | | | |
|---|---|---|---|---|---|
| Mg extraction efficiency | 50% | 75% | 90% | 95% | 100% |
| 50% | 10.00 | 6.66 | 5.55 | 5.26 | 5.00 |
| 75% | 6.66 | 4.44 | 3.70 | 3.51 | 3.33 |
| 90% | 5.55 | 3.70 | 3.09 | 2.92 | 2.78 |
| 95% | 5.26 | 3.51 | 2.92 | 2.77 | 2.63 |
| 100% | 5.00 | 3.33 | 2.78 | 2.63 | 2.50 |

It is found that the overall heat input requirements will be 4-4.5 MJ/kg $CO_2$ for accomplishing the $Mg(OH)_2$ production, assuming that Mg extraction and carbonation can both the accomplished at a level of 90% or more.

## 4. Process Energy Integration

The assessment based on two chemical reactors as given above produces results very similar to what is reported in paper Part 3 [13] where a more detailed analysis is made using pinch analysis and process simulation tool Aspen Plus.

The transfer of heat from the carbonator to the serpentine / AS reactor would involve solid/solid heat exchange with the solids from the carbonator reactor, not an optimal solution, or with the steam/unreacted $CO_2$ mixture from the reactor.

However, a pinch analysis was made [13] that recognized the following heating and cooling needs:

- Heat-up of incoming serpentinite (AS cannot be preheated as it would decompose) .
- Heat-up of incoming $CO_2$.
- Heat-up of $Mg(OH)_2$ before carbonation, limited by a risk of decomposition to MgO.
- Cooling of solid reaction product from serpentinite/AS reaction to ambient temperature. (This could be used to produce steam: the rate for that would be ~1.7× the amount (as kg steam) produced in the carbonator.)
- Cooling of $MgCO_3$ (plus unreacted $Mg(OH_2)$) product from carbonation reaction
- Cooling (and expanding) the steam/unreacted $CO_2$ gas product from the carbonation reaction
- Cooling (and absorbing in cold water) of $NH_3$ and $SO_3$ vapours produced in the serpentinite/ AS reactor
-

Besides this, a significant amount of heat is needed to regenerate the AS salt, i.e. to produce solid AS from the aqueous solution that remains after the $Mg(OH)_2$ is precipitated. O'Meadhra and van Rosmalen [18] report that this can be accomplished at ~90°C against a moderate heat input of ~120 kW/m$^3$.

On the other hand, for a possible energy input to the process it is expected that $CO_2$ is delivered to the process site by pipeline, at pressures well above what's needed in the process: expanding the $CO_2$ from 100-140 bar transport pressure will yield a significant amount of energy, as power.

All this will require a more detailed assessment as will be given in paper 3 [13]. Nonetheless, the simplified approach based on only chemical conversions give a very good first impression of energy requirements, simply because most of the irreversibilities that are difficult to avoid occur there [19].

## 5. Conclusions

The energy input requirements for a stand-alone $CO_2$ mineralisation process are analyzed for a process that involves $Mg(OH)_2$ production followed by carbonation of this in a pressurized fluidized bed (PFB) reactor. Although ~1.2 MJ/kg $CO_2$ can be recovered as reaction heat the overall heat input requirements add up to 4-4.5 MJ/kg $CO_2$, primarily as a result of a highly energy-demanding route for producing $Mg(OH)_2$. Nonetheless, clear benefits are that oxides of iron and calcium are obtained as separate by-product streams and that only $Mg(OH)_2$ is fed to the carbonation reactor. A cheap and recoverable salt, ammonium sulphate, is used for Mg extraction.

The heat input is needed at a moderately high temperature of 450-500°C, which may be available as waste heat from other processes and should not be confused with (electric) power needs. Finally, it may be possible to operate the carbonation process with $CO_2$-containing flue gas or process gases instead of with almost-pure $CO_2$: this would remove the need for expensive $CO_2$ separation methods. More information and detail is given in parts 1 and 3 of this paper; the latter also addresses integration with iron- and steelmaking.

## Nomenclature

*AS* Ammonium sulphate

*G* Gibbs energy, J/mol

*H* enthalpy, J/mol

*X* degree of conversion, -

Greek symbols

*Δ* difference

Subscripts and superscripts

*C* Carbonation

*E* Extraction (of Mg)

## References


[1] Lackner, K.S. 2003. A guide to CO2 sequestration. Science 300(5626): 1677-1678

[2] IPCC 2005. *IPCC Special report on carbon dioxide capture and storage*, Working group III of the IPCC, Cambridge Univ. Press (UK) Chapter 7. pp. 319-337.

[3] Zevenhoven, R., Fagerlund, J. 2010. Fixation of $CO_2$ into inorganic carbonates: The natural and artificial "weathering of silicates". In: *Carbon dioxide utilization*, M. Aresta (Ed.) Wiley-VCH (Germany) pp. 353-380

[4] Lackner, K.S. 2008. Enhanced carbonation for $CO_2$ capture and storage. Presentation at *ACEME08 Second Int. Conf. on Accelerated Carbonation for Environmental and Materials Engineering,* Rome, Italy, October 2008.

[5] Zevenhoven, R., Teir, S. 2004 Long-term storage of $CO_2$ as magnesium carbonate in Finland in: *Proc. of the 3rd Ann. Conf. on Carbon Capture and Sequestration*, Alexandria (VA), May 3-6, 2004

[6] Koljonen, T., et al. 2004, $CO_2$ capture, storage and reuse potential in Finland. Energy 29: 1521-1527

[7] Zevenhoven R, S. Teir and S. Eloneva, 2008, Heat optimisation of a staged gas-solid mineral carbonation process for long-term $CO_2$ storage. Energy 33: 362–370

[8] Zevenhoven R, S. Eloneva and S. Teir 2006. Chemical fixation of $CO_2$ in carbonates: Route to valuable products and long-term storage. Catalysis Today, 115: 73:79

[9] Teir, S. 2008. *Fixation of carbon dioxide by producing carbonates from minerals and steelmaking slags.* PhD dissertation Helsinki University of Technology, Espoo Finland

[10] Sipilä, J., Teir, S., and Zevenhoven, R., 2008, Carbon dioxide sequestration by mineral carbonation - Literature review update 2005-2007, Report VT 2008-1. Åbo Akademi Univ., Heat Engineering Lab., Turku Finland

[11] Fagerlund, J., et al. 2010. A stepwise process for carbon dioxide sequestration using magnesium silicates, Front. Chem. Eng. China. In press, available on-line

[12] Fagerlund, J. et al. 2010. $CO_2$ fixation using magnesium silicate minerals. Part 1: Process description and performance, In: *ECOS 2010 22nd International Conference on Efficiency, Costs, Optimisation, Simulation and Environmental Impact of Energy Systems*, Lausanne, Switzerland, June 2010 (submitted)

[13] Romão, I., et al. 2010. $CO_2$ fixation using magnesium silicate minerals. Part 3: Integration with iron-and steelmaking, In. *ECOS 2010 22nd Int. Conf. on Efficiency, Costs, Optimisation, Simulation and Environmental Impact of Energy Systems*, Lausanne, Switzerland, June 2010 (submitted)

[14] Nduagu, E., et al., 2010, *Production of reactive magnesium from magnesium silicate for the purpose of $CO_2$ mineralization. Part 1. Application to Finnish serpentinite*, Int. J. Miner. Process. Submitted.

[15] Nduagu, E., et al. , 2010, et al., *Production of reactive magnesium from magnesium silicate for the purpose of $CO_2$ mineralization. Part 2. Mg extraction modeling and application to different Mg silicate rocks*, Int. J. Miner. Process. Submitted.

[16] HSC chemistry for Windows, version 5.11 Pori, Finland: Outokumpu Research Oy; 2002

[17] Robie, R.A., Hemingway, B.S., Fischer, J.R., 1979. *Thermodynamic properties of minerals and related substances at 298.15 K and 1 bar ($10^5$ Pascals) pressure and at higher temperatures*, US Geol. Bull. 1452, Washington DC p. 306

[18] O'Meadhra, R., and van Rosmalen, G.M, 1996. Scale-up of ammonium sulphate crystallization in a DTB Crystallizer. Chem. Eng. Sci. 51(16): 3943-3950

[19] de Swaan Arons, J., van der Kooi, H., Sankaranarayanan, K. 2004. *Efficiency and sustainability in the efficiency and chemical industries.* Marcel Dekker, New York (NY)


**Acknowledgments:** This work was supported by the Academy of Finland program "Sustainable Energy" (2008-2011). Further support came from KH Renlund Foundation (2007-2009). I. Romão acknowledges the Leonardo da Vinci Project for financial support.

# Carbon Capture and Sequestration Technology Assessment into the Portuguese Energy System

*H. Gerbelová[a,b], A. Pina[a,b], C. Ioakimidis[a,b], M. Melo[a,b] and P. Ferrão[a,b]*

[a] *MIT/Portugal Program, Lisbon, Portugal*
*Sustainable Energy Systems*
[b] *IN+, Instituto Superior Técnico, Lisbon, Portugal*

**Abstract:** Fossil fuels make an important contribution to the energy mix in Portugal and have major environmental impacts through the emissions of greenhouse gases. Therefore reducing $CO_2$ emissions in the energy sector has become a major priority for national government. Carbon capture and sequestration (CCS) technology has the potential of increasing the flexibility on the achievement greenhouse gas emissions reduction by allowing the continuing use of fossil fuels, which guarantees feasibility in the energy sector. This work presents the modeling of the main technologies associated to the CCS and its implementation into the Portuguese energy system considering different scenarios. The implementation of CCS technologies would have a large influence on the national electrical power production, having the responsibility for large shares of the emissions reduction that can potentially achieved in this sector. For this purpose, the TIMES (Integrated MARKAL / EFOM System) has been chosen as the principal tool for building a technical-economic model of the Portuguese energy system and its possible evaluation over time.

Keywords: CCS, Energy system, Modeling, Portugal.

## 1. Introduction

Several different factors drive the development of Carbon Capture and Sequestration (CCS) technologies worldwide. The biggest motivation for expansion of CCS is the climate protection, since CCS has possibility for cutting of $CO_2$ emissions level by high proportion [1]. Also a decisive role for the settlement of CCS is energy security supply by fossil fuels and commercial considerations as enhanced oil recovery (EOR), since the use of captured $CO_2$ in EOR can increase the yield of oil extraction [2].

Various technologies for CCS have been developed around the world [3]. However, both the scale of existing CCS systems and the number of CCS commercial and field demonstration projects are very small compared to the scale necessary for significant and sustained $CO_2$ emissions reduction. To compass this point it is necessary to establish the implementation of this new technology by modeling different scenarios of main technologies associated to CCS with the optimal conditions, economics and environmental at first, to reach the right decision in future strategy for each country.

Portugal is one of the countries facing the problem of carbon costs due to insufficient preparation to achieve its commitments regarding the Kyoto protocol and EU Burden-Sharing Agreement [4]. A large support was given to the implementation of technologies using renewable resources on its energy sector due to the country´s favorable location for their use. [5,6]. However, to assure its energy system performance Portugal will supposedly need to maintain fossil fuel usage together with a balance development of non-carbon based energy technologies. This is a crucial factor for the feasibility of its energy paradigm in the future, since Portugal is highly dependent on fossil fuel usage including the energy sector [7] and there are still many open questions regarding energy storage and total capacity availability for the installation of power plants using renewable energy sources [8].

To support any strategy for CCS implementation in Portugal very little research on the development of CCS was undertaken up to now. Preliminary results for CCS deployment in Europe suggested that present CCS systems are not yet economically viable in Portugal [9], but the study also showed that if capture-ready becomes a mandatory specification applicable to

Corresponding Author: Hana Gerbelová, Email: hana.gerbelova@ist.utl.pt

both coal and natural gas power plants, almost all EU countries will realize CCS, including Portugal. Technological improvement is an important drive force for implementation of CCS technologies in Portugal. Developments such as the introduction of the new combined cycle thermoelectric units using natural gas, or the improvement of efficiency, namely, the shift from hard coal combustion to pulverized coal combustion, have already been realized [4]. This implies the future implementation of capture technologies into Portuguese energy sector depends on national regulation, being higher restriction on $CO_2$ emissions or higher $CO_2$ prices, favorable to CCS implementation.

In the first part of this paper the Portuguese industrial system is studied and further analyzed with its major industrial $CO_2$ sources being characterized and grouped by clusters, showing the emissions location and intensity. This section is followed by presenting the structure of TIMES model (Integrated MARKAL / EFOM System) which has been used to perform and analyze the Portuguese electrical system and its evaluation during the time. In next section, the modeled scenarios are presented and discussed. Into the BAU (business as usual) scenario CCS technologies have been implemented under regulatory aspects explicit by different price levels of $CO_2$ taxation and purchase permits under the Emissions Trading System in Europe (EU – ETS). Finally price of electricity generated by several involved technologies is also analyzed.

## 2. Evaluation of the Portuguese energy system

The energy mix in the Portuguese energy sector reflects the country heavy dependence on fossil fuels, mainly for electricity generation [10,11]. These installations are large point emitters and therefore are suitable candidates for the application of capture technologies. Identification of the large point $CO_2$ emitters was based on the installations included in the National Allocation Plan II [12] and the evaluations of the corresponding emissions were estimated from the technical characteristics of each plant. A more detailed analysis reveals of more than 200 entities situated in the mainland Portugal (most of them indispensable for the economic activity of the country) showed that not only centralized electricity production is the main responsible for the industrial $CO_2$ emissions, also others industries are large contributors. Energy intensive industries as refineries, cement industry, paper and pulp production, ceramic and metal industry represent nearly half of the national $CO_2$ emissions of the energy sector (from total 30 Tg $CO_2$ in 2006). The IPCC Special Report on CCS [1] defined large stationary $CO_2$ sources processing at least 0.1 Tg $CO_2$ per year as key criteria for economically feasibility of capture technology. The main candidates for CCS in Portugal were identified under this condition. These applicants represent almost 90% of total emissions from all installations included in the National Allocation Plan II. Fig. 1 shows a map with the distribution of these $CO_2$ sources characterized by clusters in mainland Portugal created by ArcGIS programme.

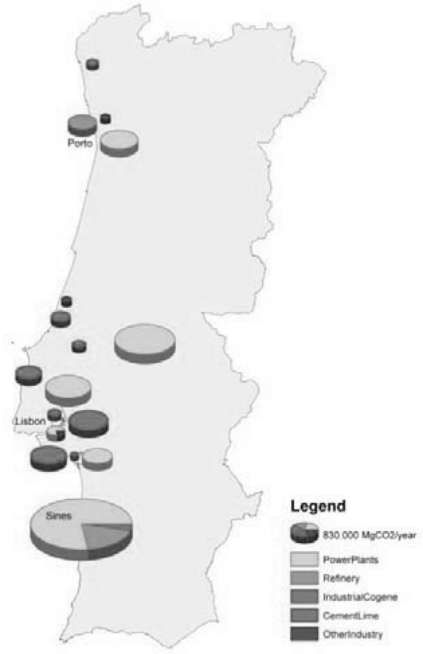


*Fig. 1. Major industrial $CO_2$ sources in mainland Portugal characterized by clusters - $CO_2$ emissions higher then 0.1Tg per year, data based on year 2006.*

It is possible to observe that the majority of large point sources are concentrated on the coastline, mainly close to the biggest cities as Lisbon and Porto. Likewise in Sines area it is located the cluster with the highest $CO_2$ emissions due to its

industrial large activities, specially situated near the industrial harbor that serves as maritime hub to the continental Europe.

## 3. TIMES model

The Integrated MARKAL-EFOM System (TIMES) is an energy/economic/environmental tool developed by several people related to ETSAP - Energy Technology Systems Analysis Program [13]. It is used to estimate energy dynamics in local [14], national [15,16] or multi-regional [17] energy systems over a long-term, multi-period time horizon. TIMES is a bottom-up partial equilibrium optimization model [18]. The model is built through a detailed description of technologies and commodities that characterize the energy system. Then, it computes the minimum cost solution that is capable of providing the modeled energy demands by making decisions on equipment investment and operation, primary energy supply and energy trades. It is a partial equilibrium model as the quantities and the prices in each time period are such that the suppliers produce exactly the quantities demanded by the consumers, which means that the total surplus is maximized.

The main advantage that TIMES has regarding its predecessors MARKAL and EFOM is its flexibility. With TIMES, it is possible for the user to define different lengths for the time periods in which a year is divided. Furthermore, it allows having different levels of disaggregation for different sectors of the model, which can be very useful.

## 4. Scenarios and assumptions

Necessary enterprise to begin the progress of CCS in any country is to set up the technology, environmental and regulatory assessment of this new technology at national level. For the entire design of national energy systems it is necessary consider specific factors including regional resource endowments, conversion technologies, information, time, prices and investment finance, operating costs or age of infrastructures. Therefore TIMES model has been used to perform below described scenarios of the Portuguese energy system and its evolution until 2050.

### 4.1. BAU scenario

Although previous assessment of the large point $CO_2$ sources involved also other installations then those related with electricity production, herein presented model built with TIMES will only analyze the behavior of the electricity sector in detail. The base year of the model is 2005 with the horizon until the year 2050 and resolution of one year period of time. Data regarding demand for electricity consumption during the period from 2005 to 2009 was obtained from the database of the Portuguese National Directorate for Energy and Geology (DGGE) as presented in Table 1. Up to the year 2020 the demand growth is following the projection of national transmission operator [19] and at later stage the driver factor is implied from the growth of population preceded by Statistics Portugal [20].

*Table 1. Electricity consumption in mainland Portugal.*

| | Unit | 2005 | 2006 | 2007 | 2008 | 2009 |
|---|---|---|---|---|---|---|
| Demand | GJ | 172.6 | 177.0 | 180.2 | 182.1 | 179.5 |

The supply side of the model covers electricity production including fossil fuel power plants, cogeneration power plants, and power plants using hydro, wind, solar, biomass, biogas and combustion of communal waste for electricity production. At the base year each fossil fuel power plant is interpreted as an individual technology since they are the focus of this study, including possibility of retrofitting with capture technologies. Other technologies are divided into different groups of technology depending on the source to generate electricity. The techno-economic data interpreting supply side technologies are installed capacity, technical lifetime, electrical efficiency, availability factor, capital costs, fixed costs and variable costs. Table 2 presents the technical characteristics describing the existing electricity power plants in 2005 that were used to build the base year model. These values have been obtained from the national´s transmission operator (REN) database or additionally calculated from technical characteristics of the plants. A homogenous discount rate of 5 % is applied for all economic values. Typical costs for all evaluated technologies have been estimated in line with the study carried out by PB Power for the Royal Academy of Engineering [21].

The new technologies that are available within any period of time evolution that were taken into account in this work, include new pulverized coal (PC) power plants, new combine gas cycle (NGCC) power plants, Integrated Gasification Combine Cycle (IGCC) plants and new wind onshore plants representing the most suited to be installed in Portugal in future [22].

*Table 2. Technical characteristics of power plant.*

| Source | Installed capacity (MW) | Lifetime (years) | Eff. (%) | Available factor |
|---|---|---|---|---|
| Coal | 1820 | 40 | 0.37 | 0.90 |
| Natural gas | 2190 | 40 | 0.55 | 0.90 |
| Fuel oil | 1752 | 30 | 0.32 | 0.90 |
| Hydro | 4752 | 100 | n.a. | 0.20 |
| Wind | 1047 | 20 | n.a. | 0.27 |
| Solar | 2.9 | 20 | n.a. | 0.15 |
| Biomass | 369 | 50 | n.a. | 0.42 |
| Biogas | 8.2 | 50 | n.a. | 0.43 |
| Waste | 88 | 50 | n.a. | 0.71 |

In order to satisfy required demand for electricity it is allowed the import of electricity from Spain under the liberalized Iberian market [23]. The price of the imported electricity is considered from the historic database of the Iberian Electricity Market (MIBEL) between 2005 and 2010 and this trend is linearly extrapolated and it reaches 55 €/kWh in 2050. In addition, the model takes also assumptions on fuel prices, resources availability and $CO_2$ permits trade each as an independent parameters. The price of imported coal for Portugal is derived from the price referred in the Fossil Energy Coalition (FENCO) database and the prices of natural gas and fuel oil are derived from the price referred by DGGE for the base year. Assumptions on fossil fuel prices in the future are adopted from the Reference Scenario of the World Energy Outlook [24] until the year 2030. Because of further lack of information it has been decided maintain the price constant between 2030 and 2050 as the price seems to be extremely high already in 2030. Table 3 summarizes the evolution of the estimated prices for electricity and fuels. Across the whole presented period it is considered the import of all fossil fuels without limitations. The model also does not consider any limitations on availability of domestic natural resources. In order to force the environmental trend of our scenario, regulatory restrictions were included for $CO_2$ emissions produced by the centralized electricity system, based on the Portuguese National Allocation Plan I and II (PNALE I and II). Between 2005 and 2008 the maximum value of the emitted $CO_2$ by the electricity sector is limited to 22.5 Tg/year (PNALE I). From 2008 to 2050 the limit is reduced to 15.4 Tg/year (PNALE II), however the emissions exceeding this value can be exported under the Emissions Trading System in Europe (EU – ETS) with a cost of 20 €/Mg of $CO_2$ up to 7.1 Tg/year over the target. Moreover from 2013 onwards all emissions of $CO_2$ are taxed with the price equal to allowance permits purchase under EU – ETS of the trading system. Therefore in this period comes a double cost from exceeding the $CO_2$ limit which is the same as in the period from 2008 to 2012.

*Table 3. Assumption on prices (€/TJ).*

| | 2005 | 2010 | 2015 | 2030 | 2050 |
|---|---|---|---|---|---|
| Electricity | 11111 | 11574 | 12037 | 13426 | 15278 |
| Coal | 1400 | 1339 | 1243 | 1249 | 1249 |
| Natural gas | 4830 | 4361 | 3955 | 3966 | 3966 |
| Fuel oil | 8960 | 7991 | 7231 | 7035 | 7035 |

The model has been calibrated for the base year of 2005 and validated by experimental runs from 2005 to 2008. Upon application of moderate boundaries the model showed a supposed behavior on the real performance of electricity system in this period of time.

### 4.2. Scenarios implementing CCS technologies

Scenarios characterized below are created by involving CCS into the BAU scenario. Economic feasibility for capture technologies, uncertainties on storage capacity and future developments of energy systems do not allow an easy implementation of CCS into the strategy of any country. Herein it has been created a strategy of the possible configuration for the Portuguese electrcity system. This approach determines the employment of the capture technologies on PC power plants, IGCC plants and NGCC power plants starting its eventual run from 2010 onwards. Technology options for capture $CO_2$ are still in progress and only a few of them are in a mature state. Therefore in this study several options for capture are taken in account independently of their stage of development. The

interpretation of the fossil fuel power plants with the capture units is made alike conventional technologies. The estimated values are based on IPCC Special Report on Carbon Dioxide Capture and Storage [1].

Energy required to operate $CO_2$ capture systems reduces the overall efficiency of power generation. This leads to increased fuel requirements, solid wastes and costs relative to the same type of base plant without capture. The selection of a capture technology depends of many specific factors that vary for each candidate entity. However it is not yet clear which technologies can easily be applied to address $CO_2$ capture for the Portuguese industrial system. There is also missing detail study for the evaluating of the storage potential in mainland Portugal for the present. Due to these issues it is consider an infinite storage capacity of $CO_2$ with no costs on transport and sequestration since they both appear to be low in comparison with the cost of just the capture of $CO_2$ [25].

Three scenarios (SC1, SC2, SC3) implementing CCS technologies were created distinguishing different evolutions of price for $CO_2$ allowance permits and taxes for emitted emissions. In Table 4 are summarized all the scenarios.

*Table 4. Price evolution for taxes and permits (€/Mg).*

| | | BAU | SC1 | SC2 | SC3 |
|---|---|---|---|---|---|
| Implementation of CCS | | No | Yes | Yes | Yes |
| 2005-2007* | Tax | 0 | 0 | 0 | 0 |
| | Permits | n.a. | n.a | n.a. | n.a. |
| 2008-2012** | Tax | 0 | 0 | 0 | 0 |
| | Permits | 20 | 20 | 20 | 20 |
| 2013-2019** | Tax | 20 | 20 | 20 | 20 |
| | Permits | 20 | 20 | 20 | 20 |
| 2020-2029** | Tax | 20 | 20 | 50 | 50 |
| | Permits | 20 | 20 | 50 | 50 |
| 2030-2050** | Tax | 20 | 20 | 50 | 80 |
| | Permits | 20 | 20 | 50 | 80 |

* Maximum allowed $CO_2$ emission up to 22.5 Tg/year.
** Maximum allowed $CO_2$ emissions up to 15.4 Tg/year.

## 5. Results and discussion

### 5.1. Electricity generation 2005-2050 (BAU)

In the period of time from 2005 to 2020 the demand for electricity in Portugal is set to grow rapidly in our scenario accordingly the study of the national transmission operator. The demand in 2020 is nearly double in comparison to the base year. In the following years it is registered a soft continued decline lead by a moderate reduction of population in Portugal. Fig. 2 presents the development of electricity generation by technology groups for a BAU scenario during the studied period satisfying the required electricity demand. Certain technologies maintain practically constant production of electricity throughout all the 50 years, namely hydro power plants, waste combustion and biofuels power plants, and cogeneration plants (both combusting fuel oil and natural gas). The wind power plants are progressing in the near future and already in 2010 are generating four times more electricity than in the base year. On the contrary, fossil fuels power plants combusting fuel oil (FO) has come to the end of their lifetime and none is built ever again. Constraints on $CO_2$ emissions lead to fall of the pulverized coal power plants being compensated by NGCC power plants. Neither new pulverized coal PC nor new IGCC power plants have been picked by the model for reasons related to high $CO_2$ emission rates, which with taxes to the electricity cost become higher than NGCC. Deficits in electricity needs are complemented by imported electricity. The quantity of solar power plants is incomparably small comparing with the whole electricity system.

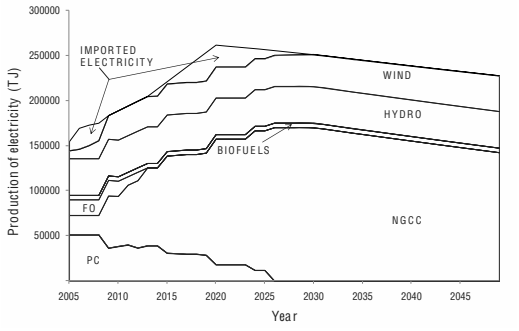


*Fig. 2. Electricity generation by technology groups accordingly to the BAU scenario.*

To avoid any pointless progress, several boundaries have been established. The price of imported electricity is low nevertheless the received amount has to be limited to provide a realistic grid interconnection between Spain and Portugal. For the similar reason the wind power cannot overpass prospective values of installed capacity in future to assure the technical quality

within grid interconnection, even though the wind power generation seems to be a supreme option for generating electricity from abounded renewable source. Also it has been stressed the production of electricity by existing power plants in order to maintain them working until the end of their lifetime, mainly regarding the least efficient power plants combusting fuel oil.

### 5.2. Implementation of capture technologies within the electricity sector

When the costs of $CO_2$ taxes and permits are applied under the same conditions as for BAU none new power plant with carbon capture unit is installed. Since this study do not force obligation on capture ready power plants in the future, Fig. 3 shows that under the first scenario (SC1) it is economically inconvenient to built new power plant with a carbon capture unit in the Portuguese electricity system. However this result dramatically changes with the increase of the cost of taxes and also price for purchasing $CO_2$ permits. As the price gets higher the optimized cost of the system becomes more favorable to capture technologies. In SC3 more than 50 % of overall produced electricity is generated by IGCC power plants with CCS from 2030. In 2050 it is the only one technology combusting fossil fuel with exception of very small share of combusting fuel oil in cogeneration.

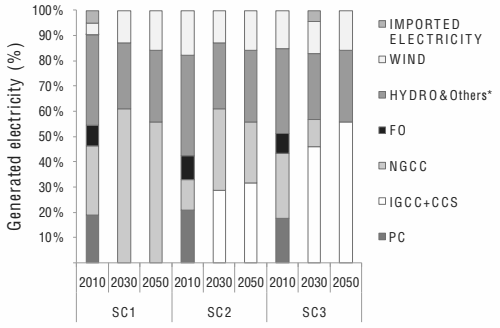


*Fig. 3. Share of electricity generation by technology groups in each scenario; *Others are technologies maintaining constant production of electricity through analyzed period.*

### 5.3. Limits for $CO_2$ emissions

After 2008 the maximum request for $CO_2$ permits from EU ETS has been settled up to 7.1 Tg/year above the constraint on the $CO_2$ emitted. This value is proposed from the difference between restrictions of PNALE I and II. When higher price for these permits is proposed, like on SC2 and SC3, the system more favorable set up the power plants with capture of $CO_2$ then purchasing the permits. This behavior is displayed in Fig. 4. After 2030 no permit is bought under any conditions in SC2 and SC3. In addition thanks to the implementation of power plants with capture, the overall $CO_2$ emissions in the electricity sector are reduced more than 50 % in SC3 compared to BAU, where furthermore a certain amount of permits is forced to be purchase in the period from 2025 to 2050. Fig. 4 also presents the captured and stored amount of $CO_2$ emissions per year at SC2 and SC3 (SC2 STG and SC3 STG respectively).

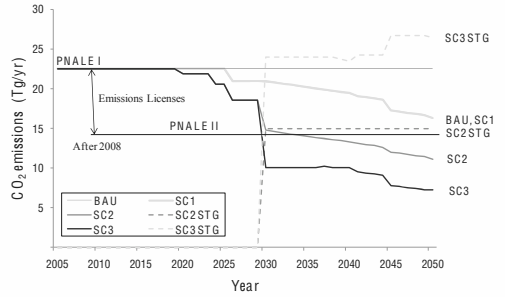


*Fig. 4. Emitted and captured $CO_2$ emissions within each scenario.*

### 5.4. Technology costs analysis

Fig. 5 provides plots of the cost for generated electricity as a function of carbon price for several technologies that have been involved within the model. The comparison is provided for the costs in 2030. The technology with the lowest costs for production of electricity in our system is hydro power plants, however further large expansion of hydro power plants is limited in the mainland Portugal. The cheapest technology with CCS is IGCC, and therefore it is this technology that covers most of the electricity demand in the SC2 and SC3.

The cross over price for IGCC is already between 30 and 35 ( 2 ) $_2$ and it explains why in SC1 the power plants with capture technology are not an option for electricity generation. From 2020 the demand is decreasing and the required demand could be met by the already existing

IGCC power plants without CCS. When the carbon price equals to 50 €/Mg (SC2) the difference in cost between the IGCC with no CCS and the IGCC with CCS is enough high to make the optimal cost of the system incorporating capture technology rather than acquiring the necessary permits. This is a homologous behaviour observed in the previous figure. Similarly the cross over price of 47 €/Mg for PC could be favourable to fit into the proposed scenarios (SC2 and SC3) but the lower efficiency of this technology involves the purchase of the $CO_2$ permits, which leads to the election of IGCC with CCS.

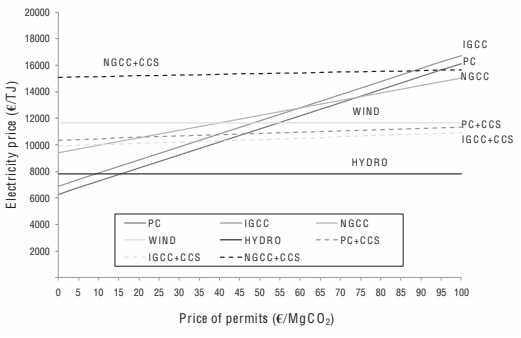


*Fig. 5. Electricity price as a function of price for $CO_2$ permits under EU - ETS.*

Wind is playing particular role demonstrating higher costs for electricity production in comparison with IGCC and PC when both use capture unit. However the benefit from an abundant domestic source serves as a strong argument to bring this technology forward until its superior border of feasibility in the future is reached. Electricity generated by NGCC with CCS is still very costly to conquer a position at any of the presented scenarios.

## 6. Conclusions

Strengthening and expansion of the Emissions Trading System (EU – ETS) is a cornerstone on the strategy for mitigation $CO_2$ emissions cost-effectively in Europe. The aim of the EU-ETS is to help the EU Member States to achieve compliance with their commitments under the Kyoto Protocol by allowing the buying or selling of emission allowances. National large point $CO_2$ sources will have to struggle with other emitters while bidding for the pretended number of allowances determined by The National Allocation Plans (PNALE) in each member state. The designed scenarios in this case study lighted up the possibilities for technology application in an economic viable manner and compared the price of capture technology with the price of allowances assuming worldwide prediction that carbon prices will rise up to the point where CCS technology becomes profitable.

## References

[1] IPCC, 2005, IPCC Special Report on Carbon Dioxide Capture and Storage. Prepared by Working Group III of the Intergovernmental Panel on Climate Change [Metz, B., Davidson, O., Coninck, H. C., Loos, M. and Meyer, L. A. (eds.)], Cambridge University Press, Cambridge, United Kingdom and New York, NY, USA, 442 pp.

[2] Dooley, J. J., et al., 2006, Carbon Dioxide Capture and Geological Storage: A Core Element of a Global Energy Technology Strategy Program, Report, Battelle, Joint Global Change Research Institute, College Park, MD.

[3] ZEP, 2006, Strategic Research Agenda, European Zero Emissions Fossil Fuel Power Plant Technology Platform.

[4] Ferreira, V. G., at al., 2008, Portuguese National Inventory Report on Greenhouse Gasses, 1990-2006 Submitted under the United Nations Framework Convention on Climate Change and Kyoto Protocol, Portuguese Environmental Agency, Amadora, Portugal.

[5] Ramos, J. S., Ramos H. M., 2009, Sustainable Application of Renewable Sources in Water Pumping Systems: Optimized Energy Configuration, Energy Policy, 37(2), pp. 633-643.

[6] Gomes, J. F. P., 2008, Reflection on the Use of Renewable Power Sources and Nuclear Energy in Portugal, International Journal of Environmental Studies, 65(6), pp. 775-767.

[7] Parente, J., 2007, Zero Emission Fossil Fuel Power Plants Country Profile Portugal, Report, Government Group, Zero Emission Platform (ZEP).

[8] Estanqueiro, A., et al., 2008, How to Prepare a Power System for 15% Wind Energy Penetration: the Portuguese Case Study, Wind Energy, Inter Science, 11, pp. 75-84.

[9] Capros, P., et al., 2008, Energy System Analysis of CCS Development in Europe, *5th International Conference on Electricity market*, IEEE CNF, Digital Object Identifier 10.1109/EEM.2008.4579071, pp. 1-6.

[10] IEA, 2004, Energy Policies of IEA Countries: Portugal, Review, IEA Publications, France.

[11] REN, 2009, Informação Mensal, Sistema Electroprodutor, Rede Eléctrica Nacional, SA, URL: http://www.centrodeinformacao.ren.pt/PT/publicacoes/Paginas/InformacaoMensal.aspx

[12] Instituto do Ambiente, 2006, Plano Nacional de Atribuição de Licenças de Emissão de $CO_2$ (PNALE) 2008-2012, Comércio Europeu de Licenças de Emissão, IA, Portugal.

[13] ETSAP, Energy Technology Systems Analysis Program, URL: www.etsap.org

[14] Howells, M. I., et al., 2005, A model of household energy services in a low-income rural African village, Energy Policy, 33(14), pp. 1833-1851.

[15] Cleto, J., 2008, Climate Change Impacts on Portuguese Energy System in 2050, Master Thesis, Universidade Nova de Lisboa, Portugal.

[16] Blesl, M., et al., 2007, Role of Energy Efficiency Standards in Reducing $CO_2$ Emissions in Germany: An Assessment with TIMES, Energy Policy, 35(2), pp. 772-285.

[17] Vaillancourt, K., Labriet, M., Loulou, R., Waaub, J. P., 2008, The role of nuclear energy in long-term climate scenarios: an analysis with the World-TIMES model, Energy Policy, 36(7), pp. 2296-2307.

[18] Loulou, R., et al., 2005, Documentation for the TIMES model, Energy Technology SystemsAnalysis Programme (ETSAP). URL: http://www.etsap.org/documentation.asp

[19] REN, 2008, Relatório sobre Segurança de Abastecimento ao Nível da Produção de Electrcididade, Analíse Intercalar, Período 2009-2020, Executive Summary, Rede Eléctrica Nacional, SA, Portugal.

[20] Instituto Nacional de Estatística Portugal, 2003, Projecções de População Residential em Portugal 2000-2005, INE, Portugal.

[21] The Royal Academy of Engineering, 2004, The Costs of Generating Electricity, The Royal Academy of Engineering, Westminster, London.

[22] REN, 2005, Perspectivas de Evolução do Sistema Electroprodutor Português, período 2006-2025, Rede Eléctrica Nacional, SA, Portugal.

[23] Eybalin, A., and Shahidehbour, M., 2003, Electricity Restructuring in Iberian Peninsula, *IEEE Power Engineering Society General Meeting*, IEEE, Digital Object Identifier 10.1109/PES.2003.1267193, Volume 1, pp. 13-17.

[24] IEA, World Energy Outlook 2007, China and India Insights, OECD/IEA, IEA Publications, France.

[25] Rubin, E. S., Chen, C. and Rao A., B., 2007, Cost and Performance of Fossil Fuel Power Plants with $CO_2$ Capture and Storage, Energy Policy, 35, pp. 4444-4454.

Acknowledgments: The authors would like to thank Prof. Alvaro Martins for providing of specific input data and PhD candidate Sérgio Casimiro for valuable comments on this paper. This work was supported under the Project PTDC/ENR/70767/2006 and ERA-FENCO/ 0001/2008 funded by the Fundação para a Ciência e a Tecnologia (FCT), Portugal.

# Utility Optimization in a Brewery Process Based on Energy Integration Methodology

*Monika Dumbliauskaite* [a], *Helen Becker* [a], *François Maréchal* [a]

[a] *Industrial Energy Systems Laboratory (LENI), Ecole Polytechnique Fédérale de Lausanne (EPFL), CH-1015 Lausanne, Switzerland*

**Abstract:** This paper presents a methodology aimed at improving the energy efficiency of a brewery applying process integration techniques. The different steps of the analysis are presented. The first step is the identification of the process energy requirements and the corresponding heat loads, which allows the definition of the process hot and cold streams. The Pinch Analysis of the brewery reveals a heat recovery potential of 36% by improving the heat exchanger system. In order to satisfy the minimum energy requirements, optimal energy conversion technology configurations are calculated, taking into account economic and environmental criteria. The integration of suitable utilities is considered (cogeneration engine combined with heat pumping and refrigeration systems) and the interaction between them is analyzed. In addition, a thermo-economic optimization is performed in order to determine the optimal heat pump operating temperatures. The results show the opportunity to reduce by 36% the brewery heating bill and by 44% the $CO_2$ emissions through the set up of an optimized utility configuration when compared to the current one. In addition, the optimal integration shows that the cooling water consumption of the refrigeration can be suppressed and appropriately be replaced by a heat pumping effect. The comparison between French and German conditions shows that contrasting results can be obtained due to the different economic and energy supply configurations. The process system analysis shows that when considering the recovery of the plant organic waste, bio-methane can be produced and valorized in the cogeneration engine. In that case, it is demonstrated that the process can become self sufficient in terms of energy.

**Keywords:** process integration, pinch analysis, brewery, thermo-economic optimization.

## 1. Introduction

Beer production (28Mt in 1999, EU-15) ranks $5^{th}$ in European food industry and the European beer is widely exported. Breweries use significant amounts of water and energy to produce this fresh and tasty drink. In the current trend of high energy price, energy efficiency improvement of industrial processes represents an important way to reduce production costs. In addition, growing environmental concern encourages companies to consider innovative solutions not only to reduce the carbon footprint but also the water consumptions.

In the Top-Down approach developed by D. Muller et al. [9] for analyzing the energy efficiency of industrial processes in the food industry, Pinch Analysis is used to identify the possible heat recovery by heat exchange between the streams to be cooled down and the streams to be heated up. Pinch Analysis [6] targets the minimum heat requirement of a process through the graphical representation of the process energy requirements, called *composite curves*, and describes how it is possible to achieve the determined energy targets with a correctly designed network of heat exchangers.

The systemic approach consists of the identification and characterization of the main Process Unit Operations (PUOs). The Top-Down approach [9] shows that more than 80% of the energy consumption can be explained by describing only 20% of the units of a factory. For these important PUOs, models are used to characterize the set of hot and cold streams that are needed to achieve the operation. The choice of the minimum approach temperature $\Delta T_{min}$ allowed by the heat exchangers enables the determination of the process Minimum Energy Requirements in heating and cooling. Grand composite curve analysis helps towards identifying opportunities for energy-efficient utility integration to satisfy the energy requirements, such as combined heat and power (CHP) systems or heat pumps (see for example [3]). Optimal utility inte-

Corresponding author: Monika Dumbliauskaite, Email: monika.dumbliauskaite@gmail.com

gration can be achieved using a Mixed Integer Linear Programming (MILP) formulation, as described by Maréchal and Kalitventzeff [7].
This paper presents the implementation of the process integration methodology on a brewery. The results are presented based on two different scenarios in terms of equivalent $CO_2$ emissions according to the substitution options of the electricity mix. In addition the methodology will be used to assess renewable energy integration using bio-methanation of the process waste.

## 2. Pinch analysis of a brewery

### 2.1. Process Description

The brewery studied corresponds to a typical brewing process. The target temperatures of the streams and the proportions of ingredients are determined by the product recipe. The brewing house is associated with beer production and is split into two parts:

- **a hot part**(*mashing*), described by the block flow diagram of Figure 1, where the blend of water and malt (*Mash*) is firstly brewed at high temperature (76°C) so that the activated enzymes transform malt starch into sugar. The *Mash* is then filtered to obtain the wort, which is boiled with hops to develop beer flavors. Wort boiling is an energy intensive operation. The wort is clarified in a whirlpool to remove the hops and eventually cooled to the pitching temperature.

- **a cold part**, illustrated in Figure 2, mainly consisting of the wort fermentation by yeast, at constant temperature (11°C), during 2 weeks. The beer is then chilled (-2°C) and clarified before being stored in insulated tanks where it ends its maturation.

The rest of the process consists of the beer packaging. In the process under study, four conditioning lines package the beer in new bottles, in kegs and in returnable bottles that are washed beforehand. The bottles filled with beer are then pasteurized.
A Cleaning in Place (CIP) system with effluent recovery, designed to wash the tanks, is also modeled in the study.

*Figure 1:* Block Flow Diagram of the Hot Part

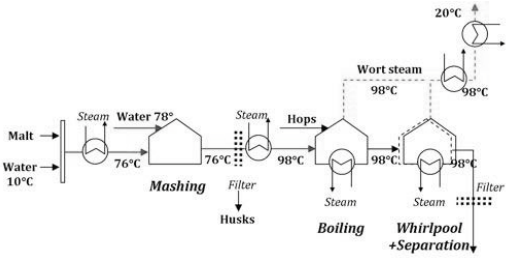


*Figure 2:* Block Flow Diagram of the Cold Part

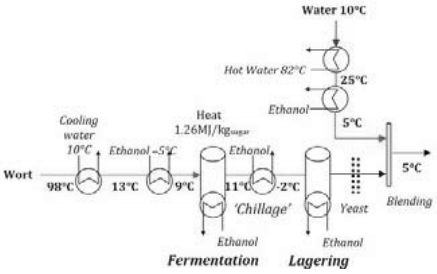


### 2.2. Process Integration Assumptions

*Table 1:* Chosen Values of $\Delta T_{min}/2$

| Stream State | $\Delta T_{min}/2$ [$\Delta$°C] |
|---|---|
| Liquid | 2.5 |
| Evaporating | 0.8 |
| Condensing | 1.7 |

The Pinch Analysis of the brewery is performed using the following key hypotheses:

- Thermal losses during heat transfers are not taken into account.

- Despite the fact that the units are operated in batch mode, we consider a time averaging approach, where all the process operations are considered as being simultaneous. This is done by calculating the overall energy consumed per unit of product and dividing it by the mean hourly production. The yearly operating time of the brewery is 4992h.

- For each stream, the corresponding $\Delta T_{min}/2$ was chosen according to the existing equipments. The associated values of $\Delta T_{min}/2$ may not be optimal; however they are used in the study, as they correspond with the existing heat exchangers available in the factory.

### 2.3. Modeling of the Conditioning Lines

The opportunity of recovering heat from the conditioning lines is worth studying, since bottle washing and pasteurization devices represent important energy consumers in breweries. In the process under study, the conditioning lines account for more than 32% of the current heating demand, which reveals the importance of modeling and integrating these units when undertaking the Pinch Analysis of breweries.

As an example, the modeling of the bottle pasteurization device is presented in this paragraph. The device is considered as a sequence of soaking baths transferring their heat to the beer bottles passing through them. The bottles are successively heated and cooled; the baths thus require respectively heating and cooling supplies in order to keep a constant temperature level.

The model considers the different baths at their corresponding temperatures. This representation enables the determination of internal heat recovery potential, as well as between the baths and other process streams.

In the study, permanent regime is considered. The current bottle pasteurization device consists of ten baths maintained at constant temperature levels. The input and output temperatures of the bottles are respectively 8°C/281K and 30°C/303K. The main soaking bath is kept at 62°C/335K.

The computed heat loads of the different baths correspond to the sum of the bottle heat loads and the heat losses to the surroundings (from conduction-convection and from radiation). The composite curves associated with the device can thus be obtained and represented in a $(T - \dot{Q})$ diagram. Figure 3 shows the composite curves corresponding to the device operating on the production line n°4. 40000 bottles of 0.33L/unit are currently pasteurized per hour by the machine.

In Figure 3, the hot streams are associated with the baths in heat excess and the cold ones with those requiring heat. The grand composite curve corresponds to the enthalpy (heat) difference between the hot and cold streams for each temperature interval. In Figure 4, the integration shows the possible heat recovery that can be obtained by transferring hot water from one cooling bath (hot stream at constant temperature) to a heating bath (cold stream at constant temperature).

*Figure 3:* Bottle Pasteurization Device (Line 4) Composite Curves

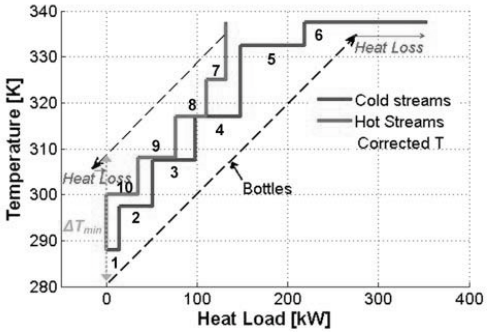


*Figure 4:* Bottle Pasteurization Device (Line 4) Grand Composite Curve

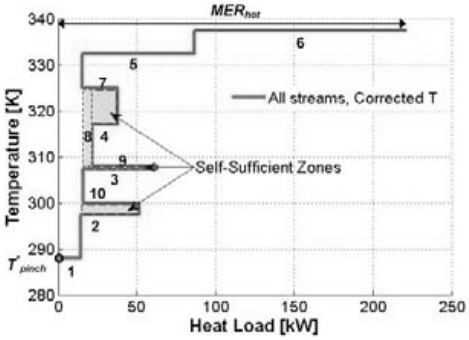


The chosen value of $\Delta T_{min}/2$ (2.5°C) leads to a pinch corrected temperature $T^*_{pinch}$ =15°C (288.2K), which corresponds to the minimal bath temperature ($T_{pinch,cold}$ = 12.5°C= $T^*_{pinch}$ − $\Delta T_{min}/2$). As a result, the device does not need external cooling, since it is possible to transfer all the heat excess from the hot streams to the cold ones. The chosen value of $\Delta T_{min}$ is an optimal one, since it is associated with the minimal MER feasible for the current device (220kW in heating and 0kW in cooling).

In addition, it can be noted that the device heat recovery potential is determined not only by the $\Delta T_{min}$, but also by the number of baths and by their temperature levels. Thus, the bottling system design can be optimized using Pinch Analysis, in particular through the definition of the minimum number of baths and their corresponding volumes that can be expressed as a function of the speed of the bottle processing.

### 2.4. Process Integration

The process requirements identified for the PUOs are used to calculate the maximum energy recovery in the system. Figure 5 presents the brewery composite curves resulting from the definition of the hot and cold streams identified in the process.

*Figure 5:* Brewery Process Composite Curves

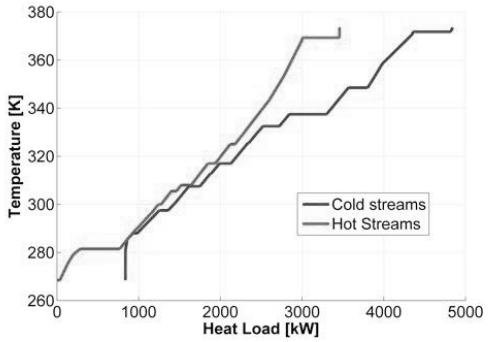


*Figure 6:* Brewery Process Grand Composite Curve

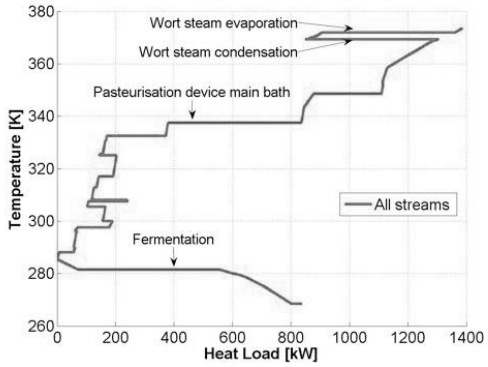


The first observation that can be established is related to the pinch, detected at the corrected temperature $T^*_{pinch}$ =285.5K (or 12.5°C). The pinch point coincides with the temperature of cold water entering the process at ambient temperature. As a consequence, all the effluents (hot streams) leaving the process at a temperature above the ambient temperature must deliver their heat to the process cold streams.

The computation of the MER for the identified PUOs enables the identification of opportunities for energy saving. The results are shown in Table 2 and reveal a heat recovery potential of **1143kW**. The remaining heating requirements of the Non Identified Process Units (NIPUs), i.e. $604kW_{th}$, are added to define consistently the minimum heat requirement for the entire process. The targeted heating savings represent 36% of the total heat consumptions.

*Table 2:* Estimated minimum energy requirement for $\Delta T_{min,liquid}$ =5°C

| Type | MER [kW] | Present [kW] | Savings [kW] | Savings |
|---|---|---|---|---|
| Hot Utility | 1386<br>**1990**$_{total}$ | 2529 $_{identified}$<br>3133 $_{total}$ | **1143** | 45%<br>**36%** |
| Cooling Water (>10°C) | **0** | NA | NA | NA |
| Refrigeration (<10°C) | **837** | NA | NA | NA |

## 3. Energy conversion integration

The analysis of the energy conversion system integration is based on the energy costs [4] and the $CO_2$ emissions [1] of the French industrial sector in 2007 and will be compared to the German case (table3).

*Table 3:* Energy Costs (without taxes) and $CO_2$ Emissions- France FR and Germany GER (2007)

| | Cost | $CO_2$ Emissions |
|---|---|---|
| Electricity FR | 54.1 €/MWh$_e$ | 55kg$_{CO2}$/MWh$_e$ |
| GER | 92.7 €/MWh$_e$ | 624kg$_{CO2}$/MWh$_e$ |
| Nat. Gas FR | 27.1 €/MWh$_{LHV}$ | 231kg$_{CO2}$/MWh$_{LHV}$ |
| GER | 41.7 €/MWh$_{LHV}$ | 231kg$_{CO2}$/MWh$_{LHV}$ |
| Water | 0.00657 €/m$^3$ | - |

### 3.1. Grand Composite Curve analysis

The analysis of the Grand composite curve (Figure 6) leads to the following observations:

- Heat is required at relatively low temperature levels which offers the opportunity to integrate combined heat and power (CHP) and heat pumping systems.
- The pinch temperature ($T^*_{pinch}$ =12.5°C) corresponds to the ambient conditions. It allows for integrating the hot stream of the refrigeration system as a heat source for the process.
- Provided that a heat pumping system is used to satisfy the needs at medium temperature, an MVR system can be used to recover the condensation of wort steam at high temperature.

This would enable lower temperature heating requirements to be satisfied by the cooling water of a cogeneration engine. Thus, the size of the MVR system will be related with the heat delivered by the cogeneration system.

- A refrigeration utility with multiple levels of evaporation represents an appropriate solution in order to minimize the exergy losses below the pinch temperature.

Using a linear programming formulation [7] the flows of the utility streams are calculated to satisfy the process requirements at minimum cost.

### 3.2. Improving the conversion system

Currently, a natural gas boiler generates steam at high pressure (8.5bar) that is distributed and condensed after expansion at 2.2bar and 123.3°C. For the cooling supply, the factory uses cold water and an $NH_3$-refrigeration cycle with two levels of evaporation, at -4°C and -8°C.
The flows in the utility system are computed to minimize the yearly operating costs. In practical terms, the stream heat loads of the energy conversion technologies are optimized and added to the process hot and cold streams

*Figure 7:* Current Utility Setup: Boiler & Refrigeration Cycle (RC)

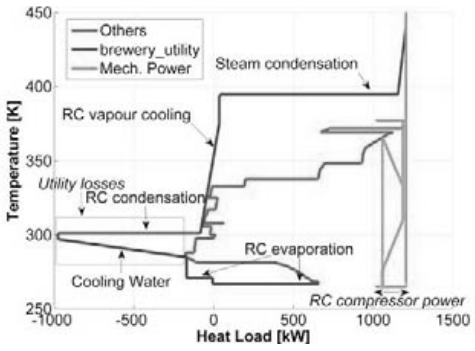


Figure 7 shows the integrated composite curves of the utility system. The utility streams are represented by the line "brewery_utility" and the process requirements correspond to the grand composite curve "Others". The mechanical work supplied to compressors (heat pump and refrigeration cycle) is represented by the line "Mech. Power". The analysis of Figure 7 reveals that the current utility configuration does not prove optimal for multiple reasons. On the one hand, the use of steam at high pressure and temperature generates exergy losses, since the process requires heat at lower temperatures. On the other hand, it can be seen that below the condensation temperature of the refrigeration cycle, the process heating requirements are lower than the heat provided by the condensation of the refrigerant. This excess of heat must be evacuated by cooling water. It is therefore necessary to consider solutions allowing the improvement of the current utility configuration.

In order to reduce the exergetic losses due to the use of high pressure steam, the integration of a cogeneration internal combustion engine is considered as an alternative to the boiler currently in operation. It appears to be the most relevant technology, as it is possible to recover heat from both exhaust gases and cooling water, which can be used in low temperature processes like breweries. Natural gas is firstly considered. As can be seen in Figure 8, the exhaust gases enable wort evaporation (T*=373K), whereas the engine cooling water provides heat to the process streams below 360K. Fuel conversion leads to the generation of 1047kW of mechanical power. Part of this power can be used to drive the refrigeration cycle compressors, which represents an important reduction in process electricity bill.

*Figure 8:* Boiler Replaced with a CHP System

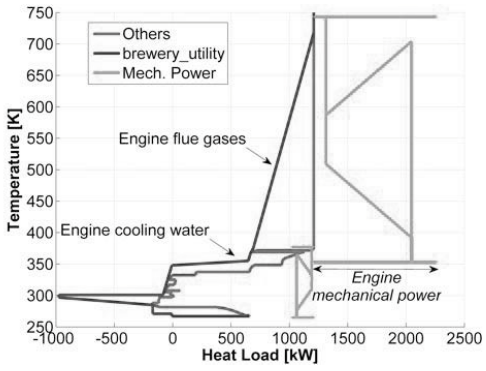


However, the size of the CHP system can still be optimized and the losses caused by refrigeration cycle condensation remain a problem that has not been solved yet. The integration of heat pumps is eventually considered. The mechanical vapor recompression (MVR) of the wort vapor can assist the evaporation and will reduce the CHP system size. In addition, this high temperature heat pump is

making the condensation of the refrigeration cycle useful for process water preheating.
The heat pump operating conditions may influence the flows and the sizes of the other utility systems. In order to determine the optimal heat pump operating temperatures, a multi-objective thermo-economic optimization is performed. Three decision variables are considered: the heat pump condensation temperature, the refrigeration cycle condensation and high pressure evaporation temperatures. Using the evolutionary algorithm *QMOO* ([5],[8]) a set of Pareto-optimal points is obtained, representing the trade-off between investment costs and operating costs. The Pareto-optimal set of figure 10 is divided into two distinct clusters, characterized by a single value of the heat pump condensation temperature (see Figure 9), namely 66.5°C for cluster 1 and 77.5°C for cluster 2, which corresponds to the maximal temperatures of the conditioning line units.

*Figure 9:* Pareto Front (84 Pareto-optimal points after 2000 iterations)

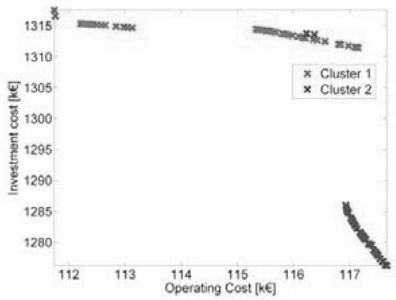


*Figure 10:* Two Pareto-Optimal Clusters of Heat Pump Condensation Temperatures

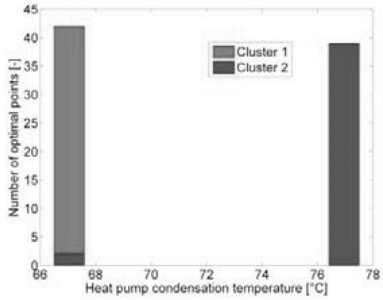


The high pressure evaporation temperature of the refrigeration cycle is converged at 6°C. The condensation temperatures are preferably distributed between 45°C and 50°C.

Two optimized configurations, including the integration of MVR and heat pump systems, are presented in Figures 11 and 12. It can be seen a clear reduction of exergy losses: utility temperatures are as close as possible to the temperatures of the process energy requirements. One can also observe a drastic reduction in the energy losses: for the case where the heat pump condenses at 77.5 °C (351K), external cooling water requirement is close to zero. Table 4 presents the results associated with the different utility setups. It is considered that the remaining heating needs of the NIPUs can be fulfilled by the use of the current boiler (efficiency 85%), fed by natural gas. The French case is compared with the German case where the electricity supply is sensibly different : higher electricity price when compared to natural gas cost and electricity being mainly produced by coal power plants (Table 3). One can observe that in France, from both an economic and an environmental point of view, the most interesting utility setup consists of using heat pumping systems. The best configuration feature a decrease by 36% of the operating costs and 18% of the total costs when compared with the current utility setup. It shows a drastic reduction in $CO_2$ emissions (44%) and in water consumption. On the contrary, in Germany, the higher electricity to gas price ratio favors cogeneration systems, which in turn enables important reductions in operating costs and $CO_2$ emissions. It is important to note that only energy costs are taken into account in the yearly operating costs. If carbon taxation was considered, the most environment-friendly setups would be associated with an increased economic savings.

*Figure 11:* CHP System+MVR, Heat Pump Condensing at 66.5°C, COP=5.37

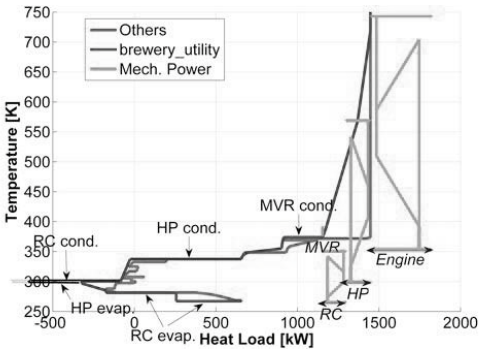

*Figure 12:* CHP System+MVR, Heat Pump Condensing at 77°C, COP=5.71

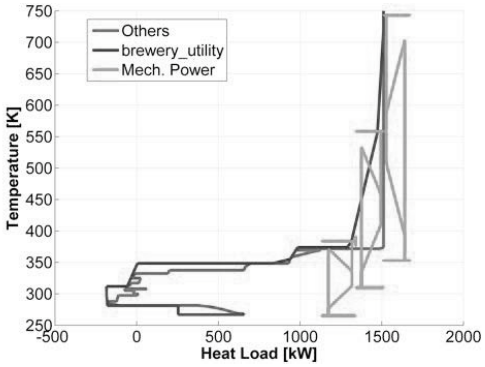


*Table 4: Results with maximum heat recovery*

*1. Boiler, 2. CHP, 3. CHP+MVR +HP($T_{cond}$=66.5°C), 4. CHP+MVR+HP($T_{cond}$=77.5°C)*

| | Unit | 1. | 2. | 3. | 4. |
|---|---|---|---|---|---|
| Fuel consumption | [kW$_{LHV}$] | 2088 | 3279 | 1677 | 1140 |
| Electricity | [kWe] | 184 | -863 | -80 | 142 |
| Operating Costs FR | [k€/year] | 332 | 210 | 205 | 212 |
| *Saving potential* | *[%]* | *0* | *-37* | *-38* | *-36* |
| Operating costs GER | [k€/year] | 520 | 283 | 312 | 336 |
| *Saving potential* | *[%]* | *0* | *-46* | *-40* | *-35* |
| TOTAL COSTS FR[4] | [k€/year] | **332** | **308** | **274** | **274** |
| *Saving potential* | *[%]* | *0* | *-7* | *-17* | *-18* |
| TOTAL COSTS GER | [k€/year] | **520** | **380** | **381** | **398** |
| *Saving potential* | *[%]* | *0* | *-27* | *-27* | *-24* |
| $CO_2$ (EDF mix) | [tons/year] | **2459** | **3544** | **1912** | **1372** |
| *Saving potential* | *[%]* | *0* | *+44* | *-22* | *-44* |
| $CO_2$ (GER mix) | [tons/year] | 2987 | 1094 | 1686 | 1976 |
| *Saving potential* | *[%]* | *0* | *-63* | *-44* | *-34* |
| Cooling water | [kg/s] | 17.1 | 17.1 | 3.0 | 0.1 |
| *Saving potential* | *[%]* | *0* | *0* | *-82* | *-99* |

### 3.3. Husk Bio-Methanation

Breweries offer the opportunity of recovering energy through husk bio-methanation. The recovered biogas can be used as an alternative to natural gas to feed the cogeneration engine. Knowing the amount of husk produced per year, it is possible to calculate the primary energy that can be recovered :

$$Q_{LHV} = \frac{M_{husk} \times \widetilde{M}_{CH_4} \times v_{CH_4} \times LHV_{CH_4}}{\widetilde{v}}$$

75 $Nm^3$ of methane can be recovered from 1 ton of husk [2], which represents, for the brewery studied, 8287MWh$_{LHV}$/year=**1660kW$_{LHV}$**, corresponding to a combined production of 677kW$_e$ of electricity and the corresponding heat load. The organic matter is blended and its transformation into biogas by microorganisms requires a specific operating temperature (35°C) [2], which results in additional electricity and heat consumptions.

*Table 5: Results Bio-Methanation integration with maximum heat recovery*

*1. Boiler, 2. CHP, 3. CHP+MVR +HP($T_{cond}$=66.5°C), 4. CHP+MVR+HP($T_{cond}$=77.5°C)*

| | Unit | 1. | 2. | 3. | 4. |
|---|---|---|---|---|---|
| Biogas Engine Size | [kW$_e$] | 0 | -1232 | -677 | -677 |
| Process Identified Elec. | [kW$_e$] | 184 | 184 | 295 | 379 |
| Digester Elec. | [kW$_e$] | 80 | 123 | 80 | 80 |
| Total Elec. | [kW$_e$] | 264 | -925 | -298 | -219 |
| Biogas Extra Heat | [kW$_{th}$] | 39 | 0 | 196 | 434 |
| Boiler (NIPU) | [kW$_{LHV}$] | 664 | 711 | 480 | 200 |
| Operating Costs FR | [k€/year] | 161 | -31 | -16 | -32 |
| Operating Costs GER | [k€/year] | 260 | -280 | -38 | -60 |
| Invest. Bio-methanation | [k€] | 895 | 2030 | 1418 | 1418 |
| Invest. Heat Pumps | [k€] | 0 | 0 | 198 | 290 |
| TOTAL COSTS FR | [k€/year] | **238** | **145** | **124** | **115** |
| *Savings /ref.* | *[%]* | *-28* | *-56* | *-63* | *-65* |
| TOTAL COSTS GER | [k€/year] | **338** | **-105** | **101** | **88** |
| *Savings /ref.* | *[%]* | *-35* | *-120* | *-81* | *-83* |
| $CO_2$ (EDF mix) | [tons/year] | **839** | **566** | **471** | **170** |
| *Savings /ref.* | *[%]* | *-66* | *-77* | *-81* | *-93* |
| $CO_2$ (GER mix) | [tons/year] | **1588** | **-2060** | **-377** | **-452** |
| *Savings /ref.* | *[%]* | *-47* | *-169* | *-113* | *-115* |

Table 5 presents the comparison between the different options when converting the biogas. The calculated energy consumptions include the NIPU heat loads that are satisfied by the current boiler supplied with biogas. The reference investment cost of a biogas installation is 450k€(digester+cogeneration of 100kW$_e$) [2].

Table 5 reveals that bio-methanation on site is the most economic and environmental solution. Indeed, the investment in a bio-methanation installation is highly profitable and makes the process self-sufficient. In France, bio-methanation allows the yearly total energy bill to be reduced by 65% and 2'289tons of $CO_2$/year to be saved (93% with respect to reference). The results are also very different between France and Germany. The higher cost and $CO_2$ content of German grid electricity promotes the cogeneration operated with biogas, which results in important economic and environmental profits.

## 4. CONCLUSION

A methodology based on process integration techniques has been applied to improve the energy efficiency of a brewery.

The definition and the modeling of the identified process units allows the determination of the heat recovery potential between process streams using Pinch Analysis. The analysis of the process composite curves enables a first identification of the utilities that can be used to fulfill the determined Minimum Energy Requirements.

[4]Total Yearly Costs = Operating Costs+Annualized Investment (interest rate=5%, payback time=15 years)

A multi-objective optimization method is applied to define the best utility setup and the corresponding operating conditions that minimize the operating and investment costs. It has been shown that integrating combined heat and power system together with heat pumps can be profitable from both an economic and an environmental point of view. A special focus is made on the dependance on the electricity cost and production mix. The comparison between France and Germany is presented: the contrasted electricity economic and environmental costs with respect to gas result in a solution promoting heat pumps in France whereas in Germany cogeneration systems prove more profitable.
The opportunity of recovering energy from brewery organic waste through bio-methanation has been studied. A quantitative analysis shows that the production and use of biogas on site leads to a drastic reduction in the total costs for both cases. However, the reduction in CHP system operating cost is not sufficient to substitute heat pumps by cogeneration if the brewery studied was located in France.
The energy requirements of the brewery are evaluated considering a continuous process functioning, which limits the accuracy of the results presented. Indeed, the identified units may not operate simultaneously, hence the interest of performing a multi-period analysis, which would require additional information on instantaneous material flows. The quantitative results presented are specific to the brewery studied and it is important to keep in mind that any process has singularities that can hardly be transposed into another case study, without prior verification.

## Nomenclature

$COP$ Coefficient Of Performance [-]

$\dot{Q}_{th}$ Heat Load [kW]

$LHV$ Lower Heating Value [MWh/kg]

$M$ Mass[kg]

$MVR$ Mechanical Vapor Recompression

$v_{CH_4}$ Methane Content of Brewery Waste [$m^3$/kg]

$MER$ Minimum Energy Requirement [kW]

$\widetilde{M}$ Molar Mass [kg/kmol]

$\widetilde{v}$ Molar Volume of Perfect Gases [$m^3$/kmol]

$NIPU$ Non Identified Process Unit

$PUO$ Process Unit Operation

$T$ Temperature [K]

## References

[1] ADEME. Note de cadrage sur le contenu $co_2$ du kwh par usage en france, 2005.

[2] ADEME. La méthanisation à la ferme, 2006.

[3] H. Becker, F. Marechal, and A. Vuillermoz. Process integration and opportunity for heat pumps in industrial processes. In *Proc. 22nd International Conference on Efficiency, Cost, Optimization, Simulation and Environmental Impact of Energy Systems*, 2009.

[4] Observatoire de l´ Energie. Prix du gaz et de l'électricité en europe au $1^{er}$ janvier 2007, 2007.

[5] G.B. Leyland. *Multi-Objective Optimisation applied to Industrial Energy Problems*. Ph.d. dissertation, Lausanne: EPFL-STI, Industrial Energy System Laboratory, 2002.

[6] B. Linnhoff et al. A user guide on process integration for the efficient use of energy. *Institution of Chemical Engineers, IChemE; Revised Sub-Edition*, 1994.

[7] Kalitventzeff B. Marechal, F. Energy integration of industrial sites: tools, methodology and application. *Applied Thermal Engineering*, 18:921–933, 1998.

[8] A. Molyneaux. *A Practical Evolutionary Method for the Multi-Objective Optimisation of Complex Energy Systems, including Vehicle Drivetrains*. Ph.d. dissertation, Lausanne: EPFL-STI, Industrial Energy System Laboratory, 2002.

[9] D. Muller. *Web-based tools for energy management in large companies applied to food industry*. Ph.d. dissertation, Lausanne: EPFL-STI, Industrial Energy System Laboratory, 2007.

**Acknowledgments:** The authors wish to thank ECLEER (European Centre and Laboratories for Energy Efficiency Research (http://www.ecleer.com) for supporting this research and collaborating in its realization.

# The Analysis of the Possibilities of the Efficiency Improvement of the Supercritical Power Plant Integrated with CCS Installation

*Janusz Kotowicz, Katarzyna Janusz-Szymańska and Łukasz Bartela*
*Institute of Power Engineering and Turbomachinery,*
*Silesian University of Technology, Gliwice, Poland*

**Abstract:** The method of integration of a supercritical coal-fired power unit with CCS installation was presented in the paper. The proposed installation is equipped with membrane modules, $CO_2$ compressors and vacuum pumps. It allows for separation and compression of 90% of $CO_2$ emitted from a coal-fired boiler. The way of minimization of the energy need of the mentioned installation was developed. It was brought to the optimization of the pressure ratio selection in the compressors and vacuum pumps used, to the use of gas cooler at the inlet to the mentioned machines and to the use of waste heat in the steam cycle. It permits to significantly decrease the energy need for the CCS installation. In details two possible systems of the integration of recycled heat from separated and compressed carbon dioxide with steam cycle were shown. It causes an increase the efficiency of power generation. Also, the cost of electricity production was calculated for a supercritical power plant with CCS installation.

**Keywords:** CCS, Membrane Separation, Supercritical Power Plant

## 1. Introduction

The European Union accepted the climate - energy package, under this validity the member's Countries of EU took on the obligation of realization of several aims:

- limitation of greenhouse gases emission by about 20% in relation to the base year (1990),
- reduction of energy consumption by about 20% in comparison to prognoses for EU for the year 2020,
- increase to 20% of total consumption of the utilization of energy from renewable sources
- increase of biofuels use in transport fuels up to 10%.

Reduction of the $CO_2$ emission about 20% to the year 2020 is possible to achieve by replacement of fossil fuels by renewable sources of energy and through reduced $CO_2$ emission in blocks applying modern technologies of electricity production connected with $CO_2$ capture and storage (CCS) in geological structures.

The connection of "clean coal" technology with CCS will permit the electricity production from coal at almost zero $CO_2$ emission [3]. The driving force of the development of the zero-emission technology is the European Trading System of allowances for the $CO_2$ emission.

The task of CCS installation is firstly the separation of $CO_2$, and further the preparation of carbon dioxide for transportation to the place of storage. There are several different types of CCS systems:

- post-combustion,
- pre-combustion,
- oxyfuel combustion.

For $CO_2$ separation from flue gases, absorption processes, adsorption processes (using for example active carbon), cryogenic fractionation, and membranes can be used. Absorption processes are well known and commonly used in the chemical industry. Thus, it is predicted that in the near future, chemical absorption using monoethanolamine (MEA), ammonia will play an essential role in $CO_2$ capture from flue gases in power plants [9].

However, separation with use of MEA requires substantial flue gas cleaning, especially in terms of $SO_2$ and $NO_x$. Removal of these components is connected to the increase of working time of the solvent (MEA), which has to be regenerated with a great amount of medium and low-pressure steam. Separation also results in decreased power plant efficiency, as regeneration consumes around 4 – 6 MJ/kg of $CO_2$ removed [19].

Corresponding Author: Katarzyna Janusz-Szymańska, Email: katarzyna.janusz@polsl.pl

These drawbacks provide a rationale for searching a new, more competitive techniques for $CO_2$ separation from flue gases, including membrane separation. Membrane separation is used both in the petrochemical industry and in the cleaning of natural gas before transport. The use of polymer membranes in the 1980s contributed to the commercial success of this separation technique in comparison to absorption processes or cryogenic fractionation [10,11]. In the industrial scale a membrane processes of air separation ($O_2/N_2$) was also developed.

Within the last several years, dynamic developments in membrane technology for $CO_2/N_2$ separation have occurred. The use of highly selective materials, especially polymers, has allowed for production of membranes with selectivity over 200 and even up to 400 [8,16].

Several projects are realized currently in which membrane separation of carbon dioxide is applied.

The industrial tests of $CO_2$ capture from flue gases from coal combustion using membranes has been run in the EnBW power plant from 2008, as a part of the METPORE project [15]. The study is conducted on polymer membranes as well as cement-type membranes, with the participation of such companies as RWE and EON.

Another project which is realized from October 2007 is MEM-BRAIN project – Gas separation membranes for zero-emission fossil power plants. It is realized by 12 research groups and 5 industrial partners, among others Shell and Siemens. Project bases not only on the application of membranes for the capture of $CO_2$ from flue gases, but also in processes of the $H_2/CO_2$ separation from the synthesis gases and for the $N_2/O_2$ separation in oxyfuel combustion. In the investigations the polymeric membranes, zeolit membranes, ceramic and hybrid membranes are used [4].

Also, in Norway the Membrain Research Group (MEMFO) deals with investigations on the use of membranes in industrial installation for separation of such gases as: $CO_2$ and $H_2$. In 2006/7 MEMFO joined a consortium with 26 European partners from 14 countries and formed a project named NanoGloWa – Nanostructured Membranes against Global Warming [17]. NanoGloWa is funded by the European Commission (EC) under the 6$^{th}$ Framework Programme.

## 2. Characteristic of power plant and power need of CCS installation

A modern power engineering rely on supercritical coal fired plant or ultra supercritical coal power plant. The application of CCS installation is very energy-consuming in the energy block and it causes a considerable efficiency losses of the electricity production.

The model of the supercritical coal power plant was applied for the thermodynamic analysis. Electric power of this power plant is equal $N_{el,REF} = 601.55\ MW_{el}$ and the efficiency of the electricity production equals 0.4878 without CCS installation [2,13]. The temperature of live and reheated steam is 600°C and 620°C, respectively. The pressure of live steam is 28.5 MPa. For this power plant the membrane CCS installation was applied. The $CO_2$ emission from such systems decreases from 726 kg/MWh to 73 kg/MWh. The membrane separation ensure 90% of $CO_2$ capture.

The analysis presented in [13,14] permitted to determine flue gases pressure and the pressure for the membrane module what is connected with the minimum power need for this process. The driving force in the process was subatmospheric pressure after the membrane module. In the system presented in [13] one vacuum pump was used, which assured the pressure at 2.8 kPa.

This pressure value assure the mole fraction of separated carbon dioxide in the stream at the level of 80% [13]. For the liquefaction of $CO_2$ for transport purposes, the compression of $CO_2$ to the pressure around 15 MPa [6] is needed, depending on the purity of the separated $CO_2$, and then cooling of the $CO_2$ stream is required. The CCS installation presented in [13] also consisted of one $CO_2$ compressor, what as a results of large compression caused a serious energy need for its driving. For the efficiency improvement of a power block integrated with CCS installation the membrane separation unit consisting of two vacuum pumps generating pressure equal to 2.8 kPa and the heat exchanger were proposed to be added to the system. For that purpose also two compressors and the additional heat exchangers were proposed. The use of the heat exchangers has the aim to decreases the $CO_2$ temperature at the inlet to machines.

Diagram of the installation for $CO_2$ capture from flue gases is presented in Fig. 1.

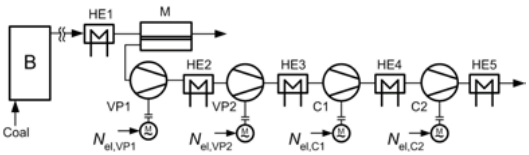


*Fig. 1. Diagram of the CCS installation for $CO_2$ capture from flue gases (B – boiler, HE – heat exchanger, M – membrane module, VP – vacuum pump, C – compressor).*

The efficiency of electricity production in the power plant with the CCS installation can be written as

$$\eta_{el,CCS} = \eta_{el,REF}\,(1-\delta_1)\,, \qquad (1)$$

where $\delta_1$ - power station internal load rate for the $CO_2$ capture installation, which is the ratio of the electric power of the compressors and vacuum pumps to power system:

$$\delta_1 = \frac{N_{\mathrm{el,VP}} + N_{\mathrm{el,C}}}{N_{\mathrm{el,REF}}}\,. \qquad (2)$$

About the energy consumption of the $CO_2$ capture process decides the power demand for vacuum pumps and $CO_2$ compressors. Power demand to the process of the $CO_2$ separation is presented in Fig. 2 as a function of variable pressure ratios ($\beta$) in machines $\sum_i N_{\mathrm{el,i}} = f(\beta_{\mathrm{C1}}, \beta_{\mathrm{VP1}})$, (i = C1, C2, VP1, VP2).

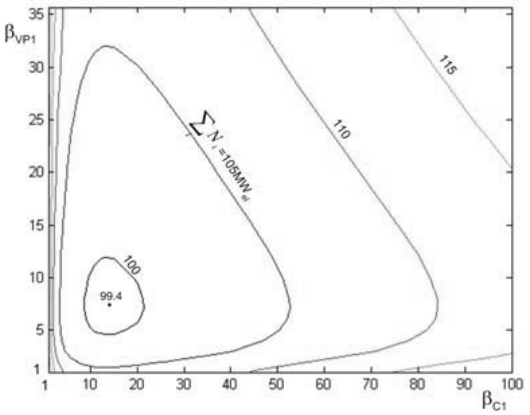


*Fig. 2. Line of constant value of $\Sigma N_{\mathrm{el,i}}$ in the plane $\beta_{C1}$ - $\beta_{VP1}$.*

As a result of the operation of both vacuum pumps, and the separated $CO_2$ compressors the rise of medium temperature is observed. It is possible to use the heat from separated and compressed $CO_2$ for replacement of the regenerative heat exchangers in the steam cycle of power system.

For this purpose, the quantity of heat that can be obtained from flue gases and separated $CO_2$, and than used in the power system was defined. The necessary quantity of heat for replacement of the heat exchangers in the reference energy block was also calculated.

Low temperature of flue gases required before the membrane module forced us to the use of the flue gases heat exchanger (HE1 in Fig. 1) through which condensate taken from behind the condenser is flowing. The condensates preheats to the temperature above 70°C. The amount of the received heat was enough to replace the first heat exchanger in regeneration in the steam turbine cycle (RH1).

Based on preliminary calculations, the quantity of heat possible to take from carbon dioxide separation process was estimated. The quantity of possible to obtain from all the exchangers (from HE1-HE5) heat load was presented in Fig. 3 as a function of compression ratio of vacuum pump (VP1) and compressor (C1). This characteristic was made for the assumption, that pressure of carbon dioxide prepared to transport equal to 15 MPa and its temperature equal to 80°C. For the transport of separated $CO_2$ lower temperature level is required, but in calculation it was assumed, that the next step of cooling is carried out without transportation of cooling heat into steam cycle. The temperature of carbon dioxide at inlet to machines is equal 70°C.

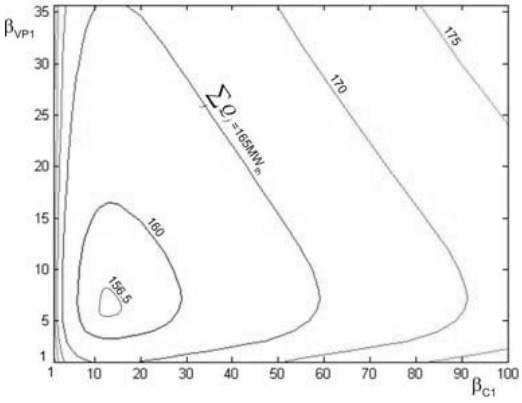


*Fig. 3. Line of constant value of $\Sigma Q_{\mathrm{j}}$ in the plane $\beta_{C1}$ - $\beta_{VP1}$ (j=HE1-HE5).*

Heat power requirement for the replacement of all the low-pressure regenerative heat exchangers is equal to 156.5 $MW_{el}$. This amount of heat is sufficient to carry out the analysis on the possibility of replacement of these heat exchangers.

In order to decrease the efficiency losses, the cooling heat of the flue gases and separated carbon dioxide may be used into the steam-water cycle in the reference system. Such an integration allows to eliminate the respective steam bleedings, causing a corresponding increase in steam flow to the steam turbine and increase the power by $\Delta N_{el}$, for example removal of the steam bleedings 10 – 13 (Fig. 4), causes an increase of steam turbine electric power by 27.74 $MW_{el}$.

Simultaneously, the efficiency of electricity production in the reference system grows according to the equation (1) where in the place of $\delta_1$, $\delta_2$ should be inserted, which can be defined by the equation:

$$\delta_2 = \frac{N_{el,VP1} + N_{el,VP2} + N_{el,C1} + N_{el,C2} - \Delta N_{el}}{N_{el,REF}} . (3)$$

In the paper [13] the results of analysis of the replacement of low-pressure regeneration for the CCS installation, consisting of a vacuum pump and a carbon dioxide compressor were presented. For comparison purposes the results of analysis presented in [13] were shown in Table 1.

Power station internal load rate $\delta_2$ is equal to 0.1642 [13], and as a result of optimization analysis decreases to 0.1201. The detailed scheme of the power plant utilizing cooling heat is shown in Fig. 4.

The next step in raising of the efficiency of power plant integrated with CCS installation had the aim to eliminate heat exchanger in high-pressure regeneration.

The amount of heat required to replace the heat exchanger in high-pressure regeneration (RH5) and in low-pressure regeneration equals to 210 $MW_{th}$.

Such a quantity of heat cannot be obtained for the assumptions made (characteristic in Fig. 3), therefore the analysis of replacement of a part of low-pressure regeneration (RH1-RH4).

For such configuration eight heat exchangers were applied in the CCS installation model. Also, one heat exchanger was installed on the stream of flue gases in order to cool flue gases to the temperature of 40ºC before the membrane module. Four heat exchangers installed directly after each vacuum pump and compressor for preheating of feed water in steam cycle. This water obtain at the temperature 222ºC allows to eliminate the regenerative heat exchanger RH5. The next four heat exchangers had the aim to reduce the temperature of separated $CO_2$ at the inlet to the vacuum pumps and the compressors. These heat exchangers preheated condensate from 35ºC to 118ºC.

In order to replace heat exchangers RH1-RH3 and RH5 167 $MW_{th}$ of heat flux was demand. It will allow to increase the electric power of steam turbine by 36.12 $MW_{el}$. Thanks to an decrease of the power demand for vacuum pumps and compressors to value 105 $MW_{el}$ and also an increase of the power obtained in the steam turbine, power station internal load rate $\delta_2$ reduced to 0.1149. Results of this analysis are presented in Table 1. Fig. 5 presents the detailed scheme of the integration of CCS installation with the power plant.

*Table 1. The parameters of the particular equipment connected to the CCS installation.*

| Characteristic parameters | | Power block | Power in block from Fig.4 | Power block from Fig.5 |
|---|---|---|---|---|
| Value | Unit | [13] | | |
| $N_{el,VP1}$ | $MW_{el}$ | 45.07 | 26.32 | 38.46 |
| $N_{el,VP2}$ | $MW_{el}$ | - | 12.81 | 3.89 |
| $N_{el,C1}$ | $MW_{el}$ | 81.41 | 27.67 | 45.79 |
| $N_{el,C2}$ | $MW_{el}$ | - | 33.21 | 17.12 |
| $\Delta N_{el}$ | $MW_{el}$ | 27.74 | 27.74 | 36.12 |
| $\beta_{VP1}$ | - | 35.714 | 10.79 | 24.1 |
| $\beta_{C1}$ | - | 150 | 9.94 | 32.27 |
| $\delta_1$ | - | 0.2103 | 0.1663 | 0.1749 |
| $\delta_2$ | - | 0.1642 | 0.1201 | 0.1149 |
| $\eta_{el,REF}$ | - | 0.4878 | 0.4878 | 0.4878 |
| $\eta_{el,CCS}$ | - | 0.4077 | 0.4292 | 0.4318 |

## 3. Economic analysis

In the conducted analysis of the economic effectiveness the net present value (*NPV*) method was used. *NPV* is one of the fundamental and most frequently applied economic coefficient used for the assessment of the economical effectiveness of the investments.

*NPV* can be described by the equation:

$$NPV = \sum_{\tau=1}^{N} \frac{CF_\tau}{(1+r)^\tau} . \quad (4)$$

In order to determine the cash flow $CF_\tau$, the total investment costs ($J$), profits from sales ($S_{el}$), overall production costs ($K_{PR}$), the income tax ($P_d$), changes of the working capital ($K_{obr}$), amortization charges ($A$), interests ($F$) and clearance value of the designed installation ($L$) ($L_\tau = 0$ when $0 \le \tau \le N-1$) had to be known.

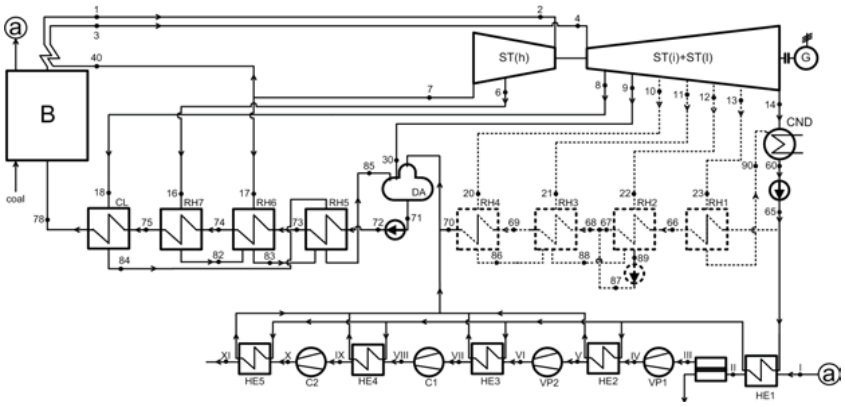


*Fig. 4. Reference system of the power plant utilizing cooling heat.*

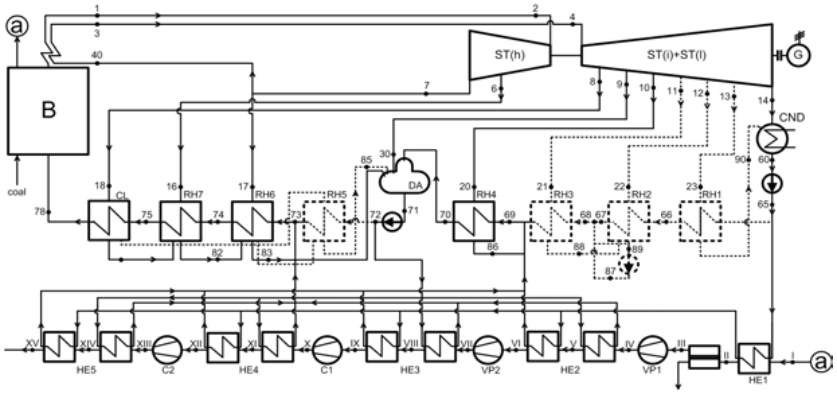


*Fig. 5. Scheme of the method of the replacement of high- and low-pressure regenerative exchangers in steam cycle of reference block.*

Thus, the equation describing the cash flow $CF_\tau$ can be written as

$$CF_\tau = \left[-J + S_{\mathrm{el}} - \left(K_{\mathrm{PR}} + P_{\mathrm{d}} + K_{\mathrm{obr}}\right) + A + F + L\right]_\tau . \quad (5)$$

A very important element of economic analysis is determination of the investment cost for a power plant. The total investment costs may be expressed as the product of the cost of machines and installations *K*, and coefficient *B*, which takes into account the costs of construction [12]

$$J = B \cdot \sum_{\mathrm{i}} K_{\mathrm{i}} . \quad (6)$$

The cost of boiler, steam turbine, pump, generator, condenser and heat exchanger in the form of approximation equations was presented in the paper [1,12]. On this basis, the investment on a supercritical power plant was determined. Cost of machines and devices connected to the CCS installation was defined in the paper [18]. In the present paper the following relations were applied:

$$K_{\mathrm{HE}} = 3{,}381 \cdot 35000 \cdot (k_{\mathrm{HE}} A_{\mathrm{HE}})^{0.6} , \quad (7)$$

$$K_{\mathrm{M}} = k_{\mathrm{M}} \cdot A_M + 250000 \cdot \left(\frac{A_M}{2000}\right)^{0,7} , \quad (8)$$

$$K_{\mathrm{C}} = 1{,}051 \cdot \frac{39{,}5 \cdot m}{0{,}9 - \eta_{\mathrm{i,C}}} \beta_{\mathrm{C}} \cdot \ln \beta_{\mathrm{C}} , \quad (9)$$

$$K_{\mathrm{VP}} = 4 \cdot 1{,}051 \cdot \frac{39{,}5 \cdot m}{0{,}9 - \eta_{\mathrm{i,VP}}} \beta_{\mathrm{VP}} \cdot \ln \beta_{\mathrm{VP}} . \quad (10)$$

The economic analysis were made for the reference system and also for a power unit itself, taking into account the investments and costs connected to the $CO_2$ capture installation. For the system with $CO_2$ separation calculated earlier, values of purity of separated $CO_2$ equal to 0.848 and carbon dioxide recovery ratio 0.9 were assumed. The rest components was nitrogen equal 0.135 and oxygen equal 0.017. The analysis takes into account total power station internal load rate ($\delta$).

For the economic analysis of the supercritical power plant the following assumption were made [1,7,14,18]:

- the investment costs were assumed at 1600 €/$kW_{el}$ for the coal fired power plant,
- the investment costs of the membranes module and CCS installation were assumed at 540 €/$kW_{el}$ for solution from Fig. 4 and 540 €/$kW_{el}$ for solution from Fig. 5, (these investments cost were estimated using equations (6÷10) for the coefficient $B$ =1.8),
- cost of membranes was assumed at 15 €/$m^2$,
- lifetime membranes was assumed at 5 years,
- operating costs of the CCS installation were assumed at 3 €/MWh,
- the annual operation time was 7500 hours,
- internal load rate for the reference system was 6%,
- the discount rate was assumed at 6.2%,
- amortization rate was given at 6.67%,
- the constant of repairs was determined at the level of 0.5% of the capital costs for the first ten years of operation and 1% for the remaining ten years,
- the investment costs are spread into three years of the construction (15/30/55%),
- the conduction of the power generating plant is financed in 75% by the commercial credit at the interest of 6% and it is paid through 10 years,
- the income tax rate was assumed at 19%,
- the average cost of fuel was 55 €/Mg.

In the economic analysis the limit sale price of electricity $C^{gr}$ was calculated. For the power plant without $CO_2$ capture it was described by the index REF and for the power plant with carbon capture installation it was described by the index CCS.

For both systems the limit sale price of electricity is a quantity determined by the condition:

$$NPV(C^{\mathrm{gr}}) = 0 . \tag{11}$$

If the price of electricity is sold over the determined limit sale price of electricity, the power plant will be economically effective (NPV > 0).

An important economic index for the power system with $CO_2$ capture is also the $CO_2$ avoided emission ($E_{AV}$) and its cost [5]. The cost of $CO_2$ emission avoidance ($C_{AV}$) is calculated according to the equation [14]:

$$C_{\mathrm{AV}} = \frac{C^{\mathrm{gr}}_{\mathrm{CCS}} - C^{\mathrm{gr}}_{\mathrm{REF}}}{E_{\mathrm{AV}}}, \tag{12}$$

where:

$$E_{\mathrm{AV}} = E^{(\mathrm{n})}_{\mathrm{REF}} - E^{(\mathrm{n})}_{\mathrm{CCS}} . \tag{13}$$

The cost of $CO_2$ emission avoidance is important when comparing with other $CO_2$ capture technologies, and also when comparing with the cost of purchase of allowances for $CO_2$ emission.
The results of the economic analysis are presented in Table 2.

*Table 2. The results of the economic analysis.*

| Characteristic parameters | Power block from Fig.4 | Power block from Fig.5 |
|---|---|---|
| The investment costs for the system (€/$kW_{el}$) | 1600 | 1600 |
| The investment costs for CCS installation (€/$kW_{el}$) | 540 | 560 |
| Unit sale price of electricity $C^{gr}_{REF}$ (€/MWh) | 43.04 | 43.04 |
| $CO_2$ emission from reference unit $E_{\mathrm{REF}}$ (kg/MWh) | 726 | 726 |
| $CO_2$ emission after separation $E_{\mathrm{CCS}}$ (kg/MWh) | 73 | 73 |
| $CO_2$ avoided emission $E_{\mathrm{AV}}$ (kg/MWh) | 653 | 653 |
| Power station internal load rate CCS installation $\delta_2$ | 0.1201 | 0.1149 |
| Unit sale price of electricity after $CO_2$ separation $C^{\mathrm{gr}}_{\mathrm{CCS}}$ (€/MWh) | 64.38 | 64.31 |
| Costs of $CO_2$ avoided emission $C_{\mathrm{AV}}$ (€/$MgCO_2$) | 31.23 | 31.11 |

Fig.6 presents the influence of the price of $CO_2$ emission allowances purchase ($C_{EA}$) on the limit sale price of electricity. The analysis was made for three systems:

A. Power Plant without $CO_2$ capture,
B. Power Plant with CCS installation, where the heat received from separated $CO_2$ was used in the steam cycle of the reference system (scheme of this structures is presented in Fig.5),
C. Power plant with CCS installation, where separated $CO_2$ is cooled, but this heat is not used in the steam cycle of the reference system.

Comparison of the characteristics from systems A and B allows on the assessment of the integration of CCS installation with the steam cycle of the power plant.

The sensitivity analysis on the influence of the investment costs and the fuel cost on the limit sale price of electricity was also conducted. The price

of fuel was changed by 20% from basic value. A change of fuel price has the influence on the change of the limit sale price of electricity by around 4 €/MWh. Whereas, the decrease of CCS installation investment cost to 500 €/$kW_{el}$ causes the decrease of electricity price by about 1 €/MWh.

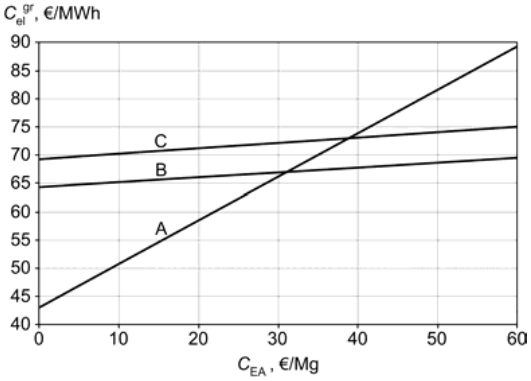


*Fig. 6. The effects of change of emission allowance cost on the changes of the limit sale price of electricity.*

## 4. Discussion and conclusions

The energy need for the CCS installation with the membrane module may be limited by the selection of optimum pressure ratio in the compressors and vacuum pumps used in the CCS installation and also by the use of gas cooling at the inlet to the mentioned machines. The heat obtained by cooling of the flue gases and separated carbon dioxide may be serve into the reintegration of steam cycle of the power block. Such an integration allows to eliminate of regenerative heat exchangers and in consequence to eliminate of the steam bleedings, causing a corresponding increase in steam flow to the steam turbine and increasing its power. It is a method for increasing of the efficiency of electricity production in the analysed system. As a result of calculations internal load rate of the CCS installation decreased from 0.1642 to 0.1201 for optimum pressure ratio (compressor and vacuum pump). It causes an increase of the efficiency of electricity production from 40.77% to 42.92%. This quantity may be further improved through better organization of the use of cooling heat in the steam cycle. For the case of replacement of heat exchangers RH1 – RH3 and RH5, internal load rate of the CCS installation decreased to 0.1149, what caused that the overall efficiency of electricity production in the power system is equal to 43.18%. In economic analysis an important element for the power system with $CO_2$ capture is the limit sale price of electricity and also the cost of $CO_2$ emission avoidance. The price of electricity for power plant without CCS installation was determined at 43.04 €/MWh and increases to above 64.3 €/MWh for a power plant integrated with the CCS installation. The price level of $CO_2$ emission avoidance was calculated at the level of approximately 31 €/$MgCO_2$.

The results of calculation of the influence of the price of $CO_2$ emission allowances purchase on the limit sale price of electricity indicate the rightness of integration of CCS installation with the supercritical coal-fired power plant for the price of $CO_2$ emission allowances above 31 €/$MgCO_2$. The results show that the use of cooling heat of separated $CO_2$ in the steam cycle power plant is very important. In analyzed cases this process permitted to decrease the limit sale price of electricity by about 5 €/MWh. In this case break even point (BEP) was displaced for the power plant integrated with CCS installation by about 8 €/$MgCO_2$ for the price of $CO_2$ emission allowance.

Nomenclature

| | |
|---|---|
| $A$ | surface area, $m^2$ or amortization charges, € |
| $B$ | coefficient |
| $C$ | cost, €/$MgCO_2$ |
| $CF$ | cash flow, € |
| $C^{gr}$ | unit sale price of electricity, €/MWh |
| $E$ | $CO_2$ emssion, kg/MWh |
| $F$ | interests, € |
| $m$ | mass flow rate, kg/s |
| $J$ | total investment costs, €/$kW_{el}$ |
| $K$ | cost, € |
| $k$ | unitary cost, €/$m^2$ |
| $L$ | clearance value of the designed installation, € |
| $N$ | power, $MW_{el}$ |
| $NPV$ | net present value, € |
| $P_d$ | income tax, € |
| $Q$ | heat stream, $MW_{th}$ |
| $r$ | discount rate |
| $S$ | profits from sales, € |
| $T$ | temperature, K |
| $\beta$ | pressure ratio |
| $\eta$ | efficiency, % |
| $\Delta$ | increase |
| $\delta$ | power station internal load rate for the $CO_2$ capture installation |

$\tau$ the next years of the construction and operating block

Indices

*AV* avoided
*C* compressor
*CCS* power plant with CCS installation
*EA* emission allowance
*el* electric
*HE* heat exchanger
*i* internal
*M* membrane
*(n)* net energy production
*obr* changes of the working capital
*PR* production
*REF* power plant without CCS installation
*th* thermal energy
*VP* vacuum pump

References

[1] Attala L., Facchini B., Ferrara G., 2001, Thermoeconomic optimization method as design tool in gas-steam combined plant realization, Energy Conversion and Management, 42(18), pp. 2163-2172.

[2] Chmielniak T., Supercritical Coal-fired Power Plants, project research. In: PBZ–MEiN–4/2/2006.

[3] Communication from the Commission to the Council and the European Parliament, Sustainable power generation from fossil fuels: aiming for near-zero emissions from coal after 2020, Brussels, 10.1.2007, COM(2006) 843 final.

[4] Czyperek M., et al., 2009, MEM-BRAIN gas separation membranes for zero-emission fossil power plants, Energy Procedia, 1, pp.303-310.

[5] Davison J., 2007, Performance and cost of power plants with capture and storage of $CO_2$, Energy, 32, pp.1163–1176.

[6] Davidson J., Thambimuthu K., 2004, Technologies for capture of carbon dioxide, *Proceedings of the 7th Greenhouse Gas Technology Conference*, Vancouver, Canada, International Energy Association (IEA), Greenhouse Gas R&D Programme.

[7] Grainger D., Hägg M-B., 2008, Techno-economic evaluation of PVAm $CO_2$-selective membrane in an IGCC power plant with $CO_2$ capture, Fuel, 87, pp. 14-24.

[8] Hägg M.-B., Lindbråthen A., 2005, $CO_2$ Capture from Natural Gas Fired Power Plants by Using Membrane Technology, Ind. Eng. Chem. Res., 44, pp. 7668-7675.

[9] Herzog H, 2001, What future for carbon capture and sequestration? Environmental Science & Technology,35(7), pp.148–53.

[10] Kohl A., Nielsen R., Gas purification. 5th ed. Houston, Texas: Gulf Publishing Company; 1997.

[11] Koros W. J., Fleming G. K., 1993, Membrane based gas separations. Journal of Membrane Science,83(1), pp.1–80.

[12] Kotowicz J., Bartela Ł., 2010, The influence of economic parameters on the optimal values of the design variables of a combined cycle plant, Energy, 35, pp. 911-919.

[13] Kotowicz J., Chmielniak T., Janusz-Szymańska K., 2010, The influence of membrane $CO_2$ separation on the efficiency of a coal-fired power plant, Energy, 35, pp.841-850.

[14] Kotowicz J., Janusz-Szymańska K., 2009, The Thermodynamic And Economic Analysis Of The Supercritical Coal Fired Power Plant With CCS Installation, Journal of POLISH CIMAC, Vol. 4, No 1, pp.75-82.

[15] METPORE (Nano-structured Ceramic and Metal Supported Membranes for Gas Separation), together with the University of Queensland, Australia, funded by Federal Ministry of Economics and Technology (BMWi), Germany and industrial companies EON, EnBW, RWE, start January 1st, 2007.

[16] Powell C. E., Qiao G. G., 2006, Polymeric $CO_2/N_2$ gas separation membranes for the capture of carbon dioxide from power plant flue gases, Journal of Membrane Science, 279 (1-2), pp.1-49.

[17] Project NanoGloWa – Nanostructured Membranes against Global Warming, URL: http://www.nanoglowa.com

[18] Zhao L., et al., 2009, Concepts and investment cost analyses of multi-stage membrane systems used in post-combustion processes. Energy Procedia, 1, pp. 269–278.

Zheng F., Tran D. N., Busche B. J., Fryxell G. E., Addleman R. S., Zemanian T. S., et al., 2005, Ethylenediamine modified SBA-15 as regenerable $CO_2$ sorbent, Industrial and Engineering Chemistry Research, 44(9), pp.3099–105.

# ANALYSIS OF A LIGNITE POWER PLANT WITH CARBON SEQUESTRATION

*C. Koroneos*, Th. Grigoriadis, M. Kosmidou*

*Laboratory of Heat Transfer and Environmental Engineering,*
*Aristotle University of Thessaloniki, Box 483, 54124 Thessaloniki, Greece*

**Abstract**

In this work the possibility and conditions for the inclusion of a system of separation and retention of $CO_2$ from flue gas (CCS) to existing lignite-fired steam power stations of the Greek energy system is investigated. An exergy and economic analysis is performed. The results show that it is possible to add a system to capture $CO_2$ from flue gas using absorption with monoethanolamine (MEA). The case considered is the absorption of 90% carbon dioxide from the exhaust gases. The paper focuses on the impact of the inclusion of CCS in the power plant and the performance and emissions from the plant. The addition of this system reduces the emissions of carbon dioxide to the atmosphere, but increases the specific production of $CO_2$/kWh. It also causes a substantial reduction in net exergy efficiency of the power plant, reduces electricity production and increases costs. As regards to the economics, the feasibility of CCS assembly depends on the price of $CO_2$ emissions in the global market. It certainly must not be forgotten that there is a drastic reduction in carbon dioxide with the addition of the CCS unit. However, the benefits coming from this action are offset by the increase in fuel consumption. Also, the storage technologies available, raise questions about their reliability over time, in other words, the time horizon for safe storage of carbon dioxide without ultimately getting back to the atmosphere. It is concluded that the technologies to capture the $CO_2$, as the one considered in this work, and others developed so far, are not attractive and valuable solution to reduce greenhouse gas emissions and to achieve the environmental goals set by international agreements.

**Keywords:** carbon sequestration; monoethanolamine absorption (MEA); lignite power plant; Greece

## 1. Introduction

One of the major environmental problems that our planet faces is the greenhouse effect, which is a phenomenon that is provoked by emissions of CO2 and other "greenhouse gases". The need to constrain these emissions is immediate and urgent. For this purpose, the international community has adopted several actions [1] that aim at the reduction of emissions in electricity production processes, the improvement of energy efficiency, the energy savings, the enhancement of the proportion of renewable energy in production, and technological development in the use of renewable energy sources [2]. In the context of reducing greenhouse gas emissions by electricity production and other industrial processes, some technologies for reducing $CO_2$ emissions by large industrial boilers (> 20MW) that are fueled by various forms of carbon (coal, lignite, etc.), have been developed. These technologies fall into three main categories [3]:

o The segregation of carbon is before the fuel combustion

o The fuel combustion takes place under conditions of pure oxygen

o The separation and retention of $CO_2$ takes place after the fuel combustion, at the exhaust gases.

In this work, these technologies are examined and the impacts of adding a complex of separation and retention of $CO_2$ in an existing thermal power station operating with pulverized lignite are analyzed. Today, it is necessary to install programs for energy savings in the developed countries in order not to deplete all the resources and not to degrade the environment further. Today, the world's daily oil consumption is 9 million $m^3$. Despite the well-known environmental consequences of combustion of fossil fuels, this number is expected to increase to 14.6 million $m^3$ per day by the year 2025 [4]. The fossils substitution with other forms of fuel, such as renewable energy sources, that will produce fewer pollutants, as well as the energy saving, are necessary actions. On the other hand, the European Union (EU) wants to make cleaner use of fossil fuels in energy production [5] promoting the environmentally safe use of a promising

technology, known as separation and retention of carbon dioxide (CCS). This technology allows the capture of carbon dioxide ($CO_2$) emissions from industrial processes before the gases reach the atmosphere and then pump them underground for long term storage.

## 2. Capture of CO2 from lignite and natural gas in power plants

There have been limited measures taken by all countries in order to reduce global warming and in order to achieve the objectives of the Kyoto Protocol [1]. Moreover, the growing market of $CO_2$ and the growing interest in optimal recovery of petroleum are the economic incentives to medium term application of technologies to capture $CO_2$. Sequestration and safe storage of $CO_2$ permits the use of fossil fuels and simultaneously reduces emissions of $CO_2$ in the atmosphere, leading to the prevention of climate change. Today, fossil fuels are the world's dominant primary energy sources. Despite the considerable efforts and investments by many countries to promote renewable energy and energy saving in order to address the problem of climate change, capture technologies and storage technologies of $CO_2$ will have to be included. Capture technologies of $CO_2$ from the thermoelectric stations (almost 1/3 of global emissions of $CO_2$ in the atmosphere) are expected to contribute significantly to reduction of greenhouse gases globally [6]. There is a very intense research activity internationally towards isolation and capture of $CO_2$ in thermoelectric plants. The main commercial and developing technologies [7] for capture of $CO_2$ in thermoelectric stations can be classified into three categories [8]:

1. Separation of $CO_2$ from the exhaust gas

The following processes can be used to remove $CO_2$ from the exhaust gas on a large scale:

- Absorption (separation of $CO_2$ injection in liquid by absorption column)
- Adsorption (separation by adsorption of $CO_2$ in a solid)
- Membranes (based on differential permeability of gases through membranes)
- Cryogenic technologies (cooling or condensation of $CO_2$)

2. Combustion of fossil fuels in pure oxygen conditions

3. Lignite gasification

The combustion of solid fuel, hydrocarbons or synthetic gas takes place in pure oxygen and the produced exhaust gas contains mainly carbon dioxide and water vapor. Carbon is removed from the fuel before it is burned. In the formal process of gasification combined cycle (IGCC), the solid fuel is pulverized and dissolved in water. After sequestration, $CO_2$ can be stored or reused, e.g. as an additive to refreshments or in greenhouses for plant growth enhancement. Because of the limited market for reuse of $CO_2$, the majority of the sequestrated $CO_2$ should be stored. $CO_2$ can be stored in geological formations (including exhausted reservoirs of oil and natural gas, deep saltwater aquifers and non-extracted coal layers). $CO_2$ can also be secured in the form of minerals. Deep saltwater aquifers are underground formations typically sandstones, containing salt water. Storage of carbon dioxide ($CO_2$) in oceans may be useful for the climate change that is caused by fossil fuel combustion.

## 3. The lignite power plant in Melite, Greece

The electricity power station of Melite in Florina, Greece [9], has nominal power 330 MWel, steam pressure 240 atm and temperature steam 813.15 K. It is a unit of supercritical operating point with low-NOx combustion, with a device of exhaust gas desulphurization, and belongs technologically to the latest generation of lignite units. This unit is the newest of the Greek system (started operating in 2006) and due to its technological level requires the least modifications to add complex capture of CO2, compared with other Lignin units in Greece. The lignite used in the power plant is specified in table1. The basic characteristics of the power plant are shown in table 2. The LHV of this lignite is $7955 * 10^3$ J/kg. These figures refer to turbine load 100% (330 MWel), ambient temperature 816.15 K and atmospheric pressure 976 mbar.

*Table 1: Basic quality analysis of lignite*

| **Composition** | **% w./w.** |
|---|---|
| Humidity | 36,80 |
| Ash | 27,36 |
| Total carbon (C) | 22,58 |
| Hydrogen (H) | 2,07 |

| | |
|---|---|
| Nitrogen (N) | 0,37 |
| Sulfur (S) | 0,94 |
| Oxygen (O) | 9,88 |
| **Total** | **100** |

*Table 2: Functional size of the unit of electricity power station of Melite in Florina*

| | | Unit | Rate |
|---|---|---|---|
| | Nom. Power | MW | 330 |
| **Boiler parameters** | Nom. steam | Kg/s | 268.9 |
| | Max. steam | Kg/s | 282.4 |
| | Fuel | Kg/s | 101.4 |
| | Heat | kJ/s | 806,637 |
| | Boiler eff. (LHV) | | 89.6% |
| | Specific heat cons. | kJ/kWh | 7784 |
| **Steam cycle parameters** | Eff. of steam cycle | | 46.2% |
| | Internal energy cons. | MW | 37.8 |
| | Electricity of network | MW | 292.1 |
| | Unit eff. (LHV) | | 36.21% |
| **Exhaust gases** | Total exhausts | Kg/s | 554 |
| | Emissions of $CO_2$ | Kg/s | 81.85 |

A typical lignite unit consists of the following: Fuel system, Combustion air system, Boiler, Draft exhaust system - Fly ash collection, Steam turbine – Generator, the main Refrigerator (condenser) and cooling tower, Preheaters, Main feed pumps, Main transformer. The unit operates with pulverized lignite. The fuel is sprayed from the mill to the boiler with warm air. The combustion produces heat that it is needed to produce super-heated and reignited steam. Fuel consumption is 100 kg/s, and air consumption 337.5 kg/s. The quantities of the exhaust gases after the ID Fans are 528 kg/s and after desulphurization (FGD) are 554 kg/s. The composition of exhausts after desulphurisation, which is based on the assessment of energy quantities of CO2 capture, is shown on table 3.

*Table 3. Exhaust gas composition*

| **Ingredient** | **Kg/s** | **Kmoles/s** | **Kmole %** |
|---|---|---|---|
| $CO_2$ | 0.08185 | 1.86 | 9.12 |
| $O_2$ | 0.01604 | 0.501 | 2.46 |
| $H_2O$ | 0.08848 | 4.91 | 24.1 |
| $N_2$ | 366.63 | 13.1 | 64.23 |
| $SO_2$ | 1.12 | 17.5 | 0.086 |
| Particles | 50($mg/Nm^3$) | | |
| Total | 554.12 | | |

**4. Absorption of CO2 - Necessary modifications**

It is generally accepted that the most successful technique for $CO_2$ capture from exhaust gases in power stations is the leaching method of chemical absorption with monoethanolamine [10]. This method may capture up to 98% of carbon dioxide from exhaust gas and give a final product purity reaching over 99%. Most systems use MEA dissolved in water containing only 15-30% by weight to avoid erosion conditions. For the smooth operation of the absorption system of $CO_2$, the exhaust gas that enters into the absorption column must have content of $NO_X$, $SO_2$, $O_2$, hydrocarbons and particles that do not overcome a maximum level so as not to destroy the solution of MEA and to avoid creating deposits or corrosion. $CO_2$ is absorbed by the liquid solution into the absorption column which operates at 313-333 K. The exhaust gas and the liquid solution are in contact in different flow. The exhaust gas, before entering the column, is compressed to 1.3 bar and enters from the bottom. The solution enters into the top of the absorption column directed downward. The heat required for regeneration of the solution is about 4 MJ per kg of bound CO2. Taking into account that the regeneration of sodium absorption takes place at about 150 ºC, the abstraction is at 5 bar. The energy required to compress the exhaust before it enters the absorption column and the movement of the solution in the system amounts to 0.11 MJ/kg of captured $CO_2$. Then, the compression, dehumidification and liquefaction of $CO_2$, follows. The steam allotment of low pressure turbine is reduced by approximately 2/3 when the application of the chemical absorption takes place. Energy use corresponds to 80% of the total energy required for the process of chemical absorption. The produced power is reduced by 20-25% and the efficiency of the plant by 11-14 %. For a typical station, the rate of removal for economic operation of the system is 85%, when the concentration of

CO2 in exhaust gas is 3% and respectively when the concentration of CO2 in exhaust gas is 8% it is 90-92%.

### 4.1 Necessary interventions in the plant

Since the amine solution is impaired with the $SO_2$, $NO_x$ and $O_2$, it will be expected to ensure that they are at maximum levels in the exhaust stream [11]. This means that changes and additions to the combustion system-boiler, in electrostatic filters and desulphurization unit should be made. These changes are necessary to be compatible with the $CO_2$ capture system. Also, to provide heat and electricity to the capture unit, changes should take place in the low pressure turbine to allow the abstraction of the necessary steam [12].

Actions to improve the quality of exhaust: The presence of $NO_2$ should be limited in the exhaust gases because it reacts with amine, and destroys it. The maximum $NO_2$ content, which is tolerated by the process, is 40 mg/Nm3 (6% $O_2$ v / v dry), that corresponds to $NO_X$ content of 600 mg/$Nm^3$. For NOx and $O_2$ control in the exhaust gases, steps should be taken such as: 1. Conversions in the boiler: a) Replacement of boilers with boilers of low NOX content and b) convert of the combustion air system in two stages. 2. Installation of SCR system (Selective Catalytic Reduction) to further reduce NOx. The power station of Melite has low NOx combustors which create under stoichiometric combustion zone. However, there are not data on the NOx content in exhaust gases and therefore it is not clear whether the system requires the addition of SCR. The maximum $SO_2$ content in the exhaust gases must not exceeds 30 mg/$Nm^3$ (6% $O_2$ v / v dry). It is a limit that is much lower than the limit which is imposed by European legislation on environmental protection and it means that the existing desulphurization unit is not sufficient. For further reduction of $SO_2$, a secondary desulphurization unit must be installed. To control of $O_2$ in the exhaust gases, proper air quantity in the boiler must be ensured and measure must be taken to control extra air into the boiler if it exceeds the baseline design of the boiler.

Turbine modifications: To feed the capture unit, heat energy is required for the reboiler separator and regenerator of MEA solution, and electricity for electric fans, pumps and compressors of the unit. The requirements of the absorption and liquefaction energy are shown in table 4.

*Table 4. Absorption and liquefaction energy requirements*

| | | |
|---|---|---|
| Captured $CO_2$ | tn/day | 6365 |
| Captured $CO_2$ | Kg/sec | 73,67 |
| Heat energy | kJ/kg $CO_2$* | 3600 |
| Steam in the separator | Kg/ kg $CO_2$* | 135,9 |
| Steam pressure | Pa | 320,000 |
| Steam temperature | K | 408 |
| Required solution | $m^3$/kg $CO_2$* | 0.017 |
| Electricity | MW | 45,8 |
| Cooling water | $m^3$/kg $CO_2$* | 0.046 |

* Refers to the amount of the bounded CO2

A stream of steam from the average pressure gradient of the turbine must be taken to overcome the needs of heat energy, so: a) this flow is equivalent to 50% of the total steam production and the total quantity of steam that goes to low pressure gradient and b) the steam characteristics at the exit of low pressure must be P = 320,000 Pa and T = 408 K. The existing low-pressure gradient should be abolished because it cannot operate effectively with the new characteristics of steam requirements. The solution under consideration is the new low-pressure turbine setting, which operates independently of the old one and it will have its own generator which is suitable for an operation under the new circumstances. This turbine will give steam with the characteristics needed for the absorption – separation process, and the power needed will be about 40 MW.

Modifications to the cooling water circuit: Only pipe manufactures need for this system to supply cooling water.

### 5. Capture and liquefaction system of $CO_2$

The amine technology is similar to existing amine procedures of MEA. The presence of oxygen is tolerated in the exhaust gas and a limited amount of $SO_2$ [11, 12, 13]. The process uses an oxygen-activated corrosion factor, which also prevents degradation of the amines. The low degree of erosion and the minimal loss of solvent that is used to absorb the $CO_2$, promote economical and reliable operation of the complex. This case considers a capture of 90% of CO2 from exhaust gas, which requires treatment throughout the exhaust gas allotment. There are many levels of sequestration (70%, 50% and 30%) which have

two options: a) treatment of the exhaust stream and bypass of the remaining power through the chimney. This method allows the sequestration and separation system to be smaller and less expensive b) passing the entire exhaust stream sequestration and separation system and in that case, the amine solution has different characteristics as the other parameters of the plant to be less absorption. The method has a disadvantage by the fact that it requires large absorber and amine regeneration system, which is significantly more expensive than the first method of bypassing part of the exhaust.

### 5.1 Description of removal process of $CO_2$, compression, and realization system

The $CO_2$ Recovery Unit is comprised of the following sections:

- Flue Gas Pretreatment
- Absorption
- Stripping
- CO2 Compression and Liquefaction
- Drying

The flue gas pretreatment section cools and conditions the flue gas, which is then fed to the $CO_2$ Absorber (or $CO_2$ contactor as it is often called). In the Absorber, $CO_2$ is removed from the gas by contacting it, in countercurrent fashion, with monoethanolamine (MEA). The recovered $CO_2$ is then stripped off in the Stripper (or Regenerator) from where the lean solvent is recycled back to the Absorber. Solvent regeneration for requires 4,958.5 kJ/kg $CO_2$. The overhead vapor from the Stripper is cooled to condense most of the water vapor. The condensate is used as reflux in the Stripper and the wet $CO_2$ stream is fed forward to the $CO_2$ Compression and Liquefaction System. Here the $CO_2$ product is compressed and dried so it can be pumped to its final destination. No specific destination has been chosen for the product pipeline. It has been assumed to end at the battery limit for costing purposes. Description of the package units is indicative.

### 5.2 Performance of the $CO_2$ capture system

The expected efficiency of the system [12] is represented in table 5. It is shown that there is 100% removal of Nitrogen and water from the stream. The material that is used for the operation of the $CO_2$ capture system is mostly MEA (Table 6) and then $Na_2CO_3$ with Anticorrosion inhibitor, Diatomaceous earth, Molecular sieve (Silica gel), and activated coal.

*Table 5. Capture system performance*

| | **Before the separator** | **Exhausts** | **Captured masses** |
|---|---|---|---|
| Ingredient | moles/s | moles/s | moles/s |
| $CO_2$ | 1.8598 | 0.1854 | 1.6743 |
| $H_2O$ | 4.9155 | 7.3062 | 0.2088 |
| $N_2$ | 13.089 | 13.089 | 0 |
| $O_2$ | 0.5012 | 0.5012 | 0 |
| Total | 20.365 | 21.082 | 1.8831 |

*Table 6. Material use*

| **Chemical substance** | **Quantity Kg/s** |
|---|---|
| MEA | 0.12071 |
| $Na_2CO_3$ | 0.01221 |
| Anticorrosion inhibitor | 0.00544 |
| Diatomaceous earth | 0.00243 |
| Molecular sieve (Silica gel) | 0.00131 |
| Activated coal | 0.00810 |

## 6. Results

A retention system of $CO_2$ from the exhaust lignite steam electric station was presented at the previous chapter, with the technical conditions for its operation, the mode of operation, the required energy and its efficiency. Based on these data, the efficiency of the Melite power plant before the use of CCS and after the use of CCS is presented in table 7. It should be noted here that the required energy for transport and the underground compression of carbon, are not taken into consideration. These factors will have an extra effect on the total efficiency of the system.

*Table 7: Comparative table of energy and technical parameters of the two cases*

| Parameter | Unit | Plant without CCS | Plant with CCS |
|---|---|---|---|
| **Boiler** | | | |
| Steam prod. | Kg/s | 0.0744 | 0.0744 |
| Steam pres. | Pa | $240*10^6$ | $240*10^6$ |
| Steam tem. | K | 813 | 813 |

| | | | |
|---|---|---|---|
| Reignited temperature | K | 813 | 813 |
| Boiler eff. | % | 89,6 | 89,6 |
| Lignite cons. | kg/s | 101.39 | 101.39 |
| **Steam cycle power** | MW | 330 | 275 |
| Power (generator) | | | |
| Power (new turbine) | MW | - | 40 |
| Tot. output power | MW | 330 | 315 |
| Specific heat cons. | kJ/kWh | 7784 | 8054 |
| Eff. of steam cycle | % | 46,2 | 44,7 |
| Consumption (unit) | MW | 37,88 | 37,88 |
| Consumption (CCS) | MW | - | 45,80 |
| Net power (network) | MW | 292,12 | 231,32 |
| **Station eff.** | % | 36,21 | 28,68 |
| Exergy eff. (LHV) | | | |
| Reducing eff. | % | 0 | 7,53 |
| Reducing production | % | 0 | 20,8 |
| **Emissions $CO_2$** | Kg/s | 81.85 | 81.85 |
| Produced $CO_2$ | | | |
| Specific cons. of $CO_2$ | Kg/kWh | 1,019 | 1,274 |
| Emitted $CO_2$ | Kg/s | 0 | 73.665 |
| Rate of captured $CO_2$ | % | 0 | 90 |
| Emitted $CO_2$ | Kg/s | 81.85 | 81.85 |

### 6.1 Effects on the performance of the power plant

It is very obvious from table 7 that adding the $CO_2$ capture system in the power plant will have a significant negative impact on the efficiency of the unit and of the electricity production. This is expected since the process of liquefaction engagement and the storage of $CO_2$ are processes that use heat and electricity. Figure 1 represents graphically the impact and the efficiency of the power plant.

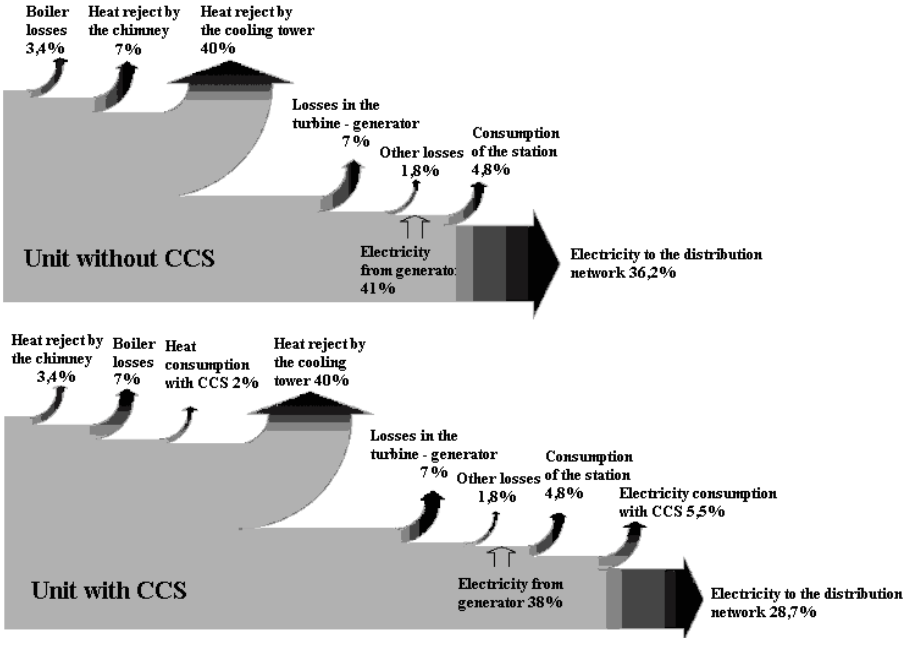


*Figure 1. Impact of CO2 capture system of the Melite power plant*

(Figure 2) and will also increase the emissions of $CO_2$ per kWh of electricity production (Figure 2).

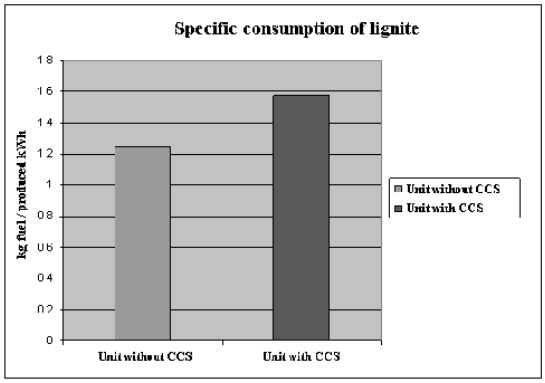


*Figure2. Specific consumption of lignite*

Also, as it is shown in Table 7 and in Figure 3, the specific production of $CO_2$ will be increased. 90% of carbon will be captured and eventually the carbon dioxide in the atmosphere will be significantly reduced.

### 6.2 Economic impacts

The addition of the capture $CO_2$ system along with other modifications of existing equipment that they are needed, have an estimated cost of $ 300,000,000. This cost was based on recent publications (November 2007) of National Energy Technology Laboratory (NETL) of US and it may deviate + / - 30% depending on the unit.

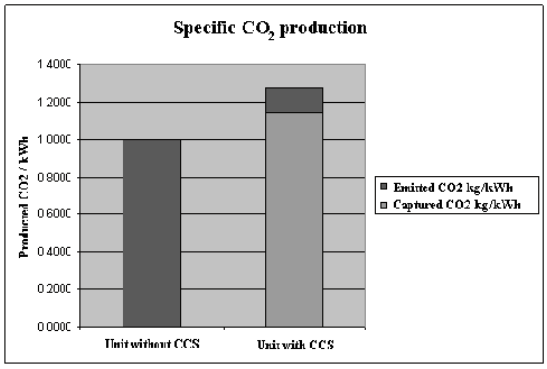


*Figure 3. Specific production of $CO_2$*

Apart from the cost of initial investment, there are costs of operating and maintaining of the facility, which they will charge the price of electricity to about 0,055 €/kWh. It is estimated that the cost will be 30 €/tn of captured $CO_2$ by 2012 and it will be reduced to 25 €/tn because of the further improving efficiency of the process. On the other hand, the $CO_2$ capture system will reduce the cost of the emission rights

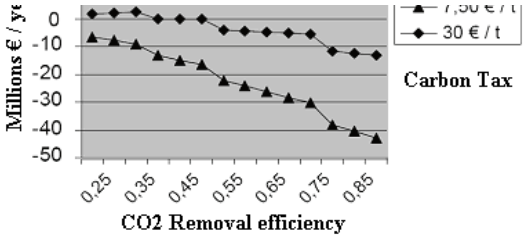


*Figure 4. The effect of removal of $CO_2$ on the financial effect of the plant*

Figure 4 shows whether the removal of $CO_2$ will have a positive or negative economic impact depending on the price of $CO_2$ in the international carbon market. The y axis of figure 4 represents the yearly earnings and the x axis the selling price of $CO_2$ rights in the market. As it is shown, the $CO_2$ capture use will have a positive financial result for the power plant only if the market price of pollutants is over 30 €/tn and for capture rate of less than 50% or the price reaches 50 €/tn so it is economically capture a greater proportion of carbon. The amount of energy required is 3600 kJ/kg of captured $CO_2$, and with technology improvements it is possible to reduce it to 2800 kJ/kg of captured $CO_2$.

### 6.3 Environmental impacts of CCS

The environmental impacts resulting from the use of the CCS system are the following:

a) The application of carbon capture on a large scale will increase the rate of consumption of conventional energy resources, which are not consistent with the principles of sustainability.

b) The $CO_2$ produced per unit of kWh is increased (in this case the increase is 25%).

c) The carbon storage is safe. Some methods of geological storage of carbon are considered very safe and tested at normal rate of production for many years.

d) The storage capacity

e) An alternative to reduce emissions is to upgrade or replace older power plants with new, which will have significantly better efficiency and therefore will have fewer emissions per kWh.

f) The process of absorption with monoethanolamine (MEA) requires consumption of large amounts of MEA on a daily basis (for the case that is examined: 10.43 tn/day). The MEA has index 3 for health risk and 2 for flammability by NFPA, so it is a hazardous substance.

## 7. Conclusions

The installation of $CO_2$ capture systems in the

technical specifications. The cost effectiveness, in addition to the construction and operating costs, is determined by the rate of CO2 in the global market emissions, by other financial penalties that might arise, by the energy required per mass unit of captured CO2 and by the rate of other energy sources except of lignite. Also, on the economic evaluation, the replacement of the deficit of electric energy must take into account. Currently the rate of carbon emissions and the commercially technology make this installation unprofitable because they reduce the economic impact of power plants. The obvious advantage of the CO2 capture system is the reduced emissions in the atmosphere. In contrast, there is the increase of fuel consumption. Also the storage technologies that are available make questions about their reliability. Summarizing all the above, the conclusion that emerges is that the CO2 capture technologies are not attractive and valuable to reduce greenhouse gas emissions and to achieve the environmental targets. Also, the general overall philosophy of this process, "still produce pollutants, but store them", does not comply with any environmental policy. Possible objective of these technologies is the short-term adjustment of the parts of the world energy market that it is based and has interests in solid fossil fuels, by international agreements.

**8. References**

1) Kyoto Protocol to the United Nations Framework Convention on Climate Change, 1-10 December 1997, English Conference of the Parties, Third session Kyoto

2) DG Environment ,"Future Climate Action beyond 2012", 9/2004, Background Document for the 14th September 2004 workshop on "Future Climate Action beyond 2012".

3) European Commission - Environment for Europeans, March 2007, Magazine of the Directorate General Environment, Issue 26.

4) IEA, International Energy Agency, Key World Energy Statistics, 9, rue de la Fédération, 75739 Paris Cedex 15, www.iea.org

5) European Commission, http://cordis.europa.eu/fp7/energy/about-coal_en.html

6) NETL, National Energy Technology Laboratory, 2007, What are the costs and benefits of Carbon Capture and Sequestration?, http://www.netl.doe.gov/technologies/carbon_seq/FAQs/benefits.html#

7) IEA, International Energy Agency, May 2007, $CO_2$ Capture ready power plants

8) NETL, National Energy Technology Laboratory of U.S., April 2005, Carbon Capture and Sequestration Systems Analysis Guidelines.

9) Greek Public Power Corporation, http://www.dei.gr/

10) Hongyi Dang, Gary T. Rochelle, May 14-17/ 2001, $CO_2$ Absorption Rate and Solubility in Monoethanolamine/Piperazine/Water, the First National Conference on Carbon Sequestration, Washington, DC

11) NETL, National Energy Technology Laboratory of U.S., November 2007, Carbon Dioxide Capture from Existing Coal-Fired Power Plants, Final Report.

12) Alstom Power Inc. & Abb Lumus Global Inc, Engineering feasibility and economics of $CO_2$ capture on an existing coal-fired power plant, Final Report.

13) IEA, International Energy Agency, May 2007, $CO_2$ Capture ready power plants.

# Tech-economical analysis of waste heat recovery and utilization at Ruukki metals, Raahe Steelworks

*Chuan Wang[a] and Jorma Perander[b]*

[a] *Centre for Process Integration in Steelmaking, Swerea MEFOS AB*
*Luleå, Sweden*
[b] *Rautaruukki Oyj, Ruukki Metals, Raahe, Finland*

**Abstract:** Steel industry is one of energy-intensive industries. Recovery and utilization of waste heat is important for reduction of energy consumption in the steel industry. Waste heat occurs in every plant of iron and steel works in the form of gases, liquid and solid. In this work, the waste heat considered is the flue gases from various process units. The studied steel works is Raahe steelworks (Ruukki), which is a fully integrated steel plant. The major process units to generate flue gases at Ruukki are batteries at coking plant, cowper at iron making plant and heat furnaces at the rolling mill. The flue gas temperatures are in the range of 230 ~ 550 ℃, and the flow rates are in the range of 25000 ~ 127000 Nm3/hour at each stack. The potential thermal energy recovered at each unit is calculated. Organic Rankine Cycle (ORC) technique has been applied for electricity generation from the recovered waste heat. Some economical parameters such as net present value (NPV), Internal return rate (IRR) and pay-back time are presented to show projects' economical feasibility. Sensitivity analysis of some key influence factors, such as equipment cost, electricity price and discount rate, etc. has been made. Furthermore, a concept of optimized use of waste heat from an integrated point of view has been studied, in which the power plant is also covered. Analysis and discussions on how to utilize waste heat to produce steam or electricity towards a more economical solution are presented.

**Keywords:** Waste heat recovery, Organic Rankine Cycle (ORC), Steelworks.

## 1. Introduction

Waste heat occurs in every plant of iron and steel works. The reuse of waste heat is important for the steel industry to reduce $CO_2$ emission and energy consumption. Furthermore, it can help reduce thermal pollution to the air and water body. Therefore, to recover and reuse the waste heat within the steel industry is an interesting research topic.

Waste heat exists in many forms, for instance, flue gas from furnaces, hot/cooling water in the heating system, hot slag from BF and BOF, radiation and convection from hot slabs. The presented paper is focusing on the recovery and reuse of waste heat from the flue gases at different process units in an integrated steel plant.

There are many ways of using the waste heat sources to produce useful products, such as electricity, process steam and hot water. Recent years, more attentions have been paid on using Organic Rankine cycle (ORC) technique to recover waste heat from flue gas for electricity production. The ORC unit is based on a closed Rankine cycle performed adopting a suitable organic fluid as working fluid. Conventional steam power cycles cannot give a better performance to recover low grade waste heat. There are several advantages in using an ORC to recover low grade waste heat, including economical utilization of energy resources, smaller systems and reduced emissions of CO, $CO_2$, $NO_x$ and other atmospheric pollutants. The main advantage of the ORC is its superior performance in recovering waste heat with a low temperature.

The ORC is not a new concept, and it has been investigated a lot for power generation the last decade [1, 2]. Thermodynamic analysis of the ORC has been presented in many studies, for instance, by Wei et al. [3]. The selection of the proper working fluids from the many different working fluids plays a significant role for the use of ORC process to recover a given waste heat, and is determined by the application and the waste heat level. The examples of working fluids and their thermo physical properties can be found in [2, 4-5]. The important parameters are for example critical temperature, boiling temperature, critical pressure and vapour pressure. Unlike water, most organic fluids suffer chemical decomposition and

Corresponding Author: Chuan Wang, Email: chuan.wang@swerea.com

deterioration at high temperatures and pressures. Therefore, an ORC system must be operated well below the temperature and pressure at which the fluids are chemically unstable. Most organic fluids have relatively low critical pressures and are therefore usually operated under low pressures and with much smaller heat capacities than water-vapor cycles.

ORC technique has been used for electricity production in some industries. For example, it has been applied to biomass combustion biomass CHP [6-8], geothermal plants [9-10] and cement industry [11-12]. However, according to authors' knowledge, the ORC application to the steel industry has not been reported yet.

In this paper, ORC technology is used to generate electricity by recovering waste heat from flue gases streams in a fully integrated steel plant. In addition, the other way to reuse the waste heat within the plant is also presented for comparison.

## 2. An overview of flue gases at Ruukki metals and their potential utilization

Raahe steelworks is a fully integrated steel plant including production units for coke, sinter, burnt lime, oxygen, electricity, hot metal, steel and final products of steel plates and coils. Annual crude steel production is about 2.8 Million tons.

The main flue gas sources at Ruukki metals are from batteries at the coking plant, cowper stoves at the blast furnaces and preheating furnaces at strip mill and plant mill. Table 1 shows the stack number in each process unit, the distance between each stack and the available cooling sources.

Table 1. Stack and cooling water information at different process units.

| | Stack number | Stack distance | Cooling water |
|---|---|---|---|
| Coking plant | 2 | 150 m | Sea water |
| Cowper | 2 | 100 m | Sea water |
| Plate mill | 4 | 40 m | Lake water or air |
| Strip mill | 2 | 50 m | Lake water or air |

Table 2 shows the fuel types used in each process unit. Basically three types of fuel are in use, i.e. coke oven gas (COG), blast furnace gas (BFG) and liquefied petroleum gas (LPG). COG and BFG are generated on site from coking plant and blast furnace as by-products in form of process gases.

Table 2. Fuel used in different process units

| Process unit | Fuel used | | |
|---|---|---|---|
| | COG | BFG | LPG |
| Coking plant 1 | √ | √ | |
| Coking plant 2 | √ | | |
| Cowper 1 | | √ | |
| Cowper 2 | | √ | |
| Plate mill 1 | √ | | |
| Plate mill 2 | √ | | |
| Strip mill 1 | √ | | √ |
| Strip mill 2 | √ | | √ |

As shown in Table 3, the flue gas flow rate is high in preheating furnaces at strip mill which corresponds to preheating furnaces. Meanwhile, the flow rate is low in preheating furnaces at the plate mills. The flue gas temperatures are in rang of 250 – 550 ℃. Table 3 also shows the heat capacity, $C_p$ value. The chemical composition of the flue gas from each process unit is presented in Table 4.

Table 3. Flow rate, temperature and the specific heat of flue gases.

| Process unit | Flow rate | Temp. | $C_p$ |
|---|---|---|---|
| | $Nm^3/h$ | ℃ | kJ/Kg·K |
| Coking plant 1 | 109222 | 250 | 1.053 |
| Coking plant 2 | 114749 | 230 | 1.100 |
| Cowper 1 | 109991 | 320 | 1.090 |
| Cowper 2 | 127723 | 320 | 1.089 |
| Plate mill 1 | 28305 | 550 | 1.186 |
| Plate mill 2 | 24903 | 550 | 1.175 |
| Strip mill 1 | 73414 | 450 | 1.151 |
| Strip mill 2 | 73414 | 370 | 1.151 |

In this paper, case studies of waste heat recovery and reuse are performed for cowper and preheating furnaces at the strip mill due to high amount of sensible heat in these two cases.

Table 4. Chemical composition of flue gases.

| Process units | Exhaust gas composition, % | | | | | | |
|---|---|---|---|---|---|---|---|
| | $H_2$ | CO | $CO_2$ | $N_2$ | $O_2$ | $H_2O$ | Others |
| Coking plant 1 | 0.0 | 0.0 | 17.0 | 66.2 | 8.6 | 8.1 | 0.0 |
| Coking plant 2 | 0.0 | 0.0 | 4.3 | 73.0 | 9.6 | 13.1 | 0.0 |
| Cowper 1 | 0.0 | 0.0 | 27.8 | 65.1 | 0.7 | 6.4 | 0.0 |
| Cowper 2 | 0.0 | 0.0 | 27.6 | 65.2 | 0.7 | 6.5 | 0.0 |
| Plate mill 1 | 0.0 | 0.0 | 7.7 | 69.2 | 0.7 | 22.3 | 0.1 |
| Plate mill 2 | 0 | 0 | 7.7 | 69.2 | 0.7 | 22.3 | 0.1 |
| Strip mill 1 | 0.0 | 0.0 | 8.9 | 70.3 | 0.7 | 20.0 | 0.1 |
| Strip mill 2 | 0.0 | 0.0 | 8.9 | 70.3 | 0.7 | 20.0 | 0.1 |

## 2.1. Electricity production from flue gas by use of ORC technique

The distance between two stacks at the cowper plant is 100 meters. As shown in Fig. 1, two heat exchangers are planned for installation, one for each stack, to recover the sensible heat from the flue gases. The hot source after the heat exchanger is slightly pressurized water at 190 ℃. The hot source is connected to one ORC unit for electricity production.

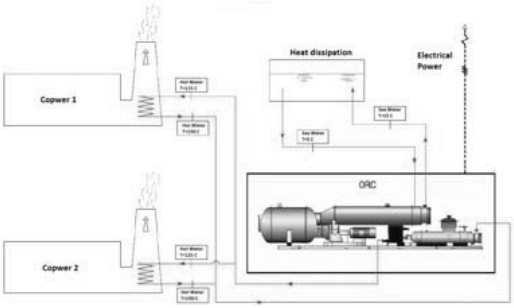


*Fig1. Process layout of ORC solution for cowpers.*

The thermal power recovered from flue gas in Cowpers is shown in Table 5.

*Table 5. Heat recovery from Cowpers.*

| | Cowper 1 | Cowper 2 |
|---|---|---|
| Inlet Temperature, ℃ | 320 | 320 |
| Outlet Temperature, ℃ | 160 | 160 |
| Recovered Thermal power, MW | 7.329 | 8.504 |

As shown in Fig. 2 for the strip mill, for taking advantage of the higher temperature level of the strip mill, the ORC is fed by thermal oil. Two heat exchangers are installed (one for each stack at the strip mill) to recover waste heat through the thermal oil.

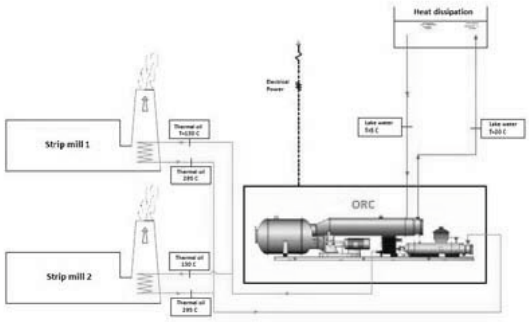


*Fig. 2. Process layout of ORC solution for the strip mill.*

As shown in Table 6, 15.15 MW thermal power will be recovered from the flue gas in the strip mill.

*Table 6. Heat recovery from the strip mill.*

| | Strip mill No. 1 | Strip mill No.2 |
|---|---|---|
| Inlet Temperature, ℃ | 450 | 370 |
| Outlet Temperature, ℃ | 150 | 150 |
| Recovered Thermal power, MW | 8.777 | 6.373 |

Table 7 shows a summary of main technical and economical parameters at strip mill and cowper by using of ORC technology. As shown in the table, the net electricity output for the strip mill and cowper are 3.05 MW and 2.70 MW, respectively.

*Table 7. Tech- economical data for ORC solution.*

| | Strip mill | Cowper |
|---|---|---|
| ORC investment, Million € | 3.73 | 3.55 |
| Thermal oil investment | 3.20 | |
| Hot water investment | | 3.45 |
| Total equipment cost, Million € | 6.93 | 7 |
| Other cost, Million € | 0.373 | 0.355 |
| Total investment, Million € | 7.303 | 7.355 |
| Operation cost, Million € per year | 0.1 | 0.1 |
| Operating hours | 7148 | 8519 |

| | | |
|---|---|---|
| Overall thermal power, MW | 15.15 | 15.83 |
| Gross electric output, MW | 3.55 | 3.19 |
| Net electric output, MW | 3.05 | 2.70 |
| Annual utilized heat energy, MWh | 108000 | 134600 |
| Annual electric output, MWh | 21800 | 23000 |
| Gross efficiency, % | 23.4 | 20.2 |
| Net efficiency, % | 20.2 | 17.1 |

## 2.2. Steam production from flue gas

The power plant at Ruukki metals produces electricity, which is used within the steelworks. The electricity is generated from the steam turbines. The high pressure steam (82 bar) is provided from the coking plant and from two steam boilers in the power plant, as shown in Fig.3. Except for the electricity production, some amounts of low pressure steam is tapped out for the process use, for example steam extraction from 82 bar to 30 bar (80/30), 80/10 bar. Some other process steam (8 bar and 4 bar) are also needed and taken from the steam tapping. However, less electricity will be generated when process steam is tapped from high pressure steam or from lower pressure tapping. Other ways to increase the electricity production are to generate the process steam in separate boilers to reduce steam tapping.

As shown in Fig. 3, there are three turbines of condensing type at the power plant. TG 65 is producing 65 MWel and it has many tapping points. TG 21 is an older turbine which produces 21 MWel. The third one, TP01, is used to drive blower for blast furnaces representing 10 MWel and does not have any tappings. Each turbine has its own condenser.

The recovered waste heat from the flue gas can be used to run boilers for steam production. For the strip mill case, the thermal oil solution or steam boiler can be used to generate 26 bar steam. 100,000 MWh steam flow in 26 bar is taken from early planning in the plant. This steam is used to substitute 50% 30 bar and 10 bar, as well as 50% 8 bar tapped process steam.

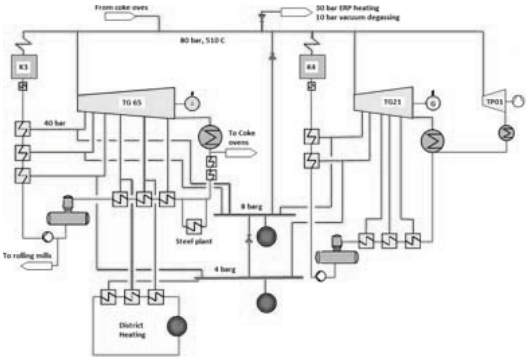


*Fig. 3. Overviews of steam turbine process at the power plant.*

All steam used in 30 bar and in 10 bar has taken from direct reduction. 30 bar steam can be reduced to 26 bar, therefore, we can substitute 30 and 10 bar steam by using 26 bar steam generated from the strip mill. As shown in Fig. 3, steam from tappings in 30 and 20 bar are going into 8 bar steam net.

Changing factors is used to calculate how much electricity could be generated from the untapped process steam. Fig. 4 illustrates the correlation between steam tapping and electricity production in the turbine process. The pressure on curve means pressures inside turbine, as shown in Fig.4. For 30 bar and 10 bar steam which is directly reduced from 80 bar steam, a factor of 3 is used. This factor means that 3MW thermal steam (82 bar) will not go through the turbine for electricity production, which can generate 1 MW electricity. As for 8 bar steam taken 30 bar and from 20 bar tapping, an average factor of 3.75 is adopted. Therefore, factor for utilizing 26 bar steam from mill plant will be calculated as (3 + 3.75)/2 = 3. 375. This factor used in this work, which corresponds to gross efficiency of 29.6%. By calculation, 3.45 MW gross power output will be achieved. For the 26 bar steam system, the additional electricity is needed for feed water pumping and flue gas funs in the strip mill. By estimation, the net output will be 3.3 MW if 4-5% electricity consumption is assumed.

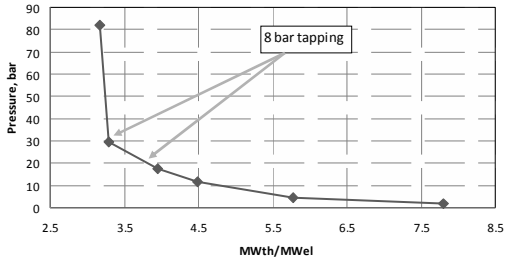


*Fig. 4. The ratio of thermal energy and electricity from the steam turbine process.*

As for the cowper plant, the other option is to produce 190 ℃ water (same as for ORC process) by installing heat exchangers at the cowper plant to recover the waste heat from the flue gas. This hot water can be used to substitute preheating of feed water to mill plant, coking plant and feed water tank. At the moment, the feed water in these two units is preheated to 80-100℃ by hot water from a feed water tank, which is heated by other tapped process steams in temperature to 150℃. For this solution, the flue gas temperature is assumed to be lowed down to 120 ℃ from 320 ℃. By calculation, 20 MW of hot water (190 ℃) will be produced. This amount of hot water is assumed to feed into the power plant to avoid tapping out 4 bar steam from the turbine. The gross electricity output will be 3.33 MW when changing factor of 6 is used. The net electricity is assumed to be 3.2 MW.

As shown in Table 8, the additional net power output from the strip mill and cowper using the steam turbine solution are 3.3 MW and 3.2 MW, respectively. A high investment, 9 million Euro, is noticed for steam boiler in the strip mill. The thermal oil solution could make the investment lower.

*Table 8. Tech- economical data for the steam turbine solution.*

| | Strip mill | Cowper |
|---|---|---|
| Hot water investment | | 3.5 |
| Steam (26 bar) production | 9.0 | |
| Total equipment cost, Million € | 9.0 | 3.5 |
| Other cost, Million € | 0 | 0 |
| Total investment, Million € | 9.0 | 3.5 |
| Operation cost, Million € per year | 0.1 | 0.1 |
| Operating hours | 8485 | 8438 |
| Overall thermal power, MW | 15 | 20 |
| Gross electric output, MW | 3.45 | 3.33 |
| Net electric output, MW | 3.3 | 3.2 |
| Annual utilized heat energy, MWh | 100000 | 170000 |
| Annual electric output, MWh | 28000 | 27000 |
| Gross efficiency , % | 29 | 16.5 |
| Net efficiency, % | 28 | 16.0 |

## 2.3. Economic parameters

The following economic parameters have been considered to evaluate the project's economical feasibility.

Net present value (NPV) is a traditional valuation method used in the discounted cash flow measurement methodology. NPV is expressed by the value of difference between the present value of all in-flow cash and outflow cash. The value of NPV determines whether or not the project is profitable. Positive NPV values are an indicator of a potentially feasible project.

The calculation of NPV can be expressed in Equation (1),

$$NPV = \sum_{t=1}^{T} \frac{C_t}{(1+r)^t} - C_0 \qquad (1)$$

where,

$C_0$, initial investment including machinery, installation, employee training cost, etc.

$C_t$, cash flow from year *1-t*

*t*, the time of the case flow

*r*, the discount rate (the rate of return that could be earned on an investment in the financial markets with similar risk).

The internal rate of return (IRR) represents the true interest provided by the project over its year. It is the discount rate at which the NPV of a project equals to zero. If the project's IRR is equal to or greater than the rate required by the investor, this project is likely to be considered acceptable, and vice versa.

The pay-back time represents the length of time that it takes for the owner of a project to recoup the initial investment out of the generated project cash flow. It is the year in which the NPV of a project equals to zero, and can be easily obtained by reading the NPV vs. Year curve.

## 3. Results

This section presents the financial results of different solutions. The present economic analysis has been based on the following assumptions as shown in Table 9.

*Table 9. Input economic data.*

| | |
|---|---|
| Discount rate, % | 10 |
| Project lifetime, year | 20 |
| Tariff, €/MWh | 60 |

### 3.1. ORC solution

Fig. 5 presents NPV and IRR value for ORC solution at the strip mill and cowper. NPVs are positive for both strip mill and cowper indicating profitable results for ORC solution. This can also be shown from IRR values. IRR values for strip mill and cowper are 15.6% and 16.6%, repectively. They are greater than the rate required at Ruukki, i.e. 10%.

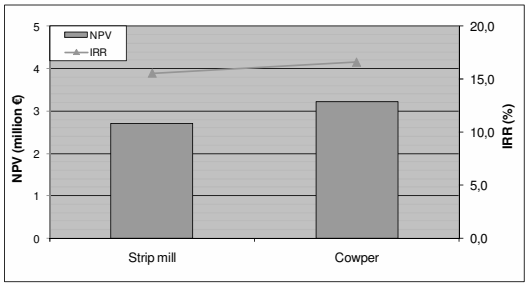


*Fig. 5. NPV and IRR for ORC solution*

As shown in Fig. 6, the pay-back time for these two cases are 5.7 years and 6.0 years, respectively.

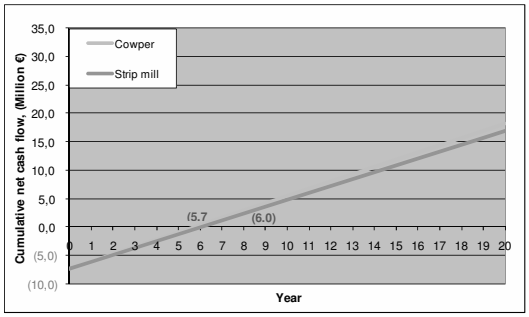


*Fig. 6. Pay-back time for ORC solution*

### 3.2. Steam turbine solution

As shown in Fig. 7, NPVs for the steam turbine solution at strip mill and cowper are 4.0 and 8.6 million Euro, respectively.

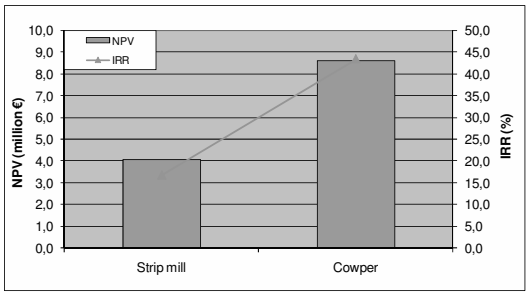


*Fig.7. NPV and IRR for steam turbine solution*

Fig. 8 indicates a pay-back time of 2.3 year for the cowper case and 5.7 year for the strip mill case.

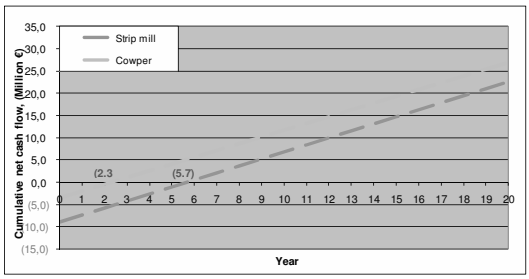


*Fig. 8. Pay-back time for steam turbine solution.*

All the economical parameters indicate that the steam turbine solution are enomically profitable.

## 4. Discussions

The economic analysis performed in this work shows that all solutions to recovery and reuse the waste heat from the strip mill and cowper are economically profitable.

In general, the project profitability is higher when utilizing the recovered waste heat to substitute process steam or hot water, which otherwise has to be tapped from the steam turbine in the power plant. Compared to the ORC solution, more electricity will be generated from the steam turbine solution. However, the approaches are not the same for these two cases. For the strip mill case, a higher efficiency in the steam turbine solution leads to a more profitable situation than ORC solution. As for the cowper case, a lower investment for the steam turbine solution makes a better profitability than the ORC solution.

The ORC solution could be chosen when the recovered heat could not be used to substitute some process related heat. However, a relative long pay-back time is expected.

The project's profitability is sensitive to some economic parameters, such as tariff, investment and discount rate. Fig. 9 illustrates that NPV increases with increasing electricity price.

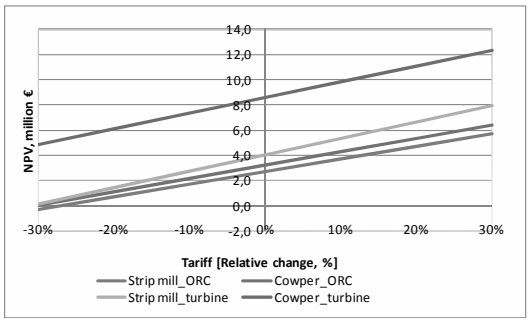


*Fig. 9. Tariff relative change vs. NPV*

The influence of investment change on NPV is shown in Figure 10. It shows a decreasing tendency of NPV with increased investment. Compared Figure 9 with Figure 10, it is found out that tariff is more sensitive than investment.

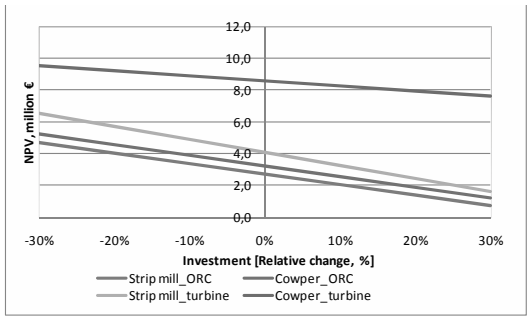


*Fig. 10. Investment relative vs. NPV*

To illustrate the uncertainties of discount rate's influence on NPV, Figure 11 shows that a low discount rate will lead to a relative high NPV, and vice versa.

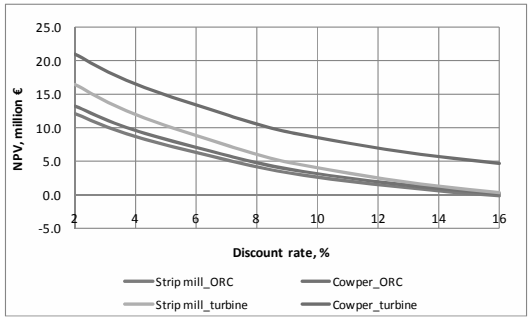


*Fig. 11. Discount rate vs. NPV*

## 5. Conclusions

Waste heat recovery and utilization from flue gases in selected process units were studied. Two different utilization approaches have been considered and compared, i.e. to produce electricity by using ORC technique and to substitute process steam or hot water in the power plant.

The economic analysis performed in this paper shows that all technical options considered are economically feasible. The comparisons indicate that it is more profitable to utilize the recovered waste heat to substitute process steam and hot water instead of generating electricity directly from ORC units.

We can conclude that it is better to apply a site-oriented approach for waste heat recovery and reuse in order to achieve a maximum profitability.

## Acknowledgements

This work was carried out in PRISMA - Center for Process Integration in Steelmaking. PRISMA is an Institute Excellence Centre (IEC) supported by the Swedish Agency for Innovation Systems, the Knowledge Foundation, the Foundation for Strategic Research, and by the industrial participants Luossavaara-Kiirunavaara AB, SSAB Tunnplåt AB and Rautaruukki Oyj, located at Swerea MEFOS AB.

The authors would like also thanks the ORC company, Turboden Italy; and the engineering company, Planora Oy Finland, for providing us technical and cost data needed for this work.

## References

[1] Lee K, Kuo S, Chien M, Shih Y, 1998, Parameters analysis on organic Rankine cycle energy recovery system. Energy Convers Manage 28, pp.409–18.

[2] Hung T-C, Shai T-Y and Wang S-K, 1997, A review of organic rankine cycles (ORCs) for the recovery of low-grade waste heat. Energy, 22(7), pp. 661-667.

[3] Dai Y-P, Wang J-F, Gao L, 2009, Parametric optimization and comparative study of organic Rankine cycle (ORC) for low grade waste heat recovery. Energy Conversion and Management 50, pp. 576-582.

[4] Schuster A, Karellas S, Kakaras E and Spliethoff H, 2009, Energetic and economic investigation of Organic Rankine Cycle applications. Applied thermal engineering 29, pp. 1809-1817.

[5] Wei D-H, Lu X-S, Lu Z and Gu J-M, 2007, Performance analysis and optimization of organic Rankine cycle (ORC) for waste heat recovery. Energy conversion and management 48, pp. 1113-1119.

[6] Obernberger I, 1998, Decentralized biomass combustion: state of the art and future development, Biomass and Bioenergy, 14 (1) pp. 33-56.

[7] Duvia A and Gaia M, 2002, ORC plants for power production from 0.4 MWe to 1.5 MWe: technology, efficiency, practical experiences and economy, in: Seventh Holzenergie Symposium, Zürich, Switzerland.

[8] Obernberger I, Thonhofer P and Reisenhofer E, 2002, Description and evaluation of the new 1000 kWel Organic Rankine Cacle process integrated in the biomass CHP plant in Lienz, Austria, Euroheat & Power 10.

[9] A. Borsukiewcz-Gozdur, W. Nowak, Maximising the working fluid flow as away of increasing power output of geothermal plant, Applied ThermalEngineering 27 (2007) 2074–2078.

[10] Vasile M, 2007, Using geothermal energy and insutrial waste heat for power generation. 2007 IEEE Canada Electrical Power Conference, Montreal, QC, Canada.

[11] Legmann, H, 2002, Recovery of industrial heat in the cement industry by means of the ORC process, IEEE Cement Industry Technical Conference (Paper), pp. 29-35.

[12] Huckauf H and Sankol B, 2000, Using the ORC process for waste heat utilization when burning cement clinker. ZKL International, 3, pp. 146-151.

# Enhanced Training on Marine Gas Turbine Degradation Effects

*I. Roumeliotis [a], N. Aretakis[b], E. A. Yfantis[a], K. Mathioudakis[b], P. Kapasakis[a]*

[a] *Hellenic Naval Academy, Section of Naval Architecture & Marine Engineering, Piraeus, Greece*
[b] National Technical University o*f Athens, Laboratory of Thermal Turbomachines, Athens, Greece*

**Abstract:** This paper focuses on the degradation effects on marine gas turbine engines and is introducing the aspect of enhanced training in the field of performance monitoring and diagnostics via fault simulation. A particular performance model, TEACHES, built for on board training purposes in the frame of Virtual Lab, is employed to demonstrate the effects of typical faults on the operation and performance of a specific marine engine of interest. The model allows the presentation of basic rules of gas turbine engine behavior and enables users to indulge in different aspects of its operation using a graphics user interface. The faults can be easily introduced into different engine components and their impact on engine performance can be studied and evaluated allowing the derivation of faults signatures on monitoring parameters. A literature review was materialized in order to simulate the degradation effects on each component accurately.

**Keywords:** Gas Turbine, Fouling, Erosion, Diagnosis, Simulation.

## 1. Introduction

Marine gas turbines have been in service for more than three decades and have proved to be reliable and offer significant advantages to the user. Despite the well-proven reliability of these machines, their operation in hostile marine environment results in the degradation of their performance characteristics.

Several mechanisms result in engine degradations, such as fouling, corrosion, erosion and FOD causing a change of rotating components swallowing capacity and a reduction in their isentropic efficiency. The components performance degradation leads to a deviation of the engine monitoring parameters. These deviations are the symptoms the users will observe. It is of major importance for the engineers who will operate these marine propulsion systems to realize the engine degradation phenomena and to be prepared to face the "real" engine behavior. In this paper data from the bibliography is used in order to simulate the most common faults and a thorough discussion of their impact on engine performance is featured, while typical fault signatures are presented. A specific marine gas turbine configuration has been considered for the implementation of the proposed simulation and for the derivation of the fault signatures. Namely the GE LM2500, an engine widely used for marine propulsion purpose, is examined in this study.

Diagnostic capabilities of the existing performance model might be examined and tested using the measurement data from an actual operating marine gas turbine. Model results and real engine performance data could be compared by the user to assess proper engine rating and ultimately to reconsider force engine maintenance schedule.

## 2. Computer Models and Gas Turbin Performance Training

Employing computer models for training gives seve possibilities that could only be offered by observing an act gas turbine in operation. A computer model produces ve easily a lot of information that would be difficult, expensi and some times even impossible to obtain on an actual engi Engine behavior can be studied at all possible permissible even non-permissible operating conditions, depending on t level of modeling.

Any physical quantity can be observed, without the need expensive instrumentation, which must be used on an act engine. Even quantities that would be impossible to obta due to geometrical or operating restrictions, can be observ (for example, turbine entry temperature, interstage pressure a multistage compressor or turbine etc).

A model provides also advantages over observing engine operating in the field. Operating restrictions usua impose a narrow envelope of operation, thus the time need before the operators can get the hands-on experience may long. The possibilities for understanding the principles of g turbines operation, offered by a computer model, have be discussed in more detail by Mathioudakis et al. [1].

These advantages become even more pronounced wh operation under abnormal conditions, namely deteriorat engines or engines with faults, is considered. If experience to be gained by observing actual engines this will have happen either by (a) studying cases where faults have occurr

Corresponding Author: Ioannis Roumeliotis, Email: jroume@ltt.ntua.gr

an operating gas turbine or (b) by setting up tests in which ılts have been artificially introduced. Case (a) is a situation ıt may or may not happen and any operator would try to ɔid anyway. Case (b) can result to costly tests while many ılts would not be implemented in fear of confronting more ious damage. For these reasons, both approaches cannot be nsidered as suitable for training purposes, leaving the most ıble option to be the use of an engine simulation model.

## 1 Modeling of Engine Deterioration

In order to have the ability to examine the operation of a s turbine of different configuration, under various operating nditions and control variables, a generic 0-D non-linear aptive performance model was developed by the research ɔup of the LTT/NTUA. The model was created in order to nulate all existing gas turbine configurations from a single aft engine, to a three spool engine with power turbine, ieating, recuperation and water injection at various positions ɔng the engine. The model is capable to acknowledge veral parameters as control variables like TIT, CDP, Load, . depending on the engine configuration. The model layout d the system of equations to be solved are modified in cordance with the engine configuration under consideration.

A schematic representation of the generic model and its eak down scheme to individual components is shown in gure 1. The components operation is modeled via maps (e.g. bomachinery component maps), via analytical relationships g water/steam injection [2]) or a combination of analytical ationships including empirical constants (e.g. duct pressure s).

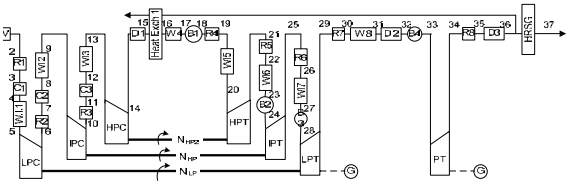


*gure 1: Schematic representation of a three spool gas bine and its components discrimination*

The model is employing the adaptive modeling technique, introduced by the research group of the LTT/NTUA [3], ıich will be used in order to model engine faults. The basic a behind the adaptive modeling is that component aracteristics (e.g compressor map) are allowed to change ough the introduction of appropriate modification factors. e values of these factors in the case of adaptive modeling determined by requiring that the available engine formance data are matched by the engine model results. In end of the adaptive procedure a unique set of components aracteristics is produced. The engine model incorporating s set is capable of simulating the specific engine operation th great accuracy (Tsalavoutas et al. [4]).

When diagnostic applications on an actual engine are considered, the modification factors can be used as engine health indices as, for example, presented in [5] and [6], in order to identify engine components faults. This requires that prior an accurate model of the healthy engine has been created by performing adaptation.

The adaptive (or modification) factor for each component parameter is defined via eq. (1).

$$f = \frac{X_{act}}{X_{ref}} \tag{1}$$

Specifically, if a particular component parameter has a value $X_{ref}$ on the reference map and a value $X_{act}$ on the actual "engine" map, then the relation between the two can be expressed by means of the modification factor f. The value of this factor shows how strong is the deviation of a particular performance parameter with respect to its reference/nominal value.

Each rotating component (compressors and turbines) employs two modification factors, one related to pumping (or swallowing) capacity and the other related to efficiency. The swallowing capacity factor is:

$$f_{SWi} = \frac{\left(W \cdot \sqrt{T}/p\right)_{act}}{\left(W \cdot \sqrt{T}/p\right)_{ref}} \tag{2}$$

The efficiency factor is:

$$f_{SEi} = \frac{\eta_{act}}{\eta_{ref}} \tag{3}$$

In the case of the combustion chamber, the modification factors correspond to the pressure losses and the combustion efficiency (see for example [2]), while there are also modification factors associated to the bleed flows.

Pertaining to all modification factors the term i corresponds to a specific component of the selected engine configuration. For example in the case of a twin shaft arrangement and for the rotating turbomachinery factors i=1 corresponds to the compressor, i=2 to the gas generator turbine and i=3 to the power turbine.

The faults are simulated by modifying the performance characteristics of the components from their “healthy” values, using the appropriate modification factors. The modified characteristics are used by the engine model and the deviations of the performance parameters are established.

For example, setting the value of the swallowing capacity of the compressor 0.97 it represents a 3% reduction in compressor pumping capacity from the nominal (healthy) operation. To simulate the existence of a malfunction, modification factors with values different from unity should be introduced.

Corresponding Author: Ioannis Roumeliotis, Email: jroume@ltt.ntua.gr

## 2.2 Visual Interface

A key factor for the effectiveness of software, used for training purposes, is the display feature of the visual interface in a user friendly aiming. The visual interface contains:

- The variables associated with gas turbine performance grouped in three different kinds, namely, operational input, component parameter input and output.
- A comprehensive plotting of the actual engine.
- A graphic window display of parameters, selectable by the user.

The layout of the basic s/w visual interface is shown in Figure 2 for the case of GE LM2500. Data can be introduced for all operational variables, i.e. ambient conditions, fuel type and synthesis etc.

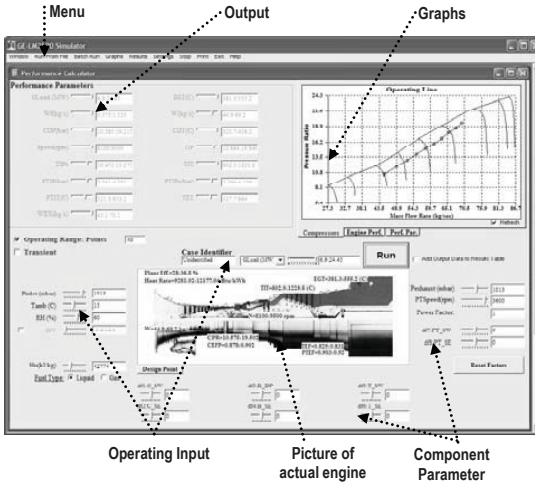


*Figure 2: The layout of the basic screen of the engine performance simulation and diagnostics software*

As previously mentioned the model is capable to treat several parameters as control variables, thus the user can select the exact mode (maximum power, continuous rating etc) in which the engine is working. The visual interface allows the easy introduction of modification factors values, as shown in Figure 3. To facilitate the interpretation, the actual value fed to the model is the quantity (f-1)*100, i.e. the percentage deviation of each component parameter.

In the partial s/w window displayed in Figure 3, a particular case is shown, in which the compressor has suffered a 3% reduction in mass flow capacity and a respective 1% reduction in efficiency. The users are capable to perceive the possible shift of the operating line and evaluate the effect of malfunctions on the compressor surge margin, which is one of the most important engine operational parameters, via a graphical interface as presented in [7].

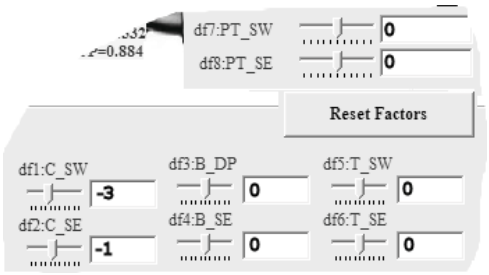


*Figure 3: Engine modification factors characterizing engi component condition.*

The introduction of malfunctions gives several possibilit to demonstrate their effect on engine performance paramete First of all, by performing simulations for healthy and fau engines the impact of faults can be directly assessed. T important notion of ¨fault signature¨ can be very eas introduced, when the above-mentioned possibility exis Values of measured quantities can be calculated for bo healthy and faulty operation and their differences a calculated to provide the signatures. The present model equipped with the capability of directly evaluating such signature, whenever a fault is simulated. A picture of a fa signature in the form of measurement deviations with resp to specific reference values, provided by the model is sho in Figure 4. The fact that different signatures are produced different faults can be easily demonstrated, while the effect the selected control variable on the fault signature can also examined.

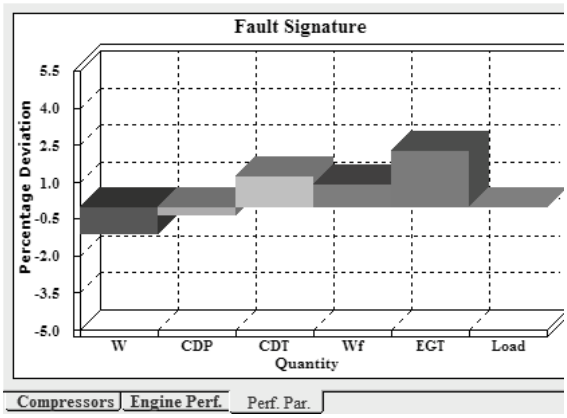


*Figure 4: Example of fault signature for main engi parameters.*

## 3. Faults Representation

Prior to implement any engine performance degradati effects, it is necessary to describe the most common faul investigate the physics of the alternations on the engi operation and correlate them with suitable modification facto variations.

Corresponding Author: Ioannis Roumeliotis, Email: jroume@ltt.ntua.gr

pical faults that are considered herein are:

Compressor Fouling

Compressor Erosion

Compressor Tip Clearance Increase

Turbine Fouling

Turbine Erosion

Foreign Object Damage (FOD)

## 1 Compressor Fouling

Fouling is one of the main reasons which lead to nificant performance loss in gas turbines. According to mji [8] some estimates have rendered fouling responsible 70 to 85% of all gas turbine performance loss accumulated ring life service.

All compressors are susceptible to fouling due to the gestion of air impurities that accumulate on and stick to gas h free surfaces, blades and shrouds, modifying in this way foil geometry [9]. In addition oil leaks from compressor ls and bearings mix with some of the ingested particles and posit on the blade surfaces [10]. The result would be the terioration of airfoils aerodynamic behavior and a relative luction of flow area, leading to the compressor and whole gine performance degradation. According to Tarabrin et al. ] the first 5 to 6 stages of axial compressors are mainly jected to blade fouling due to deposits while the first two ges are significantly more prone to fouling than the sequent ones (Tarabrin et al. [11], Syverud et al. [12]).

Fouling is be represented by a reduction in swallowing pacity of the component inlet (reduce of flow area) plus a luction in the component efficiency (due to the increase of face roughness). Field tests for fouling effect referenced by q and Saravanamuttoo [13] show a ratio between mass w and efficiency reduction in the order of 2.67 (0.8/0.3). sults presented by Zaba [14] for two different engines, fering from high fouled compressor first stages, indicated a nd between mass flow and efficiency reduction in the order 2.5. Diakunchak [9] reported site test data, obtained by a ge industrial gas turbine, which indicate that compressor uling account for a 5 percent reduction in inlet mass flow d 1.8 percent reduction in compressor efficiency, giving a io of 2.78. Thus, for the compressor fouling simulation it is itimate to use a ratio between swallowing capacity luction and efficiency reduction equal to 3.

## 2 Compressor Erosion

While in service, the engine will swallow dust and small nd particles resulting to the exfoliation of blade material. is material removal causes increased tip clearances and luced chord lengths. The erosion of the blade, results in reased surface roughness, changes in the inlet metal angle ence, a change in airfoil incidence), change in airfoil profile, change in airfoil throat opening, and an increase in blade tip and seal clearances**.** The results of these changes are increased losses and therefore a decrease in the compressor performance. Erosion has been manifested to be more severe in the tip region at the rear part of the compressor due to the existence of centrifugal forces which cause the migration of solid particles to the outer diameter, as discussed by Tabakoff [15] and adopted by Zaita et al. [16]. The effect of erosion on the compressor parameters is the significant decrease in the swallowing air mass flow.

No experimental data on the degradation ratio of these parameters is available in literature. The results derived by Aretakis et al. [17] through the application of a stage stacking model for the compressor, accounting for erosion effect, coupled with an engine model will be used herein.

The results indicate that the blade erosion effect, not accounting for the tip clearance increase, will affect mainly the air mass flow and will slightly decrease the compressor efficiency. Thus for the compressor erosion simulation, excluding the tip clearance effect, a ratio between swallowing capacity reduction and efficiency reduction equal to 8 will be used.

### 3.3 Compressor Tip Clearance Increase

Excessive compressor blade tip wear is a typical fault for in service engines, in case the compressor rotor becomes unbalanced or misaligned due to front or rear compressor bearing damage. Depending on the operation, it may be the result of differences in thermal growth of the rotors and casing during transients phenomena as discussed by Zaita et al. [16].

Also in the case that the blades are not in contact with the casing, the clearance may be increased by erosion as discussed by Schmücker and Schäffler [18]. In any case, compressor tip clearance increase results in a severe reduction of air mass flow rate and pressure ratio as reported by MacLeod et al. [19]. According to the experimental results given by Schmücker and Schäffler [18] compressor tip clearance increase should be represented by reduced swallowing capacity at the component inlet as well as by a reduction in the component efficiency.

According to the experimental results presented by Schmücker and Schäffler [18] the mean loss for a 1% change in tip clearance, is 2% in both efficiency and mass flow rate, thus giving a ratio of change equal to 1.

### 3.4 Turbine Fouling

Turbine fouling is mainly depending on type and quality of the operating fuel [20]. If gas turbine is running on clean fuel such as natural gas, the turbine degradation will be much slower, while when heavy fuel oil or crude oil is used, the turbine degradation is likely to appear earlier. Low melting

Corresponding Author: Ioannis Roumeliotis, Email: jroume@ltt.ntua.gr

point ashes, metals and unburned hydrocarbons can be aggregated in the turbine in the form of scale.

The contaminants deposition will have an impact over blade, by changing the airfoil shape, the inlet angle and increasing the surface roughness. These effects will result to the reducing of the airfoil throat area and apparently reducing the performance characteristics and the service life of the component. Also, especially in marine gas turbines, sulfidication may occur resulting in turbine corrosion. As a result, fouling rate will increase, as discussed by Basendwah et al. [21].

Turbine fouling is liable for the decrease of both turbine swallowing capacity and efficiency. According to the experimental results presented by Zaba [14] the ratio of the factors is expected to be in the range of 1. Thus, for the turbine fouling simulation, a ratio between turbine swallowing capacity reduction and efficiency reduction equal to 1 will be used.

### 3.5 Turbine Erosion

Erosion is caused by the impingement attack of particles against the surface of the turbine blade. Due to the high speeds, at which the blades rotate, a collision with even a very small particle induces a significant damage effect on the turbine blade affecting the performance of the turbine. Erosion is generally attributed to the larger particle sizes in excess of approximately 20 μm in diameter. According to the 1-D analysis by Morini et al. [22], erosion causes a shift of the non-dimensional corrected mass flow rate curves towards higher values, while efficiency curves are in practice unaffected by this type of deterioration. The same effect of erosion was considered by Zhu and Saravanamuttoo [23] in their simulation, although they suggested that turbine erosion may cause efficiency degradation as well.

No experimental data is available in the open literature thus, for the turbine erosion simulation, a ratio between swallowing capacity increase and efficiency reduction of (-) 8 will be used since the effect on swallowing capacity is predominant.

### 3.6 Foreign Object Damage

There are several other factors, like foreign-object ingestion and cracking during thermal cycles on the hot section that can also lead to mechanical damage and performance deterioration of the engine. However, as the levels of damage from these phenomena can vary it is difficult to provide general, quantifiable guidance concerning their effects and as a result to realistically simulate their impacts on the engine's performance.

Foreign Object Damage (FOD) is the result of a body striking the internal surfaces of the component. For the compressor, according to Homji [8], the damage is typically realized in the early compressor stages, though in some cas the object may reach the later stages damaging them. FOD c be caused by ice, failed intake section component and even materials or tools left in the inlet plenum sucked in by t compressor. Turbine FOD may occur due to carbon build on fuel nozzles and by a subsequent potential breaking off the stiff residues. The damage is a function of size, forei object composition, blade construction and impact location. is common practice the mechanical damage in bo compressor and turbine to be modeled by a degradation of t component efficiency, while assuming the swallowi capacity to be unchanged ([22], [23]).

## 4. Faults Simulation

The GE LM2500 is selected as a test engine in order simulate the aforementioned degradation phenomena. T engine model used is capable to reproduce the engin operation with acceptable accuracy as discussed by Yfan and Kapasakis [24]. The GE LM2500 is a twin shaft engine.

The representation of the components degradation implemented following the data depicted above. Specifical in Table 1 the way in which the component corrected air ma flow as well as the efficiency change, for each case of fault, presumed. In Table 2 the values of the modification factors for fault severity 100% are presented. These values are t maximum ones, used herein, and are defined for the g generator rotating components in order to give a reduction the thermal efficiency of about 2% for 75% of Load. This w done in order the results to be comparable. In the case power turbine (LPT), the same values of gas generator turbi (HPT) are used.

*Table 1: Component Performance Parameter Variation w Degradation*

| Physical Fault | Swallowing Capacity Change ($f_{SW}$) | Component Efficiency Change ($f_{SE}$) | $f_{SW}$ rati |
|---|---|---|---|
| Compressor Fouling | $f_{SW,C} \downarrow$ | $f_{SE,C} \downarrow$ | 3:1 |
| Compressor Erosion | $f_{SW,C} \downarrow$ | $f_{SE,C} \downarrow$ | 8:1 |
| Compressor Tip Clearance | $f_{SW,C} \downarrow$ | $f_{SE,C} \downarrow$ | 1:1 |
| Turbine Fouling | $f_{SW,T} \downarrow$ | $f_{SE,T} \downarrow$ | 1:1 |
| Turbine Erosion | $f_{SW,T} \uparrow$ | $f_{SE,T} \downarrow$ | 8:1 |
| FOD | $f_{SW,C/T} \leftrightarrow$ | $f_{SE,C/T} \downarrow$ | - |

The faults described were simulated for different severit and for constant TIT operation at different power settings the range a gas turbine usually operates. More specifically t TIT values corresponding to different power settings (30, 5 75, 100 and 104%) and healthy operation were also used faulty operation simulation. This choice was based on the fa that gas turbines usually operate with TIT as control variab In all examined cases power turbine speed was kept consta

Corresponding Author: Ioannis Roumeliotis, Email: jroume@ltt.ntua.gr

Figure 5 the faults signatures, for compressor faults based performance related quantities deviation, are presented for 0% severity and different power settings.

*ble 2: Component Performance Parameter values for fault erity 100%*

| hysical Fault | Component performance parameter values | |
|---|---|---|
| ompressor Fouling | $f_{SW,C}$ : -3% | $f_{SE,C}$: -1% |
| ompressor Erosion | $f_{SW,C}$ : -7% | $f_{SE,C}$: -0.875% |
| ompressor Tip Clearance | $f_{SW,C}$ : -1.2% | $f_{SE,C}$: -1.2% |
| ompressor FOD | $f_{SW,C}$ : 0 | $f_{SE,C}$: -1.2% |
| urbine Fouling | $f_{SW,T}$ : -1.5% | $f_{SE,T}$: -1.5% |
| urbine Erosion | $f_{SW,T}$ : 7% | $f_{SE,T}$: -0.875% |
| urbine FOD | $f_{SW,T}$ : 0 | $f_{SE,T}$: -1.5% |

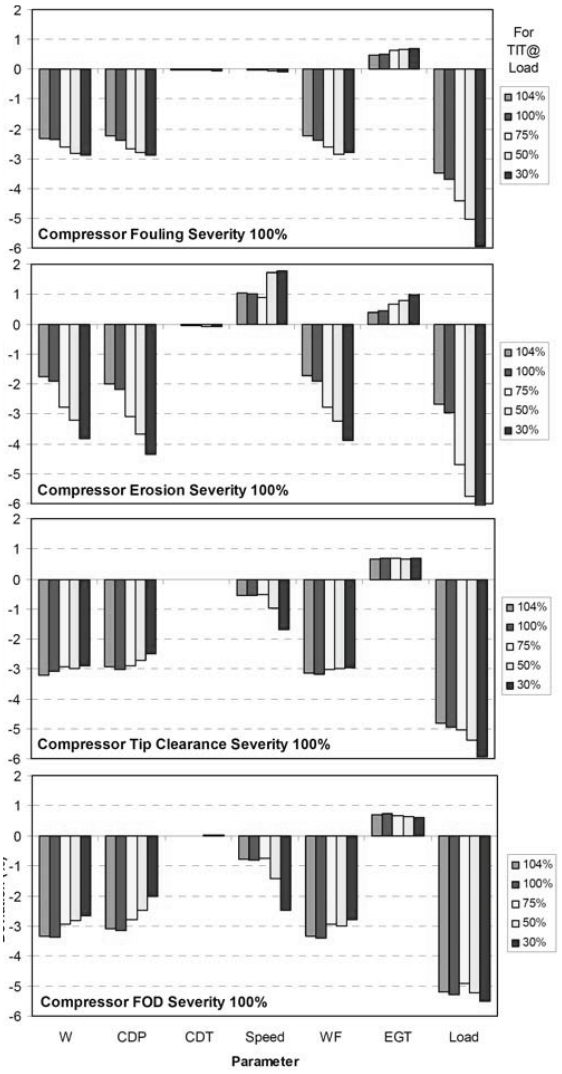


*gure 5: Fault signatures for compressor faults at fault erity 100% and for constant TIT @different power settings.*

It can be seen that all faults produce a significant reduction in inlet mass flow, fuel flow and CDP for all power settings. These effects result in a severe reduction of engine power output. For the case of erosion, the gas generator speed increases noticeably. In the case of fouling rotational speed is almost unchanged, while in the case of tip clearance and FOD decreases.

All faults have negligible impact on CDT while the effect on EGT may be noticeable depending on measurement accuracy. Based on fault signatures, the main compressor fault distinction can be made using the deviation of gas generator speed, which is usually an accurate measurement. Although tip clearance and FOD faults produce similar fault signatures, the distinction between them can be based on the fact that FOD effect is expected to appear as a sudden deviation of the measurements.

Similar conclusions can be drawn from Figure 6 where the deviation of performance related quantities versus fault severity is presented for constant TIT@100% Load. The parameters deviation is almost linear with increasing fault severity. The effect of tip clearance and fouling is expected to be noticeable prior to erosion, while the predominant measurement deviation for all faults is Load.

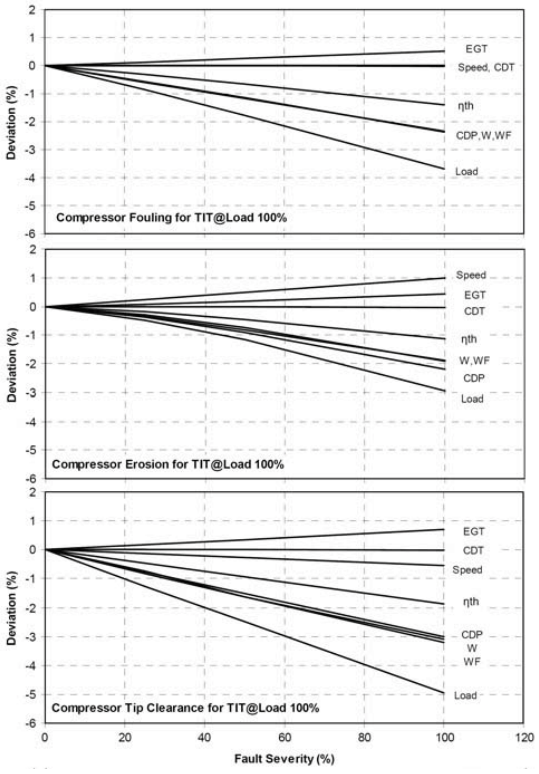


*Figure 6: Performance related quantities deviation in function of fault severity for compressor faults and constant TIT (@Load 100%).*

Corresponding Author: Ioannis Roumeliotis, Email: jroume@ltt.ntua.gr

The same variables deviation for the case of faulty gas generator turbine is shown in Figure 7 and Figure 8. It can be realized that erosion produces a distinct fault signature due to the significant reduction of CDP. Also it should be noted that for the case of fouling the predominant deviation is that of the power output (Load). Erosion is expected to be identified more rapidly than fouling as the CDP reduction is more intense.

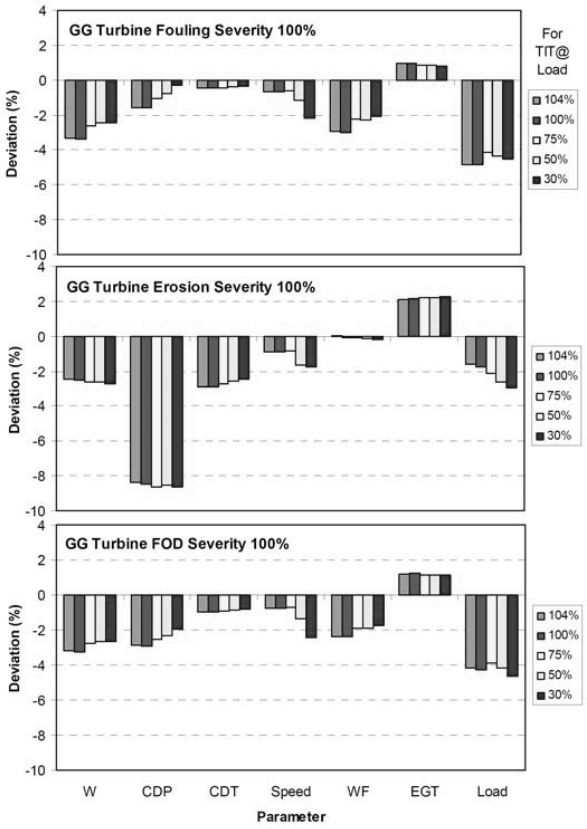


*Figure 7: Fault signatures for GG Turbine faults at fault severity 100% and for constant TIT @different power settings.*

In the case of power turbine faults the effect on the engine measured quantities of interest are presented in Figure 9 for different Load settings and in Figure 10 for increased fault severity. In this case the faults give distinct fault signatures, with erosion being the one that is expected to produce the greatest measurement deviation. The increase of the turbine mass flow due to erosion result to the shifting of the compressor operating point towards higher pressure ratios and rotational speeds. The off-design operation of the engine results in a decrease of the thermal efficiency. FOD is expected to influence the engine load, while erosion produces a deviation in CDP, CDT and Load.

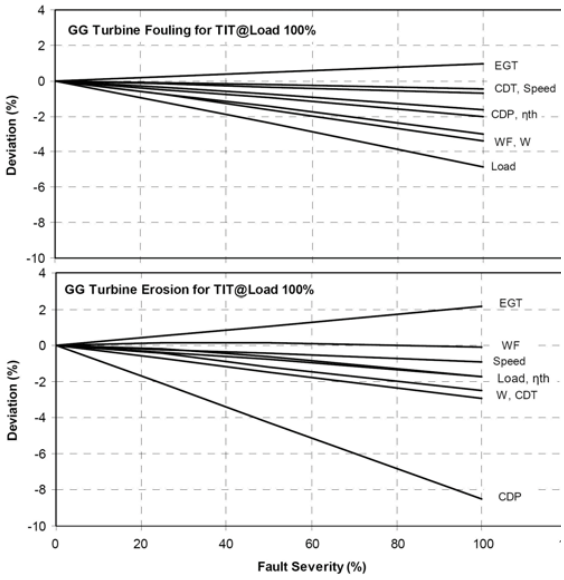


*Figure 8: Performance related quantities deviation in functi of fault severity for GG Turbine faults and constant T (@Load 100%).*

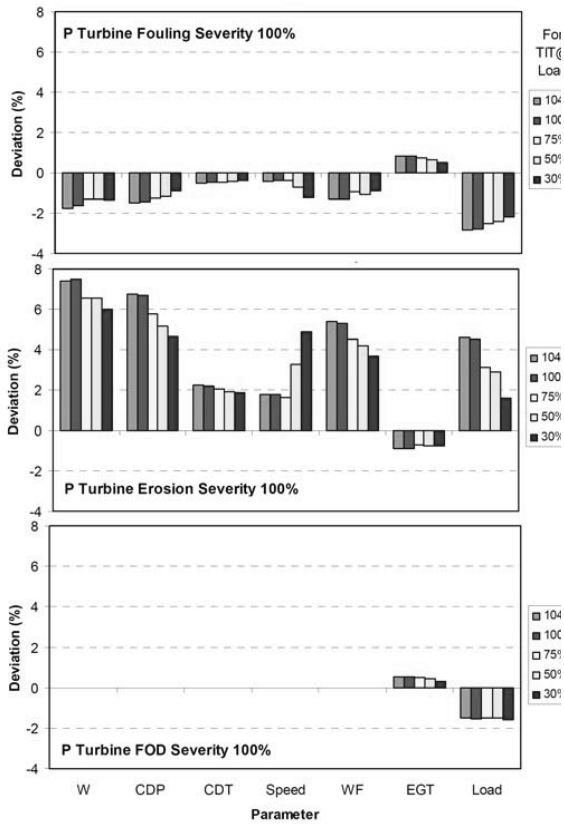


*Figure 9: Fault signatures for Power Turbine faults at fa severity 100% and for constant TIT @different power setting*

Corresponding Author: Ioannis Roumeliotis, Email: jroume@ltt.ntua.gr

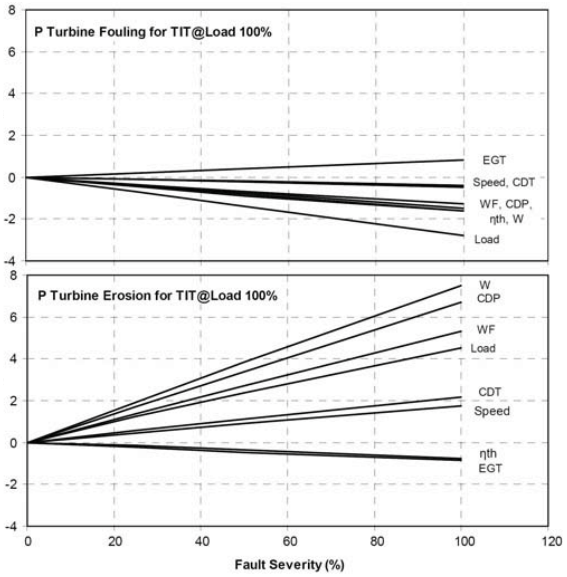


*gure 10: Performance related quantities deviation in nction of fault severity for Power Turbine faults and nstant TIT (@Load 100%).*

The power turbine erosion produces a significantly fferent signature than the gas generator turbine erosion. us, the faulty hot section component can be easily ntified. In case that both turbines are eroded a third nature is produced, a distinct fault signature, which is the mbination of the individual ones, as presented in Figure 11.

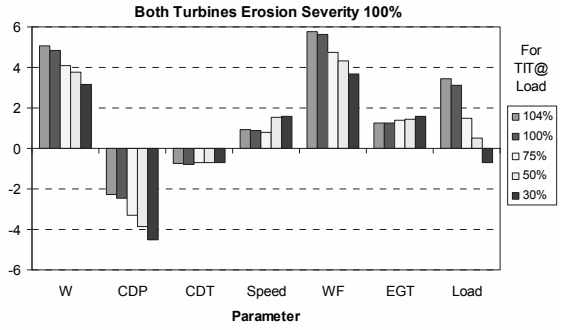


*gure 11: Fault signatures for the case of both turbines oded at fault severity 100% and for constant TIT @different wer settings.*

## Concluding Remarks

The variation, of certain engine performance parameters mely CDP, CDT, W, WF, EGT, LOAD engine rotational eed), in the presence of faults is clearly of prime importance the individual customer requirements. As far as the model is concerned, the study and pursuit of this variation enables the user to make a pre assessment with respect to what is going to face in an actual engine running environment.

The evaluation of the performance of an actual gas turbine can be accurately predicted by exploiting data out of an installed parametric observation system coupled with data from a software related tool (a computer model).

The use of a performance model allows an ad hoc comparison between engine actual performance and this of a new and clean engine. This could be done in order to assess proper rating and potential malfunction. The results motivate the user to reconsider engine maintenance schedule, going through all necessary engine and ancillary systems refinements.

The user could use the performance model in order to simulate a harsh and hostile for the propulsion plant environment. This would give the user an opportunity to investigate engine operation extremities (e.g. transient operation, or fouled operation), thus gaining operational experience.

Performance model usefulness has to be remarked, in particular, when on board training is desired. In this case, on board program installation is feasible and facile. Provided that installation has been accomplished, after all available measurements having been gathered, simulation program may be applied to reliably implement:

a) Engine condition and operation summary and assessment.

b) Trend analysis of certain parameters.

c) Furthermore, the risk of engine fault occurrence can be minimized.

The user is encouraged to take advantage of these software abilities, which can go as far as diagnostics, and at the same time, provides an excellent learning experience for the technical personnel involved. The use of computer models is an issue of major importance that might substantially increase propulsion operational capabilities.

### NOMENCLATURE

| | |
|---|---|
| CDP | Compressor Delivery Pressure |
| CDT | Compressor Discharge Temperature |
| EGT | Exhaust Gas Temperature |
| $f_i$ | Modification factor |
| Load | Engine Power |
| p | Pressure |
| T | Temperature |
| TIT | Turbine Inlet Temperature |
| W | Mass Flow |
| WF | Fuel Flow |
| X | Component parameter value |

**Greek Symbols**

| | |
|---|---|
| η | Efficiency Coefficient |

Corresponding Author: Ioannis Roumeliotis, Email: jroume@ltt.ntua.gr

**Subscripts**

| | |
|---|---|
| act | actual |
| C | compressor |
| ref | reference |
| SE | component efficiency |
| SW | swallowing capacity |
| T | turbine |
| th | thermal |

## REFERENCES


[1] Mathioudakis K., Politis, E., Stamatis,A. , 1999, "A computer model as an educational tool for gas turbine performance", International Journal of Mechanical Engineering Education, Vol 27, No 2, April 1999, pp 113-125.

[2] Roumeliotis I., Mathioudakis K., Aretakis N., Performance analysis of twin-spool water injected gas turbines using adaptive modeling, ASME paper No. GT2003-38516.

[3] Stamatis A., Mathioudakis K., Papailiou D.K., Adaptive Simulation of Gas Turbine Performance, ASME J Eng Gas Turbines Power 1990, 112(2): 168-175

[4] Tsalavoutas A., S. Pothos, Mathioudakis K., Stamatis A., Monitoring the performance of a twin-shaft ship propulsion turbine by means of adaptive modeling, RTO Symposium on Gas Turbine Operation and Technology for Land, Sea and Air Propulsion and Power Systems, Ottawa, Canada, 18-21 October 1999

[5] Stamatis, A., Mathioudakis, K., Smith, M., Papailiou, K.D., "Gas Turbine Component Fault Identification by Means of Adaptive Performance Modelling". ASME Paper 90-GT-376, 1990

[6] Aretakis N., Mathioudakis K.,Stamatis A., Non-Linear engine component fault diagnosis from a limited number of measurements using a combinatorial approach, ASME J Eng Gas Turbines Power 2003; 125(3): 642-650

[7] Mathioudakis K., Aretakis N., Yfantis E., "A Possibility for on-board Training for Marine Gas Turbine Performance Monitoring and Diagnostics" Conference Proceedings MECON 2006, 29 August-1 September 2006 Hamburg.

[8] Meher-Homji, C. B., 1990, "Gas Turbine Axial Compressor Fouling - A Unified Treatment of its Effects, Detection and Control", ASME Cogen Turbo IV, New Orleans, LA, August 27-29, 1990, Also in International Journal of Turbo and Jet Engines, Vol. 9, No. 4, 1992, pp 99-111.

[9] Diakunchak, I. S. , 1992, "Performance Deterioration in Industrial Gas Turbines» Asme J. of Engineering for Gas Turbines and Power, Vol. 114, pp. 161-168

[10] Lakshminarasimha, A. N., Boyce M. P., Meher-Homji C. B., 1994, "Modelling and Analysis of Gas Turbine Performance Detrerioration» ASME J. of Engineering for Gas Turbines and Power, Vol. 116, pp. 46-52

[11] Tarabrin, A. P., Schurovsky, V. A., Bodrov A. I., Stadler J-P, 1996, "An Analysis of Axial Compressors Fouling and a Cleaning Method of ther Blades" ASME Paper No. 96-GT-363

[12] Syverud, E., Brekke, O., Bakken, L. E., 2005, "Axial Compressor Deterioration Caused by Saltwater ingestion" ASME Paper No. GT2005-68701

[13] Haq, U., I., Saravanamuttoo, H. I. H.., 1993, "Ax Compressor Fouling Evaluation at High Speed Settings usi an Aerothermodynamic Model" ASME Paper No. 93-GT-40

[14] Zaba, T., 1980, "Losses in Gas Turbines Due to Depos on the Blading," Brown Boveri Review, Volume 67, Numb 12, December 1980.

[15] Tabakoff, W., 1986, "Compressor Erosion a Performance Deterioration," ASME Publication FED-Vol. presented at the AIAA/ASME 4th Joint Fluid Mechani Plasma Dynamics, and Lasers Conference, Atlanta, Georgia.

[16] Zaita, A. K., Buley, G, Karslons, G., 1997 "Performar Deterioration Modeling in Aircraft Gas Turbine Engine ASME paper No. 97-GT-278

[17] Aretakis N., Roumeliotis, I., Mathioudakis K, 20 "Performance Model "Zooming" for In-Depth Compone Fault Diagnosis", ASME paper No. GT-2010-23262, to presented at ASME Turbo Expo 2010.

[18] Schmücker, J., Schäffler, A., 1994, "Performar Deterioration of Axial Compressors Due to Blade Defec Paper presented at the Propulsion and Energetics Panel (PE Symposium held in Rotterdam, the Netherlands in April 199

[19] MacLeod, J. D., Taylor, V., Laflamme, J. C., 19 "Implanted Component Faults and Their Effects on C Turbine Engine Performance" ASME J. of Engineering Gas Turbines and Power, Vol. 114, pp. 174-179

[20] Meher-Homji. C. B, 1989, "Compressor and Hot Secti Fouling in Gas Turbines – Causes and Effects", Proceedir of the 9th Industrial Energy Technology Conference, Houst September 16-18. 1987, Texas A&M University.

[21] Basendwah A. A., Pilidis P., Li Y. G., "Turbine Off- Li Water Wash Optimization Approach for Power Generatio ASME paper No. GT2006-90244

[22] Morini M., Pinelli M., Spina P. R., Venturini M "Influence of Blade Deterioration on Compressor and Turbi Performance", ASME paper No. GT2008-50043

[23] Zhu P., Saravanamuttoo H.I.H., 1994, "Simulation of Advanced Twin – Spool Industrial Gas Turbine", Asme J. Engineering for Gas Turbines and Power, Vol. 114 , pp. 18 185

[24] Yfantis E. A., Kapasakis P., "Marine Gas Turbi Performance Diagnostics: A Case Study", Diagnostyka 3(47)/2008, September 2008, ISSN 1641-6414,pp. 61-64.


Corresponding Author: Ioannis Roumeliotis, Email: jroume@ltt.ntua.gr

# Thermodynamic Analysis of a Post Combustion $CO_2$ Capture Process

*Zeinab Amrollahi[a],[1] Ivar S. Ertesvåg[a] and Olav Bolland[a]*

[a] *Department of Energy and Process Engineering, Norwegian University of Science and Technology, Trondheim, Norway*

**Abstract:** A chemical absorption, post-combustion CO2 capture unit is simulated and an exergy analysis was conducted, including irreversibity calculations for all process units. With pinpointing major irreversibilities, new proposals for efficient energy integrated chemical absorption process were suggested. Moving further to the whole natural gas combined cycle plant with a $CO_2$ capture unit, it has been analyzed on an exergetic basis. By defining exergy balances and black-box models for plant components, investigation has been made to determine effect of each component on overall exergy efficiency. Simulation of chemical absorption plant was done using UniSim Design software with Amine Property Package which maintains thermodynamic data. For overall power plant design, GT PRO software (Thermoflow, Inc.) was used for simulation of a natural gas combined cycle. For exergy calculations, spreadsheets were created with Microsoft Excel by importing data from UniSim and GT PRO. By pinpointing major irreversibilities, new proposal for energy-efficient integrated chemical absorption process is suggested. Results show that for current chemical absorption plant, the exergetic efficiency compared to the reversible separation work lies between 15% and 22%.

**Keywords:** $CO_2$ capture, Absorption, Exergy analysis

## 1.Introduction

For a natural gas-capture from flue gases, using chemical absorption with aqueous monoethanolamine (MEA) is one of the most near-term technologies.

Flue gas containing $CO_2$ is flowing through absorber while contacting with MEA solvent counter-currently. Meanwhile reaction is happening between MEA solvent and $CO_2$ forming a water soluble salt. A rich MEA stream which contains the chemically bound $CO_2$, preheated in a heat exchanger is entered to a stripper column to reverse the reaction by means of heat maintained by a reboiler and lose $CO_2$ content as a stream leaving at the top of the column. The lean MEA is recycled back to the absorption column while the $CO_2$ stream is going to compression section.

Although it is a well-established separation method, the energy consumption and the costs of $CO_2$ separation are substantially high and lead to consumption of more fossil fuel for the same power generation. In order to increase the energy efficiency and prevent forced extra costs and energy consumption, it is beneficial to optimize the process and evaluate the performance of the whole system by means of exergy analysis which identifies the energy consumption, potential improvements and thermodynamic irreversibilities. It should be noted that although the nature of exergy losses in power plants specially combustion chambers are higher than those of post combustion $CO_2$ capture plant, but because the capture plants are add-ons to existing power plants and their design and set-up is still under investigation and development, energy and exergy analysis, shows more potential of energetic and exergetic improvement in these processes.

## 2. Exergy analysis

The exergy method of evaluating energy-intensive systems integrates the first and second laws of thermodynamics at the state of particular environmental conditions. Exergy analysis with its own certain methods of process evaluation has proven to be an efficient method to define the second law efficiency of processes. It combines the principles of conservation of mass and conservation of energy together with the second law of thermodynamics to characterize the thermodynamic losses of each component of a

[1] Corresponding author. Email: zeinab.amrollahi@ntnu.no

system through the whole design and it enables to make possible improvements of work and energy consumption. This is an advantageous method to approach the goal of more efficient energy-resource use, since it specifies the locations, types, and real magnitudes of irreversibilities either to be recovered or inevitably lost.

In absence of potential and kinetic energy, exergy of stream is divided into physical exergy and chemical exergy. Physical exergy equals to maximum amount of work obtainable when the stream of substance is brought from its actual state to the environmental state defined by $P_0$ and $T_0$ [4] by physical processes involving only thermal interaction with the environment. It is depicted as:

$$\varepsilon_{ph} = (h - h_0) - T_0(s - s_0) \quad (1)$$

Where h and s are the specific enthalpy and entropy and $h_0 = h(T_0, P_0)$ and $s_0 = s(T_0, P_0)$ for the flowing matter.

The chemical exergy of a substance is the minimum work requirement to deliver it in the environmental state from the environmental substances by means of processes involving heat transfer and exchange of substances only with the environment. There are tables of calculated standard chemical exergy of various substances in literature [1]. Molar chemical exergy of an ideal mixture is expressed as

$$\tilde{\varepsilon}_{0M} = \sum_i x_i \tilde{\varepsilon}_{0i} + \tilde{R}T_0 \sum_i x_i \ln x_i \quad (2)$$

Exergy loss of each individual unit can be calculated by finding the difference between the exergy of input and output streams of a unit operation. To pinpoint irreversible losses in each unit operation, the exergy balance for steady state steady flow is used;

$$\sum_{in} \dot{m}_j \varepsilon_j + \sum_l \dot{Q}_l \left(1 - \frac{T_0}{T_l}\right) = \sum_{out} \dot{m}_k \varepsilon_k + \dot{W} + \dot{I} \quad (3)$$

Flow exergy into system | Heat exchange | Flow exergy out of system | Work | Irreversibility

Exergy analysis can be done when composition and thermodynamic properties of all streams involving in capture process are available. For this purpose, a simulation software model is used to simulate the whole $CO_2$ capture process. By transferring stream physical properties and compositions to excel spreadsheets, exergy calculations are performed and reported.

To calculate the chemical exergy of each stream containing MEA component there is a need of chemical exergy of the MEA molecule in the liquid phase. The value which is used in these calculations is not found directly from literature but estimated. The value is $1.274 \cdot 10^6$ kJ/kmol.

## 3. Methodology

In the analysis, the mass, energy and exergy balances were applied to each unit (valve, pump, heat exchanger, etc.) of the plant. For presentation purposes, the plant was subdivided into sections comprising one or more units. These sections were the gas turbine, heat recovery steam generator (HRSG), steam turbine and condenser, $CO_2$ absorption column, main heat exchanger of $CO_2$ capture plant, stripping section, compression

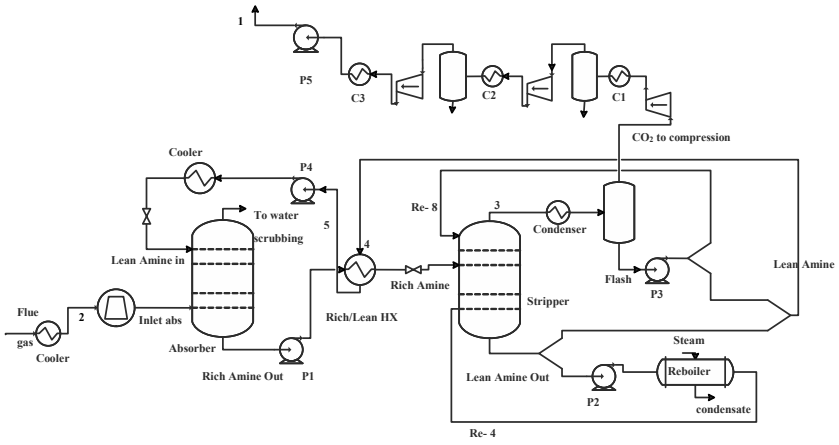


*Figure 1: Flow sheet of $CO_2$ capture and compression units designed by UniSim Design*

section. The irreversibility of a section was the sum of the irreversibilities of the contained units.

Chemical and physical exergy of all streams was functioned in excel spreadsheets. Furthermore, exergy analysis calculations for the designed power plant were derived from GTPro Thermoflow software calculation which will be depicted later. The reference environment is the local environment of the place where the natural gas fired power plant is located which it is assumed in here with ambient temperature $T_0$= 298.15 K and pressure $P_0$=101.325 kPa.

As mentioned before, this study is limited to the analysis of the physical exergy and chemical exergy. Other forms of exergy as kinetic and potential are insignificant in these processes so they are ignored. The degradation and consumption of the MEA solvent was neglected in $CO_2$ capture unit.

## 4. Base case model

As a base case, the $CO_2$ separation with MEA absorption model shown in Figure 1 is designed according to the capture rate that is set to 90.5%.

This capture rate for the base case was attained by MEA weight percentage of 30 and solvent circulation rate of 2500 t/h and reboiler duty of $5.12 \cdot 10^8$ kJ/h. Reboiler energy consumption is 3.86 (MJ/kg of separated $CO_2$) which is produced by the steam flow of 64.35 kg/s .Total mechanical work needed for the capture and compression unit is mentioned in Table 1. $CO_2$ compression was done in 3 stages with adiabatic efficiencies of 85%, 85% and 80% respectively with intermediate cooling after each stage. A pump further raised the pressure from 79.7 bara to 110 bara. The pump adiabatic efficiency was set to 75%.

*Table 1: Total mechanical work demand for post combustion $CO_2$ capture plant*

| Work demand | MJ/kg $CO_2$ separated |
|---|---|
| Power production penalty | 0.89 |
| compression work | 0.29 |
| Auxiliary power | 0.16 |
| Total | 1.34 |

*Table 2: Power plant summary*

| | Power Output MW | | Elect. Eff. LHV% | |
|---|---|---|---|---|
| | gross | net | gross | net |
| Gas Turbine | 282.7 | | 39.22 | |
| Steam | 92.7 | | | |
| Plant Total | 375.4 | 368.2 | 52.08 | 51.09 |

The virtual power plant that is connected to the $CO_2$ capture process provides mechanical work to cover the demand of the $CO_2$ capture unit as well as the steam demand of the regeneration reboiler. A complete schema of the designed combined cycle power plant is shown in Figure 2 with key stream information. The plant key data are shown in Table 2.

*Figure 2: Flowsheet of the designed power plant*

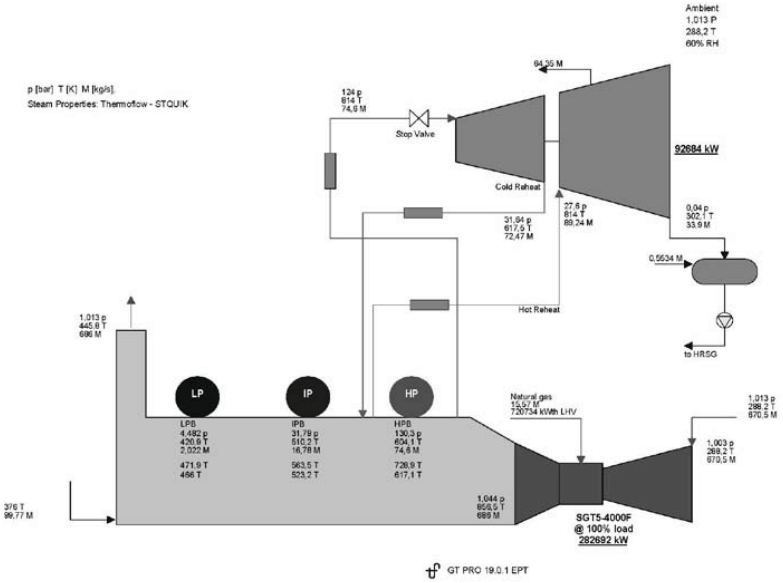

The fuel was considered as natural gas without $H_2S$ with 722087 kW thermal as lower heating value and flow of stack gas is 686.4 kg/s with molar composition of 3.82% $CO_2$, 12.54% $O_2$, 8.24 % $H_2O$, 75.4% $N_2$ and temperature of 412.5 K which is going to be cooled in capture unit.

## 5. Results

### 5.1 Natural gas fired power plant

The results of exergy calculation for specified natural gas fired power plant designed by GTPro Thermoflow software are shown in Table 3.

*Table 3: Plant exergy analysis*

| | kW | MJ/kg $CO_2$ separated |
|---|---|---|
| Exergy In | 739008 | 19.96 |
| Fuel exergy | 727460 | 19.65 |
| Ambient air exergy | 0 | 0,00 |
| Condenser cooling water in | 6359 | 0.17 |
| Process condensate return | 5072 | 0.14 |
| Makeup water | 1.633 | 0.00 |
| Exergy Out | 435668 | 11.77 |
| Net electric output | 368193 | 9.94 |
| Process steam exergy | 45870 | 1.24 |
| Condenser cooling water out | 1391.5 | 0.04 |
| Stack gas exergy | 20214 | 0.55 |
| Exergy Loss | 303340 | 8.19 |
| GT exergy loss | 255216 | 6.89 |
| HRSG exergy loss | 22140 | 0.60 |
| Steam turbine exergy loss | 10584 | 0.29 |
| Condenser exergy loss | 5960 | 0.16 |
| Non-heat balance related auxiliaries | 2616 | 0.07 |
| Transformer loss | 1876.9 | 0.05 |
| Miscellaneous exergy loss* | 2369.9 | 0.06 |
| Unaccounted exergy loss** | 2577.6 | 0.07 |

* Includes piping loss, ST leakage to external sink, fuel compressor loss, condensate pump loss
** Includes losses from desuperheating, mixing, and throttling, small water streams, misc. aux. and heat rejection

### 5.2 Base case $CO_2$ capture plant

In Table 4, physical stream characteristics and relevant calculated exergy which is used to find irreversibility amounts according to exergy balance formula are shown. It should be noted here that for simulation of streams containing amine component, UniSim Design software [3] developed a specific property package which predicts behavior of systems containing MEA solvent. For simulation of other streams Peng-Robinson equation of state is used.

*Table 4: Themodynamical data and exergy of streams for the base case model*

| Stream | Temperature (°C) | Pressure (kPa) | Mass Flow (kg/s) | Exergy (MJ/kg $CO_2$ separated) |
|---|---|---|---|---|
| 1 | 24.66 | 11000.00 | 37 | 0.67 |
| $CO_2$ to compression | 28.00 | 167.20 | 37.3 | 0.486 |
| 2 | 43 | 101.30 | 686.4 | 0.6 |
| Inlet abs | 49.6 | 107.30 | 686.4 | 0.49 |
| Flue gas | 139.4 | 101.30 | 686.4 | 1 |
| To water scrubbing | 52 | 101.30 | 663.1 | 0.61 |
| 3 | 100.3 | 172.4 | 70.22 | 0.89 |
| 4 | 119.1 | 186.20 | 710.5 | 129.1 |
| 5 | 55.5 | 146.20 | 710.5 | 126.1 |
| Lean Amine Out | 119.5 | 186.20 | 809 | 143.2 |
| Steam | 177 | 400.00 | 64.35 | 2.4 |
| Condensate | 143 | 392.00 | 64.35 | 1.3 |
| Lean Amine in | 39.5 | 107.00 | 680.4 | 126.9 |
| Rich Amine Out | 46 | 106.30 | 748 | 125.9 |
| Rich Amine | 110.5 | 106.30 | 748 | 128.7 |

### 5.3 Improved model

Observing the exergy amounts of streams and process sections irreversibilities, a new model - see Figure 2- with lower energy consumption and irreversibility is investigated. The first configuration change is to split the *Rich Amine* stream which carries mainly the absorbed $CO_2$ and MEA amine and integrating those split streams with two streams returning from stripper; the first stream is *Lean Amine* which is also in the base case model, but the second stream is *Semi-Lean* stream which is a liquid side stream taken from the stripper. The concept behind these modifications is to divide the driving force along the stripper into smaller segments which makes the separation processes closer to its reversible situation and decreases the irreversibilities. The largest portion

of *Rich Amine* stream coming out of absorber is still passing through the *Rich/Lean heat exchanger 1* while its smaller portion is heated through *Rich/Lean heat exchanger 2* with the *Semi-Lean* stream that is taken from the stripper column and recycled back to the absorber. With these new changes, there is a chance of approaching exergy recovery and decreasing irreversibility amount of the whole system.

*Table 5: Total mechanical work demand for new process configuration of $CO_2$ capture unit*

| Work demand | MJ/kg $CO_2$ separated |
|---|---|
| Power production penalty | 0.88 |
| compression work | 0.29 |
| Auxiliary power | 0.17 |
| Total | 1.34 |

The $CO_2$ capture rate for this modified model which is shown in Figure 3 is 90.3% and the new reboiler duty is $5.1 \cdot 10^8$ kJ/h which is less than base case model. Reboiler energy consumption is 3.83 (MJ/kg of separated $CO_2$) which is produced by the steam flow of 63.71 kg/s .Total mechanical work needed for the capture and compression unit is given in Table 5.

*Table 6: Themodynamical data and exergy of streams for new process configuration of $CO_2$ capture unit*

| Stream | Temperature (°C) | Pressure (kPa) | Mass Flow (kg/s) | Exergy (MJ/kg $CO_2$ separated) |
|---|---|---|---|---|
| 1 | 24.88 | 11000.00 | 37 | 0.675 |
| $CO_2$ to compression | 28 | 167.20 | 37.3 | 0.49 |
| 2 | 43 | 101.30 | 686.4 | 0.6 |
| Inlet abs | 49.6 | 107.30 | 686.4 | 0.49 |
| Flue gas | 139.4 | 101.30 | 686.4 | 1 |
| To water scrubbing | 51.7 | 101.30 | 662.5 | 0.6 |
| 3 | 100.1 | 172.4 | 70 | 0.9 |
| 4 | 118.5 | 186.20 | 714.6 | 129.2 |
| 5 | 56.2 | 146.20 | 714.3 | 126.1 |
| Lean Amine Out | 118.6 | 186.20 | 809 | 143.1 |
| Steam | 176.9 | 400.00 | 63.7 | 2.37 |
| Condensate | 143 | 392.00 | 63.7 | 1.26 |
| Lean Amine in | 39.4 | 107.00 | 723.8 | 127.4 |
| Rich Amine Out | 50 | 106.30 | 881 | 148.3 |
| Semi- Lean | 114.5 | 184.1 | 130 | 22 |
| RA 1 | 110.1 | 610 | 766.3 | 128.4 |
| RA 2 | 114.4 | 650 | 136.6 | 23.6 |

*Figure 3: Flow sheet of new configuration for $CO_2$ capture and compression units*

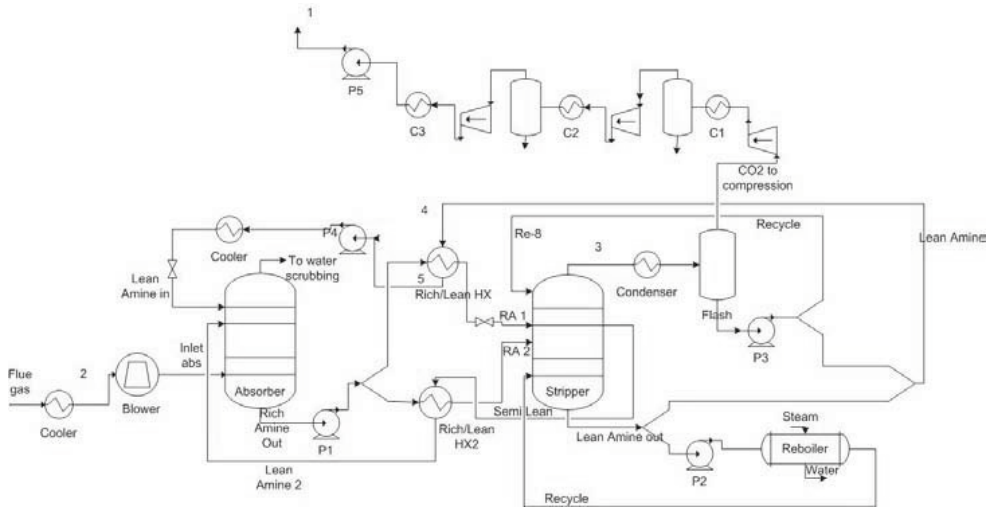

*Table 7: Irreversibilities by process sections*

| Irreversibility [MJ/kg $CO_2$] | Base case | New design |
|---|---|---|
| Flue gas cooler | 0.48 | 0.48 |
| Blower | 0.04 | 0.04 |
| Absorption section | 0.61 | 0.64 |
| Rich /lean heat exchanger 1 | 0.01 | 0.0 |
| Rich /lean heat exchanger 2 | - | 0.01 |
| Stripping section | 0.59 | 0.51 |
| compression section | 0.12 | 0.12 |
| **Total** | **1.85** | **1.80** |

## 5. Discussion

As the exergy calculation results show- Tables 6 and 7- the magnitude of irreversibilities which is currently happening in the absorption and stripping sections, motivates the design of similar process with configuration changes, which is mainly stream splitting and recycling of the streams. By taking out a side stream from stripper and recycling it through a heat exchanger to the absorber, the stream is taking out a considerable amount of irreversibility from stripper; but since this side stream is cooled before absorber, it affects the absorber irreversibilities less. Additionally, in the improved model, by splitting the feed stream before the absorber and feeding them into different trays, the driving forces are distributed more evenly along the column height which results in lower irreversibility. Furthermore, reboiler duty is decreased which will show its deduction in the stripper irreversibility amount.
More to add is since flue gas temperature entering chemical absorption plant is fairly the same in both models, the irreversibilities of flue gas cooler and blower for both of cases are equal.
Finally, from efficiency point of view, power plant with the modified model for $CO_2$ capture has slightly higher net electrical efficiency i.e 51.14% comparing to the power plant with base case model i.e. 51.09%. Since the steam demand in the reboiler in the improved model is decreased comparing to the reboiler duty of the base case, power plant's steam turbine has higher power output (93MW) and electrical efficiency (LHV%) increases. It should be mentioned that power plant efficiency (LHV%) without $CO_2$ capture is 56.34% that is higher than the efficiency of power plants with $CO_2$ capture .

## 6. Concluding remarks

Although the exergy loss in $CO_2$ capture and compression units are rather small comparing to those lost in Gas turbine, HRSG and steam turbine, there are points of potential improvements in $CO_2$ capture process. By process configuration changes and decreasing regeneration duty, improved $CO_2$ capture process with lower heat consumption and less irreversibility amount was designed.
Minimum reversible separation work for the flue gas stream coming to the $CO_2$ capture plant is 0.247 MJ/kg$CO_2$. When looking to the actual work demand Tables 1&5, it was calculated that for base case chemical absorption plant exergy efficiency was 18.36% and the modified case gave exergy efficiency of 18.37%.
Current study -as in Table 7- shows that by splitting the out-coming streams from the absorber and encountering them to various lean MEA recycles from the stripper, the irreversibility amounts through stripper decreases sensibly. Use of other solvents with lower binding energy is suggested to decrease the exergy loss of reboiler section. In order to minimize the exergy loss, it is important to have uniform exergy degradation along equipments, which can be an optimization idea for the regeneration column, flasher and reboiler. Furthermore in order to divide exergy losses through the absorption column and stripping column, process configuration changes such as stream splitting can be performed [5].

**References:**

[1] Kotas, TJ. , 1995, *The exergy method of thermal plant analysis*, Malabar (FL): Krieger Publishing Company.

[2] Cengel, Y. A. and Boles, MA. , 2006, *Thermodynamics: An Engineering Approach, 6th* edition, McGraw-Hill.

[3] UniSim design user guide; Honeywell; 2008 R380 Release

[4] Szargut J, Morris DR, Steward FR., 1988, *Exergy analysis of thermal, chemical and metallurgical processes*, New York: Hemisphere Publishing Corp.

[5] Adisorn Aroonwilas, 2005, Integration of $CO_2$ capture unit into supercritical coal-fired power plants: Implications for emission and energy management, International journal of Greenhouse Gas Control Technologies, 1(2), pp. 1841-1844.

# ECOS: Application of the effective heat absorbing and emitting temperatures to determining power losses of industrial processes

*Henrik Holmberg[1], Pekka Ruohonen[1,2], Jaana Federley[1]*

[1]*Aalto University, School of Science and Technology, Department of Energy Technology, Finland,*
[2]*Pöyry Finland Oy*

**Abstract:** All real processes generate entropy, and loss of power/exergy is usually determined by means of the Gouy-Stodola law. The Gouy-Stodola law gives the exact loss of power/exergy if the system only exchanges heat at the real environmental temperature or the standard temperature of 298.15K. However, most industrial processes emit or absorb heat at a temperature level other than this temperature. In these cases, the Gouy-Stodola law does not give the real loss of power/exergy. This paper uses an effective heat emitting or absorbing temperature to calculate the real loss of power. The aim of the study is to show the importance of using effective temperatures to calculate the real power loss of the system. Power losses are calculated for three industrial unit processes using the effective temperature and the standard temperature of 298.15 K. These processes are: 1) heating of water with steam in a recuperative heat exchanger, 2) preheating of chips with steam, and 3) refining of chips into pulp in the thermo mechanical pulping process (TMP process). Results show that, in addition to the entropy generation rate, the real power loss depends on the temperature level at which the system exchanges heat with the surroundings. The conventional way to calculate the exergy loss does not take this into account. The difference between power losses may become significant if the actual heat exchange takes place at a temperature level much higher than the real environmental or standard temperature.

**Keywords:** Gouy-Stodola law, effective temperature, exergy loss, power loss, second law analysis.

## 1. Introduction

Exergy is usually defined as the maximum work output attainable in the natural environment, or the minimum work input necessary to realise the reverse process [1]. All real processes generate entropy, and loss of exergy is determined by means of the Gouy-Stodola law:

$$E_{loss} = T_o \delta \quad (1)$$

where $T_o$ is the reference temperature and $\delta$ the entropy generation rate. From the viewpoint of the system, loss of exergy means loss of work or power due to irreversibilities caused by the system. In this paper the loss in Eq. (1) is always called power loss. Equation (1) also expresses the thermodynamic improvement potential of the system.

In most cases [2-8], the reference temperature $T_o$ in Eq. (1) is the real temperature of the environment or the standard temperature of 298.15K. The Gouy-Stodola law gives the exact loss of power if the system only exchanges heat at the temperature $T_o$ [9,10]. However, balance boundaries of the thermodynamic system can always be defined in several different ways, depending on the case, and therefore thermodynamic systems may emit or absorb heat at a temperature level other than the real temperature of the environment or the standard temperature. In most industrial processes, this heat is not surplus heat but useful heat needed in processes (e.g. district heating, paper drying). In these cases, the Gouy-Stodola law does not give the correct loss of power (i.e. the improvement potential of the system) if the real temperature of the environment $T_o$ is used [9, 10].

Determination of the temperature $T_o$ in exergy analysis is discussed in some papers. In [11], the authors state that there is no common agreement on a proper definition of the reference

Corresponding Author: Henrik Holmberg, Email: henrik.holmberg@tkk.fi

environment/temperature for steady state exergy analysis of buildings. Kamate et. al. [12] define the exergy loss of a component in a cogeneration plant as a function of the entropy generation rate and air temperature surrounding the component. However, the temperature may change substantially from place to place [12]. In steam expansion, Bejan [13] states that the temperature in Eq. (1) falls somewhere between $T_{out,rev}$ and $T_{out,real}$ when the loss term is calculated ($T_{out,rev}$ outlet temperature after isentropic expansion, $T_{out,real}$ outlet temperature after real expansion). However, Bejan does not elucidate on what the temperature in Eq. (1) should be. In [14], the thermodynamic equivalent temperature has been introduced in connection with exergy analysis of thermodynamic power cycles. This temperature takes into account that the heat transfer temperature changes during the process. However, this temperature has not been used as a reference temperature in exergy analysis. Lampinen et. al. [9] have presented an in-depth theory of the determination of the temperature in Eq. (1) to calculate the real loss of power. The temperature is called the effective heat absorbing or emitting temperature.

The aim of the study is to show the importance of using the effective absorbing or emitting temperature in the Gouy-Stodola law to calculate the real power loss of the system. The paper also tries to explain what differences between power losses mean from the viewpoint of the selected unit processes.

Power losses are calculated for three industrial unit processes using the effective temperature and the standard temperature of 298.15K. The industrial processes are: 1) heating of water with steam in a recuperative heat exchanger, 2) preheating of chips with steam, and 3) refining of chips into pulp in mechanical pulping. All the above-mentioned processes are selected unit processes of the thermo mechanical pulping process (TMP process). Unit processes can be studied as stationary flow systems.

## 2. Theory

This chapter only summarises the main results of the theory presented in more detail in [13].

The correlation between the real power and maximum power output (Eq. 2a) or minimum power input (Eq. 2b) to realise the reversible work is expressed as follows:

$$P = P_{max} - T_{eff}\delta \quad (2a)$$

$$P = P_{min} + T_{eff}\delta \,, \quad (2b)$$

where P is the power and δ the entropy generation rate. $T_{eff}$ is either the effective heat emitting temperature $T_{\_}$ or the effective heat absorbing temperature $T_{+}$, depending on whether the heat flows in or out over the system boundaries. These temperatures are defined a little later in this chapter. The entropy generation rate for a stationary flow system can be written as:

$$\dot{m}\left(s_{out} - s_{in}\right) - \int_1^2 \frac{dQ}{T} = \delta \quad (3)$$

where $s_{in}$ is the specific entropy at the inlet, $s_{out}$ the specific entropy at the outlet, and δ the entropy generation rate. The temperature T in the integral represents the temperature of the boundary over which the heat dQ flows to or from the system. The first term in Eq. (3) represents the entropy generation of the system, and the heat integral the entropy generation of the surrounding.

According to the theory of Lampinen et. al. effective heat emitting and absorbing temperatures $T_{\_}$ and $T_{+}$ are defined as follows [13]:

$$\frac{Q_{\_}}{T_{\_}} = \int_1^2 \frac{dQ_{\_}}{T} \quad (4a)$$

$$\frac{Q_{+}}{T_{+}} = \int_1^2 \frac{dQ_{+}}{T} \quad (4b)$$

where $Q_{\_}$ is heat emitted from the system and $Q_{+}$ is heat absorbed into the system.

Most industrial stationary flow systems can be approximately treated as adiabatic systems which do not exchange heat with the surrounding. In this case, the entropy generation rate becomes:

$$\delta = \sum_{i=1}^{n} \dot{m}_i s_{i,out} - \sum_{j=1}^{m} \dot{m}_j s_{j,in} \quad (5)$$

where $\dot{m}$ is the mass flow and s the specific entropy of the flow. Balance boundaries of the system can always be defined case-specially. Instead of an adiabatic system, balance boundaries can also be defined in such a way that one of the flows emits or absorbs heat to or from the system representing the surroundings. Let assume that the system only emits heat and one flow absorbs it. In this case, the entropy generation rate of the system becomes:

$$\delta_{sys} = \sum_{i=1}^{n-1} \dot{m}_i s_{i,out} - \sum_{j=1}^{m-1} \dot{m}_j s_{j,in} \quad , \qquad (6)$$

where the missing flow is the flow which absorbs heat from the system.

Substituting Equations (4a) and (5) in (3), we obtain

$$\sum_{i=1}^{n-1} \dot{m}_i s_{i,out} - \sum_{j=1}^{m-1} \dot{m}_j s_{j,in} - \frac{\dot{Q}_-}{T_-} = \sum_{i=1}^{n} \dot{m}_i s_{i,out} - \sum_{j=1}^{m} \dot{m}_j s_{j,in} \quad , \qquad (7)$$

Equation (7) reduces to

$$-\frac{\dot{Q}_-}{T_-} = \dot{m}(s_{out} - s_{in}) \quad , \qquad (8)$$

where $\dot{m}$ is the flow which absorbs heat from the system (i.e. the surroundings) and $s_{out}$ and $s_{in}$ are outlet and inlet entropies of this flow, respectively. Taking into account that $\dot{Q}_-$ has a negative value, the effective heat emitting temperature becomes

$$T_- = \frac{\dot{Q}_-}{\dot{m}(s_{out} - s_{in})} = \frac{h_{out} - h_{in}}{(s_{out} - s_{in})} , \qquad (9)$$

where $h_{out}$ and $h_{in}$ are inlet and outlet enthalpies of the flow which absorbs heat. If the heat capacity of the flow remains constant, Eq. (9) becomes

$$T_- = \frac{T_{out} - T_{in}}{\ln \frac{T_{out}}{T_{in}}} \quad , \qquad (10)$$

where $T_{out}$ and $T_{in}$ are inlet and outlet temperatures of the flow which absorbs heat.

If the system absorbs heat, the heat absorbing temperature $T_+$ is also calculated from Equations (9) or (10). In this case, enthalpies, entropies and temperatures refer to the flow which emits heat to the system.

## 3. Description of unit processes

All processes studied in this paper are selected unit processes of the thermo mechanical pulping (TMP process). The entire TMP process consists of the following unit processes: 1) chipping, 2) chip washing, 3) preheating of chips, 4) refining of chips with a TMP-refiner, 5) latency removal, 6) screening and 7) bleaching. This study focuses on the preheating of chips (Fig. 2) and the refining of chips (Fig. 3).

The third unit process in this study is water heating with steam in a recuperative heat exchanger (Fig. 1). The hot water is used as washing water in washing of the chips. Sand, metal pieces etc. are removed from the chip stream in washing.

In preheating, chips are moistened and heated to soften the fibre and middle lamella lignin. Steam is used as the heating medium in preheating. Most of liquid water is absorbed into the chips before preheating.

After preheating the chips are refined into pulp in the TMP refiner. A considerable amount of electricity is consumed in the refining process. Most of the electricity supplied to the refiner is converted into steam/heat. Steam is generated from the dilution water and water absorbed into the chips. The inside of the closed refiner is under pressure and the pulp is blown out of the refiner by means of the steam generated inside the refiner. Part of the steam generated ("Steam out" in Fig. 3) is used as a heating medium in the paper machine. Usually, refining takes place in two stages. Figure 3 shows the second stage of the refining process. In Figure 3, the steam flow $m_v$ in the "Chips in" stream is steam generated in the first stage.

Figures 1-3 also show process values used in example calculations. Process values have been calculated using Balase simulation programme.

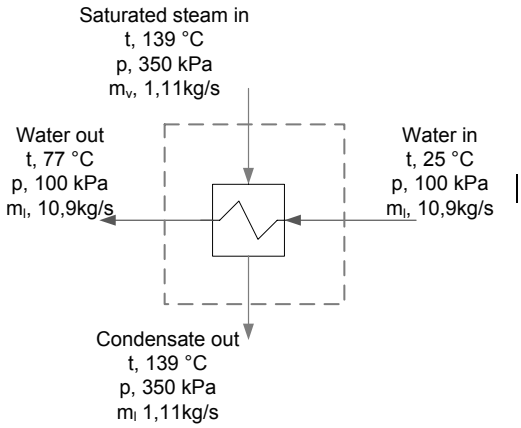


*Figure1. Water heating (t temperature, p pressure, $m_l$ mass flow rate of water, $m_v$ mass flow rate of vapour/steam)*

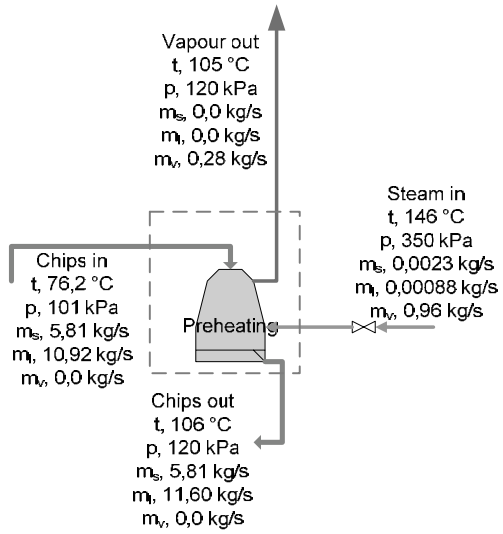


*Figure 2. Preheating of chips (t temperature, p pressure, $m_l$ mass flow rate of water, $m_v$ mass flow rate of vapour/steam, $m_s$ mass flow rate of dry chips)*

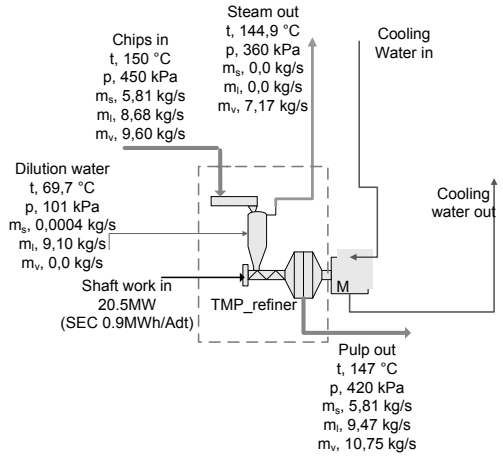


*Figure 3. Refining of chips with a TMP refiner (t temperature, p pressure, $m_l$ mass flow rate of water, $m_v$ mass flow rate of vapour/steam, $m_s$ mass flow rate of dry chips)*

## 4. Results and discussion

Entropy generation rates over each unit process have been calculated using Eq. (5). Entropy values of each flow have been taken from the Blase data bank and are shown in Table 1.

*Table1. Specific entropy values (kJ/kgK) for flows in Figures 1-3.*

| Flow | Water heating kJ/kgK | Chips preheating kJ/kgK | TMP process kJ/kgK |
|---|---|---|---|
| Chips in | | | |
| *$m_s$ | | 4.54 | 4.78 |
| $m_l$ | | 1.03 | 1.84 |
| $m_v$ | | | 6.87 |
| Water in | 0.37 | | |
| Steam in | 6.94 | 6.98 | |
| Dilution water in | | | 0.95 |
| Water out | 1.04 | | |
| steam/vapour out | | 7.30 | 6.96 |
| Condensate out | 1.73 | | |
| Chips/Pulp out | | | |
| $m_s$ | | 4.64 | 4.77 |
| $m_l$ | | 1.37 | 1.81 |
| $m_v$ | | | 6.88 |

*$m_s$ solid, $m_l$ liquid, $m_v$ steam/vapour

To be able to define the effective absorbing or emitting temperature a heat flow representing the surroundings must be defined. These flows are defined as follows:

- **Water heating**: The water flow absorbing heat from the condensing steam.
- **Preheating of chips**: The condensing steam flow emitting heat to the mixture of chips and water flow.
- **Refining of chips**: The superheated steam generated from the dilution water.

Effective heat absorbing ($T_+$) and emitting ($T\_$) temperatures depend on whether the system absorbs or emits heat. In unit processes, these temperatures are the following:

- **Water heating**: heat emitting temperature $T\_$
- **Preheating**: heat absorbing temperature $T_+$
- **Refining**: Heat emitting temperature $T\_$

Effective temperatures have been calculated using Equations (9) or (10).

Entropy generation rates, effective temperatures and power losses for all unit processes are shown in Table 2. Power losses have been calculated using the effective temperature ($P_{loss1}$) and the standard temperature 298.15K ($P_{loss2}$) in the Gouy-Stodola law.

*Table 2. Power losses of unit processes*

| Process | δ kJ/kgK | $T_-$ K | $T_+$ K | $*P_{loss1}$ kW | $**P_{loss2}$ kW |
|---|---|---|---|---|---|
| Water heating | 1.6 | 323 | - | 509 | 470 |
| Chips heating | 0.63 | - | 411 | 258 | 187 |
| Refining | 50.4 | 408 | - | 20600 | 15040 |

$*P_{loss1} = T_-\delta$ or $T_+\delta$ , $**P_{loss2} = T_o\delta$ , $T_o = 298.15$

What do the power losses in Table 2 then tell us? In water and chips preheating, both systems generate entropy and $P_{loss1}$ expresses what the *real loss of mechanical work* is compared to a reversible process. In a reversible process, water and chips heating would be carried out in such a way that no entropy generation occurs. It is impossible to design a reversible process, but the entropy generation should be minimised in process design. Szargut has published in [1] a good list of guidelines to minimise the entropy generation rate and power losses in process design.

In water and chips preheating, the $P_{loss2}$ expresses what the loss of mechanical work is if the system exchanges heat with the surroundings only at the temperature of 298.15K and the entropy generation rate does not change compared to the basic process (Fig. 1 and 2). This means that the system does not heat water or the chips flow to the desired final temperature, but part of the heat is converted into mechanical work inside the system. To do this there must be a heating engine inside the system. Without the heat engine the entropy generation will increase if the heat exchange takes place only at the temperature of 298.15K. In practice, there is probably not any heat engine inside the system and therefore the entropy generation rate increases if the effective heat emitting or absorbing temperatures decrease.

In the refining process, the loss term $P_{loss1}$ is equal to the shaft work supplied to the system (see Table 2 and Figure 3). The small difference in $P_{losss1}$ and shaft work values results from rounding. It is an obvious result that these values are equal because in practice all shaft work is converted into heat in refining. Only a very small part of the shaft work is needed to break the bonds between fibres. The energy needed to break the bonds represents the minimum work of the pulping process, and all work inputs over this are losses from the viewpoint of the process.

To show that losses are indeed equal to the shaft work, power losses have also been calculated for two other shaft work inputs. Various shaft work inputs have been calculated by changing the specific energy consumption (SEC) of the refining process. Results of these calculations and the basic case (see Fig. 3) are shown in Table 3. Table 3 also shows the specific energy consumptions used in the calculations.

In refining, the loss term $P_{loss2}$ describes the minimum power loss for the entropy generation rate of 50.4kJ/kgK. The real power loss could be reduced by letting the outlet steam expand through the turbine. In this case, the cooling water of the condenser represents the surroundings and the effective heat emitting temperature $T_-$ is calculated on the basis of the inlet and outlet temperatures of the cooling water. Table 4 shows an example of how much the power loss would be reduced if the outlet steam could expand through the turbine. The example assumes that the turbine and condenser do not generate any entropy, and therefore the entropy generation rate does not change compared to the basic process (Fig. 3). In reality, both components generate entropy and the power loss is higher than the one in Table 4.

Normally, the outlet steam from the refining process is used in the drying section of the paper machine. This either reduces the need for heat production or increases power generation in the power plant.

*Table3. Influence of specific energy consumption (SEC) on shaft work and power loss in refining*

| SEC MWh/Adt | Shaft work MW | δ kJ/kgK | $T_-$ K | $P_{loss1}$ MW |
|---|---|---|---|---|
| 0.6 | 13.7 | 33.8 | 408 | 13.8 |
| 0.9 | 20.5 | 50.4 | 408 | 20.6 |
| 1.2 | 27.3 | 67.0 | 408 | 27.4 |

*Table 4.Example of a refining process with a turbine and a condenser*

| Parameter | Value |
|---|---|
| Cooling water into the condenser $T_{in}$, K | 298 |
| Cooling water out of the condenser $T_{out}$, K | 336 |
| Effective temperature T_, K | 314 |
| Entropy generation rate δ, kW/K | 50.4 |
| Power loss $P_{loss1}$ , kW | 15850 |

The difference between $P_{loss1}$ (effective temperature) and $P_{loss2}$ (standard temperature) in Table 2 depends on the value of the effective temperature which is determined by the process values. The influence of the process values on the difference between the power losses has been evaluated in the case of water heating (Fig. 1). Figure 4 shows power loss values when the temperature of the saturated steam is changed. Correspondingly, Figure 5 shows the power losses for a case where the outlet temperature of the water is changed.

In both cases, the absolute difference between the power losses increases as the temperature rises. However, the relative difference ($T_/T_o$-1) does not change in the case of Figure 4, because the inlet and outlet temperatures of the water remain constant (see Eq. 10). In the case of Figure 5, the relative difference between the power losses increases constantly, because the effective temperature T_ depends on the outlet temperature of the water. However, for outlet temperatures below 60°C, the relative difference is less than 6%, which is quite a small difference.

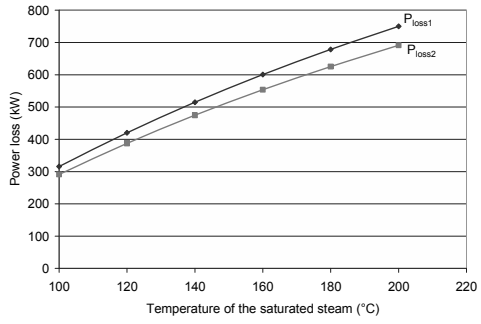


*Figure 5. The influence of the saturated steam temperature on $P_{loss1}$ (effective temperature) and $P_{loss2}$ (standard temperature 298K) in the case of the water heating process (see Fig. 1)*

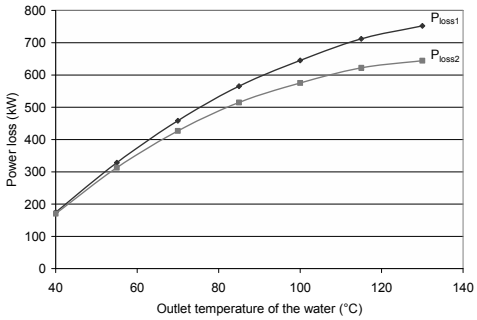


*Figure 6. The influence of the outlet temperature of the water on $P_{loss1}$ (effective temperature) and $P_{loss2}$ (standard temperature 298K) in the case of the water heating process (see Fig. 1)*

## 5. Conclusions

The results of this study show that the entropy generation rate is not an adequate tool for comparing the performance of different thermodynamic systems. The real power loss also depends on the temperature level at which the system exchanges heat with the surroundings, and therefore the effective heat absorbing or emitting temperature must be defined. The results of the refining process best show the importance of defining the effective temperature.

The conventional way to calculate the power/exergy ignores the influence of the temperature because the entropy generation rate is usually multiplied with the real environmental temperature or the standard temperature. The difference between the power losses may become significant if the actual heat exchange takes place at a temperature level much higher than the real environmental or standard temperature (see results of the refining process). For this reason_the conventional way to calculate power/exergy losses may give misleading information on the performance of thermodynamic systems.

## Nomenclature

*h specific enthalpy [J/kg]*
*$\dot{m}$ mass flow rate [kg/s]*
*P Power [W]*
*$P_{loss}$ Power loss [kW]*
*$Q_-$ emitted heat flow [W]*
*$Q_+$ absorbed heat flow [W]*
*s specific entropy [J/kgK]*
*$T_-$ effective heat emitting temperature [K]*
*$T_+$ effective heat absorbing temperature [K]*
*$T_{eff}$ effective temperature [K]*
*$T_o$ standard temperature 298.15K*

*Greek*
*$\delta$ entropy generation rate [W/K]*

## References


[1] Szargut J., 2005, *The Exergy Method: Technical and Ecological Applications*, WITPress, UK, USA.

[2] Gelein de K., Ricardo R., 2003, Entropy production and exergy loss in experimental distillation columns, Chemical Engineering Science, 58(8), pp. 1587-1597.

[3] Wølneberg P.W., Ertesvåg I.S., 2008, Alternatives for power supply to natural-gas export compressors combined with heat production evaluated with respect to exergy utilization and CO2 emissions, Energy Conversion and Management, 49(12), pp. 3531-3540

[4] Zheng J.,Sun F., Chen L.,Wu C., 2001,Exergy analysis for a Braysson cycle Exergy, An International Journal, 1(1), pp. 41-45

[5] Khaliq A., 2009 Exergy analysis of gas turbine trigeneration system for combined production of power heat and refrigeration, International Journal of Refrigeration, 32(3), pp. 534-545

[6] Castro M.B.G., Remmerswaal J.A.M., Brezet J.C., Reuter M.A., 2007 Exergy losses during recycling and the resource efficiency of product systems Resources, Conservation and Recycling, 52(2), Issue pp. 219-233

[7] Suphanit B., Bischert A., Narataruksa P., 2007, Exergy loss analysis of heat transfer across the wall of the dividing-wall distillation column Energy, 32(11), pp. 2121-2134

[8] Durmu A., 2004, Heat transfer and exergy loss in cut out conical turbulators, Energy Conversion and Management, 45(5), pp. 785-796

[9] Lampinen M., Wiksten R., 2006, Theory of Effective Heat-absorbing and Heat Emitting Temperatures in Entropy and Exergy analysis with Applications to Flow Systems and Combustion Process. Journal of Non-Equilibrium Thermodynamics, 31(3), pp. 257-291.

[10] Holmberg H, Ruohonen P, Ahtila P, 2009, Determination of the Real Loss of Power for a Condensing and a Backpressure Turbine by Means of Second Law Analysis, Entropy 11(4), pp. 702-712

[11] Torio H., Angelotti A., Schmidt D., 2009, Exergy analysis of renewable energy-based climatisation systems for buildings: A critical review. Energy and Buildings 41(3), pp. 248-271.

[12] Kamate S.C., Gangavti P.B., 2009, Exergy analysis of cogeneration power plants in sugar industry. Applied Thermal Engineering 29(5-6), pp. 1187-1194.

[13] Bejan A., 1996, Entropy generation minimisation, CRCPpress, BocaRaton, New York, London, Tokoy.

[14] Woudstra N., Woudstra T., Pirone A., van der Stelt T., 2010, Thermodynamic evaluation of combined cycle plants, Energy Conversion and Management, in press.

# Combined Cycle Analysis through an Optimal Control Formulation

*Rogério R. dos Santos[a], Rosiane C. de Lima[a], Geraldo L. S. Ribeiro[a]*

[a] *Vale Solutions in Energy, São José dos Campos, SP, Brazil*

**Abstract:** Power generation is an important issue nowadays. The high demand for energy in modern life means that the performance of power generation systems is a subject of paramount importance. In modern engineering projects, numerical simulation plays a key role in the development and evaluation of devices. In this context, an important aspect of the numerical computation of power generation systems is the ability to propose a representative model of the system. Since there exist a number of known and unknown parameters that may affect the performance of the system and compromise the fidelity of the model, the ability to deal with uncertainty is a desirable characteristic. In this paper, a combined power cycle, that couples two power cycles such that the energy discharged by heat transfer from one cycle is used partly or wholly as the input for the other cycle, is considered. The combined cycle has the gas turbine's high average temperature of heat addition and the vapor cycle's low average temperature of heat rejection and, thus, a thermal efficiency greater than either cycle would have individually. For many applications combined cycles are economical, and they are increasingly being used worldwide for electric power generation. The major challenges in modeling and simulation of the device are the system degradation, measurement errors, and the presence of disturbances of unknown sources. To address this issue, an optimal control framework for system modeling and optimization is proposed. Aiming to capture the system behavior, a meta-modeling that requires only deterministic information is developed. Such approach is shown to be able to deal with the random noise of unknown sources, and furthermore is able to build a model by using information from computational and experimental sources. Transitions between stages and components of the system are modeled by means of an optimal control formulation. It captures the nonlinearities of the system dynamics through a cost functional inspired by the Lagrangian formalism. First order dynamic constraints are then defined to guide the system to the optimal configuration, subject to algebraic path constraints. A feature of the proposed framework is the ability to evaluate both computational and experimental power generation plants. Numerical results show the viability of the proposed methodology.

**Keywords:** power generation, combined cycle, optimal control.

## 1. Introduction

The combined power cycle has increasingly been used worldwide not only for generating electricity but also for generating steam for desalinization plants, pulp factories, paper mills, and all types of chemical plants. The conventional combined cycle couples two thermodynamic cycles (Brayton and Rankine cycles) such that the energy discharged by heat transfer from one cycle is used partly or wholly as the input for the other cycle, which improves overall efficiency.

In a competitive, market-driven economy, it is more important than ever to reduce power generation costs and to find solutions that provide a rapid return on investment without sacrificing long-term reliability and flexibility. Thus, combined cycle power plants have become a well-known and substantial technology for power generation due to its numerous advantages including high efficiency and low emissions. It is a very effective way to increase the thermal efficiency. Producing only electrical power the overall net efficiency can approach 60% for large units above 300 MWe [1-3].

The combined cycle technology provides further advantages [4, 5]:

- thermal efficiencies in excess of 55% are possible with current designs;
- capital cost is relatively low;
- construction times are short (often 2–3 years);
- plant is available in a wide range of configurations and capacities;

Corresponding Author: Rogério R. dos Santos, E-mail: rogerio.santos@vsesa.com.br

- the scheme is compatible with a range of fuels and, in particular, with gas produced by coal gasification plants;
- less space requirements than the space required for equivalent coal or nuclear stations, which reduces site constraints;
- atmospheric emissions are relatively low since natural gas produces no ash or $SO_x$, less quantities of volatile hydrocarbons, carbon monoxide, and $NO_x$ than oil and coal, and much less $CO_2$.

Since the efficiency and performance of a combined cycle are subjects of paramount importance, in this paper a framework for the optimal control of a power plant is proposed.

This subject is addressed as follows. Section 2 presents the mathematical background for the modeling of a standard combined cycle. The formulation of system dynamics as differential equation in terms of time and Laplace domains are presented in Section 3. Section 4 shows the state-state-space representation, and the optimal control formulation is presented in Section 5. The numerical result is addressed in Section 6. Finally, conclusions are presented in Section 7.

# 2. Combined Cycle

## 2.1 Description

Combining gas turbine cycle (Brayton cycle) with a medium or low temperature bottoming cycle (like the Rankine cycle), is the most effective way to increase the thermal efficiency of a gas turbine cycle, [6].

The Brayton Cycle arrangement, also known as the gas cycle, is composed of a compressor, a combustion chamber, and a gas turbine. The Rankine Cycle, whose working fluid is the steam, is composed of a pump, a condenser, a heat exchanger, and a steam turbine.

The exhaust gas of the Brayton Cycle is input for the superheater. After that, it goes through the remainder of the heat recovery steam generator (HRSG).

Energy in the heat exhaust gases is transferred to the water, converting the feedwater to steam. After expansion in the steam turbine where it is condensed. This arrangement is presented in Fig. 1.

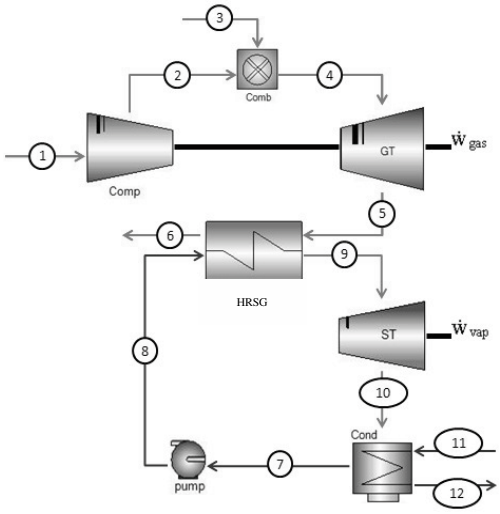


*Fig. 1. Sketch of the combined cycle (Brayton/Rankine).*

## 2.2 Mathematical Modelling

In the current analysis, some assumptions are taken into account:

- the system is in steady state;
- the gas is modeled as an ideal gas;
- turbines, compressor and pump are adiabatic;
- kinetic and potential energy variations are negligible;
- the isentropic efficiencies of the gas turbine, compressor, pump, and steam turbine are $\eta_{GT} = 88\%$ , $\eta_c = 84\%$ , $\eta_p = 80\%$ and $\eta_{ST} = 80\%$, respectively;
- the pressure drop of the combustion chamber is 3%;
- the pressure drop of both streams (gas and steam) in the HRSG is 3%;
- any pressure loss in the condenser is not considered;
- natural gas with LHV=47,500kJ/kg.

The steam mass flow $\dot{m}_{vap}$ and the flue gas mass flow $\dot{m}_{gas}$ can be determined by applying mass and energy balances to the HRSG, [6], as follows:

$$0 = \dot{m}_{gas}(h_5 - h_8) + \dot{m}_{vap}(h_9 - h_{10}) \qquad (1)$$

The mass and energy balances applied to the power cycle provide the net power produced by the gas and steam turbines, namely,

$$\dot{w}_{gas} = \dot{m}_{gas}\left[(h_4 - h_5) - (h_2 - h_1)\right] \quad (2)$$

$$\dot{w}_{vap} = \dot{m}_{vap}\left[(h_{10} - h_9) - (h_8 - h_7)\right] \quad (3)$$

$$\dot{w}_{liq} = \dot{w}_{gas} + \dot{w}_{vap} \quad (4)$$

The temperature (T), pressure (p), and enthalpy (h) of the gas and steam states are presented in Table 1 and Table ***2***, respectively. The conditions of the air inlet are $T_1$=300 K and $p_1$=100 kPa; the pressure ratio ($p_2/p_1$) is 12.38; the gas turbine inlet temperature is $T_4$=1400 K; the gas turbine inlet pressure is $p_4$=1200 kPa; the exhaust temperature is $T_5$=867.34 K; the steam turbine inlet pressure is $p_{14}$=8 MPa and the outlet pressure is $p_{15}$=8 kPa. The steam property method is the IAPWS-IF97 [7], and the gas property method is the NASA [8].

*Table 1. Gas cycle states.*

| *Gas Cycle (GC)* | | | |
|---|---|---|---|
| *State* | *T (K)* | *p (kPa)* | *h (kJ/kg)* |
| 1 | 300 | 100 | 11.48 |
| 2 | 663.53 | 1238 | 390.12 |
| 4 | 1400 | 1200.86 | 1297.89 |
| 5 | 867.34 | 111 | 639.46 |
| 6 | 438.39 | 101.31 | 158.72 |

*Table 2. Steam cycle states.*

| *Steam Cycle (SC)* | | | |
|---|---|---|---|
| *State* | *T (K)* | *p (kPa)* | *h (kJ/kg)* |
| 7 | 314.68 | 8 | 173.87 |
| 8 | 318.04 | 8502.05 | 195.29 |
| 9 | 827.82 | 8000 | 3530.97 |
| 10 | 314.68 | 8 | 2296.02 |

From equation (1), the mass flow ratio is

$$\frac{\dot{m}_{vap}}{\dot{m}_{gas}} = \frac{14.24}{99.79} = 0.1427 \quad (5)$$

The combined cycle net power is obtained applying the data of Table 1 and Table ***2***, i.e.,

$$\dot{w}_{liq} = \dot{w}_{gas} + \dot{w}_{vap} = 45\,\text{MW} \quad (6)$$

## 3. System dynamics

The state-space approach is a generalized time-domain method for modeling, analyzing and designing a range of control systems. When the state-space X is a finite-dimensional normed linear space, it is known as a finite-dimensional dynamical system. Also, when all motions of a continuous-time dynamical system are continuous with respect to time *t*, it is called a continuous dynamical system.
Continuous-time, finite-dimensional dynamical systems may be determined, for example, by the solutions of ordinary differential equations and ordinary differential inequalities. These arise in a number of areas in science and engineering, including mechanics, circuit theory, power and energy systems, chemical processes, and feedback control systems, among others.
When a second-order differential equation

$$a\frac{d^2x_0}{dt^2} + b\frac{dx_0}{dt} + cx_0 = ex_i(t) \quad (7)$$

is considered, the Laplace transform of the equation with zero initial conditions gives

$$as^2X_0(s) + bsX_0(s) + cX_0(s) = eX_i(s) \quad (8)$$

$$\Rightarrow (as^2 + bs + c)X_0(s) = eX_i(s) \quad (9)$$

The corresponding transfer function is

$$G(s) = \frac{X_0}{X_i}(s) = \frac{e}{as^2+bs+c} \quad (10)$$

By dividing the equation by *c* and making the coefficient of $s^2$ equal to unity, the following standard form is obtained

$$G(s) = \frac{K\omega_n^2}{s^2+2\zeta\omega_n s+\omega_n^2} \quad (11)$$

Equation (11) is the standard form of the transfer function for a second-order system, where K is the steady state gain constant; $\omega_n$ (rad/s) is the undamped natural frequency, and $\zeta$ is the damping ratio.

The transient response of a system is independent on the input ([10]). Thus, for transient response analysis, the system input can be considered to be zero, and equation (9) can be written as

$$(as^2 + bs + c)X_0(s) = 0 \quad (12)$$

If $X_0(s) \neq 0$ then

$$as^2 + bs + c = 0 \quad (13)$$

This polynomial in $s$ is called the characteristic equation and its roots $s_1$ and $s_2$ determine the system transient response. This response is given by the general solution

$$x_0(t) = Ae^{s_1 t} + Be^{s_2 t} \quad (14)$$

The transient response is classified according the criteria given in Table 3.

*Table 3. Transient behaviour of a second-order system.*

| *Discriminant* | *Roots* | *Response type* |
|---|---|---|
| $b^2 > 4ac$ | $s_1$ and $s_2$ real and different | Overdamped |
| $b^2 = 4ac$ | $s_1$ and $s_2$ real and equal | Critically damped |
| $b^2 < 4ac$ | $s_1$ and $s_2$ complex conjugate | Underdamped |

When the damping coefficient $d$ of a second order system has its critical value $d_c$ the system, when disturbed, reaches its steady-state value in the minimum time without overshoot. The ratio between the damping coefficient and its critical value defines the damping ratio, i.e.,

$$\zeta = \frac{d}{d_c} \quad (15)$$

with damping characteristic defined in Table 4.

*Table 4. Damping coefficient.*

| | |
|---|---|
| $\zeta$=0 | No damping |
| $\zeta$<0 | Underdamping |
| $\zeta$=1 | Critical damping |
| $\zeta$>1 | Overdamping |

In this paper, the general model of second order is supposed to capture the main behavior of a combined cycle power plant.

The inlet flow at the compressor is the control variable and the plant net power is the output variable. A reference input value is $\dot{m}_{ref} = 98\,kg/s$ and the corresponding plant net power is $P_{ref}$ =45 MW. A detailed discussion about plant model is presented by [9].

Small deviations of the nominal mass flow value $\dot{m}_{air}$ (kg/s) and the corresponding plant net power $P$ (MW) are presented in Table 5.

*Table 5. Mass flow and net power.*

| $\dot{m}_{air}$ | $P$ | $\dot{m}_{air}$ | $P$ | $\dot{m}_{air}$ | $P$ |
|---|---|---|---|---|---|
| 87 | 40.01 | 95 | 43.69 | 103 | 47.37 |
| 88 | 40.47 | 96 | 44.15 | 104 | 47.83 |
| 89 | 40.93 | 97 | 44.61 | 105 | 48.29 |
| 90 | 41.39 | 98 | 45.07 | 106 | 48.75 |
| 91 | 41.85 | 99 | 45.53 | 107 | 49.21 |
| 92 | 42.31 | 100 | 45.99 | 108 | 49.67 |
| 93 | 42.77 | 101 | 46.45 | 109 | 50.13 |
| 94 | 43.23 | 102 | 46.91 | 110 | 50.59 |

There is a high correlation between the input $\dot{m}_{ref}$ and the output $P$ variables. Furthermore, normalization of input and output reference values, $\dot{m}_{ref}$ and $P_{ref}$, enables writing the system model through dimensionless values. The practical aspect of such an approach is that the input $\dot{m} = 1$ gives output $P$=1, input $\dot{m} = 0.9$ has output $P$=0.9 and so on.

Additionally, system dynamics is supposed to be an underdamped, second-order system. The

workflow proposed in this paper can easily be adjusted to also deal with overdamped and critically damped systems.

Without loss of generality, for K=1, $\zeta = 0.7$ and $\omega_n = 1$, Equation (11) gives

$$\mathrm{G(s)} = \frac{1}{\mathrm{s^2+1.4s+1}} \quad (16)$$

Different damping conditions will be considered as disturbance over nominal conditions and will be addressed through the numerical methodology.

A fine tuning can be performed for the determination of coefficients. However, the current study reinforces the generality of the proposed methodology to ensure the convergence and stability of the solution for a range of values.

It should be pointed out that different damping factors and natural frequencies are considered by means of a straightforward replacement in Equation (11).

## 4. The state-space approach

The state of a system is described by a set of first order differential equations in terms of the state variables $\mathbf{x} = (x_1, \ldots, x_n)$ and control variables $\mathbf{u} = (u_1, \ldots, u_m)$ and can be expressed in matrix form by

$$\dot{\mathbf{x}} = A\mathbf{x} + B\mathbf{u} \quad (17)$$

where $A$ is the $n \times n$ system matrix and $B$ is the $n \times m$ control matrix.

According to this convention, the system plant defined by equation (16) can be rewritten as

$$\dot{\mathbf{x}} = \begin{bmatrix} 0 & 1 \\ -1 & -1.4 \end{bmatrix}\mathbf{x} + \begin{bmatrix} 0 \\ 1 \end{bmatrix}\mathbf{u} \quad (18)$$

This is the standard form of the dynamic system addressed by optimal control theory.

## 5. Optimal control

Optimal programming problems for continuous systems are problems in the calculus of variations. A continuous-step dynamic system is described by an $n$-dimensional state vector $\mathbf{x}(t)$ at time $t$. Choice of an $m$-dimensional control vector $\mathbf{u}(t)$ determines the time rate of change of the state vector through the relations

$$\dot{\mathbf{x}} = g(\mathbf{x}, \mathbf{u}, t) \quad (19)$$

The general optimization problem for such a system is to find the time history of the control vector $\mathbf{u}(t)$ for $t_0 \le t \le t_f$ to minimize a performance index of the form

$$\mathrm{J} = \phi[\mathbf{x}(t_\mathrm{f})] + \int_{t_0}^{t_\mathrm{f}} \mathrm{L}(\mathbf{x}, \mathbf{u}, t)\mathrm{dt} \quad (19)$$

subject to equation (19) with $t_0$, $t_\mathrm{f}$ and $\mathbf{x}(t_0)$ specified.

In the present study, the formulation of interest is to find the control vector function $\mathbf{u}(t)$ that minimizes

$$J = \frac{1}{2}\mathbf{e}_f^T Q_f \mathbf{e}_f + \frac{1}{2}\int_{t_0}^{t_f} [\mathbf{x}^T \ \mathbf{u}^\mathbf{T}] \begin{bmatrix} Q & N \\ N^T & R \end{bmatrix} \begin{bmatrix} \mathbf{x} \\ \mathbf{u} \end{bmatrix} dt \quad (20)$$

subject to

$$\dot{\mathbf{x}} = A\mathbf{x} + B\mathbf{u} \quad (21)$$

$$\mathbf{x}(t_0) = \mathbf{x}_0 \quad (22)$$

$$\mathbf{e}_f = M_f \mathbf{x}(t_f) - \psi \quad (23)$$

where $M_\mathrm{f}$, $Q_\mathrm{f}$ are given matrices and $A$, $B$, $Q$, $N$, and $R$ are given constant matrices or matrix time functions. The control designer chooses $Q_\mathrm{f}$, $Q$, $N$ and $R$.

Variational calculus ([11]) may be employed to obtain a set of differential equations with boundary condition properties, known as the Euler-Lagrange equations. The maximum principle of Pontryagin [12] can also be applied to provide the same boundary conditions by using the Hamiltonian function. The Hamilton-Jacobi equation is usually solved for the special case of the linear time invariant plant with quadratic performance index (considered in the present study), which takes the form of the matrix Riccati equation. This produces

an optimal control law as a linear function of the state vector components which is always stable, providing the system is controllable.

From Equations (19) and (20), a Hamilton-Jacobi equation may be expressed as

$$\frac{\partial f}{\partial t} = -\min_{\mathbf{u}} \left[ L(\mathbf{x}, \mathbf{u}) + \left( \frac{\partial f}{\partial \mathbf{x}} \right)^T g(\mathbf{x}, \mathbf{u}) \right] \quad (25)$$

For a linear, time invariant plant, Equation (19) becomes

$$\dot{\mathbf{x}} = A\mathbf{x} + B \quad (26)$$

and for a quadratic performance index, Equation (21), the equality

$$\frac{\partial f}{\partial t} = -\min_{\mathbf{u}} \left[ \mathbf{x}^t Q \mathbf{x} + \mathbf{u}^T R \mathbf{u} + \left( \frac{\partial f}{\partial \mathbf{x}} \right)^T (A\mathbf{x} + B\mathbf{u}) \right] \quad (27)$$

follows. Introducing the relationship

$$f(\mathbf{x}, t) = \mathbf{x}^T P \mathbf{x} \quad (28)$$

where $P$ is a square, symmetric matrix, the optimal control law after some computation is

$$\mathbf{u}_{opt} = -R^{-1} B^T P \mathbf{x} \quad (29)$$

is obtained. Furthermore, some development yields

$$\dot{P} = -PA - A^T P - Q + PBR^{-1}B^T P \quad (30)$$

which belongs to a class of nonlinear differential equations known as the Riccati equation. To ensure that the solution is unique and finite, matrices $Q_f$ and $Q$ must be positive semidefinite and matrix $R$ must be positive definite.

## 6. Numerical result

A numerical simulation was performed to evaluate the performance of the proposed methodology. For a system dynamics defined according to Equation (18) and a performance index given by Equation (21), the following parameters were adopted:

$$Q = \begin{bmatrix} 10 & 0 \\ 0 & 10 \end{bmatrix}, R = [20], N = \mathbf{0}, Q_f = \mathbf{0} \quad (31)$$

These values can be adjusted to represent different priorities on the performance of states and controls.

By using the Riccati expression, Equation (30), the optimal design $K = [1.0 \quad 1.4]$ is obtained. Initial and optimal designs are presented in Fig. 2 and show the response against impulse signal.

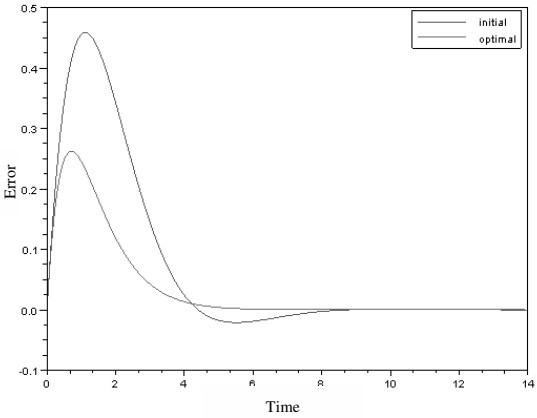


*Fig. 2. Initial and optimal impulse response.*

The response of the initial design has a peak value of 0.458. After the optimization, the response peak is successfully decreased to 0.262. The settling time is also decreased. Since the procedure is independent of the system damping and natural frequency, it is able to find the optimal gain even after system changes are required (Equation (16)).

Furthermore, the robustness of the optimal design is numerically evaluated. Disturbances between 0 and 10% on system parameters are artificially included. These aim to represent sensor or actuator noise, system degradation and unexpected operational conditions.

As a result, K=1±0.1, $\zeta$=0.7±0.07 and $\omega_n$=1±0.1 in equation (16). Deviations in system damping is summarized on Fig. 3 and deviations in the natural frequency is summarized on Fig. 4, according to the Gaussian distribution.

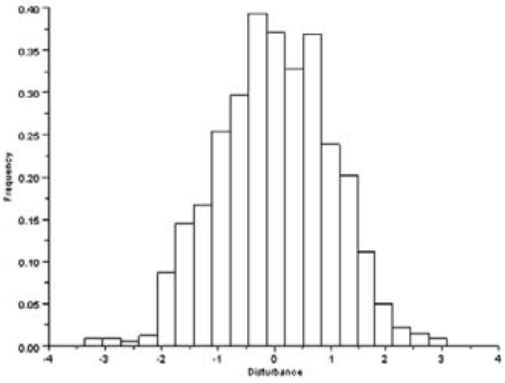


*Fig. 3. Histogram of damping coefficient disturbance.*

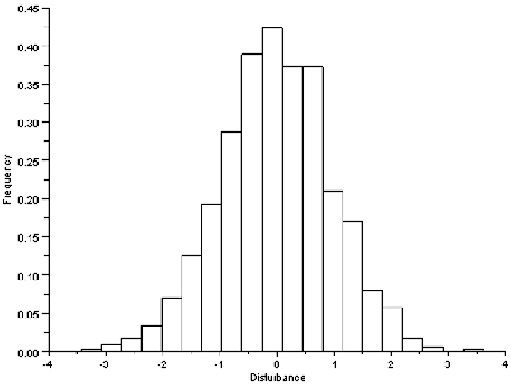


*Fig. 4. Histogram of natural frequency disturbance.*

In agreement with the Monte Carlo methodology, one thousand simulations with noisy designs were run.

Figure 5 shows the impulse response of a disturbed system using the same optimal design previously determined.

The design $K$ = [1.0 1.4] is optimal only for the initial problem (Equation (16)). However, it was shown to be robust with regard to the presence of small deviations in the nominal value. It is confirmed by the fact that the worst peak response is lower than 0.33 and still smaller than the initial peak response of 0.458.

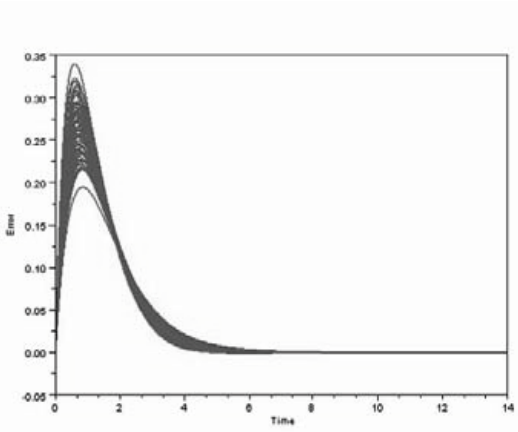


*Fig. 5. Impulse response for several plant disturbances.*

Similar numerical results are found for other experiments conducted by the authors.

## 7. Conclusion

In this paper a strategy for the optimal control of a combined cycle power plant are presented. Initially, the efficiency of commercially available arrangements is discussed. Later, the mathematical modeling of a standard combined cycle is outlined.

The contribution of this paper is the evaluation of the system from the dynamical point of view. The concept of a dynamic system represented by a differential equation is presented. The standard form and the equivalent state-space representation are shown.

The optimal control formulation is applied to the computation of the optimal design, leading the system to a steady state presenting a smaller overshoot and smaller settling time when compared with its initial design.

Latter, the presence of a disturbance in the original plant is taken into account, and the same optimal design is applied. Despite the fact that in this situation the design previously obtained is not optimal, it is shown to be able to guide the system to the steady state with better performance than the initial (not optimized) design.

If a maximum performance is required from the plant, the optimal design can be computed every time a structural change is detected. There exist technical solutions of low cost that provide this behavior.

The main conclusion of this study is that the Linear Quadratic Regulator was able to provide significant improvement in system performance and has proven to be robust with regard to system deviations.

Future research on this topic includes the calibration of the transfer function according to data provided by commercial devices and the analytical expression for the optimal design.

Finally, due to the ease of implementation and significant improvement of system performance the authors believe that the proposed framework is a useful tool for power plant control.

## Nomenclature

$A$ system matrix
$B$ control matrix
$h$ enthalpy, kJ/kg
$LHV$ Low heating value, kJ/kg
$\dot{m}$ mass flow rate, kg/s
$p$ pressure, kPa
$P$ power, MW
$s$ Laplace domain
$t$ time, s
$T$ temperature, K
$\mathbf{u}$ control vector
$\mathbf{x}$ state vector

### *Greek symbols*

$\eta$ isentropic efficiency, %
$\omega_n$ undamped natural frequency, rad/s
$\zeta$ damping ratio

### *Subscripts and superscripts*

air air
C compressor
gas gas
GT gas turbine
liq net
P pump
ref reference
ST steam turbine
vap steam

## References


[1] http://www.energy.siemens.com/hq/en/power-generation/power-plants/gas-fired-power-plants/combined-cycle-power-plant-concept/

[2] http://www.power.alstom.com

[3] http://www.gepower.com/prod_serv/products/gas_turbines_cc/en/stag/index.htm

[4] Heppenstall, T., 1998, Advanced gas turbine cycles for power generation: a critical review, Applied Thermal Engineering, 18, pp. 837-846.

[5] Poullikkas, A., 2005, An overview of current and future sustainable gas turbine technologies, Renewable and Sustainable Energy Reviews, 9, pp. 409-443.

[6] Moran J., and Shapiro N.M., 2006, *Fundamentals of engineering thermodynamics*. 5th ed., John Wiley & Sons, Inc.

[7] Wagner, W., and Kruse, A., 1998, Properties of Water and Steam, The Industrial Standard IAPWS-IF97, Springer-Verlag, Berlin Heidelberg New York ISBN: 3-540-64339-7.

[8] Gordon, S., and McBride, B.J., 1999, Thermodynamic Data to 20,000 K for Monatomic Gases, NASA/TP – 208523.

[9] Sontag, R.E., et al., 2003, *Fundamentals of Thermodynamics*, John Wiley & Sons, Inc.

[10] Burns, R.S., 2001, *Advanced control engineering*, Butterworth-Heinemann.

[11] Dreyfus, S.E., 1962, Variational Problems with Inequality Constraints, J. Math. Anal. Appl., 4, p. 297.

[12] Pontryagin, L.S., et al., 1962, *The Mathematical Theory of Optimal Processes*, John Wiley & Sons, New York.

# Boiler Calculation Software

*Renan Heck Saccomani[a], Juan Harold Sosa-Arnao[a] and Silvia Azucena Nebra[b]*

*[a] Equipalcool Sistemas Ltda, Sertãozinho, Brazil*
*[b] Interdisciplinary Center of Energy Planning – NIPE/UNICAMP, Campinas, Brazil*

**Abstract:** The cogeneration systems fueled by biomass are enhancing considerably the electrical energy sales to the national grid. This fact has produced the increase of steam generation parameters and the research for more efficient generation systems. The steam boiler represents the most important device in the cogeneration systems from the technical and economical point of view. Consequently, the boiler performance study could reduce its cost, increasing its thermal efficiency and thus could improve the cogeneration systems performance. Therefore, Equipalcool Sistemas developed the software INKA´S BOILER, which allows the simulation of the biomass boiler at several arrangements of its devices (furnace, super-heater, boiler bank, economizer and air heater). Also, the cogeneration system study can be carried out by this software, whose patent has been requested. Aiming to validate this software, a bagasse boiler that operates with 200 t/h of steam at 6.57 MPa and 520 °C, located at the Cerradinho II mill, was simulated. The results simulated were compared with measurements done "in loco" and presented good agreement.

Keywords: Boiler, Biomass, Cogeneration, Efficiency.

## 1. Introduction

Conventional engineering analysis relies heavily on empirical correlations and experience to develop boiler and auxiliary equipment designs. Today design processes must be more accurate while minimize development costs to compete in a world economy. This fact forces engineering companies to take advantage of design tools, which enlargeexisting experience and empirical data while minimize cost. One tool which excels under these conditions is numerical modeling [1].

Nowadays there are softwares in the market, capable of making the thermal calculation of a complete boiler. For instance, the Grate Fired Boiler Software [2] is used to design all types of stoker fired boilers up to a steam capacity of 200,000 kg/h. The types of Boilers that can be designed include coal, lignite and biomass as fuel. Another one is the Heat Recovery Steam Generators simulation program – HRSGs [3] that is a thermal simulation tool capable of obtaining temperature profiles for different configurations and also able of simulating the complete plant cogeneration cycle.

It was developed in Brazil the Steam Boiler Calculations – SBC [4] which allows the thermal and aerodynamic calculation of natural circulation boilers with a capacity between 20,000 and 900,000 kg/h using oil, gas and coal as fuel. With the help of this program it is possible to: Project new boilers, optimize the boiler's thermal and aerodynamical scheme, research the partial load boiler operation regimes, select the blower and the induced draft fan, and elaborate performance tests data.

The biggest manufacturers of boilers in the world, such as Foster Wheeler, Metso, Mitsubishi, Kawasaki and the Babcock & Wilcox Company, also have softwares for thermal and aerodynamic calculations including Computational Fluid Dynamics software.

This work presents the simulation results obtained from the bagasse boiler aerodynamic and thermal calculation carried out through INKA'S BOILER Software. Also, compares this values with that one's measured in the field.

## 2. Software INKA´S BOILER

This calculation tool was developed by Saccomani and Sosa-Arnao for the utilization of Equipalcool Sistemas, boilers manufacturer in Brazil. It's in the process of obtaining patent registration and your temporary protocol number is 0000220908082549 issued in December of 2009.

Corresponding Author: Renan H. Saccomani, Email: renan@equipalcool.com.br

This software is capable of aerodynamically and thermically simulating any type of boiler, of different configurations and quantities of superheaters, screens, boiler banks, economizers, air heaters, and other devices that compose the boiler.

The user is free to assemble the boiler and use any desired fuel, filling up only with the ultimate composition and its Lower Heating Value (LHV).

Also, the Rankine Cycle can be completely simulated, because its virtual library contains the blocks of condensation and back-pressure turbine, deaerator, condenser, regenerator and radiator steam.

### 2.1. Simulated boiler

The boiler considered in the simulation was a bagasse boiler with 200,000 kg/h of steam at 6.57 MPa and 520 °C, which was manufactured, by Equipalcool Sistemas Ltda, in 2007 and is installed in the Cerradinho II mill, in Potirendaba, São Paulo State, Brazil, as can be seen in Fig. 1.

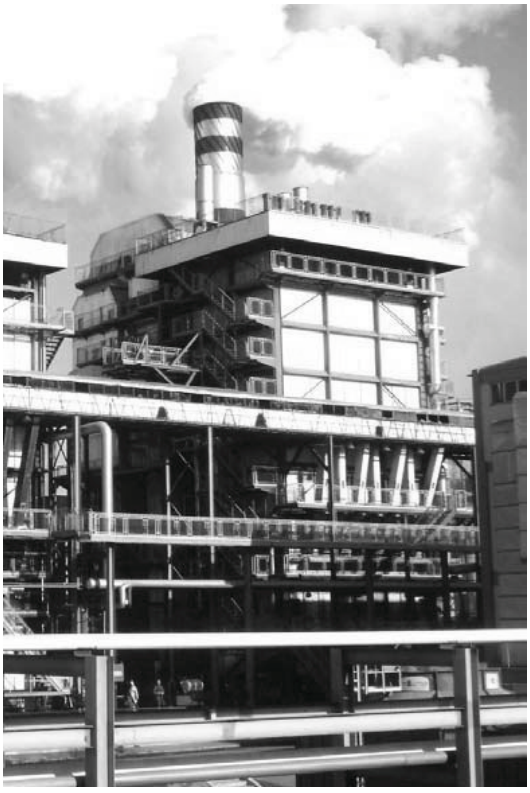

*Fig. 1. Boiler installed in the Cerradinho II mill.*

The boiler configuration assembled in INKA'S BOILER can be observed in the Fig. 2 and the identification of each device is shown in the Table 1.

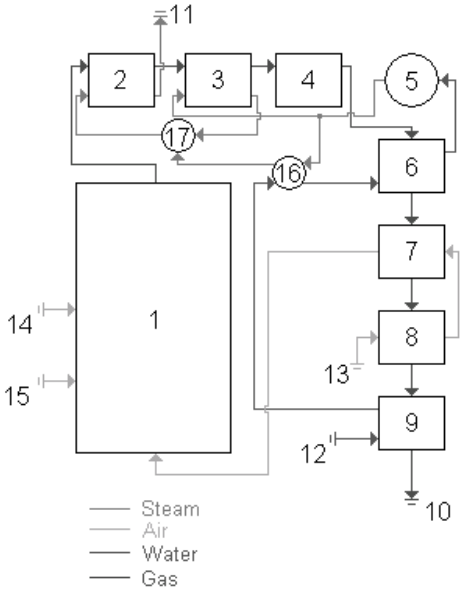


*Fig. 2. Boiler considered in the simulation.*

*Table 1. Identification of the boiler devices.*

| Position | Identification | Position | Identification |
|---|---|---|---|
| 1 | Furnace | 10 | Output Gas |
| 2 | Secondary Superheater | 11 | Output Steam |
| 3 | Primary Superheater | 12 | Water Inlet |
| 4 | Boiler Bank | 13 | Primary Air Inlet |
| 5 | Steam Drum | 14 | Secondary Air Inlet |
| 6 | Secondary Economizer | 15 | Air feeding flue |
| 7 | Secondary Air Heater | 16 | Condenser |
| 8 | Primary Air Heater | 17 | Desuperheater |
| 9 | Primary Economizer | | |

## 3. Methodology

The simulation is made by blocks, in other words, each block has its own internal function where the calculations are performed according to input data specified by the user, as well as data coming from

other blocks, generating the output data, which will be passed to the next block of the sequence.

The main input data for the simulation are: mass flow, pressure and temperature of the steam at the outlet of the boiler, besides fuel ultimate composition and its HHV. However, each block has its own specific input data. For instance, in the superheater are inserted: external diameter and thickness of the tubes, tubes number per serpentine, serpentines number, serpentine length, height and depth of the involucre, longitudinal and transversal pass, arrangement type: parallel or counterflow, as well as steam inlet and outlet pressure.

The calculation starts at the furnace block, however this block needs previous data coming from others, like the air temperature coming from the air heater, so, for the first calculation cycle, that data are estimated.

The convergence is made through the gas outlet temperature, which is calculated at the last block present in the configuration, see Fig. 2. The current calculated temperature is compared to the previous one and the cycle is repeated until the difference is lower than the parameter established by the software.

### 3.1. Furnace

The furnace is the most important boiler component. Its primary function is to provide adequate space for fuel particles to burn completely and to cool the flue gas to a temperature at which the convective heating surfaces can be operated safely [5].

In the furnace block the following calculations are carried out: combustion, gas outlet temperature and also boiler efficiency.

#### 3.1.1. Flue Gas Temperature at the Furnace Exit (FEGT)

A typical boiler design calculation starts with the stoichiometric calculations for the fuel fired followed by the energy balance calculations. From the stoichiometric and energy balance calculations, the rated fuel consumption $\dot{m}_b$, the heat retention coefficient Ø, and the average specific heat $Cp$ of the flue gas can be determined. To use (1) to calculate the flue gas temperature at the furnace outlet $T_{g,fo}$, the flat surface area A of the waterwall tubes, the coefficient $\psi$ of thermal efficiency, and the coefficient $M$ and the emissivity $\alpha$ of the furnace must be supplied or calculated [5].

$$T_{g,fo} = \frac{T_{af}}{M\cdot\left(\frac{\sigma\cdot\alpha\cdot\psi\cdot A\cdot T_{af}^{\,3}}{\phi\cdot\dot{m}_b\cdot Cp}\right)^{0,6}+1} \quad (1)$$

#### 3.1.2. Boiler Efficiency

The bagasse boiler efficiency is the most important parameter on a sugar mill cogeneration system; therefore, its calculation helps on cogeneration system optimization [6].

On the A ( . , ( , the boiler first law efficiency is analyzed through two proposals: Beatón and Lora [7] and ASME Code PTC 4.1 [8]. This last one was adapted to bagasse boilers, since it has been formulated for coal boilers.

O 6 6 to evaporate the water formed by oxidation of bagasse hydrogen content and also by bagasse moisture content are discounted in the LHV calculation. The boiler efficiency is determined from the sum of all heat loss fraction, taking into account: exhaust gas $q_2$, incomplete chemical combustion $q_3$, incomplete combustion due to mechanical causes $q_4$, surface radiation and convection $q_5$, slag and ashes $q_6$ and bleeding in the boiler $q_7$, according (2).

$$\eta_I = 100 - (q_2 + q_3 + q_4 + q_5 + q_6 + q_7) \quad (2)$$

The first law efficiency by the input / output method is calculated through (3).

$$\eta_I = \left(\frac{\dot{m}_s\cdot(h_s - h_{w,o})}{\dot{m}_b\cdot LHV_b}\right)\cdot 100 \quad (3)$$

Code ASME PTC 4.1 proposal requires the determination of losses, heat credits, ultimate analysis and higher heating value (HHV) of the fuel .The heat losses, considered in the calculation, 6 9 6 $q_3$, $q_4$, $q_5$, $q_6$ and $q_7$), but the calculation base is the HHV. There are some differences in the analysis of the boiler exhaust gas heat loss $q_2$ between the two proposals. According to ASME PTC 4.1, this heat loss is divided up in three ones: dried gas heat loss $q_2^*$, heat loss due to water vapor from burning hydrogen $q_8$ and heat loss due to bagasse moisture content $q_9$. The boiler efficiency is determined from the sum of all heat loss fractions, according (4).

$$\eta_{II} = 100 - (q_2^* + q_3 + q_4 + q_5 + q_6 + q_7 + q_8 + q_9) \quad (4)$$

The first law efficiency by the input / output method is calculated trough (5).

$$\eta_{II} = \left(\frac{\dot{m}_s \cdot (h_s - h_{w,o})}{\dot{m}_b \cdot HHV_b}\right) \cdot 100 \qquad (5)$$

These proposals were discussed by Sosa-Arnao et al. [9], who concluded that due to the high bagasse moisture content to use the HHV as calculation base is more adequate.

### 3.2. Heat Exchangers

The heat exchangers as superheater, screen, boiler bank, economizer and air heater, follow the same calculation line, and it was modeled according Babcock & Wilcox Company Handbook[10]. The main calculation involves the heat flux through heat transfer coefficient, heat transfer area and log mean temperature difference (LMTD) as inlet parameters, being this last one calculated according the flux type (parallel or counterflow).

Sometimes, the heat exchangers, as superheater, is exposed to radiation from furnace, in this case, besides the heat transferred by convection and intertube radiation also, the radiated heat from furnace is considered.

The heat transfer coefficient *U* is a composition of the convective and radiation heat transfer coefficient from the gas side, and the heat transfer coefficient of the fluid (air or steam).

### 3.3. Input data

To initiate the simulation, it was considered the input data that represent the measured physical parameters.

The bagasse ultimate composition (wet basis) according [11] and its HHV are showed in the Table 2.

*Table 2. Fuel ultimate composition*

| Bagasse | | |
|---|---|---|
| Moisture | 50.00 | % |
| Ash | 1.25 | % |
| Carbon | 23.50 | % |
| Hydrogen | 3.25 | % |
| Nitrogen | 0.00 | % |
| Oxygen | 22.00 | % |
| HHV | 9,325 | kJ/kg |

The boiler was simulated at the same conditions at which the field measurements were made. The steam parameters are presented in Table 3.

*Table 3. Steam parameters at the boiler outlet , in operation.*

| Steam | | |
|---|---|---|
| Mass flow | 188,000 | kg/h |
| Pressure | 6.57 | MPa |
| Temperature | 520 | °C |

Just like it is in the real boiler, the air excess considered in the burn was 35% and the ambient temperature around the boiler was 30 °C. That air excess quantity guarantees a complete combustion aiming to avoid the formation of carbon monoxide CO.

From the total quantity of air necessary for the burn, including air excess, 85% are destined to the primary air, which passes by the air heaters, 5% for the fuel feeding and the rest are secondary air.

The temperature of the boiler inlet water coming from the deaerator was considered as 120 °C.

The superheaters are vertical and their tubes are arranged in a square format. The secondary superheater presents parallel arrangement while the primary superheater is counterflow.

Also, the boiler tubes bank is vertical and have its tubes arranged in a square format. The tubes are connected directly to the upper and lower boiler drums.

The economizers are horizontal, having their tubes arranged in square format. The secondary economizer has flat tubes while the primary economizer has spiral fin.

The air heaters are vertical, with staggered arrangement of tubes, where the gas passes internally and the air passes outside.

The software has capacity to calculate other air heaters types, such as, horizontal air/gas and air/steam radiator, if necessary.

The fig. 3 presents the several measured point along the bagasse boiler. Which permits to validate the software calculation development.

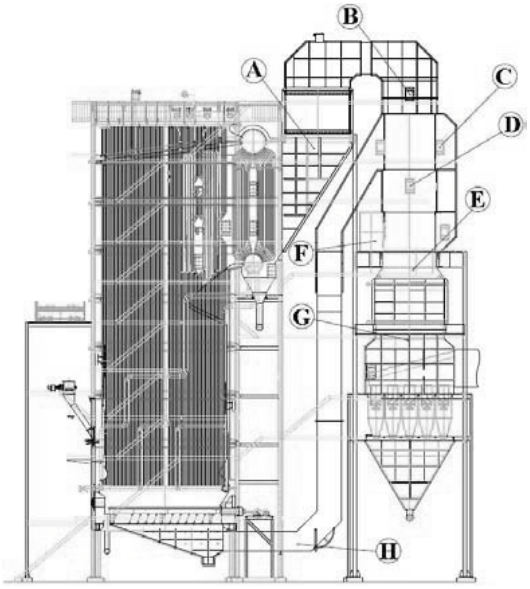


*Fig. 3. Measured points along the bagasse boiler.*

*Table 4. Localization of measuring points.*

| Localization | Point |
|---|---|
| Gas outlet of the Boiler Bank | A |
| Gas outlet of the Secondary Economizer | B |
| Air outlet of the Primary Air Heater | C |
| Gas outlet of the Secondary Air Heater | D |
| Gas outlet of the Primary Air Heater | E |
| Air inlet of the Primary Air Heater | F |
| Gas outlet of the Primary Economizer | G |
| Air outlet of the Secondary Air Heater | H |

## 4. Results

After inserting the input data that are specified by the user in each device, the simulation runs until convergence is obtained and the results are showed in the computer's screen.

The first parameter to be evaluated in a boiler project is its efficiency. For the simulated boiler, the efficiency was calculated in 86.71 % using LHV as calculation base and 69.32 % using HHV. The Sankey diagram is presented in Fig. 4.

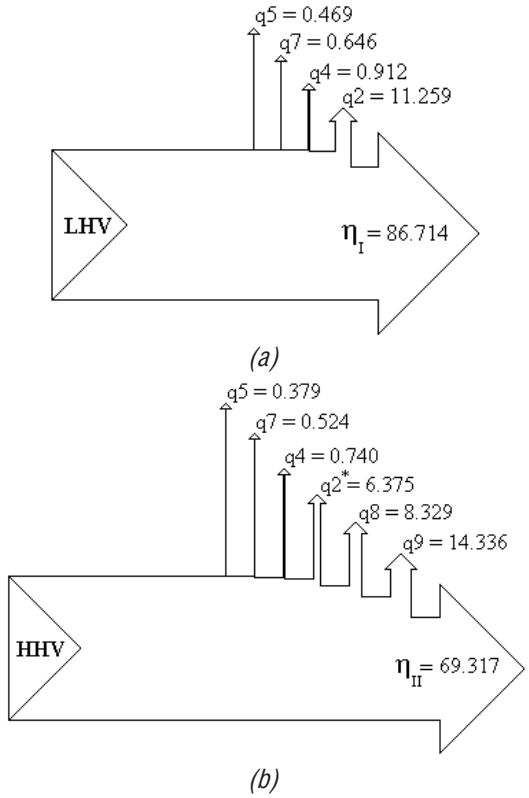


*Fig. 4. Efficiency calculated using: a) LHV, b) HHV.*

The HHV calculate base highlights the main effect of the moisture in the fuel. This can be observed by high values of $q_9$, which represents the heat losses due to water evaporation from bagasse moisture content.

In the Table 5, the mass flow data calculated by INKA'S BOILER software are showed.

*Table 5. Mass Flow calculated in the simulation.*

| Flow data | | |
|---|---|---|
| Steam | 52.22 | kg/s |
| Bagasse | 23.58 | kg/s |
| Gas | 114.01 | kg/s |
| Primary air | 77.11 | kg/s |
| Secondary air | 9.07 | kg/s |
| Air Supply | 4.54 | kg/s |

Since Table 5, the relation steam/fuel is 2.21, while the relation gas/fuel is 4.84. That last relation is very dependent of the bagasse moisture content.

In Table 6, the global coefficients of heat transfer for the various heat exchangers are shown and compared with typical values for coal boilers [10].

*Table 6. Heat transfer global coefficient.*

| Heat Exchanger | $U$ (W/m$^2$ K) | Typical (W/m$^2$ K) |
|---|---|---|
| Secondary Superheater | 60,71 | - |
| Primary Superheater | 57,73 | 46,73 |
| Boiler Bank | 49,49 | 52,75 |
| Secondary Economizer | 68,54 | 76,32 |
| Secondary Air Heater | 24,32 | - |
| Primary Air Heater | 24,79 | 28,79 |
| Primary Economizer | 44,11 | - |

As it was expected the air heaters present lower thermal exchange coefficients, what confirms that the heat exchange gas/water is more efficient than gas/air.

*Fig. 5. Measuring equipment - Testo 330*

In the field, using a Testo 330 portable analyzer, see Fig. 5, the gas temperature and composition was measured along the boiler, in each heat exchanger, starting from the Boiler Bank. In the furnace, secondary and primary superheater, the 9 A 9 B limitations of measure equipment. Those numbers were compared with the simulated ones, see Table 7.

*Table 7. Measured and calculated gas Temperature along the boiler.*

| Outlet of: | Measured (°C) | INKA'S BOILER (°C) | Error (%) |
|---|---|---|---|
| Furnace | - | 956.8 | - |
| Secondary Superheater | - | 839.8 | - |
| Primary Superheater | - | 717.3 | - |
| A - Boiler Bank | 449.7 | 461.1 | 2.5 |
| B - Secondary Economizer | 409.2 | 376.2 | 8.1 |
| D - Secondary Air Heater | 315.2 | 310.4 | 1.5 |
| E - Primary Air Heater | 235.1 | 237.5 | 1.0 |
| G - Primary Economizer | 187.1 | 172.3 | 7.9 |

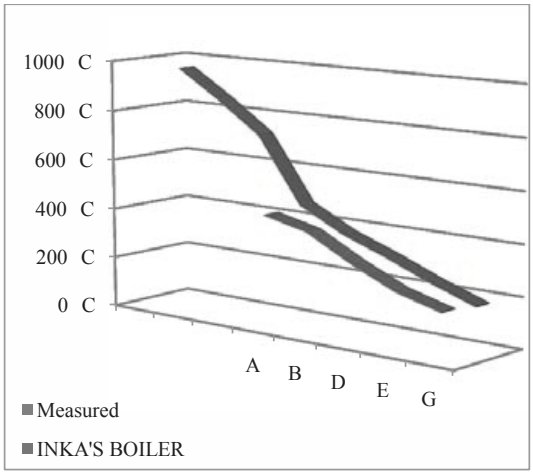


*Fig. 6. Comparison between the simulated and the measured gas temperature*

In Table 7 it can be appreciated that the higher differences happened in the Economizers (8.1 %). It is noteworthy that our measuring device has a short stem (0,8 m) and measurements of temperatures are made near the sides of the envelope, not reaching the center of the measured device. Fig. 6 compares the simulated with measured gas temperature.

Table 8 shows the air temperature along bagasse boiler, while Fig. 7 presents the comparison between these values.

*Table 8. Air Temperature along the boiler.*

| Outlet of the: | Measured (°C) | INKA'S BOILER (°C) | Error (%) |
|---|---|---|---|
| F - Forced Fan | 31.0 | 30.0 | 3.23 |
| C - Primary Air Heater | 155.5 | 165.6 | 6.50 |
| H - Secondary Air Heater | 295.0 | 286.4 | 2.92 |

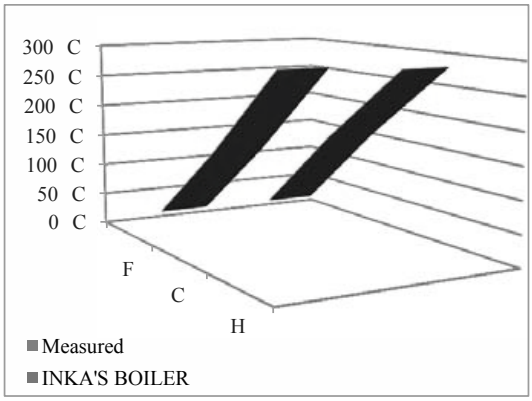


*Fig. 7. Comparison between the simulated and the measured air temperature.*

From Table 8, it can be observed that the error kept practically at the same level, with 6.5% as highest ones. For the water/steam flow, the simulated temperature in each point of the boiler is shown in the Table 9. Measured temperatures are not available.

*Table 9. SimulatedTemperature of the water/steam along the boiler.*

| Outlet of the: | INKA'S BOILER (°C) |
|---|---|
| Feed Pump | 120.0 |
| Primary Economizer | 162.7 |
| Secondary Economizer | 235.2 |
| Boiler Bank | 283.9 |
| Primary Superheater | 374.9 |
| Secondary Superheater | 527.4 |

Other important factor in boilers is the composition of flue gas, this is reported in Table 10. The measured values presented in the table are an average of collected along the boiler.

*Table 10. Flue gas composition (mole fractions - dry base).*

| Element | Simulated (%) | Measured (%) |
|---|---|---|
| $CO_2$ | 15,85 | 15,86 |
| $N_2$ | 79,75 | - |
| $O_2$ | 4,40 | 4,30 |

The software does not consider the production of CO in the combustion. The combustion model is complete combustion with excess air. Nevertheless, the average value of CO measured along the boiler was 691 ppm. $NO_x$ was not measured in field.

Because of the high humidity of the fuel, the calculated percentage of water mass dragged by the gas is 17.24 %, which corresponds to a flow of 29.89 kg/s. Of this total water, 63.25 % is due to moisture in the fuel and the remainder is formed in the combustion

## 5. Conclusions

In this work, it was presented the simulation of a bagasse boiler with 200,000 kg/h of steam at 6.57 MPa and 520 °C. The boiler was simulated at the same conditions of operation and the results obtained by the A ( . , ( were compared with that obtained in the field. It was observed good agreement between measured and simulated values, considering that the measured points were not adequate, since it should take on the middle point of boiler.

The next stage will be to implement the second law analysis in the ( . , ( software. Also the analysis of boiler cost will be executed. That will permit to reduce the boiler cost attaining high thermal performance.

## Nomenclature

$A$ effective flat surface area of the furnace, $m^2$

$HHV$ higher heating value, kJ/kg

$h$ specific enthalpy of water vapor at boiler outlet, kJ/kg

$LHV$ lower heating value, kJ/kg

$LMTD$ log mean temperature difference, K

$M$ temperature field coefficient,

$\dot{m}$ mass flow, kg/s

$q_2$ heat losses due to exhaust gas, %

$q_2^*$ heat losses due to dried gas, %

$q_3$ heat losses due to incomplete chemical combustion, %

$q_4$ heat losses due to incomplete combustion related to mechanical causes, %

$q_5$ heat losses due to surface radiation and convection, %

$q_6$ heat losses due to slag and ashes, %

$q_7$ heat losses due to bleeding in the boiler, %

$q_8$ heat losses due to evaporation of water formed from hydrogen in the fuel, %

$q_9$ heat losses due to evaporation of water from Bagasse moisture content, %

$T$ temperature, K

$U$ heat transfer coefficient, kW/(m$^2$ K)

$Cp$ average specific heat, kJ/(kg K)

Greek symbols

$\eta_I$ boiler efficiency (LHV as the basis for calculating), %

$\eta_{II}$ boiler efficiency (HHV as the basis for calculating), %

$\phi$ coefficient of heat retention

$\alpha$ excess air coefficient at the furnace exit

$\sigma$ Stefan-Boltzman constant, W/m$^2$ K$^4$

$\psi$ thermal efficiency factor

Subscripts and superscripts

$af$ Adiabatic flame

$b$ Bagasse

$fo$ Furnace outlet

$g$ Gas

$o$ State reference

$s$ Steam

$w$ Water

## References

[1] Mull Jr., T. V., et al., 1996, Numerical Simulation Models for a Modern Boiler Design, Power-Gen International '96, Orlando USA.

[2] GFBS, Grate Fired Boiler Software, 2004, Software Package, FireCAD Technologies, Visakhapatnam, India, URL: http://www.firecad.net/boiler/Grate-Fired-Boiler.aspx.

[3] HRSGS, Heat Recovery Steam Generators, 2009, Software Package, Boiler and HRSG Consultancy Services, Chennai, India, URL: http://vganapathy.tripod.com/boilers.html.

[4] SBC, Steam Boiler Calculations, 2005, Software Package, Núcleo de Excelência em Geração Termelétrica e Distribuída, Itajubá, Brasil, URL: http://www.nest.unifei.edu.br/portugues/pags/softwares/sbc/sbc_pt.html.

[5] Basu, P., 2000, *Boilers and Burners – Design and Theory*, Springer-Verlag, New York, Chap. 6.

[6] Sosa-Arnao, J. H., and Nebra, S. A., 2009, First and Second Law to Analyze the Performance of Bagasse Boilers, ECOS 2009, Foz do Iguaçu, Brazil.

[7] Beatón, P., and Lora, E., 1991, Thermal Balance Tests in Bagasse Boilers, Departamento de Termoenergética, Facultad de Ingenieria Mecánica. I.S.P.J.A.M., Cuba.

[8] ASME PTC 4-1998, *Fired Steam Generators*, The American Society of Mechanical Engineers, New York, USA, 10016 - 5990.

[9] Sosa-Arnao, J. H., et al., 2006, Two Proposals to Determine the Efficiency of Bagasse Boiler". 6$^{TH}$ International Congress on Distributed Generation and Energy in Rural Environments [CD-ROM], Campinas, Brazil.

[10] The Babcock & Wilcox Company, 2005, Steam/its generation and use, 41$^{st}$ ed., Ohio, USA, Chap 22.

[11] Hugot, E., 1986, *Handbook of Cane Sugar Engineering*, Elsevier Science Publishers B. V., Amsterdam, Chap. 41.

Acknowledgments: The authors wish to thank Equipalcool Sistemas Ltda, CNPq (National Research Council) and FINEP (Financier of Studies and Projects) for their support during the development of this work.

# Fuel Impact Reconciliation Method. Part II: Effect of the Regulation System

*J. J. Pacheco Ibarra[a], V. H. Rangel Hernandez[b], C. Rubio Maya[a], J. M. Medina Flores[c], A. Zaleta Aguilar[b], J.M. Belman-Flores[b]*

[a] *Faculty of Mechanical Engineering, UMSNH, Morelia, Michoacán, México*
[b] *Mechanical Engineering Department, University of Guanajuato, Salamanca, Guanajuato. Mexico*
[c] *Manufacturing Process Engineering, Polytechnic University of Guanajuato, Cortazar, Guanajuato. Mexico*

**ABSTRACT.** The present work is the second part of a paper titled *Reconcilied Fuel Impact Method: An Integral Tool of Thermoeconomic Diagnosis,* presented in ECOS 2008 (Recently published in Energy). In that paper a new diagnosis technique based basically on two of the main diagnosis techniques, namely, the fuel impact method and the power and heat rate analytical reconciliation method was unveiled. In this same work, a method for filtering the effects induced by the control and regulation system was included too. This filtering method however was performed in a graphical mode, thus having a cumbersome process. Hence a second part is proposed in which a mathematical algorithm used to simplify and accelerate the filtering process of the induced effects. The filtering tool is performed on each one of the malfunctions in such a way that the energy system will be characterized through filtering maps of Induced Effects in terms of load. This method differs from others, in which the anomalous and the reference conditions are characterized by means of a graph which shows the heat rate or fuel impact versus the control and regulation system (IGV position in the particular case of gas turbines and combined cycles, and TFR load in the case of conventional power plants). For validation of the model, a pilot case is presented.

Keywords: *Control System Regulation*, *Induced Effects, Filtering Maps.*

## 1. Introduction

The thermoeconomic diagnosis embarked on in 1992 with a ground-breaking work that proposed a method of thermoeconomic diagnosis for industrial process, which was called as the Exergy Cost Theory (ECT, henceforward) [1]. Such method was promptly adopted by others in order to evaluate the change in fuel consumption due to the local irreversibilities present in thermal systems [2]. Later, by using the fundamentals of the ECT, Lozano et. al. [3] proposed a method of thermoeconomic diagnosis that is called as the Fuel-Impact Method. There he links the individual variation of the specific consumptions of resources in each one of the components to the total variation of resources in the system. The method has also been used by other researchers so as to investigate its accuracy in detecting anomalies in different systems [4, 5]. In general, the philosophy of these methods is to compare conditions of real operation with conditions of reference, while maintaining the product (power) of the system constant as well as the environmental conditions.

Alternatively, there are the methods which only make use of energy indicators to diagnose variations in the operation variables of the system; this is the case of the works unveiled by Zaleta [6]. He proposes a method through which the diagnosis is performed by *Reconciliation of the Heat Rate and Power*. Such as, it is based on the comparison between two operating conditions characterized by the same mass flow rate: one concerning the test operation condition (TOC), and the other regarding the reference operation condition (ROC). In order to give evidence of its use in real systems, it should be mentioned that it is currently installed in many of the Mexican power plants.

On the ground that there were different ways of performing thermoeconomic diagnosis methods, then a group of researches compiled in a series of papers the evolution of the different tendencies of diagnosis methods [7, 8]. However, most of these methods have the disadvantage that require of a great capacity of hardware and software, are complex in their mathematical formulations and

matrix resolutions. Besides in order to to increase the accuracy of results, hi-tech measurements systems are required. Most importantly, the quantitative comparison of their results cannot be undertaken because of their dissimilarities in indicators and methodologies.

In view of the fact, Pacheco et al [9,10] put forward the Fuel Impact Reconciliation Method (FIRM, henceforward), which is able of joining the advantages of the Fuel Impact Formula Method [5] and the Heat Rate and Power Analytic Reconciliation Method [8]. In that paper the development of the Hybrid Fuel Impact Reconciliation Method is explained as well as its fundamental idea and mathematical model. Likewise it is introduced a technique for filtering the effects induced by the regulation system in the results of the thermoeconomic diagnosis. However, the technique through which the filtering is achieved is not well explained thereat, therefore, the goal of this paper is to explain at large the mathematical fundamentals of such filtering technique.

## 2. Analytical reconciliation method

The thermodynamic reconciliation method consists basically in a comparison between the test operation condition and reference operation condition as defined in [8]. Both states are assumed to be operating at the same mass flow rate and not at constant power as the Fuel Impact Method does. Results from such conditions are then compared on a free variables basis, which have been chosen previously as the most probable malfunction causes. Such variables are classified as: internal, control and external variables, which are thought to be the main causes of deviations in the Heat Rate (HR) and in the Power Output (W).

This method permits evaluating the impact of the malfunction caused by each free variable (M) on both the heat rate and the power output, by maintaining the condition of flow rate constant, as shown in the following equations (1).

$$\begin{array}{ll} DHR & \frac{HR}{M_1} dM_1 \quad \frac{HR}{M_2} dM_2 \quad \ldots \quad \frac{HR}{M_m} dM_m \\ DW_B & \frac{W_B}{M_1} dM_1 \quad \frac{W_B}{M_2} dM_2 \quad \ldots \quad \frac{W_B}{M_m} dM_m \end{array} \tag{1}$$

## 3. The fuel impact reconciliation formula

In the conventional reconciliation method, the mathematical models used for evaluating both the heat rate ($HR$) and power ($\dot{W}$) are defined as a function of the number of independent variables (i.e. $M$):

$$\begin{array}{ll} HR & RT(M_1, M_2, M_3, ....., M_n) \\ W & W(M_1, M_2, M_3, ....., M_n) \end{array} \tag{2}$$

In the methodology proposed in the Reconcilied Fuel Impact, both the test and the reference operating conditions operate at the same power, hence the W term is eliminated from Eq. (2) and a new term is proposed to calculate the Fuel Impact as:

$$\begin{array}{ll} HR & HR(M_1, M_2, M_3, ....., M_n) \\ FI & FI(M_1, M_2, M_3, ....., M_n) \end{array} \tag{3}$$

It should be noted that the expression for calculating the heat rate has not been changed, however, in order to evaluate the Fuel Impact the following expression is proposed:

$$FI \quad \left( \sum_{i=1}^{n} \frac{HR}{M_i} dM_i \right) * W_N \Big/ 3600 \tag{4}$$

where $\dot{W}_N$ is the net power of the system.

On the whole, Eq. (4) represents the Fuel Impact caused by the M independent variables, expressed in terms of the additional fuel consumption, kW, necessary to compensate the impact of each malfunction.

In general, the methodology of the Fuel Impact Reconciliation Method, FIRM, consists in:

1. Simulating the power plant with no anomalies in order to obtain the optimum thermodynamic

state (the reference), but keeping the power at the same value of that of the test operation
2. Defining the free variables for the test condition, $M_{1....n,}$ in accordance to the mathematical method.
3. Providing the value of the free variables at the reference condition, these have to be the same defined in the test condition, $M_{1....n, R}$, but subject to the same power of the test condition.
4. Determining the additional information required for the reconciliation module, i.e., design data of devices and correlations between design values with no malfunctions.
5. Developing the Fuel Impact Reconciliation module to detect the impacts on fuel due to each free variable, while maintaining steady power and allowing the system to calculate the flow conditions of the main operation.
6. Filtering the effects induced by the control and regulation system to hold constant the power of the system.

However, as mentioned above, the objective of the paper is to explain the technique for filtering the induced effects. So, in order to show the meaning of filtering the effects coming from the control system, the following explanation is provided.

## 4. Effect of the control and regulation system

With regard to Figure 1, there it is plain to differentiate two lines: one representing the reference state condition and the other one corresponds to the actual state condition (i.e. the malfunctioning state). Both lines are constructed by considering all the operating range of the control system; hence each point plotted on the graph corresponds to a different position of the Inlet Guide Vanes (IGV´s) that represents indirectly the load as a function of the mass flow.

Thus, if a malfunction appears in the system, the total power drops with respect to its reference value as shown in path BC. So, if the power is wanted to be restored, then the regulation system intervenes as shown in path AB, producing the induced effects thereof. When the control system intervenes, it permits a major flow of work to compensate for the loss of power, thereby appearing the induced effects. This is known in classical thermoeconomics as induced effects due to the regulation system.

When it comes to quantify the anomalies in a system, there is always a difference in the total value of such malfunctions. This difference is originated by the effects induced by the regulation system. Hence the necessity of a mathematical model to filter such induced effects and that permits to isolate intrinsic malfunctions from induced malfunctions, in particular, those induced by the control system.

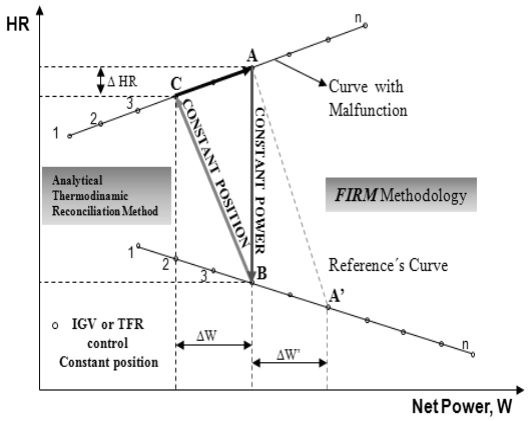


*Figure 1. Schematic representation of the regulation system control.*

In this respect, the works of Verda [10, 11] can be highlighted as the pioneering applications of these techniques. In his work he proposes a procedure to filter the effects induced by the regulation system. The method is performed using exergoeconomics indicators to disaggregate most of the malfunctions induced by the control system. The procedure is based on the comparison between the two conditions of operation (i.e., reference and test conditions) and an assumed set of working conditions characterized by the same regulation as in the reference condition.

In an earlier work [9], it was discussed that the filtering procedure did consist basically in the characterization of the system through a series of plots known as “Maps of Induced Effects”, instead of exergoeconomic indicators, as seen in Figure 1. Accordingly, it is assumed that point A corresponds to the test condition or abnormal condition, point B represents the reference condition characterized by

the same power output as in the test conditions; whereas, point C stands for the fictitious condition that is characterized by the same position in the regulation system as in the reference condition. The path BC corresponds to the classical analytical reconciliation method for diagnosis which is performed between the fictitious condition and the reference condition. The hybrid fuel impact reconciliation method, on the other hand, is characterized by path AB. In this particular case, the method has been carried out using the *Heat Rate* as diagnosis indicator instead of the fuel impact; however, both indicators can be used indifferently.

For the particular case analyzed in this paper, the results of the diagnosis are plotted on a Heat Rate versus Net Power graph instead of a Fuel Impact versus Net Power graph.

Accordingly, the effects induced by the regulation system are graphically represented by the difference in heat rate between C and A states. The shortcoming at this particular point, however, is that for each malfunction occurring in the system it should be required to draw it on the graph. Hence an analytical method is presented in the following section.

## 5. Analytical method for filtering induced effects

As an alternative, the filtering process for removing the effects induced by the control and regulation system from the diagnosis through maps can also be carried out by including an additional equation into reconciliation module, see Figure 2. The mathematical procedure consists in integrating a polynomial expression, corresponding to the malfunction, into the reconciliation module. Then whenever the module is called, it carries out the differences between the different states for each variable, as done in the fuel impact method. So the Fuel Impact Reconciliation Method now incorporates an additional equation and not only the Heat Rate and Fuel Impact indicators, as done before, in order to determine the fictitious state and the test condition.

Turning to Equation (5), it shows the three main equations governing the modified Fuel Impact Reconciliation Method. The third equation has to do precisely with the mathematical procedure proposed as filtering technique:

$$\Delta HR = \sum_{i=1}^{n} \frac{\partial HR}{\partial M_i} dM_i \Big|_{W_N = Cte.}$$

$$\Delta FI = \sum_{i=1}^{n} \frac{\left( \frac{\partial HR}{\partial M_i} dM_i \right) * W_N}{3600} \qquad (5)$$

$$\Delta HR_F = \sum_{i=1}^{n} \left[ \frac{\partial HR_F}{\partial (setpoint)\big|_i} d(setpoint)_i - \frac{\partial HR}{\partial M_i} dM_i \right]_{W=Cte.}$$

set point = IGV o TFR

Finally, the module to perform the modified fuel impact reconciliation method, considering the five steps explained before as well as including step 6, is shown in Figure 2.

Methodology FIRM modified

MODULE RECMOD ($M_1$, $M_2$, . . . , $M_n$: HR)
$HR = HR(M_1, M_2, \ldots, M_n)$
$HR_F = a + b \cdot IGV + c \cdot IGV^2 + d \cdot IGV^3 + ..$
$W_{net} = const.$
END

CALL RECMOD($M_{1,P}$, $M_{2,P}$, . . . , $M_{n,P}$: $HR_P$, $IGV_P$, $HR_{F,P}$)
CALL RECMOD($M_{1,R}$, $M_{2,P}$, . . . , $M_{n,P}$: $HR_{M1,R}$, $IGV_{M1,R}$, $HR_{F,M1,R}$)
$\Delta HR_{M1R} = HR_P - HR_{M1,R}$
$\Delta FI_{M1R} = (\Delta HR_{M1,R} * W_N) / 3600$
$\Delta IGV_{M1R} = IGV_P - IGV_{M1,R}$
$\Delta HR_{F,M1R} = HR_{F,P} - HR_{F,M1,R}$
$COSTO_{M1,R}$ [\$/ h] = $\Delta FI_{M1,R}$ (kW) * PRECIO COMBUSTIBLE (\$/ kJ)
.
.
CALL RECMOD($M_{1,R}$, $M_{2,R}$, . . . , $M_{n,R}$: $HR_R$, $IGV_R$, $HR_{F,R}$)
$\Delta HR_{Mn,R} = HR_{M(n-1),R} - HR_R$
$\Delta FI_{Mn,R} = (\Delta HR_{Mn,R} * W_N) / 3600$
$\Delta IGV_{Mn,R} = IGV_{M(n-1),R} - IGV_R$
$\Delta HR_{F,M1R} = HR_{M(n-1),R} - HR_{F,R}$
$COSTO_{Mn,R}$ [\$/ h] = $\Delta FI_{Mn,R}$ (kW) * PRECIO COMBUSTIBLE (\$/ kJ)

*Figure 2 Modified Fuel Impact Reconciliation Method.*

In figure 2, the $HR_F$ term (in CALL module) refers to the Heat Rate evaluated at the fictitious condition. It is important to mention that in this particular example, the variation in fuel impact was not taken into account only the impact on heat rate.

The difference seen in the IGV (regulation of the control system) is determined with the aim of

indicating in the diagnosis results the weight that each different position in the set point of the control system has upon the total impact on the heat rate. The sum of all the contributions to the Heat Rate evaluated at the fictitious condition will have to be equivalent to the impact on heat rate due to the control system, which is obtained by direct difference or graphically between the individual reconciliations (A-B and B-C) marked up on Figure 1.

## 6. Application of the technique to a study case

In order to prove the reliability of the method a study case is taken as bench test. A third-generation combined cycle power plant is considered. This consists of a sequential double-combustion chamber gas turbine (GT), a three-pressure-level heat recovery steam generator (HRSG) with reheating, a three-pressure-level steam turbine (ST) connected to the same GT shaft, a cooling system operated by an aircondenser. The gas turbine blades are cooled by air which is bled from the air compressor. The combined cycle net power output is 240 MW, 144 MW generated by the GT and 96 MW generated by the ST. A brief description of the working flows is provided in Table 1.

As an example of the application of the filtering technique, an anomaly in the low pressure gas turbine is hypothetically assumed. The anomaly consists in increasing the temperature of the outlet gases up to 3 Celsius degrees.

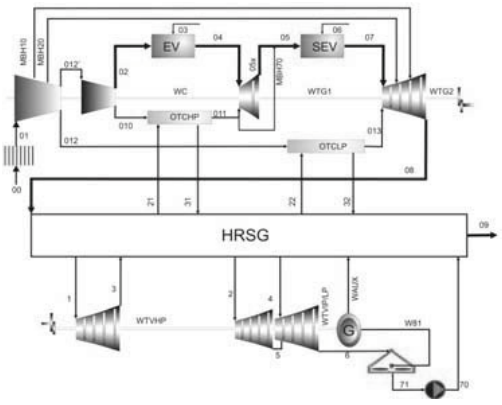


*Figure 3. Scheme of the study case.*

## 7. Results

In order to begin with, it is considered to perform the diagnosis of the case of study following the A-B path, as shown in Figure 1. Results are shown in Table 2. Analysis of these results provide a total fuel impact of about 2682 kW, whereas the Heat Rate impact, it can be viewed that the anomaly caused an impact on the low-pressure gas turbine of 46.41 kJ/kW-h. After analyzing the results, it is concluded that this impact is partly caused because of the effect induced by the regulation system, as shown in Figure 1.

The next step consists in diagnosing the system in accordance to the BC path (as previously explained) or known as the "fictitious" state. Unlike the previous diagnosis (the AB path), this process is performed by means of the conventional reconciliation method and not with the proposed here since the system is operating at constant IGV and not at constant power. A fundamental characteristic of the "fictitious" state is that it has to hold the anomalies present in the test condition as well as to keep the same regulation system conditions as those of the reference condition. Results can be seen in Table 3.

The results of the reconciliation procedure between the reference state and the fictitious state present a malfunction value, as impact on the Heat Rate, of 42.3 kJ/kWh. Besides results show that operating at constant IGV´s in presence of anomalies, it causes a power output drop of approximately 1.2 MW.

The difference between the results obtained in the Fuel Impact Reconciliation Method, AB path, and those provided in the Analytical Reconciliation Method, BC path, reveals the malfunctions induced by the control system. Recall that the control system modifies the IGV position in order to compensate the power output drop while anomalies are present.

In general, the total effect induced by the control system to maintain constant the power when an anomaly is present, turned out to be as high as 4 units (kJ/kW-h). It should be said that after applying the mathematical procedure, Equation (5) and Figure 2, 4.1306 kJ/kWh were calculated. In view of this, it can be concluded that the procedure is acceptable at all. Table 4 provides evidence of the results.

## 8. Conclusions

A new technique to filter the effects induced by the control system was proposed herein. It is well known that induced effects do disturb the thermoeconomic diagnosis when the system is operating at constant power and the control system intervenes so as to recover the loss of power. Such filtering technique has been introduced into the procedure proposed by the Fuel Impact Reconciliation Method, and now is known as the Modified Fuel Impact Reconciliation Method.

The method permits to disaggregate the effects induced by the regulation of the control system through a series of filtering maps induced by load. The particular characteristic of the method is that it is able to diagnose even when several malfunctions occur simultaneously.

By means of the present paper it has been provided an alternative tool to discern induced malfunctions from intrinsic ones inasmuch as to provide more reliable and accurate diagnosis results. To prove its consistency this is nowadays being applied to real cases in some of the power stations where the Reconciliation Method has already been installed,

## References


[1] Valero, A., Torres, C., Serra, L., and Lozano, M. A. *A General Theory of Thermoeconomics, Parts I and II*, ECOS 92 Ed. By A. Valero and G. Tsatsaronis, Zaragoza. ASME Bok No. 100331 pp 147 – 154. 1992.

[2] M. A. Lozano and A. Valero. *Theory of the exergetic cost*. Energy, Vol. 18, No. 9, pp 939-960, Printed in Great Britain. Pergamon Press Ltd.1993.

[3] M. A. Lozano, J. L. Bartolome, A. Valero, M Reini. *Thermoeconomic diagnosis of energy systems*. Proceeding of the third Florence World energy research symposium, Florence; July 1994.

[4] Reini M. *Analisi e sviluppo dei metodi termoeconomico per lo studio degli impianti di converione dell' enegia,* PhD. Thesis, University of Padova, Italy, Department of Mechanical Engineering. 1994.

[5] A. Valero, L. Correas, A. Zaleta, A. Lazzaretto, V. Verda, M. Reini and V. Rangel. On the Thermoeconomic Approach to the Diagnosis of Energy Malfunctions. Part I: The TADEUS Problem. In Proceedings of ECOS 2002, VOL. I. Berlin, Germany, June 2002.

[6] Zaleta A, Gallegos A., Rangel V. H. and Valero A., *A Reconciliation Method Based on a Module Simulator*. An approach to the Diagnósis of Energy System Malfunctions, Int. J. Thermodynamics Vol. 7, (No. 22), 2004.

[7] Lazzaretto A, Toffolo A, Reini M, Taccani R, Zaleta A, Rangel V, Verda V. Four approaches compared on the TADEUS (thermoeconomic approach to the diagnosis of energy utility systems) test case. Energy Volume 31, 2006.

[8] A. Zaleta, V. Rangel, A. Valero. On the Thermodynamic Approach to the Diagnosis of Energy System Malfunctions: Part 6. Model of Thermodynamic Reconciliation for the Diagnosis of Power Plants. Proceedings of ECOS 2003. Copenhagen, Denmark, pp. 365-372.

[9] Pacheco JJ, Rangel VH, Zaleta A, Gallegos A y Riesco JM. Reconcilied Fuel Impact Method: An Integral Tool of Thermoeconomic Diagnosis. ECOS 2008 21st International Conference on Efficiency, Cost, Optimization, Simulation and Environmental Impact of Energy Systems. Vol. II, Session 14, pp. 1043-1050. Jun. 2008. Krakow, Poland. ISBN: 978-83-922381-4-0.

[10] Pacheco Ibarra, J.J. (2007). *Development of a methodology for the diagnosis of advanced energy systems.* FIMEE, University of Guanajuato, PhD Thesis [In Spanish]

[11] V. Verda. *Thermoeconomic Diagnosis of an urban District Heating System Based on Cogenerative Steam and Gas Turbine*. PhD thesis, University of Zaragoza and Polytechnic di Torino, 2001, In Spanish.

[12] V. Verda, L. Serra and A. Valero. *Effects of the regulation system on the thermoeconomic diagnosis of a power plant. Part II: The Diagnosis procedure.* In Proceedings of the ECOS'01, pages 777-784. July 4-6, Istanbul, 2001.

*Table 1. On-design properties of the main energy streams for steam and gas turbine sections*

| ID | Description | Pressure P [Bar] | Temperature T [°C] | Mass flow rate, [kg/s] | Exergy B [kW] |
|---|---|---|---|---|---|
| 00 | Environmental condition | 0.97 | 18.92 | - | 0 |
| 01 | Air flow entering compressor | 0.95 | 19.81 | 366 | 0 |
| 02 | Compressed air entering combustion chamber | 27.00 | 520 | 176 | 89175 |
| 03 | Combustor (EV) fuel inlet | - | - | 3.50 | 179655 |
| 04 | Flue gas entering HPGT | 26.00 | 1233 | 179 | 251904 |
| 05 | Exhausted flue gas entering combustor (SEV) | 14.96 | 953 | 218 | 225619 |
| 06 | Combustor (SEV) fuel inlet | - | - | 4.86 | 251853 |
| 07 | Flue gas entering LPGT | 13.43 | 1819 | 223 | 454945 |
| 08 | Exhausted flue gas entering HRSG | 0.98 | 617 | 374 | 238285 |
| 09 | Stack flue gas | 0.97 | 104 | 374 | 31409 |
| 010 | Air flow cooling entering OTCHP | 26.95 | 520 | 38.84 | 19686 |
| 011 | Air flow for HPGT cooling | 26.95 | 337 | 38.84 | 15153 |
| 012 | Air flow to low pressure OTC | 18.29 | 435 | 127.53 | 53128 |
| 013 | Air flow cooling entering OTCLP | 16.42 | 348 | 127.53 | 45231 |
| MBH10 | Air flow cooling entering LPGT | 4.67 | 197 | 4.65 | 810 |
| MBH20 | Air flow cooling entering LPGT | 14.67 | 384 | 19.25 | 7049 |
| MBH70 | Air flow for HPGT cooling | 26.95 | 337 | 6.10 | 2376 |
| WC | Compressor work input | - | - | - | 175704 |
| WTG1 | High pressure gas turbine work output | - | - | - | 39184 |
| WTG2 | Low pressure gas turbine work output | - | - | - | 265483 |
| 1 | High pressure live steam flow | 136.30 | 555 | 51.10 | 79380 |
| 2 | Intermediate pressure superheated steam flow | 30.90 | 532 | 50.54 | 70516 |
| 3 | High pressure exhausted steam flow | 34.02 | 361 | 50.54 | 59346 |
| 4 | Low pressure superheated steam flow | 6.19 | 343 | 14.32 | 13757 |
| 5 | Low pressure superheated steam flow | 6.19 | 310 | 50.40 | 46666 |
| 6 | Low pressure exhausted steam flow | 0.09 | 44.30 | 65.41 | 11829 |
| 70 | HRSG feed water | 21.04 | 44.42 | 67.31 | 433 |
| 71 | Condensate water flow | 0.09 | 44.31 | 67.31 | 288 |
| W81 | Air Condenser work inlet | - | - | - | 1260 |
| WAUX | Auxiliary equipments work | - | - | - | 4.30 |
| WTV | Steam Turbine total work | - | - | - | 66720 |
| WNETA | Net work output | - | - | - | 208056 |
| QCOND | Heat dissipation in the condenser | - | - | - | 11567 |

*Table 2. Results provided by the proposed method at the test and reference conditions: process A-B*

| Diagnosis variable | Test | Reference | Difference | HR Impact [kJ/kW-h] | Fuel Impact [MW] | Cost [$/h] |
|---|---|---|---|---|---|---|
| Environment | | | | | | |
| $P_0$ [bar] | 0.97 | 0.97 | 0 | -1.5E-09 | -8.9E-08 | -4.2 E-08 |
| $T_0$ [C] | 18.9 | 18.9 | 0 | 0 | 0 | 0 |
| $HR_0$ [%] | 47.5 | 47.5 | 0 | -1.2E-08 | -7.4E-07 | -3.4E-07 |
| Gas Cycle | | | | | | |
| Pressure drop in filters, DP0E [mbar] | 10 | 10 | 0 | 0 | 0 | 0 |
| CBP efficiency, $\eta_{CBP}$ [%] | 89 | 89 | 0.0049 | -0.135 | -7.83 | -3.6 |
| OTCBP outlet temperature, T013, [C] | 348 | 348 | 0 | 0 | 0 | 0 |
| CAP efficiency, $\eta_{CAP}$ [%] | 89.8 | 89.7 | 0.031 | -0.132 | -7.62 | -3.56 |
| OTCAP outlet temperature, T011, [C] | 337 | 337 | 0 | 0 | 0 | 0 |
| Pressure drop in 1st combustion, DPCEV [bar] | 0.95 | 0.95 | 0 | 0 | 0 | 0 |
| Pressure drop in 2nd combustion, DPCSEV [bar] | 1.5 | 1.5 | 0 | 0 | 0 | 0 |
| 1st. Combustion chamber efficiency, $\eta_{CEV}$ [%] | 99.8 | 99.8 | 0 | 0 | 0 | 0 |
| 2nd. Combustion chamber efficiency, $\eta_{CSEV}$ [%] | 99.8 | 99.8 | 0 | 0 | 0 | 0 |
| High heating value, HHV [kJ/kg] | 51825 | 51825 | 0 | 0 | 0 | 0 |
| HPGT efficiency, $\eta_{HPGT}$ [%] | 89.1 | 89.1 | -4. 1 E-06 | 3.7E-05 | 2. E-03 | 1.0E-03 |
| LPGT efficiency, $\eta_{LPGT}$ [%] | 90.1 | 90.5 | -0.3732991 | 46.70 | 2697.64 | 1262.50 |
| Steam Cycle | | | | | | |
| Main steam pressure, P1 [bar] | 136 | 136 | 0 | 0 | 0 | 0 |
| Main steam temperature, T1 [C] | 555 | 555 | 0 | 0 | 0 | 0 |
| Hot reheated steam temperature, T2 [C] | 532 | 532 | 0 | 0 | 0 | 0 |
| Low pressure steam temperature, T4 [C] | 343 | 343 | 0 | 0 | 0 | 0 |
| HPST Temperature, $\eta_{HPST}$ [%] | 82 | 82 | 0 | 0 | 0 | 0 |
| IPST Temperature, $\eta_{IPST}$ [%] | 90 | 90 | 0 | 0 | 0 | 0 |
| LPST Temperature, $\eta_{LPST}$ [%] | 93 | 93 | 0 | 0 | 0 | 0 |
| Mass flow rate Inlet coefficient $\phi_{IP}$ | 46 | 46 | 0 | 0 | 0 | 0 |
| Mass flow rate Inlet coefficient $\phi_{LP}$ | 17 | 17 | 0 | 0 | 0 | 0 |
| Condenser vacuum pressure, P6 [bar] | 0.09 | 0.092 | 0 | 2.5 E-08 | 1.5 E-06 | 6.8 E-07 |
| TOTAL | | | | 46.41 | 2682.20 | 1255.30 |
| DIRECT DIFFERENCES, HR | 7512.87 | 7466.47 | 46.41 | | | |
| DIRECT DIFFERENCES, FI | 434193.96 | 431511.76 | 2682.20 | | | |

*Table 3. Reconciliation between the fictitious and the reference state: process B-C*

| Diagnosis variable | Test | Reference | Difference | HR Impact [kJ/kW-h] | $W_N$ Impact [MW] | Cost [$/h] |
|---|---|---|---|---|---|---|
| Environment | | | | | | |
| $P_0$ [bar] | 0.97 | 0.97 | 0 | -0.0004 | -4.57E-07 | -0.001 |
| $T_0$ [C] | 18.92 | 18.92 | 0 | 0 | 0 | 0 |
| $HR_0$ [%] | 47.53 | 47.53 | 0 | 0 | 0 | 0 |
| Gas Cycle | | | | | | |
| Pressure drop in filters, DP0E [mbar] | 10.22 | 10.22 | 0 | 0 | 0 | 0 |
| CBP efficiency, $\eta_{CBP}$ [%] | 89.80 | 89.80 | 0 | 0 | 0 | 0 |
| OTCBP outlet temperature, T013, [C] | 348 | 348 | 0 | 0 | 0 | 0 |
| CAP efficiency, $\eta_{CAP}$ [%] | 89.80 | 89.80 | -1E-07 | 3.22E-07 | -3.78E-09 | 8.66E-06 |
| OTCAP outlet temperature, T011, [C] | 337 | 337 | 0 | 0 | 0 | 0 |
| Pressure drop in 1st combustion, DPCEV [bar] | 0.94 | 0.94 | 0 | 0 | 0 | 0 |
| Pressure drop in 2nd combustion, DPCSEV [bar] | 1.53 | 1.53 | 0 | 0 | 0 | 0 |
| 1st. Combustion chamber efficiency, $\eta_{CEV}$ [%] | 99.8 | 99.8 | 0 | 0 | 0 | 0 |
| 2nd. Combustion chamber efficiency, $\eta_{CSEV}$ [%] | 99.8 | 99.8 | 0 | 0 | 0 | 0 |
| High heating value, HHV [kJ/kg] | 51825 | 51825 | 0 | 0 | 0 | 0 |
| HPGT efficiency, $\eta_{HPGT}$ [%] | 89.10 | 89.10 | -0.0000041 | 3.06172E-05 | -1.88E-06 | 0.0008 |
| LPGT efficiency, $\eta_{LPGT}$ [%] | 90.14 | 90.52 | -0.38 | 42.40 | -1.17 | 1139.50 |
| Steam Cycle | | | | | | |
| Main steam pressure, P1 [bar] | 136 | 136 | 0 | 0 | 0 | 0 |
| Main steam temperature, T1 [C] | 555 | 555 | 0 | 0 | 0 | 0 |
| Hot reheated steam temperature, T2 [C] | 532 | 532 | 0 | 0 | 0 | 0 |
| Low pressure steam temperature, T4 [C] | 343 | 343 | 0 | 0 | 0 | 0 |
| HPST Temperature, $\eta_{HPST}$ [%] | 82 | 82 | 0 | 0 | 0 | 0 |
| IPST Temperature, $\eta_{IPST}$ [%] | 90 | 90 | 0 | 0 | 0 | 0 |
| LPST Temperature, $\eta_{LPST}$ [%] | 94 | 94 | 0 | 0 | 0 | 0 |
| Mass flow rate Inlet coefficient $\phi_{IP}$ | 46.41 | 46.41 | 0 | 0 | 0 | 0 |
| Mass flow rate Inlet coefficient $\phi_{LP}$ | 17.15 | 17.15 | 0 | 0 | 0 | 0 |
| Condenser vacuum pressure, P6 [bar] | 0.092 | 0.092 | 0 | 0.0004 | 0 | 0.0101 |
| TOTAL | | | | 42.37 | -1.17 | 1139.50 |
| Differences, HR | 7508.77 | 7466.40 | 42.37 | | | |
| Differences, WN | 206.88 | 208.05 | -1.17 | | | |

*Tabla 4. Filtering Curves Load-Induced Effects*

| Diagnosis variable | Test | Reference | Difference | Delta IGV | Effect induced by HR [MW] |
|---|---|---|---|---|---|
| Environment | | | | | |
| $P_0$ [bar] | 0.97012384 | 0.97012384 | 0 | -3.51905E-11 | -2.18279E-10 |
| $T_0$ [C] | 18.9243889 | 18.9243889 | 0 | 0 | 0 |
| $HR_0$ [%] | 47.5320702 | 47.5320702 | 0 | -4.0025E-10 | -2.48201E-09 |
| Gas Cycle | | | | | |
| Pressure drop in filters, DP0E [mbar] | 10.2175607 | 10.2175607 | 0 | 0 | 0 |
| CBP efficiency, $\eta_{CBP}$ [%] | 89.8005464 | 89.8005464 | 0 | 0.018803592 | 0.11665861 |
| OTCBP outlet temperature, T013, [C] | 348.391164 | 348.391164 | 0 | 0 | 0 |
| CAP efficiency, $\eta_{CAP}$ [%] | 89.7926852 | 89.7926853 | -1E-07 | -0.003981882 | -0.024711495 |
| OTCAP outlet temperature, T011, [C] | 336.656698 | 336.656698 | 0 | 0 | 0 |
| Pressure drop in 1st combustion, DPCEV [bar] | 0.943935633 | 0.943935633 | 0 | 0 | 0 |
| Pressure drop in 2nd combustion, DPCSEV [bar] | 1.53062034 | 1.53062034 | 0 | 0 | 0 |
| 1st. Combustion chamber efficiency, $\eta_{CEV}$ [%] | 99.8 | 99.8 | 0 | 0 | 0 |
| 2nd. Combustion chamber efficiency, $\eta_{CSEV}$ [%] | 99.8 | 99.8 | 0 | 0 | 0 |
| High heating value, HHV [kJ/kg] | 51824.6368 | 51824.6368 | 0 | 0 | 0 |
| HPGT efficiency, $\eta_{HPGT}$ [%] | 89.08072 | 89.0807241 | -0.0000041 | 1.06953E-06 | 6.63694E-06 |
| LPGT efficiency, $\eta_{LPGT}$ [%] | 90.144 | 90.5172991 | -0.3732991 | 0.647933586 | 4.03871956 |
| Steam Cycle | | | | | |
| Main steam pressure, P1 [bar] | 136.296371 | 136.296371 | 0 | 0 | 0 |
| Main steam temperature, T1 [C] | 555.312561 | 555.312561 | 0 | 0 | 0 |
| Hot reheated steam temperature, T2 [C] | 532.146912 | 532.146912 | 0 | 0 | 0 |
| Low pressure steam temperature, T4 [C] | 343.268677 | 343.268677 | 0 | 0 | 0 |
| HPST Temperature, $\eta_{HPST}$ [%] | 82.0033436 | 82.0033436 | 0 | 0 | 0 |
| IPST Temperature, $\eta_{IPST}$ [%] | 90.1651048 | 90.1651048 | 0 | 0 | 0 |
| LPST Temperature, $\eta_{LPST}$ [%] | 93.6736586 | 93.6736586 | 0 | 0 | 0 |
| Mass flow rate Inlet coefficient $\phi_{IP}$ | 46.4142277 | 46.4142277 | 0 | 0 | 0 |
| Mass flow rate Inlet coefficient $\phi_{LP}$ | 17.1546278 | 17.1546278 | 0 | 0 | 0 |
| Condenser vacuum pressure, P6 [bar] | 0.092540441 | 0.092540441 | 0 | 6.79961E-09 | 4.20705E-08 |
| TOTAL | | | | 0.66276 | 4.130673 |
| Differences directly, IGV | 5.655 | 4.992 | 0.663 | | |

# Review of Methods for Thermal Management and Design for Energy Efficiency

*David J. Moorhouse, David M. Pratt*

*Air Force Research Laboratory*
*Wright-Patterson AFB, OH 45433*

**Abstract:** Aircraft are extremely complex machines posing a highly integrated design problem, including many systems that are all interrelated and dependent on power (or energy) in some form. In some of the systems there is also the creation of by-products, in the form of heat energy, that have to be removed from that equipment. The more we depart from existing data bases and experience levels, the less confidence we can have that we are close to an optimal design. In addition, many of the classical techniques are based on simplifying assumptions that were used in the original derivation. AFRL research has been accomplished for advanced thermal management and also to progress towards a methodology in a 'common currency' for the design of the complete integrated system of systems. The objective of this paper is to review the results of this research in a general way for application to any system.

**Keywords:** exergy, thermal management, design

## 1. Introduction

Aircraft have evolved to a point where they are extremely complex machines posing a highly integrated design problem. Any flight vehicle includes many systems that are all interrelated and dependent on power (or energy) in some form. For military vehicles the problems can be more intense, such as the use of directed energy weapons (DEW) such as high power microwaves (HPM) and high energy lasers (HEL). These devices present unique energy challenges are inefficient, therefore a large portion of the energy required to operate the device is converted to waste heat and must be transferred to a suitable heat sink. For HPM, the average heat load during one 'shot' is on the same order as traditional subsystems and thus designing a thermal management system is possible. The challenge is transferring the heat from the HPM device to a heat sink. The power density of each shot could be hundreds of megawatts. This heat must be transferred from the HPM beam dump to a sink. The heat transfer must occur at a rate that will support shots in the 10-100Hz range. For HEL systems, in addition to the high intensity, there are substantial system level thermal loads required to provide an 'infinite magazine.' Present models are inadequate to analyze these problems, current systems are unable to sustain the energy dissipation required and the high intensity heat fluxes applied over a very short duration phenomenon is not well understood. Such systems are discussed generically as examples of the problem of design for energy efficiency.

In some of the systems there is also the creation of by-products, in the form of heat energy, that have to be removed from that equipment. There obviously exist methods for the design of all these systems, based on the evolutionary nature of vehicle development. However, the more we depart from existing data bases and experience levels, the less confidence we can have that we are close to an optimal design. In addition, many of the classical techniques are based on simplifying assumptions that were used in the original derivation. If these are not considered, then there is no guide to when those classical techniques no longer give an acceptable solution because they do not incorporate the requisite multi-physics and multi-scale integration. We consider the question of when traditional methods are appropriate and when other approaches are necessary. AFRL research has been accomplished for advanced thermal management and also to progress towards a methodology in a 'common currency' for the design of the complete integrated system of systems. The objective of this paper is to review the results of this research. In addition, the work

has shown the complexities of 'integrating' the various forms of energy and work. The paper will discuss this aspect in a general way for application to any system.

## 2. Background

In the design problem for a complex system, such as flight vehicular design, we suggest that it should be recognized that the laws of the physics were often written in a form convenient for an application. We start with a simple example, for a flight vehicle in cruise there is no net vertical force, which could imply that no work is being done in the vertical direction. Work must be done in the vertical axis, however, in order to support the weight. L – W = 0 and it is correct physics to say that no work is being, but not for this application. This can be visualized with a control volume around the vehicle which must do work to oppose the external force of gravity. One physical theory is to calculate the rate of change of vertical momentum that must be transmitted to the volume of air 'flowing into the control volume'. Actually, the 'freestream air' is typically at rest with zero kinetic energy. Since all the required 'vertical work' is accomplished by the thrust of a conventional configuration, then for design application it was book-kept as induced drag (calculated as a function of lift). This component of drag multiplied by velocity is 'the rate of doing the required vertical work'. A certain amount of this vertical work is an absolute requirement to perform the mission but there may be inefficiencies that can be reduced. Any unnecessary component of weight increases the required lift and the resultant induced drag, so that there is some benefit from weight minimization. We suggest, however, that such minimization should not be done independent of other considerations. Of course, there is also the friction drag component which is part of the work required to maintain the cruise speed, i.e. 'the rate of doing required horizontal work'. Thus, minimizing drag is an obvious component of traditional optimization, and a component of that is weight. For system-level optimization, we suggest that lift and drag can be represented in the terms of rate of doing work in a format that is consistent with other components of the total design process. As an example, the propulsion system and power-related equipment are connected to a very strong degree in thermal terminology, which means they could be optimized as a total energy subsystem. However, optimizing by minimizing the weight of a component to reduce the 'work done in the vertical axis' could lead to system-level inefficiency wasting more fuel than saved by reducing weight. Thus, we should consider the question what is 'good weight', versus the conventional metric that all weight is bad and should be minimized.

Now, we are going to suggest that many revolutionary concepts cannot be decomposed into relatively independent components. Such design integration would be facilitated by energy-based design methods to define the available design space early in the process. Alternatively, an evolutionary design could be audited by the new methodology before the system design was finalized. This would identify where and how the available energy, i.e. fuel, was being used. This would involve items of required work and use of energy as described above, unavoidable irreversibility such as combustion losses, or identify components and/or configuration elements yielding avoidable waste. The design team could then assess which avoidable inefficiencies could be improved in an acceptable design change.

## 3. Thermal Management Challenge

Heat generated by numerous sources in any vehicle must be collected, transported and rejected by a thermal management system (TMS) and prevent components and subsystems from exceeding specified temperature limits, while meeting an overall thermal balance for the vehicle. On aircraft we have traditionally used ram air and fuel as our primary heat sinks. This was adequate until about 20 years ago. Prior to which thermal loads generated were sufficiently small and thermal reserves were great enough to overcome problems that appeared late in the development cycle. Legacy aircraft such as the F-15 and F-16 had no TMS-induced operating constraints; their available heat sink capacity significantly exceeded their total thermal load under all operating conditions. Recently, however, thermal loads in systems such as the F-22 and F-35 have increased substantially while low-observability (LO) constraints have dramatically reduced the availability of heat sinks. This results in thermal deficits during some portion of typical missions, including ground operations. These thermal deficits can lead to hardware failures which in turn lead to increased maintenance costs and potential

aircraft loss. Thermal management challenges will be even greater in future systems including Long Range Strike aircraft, advanced Intelligence, Surveillance and Reconnaissance aircraft, and airborne Directed Energy Weapon (DEW) systems. In these systems, heat loads will be up to an order of magnitude higher than in today's fighters, which are already encountering thermal constraints in their operation. To prevent thermal management from becoming a show stopper, solutions are required to reduce heat loads, raise allowable temperature limits, improve heat rejection, increase the capacity of existing heat sinks, and provide new heat sinks.

Many component-level and subsystem-level thermal management technologies exist that could have important benefits for the TMS. One example is the research into feasibility of energy recovery from aircraft avionics via thermoelectric devices, e. g. [1]. No one of these technologies, however, will radically simplify the challenges faced in thermal management across widely differing systems. The benefits of a given technology depend strongly on the particular thermal management architecture into which it is integrated. A system-level thermal management analysis capability, centered on modeling and simulation (M&S), is the single most important technology that requires development. It can be implemented in the near-term from existing subsystems and component-level models, and the fidelity can increase over time as these models are refined.

The technology assessment area can be divided into two broad sub-areas. That of traditional physics based modeling and that of advanced concepts to enable energy optimized systems. Both of which require information technologies to enable interchange of information across remote networks, insurance of shared proprietary rights, non-unique data fusion and output and a common basis for interfacing eclectic disciplines. In the traditional physics based modeling sub-area, advances must be made in the description of the fundamental physics associated with the energy and mass transport within DEW as well as their integration and the quantification of uncertainties. Exergy, entropy generation minimization, and energy optimization are examples of technologies that can enable the creation of energy optimized systems. These approaches allow the manipulation of fundamental equations governing thermodynamics, heat transfer, and fluid mechanics to produce minimized irreversibilities at the vehicle, subsystem of device levels. Applying these techniques to the aircraft systems would identify not only which subsystems are inefficient but also those that are close to their maximum theoretical efficiency.

Heat transport systems capable of dissipating high intensity heat energy and transporting large amounts of thermal energy over distances are required to cool the DEW devices and to integrate these devices at the system and platform level. Of the heat transport concepts under consideration in this regime, the most attractive utilize the latent heat of vaporization through liquid-vapor phase change or two phase flow. However, the risk associated with two phase systems is beyond that which is acceptable to air platform system integrators. To fully reap the potential benefits of these concepts, they must be matured. Additionally, working fluids that change phase in the 200-400ºC range require development.

### 3.1. System Level

Preliminary assessments have shown that high powered microwave systems will require

- 5-10 MW electrical
  - 4 kW Input Power for Cryogenic Cooler (30K) for Magnet
  - ~1 kW Input Power for Cathode Heater

They are typically less than 50% efficient, and an added complication occurs when including the users' desire for near continuous duty cycle. These preliminary assessments also gave insight into High Power Laser (HPL) requirements that include

- 1-2 kHp input power
- ~10% device efficiency
- 1000 W/cm2 heat fluxes

While the user desires only seconds between shots but an infinite magazine. This leads to demands on the thermal management systems of

- High heat flux of 100-1200 W/cm2
- High thermal power of 10-100's kW – 10's MW
- Duty cycle of seconds to minutes to near continuous
- Isothermality for solid state lasers of less than 2C and device defined performance generally <50C

• Operational temperatures consistent with device performance
  – Electronics 100-400C
  – Laser devices 0-200C
  – High power microwave devices 300-400C
• Operation in high-g environments

These parameters define the system constraints. The preliminary assessments also determine that the integration of DEW system allows or requires the examination of the thermal management concepts into discrete classifications, those of local or device cooling, intermediate or capacitor/damping concepts and finally subsystem or platform energy dissipation.

### Device cooling and two-phase flow

Table 1 details high heat flux device level technologies that may be feasible to meet the parameters mandated for the detailed for device level components.

*Table 1. High heat flux cooling technologies*

| | Heat flux, W/cm2 | Temp., 0C/heat flux, W/cm2 | Transport capacity, W-m |
|---|---|---|---|
| Heat pipes | <10-20 | | 100's |
| Loop heat pipes, capillary pumped loops | 10-20 | | 1000's |
| Single phase liquid flow cooling | 1,000's (high flow rate/pumping penalty) | | 1000's |
| Two phase flow cooling | | 50-70/100 | 1000's |
| - | 100-1000 | 20/200 | |
| - | 100-1000 | 20/500 | |
| - | 100-1000 | 100/1000 | |
| *Thermal energy storage | <1kW/s | | |

Now to differentiate and do the trades between the two most feasible solutions shown in Table 1, i.e. that of single phase liquid flow cooling and two phase flow cooling, Fig. 1 is presented. This figure is a comparison of these two cooling phenomena for a given working fluid. It yields insight into the advantages of using two phase flow systems which is an order of magnitude increase in the local heat flux. Another advantageous aspect of two phase systems as shown in the figure is that they acquire these large heat fluxes isothermally. Both of these parameters are required for DEW systems.

Concepts for single phase liquid cooling heat fluxes such as single phase jet impingement cooling and sub-cooled nucleate boiling have demonstrated the ability to meet the local flux requirement but the single phase problem is what do you do with all that liquid. It takes a huge flow rate to remove the requisite heat using single phase schemes. This problem is highlighted in the following equation which is a comparison of the required mass flow rate for single and two phase flow systems. Two phase systems are not problem free. The two phase problem is what do you do with all that vapor and how do you do separate it from the liquid during high-g maneuvers? As opposed to the single phase problem which is inherent to thermophysics, the latter is a design consideration which can be overcome by maturation of the technology.

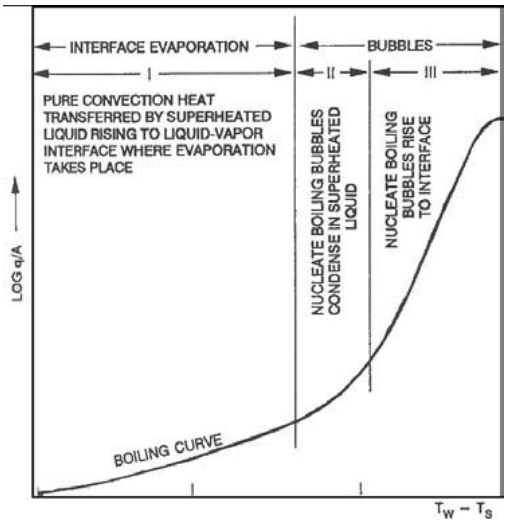


*Fig. 1. Fluid Thermophysics (ASHRAE)*

$$\dot{m}_{SP} = \frac{\dot{Q}}{Cp\Delta T} \Rightarrow \left[\frac{\dot{m}_{SP}}{\dot{m}_{TP}}\right]_{lim} = \frac{h_{LV}}{Cp\Delta T} = \frac{2454\ kJ/kg}{(4.8\ kJ/kgK)(1K)} \quad {}_2O$$
$$\dot{m}_{TP} = \frac{\dot{Q}}{h_{LV}} \qquad (1)$$

So now we have a concept to locally remove the energy but there still exist considerations for the required duty cycles. Fig. 2 shows an approximate duty cycle for a HPM system integrated into a vehicle. Fig. 3 shows the thermal management considerations for an HEL. For HEL the minimum useful duty cycle is ten seconds between shots or a 40% Duty Cycle with 100kW output, 10% efficient continuously pulsed laser of 4sec on, 10 sec off. However an infinite magazine is desirable. So, we must evaluate impacts as the numbers are reduced. Duty cycles of these types lead to the incorporation of a thermal capacitor between the local energy removal system and the platform thermal management system.

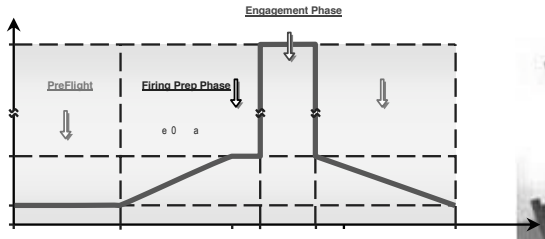


*Fig. 2. Approximate AAD mission profile*

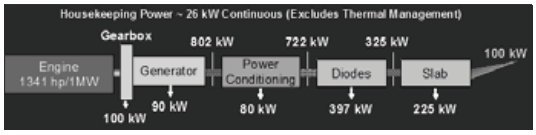


*Fig. 3. HEL thermal requirements*

### 3.2. Thermal Capacitors

Traditional thermal capacitors include phase change materials (PCMs) [2] such as waxes, chemical adsorption beds, chemical reaction systems, among others. Of these the one most commonly considered is a PCM bed. These beds have drawbacks in that they have relatively huge capacities however they have very low thermal conductivity. This leads to unacceptable time constants associated with the energy transport into the bed. Thus research must be pursued in the optimally embedding high conductivity material in the PCM to decrease the time constant associated with the energy storage systems. Means of doing this include infiltrating PCM into high conductivity foams and example of which is shown in Fig. 4 [3,4,5], into fin or honeycomb structures like in Fig. 5, or into graphite heat exchanges as in Fig. 6 or encapsulating them in a micro encapsulation process as shown in Fig. 7 [6].

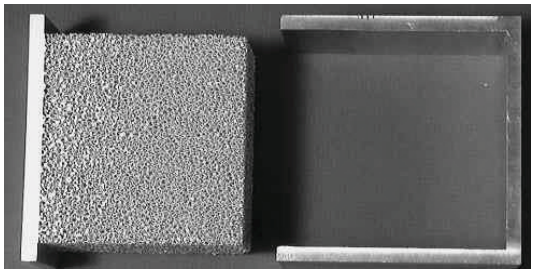

*Fig. 4. High conductivity foams (http://widget.ecn.purdue.edu)*

*Fig. 5. Finned heat sink (www.trade-taiwan.org)*

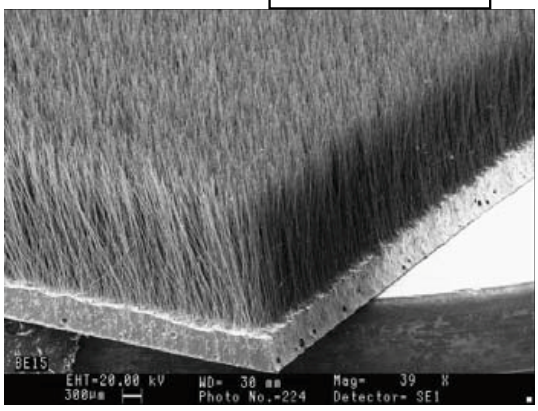


*Fig. 6. Carbon Heat Exchanger (http://www.esli.com)*

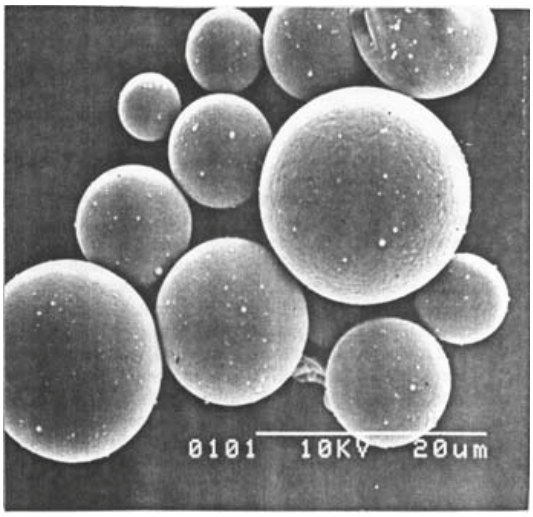


*Fig. 7. Microencapsulated Phase Change Materials [7]*

### 3.3. Energy Conversion

DEW systems are extremely inefficient and thus have large quantities of high quality energy that must be removed from the weapon. In general this energy must then be dissipated. However, if devices that could convert this energy into useful work were available, the overall efficiency of the weapons system would be increased. This requires the development of energy harvesting or the recovery, conversion and re-use concepts. Sodano reviewed and detailed some of the topics in power harvesting that have been undergoing recent research. These included energy harvesting from mechanical vibration, biological systems, and the effects of power harvesting on the vibration of a structure but like most other recent researches Sodano emphasized the conversion of vibrational energy into electrical power. DEW systems are concerned more with thermal energy conversion into useful work. Systems of this nature include heat engines and heat pumps. Heat engines are defined as devices that convert heat energy into mechanical energy or more exactly systems which operate continuously and only heat and work may pass across the boundaries (Fig. 8).

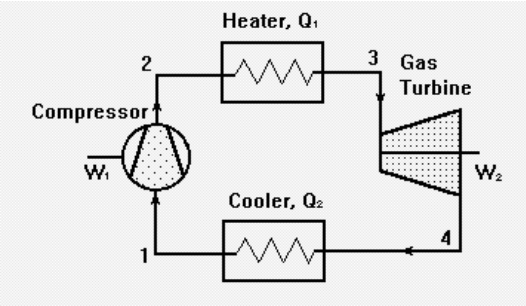


*Fig. 8. Typical Heat Engine (Brayton Cycle) (http://www.taftan.com/thermodynamics)*

While these systems have been under development for decades, consideration for the isothermal constraints, heat flux levels, and total energy dissipation requirements associated with DEW integration must be explored.

Heat pumps are devices that transfer heat energy from a low temperature reservoir to a high temperature reservoir requiring the input of energy such as refrigeration cycles. If however you 'drive' these devices in reverse that is if a temperature gradient exists, you can produce useable output energy. An example of such a system is a thermoelectric device. Thermoelectric devices are solid-state devices that convert thermal energy from a temperature gradient into electrical energy by the Seebeck effect or convert electrical energy into a temperature gradient by the Peltier effect. Heat pumps like heat engines have been under development for decades however they too require substantial work to overcome the constraints associated with DEW integration.

## 4. System Integration

In addressing the problems of designing a system integrating a variety of dissimilar components, [8] proposed consideration of a flight vehicle as a device to do work, and the use of a design methodology to minimize exergy destruction. Exergy destruction as a 'common currency' for design has been investigated in a variety of ways.

An early focus was to address if optimizing to minimize exergy destruction made a difference and how. An analysis was performed [9] to optimize a notional fighter configuration over a mission with conflicting segment requirements, e.g. supersonic and subsonic. The intent was to compare the traditional minimization of takeoff gross weight (W TO) against minimization of

exergy destruction (including unburnt fuel losses). Two other metrics were included: maximize the 'thrust efficiency' defined as thrust divided by fuel mass flow times the heating value; and maximize 'thermo effectiveness' defined as thrust divided by the maximum thrust if there were no irreversibilities. The first result is presented in Fig. 9 which compares the exergy destruction for the four different optimization metrics. It can be seen that there is no significant difference in the result from these four design metrics, and only the first two were used in follow-on analysis. We deduced that the optimization metric made little difference if the system was all related components, such as propulsion and power-related subsystems. Alternatively, there was a significant difference when a variable airframe system was included with the propulsion related systems in the optimization process. We consider this as integrating a 'force-based system' with a 'thermo-based system'. The result is shown in Fig. 10, where fuel weight required to accomplish the mission is used as the metric as an obvious function of total exergy destruction. With AirFrame Subsystem – Aerodynamics Degrees of Freedom (AFS-A, DOF) included in the optimization there is a reduction in fuel required. The results also show a far more significant benefit from optimizing to minimize exergy destruction rather than traditional minimization of weight in terms of required fuel.

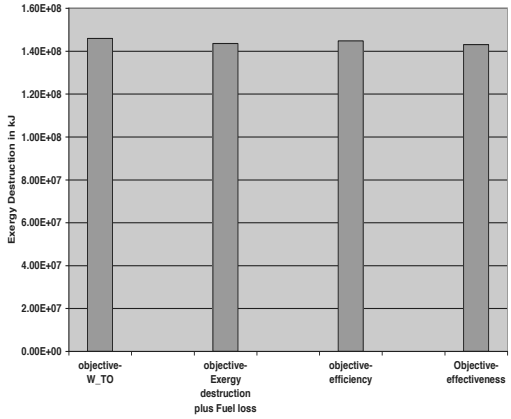


*Fig. 9. Effect of Different Design Optimization Metrics on Exergy Destruction*

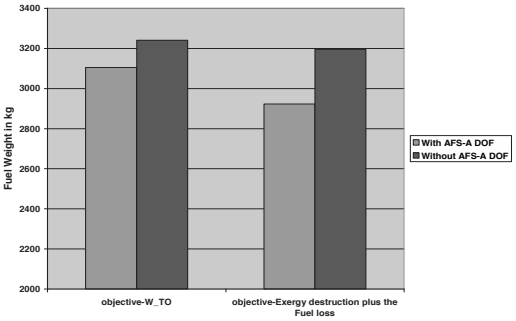


*Fig. 10. Effect of Optimization with and Without Airframe Degrees of Freedom*

Additional research has also shown the benefits of integrating the external and internal flow fields of high-speed vehicles [10]. This reference provides analytical and numerical applications and studies relevant to the vehicle performance-entropy relationship. A simplified configuration of a two-dimensional blunt body at high Mach number was examined utilizing a Navier-Stokes CFD code for cases with forward-facing injection and forward-facing injection with upstream energy deposition (as heat), The problem of upstream-directed injection jet instability has been shown to be significantly reduced by the coupling of the two techniques (injection and upstream energy deposition); this allows the jet to penetrate far upstream and stabilize within bounds. When hydrogen is used as the core injectant, the substantial production of water in and near the zone of upstream energy deposition may assist in the efficiency of energy deposition systems. Additionally, by sheathing the hydrogen core with an inert injectant such as nitrogen, the body is cooled and the heat release and resulting zones of water production are removed from the vicinity of the blunt body. Cases have been shown in which the overall drag is only 20 to 30% of the base-line drag, heat transfer is minimal, and jet stabilization and forward penetration is ensured. The comparisons of the computed drag for all configurations provide an excellent endorsement of the entropy method, i.e. potentially allowing a direct assessment of losses in terms of the *common currency* of entropy generation. The entropy characteristics of the flow-fields for these cases clarified the relative performance of these cases and demonstrated the utility of the direct link between entropy generation and vehicle

performance for configuration analysis, design and optimization.

A second part of the investigation demonstrates the potential advantage of distributing energy in both external airstreams upstream and adjacent to an actual hypersonic vehicle configuration as well as in the 'traditional' location of the engine combustor. Second-law analysis was performed on a number of entire vehicle flow-fields and the performance related to the generation of entropy due to flow irreversible losses in both the vehicle flow-field as well as in the vehicle wake. The results showed the significant benefits of external flowfield use of the energy vs the conventional use just in the combustor. A system design application would have to assess the 'cost' of depositing that external energy, but the research shows that there is definitely a potential benefit that does appear to be worth pursuing.

## 5. Conclusions

Overall, the paper is intended to show that the proposed technique of minimizing system-level exergy destruction provides a method to facilitate system-level optimization for energy efficiency at all stages of the design process. We also suggest that the 'thermal management challenge' can be addressed by designing all components to the system-level metric. It was also intended to discuss exergy methods in a form that could apply to any system, not just flight vehicles.

## References

[1] Hallinan, K. P., B. Sanders, T. Somphone and G. Ephrem, February 2005, "Entropy Generation Metric for Evaluating and Forecasting Aircraft Energy Management Systems", Int. Journal of Exergy, Vol. 2, No. 2,

[2] Hale, D. V., M. J. Hoover, and M. J. O'Neil, 1971, *Phase Change Materials Handbook*, NASA CR-61363.

[3] Klett, James, 2004, "Pitch-Based Carbon Foam Heat Sink with Phase Change Material," United States Patent # 6,780,505.

[4] Hagar, J. W. and Lake, M.L., 1992, "Novel Hybrid Composites Based on Carbon Foams," *Materials Research Society Symposium Proceedings*, Vol 270.

[5] Wierschke, K.W., Franke, M.E., Watts, R., and Ponnappan, R., 2005, "Heat Dissipation with Pitch Based Carbon Foams and Phase Changer Materials", *38th AIAA Thermophysics Conference Proceedings.*

[6] Fossett, A.J., Maguire, M.T., Kudirka, A.A., Mills, F.E.and Brown, D.A., 1998, "Avionics Passive Cooling with Microencapsulated Phase Change Material", Journal of Electronic Packaging, Vol. 120, pps. 238–242.

[7] Colvin, D.P., Mulligan J.C. and Bryant Y.G., 1992, "Enhanced Heat Transport in Environmental Systems Using Microencapsulated Phase Change Materials", SAE Technical Paper Series, Vol 921224, pg. 2.

[8] Moorhouse, D. J., January 2003, "A Proposed System-Level Multidisciplinary Analysis Technique Based on Exergy Methods", AIAA Journal of Aircraft, Vol. 40, No. 1.

[9] Periannan, V., M. R. von Spakovsky and D. J. Moorhouse, August 2008, "A Study of Various Energy- and Exergy-Based Optimization Metrics for the Design of High Performance Aircraft Systems", Royal Aeronautical Society, Aeronautical Journal, Vol. 112, No. 1134.

[10] Riggins, D. W., T. Taylor, L. Terhune and D. Moorhouse, May 2007, "Methods for the Design of Energy-Efficient High-Speed Aerospace Vehicles", Royal Aeronautical Society, Aeronautical Journal, Vol. 111, No. 1119.

# Thermoeconomic Analysis of Energy System Control Strategies

*Giorgia Baccino[a], Matteo Dalla Vedova[b], Vittorio Verda[a]*

[a] *Department of Energetics, Politecnico di Torino, Italy*

[b] *Department of Aerospace, Politecnico di Torino, Italy*

**Abstract:** In this paper an exergoeconomic approach is applied to the dynamic model of a Power System in order to investigate the effects of the control system on the primary energy consumption. To achieve this objective, various control strategies are compared when variations of the operation condition, due to some internal or external causes, are produced.
Those variations causes the intervention of the control system, which rearranges the operating condition in order to have the controlled quantities within acceptable ranges. Generally the plant efficiency changes, depending on the selected strategy.
A microturbine is considered as the case study.
The analysis here proposed allows one to quantify the effect of the control on the performance variation of the components. The exergoeconomic approach associates a cost to the control system operation, which expresses the additional fuel consumption that may be associated to the control. The impact on the initial and final steady states as well as the transient evolution are considered.

**Keywords:** Control system, Transient analysis, Thermoeconomics.

## 1. Introduction

Control system is one of the main parts of a power plant. Its intervention occurs when the working condition changes, which can be due to external or internal causes, such as variations in load or ambient conditions, changes in the set points, performance degradation of components, etc.

Control technology has focused its attention on minimizing the deviation of variables (the controlled variables) from set points. Often the problem of control is faced referring to response stability and robustness, to allow the system operate correctly in the various operating conditions (see for example [1], [2]). A proper control can obtain more production out of limited plant equipment and can contribute more to reducing operating costs than any other device; however, also a control technology entails costs that cannot be neglected [3].

The control system must be taken into account whatever is the aim of the analysis: cost accounting, performance/cost evaluation [4], operation and management optimization [5], detection and location of malfunctions [6], etc. In this paper, the analysis of the control system is performed using thermoeconomics.

In a previous paper [7], thermoeconomic analysis was used to compare various control strategies for a gas turbine and to define the cost of a control system. The analysis was conducted considering the initial and final steady states, without including the impact of the control system on the transient process and the deviation with respect to the desired operating condition. Here, some work is presented with the aim of starting to fill the gap.

Two control strategies for a microturbine are analyzed. The common goal for these strategies is the obtainment of the desired electric power. A second objective consists in keeping the operating temperatures within proper limits in order to avoid too low efficiencies or low lifetime due to creep. The first strategy is operated considering the turbine outlet temperature as constant. This is a typical operating mode for microturbines. The second strategy consists in keeping the turbine inlet temperature (TIT) close to the reference value. As this variable is not measurable in real installations, a correlation between turbine outlet temperature (TOT) and the net power is obtained,

Corresponding Author: Vittorio Verda, Email: vittorio.verda@polito.it

so that the inlet turbine temperature is kept almost constant in the various operating conditions. This correlation is obtained through a steady state model of the microturbine that has been built in EES. Details of the model are available in the Annex.

In order to comply these strategies, two independent parameters can be adjusted: the fuel mass flow rate and shaft rotational speed.

## 2. Thermoeconomic analysis

The use of thermoeconomic methodologies has been widely applied to the analysis of energy systems [8]. In the last decade, it has been applied also to system diagnosis, as a tool for the detection and the location of the anomalies causing reductions of the overall efficiency [9]. This is not a simple task, as several physical factors affects the behavior of the components in a plant.

In the framework of thermoeconomic diagnosis, a tool called the "fuel impact formula" has been developed [10, 11]. This quantities expresses the additional fuel consumption of the system, when the operating condition deviates from the reference condition. In this paper, the fuel impact formula is used to calculate the additional fuel consumption due to the control system.

To apply this formula, a productive representation of the system must be defined. It consists on expressing the role of each component by means of the exergy flows which associated to the consumed resources and the obtained product (see the Annex). The structural approach to the thermoeconomic analysis [11] can be used for this goal.

Two terms contribute to the fuel impact: the variations in the efficiency of components due to off-design conditions or intrinsic malfunctions and the variations in the overall plant production:

$$\Delta F_T = \sum_{i=1}^{n}\left(\sum_{j=0}^{n} k^*_{p_j}\cdot\Delta k_{ji}\right)\cdot P_i^0 + \sum_{i=1}^{n} k^*_{p_i}\cdot\Delta P_{e_i} \quad (1)$$

$k_{Pj}^*$ is the exergetic unit cost of the product of the $j^{th}$ component (calculated in operating condition), $P^0_j$ is the total product of $i^{th}$ component in reference condition and $k_{ji}$ is the unit exergy consumption defined as:

$$k_{ji} = \frac{E_{ji}}{P_i} \quad (2)$$

where $E_{ji}$ is the resource of the $i^{th}$ component produced by the $j^{th}$ component ($0^{th}$ component is the ambient). $\Delta k_{ji}$ is the variation of $k_{ji}$ between the operating condition and the reference condition. The term $\Delta P_{ei}$ is the variation in the product of $i^{th}$ component between the operating condition and the reference condition also resulting in a corresponding variation of the overall system product.

The first term on the right hand side of equation (1) expresses the additional fuel consumption required to obtain the same overall production. This quantity can be used to evaluate the impact of the system together with its control in a particular steady state operating condition. When comparing alternative control strategies, differences in its value can be directly associated with inefficiencies caused by the control system.

Proper analysis of the control system should include the transient operation from the initial operating condition to the final operating condition. Such analysis requires to consider the contribution of exergy storage in the fuel impact formula.

To analyze this contribution, we may start from the general exergy equation for a component:

$$\sum_{i=1}^{m}\Psi_{q_i} - W_t = \sum_{j=1}^{n} m_j\cdot b_j^t + \Psi_{irr} + \left(\frac{\partial A^t}{\partial t}\right)_{cv} \quad (3)$$

where $\Psi_q$ is the exergy associated with heat fluxes exchanged between the component and other systems, $W_t$ is the mechanical work, m is the general mass flow rate exiting (+) or entering (-) the system and b the corresponding total specific exergy, $\Psi_{irr}$ accounts for the irreversibilities, A is the total internal exergy in the control volume (cv):

$$A^t = U + p_0\cdot V - T_0\cdot S + E_c + E_p \quad (4)$$

where U is the internal energy, $p_0$ is the biosphere pressure, V the system volume, $T_0$ the biosphere temperature, S the system entropy, $E_c$ the kinetic energy and $E_p$ the potential energy.

The same equation can be rewritten in terms of entering and exiting exergy flows and fluxes or, which is the choice operated here, productive

flows, i.e. resources (F), products (P) and losses (L):

$$\Psi_F = \Psi_P + \Psi_L + \left(\frac{\partial A^t}{\partial t}\right)_{cv} + \Psi_{irr} \quad (5)$$

where productive flows may be in the form of thermal exergy, mechanical exergy or exergy associated to mass flows. Equation (5) shows that, in a general process, the exergy flow entering with the resources is converted into products, dissipated in losses, stored or destroyed in irreversibilities.
The corresponding exergetic cost balance is:

$$\Psi_F^* = \Psi_P^* + \left(\frac{\partial A^t}{\partial t}\right)_{cv}^* \quad (6)$$

To calculate the exergetic costs, the unit cost of stored exergy is assumed equal to the exergetic unit cost of the products.
The storage term in equation (1) is considered as an external product.

## 3. Control system of a microturbine

To perform a thermoeconomic analysis of possible control systems, a simplified transient model of the microturbine is build in Matlab-Simulink. Figure 1 shows a schematic of this model.

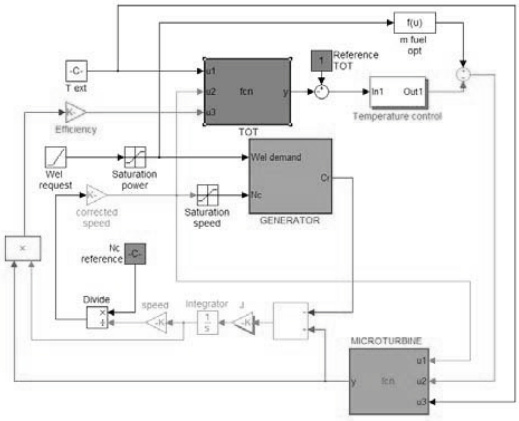


*Fig. 1. Schematic of the first model*

The system may be represented as divided in two different parts. In the lower part, there is a loop representing the spontaneous system operation. Input of the Generator are the requested electric load and the current rotational speed of the shaft. Its output is the corresponding torque.
The Microturbine block synthesizes compressor and microturbine behaviour, using a quadratic regression function linking the net torque (output variable) with external air temperature, fuel mass flow rate and current shaft rotational speed (input variables). This function has been obtained using the complete thermodynamic model presented in the Annex:

$$C_{net} = c_1 + c_2 \cdot X_1 + c_3 \cdot X_2 + c_4 \cdot X_3 + \\ + c_5 \cdot X_1 \cdot X_2 + c_6 \cdot X_1 \cdot X_3 + c_7 \cdot X_2 \cdot X_3 + \\ + c_8 \cdot X_1^2 + c_9 \cdot X_2^2 + c_{10} \cdot X_3^2 \quad (7)$$

where $C_{net}$ is the net torque (i.e. the difference between the turbine torque and the compressor torque), the $c_i$ are regression coefficients, $X_1$ is the ratio between the current speed and the nominal shaft speed, $X_2$ is the ratio between the fuel mass flow rate and its nominal value, $X_3$ is the ratio between the external air temperature and the nominal temperature. A comparison between 300 values, corresponding with different values of the input parameters (free operation parameters) calculated using the model and those obtained with equation (1) is shown in Figure 2.

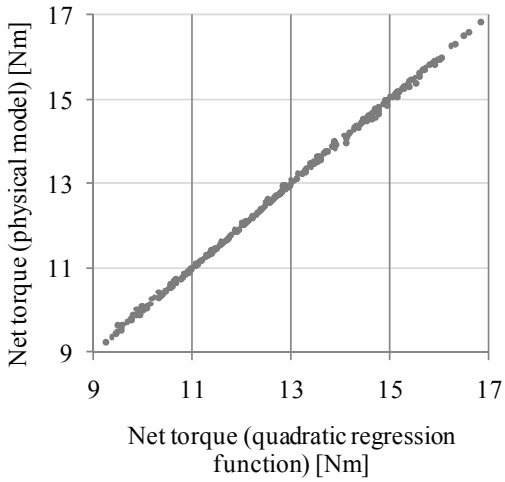


*Fig. 2. Comparison between the net torque calculated with the physical model and with equation (7)*

Net torque and generator torque ($C_g$) complies the mechanical balance:

$$C_{net} = C_g + J\frac{d\omega}{dt} \quad (8)$$

where J is the total moment of inertia (shaft, compressor and turbine) and ω is the angular rotational speed of the shaft. The integrator allows one to obtain the current rotational speed. A saturation on generator speed input restricts possible speed peaks to maximum speed value.

The upper part of the figure contains the temperature control. A quadratic function calculates the turbine outlet temperature as the function of rotational speed, ambient temperature and the current electric power (generally different than the requested power). This quantity is compared with the reference value and, in the case there is a difference, the control system operates on the fuel mass flow rate. The block on the upper right corner is a function calculating the optimal fuel mass flow rate depending on the requested electric load. This is a reference value and the control system may correct the final value if the TOT differs from the set point (in the case of the first control strategy). A proportional control has been selected. This difference also corrects the resistance torque felt by the system, which allows one to modify the rotational velocity.

The control strategy is evaluated considering an increase in the requested electric power from 75 kW to 110 kW in about 35 s (signal source is a ramp with a slope of 0.99, so it has been considered as a step).

Figure 3 shows a comparison between electricity request and the actual electric power. When the request in the electric power increases the electric power decreases to about 50 kW. This is due to the increase in the rotor velocity, as shown in Figure 5, which originates an inertial term.

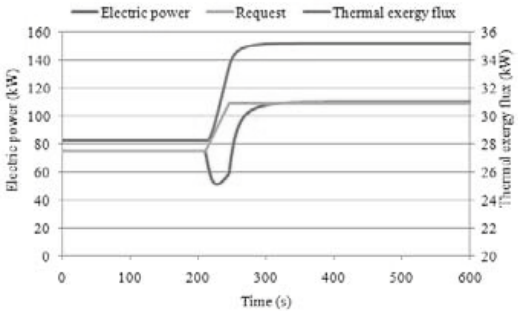


*Fig. 3. Exergy fluxes produced by the first system configuration*

Then the electric power increases, reaching the target value after about 100 s.

Thermal exergy flux produced by the system increases from 28 kW to about 35 kW, as is shown aloft in Figure 3.

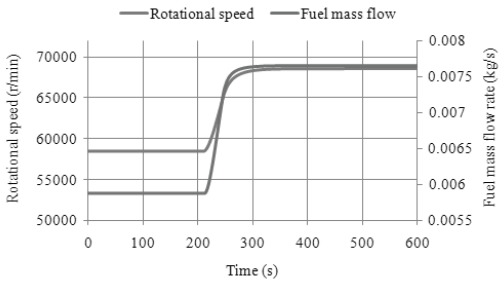


*Fig. 4. Control quantities in the operation the first system configuration*

Figure 4 displays the variation in control parameters, i.e. shaft rotational speed and fuel mass flow rate. Rotational speed rises from about 57000 rpm to about 68000 rpm. The speed course shows that the system progressively decreases its acceleration (parabolic speed course) and reaches the full load speed in about 150 s. The contribution due to inertia reaches a pick of about 40 kW in 50s, then returns to zero in about 100s.

Fuel mass flow rate increases from about $5.8 \cdot 10^{-3}$ kg/s to about $7.7 \cdot 10^{-3}$ kg/s, that corresponds to the nominal flow rate value. Whereas electricity request changes from 75 kW to 110 kW in about 35 s, fuel mass flow rate reaches nominal value in more than 200 s.

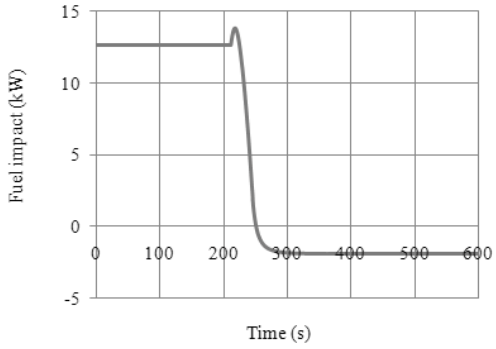


*Fig. 5. Fuel impact corresponding with the first control strategy*

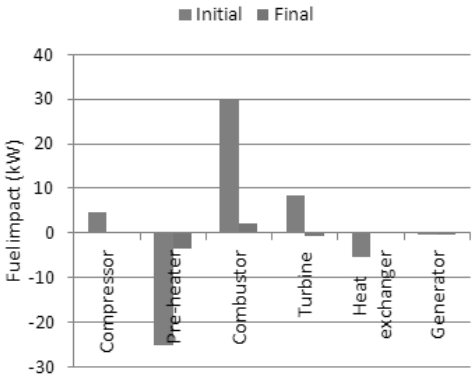


*Fig. 6. Fuel impact in the various components*

Figure 5 shows the total fuel impact corresponding with the use of the presented control strategy. In the initial operating condition, the fuel impact due to inefficiencies is about 13 kW. When the electricity request increases, there is a small pick in the fuel impact, then there is a reduction to the final value, which is about -2 kW. The contributions of the various components to the fuel impact are shown in Figure 6 for the initial and the final operating condition. The effect that mostly contributes to the reduction in the total fuel impact is that in the combustion chamber. This is caused by the smaller value in the turbine inlet temperature at reduced electric load.

A second control strategy is now considered. Instead of a constant outlet turbine temperature, the reference value is modified according with a linear function of the requested electric load, as shown in Figure 7.

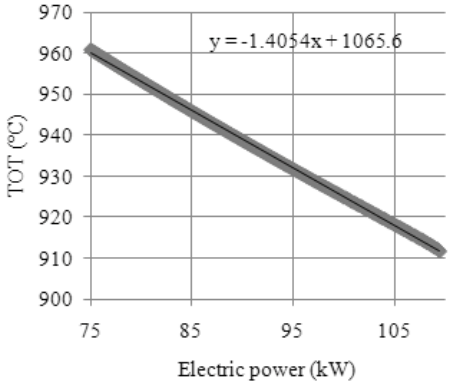


*Fig. 7. Turbine outlet temperature as the function of the electric load*

This expression allows one to reduce variations in the inlet turbine temperature at partial load. The corresponding fuel impact is shown in Figure 8.

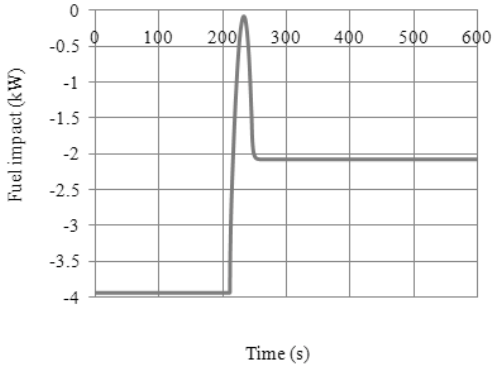


*Fig. 8. Total fuel impact using the second control strategy*

Additional improvements may be obtained acting on the control parameters. Figure 9 shows the effects on the energy consumption in the transient process provoked by modifying two control parameters: the proportional coefficient in the higher loop (red line) and the proportional coefficient in the lower loop (blue line).

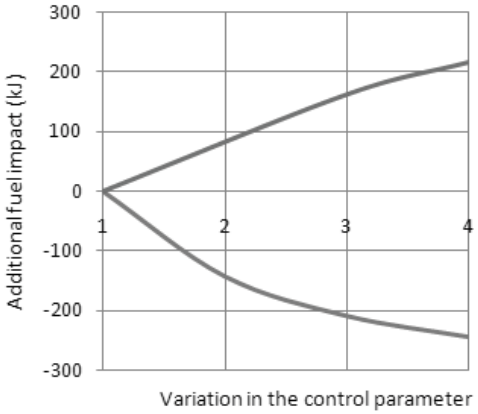


*Fig. 9. Effect provoked by variations in control parameters*

Both parameters are increased with respect to the design value, by multiplying for a term larger than 1. It is shown that an increase in the first parameter causes an additional fuel impact. A reduction has not been considered as it affect the steady state values, causing additional fuel impact. The second parameter allows one to reduce the fuel impact.

This basically corresponds to the elimination of the pick appearing in Figure 8 and a linear passage from the fuel impact corresponding with the initial steady state to that of the final steady state.

## Conclusions

Control systems are usually analyzed on the basis of their stability and robustness. In this paper thermoeconomic analysis is used to evaluate, compare and improve control strategies for an energy system, considering their effects on primary energy consumption. The fuel impact formula, written for a transient system is used for this goal. This tool has shown to be used both as an indicator to evaluate the control performance and as a way to improve the control strategy.

Further work is focused on the evaluation of economic aspects of the control system. This is particularly important as some of the control strategies may be very effective in terms of energy savings but they may affect the plant lifetime.

## References

[1] L.M. Hajagos, G.R. Bérubé (2001). Utility experience with gas turbine testing and modeling. IEEE PES winter meeting. Vol. 2. 152-158.

[2] F. Jurado (2002). Study of molten carbonate fuel cell-microturbine hybrid power cycles. Journal of Power Sources.

[3] F.G. Shinskey (1978). Energy Conservation through control. Academis Press. New York.

[4] Y.M. El-Sayed (1999). Thermoeconomics of some options of large mechanical vapor-compression units. Desalination 125: 251-257.

[5] D.F. Rancruel, M. R. von Spakovsky (2006). Decomposition with thermoeconomic isolation applied to the optimal synthesis/design and operation of an advanced tactical aircraft system. Energy 31: 3327–3341

[6] V. Verda, L. Serra, A. Valero (2004). The effects of the control system on the thermoeconomic diagnosis of a power plant. Energy 29: 331-359

[7] V. Verda, R. Borchiellini (2004). Exergetic and economic evaluation of control strategies for a gas turbine plant. Energy 29:2253-2271

[8] Bejan A, Tsatsaronis G, Moran M. Thermal Design and Optimization. New York: John Wiley and Sons, 1996

[9] Lozano MA, Bartolomé JL, Valero A, Reini M. Thermoeconomic Diagnosis of Energy Systems. In: Carnevale E, Manfrida G, Martelli F. Flowers 94. Florence World Energy Research Symposium. Padova: Sge, 1994. 149-156.

[10] Reini M., Taccani R. On Energy Diagnosis of Steam Power Plants: a Comparison among three Global Losses Formulation. International. Journal of Applied Thermodynamics. 2002; 5: 177-188.

[11] Valero A, Torres C, Lerch F, Royo J, Serra L. Structural Theory and Thermoeconomic Diagnosis. Part I: On Malfunction and Dysfunction Analysis. Energy Conversion and Management 2002; 43: 1503 – 1518.

## Annex

The microturbine is a power generation system that is based on a combination of a small gas turbine and a directly driven high-speed generator.
The basic components of the microturbine system modelled are the compressor, the recuperator (air pre-heater), the combustion chamber and the turbine generator.
The heart of the microturbine is the compressor – turbine package, which is commonly mounted on a single shaft along with the electric generator.
Recuperators are heat exchangers that use the turbine hot exhaust gas to preheat the compressed air going into the combustor, thereby reducing the fuel needed to heat the compressed air to turbine inlet temperature. The generator is placed on the same shaft as the compressor and the turbine.
The electricity created by the high-speed generator is converted into AC voltage with a constant frequency by a power converter that is a part of the power electronics. The power electronics control the electric variables of the microturbine and the machine can readily be connected to the power grid.
Only compressor – turbine package, recuperator and combustion chamber have been modelled; electric generator equations are been neglected, and so friction.
The model is built in Engineering Equation Solver (EES). System components modelled are

compressor, air pre-heater, combustion chamber, gas turbine and heat exchanger.
Inlet air temperature, induction pressure and rotation speed (number of revolutions) have been assigned; in design conditions the air compressor is characterized by a pressure ratio of 4.9 and an isentropic efficiency of 0.8. Delivery temperature has been calculated assuming the transformation as adiabatic.
Off design conditions are modelled through proper characteristic maps; the compressor maps express pressure ratio ($\beta_c = p_2/p_1$) and isentropic efficiency as the function of the non-dimensional mass flow rate (corrected air mass flow rate, $\frac{G_{ac} \cdot \sqrt{T}}{p}$ ) and the non-dimensional speed (corrected shaft rotation speed, $\frac{N_c}{\sqrt{T}}$).

Heat exchangers (air pre-heater and exhaust gas – water heat exchanger) are modelled using the ε-NTU method. This consists of the energy equation applied to hot and cold fluids as well as a set of equations depending on the heat exchange configuration. These equations relate one of the outlet temperatures to the inlet temperatures, the two heat capacities, the heat transfer area and the overall heat transfer coefficient. This approach can be used both for the design conditions and the off-design conditions.
The product of exchange area and heat transfer coefficient (UA) has been set to 4.13.
The combustion chamber is modeled with energy conservation equations. The microturbine burns natural gas, with a lower heating value of 47432 kJ/kg. The burner has an efficiency of 0.98.
In nominal conditions, the fuel mass flow rate has been set to 0.007667 kg/s, but in off-design conditions it changes according to energy balance wrote for system component and on the basis of the off design value of air and gas mass flow rates.
The turbine is installed on the same shaft as the compressor, producing enough torque to power the compressor and the generator. In design conditions the microturbine isentropic efficiency is equal to 0.84 and the pressure ratio about to 4.6; off-design conditions of the microturbine are modelled through proper characteristic maps. Similarly as the compressor, turbine maps express the pressure ratio ($\beta_t = p_4/p_5$) and the turbine isentropic efficiency as function of corrected mass flow and the corrected speed:

$$\beta_t = \beta_t(G_t/G_{t,N}, N_t/N_{t,N})$$

$$\eta_t = \eta_t(G_t/G_{t,N}, N_t/N_{t,N})$$

where $\frac{G_t \cdot \sqrt{T}}{p}$ is the corrected mass flow and $G_{t,N}$ the corresponding value in design conditions, $\frac{N_t}{\sqrt{T}}$ is the corrected speed, $N_{t,N}$ is the corresponding value in design conditions, $\beta_t$ is the pressure ratio in off design conditions and $\eta_t$ is the efficiency in off design conditions.
The end point of the system is an heat exchanger that interfaces exhaust gases and use water. Inlet and outlet water temperature is fixed respectively to a value of 333 K and 353 K , whereas it has been assumed that water flow rate can vary. As for the air pre – heater, heat exchanger has been modelled using ε-NTU method. The product of exchange area and heat transfer coefficient (UA) has been set to 3.32.

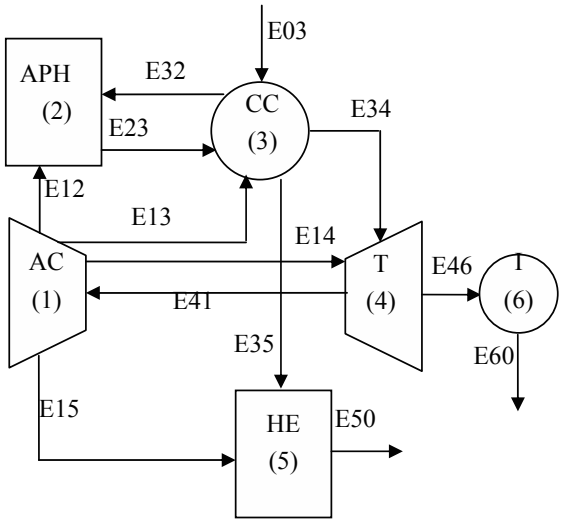


*Fig. A1. Productive structure of the microturbine.*

The heart of thermoeconomic analysis is represented by the productive structure of the power plant, which is the mathematical expression of the role played by every component in the system. This description leans on the concepts of fuel and product. In modern thermoeconomics

fuels and products are expressed as exergy flows. A general representation of the productive structure can be obtained by using the structural theory. A possible productive structure corresponding to the analyzed plant is represented in figure A1.

The compressor has one resource, the mechanical power supplied by the turbine ($E_{41}$) and four products: mechanical and thermal exergy supplied to the air pre-heater ($E_{12}$) and mechanical exergy supplied to the combustion chamber ($E_{13}$), to the turbine ($E_{14}$) and to the heat exchanger ($E_{15}$).

The air pre-heater uses thermal exergy, that is considered as produced by the combustion chamber ($E_{32}$) and mechanical exergy (associated with pressure losses) to increase the thermal exergy of the air flow ($E_{23}$). The combustor (CC) has three resources: the total exergy flow of the fuel ($E_{03}$), the mechanical exergy supplied by the compressor and the thermal exergy supplied by the air pre-heater and produces thermal exergy to feed the other components.

The turbine produces mechanical power, which is supplied to the air compressor and to the generator, which produces electricity ($E_{60}$).

The heat exchanger uses mechanical and thermal exergy to increase the thermal exergy of a water flow, supplied to the users ($E_{50}$).

$$E_{03} = m_3 \cdot H_i \tag{A1}$$

$$E_{12} = m_a \left[ c_{pa} \left( T_1 - T_0 - T_0 \ln \frac{T_1}{T_0} \right) + R \cdot T_0 \cdot \ln \frac{p_1}{p_2} \right] + m_g \cdot R \cdot T_0 \cdot \ln \frac{p_5}{p_6} \tag{A2}$$

$$E_{13} = m_g \cdot R \cdot T_0 \cdot \ln \frac{p_2}{p_4} \tag{A3}$$

$$E_{14} = m_g \cdot R \cdot T_0 \cdot \ln \frac{p_4}{p_5} \tag{A4}$$

$$E_{15} = m_g \cdot R \cdot T_0 \cdot \ln \frac{p_6}{p_0} \tag{A5}$$

$$E_{23} = m_a \cdot c_p \left( T_2 - T_1 - T_0 \ln \frac{T_2}{T_1} \right) \tag{A6}$$

$$E_{32} = m_g \cdot c_{pg} \left( T_5 - T_6 - T_0 \ln \frac{T_5}{T_6} \right) \tag{A7}$$

$$E_{34} = m_g \cdot c_{pg} \left( T_4 - T_5 - T_0 \ln \frac{T_4}{T_5} \right) \tag{A8}$$

$$E_{35} = m_g \cdot c_{pg} \left( T_6 - T_7 - T_0 \ln \frac{T_6}{T_7} \right) \tag{A9}$$

$$E_{41} = W_8 \tag{A10}$$

$$E_{46} = W_9 \tag{A11}$$

$$E_{50} = m_w \cdot c_w \left( T_{12} - T_{11} - T_0 \ln \frac{T_{12}}{T_{11}} \right) \tag{A12}$$

$$E_{60} = W_{10} \tag{A13}$$

# Exergoeconomic Optimization of Coupling MSF Desalination with Conventional Gas Fired Steam Power Plant

*M. H. Khoshgoftar Manesh [a, b], M. H. Hamedi [b], M. Amidpour [b] and L. Khoshgoftar [c]*

[a] *Iran Power Plant Project Management Co, (MAPNA GROUP), Neyrperse Co, Tehran, Iran*
[b] *Mechanical Faculty, K.N.Toosi University of Technology, Tehran, Iran*
[c] *Faculty of Economic, Allame Tabatabai University, Tehran, Iran*

**Abstract:** Steam power plants can provide both electrical and thermal energy in an integrated, co-generated fashion to produce a spectrum of energy products including electricity, desalted water, process heat, and district heating. Thermodynamic simulation programs are widely used for designing complex thermal systems but most of them don't incorporate second law optimization techniques. In this study, an efficient optimization strategy is presented, which integrates a well-known Evolutionary Algorithms optimization technique with a professional power plant and cogeneration simulator, so as perform exergoeconomic optimization of complex thermal systems and generating combined pinch and exergy representations. This paper deals with the application of an evolutionary algorithm to multiobjective exergoeconomic optimization of coupling desalination plant with steam power plant. The thermodynamic simulation of this plant has been performed in THERMOFLEX simulator. An Excel Add in called THERMOFLEX Link has been developed to calculate the exergy of each stream from a THERMOFLEX simulation results. In addition, computer code has been developed for thermoeconomic and improved combined pinch-exergy analysis in MATLAB environment. Both design configuration and the process variables are optimized simultaneously. The optimization algorithm can choose among several design options included in a superstructure of the feed water heaters and MSF desalination in dual purpose plant. For the assumptions and simplifications made in this study, a 315 MWe gas fired steam power plant similar to RAMIN power plant has been considered.

**Keywords:** Optimization, Exergoeconomic, Evolutionary Algorithm, Steam power plant, MSF

## 1. Introduction

Man is by nature an exploiter of resources. In time, it became apparent that there is a constraint on the rate of his exploitation since it is not practical to accelerate the renewal rate of resources set by nature and that human developments have to be sustainable. The depleting fuel resources, the depleting ozone layer, and the increasing carbon dioxide in the atmosphere offered the sufficient evidence that man has to live within nature's recycling rate of the essential life support elements. This is a basic law of life and is embodied in the laws of thermodynamics.

The main objective of a designer is to define the optimal plant configuration and operative conditions according to specified environmental constrains and to the user's requests. The most efficient configuration is not always the optimal one in term of product cost, since capital, labor and energy costs play a non-negligible role. A thermoeconomic analysis takes into account both fuel (i.e. energy and material) and capital costs (the latter include labor costs), and allows to determine the products cost on the basis of exergy criteria. This requires the determination of a functional quantitative interdependence between equipment, operations costs and efficiency.

Exergy, exergoeconomic and pinch methods can be applied for process analysis. Exergy analysis usually predicts the thermodynamic performance of an energy system and the efficiency of the system components by accurately quantifying the entropy-generation of the components.

Corresponding Author: Majid Amidpour, Email: amidpour@kntu.ac.ir

Furthermore, exergoeconomic analysis estimates the unit cost of products such as electricity, steam and quantifies monetary loss due to irreversibility [1], [2]. Also, this analysis provides a tool for the optimum design and operation of complex thermal systems. At present, such analysis is in great demand because proper estimation of the production costs is essential for companies to operate profitably [3].

In addition, combined pinch and exergy analysis help us to better understanding of system by graphical representation of each component information as Feng proposed in 1997 [4]. The strength of pinch analysis is that system information can be represented using simple diagrams and thus targets for the system under consideration can be readily obtained prior to design. In contrast, the power of exergy analysis is that it can identify the major causes of thermodynamic imperfection of thermal and chemical processes and thus promising modifications can be determined effectively [5]. The proposed method can represent a whole system, including individual units on one diagram, which helps to screen the promising modifications quickly for improving a base case design.

Furthermore, heuristic rules are often applied in the design and improvement of energy conversion systems to master the complexity of such systems and the uncertainties involved in some design decisions. Meanwhile, graphical representation as combined pinch and exergy analysis can help us to determination of promising modification and constraints for optimization. Particularly, interactions among the plant components, the very large number of possible design alternatives, and the lack of accurate cost data for all plant components at an early stage of the design process make the optimization of complex energy conversion systems a difficult task. Principles taken from the fields of artificial intelligence (e.g., expert systems [6]) and computational intelligence (e.g., fuzzy systems [7] and evolutionary algorithms can assist the process designer in the development of a cost-effective power plant concept. [8], [9], [10], [11], [12].

In general, the cost of electricity and desalted water are more sensitive to changes in the configuration of the plant components (process structure) than to modified values of the process variables. The objectives of this study are to optimization with an evolutionary algorithm by a commercial power plant and desalination simulation program. The approach is demonstrated for optimization of 1000 MWth PWR power plant such as Ramin power plant.

## 2. General information

A 315-MW gas fired steam power plant such as Ramin power plant was studied here, As shown in (Fig.1). RAMIN 315-MW gas fired steam power plant that is located in southwest of Iran in Ahvaz city. The detail specification of RAMIN plant at full load condition based on plant data and simulation results has been demonstrated in Table 1. As shown in Table 1, the type of fuel is natural gas that its Low Heating Value (LHV) is 48748 kJ/kg and the net plant efficiency based on LHV is about 38.54 %.

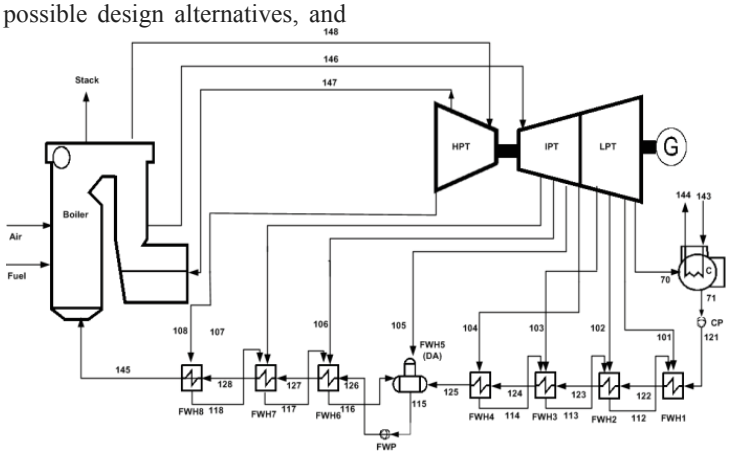


*Fig.1. PFD of a 315 MW steam power plant*

*Table 1. Detail specification of RAMIN plant*

| Parameter (Unit) | Plant data | Simulation |
|---|---|---|
| Fuel :NG, LHV (kJ/kg) | 46272 | 46272 |
| Boiler efficiency (%) | 93.87 | 93.89 |
| HPT efficiency (%) | 86.39 | 86.74 |
| LPT efficiency (%) | 87.99 | 88.12 |
| IPT efficiency (%) | 88.42 | 88.76 |
| Net heat rate (kJ/kWh) | 9340 | 9352 |
| Gross efficiency (%) | 40.20 | 40.71 |
| Net efficiency (%) | 38.54 | 38.73 |
| Net power (MW) | 315.019 | 316.11 |
| Net efficiency (%) | 38.54 | 38.59 |

Steam Pro Results is very similar to plant data that is shown high accuracy of simulation. Steam Pro is more reliable and accurate result for steam power plant rather other power plant or process simulation software such as IPSE-Pro, HYSYS and Aspen Plus.

## 3. Analysis

### 3.1. Exergy analysis

Exergy is the maximum theoretical useful work attainable from an energy carrier under the conditions imposed by an environment at given pressure p0 and temperature T0, and with given amounts of chemical elements [8], [9]. The purpose of an exergy analysis is generally to identify the location, the source, and the magnitude of true thermodynamic inefficiencies in thermal systems. Disregarding kinetic and potential energy changes the specific flow exergy of a fluid at any cycle state is given by [10]:

$$e = h - h_o - T_o(s - s_o) \quad (1)$$

The reversible work as a fluid goes from an inlet state to an exit state is given by the exergy change between these two states. That is:

$$e_2 - e_1 = h_2 - h_1 - T_o(s_2 - s_1) \quad (2)$$

where the subscripts 1 and 2 represent the inlet and the exit state for a flowing fluid. Now, we present the exergy destruction and exergy efficiency relations for various cycle components in plant [11], [12], [13].

### 3.2. Cost equation for plant component

All costs due to owning and operating a plant depend on the type of financing, the required capital, the expected life of a component, and so on. The annualized (levelized) cost method of Moran was used to estimate the capital cost of system components in this study. The amortization cost for a particular plant component may be written as:

$$PW = C_i - S_n PWF(i,n) \quad (3)$$

$$\dot{C}(\$/year) = PW \times CRF(i,n) \quad (4)$$

The present worth of the component is converted to annualized cost by using the capital recovery factor CRF(i,n), i.e [2],[14], [15]. Dividing the levelized cost by 8000 annual operating hours, we obtain the following capital cost for the kth component of the plant.

$$Z_k = \Phi_k \dot{C}_k / (3600 \times 8000) \quad (5)$$

The maintenance cost is taken into consideration through the factor $\Phi_k = 1.06$ for each plant component whose expected life is assumed to be 15 years [2], [16].

### 3.3. Thermoeconomic Modeling

The results from an exergy analysis constitute a unique base for exergoeconomics, an exergy-aided cost reduction method. A general exergy-balance equation, applicable to any component of a thermal system may be formulated by utilizing the first and second law of thermodynamics [1], [2], [14], [15]. The cost balance expresses that the cost rate associated with the product of the system (CP), the cost rates equals the total rate of expenditure made to generate the product, namely the fuel cost rate (CF), the cost rates associated with capital investment (ZCI), operating and maintenance (ZOM) [16], [17].

In a conventional economic analysis, a cost balance is usually formulated for the overall system (subscript tot) operating at steady state [8]:

$$C_{P,tot} = C_{F,tot} + Z_{tot} \quad (6)$$

To solve for the unknown variables, it is necessary to develop a system of equations applying Eq. (6) to each component, and it some cases we need to apply some additional equations, to fit the number

of unknown variables with the number of equations.

A general exergy-balance equation, able to any component of a thermal system may be formulated by utilizing the first and second law of thermodynamics.

## 4. Methodology

### 4.1. Mathematical Programming

In this, research Mixed Integer Non-Linear Programming (MINLP) as mathematical optimization method has been applied for finding optimum solution. The objective function is minimum production cost that related to summation of desalted water and electricity generation. However, in this step optimization method is based on one objective.

### 4.2. Evolutionary algorithms

Evolutionary algorithms apply an iterative, stochastic search strategy to find an optimal solution. Principles of biological evolution are imitated in a very simplified manner. Characteristic feature of an evolutionary algorithm is a population of individuals. An individual consists of the values of the decision variables (here: structural and process variables) and is a potential solution to the optimization problem. A "black box" model of the power plant and an objective function are used to evaluate the fitness of each individual. Pairs of individuals are selected to create new individuals based on their performance to optimize the objective function. In general, a constant number of individuals constitute the population in which deterministic and stochastic operators select and manipulate parts of the individuals. Individuals of the initial population are often generated randomly, but the results of previous optimization runs or expected optimal solutions might also be included. Each individual is evaluated to calculate its fitness. Here, the evaluation involves the simulation of the thermodynamic behavior of the power plant, estimates for the purchased-equipment costs, and an economic analysis. [7], [8], [10] and [11].

After a fitness value has been assigned to each individual in the initial population, some of the individuals are selected for the mating pool. Better individuals are given more opportunities to contribute to the next generation of new individuals ("survival of the fittest"). Next, recombination and mutation operators are applied to the individuals in the mating pool, producing the offsprings. These operators randomly combine and slightly modify the decision variables of different individuals in the mating pool so that an offspring might achieve a better fitness than its parents. Since the evolutionary algorithm maintains a fixed-size population, individuals with a higher fitness value are selected with a higher probability for the next generation (replacement, Fig. 3). The iteration loop is repeated several times until the maximum number of generations is reached. Evolutionary optimization techniques include genetic algorithms and evolution strategies among others.

The Pareto approach is not the only possible way to deal with multi-objective optimization. In fact, single objective approaches do not necessarily deal with fewer objectives than multi-objective approaches since they can weigh explicitly or implicitly multiple objectives into an overall single-objective function. The different optimal solutions on the Pareto front can then be obtained by varying the weight coefficients.

Thermo-economic or environomic analyses performed in the literature include more cost terms into a single objective function, so that a pure economic function with fixed weighting is considered in both cases. For clarity of presentation, the discussion on the difference between single- and multi-objective optimizations is limited in the following to the comparison between the traditional thermo-economic and the two-objective (energetic and economic) optimization. The same conclusions would be conceptually drawn by comparing the environomic and the three-objective (energetic, economic and environmental) approaches. The thermo-economic objective function to be minimized expresses the total cost rate as the sum of fuel and investment (equipment/maintenance) cost rates :

$$C_{tot} = C_{fuel}(C_w(X)) + C.\mathrm{inv}(X) \quad (7)$$

Where ε is the exergetic efficiency, and $X$ is a vector containing the design variables. $C_{tot}$ includes information in the fuel cost rate ($C_{fuel} = c_{fuel}.E_{fuel}$) through $E_{fuel}$ (fuel exergy flow rate), which directly depends on the desalted water production cost $C_w$ when the analysis is performed at constant total product. This dependence does not change the nature of the objective function, which still accounts for the total money to be spent. Thus, the two terms of the function, that in

principle are associated with two different objectives, merge into a single objective $C_{tot}$ implicitly including the desalted water production cost $C_w$ with the unit cost of fuel as a transformation coefficient. If $C_{tot}$ is minimized for a particular unit cost of fuel, only the extremum of the Pareto front corresponding to the economic minimum is found. On the other hand, in a single-objective approach considering both the thermodynamic and economic objectives ($C_w$ and $C_{tot}$), the overall single-objective function (to be maximized) would be constructed by combining the two functions through appropriate weights, as follows [11], [12]:

$$F(X) = w_1 \cdot C_w(X) - w_2 \cdot C_{tot}(X, C_w(X)) = w_1 \cdot C_w(X) - w_2 \cdot C_{tot}(X) \quad (8)$$

With $w_1 \geq 0$, $w_2 \leq 1$ and $w_1 + w_2 = 1$.

By varying the weight coefficients $w_1$ and $w_2$, the same optimal solutions belonging to the Pareto front of the multi-objective approach are obtained, one for each value of the weight coefficients.

The class of search algorithms that implement the Pareto approach for multi-objective optimization in the most straightforward way is the class of multi-objective evolutionary algorithms (MOEAs). MOEAs have been developed over the past decade [12]; severe tests on complex mathematical problems and on real-world engineering problems have shown that they can eliminate the above cited difficulties of classical methods. An evolutionary algorithm is a hybrid stochastic/deterministic optimization tool that imitates the natural evolution of biological organisms, i.e. a randomly initialized population of individuals (a set of points in the search space) evolves following the Darwinian principle of survival of the fittest. New individuals are created using some simulated evolutionary operators, such as crossover and mutation, and the probability of survival for these newly generated solutions depends on their fitness, that is on how well they perform with respect to the objective(s) of the optimization problem. Since MOEAs use a population of solutions during the search, a single run will find multiple Pareto-optimal solutions.

Multi-objective optimization problems generally show a possibly uncountable set of solutions, whose evaluated vectors represent the best possible trade-offs in the objective function space. Pareto optimality is the key concept to establish a hierarchy among the solutions of a multi-objective optimization problem, in order to determine whether or not a solution is really one of the best possible trade-offs. Let us first introduce the definition of Pareto dominance: a vector $u = (u_1,...,u_m)$ in the objective function space is said to dominate $v = (v_1,...,v_m)$ if and only if all the components of u are less or equal to the ones of v and at least one component of u is strictly less than the corresponding one in v . Then a solution $X = (X_1,...,X_n)$ of a multi-objective optimization problem is said to be Pareto optimal with respect to the entire decision variable space if and only if there is no other solution $X'$ for which $F(X') = (f_1(X'),...,f_m(X'))$ dominates $F(X) = (f_1(X),...,f_m(X))$. The set of Pareto optimal solutions is also called the Pareto Optimal Set and the set of the corresponding evaluated vectors in the objective function space is called the Pareto Front.

### 4.3. Computer Program

In this research, the proposed integrated exergoeconomic analysis and optimization technique exploits the power of the Thermofloex simulator. Exergy analysis has been performed in Excel environment. An Excel Add-in called Steam PRO/Thermoflex Link has been developed to calculate the exergy of each stream from a Steam PRO/Thermoflex simulation results. Meanwhile, the thermodynamic data from Excel environment as simulation data of Thermoflex has been exported to Matlab code. All optimization runs are controlled by a Matlab program which calls each program for (a) simulating a selected design, (b) estimating costs in Thermoflex and (c) conducting an exergy and exergoeconomic analysis in Excel-Thermoflex and Excel-Thermoflex-Matlab environment. The Matlab program also coordinates the data exchange (values of the decision variable and the objective function) between these programs and the evolutionary algorithm. The Genetic and Evolutionary Algorithm program for use with MATLAB 7.1 (Genetic Algorithm Tool Box) used in this study provides many useful functions and routines for applying an evolutionary algorithm to complex optimization problems. Figure 2 shows integration of optimization procedure with power plant simulator.

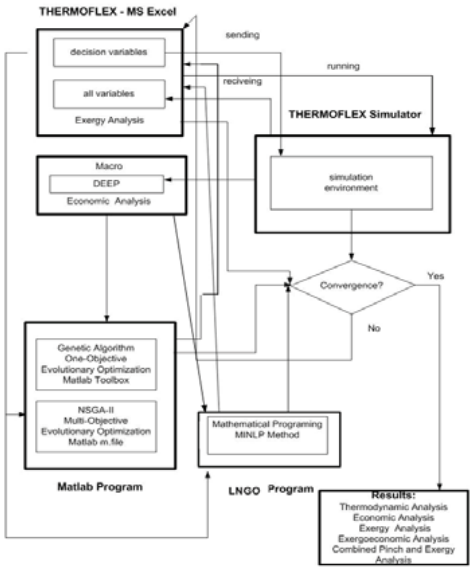


*Fig.2. Schematic of proposed algorithm*

### 4.4. Superstructure

The basic idea in the development of a superstructure is to include as many (promising) design configurations as possible. Here, the main focus is on a selected set of different design options such as using different Feed Water Heaters (FWHs) and connection of them to steam turbines. However, not all possible designs reconsidered. Nevertheless, the superstructure is complex enough to be a challenge for any optimization algorithm. In general, the superstructure can easily be extended. A discussion of coupling Multi Stage Flash Desalination (MSF) with steam powerplant (as dual purpose plant is considered, for example, provided here. Figure 3 shows the superstructure of a dual purpose plant used in this study. As shown, boiler and steam turbines are fixd and number, configuration and connection of FWHs and MSF desalination process are variables.

### 4.5. Decision variables

The evolutionary algorithm can modify both the structure of the plant and the values of the process variables whenever a new individual in the population considered by the algorithm is created. Structural variables take binary values (0 or 1) while process variables are real numbers restricted by the precision of the bit-string. Different values of the structural variables represent different interconnections among the plant components. For example, the evolutionary algorithm can select different connection of MSF process system with steam extraction paths from steam turbines. The term process variable denotes independent design specifications such as mass flow of desalted water production or net electricity production.

A total of 40 decision variables (22 structural variables and 18 process variables) can be simultaneously modified by the evolutionary algorithm. However, some constraints must not be ignored. If/then rules in the main control program add a penalty term to the fitness value whenever such a constraint is violated.

## 5. Results

In this paper, multi-objective optimization has been performed for finding minimum desalted water cost and minimum electricity cost in a dual purpose plant. In addition, one objective genetic and mathematical programming (MINLP) have been evaluated and comprised.

Optimum solution based on Pareto Front solution through evolutionary algorithm (NSGA-II) is shown in Fig. 4. Sensitivity analysis of multi-objective optimization by modification of specific fuel cost corresponding to Pareto optimal sets has been illustrated in Fig.5. Best configuration after multi-objective optimization of dual purpose plant is illustrated in Fig.6. As shown in Table 2, the minimum value of desalted water production rates obtained by multi-objective evolutionary algorithm is 3.65 ($/m$^3$) and minimum value for electricity generation is 0.055 ($/MJ); whereas the minimum values calculated by one objective genetic and MINLP approaches that are summarized in Table.1, are more than multi-objective evolutionary algorithm values. This reveals that the utilized multi-objective evolutionary algorithm for cost minimization of coupled plant is more efficient than the mathematical and one objective genetic optimization methods.

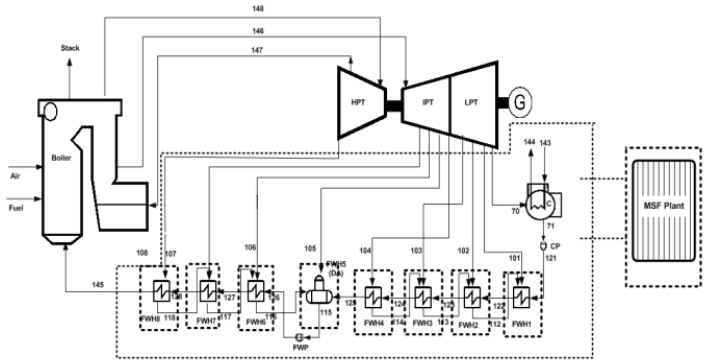


*Fig.3. Superstructure of dual purpose plant*

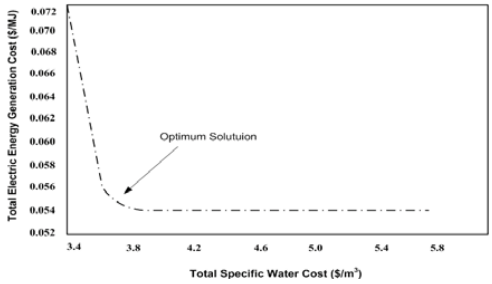


*Fig.4. Pareto optimum solution*

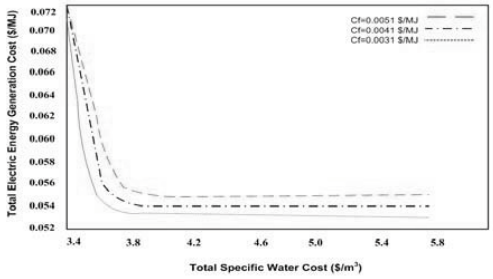


*Fig.5. Sensitivity analysis*

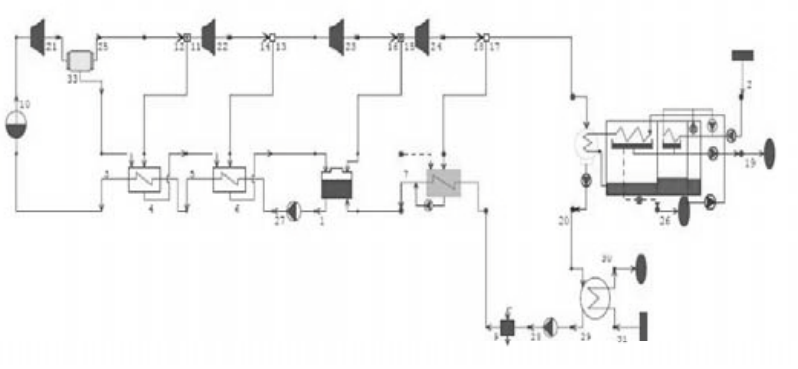

*Fig.6.Best configuration of dual purpose plant*

*Table.2. The result comparison of different optimization approaches*

| Variables | MINLP | One Objective Genetic Algorithm | Multi-Objective Genetic Algorithm (NSGA-II) |
|---|---|---|---|
| Specific Water Cost ($/m$^3$) | 4.19 | 4.21 | 3.65 |
| Electricity Generation Cost ($/MJ) | 0.064 | 0.062 | 0.055 |
| Net Electricity Generation (MW) | 163.41 | 164.0 | 170.979 |
| Electricity Consumption (MW) | 31.0 | 29.24 | 30.638 |
| Electricity Efficiency (%) | 16.01 | 18.12 | 20.92 |
| Total Desalted Water Flow Rate (kg/s) | 1705.1 | 1700.2 | 1794.6 |
| Brine Source Flow Rate (kg/s) | 8320 | 8321 | 8494 |

## 6. Conclusion

Thermodynamic simulation program are widely used for designing complex thermal systems but most of them don't incorporate second law optimization techniques. In this study, an efficient optimization strategy is presented, which integrates a well-known Evolutionary Algorithms optimization technique with a professional steam power plant and MSF desalination plant simulator, so as perform exergoeconomic optimization of complex thermal systems and generating combined pinch and exergy representations. Evolutionary algorithms are powerful tools to optimize process structure and process variables in view of thermoeconomic. About 53% of the time needed for applying this approach is spent to developing robust simulation of the thermodynamic behaviour of all possible process designs and to link this program to MATLAB where the evolutionary algorithm controls the optimization run.

An exergy-costing method has been applied to a dual plant to estimate the unit costs of electricity produced electricity and desalted water. The computer program that was developed which shows that the exergy and exergoeconomic analysis and thermoeconomic optimization of process configuration and process variables. Evolutionary Algorithm (NSGA-II) presented here can be applied to MSF- Steam Gas Fired Power plant as dual purpose plant systematically and elegantly.

## Nomenclature

| | |
|---|---|
| $c$ | cost per unit exergy ($/MW) |
| $cp$ | molar specific heat capacity (J/kmol.K) |
| $C$ | cost flow rate ($/hr) |
| $CP$ | heat capacity (J) |
| $CRF$ | capital recovery factor |
| $e$ | exergy rate per mass (MW/kg) |
| $E$ | specific exergy (MW) |
| $h$ | specific enthalpy (kJ/kg) |
| $i$ | interest rate |
| $m$ | mass flow rate (kg/s) |
| $N$ | Molar mass flow rate of saline water |
| $PWF$ | Present forth factor |
| $PW$ | Present worth |
| $P$ | pressure (bar) |
| $Pm$ | Probability of mutation |
| $R$ | universal gas constant (bar.m$^3$K$^{-1}$) |
| $s$ | specific entropy (MJ/K) |
| $T$ | temperature (°C) |
| $T_0$ | ambient temperature (°C) |
| $x$ | mol fraction |
| $W$ | shaft work, electricity (MW) |
| $Z$ | capital cost rate of unit ($/hr) |

**Greek symbols**

| | |
|---|---|
| $\Phi$ | Maintenance factor |
| $\rho$ | density (kg/m$^3$) |

**Superscript**

| | |
|---|---|
| CI | capital investment |
| OM | operating and maintenance cost |
| ph | Physical |
| ch | Chemical |

**Subscript**

| | |
|---|---|
| p | Product |
| f | Fuel |
| tot | Total |
| D | Destruction |
| L | Loss |
| k | kth component |
| 0 | without considering capital investment |
| d | Distillate |
| b | Brine |
| w | Water |
| dis | Discharge |
| Q | Heat transfer |
| i | Inlet |
| o | outlet |
| st | steam |
| s | saline water |
| m | mixture |
| W | shaft work |

## References


[1] Sanjay Y, Singh O, Prasad BN. Energy and exergy analysis of steam cooled reheat gas–steam combined cycle. *Applied Thermal Engineering* 2007; 27: 2779–2790.

[2] Chao Z, Yan W. Exergy cost analysis of a coal fired power plant based on structural theory of thermoeconomics. *Energy Conversion and Management* 2006; 47:817–843.

[3] Modesto M, Nebra SA. Analysis of a repowering proposal to the power generation system of a steel mill plant through the exergetic cost method, *Energy* 2006; 31: 3261–3277.

[4] Feng X, Zhu XX. Combining pinch and exergy analysis for process modifications. *Applied Thermal Engineering* 1997*;* 17: 250-260.

[5] Kotas TJ. The exergy method of thermal plant analysis. New York:Krieger; 1995.

[6] Cziesla F. Produktkostenminimierung beim Entwurf komplexer Energieumwandlungsanlagen mit Hilfe von wissensbasierten Methoden, no. 438 in Fortschr. -Ber. VDI, Reihe 6, VDI Verlag, D¨usseldorf, 2000.

[7] Cziesla F, Tsatsaronis G. Iterative exergoeconomic evaluation and improvement of thermal power plants using fuzzy inference systems. *Energy Conversion and Management* 2002; 43: 1537–1548.

[8] Uhlenbruck S, Lucas K. Exergoeconomically-aided evolution strategy applied to a combined cycle power plant. *International Journal of Thermal Science* 2004; 43: 289–296.

[9] Bejan A, Tsatsaronis G, Moran M. Thermal design and optimization. New York: Wiley; 1996.

[10] Dobrowolski R, Witkowski A, Leithner R, Simulation and optimization of power plant cycles, in: G. satsaronis, M. Moran F. Cziesla T. Bruckner (Eds.), ECOS 2002, Proceedings of the 15th International Conference on Efficiency, Costs, Optimization, Simulation and Environmental Impact of Energy Systems, Berlin, Germany, 2002, pp. 766–772.

[11] Emmerich M, Gr¨otzner M, Gross B, Sch¨utz M. Mixed-integer evolution strategy for chemical plant optimization with simulators, in: I. Parmee (Ed.), Evolutionary Design and Manufacture, Springer Verlag, Berlin, 2000, pp. 55–67.

[12] Emmerich M, Schutz M. Design of graph-based evolutionary algorithms: A case study for chemical process networks. *Evolutionary. Computation* 2001; 9 (3): 329–354.

[13] Durmayaz A, Yavuz Y. Exergy analysis of a pressurized water reactor nuclear power plant. *Applied Energy 2001;* 69: 39-57.

[14] Nafey AS, Fath HES, Mabrouk AA. Exergy and thermoeconomic evaluation of MSF process using a new visual package. *Desalination 2006;* 201: 224-240.


**Acknowledgments:** The author thanks MAPNA Group for financial and data support.

# Energy and Exergy Analysis of a Gas Turbine Power Plant with Inlet Evaporating Cooling Systems

*Mohammad Ameri*[*1], Mohammad Karimi[2], Pouria Ahmadi[3]*

[1]*Associate Professor, Energy Engineering Department, Power & Water University of Technology (PWUT), Tehran, Iran*
[2]*M.Sc Student, Energy Engineering Department, Power & Water University of Technology (PWUT), Tehran, Iran*
[3]*Ph.D Candidate, Department of Mechanical Engineering, Sharif University of Technology (SUT), Tehran, Iran*

**Abstract**

The gas turbine (GT) is known to feature low capital cost to power ratio, high flexibility, high reliability without complexity, short delivery time, early commissioning and commercial operation and fast starting–accelerating. Hence, researchers all over the world are working to increase the output power and efficiency of gas turbine cycle. One of the important techniques to increase the output power of such cycles is the compressor inlet air cooling method. The objective of this paper is to analysis the gas turbine cycle from both energy and exergy point of view. Thus, two important methods for increasing the output power, i.e. fog and media inlet air cooling systems are discussed. Moreover, the effect of some key parameters such as ambient temperature, air humidity and pressure drop at the compressor inlet are discussed. Finally, it has been shown that fog inlet air cooling method is slightly a better option in comparison with the media inlet air cooling. Moreover, it is concluded that by using evaporative cooling there is no change in compressor and turbine efficiency. Nevertheless, it reduces the thermal and exergy efficiencies of combustion chamber and increases the total cycle efficiency.

**Key words**: Gas turbine, inlet air cooling, exergy analysis, Fog, Media

## 1. Introduction

Gas turbines are almost constant volume machines at a given constant shaft speed. On the other hand, the gas turbine output power depends strongly on the inlet air mass flow rate. Therefore, the available output power considerably reduces when the air density decreases at high ambient temperatures [1]. In fact, the gas turbine performance is highly sensitive to the compressor inlet temperature. The output of gas turbine falls to a value that is less than the rated output under high temperature conditions. An increase of inlet air temperature by 18°C will decrease the output power by 0.7% approximately [2]. The solution of this problem is very important because the peak demand season also happens in the summer. One of the convenient methods for inlet air cooling is evaporating cooling which is appropriate for warm and dry weather. If the compressor works at the constant speed and constant position of inlet guide vane, the volume flow rate will be constant. Moreover, air mass flow rate decreases with increase in temperature. Therefore, increasing the ambient temperature results in the decrease of density as well as mass flow rate according to the following formula:

$$\left.\begin{array}{l} P=\rho RT \;\rightarrow\; \rho \propto \dfrac{1}{T} \\ m=\rho V \;\rightarrow\; m \propto \rho \end{array}\right\} \Rightarrow m \propto \frac{1}{T}$$
$$\frac{\dot{W}_{comp}}{\dot{m}} = \frac{h_2-h_1}{\eta_{comp}} = \frac{C_P(T_2-T_1)}{\eta_{comp}} = \frac{C_P T_1}{\eta_{comp}} \times \left[ \left( \frac{P_2}{P_1} \right)^{\frac{k-1}{k}} - 1 \right] \quad (1)$$

According to this formula, compressor work per unit of air mass flow rate is a function of compressor pressure ratio and compressor inlet temperature. At the constant compressor pressure ratio when inlet temperature increases the compressor work increases as well. There are a lot of researchers all over the world who have worked on gas turbine inlet air cooling method. Ameri *et al.* [3] have studied the installation of fog inlet air cooling system for six Frame5 (25MW) gas turbines. The results of that study showed that the

* Corresponding Author: Mohammad Ameri, Email: ameri_m@yahoo.com

output power of each gas turbine was increased by 3 MW. Also, they showed that the fog system was very cheap in comparison with the installation of new gas turbines. Mahmoudi *et al.* [4] investigated the energy and exergy analysis of gas turbine inlet air cooling method by absorption chiller. The results showed that effect of inlet air cooling at higher compressor pressure ratio has a great effect on increasing the efficiency and output power. Moreover, it results decrease of simple cycle irreversibilities. Shanbghazani *et al.* analyzed the thermodynamic modeling of a gas turbine power plant equipped with media evaporative cooler [5]. They also investigated the effect of cycle key parameters in order to enhance the output power and efficiency.

Moreover, there are a lot of researches which have studied the economical benefits of gas turbine inlet air cooling methods. Kakaras *et al.* [6] investigated the effect of three different inlet air cooling methods including evaporative air cooling, wet compression air cooling and absorption air cooling systems. The results showed that absorption cooling method has the major effect on increase of the output power while evaporative air cooling method is important from the economical point of view. Ameri *et al.* analyzed the effect of using the media and fog inlet air cooling method in some gas turbine power plants [2]. They used the installation test data to compare these two methods respectively. The results showed that both methods are suitable for the dry and hot areas for gas turbine power augmentation.

The objective of this study is to use the energy and exergy analysis methods to evaluate the air cooling method used for enhancing the gas turbine power plant. Therefore, two common important methods (i.e. media and fog systems) have been considered. The energy and exergy analysis of a gas turbine power plant have been carried out based on the performance test data obtained from evaporative air cooling methods. Also the effects of evaporative cooling on the exergy loss of each component have been investigated. Finally, the difference of these two methods will be discussed by using a theoretical thermodynamic modeling.

## 2. Thermodynamic Modeling

### 2.1. Compressor

The schematic of a gas turbine power plant with compressor inlet air cooler is shown in Fig.1. Air enters the compressor after passing through the cooler. If the cooler is of evaporative type, the outlet condition will be derived as it follows:

$$\begin{aligned} &T_1 = T_0 - (T_0 - T_{wb}) \times \eta_{hu} \quad , \quad P_1 = P_0 \\ &\varphi_1 = F(T_0, P_0, \varphi_0, T_1, P_1, T_{wb}) \end{aligned} \tag{2}$$

In which $\eta_{hu}$ is the evaporative cooler efficiency. This efficiency is from 90% to 98% for fog system and it is from 80% to 90% for media air cooling system respectively. The compressor outlet temperature is obtained by considering a compressor isentropic efficiency:

$$T_2 = T_1 = \frac{T_1}{\eta_C}\left[r_C^{(k_a-1)/k_a} - 1\right] \quad , \quad r_C = \frac{P_2}{P_1} \quad , \quad w_1 = w_2 \tag{3}$$

In which $r_c$ and $k_a$ are compressor pressure ratio and specific heat ratio. Also $\eta_C$ is compressor isentropic efficiency which is considered to be 0.83 in this study.

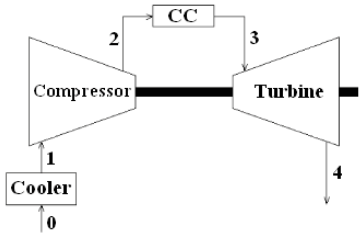


*Fig. 1 Schematic of a GT power plant with cooler.*

### 2.2. Combustion chamber (CC)

Fuel is injected into the combustion chamber and results in increase of the combustion products temperature. By applying the energy balance for a control volume around the CC the following relation is obtained:

$$\begin{aligned} \eta_{CC} &= \frac{\dot{m}_{total} \times h_3 - \dot{m}_{air} \times h_2}{\dot{m}_{fuel} \times LHV} \\ &= \frac{(1 + AF) \times Cp_{gas} \times T_3 - AF \times Cp_{air} \times T_2}{LHV} \\ P_3 &= P_2 - \Delta P_{CC} \quad , \quad w_3 = w_2 \end{aligned} \tag{4}$$

In which $\eta_{CC}$ is combustion chamber efficiency, LHV is the lower Heating Value of the fuel. In the present study, the fuel injected into the combustion chamber is $CH_4$ with the lower heating value (LHV) of 5000 kj/kg. In Eq. (4) AF is the air to fuel ratio. Combustion products leave the combustion chamber and enter the gas turbine to produce power.

### 2.3. Gas Turbine (GT)

The outlet temperature of the GT is obtained by considering the GT isentropic efficiency as it follows:

$$T_4 = T_3 \times \left(1 + \frac{\eta_t}{r_t^{(k_{gas}-1)/k_{gas}}} - \eta_t\right) \qquad r_t = \frac{P_3}{P_4} \quad , \quad w_4 = w_3 \quad , \quad P_4 = P_0 + \Delta P_0 \tag{5}$$

Here $\eta_t$ is the GT isentropic efficiency which is considered to be 0.9 in this study.

## 3. Exergy analysis

Exergy can be divided into four distinct components. The two important ones are the physical exergy and chemical exergy. In this study, two other components which are kinetic exergy and potential exergy are assumed to be negligible as the elevation and speed have negligible changes [7-11]. The physical exergy is defined as the maximum theoretical useful work obtained as a system interact with an equilibrium state. The chemical exergy is associated with the departure of the chemical composition of a system from its chemical equilibrium. The chemical exergy is an important part of exergy in combustion process.

In order to do the exergy analysis, mass and energy balances for the control volume are required to determine the flow rates and energy transfer rates at the control surface. If one applies the first and second laws of thermodynamics, one can find the formula for exergy balance as the following [7]:

Continuity equation:

$$\sum \dot{m}_i = \sum \dot{m}_e \tag{6}$$

Energy equation:

$$\dot{Q} - \dot{W} = \sum \dot{m}_e h_e - \sum \dot{m}_i h_i \tag{7}$$

Exergy balance equation:

$$\dot{E}_Q + \sum_i \dot{m}_i e_i = \sum_e \dot{m}_e e_e + \dot{E}_W + \dot{E}_D + \dot{E}_L \tag{8}$$

where subscripts i and e refer to streams entering and leaving the control volume, respectively. In this equation, (e) is the total specific exergy and $\dot{E}_D$ is the exergy destruction.

$$\dot{E}_Q = \left(1 - \frac{T_\circ}{T_i}\right)\dot{Q}_i \quad , \quad \dot{E}_W = \dot{W} \tag{9}$$

The physical exergy is defined by:

$$e_{physical} = (h - h_\circ) - T_\circ (S - S_\circ) \tag{10}$$

Where $T_0$ is the absolute temperature (K) and subscripts (i) and (o) refer to inlet and ambient conditions respectively.

Also chemical exergy is defined by:

$$\bar{e}_{Chemical} = \sum x_k \bar{e}_k^{Chemical} + \bar{R} T_0 \sum x_k \ln x_k \tag{11}$$

where $\bar{e}_k^{CH}$ is the molar chemical exergy of the *k*th component.

$$\dot{E} = \dot{E}_{ph} + \dot{E}_{ch} \quad \& \quad \dot{E} = \dot{m} e \tag{12}$$

Firs law and exergy efficiency of the GT cycle are defined as follow:

$$\eta_{ex} = \frac{\dot{W}_{net}}{\dot{m}_{fuel} \times e_{fuel}} \tag{13}$$

$$\eta_I = \frac{\dot{W}_{net}}{\dot{m}_{fuel} \times LHV} \tag{14}$$

## 4. Fog & media inlet air cooling systems test data

In this part two typical and practical cases installed for Iranian gas turbine power plants are considered. The Fog inlet air cooling system is installed in Yazd gas turbine power plant and media evaporating cooling is installed in Fars gas turbine power plant.

*Table 1. Exergy efficiency for gas turbine components.*

| | Turbine or Expander | Compressor, Pump, or Fan | Gasifier or Combustion Chamber |
|---|---|---|---|
| Component | 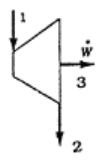 | 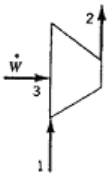 | 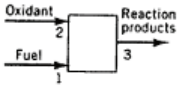 |
| $\dot{E}_P$ | $\dot{W}$ | $\dot{E}_2 - \dot{E}_1$ | $\dot{E}_3$ |
| $\dot{E}_F$ | $\dot{E}_1 - \dot{E}_2$ | $\dot{W}$ | $\dot{E}_1 + \dot{E}_2$ |
| $\varepsilon$ | $\frac{\dot{W}}{\dot{E}_1 - \dot{E}_2}$ | $\frac{\dot{E}_2 - \dot{E}_1}{\dot{W}}$ | $\frac{\dot{E}_3}{\dot{E}_1 + \dot{E}_2}$ |

### 4.1. Yazd Gas Turbine with fog system

Unit 1 of Yazd GT power plant is considered to analyze its performance with fog system. The system exergy is obtained before and after fog operation. The results are shown in Table (2).

*Table 2. Yazd gas power plant specification with fog system.*

| Parameter | Unit | Before Fog | After Fog | Variation | % of Variation |
|---|---|---|---|---|---|
| Ambient temperature | ºC | 37.58 | 38.66 | 1.08 | 2.87 |
| Ambient relative humidity | % | 7.4 | 7.1 | -0.4 | -4.9 |
| Ambient pressure | kPa | 87.17 | 87.15 | -0.02 | -0.02 |
| Compressor inlet temperature | ºC | 38 | 25.2 | -13.2 | -34.3 |
| Compressor outlet temperature | ºC | 377 | 359 | -18 | -5 |
| Compressor outlet pressure | bar | 8.7 | 9.29 | 0.59 | 6.86 |
| Supply water in Fog | lit/h | - | 9117 | - | - |
| Turbine outlet temperature | ºC | 565 | 555 | -10 | -2 |
| Power | MW | 89.9 | 100.5 | 10.6 | 11.8 |
| Thermal Efficiency | % | 29.38 | 30.28 | 0.9 | 3.07 |

Figures 2-4 demonstrate a better comparison between exergy efficiency and its losses for two different cases; i.e. with and without fog system.

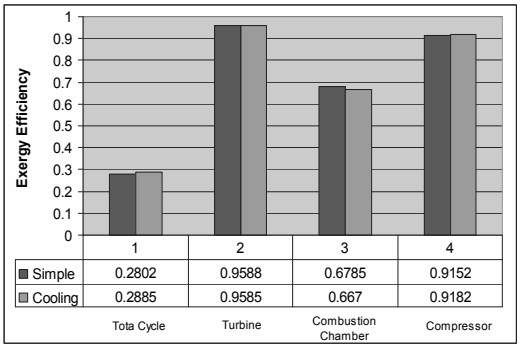


*Fig. 2 Exergy Efficiency for each GT component with and without fog system.*

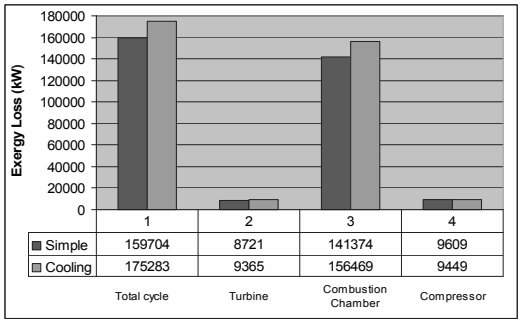


*Fig. 3 Exergy losses for each GT component with and without fog system.*

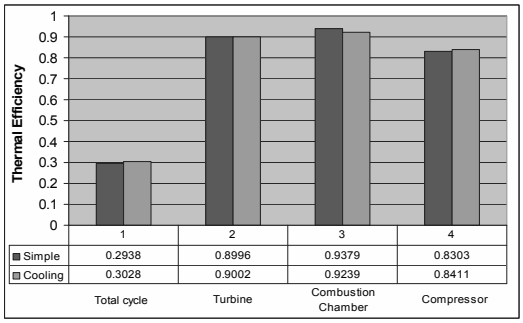


*Fig. 4 Exergy efficiency for each component with and without fog system.*

As it is clear, there are no significant changes in exergy efficiencies. However; combustion chamber has the most exergy loss, which leads to increase in cycle total exergy loss. Although increasing mass flow rate is the main purpose of inlet air cooling and it is the main cause of the increase in total exergy loss. Figure 4 compares the first law efficiencies, which has the same trend as the exergy efficiencies.

### 4.2. Fars gas turbine with media system

Table 3 presents the thermodynamic data for unit 1 Fars gas turbine power plant before and after media system operation.

According to the relations similar to what have been performed for fog system, total exergy for each point is calculated. Following figures give a better comparison of efficiency and losses for both cases. As it is seen, the variation trend is the same for both fog and media systems.

*Table 3. Fars gas turbine specification before and after media system operation.*

| Parameter | Unit | Before Media | After Media | Variation | % of Variation |
|---|---|---|---|---|---|
| Ambient temperature | ºC | 38.2 | 38.3 | 0.1 | 0.3 |
| Ambient relative humidity | % | 8.3 | 8.3 | 0 | 0 |
| Ambient pressure | kPa | 83.8 | 83.8 | 0 | 0 |
| Compressor inlet temperature | ºC | 40.6 | 22.7 | -17.9 | -44.2 |
| Compressor outlet temperature | ºC | 371 | 347 | -24 | -6.5 |
| Compressor outlet pressure | bar | 8.2 | 8.9 | 0.7 | 8.4 |
| Supply water in Media | $m^3/hr$ | - | 8.4 | - | - |
| Turbine outlet temperature | ºC | 560 | 549 | -11 | -1.9 |
| Power | MW | 76.6 | 87.7 | 11.1 | 14.5 |
| Thermal Efficiency | % | 28.19 | 29.10 | 0.91 | 3.23 |

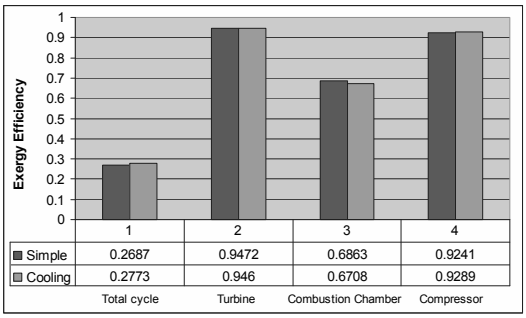


*Fig. 5 Exergy efficiency for each GT component with and without cooling system.*

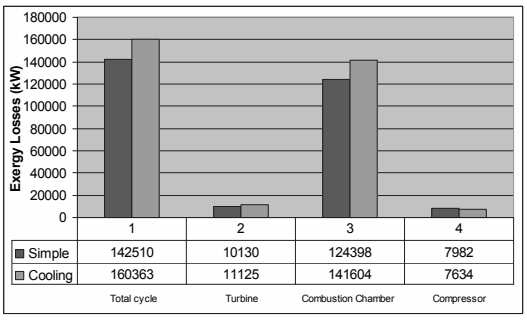


*Fig. 6 Exergy loss for each component with and without cooling system.*

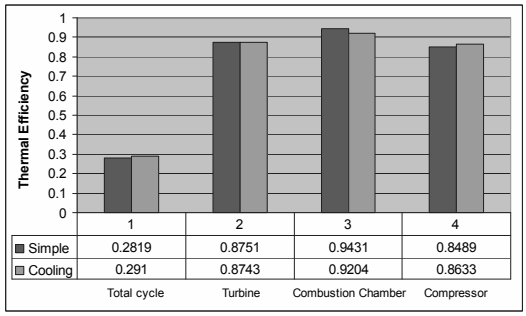


*Fig. 7 Thermal efficiency for each GT component with and without cooling system.*

## 5. Exergy efficiency

According to table 1, compressor exergy efficiency is the ratio of the change in inlet and outlet exergy to the change in enthalpy. Since for ideal gases, enthalpy is only a function of temperature, using a cooling system reduces both the inlet and outlet enthalpies. Moreover, this trend is true about exergy. Therefore; exergy efficiency for the compressor is nearly constant. This fact is also true for the turbine.

The decrease in the combustion chamber exergy efficiency is due to decrease in air to fuel ratio (A/F). In fact, the turbine inlet temperature (TIT) is kept nearly constant by GT control system. As the compressor outlet temperature & TIT is reduced due to the compressor inlet cooling system, more fuel is added to the combustion chamber to increase the TIT to its setting point. Therefore, air to fuel ratio will reduce as well.

$$\eta_{CC} = \frac{\dot{E}_3}{\dot{E}_{fuel} + \dot{E}_2} = \frac{(\dot{m}_{air} + \dot{m}_{fuel})e_3}{\dot{m}_{fuel} e_{fuel} + \dot{m}_{air} e_2} = \frac{(AF+1)e_3}{e_{fuel} + AF \cdot e_2} \quad , \quad AF = \frac{m_{air}}{m_{fuel}} \tag{15}$$

While the enthalpy of point 3 remains constant and the enthalpy of point 4 has a sensible decrease, the overall exergy efficiency increases. This is evident by the following equation:

$$\eta_{II} = \frac{\dot{W}_{net}}{\dot{E}_{Fuel}} = \frac{(AF+1)\times(h_3 - h_4) - AF \times (h_2 - h_1)}{e_{Fuel}} \tag{16}$$

## 6. Exergy loss

The inlet air mass flow has a significant effect on the exergy loss. Therefore, application of GT inlet air cooling system will increase the air mass flow

rate, which results in an increase in exergy loss. It was found that the combustion chamber is the greatest exergy destructor. However, the decrease in compressor loss is due to the significant decrease in enthalpy and exergy at its outlet, which overcomes the increase in exergy loss due to increase in inlet air mass flow rate. The GT cycle overall exergy loss increases due to considerable increase in combustion chamber loss.

## 7. Compressor & turbine thermal efficiency

Compressor and turbine efficiencies are given by Eq.(17) [12].

$$\eta_c = \frac{T_1\left[r_c^{\frac{k_{air}-1}{k_{air}}}-1\right]}{T_2-T_1} = \frac{r_c^{\frac{k_{air}-1}{k_{air}}}-1}{\frac{T_2}{T_1}-1}$$

$$\eta_t = \frac{T_3-T_4}{T_3\left[1-\frac{1}{r_t^{\frac{k_{gas}-1}{k_{gas}}}}\right]} = \frac{1-\frac{T_4}{T_3}}{1-\frac{1}{r_t^{\frac{k_{gas}-1}{k_{gas}}}}} \qquad (17)$$

## 8. Comparison of fog and media systems

The differences between fog and media systems are:

- There is a higher pressure drop in the inlet duct of the media system
- Evaporating efficiency (relative humidity after air cooling) in the media system is lower than in the fog system. Maximum evaporating efficiency in the media system is 90% and in the fog system is 98%.
- Media system needs a lower pressure pump. However, it needs a higher amount of water mass flow rate.

Now, one should evaluate those systems based on the differences.

### 8.1. First difference: Inlet air pressure drop

Figure 8 shows the effects of compressor inlet air pressure drop on the output power ratio and simple GT cycle efficiency ratio, with respect to standard ambient condition (P = 101.3kPa , T = 15˚C and relative humidity = 60%) . In this figure, PW and PE are obtained based on the following relations:

$$PW = \frac{\dot{W}-\dot{W}_S}{\dot{W}_S} \quad , \quad PE = \frac{\eta-\eta_S}{\eta_S} \qquad (18)$$

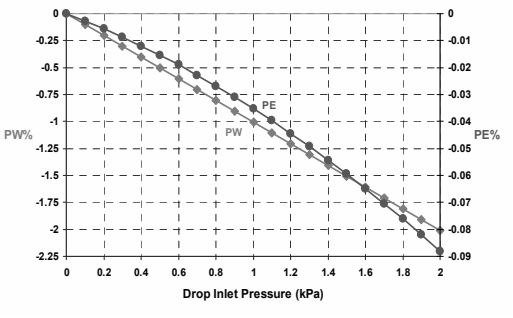


*Fig. 8 Effect of compressor inlet pressure drop on PW% and PE%.*

The parameters without subscript show the final state regarding the changes and subscript "s" refers to standard condition. As it is obvious, pressure drop does not have a strong effect on efficiency. In fact, there is a slight decrease (0.035% per 1 kPa pressure drop), which is less than 0.01% for the GT cycle efficiency. There is about 1% decrease in GT output power for each 1 kPa pressure drop in the compressor inlet duct. Media system always encounters a fixed pressure drop (i.e. 60 Pa) even if it is not working. Therefore, in this case, the priority should be given to fog system although its advantage is marginal.

### 8.2. Second difference: Evaporation efficiency

The maximum evaporation efficiency of the media system is around 90% (8% less than the maximum evaporation efficiency of the fog system i.e. 98%). Therefore the media system can not use the maximum available cooling capacity. Figure 9 shows the percentage of differences in output power ratio (PW) and efficiency ratio (PE) for two common evaporating systems efficiencies, i.e. 95% (fog), and 85% (media).

As one can see, this 10% difference of evaporating efficiency has a notable effect on both output power and efficiency. For example, for ambient temperature of 40˚C, there is 2.1% increase in output power and 0.47% increase in effective efficiency. Therefore; if the output power for the simple GT cycle is 100 MW and the efficiency is 30%, the 10% difference is evaporating efficiency

results in 2.1 MW and 0.141% increase in output power and overall efficiency respectively.

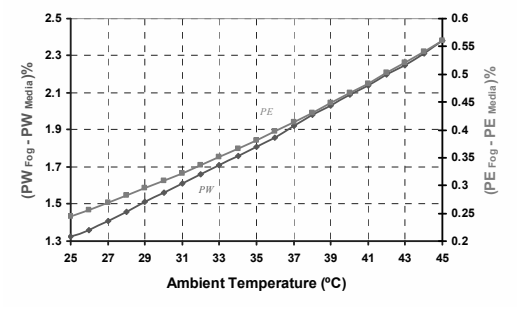


*Fig. 9 Difference between PW% and PE% terms for $\eta_{Eva} = 95\%$ (Fog) and $\eta_{Eva} = 85\%$ (Media) versus ambient temperature.*

### 8.3. Third difference: pump power demand

The required water mass flow is $\dot{m}_{air}(\omega_2 - \omega_1)$. The design value is more than the calculated one to guarantee the evaporating process efficiency. For the above mentioned example the surplus water is near 2 to 4 kg/s. The pump power demand is:

$$\dot{W}(kW) = \dot{m}(kg/s) \times P(kPa) / \rho(kg/m^3) \quad (19)$$

The pump pressure for the media system is around 200 kPa. Nevertheless, the fog system pressure is from 130 to 200 bar. If one assumes the water density of 1000 kg/m$^3$, the pump power demand can be estimated:

$$\begin{aligned} \dot{W}_{Media} &= 4 \times 200/1000 = 0.6\,KW = 8 \times 10^{-4}\,MW \\ \dot{W}_{Fog} &= 3 \times 15000/1000 = 45\,KW = 0.045\,MW \end{aligned} \quad (20)$$

As it is clear, pump power demand of the media system is negligible, while it is nearly 50 times for the fog system. Although the power demand for the fog system is considerably higher than the media system, it still is in priority while choosing an inlet air cooling system for GT cycles.

## 9. Conclusion

In summary, the results of fog and media inlet air cooling systems for gas turbine power plants are briefed as it follows:

- Compressor isentropic efficiency and turbine efficiency remain almost constant.
- Combustion chamber efficiency is reduced.
- Combustion chamber is the main source of exergy destruction due to the high temperature difference between the flame temperature and flow which results in increase of the irreversibility.
- During cooling the exergy losses are reduced only in the compressor.
- The main source of exergy destruction is for increase in mass flow rate.
- Pressure drop in compressor inlet causes the decrease of output power. However, it does not have any considerable effect on the efficiency.
- The difference of output power for fog and media system with evaporative efficiencies of about 95% and 85% was significant and is not negligible.
- The pump power demand for fog system is very much higher than its demand for media system.
- Finally, it can be concluded that fog system is slightly a better option in comparison with media system as it has been shown in this research.

## 10. Nomenclatures

| | |
|---|---|
| Cp | Specific heat at constant pressure |
| e | Specific exergy (kJ kg $^{-1}$) |
| E | Exergy (kJ) |
| $E_D$ | Exergy destruction (kJ) |
| $E_L$ | Exergy loss (kJ) |
| h | Specific enthalpy (kJ kg $^{-1}$) |
| k | Specific heat ratio |
| LHV | Lower heating value (kJ kg $^{-1}$) |
| m | Mass (kg) |
| P | Pressure (kPa) |
| PE | Percent of efficiency change |
| PW | Percent of net power change |
| Q | Heat transfer (kJ) |
| R | Gas constant (kJ kg $^{-1}$K $^{-1}$) |
| r | Pressure ratio |
| s | Specific entropy (kJ kg $^{-1}$K $^{-1}$) |
| T | Temperature ($^o$C) |
| W | Work (kJ) |
| *w* | Specific humidity |
| x | Molar fraction |

**Greek symbols**

| | |
|---|---|
| $\eta_I$ | Thermal efficiency |
| $\eta_{II}$ | Exergy efficiency |
| $\eta_{\text{Eva}}$ | Evaporative cooler saturation efficiency |
| ρ | Density [kg/m$^3$] |
| $\varphi$ | Relative humidity |

**Subscripts and superscripts**

| | |
|---|---|
| cc | Combustion chamber |
| c | Compressor |
| t | Turbine |
| 0 | Reference ambient condition |
| • | Rate |
| 1 | Before cooler |
| 2 | After cooler |

## 11. References


[1] Kraneis.W., 2000, Increased importance of Evaporative coolers for gas turbine and Combined cycle power plants, VGB Power Tech, 80(9):22-25.

[2] Ameri, M., et al., 2007, Comparison of evaporative inlet air cooling systems to enhance the gas turbine generated power, Int. J. Energy Research, 31(15), 1483-1503.

[3] Ameri, M., et al., 2004, Gas turbine power augmentation using fog inlet air-cooling system, Proceedings of the ASME 7th Biennial Conference on Engineering Systems Design and Analysis, Manchester, U.K., 1: 73–78.

[4] Mahmoudi, S.M.S., and et al. 2009, Energy and exergy analysis of simple and regenerative gas turbines inlet air cooling using absorbtion refrigeration, Journal of Applied Sciences, 9(31), pp. 2399-2407.

[5] Shanbghazani, M., and Khalilarya, Sh., 2008, Exergy analysis of a gas turbine system with evaporative cooling at compressor inlet, Int. J. Exergy, 5(3), pp. 309-325.

[6] Kakaras, E., et al., 2006, Inlet Air Cooling Methods for Gas Turbine Based Power Plants, Journal of Engineering for Gas Turbines and Power, 128: 312-317.

[7] Ameri, M., et al., 2008, Exergy analysis of a 420 MW Combined Cycle Power Plant, Int. J. Energy Res., 32: 175–183.

[8] Cihan, A., et al., 2006, Energy-exergy analysis and modernization suggestions for a combined cycle power plant, Int. J. Energy Res. 30: 115–126.

[9] Bejan, A., et al., 1996, Thermal Design and Optimization, Wiley: New York Conference.

[10] Moran, M., 1989, Availability Analysis, Guide to Efficient Energy Use, Englewood Cliffs, NJ: Prentice-Hall.

[11] Ameri, M., et al., 2009, Energy exergy and exergoeconomic analysis of a steam power plant (A Case Study), Int. J. Energy Res., 33: 499–512.

[12] Weisman, J., Eckart, R., 1988, Modern Power Plant Eng., Prentice Hall of India.

# Thermoeconomic Diagnosis of 300 MW conventional fuel-oil based power plant, from exergetic cost to malfunctions analysis.

*Sanchez Cifuentes Augusto*[a], *Acevedo Galicia Luis E*[a].

[a]*Facultad de Ingeniería-UNAM,México D.F., Mexico*

**Abstract:** Exergy and thermoeconomic cost are the fundamental concepts for energy saving and optimization of systems. For this purpose, the diagnosis is the first step to discover and infer signs of malfunctions and dysfunctions quantifying the effects in terms of additional consumption of fuel resources. This work presents an exergetic cost analysis, its impact on the fuel, malfunction, dysfunction analysis and the thermoeconomic cost based on the F-P-L representation of a 300 MW conventional fuel-oil based power plant sited in Colima (México). A complete thermoeconomic diagnosis is presented for a 300 MW conventional fuel-oil based power plant. Exergetic efficiencies, irreversibilities, the thermoeconomic cost due to malfunctions and dysfunctions and the impact on the fuel consumption in each component of the power plant could be determined with The Theory of Exergetic Cost and The General Theory of Exergy Saving. Finally, the results of this analysis are complemented and compared at the same time with the analysis made by the computer program developed in CIRCE and the Dpt. of Mechanical Engineering of the University of Zaragoza (Spain), *Thermoeconomic Analysis of Energy System Software (TAESS)*.

**Keywords:** Diagnosis, Thermoeconomics, Exergetic Cost, Malfunctions, Dysfunctions, Fuel Impact.

## 1. Introduction

An optimal use of energy is fundamental when deciding on operation, evaluation, diagnosis and rehabilitation of power plants [1]. Thermoeconomic diagnosis refers to improving energy systems efficiency by locating and quantifying anomalies that cause additional fuel consumption.

In this paper, a complete thermoeconomic diagnosis is applied to the fourth unit of Manzanillo II, a 300 MW conventional fuel-oil based power plant sited in Colima (México) on the Pacific coast.

The physical structure of the power plant is presented first, followed by the productive structure which is built for determining exergetic cost, exergoeconomic cost of the internal flows, and final products in the power plant. The complete thermoeconomic diagnosis is also presented including exergetic efficiencies, irreversibilities, the thermoeconomic cost due to malfunctions and dysfunctions, and the impact on the fuel consumption in each component of the power plant. To obtain thermoeconomic diagnosis, a comparison was made between the reference operation mode and the real operation mode for three load cases: 100%, 75% and 50%. The monetary cost is calculated only for the 100% load case, in this particular research work.

## 2. Description of the Manzanillo II power plant

Manzanillo II is a 300 MW conventional fuel-oil based power plant sited in Colima (México). The structure of the plant contains the most significant mass and energy flow-streams considered in the analysis as shown in Figure 1.

The steam cycle is a conventional Rankine Cycle with superheating, reheating and feedwater heaters. The steam is expanded in three different turbine sections. In each section, steam is sent to feedwater heaters at different pressures. The low pressure turbine is a condensing turbine which transfers steam to a condenser where the cooling medium is the ambient. Depending on the required power, some streams are void. In the cases of 75% and 100% loads, flow “f” has neither mass nor energy. The same happens in the case of 50% load with flow “s”.

### 2.1. Thermodynamic simulation

With the operation data, both reference and real, from the power plant Manzanillo II and with the aid of spreadsheet, a complete model of the power plant was calculated for a 50% load, a 75% load and a 100% load.

Thermodynamic properties have been calculated applying the complement IAPWS IF97 Excel Steam Tables.

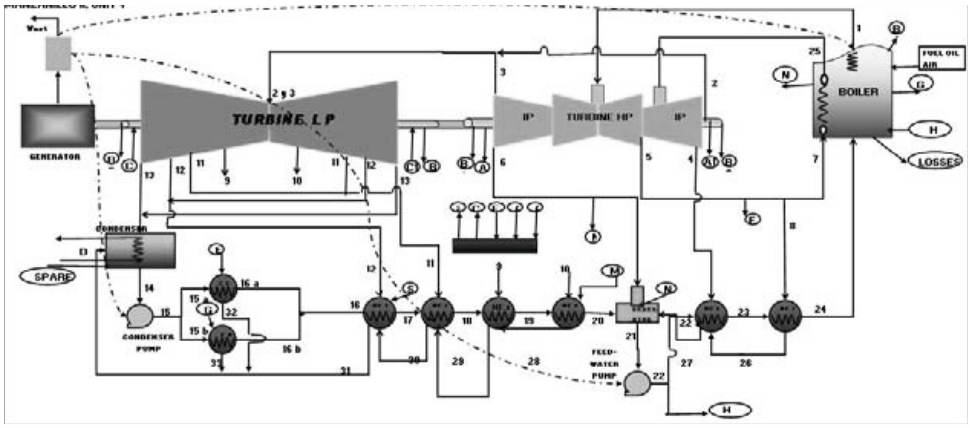


*Figure 1. Physical Structure of Manzanillo II, Unit 4.*

In order to perform the thermodynamic analysis of the plant, exergy flows are calculated through temperature and pressure values of reference environment considered in this analysis as: $T_0$=25 °C and $P_0$=101.3 kPa. The exergy of the plant fuel was calculated following the Methodology for Calculating Exergy in Chemical Process (Lozano and Valero, 1988) [2].

| Fuel oil: | |
|---|---|
| HHV [kj/kg] | 41,309.87 |
| Atomic composition by carbon atom (1/C): | |
| Carbon | 1.0000 |
| Hydrogen | 1.4439 |
| Oxygen | 0.0035 |
| Nitrogen | 0.0030 |
| Sulfur | 0.0159 |

| Conversion factor: | |
|---|---|
| Fi [mol C/kg] | 70.768 |
| HHV [kj/mol C] | 583.73 |
| $\Delta h^0$ [kj/mol C] | - 21.60 |
| $s^0$ [kj/mol C-K] | 0.03 |

| | [kj/mol C] |
|---|---|
| eI | 551.92 |
| eII | 583.74 |
| eIII | 589.12 |
| b fuel oil | 589.47 |
| b fuel oil [kj/kg] | 41716 |
| Diference with HHV | -1% |

*Table 1. Fuel Oil Exergy*

### 2.2. Physical structure

Once all thermodynamic properties were calculated, we reorganized the power plant as a set of subsystems linked firstly among themselves, then to the environment by means of matter, heat and work flows. Consequently, diagnosis was carried out in a better way.

This is to say: *energy systems =subsystems + matter and energy flows* [3]

So this can be considered as the incidence matrix (A) which is the basis for the balances of matter, energy and destroyed exergy, through:

$$A \times M = 0 \qquad (1)$$

$$A \times E = 0 \qquad (2)$$

$$A \times B = D \qquad (3)$$

Where A (18x63), M, E, and B are the column vectors (m=63) calculated in the thermodynamic simulation corresponding to mass, energy and exergy, respectively.

The destroyed exergy analysis is the first step to notice the possible changes between reference and real behaviour of the plant. An exergy efficiency comparison between them both will help to better understand how real irreversibilities affect the system. Figure 2 shows exergy efficiency for the three cases in the power plant.

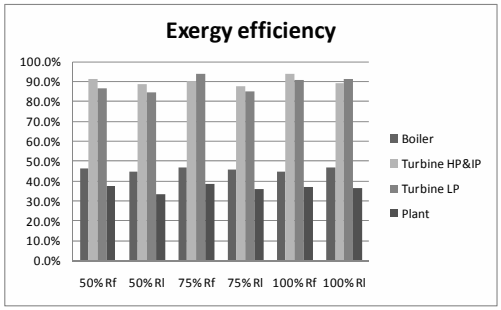


*Figure 2. Differences between reference (Rf) and real (Rl) exergy efficiency for the most representative units in the power plant.*

## 3. Exergetic Cost

Since any real process has irreversibilities, it is necessary to invest a bigger amount of exergy (exergetic cost) to obtain an exergy flow. Similarly, it is essential to know the connection among product, irreversibility increase and resources consumption for the diagnosis of the plant. With a higher irreversibility always comes a higher consumption of resources of the plant when product remains constant.

### 3.2. Productive structure

Flows and units are part of the physical structure; each unit with its flows has a particular productive function that contributes to get the final product, in this case, the net electrical power. In order to

define this productive function, the energetic transformations taking place in the plant are examined as Fuel (F), Product (P) and Losses (L).

Table 2 shows the F-P-L definition assigned to the units or subsystems of the power plant. Using the F-P-L definition, it is possible to develop matrices for each one: $A_F$, $A_p$, and $A_L$.

| SUBSYSTEM | | FUEL F | PRODUCT P | LOSSES L |
|---|---|---|---|---|
| BOILER | GV | Fuel + Air | B1+N-H<br>G+25-24<br>1-7 | Loss+ Heat loss in Boiler<br>+Combustion gases |
| TURBINE HP&IP | TAI | 1+25<br>2+3<br>4+7<br>8+6<br>A1+A2<br>B2+B3) | WTAI | |
| TURBINE LP | TB | 2-9-10<br>3-11-12<br>C1-13-B4<br>C2-B5 | WTB | |
| CONDENSER | C | 13+31<br>32+33+Spare | 14 | Condenser heat rejected |
| CONDENSER PUMP | BB | WBB | 15A+15B-14 | |
| FEED-WATER PUMP | BA | WBA | 22A+H-21 | |
| STEAM SEALING CONDENSER | CS | B1+B2<br>B3+B4<br>B5+15A | 16A+32 | |
| EJECTOR | EA | G+15B | 16B+33 | |
| HEATER 1 | C1 | 12+S<br>30-31<br>*12+30-31 | 17-16A-16B | |
| HEATER 2 | C2 | 11+29-30 | 18-17 | |
| HEATER 3 | C3 | 9+28+18 | 19+29 | |
| HEATER 4 | C4 | 10+M-28 | 20-19 | |
| DEAERATOR | D | 6+N<br>27+20 | M+21 | |
| HEATER 6 | C6 | 4+26-27 | 23-22A | |
| HEATER 7 | C7 | 8+23 | 24+26 | |
| STEAM REGULATOR | RVS | A1+A2<br>*A1+A2+F | S+C1+C2<br>*C1+C2 | |
| ELECTRIC GENERATOR | GE | WTAI+WTB | E GE | Heat EG |
| ELECTRIC TRANSFORMER | T | E. GE | Wnet+WBB+WBA | Heat T |
| PLANT | PLANT | Fuel+Air+Spare | Wnet | Loss+ Heat loss in Boiler<br>+Combustion gases+Condenser H.R.<br>+ Heat EG+Heat T |

*Table 2. Productive structure of the Manzanillo II power plant. *Equations used only in the 50% load case.*

### 3.3. Determination of the exergetic cost

For this purpose, it must have been taken into account the four propositions developed by Valero at al [3].

1. The exergetic cost of a flow, fuel or product is the quantity of exergy needed to produce it.
2. In the absence of an external assessment, the exergetic cost of the flows entering the plant equals the exergy
3. All cost generated by the productive process must be included in the cost of final products.
4. If an output flow of a subsystem is a part of the fuel of this subsystem, or if a subsystem has a product composed by several flows, then the same unit exergetic cost will be assigned to all of them.

The exergetic cost balance of the subsystems corresponds to the next equation:

$$A \times B^* = 0 \qquad (4)$$

It is already known that the number of flows is bigger than the number of subsystems, and to solve the assign cost problem, (m-n) equations are needed. This entails the need of a $\alpha$ matrix (m-n, m) and a vector column $\omega$ (m-n) that satisfy [3]:

$$\begin{bmatrix} A \\ \alpha \end{bmatrix} \times B^* = \begin{bmatrix} 0 \\ \omega \end{bmatrix} \rightarrow A \times B^* = Y^* \qquad (5)$$

Table 3 contains the auxiliary equations for calculating the exergetic cost; these equations were obtained using the propositions 1 to 4 in the analyzed power plant.

| α Equations uisng propositions 1 to 4 | | | |
|---|---|---|---|
| 1 | Bfuel=B*fuel | 24 | B*10/B10-B*11/B11=0 |
| 2 | Bair=B*air | 25 | (B*29-B*30)/(B29-B30)-B*11/B11=0 |
| 3 | Bspare=B*spare | 26 | B*12/B12-B*13/B13=0 |
| 4 | Bloss=0 | 27 | B*13/B13-B*B4/BB4=0 |
| 5 | Bheat loss in boiler=0 | 28 | B*B4/BB4-B*B5/BB5=0 |
| 6 | B combustion gases=0 | 29 | B*C1/BC1-B*C2/BC2=0 |
| 7 | B*17/B17-(B*16A+B*16B)/(B16A+B16B)=0 | 30 | B*C2/BC2-B*S/BS=0<br>[1]B*B3/BB3-B*F/BF=0 |
| 8 | Bheat EG=0 | 31 | B*15A/B15A-B*15B/B15B=0 |
| 9 | Bheat ET=0 | 32 | B*16A/B16A-B*32/B32=0 |
| 10 | B*1/B1-B*25/B25=0 | 33 | (B*26-B*27)/(B26-B27)-B*4/B4=0 |
| 11 | B*25/B25-B*N/BN=0 | 34 | B*16B/B16B-B*33/B33=0 |
| 12 | B*N/BN-B*G/BG=0 | 35 | B*17/B17-B*31/B31=0 |
| 13 | B*G/BG-B*B1/BB1=0 | 36 | B*18/B18-B*30/B30=0 |
| 14 | B*2/B2-B*3/B3=0 | 37 | B*19/B19-B*29/B29=0 |
| 15 | B*3/B3-B*6/B6=0 | 38 | B*20/B20-B*28/B28=0 |
| 16 | B*6/B6-B*7/B7=0 | 39 | B*21/B21-B*M/BM=0 |
| 17 | B*7/B7-B*8/B8=0 | 40 | B*23/B23-B*27/B27=0 |
| 18 | B*8/B8-B*4/B4=0 | 41 | B*WTA/BWTA-B*WTB/BWTB=0 |
| 19 | B*4/B4-B*A1/BA1 | 42 | B*22A/B22A-B*H/BH=0 |
| 20 | B*A1/BA1-B*A2/BA2=0 | 43 | B*ET/BET-B*WBB/BWBB=0 |
| 21 | B*A2/BA2-B*B2/BB2=0 | 44 | W*WBB/BWBB-B*WBA/BWBA=0 |
| 22 | B*B2/BB2-B*B3/BB3=0 | 45 | (B*M-B*28)/(BM-B28)-B*10/B10=0 |
| 23 | B*9/B9-B*10/B10=0<br>[1](B*15A+B*15B)/(B15A+B15B)-B*14/B14=0 | | |

*Table 3. Auxiliary α equations. *Equations used only in the 50% load case.*

After calculating the exergetic cost of the flows, it is possible to determine the exergetic cost of fuels and products, and the unit cost of all of them. Table 4 shows results for the real operation state at the three different percentages of loads.

### 3.4. Exergoeconomic cost

Calculating the monetary cost of the internal flows and final products in energy or chemical plants is a problem of the utmost importance [3]. When economics and thermodynamics work together, a direct link between productive process and monetary cost appears. This provides the capital cost and the operating and maintenance cost associated with each system component separately [4].

In most of the cases, inputs to analyze are the initial capital expenses, annual expenses, fuel cost and the escalation rates. Finally, the result of a conventional economic analysis is the cost of the final product of the system.

| Real operation state at: | 50% load | | | | 75% load | | | | 100% load | | | |
|---|---|---|---|---|---|---|---|---|---|---|---|---|
| Subsystem | $B_F$ [kw] | $k_F$* | $B_P$ [kw] | $k_P$* | $B_F$ [kw] | $k_F$* | $B_P$ [kw] | $k_P$* | $B_F$ [kw] | $k_F$* | $B_P$ [kw] | $k_P$* |
| BOILER | 448,891.44 | 1.00 | 202,016.77 | 2.22 | 622,481.46 | 1.00 | 284,070.26 | 2.19 | 802,450.52 | 1.00 | 374,919.82 | 2.14 |
| TURBINE HP&IP | 111,130.61 | 0.99 | 98,387.32 | 1.12 | 154,196.88 | 2.13 | 135,140.69 | 2.43 | 192,168.69 | 2.23 | 171,465.97 | 2.50 |
| TURBINE LP | 78,561.58 | 0.95 | 66,422.74 | 1.12 | 111,436.38 | 2.07 | 95,060.36 | 2.43 | 154,040.76 | 2.28 | 140,637.09 | 2.50 |
| CONDENSER | 10,206.51 | 26.81 | 87.78 | 47.54 | 15,876.96 | 4.63 | 87.30 | 3.71 | 25,562.72 | 1.65 | 636.61 | 1.03 |
| CONDENSER PUMP | 535.47 | 1.19 | 13.42 | 47.54 | 545.33 | 2.45 | 117.29 | 11.37 | 482.05 | 2.61 | 194.52 | 6.48 |
| FEED-WATER PUMP | 4,104.46 | 1.19 | 2,865.35 | 1.71 | 3,747.04 | 2.45 | 3,452.09 | 2.65 | 6,921.32 | 2.61 | 5,385.28 | 3.36 |
| STEAM SEALING CONDENSER | 132.24 | 28.57 | 65.77 | 57.44 | 132.68 | 6.95 | 122.39 | 7.54 | 452.12 | 2.28 | 451.35 | 2.28 |
| EJECTOR | 91.42 | 27.84 | 65.66 | 38.76 | 159.42 | 6.06 | 121.28 | 7.96 | 475.43 | 2.29 | 450.03 | 2.42 |
| HEATER 1 | 917.17 | 25.58 | 487.74 | 48.10 | 1,932.63 | 4.56 | 1,138.48 | 7.75 | 2,870.05 | 1.62 | 1,974.71 | 2.35 |
| HEATER 2 | 1,778.71 | 9.93 | 1,175.27 | 15.03 | 2,812.04 | 3.70 | 1,992.04 | 5.22 | 4,104.97 | 1.49 | 3,191.63 | 1.92 |
| HEATER 3 | 3,896.11 | 18.82 | 3,435.75 | 21.34 | 6,840.46 | 5.04 | 6,127.95 | 5.62 | 11,313.20 | 1.85 | 10,552.00 | 1.98 |
| HEATER 4 | 3,654.05 | 9.93 | 2,728.90 | 13.30 | 5,513.24 | 3.70 | 4,245.86 | 4.81 | 5,170.15 | 1.49 | 4,532.60 | 1.70 |
| DEAERATOR | 13,981.78 | 10.50 | 13,549.09 | 10.83 | 23,318.02 | 3.81 | 22,575.07 | 3.94 | 35,384.17 | 2.07 | 33,603.89 | 2.18 |
| HEATER 6 | 7,602.43 | 4.51 | 6,042.90 | 5.68 | 11,990.48 | 2.50 | 10,679.93 | 2.81 | 17,233.12 | 2.13 | 14,398.39 | 2.55 |
| HEATER 7 | 26,683.33 | 7.13 | 26,100.82 | 7.29 | 45,361.47 | 3.20 | 44,839.24 | 3.24 | 72,480.28 | 2.33 | 70,963.98 | 2.38 |
| STEAM REGULATOR | 105.45 | 4.51 | 105.44 | 4.52 | 276.32 | 2.50 | 276.26 | 2.51 | 301.41 | 2.13 | 301.34 | 2.13 |
| ELECTRIC GENERATOR | 164,810.06 | 1.12 | 159,865.76 | 1.16 | 230,201.06 | 2.43 | 229,510.45 | 2.44 | 312,103.06 | 2.50 | 305,861.00 | 2.55 |
| ELECTRIC TRANSFORMER | 159,865.76 | 1.16 | 155,240.85 | 1.19 | 229,510.45 | 2.44 | 228,893.32 | 2.45 | 305,861.00 | 2.55 | 298,605.36 | 2.61 |
| PLANT | 448,892.18 | 1.00 | 150,600.91 | 1.19 | 622,482.98 | 1.00 | 224,600.95 | 2.45 | 802,451.42 | 1.00 | 291,202.00 | 2.61 |

*Table 4. Exergetic Cost in the units of the power plant shown in Fig. 1.*

A conventional economic analysis is conducted for this 300 MW power plant. The procedure by Tsatsaronis [5] is used to evaluate the monetary cost of the internal flows and products of the plant.

Considering the previous equations for all the units of the plant, and following the equation:

$$\mathrm{A} \times \Pi = -Z \qquad (6)$$

Where Π is the unknown exergoeconomic costs of the (m) flows. Similar to the exergetic cost, auxiliary equations are needed to solve the problem, as follows: [5]

$$\begin{bmatrix} A \\ \alpha \end{bmatrix} \times \Pi = \begin{bmatrix} -Z \\ \omega_Z \end{bmatrix} \rightarrow \mathrm{A} \times \Pi = \vec{Z} \qquad (7)$$

Where $\vec{Z}$ is the vector that contains the external economic assessment.

Vector $\vec{Z}$ was defined with the data collected in the plant. In this case the capital expenses referring to the existing facility represent a sunk cost and do not need to be considered in this economic analysis. All costs are added to the fuel cost as a total cost. See Table 5.

| Manzanillo II | | | |
|---|---|---|---|
| **Energy production factors** | | | |
| Fuel Cost | $ | 3.12 | Doll/s |
| **Non-energy production factor** | | | |
| Cost level & Oparetion and Maintenance | $ | 1.57 | Doll/s |
| **Total** | $ | 4.69 | Doll/s |

*Table 5. Costs of Manzanillo II Power Plant.*

These data are for the 100% load case, after calculating the exergoeconomic cost of the flows. It is possible to determine the exergoeconomic cost of fuels and products, and the unit exergoeconomic cost of all of them. Table 6 shows results for the reference and real operation state at 100% load case.

| | Reference | | Real | |
|---|---|---|---|---|
| Subsystem | $c_F$ [doll/Gj] | $c_P$ [doll/Gj] | $c_F$ [doll/Gj] | $c_P$ [doll/Gj] |
| BOILER | $ 5.96 | $ 13.26 | $ 5.83 | $ 12.47 |
| TURBINE HP&IP | $ 13.01 | $ 13.84 | $ 13.00 | $ 14.57 |
| TURBINE LP | $ 12.56 | $ 13.84 | $ 13.31 | $ 14.57 |
| CONDENSER | $ 25.68 | $ 29.31 | $ 9.60 | $ 6.03 |
| CONDENSER PUMP | $ 14.25 | $ 43.53 | $ 15.23 | $ 37.75 |
| FEED-WATER PUMP | $ 14.25 | $ 20.19 | $ 15.23 | $ 19.58 |
| STEAM SEALING CONDENSER | $ 32.04 | $ 32.25 | $ 13.28 | $ 13.31 |
| EJECTOR | $ 29.44 | $ 33.76 | $ 13.34 | $ 14.09 |
| HEATER 1 | $ 23.91 | $ 33.00 | $ 9.43 | $ 13.70 |
| HEATER 2 | $ 8.43 | $ 10.12 | $ 8.68 | $ 11.17 |
| HEATER 3 | $ 15.59 | $ 16.25 | $ 10.77 | $ 11.54 |
| HEATER 4 | $ 8.43 | $ 9.25 | $ 8.68 | $ 9.90 |
| DEAERATOR | $ 14.39 | $ 15.16 | $ 12.09 | $ 12.73 |
| HEATER 6 | $ 13.93 | $ 14.35 | $ 12.43 | $ 14.88 |
| HEATER 7 | $ 14.73 | $ 14.73 | $ 13.58 | $ 13.87 |
| STEAM REGULATOR | $ 13.93 | $ 13.93 | $ 12.43 | $ 12.44 |
| ELECTRIC GENERATOR | $ 13.84 | $ 14.05 | $ 14.57 | $ 14.87 |
| ELECTRIC TRANSFORMER | $ 14.05 | $ 14.25 | $ 14.87 | $ 15.23 |
| PLANT | $ 5.96 | $ 14.25 | $ 5.83 | $ 15.23 |

*Table 6 . Unit exergoeconomic cost for the power plant working at 100% load.*

## 4. Thermoeconomic Diagnosis

Thermoeconomic diagnosis consists of identifying deviation of the components behavior, assessing and quantifying their effects in terms of additional fuel plant consumption [6]. Diagnosis procedures are based on comparison between working conditions of two systems (reference and real). The main goal is to show where and which part of the consumed resources can be saved for the same quantity and quality products.

### 4.1. Fuel impact

Fuel impact is an evaluation of the participation of the malfunctioning component on the total power plant fuel consumption. In order to analyze the fuel impact, it is necessary to know about the increase of the unit exergy consumption of each component of the plant. Table 7 shows these increments.

These variations increase the resources consumptions and the irreversibilities according to $\Delta k_i P^0$. If this is multiplied by the unit exergetic cost of the fuel, it results in the fuel impact [7].

The local variation of the fuel consumption corresponds to:

$$\Delta F = K^*_{F,i}\Delta k_i P^0 \quad (8)$$

| Subsystem | 100% $\Delta k_i$ | 75% $\Delta k_i$ | 50% $\Delta k_i$ |
|---|---|---|---|
| BOILER | -0.082 | 0.068 | 0.067 |
| TURBINE HP&IP | 0.057 | 0.031 | 0.034 |
| TURBINE LP | -0.007 | 0.105 | 0.031 |
| CONDENSER* | -0.030 | 0.955 | 1.576 |
| CONDENSER PUMP | -0.577 | -0.292 | 35.783 |
| FEED-WATER PUMP | -0.132 | -0.475 | 0.001 |
| STEAM SEALING CONDENSER | -0.005 | 0.082 | 0.772 |
| EJECTOR | -0.090 | 0.206 | 0.337 |
| HEATER 1 | 0.073 | 0.235 | 0.690 |
| HEATER 2 | 0.086 | 0.136 | 0.159 |
| HEATER 3 | 0.030 | 0.034 | 0.064 |
| HEATER 4 | 0.044 | -0.175 | -0.091 |
| DEAERATOR | 0.000 | -0.032 | -0.069 |
| HEATER 6 | 0.167 | -0.039 | 0.112 |
| HEATER 7 | 0.021 | -0.012 | 0.005 |
| STEAM REGULATOR | 0.000 | 0.000 | 0.000 |
| ELECTRIC GENERATOR | 0.005 | -0.012 | 0.021 |
| ELECTRIC TRANSFORMER | 0.010 | -0.011 | 0.020 |
| PLANT | 0.063 | 0.171 | 0.322 |

*Table 7. Increase of unit exergy consumption. $\Delta k_i = k_i - k_i^0$ *$k_{condenser}$ taking the product of the condenser as negentropy*

## 4.2. Malfunction and dysfunction analysis

The diminution of a local irreversibility is obtained by making a unit work exactly as the reference operation [7].

$$I_i = F_i - P_i = (k_i - 1)P_i \quad (9)$$

If the working conditions are modified, the efficiency and the total product could change, resulting in the increase of the irreversibility.

The irreversibility increase of a generic system component is:

$$\Delta I = P_i\Delta k_i + (k_i - 1)\Delta P_i \quad (10)$$

From this expression, we can find two kinds of irreversibilities [7]:

- Malfunction: referring to the irreversibility originated by the low efficiency of the unit. It can be repaired working over it:

$$MF_i = P_i\Delta k_i \quad (11)$$

- Dysfunction: applying to the irreversibility produced in unit *i*. After varying the efficiency of other units in the power plant, unit *i* needs to produce more product. It can be repaired acting on the rest of the plant.

$$DF_i = (k_i - 1)\Delta P_i \quad (12)$$

The deviation of a component forces other components to adapt their behavior in order to maintain their production conditions, and thus modify their irreversibilities. Malfunctions, dysfunctions and fuel impact for Manzanillo II are shown in Tables 8-10.

## 4.3. TAESS Analysis

TAESS is a software tool designed to make the thermoeconomic analysis of energy systems from their thermodynamic model and productive structure. It is based on the works on thermoeconomics developed in CIRCE and the Dpt. of Mechanical Engineering of the University of Zaragoza (Spain) [8].

TAESS software works with two thermodynamic states, one for reference operation and one for real operation. [9, 10].

TAESS computes the exergy cost of the productive structure flows $E^*_{ij}$:

$$C_{F,i} = E^*_{i,0} + \sum_{j=1}^{n} E^*_{j,i} \quad v_i \in V \quad (13)$$

$$C_{P,i} = E^*_{0,i} + \sum_{i=1}^{n} E^*_{i,j} \quad v_i \in V$$

builds the malfunction vector and matrices:

$$MF = K_D P^0 \quad (14)$$

$$[MF] \equiv \left(\Delta k_{ij} P^0_j\right)_{i,j=1\ldots n} \quad (15)$$

$$MF_e \equiv \left(\Delta k_{0,i} P^0_j\right)_{j=1\ldots n} \quad (16)$$

computes the dysfunction vector and matrices:

$$DF = (K_D - U_D)\Delta P \quad (17)$$

$$[DF] = |I|[MF] \quad (18)$$

and builds the irreversibility table that decomposes the irreversibilities in malfunctions and dysfunctions to finally compute the fuel impact.

$$\Delta F_T = {}^t u MF_e + {}^t c^e_p [MF] u + {}^t c^e_p \Delta\omega_0 \quad (19)$$

| Subsystem | MF [kW] | DF [kW] | Fuel Impact [kW] |
|---|---|---|---|
| BOILER | 18614.7 | 10725.7 | 18614.7 |
| TURBINE HP&IP | 4182.0 | 164.5 | 8913.9 |
| TURBINE LP | 10998.9 | -1612.5 | 22819.1 |
| CONDENSER | 9271.6 | -4130.0 | 42887.6 |
| CONDENSER PUMP | -31.0 | 40.3 | -75.9 |
| FEED-WATER PUMP | -1983.8 | -61.7 | -4852.2 |
| STEAM SEALING CONDENSER | 16.2 | -6.3 | 112.4 |
| EJECTOR | 40.2 | -23.3 | 243.7 |
| HEATER 1 | 208.9 | 173.7 | 953.6 |
| HEATER 2 | 290.1 | -57.0 | 1073.7 |
| HEATER 3 | 196.8 | 32.5 | 990.9 |
| HEATER 4 | -416.9 | 556.9 | -1543.0 |
| DEAERATOR | -519.6 | 214.4 | -1981.2 |
| HEATER 6 | -280.2 | 421.9 | -701.8 |
| HEATER 7 | -460.3 | 90.0 | -1474.3 |
| STEAM REGULATOR | 0.0 | 0.0 | 0.1 |
| ELECTRIC GENERATOR | -2869.3 | -16.0 | -6978.4 |
| ELECTRIC TRANSFORMER | -2553.9 | -7.4 | -6229.8 |
| POWER PLANT 75% | | | 38343.3 |

*Table 8. Malfunctions, Dysfunctions and Fuel Impact for all subsystems in Manzanillo II power plant at a 75% load.*

| Subsystem | MF [kW] | DF [kW] | Fuel Impact [kW] |
|---|---|---|---|
| BOILER | -29002.1 | 25206.3 | -29002.1 |
| TURBINE HP&IP | 9807.5 | -1.6 | 21880.5 |
| TURBINE LP | -904.2 | 349.7 | -2064.0 |
| CONDENSER | -443.4 | 1375.4 | -20.8 |
| CONDENSER PUMP | -105.4 | 17.6 | -275.5 |
| FEED-WATER PUMP | -727.8 | -40.6 | -1902.0 |
| STEAM SEALING CONDENSER | -1.6 | 0.2 | -3.7 |
| EJECTOR | -30.2 | 6.5 | -69.0 |
| HEATER 1 | 174.3 | -188.9 | 281.9 |
| HEATER 2 | 347.1 | -248.0 | 517.0 |
| HEATER 3 | 344.9 | -70.1 | 637.2 |
| HEATER 4 | 153.7 | 141.3 | 228.9 |
| DEAERATOR | -3.2 | 219.5 | -6.7 |
| HEATER 6 | 2193.8 | 246.4 | 4680.5 |
| HEATER 7 | 1190.3 | 313.0 | 2773.4 |
| STEAM REGULATOR | 0.0 | 0.0 | 0.0 |
| ELECTRIC GENERATOR | 1573.7 | 41.6 | 3934.8 |
| ELECTRIC TRANSFORMER | 3049.2 | -23.9 | 7779.6 |
| POWER PLANT 100% | | | **18304.6** |

*Table 9. Malfunctions, Dysfunctions and Fuel Impact for all subsystems in Manzanillo II power plant at a 100% load.*

| Subsystem | MF [kW] | DF [kW] | Fuel Impact [kW] |
|---|---|---|---|
| BOILER | 12353.8 | 19898.5 | 12353.8 |
| TURBINE HP&IP | 3110.0 | 834.0 | 3089.9 |
| TURBINE LP | 2074.3 | 89.2 | 1968.1 |
| CONDENSER | 12962.9 | -6999.4 | 347537.8 |
| CONDENSER PUMP | 3896.5 | -3714.4 | 4642.3 |
| FEED-WATER PUMP | 2.1 | 123.5 | 2.5 |
| STEAM SEALING CONDENSER | 153.9 | -135.0 | 4395.9 |
| EJECTOR | 67.2 | -52.4 | 1869.3 |
| HEATER 1 | 247.7 | 113.3 | 6335.4 |
| HEATER 2 | 200.0 | -40.3 | 1985.6 |
| HEATER 3 | 227.0 | -12.5 | 4271.5 |
| HEATER 4 | -127.5 | 450.4 | -1266.4 |
| DEAERATOR | -669.9 | 120.5 | -7031.5 |
| HEATER 6 | 482.2 | 452.9 | 2176.9 |
| HEATER 7 | 102.1 | 86.7 | 727.6 |
| STEAM REGULATOR | 0.0 | 0.0 | 0.1 |
| ELECTRIC GENERATOR | 3255.3 | 110.2 | 3653.2 |
| ELECTRIC TRANSFORMER | 3048.6 | 14.8 | 3527.0 |
| POWER PLANT 50% | | | **48535.2** |

*Table 10. Malfunctions, Dysfunctions and Fuel Impact for all subsystems in Manzanillo II power plant at a 50% load.*

Modeling the Manzanillo II power plant in this powerful software tool is useful to compare the results between the analysis applying the Theory of Exergetic Cost and the General Theory of the Exergy Saving (TEC&GTES) with the aid of a spreadsheet and TAESS analysis. Using the same F/P structure, the fuels and products were defined for the three cases under study.

| No. Device | DEVICE |
|---|---|
| 0 | Environment |
| 1 | BOILER |
| 2 | TURBINE HP&IP |
| 3 | TURBINE LP |
| 4 | CONDENSER PUMP |
| 5 | FEED-WATER PUMP |
| 6 | STEAM SEALING CONDENSER |
| 7 | EJECTOR |
| 8 | HEATER 1 |
| 9 | HEATER 2 |
| 10 | HEATER 3 |
| 11 | HEATER 4 |
| 12 | DEAERATOR |
| 13 | HEATER 6 |
| 14 | HEATER 7 |
| 15 | STEAM REGULATOR |
| 16 | ELECTRIC GENERATOR |
| 17 | ELECTRIC TRANSFORMER |
| 18 | CONDENSER ** |

*Table 11. Device Configuration in TAESS for the three cases.*

Device configuration is defined as shown in table 11. The condenser was originally defined as a dissipative device. However, an error occurred indicating that the sum of distribution of residues of dissipative devices was different to 1.0. In this particular case, the total sum of distribution of residues was 1.00002, different enough for blocking the functions of TAESS software. Therefore, the condenser had to be modelled as a productive device. As entropy must be rejected to the environment through the condenser, then the condenser product had to be modelled as negentropy, necessary in the Rankine cycle for the correct cyclical operation of the system [12].

TAESS software uses the condenser product like any other exergetic product in a productive device; for this reason, we split the total condenser product in two: the exergy-fuel of the feed-water pump and the negentropy rejected to the environment.

Table 12 shows the F/P structure used for TAESS analysis. Flows 8 and 55 represent the exergy sent as fuel to the feed-water pump and the negentropy rejected to the environment, respectively.

| Flow | Ouput Device | F/P | Input Device | F/P | Flow | Ouput Device | F/P | Input Device | F/P |
|---|---|---|---|---|---|---|---|---|---|
| **1** | 1 | P | 2 | F | **30** | 10 | P | 9 | F |
| **2** | 2 | F | 3 | F | **31** | 9 | F | 8 | F |
| **3** | 2 | F | 3 | F | **32** | 8 | F | 18 | F |
| **4** | 2 | F | 13 | F | **33** | 6 | P | 18 | F |
| **5** | 2 | F | 12 | F | **34** | 7 | P | 18 | F |
| **6** | 2 | F | 1 | P | **35** | 2 | F | 15 | F |
| **7** | 2 | F | 14 | F | **36** | 2 | F | 15 | F |
| **8** | 3 | F | 10 | F | **37** | 1 | P | 6 | F |
| **9** | 3 | F | 11 | F | **38** | 2 | F | 6 | F |
| **10** | 3 | F | 9 | F | **39** | 2 | F | 6 | F |
| **11** | 3 | F | 8 | F | **40** | 3 | F | 6 | F |
| **12** | 3 | F | 18 | F | **41** | 3 | F | 6 | F |
| **13** | 18 | P | 4 | P | **42** | 15 | P | 3 | F |
| **14** | 4 | P | 6 | F | **43** | 15 | P | 3 | F |
| **15** | 4 | P | 7 | F | **44** | 1 | P | 7 | F |
| **16** | 6 | P | 8 | P | **45** | 5 | P | 1 | P |
| **17** | 7 | P | 8 | P | **46** | 12 | P | 11 | F |
| **18** | 8 | P | 9 | P | **47** | 1 | P | 12 | F |
| **19** | 9 | P | 10 | F | **48** | 15<br>2* | P<br>F* | 8<br>15* | F |
| **20** | 10 | P | 11 | P | **49** | 0 | P | 18 | F |
| **21** | 11 | P | 12 | F | **50** | 0 | P | 1 | F |
| **22** | 12 | P | 5 | P | **51** | 0 | P | 1 | F |
| **23** | 5 | P | 13 | P | **52** | 17 | P | 5 | F |
| **24** | 13 | P | 14 | F | **53** | 2 | P | 16 | F |
| **25** | 14 | P | 1 | P | **54** | 3 | P | 16 | F |
| **26** | 1 | P | 2 | F | **55** | 18 | P | 0 | F |
| **27** | 14 | P | 13 | F | **56** | 17 | P | 4 | F |
| **28** | 13 | F | 12 | F | **57** | 16 | P | 17 | F |
| **29** | 11 | F | 10 | F | **58** | 17 | P | 0 | F |

*Table 12. F/P structure for the Manzanillo II power plant. *Equations used only in the 50% load case.*

The Fuel Impact in TAESS calculation was very similar to the results found with TEC&GTES. Table 13 shows that TEC&GTES analysis

represents the 99% of the Fuel Impact calculated with TAESS.

In Tables 8-10 and 14, we can see that the results for Malfunctions and Dysfunctions are identical for both, TAESS and TEC&GTES, when we define the condenser product like negentropy as explained in this section.

| Fuel Impact | TEC&GTES | TAESS | Δ |
|---|---|---|---|
| Power plant 100% of load | 18304.6 | 18310.0 | 5.4 |
| Power plant 75% of load | 38343.3 | 38345.7 | 2.4 |
| Power plant 50% of load | 48535.2 | 48536.2 | 1.0 |

*Table 13. Differences between TEC&GTES and TAESS analyses in Fuel Impact for the Manzanillo II power plant.*

## 5. Conclusions

The thermoeconomic diagnosis of the Manzanillo II power plant has been performed applying The Theory of Exergetic Cost for a systematic use of the exergy concept and the fuel- product based on the productive purpose of a component. The General Theory of the Exergy Saving was used for the same idea of exergetic cost to obtain the thermoeconomic cost.

Throughout this article, three different stages in the power plant have been examined.

It is obvious that operating the plant at a 100% load is possible to be closer to the reference operation behavior. In this case, we found that the boiler works well and the savings in this unit are almost completely exogenous. The contrary happens for most of the heaters.

For the 75% load case, the boiler has the most important savings by acting on itself; malfunctions represent the most irreversibilities in this unit. Also for the turbines the most important savings are by acting in the malfunction or endogenous irreversibility

Typically in Rankine cycles, the most important technical saving occurs in the boiler. In the 50% load case, we can see that the dysfunctions are the most affecting irreversibility in the boiler. This means that when the power plant is at 100% or 50% of load, the other units are more involved in the performance of the boiler than when the plant is working at 75% its capacity. Most of the units are more affected by the exogenous irreversibility than by the endogenous. Acting on a global way, we can improve the working of the plant.

This work presented the analysis of a conventional power plant at three different percentages of loads and compared the results between TEC&GTES and TAESS analyses, finding identical results (Tables 14 and 8-10). Once again, as supported by the bibliography of this paper, it was proven that whatever irreversibility comes this way, either endogenous or exogenous, the thermodynamic diagnosis methods will be able to detect it for a thermal optimization, subjected to a further stage.

| TAESS Results | 100% load | | 75% load | | 50% load | |
|---|---|---|---|---|---|---|
| Subsystem | MF [kW] | DF [kW] | MF [kW] | DF [kW] | MF [kW] | DF [kW] |
| BOILER | -29002.1 | 25206.3 | 18614.7 | 10725.7 | 12353.8 | 19898.5 |
| TURBINE HP&IP | 9807.5 | -1.6 | 4182.0 | 164.5 | 3110.0 | 834.0 |
| TURBINE LP | -904.2 | 349.7 | 10998.9 | -1612.5 | 2074.3 | 89.2 |
| CONDENSER | -443.4 | 1375.4 | 9271.6 | -4130.0 | 12962.9 | -6999.4 |
| CONDENSER PUMP | -105.4 | 17.6 | -31.0 | 40.3 | 3896.5 | -3714.4 |
| FEED-WATER PUMP | -727.8 | -40.6 | -1983.8 | -61.7 | 2.1 | 123.5 |
| STEAM SEALING CONDENSER | -1.6 | 0.2 | 16.2 | -6.3 | 153.9 | -135.0 |
| EJECTOR | -30.2 | 6.5 | 40.2 | -23.3 | 67.2 | -52.4 |
| HEATER 1 | 174.3 | -188.9 | 208.9 | 173.7 | 247.7 | 113.3 |
| HEATER 2 | 347.1 | -248.0 | 290.1 | -57.0 | 200.0 | -40.3 |
| HEATER 3 | 344.9 | -70.1 | 196.8 | 32.5 | 227.0 | -12.5 |
| HEATER 4 | 153.7 | 141.3 | -416.9 | 556.9 | -127.5 | 450.4 |
| DEAERATOR | -3.2 | 219.5 | -519.6 | 214.4 | -669.9 | 120.5 |
| HEATER 6 | 2193.8 | 246.4 | -280.2 | 421.9 | 482.2 | 452.9 |
| HEATER 7 | 1190.3 | 313.0 | -460.3 | 90.0 | 102.1 | 86.7 |
| STEAM REGULATOR | 0.0 | 0.0 | 0.0 | 0.0 | 0.0 | 0.0 |
| ELECTRIC GENERATOR | 1573.7 | 41.6 | -2869.3 | -16.0 | 3255.3 | 110.2 |
| ELECTRIC TRANSFORMER | 3049.2 | -23.9 | -2553.9 | -7.4 | 3048.6 | 14.8 |
| POWER PLANT | Fuel impact [kW] | 18310.0 | Fuel impact [kW] | 38345.7 | Fuel impact [kW] | 48536.2 |

Table 14. *TAESS Malfunctions and Dysfunctions for all subsystems in Manzanillo II power plant at 50%, 75% and 100% loads.*

## Nomenclature

*Abbreviations*

TEC Theory of Exergetic Cost
GTES General Theory of Exergy Saving

*Scalars*

n Number of components
m Number of flows
$T_0$ Temperature reference [c]
$P_0$ Pressure reference [kPa]
$F_i$ Conversion factor [mol C/kg]
HHV Higher heating value
$h^0$ Specific enthalpy at standard environment state [kj/mol C]
$s^0$ Specific entropy at standard environment state [kj/mol C-K]
e Specific energy at standard environment state [kj/mol C]
b Specific exergy [kj/kg]
E Exergy of a flow [kW]
$C_F$ Exergy cost of fuel [kW]
$C_P$ Exergy cost of product [kW]
$F_T$ Exergy of the external resources [kW]

*Matrices and vector*

A Incidence matrix (n *x* m)

$A_F$ Fuel incidence matrix (n *x* m)
$A_P$ Product incidence matrix (n *x* m)
$A_L$ Losses incidence matrix (n *x* m)
M Mass flow vector (m x 1)
E Energy flow vector (m x 1)
B Exergy flow vector (m x 1)
D Destroyed exergy vector (m x 1)
$B^*$ Exergetic cost vector (m x 1)
$Y^*$ Exergetic amortization cost vector of a system
Z Non-energy production factors
$\dot{Z}$ External economic valuation
Π Exergoeconomic cost vector (m x 1)
I Irreversibility vector (n x 1)
MF Malfunction vector (n x 1)
DF Dysfunction vector (n x 1)
[MF] Malfunction matrix (n x n)
[DF] Dysfunction matrix (n x n)

*Greek letters*

α Cost sub-matrix of a system associated with efficiencies ((m-n) x m)
κ Exergetic unit consumption of a subsystem
$\kappa^*$ Exergetic unit cost of a flow. I.e. $\kappa^* = B^*/B$
η Exergetic efficiency of a subsystem. I.e. the inverse of κ
ω Vector of numerical values in kilowatts ((m-n) x 1) associated with matrix α
Δ Increment

*Subscripts and Superscripts*

I…n Chemical species.
0 reference state
e Related to external resources
*i, j, h* Index for number of components

## References


[1] Juan M. Belman. et al, 2002, Procedimiento Termoeconómico de Diagnostico y Evaluación de Ciclos Combinados, Tecnología y Desarrollo, 1(1), pp. 6-11.

[2] M. A. Lozano. Valero A., 1986, Methodology for Calculating Exergy in Chemical Process, Chemical engineering, March 1986, Pages 119-128

[3] M. A. Lozano. Valero A., 1993, Theory of the Exergetic Cost, Energy, Volume 18, Issue 9, September 1993, Pages 939-960

[4] G. Tsatsaronis, A. Valero, Combining Thermodynamics and Economics in Energy Systems.

[5] Tsatsaronis, G., Winhold, M., 1985, Exergoeconomic Analysis and Evaluation of energy conversion Plants. I: A New General Methodology, Energy, vol. 10.

[6] Valero A, M. A. Lozano, M Muñoz., 1986, A General Theory of Exergy Saving I. On the Exergetic Cost, Computer-Aided Engineering of Energy System

[7] César Torres, Antonio Valero, Luis Serra, Javier Royo, 2002, Structural Theory and Thermoeconomic Diagnosis: Part I. On Malfunction and Dysfunction Analysis, Energy Conversion and Management, Volume 43, Issues 9-12, June-August 2002, Pages 1503-1518

[8] César Torres, Ericka Perez, 2007, TAESS User Guide V. 1.0

[9] Valero A, César Torres, Ericka Perez, 2007, Guidelines to Developing Software for Thermoeconomic Analysis of Energy Systems. Part I: The Thermoeconomic Model, ECOS 2007.

[10] Valero A, César Torres, Ericka Perez, 2007, Guidelines to Developing Software for Thermoeconomic Analysis of Energy Systems. Part II: Application to Thermoeconomic Diagnosis, ECOS 2007.

[11] Valero A, M. A. Lozano, M Muñoz., 1986, A General Theory of Exergy Saving II. On the Thermoeconomic Cost, Computer-Aided Engineering of Energy System

[12] M. A. Lozano, A. Valero, L Serra, 1993, Theory of Exergetic Cost and Thermoeconomic Optimization. Proceedings of The Internal Conference ENSEC'93


**Acknowledgments:**

We thank the Manzanillo II power plant & CFE engineers for their helpful, technical support and availability for developing this work.

Trad. Por Ma. Susana García A.

# Evaluation of Quasi-Stationary Simulation for the Analysis of Industrial Energy Systems

*Philip Voll[a], Stefan Kirschbaum[b] and André Bardow[a]*

[a] *Chair of Technical Thermodynamics, RWTH Aachen University, Aachen, Germany*
[b] *Society for the Promotion of Applied Computer Science, Berlin, Germany*

**Abstract:** The analysis and optimization of industrial energy systems pose non-trivial, multi-criteria problems. Today, solving these problems can be supported by system simulation. A simulation's applicability to practical problems, however, is strongly depending on the level of detail of the physical models employed. This paper evaluates quasi-stationary simulation based on rather simple models with regard to its applicability to industrial energy consultancy. For this purpose, a simplified quasi-stationary and a full dynamic model of an actual heating system are developed. Simulation is used to quantify the impact of two measures for the reduction of the heating system's energy use. Both models are compared with regard to time and effort to perform the system modeling, the quality of their simulation results, and necessary computing time. It is shown that the simplified quasi-stationary approach minimizes time and effort to perform the system modeling and simulation. Moreover, it yields sufficiently accurate results when integral values are of main interest. This is demonstrated for the case studies investigated within this paper and applies to most tasks within the scope of industrial energy consultancy.

**Keywords:** industrial energy systems, quasi-stationary simulation, TOP-Energy, ThermoPower.

## 1. Introduction

Industrial energy systems are manifold and often highly integrated. Thus, the analysis and optimization of these systems pose non-trivial, multi-criteria problems. Typical tasks are the identification of energy paths through energy systems, the design of energy schemes, or the assessment of improvement measures. Today, solving these problems can be supported by system simulation. A simulation's applicability to practical problems, however, is strongly depending on the level of detail of the physical models employed. Simulation in energy consultancy requires an approach that allows system modeling based on the few data an energy consultant maps during site inspections; this includes the single machines' characteristics, the system's infrastructure and in-operation-measured values of pressure and temperature. In energy consultancy, system simulation is then used to compute economic, energy-related and environmental key figures that are strongly depending on the actual state of operation. Thus, it is not enough to consider only specific points in time; in fact, for most applications the necessary period under consideration is a whole year ([1]).

In [2] several approaches for system modeling and simulation are discussed, but only few meet the demands of practical applications in industrial energy consultancy. This paper presents a simplified quasi-stationary approach for system modeling and simulation that is tailored to meet these requirements. Easy model parameterization is achieved by assuming model parameters, like machine characteristics, or pressure drop and heat loss coefficients, to be constant. Moreover, this approach considers energy demand profiles as specified input for the simulation. The time resolution of these profiles is typically not better than one hour ([1]). This allows to model the system behavior quasi-stationary or quasi-steady-state; i.e., the system is assumed to reach steady-state conditions instantly based on the current constraints. A time trajectory is thus modeled as a sequence of quasi-stationary operating points. This in turn reduces simulation time considerably compared to dynamic simulation.

The presented approach is evaluated with regard to its applicability to practical problems. For this purpose, an actual heating system is considered. The simplified quasi-stationary model of this heating system is compared to a full dynamic model. Simulation is used to quantify the impact

Corresponding Author: Philip Voll, Email: voll@ltt.rwth-aachen.de

of two measures for the reduction of the heating system's energy use. Both models are compared with regard to time and effort to perform the system modeling, the quality of their simulation results, and necessary computing time. It turns out that the simplified quasi-stationary approach meets the requirements of practical applications in industrial energy consultancy.

## 2. Investigated heating system

Fig. 1 schematically depicts the heating system in normal operation. It includes field data of the actual heating system.

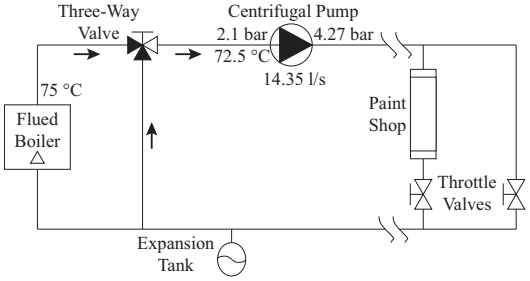


*Fig. 1. Schematic depiction of the heating system in normal operation.*

The flued boiler is operated in intermittent on/off control with a set-tempetature of 75 °C; accordingly, it provides heating water with temperatures between 70 °C and 80 °C. It has a thermal efficiency of 92%, a nominal burner power of 100 kW and a storage volume of 1.7 m³. The three-way valve mixes water from the return flow to the supply flow in order to adjust the supply temperature to 72.5 °C. The heating water is delivered to the paint shop with a fixed speed centrifugal pump actuated in throttle control. The pump's nominal electric power is 11 kW, its electric efficiency is 87%. The expansion tank imposes a system pressure of 2.1 bar. In the following a system start-up is described in detail; later, this procedure is considered to validate the detailed model of the heating system.

### 2.1. System start-up

During start-up operation no heat consumers are connected to the pipe network; the heating water is heated from ambient temperature to 70 °C. Only then the on/off controller is adjusted to a set-temperature of 75 °C. Fig. 2 depicts the run of the temperature curve recorded during system start-up of the actual heating system. After about fifteen minutes the boiler is providing pre-heated heating

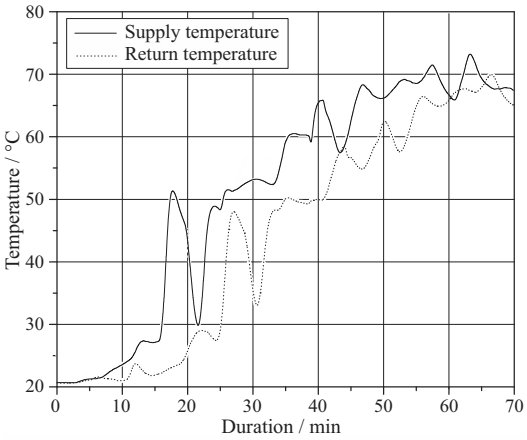


*Fig. 2. Supply and return temperature curves during system start-up.*

water to the pipe network. The cold return water causes an immediate temperature drop in the boiler. From that point the boiler is only gradually opened to provide heating water to the pipe network; it is opened entirely after about twenty-five minutes. System start-up is completed after about fifty-five minutes when the supply temperature rises above 70 °C. At this point the boiler control switches to normal operation in intermittent on/off control.

### 2.2. Hydraulic and thermal piping losses

In normal operation the pump delivers a volume flow of 14.35 l/s. Supply and return flow pressures are measured to be 4.27 bar and 2.1 bar, respectively. When the system is operated without any heat consumers the averaged temperature spread between supply and return flow is 1.1 K.

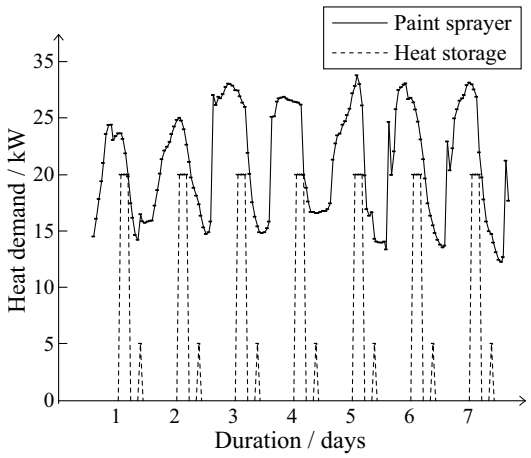


*Fig. 3. Heat demand profiles of the paint shop's paint sprayer and its heat storage.*

### 2.3. Heat demand of the paint shop

Fig. 3 depicts two demand profiles for a typical week in summer time; one curve represents the heat demand for the direct heating of the paint sprayers, the other curve represents a periodic loading of the paint shop's heat storage. While the paint sprayer's demand profile ranges from 12.1 kW to 34.3 kW, the heat storage is loaded regularly every day; the loading power is 20 kW between 4pm and 8pm, and 6 kW between 11pm and 12am. The cumulative demand profile holds 168 values; one value for every hour. Its integral value is 4.2 MWh.

## 3. Modeling

The simplified quasi-stationary and the full dynamic model of the heating system are presented in the following.

### 3.1. Simplified quasi-stationary model

The simplified quasi-stationary model of the heating system is developed using the "The Toolkit for Optimization of Industrial Energy Systems" (TOP-Energy). TOP-Energy is designed to support energy consultants in an overall analysis and optimization of industrial energy systems ([3-5]).

Section 1 describes the general requirements for system modeling and simulation in energy consultancy. The simple approach pursued by TOP-Energy meets these requirements by assuming quasi-stationary system behavior and by enabling an easy model parameterization.

$$\frac{\Delta m}{\Delta t} = \sum_i \dot{m}_i \tag{3}$$

$$\frac{\Delta U}{\Delta t} = \sum_i (\dot{m}_i \cdot h_i) - \sum_j \dot{Q}_j - \sum_k P_k \tag{4}$$

Its models are based on simple mass (3) and energy balances (4). Model parameters, like machine characteristics, or pressure drop and heat transfer coefficients, are assumed to be constant during operation. In turn, the models need to be parameterized only with easy accessible data, like the machines' characteristics and in-operation-measured temperature and pressure values.

Fig. 4 shows a screenshot of the TOP-Energy model of the heating system. In addition to the symbols representing models of technical components, it includes symbols that represent models of the environment, and electricity and natural gas suppliers. Heating water is assumed to behave like an ideal liquid with a specific volume of $v^{il}$ = 0.001 m³/kg. The most important models are described in detail in the following.

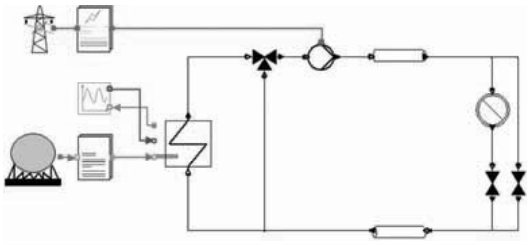

*Fig. 4. TOP-Energy screenshot of the heating system model.*

#### 3.1.1. Single component models

##### 3.1.1.1. Three-way valve

The model of the three-way valve computes the mixing ratio of the supply and the return flow by simple mass and energy balances according to the set value of the mixing temperature. Water storage inside the valve is neglected. The user has to parameterize the set value for the mixing temperature of the supply flow.

##### 3.1.1.2. Flued boiler

The flued boiler model computes the fuel consumption for a given load case by simple mass and energy balances. While the actual flued boiler is operated intermittently in on/off control, this model constantly provides heating water with the boiler's set-temperature. Its part load behavior is modeled by a characteristic curve, which relates the heat output with the fuel consumption. Water storage inside the boiler is neglected. The user has to parameterize the boiler's supply temperature, its thermal efficiency and the characteristic curve representing its part load behavior.

##### 3.1.1.3. Centrifugal pump

Equation (5) of the centrifugal pump model computes the electric input power $P_{el}$ from the present pressure head $z(n)$, the delivered volume flow $\dot{V}(n)$ and its electric efficiency $\eta_{el}$.

$$P_{el} = \eta_{el} \cdot \dot{V}(n) \cdot z(n) \tag{5}$$

To determine the pump's operating point in interaction with the pipe network, the user has to parameterize the pump's characteristic curve at nominal speed $n_0$. The pump affinity laws (6) to

(8) are then used to model the pump's behavior at arbitrary speeds $n$.

$$\dot{V}(n) = \dot{V}(n_0) \cdot n / n_0 \quad (6)$$

$$z(n) = z(n_0) \cdot (n / n_0)^2 \quad (7)$$

$$P(n) = P(n_0) \cdot (n / n_0)^3 \quad (8)$$

In (6) to (8) a constant pump efficiency is assumed to scale the characteristic curve with regard to the pump's delivery flows $\dot{V}(n)$, its pressure heads *z(n)* and its hydraulic powers *P(n)* at arbitrary speeds *n* ([6]).

#### 3.1.1.4. Pipe

Fig. 5 depicts a schematic representation of the pipe model with its variables and parameters. The model accounts for hydraulic and thermal piping losses, that are computed by a reduced momentum balance (9) and a heat transfer law (10).

$$p_2 - p_1 = \frac{1}{2} \cdot \xi \cdot A_{\Delta p} \cdot \frac{\dot{V}^2}{v^{il}} \quad (9)$$

$$\dot{Q} = k \cdot A_{\Delta T} \cdot \frac{T_1 - T_2}{1/2 \cdot (T_1 - T_{amb}) + 1/2 \cdot (T_2 - T_{amb})} \quad (10)$$

To parameterize the model, the user has to enter measured values for the volume flow $\dot{V}$, the ambient temperature $T_{amb}$, and the corresponding pressure ($p_2 - p_1$) and temperature drops ($T_2 - T_1$). These values are then used to compute the product between the pressure drop coefficient $\xi$ and the pipe's cross section $A_{\Delta p}$ as well as the product between the heat loss coefficients $k$ and the pipe's surface area $A_{\Delta T}$. All of these values are assumed to remain constant for the modeled pipe.

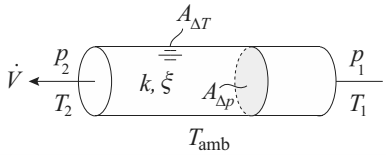


*Fig. 5. Variables and parameters of the pipe model.*

### 3.2. Full dynamic model

The full dynamic model of the heating system is based on the free available Modelica ThermoPower model library ([7]). This library was originally designed for the dynamic simulation of thermal power plants. It includes models of technical components, like pumps, compressors, evaporators, condensers, combustion chambers, turbines, valves, tubes and tanks. It accounts for the dynamic mass, momentum und energy balances. Pressure drop and heat transfer phenomena are described by constitutive laws taking into account non-constant coefficients, like the Fanning friction coefficient computed by the Colebrook equation ([6]) to describe wall friction of a liquid inside a tube.

Building up a model that is capable of predicting the dynamic behavior of the heating system, requires very detailed information about the system's single components and their interconnections. Moreover, a whole range of aggregate models must be generated by assembling standard models from the ThermoPower and the Modelica Standard Library ([8]); these include models of insulated pipes, fixtures and fittings, pump control systems, a flued boiler in intermittent on/off control and different valves. Heating water is modeled as an ideal liquid with a specific volume of $v^{il} = 0.001$ m³/kg.

#### 3.2.1. Data acquisition

In this specific case the major time and effort for the system modeling is due to acquire all necessary data for the network modeling. The actual pipe network covers a length of more than 1,400 meters and consists of more than two hundred different pipe sections, fixtures and fittings. The pipe network is mapped during site inspections to acquire all of the following data for each pipe section

- topology (length, diameter and wall thickness of the single pipes)
- pipe material conditions (surface roughness)
- pipe material properties (tube sheet heat capacities and thermal conductivities)
- insulation material properties (heat capacities and thermal conductivities)
- dimensions of valves, tees, wyes, reducers, orifices and flarings, bends and elbows

The corresponding network model needs to be parameterized by pressure drop and resistance coefficients. These are determined by [9] from the listed data of all single devices.

#### 3.2.2. Rough spatial discretization

The ThermoPower model library uses a rough discretization to model thermal dynamics linked to transport phenomena inside pipes. Thus, a number of equally spaced nodes are introduced to resolve

the enthalpy across the pipe length. A number of two nodes (one each at the pipe's in- and outlet) implies ideal mixing and thus neglects the dynamic behavior of the thermal enthalpy inside the pipe. The pipe model of the heating system contains one node for each 10 cm³ of inner pipe volume. A finer discretization does not improve the quality of the simulation results, but causes longer computing times.

#### 3.2.3. Model validation

Section 2.1 describes the start-up process of the heating system. This procedure is simulated in order to validate the full dynamic model of the heating system. Simulation is based on the recorded three-way mixing temperature curve. It holds one temperature value every five seconds, in total 720 values; simulation of this time series takes 11.8 hours on an Intel Core2 2.13 GHz with 2GB RAM. In the following results from the start-up simulation are compared to measured values.

##### 3.2.3.1. Hydraulic variables

Table 1 lists recorded and simulated values for the pressure field and the mass flow of the heating water during start-up operation. Comparison shows, that the relative error does not exceed 2%.

*Table 1. Hydraulic variables during start-up operation. Comparison of recorded and simulated values.*

| | Supply pressure | Return pressure | Mass flow |
|---|---|---|---|
| Measurement | 4.27 bar | 2.10 bar | 14.35 kg/s |
| Simulation | 4.35 bar | 2.11 bar | 14.64 kg/s |
| Relative error | 1.9% | 0.5% | 2.0% |

##### 3.2.3.2. Thermal variables

Fig. 6 contrasts the recorded and the simulated return temperature curves. Major deviations occur for simulation times between thirty and thirty-five minutes; these are attributed to operational irregularities during measurement. As described in section 2.1, system start-up is completed after about fifty-five minutes when the supply temperature rises above 70 °C. At this point the boiler control switches to normal operation in intermittent on/off control. In this operational state the absolute difference between simulated and recorded temperature is less than 1 K. Simulation yields an averaged temperature drop of 1.2 K between supply and return temperature. This is in good argument with the measured value of 1.1 K.

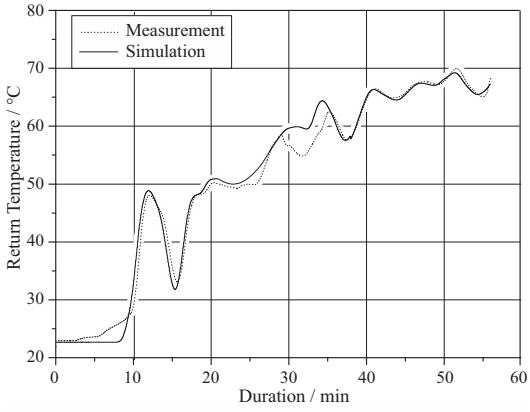


*Fig. 6. Recorded and simulated return temperature curves.*

##### 3.2.3.3. Conclusion

The full dynamic model is capable of predicting the heating system's dynamic behavior with sufficient accuracy. In the following, it serves as reference model for the evaluation of the simplified quasi-stationary model.

## 4. Simulation

This section describes the application of system simulation for the assessment of improvement measures to reduce the heating system's energy use. Starting with the present situation, simulation is used to compute the energy use for two different system alternatives. It is based on the cumulative demand profile, which holds 168 values (compare Fig. 3).

### 4.1. Present situation

In the present situation, heating water is pumped by a fixed speed centrifugal pump actuated in throttle control. While throttle control systems can be installed rather easily, their use leads to considerable exergy losses due to frictional heat production in the throttle valve. Further exergy losses occur due to running the pump in lower efficiency: Fig. 7 illustrates how throttling of the control valve causes an increase of the system's

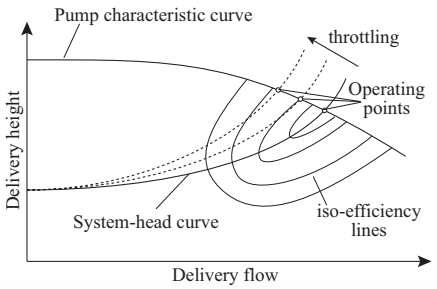


*Fig. 7. Movement of a fixed speed centrifugal pump's operating point due to throttling.*

flow resistance. This in turn causes an increase of the backpressure at the pump, so that the pump's operating point is moved to higher pressure heads and lower delivery flows at lower efficiencies.

Table 2 lists the integral simulation results for the boiler's natural gas and the pump's electricity consumption. The relative differences between the results from the simplified quasi-stationary (sQS) and the full dynamic (fD) models are smaller than 2%.

*Table 2. Simulation results for the "present situation" case.*

| | Natural gas consumption / MWh | Electricity consumption / MWh |
|---|---|---|
| fD model | 31.50 | 0.65 |
| sQS model | 30.96 | 0.66 |
| Relative difference | -1.66% | +1.54% |

### 4.2. Speed control

Other than for a fixed speed pump, the system-head curve of a speed-controlled pump remains unchanged when changing the delivery flow. Fig. 8 illustrates the movement of the pump characteristic curve to lower pressure heads for reduced speeds. This implies less exergy losses than for a fixed speed pump in throttle control; on the one hand this is due to running the pump at better efficiencies for equal delivery flows, on the other hand it is due to the avoidance of frictional losses in the throttle valve.

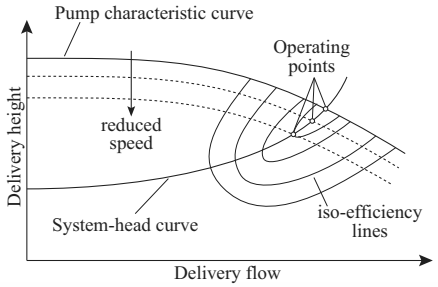


*Fig. 8. Movement of a speed-controlled centrifugal pump's operating point due to speed reduction.*

Table 3 lists the integral simulation results for the pump's electricity consumption when it is operated in speed control. The use of a speed controlled pump reduces its electricity consumption by 45.5% compared to throttle-controlled pump. Again, the results from the simplified quasi-stationary (sQS) and the full dynamic (fD) model differ only slightly; the relative difference is about 4%.

*Table 3. Simulation results for the "speed control" case.*

| | Electricity consumption / MWh |
|---|---|
| fD model | 0.296 |
| sQS model | 0.284 |
| Relative difference | -4.05% |

### 4.3. Improved pipe insulation

In most part of the pipe network the pipes are insulated with 7.5 cm thick polyurethane layers. However, along 160 meters of the older part of the network the pipes are insulated with only a 0.5 cm thin layer of glass wool. The heat conductivities of the modern and the outdated insulation materials are 0.033 W/(m K) and 0.045 W/(m K), respectively.

Table 4 lists the integral simulation results for the boiler's natural gas consumption when the outdated insulation is substituted by modern polyurethane insulation. By doing so, the natural gas consumption can be reduced by 20%. Once again, the results from both models differ only slightly; the relative difference is less than 5%.

*Table 4. Simulation results for the "improved insulation" case..*

| | Natural gas consumption / MWh |
|---|---|
| fD model | 25.08 |
| sQS model | 23.89 |
| Relative difference | -4.74% |

## 5. Discussion and conclusions

### 5.1. Discussion

The simplified quasi-stationary and the full dynamic approaches are used to quantify the impact of two measures for the reduction of the heating system's energy use. In the following both approaches are compared with regard to the quality of their simulation results, time and effort to perform the system modeling, and necessary computing time.

#### 5.1.1. Quality of the simulation results

Sections 4.1 to 4.3 list integral results for the energy use of three different system simulations. In all cases the relative differences between the results of the simplified quasi-stationary and the full dynamic models are less than 5%.

Major differences occur when the simulated time behavior is regarded. Simulation of the full

dynamic model respects effects like the run of the control systems to track the machines' set values and storage of the heating water inside the flued boiler. Simulation of the simplified quasi-stationary model neglects these phenomena; in this case the machines run stationary in one operational state for each load case. Fig. 9a and 9b illustrate the boiler's time behavior of both models during two hours of the simulation. The heat load at the boiler is 65.3 kW during the first and 26.7 kW during the second hour. In case of the dynamic simulation the boiler operates in full load in 42.6 minutes during the first and in 17.4 minutes during the second hour. This is due to the dynamic behavior of the intermittent control and water storage inside the boiler. In case of the quasi-stationary simulation this behavior is represented by a stationary boiler operation for each load case; the burner power is 71 kW during the first and 29 kW during the second hour. The integral results of the natural gas consumption are identical, but the operation times differ considerably.

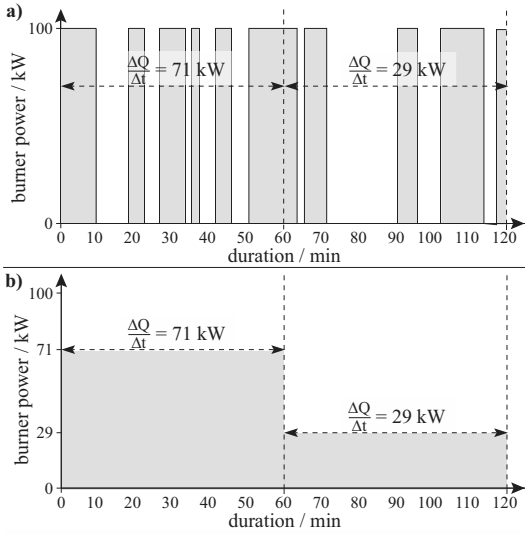


*Fig. 9. Simulated time behavior of the flued boiler. a) Full dynamic model. b) Simplified quasi-stationary model.*

A similar difference can be observed when looking at the pump's input power, compare Fig. 10. While simulation of the quasi-stationary model yields constant input powers for each load case, the dynamic model yields an oscillating curve due to the controller tracking. Particular attention has to be paid to peak loads that occur in the dynamic simulation, but are neglected in the quasi-stationary model. These peak loads occur due to load transitions, e.g. at the load shift from hour three to four.

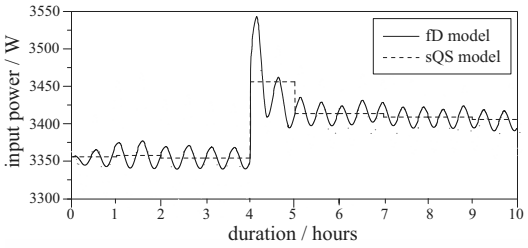


*Fig. 10. Simulated pump input power of the full dynamic (fD) and the simplified quasi-stationary (sQS) model.*

### 5.1.2. Time and effort to model the heating system

Building the full dynamic model requires considerable additional work compared to the simplified quasi-stationary model; this is due to the necessity of modeling all single controllers and due to the detailed modeling of the pipe network including all fixtures and fittings. In contrast, for the simplified quasi-stationary model it is sufficient to define control strategies by simple algebraic constraints; also, the simple model of the pipe network requires only in-operation-measured values for volume flow, pressure drop and temperature drop.

### 5.1.3. Computing time

The differential algebraic equation system of the full dynamic model consists of more than 30,000 equations. Simulation takes about thirty-four hours on an Intel Core2 2.13 GHz with 2GB RAM; in contrast to this the simplified quasi-stationary model is simulated in only a couple of minutes; it consists of less than one thousand algebraic equations. In order to reduce computing time, the full dynamic model may be simplified by neglecting thermal dynamics linked to transport phenomena inside the pipe models. For this simplified dynamic model only 4,600 equations are left to be solved. When simulation is repeated with this model the integral results remain practically unchanged, but computing time shrinks to 2.7 hours (-92%). It should be noted though, that this simplified dynamic model is not anymore capable of predicting the dynamic behavior of the heating system. This is because neglecting the thermal dynamics inside the pipe models implies ideal mixing and thus neglects the dynamic behavior of the thermal enthalpy inside the pipe, compare section 3.2.2.

### 5.2. Conclusions

The simplified quasi-stationary approach minimizes time and effort to perform the system modeling and simulation. This approach has its limitations when addressing problems for which one has to resolve the dynamic system behavior, such as the design of controllers or peak load management systems. Nevertheless, the presented approach yields sufficiently accurate results when integral values are of main interest. This is demonstrated for the case studies investigated within this paper and applies to most tasks within the scope of industrial energy consultancy.

## Nomenclature

| | |
|---|---|
| $A$ | area, m² |
| $c$ | specific heat capacity, J/(kg K) |
| $h$ | specific enthalpy, J/kg |
| $k$ | heat loss coefficient, W/m$^2$ |
| $\dot{m}$ | mass flow, kg/s |
| $n$ | rotational speed, 1/s |
| $p$ | pressure, Pa |
| $P$ | power, W |
| $\dot{Q}$ | heat flux, W |
| $T$ | temperature, K |
| $U$ | internal energy, J |
| $v$ | specific volume, m$^3$/kg |
| $\dot{V}$ | volume flow, m³/s |
| $z$ | pressure head, m |

Greek symbols

| | |
|---|---|
| $\xi$ | pressure drop coefficient, 1/m$^2$ |
| $\eta$ | efficiency, 1 |

Subscripts and superscripts

| | |
|---|---|
| 0 | nominal |
| 1 | in, inlet; state 1 |
| 2 | out, outlet; state 2 |
| amb | ambient |
| el | electric |
| il | ideal liquid |

## References


[1] Augenstein, E., et. al., 2002, EUSEBIA Decision-Support-System for Technical, Economical and Ecological Design and Evaluation of Industrial Energy Systems, Proc. 15th International Conference on Energy, Cost, Optimization, Simulation and Environmental Impact of Energy Systems, G. Tsatsaronis, M. J. Moran, F. Cziesla, and T. Bruckner, eds., Berlin, Germany, pp. 446–453.

[2] Elmegaard, B., and Houbak, N., 2002, Software for the Simulation of Power Plant Processes, Part A and B, *Proc. 15th International Conference on Energy, Cost, Optimization, Simulation and Environmental Impact of Energy Systems*, G. Tsatsaronis, M. J. Moran, F. Cziesla, and T. Bruckner, eds., Berlin, Germany, pp. 742–772 .

[3] Augenstein, E., et al., 2004, TOP-Energy – Computational Support for Energy System Engineering Processes, *Proc. 1st International Conference from Scientific Computing to Computational Engineering*, D. T. Tsahalis, ed., Athens, Greece, 3, pp. 1284-1291.

[4] Kirschbaum, S., et al., 2008, Multi-Objective Approach to Analysis of Industrial Energy Systems, *Proc. 21st International Conference on Energy, Cost, Optimization, Simulation and Environmental Impact of Energy Systems*, A. Ziebik, Z. Kolenda, and W. Stanek, eds., Crakow-Gliwice, Poland.

[5] Voll, P., et. al., 2009, Time Series Analysis and Manipulation in Industrial Energy Systems, *Proc. 5th European Conference Economics and Management of Energy in Industry*, A. Reis, R. W. Grubbström, and G. P. Hammond, eds., Vilamoura, Portugal.

[6] Mott, R. L., 2005, *Applied Fluid Mechanics*, 6th ed., Prentice-Hall, New Jersey.

[7] Casella, F., and Leva, A., 2006, Modelling of Thermo-Hydraulic Power Generation Processes Using Modelica, Mathematical and Computer Modelling of Dynamical Systems, 12(1), pp. 19-33.

[8] Fritzson, P., 2004, *Principles of Object-Oriented Modeling and Simulation with Modelica 2.1*, 1st ed., Wiley-IEEE Press, New Jersey.

[9] Crane Co., 2009, *Flow of Fluids Through Valves, Fittings, and Pipe*, Crane Co., Stamford, USA.

# The efficiency of the manufacturing of chemical products through the overall industrial metabolism

*Jo Dewulf, Geert Van der Vorst, Wang Kang and Herman Van Langenhove*

*Research Group ENVOC, Ghent University, Coupure Links 653, B-9000 Ghent, Belgium*

**Abstract:** This contribution reports a detailed efficiency analysis of the manufacturing of chemical products through the overall industrial metabolism. Based on the life cycle database of ecoinvent, we consider 26 plastics, 59 organic solvents, 33 inorganic chemicals as well as 12 plastic monomers and analyse their production efficiency by quantifying the raw materials extracted from natural environment. Based on the concept of exergy and the database of cumulative exergy extraction from the natural environment (CEENE), three indicators are used to determine the resource efficiency for each group: (1) exergy content of the final products, MJ exergy per kg product, (2) CEENE score, i.e. MJ raw materials extracted from natural environment per kg product, (3) cumulative degree of perfection (CDP), the ratio of the exergy of the final product to the CEENE value to make the product. Finally, a comparison in metabolic efficiency among different sectors is made.

The results show that the production of 1 kg plastics needs on average the largest input of natural resources, being 130.08 MJ. In contrast, the production of inorganic chemicals requires on average the lowest resource intake, being 43.56 MJ/kg. Overall, the fossil resources are the main natural resource base to manufacture the chemicals, with about 76% of the total requested exergy extracted from the environment.

The study has also shown that in the production of plastics, organic solvents and plastic monomers, these industrial chemicals processes are quite efficient if they are compared to natural processes. In these three groups the average CDP values are all higher than 30%. However, in the production of inorganic chemicals, the production efficiency is quite low (8.99%), as it is compared with other groups.

Keywords: chemicals, plastics, industrial metabolism, exergy, Cumulative Exergy Extracted out of the Natural Environment (CEENE)

## 1. Introduction

Today, people enjoy a set of chemical products that are delivered through an industrial complex network. It is obvious that the resources that are the basis for this production chain are limited. A number of them such as fossil fuels are exhaustible. So, in this sense sustainable technology should be able to maximize the conversion efficiency of resources into products. The method to quantify the efficiency is based on thermodynamics: exergy. Exergy has been put forward as an indicator for the quality of resources. Exergy measures are traditionally applied to assess efficiency, regarding the exergy losses in a process system. However, the measure can be utilised as an indicator of resource quality demand when considering the specific resources that contain the exergy. Such an exergy measure indicates the required resources and assesses the total exergy removal from nature in order to provide a product, process or service. In this work, the exergetic content of the final chemical products is quantified. At the same time, the cumulative exergy extracted out of the natural environment as resources are quantified.

Based on the life cycle database of ecoinvent, different subgroups of chemical products are considered (plastics, organic solvents, inorganic chemicals and plastic monomers). Next to the efficiency, a distinction will be made for the kinds of resources which are used in the conversion processes to show the bottlenecks and opportunities for each sector.

## 2. Material and methods

### 2.1 Materials studied

The ecoinvent LCA database, which contains over 3900 datasets of products and services (processes),

is the product of the Swiss Centre for Life Cycle Inventories. In order to quantify the resources which are extracted out of the natural environment, based on the life cycle data of ecoinvent, different groups are considered, such as plastics, organic solvents, inorganic compounds and plastic monomers. As for each group, some major products are studied as presented below. In the group of plastics, it should be noticed that some polymers have more than one type of final products. To produce each type of those products, the specific manufacture processing is required. For polyethylene (PE), for example, there are three different types of final plastics, such as high density polyethylene (HDPE), low density polyethylene (LDPE) and linear low density polyethylene (LLDPE). All reactions for the production of plastics, organic solvents, inorganic compounds and plastic monomers are provided in specific ecoinvent report [1].

The list of plastics which are selected from ecoinvent database are: acrylonitrile-butadiene styrene, ethylene vinyl acetate, nylon 66, polybutadiene, polyethylene terephthalate, polyethylene HDPE, polyethylene LDPE, polyethylene LLDPE, polymethyl methacrylate, polypropylene, polystyrene EPS, polystyrene GPPS, polystyrene HIPS, polyvinyl chloride, polyvinylidene chloride, terephthalic acid, styrene-acrylonitrile copolymer, polyphenylene sulfide,

The list of plastic monomers which are selected are: acrylic acid, vinyl chloride, bisphenol A, propylene, butadiene, styrene, butane, toluene diisocyanate, ethylene, vinyl acetate, methyl methacrylate, methylene diphenyl diisocyanate.

The following organic solvents are analysed: 1-pentanol, cyclohexane, 2-butanol, cyclohexanone, 2-methyl-1-butanol, diethyl ether, 2-methyl-2-butanol, dimethyl sulfoxide, 2-methylpentane, dimethylamine, 3-methyl-1-butanol, dioxane, 3-methyl-1-butyl acetate, ethylene glycol, diethyl ether, 4-methyl-2-pentanone, ethylene glycol dimethyl ether, N,N-dimethylformamide, dichloromethane, N-methyl-2-pyrrolidone, ethanol, acetic acid, ethyl acetate, acetic anhydride, formic acid, acetonitrile, isobutyl acetate, acrylonitrile, isopropyl acetate, benzal chloride, methyl formate, monochlorobenzene, propanal, o-dichlorobenzene, butyl acetate, tetrahydrofuran, benzaldehyde, butane-1,4-diol, benzyl alcohol, methylcyclohexane, benzyl chloride, acetone, isopropanol, 1-butanol, methanol, ethylene glycol, monoethyl ether, methyl ethylketone, ethyl benzene, methyl tert-butylether, formaldehyde, pentane, toluene, xylene, hexane, heptane, methylcyclohexane, isobutanol, isohexane, methyl acetate and 1-propanol.

The list of inorganic chemicals selected is: ammonia (partial oxidation), ammonia (steam reforming), ammonium bicarbonate, calcium carbide, calcium chloride, carbon monoxide, hydrochloric acid 30%, ammonium chloride, diborane, iron (III) chloride 40%, lithium hydroxide, lithium chloride, nitric acid 50%, phosphoric acid 70%, phosphoric acid 85%, phosphoryl chloride, potassium carbonate, potassium perchlorate, sodium carbonate, sodium chlorate, sodium chloride brine solution, sodium chloride powder, sodium hydroxide 50%, sodium hypochlorite, sodium perchlorate, sodium sulphate and sulphuric acid.

## 2.2 Methods

The calculation of the exergetic content for each plastic, plastic monomer and solvent was performed either by using the group contribution method or directly taking from the reference of Szargut [2]. In the group of inorganic compounds, the exergy data of a part of products are directly obtained from [2]. If not available, the chemical exergy can be calculated on the basis of the chemical formation reaction, utilising the Gibb's free energy of formation $\Delta G_r$ (kJ/mol) [3].

Extraction of resources out of the environment is considered in order to quantify the Cumulative Exergy Extraction from the Natural Environment (CEENE) for virgin production. In CEENE, the acquired data set is coupled with a life cycle inventory database, ecoinvent. CEENE consists of eight categories of resources withdrawn from the natural environment: renewable resources, fossil fuels, nuclear energy, metal ores, minerals, water resources, land resources, and atmospheric resources. CEENE calculation has been illustrated in previous work [4]. The reference state for the environment in the calculations is taken as in [2]. The CEENE data for the different products are

obtained from the CEENE database developed by Dewulf et al. [4].

When analyzing the production of materials and energy flows, in order to assess the thermodynamic efficiency of production process, the CEENE value can be compared with the exergy of the product, as a measure of efficiency. The ratio between the specific exergy content of the product itself and the CEENE is defined as the Cumulative Degree of Perfection (CDP). The higher the CDP is, the higher the thermodynamics perfection degree of the overall industrial system is.

## 3. Results and discussion

### 3.1 Plastics

The chemical exergies of 26 plastics are calculated straightforward as (MJ/kg): acrylonitrile-butadiene-styrene copolymer (ABS): 40.37, ethylene vinyl acetate (EVA 1, copolymer): 29.37, ethylene vinyl acetate (EVA 2, film): 29.37, nylon 6 (1): 33.00, nylon 6 (2, glass filled): 33.00, nylon 66 (1): 33.00, nylon 66 (2, glass-filled): 33.00, polybutadiene (PB): 45.16, polyethylene terephthalate (PET 1, amorphous): 23.76, polyethylene terephthalate (PET 2, bottle grade): 23.76, high density polyethylene (HDPE): 46.44, low density polyethylene (LDPE): 46.44, linear low density polyethylene LLDPE: 46.44, polymethyl methacrylate (PMMA 1, beads): 27.16, polymethyl methacrylate (PMMA 2, sheet): 27.16, polypropylene (PP): 46.31, polystyrene (EPS): 41.95, general purpose polystyrene (GPPS): 41.95, high impact polystyrene (HIPS): 41.95, polyvinyl chloride (PVC 1, bulk polymerised): 19.81; polyvinyl chloride (PVC 2, emulsion polymerised): 19.81, polyvinyl chloride (PVC 3, suspension polymerised): 19.81, polyvinylidene chloride (PVDC): 12.28, terephthalic acid (TPA): 20.85, styrene-acrylonitrile (SAN): 38.72, polyphenylene sulfide (PPS): 34.69.

The CEENE values and the fraction in total exergy inputs are presented in table 1.

Table 1 CEENE values and fraction of fossils for plastics

| Product | CEENE (MJ/Kg) | Fossil (%) |
|---|---|---|
| ABS | 106.02 | 87.76 |
| EVA(1) | 86.67 | 85.78 |
| EVA(2) | 113.26 | 72.97 |
| Nylon 6(1) | 136.83 | 87.90 |
| Nylon 6(2) | 121.98 | 79.95 |
| Nylon 66 (1) | 168.38 | 72.79 |
| Nylon 66(2) | 136.09 | 73.88 |
| PB | 100.53 | 95.14 |
| PET(1) | 87.25 | 82.39 |
| PET(2) | 92.71 | 80.55 |
| HDPE | 78.40 | 91.79 |
| LDPE | 80.94 | 87.79 |
| LLDPE | 80.03 | 88.45 |
| PMMA(1) | 132.24 | 91.43 |
| PMMA(2) | 148.95 | 88.94 |
| PP | 76.93 | 92.09 |
| EPS | 97.93 | 87.73 |
| GPPS | 94.78 | 89.37 |
| HIPS | 95.07 | 89.32 |
| PVC(1) | 59.26 | 68.09 |
| PVC(2) | 93.99 | 54.82 |
| PVC(3) | 81.20 | 57.56 |
| PVDC | 87.40 | 72.83 |
| TPA | 63.51 | 85.26 |
| SAN | 101.50 | 89.12 |
| PPS | 860.35 | 85.37 |

Eight different categories of resources withdrawn from the natural environment for producing the target product are shown in figure 1. It is obvious

that exergy extraction for plastics made from polymers is dominated by exergy from fossil energy to provide the typical fuels and feedstocks with an average of 81%. However, the second largest exergy source for each plastic production is not the same in the CEENE categories, such as nuclear energy or water resources. The difference in categories can be explained by the fact that the manufacture processing and systems needed are different to achieve the specific properties of the plastics.

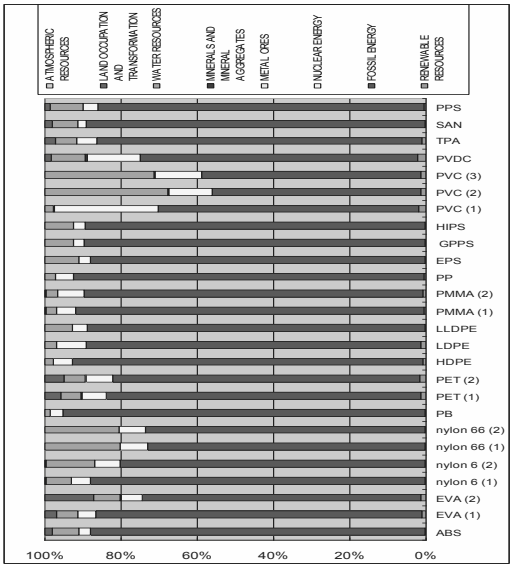


Figure 1 Comparison of the composition of CEENE for 26 plastics productions

In order to evaluate the thermodynamic efficiency of production process, the CDP values of all plastics products are separated into two groups, as represented in Figure 2.

In group (1), PP has the highest CDP value (60.2%) and the lowest one is PS (42.83). The average is 51.37%. In group (2), the range of CDP values is between 38.18% (ABS) and 14.04% (PVDC), except for PPS (4.03%).

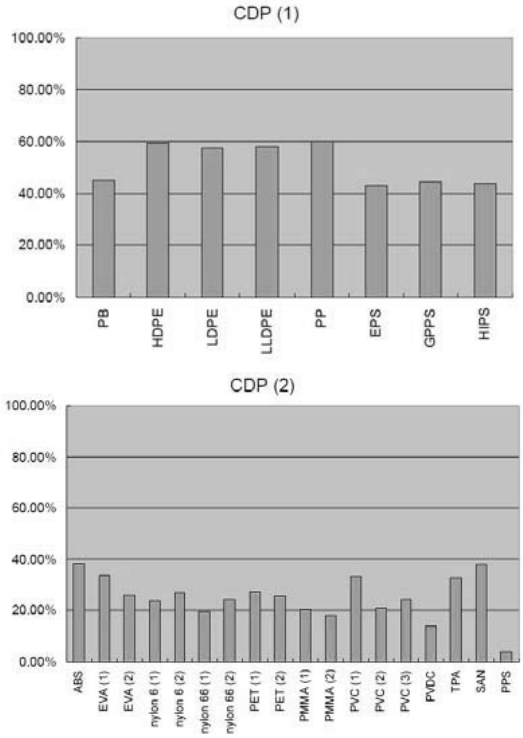


Figure 2 CDP values of plastics

The difference in the chemical exergy among polymers can be caused by the chemical structure or different degree of chemical reactions such as oxidation. In order to deliver the necessary materials and energy to the plant for the production of plastics, the industry has to extract a number of resources out of the environment. Based on the ecoinvent and CEENE database, these resources have been quantified in exergy terms. They all require exergy inputs between 59.26 (bulk PVC) and 168.38 (nylon 66) MJ per kg polymer, except for PPS (860.35 MJ/kg). The higher value for PPS is due to higher requirements of chemical inputs during the manufacturing process. To summarise the average shares of eight categories of resources intake ways within 26 plastics, it has shown that the major contribution to the CEENE scores is due to fossil energy (crude oil depletion and natural gas), accounting for instance, for 92.09% of the total in the case of PP. Secondly, in terms of thermodynamic efficiency, 32.88% (mean of CDP values) of the exergy intake is found back in the target product in case of the plastics industry.

### 3.2 Plastic monomers

The chemical exergy of 12 plastic monomers (MJ/kg) are calculated as: acrylic acid: 19.44, Methylene diphenyl diisocyanate: 30.16, bisphenol A: 35.02, propylene: 47.47, butadiene: 46.06, styrene: 42.42, butane: 47.22, toluene diisocyanate: 25.71, ethylene: 48.17, vinyl acetate: 24.38, methyl methacrylate: 27.51, vinyl chloride: 20.60. They range between 19.44 (acrylic acid) to 48.17 (ethylene) MJ/kg.

With respect to the CEENE values (Table 2), monomers require exergy inputs between 68.25 MJ/kg (butene) and 153.12 MJ/kg (bisphenol A). In the production of bisphenol A, one of the most important processes is the catalysed condensation of phenol and acetone. Such a reaction takes place at about 50 to 90 ℃ with a molar ratio of phenol-acetone of 15:1. An input amount of 0.916 kg phenol and 0.283 kg acetone are required for the production of 1 kg of bisphenol A. According to the analysis with respect to total resource inputs from technosphere in terms of exergy, it turns out that chemicals going into the manufacturing process of bisphenol A are predominant with a share of 81.10% of the total intake, 103.98 MJ (phenol) and 20.20 MJ (acetone), respectively, for the production of 1 kg of bisphenol A.

Eight categories of resources withdrawn from the natural environment for the production of 1 kg plastic monomers are shown in the figure 3. It can be seen that except for the fossil energy, only inputs of water resources and nuclear energy exhibit an important share of the total CEENE score. Depending on the plastic monomer, water resources make up between 1.34% (butadiene) and 27.03% (vinyl chloride) of the total exergy demand, with an average contribution of 8.41%.

A comparison of the cumulative degree of thermodynamic perfection (CDP) learns that ethylene, butene, butadiene and propylene exhibit the highest scores (65-70%). For the rest of the plastic monomers, the CDP scores are in the range of 21.05% (toluene diisocyanate) to 43.60% (styrene). The lowest CDP in the toluene diisocyanate is mainly due to the complex manufacturing process.

Table 2 CEENE values and fraction of fossils for monomers

| Product | CEENE (MJ/kg) | Fossil (%) |
|---|---|---|
| Acrylic acid | 69.32 | 89.03 |
| Bisphenol A | 153.12 | 81.92 |
| Butadiene | 67.59 | 96.97 |
| Butene | 68.25 | 94.80 |
| Ethylene | 68.46 | 95.84 |
| Methyl methacrylate | 125.48 | 91.66 |
| Methylene diphenyl diisocyanate | 105.97 | 76.48 |
| Propylene | 69.95 | 95.79 |
| Styrene | 97.29 | 85.39 |
| Toluene diisocyanate | 122.13 | 74.70 |
| Vinyl acetate | 79.53 | 77.19 |
| Vinyl chloride | 72.12 | 58.86 |

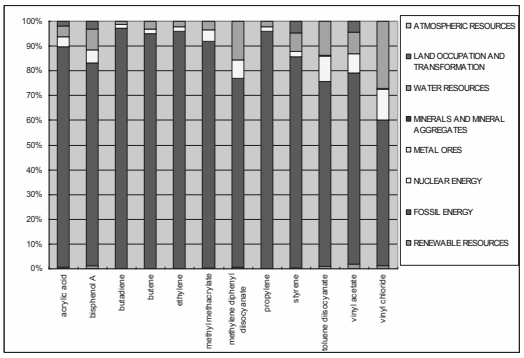

Figure 3 CEENE fingerprint of monomers

### 3.3. Organic solvents

For organic solvents, chemical exergies are not shown as this can be calculated straightforward. In Table 3, CEENE values are represented and in Figure 4 CEENE compositions.

Table 3 CEENE values and share of fossils for organic solvents

| Product | CEENE (MJ/kg) | Fossils (MJ/kg) |
|---|---|---|
| 1-pentanol | 113.51 | 94.29 |
| 2-butanol | 126.94 | 94.80 |
| 2-methyl-1-butanol | 113.51 | 94.29 |
| 2-methyl-2-butanol | 120.30 | 105.47 |
| 2-methylpentane | 65.82 | 60.49 |
| 3-methyl-1-butanol | 113.51 | 94.29 |
| 3-methyl-1-butyl acetate | 130.23 | 105.01 |
| 4-methyl-2-pentanone | 126.39 | 107.30 |
| N,N-dimethylformamide | 65.51 | 50.82 |
| N-methyl-2-pyrrolidone | 113.69 | 76.46 |
| Acetic acid | 62.03 | 47.06 |
| Acetic anhydride | 113.40 | 74.91 |
| Acetonitrile | 75.40 | 58.99 |
| Acrylonitrile | 95.41 | 86.02 |
| Benzal chloride | 83.27 | 59.45 |
| Monochlorobenzene | 494.23 | 433.04 |
| O-dichlorobenzene | 494.22 | 433.03 |
| Tetrahydrofuran | 170.75 | 111.83 |
| Butane-1,4-diol | 129.76 | 86.04 |
| Methylcyclohexane | 129.25 | 115.36 |
| Cyclohexane | 83.23 | 73.98 |
| Cyclohexanone | 118.14 | 102.20 |
| Diethyl ether | 50.63 | 46.48 |
| Dimethyl sulfoxide | 61.67 | 52.86 |
| Dimethylamine | 45.34 | 38.57 |
| Dioxane | 101.02 | 70.14 |
| Ethylene glycol diethyl ether | 103.45 | 76.05 |
| Ethylene glycol dimethyl ether | 82.84 | 69.43 |
| Ethylene glycol monoethyl ether | 73.63 | 62.05 |
| Ethanol | 50.66 | 46.50 |
| Ethyl acetate | 93.50 | 76.31 |
| Formic acid | 85.51 | 58.13 |
| Isobutyl acetate | 112.14 | 92.45 |
| Isopropyl acetate | 99.65 | 81.57 |
| Methyl formate | 113.11 | 80.33 |
| Propanal | 106.90 | 85.63 |
| Butyl acetate | 117.09 | 97.90 |
| Benzaldehyde | 146.67 | 104.81 |
| Benzyl alcohol | 122.72 | 90.01 |
| Benzyl chloride | 84.23 | 65.15 |

It can be seen that monochlorobenzene and o-dichlorobenzene have the highest CEENE values, 494.23 MJ/kg and 494.22 MJ/kg. The average CEENE value in the group of organic solvents is 103.98 MJ for producing 1 kg product. It turns out that fossil energy is the major input source, in the case of 1-pentanol, accounting for 83.07% of the total exergy inputs. Eight main intakes for the production of 1kg target organic solvent are calculated in the form of percentage (%) as presented in the figure 4.

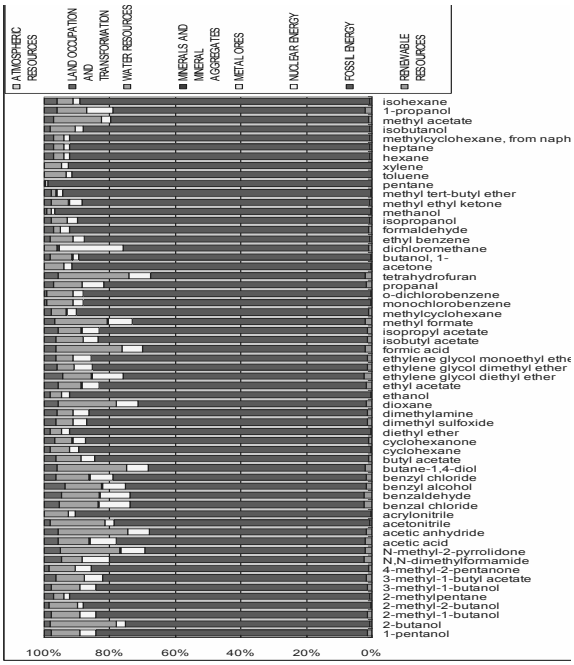

Figure 4 CEENE composition of solvents

Dimethylamine, diethyl ether, hexane, 2-methylpentane, heptane, methylcyclohexane, isohexane, toluene, methyl tert-butyl ether and xylene exhibit high CDP: above 60%. Overall low scores of CDP for methyl formate, acetic anhydride, formic acid, monochlorobenzene and o-dichlorobenzene are 14.76%, 11.29%, 7.41%, 5.78% and 4.33%, respectively. For the rest of organic solvents in the group, the values of CDP are in the range from 60% to 20%, in which the methanol has the highest value and the lowest one is for tetrahydrofuran, 58.44% and 20.37%, respectively. In the whole group of organic solvents, the average value of CDP is 38.95%.

### 3.4. Inorganic chemicals

Whereas exergy value calculations are straightforward (results not shown), CEENE values and share of fossils are presented in Table 4.

Table 4. CEENE values and fossil contribution for inorganic chemicals.

| Product | CEENE (MJ/kg) | Fossil (%) |
|---|---|---|
| Ammonia (1) | 56.52 | 92.20 |
| Ammonia (2) | 41.99 | 92.88 |
| Ammonium bicarbonate | 37.08 | 48.54 |
| Calcium carbide | 80.05 | 63.71 |
| Calcium chloride | 20.55 | 46.23 |
| Carbon dioxide | 14.59 | 61.00 |
| Carbon monoxide | 67.59 | 75.45 |
| Hydrochloric acid | 24.68 | 48.62 |
| Ammonium chloride | 89.59 | 61.39 |
| Diborane | 72.41 | 51.10 |
| Iron (III) chloride | 25.21 | 43.63 |
| Lithium hydroxide | 24.70 | 56.68 |
| Lithium chloride | 54.19 | 47.98 |
| Nitric acid | 15.65 | 83.07 |
| Phosphoric acid (1) | 47.65 | 25.18 |
| Phosphoric acid (2) | 57.65 | 31.22 |
| Phosphoryl chloride | 100.64 | 49.68 |
| Potassium carbonate | 53.79 | 59.49 |
| Potassium perchlorate | 133.07 | 48.85 |
| Sodium carbonate | 25.72 | 66.10 |
| Sodium chlorate | 84.94 | 45.91 |
| Sodium chloride (1) | 4.11 | 43.80 |
| Sodium chloride (2) | 5.67 | 44.09 |
| Sodium hydroxide (1) | 37.57 | 39.93 |
| Sodium hydroxide (2) | 27.99 | 46.45 |
| Sodium hydroxide (3) | 29.94 | 46.76 |
| Sodium hydroxide (4) | 31.32 | 44.70 |
| Sodium hypochlorite | 24.03 | 49.94 |
| Sodium perchlorate | 118.77 | 47.15 |
| Sodium sulphate (1) | 13.87 | 52.63 |
| Sodium sulphate (2) | 3.75 | 48.00 |
| Sodium sulphate (3) | 10.98 | 61.02 |
| Sulphuric acid | 5.67 | 33.51 |

It can be seen that potassium perchlorate (133.07 MJ/kg) and sodium perchlorate (118.77 MJ/kg) exhibit high CEENE values. The inputs of fossils are often over 40% of the total exergy extraction from the natural environment, especially for ammonia, where the fossil energy is up to 90% of the total CEENE score. This is due to the fact that fossil energy is used both as fuel and feedstock in the production of ammonia. Ammonia is produced basically from natural gas (steam reforming).

It can be seen from Figure 5 that except for fossil energy, the inputs of water resources and nuclear energy as well as land occupation also take up an important share of the total intake. The exergy of land use contributes on the average to 12.60% the total exergy demand, but to more than 50% in the production of phosphoric acid. It is mainly due to the large amounts of raw materials (phosphate rock and sulphuric acid) and process water needed.

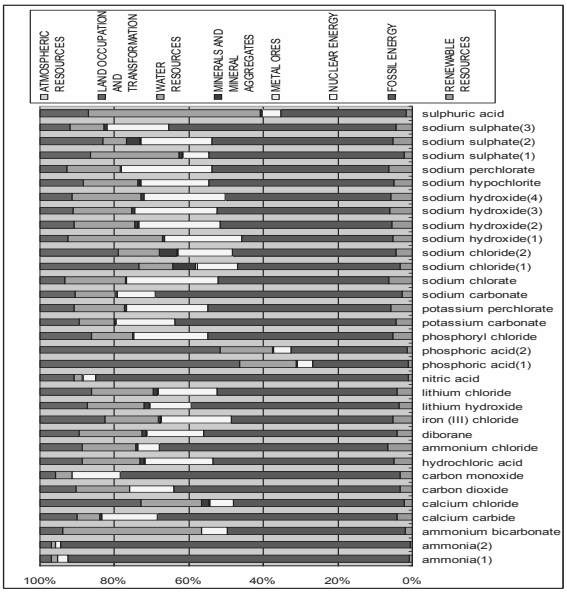

Figure 5 Composition of CEENE of inorganic chemicals

The CDP values are illustrated in Figure 6. They are obviously lower than for organics with a range of 0.93% to 50.50%, and an average value of 8.99%.

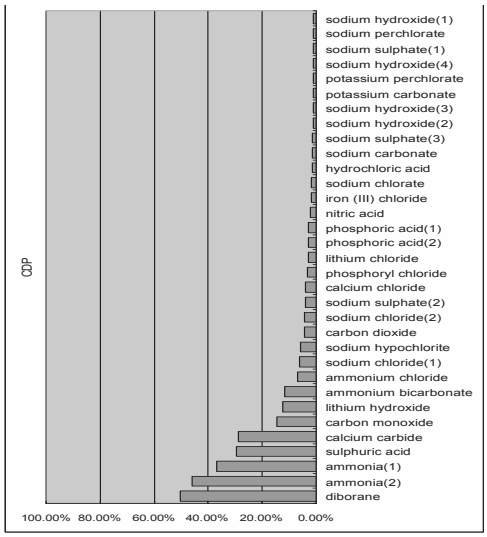

Figure 6 CDP values for inorganics

## 4. Conclusions

First of all, this work shows that the exergy concept can be operationalized in product life cycle assessments. Due to the consideration of the quality of energy and the integration of non-energetic resources, CEENE enables to account for very different natural resource intakes. This approach is helpful in substantiating the argument on sustainable use of the natural environment by humans: it expresses the physical chemical price the natural environment pays for the withdrawal toward our industrial society. Through the eight different resource categories, and the integrated development with the up-to-date life cycle inventory in ecoinvent, it shows the nature of the resources that are consumed in the chemical industry.

In terms of production efficiency, we have seen that plastics, organic solvents and plastic monomers are generally manufactured with efficient use of resources if they are compared to natural processes. In these three groups the average CDP values are all higher than 30%. The production of inorganic chemicals, the efficiency is quite low (8.99%). Overall, it can be stated that through combination of CEENE with an up-to-date life cycle inventory such as ecoinvent, decision-makers can obtain a comprehensive LCIA methods taking into consideration the impact of resource input as well as production efficiency.

References

[1] Ecoinvent, 2007. *Swiss Centre for Life-Cycle Inventories, ecoinvent database*. 2007, www.ecoinvent.org, Switzerland.

[2] Szargut, J., 2005. *Exergy method: Technical and ecological applications*. WIT Press, Southampton, UK

[3] Bosch, M. E. et al., 2007, Applying cumulative exergy demand (CExD) indicators to the ecoinvent database, International Journal of Life Cycle Assessment, 12(3), pp. 181-190.

[4] Dewulf, J. et al., 2007, Cumulative exergy extraction from the natural environment (CEENE): a comprehensive life cycle impact assessment method for resource accounting, Environmental Science & Technology, 41(24), pp. 8477-8483.

# Supervised learning for a Kraft recovery boiler: a data mining approach with Random Forests.

*Matthieu Sainlez* [a], *Georges Heyen* [b], *Sébastien Lafourcade* [c]

[a] *CRISIA, Haute-Ecole Robert Schuman, Arlon, Belgium*
[b] *LASSC, University of Liège, Liège, Belgium*
[c] *PEPITe Technologies Inc., Montréal (Québec), Canada*

**Abstract:** A data mining methodology, the random forests, is applied to predict high pressure steam production from the recovery boiler of a Kraft pulping process. Starting from a large database of raw process data, the goal is to identify the input variables that explain the most significant output variations and to predict the high pressure steam flow.

**Keywords:** data mining, Random Forests, Kraft recovery boiler, steam production.

## 1. Introduction

Data Mining refers to extracting useful knowledge from large amounts of data. Starting from a large database of raw process data, the main objective is to find interesting latent patterns ([11]). There is an increasing demand in industries for efficient data analysis tools, especially for energy management.
Pulp and paper industries, for example, account for one-third of total manufacturing energy use in Canada ([7]).
Within the framework of a Kraft pulp mill, we analyze high pressure steam production. Steam is used in other mill processes and to run a steam turbine in order to produce electrical energy. Furthermore, we want to estimate the relative importance or contribution of each input variable in predicting the response.
A promising way to achieve that is to use a combination of models. Particularly, Random Forests are a combination of tree predictors such that each tree depends on the values of a random vector sampled independently and with the same distribution for all trees in the forest ([6]).
In the end, the model relevance is assessed by its performance for predicting new observations.

## 2. Scope of this study

There are many motivations for evaluating a data mining solution in industries. In a previous study (see [15]), we analyzed recovery boiler pollutants (e.g., nitrogen oxide) using a data mining approach to classify attributes relevance for predicting pollutant emissions. In many data mining applications, only a few input variables have substantial influence on the response. Therefore, it is often useful to learn the relative importance or contribution of each input variable in predicting the response.
Supervised learning methods use a response variable to guide a statistical learning scheme.
Because of the curse of dimensionality ([12]), several methods often fail in high dimensions (e.g., nearest neighbor models). Some other popular data mining methods, like neural networks, are competitive but less interpretable compared to tree based models like Random Forests.
The main target of this paper is to highlight the interest of this technique for predicting a complex industrial response and assigning a relative importance for each input attribute.
The paper is organized as follows: firstly we present the Kraft Pulping process and particularly the recovery boiler steam production, secondly we introduce the Random Forests methodology and finally applying it for high pressure steam flow prediction.

## 3. The Kraft recovery boiler

The Kraft process is an alkaline process to produce chemical pulp. A pulp mill can be divided in two main areas ([17]): fiber line and chemical recovery loop. Cellulose fibers are dissociated from lignin by cooking the chips in a solution of sodium hydroxide ($NaOH$) and sodium sulfide ($Na_2S$), called white liquor. The residual black liquor is washed from the pulp and treated to recover the cooking chemicals.

Corresponding author: Sainlez Matthieu, Email: matthieu.sainlez@hers.be

Black liquor is the major by-product of the process and one of the most important industrial fuels ([13]). The black liquor is concentrated and burned in a recovery furnace to yield an inorganic smelt of sodium carbonate ($Na_2CO_3$) and $Na_2S$.
The smelt is dissolved to form green liquor, which is treated to recycle the calcium carbonate and to regenerate the white liquor.

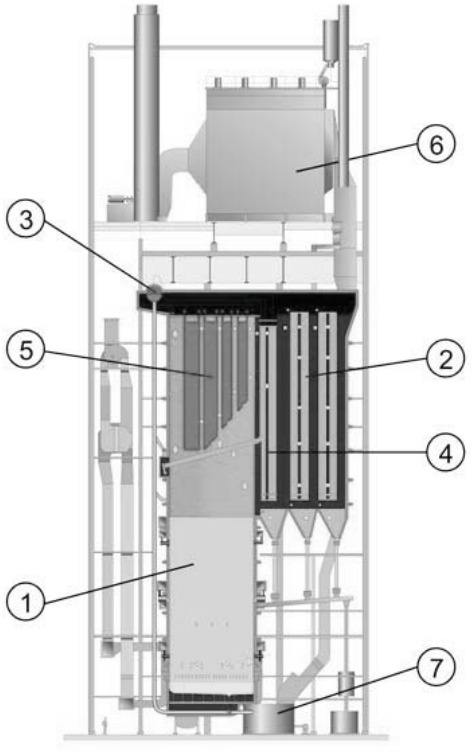


*Figure 1: Section of a modern Kraft recovery boiler*

The recovery boiler furnace can be considered as consisting of three distinct zones ([17]): a drying zone where the black liquor is fired, a reduction zone at the bottom where the smelt is formed, and the oxidation zone in the turbulent upper section. This boiler both regenerates the cooking chemicals (reducing the sulphates to sulphide) and produces high pressure steam that is typically used in the process.
It provides about 65% of the mill steam demand by the combustion of black liquor which is concentrated to about 70% dissolved solids content ([7]). Note that heavy fuel is rarely used at recovery boiler, mainly for the boiler start-up and maintenance.
The combustion air is supplied through nozzles at several levels around the furnace ([3]). Char bed reactions, its size and shape are controlled by the primary and secondary air. Tertiary and quaternary air provides oxygen to assure efficient mixing for complete combustion, these flows constitute the "over-fire air system ([3])" and assure a proper black liquor distribution above the char bed.
A modern recovery boiler, similar to the one studied, is presented in Fig.1. The black liquor is fired in the furnace (1). On the steam production side, the feed-water is preheated in the economizers (2) before entering in the steam drum (3); saturated steam is generated in the screen (4) and separated in the upper part of the steam drum and lead to the superheaters (5). High, medium and low temperature superheaters are located first in the flue gas path, close to the furnace.
We denote two auxiliary equipments: the electrostatic precipitator (6) that removes particles from the flue gas after the economizers and a dissolver tank (7) that receives the smelt to form green liquor.

## 4. Random Forests methodology

We consider a regression problem in which we are trying to predict the mass flow rate of the high pressure steam that leaves the high temperature superheater.
Let's consider a training set $\mathbf{z} = \{(x_1, y_1), \ldots, (x_n, y_n)\}$ where each $x_i = \left(x_{i1}, x_{i2}, \ldots, x_{ip}\right)^T$ is the $i^{th}$ measurement vector of $p$ input attributes, $y_i$ is the continuous response. We fit a model to $\mathbf{z}$, obtaining the prediction $\widehat{f}(x)$ at input $x$.

### 4.1. From binary trees to Random Forests

The binary tree is a widely used framework in data mining ([2, 10]); this concept can be applied both to classification or regression problems.
Basically, it's a sequence of binary decisions applied to the input variables; each non-terminal node contains a decision involving the comparison of an attribute with a given threshold, which then leads to another node or to a leaf (a terminal node). The root node contains the whole dataset which is recursively split into two branches at each node. A greedy algorithm selects the attribute and threshold that maximizes a given fitness measure.
A particular tree framework called CART (for "Classification And Regression Trees") maximizes the Gini index that selects the split with the lowest impurity at each node; CART was introduced by Breiman in 1984 ([4]). Generally, the resulting

tree is easily interpretable (giving a set of decision rules), it works with both numerical and categorical data, and it's a non parametric method (no a priori assumption is made).
Unfortunately, trees are sensitive to small changes in the learning sample ([5]). Moreover, unstable trees can be stabilized via an ensemble method: we average the predictions of a set of individual models (see for example, [9]).
Practically, we have a single training data set, and so we have to find a way to introduce variability between the different models: we use bootstrap data samples ([2]). A bootstrap replicate is a random subset of the original dataset, of the same length, taken with replacement ([8]).
We generate $m$ bootstrap samples and then use each to train a separate copy of a predictive model. This procedure is known as bootstrap aggregating or bagging ([5]). The aim of aggregating is to create an improved model. We take the average value of each prediction for a given test sample. For each bootstrap sample $z_i$ ($i = 1, \ldots, m$), we grow a full tree $T_i$ with CART. Then we aggregate the ensemble $\{T_i\}_i^m$ (see Fig.2).

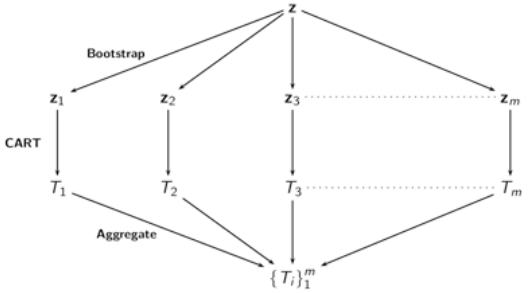


*Figure 2: Bootstrap Aggregating: Bagging*

For a giving prediction $\widehat{f_i}(x)$, the bagging estimate is the average of predictions over the $m$ trees. Bagging is very helpful for reducing variance and, for prediction, Breiman proved theoretically that a bagged predictor will always have improved accuracy over a single predictor ([5]).

### 4.2. Random Forests algorithm

A random forest is an ensemble of unpruned classification or regression trees (Breiman,[6]), induced from bootstrap samples of the training data, using random feature selection in the CART induction process.
In the Random Forests methodology ([6, 10, 12]), a second source of diversity is introduced during the growing of each tree. For each node, the method selects a small random subset of $k$ attributes (from the $p$ input attributes) and uses only this subset to search for the best split.
This random selection of features at each node decreases the correlation between the trees in the forest thus decreasing the forest error rate. We fit each tree on bootstrap sample and we select threshold and attribute at each node from a subset of attributes; the algorithm is described below ([12]):

---

- Given $\mathbf{z} = \{(\mathbf{x}_1, y_1), \ldots, (\mathbf{x}_n, y_n)\}$ a sample,
- For $i = 1$ to $m$, Do
  1. Draw a bootstrap sample $\mathbf{z}_i$ of size $n$ from $\mathbf{z}$
  2. Grow a tree $T_i$ to $\mathbf{z}_i$ by recursively repeating these steps for each non terminal node, until the minimum node size $N_{\min}$ is reached.
     (a) select $k$ variables randomly from the $p$ variables ($k < p$),
     (b) pick the best variable/split point among the $k$,
     (c) split the node into two daughter nodes.
- Output the ensemble $\{T_i\}_1^m$
- To make a prediction at a new point $\mathbf{x}$:
  $\widehat{f}_{RF}^m(\mathbf{x}) = \frac{1}{m}\sum_{i=1}^{m} T_i(\mathbf{x})$

---

Classical values for regression are $(k, N_{\min}) = (\lfloor p/3 \rfloor, 5)$, with $p$ the total number of input attributes ([12]).
Random Forests use the out-of-bag (OOB) samples for assigning variable importance measure. On average, 37% of the samples will not be present in a given bootstrap ([1, 10]): they are called OOB sets. When a tree in the forest is grown, the OOB samples are passed down the tree, and the prediction accuracy is recorded. Then, one at a time, each attribute values are randomly permuted in the OOB samples, and the accuracy is again computed. The decrease in accuracy as a result of this permuting is averaged over all trees, and is used as a measure of the importance of a variable in the random forest ([1, 12]).

## 5. Industrial case study

Our original database is a two years of historical data related to the recovery boiler: 65509 obser-

vations for 56 process variables (referred as to attributes). Those input attributes are mainly physical flow rates, pressures, temperatures for the main process flows: black liquor, fuel, air, water,...
We used a Matlab R13 implementation of Breiman's Random Forests algorithm for regression ([18], based on Breiman and Cutler's original Fortran code version 3.3).
Firstly, the database is preprocessed to make it appropriate for the analysis ([14]): all start-up and maintenance periods are eliminated. Then, the given original data set is partitioned into two independent sets ([11]): a training set (70% of the data) and a test set (the remaining 30%). The training set is used to build the model, whose accuracy is estimated with the test set.
Secondly, we select the appropriate number of trees in the forest. We analyzed the prediction score related to each $m$ varying from $m = 1$ to $m = 150$.
This is the score of correlation between the test set of real values and the predicted values computing via Random Forests.

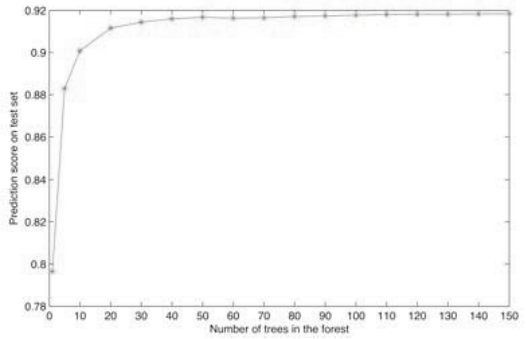


*Figure 3: Random Forests prediction score on the test set related to the number of trees in the forest.*

We can observe on Fig.3 that the prediction score increases rapidly and reaches a limiting value. In this case, Random Forests stabilize at about 80 trees. We take the following Random Forests design:

$$(m, k, N_{\min}) = (80, 18, 5)$$

Note that this step is important in terms of computational time minimization.
Then, we can observe on Fig.4 that the mean squared error on training set converges to a limiting value.
At this subject, Breiman wrote that "Use of the Strong Law of Large Numbers shows that Random Forests always converge so that over-fitting is not a problem ([6, 16])"; it explains why Random Forests do not over-fit as more trees are added.

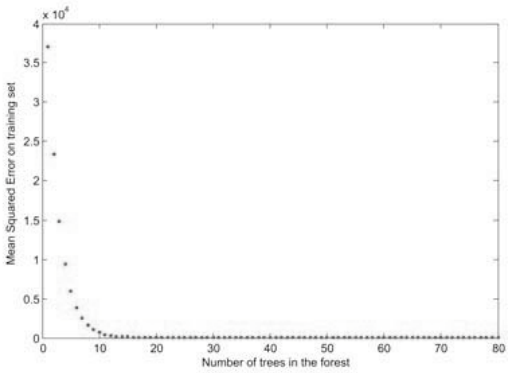


*Figure 4: Mean Squared Error on the training set related to the number of trees in the forest.*

As we said before, only a few input variables have usually a significant influence on the response. Therefore we want to learn the relative importance of each input attribute in predicting the response.
Attributes are ranked according to the importance measure (expressed as a percentage of the overall importance, see Fig.5). For a fixed number of trees, a variable with a larger importance score relative to other variables indicates that the variable is important for regression. This hierarchy presents the first 25 relevant attributes on a total of 56.

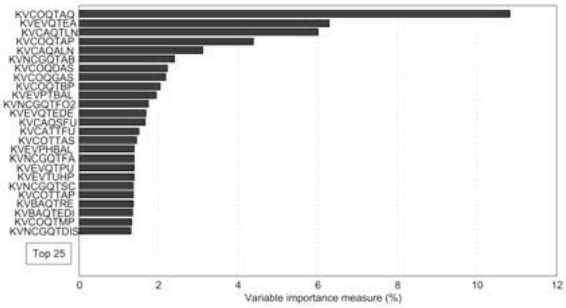


*Figure 5: Random Forest attributes score importance (%) for design* $(m, k, N_{\min}) = (80, 18, 5)$.

Quaternary air flow (KVCOQTAQ) is the more relevant attribute (10, 8%) for predicting high pressure steam flow. It regulates directly oxygen molar fraction in the flue gas which is related to boiler's load. Consequently it regulates the flue gas temperature and influences the heat exchange efficiency.
The feed water flow (KVEVQTEA) accounts for 6, 3%; this flow regulates the steam drum level and

is directly related to the steam flow.
Then, the entering black liquor flow rate (KVCAQTLN) at 6,0% is a part of the total black liquor flow rate (KVCAQALN) which is circulated in a loop around the liquor guns; these variables are highly correlated. Next, primary air flow (KVCOQTAP) accounts for 4,4% and is related to the char bed reactions.
This hierarchy is an interesting tool for better understanding which inputs affect steam prediction.
It helped operation people to better understand which parameter induce steam generation variability. In particular, quaternary air flow was not expected to be that important. Therefore it provides valuable knowledge to the mill and triggered further investigation.
Finally, we compute the Random Forests predictor on the test set (see Fig.6). The Pearson's correlation coefficient between the test set of real values and the predicted values computing via Random Forests was: 0,92.

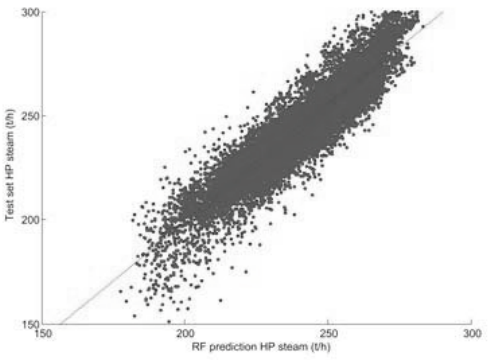


*Figure 6: Random Forests high pressure steam prediction related to test data set (units: ton/hour).*

This high correlation coefficient acts the pertinence of using Random Forests in a Kraft recovery boiler steam flow analysis.

## 6. Conclusions

This paper briefly highlighted the powerful of Random Forests in a steam flow prediction problem. Random Forests handle very large database, with mixed data types (discrete or continuous) and with missing data.
This method is easy to use and fast, requiring only a little tuning on parameters.
Its internal variable importance measure is very helpful for understanding complex interactions between attributes and discovering latent patterns.
An interesting extension of this paper is to consider boiler's operating modes separately (black liquor or heavy fuel injection) and to fit the model on these modes.

## References

[1] Kellie J. Archer and Ryan V. Kimes. Empirical characterization of random forest variable importance measures. *Computational Statistics and Data Analysis*, 52:2249–2260, 2008.

[2] Christopher M. Bishop. *Pattern Recognition and Machine Learning*. Springer, 2006.

[3] W. Blasiak, L. Tao, J. Vaclavinek, and P. Lidegran. Modeling of kraft recovery boilers. *Energy Conversion Management*, 38:995–1005, 1997.

[4] L. Breiman, J. Friedman, R. Olshen, and C. Stone. *Classification and Regression Trees*. Wadsworth, 1984.

[5] Leo Breiman. Bagging predictors. *Machine Learning*, 24:123–140, 1996.

[6] Leo Breiman. Random forests. *Machine Learning*, 45:5–32, 2001.

[7] Adrian Cakembergh-Mas, Jean Paris, and Martin Trépanier. Strategic simulation of the energy management in a kraft mill. *Energy Conversion Management*, 51:988–997, 2010.

[8] B. Efron. Estimating the error rate of a prediction rule: some improvements on cross-validation. *Journal of the American Statistical Association*, 78:316–331, 1983.

[9] Pierre Geurts, Damien Ernst, and Louis Wehenkel. Extremely randomized trees. *Computational Statistics and Data Analysis*, 36:3–42, 2006.

[10] P.M. Granitto, F. Gasperi, F. Biasioli, E. Trainotti, and C. Furlanello. Modern data mining tools in descriptive sensory analysis: A case study with a random forest approach. *Food Quality and Preference*, 18:681–689, 2007.

[11] Jiawei Han and Micheline Kamer. *Data Mining : Concepts and Techniques*. Morgan Kaufmann Publishers, 1984.

[12] Trevor Hastie, Robert Tibshirani, and Jerome Friedman. *The Elements of Statistical Learning : Data Mining, Inference, and Prediction*. Springer Series in Statistics, 2009. Second Edition.

[13] Andrej Macek. Research on combustion of black-liquor drops. *Progress in Energy and Combustion Science*, 25:275–304, 1999.

[14] Sigurdur Olafsson, Xiaonan Li, and Shuning Wu. Operations research and data mining. *European Journal of Operational Research*, 187:1429–1448, 2008.

[15] Matthieu Sainlez and Georges Heyen. Performance monitoring of an industrial boiler: classification of relevant variables with random forests. In S. Pierucci and G. Buzzi Ferraris (Editors), editors, *20th European Symposium on Computer Aided Process Engineering ESCAPE20*. Elsevier, 2010. Accepted paper.

[16] David S. Siroky. Navigating random forests and related advances in algorithmic modeling. *Statistics Surveys*, 3:147–163, 2009.

[17] Gary A. Smook. *Handbook for Pulp and Paper Technologists*. Angus Wilde Publications, 2002. Third Edition.

[18] Ting Wang. Package random forests for matlab r13. `http://lib.stat.cmu.edu/matlab/`.

**Acknowledgments:** This project was supported by the Walloon Region (FIRST Program, PHOEBUS). The authors would like to thank PEPITe S.A. (Liège, Belgium) for the expert opinion on the subject.

# A Method for Site-specific Analysis of $CO_2$-Emission and Cost Reduction Potentials of ODC-Technology in the Chlorine Industry

*Johannes Jung and André Bardow*

*Chair of Technical Thermodynamics, RWTH Aachen University, Aachen, Germany*

**Abstract:** Industrial energy efficiency is nowadays a key characteristic of technologies besides their costs. For new emerging technologies, however, its evaluation becomes complicated if different in- and outputs occur. The introduction of a new chlorine-electrolysis technology is an example for such evaluation difficulties. It is shown that existing analysis methods do not allow for a universal evaluation of energy demand, $CO_2$-emission and cost reduction potentials of the new technology. A software-based site-specific method is therefore introduced and applied to the example of chlorine production in a case study. The final results support the approach because $CO_2$-emission and energy cost reduction potentials are found to strongly depend on site-specific constraints. Hence, it is concluded that a universally valid best-available-technology for chlorine production cannot be declared anymore if the new technology is introduced. The site-specific analysis approach is found to also allow for deduction of suitable conditions for the application of the new technology for chlorine production. The approach provides a generally sound method for evaluation of multi-product systems with different product uses.

**Keywords:** Technology Assessment, Industrial Energy Efficiency, Chlorine Electrolysis

## 1. Introduction

Industrial processes account for a significant part of the world's primary energy demand and $CO_2$-emissions. Increased energy prices and public awareness of climate change are forcing industries to improve and redesign their processes towards higher efficiencies. Industrial energy efficiency has become a particular key object in many companies and industry sectors. The development of more energy-efficient processes and technologies is encouraged by economic development schemes in many countries. Hence, the evaluation of industrial energy efficiency is a scientific field of interest. Results of such evaluations are often published in documents on best-available-technologies (BATs). In an ideal case, one technology within an industry sector has superior energy-efficiency and environmental impact characteristics combined with lowest costs. It can be consequently declared as BAT without reservation. However, the ideal case does not always apply in real life. The evaluation of multi-product systems, is particularly complicated because the main function of a process or technology can vary here. Hence, a clear definition of the BAT becomes problematic: Reference documents become vague and may include many exceptions.

Chlorine production is a typical example for such a complex evaluation problem. Being amongst the most energy-intensive industrial processes [1], it has always been in focus for energy-efficiency improvements. Chlorine production in an electrolysis process is by nature a multi-product process delivering the by-products sodium hydroxide and hydrogen. The evaluation of a new electrolysis technology with promising energy-efficiency characteristics ([2]) but different by-products brings up the question of the suitability of universally declared BATs for multi-product technology assessments. The aim of this work is the development of a technology assessment strategy for cases where regular evaluation techniques may fail. Chlorine production as the motivating example is briefly described in section 2 before the approach for a software-based site-specific evaluation model is illustrated in section 3. The model is presented in section 4 and applied in a case study in section 5. Conclusions for chlorine production technology assessment and the suitability of the site-specific model approach are given in section 6.

Corresponding Author: Johannes Jung, Email: jung@ltt.rwth-aachen.de

# 2. Motivating Example: Chlorine Electrolysis

## 2.1. Industrial Chlorine Production

Chlorine is a highly reactive gas and a strong oxidant in chemical reactions. Hence, it has become an essential chemical commodity required for the production of numerous products. The European annual chlorine production peaked at 10.4 millions tons in 2007 ([3]), worldwide production was at 52 million tons in 2003 ([4]). An average energy demand of 3415 kWh per ton chlorine is given for the European capacities ([3]). Assuming this average demand for the global capacities gives an annual energy demand of approx. 178 TWh in 2003.

## 2.2. Established Industrial Chlorine Electrolysis Technologies

The process of driving a non-spontaneous reaction using electric current is called electrolysis. Electrolyzing sodium chloride solution forms gaseous elemental chlorine at the anode as well as a sodium hydroxide solution and gaseous elemental hydrogen at the cathode. This process is called chlor-alkali electrolysis and can be generally described by the following overall stoichiometry:

$$2NaCl + 2H_2O \rightarrow 2NaOH + Cl_2 + H_2 \quad (1)$$

The products of the anode (i.e. chlorine) and the cathode (i.e. hydrogen and sodium hydroxide solution) have to be separated to avoid forming of unwanted hypochlorite and explosive hydrogen-chlorine mixtures. Three technical solutions are established as today's chlor-alkali-processes. These technologies will be described briefly in the following sections, detailed information can be found in [5], [6].

### 2.2.1. Diaphragm Technology

Diaphragm electrolysis uses a porous diaphragm to separate anode and cathode products, especially to avoid transport of hydroxide-ions from cathode to anode by streaming of the complete anolyte through the diaphragm into the cathode chamber. It has major disadvantages: The sodium hydroxide mass fraction in the solution is low at ca. 12 wt % and ca. 15 wt % of sodium chloride are still included in the solution. The impurity can only be removed down to ca. 1 wt % sodium chloride by evaporation up to 50 wt % of sodium hydroxide. This requires a high consumption of thermal energy and expensive apparatus. Additionally the diaphragms are commonly made of hazardous asbestos.

### 2.2.2. Mercury Technology

This electrolysis places the formation of chlorine and hydrogen in two different reactors. Chlorine and a sodium/mercury amalgam are formed in the first reactor. The amalgam is transported to the second reactor, where it reacts with water to form hydrogen and sodium hydroxide solution while the mercury is recycled. This process delivers very pure sodium hydroxide with a mass fraction of 50 wt % in the solution, but the electrical energy demand is increased and hazardous mercury requires expensive precautions.

### 2.2.3. Membrane Technology

The membrane technology applies a nearly ideal separation principle: a semi-permeable ion-exchange membrane enables the necessary transport of sodium ions from anode to cathode and suppresses almost completely the undesired transfer of hydroxide ions in the opposite direction. It produces very pure sodium hydroxide with a mass fraction in the solution typically at 32 wt %.

### 2.2.4. Best Available Technology

The three described technologies are usually compared assuming gaseous chlorine and sodium hydroxide in a 50 wt. % solution as basis of comparison. Hydrogen as a third product is not considered because it is formed equally in all three processes. Both diaphragm and mercury electrolysis technologies have major disadvantages compared to the membrane technology: they use the hazardous materials asbestos and mercury, respectively. Furthermore, they have a higher energy demand: the diaphragm technology requires the evaporation of the catholyte (and delivers impure sodium hydroxide) and the mercury technology needs an increased cell voltage due to the intermediate sodium metal formation in the amalgam. Consequently, membrane technology is the state-of-the art solution for chlor-alkali electrolysis being declared BAT of the European Union in 2001 ([7])

## 2.3. Oxygen-Depolarized-Cathodes for Energy-Efficient Chlorine Electrolysis

The electricity demand of an electrolysis process is determined by the fundamental electrochemical characteristics of the involved materials. Thus,

new reaction paths are considered to lower the electricity demand significantly. A promising approach is the use of oxygen-depolarizing cathodes within membrane electrolysis plants. Supplying such a cathode with gaseous oxygen leads to the following stoichiometric equation for this electrolysis:

$$2NaCl + H_2O + ½\ O_2 \rightarrow 2\ NaOH + Cl_2 \quad (2)$$

A detailed description of the history, present status and future prospects of this technology can be found in [4]. The key characteristics of this electrolysis are a significantly lower cell voltage, the lack of the by-product hydrogen and oxygen as a required resource.

### 2.4. Status of Chlorine Technology Assessment

The described ODC-technology is already mentioned as an emerging technology in the BAT reference document of 2001 ([7]). A review of this document started in 2009 and results of the first meeting are available online ([8]). It is stated that more data about the still emerging ODC-technology is required to update the reference document. However, it becomes already apparent that the declaration of a universally valid BAT is then more complicated: ODC-electrolysis does not deliver hydrogen anymore. As hydrogen is not a waste product, the technologies cannot easily be compared anymore.

## 3. A Site-Specific Analysis Approach

### 3.1. Problem Specification

The four electrolysis technologies described in section 2 are used for the production of the main product chlorine. Hence chlorine producing companies have to answer the question of which is the most efficient technology. However the processes are not directly comparable because they have different in- and outputs as it is described in section 2.

The field of life-cycle-analysis (LCA) has evolved over the last two decades as a sound method for evaluation of the environmental impact of technologies, products and services. The scientific development of LCA-theory has delivered strategies for analysis of multi-product systems ([9], [10]). A possible adaption of these methods to the given problem is evaluated in the following sections.

### 3.2. System Expansion

The recommended solution for evaluating multi-product systems is a system expansion ([9], [11], [12]). System expansion is performed by adding processes to the given systems until equal outputs are obtained. A simple system expansion for a comparison of the mercury electrolysis with ODC-electrolysis is depicted in Figure 1.

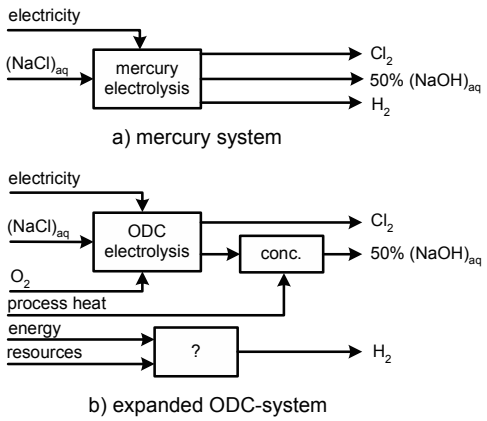


*Fig. 1. a) mercury chlorine production system*
*b) expanded ODC chlorine production system*

This approach often leads to inaccurate results because of it requires assumptions. Applying the method to the given problem, the alternative hydrogen production is one key assumption. It was found that hydrogen produced in chlorine electrolyses is used differently depending on the characteristics of the specific production site ([3]): Further processing is possible as well as thermal use for electricity generation. At some sites, hydrogen is not even used at all and treated as a waste gas ([3]). Consequently, a uniformly valid system expansion approach is not suitable for a universal analysis of chlorine electrolysis technologies.

### 3.3. Allocation

Allocating impact figures like primary energy demand or $CO_2$-emissions to single products of multi-product systems avoids the assumptions underlying the system expansion approach. A simple allocation of the used electricity to the product chlorine is illustrated in Figure 2. X and Y represent different fractions of the total electricity demand according to an arbitrary allocation rule.

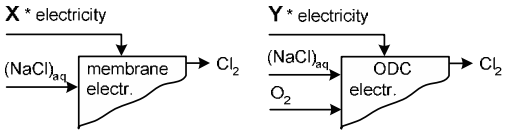


*Fig. 2. Allocation of electricity demand to main product chlorine for membrane and ODC-electrolysis.*

The obvious disadvantage is the lack of a universally valid allocation rule for technical processes. Different allocation strategies have been investigated, often applied to special cases such as in [13], [14]. The suitability of allocation for chlorine electrolysis technology assessment is evaluated in [15]. It is shown that the results of a technology assessment depend strongly on the chosen allocation rule. Consequently, allocation is not a suitable method for chlorine electrolysis technology assessment.

### 3.4. A Site-Specific Analysis Model

Chlorine production is usually at the beginning of the value-creation chain of chemical production sites. Analysis and technology comparison therefore strongly depend on the requirements of the downstream processes. Especially relevant is the site-specific use of hydrogen produced in existing electrolysis technologies. The previous explanations show that existing analysis methods cannot be applied universally to this case. It is therefore suggested to evaluate and compare the ODC-technology with existing production systems site-specifically: The system expansion approach is therefore applied under the given constraints of the actual chlorine production site. A software-based analysis model is implemented in order to analyze energy efficiency, environmental impact and costs of different chlorine electrolysis technologies. It includes physical models of the described electrolyses and other technologies required to model a chlorine production site that can include ODC-technology, i.e. technologies for oxygen supply or alternative hydrogen production. The model can be universally applied to various chlorine production sites and is suitable to derive guidelines for the introduction of the ODC-technology. The following section gives a brief overview of the software-based method.

## 4. Chlorine Production Site Models

### 4.1. Software

The TOP-Energy Software framework ([16]) is used to model chlorine production sites. Among other features, it provides a graphical user interface including a flow process chart and a simulation core for solving algebraic equation systems ([17]). The chemical production sites can be graphically assembled using the flow process chart. Key figures such as energy demand, $CO_2$-emissions or energy costs are extracted from the simulation results.

### 4.2. Plant Models

Stationary process models are implemented allowing graphical assembling of various chlorine production sites. The model library includes the described four electrolysis technologies as well as optional up- and downstream technologies which allow a site-specific system expansion. Required technologies are air fractionation plants for oxygen supply, power plants for thermal hydrogen use, concentration plants for sodium hydroxide concentration, and steam reformer plants for alternative hydrogen production. While the electrolyses are modeled using the underlying electrochemistry, the other plants are described by characteristic figures. This allows easy adaption of future developments of these technologies.

#### 4.2.1. Electrolysis

The electrolysis technologies can be modeled using fundamental electrochemical laws obtained by Faraday ([5]). The specific electricity demand per ton chlorine $w_{el}$ depends on the electrochemical characteristics of the involved materials summarized in the electrochemical equivalent $f$ as well as the voltage $U$ and current efficiency $a$ according to Faraday's first and second law:

$$w_{el} = \frac{U}{a \cdot f} \tag{3}$$

The voltage is determined by the electrochemical reactions at the electrodes. Diaphragm and membrane technology have the same reactions at the electrodes and differ only by further electrical resistances. The voltages of the mercury and ODC-technology are higher or lower than diaphragm or membrane technology voltages because of different electrode reactions [4], [5]. Voltage and current efficiency can be modified in the electrolysis model to obtain a site-specific model. Further site-specific conditions such as

plant size, current density and sodium hydroxide concentration are integrated as well.

#### 4.2.2. Air Fractionation Plant

An air fractionation plant is modeled using a specific electricity demand per produced mass of oxygen as characteristic figure. This value can be adapted according to the site-specific plant.

#### 4.2.3. Concentration Plant

A concentration plant is modeled with a mass-based steam demand per mass of water that has to be evaporated to reach a desired sodium hydroxide concentration in the solution. The pressure level of the heating steam can be adapted in order to calculate the process heat energy demand and steam generation related $CO_2$-emissions.

#### 4.2.4. Steam Reformer

A steam reformer is modeled using a specific fuel gas demand per hydrogen output. The model calculates the resulting $CO_2$-emissions from a stoichiometric reaction shifting the reaction completely to hydrogen and $CO_2$, i.e. the production of CO as a by-product is neglected. This assumption seems to be valid since the steam reformer is used to replace hydrogen production from electrolysis plants.

#### 4.2.2. Resource and Energy Supply Systems

Resource supply is modeled as a general material source. Upstream energy demand, $CO_2$-emissions and costs can be adapted for the respective resource. Energy is consequently supplied from general energy sources, where upstream emissions and costs can be adjusted to model specific grid or generation characteristics such as the $CO_2$-emission coefficient of a specific electricity grid. An on-site electricity generation model with a characteristic electrical efficiency is also included to model thermal hydrogen use for electricity generation. Conditions for combined heat and power generation can be modeled by adapting the $CO_2$-emission coefficients.

## 5. Case Study

### 5.1. Scenarios

The method and models described in the sections above are applied to a case study in order to evaluate $CO_2$-emission and energy cost saving potentials of the ODC-technology for a typical chlorine production site. The chosen case consists of a reference scenario, which is a chlorine production plant with mercury electrolysis technology. It is imaginable to retrofit either membrane or ODC-technology to improve the efficiency. Hence, these two options are compared to the reference case. Key site-specific parameters are varied to assess their influence on the results. Therefore three types of hydrogen use are considered:

- Chemical use for further processing
- Thermal use for power generation
- Hydrogen as waste product

The grid electricity $CO_2$-emission coefficient determines the $CO_2$-emissions from electricity generation. It is varied here in order to model different electricity generation characteristics. The influence of energy prices on cost reduction potentials is analyzed as well.

#### 5.1.1. Mercury Electrolysis

A model of a typical chlorine production site using mercury electrolysis technology is depicted in Figure 3. $CO_2$-emissions and energy costs result from the electrolysis electricity demand. Electricity is supplied from the grid for chemical use of hydrogen and hydrogen as a waste product as shown in Figure 3.a). For thermal hydrogen use a fraction of the electricity is supplied from a local power generation as illustrated in 3.b).

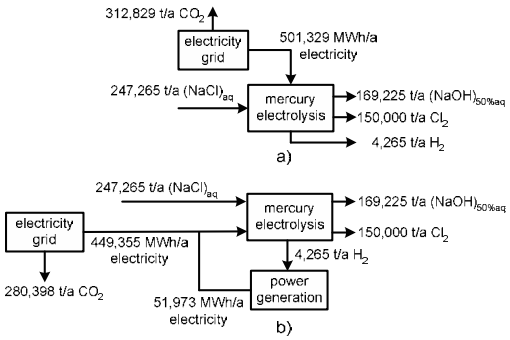


*Fig. 3. mercury electrolysis site with*
*a): chemical/no hydrogen use*
*b): thermal hydrogen use*

#### 5.1.2. Membrane Electrolysis

A scenario with membrane electrolysis technology has to be expanded by a concentration plant model as it is shown in Figure 4 for the chemical use and hydrogen waste product case. An on-site steam generation unit causes additional $CO_2$-emissions.

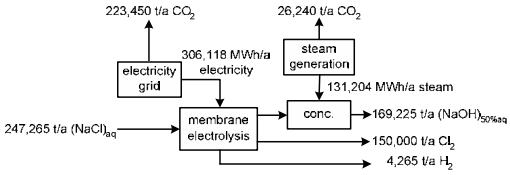


*Fig. 4. Membrane electrolysis site for chemical $H_2$ use*

### 5.1.3. ODC Electrolysis

Equipping a former mercury electrolysis site with ODC-technology causes further changes in the scenario. Figure 5 shows a site with ODC-technology for former chemical hydrogen use. Here, an air fractionation is added for oxygen supply while a steam reformer produces hydrogen for further processing.

The case of former hydrogen thermal use requires an on-site power generation unit where hydrogen is replaced with fossil fuel leading to additional $CO_2$-emissions. Hydrogen as a waste product requires neither a steam reformer nor additional fossil fuel use.

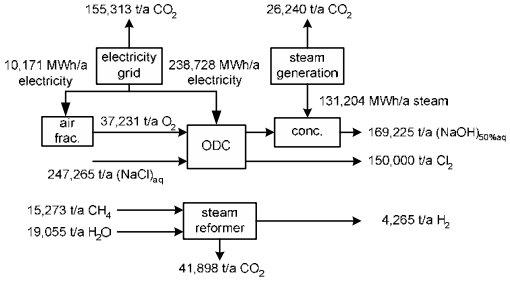


*Fig. 5. ODC electrolysis site for chemical $H_2$-use*

### 5.1.4. Key Parameters and Assumptions

The key parameters of the presented scenarios are summarized in Table 1.

*Table 1. Technical and Economical Parameters*

| Parameter | Value | Unit |
|---|---|---|
| chlorine production | 150 | kt $a^{-1}$ |
| current efficiency | 95 | % |
| electrochemical equivalent | 1.3228 | kg $kA^{-1}h^{-1}$ |
| mercury electrolysis voltage | 4.2 | V |
| membrane electrolysis voltage | 3.0 | V |
| ODC electrolysis voltage | 2.0 | V |
| ODC oxygen surplus | 10 | % |
| concentration steam demand | 0.9 | kg $kg^{-1}$ |
| air frac. electricity demand | 0.27 | MWh $t^{-1}$ |
| steam ref. fuel gas demand | 0.45 | $(m^3)_N/(m^3)_N$ |
| steam $CO_2$-emission factor | 0.2 | kg $kWh^{-1}$ |
| electricity price | 0.06 | € $kWh^{-1}$ |
| hydrogen price | 0.03 | € $kWh^{-1}$ |
| steam price | 0.02 | € $kWh^{-1}$ |

As said before, the electricity grid $CO_2$-emission coefficient determines the electricity generation related emissions. Three different electricity generation characteristics listed in Table 2 are evaluated in this study.

*Table 2. Electricity Grid $CO_2$-Emissions Coefficients*

| Value | Unit | Explanation |
|---|---|---|
| 0.624 | kg $kWh^{-1}$ | 2007 German Grid Average |
| 0.3 | kg $kWh^{-1}$ | 25% Nuclear 75% Modern Fossil |
| 0.8 | kg $kWh^{-1}$ | 25% Hydro 75% Coal Fired |

Energy costs are calculated for the prices shown in Table 1 as well as for 25% higher and lower prices. Scenarios with hydrogen production receive a financial credit based on an energy-related hydrogen price.

## 5.2. Results and Discussion

### 5.2.1. $CO_2$- Emissions

The total $CO_2$-emissions of the different chlorine production scenarios are shown in Figure 6. The displayed bars represent the absolute $CO_2$-emissions for an electricity grid $CO_2$-emission coefficient of 0.624 kg $kWh^{-1}$. The error bars give the results for higher and lower coefficient scenarios, respectively. Shaded areas mark on-site $CO_2$-emissions, i.e. for steam and power generation and steam reforming.

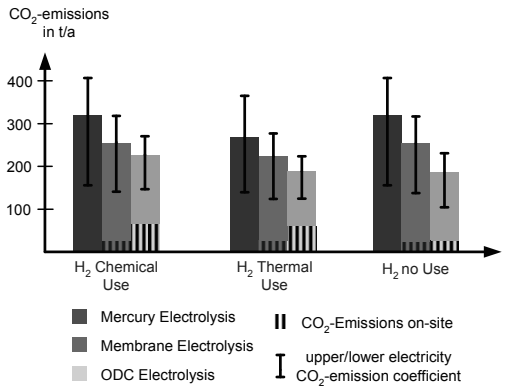


*Fig. 6. $CO_2$-Emissions of different hydrogen use scenarios*

It can be seen that ODC-technology has in all cases $CO_2$-emission reduction potentials compared to mercury and membrane technology for an electricity grid emission coefficient of 0.624 kg $kWh^{-1}$. The reduction potentials range from 41% (no hydrogen use, compared to mercury) to 10%

(chemical hydrogen use, compared to membrane). Membrane and ODC-technology both generate significant on-site emissions due to sodium hydroxide concentration and hydrogen replacement. The results also show a strong influence of the given electricity grid $CO_2$-emission coefficient. A higher coefficient leads to greater reduction potentials while a lower coefficient causes lower reduction potentials for the ODC-technology. This can be explained with the significant $CO_2$-emissions from hydrogen replacement which is not coupled to the electricity grid characteristics. For no hydrogen use the coefficient does not have a significant influence on the result.

### 5.2.2. Energy Costs

The resulting energy costs are shown in Figure 7. Membrane and ODC-technology lead to energy cost reductions of 28% and 37% compared to mercury technology. Higher energy prices lead to greater relative energy cost reduction potentials of the ODC-technology while low prices cause less reductions. This can be explained by the dominance of electricity costs. Electricity costs represent a major part of the energy costs and are significantly higher than a hydrogen credit. This dominance is enhanced by increasing energy prices and lowered by lower energy prices. Consequently the energy cost reduction of ODC-technology compared to mercury and membrane technology increases because of ODC's lower electricity demand. The hydrogen credit has a significant influence on the energy cost reduction potential of ODC-technology. In case of no financial credit, ODC's cost reduction potentials increase to 46% compared to mercury technology.

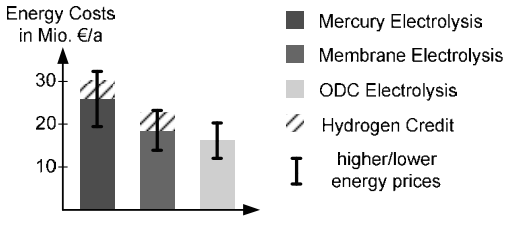


*Fig. 7. Energy costs of different electrolysis technologies*

The energy cost reduction potential is transferred to a maximum invest sum for a given payback period applying a simple net present value method with an interest rate of 8%. The results are shown in Figure 8. The difference between maximum membrane investments and maximum ODC investments are strongly depending on the hydrogen credit.

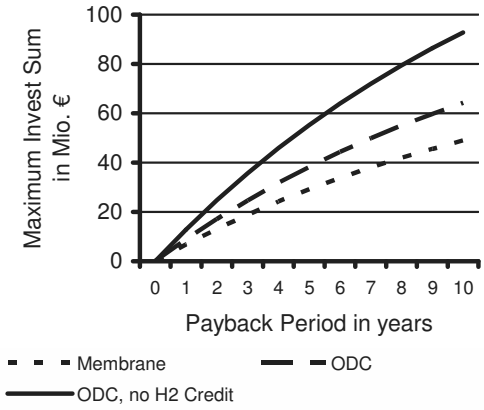


*Fig. 8. Maximum investment sum for different retrofit scenarios*

## 6. Conclusions

It is shown that the presented method can be used to evaluate multi-product processes site-specifically. Considering the given example of different chlorine production technologies, it can be concluded that the actual $CO_2$-emission reduction potential depends strongly on the site-specific constraints such as the electricity grid $CO_2$-emission coefficient. Different possible uses of hydrogen also influence the results significantly. The energy cost reduction potential strongly depends on the site-specific energy prices. A financial credit for hydrogen has a particular strong influence if ODC-technology is compared to existing technologies. Consequently, ODC-technology is more suitable for production sites where formerly produced hydrogen can be easily replaced and no alternative production method has to be installed.

The method of site-specific analysis for assessment of different multi-product systems allows for the estimation of site-specific BATs. The approach is more useful for practical application than universally declared BATs which do not take site-specific characteristics into account. Even though new calculations for different sites seem to be inevitable, the software-based approach allows for easy adaption of the model. The model can be adjusted for different technologies as long as their thermodynamic

behavior can be expressed in stationary equation systems. If statistical data about the distribution of different site characteristics is available, the presented method will be capable of estimating efficiency improvement potentials of new technologies more precisely.

A possible extension of the model would include process heat in order to also immediately evaluate heat integration potentials.

## References


[1] Neelis, M. et al., 2007, Approximation of theoretical energy saving potentials for the petrochemical industry using energy balances for 68 key processes. Energy 32, 1104-1123

[2] Bulan, A. et al., 2009, $CO_2$-Reduktion bei der Herstellung chemischer Grundstoffe (in German), in Mahammadzadeh et al (edts.), Klimaschutz und Anpassung an die Klimafolgen. ISBN: 978-3-602-45462-4

[3] EuroChlor, 2009, Chlorine Industry Review 2008-2009, available online, URL: http://www.eurochlor.org/europeanchlorineindustry

[4] Turek, T., et al., 2008, Chlor-alkali electrolysis with oxygen depolarized cathodes: historsy, present status and future prospects. Journal of Applied Electrochemistry, 8 (9), pp. 1177-1194.

[5] Schmittinger, P., 1986, Chlorine. in: Ullmann´s Encyclopedia of Industrial Chemistry, Volume A6, Ceramics to Chlorohydrins. Weinheim, Germany, VCH.

[6] Blum, K. et al., 2005, Chlor, Alkalien und anorganische Chlorverbindungen (in german). In Winnacker - Küchler, Chemische Technik, Prozesse und Produkte, Volume 3. Weinheim, Germany, Wiley-VCH.

[7] European Commission, 2001, Reference Document on Best Available Techniques in Chlor-Alkali Manufacturing Industry. Intergrated Pollution Prevention and Control (IPPC). Available online: http://eippcb.jrc.es/reference/

[8] European Commission, 2009, Meeting Report. Kick-Off Meeting for the Review of the Reference Document on Best Available Techniques in Chlor-Alkali Manufacturing Industry. Intergrated Pollution Prevention and Control (IPPC). Available online: http://eippcb.jrc.es/reference/

[9] ISO 14040, 2006, Environmental Management – Life Cycle Assessment – Principles and Framework.

[10] ISO 14044, 2006, Environmental Management – Life Cycle Assessment – Requirements and Guidelines.

[11] Ekvall, T., 1999, System Expansion and Allocation in Life Cycle Assessment, Ph.D. thesis, Chalmer University of Technology.

[12] Weidema, B., 2001, Avoiding Co-Product Allocation in Life-Cycle Assessment. Journal of Industrial Ecology 4 (3), 11-33.

[13] Azapagic, A. and Clift, R., 1999, Allocation of environmental burdens in multiple-function systems. Journal of Cleaner Production, 7, 101-119.

[14] Babusiaux, D. and Pierru, A., 2007, Modelling and allocation of $CO_2$ emissions in a multiproduct industry: The case of oil refining. Applied Energy 84, 828-841.

[15] Jung, J. and Leder, J., 2009, The Influence of Allocation Methods on Chlorine Electrolysis Technology Assessment, *Proceedings of 5th European Conference Economics and Management of Energy in Industry.* Vilamoura, Portugal**,** ISBN: 978-972-99309-4-2

[16] TOP-Energy, Toolkit for Optimization of Industrial Energy Systems, 2010, Software Package, Available online: http://topenergy.ltt.rwth-aachen.de

[17] Kirschbaum, S., et al., 2008, Multi-Objective Approach to Analysis of Industrial Energy Systems, *Proc. 21st ECOS*, Cracow-Gliwice, Poland, ISBN: 978-83-922381-4-0


**Acknowledgments:** This work has been carried out within the project "$CO_2$ Reduction during the Production of Basic Chemicals" (01LS05013). The project is funded by the German Federal Ministry of Education and Research (BMBF) within the funding priority "Research for Climate Protection and Protection from Climate Impacts". Prof. Jörissen of TU Dortmund is acknowledged for support in the presentation of the electrolysis technology.

# Tailor-Made Energy Efficiency Optimization of an ATAD Plant

***Jaime Rojas and Toshko Zhelev***

*Charles Parsons Initiative on Energy and Sustainable Environment, University of Limerick, Limerick, Ireland*

**Abstract:** Autothermal thermophilic aerobic digestion (ATAD), an activated sludge process at thermophilic temperatures used to pasteurize and stabilize the sludge, has a relatively high energy requirement with 0.3-0.5 kWh/kg. The aim of this paper is to minimize the energy requirement of the case study ATAD plant by altering the operating conditions while complying with treatment goals. The methodology selected to achieve this goal is dynamic optimization. One of the characteristics of our case study plant is that it makes use of a polymer as pre-thickening agent. The use of this polymer increases the energy requirements by a factor of 2.5 (up to 1.3 kWh/kg). The idea is, therefore, to use the polymer concentration as one of the optimization variables. Other optimization variables include the aeration flowrate, sludge flowrate, and influent temperature, which were found to significantly influence the energy requirement in our previous work. The optimization problem was implemented in MATLAB® and the optimization method employed was *fmincon*. Preliminary results show reductions in the energy requirement of up to 33%. As the objective function was found to be multimodal, future work includes the use of global optimization techniques.

**Keywords:** Wastewater treatment, ATAD, Energy efficiency, Dynamic optimization.

## 1. Introduction

Autothermal thermophilic aerobic digestion (ATAD) is an activated sludge process used in wastewater treatment to stabilize and pasteurize the sludge. In this context, stabilization refers to the reduction of the organic matter or volatile solids (VS) concentration of the sludge, while pasteurization refers to pathogen elimination via heat treatment. Several review papers are available on ATAD development, design, and operation [1-3].

The principle of the ATAD reaction can be described as follows: raw sludge containing large amounts of organic matter and pathogens is fed into a well insulated reactor, where it is aerated and mixed for a certain time. The thermophilic microorganisms present in the sludge start to feed and grow at the expense of oxygen and organic matter, thus contributing to sludge stabilization. During their digestion, the thermophiles release vast amounts of metabolic energy, therefore rising reactors' temperatures to the thermophilic range (45-60 °C). These high temperatures are lethal for pathogens, thus contributing to sludge pasteurization. After meeting required levels of stabilization and pasteurization, the reactor(s) is partially discharged (typically 20% of the total volume during 30 min) and loaded with raw sludge (with the same amount of sludge and a loading time of 30 min). During the discharge and loading phases, aeration of the reactor(s) is stopped. After loading is completed, the batch reaction phase is resumed by aerating the reactors and the cycle re-starts. The reactor is only partially discharged to prevent the reactors' temperatures from getting excessively low. The end-product is a pasteurized and stabilized sludge known as Class A Biosolids that can be used as a fertilizer on agricultural land without restrictions.

Due to the high oxygen uptake rates (OURs) of thermophilic microorganisms there is a relatively high energy requirement regarding the aeration of the reactors. As a result, ATAD is an energy-intensive process with 9-15 kWh/m$^3$ of treated sludge or 0.3-0.5 kWh/kg of VS treated [4].

In this paper, we focus on a case study ATAD facility located in Killarney (Co. Kerry, Ireland). This plant has a relatively low concentration of VS in the influent sludge (just 15 g/l) which is not high enough to reach and keep thermophilic temperatures. Hence, the influent sludge is pre-thickened with polymer so as to reach a VS concentration of 40 g/l and to ensure autothermal thermophilic operation. However, the addition of

polymer has the important drawback that it increases the energy requirement to about 1.3 kWh/kg.

## 2. Motivation and Aim

Experimental findings point out that the operating conditions (OCs) of conventional ATAD systems are often arbitrary and can be greatly improved:

- Despite the varying OURs of ATAD, conventional plants make use of invariable air supply. Further work is needed to determine the best way to accommodate the enormous and variable OURs of ATAD systems [1].
- Temperature control of conventional ATAD systems is often very poor sometimes requiring heating and cooling loops [5].
- The sludge flowrate has been found to affect the specific energy requirement for removal of defined organic matter quantities [7]. However, conventional ATAD systems make use of one single volume change per day, thus not allowing a complete exploitation of the thermophiles' efficiency [6].
- The influent organic matter concentration has also been found to strongly affect sludge stabilization [6], which in turn affects the reaction time and thus the overall energy requirement of the treatment.

In light of these considerations, several authors agree on the need to identify the optimum OCs of ATAD [1,2]. However, there is no study in the available literature devoted to the optimization of the ATAD reaction including the calculation of the potential economic and energy savings that could be attained.

Given this background, the aim of this ongoing work is to minimize the energy requirement of our case study ATAD plant by altering the OCs (including the polymer concentration in the influent sludge) while complying with treatment goals.

## 3. Methodology

The problem described above belongs to the realm of optimization. Due to the discontinuous (semi-batch) nature of ATAD, the methodology selected to solve this problem is dynamic optimization. There are some recent review papers on dynamic optimization in the context of chemical engineering [8,9]. The optimization problem in question can be formulated as per (1)-(6).

$$\min_{\vec{u}(t),t_f} E_m[\vec{x},\vec{u}] = \frac{1}{m_{in}} \int_{t_0}^{t_f} P(\vec{u}(t)) \cdot dt \,, \tag{1}$$

subject to

$$\vec{f}(\dot{\vec{x}},\vec{x},\vec{u}) = \vec{0} \,, \tag{2}$$

$$\vec{x}(t_0) = \vec{x}_0 \,, \tag{3}$$

$$0.38 - r_{VS}(t_f) \le 0 \,, \tag{4}$$

$$1 - L_P(t_f) \le 0 \tag{5}$$

$$\vec{u}_L \le \vec{u}(t) \le \vec{u}_U \,. \tag{6}$$

Where $E_m$ is the gravimetric energy requirement (kWh/kg of VS treated), $m_{in}$ the mass of VS in the influent (kg), $t_0$ and $t_f$ the initial and final time (days), respectively, $P$ the power of the aeration equipment (kW), $\boldsymbol{x}(t)$ and $\boldsymbol{u}(t)$ are the state and optimization variables, respectively, $r_{VS}$ the VS reduction (%), and $L_P$ the pasteurization lethality (%). Both concept and quantification of the VS reduction $r_{VS}$ and pasteurization lethality $L_P$ are defined in our previous work [10].

In our problem, the objective function to be minimized is $E_m$ (see (1)). Sought are the optimum trajectories of the optimization variables $\boldsymbol{u}(t)$ that minimize $E_m$ while satisfying the stabilization and pasteurization constraints. Equation 2 represents the set of differential equations describing the dynamics of the ATAD reaction which is subject to the initial value problem in (3). In other words, (2) is a model of the reaction kinetics, and for this purpose we will make use of the model presented in our previous work [10]. Equations (4) and (5) express the so-called path constraints and they represent the stabilization and pasteurization constraints, respectively. They ensure that a minimum required level of stabilization and pasteurization is achieved by the end of the reaction [10]. Equation (6) sets the lower and upper boundaries of the optimization variables.

The problem represented by (1)-(6) represents a nonlinear programming problem with differential and algebraic constraints.

### 3.1. Case study

The case study ATAD facility consists of two equally sized reactors in series, and it follows the

specifications for both design and operation set in [4]. Relevant design and operating parameters of our case study ATAD plant are shown in Table 1. The plant makes use of an aeration system with invariable speed and for convenience it is operated at a 24 hour cycle.

*Table 1. Design and operating parameters of the case study ATAD plant.*

| Parameter | Value |
|---|---|
| No. of reactors in series (-) | 2 |
| Reactor volume ($m^3$) | 100 |
| Overall energy requirement (kWh/kg VS) | 1.3 |
| Daily load ($m^3$/day) | 20-30 |
| Batch time (hours) | 24 |
| Reaction time (hours) | 23 |
| Hydraulic retention time (days) | 7-10 |
| Specific power (W/$m^3$) | 100 |
| Aeration flowrate (vvh) | 4 |
| Influent VS concentration before pre-thickening (g/l) | 15 |
| Influent VS concentration after pre-thickening (g/l) | 40 |
| Influent temperature (°C) | 10-17 |
| Temperature in first reactor (°C) | 40-50 |
| Temperature in second reactor (°C) | 50-65 |
| Annual electricity cost (€) | 60 000 |

The optimization variables considered for this case study are the loading time $t_l$ (days), the influent VS concentration of the sludge $X_{VS}$ (g/l), the influent temperature $T_{in}$ (°C), the sludge flowrate $q(t)$ ($m^3$/day), the aeration flowrate of both first stage and second stage reactors $q_a^1(t)$ and $q_a^2(t)$ (vvh), and the final time of the reaction $t_f$ (days) (see (7)). The selection of these optimization variables is based on our previous work [10], in which we showed via sensitivity analysis that they have a significant influence on the energy requirement. The lower and upper boundary $\boldsymbol{u}_L$ and $\boldsymbol{u}_U$ of the optimization variables are shown in (8) and (9), respectively. Fig. 1 illustrates the plant design of the chosen case study and the selected optimization variables.

$$\vec{u}(t) = [t_l, X_{VS}, T_{in}, q(t), t_f, q_a^1(t), q_a^2(t)] \quad (7)$$

$$\vec{u}_L = [0.02, 25, 10, 0, 0.3, 2.5, 3] \quad (8)$$

$$\vec{u}_U = [3, 42, 30, 9.6 \cdot 10^5, 3, 5, 5] \quad (9)$$

It is important to note that the influent VS concentration $X_{VS}$ before pre-thickening of the sludge is about 15 g/l. As mentioned above, this concentration is not high enough to reach and keep the thermophilic temperature range during operation. Hence, an artificial polymer is added to the sludge to raise the concentration up to 40 g/l. The addition of this pre-thickening agent is, certainly, the characteristic that makes this particular plant unique, and that is why it requires a tailor-made optimization. Additionally, it is relevant that the fraction of polymer added to the influent sludge significantly influences the energy requirement of the overall treatment (with higher fractions of polymer leading to higher energy requirements). Mathematically this phenomenon can be understood in the following manner: the mass of VS in the influent $m_{in}$ (see (1)) is considered before the polymer addition (that is, with a constant sludge concentration of 15 g/l) and is, therefore, not affected by the fraction of polymer added. However, the higher the polymer fraction the longer it will take to satisfy the stabilization constraint (see (4)), resulting in longer reaction times and, hence, higher energy requirements. This is an additional reason to choose the influent VS concentration $X_{VS}$ as one of the optimization variables (which ranges from 25 to 42 g/l).

The use the influent temperature as an optimization variable does, indeed, imply the notion of heat integration, as energy from the effluent sludge (60-65 °C) could be used to pre-heat the influent (10-17 °C).

Having the freedom to simultaneously vary influent temperature and influent VS concentration (through varying the polymer fraction) could lead to significant reductions in the energy requirement. This is due to the fact that higher influent temperatures require lower influent VS concentrations to ensure autothermal thermophilic operation; and, as stated above, lower polymer fractions lead to lower energy requirements.

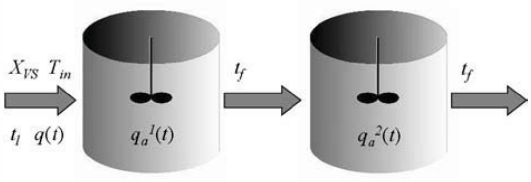


*Fig. 1. Case study ATAD plant with selected optimization variables.*

### 3.2. Details on the implementation

The problem was implemented in MATLAB® and the optimization routine employed was *fmincon* which is a gradient based method that finds the local minimum of a constrained multivariable function through the sequential quadratic programming algorithm.

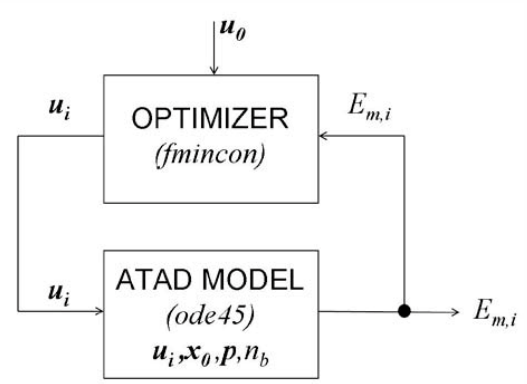


*Fig. 2. Optimization diagram showing different steps during each iteration.*

Fig. 2 describes the way how the optimization routine operates: a starting point $\boldsymbol{u}_0$ is fed into the optimizer and later into the ATAD model which also requires an initial condition $\boldsymbol{x}_0$ and a certain set of parameters $\boldsymbol{p}$ in order to determine the value of the objective function $E_m$ and to evaluate the path constraints after solving the set of differential equations. This output is then used to calculate (via gradients and Hessians) the next value of the optimization variables $\boldsymbol{u}_i$. This procedure continues until a certain tolerance criterion is satisfied.

Due to the partial discharge of the reactors after each batch, the initial condition for a given batch depends on the final condition of the previous batch. Consequently, for a given optimization vector $\boldsymbol{u}$, the constraint vector $\boldsymbol{g} = [0.38\text{-}r_{VS}(t_f), 1\text{-}L_P(t_f)]$ generally depends on the batch number $n_b$, i.e., $\boldsymbol{g} = \boldsymbol{g}(n_b)$. This dependence means that for a given vector $\boldsymbol{u}$, the path constraints may be satisfied for high $n_b$ -values (leading to a feasible solution), but may not be satisfied for low $n_b$-values (leading to an unfeasible solution), and vice versa. As we are interested only in periodic (and not in transient) solutions, it is important to set $n_b$ sufficiently high to achieve periodicity without overloading the computer. Our experience shows that periodicity is generally achieved after at least 10 batches. However, due to computer memory limitations, the value seven was used in the preliminary optimizations.

Hence, for each iteration within the optimization loop (see Fig. 2) and for a given initial condition $\boldsymbol{x}_0$ and control vector $\boldsymbol{u}$, the ATAD model simulates a total of $n_b$ consecutive batches. The path constraints $\boldsymbol{g}$ are then evaluated based on the last batch.

Periodic solutions no longer depend on the initial condition $\boldsymbol{x}_0$ of the first batch: they only depend on the characteristics of the influent sludge and the OCs. This independence of the solutions from the initial condition $\boldsymbol{x}_0$ of the first batch makes our problem unique and different to other dynamic optimization problems found in the literature [8,9,11], in which optimal values depend on the initial condition of the first batch. This is due to the fact that in those problems the entire reactor volume is replaced after each batch.

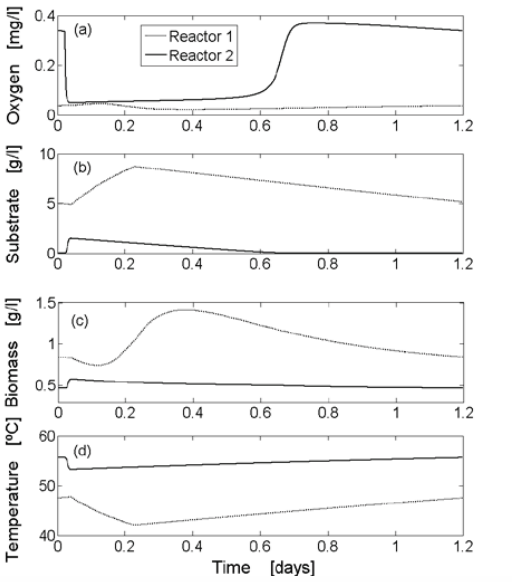


*Fig. 3. Optimal trajectories of state variables for the two reactors in series for $n_b$-value of seven: (a) oxygen concentration, (b ) readily biodegradable substrate concentration, (c) thermophilic biomass concentration, and (d) temperature.*

## 4. Preliminary Results

Fig. 3 shows the optimal trajectories of the state variables for the case study plant. The periodicity

of the state variables can be easily observed which indicates that the value chosen for $n_b$ was sufficiently high (and thus, the solution is feasible). The optimal value of the energy requirement (objective function) is 0.86 kWh/kg, which represents a reduction of 33% regarding the reference value of 1.3 kWh/kg. The starting point used was $\boldsymbol{u_0}$ = [0.125, 38.5,26,160000,1,4,3] which is very close to the current OCs of the case study plant, while the optimal control vector found was $\boldsymbol{u}^*$ = [0.187,40,26,1.2,160000,1.2,3.8, 3.2].

By comparing the starting point $\boldsymbol{u_0}$ and the optimal control vector $\boldsymbol{u}^*$, we observe the following: the algorithm reduced the loading time $u_1$, while keeping the sludge flowrate $u_5$ at a constant value. This is somewhat surprising as usually the increasing sludge flowrate minimizes the energy requirement by pushing the system towards its upper boundary. It seems also surprising that the value of the influent VS concentration $u_2$ (which increases with addition of polymer) has increased as a result of optimization with respect to the starting point. This is surprising as we saw above that, generally, increased polymer quantities increase the reaction time and thus the energy requirement. The temperature $u_3$ remains constant after the optimization, while the reaction time $u_4$ increased. The aeration flowrate for the first stage reactor $u_7$ decreased, while that of the second stage reactor $u_8$ increased. However, the aeration flowrate of the first stage reactor is still higher than that of the second stage. This is reasonable as it is well known that the first stage reactor has a higher oxygen uptake and degradation rate due to its higher load [4].

Several optimization trials were run using different starting points $\boldsymbol{u}_0$. It was found that the optimal values of the objective function differed significantly (up to 40%). This dependence of the optimum value of the objective function on the starting point $\boldsymbol{u}_0$ indicates that the objective function is multimodal. In other words, the objective function has several minima, and, generally, the optimization algorithm is "caught" in the local minimum that is closest to $\boldsymbol{u}_0$.

## 5. Conclusion

The aim of this paper was to minimize the energy requirement of the case study ATAD plant by altering the operating conditions while complying with treatment goals. The need to optimize the ATAD reaction in general and our case study plant in particular was explained. Then, the dynamic optimization problem in question was formulated. Our case study plant and its characteristics were introduced. The selection of the optimization variables was based on our previous work [10]. The singularity of the chosen case study plant lies in the addition of polymer to the influent sludge. This singularity justifies a tailor-made optimization for this particular plant. As the fraction of polymer significantly influences the energy requirement, it was used as an optimization variable. Optimal operating conditions resulting from the preliminary optimization would lead to up to 33% reduction of the current energy requirements.

Two important challenges were found during the implementation of the optimization problem:

- When optimizing the dynamics of a single batch, the solutions would correspond to non-periodic states (often being unfeasible). This is due to the partial replacement of the reactor content after each batch. Therefore, to obtain feasible periodic solutions, the path constraints are evaluated based on the last batch of $n_b$ consecutive batches. To our knowledge, this aspect of the optimization is new and different to other implementations found in the literature where the dynamics of one single batch is optimized. In our specific problem, the value of $n_b$ should be at least 10 in order to guarantee periodicity of the solutions. However, due to computer memory limitations, the value seven was used for our preliminary optimizations. This approach, though, is computationally expensive.
- After performing several optimization trials with different starting points, it was found that the optimal values of the objective function varied significantly (up to 40%). Therefore, we conclude that the objective function is multimodal. Future work will be dedicated to solving the problem with stochastic algorithms or global optimization techniques to explore a wider region of the control space in search of better solutions. In this regard, an efficient global method has to be chosen because a typical optimization run (i.e., ~200 function evaluations) with *fmincon* for an $n_b$-value of seven needs over 0.5 days to complete successfully. A potential candidate would be a scatter search method, while methods like

genetic algorithm have been ruled out as some authors have found them to be the least robust and efficient strategies [11].

## References


[1] T. M. LaPara and J. E. Alleman, 1999, 'Thermophilic aerobic biological wastewater treatment.' *Wat. Res.*, 33(4), pp. 895-908.

[2] N.M. Layden, H.G. Kelly, D.S. Mavinic, R. Moles, and J. Barlet, 2007, Autothermal thermophilic aerobic digestion (ATAD) – Part I: Review of origins, design, and process operation. *Journal of Environmental Engineering and Science*, 6(6), pp. 665-678.

[3] N.M. Layden, H.G. Kelly, D.S. Mavinic, R. Moles, and J. Barlet, 2007, Autothermal thermophilic aerobic digestion (ATAD) – Part II: Review of research and full-scale operating experiences. *Journal of Environmental Engineering and Science*, 6(6), pp. 679-690.

[4] USEPA, 1990, Environmental regulations and technology: Autothermal thermophilic aerobic digestion of municipal wastewater sludge, Technical report, United States Environmental Protection Agency, Office of Research and Development, Washington, D.C.

[5] J.P. Scisson, 2003, ATAD, the next generation: Design, construction, start-up and operation of the 1rst municipal 2nd generation ATAD, In *WEF/AWWA/CWEA Joint Residuals and Biosolids Management Conference and Exhibition 2003*, Baltimore, MD, February 2003.

[6] C. Ponti, B. Sonnleitner, and A. Fiechter, 1995, Aerobic thermophilic treatment of sewage sludge at pilot plant scale 1: operating conditions, *J. Biotechnol.* 38(2), pp. 173–182.

[7] C. Ponti, B. Sonnleitner, and A. Fiechter, 1995, Aerobic thermophilic treatment of sewage sludge at pilot plant scale. 2: technical solutions and process design, *J. Biotechnol.*, 38(2), pp. 183-192.

[8] J.R. Banga, E. Balsa-Canto, C.G. Moles, 2003, Dynamic optimization of bioreactors – a review, *Proc. Ind. Natl. Sci. Acad.* 69A, pp. 257-265.

[9] D. Bonvin, S. Palanki and, B. Srinivasan, 2003, Dynamic Optimization of Batch Processes: I. Characterization of the nominal solution, *Computers and Chemical Engineering*, vol. 27, pp. 1–26.

[10] J. Rojas, T. Zhelev, and A. D. Bojarski, 2010, Modelling and Sensitivity Analysis of ATAD, *Computers and Chemical Engineering*, vol. 34, issue 5, pp. 802-811.

[11] Banga, J. R., E. Balsa-Canto, C. G. Moles and A. A. Alonso, 2005, Dynamic optimization of bioprocesses: Efficient and robust numerical strategies, *Journal of Biotechnology*, vol. 117, issue 4, pp. 407-419.


**Acknowledgement:** This publication has emanated from research conducted with the financial support of Science Foundation Ireland under grant number 06/CP/E007. We wish to thank Robert Kovacs (BME, Budapest, Hungary) and Jairo Gomez (NILSA, Navarra, Spain) for providing data and for their continued support.

# CHP generation in heat integrated separation system

*Kazem Hasanzadeh[a], Gholam Reza Salehi[a], Majid Amidpour[a], Ali Behbahaninia[a]*

[a] *Center of Integration KN Toosi University of Technology, Tehran, Iran*

**Abstract:** This paper presents an industrial case-study: the synthesis of heat-integrated distillation systems applied to the light ends separation section of olefin and gas process plants. In this paper, the possibility of producing power in a sequence of heat integrated columns in a chemical process is inspected. The aim is to find the best sequence with heat integration and its feasible power production as a means of achieving a minimum TAC (Total Annual Cost). First, all sequences have been simulated with HYSYS and then, heat integrations and feasible power production in each sequence are examined. After finding the best values for parameters of each sequence, all sequences are compared and finally the optimum state for the process is found.

**Keywords:** Distillation, Sequence, Heat Integration, TAC, CHP.

## 1. Introduction

Separation of components of multi-component flows using simple distillation columns can be carried out using different sequences. Since distillation columns are very energy consumptive and different sequences have different values of energy requirement, choosing the best sequence is economically important. On the other hand heat integration causes a considerable reduction in heat consumption of these column sequences [1]. There are a number of different methods for heat integration of columns and numerous works have been carried out about this subject so far [1-9]. Another possible optimization for columns is increasing the possibility of power production between columns. In processes such as separation systems of olefin units in which some of columns operate in temperatures lower than that of the environment and exchange heat using cryogenic systems, the power produced between high temperatures columns can be directly consumed by cryogenic systems. Numerous works of research have been done so far related to the exergetic examination of columns and sequences [10-12]. From the thermodynamic point of view, simple sequences of columns have lower exergetic efficiencies, for instance the efficiency of the direct sequence is usually 10% [13]. Using the capability of power production between the columns greatly increases the exergetic efficiency of the process.

We use Kotas's relationship [14] to calculate the exergetic efficiency $(\psi)$ .

$$\psi = \frac{\sum \Delta E_{out}}{\sum \Delta E_{in}}, \quad (1)$$

This relationship is based on the ratio of the required output of the process to the input necessary to obtain that output. The exergies of flows have also been obtained using the following relationship.

$$E = E_{ph} + E_{ch}, \quad (2)$$

Ambient temperature and pressure are respectively 30oC and 1atm.

In order to separate multi component flows to n product groups, the number of column sequences (Sn) is calculated using King's relationship [15]:

$$S_n = \frac{[2(n-1)]!}{n!(n-1)!}, \quad (3)$$

## 2. Case study

In this paper, flow separation of compounds such as propane, propylene, butane, butylene, pentane, and hexane to four groups of products is examined. The possible sequences for this process are as follows: Distributed sequence (figure 1): AB/CD; A/B; C/D. Direct sequence (figure 4): A/BCD; B/CD; C/D. Indirect sequence (figure 9): ABC/D; AB/C; A/B. Direct-indirect sequence

Corresponding Author: Salehi, rezasalehi@kntu.ac.ir

(figure 7): A/BCD; BC/D; B/C. Indirect-direct sequence (figure 11): ABC/D; BC/D; B/C.

The aim is to find the best arrangement with its heat integrations and power production in order to achieve the minimum value of TAC.

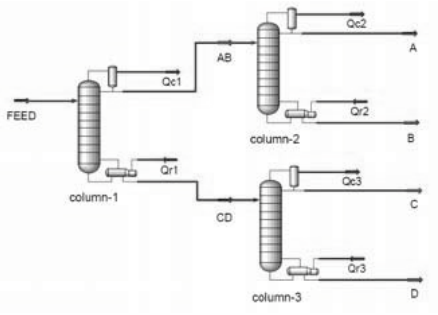


*Fig. 1. Primary Distributed sequence*

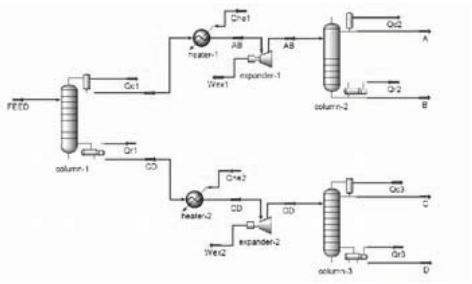

*Fig. 2. Distributed (1X2&1X3) sequence*

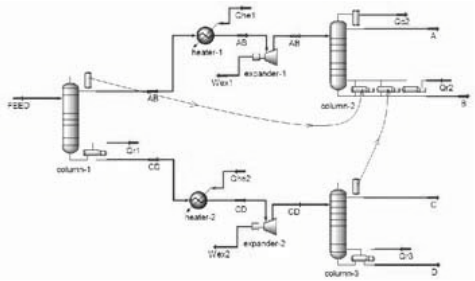

*Fig. 3. Distributed (C1&C3-R2)(1X2&1X3) Sequence*

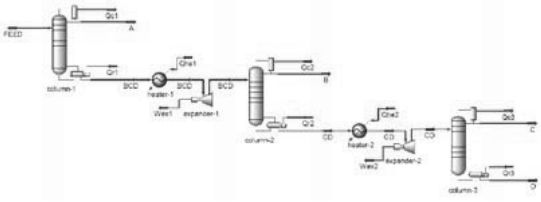

*Fig. 4. Direct (1X2&2X3) sequence*

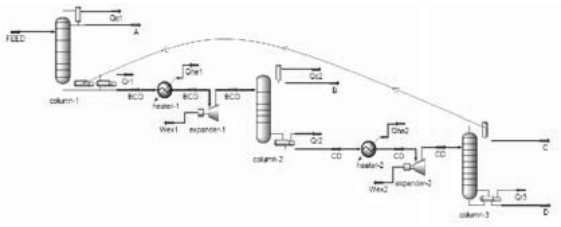

*Fig. 5. Direct (C3-R1)(1X2&2X3) sequence*

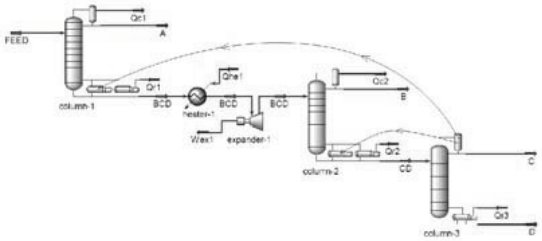

*Fig. 6. Direct (C3-R2&R1) (1X2) sequence*

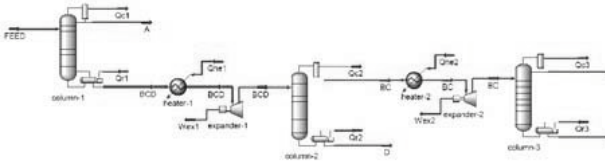

*Fig. 7. Direct-Indirect (1X2&2X3) sequence*

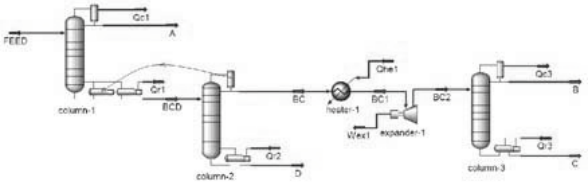

*Fig. 8. Direct-Indirect (C2-R1)(2X3) sequence*

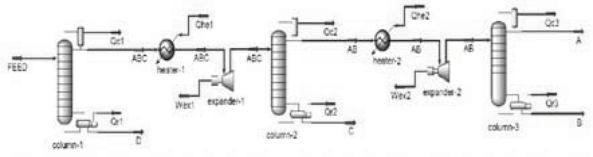

*Fig. 9. Indirect (1X2&2X3) sequence*

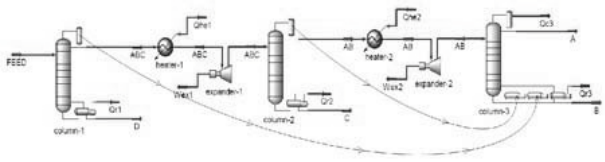

*Fig. 10. Indirect (C1&C2-R3)( 1X2&2X3) sequence*

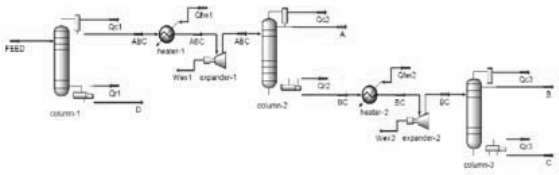

*Fig. 11. Indirect-Direct (1X2&2X3) sequence*

The process examined in this paper, is the separation of a multi-component flow to four categories of products with a purity of 0.99. The intake flow has a temperature of 59.3 oC, a pressure of 1785 kPa and a flow rate equal to 1355 kmole/hr. Compositions of process intake flow and products are shown in table 1. The initial process is illustrated in figure 1-A and it is regarded as a reference case for other states. Simulations are carried out using the software HISYS and two models, Shortcut and Rigorous, are employed for simulating the towers. The governing equations for simulating the columns are NRTL equations.

The TAC function is optimized using the optimizer of HYSYS software. The method SQP is used to minimize TAC function. Different arrangements have been obtained for the process with heat integration satisfying the constraints of the problem. These arrangements are shown in figures 1-11. In this paper, first all possible states for arrangement of columns in separation of the process intake flow are simulated and then attempts are made for optimization and heat integration of columns. Utility costs are shown in table 2[16]. Equations related to installation and start up costs of columns is provided in appendix A [17]. Results of design and optimization of arrangements are shown in table 3.

*Table 1- Feed and product specifications*

| Product groups | Feed Components | Feed Xi (Mol Fraction) |
|---|---|---|
| A | C2H4 | 0.0001 |
| | C3H4 | 0.0047 |
| | C3H6 | 0.4538 |
| B | C3H8 | 0.2912 |
| | C4H4 | 0.0003 |
| C | C4H6 | 0.0011 |
| | C4H8 | 0.1541 |
| | C4H10 | 0.0359 |
| D | C5H12 | 0.0419 |
| | C6H14 | 0.0137 |
| | C7H16 | 0.0031 |

*Table. 2. Utility costs*

| Utility | Temperature Level ( ° C) | Values |
|---|---|---|
| LP-steam ($/ton) | 158 | 13 |
| MP-steam ($/ton) | 200 | 16 |
| HP-steam ($/ton) | 250 | 20 |
| Cooling water ($/ton) | 35-45 | 0.082 |

## 3. Discussion on the results

The distributed sequence of the initial process is chosen as the base for comparison of other distributions (figure 1). The exergetic efficiency of the initial process is 0.28 .

In the sequence Distributed(1X2&1X3), power is produced using the pressure difference between columns 1 and 3 and also temperature increase and enthalpy increase of the CD flow using HP steam and passing it through the expander(figure 2). Operational costs in this state decreased by 44.03% relative to the base case. The heat consumptions of columns 2 and 3 have decreased greatly compared to the case without the expander as a result of the existence of the steam flow, while the heat outputs of condensers have increased. The total steam cost has increased because of using HP steam and high heat consumption in heat exchangers heating the flow entering the expanders. The scrutiny resulting from minimization of the TAC function showed that using HP steam for heating the intake flow of the expanders in different sequences is preferred to LP and MP steams. Reflux ratio and diameters of columns 2 and 3 have increased compared to the case without the expander which is a result of increasing the steam volume of columns. Although the costs related to steam and cold water have increased in this case, but the operational costs have shown a high improvement which is a result of the benefits involving power production of expanders.

In the distributed state the pressure difference between the two columns like 1 and 2, has no effect on the pressure difference between the columns 1 and 3, that is one can increase the pressure of column 1 and decrease the pressures of columns 2 and 3 to create a high pressure difference between the columns.

*Table 3: Optimal schemes*

| Description | Primary Distributed | Distributed (1X2&1X3) | Distributed (C1&C3-R2) (1X2&1X3) |
|---|---|---|---|
| Total actual plates | 260 | 273 | 272 |
| TAC ($/yr) | 7177384.2 | 4471592.9 | 2833536.17 |
| Op. cost saving (%) | - | 44.03 | 69.32 |
| Capital saving (%) | - | -15.57 | -13.53 |
| TAC saving (%) | - | 37.7 | 60.52 |
| TAC sav. by heat (%) | - | - | 27.86 |
| TAC sav. by power (%) | - | 37.7 | 32.66 |
| Thermo. Eff. | 0.28 | 0.97 | 0.89 |
| Description | Direct (1X2&2X3) | Direct (C3-R1) (1X2&2X3) | Direct (C3-R2&R1) (1X2) |
| Total actual plates | 264 | 263 | 270 |
| TAC ($/yr) | 5012322.9 | 4804199.6 | 5452067.48 |
| Op. cost saving (%) | 34.31 | 37.77 | 27 |
| Capital saving (%) | -4.69 | -6.51 | -0.92 |
| TAC saving (%) | 30.17 | 33.06 | 24.04 |
| TAC sav. by heat (%) | 9.85 | 13.14 | 11.1 |
| TAC sav. by power (%) | 20.32 | 19.92 | 12.94 |
| Thermo. Eff. | 0.62 | 0.59 | 0.4 |
| Description | Direct-Indirect (1X2&2X3) | Direct-Indirect (C2-1)(2X3) | Indirect (1X2&2X3) |
| Total actual plates | 264 | 265 | 294 |
| TAC ($/yr) | 4772868.1 | 5623837 | 4362824.66 |
| Op. cost saving (%) | 39.32 | 25.8 | 48.78 |
| Capital saving (%) | -15.47 | -13.34 | -41.24 |
| TAC saving (%) | 33.5 | 21.65 | 39.21 |
| TAC sav. by heat (%) | 1.2 | 6.48 | -17.31 |
| TAC sav. by power (%) | 32.3 | 15.17 | 56.52 |
| Thermo. Eff. | 0.73 | 0.43 | 0.9 |
| Description | Indirect (C1&C2-R3) (1X2&2X3) | Indirect-Direct (1X2&2X3) | |
| Total actual plates | 303 | 292 | |
| TAC ($/yr) | 2190632.5 | 4615472.6 | |
| Op. cost saving (%) | 84.39 | 42.76 | |
| Capital saving (%) | -55.96 | -23.77 | |
| TAC saving (%) | 69.48 | 35.69 | |
| TAC sav. by heat (%) | 17.15 | -8.11 | |
| TAC sav. by power (%) | 52.33 | 43.8 | |
| Thermo. Eff. | 0.85 | 0.8 | |

Capital costs have in turn increased by 15.57% because of high costs of expanders. Finally, TAC has decreased by 37.7% compared to the base case. The exergetic efficiency is 97% in this case which is a result of high ratio of power production to heat consumption and low temperature of heat transfer in the process. Since the intake flow rate to column 2 has a high value, the expander put in its way has produced a much higher power compared to the second expander.

In the case Distributed (c1&c3-r2) (1X2&1&3) power is produced by putting two expanders in the way of AB and CD flows (figure 3). Saturated liquid streams of column 1 have been superheated using HP steam. In this case, two heat integrations have been done between condensers of columns 1 and 3 and the reboiler of column 2.

The operational cost have improved by 69.32% compared to the base case which is a result of the optimization caused by two heat integrations and two expanders installed in the process.

The exergetic efficiency in this state is 0.89. Condenser heats of columns 2 and 3 have increased and their reboiler heats has decreased due to steam flow intake to these columns and since the condenser heat of columns 1 and 3 have been transferred to the reboiler of column 2, the heat consumption of the reboiler of column 2 has greatly decreased. In fact, the preheating of the heat flow to column 3, has increased the heat transfer from this column to column 2. Reflux ratio and diameters of columns 2 and 3 have also increased compared to the state without expander due to increase of steam volume. The initial cost has shown a 13.53% increase compared to the base state which is chiefly because of costs of the employed expanders. The number of trays of column 2 has also increased due to steam volume and reflux ratio of the column since when the steam volume increases; one has to increase the number of trays to enlarge the contact area of vapor and liquid. Generally TAC has improved by 60.52% which involves a thermal improvement of 27.86% and the optimization caused by power production of 32.66%. In this case also the expanders have produced a high power due to high pressure difference and high flow rate between the columns and super heating of the intake flow of expanders.

In the case Direct (1X2&2X3) a large power has been produced using the pressure difference between the columns and employing expanders

between them (figure 4). In this case the operational cost has decreased by 34.31%. The initial cost has increased by 4.69% and TAC has improved by 30.17 %

TAC has had a heat optimization of 9.85% and the optimization involving power production has been 20.32%. The exergetic efficiency of this case is 0.62. In this case also the intake flows of expanders have been heated using the HP steam. In this sequence, since light components exit from the tops of columns, column pressure reduces sequentially and therefore creating a reasonable pressure difference between the columns for the purpose of producing power has become possible. However, since products A and B have left the process in pure states in primary columns, a high potential of high pressure for power production has been lost, because products A and B constitute 45% and 29% of the intake flow rate of the process. The fact that the columns are sequential in this case has resulted in the pressure difference between two columns influencing the pressure difference of the two other columns. For instance, by increasing the pressure of column 2 in order to increase the pressure difference of the two subsequent columns 1 and 2, the pressure difference between columns 2 and 3 is reduced, assuming that column 1 has the highest pressure and column 3 has the lowest pressure. The reflux ratio and diameters of columns 2 and 3 has also increased compared to the case without the expander as a result of increasing of the volume of steam in expanders. Flow rates between columns are usually higher in sequences leaving the expanders consecutively compared to the distributed case because in the distributed case the intake flow rate of the process is divided into different parts and flows between the columns while in the consecutive state the intake flow rate gradually reduces throughout the process and therefore the total flow rate between the columns us usually more than the intake of the process. The negative point about the consecutive state is the high heat consumption of columns because the air intake flow rate of columns is high and we have limited freedom to carry out pressure changes in columns for the purpose of heat integration.

In the Direct (C3-R1) (1X2&2X3) case, a considerable amount of power is produced using the pressure difference between the columns and employing two expanders in the process. Heat integration is also performed between the condenser of column 3 and the reboiler of column 1(figure 5). The operational costs in this case have decreased by 37.77% The intake flows to the expanders have been superheated by the HP steam. The intake steam to columns2 and 3 has decreased the heat of reboilers and increased the heat of condensers. In spite of heat integration and power production in this state, the improvement in operational costs is almost equal to the case Direct(1X2&2X3) which is a result of reduction of power production as a result of pressure changes carried out with the purpose of heat integration between the columns, as in this state the pressure of column 3 has been increased to increase the temperature of its condenser and transfer heat to the reboiler of column 1 and the pressure of column 1 has also been decreased to decrease the temperature of its reboiler. The aforementioned factors have considerably reduced the power production potential between the columns. On the other hand, as a result of high temperature difference between the columns, we have less freedom to change their pressures because it rapidly increases the temperatures of condensers and reboilers beyond the allowable limits. The reason for this fact is the existence of materials with different volatilities in the columns. The exergetic efficiency in this case is 0.59 which is lower than the case Direct (1X2&2X3) . The capital costs increased by 6.51% and TAC improved by 33.06%, its heat optimization contribution and power production contribution being 13.14% and 19.92%, respectively. Increasing the volume of steam in columns 2 and 3 increases the reflux ratio and the diameter of these columns.

In the case Direct (C3-R2&R1) (1X2), since there is heat integration, the pressures of columns allows only one expander in the process, which is located between columns 1 and 2 (figure 6). The output flow from the lower part of column 1, is superheated using the HP steam. Here we have two heat integrations between the condenser of column 3 and reboilers of columns 1 and 2. From results, it is evident that the heat transferred through heat integration in this case is lower than that of the case Direct (C3-R1) (1X2&2X3) . Operational costs have decreased by 27% which represents a lower improvement compared to Direct(1X2&2X3) and Direct(C3-R1)(1X2&2X3) cases since the power production in this case has had a high decrease greatly reducing the exergetic efficiency of this case to a very modest value of 0.4. Capital costs have increased by 0.92%

compared to the base case and TAC has improved by 24.04%, its heat optimization and power production contributions being 11.1% and 12.94%, respectively. The reflux ratio and the diameter of column 2 have also increased as a result of increased volume of the steam in the column.

In the case Direct-Indirect (1X2&2X3), two expanders have been put between the columns (figure 7). Operational costs have reduced 39.32% compared to the base case. The expanders' intake flows have been superheated using the HP steam to increase the power production of expanders. The reason of power production in this case compared to the case Direct (1X2&2X3) is the separation of product B in column 3 since product B constitutes 29% of the flow rate of the total intake flow and this much flow leaving column 2 in the case Direct (1X2&2X3), have largely reduced the power production between columns 2 and 3. The exergetic efficiency of this case is 0.73 which represents high power production in the process. Capital costs have increased by 15.47% and TAC have decreased by 33.5%, heat improvement and power production contributing to 1.2% and 32.3%, respectively.

In the case Direct-Indirect (C2-R1) (2X3) it is only possible to put one expander between the columns 2 and 3. Heat integration has also been carried out between the condenser of column 2 and the reboiler of column 1 (figure 8). In this case operational costs have reduced by 25.8% relative to the base case. In spite of its heat integration, this case has had a lower improvement in operational costs compared to the case Direct-Indirect (1X2&2X3) which is a result of lack of an expander between columns 1 and 2, due to the positive pressure difference between them, greatly reducing power production. The exergetic efficiency of this case is 0.43. Capital costs have increased by 13.34% and TAC has improved by 21.65%, thermal optimization and power production contributing 6.48% and 15.17%, respectively. In this case also steam intake flow and higher steam volume in columns 2 and 3, has increased their diameters and reflux ratios.

In the case Indirect (1X2&2X3) two expanders have been put between the columns (figure 9). Operational costs have decreased by 48.47%. Capital costs increased by 41.24% and TAC reduced by 39.21% , 17.31% of the decrease in TAC was caused by changing the sequence and 56.52% of it was caused by the power produced by expanders. The exergetic efficiency of this case is 0.9 representing a very high power production in the process. In this case, separation of products A and B in column 3 has required a high flow rate for producing power between the columns since A and B form 45% and 29% of the total flow rate of the process, respectively. However, the fact that these products exist with high flow rates in columns has greatly increased the heat consumption of the process. In general, TAC has largely reduced because of high power production in the process which shows the importance of the profits brought about by power production compared to the costs imposed by more heat consumption.

In the case Indirect (C1&C2-R3) (1X2&2X3), like the former case, two expanders have been put between the columns and the intake flow of expanders have been superheated using the HP steam (figure 10). Two heat integrations are carried out between the condensers of columns 1 and 2 and the reboiler of column 3. In this case operational costs have reduced by 84.39%. Capital costs have been augmented by 55.96% and TAC has lowered by 69.84%. The improvement cause by the heat integration was 17.15% and the improvement resulted from power production was 52.33%. Since we have two heat integrations in the processes and thus, high power production in expanders, the operational costs have had a considerable reduction. The power production is so high in this case because there are high flow rates going through the expanders put between the columns. The exergetic efficiency of this case is 0.85.

In the case Indirect-Direct, a high power is produced by putting two expanders between the columns (figure 11). The operational costs have decrease by42.76% compared to the base case, capital costs have increased by 23.77% and TAC has improved by 35.69%. For the thermal part, TAC has increased by 8.11% and for the power production part; it has reduced by 43.8%. Since product A has left the column in column 2, the power production of the second expander has had a considerable reduction in this case compared to the case Indirect (1X2&2X3). The exergetic efficiency of this case is 0.8. The reason for high increase of capital costs in indirect cases as compared to the other cases is the high costs of expanders.

## 3. Conclusions

In this study, all possible states of heat integration and installation of expanders between the columns in order to produce power in different sequences for separation of a four component flow are studied, considering the constraints of the process. The results represent a very high improvement for the sequence Indirect (C1&C2-R3) (1X2&2X3) since the properties of the intake flow to the process are such that in this sequence, not only we have a high freedom for carrying out heat integration, but also a large amount of power is produced between the columns because of having high flow rate flows between the columns. Separation of products A and B in column 3 has increased the possibility of heat integration in this sequence. On the other hand, since these two products include almost 75% of the total input flow rate of the process, the power production between the columns has also been high compared to other states. A negative point of this sequence which is an example of consecutive sequences is the high volume of steam in columns which increases the costs related to heat consumption of columns compared to Distributed cases. Placing expanders between the columns, not only produces power, but also it brings about intake steam into the columns and thus reduces heat consumption of reboilers. One can say by creating suitable conditions in the process for power production, we can greatly influence operational costs.

A high temperature difference inside the columns is one of the factors making changing their pressures difficult. The reason for that is having materials with largely different volatilities in the column. Therefore, in order to have more freedom in changing pressures of columns and creating heat integration, we should select sequences in which there is a low temperature difference between condensers and reboilers of the columns.

High flow rate of flows between the columns increases the process's power production. However, it also increases the volume of steam inside the columns and thus their heat consumption. Since producing power inside the process has a high profit compared to steam costs, noticing power production is of considerable importance in designing sequences. Therefore, the best sequence should not only convey a high freedom in creating heat integration, but also it should include high flow rate flows between the columns. Regarding the calculated results, the following two rules of thumb should be considered while designing a sequence:

- Choose sequences with minimum sums of temperature differences of columns
- Choose sequences with maximum sums of flow rates between the columns

## Nomenclature

$S_n$ number of all simple configurations

$N$ number of components

$M\&S$ Marshal and swift index

$D$ Diameter of column

$A$ Area of exchanger, $m^2$

$H$ Height of column, m

## References

[1] Petlyuk, F. B., Platonov, V. M., & Slavinskii, D. M. "Thermodynamically Optimal method of separating multicomponent mixtures." International Chemical Engineering, 5 (1965) 555.

[2] Proios, P.; F. Goula, N.; N. Pistikopoulos, E. "Generalized Modular Framvork for the Synthesis of Heat Integrated Distillation Column Sequences." Chemical Engineering Science, 60 (2005) 4678-4701.

[3] Andrecovich, M.J.; Westerberg, A.W. "A simple synthesis method based on utility bounding for heat-integrated distillation sequences." AIChE J. 31 (1985) 363–375.

[4] Kattan, M.K.; Douglas, P.L. "A new approach to thermal integration of distillation sequences." Can. J. Chem. Eng. 64 (1986) 162–170.

[5] Smith, R.; Linnhoff, B. "The design of separators in the context of overall processes." Chem. Eng. Res. Des. 66 (1988) 195–228.

[6] Isla, M. A.; Cerda, J. "A Heuristic Method for the Synthesis of Heat-integrated Distillation Systems." Chem. Eng. J. 38 (1988) 161 - 177

[7] Trigueros, D.; Coronado-Velasco, C.; Gomez-Munoz, A. "Synthesize simple distillation the thermodynamic way." Chem. Eng. 96 (1989) 129–134.

[8] Agrawal, R. "Synthesis of Distillation Column Configurations for a Multicomponent

Separation." Ind. Eng. Chem. Res. 35 (1996) 1059.

[9] Yeomans, H.; Grossman, I. E. "Nonlinear Disjunctive Programming Models for the Synthesis of Heat Integrated Distillation Sequences. " Computer and Chemical Engineering, 23 (1999) 1135-1151.

[10] Sobo can, G.; Glavi c, P. "A simple synthesis method for studying thermally integrated distillation sequences." Can. J. Chem. Eng. 78 (5) (2000) 908–916.

[11] Douani, M.; Terkhi, S.; Ouadjenia, F. "Distillation of a Complex Mixture. Part II: Performance Analysis of a Distillation Column Using Exergy. Entropy, 9 (2007) 137-151

[12] Paiva, C. R.; de Lacerda, A. I. "Chemical Process Improvements by Exergy Analysis."

[13] Araújo, A. C. B.; Vasconcelos, L. G. S.; Fossy, M. F.; Brito, R. P.; "Exergetic and Economic Analysis of an Industrial Distillation Column. " Brazilian Journal of Chemical Engineering, 24 (2007) 461 - 469

[14] Kistar, H. Z. "Distillation Design." McGraw-Hill, New York, (1992).

[15] Kotas, T. J. "The Exergy Method of Thermal Plant Analysis." Krieger Publishing Company, Florida (1995).

[16] C.J. King, "Separation Processes," second ed., McGraw-Hill, New York, (1980).

## Appendix A. Cost estimation

A.1. Distillation columns

The total cost of a distillation column can be considered as a sum of the costs of column shell and trays. The number of stages and the diameter values obtained from the Aspen simulations can be utilized in the following correlations. All the correlations are valid for carbon steel construction and are updated from mid-1968 to 2009 utilizing the Marshall and Swift cost index [18].

• Column shell

$$\$ = \left(\frac{M\ \&\ S}{280}\right)(937.61)D^{1.066}H^{0.802}$$

(A.1)

$$H = (N-1)\times 0.6 + 6.0 \qquad \text{(A.2)}$$

The correlation (A.1) is valid for a pressure less than 345 kPa; otherwise a correction factor must be applied. The column height is evaluated considering 0.6m as tray spacing and 6.0m as disengagement.

• Column trays

Considering sieve trays, the following correlation has been utilized.

$$\$ = \left(\frac{M\ \&\ S}{280}\right)(97.24)D\ H^{0.802}$$

(A.3)

A.2. Heat exchangers

The heat exchanger cost evaluation is based on the heat exchanger area evaluated utilizing the usual design formula:

$$A = \frac{Q}{U\ \Delta T_M}$$

(A.4)

Mean values of 1800 kJ/ (m2 h ◦C) and 2100 kJ/(m2 h ◦C) for the overall heat transfer coefficient for condensers and reboilers are assumed respectively. Assuming shell and tube, floating head and carbon steel construction the cost correlation is as follows:

$$\$ = \left(\frac{M\ \&\ S}{280}\right)(474.67)A^{0.65}$$

(A.5)

The reported correlation is valid for design pressure less than 1034.2 kPa and an exchange area range between $18.6 < A < 464.5$m2.

A.3. Annual capital cost

The capital cost (purchase plus installation cost) is annualized over a period which is often referred to as plant life time.

Annual capital cost = Capital cost / Plant life time

TAC = Annual operating cost + Annual capital cost

Operating cost was assumed just utility cost (steam and cooling water).

- Plant lifetime = 10 years
- Operating hours = 8000 h/year

# Timing and sizing of investments in industrial processes – the use of an optimization tool

*Magnus Karlsson and Nawzad Mardan*

*Division of Energy Systems, Linköping University, Linköping, Sweden*

**Abstract:** Investments of different kinds are vital for industries to stay competitive. However, there are several issues that need to be considered before investing, e.g. the timing and size of the investment. In this paper a methodology is presented for analyzing investments from the point of view of optimal size and timing. The energy systems optimization tool reMIND is used as the basis for the modelling, and has been used in several industrial energy systems studies for various purposes. reMIND is based on Mixed Integer Linear Programming (MILP) and has been further developed to consider investments of different kinds. The different constraints needed to model the investment properly are presented together with the variables included in the objective function. A simple case study is also included to illustrate how the method is used. The results from the case study show that the timing and size of the different investments change, depending on the size of the proposed increase in production rate.

**Keywords:** Energy efficiency, Investments, MILP, Optimization.

## 1. Introduction

Investments of different kinds are vital for industries to stay competitive. The basis for the investment may for example be to increase productivity, improve quality and replace old processes. Changes in the systems are also needed to reduce environmental impact due to emissions of greenhouse gases [1]. $CO_2$-emissions related to energy use in the industrial sector are considerable and changes in the energy demand in this sector are vital [2]. Reductions in industries' energy demand can for example be accomplished by investing in processes with low energy demand. When making an investment it is important to consider how processes are process-integrated, i.e. how they are integrated with the rest of the system to achieve a low energy demand overall [3]. It is also important to consider the timing and size of the investment. The decisions that must be made are therefore complicated and tools to provide support are very valuable. Possibilities to reduce energy demand in the industrial sector may be identified by different process integrations methods, e.g. exergy [4], pinch technology [5] and mathematical programming [6]. An energy systems optimization tool called reMIND, based on mathematical programming, has been developed for analyses of industrial energy systems [7, 8] and has been used in several studies focusing on different kinds of question, e.g. operational strategies [9] and the influence on an existing system of different boundary conditions [10]. Different kinds of industry have been analyzed, such as foundries [11], pulp and paper mills [12] and steel works [13]. In these analyses it has been common to calculate the window of investment opportunity, i.e. the maximum cost of an investment. This is a very good approach when, for example, the cost of the investment is not known. However, it does not consider the optimal size or timing of the investment. The aim of this paper is to present a methodology for analyzing investments' optimal size and timing, where a further developed version of reMIND is used to consider such aspects. The different constraints needed to model the investment properly are presented together with the variables included in the objective function. A simple case study is also included to illustrate how the method is used. The case study includes different scenarios to show how different investments change as regards timing and size. Common investment theory, as found in e.g. [14], has been used as the basis for formulating the investment cost function in reMIND. To handle investments properly in the analysis it must be possible to include some input data. In the improved version of reMIND the rate of return, economic lifetime and technical lifetime can be included. The disposal residual values can

Corresponding Author: Magnus Karlsson, Email: magnus.karlsson@liu.se

also be entered as fixed values or percentages, where the latter is dependent on the size of the optimal investment.

## 2. Method

This study uses the energy systems optimization tool reMIND, which is based on the MIND method (Method for analysis of INDustrial energy systems) developed at Linköping University in Sweden [7, 8]. The method has been developed for optimization of dynamic industrial energy systems, but can also be used for other purposes as well. The dynamics of the modelled systems are considered by dividing time into different numbers of time steps, depending on the purpose of the analysis. The structure of the system is modelled using branches that represent different kinds of flow (e.g. materials and electricity), and nodes representing different kinds of process (e.g. separators and boilers). The system to be optimized is compiled in a standardized file, where all limitations and relations in the system are included. The file is optimized using an optimization solver, here CPLEX [15]. The method minimizes the system cost, based on net present value calculations.

As the basis for the optimizations, MILP (Mixed Integer Linear Programming) is used and a MILP problem is defined, in general, according to Equations 1 and 2 [6].

Objective:

$$\min \sum_{v=1}^{V}\sum_{w=1}^{W}\left(c_{1,v}x_v + c_{2,w}y_w\right) \qquad (1)$$

subject to:

$$\sum_{v=1}^{V}\sum_{w=1}^{W}\left(c_{1,v,z}x_v + c_{2,w,z}y_w\right)\begin{Bmatrix}\le\\=\\\ge\end{Bmatrix}C_z, \forall z = 1,2,...,Z \qquad (2)$$

$x \ge 0; y \in \{0,1\}$ and integer.

### 2.1. Constraints describing the cost of investments

When investing in any kind of equipment, both the size of the unit and when to invest need to be considered. The constraints generated when using the investment cost functionality extract the largest size of the equipment used in the model, found in any of the time steps, and assign an appropriate price for that size. The investment cost functions may have different shapes and Figures 1 and 2 show two examples of investment cost functions.

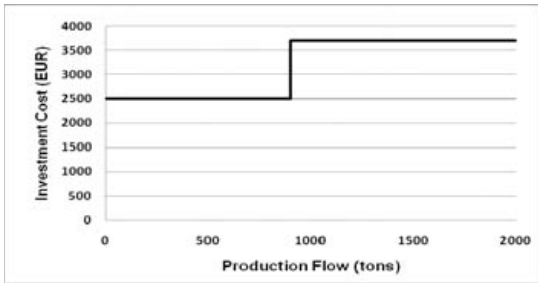


*Fig. 1. First example of an investment cost*

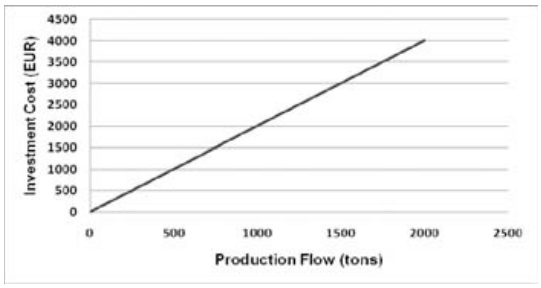


*Fig. 2. Second example of an investment cost*

Equations 3 to 21 are needed to visualize the function correctly, where Equations 3 to 13 are included as the basis for the investment. The other equations are included if economic and technical lifespan are included and if disposal residual values are inserted. Equations 3 to 5 describe the constraints that determine the maximum flow for the specific investment in all time steps included in the analysis period.

$$\sum_{i=h}^{H} x_{1,t,h} = x_{t,tot}, \forall t \qquad (3)$$

$$x_{t,tot} \le x_{\max}, \forall t \qquad (4)$$

$$\sum_{t=1}^{T}\sum_{p=1}^{P} x_{2,t,p} = x_{\max} \qquad (5)$$

$x_{t,tot}$ represents the total flow for specific time step $t$.

$x_{max}$ represents the maximum flow the specific flow assigns for all time steps $t$.

Equations 6 to 10 represent the constraints to determine that only one slope is active for each investment. $IC_{tot}$ is included in the objective function where multiplied with the factor of internal rate of return $(1+r)^{-IY}$, where $IY$ is the year the investment is to take place.

$$\sum_{p=1}^{P} IC_{t,p} + IC_{t,0} = IC_{tot}, \forall t \quad (6)$$

$$c_{t,0} \cdot Y_{t,0} = IC_{t,0}, \forall t \quad (7)$$

$$c_{3,t,p} \cdot x_{2,t,p} + c_{4,t,p} \cdot Y_{t,p} = IC_{t,p}, \forall t, p \quad (8)$$

$$c_{5,t,p} \cdot Y_{t,p} \le x_{2,t,p} \le c_{6,t,p} \cdot Y_{t,p}, \forall t, p \quad (9)$$

$$\sum_{p=1}^{P} Y_{t,p} + Y_{t,0} \le 1, \forall t \quad (10)$$

$IC_{t,0}$ is the price of the equipment unit when there is no flow through the node for the specific time step $t$. Equations 11 to 13 represent the constraints that ensure that there is no flow through the investment in the time steps that are included in the analysis period before the "investment time step", i.e. the time step when the investment is made.

$$\sum_{p=1}^{P} Y_{t,p} + Y_{t,0} = IH_{1,t}, \forall t \quad (11)$$

$$\sum_{i=h}^{H} x_{1,t,h} \le IH_{2,t} \cdot U, \forall t \quad (12)$$

$$IH_{1,t} + IH_{2,(t-IH_3)} \le 1, \forall t, IH_3 \quad (13)$$

Where

$IH_3 = 1, 2, 3, \ldots, T$

The constraints in Equation 13 are generated as long as $t\text{-}IH_3 \ge 1 \ \forall t, IH_3$.

If a technical lifespan is included, Equation 14 is used to ensure that the investment is not active in the time steps after the technical lifespan of the investment. The constraints in Equation 14 are created as long as $t+IH_3+IL_t \le IH_{t,1} \ \forall t, IH_3$.

$$IH_{t,1} + IH_{(t+IH_3+IL_t),2} \le 1, \forall t, IH_3 \quad (14)$$

Where

$IH_3 = 0, 1, 2, \ldots, T$

$IL_t$ is calculated according to the example shown in Figure 3 and the subsequent text, where a technical lifespan of 2 years has been assumed. The analysis period is 5 years (Year1-Year5) divided into different amounts of time steps:

Year1 = 3, Year2 = 2, Year3 = 2, Year4 = 1 and Year5 = 2.

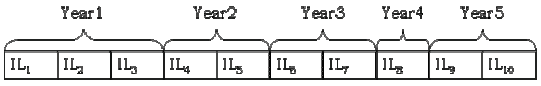


*Fig. 3. Schematic example of the basis for the calculation of the values for $IL_t$.*

From Figure 3 it is possible to calculate the corresponding values for $IL_t$ according to the following:

$IL_1 = 7 = (\text{Year1} - 0) + \text{Year2} + \text{Year3} = (3 - 0) + 2 + 2$

$IL_2 = 6 = (\text{Year1} - 1) + \text{Year2} + \text{Year3} = (3 - 1) + 2 + 2$

$IL_3 = 5 = (\text{Year1} - 2) + \text{Year2} + \text{Year3} = (3 - 2) + 2 + 2$

$IL_4 = 5 = (\text{Year2} - 0) + \text{Year3} + \text{Year4} = (2 - 0) + 2 + 1$

$IL_5 = 4 = (\text{Year2} - 1) + \text{Year3} + \text{Year4} = (2 - 1) + 2 + 1$

$IL_6 = 5 = (\text{Year3} - 0) + \text{Year4} + \text{Year5} = (2 - 0) + 1 + 2$

$IL_7 = 4 = (\text{Year3} - 1) + \text{Year4} + \text{Year5} = (2 - 1) + 1 + 2$

$IL_8$ to $IL_{10}$ are not valid as the technical lifespan in the example is 2 years and would be outside the analysis period and are therefore not calculated.

If an economic lifespan is included for the investment, Equations 15 and 16 are included as long as $IE\text{-}YA+YT_t \ge 0$. $IR_{tot}$ is included in the objective function.

$$\sum_{t=1}^{T} \sum_{p=1}^{P} IR_{t,p} = IR_{tot} \quad (15)$$

$$IC_{t,p} \cdot \frac{(IE - YA + YT_t)}{IE} \cdot (1+r)^{-YA} = IR_{t,p}, \forall t, p \quad (16)$$

Constraints for $IR_{t,0}$ are only included in the model when $IC_{t,0} \neq 0$. $YT_t$ is calculated according to the example shown in Figure 4 and the subsequent text. The analysis period is 5 years (T1-T5) divided into different numbers of time steps: T1 = 3, T2 = 2, T3 = 2, T4 = 1 and T5 = 2.

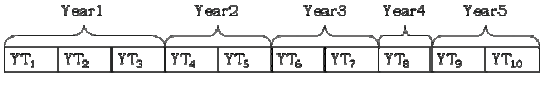


*Fig. 4. Schematic example of the basis for the calculation of the values for $YT_t$.*

From Figure 4 it is possible to calculate the corresponding values for $YT_t$ according to the following, i.e. each $YT_t$ is assigned the same number as the year $YT_t$ is included in: $YT_1 = 1$, $YT_2 = 1$, $YT_3 = 1$, $YT_4 = 2$, $YT_5 = 2$, $YT_6 = 3$, $YT_7 = 3$, $YT_8 = 4$, $YT_9 = 5$, $YT_{10} = 5$

It is possible to choose whether to include a percentage disposal residual value or a fixed disposal residual value. The disposal residual values may be positive or negative depending on whether there is a cost or a profit after shut-down. If a percentage disposal residual value is entered in the model, the constraints shown in Equations 17 and 18 are included. $IP_{tot}$ is included in the objective function.

$$\sum_{t=1}^{T}\sum_{p=1}^{P} IP_{t,p} = IP_{tot} \quad (17)$$

$$IC_{t,p} \cdot ip \cdot (1+r)^{-ID_t} = IP_{t,p}, \forall t, p \quad (18)$$

Constraints for $IP_{t,0}$ are only included in the model when $IC_{t,0} \neq 0$. $ID$ is calculated according to the example in Figure 5 and the subsequent text, where a technical lifespan of 2 years has been assumed. The analysis period is 5 years (T1-T5) divided into different numbers of time steps: T1 = 3, T2 = 2, T3 = 2, T4 = 1 and T5 = 2.

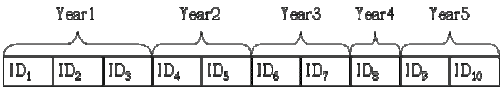


*Fig. 5. Schematic example of the basis for the calculation of the values for $ID_t$.*

From Figure 5 it is possible to calculate the corresponding values for $ID_t$ according to the following, i.e. each $ID_t$ is assigned the number of the year that the technical lifespan for the investment ends, depending on what year the investment is made (when the investment is made late in the analysis period the technical lifespan exceeds the timeframe of the analysis and are therefore assigned the number for the last year): $ID_1 = 3$, $ID_2 = 3$, $ID_3 = 3$, $ID_4 = 4$, $ID_5 = 4$, $ID_6 = 5$, $ID_7 = 5$, $ID_8 = 5$, $ID_9 = 5$, $ID_{10} = 5$

If a fixed disposal residual value has been entered in the model the constraints shown in Equation 19 and 20 are included. $IF_{tot}$ is included in the Objective function.

$$\sum_{t=1}^{T}\sum_{p=1}^{P} IF_{t,p} = IF_{tot} \quad (19)$$

$$Y_{t,p} \cdot if \cdot (1+r)^{-ID_t} = IF_{t,p}, \forall t, p \quad (20)$$

Constraints for $IF_{t,0}$ are only included in the model when $Y_{t,0} \neq 0$.

A constraint according to Equation 21 is included in the model to supplement the equations stated above to ensure that the solution does not include disposal residual values even though the investment is not in operation.

$$IC_{tot} - IR_{tot} - IP_{tot} - IF_{tot} \geq 0 \quad (21)$$

In Figure 6 and the subsequent text an example is presented of the use of the investment cost functionality.

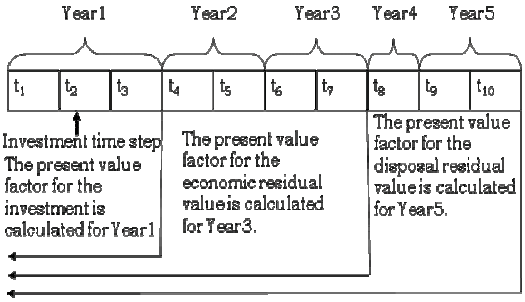


*Fig. 6. Schematic illustration of the use of the investment cost functionality.*

As can be seen from Figure 6 the present value of the investment is calculated at the end of the year the investment is made. However, the investment in the example is in operation from time step $t_3$. The economic lifespan is 2 years and the residual value is therefore calculated from Year3. It should be noted that the economic residual value is zero in this example as the economic lifespan is shorter than the remaining length of the analysis after the year the investment is made. The technical lifespan is set to 6 years, but as the analysis period is 5 years and the there are only 4 years for the investment to be in operation after the "investment time step", the disposal residual value is calculated

from Year5. According to investment theory the disposal residual value should be calculated from the end of the last year of the economic lifespan. However, as seen in Figure 6, the present value factor for the disposal residual value is calculated two years after the economic lifespan has ended. Firstly, this is made possible in the tool due to the possibility for the investment to continue working during the entire technical lifespan and, secondly, due to the complexity of estimating extra costs, e.g. maintenance cost, after the economic lifespan have been completed. If setting the same economic and technical lifespan a situation according to investment theory is possible to achieve. However, the way the constraints from the above presented equations are created, allows modelling of real industrial situations, e.g. when investing in large process equipment that is used after the economic lifespan has ended. It should be noted that the residual values are calculated as a linear depreciation and that the economic lifespan is always shorter than or equal to the technical lifespan. The interest rate for the different investment alternatives may also have different values compared to the analysis as a whole.

## 3. Case study model description

The energy systems optimization tool reMIND is used to model the system. The modelled system in this case study represents a fictive company that is planning to increase its production capacity and the production rate gradually every year. The company therefore plans to invest in new processes to meet the increased demand. To produce the product, raw materials are processed in different processes and change states to result in a finished product, see Figure 7. Process I is an existing process and Processes II and III are new processes in which the company plans to invest. The different processes have different electricity demand and different efficiency. Processes II and III also have different economic lifespan, technical lifespan and residual disposal value. The input data for the processes are shown in Table 1. The investment cost for Process II rises sharply and is a function of production flow as shown in Figure 2. In Process III two different sizes of the investment are possible, depending on production capacity, as shown in Figure 1. In this study, 10 production years were modelled using 10 time steps. A discount rate of 6% is used. Both electricity and material prices are assumed to fluctuate over the analysed period, as shown in Figure 8. The prices are fictive and are used here to illustrate the use of the investment cost functionality. The system cost of the model considers costs for investments, energy and raw materials.

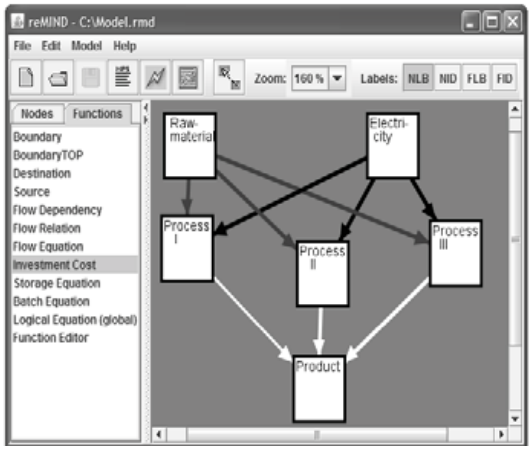


*Fig. 7. A schematic outline of the modelled system derived from reMIND. The arrows represent different flows of electricity, raw material and finished product.*

*Table 1. The input data for the processes.*

| | Process I | Process II | Process III |
|---|---|---|---|
| Electricity demand (kWh/ton) | 1.1 | 0.86 | 0.83 |
| Efficiency | 0.95 | 0.96 | 0.98 |
| Technical lifespan | - | 4 | 5 |
| Economic lifespan | - | 4 | 5 |
| Residual disposal value | - | 400 EUR | 15% of investment cost |

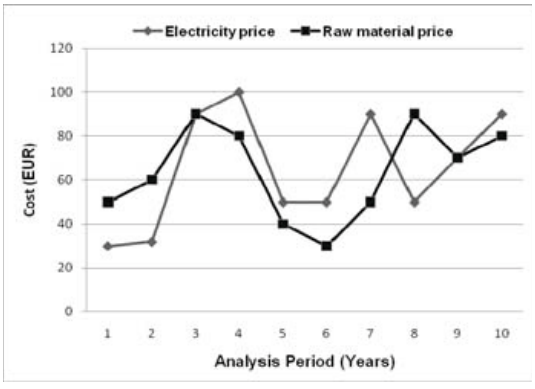


*Fig. 8. Electricity and raw material prices over the analysed period.*

## 4. Case study scenarios

In order to investigate the usefulness of using reMIND for investment decision support, two different scenarios were devised. In Scenario 1, the company increased its production rate by 5% each year and in Scenario 2 by 10% each year.

## 5. Case study results

In Scenario 1, when the company increases its production capacity by 5% each year, the size of Process II and Process III differs. The optimization result from Figure 9 shows that the company should invest in Process III the first year. Process III should be used from the second year to the sixth year. The optimization result also shows that the optimal size for Process III can handle production flows up to 900 tons/year, i.e. the investment that costs 2,500 EUR (see Figure 1). The company should also invest in Process II during year 6 and use this investment for the rest of the analyzed period, i.e. from year 7 to year 10. The optimal size for Process II can handle up to 1,086 tons/year, i.e. the investment costs 2,172 EUR (see Figure 2). Scenario 1 therefore gives the lowest cost using Process III when the amount of produced unit per year is less than 900 tons, i.e. until year 6, and using Process II during the rest of the analyzed period, when the quantity of produced unit per year is more than 900 tons.

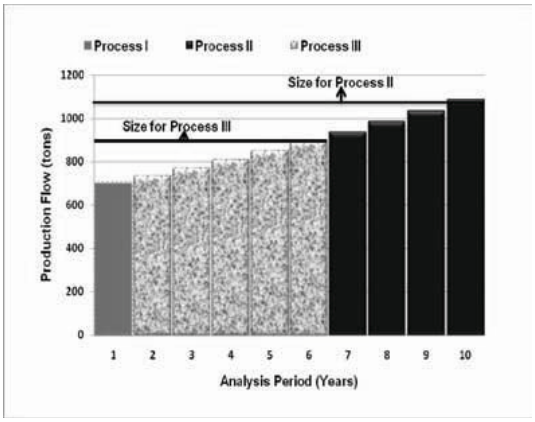


*Fig. 9. The optimization results for the first scenario*

In Scenario 2, the company increases its production capacity by 10% each year and in the same way as in Scenario 1 different investment sizes are also used for both Process II and Process III. While in Scenario 1 the optimization results indicated that the company should start to invest in Process III, Scenario 2 shows that the company should begin by investing in Process II, see Figure 10. Process II is invested in during the first year and operates from the second year to the fifth year. The optimal size for this investment is slightly smaller than in Scenario 1 and can handle production flows up to 1,025 tons/year, i.e. the investment costs amount to 2,050 EUR (see Figure 2). The remainder of the analyzed period, i.e. from year 6 to year 10, the company should operate Process III by making the investment in year 5. The optimal size for Process III is much larger than in Scenario 1 and is capable of handling up to 2,000 tons/year, i.e. the investment costs 3,700 EUR (see Figure 1). Scenario 2 therefore gives the lowest cost using Process II when the amount of produced unit per year is less than 1,025 tons, until year 5, and using Process III during the rest of the analyzed period, when the quantity of produced unit per year is more than 1,025 tons.

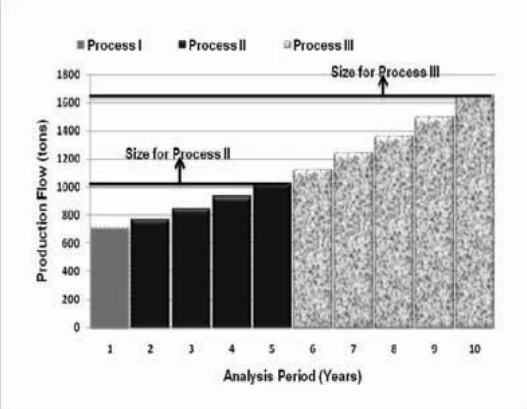


*Fig. 10. The optimization results for the second scenario*

## 5. Concluding discussion

As the case study indicates it is difficult to know when to make different investments. When the production rate is increased by 5%, Process III is invested in and used during the years before investment in Process II. When the production rate is increased by 10%, the first investment is Process II, which is used during the first years of the analysis period, before investing in Process III. In this simple case study, only one future change is included, i.e. the production rate change. In more

complex situations there may be several different future changes to consider, which complicates the analysis.

The size of the investment is yet another complicating factor, which is indicated by the simple case study, as the size of the investments depends on what investment to make and when to make it. As for the timing of the investment, more complex situations than the one shown in the simple case study in this paper will complicate the analysis of the sizing of the investment.

Both the timing and sizes of investments are difficult issues to deal with. This indicates a need for tools that consider investments accurately to provide a solid foundation for investment decisions.

Using a window of investment opportunity is a good way to estimate the maximum cost of an investment, especially when the investment cost is unknown. However, when investment cost functions for different processes are known the possibility to calculate the timing and size of investments enhances the use of the results. Also, it is not possible to use the window of investment opportunity method when more than one investment alternative is potentially included in the solution, as is the situation in the case study in this paper. The complicating factor is the technical lifespan, which can not be considered in the window of investment opportunity method and therefore a comparison between such an analysis and including an investment functionality is not shown in this paper.

The possibility to include an economic and technical lifespan, including fixed or percentage disposal residual value, enhances the use of the results from the analysis and more intricate problems may be analyzed with this method. The simple case study in this paper is only included to show the use of the method.

One drawback of including the investment cost functionality is that large numbers of constraints are needed to picture the investments correctly. Integers are also needed for the functionality, which might lead to longer solution times. This simple case study has a solution time of approximately 0.2 seconds. However, including more time steps and representing the investments with more information, e.g. more steps in the investment function, will increase solution time.

## Nomenclature

*Parameters*

c a coefficient: represents e.g. (1) a slope of a function [slope] and (2) a step in a function [step] (real)

C a constant (real)

h flow included as basis for the investment cost (integer)

H total number of flows included as the basis for the investment cost (integer)

if fixed disposal residual value of an investment (real)

ip percentage disposal residual value of an investment (real)

ID represents a parameter stating the year the technical lifespan for a specific investment ends (integer)

IE represents the economic lifespan of an investment (integer)

IL represents a parameter stating the number of time steps an investment is in operation after the time step the specific investment is made (integer)

p a slope within the function (integer) (p=0 represents the point when the production flow, as shown in Figure 1, is exactly zero. Slope 1 begins when the production flow is larger than zero)

P total number of slopes within a function (integer)

r interest rate (real)

t time step (integer)

T total amount of time steps (integer)

U a large number (real)

v the number of a specific real variable

V the total number of real variables in the problem

w the number of a specific integer variable

W the total number of integer variables

YA specifies the amount of years in the analysis

YT specifies the year a specific time step is included (integer)

z the number of a specific constraint (integer)

Z total number of constraints (integer)

*Variables*

x represents a flow of any kind (real)

Y (binary) (only attaining the values 0 or 1)

IC represents the investment cost (real)

IH represents a help variable (integer)

IF represents the fixed disposal residual value of an investment (real)

IP represents the percentage disposal residual value of an investment (real)

IR represents the economic residual value of an investment (real)

IY represents the year the investment takes place (integer)

## References

[1] Intergovernmental Panel on Climate Change. Fourth assessment report; 2007. http://www.ipcc.ch.

[2] IEA, 2006, Energy technology perspectives, Scenarios & Strategies to 2050, ISBN: 92-64-10982-X – 2006, Stedi Media, France.

[3] Gundersen, T., 2002, A process integration primer, (Int Energy Agency) SINTEF Energy Research, Trondheim, Norway

[4] Rosen, M.A., 2002. Does industry embrace exergy?, Exergy, An International Journal, 2(4), pp. 221-223.

[5] Linnhoff, B., Townsend, et al., 1982, A User Guide on Process Integration for the Efficient Use of Energy, IChemE, Rugby, UK.

[6] Rardin, R.L., 1998, Optimization in operations research, Prentice-Hall Inc., Upper Saddle River, New Jersey, US.

[7] Nilsson, K., 1993, Cost-Effective Industrial Energy Systems – Multiperiod Optimization of Operating Strategies and Structural Choices, Linköping Studies in Science and Technology, Dissertation No. 315, Linköping University, Linköping, Sweden.

[8] Karlsson, M., 2010, The MIND method: a decision support for optimization of industrial energy systems - principles and case studies, To be submitted.

[9] Larsson, M. and Sandberg, P., 2003, Analysing the Influence of Variations when Optimising the Energy and Material System for an Integrated Steel Plant, *Proceedings of the 4th International Conference on Fluid and Thermal Energy Conversion, FTEC 2003*, Bali, Indonesia.

[10] Karlsson M., 2004, A systems approach to the reduction of oil demand in a Swedish board mill, Energy – The International Journal 29(1), Elsevier.

[11] Thollander, P., Mardan, N. and Karlsson, M., 2009, Optimization as investment decision support in a Swedish medium-sized iron foundry – a move beyond traditional energy auditing, 86(4), pp 433-440.

[12] Klugman, S., Karlsson, M. and Moshfegh, B., 2009, A Swedish integrated pulp and paper mill - Energy optimisation and local heat cooperation, Energy Policy, 37(7), pp 2514-2524.

[13] Larsson M, et al., 2004, System profits of widening the system boundaries - renovation of the coke oven battery at an integrated steel plant. International Journal of Energy Research 28, pp. 1051-1064.

[14] Andersson, G., 2008, Kalkyler som beslutsunderlag – Kalkylering och ekonomisk styrning, ISBN: 978-91-44-05024-9, Studentlitteratur, Pozkal, Poland [in Swedish].

[15] CPLEX, 1995, Using the CPLEX Callable Library. CPLEX Optimization Inc, Incline Village: NV, US.

**Acknowledgments:** We kindly thank the Swedish Energy Agency (SEA) for their financial support.

# Prediction of Oxy-Coal Combustion Through an Optimized Weighted Sum of Gray Gases Model

*Tanin Kangwanpongpan[a], Rodrigo Corrêa da Silva[a], Hans Joachim Krautz[a]*

[a] *Chair of Power Plant Technology, Brandenburg University of Technology Cottbus, Germany*

**Abstract:** Oxyfuel combustion is pointed as one of the main options for carbon dioxide capture in future coal power plants. In this technology, coal is burned in a mixture of recycled flue gas and oxygen instead of air to provide a flue gas with a high amount of carbon dioxide. Currently models available in commercial CFD codes could not be appropriate to predict accurately the radiative heat transfer in oxyfuel cases due to higher pressure of carbon dioxide and water vapor. This paper concerns numerical investigation of a reference case, where the radiative heat transfer is calculated by discrete ordinate method (DOM) coupled to an optimized weighted sum of gray gases model (WSGG). Three band's formulations are examined aiming an accurate prediction of radiative properties. The first case relates to the domain-based approach using air-firing parameters. In the last two cases, the optimized parameters of 3 and 4 gray gases fitted to oxy-fired conditions are implemented through non-gray gases approach. Numerical results applying the different set of band's parameters are evaluated through a comparison with experimental values.

**Keywords:** CFD, Oxy-fuel Combustion, Radiation Modeling.

## 1. Introduction

Although in recent years have seen a significant pressure on coal-fired power stations to limit pollutant emissions, it is expected that coal will continue to play a significant role in power generation. It is projected that by 2030 coal will account for around 29% of the world energy [1]. However, to maintain its position in the global energy mix, technological solutions for reducing greenhouse gas emissions become an important issue. Among the possible technologies for emissions control from coal-fired power generation, $CO_2$ capture and storage (CCS) has been recognized as a promising option for achieving significant results. This offers the prospect of a power plant with near-zero emissions.

Oxy-fuel combustion is pointed as one of the main options for CCS technologies. In this technology, a combination of oxygen typically of greater than 95% purity and recycled flue gas are used for combustion of the fuel instead of air. By recycling the flue gas, a gas consisting mainly of $CO_2$ is generated ready for sequestration [2]. Besides, the recycled flue gas is used to control flame temperature and make up the volume of the missing $N_2$ to ensure there is enough gas to keep an approximated heat transfer in the convective section of the boiler. It is known that the combustion behavior, pollutant emissions and heat transfer characteristics in such atmospheres could differ considerably with air combustion [3].

In terms of heat transfer, changes can be expected within the furnace mainly due to higher concentration of participating gases. However, models available in commercial CFD codes could not predict accurately the heat transfer characteristics. Basically, such models were developed for air combustion with conventional partial pressure of $CO_2$ and $H_2O$ and could fail in the calculation of gaseous radiative properties under oxy-fuel atmospheres.

The goal of this work is to investigate the predicted results obtained by different polynomial coefficients for the calculation of spectral emissivity and absorptivity through the weighted sum of gray gases (WSGG) model. Numerical simulations of a test case are performed applying the discrete ordinate method (DOM) to solve the radiative transfer (RTE) equation.

Corresponding Author: Rodrigo Corrêa da Silva, Email: correa@tu-cottbus.de

## 2. The weighted sum of gray gases model

Previous studies [4-5] demonstrated application feasibility of WSGG to solve the radiative transfer equation (RTE) by $P_N$ approximation or discrete ordinates method (DOM). In this method, the radiative properties such as the fraction of black body radiation (weighting factor) and the absorption coefficient are spatially assumed to be constant over a number of $j$ gray gases. The total emissivity can be approximated as:

$$\varepsilon = \sum_{j=1}^{N} w_j \left[1 - \exp\left(-k_j PL\right)\right] \quad (1)$$

The spectrally clear windows (with an implied $\kappa_0 = 0$) are accounted for by the weighting factor at $j = 0$ according to (2).

$$w_{j=0} = 1 - \sum_{j=1}^{N} w_j \quad (2)$$

In the gray gas formulation, the total absorption coefficient is calculated from the total emissivity as:

$$a = -\ln\left(1-\varepsilon\right)\big)/L \quad (3)$$

For an entire uniform isothermal medium volume, the path length is approximated as the mean beam length, which is calculated from the cell volume and the cell surface area [6] according to (4).

$$X = 3.6V/S \quad (4)$$

Although the weighting factors and the absorption coefficients from air-fired condition are already available [7], this set of parameters should be validated when applying to the calculation in radiative heat transfer under oxy-fired conditions. In this work, this set of parameters is denoted as WSGG-SmithG. Recently, a new set of parameters was proposed for the application of the WSGG model in oxy-fired atmospheres [8]. Where one set is related to the three gray-one clear gases, denoted here as WSGG-Oxy3NG, while another set is related to the four gray-one clear gases, denoted as WSGG-Oxy4NG.

The emissivities calculated by these three different sets are illustrated in Fig. 1 for dry recirculation ($P_{H2O}/P_{CO2} = 0.125$) and wet recirculation ($P_{H2O}/P_{CO2} = 1$). The path length adopted here is 0.33 m. Significative differences in the prediction of emissivity are observed mainly in the case of dry recirculation. The WSGG-SmithG parameters result in higher emissivities in all temperature range. In the other hand, similar emissivity values in the case of wet recirculation are obtained for all temperature range except in temperatures lower than 600 °C. No discrepancies between the values calculated by WSGG-Oxy3NG and WSGG-Oxy4NG are observed.

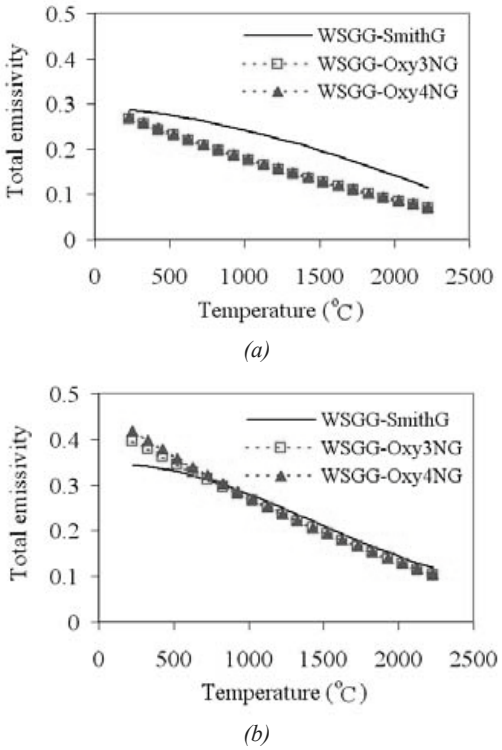


*Fig. 1. Comparison of the total emissivities calculated by different WSGG parameters: (a) dry recirculation, (b) wet recirculation.*

## 3. Mathematical model

Numerical simulations were performed by using the commercial code ANSYS FLUENT 12. The geometry and operating conditions adopted in this research are based on experiments performed in a 100 $kW_{th}$ dry vertical pilot-scaled furnace [9]. The 1/6-scaled computational mesh is composed of approximately 100,000 cells with the periodic boundary condition in the swirling direction of flow.

The rate of devolatilization is estimated from coal proximate analysis using the chemical percolation devolatilization (CPD) model [10]. The Reynolds stress model (RSM) is applied for the prediction of

turbulent flow while the pressure-velocity coupling is solved by the SIMPLE method.

For the hydrocarbon volatile combustion, the global 3-step mechanism similar to the simplified mechanism optimized for the perfectly stirred reactor [11], is used with some adaptations. In this work, the oxidation rate of CO is modified to take into account also the reverse rate of reaction [12]. The kinetic rates of volatile production are calculated from the experiments performed by [13]. The reaction of $H_2$ oxidation is assumed to be irreversible in which kinetic parameters are obtained according to [14]. The reaction mechanisms are written in (5)-(8) and the kinetic parameters of volatile combustion are summarized in the Table 1.

$$C_m H_n O_x N_y S_z + (m/2 + z - x/2) O_2 \rightarrow mCO + (n/2) H_2 + (y/2) N_2 + z\,SO_2 \quad (5)$$

$$CO + 1/2\,O_2 \rightarrow CO_2 \quad (6)$$

$$CO_2 \rightarrow CO + 1/2\,O_2 \quad (7)$$

$$H_2 + 1/2\,O_2 \rightarrow H_2O \quad (8)$$

*Table 1. The kinetic parameters of volatile combustion.*

| R1[a] | A | E, × $10^7$ | Species concentration (n) |
|---|---|---|---|
| VM[b] | $1.623\times10^6$ | 5.066 | VM(1), $O_2$(1) |
| CO | $2.238\times10^6$ | 4.187 | CO(1), $O_2$(0.25), $H_2O$(0.5) |
| $CO_2$ | $1.095\times10^{13}$ | 32.820 | $CO_2$(1), $O_2$(-0.25), $H_2O$(0.5) |
| $H_2$ | $1.000\times10^8$ | 0.837 | $H_2$(1), $O_2$(1) |

[a] R1 means reactant, [b] VM means the volatile matter in coal, [b] n means reaction order.

All reactions in Table 1 react with oxygen and have zero temperature exponent ($\beta = 0$), excepting the third reaction ($CO_2$), which is the reverse reaction from the second reaction (CO). This $CO_2$ reverse reaction has influence from the temperature exponent of -0.97 in the Arrhenius equation.

The finite rate eddy dissipation (FR-ED) is used to estimate the turbulent gaseous combustion in the furnace accounting for both chemical kinetic rate and turbulent mixing rate simultaneously. In this model, the governing rate is assumed to be a minimum of three rates, which are the chemical kinetic rate, the rate of dissipation of reactant eddies, and the rate of dissipation of product eddies.

For the char combustion, the assumption of three-heterogeneous reactions is applied. The char particles react with $O_2$, $CO_2$, and $H_2O$ in order to produce CO and $H_2$ by the following reactions:

$$C + 1/2\,O_2 \rightarrow CO \quad (10)$$

$$C + 1/2\,CO_2 \rightarrow 2CO \quad (11)$$

$$C + H_2O \rightarrow CO + H_2 \quad (12)$$

The kinetic rates of char oxidation are determined from the thermogravimetric analysis (TGA) [15]. The kinetic rates of char reacting with $CO_2$ and $H_2O$ are obtained from experiments [16-17]. These kinetic parameters of char oxidation and gasification are summarized in Table 2.

*Table 2. The kinetic parameters of the char heterogeneous surface reactions.*

| R2[a] | A, × $10^{-3}$ | n | E, × $10^7$ | T[b] |
|---|---|---|---|---|
| $O_2$ | 3.450 | 0.5 | 6.57 | 800-1000 |
| | | | 2.90 | 1000-1080 |
| $CO_2$ | 0.135 | 1 | 13.56 | 850-950 |
| | 6.350 | | 16.22 | 950-1400 |
| $H_2O$ | 319 | 1 | 20.81 | 860-960 |
| | 1.920 | | 14.71 | 1000-1160 |

[a] R2 means oxidizer, [b] T means the particle temperature in °C.

The discrete ordinate method (DOM) is applied to solve the radiative transfer equation (RTE), which takes into account the effect of the non-gray gases and the scattering particles. In the DOM, the RTE is discretized into a set of *n* different direction in a $4\pi$ solid angle according to (13).

$$dI(r,s)/ds = -(\kappa + \sigma) I(r,s)) + \kappa I_b + [\sigma/(4\pi)] \sum_{j=1}^{N} w_j I(r,s_j) \Phi(r,s_i,s_j), i = 1,2,..N \quad (13)$$

## 4. Results

Fig. 2 shows the comparison between the predicted axial velocities and experiments at 0.05 and 0.2 m distant from burner quarl. The results show a good prediction against experimental results. However, under predicted values are observed before 0.05 m. This behavior could be related to either insufficient mesh refinement close to the burner quarl or incorrect assumption of uniform velocity profiles at burner inlet. From the plot, it is also clear that all applied models for calculation of radiative properties provide same results of velocity profiles, once the selection of turbulent model impacts directly into the results.

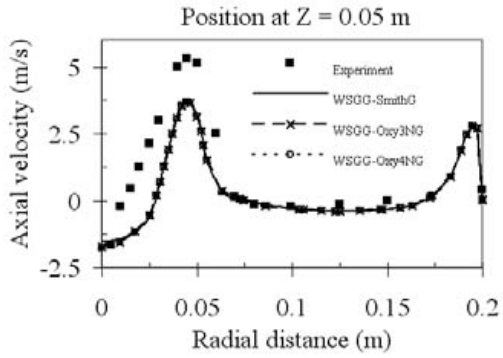


*(a)*

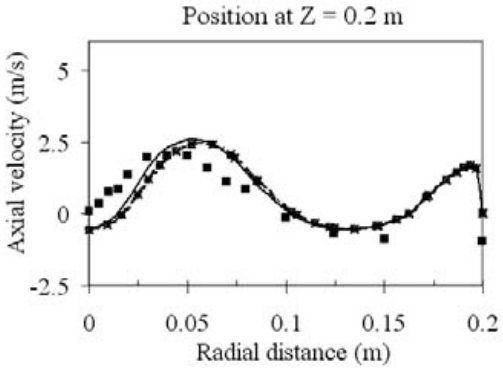


*(b)*

*Fig. 2. Plot of axial velocity at (a) 0.05 and (b) 0.2 distant from burner.*

The oxygen molar concentration at 0.2 m distant from the burner quarl is plotted in the Fig. 3. The predicted values from the WSGG-Oxy3NG and WSGG-Oxy4NG are nearly the same as the prediction obtained from the WSGG-SmithG. The numerical results tend to be over predicted near to the wall. This may be caused due to the insufficient mesh in this region and the stagging flow inlet in computational domain. However, the oxygen molar fraction at post flame region is approximately 0.013 in all cases, which imply that the overall predictions of oxygen concentration are accurate when compared to experiments.

Temperature profiles are compared in Fig. 4 at two different locations. From the plot, it is clear that the results of temperature profile calculated by WSGG-Oxy3NG and WSGG-Oxy4NG are closer to experimental results. In addition, the predicted temperature profiles from both models are similar. The temperature distribution within the furnace for the three cases in the first 1.5 m are illustrated in the Fig. 5. Similar flame shape and length are observed for all cases. Lower temperature levels are, nevertheless, obtained when applying the optimized parameters for oxy-fuel atmospheres (WSGG-Oxy3NG and WSGG-Oxy4NG).

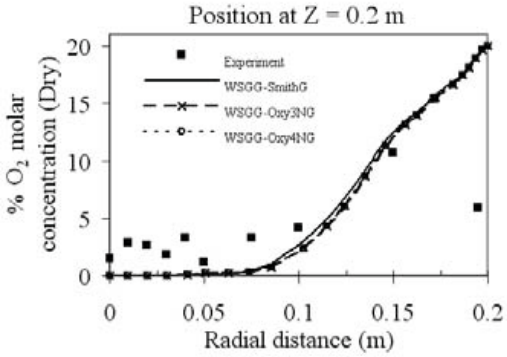


*Fig. 3. Plot of oxygen concentration at axial distance of 0.2 m from burner.*

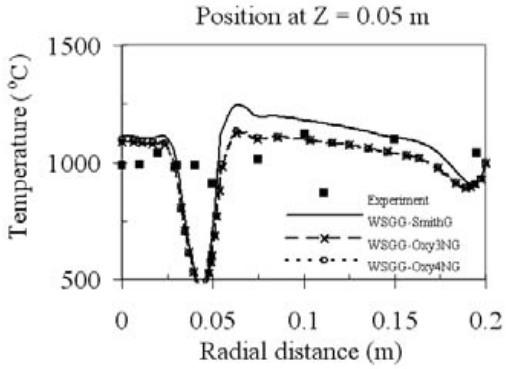


*(a)*

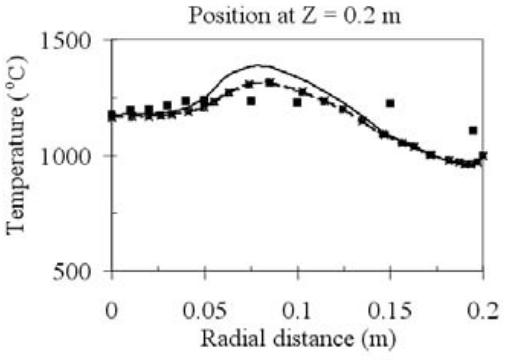


*(b)*

*Fig. 4. Plot of temperature at axial distance of 0.2 m from burner.*

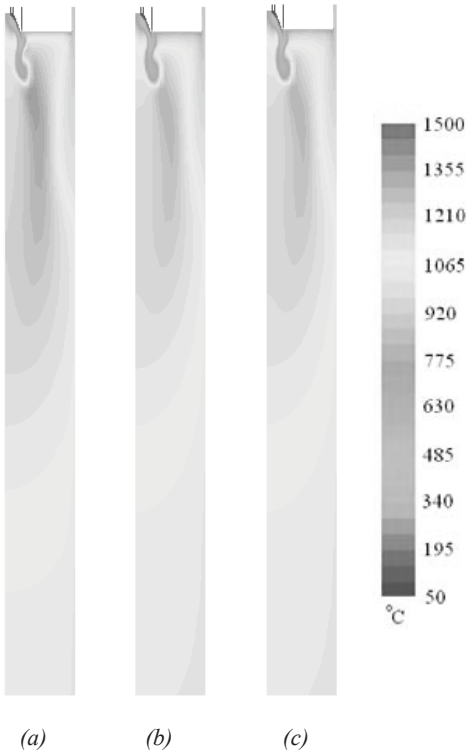


*Fig. 5. Temperature distribution within the furnace (a) SmithG, (b) WSGG-Oxy3NG and (c) WSGG-Oxy4NG.*

The radiative heat fluxes at the lateral wall are plotted in the Fig. 6. Higher heat flux distribution is observed when the WSGG-SmithG is applied. This behavior could be related to the higher flue gas emissivity and temperatures predicted by this set of radiative parameters.

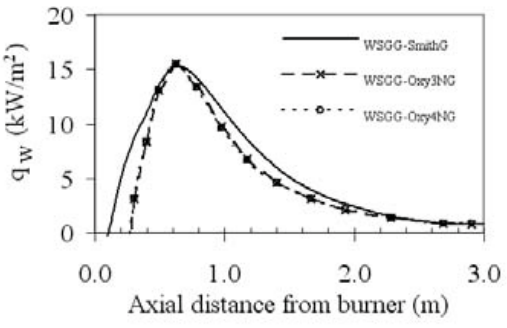


*Fig. 6. Plot of radiative heat flux along the lateral wall.*

The computational time for the three cases are compared in the Fig. 7. The usage optimized parameters for oxy-fuel condition require 35 % and 50 % higher computational effort in the case of WSGG-Oxy3NG and WSGG-Oxy4NG.

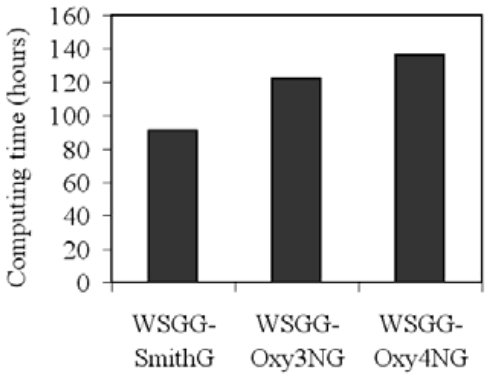


*Fig. 7. Computational time usage from different WSGG parameters.*

## 5. Conclusions

The final results from this research show the possibility to implement the non-gray WSGG model through optimized polynomial coefficients for an accurate prediction of coal combustion under oxyfuel conditions. Velocity and oxygen profiles predicted by three evaluated models show similar behavior and present a good agreement when compared to experiments. Significant differences are observed mainly when temperature and heat fluxes profiles are compared. Predicted values of temperature are closer to experimental results when optimized models for oxy-fuel atmospheres are applied (WSGG-Oxy3NG and WSGG-Oxy4NG). In addition, it is observed lower temperatures in such cases due to lower gaseous emissivities. The radiative heat flux are also compared and the optimized models provide lower heat flux through lateral wall.

The WSGG-Oxy3NG should be applied preferentially due to the less computational effort without loss of accuracy. Although the prediction has a good agreement in the laboratory scaled oxyfuel simulation, the validity of these non-gray WSGG models should still be applied by caution in the pilot scaled and full scaled test facility when the path length differ considerably. Additionally, wall heat transfer increases in full scaled boilers due to water wall cooling.

Further investigations will be performed in parallel to the experimental work in the new 0.4 $MW_{th}$ test facility, which has been constructed at Chair of Power Plant Technology at Brandenburg University of Technology Cottbus. Thus, the validity of these and additional models for the prediction of radiative properties will be evaluated with experiments.

## Nomenclature

| | |
|---|---|
| $A$ | pre-exponential factor |
| $E$ | activation energy, J/kmol |
| $I$ | radiation intensity, W/(m$^2$·sr) |
| $L$ | path length, m |
| $P$ | partial pressure of the absorbing gases, atm |
| $r$ | position vector for RTE |
| $s$ | direction vector for RTE |
| $S$ | boundary area of computational cells, m$^2$ |
| $V$ | volume of computational cells, m$^3$ |
| $w$ | weighting factor |
| $X$ | mean beam length, m |

### Greek symbols

| | |
|---|---|
| $\varepsilon$ | total emissivity |
| $\kappa$ | absorption coefficient, 1/m |
| $\Phi$ | scattering phase function, sr$^{-1}$ |

### Subscripts and superscripts

| | |
|---|---|
| $b$ | blackbody |
| $j$ | index of gray gases |
| $H_2O$ | water |
| $CO_2$ | carbon dioxide |

## References

[1] International Energy Agency, 2009, World Energy Outlook 2009, IEA, Paris, France.

[2] Buhre, B.J.P., et al., 2005, Oxy-fuel combustion technology for coal-fired power generation, Prog. Energy Combust. Sci., 31, pp. 283-307.

[3] Corrêa da Silva, R., Krautz, H.J., 2009, Theoretical investigation of pulverized coal combustion in air and in $O_2/CO_2$ atmospheres. *Proc. 24th German Flame Day*, Bochum, Germany.

[4] Hottel, H.C., Sarofim, A.F., 1967, *Radiative Transfer*, McGraw-Hill, New York.

[5] Modest, M.F., 1991, The weight-sum-of-gray-gases model for arbitrary solution methods in radiative transfer, Journal of Heat Transfer, 113, pp. 650-656.

[6] Siegel, R., Howell, J.R., 2008, *Thermal Radiation Heat Transfer*, 4th ed., Taylor & Francis, New York.

[7] Smith, T.F., Shen, Z.F., Friedman, J.N., 1982, Evaluation of coefficients for the weighted sum of gray gases model, ASME Journal of Heat Transfer, 104, pp. 602-608.

[8] Johansson, R., 2008, Modelling elements in conversion of solid fuels-fixed bed combustion and gaseous radiation, Ph.D. Dissertation, Chalmers University of Technology, Göteborg, Sweden.

[9] Toporov, D., et al., 2008, Detailed investigation of a pulverized fuel swirl flame in $CO_2/O_2$ atmosphere, Combust. Flame, 155, pp. 605-618.

[10] Fletcher, T.H., et al., 1992, Chemical percolation model for devolatilization. 3. Direct use of $^{13}C$ NMR data to predict effect of coal type, Energy & Fuels, 6, pp. 414-431.

[11] Brink, A., 1998, Eddy break-up based models for industrial diffusion flames with complex gas phase chemistry, Ph.D. Dissertation, Abo Akademi University, Finland.

[12] Andersen, J., et al., 2009, Global combustion mechanisms for use in CFD modeling under oxy-fuel conditions, Energy & Fuels, 23, pp. 1379-1389.

[13] Shaw, D.W., et al., 1991, Determination of global kinetics of coal volatiles combustion, Symp. (Int.) Combust., 23, pp. 1155-1162.

[14] Rückert, F.U., et al., 2003, Comparison of different global reaction mechanisms for coal-fired utility boiler, Progress in Computational Fluid Dynamics, 3, pp. 130-139.

[15] Tappe, S., Krautz, H.J., 2009, Experimental investigations of combustion behaviour in various $O_2/CO_2$-atmosphere, *Proc. 4th International Conferences on Clean Coal Technologies*, Dresden, Germany.

[16] Mayers, A.M., 1934, The rate of reduction of carbon dioxide by graphite, Journal of the American Chemical Society, 56, pp. 70-76.

[17] Mayers, A.M., 1934, The rate of reduction of graphite by steam, Journal of the American Chemical Society, 56, pp. 1879-1881.

**Acknowledgments:** The authors acknowledge the support by the Federal Ministry of Education (BMBF) through the Innoprofile research program and the International Graduate School at Brandenburg University of Technology Cottbus.

# Modelling the French Primary Aluminium production under several carbon constraints

*D. Bory[a], A. Hita[a], A. Djemaa[a]*

[a]*Eco-efficiency and Industrial Processes Department, EDF R&D, Moret Sur Loing, France*

**Abstract:** Up to now, the Aluminium sector has not been included in the European Trading Scheme (ETS). The sector is already affected by the global economic crisis and the carbon emissions limit could accelerate the effect and move the production towards the regions with lower carbon emissions constraints. The electro intensive character of the aluminium sector requires consideration. Indeed, amongst the fuel oil, natural gas and coke, electricity represents the major energy consumed in the aluminium sector. A TIMES (MARKAL) model allows us to build the Reference Energy System (RES) of the French Aluminium sector in order to follow the evolution of the sector under different conditions of electricity prices and carbon taxes. The methodology applied is a "bottom up" one: the RES is described in detail with specific economic and technical parameters (Investment cost, technology lifetime, availability factor, energy and raw materials costs, etc.). In a prospective point of view, we added the possibility in the future to evolve towards more efficient technologies. These technologies, nowadays in development, can be industrially feasible in the future but require efficiency and cost hypothesis that have been studied through the scientific literature and publications on the aluminium technologies.

**Keywords:** industry model, GHG emissions, energy, aluminium sector, bottom-up, scenarios.

## 1. Introduction

The industry sector is under pressure because of the economic conjuncture and new regulations due to climate change concerns. It induced a global industrial system were the country limits have no signification anymore and the politic decisions play an important role on a wider scale than the country barriers.

The European Community has set several measures for the emissions regulation, the most important is the emissions trading scheme (ETS), the first part of which ended in 2007, that created a carbon market. The carbon prices are at present low, thanks to the economic crisis that reduced the energy consumption for the sectors most affected and made the quota easier to be satisfied. A second part is ongoing (2008-2012), after this pilot phase A longer phase is planned (2013 to 2020). In the second part, the emission quotas are free for the industrial sectors but for the third phase there is uncertainty about the mechanism of allocation and probably a part of the quota will be put up for auction. This way, the ETS will influence directly the European industry through the sectors under quota or indirectly through the effect of the ETS on energy prices.

For the mid term vision of the energy market, it is very important to understand how this mechanism (or other emission reduction measures such as the carbon tax) can impact an industrial sector and push him toward a better energy management and process innovation that are necessary to obey the new emissions allocation allowed, at the lower cost. This sensitivity analysis can help the energy sector to adapt its energy offer and production means to the possible changes through the study of different scenarios.

Up to now, the aluminium sector was not included in the ETS scheme, but it will probably be included in the third phase (2013-2020). The aluminium sector is also an important source of greenhouse gases other than $CO_2$, particularly perfluorocarbon gases (PFCs). The EU-ETS phase, including the primary and secondary aluminium sector, could cover $CO_2$ emissions and PFCs as well.

We performed, with the help of an energy model, several scenarios for the French Aluminium sector in order to understand the technological changes of the sector and the effect of a cost associated to the emissions.

## 2. The bottom-up methodology and the TIMES Model

The bottom-up methodology applied to an industrial sector consists in a description of the sector based on an aggregated simple representation of the process parameters (raw materials and energies consumption). Specific ratios are obtained from a large amount of data collected from real measurements by statistical treatment and detailed expert analysis.

TIMES (an acronym for The Integrated MARKAL-EFOM System) is an evolution of the MARKAL framework, created by the Energy Technology System Analysis Programme (ETSAP) of the IEA [1]. Like MARKAL, TIMES is a bottom-up economic linear programming model generator for local, national or multi-regional energy systems, which provides a technology-rich basis for estimating energy dynamics over a long-term, multi-period time horizon. It is usually applied to the analysis of the energy sector, but may also be applied for an in depth single sector (e.g. the electricity and district heat sector, the industrial sector, etc.). The TIMES model computes energy balances at all levels of an energy system: primary resources, secondary fuels, final energy or products, and energy services. The model aims to supply an energy system at minimum global cost by simultaneously making equipment investment and operating, primary energy supply, and energy or product trade decisions, by region.

In our model, we described a detailed industrial sector in only one region. TIMES is a demand driven model, the demand can be set up directly by the user (as we did in our study) or indexed to other determinants such as population, GDP, family units, etc., which are obtained externally, via other models or from accepted other sources. The set of supply, primary energy, material resources and trading possibility represent the potential of the resources available at particular cost. The policy component concerns a panel of various parameters such as tax or subsidies for set of technologies, material resources or energy, carbon tax or permit trading system, etc. The technologies assumed for the transformation of primary resources into energy services or material resources into final product.

## 3. The aluminium production

aluminium is manufactured by the electrolysis of the alumina ($Al_2O_3$). The alumina is obtained from the bauxite through the Hall Heroult process mainly in the countries where this raw product is available (Guinea, Australia etc.). The electrolysis occurs between a carbon cathode that covers the pot walls and a carbon anode (Fig. 1) where alumina is supplied in a molten salts bath. The aluminium produced is called “primary aluminium”.

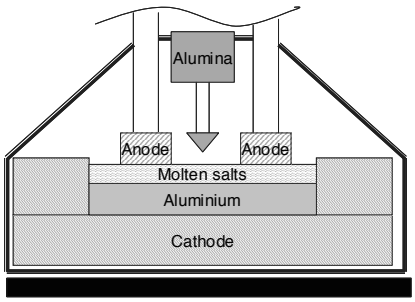


*Fig. 1. Electrolysis cells scheme for aluminium production.*

Two types of electrolysis cells exist, which differ mainly in the anodes manufacturing: the prebake and the Søderberg. In the prebake cells, the anodes are manufactured and baked in specific plant annexed to the aluminium plant and they are changed in the cells once they worn. In the Søderberg cells, a carbon paste is directly introduced in the cell and the heat of the cell itself bakes the anode. This kind of cells is less and less used because of the large amount of dangerous and greenhouse gases emissions.

The direct emissions in the process come from the anode consumption during the electrolysis (it produces $CO_2$, $C_2F_6$ and $CF_4$) and from the use of the energy for the anodes manufacture (baked in kiln using fossil energy or natural gas). Indirect emissions are due to the large amount of electricity used in the electrolysis.

The aluminium can also be obtained by recycling the aluminium scrap, commonly using natural gas furnaces, strongly reducing the energy consumption for the production. It is called “secondary aluminium”.

The global direct emissions for the French production sector are represented in Fig. 2.

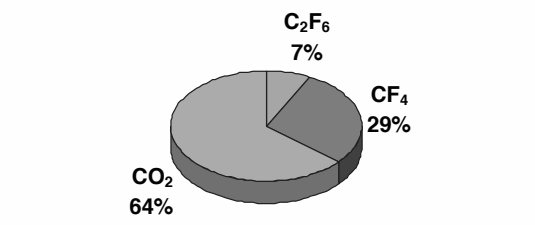


*Fig. 2. Global direct emission shares for the French aluminium production (primary and secondary in $CO_2$eq) in 2005 [2].*

## 4. The French Aluminium sector

Because of the high electric intensity of the electrolysis, the primary production is very sensitive to the electricity price and primary aluminium smelters are located in countries were the electricity supply is reliable and at low cost.

A small number of industrial companies controls the world primary aluminium while the secondary aluminium is produced by a multitude of smaller smelters.

France has a long history in the aluminium production (the first site was founded in 1888). But in the last years the primary production suffered from the increase of the energy (electricity) prices and we observe a transfer toward countries with lower electricity prices.

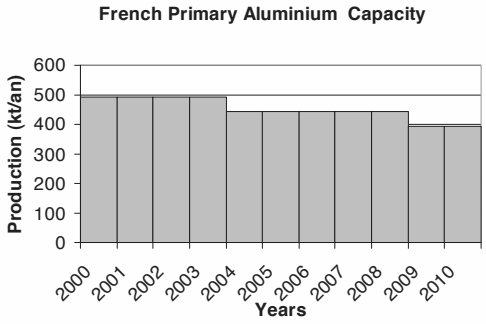


*Fig. 3. French primary aluminium capacity evolution since year 2000.*

The European production is generally decreasing, although a growing demand, the aluminium being used more and more.

In France, amongst the four existing primary plants, two of them closed in 2003 and 2008, and the primary production decreases since 2003 as showed in Fig. 3.

For the moment, no new investments are forecasted to increase the primary aluminium capacities. The production capacities are moving more and more from Europe towards the Middle East and India according to [3].

The secondary production is ensured by a large number of small refiners and smelters that uses scrap aluminium recycled from the automotive industry, and packaging collection, but it is still a limited amount, compared with the national demand. Therefore France needs to import most of the aluminium demand. The increase of the recycled part is linked to the capacity of the scrap collection and scrap prices. The energy use is mostly natural gas and the sector evolution is linked to its price. A slow improvement of the scrap availability is forecasted in our model (doubled by 2050).

## 5. Technology reference and improvements

The TIMES Model is based on a Reference Energy System (RES), which is a network describing the flows of commodities through various processes. The basic components of an energy system model are commodities, processes and commodity flows.

The system references for the existing technologies used for the primary and secondary aluminium are obtained through the energy consumption related in [4]. We can represent the production process in the RES as in the figure below.

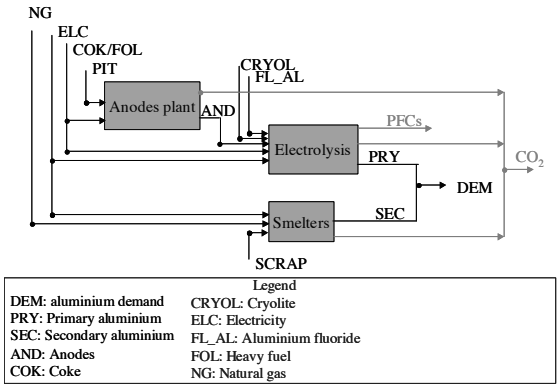


*Fig. 4. Reference production system for the primary and secondary aluminium production.*

For the new technologies, the research and development (R&D) in the aluminium sector is mainly focused on the improvement of the cell configuration, in order to improve the efficiency of the cell and to reduce the secondary chemical, electric and thermal effects.

We made reference to three main evolutions as reported in [7-9].

The "optimised electrolysis" is a control system that allows improving the distance between the electrodes through a computer control. It improves the efficiency of the electrolysis (more the electrodes are close, less voltage is needed). This technique although already available is not yet generalised, the efficiency improvement is about 10% of our reference technique.

Innovative design and materials covering the cathode also allow reducing this distance and improving the efficiency (15-20 %): this technique is known as wettable cathode or drained cell. A lot improvement are recently done to develop economically feasible and resistant materials, and we consider this technique available by 2015.

The technique of the inert anode (non carbon) allows avoiding the anodes consumption, improves the cell efficiency (10 %) and reduces the operation costs due to the anodes replacement. Nowadays the materials considered (metallic and ceramic) do not resist to the high corrosive and temperature cell environment and R&D efforts are needed. The inert anode will be commercially available in 2020 in our model. This technique allows also to considerably reduce the emissions due to the anodes consumptions.

Following the reference [6], combining these last two technologies would allow obtaining the largest efficiency improvement and emissions abatement for the primary aluminium production.

For the secondary production, a more efficient recycling technology will be available from 2010 by improving the existing technology.

## 6. Main hypothesis and scenarios

The aluminium demand (Fig.5) satisfied by the local aluminium production in France (without the part provided by the importation) takes into account the evolution of the primary production, the absence of new large investment in primary production and a light increase of the production related to the improvement in the scrap collection.

At present, the model only considers the French region and does not take into account effects due to possible exchanges with other countries.

We carried out several scenarios. The business as usual (BAU) scenario observes the evolution of the sector without the availability of the new technologies at the considered horizon.

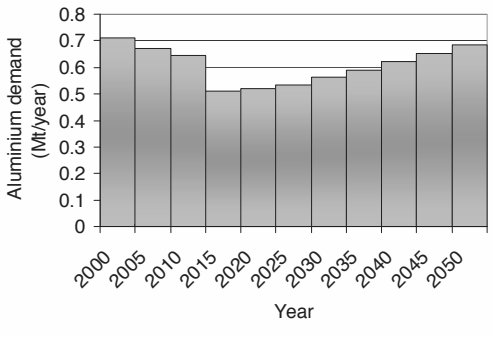


*Fig.5. French Aluminium demand scenario*

The energy prices of reference scenarios, take into account the electricity price resulting from the last negotiation between EDF and the consortium of the biggest French industries, this set up the electricity price at 42 €/MWh for a duration of twenty four years. After that period, it will be renegotiated and two price scenarios are considered : in the scenario ELEC1 the electricity price will be increased by 10 %, and then constant

for the next 20 years, the second scenario (ELEC2) takes the same shape with an increase of 20%. This second scenario translates the hypothesis of stronger impact of the increase of the other energies prices on the electricity price.

The other energies prices increase linearly until 2050: the natural gas prices follow closely the hypothesis in [10] while the oil and petroleum coke prices are similar but increase more slowly in order to better fit with the French prices.

The existing capacities of the primary production will stop in 2015. The secondary production needs for renovation from 2020. Since 2015, new investments are required to satisfy the demand. The importations and exportations mechanisms are not taken into account.

We performed iteratively the model and it allowed us to model a gross evolution of the aluminium production costs and to adjust the prices evolutions of the aluminium scrap.

During the first simulations, we observed that the model results showed a strong carbon emissions reduction in all the considered scenarios, because of the decreasing demand and of the efficiency improvement due to the new technologies. To establish a scenario with a global carbon constraints (i.e. to halve the emissions of the sector by 2050) has no longer sense, because this type of constraints would be satisfied anyway in the scenarios without carbon constraints with our technology hypothesis. We chose to observe the effect of a carbon tax at different levels in order to simulate the sector evolution for different carbon prices. This carbon tax is considered under two types of scenarios: the tax will be applied only to the $CO_2$ emission and, the tax will also take into account the equivalent emission of PFCs. The $CO_2$ equivalence factors (GWP, 100 yrs) of $CF_4$ is 5700 and $C_2F_6$ is 11900 [9].

## 7. Model results

The first BAU scenario was performed without any technology innovation and the comparison with the scenarios ELEC1 and ELEC2, which include the new technologies penetration under different electricity prices, gave the emission evolution in Fig. 6.

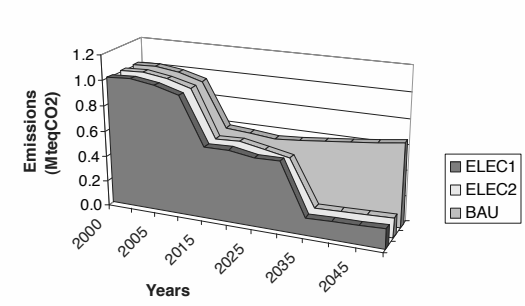


*Fig. 6. Evolution of the global emissions (including PFCs) in $MtCO_2eq$.*

The introduction of the new technologies is a key factor in the energy consumption reduction and they will be economically profitable even with no carbon pressure. The increased electricity cost in the scenario ELEC2 is translated in the model by a large effort in the secondary production between 2020 and 2030 although limited by the availability of the scrap set in the model.

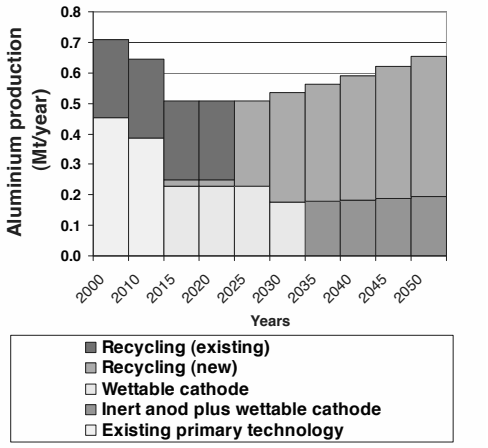


*Fig. 7. Technology selection for the scenario ELEC1*

In the scenario ELEC1, the primary production progresses from 2015 when a more efficient technology is available, towards the wettable cathode and waits until 2035 to upgrade to the combined technology of the inert anode and wettable cathode (yellow and orange bars in Fig. 7).

The secondary production is largely renovated from 2020 and nearly all the scrap available is recycled using the new technology (green bars in

Fig. 7). All the performed scenarios gave similar technology emergence profiles.

The recycling process uses ten times less energy than the primary production (Fig. 8) and the model always converges in order to maximise the recycling part.

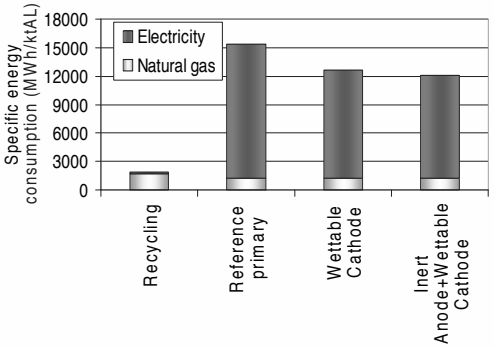


*Fig. 8. Specific energy consumption for the considered technologies.*

The sector would naturally take advantage of the new available technologies under the energy prices modelled independently of the carbon tax level.

The effect of the carbon tax does not modify globally the technologies chosen by the model but it influences mainly the timeline of the investment: the inert anode technology is anticipated for a carbon tax over 150 €/t$CO_2$ (if extended to the PFCs gases) and more Fig. 9.

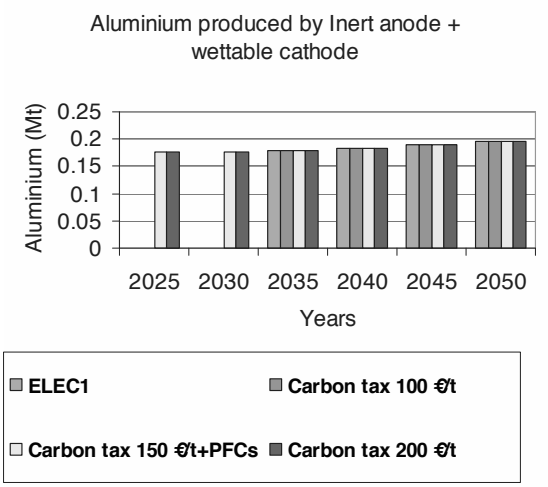


*Fig. 9. Inert anode + wettable cathode technology emergence following the scenario*

The emergence of this technology allows a large emission abatement for the sector and becomes competitive with the secondary production in term of emissions. In terms of production costs (sum of the fix and variable costs plus the costs associated to the energy), the inert anode would allow reducing the costs of the production, balancing the global increase of the energy costs with the improvement of the efficiency, and the strong reduction of the costs associated with the anodes replacement.

In terms of emissions, a carbon tax over 150 € including the PFC, pushes the sector to decrease emissions from 2020, when the more efficient technique is available, of 40 % of the BAU scenario (from 0.58 MteqCO2 to 0.33 MteqCO2).

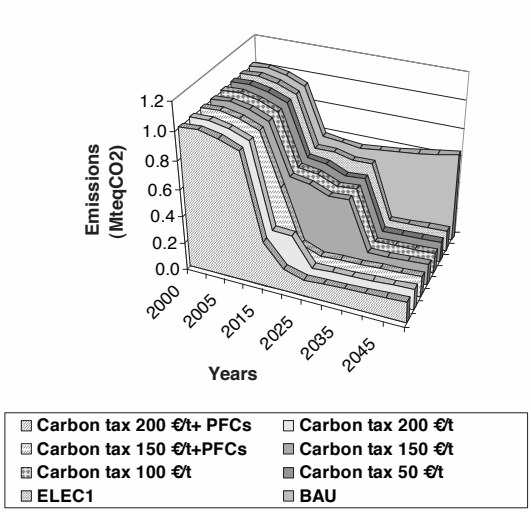


*Fig. 10. Total emission (CO2+PFCs) evolutions for different carbon taxes levels.*

## Conclusions

The French aluminium sector can be involved in the coming years in participating to the industry effort in the reduction of the emissions of GHG. Especially if the PFC gases emissions are taken into account.

Today, the emissions reduction in the aluminium production can be obtained through the recycling (that uses ten times less energy than the primary) and through the improvement of the existing techniques for the electrolysis. The inert anode technique and the wettable cathode are the major R&D challenges that could allow considerable

changes in the energy consumption of the aluminium sector. These techniques are a key factors both at emission and profitability levels and if they become mature as sooner as possible, the production methods will naturally converge toward these techniques, independently of the carbon pressure on the sector.

A carbon tax can anyway stimulate the R&D efforts and accelerate the emergence of this techniques improving their profitability.

A European model for the aluminium sector is in development in our research centre in order to highlight the differences between the European country production systems and the effects of the carbon pressure on the sector at an European level.

## References

[1] http://www.etsap.org

[2] CITEPA « Organisation et méthodes des inventaires nationaux des émissions atmosphériques en France » 3rd edition 2006

[3] CRU International Limited Aluminium Quarterly Report January 2010

[4] CEREN- Centre d'Etude et de Recherche Economique sur l'Energie « Le profile énergétique du secteur de la métallurgie et de la mécanique». 2009.

[5] Aluminium Benchmark Model 2006, CRU Group

[6] Industry Zheng Luo "Antonio Soria Prospective Study of the World Aluminium" JRC Sceintific and Technical Reports, EUR 22951 EN – 2007

[7] ICARUS-4 Sector study for the Non-Ferrous Metals Industry NWS-E-2000-08

[8] Ybema J.R., Lako P., Gielen D.J., OOSTERHEERT R.J., KRAM T., « Prospects for Energy technologies in the Netherlands » vol 2. ECN-C--095-039; 1995

[9] Gibbs Michael J., Bakshi Vikram, Lawson Karen,Pape Diana (ICF Consulting) and Dolin Eric J. (USEPA) "Inventories PFC Emissions from Primary Alumium Production" Good Practice Guidance and Uncertainty Management in National Greenhouse Gas pgs197-216, IPCC 2000

[10] AIE "Energy Technology transition for industry, strategies for the Next Industrial revolution" ISBN: 978-92-64-06858-2, 2009

# Dispersion of Pollutants, Environmental Externalities due to a Pulverized Coal Power Plant and their Effect on the Cost of Electricity

*Lucyna Czarnowska[a] and Christos A. Frangopoulos[b]*

[a] *Silesian University of Technology, Gliwice, Poland*
[b] *National Technical University of Athens, Athens, Greece*

**Abstract:** Energy conversion systems generate pollution which causes damages to human health, building materials, crops, land, etc. The objective of this work is to study the dispersion of pollutants and assess the cost of pollution of such a system to the society and environment. For this purpose, a pulverized coal power plant is selected. Using thermodynamic principles combined with empirical techniques, the quantities of pollutants emitted by this plant are estimated, then using the EcoSenseWeb software, which is based on the results of the ExternE project, the external environmental cost (externalities) of pollution are assessed. This plant is considered as located in four different cities in Poland and the externalities are calculated for each city separately. It is shown that the external environmental cost has a strong influence on the unit cost of electricity. In addition, the dispersion of pollutants is presented for the plant located in Olsztyn city. Furthermore, the plant has been also located near the capitals of European countries. The environmental externalities are calculated for each city and, in addition, the neighbouring countries that are strongly affected by the plant in each particular city are identified. The sensitivity of the unit cost of electricity to certain important parameters is investigated.

**Keywords:** Cost of electricity, EcoSenseWeb, External environmental cost, Externalities, Pollution abatement, Pulverized coal power plant.

## 1. Introduction

The emission of pollutants from energy conversion systems causes damages to the environment and the society not only in the vicinity of the system but also in distant areas, even in other countries, that are in the trajectory of pollutants dispersion. It is necessary to identify these damages and estimate the cost they cause, and then internalise this cost in order to reveal the true economic performance of a system. These issues have been studied having in mind a pulverized coal power plant as an example and the results are presented in the following.

## 2. Procedure for estimation of environmental externalities

### 2.1. The EcoSenseWeb software

The externalities of pollutants from power plants or other industrial activities depend primarily on the location of this activity. The same amount and types of the emissions of harmful pollutants give different effects at different locations, because the adverse effects on the society and the environment are strongly related with population density, site-specific meteorological data, infrastructure, etc.

The EcoSenseWeb software has been developed for the assessment of impacts on the environment and the society from electricity generation and other industrial activities, and for the estimation of the external costs due to these impacts. The assessment of impacts is based on the Impact Pathway Approach (IPA) developed in the ExternE (Externalities of Energy) project, funded by the European Commission, and it provides data for an integrated impact assessment associated with pollutants. The environmental cost of pollutants is obtained in Euro-cents of year 2000 per kWh [1].

### 2.2. The Impact Pathway Approach (IPA)

The IPA starts with the quantities of various pollutants emitted at a certain location in one of the 65 sub-regions in Europe or six regions outside Europe, such as Turkey or Egypt. In the second step, using the atmospheric pollutant transport module, which takes into account wind speed and

Corresponding Author: Christos A. Frangopoulos, Email: caf@naval.ntua.gr

direction, baseline (current) concentrations of pollutants and chemical transformation of pollutants, the marginal changes in the ambient conditions are modelled. The third step consists of the impact assessment of damages such as impacts on health, building materials, crops and land, due to harmful pollutants. For this purpose, the dose-response function is used, which relates the quantity of pollutants with the physical effect on the receptors, e.g. number of hospitalizations [2]. Then, the results from the three steps are aggregated and converted to monetary values, in order to obtain the external cost.

### 2.3. Methods for estimation of the impact of pollution on human health

The user of EcoSenseWeb may select one of three different methods in order to calculate the external cost associated with human health[1]:

1. "SIA_E_PPM". It considers 30 endpoints in total: eight due to each of PPM10 and SIA10, four due to each of PPM2.5 and SIA2.5, and six due to SOMO 35.
2. "SIA_D_PPM_Core". It considers 42 endpoints in total: eight due to each of PPM10, Nitr10 and Sulf10, four due to each of PPM2.5, Nitra2.5 and Sulf2.5, and six due to SOMO 35. In addition, it takes into consideration different toxicity of primary and secondary particles. For this purpose, the value of concentration response function (CRF) is multiplied by 0.5 in case of nitrates, 0.7 in case of sulphates and 1.3 in case of primary particles.
3. "SIA_E_PPM_AddSens". It considers 48 endpoints in total: 14 due to each of PPM10 and SIA10, five due to each of PPM2.5 and SIA2.5, and ten due to SOMO 35.

These endpoints refer to the concentration response function for assessment of impacts on human health, the various age groups of people and different monetary values. Examples of endpoints (EP) for primary pollutants and SIA less than 2.5 μm are are the following: 1) Life expectancy reduction: years of life lost (YOLL). 2) Net restricted activity days (netRADs). 3) Work loss days (WLD), 4) Minor restricted activity days (MRAD), 5) new cases of chronic bronchitis (for the third method only).

[1] Abbreviations are explained at the end of the main text.

### 2.4. Division of geographic area

The results of EcoSenseWeb refer to local, regional, local/regional and hemispheric scale. The local scale is defined as an area of 10000 $km^2$ and the calculations in this area are performed using a 10×10 $km^2$ grid. The regional scale covers the whole of Europe and the calculations in this area are performed using a 50×50 $km^2$ grid. The hemispheric scale uses a 100×100 $km^2$ grid and covers the entire northern hemisphere. In local/regional scale, the results from local scale and the results from regional scale are taken into account and they are used with the Monte Carlo Method in order to obtain better results at the regional scale, but only for PPM. The grid of Europe has been created by the European Monitoring and Evaluation Programme (EMEP) [3].

Fig. 1 shows a 50×50 $km^2$ grid of Poland, which is a relatively large country (312 679 $km^2$) [4] and it is divided into three sub-regions. In the diagram, the sub-regions are separated by darker lines [5], so the three cities selected for this study, i.e. Gliwice, Olsztyn and Szczecin, are located in different sub-regions. Additionally, Warsaw is considered, which is capital of Poland and it is in the same sub-region with Olsztyn. A smaller country, such as Greece (131 957 $km^2$) [4], is not divided into sub-regions. Each element has its own grid coordinates (x, y), which are in correlation with the geographical coordinates, so as to make it easier and clear to find it. Fig. 1 also shows the coordinates of grid; for convenience in reading the figure, one of the coordinates is underlined.

### 2.5. Background concentration of pollutants

Another important element used by the EcoSenseWeb is the background concentration of pollutants, which is partly presented in Fig. 1. Varying degrees of darkened elements in the grid of Fig. 1 show the concentration PMcoarse in year 2007 due to combustion in energy and transformation industries (stationary sources); in the literature it is also called Sector 1. PMcoarse denotes coarse particulate matter, defined as the integrated mass of aerosol with dry diameter between 2.5μm and 10μm.

For each pollutant, there is a different background. In case of SIA, the least polluted areas are Norway and north and central Sweden. The highest

concentration is in the centre of Europe, where it is possible to separated six regions with the highest emissions: 1) Netherlands, Belgium and north France; 2) south Romania, west Bulgaria; 3) north Italy; 4) Hungary; 5) Poland; 6) west Ukraine. For PPM, the background is similar with the background of SIA, but the highest concentration is over the capital of Russia, Moscow. In case of SOMO, the background is completely different than the previous two cases: the lowest concentration is in north of Europe, but the highest is in south of Europe, over the Mediterranean Sea. Therefore most at risk are Greece and Italy.

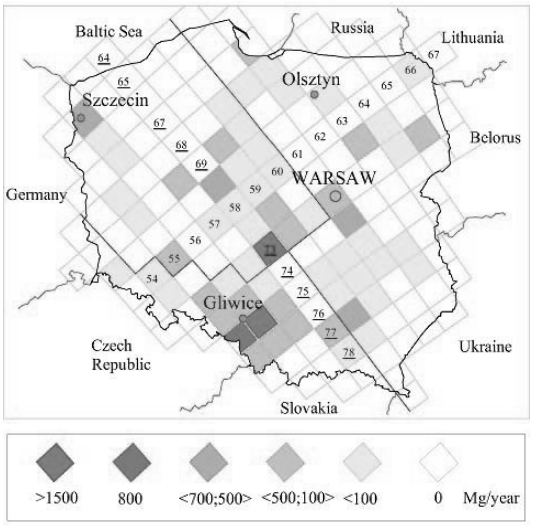


*Fig. 1: 50×50 km² grid of Poland with concentration of PMcoarse in year 2007.*

*Table 1: Emission of pollutants due to Sector 1 in year 2007, Mg/year [5].*

| Grid | $NO_X$ | $SO_2$ | PM10 |
|---|---|---|---|
| 75/56 | 55 972 | 142 282 | 3 198 |
| 73/58 | 48 267 | 188 050 | 2 758 |
| 75/55 | 23 155 | 37 747 | 1 323 |

Table 1 gives the annual emission of various pollutants from Sector 1 in 2007 in the elements of polish grid with the highest concentration.

EcoSenseWeb has two different scenarios of background: present concentration (year 2010) and future concentration (year 2020) of pollutants; the second scenario has estimated a lower concentration of emissions. Both scenarios have different values for each element than those shown in Table 1, because they take into consideration the concentration of pollutants from all sectors. The grid elements with the highest values in this table, e.g. 75/56 for $NO_x$, have the highest values in both scenarios, because it is assumed that the location of emission sources remains the same, but the emissions in 2020 are lower than those in 2010 due to policy instruments.

### 2.6. Air dispersion model

The Industrial Source Complex Model (ISC), used by EcoSenseWeb for the damage cost due to pollutants, is such that there is differentiation between local and regional scale for PPM only. For $SO_2$ and $NO_X$, the local scale is embedded in the regional scale and the values are the same in the whole sub-region.

The ISC model is a widely used steady-state Gaussian plume model, which is a mathematical model typically applied to point source emitters, such as coal plants, in order to assess pollutant concentration. Air pollution is represented by an idealized plume coming from the top of a stack of certain height and diameter. The vertical displacement depends on the stack gas exit velocity and temperature, and the temperature of the surrounding air [6].

For regional modelling by the EcoSenseWeb, the Eulerian dispersion model is used, which quantifies pollution transport by subdividing the atmosphere into a fixed grid of calculation points, where the fundamental equations are explicitly solved. The model takes into consideration the movement of a large number of pollution plume parcels as they move from their initial location in the atmosphere and model the motion of the parcels as a random walk process. The Eulerian model uses a fixed three-dimensional Cartesian grid as a frame of reference [1].

## 3. Evaluation of externalities for the plant without and with abatement equipment

### 3.1. Brief description of the plant

A pulverized coal power plant with steam at supercritical conditions is selected for the study, which achieves a gross electric efficiency at a level of 48%. It is considered that the plant operates for 6500 h per year. The following composition of fuel is considered on a mass basis: carbon 0.557, hydrogen 0.036, nitrogen 0.011,

oxygen 0.046, moisture 0.09, sulphur 0.01 and ash 0.25.

Abatement equipment for flue gas desulfurization is considered that uses wet limestone, which has two advantages: it achieves a high efficiency, namely 95% [7], and gives gypsum as a useful product.

Dust is removed from the exhaust gas with the use of a patented electrofilter bag, which is the most proven method and has an efficiency of about 99.5% [7].

Abatement of $NO_x$ with Selective Catalytic Reduction (SCR) is considered. The method consists of injecting ammonia ($NH_3$) into the boiler flue gas and passing the flue gas through a catalyst, where the $NO_x$ and $NH_3$ react to form nitrogen and water vapour [8].

### 3.2. Selection of options for estimation of externalities

The options selected for estimation of externalities in this study are the following:

- Human health damages are estimated by the SIA_E_PPM_AddSens model.

- The dispersion module based on the background of present concentration of pollutants in the atmosphere is used, which influences the secondary pollutant transformation (Emission-Scenario 2010).

- The dispersion is estimated also in combination with meteorological data in the form of average values of atmospheric condition of several representative years, such as 1996, 1997, 1998 and 2000.

Other conditions for a complete analysis of the results from EcoSenseWeb software are the following:

- The European currency unit with background value of year 2000 (Euro 2000) is used.

- The results of this study refer to the combined local/regional model.

Table 2 gives the technical data used with EcoSenseWeb software to obtain the external cost of pollutants in the case studies presented here. The externalities are calculated for the aforementioned three polish cities, which have the following coordinates: Gliwice (18º33´E, 50º21´N); Olsztyn (20º27´E, 53º47´N) and Szczecin (14º42´E, 53º26´N). The three cities are located in three different sub-regions of Poland (Fig. 1). In order to show the relation within one sub-region, calculations for Warsaw (21°3´E, 52°11´N), which is located in the same sub-region as Olsztyn, are carried out.

*Table 2: Technical data for EcoSenseWeb software. A: without pollution abatement equipment. B: with pollution abatement equipment.*

| Parameter | Value | | Units |
|---|---|---|---|
| | A | B | |
| Net electric production | 4052.6 | 3900 | GWh/a |
| Flue gas volume (dry) | 1 451 522 | 1 449 303 | $Nm^3/h$ |
| Stuck height | 250 | | m |
| Flue gas temperature | 393 | | K |
| Emissions: | | | |
| $SO_2$ | 2946 | 177 | $mg/Nm^3$ |
| $NO_2$ | 1326 | 200 | $mg/Nm^3$ |
| PM10 | 5523 | 26 | $mg/Nm^3$ |
| PM2.5 | 1104 | 5.3 | $mg/Nm^3$ |

### 3.3. External cost of pollutants for Gliwice, Olsztyn, Szczecin and Warsaw.

Table 3 shows, the external cost of each pollutant, which is obtained by dividing the results of EcoSenseWeb in €-$cent_{2000}$/kWh by the quantity of each pollutant. Values in Euros of the year 2000 were converted to values in Euros of the year 2008 using the annual average rate of change in Harmonized Indices of Consumer Prices in Poland, which was 5.3% in year 2001, 1.9% in 2002, 0.7% in 2003, 3.6% in 2004, 2.2% in 2005, 1.3% in 2006, 2.6% in 2007 and 4.2% in 2008 [4]. The values of externalities in €-$cent_{2000}$/kg are the same for the cases A and B because, according to the EcoSenseWeb, the impact is a linear function of the quantity of a pollutant in the range of emissions appearing in this study.

Comparing the external cost of pollutants to the concentration of pollutants as illustrated in Fig. 1, a simple conclusion could be reached: the higher the concentration of pollutants in the region, the higher external cost.

The external cost due to $NO_X$ and $SO_2$ obtained with EcoSenseWeb for Warsaw are exactly the same like for Olsztyn, but for PM this value is

slightly different, it equals 6.44 €$_{2008}$/kg and it is about 6% higher than the value obtained for Olsztyn. This is due to the different dispersion model used for local and regional scale.

*Table 3. External cost of pollutants, €$_{2008}$/kg.*

| City | $SO_2$ | $NO_x$ | PPM |
|---|---|---|---|
| Olsztyn | 12.04 | 10.00 | 6.07 |
| Warsaw | 12.04 | 10.00 | 6.44 |
| Gliwice | 14.52 | 7.91 | 8.75 |
| Szczecin | 12.64 | 9.72 | 6.72 |

### 3.4. Impact of power plant in Olsztyn on other countries

The external cost at regional scale due to a power plant located in Olsztyn is 8.377 €$_{2000}$/MWh and it is related to human health (91.37%), crops (1.07%), buildings material (3.44%) and biodiversity losses due to acidification and eutrophication (4.12%).

The external cost in relation to health in 64 countries located in three continents (Europe, Africa and Asia) is 7.7 €$_{2000}$/MWh. As can be foreseen, the highest cost is in Poland and equals 2.08 €$_{2000}$/MWh. The power plant located in Olsztyn adversely affects the population of Ukraine, where the external cost is 1.14 €$_{2000}$/MWh and the people of Germany and Russia, where the cost is 0.66 and 0.54 €$_{2000}$/MWh, respectively.

### 3.5. Externalities in a few selected countries

A further step in this study was the estimation of the external cost due to a power plant located near the capitals of European countries. For this purpose the EcoSenseWeb has been used with the dispersion models described in Sub-section 2.6.

For $SO_2$, the highest value of the external cost is received for Switzerland (15.08 € per kg of $SO_2$), while the lowest value is for Norway (3.27 € per kg of $SO_2$). The average value of external cost of $SO_2$ for Europe is 8.62 € per kg of $SO_2$. When considering $NO_X$ emissions and their harmful effects on the environment, the highest external cost is also for Switzerland (20.27 € per kg of $NO_X$), but the lowest value is for Portugal (1.09 € per kg of $NO_X$). The average external cost due to $NO_X$ in Europe is 7.14 € per kg of $NO_X$.

Figure 2 shows the ten countries with the highest external cost of one selected pollutant, namely $SO_2$, emitted from a plant located near the capital of each country.

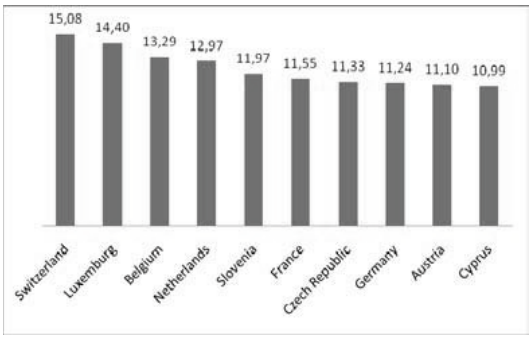


*Fig. 2. The ten highest values of external cost of $SO_2$ in European countries, €/kg .*

Taking into consideration the background concentration of pollutants, the population density and the concentration of industry, it can be understood why certain areas are more sensitive to additional pollution and consequently the environmental cost is higher, as it is shown by the calculated externalities. But there is also one other significant factor, which affects the results: the dispersion of pollutants, that is to which countries and how much pollution is transferred. For example, Switzerland is not the most polluted country, but about 34% of pollutants go to Italy, 23% to Germany and only 10% stay in Switzerland. Comparing this distribution with the background, it is visible that Germany and Italy are very polluted.

The highest value of external cost of PPM appears in the Netherlands, 9.83 € per kg of PPM, but the lowest value was obtained for Finland, 1.54 € per kg of PPM. According to the results of EcoSenseWeb, the total environmental cost due to PPM emissions in the Netherlands is distributed primarily to the Denmark (32%), the Netherlands itself (29%) and Belgium (13%). Thus, emission of particulates in the Netherlands increases the concentration of this pollutant in one of the most polluted areas in Europe. But in case of Finland, 37% of PPM stay in Finland and 28% is transferred to Russia.

In order to investigate the effect of the method used on the results of the external costs, calculations have been performed with each one of

the three methods described in Sub-section 2.3 for a plant located near the capital of each country.

The results related to $SO_2$ for the three European countries with the highest cost and the three European countries with the lowest cost are presented in Fig. 3. The results with method 2 are 43-57% lower than those with method 3, while the results with method 1 are 29-35% lower than those with method 3. Even though not shown here, similar is the effect of the method on the externalities due to PPM and $NO_X$. These differences are due to the number of endpoints (in other words adverse effects on the environment and the society) and the weighting factors considered by each method. The different results influence the cost of electricity, as it is shown in Section 4.

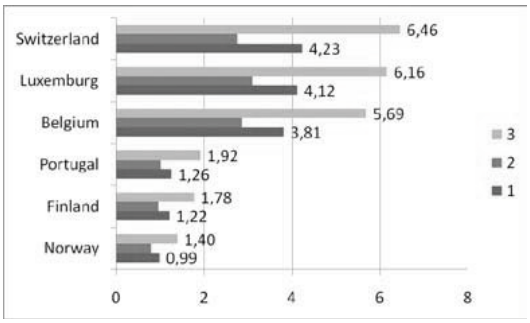


*Fig. 3. Three European countries with the highest and three with the lowest external cost of $SO_2$, in €/MWh, derived with the three methods described in Sub-section 2.3.*

Comparing the highest and the lowest external cost in Europe, it is visible that the difference is significant. In case of $SO_2$, the cost in Switzerland is 4.6 times higher than the cost in Norway. Even though not shown here due to space limitations, the cost due to PPM in the Netherlands is 6.4 times higher than the cost in Finland and the cost due to $NO_x$ in Switzerland is 18.6 times higher than the cost in Portugal.

One of the most important results obtained with EcoSenseWeb is the influence of a power plant located in a certain area to other areas. Table 4 shows the most vulnerable countries due to a plant located in certain selected countries with respect to three pollutants, $SO_2$, $NO_X$ and PPM, taken into account together. It is important to note that the results for these pollutants calculated separately are a bit different.

The relative location of the various countries and the dispersion of pollutants due to meteorological conditions, e.g. wind speed and direction, make Germany, Poland, Italy, Romania, Russia and France the most vulnerable countries from the point of view of pollution, partially shown in Table 4.

*Table 4 The most vulnerable countries due to a power plant located close to the capital of each selected country.*

| Location of power plant | | Vulnerable countries | | |
|---|---|---|---|---|
| CH | Switzerland | IT | DE | FR |
| LU | Luxembourg | FR | DE | NL |
| BE | Belgium | DE | FR | NL |
| PT | Portugal | PT | ES | DZ |
| FI | Finland | RU | FI | UA |
| NO | Norway | DE | UK | PL |

# 4. Cost of electricity without and with abatement equipment

## 4.1. Estimation of the unit cost of electricity

The net present value (NPV) of the system is a function of the selling price of electricity. The price that makes the NPV equal to zero is the unit cost of electricity. The NPV is calculated by taking into consideration the total net cash flow [9].

For the calculation, the following values are adopted: time horizon of analysis 40 years, cost of coal 1.91 €/GJ, cost of coal transport 4.24 €/ton, cost for ash and dust removal from power plant 5.83 €/ton.

It is considered that the construction of the plant starts in year 2010 and its operation starts in 2014.

Capital expenditures were estimated assuming 1300 €/kW in the case of power plant with supercritical parameters with abatement equipment and 1100 €/kW without abatement equipment. It is considered that the power output of the plant with abatement is 600 MW, while the power output of the plant without abatement is 623 MW. The share of own capital in financing the investment is assumed equal to 20% of investment.

For the general inflation rate a value of 2% is assumed, but for the cost of coal, coal transport, removal of dust from the power plan, compensation of employees and electricity an annual inflation rate of 3% is assumed. According to [10], the cost of $CO_2$ equals 19 €/Mg until 2020,

23 €/Mg in 2025, 30 €/Mg in 2030, 46 €/Mg in 2040 and 61 €/Mg in 2050. For others years, a linear approximation is considered. For the environmental cost of CO, a constant value of 1.16 €/kg CO has been considered.

The results are presented in Table 5 for power plant with and without abatement equipment and with and without externalities.

*Table 5: Cost of electricity in Olsztyn, in €$_{2008}$/MWh.*

| Case | Abatement | |
|---|---|---|
| | without | with |
| Without externalities | 30 | 33 |
| With externalities | 200 | 53 |

According to the results in Table 5, the unit cost of electricity for the power plan with abatement is by about 10% higher than for the same plant with no abatement, if the external cost of pollution is omitted. The environmental externalities strongly increase the unit cost of electricity by about 566% for the plant with no abatement equipment and by about 70% for the plant with abatement equipment. Furthermore, the cost of electricity including environmental externalities from a power plant without abatement is about four times higher than the cost of electricity of the same power plant with abatement (200 versus 53 €$_{2008}$/MWh).


*Fig. 4 Cost of electricity in Olsztyn, in €$_{2008}$/MWh, obtained by different methods – A without abatement and B with abatement.*

The unit cost of electricity obtained with all three methods available in EcoSenseWeb is presented in Fig. 4 for the power plant with and without abatement equipment. The difference between the highest and the lowest cost is about 32% in case without abatement and 3.5% with abatement. The differences among the results of these three methods indicate the uncertainty in understanding the adverse effects and calculating the externalities. Thus, an improvement of the methodology is necessary.

### 4.2. Sensitivity analysis

Figure 5 shows the effect of externalities and of the fuel cost on the unit cost of electricity, $c_e$, for the power plant with abatement equipment. The straight line corresponds to the $c_e$ obtained with the nominal set of parameters values. The dark bars indicate $c_e$ for an increase of the externalities or cost of fuel by 10%, while the light bars indicate $c_e$ for a decrease of the externalities or cost of fuel by 10%.

A 10% increase of the environmental cost of all pollutants together causes 8.51 % increase of the cost of electricity, if there is no pollution abatement, but only 2.86 % increase when the plant has abatement equipment, which is in the same order of magnitude (2.76%) with the effect of a 10% increase of the cost of coal.

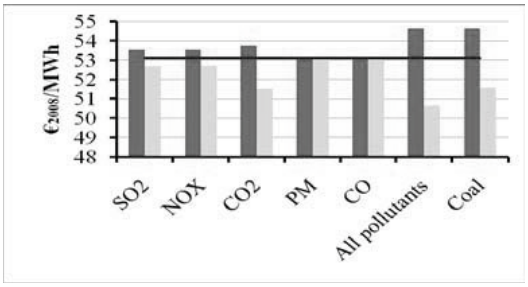


*Fig. 5. Cost of electricity for a plant with abatement in Olsztyn, in €$_{2008}$/MWh, for a change in cost of externalities and coal by ±10%.*

Due to nonlinear change of environmental cost of $CO_2$ with time, the influence of this externality on the $c_e$ is different from the influence of the externalities of other pollutants.

In case of no abatement, the most severe effect is due to $SO_2$ and PM. However in case of abatement, the most severe impact is due to $CO_2$.

## 5. Conclusions

The results presented in the preceding sections lead to the following conclusions.

The external environmental and social cost due to pollution has a significant impact on the cost of

electricity and should not be ignored. The studies have to be performed for particular plants and locations and at various levels (local, regional, global), in order for the complete effect of pollution on the environment to be properly assessed.

If externalities are accounted for, installation of pollution abatement equipment decreases the unit cost of electricity drastically (to the 1/4 of the cost without abatement, in the particular example).

The location of the source of emissions (e.g. a power plant) has a significant effect on the external cost due to pollution, which is a function of the background concentration in the particular place, the pollution dispersion (which is strongly related with meteorological conditions), the population density, the infrastructure, etc.

The transboundary pollution increases the background concentration of pollutants, which, in turn, causes a strong increase in the environmental cost due to pollutants emitted from a plant located in the area receiving the transboundary pollution.

## Abbreviations

| | |
|---|---|
| CRF | Concentration Response Function |
| EMEP | European Monitoring and Evaluation Programme |
| IPA | Impact Pathway Approach |
| ISC | Industrial Source Complex Model |
| Nitr | nitrate particles |
| PM10 | particulate matter, defined as the integrated mass of aerosol with dry diameter up to 10 μm. |
| PM2.5 | fine particulate matter, defined as the integrated mass of aerosol with dry diameter up to 2.5 μm. |
| PMcoarse | coarse particulate matter, defined as the integrated mass of aerosol with dry diameter between 2.5μm and 10μm. |
| PPM | Primary Particulate Matter |
| SCR | Selective Catalytic Reduction |
| SIA | Secondary Inorganic Aerosols (a mixture of $SO_4$, $NO_3$, $NH_4$) |
| SOMO35 | Sum of Ozone Means Over 35 ppb, yearly sum of the daily maximum of 8-hour running average over 35 ppb |
| Sulf | sulfate particles |

## References


[1] Preiss P., and Klotz V., 2007, Description of updated and extended draft tools for the detailed site-dependent assessment of external costs. Technical Paper, 7.4 RS 1b, University of Stuttgart, Germany, URL: http://www.needs-project.org/docs/results/RS1b/NEEDS_Rs1b_TP7.4.pdf .

[2] Torfs R., et al., 2007, A set of concentration-response functions, Deliverable 3.7–RS1b/WP3, URL: http://www.needs-project.org/2009/Deliverables/Rs1b%20D3.7.pdf

[3] http://www.emep.int/

[4] http://epp.eurostat.ec.europa.eu

[5] Preiss P., and Scasny M., 2009, Generalization–Aggregation–Transferability, *External cost of energy technologies*, Brussels 2009 URL: http://www.needs-project.org/2009/17-02-09/afternoon/Philipp & Milan.ppt

[6] Atkinson D., et al., 1997, Improvements to the EPA Industrial Source Complex Dispersion Model, Journal of Applied Meteorology, 36, pp. 1088-1095.

[7] Konieczyński J., 2004, *Ochrona powietrza przed szkodliwymi gazami* (Air protection against harmful gases), Wydawnictwo Politechniki Śląskiej, Gliwice, PL.

[8] Control of Nitrogen Oxide Emissions: Selective Catalytic Reduction (SCR), Technical Report, The U.S. Department of Energy and Southern Company Services, Inc., 2007, URL:

http://www.netl.doe.gov/technologies/coalpower/cctc/topicalreports/pdfs/topical9.pdf

[9] Sierpińska M., and Jachna T., 2007, *Metody podejmowania decyzji finansowych – analiza przykładów i przypadków* (Methods of financial decision-making - an analysis of examples and cases), PWN, Warszawa.

[10] Onno Kuik, 2007, The avoidance costs of greenhouse gas damages: a meta-analysis, CASES project, WP3, University of Amsterdam.


**Acknowledgments:** The financial support of the European Commission through the INSPIRE Project is gratefully acknowledged.

# Energetic optimization of Wet Air Oxidation coupling process simulation and experimental design

*Sébastien LEFEVRE[a,b], Jean-Henri FERRASSE[a], Rémy FAUCHERAND[b], Alain Viand[b] and Olivier BOUTIN[a]*

[a] *Aix-Marseille Université, Laboratoire M2P2 UMR CNRS 6181, Aix en Provence, France*
[b] *A3i, Donzère, France*

**Abstract** Wet air oxidation process is used for wastewater treatment, especially when it contains high chemical oxygen demand. With non catalytic processes, temperatures between 200 and 350°C and pressures between 15 and 30 MPa are generally applied. A method, based on the coupling of simulations and experimental design, to optimize from an energetic point the process has been developed. The interest of an experimental design approach is to plan the combination of simulation to describe the functioning of the process. Five parameters have been selected; temperature, pressure, chemical oxygen demand, air ratio and temperature of steam. After achieving the 41 simulations of the *"numerical design"*, mass and energy balances were analysed through three energetic values integrated as the design responses: exergetic efficiency, minimum heat required by the process, and work balance during the process functioning. The surface response methodology determines which are the most influencing parameters on design responses. It also shows eventual interaction between parameters. For the flowsheet presented in this work, the best functioning conditions are the following: a pressure of 20.5 MPa, a temperature of 294°C, a ch emical oxygen demand of 47.6 g.L$^{-1}$, an air ratio of 1.7 and a steam temperature of 183°C.

**Keywords:** wet air oxidation, experimental design, energetic efficiency, exergy.

## 1. Introduction

Due to new legislation on environmental protection, it is necessary to improve the water treatment processes for urban and industrial aqueous wastes.

Domestic wastewaters essentially carry organic pollution such as cleaners, fats, solvents and organic matter. Industrial waters have characteristics which vary from one industry to another: refineries, pharmacy, microelectronics, distilleries, food processing. Besides, organic nitrogenous or phosphorous matters, the effluents can also contain toxic products such as solvents, heavy metals, organic micropollutants and hydrocarbons. The classical methods used to treat these wastes are based on biological processes or physico-chemical treatments. Other technologies are still under research and development, as for instance Wet Air Oxidation (WAO).

When an effluent contains hard chemical oxygen demand this process is adapted. It consists in oxidizing the organic fraction of an effluent containing a strong concentration of organic matter, biodegradable or not (COD included between 10 and 150 g.L$^{-1}$), by putting in contact an oxidizer (air, pure oxygen, hydrogen peroxide) with the liquid effluent. The WAO process works in sub-critical conditions with a pressure of 5 to 20 MPa and a temperature of 100 to 320°C. High pressures allow keeping the reactions mostly in the liquid phase. The yield of the oxidation of organic matter depends on various parameters such as temperature, partial pressure of oxygen and residence time. The oxidation reaction can be catalysed or not ([1]). More information and discussion about WAO process can be found in several reviews ([2-5]).

In the literature, there are many kinetic studies to find the conditions for the degradation of different

Corresponding Author: Olivier BOUTIN, Email: olivier.boutin@univ-cezanne.fr

molecules (carboxylic acid, aromatic compounds) or real effluents (pulp and paper, textile). But there are few studies considering economic aspects and energy recovery.

The purpose of this work is to present an original method, based on coupling process simulation, calculation of energy parameters and experimental design methodology.

The difficulty is to determine the influence of operating parameters (like pressure, temperature or chemical oxygen demand) on the calculated energetic values (presented in point 2.3). The experimental design methodology is used to minimize the number of cases studied and to interpret the results for a fixed process flowsheet.

## 2. Material and methods

### 2.1. Process simulation

The simulation of the process has been done with the ProsimPlus software (version 3.0, France). The basic process is composed of different gas/liquid streams and equipment that could be implemented in the flowsheeting tool of the software represented on Figure 1. The selected thermodynamic model (equation of state and mixing rule) is the Predictive Soave-Redlich-Kwong one. Then, the mass and energy balances are calculated.

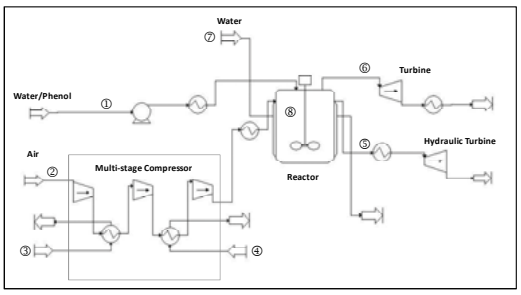


*Fig. 1. Flowsheet of the WAO process (ProsimPlus®).*

The details about streams, apparatus and the hypothesis made for the calculations are given below.

The stream ① is the feeding of the waste water, with a flowrate of 1 $kg.h^{-1}$. The organic waste is represented by phenol. This compound and its derivatives are often presented in industrial wastewaters with concentrations of 15 $g.L^{-1}$ ([6]). The amount of phenol in the feeding is expressed in chemical oxygen demand (COD) in $g.L^{-1}$, using the oxidation reaction between phenol and oxygen:

$$C_6H_6O + 7\ O_2 \rightarrow 6\ CO_2 + 3\ H_2O \quad (1)$$

Before entering the reactor, the stream flows through a volumetric pump to reach the chosen pressure, and through a virtual exchanger to be heated at the desired temperature. The heat exchanges are considered independently, the positioning of heat exchangers being done later.

The flowrate of air ② is calculated according the aeration ratio chosen. It corresponds to the ratio between the air introduced in the reactor and the air required by the stoechiometry of the reaction (1). The air stream is pressurised at the same pressure than the liquid stream using a multi-stage compressor. Every stage is cooled using heat exchanger (③,④) in order to obtain a stage entrance temperatures of 30°C.

At the exit of the reactor, the gas and liquid phases (⑤,⑥) are injected respectively in a wet air turbine and in a hydraulic turbine to be expanded at 0.1 MPa. The two streams are then cooled at 20°C by virtual heat exchangers.

The reactor ⑧ is isothermal with any pressure loss and the oxidation reaction is supposed to be total. The heat of reaction is calculated from the Hess law, as the difference between the heat of formation of the products minus the heat of formation of the reactants: $\Delta_r H^\circ = -3054\ kJ.mol^{-1}$. To keep the temperature constant in the reactor, the exothermic energy of reaction is evacuated by a double shell where water circulates ⑦. The water flowrate is adjusted to generate steam at the temperature $T_v$.

### 2.2 Experimental design

The experimental design is a statistical method that consists in selecting and ordering experiments to identify the quantitative effects of the chosen parameters on the responses of the system. The implementation of these methods contains different steps:

- Postulating a mathematic model of the system,

- Defining an experimental design (trials allowing the identification of the model coefficients),
- Achieving the experiments,
- Identifying the coefficient and analyse the results.

In this study, the experiments are simulations done with commercial software. This kind of design will be called "numerical design". The objective of the study is to explore the relationships between the chosen parameters of the process and the three responses (the energetic values) by using a sequence of experiments in order to obtain an optimal response. This is called response surface methodology.

The production of the experiment plan and the interpretation of results has been done with, the NEMRODW software (2000-D, LPRAI Corporation, France). The selected model is a second order polynomial model in order to take into consideration interaction effects between the parameters.

The five parameters are: temperature, pressure, air ratio, COD input and steam temperature $T_V$ of the reactor double shell. To estimate the coefficients of the model, a Box Benhken design was chosen. It is a particular model adapted to the parameters with three levels. The variation domains are the following: pressure (20-30 MPa); temperature (200-300 °C); COD (23-143 $g.L^{-1}$); air ratio (1.2-2); temperature of steam (160-200 °C). The experiment plan contains 41 simulations.

## 2.3. Energetic values

With the data of mass and energy balances obtained with ProsimPlus®, it is possible to calculate three energetic values: exergetic efficiency, work balance and minimum heat required (or furnished) by the process evaluated by Pinch analysis.

To explain the calculation of these energy values, an example is given for the following parameters: pressure=20MPa, temperature=250°C, COD=143$g.L^{-1}$ (6% phenol in the feeding), aeration ratio=1.6 and temperature of steam $T_V$=180°C.

The exergetic efficiency η is the ratio between exiting exergies (turbines, streams, heat exchanges) and entering exergies (compressor, volumetric pump, heat exchanges, streams).

The different exergies calculated in this example are shown in Table 1.

*Table 1. Case studied: exiting and entering exergies*

| | Exergy (W) |
|---|---|
| Compressor | 210.4 |
| Volumetric pump | 8.5 |
| Heating exchangers | 269.7 |
| Compressor cooling | 130.4 |
| Entering mass flows | 541.2 |
| Vapour utility | 145.4 |
| Turbines work | 157.5 |
| Cooling exchangers | 172.8 |
| Exiting mass flows | 0 |

The entering and exiting mass flows are at the reference conditions (T=20°C, P=0.1 MPa) so their exergy is null. However for the liquid entering flow, the phenol exergy as fuel must be considered. It corresponds to the maximum fraction of its energy convertible in mechanical energy. In the case studied, this maximum is obtained with a complete oxidation of phenol. By convention, the exergy of smokes ($CO_2$, $H_2O$ and Air) in equilibrium with the environment is null.

Then the exergy of phenol (in kW) is equal to:

$$E_x = \frac{006 \times F \times \Delta H_r^\circ}{M_{phenol} \times 3.6} \qquad (3)$$

where F is the flowrate of wastewater ($kg.h^{-1}$) and $M_{phenol}$ the molar mass of phenol (94 $g.mol^{-1}$). In the case studied, Ex=541.2 W.

To calculate the exergies due to heat exchanges, different equations have been used ([7]). For the vapour utility, the exergy contained in the steam stream is:

$$E_{xV} = Q\left(1 - \frac{T^\circ}{T_V}\right) \qquad (4)$$

where Q is the energy of the vapour flow (Watts), $T_V$ the temperature of the vapour and T° the temperature of reference (293K).

In the case studied, the simulation shows that 411.7 W are transferred from the reactor to the

water flow in the double shell. The temperature of the vapour is 180°C so the exergy of the vapour utility is:

$$E_{xW} = 411.7 \times \left(1 - \frac{293}{453}\right) = 145.4\ W$$

For the virtual heat exchangers, the heat Q is exchanged between $T_{in}$ and $T_{out}$ and the corresponding exergy variation is equal to:

$$\Delta E_x = Q\left(1 - \frac{T^*}{T_{la}}\right) \quad \text{with} \quad T_{la} = \frac{T_{out} - T_{in}}{\ln \frac{T_{out}}{T_{in}}} \quad (5)$$

For the exiting liquid phase, the virtual exchanger is cooling the stream from 250°C to 20°C leading to Q=172.8W.

$$T_{la} = \frac{293 - 523}{\ln \frac{293}{523}} = 397K$$

$$T^* \text{ and } \Delta E_x = 172.8\left(1 - \frac{293}{397}\right) = 45.3W$$

By definition, the work is pure exergy. So the exergies corresponding to the compressor, pump and gas turbine are directly obtained by the simulation data. For the hydraulic turbine, the following formula is used:

$$W = q\left(\frac{P_{out}}{\rho_{out}} - \frac{P_{in}}{\rho_{in}}\right) \quad (6)$$

Using data from Table 1, the entering exergy is 781.5 W and the exiting exergy is 406.7 W. The exergetic efficiency is 0.52. This value allows estimating the performance of the process in these conditions of functioning and easily comparing several technological solutions. The COD of 143 $g.L^{-1}$ involves an important air flowrate, and the energy needed to compress this air has a negative impact on the efficiency.

The work balance ΔW is a non conventional parameter that is customised to enlarge the purpose of the paper. It is the sum of power used to pressurize (compressor, pump) and power recovered (turbines). If this term is negative, some work could be really recovered. In the case studied, ΔW= 61.5W.

Finally the third energetic value is the minimum hot utility requirement ($Q_{Hmin}$) which is evaluated using Pinch analysis ([8-10]). It corresponds to the energy which must be supplied by utilities (electric heating, hot oil or gas circuit, etc.). The Pinch analysis allows optimising the use of energy for various processes, in different fields of industry: chemistry, petrochemistry, refining and food-processing industry. By analysing the various energy streams of a process, it allows determining the methods to get back a maximum of heat and reduce the use of utilities.

The main tool of Pinch analysis is the composite curves diagram ([11]). These curves, representing the available sources of heat (hot curve) and the thermal needs of the process (cold curve), are used to determine the targets of minimal energy consumption. According to the shape and the position of these curves, the potential energy recoveries could be known. To build these curves, it is necessary to assess mass and energy balances to represent the various streams according to their level of temperature and their needs of heating or cooling.

The list of streams in the studied case is shown in Table 2. A "cold" stream needs heat; a "hot" stream gives heat.

*Table 2. Characteristics of the process flows*

| | Ti (°C) | Ti (°C) | CP ($W.°C^{-1}$) |
|---|---|---|---|
| Water/Phenol ① | 20 | 250 | 1.21 |
| Air ② | 20 | 250 | 0.35 |
| Compressor coolings ③,④ | 15 | 42.1 | 4.81 |
| Liquid exit ⑤ | 250 | 20 | 0.75 |
| Gas exit ⑥ | 250 | 20 | 1.29 |
| Vapour utility ⑦ | 15 | 180 | 2.49 |
| Reactor ⑧ | 270 | 250 | 27.1 |

The variation of enthalpy between the initial and the final point of each stream or "heat capacity flowrate" CP is calculated using equation 8.

$$\Delta E_x = \frac{\Delta H \times \text{Flowrate}}{T_f - T_i} \quad (7)$$

Composite curves are representing the temperature level as a function of the heat load. To establish the targets of minimal consumption of energy, the hot and cold curves are placed on the same

diagram. The smaller vertical distance between both curves is determined by the difference $\Delta T_{min}$, representing the minimal temperature between the fluids of a heat exchanger (usually recommended to 20°C in the chemical processes).

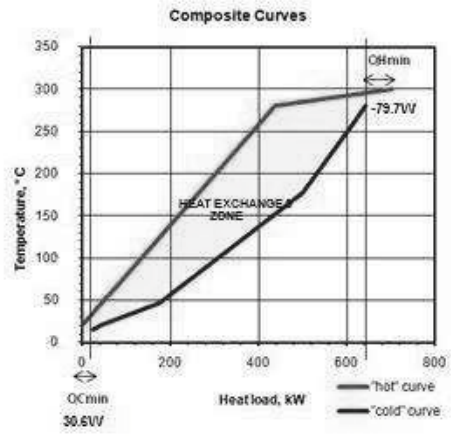


*Fig. 2. Composite curves of Pinch Analysis.*

On Figure 2, the coloured zone between the composite curves indicates the maximal quantity of heat energy which can be recovered by heat exchange. The quantities of energy outside of this zone indicate the loads of heating and cooling which must be filled by the utilities of the process.

In this figure, $Q_{Hmin}$= -79.7W, indicating that there is no heat supply needed for the functioning of the process in these conditions, and even that energy is produced.

## 3. Results and discussion

After achieving the simulations and calculate the energetic values for the 41 experiments of the Box-Behnken design, the estimation of the model coefficients is done using multi-linear regression. For the three responses, all the results are taken into account after analysing the statistical tests of significance for the model and for the different coefficients of the linear regression.

The variance analysis is done with a Fischer-Snedecor statistical test and presented in Table 3.

*Table 3. Variance analysis for the model of exergetic yield*

| | $\Sigma ei^2$ | p | S | F-test | Signif. |
|---|---|---|---|---|---|
| Regression | 0.5055 | 20 | 0.0253 | 66.35 | < 0.01 |
| Residual | 0.0076 | 20 | 0.0004 | | |
| Total | 0.5131 | 40 | | | |

For the exergetic efficiency the regression is significant then the linear model (polynomial of 2nd order) is validated. The same conclusions can be derived from the results obtained for $Q_{Hmin}$ and work balance. All the coefficients of the regression must be tested to know whether they are significant or not. It is done with a Fisher statistical test. These coefficients represent the influence of the corresponding parameter on the response and indicate the possible interactions between the parameters.

For exergetic efficiency $\eta$, which varies between 0.49 and 0.84, the Fisher test shows that COD of the liquid feed is the main influencing parameter. The more COD increases, the lower efficiency is. Indeed if the COD increases, the stoechiometric amount of air is more important quite as the energy expense for warming and compressing this air.

The results can be represented graphically, as on Figure 3, where the evolution of the exergetic efficiency is plotted in function of COD and temperature. It shows that $\eta$ decreases until a minimum, corresponding to a medium value of COD. The other parameters have no significant influence.

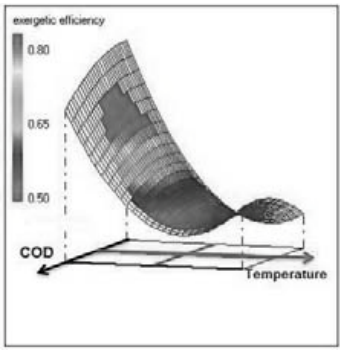


*Fig. 3. Isoresponse curves of exergetic yield with COD and temperature (P=25 MPa, AR=1.6, Tv=180°C).*

Concerning $Q_{Hmin}$, two parameters have an influence: temperature and pressure. On Figure 4, negative values are obtained for the highest pressures and medium temperatures. With this kind of conditions, the liquid phase is favoured at the reactor exit. A less important part of the reaction exothermic energy is lost to vaporise water in the reactor and heat is produced by the process.

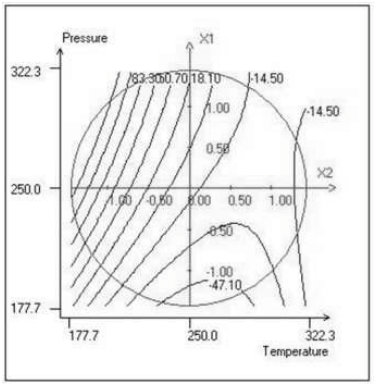


*Fig. 4. Isoresponse curves of $Q_{Hmin}$ with pressure and temperature (COD 83 g.L$^{-1}$, AR=1.6, Tv=180°C).*

Finally, the work balance is mainly influenced by COD and temperature. The best negative values (work recovery) are obtained for the highest values of temperature and medium COD, as seen on Figure 5.

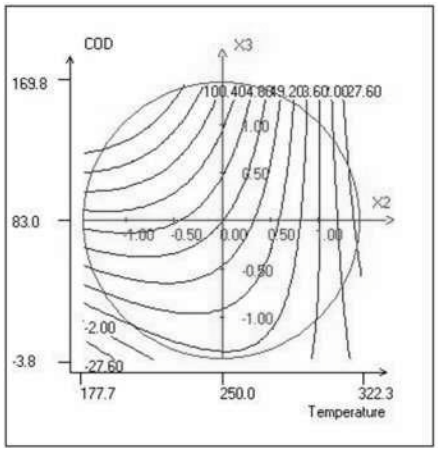


*Fig. 5. Isoresponse curves of work Balance with COD and temperature (pressure 25 MPa, AR=1.6, Tv=180°C).*

The experimental design allows the calculation of the desirability for the 3 energetic values in order to reach an optimum (Figure 6). This function is a multicriteria mathematical optimisation based on the different polynomial obtained from the numerical design. It necessitates giving the desirable values for each energetic parameter and a range of forbidden values. The optimisation will determine the maximum response values in the determined ranges.

For each response, a chosen range is specified with forbidden values (exergetic yield < 0.6, $Q_{Hmin}$ > 0 W, WR > 0 W) and target values (exergetic yield = 1, $Q_{Hmin}$ = -50 W, WR = -15 W).

From an energetic point of view of the process, this optimum is considered as the good conditions of functioning.

In this study, the values obtained are a pressure of 20.5 MPa, a temperature of 294 °C, an aeration ratio of 1.7 and a chemical oxygen demand of 47.6 g.L$^{-1}$. In these conditions, the exergetic efficiency is 0.7, $QH_{min}$ is -8.1W and work balance is -12,1W.

This method of energetic optimization based on coupling process simulation and experimental design is validated.

By improving process flowsheet with technologies of energy recovery, updating the technical data according current industrial equipments, and achieving kinetic studies on phenol degradation to take in account the conversion rate of the waste, this method will be relevant for the development of a non-catalysed WAO process energetically optimised, but for other kind of industrial processes as well.

## Nomenclature

| | |
|---|---|
| AR | aeration ratio |
| COD | chemical oxygen demand (g.L$^{-1}$) |
| CP | heat capacity flowrate (W.°C$^{-1}$) |
| $_rH°$ | heat of reaction (kJ.mol$^{-1}$) |
| ΔH | enthalpy variation (W) |
| Ex | exergy (W) |
| F | feeding flowrate (kg.h$^{-1}$) |
| $M_{Phenol}$ | mass molar of phenol (g.mole$^{-1}$) |
| P | reaction pressure (MPa) |

$P_{in}$ hydraulic turbine entering pressure (MPa)
$T_{out}$ hydraulic turbine exiting temperature (MPa)
p degrees of freedom
q flowrate through the turbine ($kg.s^{-1}$)
$Q_{Hmin}$ minimum heat (W)
Q heat exchanged (J)
T reaction temperature (°C)
$T^0$ reference temperature (K)
$T_i$ initial temperature of the stream (K)
$T_f$ final temperature of the stream (K)
$T_{la}$ logarithmic mean temperature
$T_{in}$ heat exchanger entering temperature (°C)
$T_{out}$ heat exchanger exiting temperature (°C)
$T_V$ steam temperature (°C)
$\rho_{in}$ density of entering flow ($kg.m^{-3}$)
$\rho_{out}$ density of exiting flow ($kg.m^{-3}$)
$\eta$ exergetic yield

## References


[1] Luck, F, 1999, Wet air oxidation: past, present and future, Catalysis Today, 53, pp.81-91.

[2] Debellefontaine, H, Foussard, J.N, 2000, Wet air oxidation for the treatment of industrial wastes. Chemical aspects, reactor design and industrial applications in Europe, Waste Management, 20, pp. 15-25.

[3] Barghava, S.K, Tardio, J, Prasad, J, Akolekar, D.B, Grocott, S.C, 2006, Wet oxidation and catalytic wet oxidation, Industrial and Engineering Chemistry Research, 45, pp.1221-1258.

[4] Levec, J, Pintar, A, (2007), Catalytic wet air oxidation process: A review, Catalysis Today, 124, pp.172-184.

[5] Luck, F, (1996), A review of industrial catalytic wet air oxidation process, Catalysis Today, 27, pp.195-202.

[6] Portela, J.R, Nebot, E, Martinez de la Ossa, E, 2001, Kinetic comparison between subcritical and supercritical water oxidation of phenol, Chemical Engineering Journal, 81, pp.287-299.

[7] Rivero, R, De Oliveira, J.R, Le Goff, P, 1990, Température de Carnot θ, diagramme θ/Q, méthode du pincement. Application à l'analyse exergétique des procédés industriels, Entropie, 26, pp.13-20.

[8] Linhoff, B, Towsend, D.W, Boland, D., Hewitt, G.F, Thomas, B.E.A, Guy, A.R, Marsland, R.H, 1982, *User guide on process integration for the efficient use of energy*, IchemE, Rugby, UK.

[9] Staine, F, Favrat, D, 1996, Energy integration of industrial processes based on the pinch analysis method extended to include exergy factors, 16, pp.497-507.

[10] Borel, L, Favrat, D, 2005, *Thermodynamique et Energétique Vol.1 De l'Energie à l'Exergie*, Presses Polytechniques et Universitaires Romandes.

[11] Giquel, R, 1995, Méthode d'optimisation systématique basée sur l'intégration thermique par extension de la méthode du pincement, Revue Générale de Thermique, 34, pp.579-607.

# Exergy Analysis of the Oil and Gas Separation Processes on a North Sea Oil Platform

*Mari Voldsund* [a], *Ivar Ståle Ertesvåg* [a], *Audun Røsjorde* [b], *Wei He* [b] *and Signe Kjelstrup* [a]

[a] *Norwegian University of Science and Technology, Trondheim, Norway*
[b] *Statoil ASA, Norway*

**Abstract:** The oil industry is in need for tools to monitor the performance of the processes on oil platforms. The irreversibility of different parts of an oil platform can be used to see where in the process exergy is wasted. We investigate a typical North Sea platform, to find where the highest irreversibilities take place. The platform in question consists mainly of a power plant, and a gas and oil processing plant. A detailed exergy analysis is done on the oil and gas processing part. Here 12 MW exergy is lost. Out of this is 20 % lost in the separation train, 11 % is lost in the gas re-compression train, 66 % is lost in the gas injection trains and 3.1 % is lost in the oil export section. We propose to improve this by focusing on the injection trains, where the gas is compressed before injection back into the reservoirs. The project is the first approach to a more detailed study of the exergy efficiency of the platform.

**Keywords:** Energy efficiency, Exergy analysis, Oil platform.

## 1. Introduction

In 2008, gas turbines and diesel engines on oil platforms were responsible for 21 % of Norway's total $CO_2$ emissions [1]. More efficient use of energy on platforms will therefore be important to reduce the total emissions of greenhouse gases. The oil industry is in need for tools to monitor the energy performance of the platform processes. Platforms can have different working conditions, where some have a higher potential than others for exergy saving. The exergetic efficiency, or second law efficiency, compares the work used in a process with the work needed for the same process if it was reversible. This can give a fair picture of the efficiency of each platform. The entropy production, or irreversibility, of different parts of a platform can be used to see where in a process potential work is lost, and by this also point to where the process can be improved. Exergy analysis is a method in thermodynamics which is not yet systematically used in the industry.

In 1997 [2] made an exergy analysis of the petroleum separation processes on a Brazilian offshore platform. On this platform the exergy is consumed in order to heat the petroleum for separation, to compress natural gas and to pump oil to the coast. There is recovery of exhaust gases for heat purposes. The analysis shows that the exergy consumption on this platform is dominated by the heating of oil in the separation process, despite the heat recovery system, and by the compression of gas.

In 2003 [3] studied chemical processes like absorption, stripping and heat transfer to identify ways of reducing exergy consumption. They discussed the state of the art on second law methods for reducing exergy losses. The paper concludes with 12 commandments for industrial processes, using the principle that the driving forces in a process should be held uniform, and as small as possible. While this may be a useful approximation for a single process unit, it does not hold for a process plant due to restrictions imposed by boundary conditions of the units [4]. In those cases, exergy losses must be minimized, taking boundary conditions into account, see [5]. As a first step in this direction, an exergy analysis is useful.

In this project an exergy analysis is given for the oil and gas separation processes of a North Sea oil platform. This is the first approach to a detailed study on how exergy can be saved on this platform.

## 2. Theory

This section is based on [6] and derivations of the equations below can be found there.

Corresponding author: Mari Voldsund, Email: mari.voldsund@chem.ntnu.no

The exergy balance for a system in steady state and steady flow is given by:

$$T_\circ \dot{\sigma} = \dot{W} + \sum_k \int_{T_k} \left(1 - \frac{T_\circ}{T_k}\right) \delta\dot{Q}_k + \sum_j \dot{n}_j \varepsilon_j \quad (1)$$

Subscript $\circ$ refers to environmental temperature and/or pressure. $\dot{\sigma}$ is the entropy production, and the term $T_\circ \dot{\sigma}$ is the lost work, or the exergy loss of the process due to irreversibilities, often called the *irreversibility*. The other terms are exergy entering or leaving the system different ways. The first term is exergy entering or leaving as work. The second term is exergy entering or leaving with streams of heat. It is equal to the Carnot efficiency multiplied with the heat stream. The last term is exergy entering and leaving the system with streams of matter. In streams of matter we have physical and chemical exergy and exergy as kinetic and potential energy of the stream:

$$\varepsilon_j = \varepsilon_j^{ph} + \varepsilon_j^{ch} + e_{kin,j} + e_{pot,j} \quad (2)$$

The physical and chemical exergy of streams of matter is the work that can be obtained by bringing the stream from the current state to respectively thermophysical and chemical equilibrium with the environment using reversible processes. The physical exergy content of the stream is given as:

$$\varepsilon_j^{ph} = (h - h_\circ)_j - T_\circ (s - s_\circ)_j \quad (3)$$

The chemical exergy is:

$$\varepsilon_j^{ch} = \sum_i (x_{j,i} \varepsilon_{\circ,i} + R T_\circ x_{j,i} \ln x_{j,i}) \quad (4)$$

The first term in (4) is due to exergy contained in each pure component, while the last term is due to mixing of different components in the streams, assuming ideal mixtures. For a component present in the atmosphere, the molar component chemical exergy is given by:

$$\varepsilon_{\circ,i} = R T_\circ \ln x_{i,\circ} \quad (5)$$

where $x_{i,\circ}$ is the mole fraction of component $i$ in the environment, and the environment is assumed to be a mixture of ideal gases. For a component that is a fuel, this exergy is given by:

$$\varepsilon_{\circ,i} = -\Delta G_{\circ,i} + \sum_{prod} \nu_p \varepsilon_{\circ,p} - \nu_{O_2} \varepsilon_{\circ,O_2} \quad (6)$$

where the $\nu$'s are stochiometric coefficients and $\Delta G_{\circ,i}$ is the change in Gibbs energy for the combustion reaction of the component at environmental temperature and pressure.

To evaluate the exergetic performance of a process, the *exergetic efficiency* is defined:

$$\psi = \frac{\sum \Delta\dot{\mathcal{E}}_{out}}{\sum \Delta\dot{\mathcal{E}}_{in}} \quad (7)$$

where $\sum \Delta\dot{\mathcal{E}}_{out}$ is the exergy output of the system, while $\sum \Delta\dot{\mathcal{E}}_{in}$ is the exergy input. This efficiency is also often called *rational efficiency*, or *second law efficiency*. Following the method of [2] the exergy output is the exergy change in the mass streams, while the exergy input is the exergy added to the platform as work or heat. To see the relative importance of the efficiency of different sections of a process, [2] use a factor $f$. This factor is the ratio between the exergy input of a section and the exergy input of the whole process.

## 3. System

A platform situated in the North Sea is studied, and typical production data for this platform is used. The temperature is set to 8 °C for the air and the sea. This is the mean air temperature throughout the year in this area.

### 3.1. Entire platform

A systematic overview of the oil platform with the main exergy streams is given in Fig. 1. It is divided into two subsystems; the power plant and the oil and gas processing plant. The oil and gas processing plant is from now on called "process plant". The whole system is considered to be in steady state and steady flow.

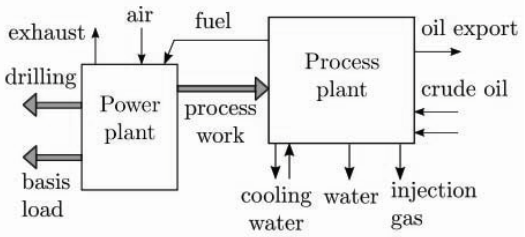


*Figure 1: Schematic overview of exergy streams in the platform. The black, thin arrows represent exergy in streams of matter, while the grey, thick arrows represent exergy as work.*

The power plant uses natural gas produced at the platform as fuel, and generates electric power for pumping and compression in the process plant, drilling and basis load. Basis load is the load needed at zero oil and gas production, and includes electricity for the accommodation part.

In the process plant, the crude oil is separated into oil, gas and water. The oil is pumped out for export, the gas is recompressed and injected back into the reservoir, and the water is rinsed and released to the sea.

### 3.2. Process plant

An overview of the process plant is given in Fig. 2.

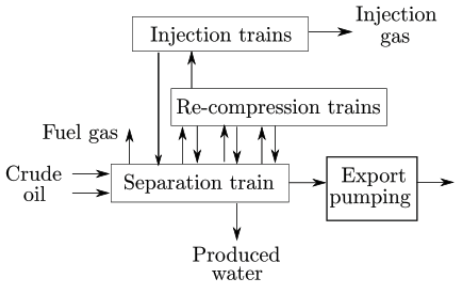


*Figure 2: Schematic overview of the oil and gas processing part of the platform.*

First the crude oil enters a separation train, see Fig. 3. Here the mixed feed stream is separated into gas, oil and water phases. This train consists of three separators and one electrostatic coalescer in series. Between the separators, the pressure is reduced, so that more gas is released from the oil. The oil shall meet specifications of water content and vapor pressure, which is why the separation process is performed in several stages at different pressures. In total the pressure is reduced from 69 to 1.9 bar during this section. Fuel gas for the power plant is supplied from gas from the 1st stage separator. The water that leaves the separators enters a water treatment process where traces of oil are removed. The water treatment process is neglected here. A pump is used for the separated water from the electrostatic coalescer. The remaining oil is exported via two pumps with cooling inbetween, see Fig. 4. Temperatures, pressures and molar flow for the separation train and the oil export section are given in Table 1.

*Table 1: Temperature, pressure and molar flow in streams in the separation train and oil export section.*

| Stream | T (°C) | p (bar) | $\dot{n}$ (kmol/h) |
|---|---|---|---|
| Crude oil | 75 | 69 | 34179.87 |
| C231 | | 6.0 | |
| C4215 | 28 | 65 | 336.50 |
| C213 | | 1.9 | |
| C541 | 60 | 8.9 | 30.89 |
| C234 | 50 | | |
| Oil export | 50 | 36 | 1955.56 |
| C217 | 60 | 1.9 | 1955.56 |
| Fuel gas | 75 | 69 | 350.00 |

The gas that is released in each stage in the separation train enters a re-compression train, see Fig. 5. Here the gas is compressed from 1.9 to 69 bar. The train consists of three stages, each with a cooler, a scrubber and a compressor. A scrubber is a separator that removes small amounts of condensed liquid. As the gas gets more compressed, the liquid that is separated enters the separation train again. Temperatures, pressures and molar flows for the streams are given in Table 2.

After the re-compression train, the gas enters three parallell injection trains, train A - C. Here the pressure is raised from 69 to 224 bar. In each of these trains there are two stages with cooling, scrubbing and compression. Separated oil from this process will go back to the separation train. After this last process, high pressure gas, for injection back into the reservoir, leaves the system. A shematic overview of one such train is given in Fig. 6 and temperatures, pressures and molar flows for the streams for all the injection trains are given in Table 3.

Composition of the crude oil entering the process plant is given in Table 7, and properties of hypothetical components used to describe the heavy oil fractions are given in Table 6. Pressure rise in all pumps are given in Table 4, and pressure drop in coolers are given in Table 5. All the compressors and pumps are assumed to have an adiabatic efficiency of 75 %.

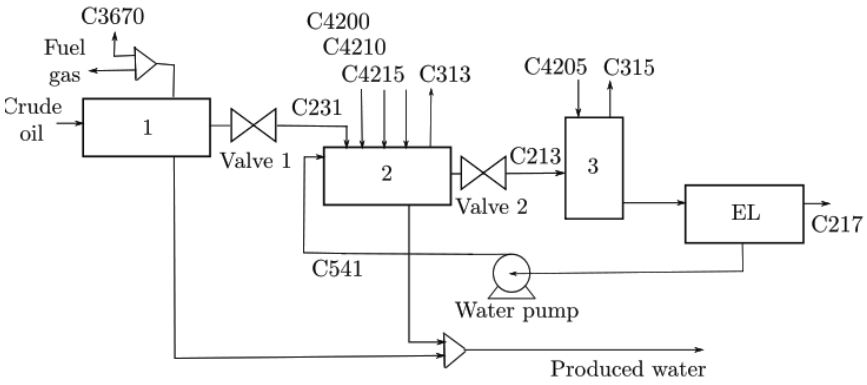


*Figure 3: Schematic overview of separation train. Boxes labelled 1-3 represent separator 1-3. Box labelled EL represents the electrostatic coalescer.*

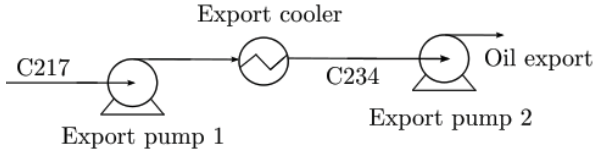


*Figure 4: Schematic overview of the oil export section.*

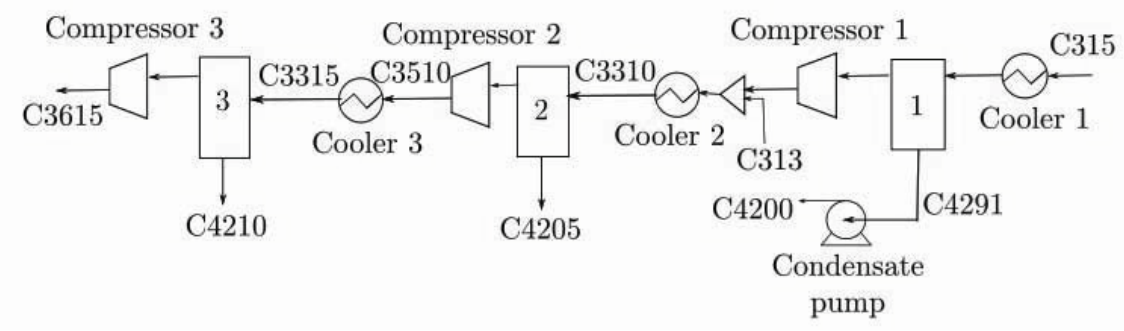


*Figure 5: Schematic overview of re-compression train. Boxes labelled 1-3 represent scrubber 1-3.*

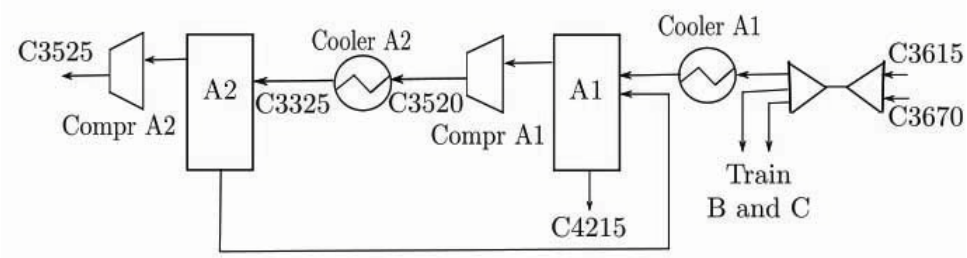


*Figure 6: Schematic overview of injection train A. Boxes labelled A1-A3 represent scrubber A1-A3. Injection train B and C have the same structure. The gas and condensate streams leaving the train are mixed with the same streams from train B and C.*

*Table 2: Temperature, pressure and molar flow in streams in the re-compression train.*

| Stream | T (°C) | p (bar) | $\dot{n}$ (kmol/h) |
|---|---|---|---|
| C3305 | 49 | | |
| C3505 | | 4.8 | |
| C3310 | 21 | | |
| C3510 | | 17 | |
| C3315 | 24 | | |
| C3515 | | 69 | |
| C3615 | 129 | 69 | 922.62 |
| C4205 | 21 | 4.1 | 85.47 |
| C4210 | 24 | 17 | 107.60 |
| C4291 | 49 | 1.4 | 3.29 |

*Table 3: Temperature, pressure and molar flow in streams in the injection trains.*

| Stream | T (°C) | p (bar) | $\dot{n}$ (kmol/h) |
|---|---|---|---|
| C3320A | 28 | | |
| C3520A | | 133 | |
| C3325A | 28 | | |
| C3525A | | 224 | |
| C4220A | 28 | 132 | 1.00 |
| C3320B | 28 | | |
| C3520B | | 137 | |
| C3325B | 28 | | |
| C3525B | | 224 | |
| C4220B | 28 | 136 | 1.02 |
| C3320C | 28 | | |
| C3520C | | 128 | |
| C3325C | 28 | | |
| C3525C | | 224 | |
| C4220C | 28 | 126 | 1.86 |

*Table 4: Pressure rise in pumps.*

| Pump | Δp (bar) |
|---|---|
| Water pump | 7.0 |
| Export pump 1 | 10.6 |
| Export pump 2 | 24 |
| Condensate pump | 4.6 |

*Table 5: Pressure drop in coolers.*

| Cooler | Δp (bar) |
|---|---|
| Export cooler | -0.50 |
| Cooler 1 | -0.50 |
| Cooler 2 | -0.70 |
| Cooler 3 | -0.20 |
| Cooler A1 | -1.0 |
| Cooler A2 | -1.0 |
| Cooler B1 | -1.0 |
| Cooler B2 | -1.0 |
| Cooler C1 | -4.0 |
| Cooler C2 | -2.0 |

*Table 6: Properties of hypothetical components used to describe the heavy oil fractions.*

| Stream | Molecular weight (g/mol) | Normal boiling pt (°C) | Ideal liq density (kg/m$^3$) |
|---|---|---|---|
| HypoA-1 | 81 | 73 | 721.2 |
| HypoA-2 | 108 | 99 | 740.1 |
| HypoA-3 | 125 | 152 | 774.6 |
| HypoA-4 | 171 | 230 | 817.1 |
| HypoA-5 | 247 | 316 | 859.3 |
| HypoA-6 | 388 | 437 | 906.2 |
| HypoA-7 | 640 | 618 | 988.5 |
| HypoB-1 | 91 | 80 | 725.2 |
| HypoB-2 | 116 | 132 | 764.8 |
| HypoB-3 | 156 | 201 | 808.6 |
| HypoB-4 | 215 | 279 | 857.3 |
| HypoB-5 | 312 | 383 | 897.4 |
| HypoB-6 | 637 | 620 | 971.6 |
| HypoC-1 | 94 | 69 | 707.5 |
| HypoC-2 | 119 | 133 | 781.7 |
| HypoC-3 | 172 | 215 | 821.3 |
| HypoC-4 | 238 | 293 | 860.3 |
| HypoC-5 | 383 | 405 | 900.7 |
| HypoC-6 | 636 | 567 | 963.7 |

*Table 7: Composition of the crude oil. The 19 last components are hypothetical components used to simulate the heavy oil fractions. Properties of these components are given in Table 6.*

| Component | Molar stream (kmol/h) |
|---|---|
| CO2 | 191.30 |
| Methane | 14 050.10 |
| Ethane | 1 269.40 |
| Propane | 714.10 |
| i-Butane | 112.15 |
| n-Butane | 260.01 |
| i-Pentane | 87.51 |
| n-Pentane | 115.84 |
| H2O | 15 456.60 |
| N2 | 139.59 |
| HypoA-1 | 180.43 |
| HypoA-2 | 151.66 |
| HypoA-3 | 191.36 |
| HypoA-4 | 151.25 |
| HypoA-5 | 110.35 |
| HypoA-6 | 62.80 |
| HypoA-7 | 41.30 |
| HypoB-1 | 91.10 |
| HypoB-2 | 112.80 |
| HypoB-3 | 110.95 |
| HypoB-4 | 113.35 |
| HypoB-5 | 81.81 |
| HypoB-6 | 54.33 |
| HypoC-1 | 62.94 |
| HypoC-2 | 81.99 |
| HypoC-3 | 59.87 |
| HypoC-4 | 60.46 |
| HypoC-5 | 39.23 |
| HypoC-6 | 25.29 |

## 4. Methodology

A model of the process plant is made, using HYSYS [7] with the Peng-Robinson equation of state to estimate properties of all the mass and energy flows. All process units are treated as a black boxes, and the irreversibility for each unit is found, using the exergy balance, (1). Contributions to the exergy from potential and kinetic energy are neglected. Since there are no chemical reactions in the process plant, apart from phase transformations, the exergy change due to streams of matter can be calculated by:

$$\sum_j \dot{n}_j \varepsilon_j = \sum_j \dot{n}_j (h - T_\circ s)_j \tag{8}$$

Here enthalpy and entropy are given for the mixed stream, so differences in physical exergy and in chemical exergy due to mixing are both included. The terms with enthalpy and entropy for each component at environmental temperature and pressure cancel out, and so does the chemical exergy contained in each component.

For separators, mixers and valves, there are only streams of matter entering and leaving the process unit, so the exergy balance reduces to:

$$\dot{I} = T_\circ \dot{\sigma} = \sum_j \dot{n}_j \varepsilon_j \tag{9}$$

In compressors and pumps, there are also work entering, so the exergy balance gives:

$$\dot{I} = T_\circ \dot{\sigma} = \dot{W} + \sum_j \dot{n}_j \varepsilon_j \tag{10}$$

Seawater is used as cooling medium for the coolers on the platform, and is later discharged irreversibly to the environment. Thus, the exergy corresponding to the heat going from the process stream to the seawater is an irreversibility due to cooling:

$$\dot{I} = T_\circ \dot{\sigma} - \int_{T_k} \left(1 - \frac{T_\circ}{T_k}\right) \delta \dot{Q}_k = \sum_j \dot{n}_j \varepsilon_j \tag{11}$$

$\delta \dot{Q}_k$ is negative, since heat is leaving the cooler. Since no heat added to the platform, the exergetic efficiency using the method of [2] is given by:

$$\psi = \frac{\sum_j \dot{n}_j \varepsilon_j}{\sum_l \dot{W}_l} \tag{12}$$

## 5. Results and discussion

The calculated total irreversibility and the exergetic efficiency of the process plant are listed in Table 8. The percentage of the total loss distributed on each process section and on the different equipment types are listed in Table 9, and the exergetic efficiencies and $f$-values of each section are listed in Table 10.

*Table 8: Performance parameters of the process plant*

| Performance parameter | Value |
|---|---|
| Process plant irreversibility (MW) | 12 |
| Exergetic efficiency process plant | 0.36 |

In some of the separators the irreversibility is zero. The reason for this is that phase changes take place

*Table 9: Percentage of total irreversibility of process plant distributed on process section and equipment type.*

| Section | % | Equipment | % |
|---|---|---|---|
| Separation | 20 | 2 valves | 13 |
| | | 4 separators | 2.9 |
| | | 1 mixer | 3.9 |
| Re-compression | 11 | 3 coolers | 5.5 |
| | | 3 compressors | 4.1 |
| | | 1 mixer | 1.4 |
| | | 3 separators | 0 |
| | | 1 pump | $1.1 \cdot 10^{-3}$ |
| Injection | 66 | 6 coolers | 39 |
| | | 6 compressors | 26 |
| | | 3 mixers | 1.3 |
| | | 6 separators | 0 |
| Oil export | 3.1 | 1 cooler | 2.6 |
| | | 2 pumps | $5.0 \cdot 10^{-1}$ |

*Table 10: Exergetic efficiency and $f$-value for each section of the process plant*

| Section | $\psi$ | $f$ |
|---|---|---|
| Separation | $(-1.7 \cdot 10^4)$ | $7.7 \cdot 10^{-5}$ |
| Re-compression | 0.51 | 0.14 |
| Injection | 0.49 | 0.83 |
| Oil export | 0.34 | $3.0 \cdot 10^{-2}$ |

before the separator, where there is a pressure or temperature change. In HYSYS, the only function of the separator is that it lets different phases that are already separated go different ways. In reality, however, the phase change takes some time, and some of it happends in the separator. Also, the flow entering the separator is turbulent, and the phases are mixed as bubbles and foam. In the separator, the gravity will separate the phases better. This process is not included in the exergy analysis, as kinetic and potential exergy is neglected. For the separators which have a calculated irreversibility, the irreversibility is due to mixing when more than one stream enter the separator.

As can be seen, the highest irreversibility (66 %) takes place in the injection trains. The pressure is here raised significantly, and this is the section where the largest part of the electric power is used ($f$ = 0.83). By using more than two steps in the compression process, the driving forces would be smaller. We would then come closer to a reversible compression, and the irreversibility would be lowered, in agreement with earlier foundings [4]. The effect of introducing a number of extra steps should therefore be examined, following [5].

The second highest irreversibility in the process plant is in the separation section (20 %). Here we have a pressure drop of 67 bar. Due to the high pressure drop, the exergy content in the process stream is lowered, and the exergetic efficiency as defined here is a very high negative number ($-1.7 \cdot 10^4$ ). What happens is that the pressure component of the exergy in the input stream is used to do the separation work. In principle we could even do the separation without any other exergy entering the system than the exergy in the input stream, and would then end up with an efficiency of $-\infty$. With the definition of efficiency used here, the exergy used for doing work will sometimes be in the numerator instead of the denominator.

To be able to use the exergetic efficiency for comparing oil platforms, more work should be done on defining it in such a way that it makes sense for all situations. One alternative is to define it as the ratio between all exergy leaving the system and all exergy entering. Then, however, the chemical exergy of the hydrocarbons flowing trough the system will dominate and the ratio will be close to unity. This means than even considerable improvements will give very small changes in the efficiency. Moreover, the uncertainties of the chemical exergies of the large amounts of through-flow components will result in a high level of uncertainity for the effciency.

Coolers are together with compressors responsible for the major part of the irreversibility of the system. Can the cooling water be useful? At the process plant, there is not any need for heating. But at other parts of the platform heat is needed. As a part of the basis load, there is heating of the accomodation part. The possibilities for reducing the need for power in the basis load by heating the accomodation part with excess heat from the process plant should be examined.

When compared to the Brazilian platform [2] we see that compression of gas needs much exergy in both cases. However, on the Brazilian platform, much exergy is also added for heating the crude oil. There, the oil entering the process has only 7.4 °C and 10.78 bar, so considerable heating is necessary

to separate it. On the North Sea platform, the oil entering has a temperature of 75 °C and a pressure of 69 bar. It contains already exergy that they have to add on the Brazilian platform.

## 6. Conclusion

The irreversibility of the process plant in the studied case is 12 MW. The injection trains is the best place to reduce the irreversibility, since 66 % of the irreversibility takes place here, and here is also most of the added work used. We shall examine this possibility in the future, following [4, 5].

## Nomenclature

| | |
|---|---|
| $e$ | molar energy, J/mol |
| $h$ | molar enthalpy, J/mol |
| $\dot{I}$ | irreversibility, W |
| $\dot{n}$ | molar flow, mol/s |
| $p$ | pressure, bar |
| $\dot{Q}$ | heat flow, J/s |
| $R$ | gas constant, J/(K mol) |
| $s$ | molar entropy, J/mol |
| $T$ | temperature, K |
| $\dot{W}$ | work flow, J/s |
| $x$ | mole fraction, - |
| $\Delta G$ | reaction gibbs energy, J/mol |

### Greek Letters

| | |
|---|---|
| $\varepsilon$ | molar exergy |
| $\dot{\mathcal{E}}$ | exergy flow |
| $\nu$ | stochiometric coefficient |
| $\psi$ | exergetic efficiency |

### Subscripts and superscripts

| | |
|---|---|
| $\circ$ | environmental temperature and pressure |
| $ch$ | chemical |
| $i$ | component i |
| $j$ | mass flow j |
| $k$ | heat flow k |
| $l$ | work flow l |
| $kin$ | kinetic |
| $ph$ | physical |
| $pot$ | potential |
| $s$ | process section |
| $tot$ | total |

## References

[1] Statistics Norway, Statistisk Sentralbyrå. Emissions of greenhouse gases. 1990-2008*. http://www.ssb.no/emner/01/04/10/klimagassn/ [29.04.10].

[2] S. de Oliveira Junior and M. van Hombeeck. Exergy analysis of petroleum separation processes in offshore platforms. *Energy Conversion and Management*, 38(15-17):1577–1584, 1997.

[3] I. L. Leites et al. The theory and practice of energy saving in the chemical industry: some methods for reducing thermodynamic irreversibility in chemical technology processes. *Energy*, 28:55–97, 2003.

[4] A. Røsjorde et al. Minimizing the entropy production in a chemical process for dehydrogenation of propane. *Energy*, 32:335 – 343, 2007.

[5] A. Zvolinschi et al. The second law-optimal operation of a paper drying machine. *Chemical Engineering Science*, 61:3653 – 3662, 2006.

[6] T. J. Kotas. *The Exergy Method of Thermal Plant Analysis*. Krieger Publishing Company, Malabar, Florida, 2nd edition, 1995.

[7] Aspen HYSYS, 2009. Software package, Ver. 7.1, Aspen Technology Inc.

**Acknowledgments:** The Faculty of Natural Sciences and Technology at the Norwegian University of Science and Technology is acknowledged for financial support.

# The Multi-objective Optimization of Small-scale LNG Mixed Refrigeration Processes

*Nipen M. Shah[a,b] and Andrew F. A. Hoadley[a]*

[a] *Monash University, Clayton Campus, Vic. 3800, Australia*
[b] *Jord International, St. Leonards, NSW 2065 Australia*

**Abstract:** A multi-objective optimization study is used to determine the optimum refrigerant composition and process conditions to minimize both the equipment costs and the shaftwork requirements for a Single Mixed Refrigerant (SMR) process. Four cases were evaluated with progressively tighter constraints on the refrigerant composition. Very low specific work requirements were achieved ranging from 5.8 to 3.5 kWhr/kmol of LNG. The highest efficiencies were achieved when the refrigerant was permitted to contain pentanes. As iso-pentane has an acceptable freezing point below the operating temperature of the SMR process, this could provide significant efficiency improvements, which could be particularly beneficial for small-scale LNG projects.

**Keywords:** Genetic Algorithm, Mixed Refrigerants

## 1 Introduction

Both compressed natural gas (CNG) and liquefied natural gas are viewed as possible transport fuels of the future, particularly as an alternative fuel which can be burnt in conventional diesel engines. Because of this, there is interest in small-scale liquefaction processes that do not require the enormous infrastructure of mega-scale LNG projects. The objective of a small-scale LNG process might be to supply a remote area that is stranded from the natural gas network with an alternative fuel to run trucks and generate electricity. The gas supply could equally come from coal seam methane or biogas.

Table 1 compares the energy requirements per kmol of natural gas liquefied over a range of LNG processes for two different feed gases. Data provided by Vink and Nagelvoort[1] shows that two mixed refrigerant processes: DMR the dual mixed refrigerant and C3/MR the propane pre-cooled mixed refrigerant process would appear to provide the lowest specific work requirements and these processes are often chosen for large scale LNG projects. Whereas efficiency is critically important in large scale projects, it may not be the dominant factor in small-scale LNG processes. For example, both DMR and C3/MR have two separate refrigeration loops, which increase the number of equipment items, the capital cost and the complexity of these processes, when compared with refrigerant systems such as the single mixed refrigerant process (SMR).

*Table 1. Specific power requirements for various LNG processes[4]*

| | Specific power (kWh/ kmol LNG) | |
|---|---|---|
| Feed Composition | Feed 1 | Feed 2 |
| Processes | (Mol%) methane 0.9693 ethane .0294, Propane 0.00059, n-butane 0.0001 & nitrogen 0.00064 feed pressure 5500 kPa | (Mol%) methane 0.851, ethane 0.065, propane 0.03, n-butane 0.012, C5 plus 0.005, $CO_2$ 0.022 & nitrogen 0.015; feed pressure 6000 kPa. |
| SMR | 5.67[2] | 6.96[1] |
| cLNG | 6.79[2] | - |
| DIEP | 6.10[3] | - |
| Optimised DIEP | 5.72[4] | 6.12[4] |
| Cascade | - | 6.67[1] |
| DMR | - | 5.99[1] |
| C3/MR | - | 5.85[1] |
| C3/N2 expansion | - | 7.49[1] |

Corresponding Author: Andrew Hoadley, Email: andrew.hoadley@eng.monash.edu.au

Remeljej and Hoadley[2] reviewed many different aspects of several small-scale LNG processes. Two processes, SMR and cLNG were both assessed to be excellent options, with cLNG having additional safety benefits for offshore, whereas SMR gave the best efficiencies. For a small-scale operation to be economic, the capital cost must be tightly controlled as the revenue used to repay capital will be limited by the plant scale. This leads to a trade-off where a lower efficiency plant may be acceptable, providing the equipment costs are also low. This paper will explore this trade-off using an optimization technique which allows the optimization of two parameters simultaneously, in this case the process efficiency and the cost of the major equipment items in the refrigeration system. The refrigerant composition is a key variable which will be manipulated.

# 2 Method

This paper investigates just the refrigeration portion of an LNG facility. Prior to liquefaction, all water and $CO_2$ must be removed and heavy hydrocarbons (C4+) must also be separated out and may be recovered as a by-product or burnt as fuel. In keeping with the small-scale focus, it has been assumed that dehydration and $CO_2$ removal will use a pressure swing/vacuum swing adsorption process, which is capable of removing both components in a single step with only a small pressure drop across the adsorbent bed[5].

## 2.1. Single mixed refrigerant process

The original commercial mixed refrigerant process is known as the PRICO process (Poly refrigerant integral cycle operation)[6]. A schematic flowsheet is shown in Fig. 1. The SMR process has been the subject of much research including Lee[7], who claimed to have reduced the specific work requirements of the PRICO process through better optimization of the refrigerant composition. This was achieved by reducing the required refrigerant flowrate and the temperature difference between the cold refrigerant streams and the hot streams. It is noted that Lee[7], and Remeljej and Hoadley[2] both assumed that butanes would comprise around 20 %mol of the refrigerant flowrate without any operational problems due to freezing.

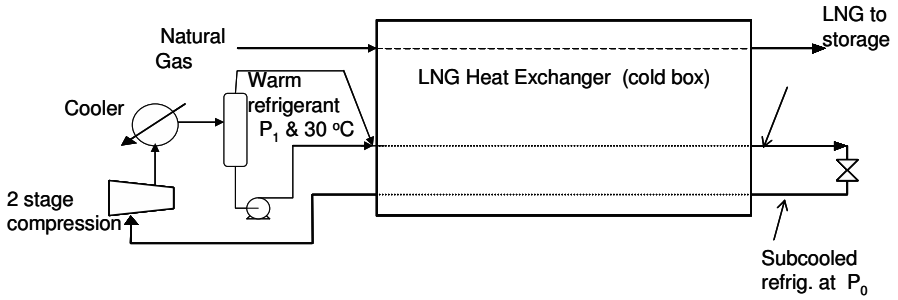


*Fig. 1. Schematic diagram of the single mixed refrigerant process.*

The inclusion of higher hydrocarbons in the mixed refrigerant stream is advantageous, because the polytropic coefficient (which governs the proportion of shaftwork converted to heat energy rather than potential or pressure energy in an adiabatic compressor) is inversely related to the molecular weight of the hydrocarbons. However, unbranched hydrocarbons, i.e. n-butane, n-pentane have relatively high melting temperatures and risk freezing out of solution in the coldest zones of the LNG exchanger. Table 2 lists the freezing characteristics of the common components in mixed refrigerant systems.

In this study a LNG production rate of 20 tonnes per day is assumed. The feed gas with a composition given by Feed 1 in Table 1 (after the removal of water and $CO_2$) is passed to the single loop SMR process, where it is liquefied by passing it through a series of plate-fin heat exchangers. The closed-loop mixed refrigerant is compressed in two compression stages of equal compression

ratios, isentropic efficiencies of 80% and inter-cooling and post-cooling to 30°C.

*Table 2. Freezing point and solubility data of alkanes*

| | Freezing point, K[8] | Solubility limit in $CH_4$ (mole fraction) at 90 K[9] |
|---|---|---|
| $CH_4$ | 90.65 | 1 |
| $C_2H_6$ | 89.85 | 1 |
| $C_3H_8$ | 85.45 | 1 |
| n-$C_4H_{10}$ | 134.8 | |
| 2- methyl propane | 113.6 | 0.29 |
| n-$C_5H_{12}$ | 142.5 | |
| 2-methyl butane | 113.3 | 0.16 |
| 2-methyl pentane | 119.5 | |

### 2.2. The Optimisation Algorithm

For a fixed refrigerant composition, the ratio of the two pressures $P_1$ and $P_0$ defines the Joules-Thomson effect achieved by the let-down valve and the refrigerant flowrate is calculated by the amount of energy which needs to be removed. However, allowing the refrigerant composition to vary introduces a strong non-linearity, as the thermodynamic parameters are all functions of composition. Lee[7] needed to develop a set of rules to ensure the LNG exchanger remained feasible, i.e. there were no temperature difference violations. Classical optimisation techniques which use gradient methods to accelerate convergence often have difficulty solving non-linear constrained problems, such as posed by the optimisation of the refrigerant composition.

An alternative approach used by Del Nogal et al[10] is to use an Evolutionary Algorithm to guide the solution. The advantage of using Evolutionary Algorithms such as the Genetic Algorithm is that although convergence is slow, no gradient information is used and infeasible solutions are easily penalised and thus eliminated. There is increasing interest in using these techniques in engineering, particularly for multi-objective optimisation[11].

In this particular work, steady-state mass and energy balance software is used to simulate the SMR process and obtain estimates of the compressor shaftwork for different input conditions. The Peng-Robinson equation of state was used to obtain the thermodynamic properties. A zonal analysis was conducted within the LNG exchanger to ensure sufficient temperature difference. The SMR process is optimised for two objectives: minimisation of specific power requirement in kW/tpd LNG and minimisation of total capital cost. The latter includes the purchased equipment cost of all the major equipment items such as heat exchangers and compressors. The optimization variables include the refrigerant composition, inlet and outlet pressures across the compressor and the refrigerant flow rate.

Minimise:

$$W_{specific} = \frac{W_{in}}{m_{product}} \qquad (1)$$
$$Capex = \left(C_{HE} + C_{Comp} + C_{cooler}\right) \times 4.7$$

where $W_{specific}$ is the specific power requirement in kW per tonnes of LNG produced per day or tpd, $m_{product}$ is the total LNG product rate in tpd and Capex is the total equipment cost in USD. $C_{HE}$, $C_{comp}$ and $C_{cooler}$ represent the purchased equipment costs of cryogenic heat exchangers, the mixed refrigerant compressor and mixed refrigerant coolers, respectively.

A single optimization problem has only one optimal solution; however, a multi-objective optimization problem has a set of optimal solutions when dealing with conflicting objectives. These optimal solutions are called Pareto-optimal solutions. Several methods have been proposed and used to generate Pareto-optimal solutions[11]. In this work, multi-platform multi-language environment developed by Bhutani et al[12] has been used for the multi-objective optimization. The working principle and the optimization methodology can be found elsewhere[4].

## 3 Results

Table 3 presents the four cases simulated for the SMR process to investigate the importance of the heavier hydrocarbons, with increasing restrictions on the heavier hydrocarbons. The Pareto curve for each case is presented in Fig. 2. The Pareto-optimal front for each case sits above the previous one, as the composition becomes more and more constrained. This is evidence that the optimisation procedure is working well. The Pareto fronts

show that the lowest specific work requirements are achieved for the highest equipment costs.

*Table 3. Case studies for multi-objective optimization*

| | |
|---|---|
| Case 1 | No constraints on compositions: $N_2$, $C_1$, $C_2$, $C_3$, $iC_4$, $nC_4$, $iC_5$, $nC_5$ |
| Case 2 | No pentanes allowed, all other compositions unconstrained |
| Case 3 | No pentanes and butanes limited < 10 mol % |
| Case 4 | No pentanes or butanes allowed |

## 4 Discussion

The value of the multi-objective approach to the design of the SMR process is immediately evident from the results presented in Fig. 2. Each point is an optimal solution and it is in the hands of the process designer to choose the solution, which best fits the project requirements. It also shows clearly when a constraint is binding, such as the different constraints imposed on the refrigerant composition.

Fig. 3 shows the specific work requirements for selected equipment costs for the different cases as a function of the refrigerant molecular weight. For each selected equipment cost, the shaftwork is reduced by allowing increasing amounts of heavier hydrocarbons.

These results raise the question as to the real limit of heavy hydrocarbons in a mixed refrigerant system. Fig. 4 shows the Pareto optimal mole fractions of propane, butanes and pentanes. Because of the overlapping volatilities of these three hydrocarbons, when the pentane composition is not restricted, the optimum butane composition is low (nearly an order of magnitude lower than propane and 25% of the pentanes). This suggests that if the refrigerant is made up from commercial grades of refinery butane, it will contain minor impurities of high freezing point components such as n-pentane and n-hexane, and these components might freeze-out at the lowest temperatures resulting in a reduction in performance. If on the other hand refinery grade propane is used together with a very pure grade of iso-pentane (freezing point -159.9 °C), then the high freezing point impurities may be eliminated.

For a fixed equipment cost of around $1million, the improvement in energy efficiency would be approximately 10%.

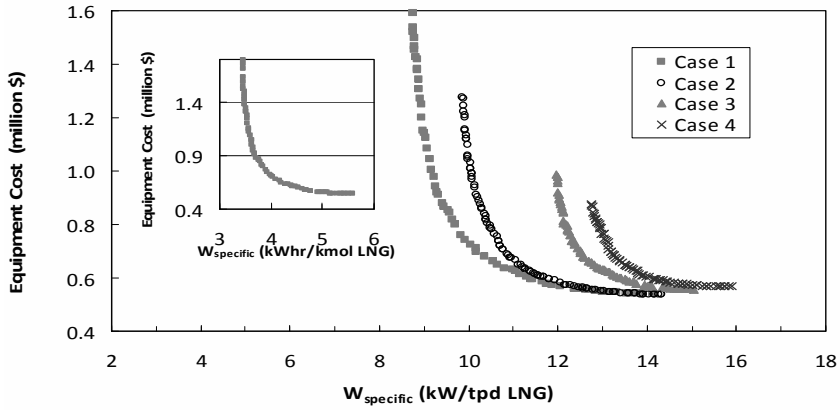


*Fig. 2. Pareto-optimal Front for Cases 1-4. The inset shows Case 1 plotted as a function of the specific power in kWhr/kmol of LNG.*

## 5 Conclusions

The four cases evaluated demonstrated that the constraints on the refrigerant composition had an increasing influence on the specific work requirements for liquefaction. The highest efficiencies were achieved when the refrigerant was permitted to contain a significant amount of pentanes. As iso-pentane has an acceptable freezing point below the operating temperature of the SMR process, it is postulated that for small-

scale SMR processes, the use of iso-pentane in the refrigerant mixture could provide significant improvements in efficiency. However, further research is required to map out in detail the temperature at which freezing first occurs.

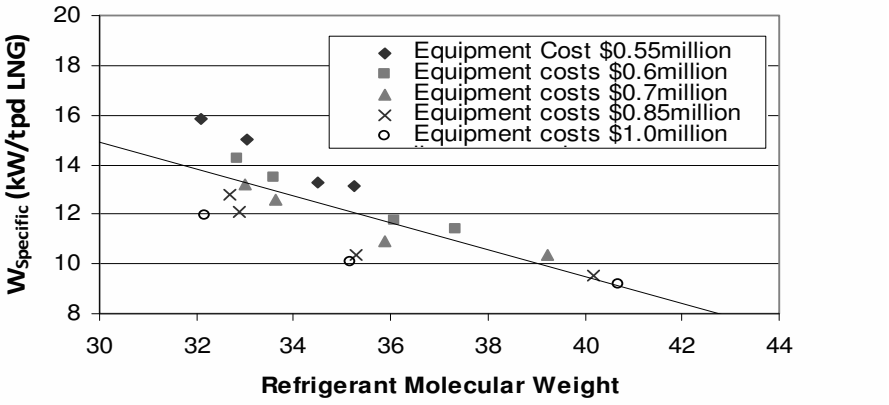


*Fig. 3. Contours of fixed equipment costs plotted.*

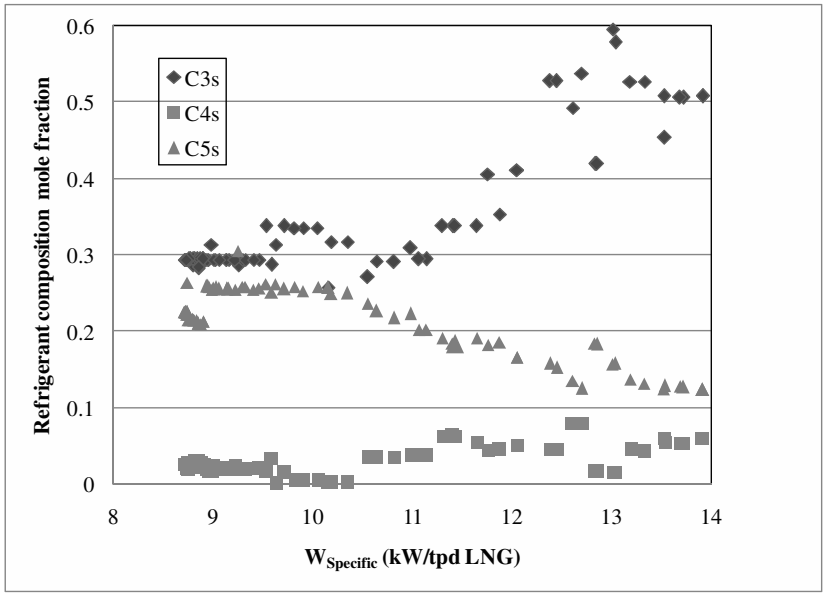


Fig. 4. Pareto optimal mixed refrigerant compositions for the higher hydrocarbons

## References


1. Vink K.J., Nagelvoort R.K., 1998, 'Comparison of base load liquefaction processes.' In: Proceedings of the LNG 12, Institute of Gas Technology, Perth, Australia, May 4–7, 1998.IPCC, *IPCC Special Report on Carbon Dioxide Capture and Storage* 2005, Cambridge University Press: Cambridge, UK. pp. 431.
2. Remeljej C.W. and Hoadley A.F.A. 2006, 'An exergy analysis of small-scale liquefied natural gas (LNG) liquefaction processes', Energy, 31, pp 2005–2019.
3. Shah N. M. and Hoadley A. F. A. 2007, 'A Targeting Methodology for Multistage Gas-Phase Auto Refrigeration Processes', Ind. Eng. Chem. Res., 46, pp 4497-4505.
4. Shah N. M., Hoadley A. F. A. and Rangaiah G. P. 2009, 'Gas phase refrigeration: A promising alternative to convention refrigeration processes for LNG', In: OPEC, Oil Prices and LNG, Ed.: Pitt, E.R. and Leung C.N., pub. Nova Science Publishers Inc., ISBN:978-1-60692-897-4, ch14.
5. Li, G., Xiao, P., Webley P. A., Zhang J. and Singh R. K., 2008, Capture of CO2 from humid flue gas streams by Vacuum Swing Adsorption using multi-layered beds, Adsorption 14, pp 415–422.
6. Price BC. 1996, PRICO—a simple, flexible proven approach to natural gas liquefaction. In: Proceedings of the 17th international LNG/LPG conference, Gastech '96, Vienna.
7. Lee G-C., 2001, 'Optimal design and analysis of refrigeration systems for low temperature processes', PhD, CEAS, The University of Manchester, Manchester, UK.
8. Griesbaum, K., Behr A., Biedenkapp D., Voges, H-W., Garbe D., Paetz, Ch., Collin G., Mayer D., Höke H., 2000, 'Hydrocarbons', Ullmann's Encyclopedia of Industrial Chemistry, publ. Wiley-VCH Verlag GmbH & Co.
9. Kittel B., 1998, Advances in Cryogenic Engineering, Proceedings of the 1997 Conference, Portland, Oregon, July 28-August 1,1997, Vol 43B, ISBN: 978-0-306-45807-1, pp1680.
10. del Nogal, F., Kim, J-K, Perry, S., and Smith, R., 2008, 'Optimal Design of Mixed Refrigerant Cycles', Ind. Eng. Chem. Res. 2008, 47, pp 8724–8740.
11. Rangaiah, G. P., 2009. Title: Introduction. In G. P. Rangaiah (Ed.), Multi-objective optimization: Techniques and applications in Chemical Engineering, Singapore, World Scientific Publication.
12. Bhutani, N., Tarafder, A., Rangaiah, G. P. and Ray, A. K., 2007. 'A Multi-Platform, Multi-Language Environment for Process Modeling, Simulation and Optimization', Int. J. of Comput. Appl. in Technology, 30(3), pp 197-214.


Corresponding Author: Andrew Hoadley, Email: andrew.hoadley@eng.monash.edu.au

# Advanced Exergetic Analysis of a Refrigeration System for Liquefaction of Natural Gas

*Tatiana Morosuk, Mohd Nazri Bin Omar, George Tsatsaronis and Rolanda Naw*

*Institute for Energy Engineering, Technische Universität Berlin, Germany*

**Abstract:** During the last years the total cost of LNG technology has decreased significantly due to improvements of the liquefaction process by developing new schematics with different mixtures as working fluids. However, many liquefaction plants, based on a three-cascade refrigeration system, are in operation in the world. In this paper, a three-cascade refrigeration system for liquefaction of natural gas is used as an example to apply the advanced exergetic analysis. With the aid of this analysis, the interactions among system components as well as the potential for improving the thermodynamic efficiency of components and of the overall system are revealed. The objective of this paper is to demonstrate (a) the potential for thermodynamic improvement of a three-cascade refrigeration system for liquefaction of natural gas, and (b) the capabilities associated with an advanced exergetic analysis.

**Keywords:** LNG, liquefaction, cascade refrigeration machine, exergetic analysis, advanced exergetic analysis.

## 1. Introduction

Liquefied Natural Gas (LNG) is expected to contribute in future more than in the past to the overall energy supply in the world. Compared with other fossil fuels, natural gas is relatively clean with respect to air pollution and to greenhouse gas emissions and has larger proven reserves than oil. Natural gas is expected to account for about 30% of total electricity generation by 2020 compared with 17% in 2000. Liquefied natural gas (LNG) is expected to have a large share in this expansion of use of natural gas.

A majority of the world's LNG supply comes from countries with large natural gas reserves. Main exporters of LNG are Indonesia, Malaysia, Qatar and Algeria, which hold significant natural gas reserves. Because of the large capital expenditure involved, economics dictate that natural gas liquefaction projects for overseas transportation are developed in conjunction with large gas reserves, able to supply large quantities of gas for at least 20 years.

Worldwide, there are 26 existing liquefaction (export) terminals, located on or off shore, in 15 countries (the start up date of earliest liquefaction terminal is given in parenthesis): USA (1969), Libya (1970), Algeria (1971), Brunei (1972), Indonesia (1977), United Arab Emirates (1977), Malaysia (1983), Australia (1989), Qatar (1997), Nigeria (1999), Trinidad and Tobago (1999), Oman (2000), Egypt (2004), Equatorial Guinea (2007), Norway, (2007). In contrast, there are over 60 regasification (import) terminals, on or off shore, spread across 18 different countries. In addition to these existing terminals, there are approximately 60 liquefaction marine terminal projects and approximately 180 regasification terminal projects that have been either proposed or are under construction all around the world [1,2].

At the production site, natural gas is converted into a liquid through liquefaction, achieved by a refrigeration cycle. Before liquefaction, the gas is purified from humidity, carbon dioxide, sulphur components, heavy hydrocarbons and other impurities.

There are three main liquefaction processes [2,3]:

- The classical cascade, where refrigeration and liquefaction of the gas is achieved in a cascade process using three pure refrigerants: Propane, ethylene and methane. This process was developed first and used in earlier design of the liquefaction plants;
- The single flow mixed refrigerant process, where the mixed refrigerant made up of nitrogen, methane, ethane, propane and isopentane, is compressed using a single compression train;
- The propane precooled mixed refrigerant process where precooling is achieved by a multi-

stage propane cycle, while liquefaction and subcooling are accomplished by a two-stage mixed refrigerant cycle, which is so far the most common process.

Other processes have been developed but are not yet in operation [2,3]:

- The cascade mixed refrigerant cycle, where three mixed refrigerant cycles are used for precooling, liquefaction, and subcooling.
- The dual mixed refrigerant process, where for both the precooling and the liquefaction cycles mixed refrigerants are used.
- The AP-X process that is based on the propane precooled mixed refrigerant process with a separate nitrogen cycle for subcooling.

During the last 20 years, the total cost of LNG technology has decreased by approximately 30% due to improvements of the liquefaction process by developing new schematics with different mixtures as working fluids. However, many liquefaction plants, based on a three-cascade refrigeration system, are in operation in the world.

In this paper, a three-cascade refrigeration system for liquefaction of natural gas is analyzed using conventional and advanced exergetic analyses. The operating conditions for the liquefaction plant as well as the environmental conditions are based on an existing export terminal in Malaysia [4].

## 2. Three-cascade refrigeration system for liquefaction of natural gas

The schematic of the three-cascade refrigeration system used for liquefaction of natural gas is shown in Figure 1. Initial data and assumptions made for the simulation are given in Table 1. The simulation of a three-cascade refrigeration system is quite difficult because many factors should be taking into account simultaneously:

- The pressure of evaporation for all working fluids within three condenser-evaporators (CD1-EV1, CD2-EV2 and CD3-EV3) should be > 1 bar. Thus, $T_{EV2}$ is assumed to be equal to –100ºC, corresponding to $p_{EV2}$ = 1.26 bar.
- The discharge temperature of compressors should not be significantly higher than 100ºC.
- Since the design of condenser CD4 is unknown, the temperature difference between $T_{CD4}$ and $T_{42}$ is assumed to be 8K [5], therefore $T_{CD4}$=50ºC.
- When $T_{EV2}$ and $T_{CD4}$ are fixed, then the middle temperature for the CD3-EV3 is $T^{m}_{CD3-EV3} = \sqrt{T_{EV2} \cdot T_{CD4}}$ =236K (–36ºC). In this way $T_{EV3}$ should be ≈ –41ºC (propane) and $T_{CD3}$ ≈ –31ºC (ethylene). Regarding the thermodynamic properties of propane, the saturation pressure of 1 bar corresponds to the saturation temperature –42ºC. If $T_{EV3}$ is assumed to be –32ºC, then $T_{CD3}$ = –22ºC.
- The energy balances are used for estimating the mass flow rates of the working fluids:

$$\dot{m}_{methane} = \frac{\dot{m}_{NG}\left(h_4 - h_3\right)}{h_{15} - h_{14}};$$

$$\dot{m}_{ethylene} = \frac{\dot{m}_{methane}\left(h_{12} - h_{13}\right)}{h_{21} - h_{24}}; \text{ and}$$

$$\dot{m}_{propane} = \frac{\dot{m}_{ethylene}\left(h_{22} - h_{23}\right)}{h_{31} - h_{34}}.$$

- Only positive displacement type compressors can be used for such a low-temperature refrigeration machine. In this way, the isentropic efficiency of the compressors is estimated as $\eta_{CM} = \frac{T_{EV}}{T_{CD}}$: $\eta_{CM1} = 0.64$; $\eta_{CM2} = 0.70$, and $\eta_{CM3} = 0.88$.

Thermodynamic data for the material streams are given in Table 2. The following simplifications (which cannot significantly affect the results obtained from the energetic and exergetic analyses) are used:

- States 4 (natural gas), 13 (methane), 23 (ethylene), and 33 (propane) are saturated liquid, and
- States 15 (methane), 21 (ethylene), and 31 (propane) are saturated vapor.

From the energetic analysis we obtain for the

- heat rates : $\dot{Q}_{RHE1}$ = 365 kW, $\dot{Q}_{CD1-EV1}$ = 728 kW, $\dot{Q}_{CD2-EV2}$ = 1109 kW, $\dot{Q}_{CD3-EV3}$ = 2304 kW, $\dot{Q}_{CD4}$ = 3778 kW, and for the
- power: $\dot{W}_{CM1}$ = 381 kW, $\dot{W}_{CM1}$ = 1194 kW, and $\dot{W}_{CM1}$ = 1475 kW.

The coefficient of performance of this three-cascade refrigeration system is calculated from

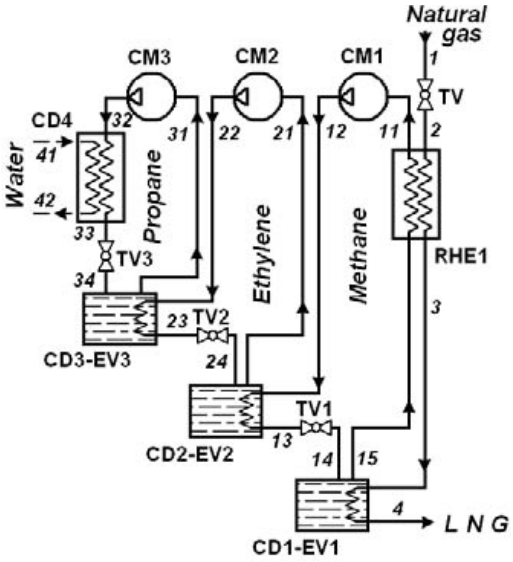


*Fig. 1. Three-cascade refrigeration system used for liquefaction of natural gas.*

*Table 1. Initial data and assumptions.*

| Natural gas | Value |
|---|---|
| Composition | $CH_4$ |
| Mass flow rate | 1 kg/s |
| Temperature of natural gas at state 1 | 50°C |
| Pressure of natural gas at state 1 | 51 bar |
| Temperature of liquefaction | –110°C |
| Heat exchangers | |
| Pressure drop ($\Delta p$) in side pipes | 3% |
| Temperature difference, $\Delta T$ in CD-EV | 10 K |
| Cooling water | |
| Inlet temperature ($T_{41}$) | 35°C |
| Inlet pressure ($p_{41}$) | 2 bar |
| Outlet temperature ($T_{42}$) | 42°C |
| Outlet pressure ($p_{42}$) | 1.5 bar |
| Reference state for the exergetic analysis | |
| Temperature ($T_0$) | 35°C |
| Pressure ($p_0$) | 1 bar |

*Table 2. Thermodynamic data for the material streams at real operating conditions.*

| Material stream | State | $\dot{m}$ (kg/s) | $p$ (bar) | $T$ (°C) | $h$ (kJ/kg) | $s$ (kJ/kg.K) | $e^T$ (kJ/kg) | $e^M$ (kJ/kg) | $e^{PH}$ (kJ/kg) |
|---|---|---|---|---|---|---|---|---|---|
| NG | 1 | 1.000 | 51.00 | 50.0 | 12.9 | –1.951 | 0.9 | 615.7 | 616.6 |
| NG | 2 | | 18.57 | 38.3 | 12.9 | –1.450 | 0.04 | 462.1 | 462.1 |
| LNG | 3 | | 18.03 | –109.2 | –351.9 | –3.048 | 132.2 | 457.5 | 589.7 |
| LNG | 4 | | 17.48 | –110.8 | –715.6 | –5.277 | 459.5 | 452.7 | 912.3 |
| Methane | 11 | 1.419 | 11.60 | –12.93 | –97.5 | –1.600 | 9.3 | 388.7 | 398.0 |
| Methane | 12 | | 36.40 | 107.7 | 170.9 | –1.333 | 18.9 | 565.3 | 584.1 |
| Methane | 13 | | 35.31 | –90.9 | –610.7 | –4.704 | 280.1 | 560.7 | 840.8 |
| Methane | 14 | | 11.96 | –120.0 | –610.7 | –4.574 | 407.3 | 393.4 | 800.7 |
| Methane | 15 | | 11.96 | –120.0 | –354.5 | –2.901 | 148.2 | 393.4 | 541.7 |
| Ethylene | 21 | 4.116 | 1.26 | –100.0 | –174.9 | –0.815 | 57.1 | 21.0 | 78.1 |
| Ethylene | 22 | | 24.01 | 108.7 | 115.2 | –0.573 | 14.5 | 279.0 | 293.5 |
| Ethylene | 23 | | 23.29 | –23.2 | –444.4 | –2.608 | 84.1 | 276.5 | 360.6 |
| Ethylene | 24 | | 1.26 | –100.0 | –444.4 | –2.372 | 267.0 | 21.0 | 288.0 |
| Propane | 31 | 11.260 | 1.55 | –32.0 | 537.9 | 2.423 | 13.4 | 25.0 | 38.4 |
| Propane | 32 | | 17.65 | 70.4 | 668.8 | 2.469 | 19.1 | 136.0 | 155.1 |
| Propane | 33 | | 16.62 | 48.6 | 333.3 | 1.440 | 0.9 | 135.8 | 136.7 |
| Propane | 34 | | 1.55 | –32.0 | 333.3 | 1.575 | 70.1 | 25.0 | 95.1 |
| Water | 41 | 129.300 | 2.00 | 35.0 | 146.8 | 0.505 | 0 | 0.1 | 0.1 |
| Water | 42 | | 1.50 | 42.0 | 176.0 | 0.600 | 0.34 | 0.05 | 0.39 |
| *Reference states for the exergetic analysis* | | | | | | | | | |
| Methane | 0 | | 1.00 | 35.0 | 21.5 | 0.078 | 0 | 0 | 0 |
| Ethylene | 0 | | 1.00 | 35.0 | 14.0 | 0.052 | 0 | 0 | 0 |
| Propane | 0 | | 1.00 | 35.0 | 647.9 | 2.905 | 0 | 0 | 0 |
| Water | 0 | | 1.00 | 35.0 | 146.7 | 0.505 | 0 | 0 | 0 |

$$COP = \frac{\dot{H}_4 - \dot{H}_2}{\dot{W}_{CM1} + \dot{W}_{CM2} + \dot{W}_{CM3}} \quad (1)$$

and is equal to 0.24.

## 3. Conventional exergetic analysis

Since in all components (except CD4) of the three-cascade refrigeration system either all temperatures are below the reference temperature $T_0$, or this temperature is crossed during system operation, the physical exergies of all states should be split into their thermal ( $e^T$ ) and mechanical ( $e^M$ ) exergy components (according to the approach presented in [6]).

The rate of exergy associated with the $j$ th material stream is $\dot{E}_j = \dot{m} \cdot e_j$ .

The exergy balance for the overall system is [7]

$$\dot{E}_{F,tot} = \dot{E}_{P,tot} + \sum_k \dot{E}_{D,k} + \dot{E}_{L,tot} \quad (2)$$

where $\dot{E}_{L,tot} = \dot{E}_{42} - \dot{E}_{41}$ , $\dot{E}_{P,tot} = \dot{E}_4 - \dot{E}_2$ , $\dot{E}_{F,tot} = \dot{W}_{CM1} + \dot{W}_{CM2} + \dot{W}_{CM3}$ , and the exergy destruction rate for each system component (subscript $k$ ) is

$$\dot{E}_{D,k} = \dot{E}_{F,k} - \dot{E}_{P,k} \quad (3)$$

The definitions of $\dot{E}_{F,k}$ and $\dot{E}_{P,k}$ for all components of the overall cogeneration system are given in Table 3 and data obtained from the conventional exergetic analysis are given in Table 4.

*Table 3. Definition of the exergy of fuel and the exergy of product for each component in the system.*

| Component | $\dot{E}_{F,k}$ | $\dot{E}_{P,k}$ |
|---|---|---|
| RHE1 [1)] | $\left(\dot{E}_{15}^T - \dot{E}_{11}^T\right) + \left(\dot{E}_{15}^M - \dot{E}_{11}^M\right) + \left(\dot{E}_2^M - \dot{E}_3^M\right) + \dot{E}_2^T$ | $\dot{E}_3^T$ |
| CM1 [1)] | $\dot{W}_{CM1} + \dot{E}_{11}^T$ | $\left(\dot{E}_{12}^M - \dot{E}_{11}^M\right) + \dot{E}_{12}^T$ |
| CD1-EV1 [2)] | $\left(\dot{E}_{14}^T + \dot{E}_{14}^M\right) - \left(\dot{E}_{15}^T + \dot{E}_{15}^M\right)$ | $\left(\dot{E}_4^T + \dot{E}_4^M\right) - \left(\dot{E}_3^T + \dot{E}_3^M\right)$ |
| TV1 | $\dot{E}_{13}^M - \dot{E}_{14}^M$ | $\dot{E}_{14}^T - \dot{E}_{13}^T$ |
| CM2 [1)] | $\dot{W}_{CM2} + \dot{E}_{21}^T$ | $\left(\dot{E}_{22}^M - \dot{E}_{21}^M\right) + \dot{E}_{22}^T$ |
| CD2-EV2 [1)] | $\left(\dot{E}_{24}^T + \dot{E}_{12}^T\right) + \left(\dot{E}_{24}^M - \dot{E}_{21}^M\right) + \left(\dot{E}_{12}^M - \dot{E}_{13}^M\right) + \dot{E}_{21}^T$ | $\dot{E}_{13}^T$ |
| TV2 | $\dot{E}_{23}^M - \dot{E}_{24}^M$ | $\dot{E}_{24}^T - \dot{E}_{23}^T$ |
| CM3 [1)] | $\dot{W}_{CM3} + \dot{E}_{31}^T$ | $\left(\dot{E}_{32}^M - \dot{E}_{31}^M\right) + \dot{E}_{32}^T$ |
| CD4 [3)] | $\left(\dot{E}_{32}^T + \dot{E}_{32}^M\right) - \left(\dot{E}_{33}^T + \dot{E}_{33}^M\right)$ | $\left(\dot{E}_{42}^T + \dot{E}_{42}^M\right) - \left(\dot{E}_{41}^T + \dot{E}_{41}^M\right)$ |
| TV3 | $\dot{E}_{33}^M - \dot{E}_{34}^M$ | $\dot{E}_{34}^T - \dot{E}_{33}^T$ |
| CD3-EV3 [1)] | $\left(\dot{E}_{34}^T + \dot{E}_{22}^T\right) + \left(\dot{E}_{34}^M - \dot{E}_{31}^M\right) + \left(\dot{E}_{22}^M - \dot{E}_{23}^M\right) + \dot{E}_{31}^T$ | $\dot{E}_{23}^T$ |

[1)] The reference temperature $T_0$ is crossed during the operation in this component.

[2)] This component operates below the reference temperature $T_0$.

[3)] This component operates above the reference temperature $T_0$.

*Table 4: Data obtained from the conventional exergetic analysis.*

| Component | $\dot{E}_{F,k}$ (kW) | $\dot{E}_{P,k}$ (kW) | $\dot{E}_{D,k}$ (kW) | $y_k$ (%) | $\varepsilon_k$ (%) |
|---|---|---|---|---|---|
| RHE1 | 208.5 | 132.2 | 76.3 | 2.50 | 0.63 |
| CM1 | 394.3 | 277.5 | 116.8 | 3.83 | 0.70 |
| CD1-EV1 | 368.1 | 322.6 | 45.5 | 1.49 | 0.88 |
| TV1 | 237.4 | 180.6 | 56.8 | 1.86 | 0.76 |
| CM2 | 1429.1 | 1121.4 | 307.8 | 10.09 | 0.79 |
| CD2-EV2 | 897.2 | 397.6 | 499.6 | 16.38 | 0.44 |
| TV2 | 1051.6 | 753.0 | 298.6 | 9.79 | 0.72 |
| CM3 | 1626.4 | 1466.3 | 160.1 | 5.25 | 0.90 |
| CD4 | 208.0 | 37.7 | 170.4 | 5.59 | 0.18 |
| TV3 | 1247.7 | 779.9 | 467.8 | 15.34 | 0.63 |
| CD3-EV3 | 708.3 | 346.0 | 362.3 | 11.88 | 0.49 |
| **Overall system** | **3050.0** | **450.2** | **2599.8** | **85.24** | **0.15** |

In a conventional exergetic evaluation the following variables are used [7]: (a) Exergy destruction rate within $k$ th system component, $\dot{E}_{D,k}$; (b) exergetic efficiency of the $k$ th component, $\varepsilon_k = \dfrac{\dot{E}_{P,k}}{\dot{E}_{F,k}}$ and of the overall system $\varepsilon_{tot} = \dfrac{\dot{E}_{P,tot}}{\dot{E}_{F,tot}}$; and (c) the exergy destruction ratio for the $k$ th plant component, $y_k = \dfrac{\dot{E}_{D,k}}{\dot{E}_{F,tot}}$.

## 4. Advanced exergetic analysis

The interactions among different components of the same system can be estimated and the quality of the conclusions obtained from an exergetic analysis can be improved, when the exergy destruction in each (important) system component is split into endogenous/exogenous and avoidable/unavoidable parts. We call the analysis based on these procedures *advanced exergetic analysis*. All publications up to date in the field of the advanced exergy-based methods are summarized and generalized in [8,9].

*Endogenous* exergy destruction is the part of a variable within a component obtained when all other components operate ideally and the component being considered operates with the same efficiency as in the real system. The *exogenous* part of the variable is the difference between the values of the variable being considered in the real system and in the endogenous case: $\dot{E}_{D,k}^{EX} = \dot{E}_{D,k} - \dot{E}_{D,k}^{EN}$. Note that the value of $\dot{E}_{P,k}^{EN}$ should be estimated for each system component when the so-called hybrid processes [8-11] are used for calculating the values of $\dot{E}_{D,k}^{EN}$.

The *unavoidable* exergy destruction cannot be further reduced due to technological limitations such as availability and cost of materials and manufacturing methods. The difference between total and unavoidable exergy destruction for a component is the *avoidable* exergy destruction that should be considered during the improvement procedure $\dot{E}_{D,k}^{AV} = \dot{E}_{D,k} - \dot{E}_{D,k}^{UN}$ where the value of the unavoidable exergy destruction within the $k$th component is calculated by $\dot{E}_{D,k}^{UN} = \dot{E}_{P,k}^{real}\left(\dfrac{\dot{E}_{D,k}}{\dot{E}_{P,k}}\right)^{UN}$.

Combining the two splitting procedures gives us an opportunity to calculate the unavoidable endogenous exergy destruction $\dot{E}_{D,k}^{UN,EN} = \dot{E}_{P,k}^{EN}\left(\dfrac{\dot{E}_{D,k}}{\dot{E}_{P,k}}\right)^{UN}$.

Using these values the following important variables can be estimated:

- The *avoidable endogenous* exergy destruction ( $\dot{E}_{D,k}^{AV,EN}$ ). This variable can be reduced by improving the $k$th component from the exergetic point of view.
- The *avoidable exogenous* exergy destruction ( $\dot{E}_{D,k}^{AV,EX}$ ) that can be reduced by a structural improvement of the overall system, or by improving the efficiency of the remaining compo-

*Table 5. Real, theoretical and unavoidable operation conditions.*

| Parameter | Real conditions | Theoretical conditions | Unavoidable conditions |
|---|---|---|---|
| Mass flow rate of natural gas | 1 kg/s | 1 kg/s | 1 kg/s |
| Pressure drop, $\Delta p$ | 3% | 0% | 5% |
| Min. temperature difference, $\Delta T$ | 5K | 0K | 2K |
| Isentropic efficiencies for compressors, $\eta_{CM}$ | CM1 - 64%, | 100% | 95% |
| | CM2 - 70%, | 100% | 95% |
| | CM3 - 88% | 1005 | 955 |
| Temperature at CD4 | 50°C | 42 °C | 44 °C |

*Table 6. Results obtained from the advanced exergetic analysis.*

| Component | $\left(\frac{\dot{E}_{D,k}}{\dot{E}_{P,k}}\right)^{UN}$ | $\dot{E}_{P,k}^{EN}$ | $\dot{E}_{D,k}^{EN,AV}$ | $\sum_{\substack{r=1 \\ r\neq k}}^{n} \dot{E}_{D,r}^{AV,EX,k}$ | $\dot{E}_{D,k}^{AV,\Sigma}$ |
|---|---|---|---|---|---|
| RHE | 0.56 | 132.20 | 0.75 | 4.92 | 5.67 |
| CM1 | 0.05 | 153.30 | 65.83 | 84.41 | 150.24 |
| CD1-EV1 | 0.06 | 320.20 | 27.16 | 164.81 | 191.97 |
| TV1 | 0.27 | 121.00 | 0 | 0.18 | 0.18 |
| CM2 | 0.04 | 596.70 | 151.91 | 76.86 | 228.77 |
| CD2-EV2 | 0.7 | 374.40 | 33.13 | 85.24 | 118.37 |
| TV2 | 0.36 | 478.10 | 0 | 27.69 | 27.69 |
| CM3 | 0.05 | 474.00 | 33.21 | 3.37 | 36.58 |
| CD4 | 2.77 | 15.52 | 28.57 | 34.13 | 62.70 |
| TV3 | 0.34 | 321.40 | 0 | 9.50 | 9.50 |
| CD3-EV3 | 0.42 | 229.50 | 30.6 | 21.87 | 52.47 |

*Table 7. Results obtained from the advanced exergetic analysis.*

| Component | $\dot{E}_{D,k}^{EN}$ [kW] | $\dot{E}_{D,k}^{EX}$ [kW] | $\dot{E}_{D,k}^{UN}$ [kW] | $\dot{E}_{D,k}^{AV}$ [kW] | Splitting $\dot{E}_{D,k}^{real}$ [kW] | | | |
|---|---|---|---|---|---|---|---|---|
| | | | | | $\dot{E}_{D,k}^{UN}$ [kW] | | $\dot{E}_{D,k}^{AV}$ [kW] | |
| | | | | | $\dot{E}_{D,k}^{UN,EN}$ | $\dot{E}_{D,k}^{UN,EX}$ | $\dot{E}_{D,k}^{AV,EN}$ | $\dot{E}_{D,k}^{AV,EX}$ |
| RHE | 54.56 | 21.74 | 53.81 | 22.49 | 53.81 | 0 | 0.75 | 21.74 |
| CM1 | 72.90 | 43.90 | 12.80 | 104.0 | 7.07 | 5.73 | 65.83 | 38.17 |
| CD1-EV1 | 44.79 | 0.35 | 17.76 | 27.38 | 17.63 | 0.13 | 27.16 | 0.22 |
| TV1 | 33.41 | 23.43 | 48.87 | 7.97 | 33.41 | 15.46 | 0 | 7.97 |
| CM2 | 174.70 | 133.0 | 42.86 | 264.84 | 22.79 | 20.07 | 151.91 | 112.93 |
| CD2-EV2 | 293.00 | 206.70 | 275.97 | 223.73 | 259.87 | 16.10 | 33.13 | 190.60 |
| TV2 | 170.40 | 128.30 | 269.21 | 29.49 | 170.40 | 98.81 | 0 | 29.49 |
| CM3 | 54.11 | 106.09 | 64.64 | 95.56 | 20.90 | 43.74 | 33.21 | 62.35 |
| CD4 | 66.22 | 104.18 | 91.36 | 79.04 | 37.65 | 53.71 | 28.57 | 50.47 |
| TV3 | 142.80 | 352.20 | 374.58 | 93.42 | 142.80 | 231.78 | 0 | 93.42 |
| CD3-EV3 | 111.50 | 250.80 | 121.96 | 240.34 | 80.90 | 41.06 | 30.6 | 209.74 |

nents, and always of course by improving the efficiency in the *k*th component.

For obtaining a deeper understanding of the interactions among components, the exogenous exergy destruction (as well as the exogenous unavoidable and the exogenous avoidable exergy destructions) within the *k*th component are split $\dot{E}_{D,k}^{EX} = \sum_{\substack{r=1 \\ r\neq k}}^{n-1} \dot{E}_{D,k}^{EX,r} + \dot{E}_{D,k}^{mexo}$ . The value of $\dot{E}_{D,k}^{EX,r}$ represents the part of the exogenous exergy destruction within the *k*th component that is caused by the irreversibilities occurring within the *r*th component. The remaining part $\dot{E}_{D,k}^{mexo}$ we call *mexogenous exergy destruction* within the *k*th component.

To identify priorities for improving components based on information obtained from an advanced exergetic analysis, we use the sum of the avoidable endogenous exergy destruction within the *k*th component and the avoidable exogenous exergy destructions within the remaining components caused by the *k*th component $\dot{E}_{D,k}^{AV,\Sigma} = \dot{E}_{D,k}^{AV,EN} + \sum_{\substack{r=1 \\ r\neq k}}^{n} \dot{E}_{D,r}^{AV,EX,k}$ .

• To calculate the unavoidable endogenous part of the exergy destruction within a system component, we apply the following equation [8,9] $\dot{E}_{D,k}^{UN,EN} = E_{P,k}^{EN}\left(\frac{\dot{E}_{D,k}}{\dot{E}_{P,k}}\right)^{UN}$ .

Table 7 presents the results obtained from splitting the exergy destruction within each component of the three-cascade refrigeration system. The values $\left(\frac{\dot{E}_{D,k}}{\dot{E}_{P,k}}\right)^{UN}$ , $\dot{E}_{P,k}^{EN}$ , and $\dot{E}_{D,k}^{AV,\Sigma}$ are given in Table 6.

## 5. Results and discussions

The results from the conventional exergetic analysis ( $\dot{E}_{D,k}$ or $y_k$ in Table 4) show that the most important components from the thermodynamic viewpoint are the CD2-EV2, TV3, CD3-EV3, CM2, and TV2.

These results are misleading to some extent because, for example, they suggest that we should try to reduce the exergy destruction within the components TV3 and TV2. However, as the results from the advanced exergetic analysis indicate (Tables 6 and 7), the endogenous avoidable exergy destruction in all throttling valves is zero. This means that the exergy destruction within these components can be reduced through changes in the remaining components or in the structure of the overall plant.

Also with respect to the relative importance of TV2 and TV3 we obtain misleading information from the conventional analysis, which suggests that TV3 is more important than TV2. The variable $\dot{E}_{D,k}^{AV,\Sigma}$ (Table 6), however, shows that TV2 is much more important than TV3.

From the advanced analysis we obtain the following additional information: Most of the exergy destruction in the components RHE, TV1, CD2-EV2, TV2, CD4 and TV3 is unavoidable (Table 7). Most of the exergy destruction in the components CM3, CD4, TV3 and CD3-EV3 is exogenous, i.e. it is caused by the interactions of the component being considered with the other components. Particularly for the components CD3-EV3 and CD2-EV2, the avoidable exogenous part of the exergy destruction is very high (last column in Table 7). Thus, the exergy destruction within these components can be reduced more effectively by improving the efficiency of the remaining components.

The variable $\dot{E}_{D,k}^{AV,\Sigma}$ indicates that, when we consider the interactions among components and only avoidable exergy destructions, the most important components of the overall system are CM2, CD1-EV1, CM1 and CD2-EV2. Thus, we obtain a completely different picture from the advanced exergetic analysis than from the conventional one, and the picture from the advanced analysis is closer to reality than the one from the conventional analysis. For example, the advanced analysis emphasizes the importance of compressors (CM1 and CM2) and reduces the importance of CD2-EV2 and CD3-EV3.

From the engineering point of view, CM1 and CM 2 can be improved by selecting, for example, a rotary (rotating vane) compressor instead of the piston compressor assumed here. In addition, a screw type refrigeration compressor can be considered only for CM1 because of the limitations associated with its operating conditions. The components CD1-EV-1 and CD2-EV2 can be improved by decreasing the

temperature difference in these heat exchangers. The assumed value for the temperature difference of 10K for all three CD-EVs is relatively high and easily can be decreased down to 6K (without selecting a different type of heat exchanger), or even down to 4 … 2K. The value $\Delta T$=2 K corresponds to standard operation conditions for plate heat exchangers.

## 6. Conclusion

We conclude that a conventional exergetic analysis provides useful information but an advanced exergetic analysis makes this information more precise and useful and supplies additional information that cannot be provided by the conventional analysis.

## Nomenclature

| | |
|---|---|
| $E$ | exergy [J] |
| $e$ | specific exergy [J/kg] |
| $k$ | $k$ th component [-] |
| $m$ | mass [kg] |
| $n$ | number of components [-] |
| $p$ | pressure [Pa] |
| $r$ | $r$ th component (different from the $k$ th component being considered) [-] |
| $T$ | temperature [K] |
| $y$ | exergy destruction ratio [-] |

*Greek symbols*

| | |
|---|---|
| $\varepsilon$ | exergetic efficiency [%] |
| $\eta$ | isentropic efficiency [%] |

*Subscripts*

| | |
|---|---|
| $D$ | refers to exergy destruction |
| $F$ | fuel |
| $P$ | product |
| $tot$ | refers to the total system |

*Superscripts*

| | |
|---|---|
| $\bullet$ | time rate |
| $AV$ | avoidable |
| $EN$ | endogenous |
| $EX$ | exogenous |
| $M$ | mechanical exergy |
| $PH$ | physical exergy |
| $T$ | thermal exergy |
| $UN$ | unavoidable |

*Abbreviations*

| | |
|---|---|
| *CD* | condenser |
| *CD-EV* | condenser-evaporator |
| *CM* | compressor |
| *RHE* | regeneration heat exchnager |
| *TV* | throttling valve |

## References


[1] http://www.energy.ca.gov/lng/international.htl

[2] *Liquefied Natural Gas: Current Expansion and Perspectives*, 2006, 19-th Informatory Note on Refrigerating Technologies. International Institute of Refrigeration, Paris, France, www.iifiir.org.

[3] Refrigeration. *ASHRAE Handbook*, 2006, American Society of Heating, Refrigerating and Air-Conditioning Engineers, Inc.

[4] Omar M.N.B., 2008, *Efficiency Improvement of a General System for the Production of Malaysia Liquefied Natural Gas (MLNG)*, Ms. Thesis, Technische Universität Berlin.

[5] Kakac S., Liu H., 1998, *Heat exchangers: selection, rating, and thermal design*, CRC Press LLC, USA.

[6] Morosuk T, Tsatsaronis G., 2005, Graphical models for splitting physical exergy. In: Kjelstrup S, Hustad JE, Gundersen T, Rosjorde A, Tsatsaronis G, editors. *Shaping our future energy systems*. vol. 1, pp. 377–384.

[7] Bejan A., Tsatsaronis G., Moran M., 1996, *Thermal Design and Optimization*, John Wiley & Sons, New York.

[8] Tsatsaronis G., Morosuk T., 2008, A general exergy-based method for combining a cost analysis with an environmental impact analysis. Part I. *Proceedings of the ASME International Mechanical Engineering Congress and Exposition, Boston, Massachusetts*, USA, 2008, files IMECE2008-67218.

[9] Tsatsaronis G., Morosuk T., 2008, A general exergy-based method for combining a cost analysis with an environmental impact analysis. Part II. *Proceedings of the ASME International Mechanical Engineering Congress and Exposition, Boston, Massachusetts*, USA, 2008, files IMECE2008-67219.

[10] Morosuk T., Tsatsaronis G., 2007, Exergoeconomic Evaluation of Refrigeration Machines Based on Avoidable Endogenous and Exogenous Costs. In Mirandola A., Arnas O., Lazzaretto A., eds. *Proceedings of the 20th International Conference on Efficiency, Cost, Optimization, Simulation and Environmental Impact of Energy Systems*, Padova, Italy, Vol.1, pp. 1459-1467.

[11] Tsatsaronis G., Morosuk T., 2007, Advanced exergoeconomic evaluation and its application to compression refrigeration machines, *Proceedings of the ASME International Mechanical Engineering Congress and Exposition*, Seattle, USA, CD-ROM, file 2007-41202.

# Two Efficient Methods for Gas Distributive Network Calculation

*Dejan Brkić*

*Ministry of Science and Technological Development, Beograd, Serbia*

**Abstract:** Today, two very efficient methods for calculation of flow distribution per branches of a looped gas pipeline are available. Most common is improved Hardy Cross method, while the second one is so-called unified node-loop method. For a gas pipeline, gas flow rate through a pipe can be determined using Colebrook equation modified by AGA (American Gas Association) for calculation of friction factor accompanied with Darcy-Weisbach equation for pressure drop while second approach is using Renouard equation adopted for gas pipeline calculation. For the development of Renouard equation for gas pipelines some additional thermodynamic properties are involved in comparisons with Colebrook and Darcy-Weisbach model. These differences will be explained. Both equations, the Colebrook's (accompanied with Darcy-Weisbach scheme) and Renouard's will be used for calculation of flow through the pipes of one gas pipeline with eight closed loops which are formed by pipes. Consequently four different cases will be examined because the network is calculated using improved Hardy Cross method and unified node-loop method. Some remarks on optimization in this area of engineering also will be mentioned.

Keywords: Calculation methods, Flow rate equation, Hydraulic pipeline systems, Natural gas distribution systems, Pipeline networks.

## 1. Introduction

A pipeline network is a collection of elements such as pipes, compressors, pumps, valves, regulators, heaters, tanks, and reservoirs interconnected in a specific way. This article is focused on pipes. The behavior of the network is governed by two factors: (i) specific characteristics of the elements and (ii) how elements are connected together. Assumption is that pipes are connected in a smooth way, i.e. so called minor hydraulic loses are neglected. The difficulty to solve the turbulent flow problem in a single pipe lies in the fact that friction factor is a complex function of relative surface roughness and the Reynolds number. Since the value of hydraulic resistance depends on flow rate, problem of flow distribution per pipes in gas distributive looped pipelines have to be solved using some kind of iterative procedures. Similar situation is with electrical resistances when diode is in circuit. With common resistors in electrical circuits where the electrical resistances are not depends on the value of electrical current in a conduit, problem is linear and no iterative procedure has to be used. So problem of flow through single tube is already complex. Despite of it, very efficient procedures are available for solution of flow problem in a complex pipeline such as looped pipeline like natural gas distribution network is.

Here has to be noted that in a municipal gas pipeline, natural gas can be treated as incompressible fluid (liquid) i.e. as water. Even under this circumstance, calculation of water pipelines cannot be literary copied and applied for calculation of gas pipelines. Assumption of gas incompressibility means that it is compressed and forced to convey through pipes, but inside the pipeline system pressure drop of already compressed gas is small and hence further changes in gas density can be neglected. This means that gas is compressible fluid in general, but inside a distribution pipeline where the pressure drops can be neglected, natural gas can be treated as incompressible fluid. This is main difference between liquid and incompressible flow. According to this, water flow in pipelines is liquid incompressible flow, while the gas flow is gaseous incompressible flow. Fact is that gas is actually compressed and hence that volume of gas is decreased and then such compressed volume of gas is conveying with constant density through gas distribution pipeline. Hence, mass of gas is constant, but volume is decreased while gas density is according to this, increased.

Corresponding Author: Dejan Brkić, Email: dejanrgf@tesla.rcub.bg.ac.rs

Operate pressure for distribution gas network is $4 \cdot 10^5$ Pa abs i.e. $3 \cdot 10^5$ Pa gauge and accordingly volume of gas is decreased four times compared to volume of gas at normal conditions. Hence, velocity of gaseous fluids depends on the pressure in pipe since they are compressible (1):

$$v = \frac{4 \cdot p_{st} \cdot Q_{st}}{p \cdot D_{in}^2 \cdot \pi} = \frac{4 \cdot Q}{D_{in}^2 \cdot \pi}, \quad (1)$$

## 2. Hydraulics frictions and gas flow rates in pipes

Each pipe is connected to two nodes at its ends. In a pipe network system, pipes are the channels used to convey fluid from one location to another. The physical characteristics of a pipe include the length, inside diameter, roughness coefficient, and minor loss coefficients. The pipe roughness coefficient is associated with the pipe material and age. When fluid is conveyed through the pipe, hydraulic energy is lost due to the friction between the moving fluid and the stationary pipe surface. This friction loss is a major energy loss in pipe flow. Losses of energy or head (pressure) losses depend on the shape, size and roughness of a channel, the velocity density and viscosity of a fluid.

Experiments show that in many cases pressure drop are approximately proportional to the square of the velocity (2):

$$p_1 - p_2 = \lambda \cdot \frac{L}{D_{in}} \cdot \frac{v^2}{2} \cdot \rho, \quad (2)$$

Equation (2) is called the Darcy-Weisbach equation, named after Henry Darcy, a French engineer of the nineteenth century, and Julius Weisbach, a German mining engineer and the scientist of the same era. In previous equation velocity and gas density must be correlated, since the gas is incompressible fluid, and hence for gas is more suitable equation in next form (3) because $Q \cdot \rho = Q_{st} \cdot \rho_{st}$:

$$p_1 - p_2 = \lambda \cdot \frac{L}{D_{in}^5} \cdot \frac{8 \cdot Q^2}{\pi^2} \cdot \rho = \lambda \cdot \frac{L}{D_{in}^5} \cdot \frac{8 \cdot Q_{st}^2}{\pi^2} \cdot \rho_{st}, \quad (3)$$

Density of gas can be noted as (4):

$$\rho = \frac{p \cdot M}{z \cdot R \cdot T}, \quad (4)$$

Considering that gas density (4) at standard pressure conditions is equal as in average pressure in pipeline, general equation for steady-state flow of gas can be written (5) [1]:

$$C = p_1^2 - p_2^2 = \lambda \frac{16 \cdot \Delta L \cdot Q_{st}^2}{D_{in}^5 \cdot \pi^2} \frac{p_{st}^2 \cdot M_{air} \cdot \rho_{st}}{z_{st} \cdot R \cdot T_{st}}, \quad (5)$$

Main parameter related to the hydraulic regime is Darcy's friction factor ($\lambda$). Note that the Darcy friction factor is defined in theory as $\lambda = (8 \cdot \tau)/(\rho \cdot v^2)$. To predict whether flow will be laminar, hydraulically 'smooth', partially turbulent or fully turbulent, it is necessary to explore the characteristics of flow. Hydraulically 'smooth' regime is characteristic of flow through plastic, i.e. polyethylene pipes and it is also sort of turbulent regime. For the steel pipes, partially turbulent regime is most common. In considerations related to the hydraulic frictions has to be very careful because some of the authors use Darcy's friction factor while the others use Fanning's factor. The Darcy's friction coefficient is four times larger than Fanning's while the physical meaning is equal. Graphically, friction factor for known Reynolds number and relative roughness can be determined using well known Moody diagram. The Darcy friction factor and the Moody friction factor are synonyms.

### 2.1. Gas flow through plastic pipes

Inner surface of polyethylene pipes which are almost always used in gas distribution networks are practically smooth and hence flow regime in the typical network is hydraulically 'smooth'. For this regime is suitable Renouard's equation [2] adjusted for natural gas flow (6):

$$C = p_1^2 - p_2^2 = \frac{4810 \cdot Q_{st}^{1.82} \cdot L \cdot \rho_r}{D_{in}^{4.82}}, \quad (6)$$

In Renouard's formula flow rate is expressed for standard conditions of pressure and temperature. Renouard's formula is adjusted for gas flow calculations in plastic pipes with no explicit determining of hydraulic resistances. This means that Darcy's friction factor is not necessary to be calculated. This is accomplished by simplification of general steady-state flow equation for gaseous fluids (5).

Using formulation for Darcy friction factor in hydraulically smooth region Renouard suggest his equation for liquid flow (7):

$$\lambda = \frac{0.172}{Re^{0.18}}, \quad (7)$$

In Renoard's equation adjusted for gas pipelines friction factor is rearranged in the way to be expressed using other flow parameters and also using some thermodynamic properties of natural gas. Using an absolute viscosity of $\mu=1.0757\cdot10^{-5}$ Pa·s, neglecting the potential energy term and assuming that temperature of natural gas is $T_{avr}=T_{st}=288.15$ K, pressure is $p_{st}=1.01325\cdot10^{5}$ Pa and compressibility factor is Z=1, general steady-state flow equation can be simplified as (8):

$$C = p_1^2 - p_2^2 = \frac{4088\cdot Q_{st}^{1.82}\cdot L\cdot \rho_r^{0.82}}{D_{in}^{4.82}}, \qquad (8)$$

It must be stressed that in the development leading to this more simplified equation (8), Renouard used a constant value for city gas kinematic viscosity $\nu=2.2\cdot10^{-5}$ $m^2/s$. Note that kinematic gas viscosity ($\nu$) and dynamic gas viscosity ($\mu$) is connected using gas density ($\rho$). Relative density of typical natural gas is 0.64. Assumed flow temperature in Renouard's equation is 15 ºC. This means that by fixing the value of gas cinematic viscosity, the density is also kept fixed, which is physically inaccurate when considering compressible gas flows at medium or high pressure, because the cinematic viscosity of gases is highly dependent upon pressure. Every time a gas with a cinematic viscosity different from the city gas is being used, a multiplying correction factor $(\nu/2.2\cdot10^{-5}\ m^2/s)^{0.18}$·must be applied in (6). This product multiplied with gas density is usually called the corrected density. Estimated error in calculation of the pressure differential by using (6) instead of (8) is no more than 9%. The use of (6) without the viscosity correction, although quite common in the daily practice, leads to an overestimation on the calculation of the pressure drop, as the quadratic pressure difference of C is about 6% to 9% higher than the value obtained through (8).

Regarding to Renouard's formula has to be careful since it does not relate pressure drop but actually difference of the quadratic pressure at the input and the output of pipe. This means that $\sqrt{C}$ is not actually pressure drop in spite of the same unit of measurement is as used for the pressure (Pa). But, for gas pipeline calculation, fact that when $\sqrt{C}\to 0$ that consecutive means that also $C\to 0$ is very useful. Parameter $\sqrt{C}$ can be noted as pseudo-pressure drop.

## 2.2. Gas flow through steel pipes

For commercial steel pipes, Colebrook [3] showed the transition region of turbulence could be described by (9):

$$\frac{1}{\sqrt{\lambda}} = -2\cdot\log\left(\frac{2.51}{Re\cdot\sqrt{\lambda}} + \frac{\varepsilon}{3.71\cdot D}\right), \qquad (9)$$

This empirical equation is developed using measurements conducted by Colebrook and White [4]. Colebrook equation also can be noted as (10):

$$\frac{1}{\sqrt{\lambda}} = 1.14 - 2\cdot\log\left(\frac{\varepsilon}{D} + \frac{9.35}{Re\sqrt{\lambda}}\right), \qquad (10)$$

Colebrook's equation describes a monotonic change in the friction factor from smooth to fully rough (Figure 1).

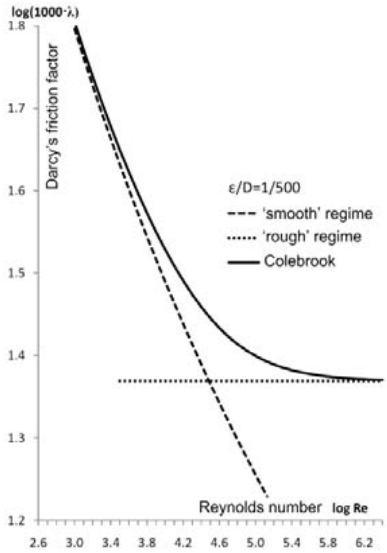


*Fig. 1. Colebrook relation make transitional curve among hydraulically "smooth" regime and turbulent rough regime*

It is also the basis for the widely used Moody diagram. Many researchers [1] adopt a modification of the Colebrook equation, using the 2.825 constant instead of 2.51 especially for gas flow calculation (modified Colebrook in Figure 2). Colebrook's equation for determination of hydraulic resistances is implicit in fluid flow friction factor and hence it has to be approximately solved using iterative procedure or using some of the approximate explicit formulas developed by many authors (Table 1). All presented approximations shown in Table 1 are very accurate.

*Table 1.* Explicit approximations to Colebrook relation.

| Relation | Name |
|---|---|
| $\lambda \approx 0.0055 \cdot \left(1 + \left(2 \cdot 10^4 \cdot \varepsilon/D + 10^6/\mathrm{Re}\right)^{1/3}\right)$ | Moody |
| $\lambda \approx 0.094 \cdot (\varepsilon/D)^{0.225} + 0.53 \cdot (\varepsilon/D) + 88 \cdot (\varepsilon/D)^{0.44} \cdot \mathrm{Re}^{-\Psi} \quad \Psi = 1.62 \cdot (\varepsilon/D)^{0.134}$ | Wood |
| $1/\sqrt{\lambda} \approx -2 \cdot \log\left((1/3.715) \cdot (\varepsilon/D) + (15/\mathrm{Re})\right)$ | Eck |
| $1/\sqrt{\lambda} \approx -2 \cdot \log\left((1/3.7) \cdot (\varepsilon/D) + 5.74/\mathrm{Re}^{0.9}\right) \Leftrightarrow 1/\sqrt{\lambda} \approx 1.14 - 2 \cdot \log\left[\varepsilon/D + 21.25/\mathrm{Re}^{0.9}\right]$ | Swamee and Jain |
| $1/\sqrt{\lambda} = -2 \cdot \log\left((1/3.71) \cdot (\varepsilon/D) + (7/\mathrm{Re})^{0.9}\right)$ | Churchill |
| $1/\sqrt{\lambda} \approx -2 \cdot \log\left((1/3.715) \cdot (\varepsilon/D) + (6.943/\mathrm{Re})^{0.9}\right)$ | Jain |
| $\lambda \approx 8 \cdot \left[(8/\mathrm{Re})^{12} + (\Theta_1 + \Theta_2)^{-1.5}\right]^{\frac{1}{12}}$<br>$\Theta_1 = \left[2.457 \cdot \ln\left[(7/\mathrm{Re})^{0.9} + 0.27 \cdot (\varepsilon/D)\right]\right]^{16}$<br>$\Theta_2 = (37530/\mathrm{Re})^{16}$ | Churchill* |
| $1/\sqrt{\lambda} \approx -2.0 \cdot \log\left[\begin{array}{l}(1/3.7065) \cdot (\varepsilon/D) - \\ -(5.0452/\mathrm{Re}) \cdot \log\left((1/2.8257) \cdot (\varepsilon/D)^{1.1098} + (5.8506/\mathrm{Re}^{0.8981})\right)\end{array}\right]$ | Chen |
| $1/\sqrt{\lambda} \approx 1.8 \cdot \log\left[\mathrm{Re}/(0.135 \cdot \mathrm{Re} \cdot (\varepsilon/D) + 6.5)\right]$ | Round |
| $1/\sqrt{\lambda} \approx -2 \cdot \log\left(\begin{array}{l}(1/3.7) \cdot (\varepsilon/D) + \\ +(4.518 \cdot \log(\mathrm{Re}/7))/\left(\mathrm{Re}\left(1 + (\mathrm{Re}^{0.52}/29) \cdot (\varepsilon/D)^{0.7}\right)\right)\end{array}\right)$ | Barr |
| $1/\sqrt{\lambda} \approx -2 \cdot \log\left[(1/3.7) \cdot (\varepsilon/D) - 5.02/\mathrm{Re} \cdot \log\left(\begin{array}{l}(1/3.7) \cdot (\varepsilon/D) - \\ -5.02/\mathrm{Re} \cdot \log\left((1/3.7) \cdot (\varepsilon/D) + 13/\mathrm{Re}\right)\end{array}\right)\right]$<br>$1/\sqrt{\lambda} \approx -2 \cdot \log\left[(1/3.7) \cdot (\varepsilon/D) - 5.02/\mathrm{Re} \cdot \log\left((1/3.7) \cdot (\varepsilon/D) + 13/\mathrm{Re}\right)\right]$ | Zigrang and Sylvester |
| $1/\sqrt{\lambda} \approx -1.8 \cdot \log\left[\left((1/3.7) \cdot (\varepsilon/D)\right)^{1.11} + 6.9/\mathrm{Re}\right]$ | Haaland |
| $\lambda \approx \left[\Psi_1 - (\Psi_2 - \Psi_1)^2/(\Psi_3 - 2\Psi_2 + \Psi_1)\right]^{-2}$<br>$\lambda \approx \left[4.781 - (\Psi_1 - 4.781)^2/(\Psi_2 - 2\Psi_1 + 4.781)\right]^{-2}$<br>$\Psi_1 = -2 \cdot \log\left((1/3.7) \cdot (\varepsilon/D) + 12/\mathrm{Re}\right) \quad \Psi_2 = -2 \cdot \log\left((1/3.7) \cdot (\varepsilon/D) + (2.51 \cdot \Psi_1)/\mathrm{Re}\right)$<br>$\Psi_3 = -2 \cdot \log\left((1/3.7) \cdot (\varepsilon/D) + (2.51 \cdot \Psi_2)/\mathrm{Re}\right)$ | Serghides |
| $1/\sqrt{\lambda} \approx -2 \cdot \log\left((1/3.7) \cdot (\varepsilon/D) + 95/\mathrm{Re}^{0.983} - 96.82/\mathrm{Re}\right)$ | Manadilli |
| $1/\sqrt{\lambda} \approx -2 \cdot \log\left\{\begin{array}{l}(1/3.7065) \cdot (\varepsilon/D) - \\ -(5.0272/\mathrm{Re}) \cdot \log\left[\begin{array}{l}(1/3.827) \cdot (\varepsilon/D) - \\ -(4.567/\mathrm{Re}) \cdot \log\left(\begin{array}{l}\left((1/7.7918) \cdot (\varepsilon/D)\right)^{0.9924} + \\ +(5.3326/(208.815 + \mathrm{Re}))^{0.9345}\end{array}\right)\end{array}\right]\end{array}\right\}$ | Romeo, Royo and Monzón |
| $1/\sqrt{\lambda} \approx 0.8686 \cdot \ln\left[(0.4587 \cdot \mathrm{Re})/S^{S/(S+1)}\right]$<br>$S = 0.124 \cdot \mathrm{Re} \cdot (\varepsilon/D) + \ln(0.4587 \cdot \mathrm{Re})$ | Sonnad and Goudar |
| $1/\sqrt{\lambda} = \alpha - [(\alpha + 2 \cdot \log(\beta/\mathrm{Re}))/(1 + 2.18/\beta)]$<br>$\alpha = ((0.774 \cdot \ln(\mathrm{Re})) - 1.41)/\left(1 + 1.32 \cdot \sqrt{\varepsilon/D}\right)$<br>$\beta = (1/3.7) \cdot (\varepsilon/D) \cdot \mathrm{Re} + 2.51 \cdot \alpha$ | Buzzelli [6] |
| $1/\sqrt{\lambda} \approx -2 \cdot \log\left(10^{-0.4343S} + (1/3.71) \cdot (\varepsilon/D)\right)$<br>$1/\sqrt{\lambda} \approx -2 \cdot \log\left((2.18 \cdot S)/\mathrm{Re} + (1/3.7) \cdot (\varepsilon/D)\right)$<br>$S = \ln\left(\mathrm{Re}/(1.816 \cdot \ln(1.1 \cdot \mathrm{Re}/\ln(1 + 1.1 \cdot \mathrm{Re})))\right)$ | Brkić [7] |

*also cover laminar regime

Percentage error for iterative formulas shown in Table 1 is less than 3% over the entire domain of Reynolds number [5]. Exceptions are Moody, Wood, Eck and Round approximations (Figure 2). These four formulas should not be used.

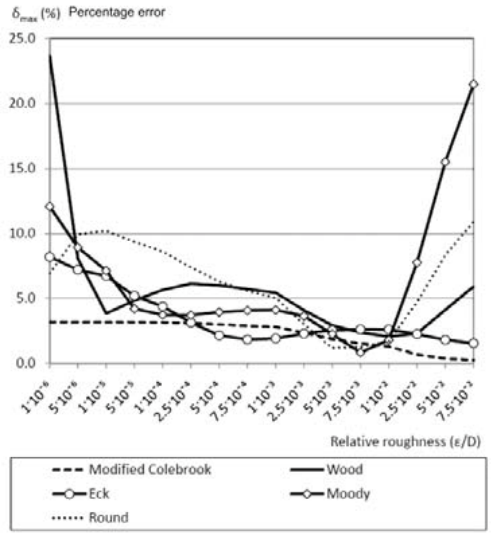


*Fig. 2. Distribution of error for most inaccurate approximations of the Colebrook's equation*

While iterative computations are trivial in the context of current computing power, iterative estimation of friction factor can significantly increase the computational burden in complex piping network like here presented where multiple calculations are necessary. So, flow distribution problem in a complex looped gas pipeline has to be solved using an iterative procedure and further to be more complex, when Colebrook equation is used, additional iterative procedure for computing of friction pipe in every pipe has to be performed. Presented approximations (Table 1) are usually used in computer programs to avoid iterative scheme. But some computers codes continue to use Newton-Raphson iteration scheme for solving to the friction factor. For these methods, finding a good starting guess is often difficult.

Initial guess and further solution can be very easily done using common software tools like MS Excel 2007. Maximal number of iterations in MS Excel 2007 is 32767. To solve for unknown friction factor $\lambda$, one must start by somehow estimating the value of friction factor on the right side of the equation, solve for the new friction factor on the left, enter the new value back on the right side, and continue this process until there is a balance on both sides of the equation within an arbitrary difference. This difference must be small without causing endless computations.

Colebrook equation consists of two parts; first part is equal to zero in first iteration i.e. $2.51/(Re\cdot\lambda)=0$, but second part has value different than zero $\varepsilon/(D\cdot 3.71) \neq 0$, so estimation of the value in the first iteration is unnecessary. Initial value in the first iteration is $\varepsilon/(D\cdot 3.71)$. Sometimes, effective solutions are too simple on a first sight, and Excel is ideal tool to solve this kind of problem. Excel allows value of accuracy much more than 0.01 (maximal accuracy can be set to 0.0000001).

To solve implicit Colebrook equation using Excel, 'Office button' in the left corner at the top of the screen has to be pressed and then in 'Excel options' in sheet 'Formulas', box 'Enable iterative calculation' has to be marked. Finally maximum number of iterations (max. allowed is 32767) have to be chosen. Also maximal change allowed between two successive iterations has to be set.

When the Darcy's friction factor is finally calculated using Colebrook's equation, it has to be put in general steady-state gas flow equation (5).

## 3. Looped gas pipeline calculations

All methods for looped gas pipeline calculations assume equilibrium among pressure and friction forces in steady and incompressible flow. As a result, they cannot be successfully used in unsteady and compressible flow calculations with large pressure drop where inertia force is important. Minor drop of pressure in the networks for gaseous fluid distribution enables to treat this fluid as incompressible, i.e. as water. Of course, some different approach must exist, but problem is not much different. Since, the resistances in hydraulic networks depend on flow, problem is not linear like in electric circuits, and iterative procedure must be used.

To solve flow distribution problem in the looped pipeline shown in figure 3, maximal consumption for each node including one of more inlet nodes has to be determined. In figure 3 inlet nodes are 1 (through pipe 20) and 5 (through pipe 21) with inlet rates shown also in Figure 3. Four outlet nodes also exist in the example network from Figure 3 and these nodes are 4, 6, 9 and 11.

All other nodes are neither inlet nor outlet nodes. First assumed flows are chosen to satisfy first

Kirchhoff's law (11). Pipe diameters and node input and output cannot be changed during the iterative procedure. Goal is to find final flow distribution for pipeline system (Figure 3). Second Kirchhoff's law has to be satisfied with demanded accuracy at the end of calculation (12), i.e. $L_{\{x\}} \approx 0$.

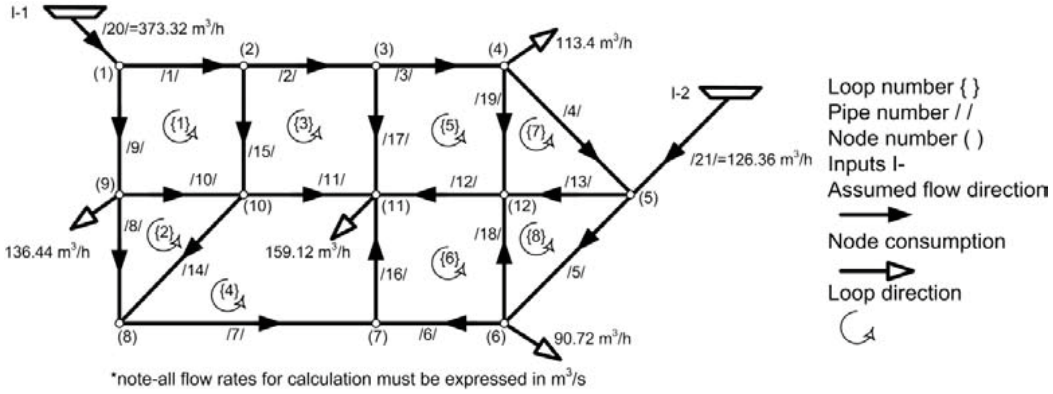


*Fig. 3. Example of looped gas distributive pipeline network*

$$
\left.\begin{array}{ll}
-Q_{/1/}-Q_{/9/}+Q_{(1)-input}=0 & node_{(1)}\\
Q_{/1/}-Q_{/2/}-Q_{/15/}=0 & node_{(2)}\\
Q_{/2/}-Q_{/3/}-Q_{/17/}=0 & node_{(3)}\\
Q_{/3/}-Q_{/4/}-Q_{/19/}-Q_{(4)-output}=0 & node_{(4)}\\
Q_{/4/}-Q_{/5/}-Q_{/13/}+Q_{(5)-input}=0 & node_{(5)}\\
Q_{/5/}-Q_{/6/}-Q_{/18/}-Q_{(6)-output}=0 & node_{(6)}\\
Q_{/6/}+Q_{/7/}-Q_{/16/}=0 & node_{(7)}\\
-Q_{/7/}+Q_{/8/}+Q_{/14/}=0 & node_{(8)}\\
-Q_{/8/}+Q_{/9/}-Q_{/10/}-Q_{(9)-output}=0 & node_{(9)}\\
Q_{/10/}-Q_{/11/}-Q_{/14/}+Q_{/15/}=0 & node_{(10)}\\
Q_{/11/}+Q_{/12/}+Q_{/16/}+Q_{/17/}-Q_{(11)-output}=0 & node_{(11)}\\
-Q_{/12/}+Q_{/13/}+Q_{/18/}+Q_{/19/}=0 & node_{(12)}-\mathrm{ref.}
\end{array}\right\} \quad (11)
$$

$$
\left.\begin{array}{ll}
-C_{/1/}+C_{/9/}+C_{/10/}-C_{/15/}=L_{\{1\}} & Loop_{\{1\}}\\
C_{/8/}-C_{/14/}-C_{/10/}=L_{\{2\}} & Loop_{\{2\}}\\
C_{/2/}+C_{/15/}+C_{/11/}-C_{/17/}=L_{\{3\}} & Loop_{\{3\}}\\
-C_{/11/}+C_{/14/}+C_{/7/}+C_{/16/}=L_{\{4\}} & Loop_{\{4\}}\\
-C_{/3/}+C_{/17/}-C_{/12/}-C_{/19/}=L_{\{5\}} & Loop_{\{5\}}\\
-C_{/6/}+C_{/12/}-C_{/16/}+C_{/18/}=L_{\{6\}} & Loop_{\{6\}}\\
-C_{/4/}+C_{/19/}-C_{/13/}=L_{\{7\}} & Loop_{\{7\}}\\
C_{/13/}-C_{/18/}-C_{/5/}=L_{\{8\}} & Loop_{\{8\}}
\end{array}\right\} \quad (12)
$$

$$
\begin{bmatrix}
L'_{\{1\}} & -\frac{\partial C(Q)_{/10/}}{\partial Q_{\{1\}}} & -\frac{\partial C(Q)_{/15/}}{\partial Q_{\{1\}}} & 0 & 0 & 0 & 0 & 0\\
-\frac{\partial C(Q)_{/10/}}{\partial Q_{\{2\}}} & L'_{\{2\}} & 0 & -\frac{\partial C(Q)_{/14/}}{\partial Q_{\{2\}}} & 0 & 0 & 0 & 0\\
-\frac{\partial C(Q)_{/10/}}{\partial Q_{\{3\}}} & 0 & L'_{\{3\}} & -\frac{\partial C(Q)_{/11/}}{\partial Q_{\{3\}}} & -\frac{\partial C(Q)_{/17/}}{\partial Q_{\{3\}}} & 0 & 0 & 0\\
0 & -\frac{\partial C(Q)_{/14/}}{\partial Q_{\{4\}}} & -\frac{\partial C(Q)_{/11/}}{\partial Q_{\{4\}}} & L'_{\{4\}} & 0 & -\frac{\partial C(Q)_{/16/}}{\partial Q_{\{4\}}} & 0 & 0\\
0 & 0 & -\frac{\partial C(Q)_{/17/}}{\partial Q_{\{3\}}} & 0 & L'_{\{5\}} & -\frac{\partial C(Q)_{/12/}}{\partial Q_{\{5\}}} & -\frac{\partial C(Q)_{/19/}}{\partial Q_{\{5\}}} & 0\\
0 & 0 & 0 & -\frac{\partial C(Q)_{/16/}}{\partial Q_{\{6\}}} & -\frac{\partial C(Q)_{/12/}}{\partial Q_{\{6\}}} & L'_{\{6\}} & 0 & -\frac{\partial C(Q)_{/18/}}{\partial Q_{\{6\}}}\\
0 & 0 & 0 & 0 & -\frac{\partial C(Q)_{/19/}}{\partial Q_{\{7\}}} & 0 & L'_{\{7\}} & -\frac{\partial C(Q)_{/13/}}{\partial Q_{\{7\}}}\\
0 & 0 & 0 & 0 & 0 & -\frac{\partial C(Q)_{/18/}}{\partial Q_{\{8\}}} & -\frac{\partial C(Q)_{/13/}}{\partial Q_{\{8\}}} & L'_{\{8\}}
\end{bmatrix}
x
\begin{bmatrix}
\Delta Q_{\{1\}}\\ \Delta Q_{\{2\}}\\ \Delta Q_{\{3\}}\\ \Delta Q_{\{4\}}\\ \Delta Q_{\{5\}}\\ \Delta Q_{\{6\}}\\ \Delta Q_{\{7\}}\\ \Delta Q_{\{8\}}
\end{bmatrix}
=
\begin{bmatrix}
L_{\{1\}}\\ L_{\{2\}}\\ L_{\{3\}}\\ L_{\{4\}}\\ L_{\{5\}}\\ L_{\{6\}}\\ L_{\{7\}}\\ L_{\{8\}}
\end{bmatrix}
\quad (13)
$$

### 3.1. The improved Hardy Cross method

Hardy Cross iterative method with its modification by Epp and Fowler [8] today is widely used for calculation of fluid flow through pipes or related pipe diameters in loops-like distribution networks of conduits with known node fluid consumptions. Original Hardy Cross method is a sort of single adjustment methods in which equations are treated one by one, while the improved version treats whole system of equations simultaneously. In both version of the Hardy Cross method, results of calculation per iterations is correction of flow $\Delta Q$ rather than flow Q (in optimization problem, results of calculation per iterations is correction of pipe diameter rather than diameter). These corrections (13) should be added to or subtracted from flow (or diameter in inverse problem) calculated in previous iteration using some kind of complex algebraic rules [9].

These rules can be implemented in a MS Excel spreadsheet. Lack of space prevents here detail discussion on these rules.

### 3.2. The node-loop method

The node matrix with all nodes included is not linearly independent [10]. To obtain linear independence any row of the node matrix [N] has to be omitted (15). No information on the topology in that way will be lost. Node 12 will be noted as referential and hence will be virtually omitted from the calculation. For the node-loop method, matrix [V] (14) and the node-loop matrix [NL] are formed to unite both, the node matrix [N] (15) and the loop matrix [L] (16). First eleven rows in [NL] matrix are from the first Kirchhoff's law (matrix [N]), and next eight rows are from the second Kirchhoff's law (matrix [L]) where each term is multiplied with first derivative (for each pipe) of C where Q is treated as variable.

$$[V]=\begin{bmatrix}
-\left|Q_{(1)-input}\right| \\
0 \\
0 \\
\left|Q_{(4)-output}\right| \\
-\left|Q_{(5)-input}\right| \\
\left|Q_{(6)-output}\right| \\
0 \\
0 \\
\left|Q_{(9)-output}\right| \\
0 \\
\left|Q_{(11)-output}\right| \\
-L_1+\left(\left|C'_{/1/}\right|\cdot Q_{/1/}+\left|C'_{/9/}\right|\cdot Q_{/9/}+\left|C'_{/10/}\right|\cdot Q_{/10/}+\left|C'_{/15/}\right|\cdot Q_{/15/}\right) \\
-C_2+\left(\left|C'_{/8/}\right|\cdot Q_{/8/}+\left|C'_{/10/}\right|\cdot Q_{/10/}+\left|C'_{/14/}\right|\cdot Q_{/14/}\right) \\
-L_3+\left(\left|C'_{/2/}\right|\cdot Q_{/2/}+\left|C'_{/11/}\right|\cdot Q_{/11/}+\left|C'_{/15/}\right|\cdot Q_{/15/}+\left|C'_{/17/}\right|\cdot Q_{/17/}\right) \\
-L_4+\left(\left|C'_{/7/}\right|\cdot Q_{/7/}+\left|C'_{/11/}\right|\cdot Q_{/11/}+\left|C'_{/14/}\right|\cdot Q_{/14/}+\left|C'_{/16/}\right|\cdot Q_{/16/}\right) \\
-L_5+\left(\left|C'_{/3/}\right|\cdot Q_{/3/}+\left|C'_{/12/}\right|\cdot Q_{/12/}+\left|C'_{/17/}\right|\cdot Q_{/17/}+\left|C'_{/19/}\right|\cdot Q_{/19/}\right) \\
-L_6+\left(\left|C'_{/6/}\right|\cdot Q_{/6/}+\left|C'_{/12/}\right|\cdot Q_{/12/}+\left|C'_{/16/}\right|\cdot Q_{/16/}+\left|C'_{/18/}\right|\cdot Q_{/18/}\right) \\
-L_7+\left(\left|C'_{/4/}\right|\cdot Q_{/4/}+\left|C'_{/13/}\right|\cdot Q_{/13/}+\left|C'_{/19/}\right|\cdot Q_{/19/}\right) \\
-L_8+\left(\left|C'_{/5/}\right|\cdot Q_{/5/}+\left|C'_{/13/}\right|\cdot Q_{/13/}+\left|C'_{/18/}\right|\cdot Q_{/18/}\right)
\end{bmatrix}, \tag{14}$$

$$[N]=\begin{bmatrix}
-1 & 0 & 0 & 0 & 0 & 0 & 0 & 0 & -1 & 0 & 0 & 0 & 0 & 0 & 0 & 0 & 0 & 0 & 0 \\
1 & -1 & 0 & 0 & 0 & 0 & 0 & 0 & 0 & 0 & 0 & 0 & 0 & 0 & -1 & 0 & 0 & 0 & 0 \\
0 & 1 & -1 & 0 & 0 & 0 & 0 & 0 & 0 & 0 & 0 & 0 & 0 & 0 & 0 & 0 & -1 & 0 & 0 \\
0 & 0 & 1 & -1 & 0 & 0 & 0 & 0 & 0 & 0 & 0 & 0 & 0 & 0 & 0 & 0 & 0 & 0 & -1 \\
0 & 0 & 0 & 1 & -1 & 0 & 0 & 0 & 0 & 0 & 0 & 0 & -1 & 0 & 0 & 0 & 0 & 0 & 0 \\
0 & 0 & 0 & 0 & 1 & -1 & 0 & 0 & 0 & 0 & 0 & 0 & 0 & 0 & 0 & 0 & 0 & -1 & 0 \\
0 & 0 & 0 & 0 & 0 & 1 & 1 & 0 & 0 & 0 & 0 & 0 & 0 & 0 & 0 & -1 & 0 & 0 & 0 \\
0 & 0 & 0 & 0 & 0 & 0 & -1 & 1 & 0 & 0 & 0 & 0 & 0 & 1 & 0 & 0 & 0 & 0 & 0 \\
0 & 0 & 0 & 0 & 0 & 0 & 0 & -1 & 1 & -1 & 0 & 0 & 0 & 0 & 0 & 0 & 0 & 0 & 0 \\
0 & 0 & 0 & 0 & 0 & 0 & 0 & 0 & 0 & 1 & -1 & 0 & 0 & -1 & 1 & 0 & 0 & 0 & 0 \\
0 & 0 & 0 & 0 & 0 & 0 & 0 & 0 & 0 & 0 & 1 & 1 & 0 & 0 & 0 & 1 & 1 & 0 & 0
\end{bmatrix} \tag{15}$$

$$[L]=\begin{bmatrix}
-1 & 0 & 0 & 0 & 0 & 0 & 0 & 0 & 1 & 1 & 0 & 0 & 0 & 0 & -1 & 0 & 0 & 0 & 0 \\
0 & 0 & 0 & 0 & 0 & 0 & 0 & 1 & 0 & -1 & 0 & 0 & 0 & -1 & 0 & 0 & 0 & 0 & 0 \\
0 & -1 & 0 & 0 & 0 & 0 & 0 & 0 & 0 & 0 & 1 & 0 & 0 & 1 & 0 & -1 & 0 & 0 & 0 \\
0 & 0 & 0 & 0 & 0 & 0 & 1 & 0 & 0 & 0 & -1 & 0 & 0 & 1 & 0 & 1 & 0 & 0 & 0 \\
0 & 0 & -1 & 0 & 0 & 0 & 0 & 0 & 0 & 0 & 0 & -1 & 0 & 0 & 0 & 0 & 1 & 0 & -1 \\
0 & 0 & 0 & 0 & 0 & -1 & 0 & 0 & 0 & 0 & 0 & 1 & 0 & 0 & 0 & -1 & 0 & 1 & 0 \\
0 & 0 & 0 & -1 & 0 & 0 & 0 & 0 & 0 & 0 & 0 & 0 & -1 & 0 & 0 & 0 & 0 & 0 & 1 \\
0 & 0 & 0 & 0 & -1 & 0 & 0 & 0 & 0 & 0 & 0 & 0 & 1 & 0 & 0 & 0 & 0 & -1 & 0
\end{bmatrix}, \tag{16}$$

Now, unknown flows can be calculated directly using (17):

$$[Q]=\text{inv}[NL]x[V], \quad (17)$$

## 4. Optimization problem

In previous text, flow distribution problem for e.g. plastic pipes is solved using (18):

$$\frac{\partial\left(p_1^2-p_2^2\right)}{\partial Q}=\frac{\partial C(Q)}{\partial Q}=\frac{\partial\left(\frac{4810\cdot Q_{st}^{1.82}\cdot L\cdot\rho_r}{D_{in}^{4.82}}\right)}{\partial Q}=, \quad (18)$$
$$=\frac{1.82\cdot 4810\cdot Q_{st}^{0.82}\cdot L\cdot\rho_r}{D_{in}^{4.82}}$$

In the problem of optimization of pipe diameters, flow is not any more treated as variable (19):

$$\frac{\partial\left(p_1^2-p_2^2\right)}{\partial D_{in}}=\frac{\partial C(D_{in})}{\partial D_{in}}=\frac{\partial\left(\frac{4810\cdot Q_{st}^{1.82}\cdot L\cdot\rho_r}{D_{in}^{4.82}}\right)}{\partial D_{in}}=, \quad (19)$$
$$=\frac{-4.82\cdot 4810\cdot Q_{st}^{1.82}\cdot L\cdot\rho_r}{D_{in}^{5.82}}$$

Of course, some other adaptations of previously shown methods should be done for optimization problem. As the diameters have to be chosen among a finite set of available nominal values, optimization problem is highly combinatorial.

## 5. Conclusions

Compared modified Hardy Cross method and the node loop method, taking as a criterion the number of iteration to achieve final results, both presented methods are equally good. For more complex networks, using the node-loop method, number of required iteration is smaller even compared with the modified Hardy Cross method. But main strength of the node-loop method lays in the fact that it does not require complex numerical scheme for algebraic addition of corrections in each of iterations. In the node-loop method, final results of each of the iterations are flows directly and not correction of flows. Both methods can be used for calculation of gas pipelines made with steel or plastic pipes using the appropriate equation according to discussion in this paper.

## Nomenclature

$p$ pressure, (Pa)
$L$ length of pipe, (m)
$D$ diameter of pipe, (m)
$Q$ flow ($m^3/s$)
$T$ temperature (K)
$z$ gas compressibility factor (-)
$M$ relative molecular mass (-)
$R$ universal gas constant = 8314.41 J/(kmol·K)

Greek symbols

$\varepsilon$ *inside pipe wall roughness (m)*
$\lambda$ *Darcy (Moody) friction factor or coefficient (-)*
$\rho$ *density ($kg/m^3$)*

Subscripts and superscripts

r relative
st standard ($T_{st}$=288.15 K, $p_{st}$=101325 Pa)
in inner

## References


[1] Coelho, P.M., and Pinho, C., 2007, Considerations about equations for steady state flow in natural gas pipelines, J. Braz. Soc. Mech. Sci. Eng., 29(3), pp. 262-273.

[2] Renouard, P., 1952, Nouvelle méthode pour le calcul des réseaux maillés de conduites de gaz, Communication au Congrès du Graz.

[3] Colebrook, C.F., 1939, Turbulent flow in pipes with particular reference to the transition region between the smooth and rough pipe laws, J. Inst. Civil. Eng. (London), 11(4), pp. 133-156.

[4] Colebrook, C.F., and White, C.M., 1937, Experiments with fluid friction in roughened pipes, Proc. Roy. Soc. Ser. A. Math. Phys. Sci., 161(906), pp. 367-381.

[5] Gregory, G.A., and Fogarasi, M., 1985, Alternate to standard friction factor equation, Oil Gas J., 83(13), pp. 120,125-127.

[6] Buzzelli, D., 2008, Calculating friction in one step, Machine Design, 80(12), pp. 54-55.

[7] Brkić, D., 2010, An explicit approximation of the Colebrook equation for fluid flow friction factor, Petrol. Sci. Technol., in press.

[8] Epp, R., and Fowler, A.G., 1970, Efficient code for steady flows in networks, J. Hydraul. Div. ASCE, 96(1), pp. 43-56.

[9] Brkić, D., 2009, An improvement of Hardy Cross method applied on looped spatial natural gas distribution networks, Appl. Energ., 86(7-8), pp. 1290-1300.

[10] Wood, D.J., and Charles, C.O.A., 1972, Hydraulic network analysis using linear theory, J. Hydraul. Div. ASCE, 98(7), pp. 1157-1170.

# The Importance of Coupling between Thermal and Molar Fluxes in a Nitrogen-Oxygen Distillation Column

*L.V. van der Ham* [a] *and S. Kjelstrup* [a,b]

[a] *Department of Chemistry, Norwegian University of Science and Technology, N-7491 Trondheim, Norway*
[b] *Department of Process and Energy, Delft University of Technology, 2628 CA Delft, The Netherlands*

**Abstract:** A model for the transfer of mass and thermal energy in a vapour-liquid region is used to investigate the influence of neglecting coupling on the transfer rates. As an example, we studied a nitrogen-oxygen distillation column. Using a combination of stage and point boundary conditions, a nitrogen transfer profile is obtained that shows the same trend as a profile based on an equilibrium stage distillation model. The distribution of the total transfer over the two column halves is not in agreement, however. This disagreement can be expected to decrease when the dependency of the vapour film thickness on the vapour flow rate and the vapour viscosity is included in the model. The effect of neglecting coupling on the calculated transfer rates changes along the length of the column. The total effect is considerable and should be taken into account in models for the transfer of mass and thermal energy through an interface.

**Keywords:** Distillation, Heat transfer, Irreversible thermodynamics, Mass transfer.

## 1. Introduction

The energy and exergy efficiencies of conventional distillation columns can be increased by distributing the thermal energy addition and removal over the entire length of the column, instead of concentrating it at the top and the bottom [6]. When optimizing the efficiencies of such columns, it is essential to model the thermal energy flows inside the column as accurately as possible. According to the theory of irreversible thermodynamics, a thermal flux is not only dependent on a temperature difference, but also on concentration differences [2]. In general, each flux is a linear combination of all driving forces. Current non-equilibrium distillation models do not explicitly include the coupling between thermal and mass fluxes [7]. Using an ethanol-water distillation column as case study, [3] showed that coupling can have a considerable effect. This is confirmed by a recent study [8] based on a single point in a cryogenic nitrogen-oxygen column.

### 1.1. Objectives

The aim of the current work is to gain more insight into the influence of coupling between thermal and mass fluxes on the calculated transfer rates in a nitrogen-oxygen distillation column. We investigate how this influence changes along the length of the column. We also provide more premises on the thermodynamic description of the transfer of mass and thermal energy through an interface.

## 2. Model of the interface region

The model we use to characterise the coupled transfer of mass and thermal energy in a vapour-liquid region is described in [8]. In this model, the interface region consists of an interface layer in between a liquid and a vapour film. Both the liquid and the vapour film can be represented by multiple control volumes, but the interface is always given by a single control volume. Figure 1 gives a schematic representation of a system consisting of five control volumes. Using a matrix of total resistivity coefficients, the model can be used to calculate the thermal and molar fluxes for a given set of boundary conditions, or driving forces. This section elaborates on the model formulation that was chosen in [8].

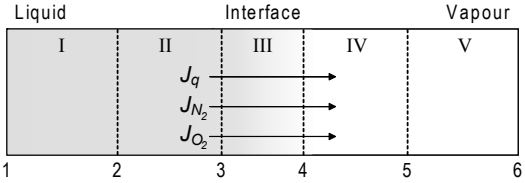


*Figure 1: Schematic of the system consisting of five control volumes: two liquid volumes (I and II), the vapour-liquid interface (III) and two vapour volumes (IV and V). Point 1 is the liquid boundary of the system and point 6 is its vapour boundary.*

### 2.1. Choosing the set of fluxes and forces

The basis of the model is an expression for the local entropy production $\sigma$ of a control volume that is located between points $a$ and $b$. According to the theory of irreversible thermodynamics, the local entropy production is given by the product-sum of conjugate fluxes and driving forces. Different sets of fluxes and driving forces can be used. Reference [1] describes two possible sets for a system with only thermal and molar fluxes. One can choose to use the total heat flux $J_q$ in combination with the chemical potentials $\mu_j$ divided by temperature $T$, as shown in 1, or one can use the measurable heat flux $J'_q$ in combination with the chemical potentials, evaluated at a constant temperature, divided by the temperature, as shown in 2 and 3.

Corresponding author: S. Kjelstrup, Email: signe.kjelstrup@chem.ntnu.no

$$\sigma = J_q \left( \Delta_{ab} \frac{1}{T} \right) + \sum_{j=1}^{n} J_j \left( -\Delta_{ab} \frac{\mu_j}{T} \right) \quad (1)$$

$$\sigma = J'_{q,b} \left( \Delta_{ab} \frac{1}{T} \right) + \sum_{j=1}^{n} J_j \left( -\frac{\Delta_{ab} \mu_j (T_a)}{T_a} \right) \quad (2)$$

$$\sigma = J'_{q,a} \left( \Delta_{ab} \frac{1}{T} \right) + \sum_{j=1}^{n} J_j \left( -\frac{\Delta_{ab} \mu_j (T_b)}{T_b} \right) \quad (3)$$

From a theoretical perspective, the three sets of fluxes and forces are equivalent. But from a practical perspective, there are some clear differences. The measurable heat flux, also known as the sensible heat flux, is a quantity that can be measured in practice. Experimental values for resistivities are always related to the measurable heat flux. The measurable and total heat fluxes are related to each other via the partial molar enthalpies $H_j$ multiplied with the molar fluxes $J_j$:

$$J_q = J'_q + \sum_{j=1}^{n} H_j J_j \quad (4)$$

In practice we rather calculate enthalpy differences, or relative enthalpies, than absolute enthalpies. It is therefore very hard to link the total heat flux to practical situations. Similar to the enthalpy, we also rather calculate chemical potential differences than absolute chemical potentials. The driving forces in 2 and 3 are therefore more practical to use than the ones in 1. These are three reasons to favour the measurable heat flux formulation over the total heat flux formulation.

The system consists of at least three control volumes: one liquid control volume, one interface control volume and one vapour control volume. In [8] it was found that more control volumes should be used to describe the liquid and vapour films. The driving forces and fluxes in a control volume can be gathered by a driving force vector and a flux vector. The driving force vector of each control volume is then given by the product of a resistivity matrix and the flux vector. The sum of the driving force vectors of all control volumes yields the total driving force vector of the system. If the flux vector is exactly the same in all control volumes, which means that the fluxes are constant throughout the system, it is straightforward to calculate them once the total resistivity matrix is known. The differences in chemical potential divided by temperature can be summed directly. But this is not possible for the differences in chemical potential evaluated in 2 and 3, because they are all evaluated at different constant temperatures. At steady state, the total heat flux is constant throughout the system, similar to the molar fluxes. But the measurable heat flux is not constant. These are two reasons to favour the total heat flux formulation over the measurable heat flux formulation.

Instead of selecting one of these two formulations, a new formulation is introduced that uses the measurable heat flux at a certain reference location $J'_{q,0}$ and evaluates all chemical potential differences at a certain reference temperature $T_0$. The choice of using such reference points must be compensated for in the resistivity matrix of the control volume. Replacing the measurable heat flux at one location by the measurable heat flux at another location can be done using the energy balance.

## 2.2. Assuming constant enthalpy

In order to replace a chemical potential difference at one temperature by a chemical potential difference at another temperature, we need to make an assumption. We start by rewriting the difference in chemical potential divided by temperature in terms of a chemical potential difference at a constant temperature $T_a$:

$$\begin{aligned} -\Delta_{ab}\left(\frac{\mu_j}{T}\right) &= -\left(\frac{\mu_j\left(T_b, x_{j,b}\right)}{T_b} - \frac{\mu_j\left(T_a, x_{j,a}\right)}{T_a}\right) \quad (5) \\ &= -\left(\frac{\mu_j\left(T_a, x_{j,b}\right)}{T_a} - \frac{\mu_j\left(T_a, x_{j,a}\right)}{T_a}\right) \\ &\quad + \frac{\mu_j\left(T_a, x_{j,b}\right)}{T_a} - \frac{\mu_j\left(T_b, x_{j,b}\right)}{T_b} \\ &= -\frac{\Delta_{ab}\mu_{j,T_a}}{T_a} + \int_{T_a}^{T_b} \frac{d}{dT}\left(\frac{\mu_{j,x_{j,b}}}{T}\right) dT \end{aligned}$$

The partial derivative of the chemical potential divided by temperature with respect to temperature is given by the Gibbs-Helmholtz equation:

$$\frac{d}{dT}\left(\frac{\mu_j}{T}\right) = \frac{H_j}{T^2} \quad (6)$$

The partial enthalpy is a function of temperature. Including this temperature dependency into the equations will eventually result into third order temperature difference terms in the entropy production expression. The theory of irreversible thermodynamics only uses terms up to the second order. So in order to avoid introducing any third order term, we assume that the partial enthalpies are independent of temperature within the control volume we are considering. If we introduce 6 into 5 with this in mind we obtain:

$$-\Delta_{ab}\left(\frac{\mu_j}{T}\right) = -\frac{\Delta_{ab}\mu_{j,T_a}}{T_a} - H_{j,x_{j,b}}\Delta_{ab}\frac{1}{T} \quad (7)$$

Instead of going to an expression containing the chemical potential at constant temperature $T_a$, we can also go to an expression at constant temperature $T_b$. The difference between the expressions for the two constant temperatures is the composition at which the partial enthalpy is evaluated. Equation 7 will be used to obtain an expression for going directly from one constant temperature to another:

$$-\frac{\Delta_{ab}\mu_{j,T_b}}{T_b} = -\frac{\Delta_{ab}\mu_{j,T_a}}{T_a} - \Delta_{ab}H_j\Delta_{ab}\frac{1}{T} \quad (8)$$

Although the partial enthalpies are considered to be independent of temperature within the control volume, we still need to choose at which constant temperature we evaluate them. They should all be calculated at the same constant temperature.

### 2.3. Formulae for total resistivities

Using the measurable heat flux at the vapour boundary $J'_{q,v}$ and the temperature at the liquid boundary $T_l$ as references and using 8, we can write the force-flux relations for a control volume:

$$\Delta_{ab}\frac{1}{T} = r^{ab}_{qq}J'_{q,v} + \sum_{j=1}^{n}\left(r^{ab}_{qj} + r^{ab}_{qq}\Delta_{vb}H_j\right)J_j \qquad (9)$$

$$-\frac{\Delta_{ab}\mu_i\left(T_l\right)}{T_l} = r^{ab}_{iq}J'_{q,v} + \sum_{j=1}^{n}\left(r^{ab}_{ij} + r^{ab}_{iq}\Delta_{vb}H_j\right)J_j + \Delta_{ab}H_i\Delta_{la}\frac{1}{T} \qquad (10)$$

Here, $r^{ab}_{mn}$ represents the resistivity in the control volume between points $a$ and $b$ that is coupling driving force $m$ with flux $n$, where $m, n \in q, i, j$. The subscript $q$ indicates the thermal driving force or flux, and the superscripts $i$ and $j$ indicate component driving forces or fluxes. The resistivity $r_{qq}$ is related to the thermal conductivity, the resistivities $r_{ij} = r_{ji}$, $r_{ii}$, and $r_{jj}$ are related to diffusion, and the resistivities $r_{iq} = r_{qi}$ and $r_{jq} = r_{qj}$ are related to the coupling between thermal and component fluxes, also known as the Soret and Dufour effects.

References [3] and [1] give formulae for the total resistivities of a system that consists of three connected control volumnes. Reference [8] shows how force-flux relations 9 and 10 can be used to derive general formulae for the total resistivities of a system consisting of a series of $m$ connected control volumes:

$$r^{tot}_{qq} = \sum_{k=1}^{m} r^{k}_{qq} \qquad (11)$$

$$r^{tot}_{qj} = r^{tot}_{jq} = \sum_{k=1}^{m} r^{k}_{qj} + r^{k}_{qq}\Delta_{k_v v}H_j \qquad (12)$$

$$r^{tot}_{ij} = r^{tot}_{ji} = \sum_{k=1}^{m} r^{k}_{ij} + r^{k}_{iq}\Delta_{k_v v}H_j + r^{k}_{qj}\Delta_{k_v v}H_i + r^{k}_{qq}\Delta_{k_v v}H_j\Delta_{k_v v}H_i \qquad (13)$$

Where $\Delta_{k_v v}$ indicates the difference between the vapour boundary of the system and the boundary of control volume $k$ that is closest to the system vapour boundary.

## 3. Calculations

The routine described in [8] allows the calculation of values for the molar fluxes and the measurable heat flux when the conditions at the liquid and vapour boundaries of the system are known. A thermodynamically consistent solution is found by requiring the entropy productions calculated using both irreversible thermodynamics and the entropy balance to be equal. This requirement is used to find the liquid film thickness for a fixed vapour film thickness. All calculations reported in this work were done using this calculation routine.

Reference [8] discussed in detail how to calculate all relevant resistivities. The influence of inaccuracies in their values on the calculation results was described in a sensitivity analysis. The influence of the number of control volumes per film, of the interface resistances, of the chosen vapour film thickness and of the order of the control volumes was also investigated. In the current study we always: used a minimum of 32 control volumes per film, included the interface resistances, used a vapour film thickness of $5\times10^{-4}$ m and described the system from the liquid to the vapour boundary.

### 3.1. Distillation column design

Reference [8] discussed the influence of coupling between thermal and mass fluxes on the transfer rates in a nitrogen-oxygen mixture at one single point in a distillation column. In this work, we investigated how this influence changes along the length of the distillation column. In order to obtain sets of boundary conditions that represent positions along the entire length of the column, we started by defining a base case distillation column design.

#### 3.1.1. Column specifications

The distillation column design we used as base case is separating a binary nitrogen-oxygen mixture with a nitrogen mole fraction of 0.80 into products with purities of 0.99. The feed and the top product are vapours at their dew points and the bottom product is a liquid at its bubble point. It is assumed that the column operates at a constant pressure of 1.4 bar. The total number of stages is 18, excluding reboiler and total condenser. At stage 11, counting from top to bottom, a feed with a flow rate of 1 mol/s enters the column. An equilibrium stage model was used to simulate the column; it was solved using the bubble point method as described in [5]. A high accuracy thermodynamic model was used to calculate the required thermodynamic properties; it is described in [4]. This model was used for all thermodynamic calculations that were done in this work.

#### 3.1.2. Column profiles

Table 1 gives an overview of how the characteristic column properties change along the length of the column. The temperature, liquid mole fraction $x$, vapour mole fraction $y$, liquid flow rate $L$ and vapour flow rate $V$ are given as function of the stage number $n$. The condenser and reboiler are represented by stage numbers $C$ and $R$.

#### 3.1.3. Stage and point boundary conditions

The point in the distillation column that was used as base case in [8] was defined by calculating average temperatures and mole fractions for a certain stage. The considered stage was located around the centre of the top part of the column, which corresponds to a position in between stages 5 and 6 in the column that was used in this work.

*Table 1: Column profiles of the temperature, the nitrogen mole fractions, the liquid flow and the vapour flow.*

| $n$ (-) | $T$ (K) | $x_{N_2}$ (-) | $y_{N_2}$ (-) | $L$ (mol/s) | $V$ (mol/s) |
|---|---|---|---|---|---|
| $C$ | 80.28 | 0.9900 | – | 0.639 | – |
| 1 | 80.45 | 0.9652 | 0.9900 | 0.634 | 1.445 |
| 2 | 80.72 | 0.9289 | 0.9791 | 0.627 | 1.440 |
| 3 | 81.09 | 0.8793 | 0.9633 | 0.618 | 1.433 |
| 4 | 81.57 | 0.8174 | 0.9420 | 0.607 | 1.424 |
| 5 | 82.13 | 0.7485 | 0.9159 | 0.595 | 1.413 |
| 6 | 82.72 | 0.6812 | 0.8874 | 0.585 | 1.401 |
| 7 | 83.25 | 0.6237 | 0.8602 | 0.576 | 1.391 |
| 8 | 83.68 | 0.5798 | 0.8373 | 0.570 | 1.382 |
| 9 | 83.99 | 0.5492 | 0.8201 | 0.565 | 1.376 |
| 10 | 84.20 | 0.5291 | 0.8082 | 0.563 | 1.372 |
| 11 | 84.34 | 0.5165 | 0.8005 | 0.561 | 1.369 |
| 12 | 84.62 | 0.4907 | 0.7839 | 0.558 | 0.367 |
| 13 | 85.23 | 0.4380 | 0.7468 | 0.551 | 0.364 |
| 14 | 86.39 | 0.3478 | 0.6702 | 0.541 | 0.357 |
| 15 | 88.17 | 0.2322 | 0.5363 | 0.530 | 0.347 |
| 16 | 90.15 | 0.1290 | 0.3603 | 0.523 | 0.337 |
| 17 | 91.71 | 0.0618 | 0.1991 | 0.519 | 0.329 |
| 18 | 92.64 | 0.0265 | 0.0926 | 0.517 | 0.325 |
| $R$ | 93.11 | 0.0100 | 0.0364 | 0.194 | 0.323 |

The vapour and liquid boundary conditions based on stage $n$ can be calculated using the following formula:

$$T_l^{n,s} = \left(T^{n-1} + T^n\right)/2 \quad (14)$$

$$T_v^{n,s} = \left(T^n + T^{n+1}\right)/2 \quad (15)$$

$$x_{N_2}^{n,s} = \left(x_{N_2}^{n-1} + x_{N_2}^n\right)/2 \quad (16)$$

$$y_{N_2}^{n,s} = \left(y_{N_2}^n + y_{N_2}^{n+1}\right)/2 \quad (17)$$

Instead of using boundary conditions based on average stage values, it is also possible to select boundary conditions based on the point in between two stages. In a packed column, the liquid flowing down from a stage meets the vapour rising up from the stage below at this point. These point boundary conditions are given by:

$$T_l^{n,p} = T^{n-1} \quad (18)$$

$$T_v^{n,p} = T^n \quad (19)$$

$$x_{N_2}^{n,p} = x_{N_2}^{n-1} \quad (20)$$

$$y_{N_2}^{n,p} = y_{N_2}^n \quad (21)$$

Using the column design presented in this section, it is possible to calculate 18 sets of stage boundary conditions. Because the points above stage 1 and below stage 18 can also be used as a set of boundary conditions, there exist 19 sets of point boundary conditions. When plotted as function of position in the column, each of the stage boundary conditions is located in between two point boundary conditions.

# 4. Results and discussion

## 4.1. Nitrogen flux profile

Using the temperature and mole fraction data given in Table 1 and using 14-21, 37 sets of system boundary conditions have been determined. Each of these sets has been used as input to the calculation model for coupled transfer of mass and thermal energy. Figure 2 gives an overview of the calculated nitrogen fluxes as function of position in the column.

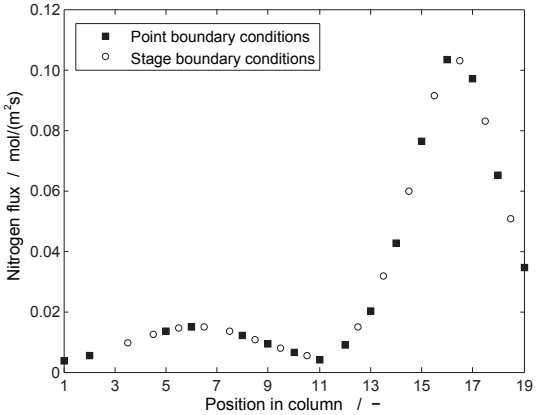


*Figure 2: Comparison between the calculated nitrogen flux as function of the position in the column for both point and stage boundary conditions.*

Only the profile of the nitrogen flux is shown in Fig. 2; the profiles of the other fluxes and of the entropy production are comparable. Although we used 37 sets of boundary conditions as input, the figure contains only 31 data points. It proved impossible to find a liquid film thickness that yielded a thermodynamically consistent system for the other 6 sets of boundary conditions.
There can be different reasons why it might be impossible to solve the model for some specific cases. It might be caused by the fixed vapour film thickness we use, or it could be related to possible inaccuracies in the calculated resistivities. It can also be related to the fact that we are using boundary conditions originating from an equilibrium stage model as input to our rather rate-based like model. At the moment we do not have sufficient understanding to predict beforehand which cases are impossible to solve.
The data points from the two different types of boundary conditions are very well in agreement with each other. The combination of the two gives a good representation of how the calculated nitrogen flux changes along the entire length of the column.

## 4.2. Nitrogen transfer profiles

Based on the mole fraction and flow data in Table 1, it is possible to calculate how much nitrogen is transferred on each of the stages. It does not make any sense to make a direct comparison between the amounts of transferred nitrogen and the calculated nitrogen fluxes shown in Fig. 2. The calculated fluxes are values at a single point and they

are given per amount of interfacial area, while the transferred amounts are the totals of complete stages. But if we assume that the interfacial area is constant along the length of the column and express the fluxes and transferred amounts as percentages of their column averages, we can still compare how the two quantities change along the length of the column. This comparison is shown in Fig. 3.

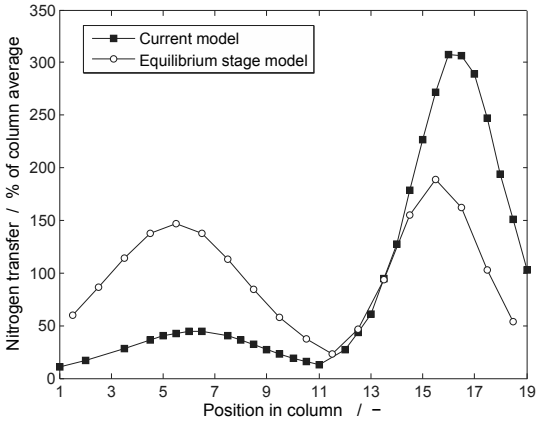


*Figure 3: Comparison between the nitrogen fluxes calculated with the model presented in this work and the total amounts of transferred nitrogen calculated from the equilibrium stage model.*

The comparison between the two nitrogen transfer profiles shows that they follow the same trend; both have a minimum around the feed stage and maxima around the centres of the top and bottom parts. But the relative magnitudes of the two maxima are different. The maxima are comparable in the equilibrium stage model profile. But in the profile based on the calculations done in this work, the bottom part maximum is almost seven times bigger than the top part maximum. A part of this difference can be related to the constant vapour film thickness that we have used in our calculations. An increase in the vapour film thickness would translate into an increase in the total resistivities, which means that a fixed set of boundary conditions yields smaller fluxes.

There are two reasons why we expect the vapour film thickness to be larger in the bottom part of the column. The first one is related to the vapour flow rates in the column. As can be seen in Table 1, the vapour flow rate is about four times larger in the top part of the column. A larger vapour flow rate corresponds to a larger superficial vapour velocity, which means a smaller vapour film thickness. The second reason is related to the viscosity of the vapour phase. When going from the top to the bottom of the column, the temperature and the oxygen fraction increase. Because oxygen has a higher viscosity than nitrogen and because the viscosity increases with an increasing temperature, the viscosity must be higher in the bottom part of the column. A higher vapour viscosity corresponds to a larger vapour film thickness. How much these two effects exactly affect the vapour film thickness should be investigated in future studies.

### 4.3. Neglecting coupling resistances

Similar to [8], we have investigated the effect of neglecting coupling between thermal and molar fluxes. This can be done by setting all control volume resistivities that couple a thermal and a molar flux equal to zero, while fixing the film thickness ratio at the value found for the coupled case. We have done this for all data points shown in Fig. 2 and calculated the relative differences between the fluxes obtained from uncoupled systems and the fluxes obtained from coupled systems. Table 2 gives the averages and standard deviations of these relative differences, summarizing the effect of neglecting coupling for the entire column.

*Table 2: The average and standard deviation of the influence that neglecting coupling resistances has on the different fluxes.*

| | $J_{N_2}$ | $J_{O_2}$ | $J'_{q,l}$ | $J'_{q,v}$ |
|---|---|---|---|---|
| Average (%) | 11 | −4.2 | −39 | −3.3 |
| Standard deviation (%) | 11 | 5.4 | 29 | 0.2 |

Similar to what was found in [8] for a single stage, the neglect of coupling mostly affects the nitrogen flux and the measurable heat flux at the liquid boundary. The column average values are lower than the values found for the single stage investigated in [8]. The standard deviations in the effects on the molar fluxes and on the measurable heat flux at the liquid boundary are of the order of their averages. There is no clear relation between these effects and the position in the column. The deviations are mainly caused by deviations in the liquid film thicknesses that were found. The vapour film thickness was fixed at the same value for all systems, which partly explains the relatively constant and small effect that neglecting coupling has on the measurable heat flux at the vapour boundary. Figure 4 shows how this effect changes along the length of the column.

The effect that neglecting coupling between thermal and molar fluxes has on the measurable heat flux at the vapour boundary is relatively constant along the length of the column. It increases slowly in the top part of the column, but towards the bottom of the column it starts decreasing. The thermal and molar fluxes are central variables in the minimization of entropy production in distillation columns.

## 5. Conclusions

Calculating fluxes from a combination of stage and point boundary conditions yields a consistent representation of how the fluxes vary along the length of the entire distillation column. The trend in the obtained nitrogen flux profile is similar to the one based on an equilibrium stage model, but the distribution of the nitrogen transfer over the two column halves does not agree. This disagreement can be partly explained by the use of a constant vapour

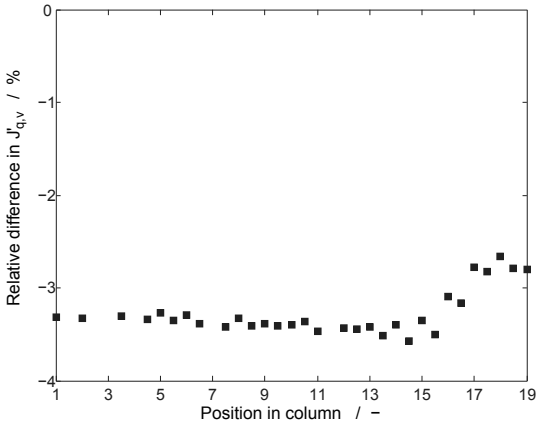


*Figure 4: Effect of neglecting coupling on the measurable heat flux at the vapour boundary, as function of the position in the column.*

film thickness. Including a dependency of the vapour film thickness on the vapour flow rate and viscosity is an important next step in the development of the model. The effect of neglecting coupling between thermal and mass fluxes on their calculated magnitudes is smaller when averaged for the entire column than it is for the single stage investigated earlier, but it is still considerable and should be considered in optimization studies.

## Nomenclature

$H_j$ partial molar enthalpy of component $j$, J/mol

$J_j$ molar flux of component $j$, mol/(s m$^2$)

$J_q$ total heat flux, J/(s m$^2$)

$J'_q$ measurable heat flux, J/(s m$^2$)

$L$ liquid flow rate, mol/s

$m$ number of control volumes, dimensionless

$r_{mn}$ resistivity coupling driving force $m$ with flux $n$, where $m, n \in q, N_2, O_2$

$S_j$ partial molar entropy of component $j$, J/(K mol)

$T$ temperature, K

$V$ vapour flow rate, mol/s

$x$ liquid mole fraction, dimensionless

$y$ vapour mole fraction, dimensionless

$\Delta_{ab}Y$ difference in property $Y$: $Y_b - Y_a$

### Greek Letters

$\mu_j$ chemical potential of component $j$, J/mol

$\sigma$ local entropy production, J/(K m$^2$)

### Subscripts and superscripts

0 reference point

$a, b$ location indices

$i, j$ component indices

$k$ control volume index

$l$ liquid

$n$ stage index

$N_2$ nitrogen

$O_2$ oxygen

$p$ point

$q$ thermal energy

$s$ stage

$tot$ total

$v$ vapour

## References

[1] D. Bedeaux and S. Kjelstrup. Irreversible thermodynamics - a tool to describe phase trasitions far from global equilibrium. *Chemical Engineering Science*, 59:109–118, 2004.

[2] S. Kjelstrup and D. Bedeaux. *Non-equilibrium thermodynamics of heterogeneous systems*. Series on Advances in Statistical Mechanics - Volume 16. World Scientific Publishing Co., Singapore, 2008.

[3] S. Kjelstrup and G.M. de Koeijer. Transport equations for distillation of ethanol and water from the entropy production rate. *Chemical Engineering Science*, 58:1147–1161, 2003.

[4] E.W. Lemmon et al. Thermodynamic properties of air and mixtures of nitrogen, argon, and oxygen from 60 to 2000 K at pressures to 2000 MPa. *Journal of Physical Chemistry*, 29(3):331–385, 2000.

[5] J.D. Seader and E.J. Henley. *Separation process principles*. John Wiley and Sons, Inc., New York, USA, 1998.

[6] A. Røsjorde and S. Kjelstrup. The second law optimal state of a diabatic binary tray distillation column. *Chemical Engineering Science*, 60:1199–1210, 2005.

[7] R. Taylor and R. Krishna. *Multicomponent mass transfer*. John Wiley and Sons, Inc., New York, USA, 1993.

[8] L.V. van der Ham, R. Bock, and S. Kjelstrup. Modelling the coupled transfer of mass and thermal energy in the vapour-liquid region of a nitrogen-oxygen mixture. *Chemical Engineering Science*, 65:2236–2248, 2010.

**Acknowledgments:** The research leading to these results has received funding from the European Community's 7th Framework Programme (FP7/2007-2013) under grant agreement number 211971 (The DECARBit project).

# Energetics aspects of the OEC in Natural Gas Confined Flames

*Alex Álisson Bandeira Santos*[a], *Ednildo Andrade Torres*[b], *Pedro Afonso de Paula Pereira*[b]

[a] *SENAI CIMATEC - Integrated Center of Manufacturing and Technology, Salvador, Brazil*
[b] *CiEnAm – Interdisciplinary Center of Energy and Environmental, Salvador, Brazil*

**Abstract:** The concept of environmental efficiency in equipments is increasingly in tariff with the unfolding of global warming, and, among the industrial equipments, the burners have a major impact in this discussion because it is an equipment of industrial combustion. Demand for environmentally more efficient burners, with the reduction of emissions is essential for the proper use of fossil fuels during the transition between this energy sources for alternatives energy, which can last more than fifty years.
This study evaluates experimentally the technique of oxygen enhanced combustion – OEC – and its interaction with the soot formation and thermal radiation in natural gas confined flames. The literature shows that works with OEC technique – technique that has important points for improving the thermal efficiency of combustion – cause under certain conditions the increase of soot formation. The soot as an important participant in the radiant heat transfer, it can, with its interaction with the OEC, bringing the increase in thermal efficiency of burners, implementing the heat transfer from the flame for heating areas, thereby reducing the consumption fuel, the temperature of flame, and, consequently, reduces the emission of NOx. In the experiment was used low enriched with oxygen, which does not require significant existing equipment changes. This technology can be an important tool for the adequacy of the industry in general, particularly in oil and gas, for the technological challenge of reducing global warming.

**Keywords:** Soot, Thermal Radiation, OEC, natural gas.

## 1. Introduction

Soot was defined as carbonaceous particulates formed in the gas phase of combustion processes [1]. They consist mainly of carbon, and contain up to 10% hydrogen on a molar basis. According to [2], soot formation and evolution proceeds in a four-step sequence: (i) formation of precursor species, (ii) soot particle inception, (iii) surface growth and particle agglomeration, and (iv) particle oxidation. The emission of soot from combustors, or from flames, results from the competition between soot formation and oxidation. Soot emission occurs when fuel is burnt in insufficient oxygen. The phenomenon of soot formation is still not fully explained due to the fact that the formation process is not slow enough to allow the precise observation of each step.

Oxygen enhanced combustion (OEC), mentioned by [3], can improve the combustion process by producing improved flame characteristics (larger inflammability limit, better ignition, stability and shape control); smaller combustion gas volumes; increased productivity and thermal efficiency (larger heat transfer process efficiency, improved product quality; fuel consumption reduction, raw material costs reduction, reduced costs of new equipment and possibly production increase in existing equipment).

Atmospheric air contains about 21% of oxygen in volume. Low levels of enrichment of the combustion air with oxygen, i.e. an $O_2$ index below 30%, are usually used in retrofit applications in which only small modifications to the existing equipment are necessary.

Data about soot, including the use of chemical additives to control its formation, has been obtained mostly from studies performed with elementary flames as in the present work. These flames are usually defined as either premixed, partially premixed, or non-premixed (diffusion) flames.

In a diffusion flame the reactants are initially separated, and reaction occurs only at the interface between the fuel and the oxidizer where mixing and reaction both take place. The addition of oxygen in diffusion flames can be carried out by direct addition to the fuel, or to the combustion air

Corresponding Author: Alex Álisson Bandeira Santos, Email: alex.santos@cimatec.fieb.org.br

in a burner with an annular, parallel or counterflow oxidizer.

The direct addition of oxygen to a methane diffusion flame has been studied by [4] and [5]. [6-9], and also [5] studied the addition to propane and butane diffusion flames. The addition of oxygen to ethane diffusion flames were studied [7-10]. The addition of oxygen to free turbulent diffusion acetylene flames over a wide range of velocities and nozzle sizes was evaluated [11].

Oxygen enhancement of the air side of a methane counterflow diffusion flame was studied [12]. They verified that with an increase in oxygen content in the oxidizer jet, soot formation was enhanced. The range of oxidizer oxygen content tested was 21% –100%. They also verified the influence of interaction among soot and NOx.

Literature about the addition of oxygen to combustion air in a burner with a parallel annular oxidizer flow includes [13-18].

The influence of the $O_2$ concentration in ethylene flames was studied [13]. The $O_2$ index was varied between 9 and 50% by the authors. They observed that soot formation reached a minimum at around 24%. This was explained by competition between fuel pyrolysis and soot oxidation in the process domain.

Lee et al. (2000) studied the influence of $O_2$ enrichment in laminar methane diffusion flames for conditions of 50 and 100% $O_2$. The authors found a reduction in soot production in both enrichment conditions with a larger reduction for 100% $O_2$.

The influence of $O_2$ enrichment on the air side of methane laminar diffusion flames also was examined, for 35, 50 and 100% $O_2$ [15]. The evaluation parameter was the integrated radial soot concentration. The authors observed a reduction in soot formation in all three situations, and predicted that soot concentration was smaller for flames with the larger $O_2$ index due to smaller flame lengths and consequently smaller residence time available for soot particle growth.

In [16] investigated the radiation intensity of a methane/oxygen flame in comparison with a methane/air flame. A laser-induced incandescence technique was used to visualize the instantaneous and average soot distribution in the flames. Different combinations of central or annular fuel-oxygen supplies were studied to find the best arrangement to increase the thermal radiation intensity. The results showed that an oxygen-enhanced inverse diffusion flame (when the diffusion direction is opposite to that in the normal diffusion flame, where fuel flows from the central tube into still air) was very effective in increasing thermal radiation compared to a normal oxygen diffusion flame. This happens due the increased soot production in the inverse oxygen diffusion flame. The authors also found a more uniform spatial distribution of soot in the methane/oxygen flames compared to methane/air flames.

Furthermore, in 2002 [17] studied the influence of the oxygen index on soot, radiation and NOx formation characteristics of turbulent jet flames for a range of oxygen indices from 21% (air) to 100% (pure $O_2$). The jet flame rig used in the experiments was designed to produce a vertical jet flame in a nearly quiescent air-oxygen coflow. The burner consisted of a 3 mm i.d. fuel tube centered in a 220 mm i.d. stainless steel flame chamber. Before entering the chamber, the air-oxygen oxidizer flow passed through a glass bead bed and a ceramic honeycomb producing a uniform, laminar coflow.

The oxidizer flow was 4 to 6 times the stoichiometric flow. The fuel-jet to oxidizer–coflow velocity ratios ranged from about 40 to 450. The combination of maintaining low coflow velocities and supplying in excess of the stoichiometric oxidizer requirements resulted in conditions close to a free flame. The fuel types used were natural gas, a methane/ethane blend, and propane.

The authors observed that soot quantities for all flames increased with the initial oxygen enhancement and then decreased as the oxygen content was further increased. The highest soot values occurred in the range of 30% to 40% oxygen index. As for the effect of the fuel type on the flame, the propane flame produced much more soot than the methane/ethane blend flame, which produced slightly more soot than the natural gas flame. The fuel jet velocity had a significant influence on soot formation and its dependence on oxygen index through residence time.

The influence of the $O_2$ index on the oxidizer side of a partially premixed acetylene/air flame was verified [18]. The flame was submerged in atmospheric air, and involved by a $N_2$ shield. It was demonstrated that soot formation increased in the flame with the shield. The first letter of which

was justified by the lack of $O_2$ available to intensify the oxidation process.

In 2005, [19] presented a comprehensive CFD model, which integrated detailed chemistry, soot formation and oxidation, radiation and NOx formation, for a propane-fueled, oxygen-enriched, turbulent, non-premixed jet flame. The results, compared with the experimental data available, gave an indication of the level of modeling that would be necessary.

Authors [20] explored the criteria for soot inception in oxygen-enriched laminar coflow flames. In these experiments an axial height in the coflow flame is selected at which to identify the sooting limit. The sooting limit is obtained by varying the amount of inert until luminous soot first appears at this predefined height. The sooting limit flame temperature is found to increase linearly with stoichiometric mixture fraction, regardless of fuel type. To understand these results, the relationships between flame structure, temperature, and local C/O ratio is explored through the use of conserved scalar relationships. Analysis of experimental results suggests that soot inception occurs when the local C/O ratio is above a critical value. The values for critical C/O ratios obtained from the analysis of experiments using several fuels are similar in magnitude to the corresponding C/O ratios for premixed flames. In addition, temperatures and PAH fluorescence were measured to identify regions in these flames most conducive to particle inception. Results indicate that the peak PAH concentration lies along a critical iso-C/O contour, which supports a theory that soot particles first appear along this critical contour, given sufficient temperature.

Authors [21] carried out a study into the evolution of products of incomplete combustion (PIC) emitted from one-dimensional, laminar, atmospheric-pressure ethylbenzene flames in the vicinity of the soot onset threshold. The objective of this study was to identify the role of the fuel-to-air equivalence ratio in the evolution of polycyclic aromatic hydrocarbons (PAH) and other PIC as soot precursors, just prior to and subsequent to soot onset in premixed flames. Temperature measurements and product sampling were conducted at various heights above the burner. Collected samples were analyzed for soot, PAH, oxygenated species, fixed gases, and light hydrocarbons. The results indicated that the soot onset limit is not a function of flame temperature alone; i.e. while the maximum measured flame temperatures was kept fairly constant, the flame could be either sooting, at the sooting limit or non-sooting depending on the equivalence ratio.

The combination of oxygen enrichment and fuel dilution for diffusion flames was studied [22]. The results suggested that an increase in the stoichiometric mixture fraction, Zst, and alters the flame structure, i.e. the relationship between the local temperature and the local gas composition. Increasing Zst has been shown to result in the reduction or even elimination of soot. In the present work, the effects of variable Zst on soot inception are investigated in normal and inverse coflow flames, using ethylene as the fuel.

The oxidation of laminar premixed natural gas flames experimentally and computationally with variable mole fractions of hydrogen (0, 20, and 60%) present in the fuel mixture was studied [23]. All flames were operated at low pressure (0.079 atm) and at variable overall equivalence ratios ($0.74 < \varphi < 1.0$) with constant cold gas velocity. At the same global equivalence ratio, there is no significant effect of the replacement of natural gas by 20% of $H_2$.

The influence of OEC in acetylene open flames was evaluated [24]. The results suggested that that the simultaneous variation of the oxygen content and of the oxidizer velocity can provide control of the soot formation and distribution along the flame to attend the retrofit load.

Evaluating the described aspects, control of the formation of soot can be an important factor for a more rational implementation of OEC. With this control, the transferred thermal radiation in heating processes can be monitored and the formation of NOx controlled. This aspect can be a factor in the use of the technology, and its peculiarities require further research.

The effects of the process variables, such as oxidizer oxygen content, fuel jet shape, diameter and velocity on soot formation and distribution are complex and coupled. In almost all the articles presented here, the work was with burners open to the atmosphere.

The objective of the present work is to explore the effect of the oxygen content in the oxidizer of the combustion on the soot concentration and thermal radiation along the length of a natural gas diffusion confined flame produced in a combustion chamber with a parallel annular

coaxial oxidizer flow, such that the natural gas discharge is surrounded by a flow of air, or oxygen-enriched air. The applied enrichment levels were 23 and 25% $O_2$ and they were used in retrofit applications where only small modifications in the existing equipment are required.

## 2. Experimental Setup and Methods

The experimental setup is shown in Fig. l. The flame was generated in a horizontal cylindrical combustion chamber, which consisted of burner with two concentric tubes: a 5mm i.d. central tube, and a 100mm i.d. external tube, and a chamber 1.35m in length. Natural gas flowed up through the internal tube, while air, or enriched air, flowed through the annular region between this tube and the larger diameter concentric tube. Gas flow rates were controlled by valves and metered by rotameters. Diffusion air and oxygen were premixed before being fed into the combustion chamber.

Soot concentrations were measured along the flame length using the laser light extinction technique. The laser system was mounted on a step-motor driven horizontal translation table, which allowed the beam coming from laser to reach the flame at any desired level. The laser was of He-Ne, with a wavelength of 632.8 nm. As the power output from the laser was only about 3mW, background radiation was blocked from the flame by narrow band pass interference filters, at the laser wavelength. The light was transformed into an electrical current signal by the photodetectors, and registered by data acquisition.

The thermal radiation was measured in the same points that the soot concentration was also measured, through radiometer in the narrow band of soot radiation influence between 0.6-3μm.

Soot volume fraction (or concentration) (ppm) was calculated from the laser light extinction data using the Rayleigh limit of the Mie theory, so that:

$$\phi = \frac{\lambda}{6\pi \,\mathrm{Im}\left|\frac{m^2-1}{m^2+2}\right|} K_{abs} \qquad (1)$$

$$K_{abs} = \frac{1}{L}\ln\left(\frac{I_o}{I_L}\right) \qquad (2)$$

$\lambda$ , is the laser wavelength, L the optical path length, $I_o$ and $I_L$ the laser beam intensity, before and after traversing the flame, and m is the refractive index, adopted as m = 1.90-0.55i, according to [25].

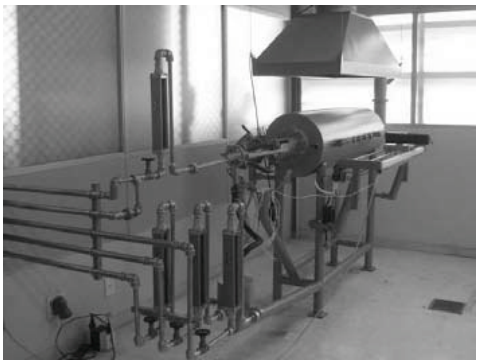

*(a) View of Combustion Chamber and Rotameters.*

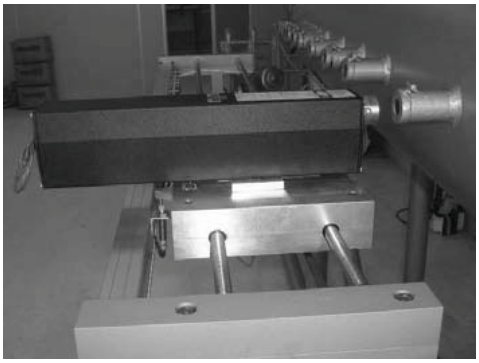

*(b) View of laser system and ten points for soot measurement.*

*Fig. 1: Experimental Setup.*

To examine the effect of the oxygen content of the combustion air, tests were performed comparing experiments with 23 and 25% $O_2$ to experiments with plain air (21% $O_2$). In the tests the equivalence ratios (φ) were maintained over a wide range (1.3 – 0.7). The natural gas flow was 0.0003$m^3$/s (18 l/min), referred to 20°C and atmospheric pressure. The burner power was 9.76kW. Table 1 summarizes the conditions used in the tests.

Some tests were performed in order to check the repeatability of results. In this work, the average uncertainty of the soot concentration measurements was in the order of 1%.

*Table 1. Conditions used in the tests.*

| $O_2$ index | φ |
|---|---|
| 21%, 23% and 25% | 1.3, 1.1, 1.0, 0.9 and 0.7 |

## 3. Results and Discussion

The analysis of the soot formation in the process was based on the values found for soot concentration located in the flame and also by its characteristics of luminous soot (radiation indicator). The analysis for the thermal radiation followed the same methodology.

Fig. 2 presents the soot concentration in the tested conditions through the average value, which is found from the performed measurements at the ten points shown in Fig. 1(b), in which the measurement was possible, representing the tendency of the tested condition. The possibility of non-detection of the concentration is caused by the frequent instability of the confined flame, as well as the possibility of non-absorption of the power of the laser by very small particles due to flames which did not encourage soot formation. Therefore, further analysis of the luminous soot becomes important.

Increased soot formation using OEC was found in particular 25% $O_2$ index compared to 23% and plain air. This possibly occurs because of the increased production of radicals that are precursors of the soot in the presence of $O_2$ in the pyrolysis of natural gas, as well as the best meeting between fuel and oxidizer in the confined flames without the influence of the external environment. Increasing the oxygen concentration increases the stoichiometric flame temperature which in turn increases the fuel pyrolysis and soot formation rates. This tendency occurs in all equivalence ratios. The variation of soot concentration with the equivalence ratio arises from the variation of temperature with the equivalence ratio.

Detection problems were seen by the flames instability in the confined condition therefore the characteristics of luminous soot in the tested conditions were also evaluated. Using the OEC with 23% or 25% $O_2$ index, a stronger yellow light, typical feature due to a greater soot concentration was verified. In all equivalence ratios, this trend was identified. On the other hand, the flames with air as oxidant have a typical blue colour under the tested conditions. The typical aspects of tested flames are shown in Fig. 3.

Fig. 4 presents the thermal radiation at combustion chamber (same points of soot measurement). There is a thermal radiation implementation using the OEC in the band of the soot influence. With the use of the OEC there was an average increase of 59% in the transferred energy by radiation, compared to burning with the plain air for all equivalence ratios.

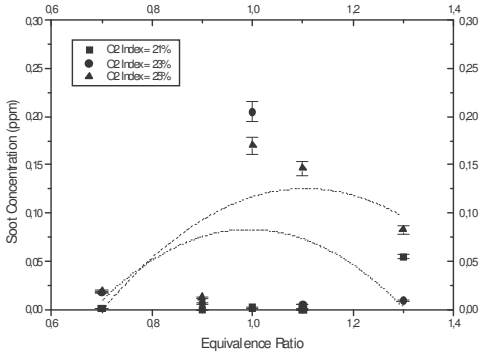


*Fig. 2: Soot concentration along combustion chamber.*

The OEC has a tendency to increase the flame temperature and consequently increases the available energy for the thermal radiation transfer. If the flame is composed of components with a higher tendency to transfer heat by radiation, more energy will be transferred to heat any kind of surface or load.

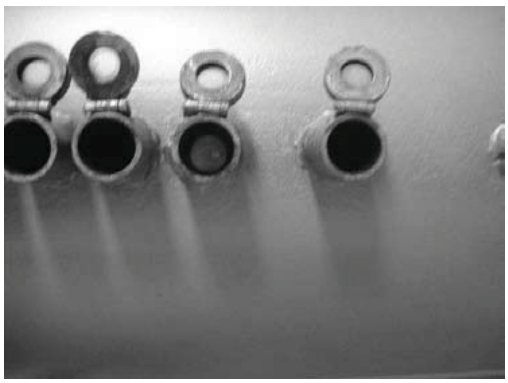

*(a) Flame without OEC utilization.*

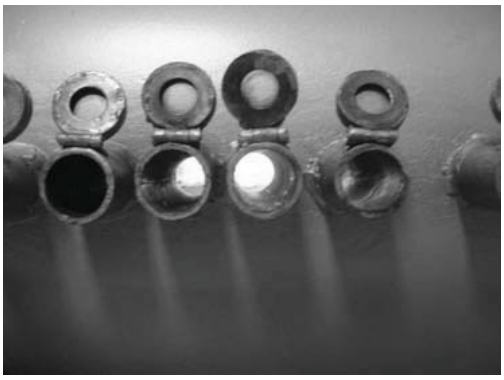

*(b) Flame with OEC utilization.*

*Figure 3: Visual Aspects of Flames with OEC.*

Therefore the temperature of the flame can be reduced. With OEC, the formation of soot was increased (increase is shown in Fig. 2), which caused an increase in the transferred energy by the flame (Fig. 4) lowering its temperature.

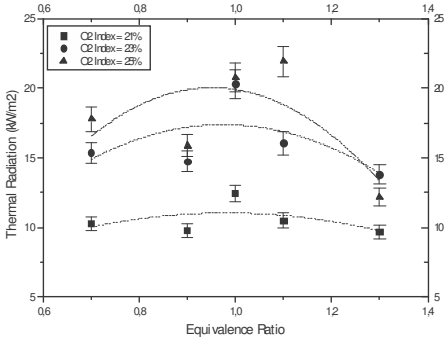


*Figure 4: Thermal radiation along combustion chamber.*

This can be indirectly seen through the temperature of the exhaust gas at the combustion chamber exit. In Fig. 5 the temperatures in question are identified. Temperature stabilization under the tested conditions was verified between 600-800K (in most tested conditions).

Even though the OEC tends to increase the flame temperature, the temperature of the exhaust gas also tends to increase. In the investigation, the temperature of the exhaust gas remains close to the values found when they are burnt with plain air; which confirms the influence of soot in the reduction of flame temperature through thermal radiation transfer.

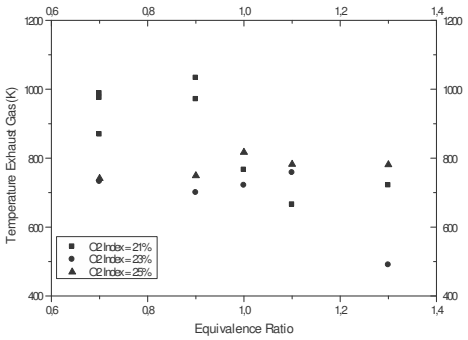


*Figure 5: Temperature of exhaust gas at exit combustion chamber.*

## 4. Conclusions

This present work investigated the effect of the oxygen index in the oxidizer of the combustion on the soot and thermal radiation along the length of a natural gas diffusion confined flame. The levels of air enrichment that were applied were 2% and 4% and can applied in retrofit burners, where only small modifications in the existing equipment are required.

The results suggest that the use of OEC in natural gas confined flames produces an increase of soot formation and consequently enhanced thermal radiation. This can be a control tool to implement radiation heat transfer and soot formation in confined burners.

## Nomenclature

$I$ signal output, V

$K$ absorption section, $m^{-1}$

$L$ laser path, m

$m$ complex index of refraction

$Z$ stoichiometric mixture fraction

### Greek symbols

$\varphi$ equivalence ratio

$\lambda$ wave length of laser, m

$\phi$ soot concentration, ppm

### Subscripts and superscripts

st stoichiometric

o incident laser signal before the flame

L emergent laser signal attenuated for the flame

## References

[1] Glassman, I., 1987, Combustion, Academic Press, New York.

[2] Turns, S.R., 1996, An Introduction to Combustion - Concepts and Applications, McGraw-Hill Int. Editions, Singapore.

[3] Baukal Jr., C.E., 1998, Oxygen-Enhanced Combustion, CRC Press, New York.

[4] Saito, K., Williams, F.A., Gordon, A.S., 1986, Effects of oxygen on soot formation in methane diffusion flames, Combustion Science and Technology, 47, pp. 117-138.

[5] Gülder, O.L., 1995, Effects of oxygen in methane, propane and n- buthane diffusion flames, Combust. Flame,101, pp. 302-310.

[6] Wey, C., 1994, Simultaneous measurements of soot formation and hydroxyl concentration in various oxidizer diffusion flames, International Society for Optical Engineering, 2122, pp. 94-106.

[7] Hura, H.S., Glassman, L., 1988, Soot formation in diffusion flames of fuel/oxygen mixtures, Proceedings of Combustion Institute, 22, pp. 371-378.

[8] Du, D.X., Axelbaum, R.L., Law, C.K., 1990, The influence of carbon dioxide and oxygen as additives on soot formation in diffusion flames, Twenty-Third Symposium (International) on Combustion, pp. 1501- 1507.

[9] Leung, K.M., Lindstedt, R.P., 1991, A simplified reaction mechanism for soot formation in non premixed flames, Combustion and Flame, 87, pp. 289-305.

[10] Hwang, J.Y., Chung, S.H., Lee, W., 1998, Effects of oxygen and propane addition on soot formation in counterflow ethylene flames and the role of C3 chemistry, Proceedings of Combustion Institute, 27, pp. 1531-1538.

[11] Kent, J.H., Bastin, S.J., 1984, Parametric effects on sooting in turbulent acetylene. Combustion and Flame, 56, pp. 29-42.

[12] Beltrame, A., et al., 2001, Soot and NO Formation in Methane–Oxygen Enriched Diffusion Flames, Combustion and Flame, 124, pp. 295-310.

[13] Glassman, I.,Yaccarino, P., 1980, The effect of oxygen concentration on sooting diffusion flames, Combustion Science and Technology, 24, pp. 107-114.

[14] Lee, K.O., et al., 2000, Soot formation effects of oxygen concentration in oxidizer stream of laminar co-annular nonpremixed methane/air flames, Combustion and Flame, 121, pp. 323- 333.

[15] Zelepouga, S.A., et al., 2000, Relative effect of acetylene and PAHs addition on soot formation in laminar diffusion flames of methane with oxygen and oxygen-enriched air, Combustion and Flame, 122, pp. 76-89.

[16] Hwang, S.S.; Gore, J.P. J., 2002, Characteristics of combustion and radiation heat transfer of an oxygen-enhanced flame burner, Power Energy - Part A, 216, pp. 379-386.

[17] Wang, L., et al., 2002, A study of the influence of Oxygen Index on soot, radiation, and emission characteristics of turbulent jet flames, Combustion Science and Technology, 174 (8), pp. 45-72.

[18] Goldstein Jr., L., et al., 2002, Experimental study of secondary air diffusion effects on soot concentration along a partially premixed acetylene/air flame, International Communications in Heat and Mass Transfer, 29 (2), pp. 223-231.

[19] Wang, L., et al., 2005, Interactions among soot, thermal radiation, and NOx emissions in oxygen-enriched turbulent nonpremixed: a computational fluid dynamics modeling study, Combustion and Flame, 141, pp. 170-179.

[20] Kumfer, B.M., et al., 2006, Measurement and analysis of soot inception limits of oxygenenriched coflow flames, Combustion and Flame, 147, pp. 233-242.

[21] Ergut, A., et al., 2007, The effect of temperature on the soot onset chemistry in one-dimensional, atmospheric-pressure premixed ethylbenzene flames, Combustion and Flame, 151, pp. 173-195.

[22] Kumfer, B.M., Skeen, S.A., Axelbaum, R.L., 2008, Soot inception limits in laminar diffusion flames with application to oxy–fuel combustion, Combustion and Flame, 154, pp. 546-556.

[23] Ferrières, S. de, et al., 2008, Experimental and numerical investigation of low-pressure laminar premixed synthetic natural gas/O2/N2 and natural gas/H2/O2/N2 flames, Combustion and Flame, 154, pp. 601-623.

[24] Santos, A.A.B., Goldstein Jr., L., Ferrari, C.A., 2009, An Experiment on the Effect of Oxygen Content and Air Velocity on Soot Formation in Acetylene Laminar Diffusion Flame Produced in a Burner with a Parallel Annular Coaxial Oxidizer Flow, International Communications in Heat and Mass Transfer, 36, pp. 445-450.

[25] Lee, S.C., Tien, C.L., 1981, Optical constants of soot in hydrocarbon flames, Proceedings of Combustion Institute, 18, pp. 1159-1166.

**Acknowledgments:** The authors are grateful for the financial support of the SENAI National Department – Brazil and the SENAI CIMATEC – Salvador – Bahia – Brazil.

# Combustion of Liquid Fuels from Renewable Sources and Liquid Wastes

*P. Bělohradský[a], V. Kermes[a]*

[a] *Institute of Process and Environmental Engineering, Faculty of Mechanical Engineering, Brno University of Technology, Brno, Czech Republic*

**Abstract:** Liquid fuels from renewable sources and liquid wastes are nowadays more and more often discussed as the source of thermal energy which can be utilized in subsequent processes. In comparison to standardized liquid fuels made from oil, these types of fuel are highly variable in their properties, such as often unstable chemical composition, changing physical-chemical properties, amount of dissolved inorganic compounds and/or presence of large amount of solid particles in fuels. The paper is focused on issues of combustion of liquid fuels from renewable sources and liquid wastes from industrial production in stationary sources. It tackles basic comparison with standardized fuels. Discussion about physical and chemical properties in the view of combustion, namely the conditions prior to entering the burner and the conditions for subsequent atomization in the combustion space makes up the main body of this text. The aim of the text is then to provide a comprehensive view on this issue mainly from technical aspect.

**Keywords:** Atomization, Liquid fuels from renewable sources, Liquid wastes, Standardized liquid fuels.

## 1. Introduction

Utilization of fuels from renewable sources and wastes for heat production or utilization of more preferred cogeneration is supported for many reasons, such as the reduction of greenhouse gases, the reduction of energy dependence on fossil fuels, or the minimization of produced wastes. From the point of view of fuel classification according to the state, it may be observed that the use of solid and gaseous fuels prevails in stationary technologies. Possibly one can meet with the combustion of products from gasification of solid fuels or waste in the facilities intended for common production of heat and electric energy.

The reasons, why the fuels from renewable sources are not more used in stationary sources, are found in the present form of legislation, availability of fuel sources, fuel prices and last but not least in technological difficulties with combustion of liquid fuels (in comparison with combustion of gaseous fuels). All four aspects then influence the economical aspect both of construction and running of technology. From the point of view of legislation and technology design, the combustion of liquid wastes is rather complicated. The wastes are often various mixtures of very badly miscible to immiscible liquids with problematic chemical composition, since the emissions may contain compounds of chlorine, fluorine and heavy metals. These liquid wastes are therefore combusted in incinerators of dangerous wastes.

As to the liquid fuels from renewable sources, their utilization is supported by legislation. The combustion technology is significantly influenced by chemical composition of fuels determining their physical-chemical properties. It is necessary to take into consideration that the available agricultural crops, which are suitable for production of liquid fuels from renewable sources, are simultaneously used for production of substances that are admixed in fuels intended for means of transport.

Next the text deals with the technological problems of application of liquid fuels from renewable sources at the stationary sources. It is assumed that the sources are of local character with small heat output. The liquid wastes are discussed mainly for the reason to realize their difference in comparison to standardized liquid fuels, even if both substances may come from the same raw material – oil.

### 1.1 Specific objectives

The text is focused on liquid wastes and fuels from renewable sources that may be used as the main

Corresponding Author: Petr Belohradsky, Email: belohradsky@upei.fme.vutbr.cz

fuel for heat and electric energy production due to their proper physical-chemical properties, but not only as the substitute of minor part of the main fuel coming from non-renewable sources for the purpose to save emission permits. The aim of the text is to give the overview of technical problems related to the substitute of fuels from fossil sources. The text does not deal with the recovery of investments and operating costs.

## 2. Liquid fuels from renewable sources

Liquid fuels from renewable sources are considered those liquids that are purposely produced from renewable sources as fuels. This definition is met by vegetable oils, ethanol and methanol. The products coming from pyrolysis or gasification of solid biomass can be also classified as fuels from renewable sources. In the Czech Republic the renewable sources for liquid fuels include rapeseed oil, sunflower oil and the products of their processing called esters. Also great potential is comprised in production of alcohol.

Capacity of individual sources for fuel production in the Czech Republic will necessitate diversification, which means certain balance between requirements on construction of individual stationary sources and fuel availability will have to be reached.

### 2.1. Fats and oils

Vegetable oils, triglycerides of fatty acids, have been known for a long time as a possible source of energy for diesel engines [1]. In comparison with diesel oil, vegetable oils are characterized for their higher viscosity and lower fraction of volatile organic substances, which leads to formation of deposits on valves and to decrease of engine power. From this fact arose an idea to transform triglycerides into methyl-esters and ethyl-esters of fatty acids with the side product of glycerin. This forms three even four substances of different physical-chemical properties which may be theoretically used as fuels for stationary sources of smaller power.

Triglycerides in the form of fats and oils are esters of glycerin and esters of fatty acids which are composed of carboxyl acids with long chains. Shares and types of individual fatty acids in fats are dependent on sources of fat (suet, lard, etc.) and oils (rapeseed oil, sunflower oil, peanut oil, linseed oil, used deep frying oil, etc.). Formation of methyl-esters and ethyl-esters may be described in short as a process of combining triglycerides with methanol and ethanol which gives rise to methyl-esters and ethyl-esters with glycerin as a side product; formation of one molecule of glycerin is accompanied with formation of three molecules of methyl-esters or ethyl-esters. Sodium hydroxide or potassium hydroxide are used as catalysts. It is necessary to supplement sufficient amount of alcohol residue due to requirements on total transesterification of fatty acids. Final product of transesterification is a liquid mixture composed mostly of esters, glycerin, alcohol residues and dissolved catalyst. This mixture is subsequently separated and esters are acquired. If it is financially beneficial and the technology allows it, methanol and ethanol are acquired from the residues. The so called G-phase is a side product if the mixture contains alcohol residue, crude glycerin is a side product if the mixture contains water instead of alcohol [2].

Utilization of G-phase and/or crude glycerin as a fuel is disputable due to presence of dissolved inorganic compounds such as sodium hydroxide, potassium hydroxide. Direct combustion is impossible as the heat transfer surfaces get fouled with sodium hydroxide and/or potassium hydroxide. G-phase or crude glycerin may be characterized as combustible substance which may be acquired from renewable sources. However, in the terms of combustion we might conclude it is more of a waste than fuel.

Utilization of vegetable oil and esters as a substitute for liquid fuels coming from fossil fuels will be discussed later on.

### 2.2. Ethanol

Production of ethanol from agricultural products is among other possibilities of substitute of liquid fossil fuels along with utilization of other products containing sugars in their structures [3]. This involves fermentation of agricultural products containing sugar (sugar cane, sugar beet) or starch (potatoes, wheat). In the Czech Republic, it is possible to use both types of products, i.e. those containing sugar or starch. If products containing starch are used, starch has to be transformed into sugar with subsequent fermentation.

Besides the above mentioned acquisition of ethanol from natural sources, it is possible to

produce it via purely chemical method of the so called synthetic ethanol. Synthetic ethanol is produced by direct catalytic hydration of ethylene, or by indirect hydration of ethylene. Pureness of the ethanol acquired by catalytic hydration may reach up to 95 to 100 %. The so called thermo-chemical method is yet another way of synthetic methanol; synthetic gas (mixture of CO and $H_2$) is an input raw material. Methanol is formed from synthetic gas in the first step which is later mixed with synthetic gas in the presence of catalyst or other chemical-technological procedures are opted.

Lower heating value of ethanol is dependent on whether it is a waterless alcohol labeled as E100 (27 MJ/kg) or alcohol with water content (e.g. 95% alcohol, 5% water) which does not necessitate energy intensive production of waterless alcohol. Waterless alcohol reaches lower heating value of 64 % compared to extra light fuel oil. Mixtures of methanol and/or ethanol and petrol for operation of motor vehicles are commonly produced and labeled as E85 (85% ethanol and 15% petrol) or M85 (85% methanol and 15% petrol), pure mixture of 95% ethanol and 5% water.

### 2.3. Pyrolysis

Technology of biomass pyrolysis for production of certain chemicals (such as methanol) has been used long before fossil fuels became prevailing product for chemical and petrochemical industry. Any appropriate material coming from renewable sources may be used for pyrolysis which is, in terms of physical-chemical actions, a thermal decomposition of biological materials with no access of oxygen. Pyrolysis results in formation of solid, liquid and gaseous products. Final products of pyrolysis may be used as a source for liquid and gaseous fuel as well as a source of hydrocarbons for subsequent chemical production. Considering the method of pyrolysis, we may either acquire more pyrolytic gas or more liquid components [1].

Both pyrolytic gas and oil may be used for combustion. Pyrolytic gas is a fuel with low to middle values of lower heating value (3.9 to 15.7 $MJ/m_N^3$). Share of individual components (carbon monoxide, carbon dioxide, methane, hydrogen, ethane, ethylene, higher hydrocarbons, and water steam) depends on type of biomass and technology used.

Liquid phase acquired by pyrolysis contains complex mixture of water and hydrocarbons which have lower average molecule weight than the input raw material. If an input raw material used for pyrolysis contains high share of cellulose, then the liquid phase contains acids, alcohols, aldehydes, ketones, esters, heterocyclic derivates and phenol compounds, which corresponds to content of heavy heat oil and pyrooil coming from processing of fossil raw material. Heavy liquid share in the form of tar then contains natural resin, hydrocarbons with mid-long chains, phenols, aromates, aldehydes and other derivates of hydrocarbons. In the terms of combustion, these tars may be compared to tars coming from processing of coal and residues from oil processing.

## 3. Liquid wastes

There is an enormous call for application of Waste-to-Energy approach with liquid waste which that looks for their utilization in production of electric energy and heat. Liquid wastes may be classified in various ways, each of them reflecting a certain aspect of their physical-chemical properties. Among the basic properties in the terms of dosing into combustion space, there are chemical composition, lower heating value, flashpoint, dependence of viscosity upon temperature, dependence of surface stress upon temperature, freezing point, miscibility and degradation of individual parts in relation to time and temperature. Properties of a specific source of liquid wastes have to be accompanied by stability of chemical composition which greatly varies depending on batch and season of the year.

Mixtures of ether and petrol and/or mixtures of ether and alcohol may be designated as liquid wastes used as sources of energy which serve for manufacturing of special optics along with various residues from processing of oil and coal, mixtures of glycerin and alcohols and/or water and other substances coming from production of esters of fatty acids, etc.

## 4. Atomization of liquid fuels

A necessary requirement for combustion of liquid fuels is a high-quality fuel atomization [4], which is necessary for complete evaporation and burnout of all droplets in the area of flame. If combusting fuel was not perfectly atomized into sufficiently small droplets, it is assumed with certainty that high concentration of carbon monoxide would be measured in flue gas indicating incomplete

combustion. Moreover insufficient atomization is characterized with deposition of unburned hydrocarbons (UHCs) on the walls of combustion chamber.

The choice of fuel atomization system itself is rather dependent on physical-chemical properties of fuel and availability of auxiliary atomizing medium. From this point of view there are three basic types of atomization, namely pressure, pneumatic and rotary atomization [5]. Besides these, there are other less frequently used types of atomization using vibrational, acoustic, ultrasonic, electrostatic forms of energy or flash atomization [6].

### 4.1. Pressure atomization

Pressure atomization utilizes transformation of pressure energy of the liquid, which after release from the atomizer into the combustion chamber changes into kinetic energy that causes fuel atomization. Depending on the type of atomized fuel, the required pressure ranges on the order of units of MPa. Quality of pressure atomization strongly depends on physical-chemical properties of the atomized fuel and is not suitable for atomization of liquid fuels of high viscosity. The main advantage of this type of atomization is the fact that no auxiliary atomizing medium is required and there are no movable components on the burner. Considering the energy intensity, pressure atomization is the least demanding of the three main types of atomization.

### 4.2. Pneumatic atomization

Pneumatic atomization (atomization with auxiliary atomizing medium) utilizes mostly compressed gas energy that secures sufficient disintegration of streaming liquid. Depending on the type of fuel, compressed air or steam are frequently used media for atomization. Compressed air is applied for fuels that do not require to be preheated prior to entering the burner (extra light fuel oil), possibly for fuels with no big temperature difference between preheated fuel and atomizing air (light fuel oil with temperature of preheating up to 50 °C). Steam is used for atomization of fuels that are necessary to preheat to high temperatures. These include medium-heavy fuel oils and especially heavy fuel oils and mazut, which require preheating temperature significantly above 100 °C. Compared to pressure atomization, pneumatic atomization is not so demanding on fuel and auxiliary medium pressures that in most applications do not exceed 1.2 MPa. Considering energy intensity, pneumatic atomization is the most demanding of the three types of atomization.

### 4.3. Rotary atomization

Rotary atomization utilizes kinetic energy transmitted to the atomized fuel by a rotating atomizer. The mechanical atomizer rotates vertically or horizontally in high revolutions and is powered by an electrical engine. Dosing of liquid is done under relatively low pressure; atomization is then caused by centrifugal force affecting fuel particles. Main disadvantage is the presence of burner components rotating in high speed. Considering energy intensity, rotary atomization is more demanding than pressure atomization but does not reach the intensity of pneumatic atomization.

### 4.4. Other types of atomization

Besides the above described main atomization methods, there are other, technically more demanding, types such as ultrasonic atomization or atomization working on the principle of flash evaporation before its injection into the combustion chamber. Ultrasonic atomization is based on contact of liquid with surface that vibrates in the range of ultrasonic waves. Some of the advantages of ultrasonic atomization are in its low energy intensity and the fact that liquid is not supplied under pressure as in the case of pressure and pneumatic atomization. The disadvantages include low jet flow rate and high investment costs, which are caused by high price of ultrasonic waves generator.

## 5. Substitute of standardized fuels

The progress in development of combustion technology of liquid fuels has come with the beginning of petroleum processing. During this period the basic types of fuels have been standardized, for which physical and chemical properties are specified [7]. The standardization of required properties has brought substantial facilitation not only in burner design and burner testing, but also in planning of flue gas cleaning technology. From this point of view, the standardization of liquid fuels from renewable sources was done more quickly, particularly in the area of fuels utilized in transportation.

The substitute of individual liquid fuels acquired from fossil sources may be done both by liquids from renewable sources, and by liquid wastes. The

comparison of standardized fuels from fossil sources with approximately corresponding liquid fuels from renewable sources is carried out in the text. The problems with the use of the fuels in combustion are discussed with respect to their physical-chemical properties.

### 5.1. Standardized liquid fuels made of oil

The possibility to substitute liquid fuels made of oil for liquid fuels made of renewable sources brings new requirements for combustion facility. The comparison of these fuels is done with basic standardized liquid fuels used at stationary combustion facilities, i.e. extra light fuel oil (ELFO), light fuel oil (LFO) and heavy fuel oil (HFO). Main differences among these fuels are their possibilities of quality atomization in the combustion chamber and the concentration of pollutants, especially of sulfur oxides.

As for the quality of atomization, ELFO is the least problematic since its viscosity is sufficiently low already at ambient temperature (no need for preheating). Further, it does not contain long chains of hydrocarbons with a tendency to crack, to form the sediments and to foul the jets. The atomization of ELFO is even characterized with the least technical constraints and is well managed by the producers of burners.

In terms of chemical composition LFO belongs to liquids with larger fraction of long-chain hydrocarbons. In order to achieve of good-quality atomization, the preheating of fuel is necessary up to 40 to 50 °C for the purpose of lowering its viscosity. This temperature does not yet constrain to use all types of atomization.

The last standardized fuel, HFO, contains large fraction of hydrocarbons with high number of carbon. The properties of HFO give good assumption for its use in stationary combustion facilities of high heat outputs. Due to high viscosity of HFO there is a need to preheat the fuel to the temperature above 100 °C. For this reason only pressure, pneumatic or rotary atomization may be used.

### 5.2. Substitute of ELFO

A comparison of basic properties of ELFO and corresponding similar liquid fuels from renewable source is shown in Table 1. By detailed investigation of individual properties, it may be concluded that the greatest differences are in lower heating values and flashpoint temperatures. The lower heating value of ELFO is about 42.5 MJ/kg and the flashpoint has to be at least 56 °C according to the standard. As to the methanol and ethanol, the temperature of flashpoint reaches to 11.1 °C and 12.8 °C, respectively. On the other hand, the flashpoint temperature of the products of transesterification of fats and oils is dependent on the base raw material that highly influences the viscosity. The values of flashpoint temperatures range in most cases above 120 °C.

Methanol and ethanol reach lower heating value approximately of half and two thirds compared to ELFO, respectively. Their viscosity is even at negative temperatures lower by order of magnitude, which enables good pumping and atomization without need of preheating. The low temperature of flashpoint enables no problematic ignition; however, it simultaneously enhances requirements for fire safety for their storage and manipulation. This fact is probably a handicap for fuel substitute mainly at the units of low heat outputs.

The products of the process transesterification of fats and oils may substitute ELFO in dependence on input raw material and on type of next processing – distillation. Further it is necessary to take into consideration the fact that compared to ELFO, which is the mixture of hydrocarbons with relatively low flashpoint, the products of transesterification reach higher viscosity and are consisted of chemical compounds with high flashpoint. As the consequence of this fact is the need to stabilize combustion of the transesterification products by a fossil fuel. Eventually the fuel has to be preheated so that it may be atomized in very fine spray.

### 5.3 Substitute of LFO

A comparison of basic properties of LFO and of corresponding liquid fuels from renewable sources is shown in Table 2. Compared to ELFO, both LFO and corresponding fuels need to be preheated prior entering the burner. The preheating should reach such temperatures that enable to use compressed air as the atomizing medium for pneumatic atomization, i.e. 60 °C. In terms of prices, the price of compressed air is lower by order than the price of steam if the pressure requirement prior the burner is about 600 kPa (which means 800 kPa for compressor). Furthermore, using of steam as the atomizing

medium requires the installation of electrical steam generator.

*Table 1 Comparison of properties of ELFO and corresponding liquid fuels from renewable sources.*

| | | | | Rapeseed Oil | | | |
|---|---|---|---|---|---|---|---|
| **Property** | **Extra-Light Fuel Oil[a]** | **Methanol[b]** | **Ethanol[b]** | **Oil[c]** | **Methylester[c]** | **Ethylester[c]** | **Distilled Methyl-ester[d]** |
| Density [kg/m$^3$] | 860 | 796 | 794 | 910 | 880 | 876 | 886 |
| Kinematic viscosity [mm$^2$/s] | max. 6 | at 20 °C 0.75 | 1.51 | 51 | 5.65 | at 40 °C 6.17 | 4.19 |
| Flash point (Pensky and Martens) [°C] | min. 56 | 11 | 13 | - | 179 | 124 | 184 |
| Freezing point [°C] | max. -10 | - | - | -21 | -15 | -10 | - |
| Ash content [wt %] | max. 0.01 | - | - | - | 0.002 | 0.002 | - |
| Sulfur content [wt %] | max. 0.2 | - | - | 0.01 | 0.012 | 0.014 | max. $1\cdot10^{-6}$ |
| Mechanical impurity content [wt %] | max. 0.05 | - | - | - | - | - | max. $5\cdot10^{-6}$ |
| Higher heating value [MJ/kg] | - | - | - | 40.17 | 40.54 | 40.51 | - |
| Lower heating value [MJ/kg] | 42.5 | 20.1 | 27 | - | - | - | - |

[a] Adapted from the material safety data sheet of UNIPETROL RPA, s.r.o. [8].

[b] Adapted from [3].

[c] Adapted from [1].

[d] Adapted from the material safety data sheet of company Agrochem a.s. [9].

LFO may be substituted by distilled residue from the distillation process of products of transesterification of fats and oils, and by some of vegetable oils that reach kinematic viscosity up to $35\cdot10^{-6}$ m$^2$/s (35 cSt) for preheating temperature 40 °C. This means the assumption that the viscosity gets lower to the value of $20\cdot10^{-6}$ m$^2$/s (20 cSt) during the preheating to 60 °C. This viscosity then enables good pneumatic atomization. The using of vegetable oils immediately after pressing and filtration highly depends on their source since the viscosity at 40 °C may differ in order of tens percents. For example, the viscosity of soybean oil is $35\cdot10^{-6}$ m$^2$/s and the viscosity of rapeseed oil is $51\cdot10^{-6}$ m$^2$/s.

Similarly as for the liquids substituting ELFO, the flash temperature of the liquids substituting LFO is approximately higher of 100 °C than the flash temperature of LFO. This fact together with the character of chemical composition (liquids from renewable sources contain minor fraction of components with low boiling point) emphasize high requirements for the quality of atomization in very fine spray. If there is a need to decrease the emissions, it is then required the stabilization by fossil fuel, either by using of gaseous (natural gas, propane, propane-butane) or liquid fuel (ELFO, LFO). Using of methanol or ethanol as the stabilizing fuel is rather complicated.

### 5.4. Substitute of HFO

Substitute of HFO or mazut for liquid fuels from renewable sources is difficult since the prerequisite is the availability of such fuel. Such fuel can be either pyrolysis oils or wastes from the process of transesterification of fats and oils, i.e. crude glycerin or G-phase (containing methanol

instead of water). The requirement for combustion of crude glycerin and G-phase has its origin in the production of products of transesterification of fats and oils where these two substances are produced in large amount. The aim of combustion of the above substances is to decrease the emissions of $CO_2$ releasing in the atmosphere during the combustion of fossil fuels. This means savings for purchase and potential profit for selling emission permits. The comparison of some typical physical-chemical properties of HFO and wastes from production of methyl-ester rapeseed-oil are shown in Table 3.

*Table 2 Comparison of properties of LFO and corresponding liquid fuels from renewable sources.*

| Property | Light Fuel Oil[a] | Soybean Oil[b] | Rapeseed Oil | |
|---|---|---|---|---|
| | | | Oil[b] | Distilled Residue of Methylester[c] |
| Density [kg/m$^3$] | 915 | 920 | 910 | 923 |
| Kinematic viscosity [mm$^2$/s] | 3.2 to 18 | 33 | at 40 °C<br>51 | 32 |
| Flash point (Pensky and Martens) [°C] | min. 66 | - | - | 218 |
| Freezing point [°C] | summer max.10<br>winter max. -5 | -12 | -21 | - |
| Ash content [wt %] | max. 0.02 | - | - | - |
| Sulfur content [wt %] | lowsulfur max. 1.0<br>midsulfur max. 2.0 | 0.01 | 0.01 | max. 1 |
| Mechanical impurity content [wt %] | max. 0.1 | - | - | max. 0.2 |
| Higher heating value [MJ/kg] | 44-46 | 39.77 | 40.17 | - |
| Lower heating value [MJ/kg] | 41.5 | - | - | 36.9 |

[a] Adapted from the material safety data sheet of company G7, Inc. [10].

[b] Adapted from [1].

[c] Adapted from the material safety data sheet of company Agrochem a.s. [9].

In terms of physical and chemical properties, particularly of viscosity, the crude glycerin and G-phase are the substances requiring high temperature for preheating. The pyrolysis oils require preheating temperature high above 100 °C. The flash point of pyrolysis oils produced by biomass pyrolysis is not much different from the flash point of oil-based liquids. As to the crude glycerin, the preheating temperature is about 80 °C depending on the water fraction in the mixture.

The problems arise during preheating of G-phase containing methanol, which starts to evaporate at temperatures above 60 °C at the atmospheric pressure (the temperature of boiling point of methanol is at the atmospheric pressure about 64 °C). However, in order to decrease the viscosity to reasonable value about $20 \cdot 10^{-6}$ m$^2$/s (20 cSt), it would be required to preheat G-phase at least to 80 °C. The manipulation and the storage of this liquid is another problem, since its flashpoint fluctuates between 20 and 30 °C depending on the content of methanol.

The above stated liquids are possible to atomize by using all three basic types of atomization. For pressure and rotary atomization it is necessary to lower the viscosity to the value required by the producers of burners. If the pneumatic atomization is used, then the steam has to be used as the atomizing medium. Unlike the compressed air, steam does not cool down atomized fuel and so

fuel is not improperly atomized due to substantial decrease of its temperature. However, the use of steam assumes the availability of the steam source at the same time.

### 5.5. Substitute with liquid wastes

Liquid fuels from fossil sources may be substituted by liquid wastes as well. This may be done if the amount of waste or of more kinds of waste with similar physical-chemical properties is large. It is necessary to take into consideration the nature of substances that pollute the primary hydrocarbon and then to analyze, whether the polluting admixtures of organic or inorganic origin may influence combustion itself and whether they may damage the fuel system both chemically and mechanically. Opting for the right type of atomization should be done with certainty, which means that in most cases the pneumatic atomization utilizing compressed air of steam is preferred. This type of atomization is able to tackle certain imbalances in viscosity of the atomized substance without affecting quality of the combustion [11].

*Table 3 Comparison of properties of HFO and corresponding liquid fuels from renewable sources.*

| | | | **G-phase** | | **Crude glycerin** | |
|---|---|---|---|---|---|---|
| | | | Composition [wt %] | | Composition [wt %] | |
| | | | Glycerol | 67 | Glycerol | 81 |
| | | | Water | 4 | Water | 11 |
| | | | Methanol | 22 | Methanol | 0 |
| **Property** | **Heavy Fuel Oil**[a] | | Inorganic | 7 | Inorganic | 7 |
| Density [kg/m$^3$] | 990 | | at 20 °C | 1100 | at 20 °C | 1274 |
| | | | at 40 °C | 1086 | at 40 °C | 1261 |
| | | | at 60 °C | 1071 | at 60 °C | 1249 |
| Kinematic viscosity [mm$^2$/s] | at 80 °C | max 118 | at 20 °C | 261 | at 20 °C | 258 |
| | at 100 °C | max. 57 | at 40 °C | 82 | at 40 °C | 67 |
| | at 150 °C | max. 10 | at 60 °C | 28 | at 60 °C | 25 |
| | | | at 80 °C | - | at 80 °C | 12 |
| Flash point (Pensky and Martens)[°C] | - | | 21 °C | | - | |
| Flash point in open crucible [°C] | min. 110 | | - | | - | |
| Freezing point [°C] | max. 40 | | - | | - | |
| Ash content [wt %] | max. 0.14 | | 7 | | 7 | |
| Sulfur content [wt %] | lowsulfur | max. 1.0 | - | | - | |
| | midsulfur | max. 2.0 | | | | |
| | highsulfur | max. 3.0 | | | | |
| Mechanical impurity content [wt %] | max. 1.0 | | - | | - | |
| Higher heating value [MJ/kg] | 42-46 | | - | | - | |
| Lower heating value [MJ/kg] | 40.9 | | 21.3 | | 20.8 | |

[a] Adapted from the material safety data sheet of UNIPETROL RPA, s.r.o. [8].

Due to enormous variety of types of ELHO, LFO and HFO, it is difficult to give a more detailed list of their waste substitutes and at least demonstrative examples will be provided. Mixtures of petrol-alcohol, petrol-ether, alcohol-ether, etc. may be given as types of wastes with properties comparable to ELFO. Polluted solvents may be considered as well. Substitutes mostly concern liquids with a low ignition point, which must be reflected in the type of storage and manipulation. Substitute of LFO with liquid wastes is possible by combustion of used deep frying oil and/or waste oil coming from production of fossil fuels which qualify thanks to their physical-chemical properties and do not contain mixtures of substances such as heavy metals. Substitute of HFO with raw glycerin and G-phase has been discussed in the previous paragraph

because of their renewable sources origin and availability in large amounts. Other options of HFO and/or mazut substitutes include combustion of waste oils such as oils coming from transformer facilities, etc.

It is vital to keep in mind that if liquid wastes are to be combusted as a fuel and not as wastes, they have to comply with related legislation which imposes restrictions on their chemical composition, especially concentration of harmful substances such as chlorine, fluorine, heavy metals, etc. Thus it is not very likely that combustion of liquid wastes will ever increase due to restrictions on these technologies which are several times stricter than technologies combustion regular standardized fuels.

## 6. Conclusion

Substitute of liquid fuels from fossil sources for liquid fuels from renewable sources and liquid wastes is generally possible from technical aspect. However, it is necessary to carry out proper consideration whether it is concerned full substitution with the aim to produce heat and eventually electric energy for own usage or for sale, or it is concerned the co-combustion conducted for economical reasons – disposal of produced waste and reduction of the amount of $CO_2$ produced by combustion of fossil fuels.

The text outlines the problems of substitute of fuels. The discussed obstacles involve the differences in basic physical-chemical properties that influence the manipulation with liquids and combustion itself. It has to be concerned several factors during the construction or reconstruction of the combustion facility. The main factors are the choice of right type of atomization and availability of suitable burner, because most of the producers (especially the producers of block burners) are reluctant to guarantee the operation of their burners with the fuels different than standardized fuels coming from fossil sources. The utilization of power burners, which enable more possibilities for setting up, is rather complicated for the reasons for higher requirements for built-up space (space required for separated air fan and for instrumentation and regulation of the burner) and for operation.

The aim of further research is to make up the overview of basic problems of combustion of liquid fuels from renewable sources based on carried out tests. The tests will be carried out on power burners enabling the co-combustion of liquid fuel from renewable sources and noble gaseous or liquid fuel as the stabilizer.

## References

[1] Klass, D., 1998, *Biomass for Renewable Energy, Fuels, and Chemicals*, Academic Press, USA.

[2] Parikka, M., 2004, Biomass Bioenergy, Global biomass fuel resources, 27, pp. 613-620.

[3] Kreith, F., and Goswami, D. Y., 2007, *Handbook of Energy Efficiency and Renewable Energy*, Taylor & Francis, USA.

[4] Lefebvre, A. H., 1989, *Atomization and Sprays*, Taylor & Francis, USA.

[5] Baukal, C. E., 2004, *Industrial Burners Handbook*, CRC Press LLC, USA.

[6] Bayvel, L., and Orzechowski, Z., 1993, *Liquid Atomization*, Taylor & Francis, USA.

[7] Netz, H., 1996, *Heat and Steam Industrial Boiler Handbook*, Verlag Dr. Ingo Resch GmbH, Germany.

[8] UNIPETROL RPA, s.r.o. [cited on the 14th February 2010]. Available on <http://www.unipetrolrpa.cz/en/>.

[9] Agrochem a.s. [cited on the 14th February 2010]. Available on <http://www.agrochem.cz/o-nas/>.

[10] G7, Inc. [cited on the 14th February 2010]. Available on <http://www.g7.cz/en/o-spolecnosti.php>.

[11] Jedelsky, J., and Jicha, M., 2006, Design of Atomizer for Waste Fuel Combustion with Decreased Exhaust Gas Emissions, *Proc. 31st International Symposium on Combustion*, Heidelberg, pp34.

# Experimental and Numerical Investigations on a Combustor Model for Syngas Swirl Flames

*Luca Casarsa [a], Andrea De Pascale [b], Diego Micheli [c] and Robert Radu [c]*

[a] *Dipartimento di Energetica e Macchine, University of Udine, Italy*
[b] *DIEM, University of Bologna, Italy*
[c] *Dipartimento di Ingegneria Meccanica, University of Trieste, Italy*

**Abstract:** An atmospheric combustor model with optical access for non-premixed swirl-stabilized flames was developed in order to investigate the combustion behavior of gas turbine fired with low-caloric syngases and to create a data-base for the validation of numerical combustion models.
In the present work, newly developed fully 3-D PIV measurements of the combustor aerodynamics at cold conditions are presented together with detailed wall temperature measurements in hot conditions. These data are respectively used to validate the combustor numerical model from an aerodynamic point of view and as boundary conditions when combustion simulations with different approaches are carried out. Thermocouple traverses data and global emissions analyzers results are then used as reference data for combustion models validation. Propane, as reference fuel, and a synthetic mixture of $CH_4$, CO, $CO_2$, $H_2$ are considered.

**Keywords:** Syngas combustion, Combustor model, Combustion simulation.

## 1. Introduction

Biomass gasification and pyrolysis enable an efficient micro scale production of syngas with LHV sufficiently high to feed a small gas turbine. Gas composition varies with both biomass nature and conversion process, and affects efficiency and power of a given generation group, usually designed for methane feeding. It follows the need of experimental and numerical tools in order to easily and reliably foresee combustion behavior and performances of small gas turbine combustors when fed with various alternative gaseous fuels.
Several examples can be found on the topic in recent open literature. In [1] gas mixtures from gasification process in IGCC power plants, composed mainly by CO and $N_2$, were tested in a swirl stabilized diffusion flame combustor. A similar device was used in [2] with a gas mixture rich of $H_2$ and $N_2$, that could be obtained from lignite by means of a suitable process. CO and $H_2$ rich mixtures usable in IGCC plants have been considered in [3] in a combustor of the same type of the previously cited ones, to study flame dynamics and stability limits. Thermoacoustic instability in combustor models was also studied numerically in [4] with reference to the experimental facility described in [1]. In [5] the atmospheric combustor model with optical access used in the present paper was described. It was designed for confined, non-premixed, swirl-stabilized flames fired with low-caloric syngases. Some preliminary experimental results were presented for two different fuels: propane, as reference one, and a synthetic mixture of $CH_4$, CO, $CO_2$, $H_2$ having a composition typical of a gas from wood pyrolysis.
In this paper new and more complete data are used to develop simplified combustion models for the considered fuels. Equivalence ratio taken constant at 0.5 is considered while thermal power varies between 4.5 kW and 8 kW, obtained with two different air flow rates. The applied measuring techniques are 3-D Particle Image Velocimetry (PIV) for the aerodynamic analysis at cold conditions, i.e. without combustion, thermocouple traverses and global emissions analyzer (CO, $CO_2$, $O_2$, HC and $NO_x$ ) in flame conditions. Numerical analysis is carried out with Fluent 6.3 CFD package. The reactive flow is solved with Eddy Dissipation Finite Rate and flamelet combustion models, adopting different levels of kinetic mechanism complexity.

## 2. The combustor model

The burner, shown in Fig. 1, is described in detail in [5]. It has an annular air nozzle with the outer diameter of 30 mm and the inner diameter of 16 mm. The concentric fuel nozzle has also an annular section with the outer diameter of 14 mm and the inner one of 10 mm, corresponding to the

Corresponding Author: Diego Micheli, Email: micheli@units.it

central bluff-body size. Flame is stabilized by a recirculation zone created by both an air swirl generator and the central bluff-body. The fuel flows through an axial swirler with a set of seven 45° vanes. The optically accessible combustion chamber consists of four fused and polished planar quartz windows of 1/8" thickness, supported at the corners by steel posts. Combustor layout and main dimensions are the same of the device presented in [1]-[4] so that present results can be directly compared with the literature ones and improve the database size.

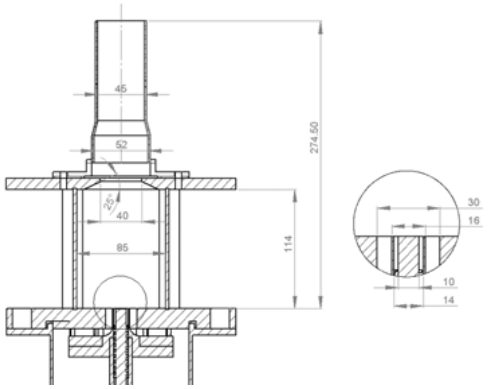


*Fig. 1. Schematic drawing of the burner and combustion chamber*

The air radial swirler has 12 variable inclination blades (Fig. 2). It allows to easily vary within certain limits the recirculation behaviour by changing swirl intensity, which is defined as [6]:

$$S = G_\theta / \left(G_y R\right), \quad (1)$$

where the reference length, R, was chosen equal to the air nozzle exit outer radius, and the axial fluxes of angular and axial momentum, are given by:

$$G_\theta = \int_0^R wr \cdot \rho u \cdot 2\pi r \cdot dr, \quad (2)$$

$$G_y = \int_0^R u \rho u \cdot 2\pi r \cdot dr, \quad (3)$$

where pressure and turbulence terms have been omitted.

Swirl number values can be obtained as a function of swirler and annular duct geometry as shown in [5], but theoretical results are strongly dependent by the calculation approach so that an experimental validation has been carried out to improve the knowledge of the burner operating limitations.

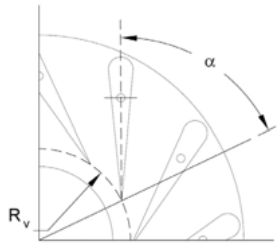


*Fig. 2. Drawing of the tested swirler*

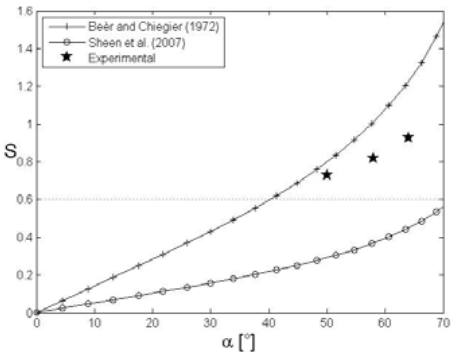


*Fig. 3. Calculated [5] and experimental swirl number for different swirler blade angles*

Experimental swirl number values have been obtained applying (1-3) to PIV flow field measurements (see paragraph 3.1) at 3 mm height from the burner plate, for three values of the swirler blade angle $\alpha$: 50°, 58°, 64°. Results are compared in Fig. 3 with the theoretical values already presented in [5]: experimental values are in the expected range and increases with $\alpha$ from 0.7 to 0.9. Note that 0.6 is generally considered a value sufficient to obtain a recirculation zone and than a stable flame. The value of $\alpha$ in the actual swirler set-up is the intermediate one.

## 3. Experimental setup and test conditions

The burner was fuelled with propane and a synthetic mixture of $CH_4$, CO, $CO_2$, $H_2$ having the composition and properties reported in Table 1 They are typical of a gas from wood pyrolysis, according to working data pertinent to the demonstrative plant described in [7].

The test bed, shown in Fig. 4, was designed to allow an easy implementation of different experimental techniques: PIV, thermocouple measurements and exhaust gas emissions measurements. Combustion air is supplied by a

radial blower, while propane and simulated syngas mixture are stored in pressurized bottles.

*Table 1. Simulated syngas composition and properties*

| Composition (vol.) | | Properties | |
|---|---|---|---|
| $CH_4$ | 21 % | Stoich. *AFR* [-] | 2.76 |
| CO | 29 % | Adiab. flame temp. [K] | 2069 |
| $CO_2$ | 38 % | Specific heat ratio [-] | 1.33 |
| $H_2$ | 7 % | Mol. weight [kg/kmole] | 29.74 |
| $N_2$ | 5 % | *LHV* [MJ/kg] | 9.008 |

The air mass flow was measured using a calibrated orifice placed upstream the air plenum while the fuel mass flow was measured with a Bronkhorst EL-FLOW thermal mass flow meter. The fuel pressure was kept constant for all the tests.
Two types of tests were carried out:
a) tests without combustion, aiming to analyze the flow field characteristics (cold tests);
b) tests with combustion, which were dedicated to temperature and exhaust emissions measurements (combustion tests).

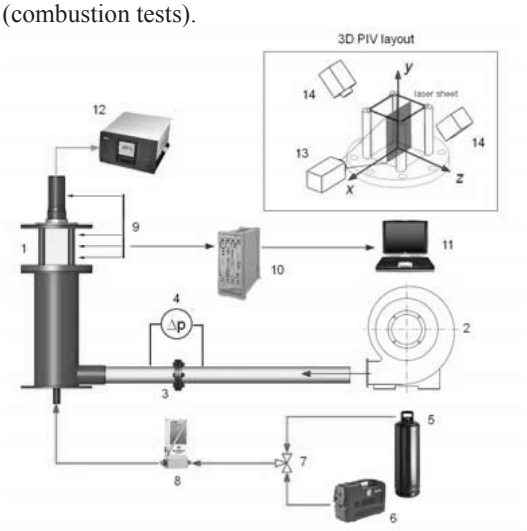


*Fig. 4. Test bed diagram (1 – combustor, 2 -radial blower, 3 – diaphragm, 4 – U tube manometer, 5 – gas cylinder, 6 – air compressor, 7 – three way valve, 8 – thermal mass flow meter, 9 – thermocouples, 10 – data acquisition system, 11 – data acquisition and processing computer, 12 – exhaust gas analyzer, 13 – laser, 14 – CCD cameras)*

### 3.1. Cold tests set up

In order to obtain a comprehensive characterization of the combustor aerodynamics, a PIV technique has been used for confined flow field measurements. Two and three-dimensional measurements were performed on both the longitudinal plane, xy, containing the burner axis and parallel to a couple of windows, and on four transversal planes, xz, normal to the burner axis and located at 3-15-55-95 mm respectively from the burner plate. Three-dimensional Stereo-PIV measurement were performed along the longitudinal xy plane, in order to avoid parallax errors due to the strong out of plane velocity component (i.e. the w tangential velocity) that characterize that measurement plane. It was not possible to obtain reliable PIV measurements closer to the fuel and air nozzles exit section, because of the background noise that would have affected the PIV images due to the unavoidable laser light reflections from the burner plate.
The PIV system set-up includes a 125 mJ double cavity Nd:Yag laser operated at a wavelength of 532 nm, two 12-bit CCD camera with a resolution of 1024 x 1280 pixels and the related synchronization and acquisition systems.
The laser sheet thickness was set at about 1.5 mm. As shown in Fig. 4, the cameras were aligned along the z direction and placed symmetrically with respect to the measurement plane xy, such that the axis of both the lenses met at an angle of 90° on the object plane. The correct focusing of all the points in the measurement plane was achieved by mounting the cameras on two Scheimplufg adapters. For camera calibration, images of a calibration target are required. The target was mounted on a micrometer for fine control, whilst traversing the out-of-plane depth (z-direction). The target contained calibration markers (black dots on white background), for which the true positions (horizontal x and vertical y in plane co-ordinates) were known a priori. The target was traversed to acquire calibration images at 5 different planes spaced at 0.35 mm covering the full thickness of the light sheet (1.5 mm). The flow was seeded with oil particles generated by a Laskin nozzle, with a characteristic size of 1.2 μm. All PIV images were processed using commercial software PIVview, with a first interrogation window of 32 x 32 pixels, a single step of window size refinement and 50% of window overlapping. Two steps of window distortion-displacement were used for each step of the refinement procedure. Finally, a Gaussian peak-fitting was adopted to perform the sub-pixel interpolation. Vector validation was performed with tests based on a normalized median filter and on criteria of primary to secondary correlation peak and minimum signal-

to-noise ratio. The percentage of invalid vectors was typically low, less than 3%, and only the valid vectors were sampled to obtain the mean velocity fields and turbulent statistics. The normalized rms errors in the statistical quantities derived from 1000 independent samples and were computed as suggested in [8]. Values of 4% and 6% can be assumed as an overall upper bound estimate of the sampling error in the mean and in the rms velocities, respectively.

### 3.2. Combustion tests set up

Two types of temperature measurements were carried out: inside the combustion chamber in order to measure the flame temperature and on the outer surface of the combustion chamber walls to establish the boundary conditions for the numerical simulation.

Flame temperatures were measured with B type thermocouples capable of measuring temperatures up to 1700 °C with a maximum error of 8.5 °C. The temperature was measured along three traverses, as reported in detail in paragraph 4.2.

Wall temperatures were measured in five points along the longitudinal axis of two adjacent walls with K type thermocouples, able to measure temperatures up to 1200 °C with a maximum error of 2.5 °C. Thermocouples were kept in contact with the outer wall surface with a spring mechanism. As effective wall temperature was considered the average of the two walls values on the same measurement level.

The temperatures were monitored with an Agilent data acquisition system composed of the E1421B mainframe and the E1419A multifunction I/O module. Values were recorded only when the system reached the steady state conditions, indicated by low temperature fluctuations (< 2°C).

The flame temperature measurements were corrected taking into account radiation and convection effects, while the error due to heat conduction effects was neglected. The equation used to calculate the corrected temperature $T_{corr}$ is:

$$T_{corr} = T + (\varepsilon\sigma/h)\left(T^4 - T_w^4\right), \quad (7)$$

where $T$ is the measured value and $T_w$ represents the combustion chamber wall temperature. The heat transfer coefficient is defined as:

$$h = k \cdot Nu/d\,, \quad (8)$$

where $d$ is the thermocouple bead diameter.

The Nusselt number was evaluated with the Collis and Williams correlation:

$$Nu = 0.24 + 0.56Re^{0.45}\,. \quad (9)$$

Thermocouple emissivity $\varepsilon$ is a function of temperature and oxidation level of the surface and ranges between 0.18 and 0.24 [9]. The maximum overall temperature error, considering the uncertainties on both the thermocouple emissivity and the characteristic velocity in *Re*, was evaluated about 5%.

Pollutant emissions were measured using a commercial gas analyzer (AVL DiGas 4000), which determines the concentrations of unburned hydrocarbon, carbon monoxide and dioxide using NDIR and the nitrogen oxides concentration with an electrochemical cell. The gas were sampled with a 5 mm tubular probe, inserted co-axially in the exhaust duct of the combustor, and dried.

## 4. Experimental results

### 4.1. Cold tests results

Tests were carried out with a main air flow of 150 or 250 slpm and a secondary air flow calculated to have the same volumetric flow rate of the syngas at the reference equivalence ratio value 0.5.

Fig. 5 shows time averaged velocity components and the related rms velocities obtained at 250 slpm. Significant radial velocities are detected only in the region close to the burner plate, where the swirling flow is expanding in the burner volume. The progressive enlargement of the swirling zone along the burner axis is obviously accompanied by a reduction of the swirling velocity, *w*. This latter increases again in the region closer to the burner top plate where the flow is forced trough the exhaust pipe. The strongest velocity fluctuations are detected at the swirler exit, with dominant components along both the axial and tangential directions. The observed high levels of turbulent fluctuations surely allows for a proper mixing between air and fuel in the first part of the burner where combustion must be triggered.

Fig. 6 allows to understand the mean flow structure inside the burner volume. Axial (*u*) and in-plane ( $\sqrt{v^2 + w^2}$ ) velocity contours are reported in the xy and xz planes, respectively. The time-averaged stream-tracers plotted in the xy plane show that the swirling air jet develops with an opening angle of about 90°. The jets are bounded by two recirculation zones: an inner one, which extends from the central bluff-body to the upper part of the combustion chamber, and an outer recirculation zone of much smaller dimension, located in the lower part of the

combustion chamber. The same behavior was observed at the flow rate of 150 slpm, and was obviously described also in [1], [2] with reference to burning conditions. The spatial evolution of the swirling motion inside the combustion chamber is clearly put in evidence by the stream-tracers plotted in the xz planes. Corner effects are also clearly visible, especially at 15 mm from the burner plate, but as a whole the core of the resulting flow field is almost axial-symmetric.

The experimental flow fields were compared with numerical results obtained by means of CFD simulations. The objective was to develop a reliable numerical model of the combustor to be used as a basis for the implementation of combustion and emissions sub-models.

Commercial software package Fluent 6.3 was used. A multi-block structured computational grid was developed, consisting of approximately 2.6 million cells. The numerical domain comprises the combustion chamber, the inlet air duct downstream the air radial swirler and the inlet fuel duct, downstream the fuel axial swirler. The flow field was solved with the SIMPLE algorithm for velocity-pressure coupling; turbulence was modelled using the k-ε model, with standard wall treatment functions. The boundary conditions set at the air and fuel inlet sections are reported in Table 2.

*Table 2. Flow field boundary conditions*

| | | |
|---|---|---|
| Inlet air mass flow [slpm] | 150 | 250 |
| Inlet air swirl/radial vel. ratio [-] | 1.804 | 1.804 |
| inlet air turbulence intensity [%] | 10 | 10 |
| Inlet air hydraulic diameter [mm] | 14 | 14 |
| Inlet fuel mass flow [slpm] | 3.1 | 5.2 |
| Inlet fuel swirl/axial vel. ratio [-] | 1 | 1 |
| Inlet fuel turbulence intensity [%] | 5 | 5 |
| Inlet fuel hydraulic diameter [mm] | 4 | 4 |

Fig. 7 compares PIV and numerical values of axial, radial and tangential components of velocity at four transversal sections of the combustor. In particular, the first section is close to the combustor entrance (h =3 mm) and the last one is in the middle of the recirculation zone (h =55mm).

As a whole, numerical and experimental data are in good agreement, in particular as far as the radial position is concerned where axial velocity becomes null, indicating the extension of the reverse flow relative to the inner recirculation vortex.

Numerical results also match the experimental radial trends of velocity components, with a not significant underestimation in few transverses.

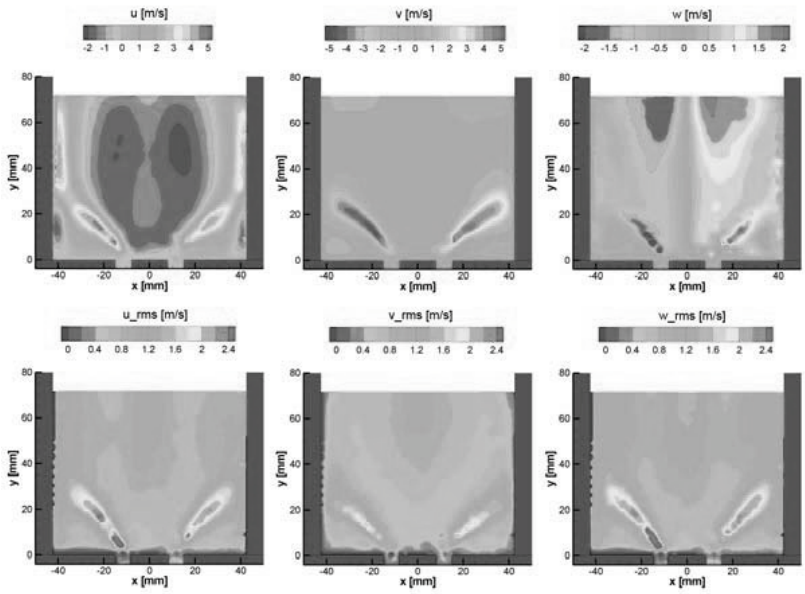


*Fig. 5. Mean and rms velocity components in the xy plane at 250 slpm flow rate.*

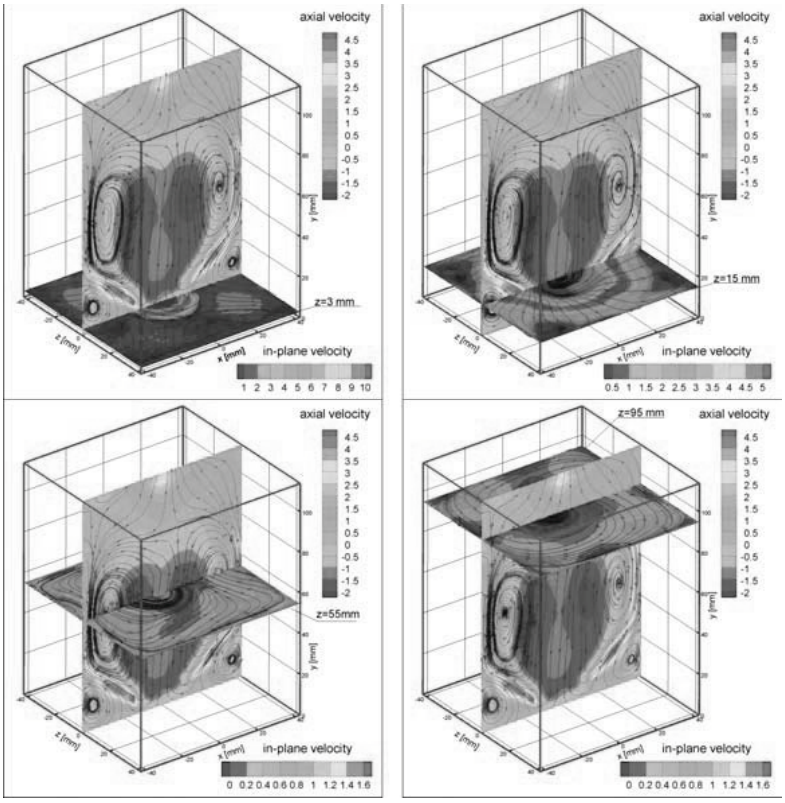


*Fig. 6. Time-averaged flow structure in the combustion chamber at 250 slpm.*

### 4.2. Combustion tests results

Flame tests were carried out with propane and simulated syngas mixture at constant equivalence ratio $\phi = 0.5$, with two air flow rates 150 and 250 slpm. The paper presents mainly the results related to the higher air flow rate. Wall temperatures, in these conditions, are reported in Table 3.

*Table 3. Measured wall temperatures*

| Propane | | | | | |
|---|---|---|---|---|---|
| $z$ [mm] | 15 | 35 | 55 | 75 | 95 |
| $T$ [K] | 365 | 447 | 461 | 450 | 436 |
| Syngas | | | | | |
| $z$ [mm] | 15 | 35 | 55 | 75 | 95 |
| $T$ [K] | 315 | 376 | 396 | 384 | 389 |

Flame temperature measurements were carried out along three half-traverses parallel to the burner plate, distant 15 - 55 - 95 mm from it and named T1, T2 and T3, respectively. They correspond to the combustion chamber transversal sections considered for the early described cold PIV analysis, so that local values of measured velocities were used as a first approximation of the effective ones to correct thermocouple response according to (7).

The experimental temperature profiles were compared with numerical results obtained by the CFD simulations. In this CFD study, the reactive flow was solved with two modeling approaches, namely the ED-FR (Eddy Dissipation Finite Rate) combustion model and the "flamelet" combustion model. The ED-FR, well proven for hydrocarbon fuels, was used to simulate both the propane and the syngas combustion case, by means of reduced chemistry.

Reduced or global mechanisms for CFD simulations are mostly developed for hydrocarbon fuels or for gasification syngas [10]-[12]. In this study the propane-air combustion simulation with the ED-FR was performed with a simple two-step reaction mechanism [13], while the syngas-air combustion case was simulated with the ED-FR with a four-step mechanism [14].

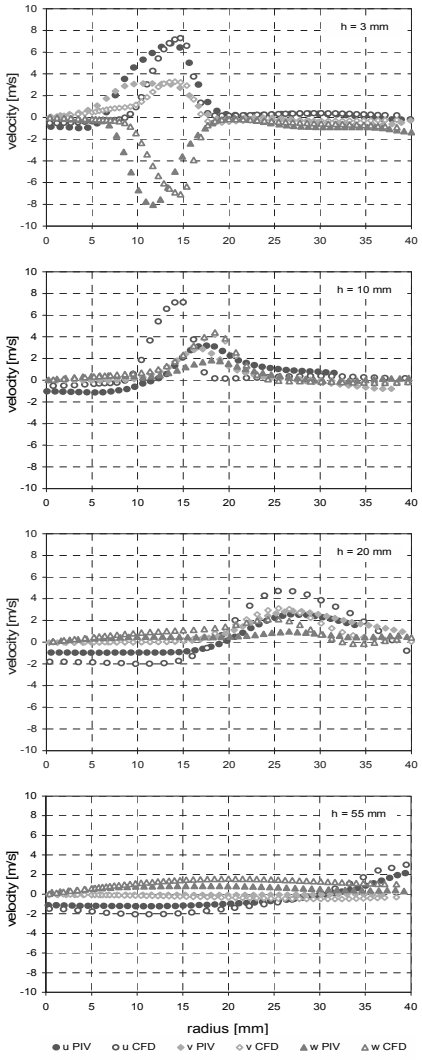


*Fig. 7. Comparison between experimental and numerical values of the axial (u), radial (v) and tangential (w) components*

Detailed multi-species and multi-step chemical mechanisms require large computational capacity, if the ED-FR model is used. The flamelet model, instead, assumes decoupling of the chemical reactions and the turbulent mixing time scales, so that it can treat multi-step chemical mechanisms with limited computational effort. Presently, comprehensive mechanisms are available for methane-air combustion, such as the GRI 3.0 (53 species and 325 reactions) [15], which involves also the key species ($H_2$, $CH_4$, CO, $CO_2$) typical of a biomass derived syngas. The GRI 3.0 has been used in this study to reproduce the syngas combustion process. Moreover, a reduced mechanism (16 species and 25 reactions), developed by Smooke [16] for methane-air combustion, has been used in case of syngas combustion.

Fig. 8 reports the results for the air flow rate of 250 slpm and both fuels. At the T1 position propane and syngas experimental curves have similar shape, characterized by a local minima between 10 and 20 mm from the burner axis, close to the inner recirculation zone. Increasingly higher temperature was detected with propane going from the window proximity to the burner axis, where the maximum difference of about two hundred degrees was reached. The corresponding numerical profiles obtained in the T1 section, with all the models and with both the fuels, show strong overestimation in the near axis region, while underestimation occurs in the region close to the wall boundary. The propane case shows the largest mismatch between experimental and numerical values.

At T2 and T3 positions practically the same temperature were measured with the two fuels at all radius values, and numerical results provide good agreement with experiments. In detail, the use of reduced mechanisms and the adoption of the ED-FR model give good results in both propane and syngas combustion. The flamelet model correctly predicts the temperature trend, but with overestimation (up to around 200°C) especially in the T2 section.

The described results can be explained considering that the T1 traverse crosses the flame, which shape depends on fuel properties, fuel/air volumetric ratio and extremely complicated local physical and chemical processes, while T2 and T3 traverses are in a more homogeneous combustion chamber zone, governed mainly by internal aerodynamics and global energy balance. So the discrepancy observed between calculated and measured values of the flame temperature fields could be due to local extinction and/or unsteady phenomena, not considered in the performed calculation, and also to the used chemical mechanisms, which were originally developed for methane-air flames.

Emissions experimental and numerical results are summarized in Table 4, where concentration values are referred on a dry sample basis.

CO values calculated with the flamelet models are very low and rather close to the experimental data (one should consider that the experimental value is

close to the resolution limit of the gas analyzer, which had a percentage scale).

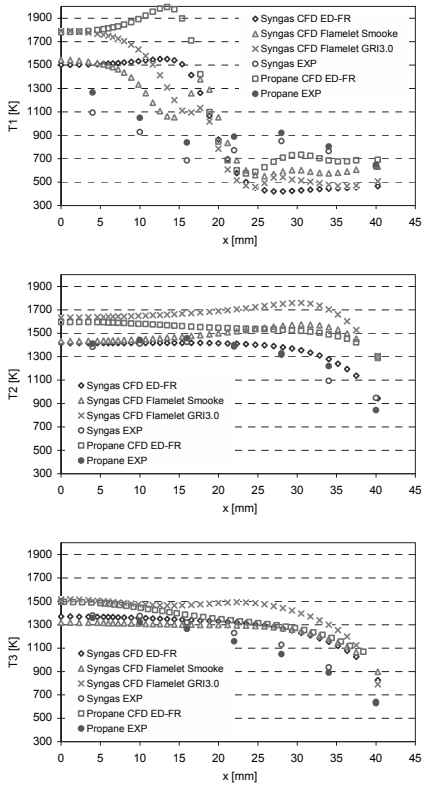


*Fig. 8. Calculated and experimental profiles of temperature at different transversal sections*

*Table 4. Syngas emissions (air mass flow 250 slpm)*

| | EXP | CFD ED-FR | CFD Flam. (GRI 3.0) | CFD Flam. (Smooke) |
|---|---|---|---|---|
| CO [$\%_{vd}$ 15%$O_2$] | 0.02 | 0.20 | 5e-4 | 3e-4 |
| NO [$ppm_{vd}$ 15%$O_2$] | 2 | 0.001 | 123 | 0.001 |
| $CO_2$ [$\%_{vd}$] | 14.9 | 13.9 | 14.5 | 14.3 |
| $O_2$ [$\%_{vd}$] | 9.7 | 10.1 | 10.0 | 10.1 |

NO concentration obtained with the GRI 3.0 (this mechanism include the NO formation path) are larger than the experimental one, while the use of Fluent post-processing $NO_x$ routines (applied in case of both ED-FR and Smooke flamelet mechanism) provides negligible NO concentration, comparable, from a practical point of view, with the measured value.

Generally, the capability to predict pollutant emissions of the tested combustion models is still quite questionable and requires further investigations. It should be also mentioned that inaccuracy in the thermal field indirectly affects the emission calculations. Anyway, in the studied case, the flamelet Smooke approach proved to be the most reliable.

## 5. Conclusions

Experimental results on internal aerodynamics and combustion behavior of an atmospheric combustor model for confined, non-premixed swirl-stabilized flames, fuelled with propane and simulated syngas, have been presented and used as validation data for the development of CFD simplified combustion models. The reactive flow was solved with two modeling approaches, namely the ED-FR and the flamelet combustion models. With the ED-FR approach the propane-air combustion simulation was performed with a simple two-step reaction mechanism, while the syngas-air combustion case was simulated with a four-step one. Because flamelet model can treat multi-step chemical mechanisms with limited computational effort, a GRI 3.0 comprehensive mechanism and a reduced mechanism developed by Smooke have been used in this study to reproduce the syngas combustion process. As a whole, ED-FR model provide good agreement with the experimental thermal field while flamelet models correctly predicts the temperature trend, but with some local overestimation. As far as emissions are concerned, the Smooke flamelet approach proved to be the most reliable.
Future work will be dedicated to further investigations on combustion models and to improve the experimental facility, taking also into account other syngas compositions.

## Nomenclature

*AFR* Air Fuel Ratio
CCD Charge-Coupled Device
CFD Computational Fluid Dynamics
IGCC Integrated Gasification Combined Cycle
*LHV* Lower Heat Value, MJ/kg
NDIR Non Dispersive Infrared
PIV Particle Image Velocimetry
$G_\theta$ axial flux of angular momentum, kg $m^2/s^2$
$G_y$ axial flux of axial momentum, kg $m/s^2$
*Nu* Nusselt number

*Re* Reynolds number
*R* reference radius, m
*S* swirl number
T1,2,3 temperature measurements traverses
*T* temperature, K
*d* diameter, m
*h* heat transfer coefficient, $W/m^2K$
*k* gas thermal conductivity, W/mK
*m* mass flow rate, kg/s
*p* pressure, Pa
*r* radius, m
*u* axial velocity, m/s
*v* radial velocity, m/*s*
*w* tangential velocity, m/s

Greek symbols

$\alpha$ swirler blade angle, °
$\varepsilon$ emissivity
$\phi$ equivalence ratio
$\rho$ density, $kg/m^3$
$\sigma$ Stefan Boltzmann constant, $W/m^2K^4$

Subscripts and superscripts

a axial direction
d dry
i inner
r radial direction
t tangential direction
v volumetric
w combustion chamber wall

## References

[1] Tsurikov M., Meier W., Geigle K.P., 2006, "Investigations of a syngas-fired gas turbine model combustor by planar laser techniques", Proc. of ASME TurboExpo 2006.
[2] Kutne P., Boxx I., Stohr M., Meier W., 2007 "Experimental analysis of the combustion behaviour of low calorific syngas mixtures in a gas turbine model combustor" Proc. Of ECM 2007.
[3] Speth R.L., Altay H.M., Hudgins D.E., Ghoniem A.F., 2008, "Dynamics and stability limits of syngas combustion in a swirl-stabilized combustor", Proc. of ASME TurboExpo 2008.
[4] Pater S. G.M., Kok J. B.W., Van der Meer T., 2006, "Thermo acoustic flame transfer function prediction for turbulent non-premixed syngas flames", Proc. of ASME TurboExpo 2006.
[5] Casarsa L., Micheli D., Pediroda V., Radu R., 2009, "Investigations of pyrolysis syngas swirl flame in a combustor model" Proc. of ASME Turbo Expo 2009.
[6] Beèr J.M., Chiegier N.A., 1972 "Combustion Aerodynamics", Applied Science Publishers LTD, London.
[7] Fantozzi F., D'Alessandro B., Desideri U., 2007, "An IPRP (Integrated Pyrolysis Regenerated Plant) microscale demonstrative unit in central Italy", Proc. of ASME TurboExpo 2007.
[8] Casarsa L., Giannattasio P., 2008, "Three-dimensional features of the turbulent flow through a planar sudden expansion", Phys. Fluids 20 (1) (2008) 015103-1-15.
[9] Struk P., Dietrich D., Valentine R., Feier I., 2003, "Comparisons of Gas-Phase Temperature Measurements in a Flame Using Thin-Filament Pyrometry and Thermocouples", NASA/TM—2003-212096.
[10] D. Bohn, J. Lepers, 1999, "Numerical simulation of swirl-stabilized premixed flames with a turbulent combustion model based on a systematically reduced six-step reaction mechanism", J. Eng. Gas Turbines Power, Vol 123, October 1999.
[11] N. Slavinskaya, M. Braun-Unkhoff, P. Frank, 2008,"Reduced Reaction Mechanisms for Methane and Syngas Combustion in Gas Turbines", J. Eng. Gas Turbines Power, March 2008.
[12] M. Braun-Unkhoff, N. Slavinskaya, M. Aigner, 2009, "A detailed and reduced reaction mechanism of biomass-based syngas fuels", Proc. of ASME Turbo Expo 2009.
[13] Westbrook, C.K., Dryer, F.L., 1981, "Simplified Reaction Mechanisms for the Oxidation of Hydrocarbon Fuels in Flames", Comb. Sci. and Tech. Vol. 27, 31-43.
[14] W.P. Jones, R.P. Lindstedt, Global reaction schemes for hydrocarbon combustion, Combust. Flame 73 (1988) 233-249.
[15] http://www.me.berkeley.edu/gri_mech.
[16] M.D. Smooke, I.K. Puri, K. Seshadri, Proc. Combust. Inst. 21 (1986) 1783–1792.

**Acknowledgments:** Research supported by the MIUR-COFIN 2008 found. Special thanks to Nicola Zuliani for his support during the experimental phase and to Paolo Cescot for his support to the numerical processes.

# The Fate of Ammonia and Hydrogen Cyanide during Flameless Combustion of Low Calorific Value Gases

*Mariusz Zieba[a], Mathias Fink[a], Anja Schuster[a], Günter Scheffknecht[a] and Roland Berger[b]*

*a Institute of Combustion and Power Plant Technology (IFK), University of Stuttgart, Germany*
*b e-flox GmbH, Renningen, Germany*

**Abstract:** In this paper, the review of the experimental investigations on the fuel-$NO_x$ formation during flameless combustion is presented. The first series of experiments described in the paper were conducted using ammonia doped synthetic gases with different compositions. During these experiments, the influence of gas composition on the conversion of ammonia ($NH_3$) to $NO_x$ is investigated. In the second part experiments, in which product gas generated in fluidized bed gasifier is subsequently combusted in FLOX®-Burner are presented. These results show the dependences between the gasifier operating parameters, product gas composition and final $NO_x$ emissions. Moreover, the concentrations of the ammonia and hydrogen cyanide (HCN) in the product gas were measured in order to calculate the conversion ratios of these compounds to $NO_x$. The results show a significant influence of the gas composition and the gasifier process parameters on the final fuel-$NO_x$ emission. In particular, the hydrocarbon content influences the ammonia to $NO_x$ conversion. Lowest $NO_x$ emissions and therefore lowest conversion ratios were measured when burning gases with lower hydrocarbons content. An increase in hydrocarbon concentration of the gas corresponded to a rapid increase in the conversion ratios.

**Keywords:** Fuel-$NO_x$, Flameless Combustion.

## 1. Introduction

The wide-ranging applicability of the Flameless oxidation (FLOX®) technology for the utilization of natural and low calorific value gases has already been proven and reported in the literature [1-3]. This technology became of interest due to its great potential in reducing thermal nitrogen oxides (thermal-$NO_x$) while burning natural gas. In addition to excellent burn-out, the fact that fluctuations in the fuel composition do not lead to combustion instabilities, is a reason for the high interest in combusting low calorific value gases (LCV) in flameless burners. However, the tests with biogenous gaseous fuels have shown a limited ability to reduce $NO_x$, where most of the $NO_x$ emissions originate from the fuel-bound nitrogen [4,5]. During the gasification process, the nitrogen contained in the solid fuel is partly released to the product gases as ammonia ($NH_3$) or hydrogen cyanide (HCN). These compounds are formed as a result of thermal destruction of proteins and thus amino acids contained in the biomass [6,7]. The $NH_3$ and HCN compounds are either converted to $NO_x$ or reduced to neutral $N_2$ in the combustion process. The selectivity of this process depends on the gas composition, temperature and mixing of the reactants during combustion. In this paper, the review of the experimental investigations on the fuel-$NO_x$ formation during flameless combustion is presented. The first series of experiments described in the paper were conducted using synthetic gases with different compositions. During these experiments, ammonia was added to the fuel stream in order to investigate the fuel nitrogen conversion. The goal of these experiments was to investigate the influence of gas composition on the conversion of ammonia to $NO_x$. Moreover, experiments in which product gas generated in a bubbling fluidized bed (BFB) gasifier is subsequently combusted in a FLOX®-Burner are presented. Since the gasifier product gas composition depends on the gasification process parameters such as air ratio (AR) and temperature, the final $NO_x$ emission is also influenced by these factors. The goal of these experiments was to investigate the dependences between gasifier operating parameters, product gas composition (combustibles, $NH_3$ and HCN concentration) and final $NO_x$ emission during flameless combustion of these gases.

## 2. Experimental

In this section the burner test rig, gas mixing unit, fluidised bed gasifier, characterization of the tested synthetic and solid fuels, gasifier settings and the analysis and measurement methods are presented.

### 2.1. Burner test rig

The experimental facility consists of 20 kW FLOX®-Burner coupled either with the gas mixing unit during experiments with synthetic gases or with the fluidised bed gasifier during experiments with solid fuels. The burner, shown in Fig. 1, has been originally developed for natural gas and was subsequently modified to combust low calorific value gases. During start-up the combustion chamber is heated in flame mode up to 850 °C using natural gas. Above this temperature the burner can be switched to flameless mode and fired either with low calorific value gas prepared in the gas mixing unit or with product gas generated in the gasifier. The combustion air is preheated while passing through a ceramic recuperator pipe. The temperature of the combustion chamber is controlled using an air-cooled pipe. In this type of burner the preheated combustion air is introduced separately to the fuel into the combustion chamber. The air velocity of about 70 to 100 m/s causes high internal recirculation of the hot flue gases. These hot products are partially mixed with the fuel and oxidizer before the mixture ignites. As a result, there is no identifiable flame front. The reactants are strongly diluted and the temperature field is homogeneous without high peaks.

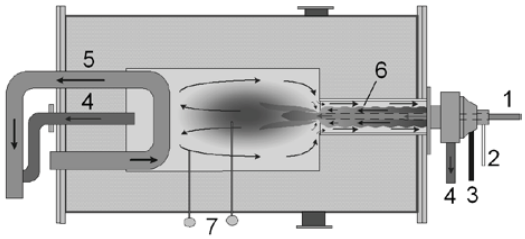


*Fig. 1. Scheme of FLOX®-Burner test rig (1 – natural gas or LCV gas with ammonia, 2 – natural gas, 3 – combustion air, 4 – flue gas, 5 – cooling pipe, 6 – recuperator pipe, 7 – thermocouples)*

### 2.2. Gas mixing unit

The gas mixing unit where the fuel gas is prepared allows mixing of $CH_4$, CO, $CO_2$, $H_2$ and $N_2$. The flow of each gas is controlled by digital mass flow controller. The gases were mixed and supplied to the burner at room temperature. Additionally ammonia was introduced to the fuel stream to simulate the fuel nitrogen oxides precursors.

### 2.3. Bubbling Fluidised Bed (BFB) gasifier

The reactor is made of high-temperature steel and is heated by five electrical heating zones which can be controlled separately. The heating zone at the bottom of the reactor vessel, where the bed material is fluidized and the biomass is fed has a heating capacity of 11 $kW_{el}$. Every other heating zone above has a heating capacity of 4 $kW_{el}$. The maximum heating zone temperature is 1000 °C, while the resulting maximum process temperature can be 950 °C.

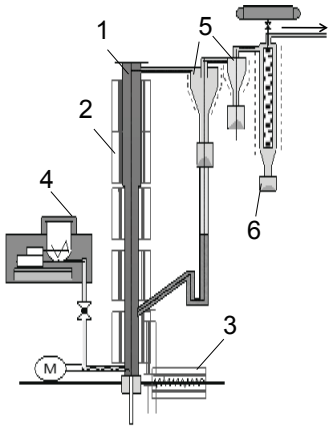


*Fig. 2. Scheme of BFB gasifier (1 –reactor tube, 2 – electrical heaters, 3 – air preheater, 4– fuel feeding unit, 5 – cyclones, 6 –candle filter)*

The fluidization air can be preheated up to 900 °C in a two zone electrical gas preheater. The absolute pressure in the BFB is controlled through a pressure control valve in the range of 0-100 mbar. The fuel feeding system is a screw feeder system where the fuel volume flow rate is controlled. The fuel rate can be set between 1 and maximum 7 kg/h depending on the type of fuel used. The product gas exits the reactor vessel and proceeds to two in series connected and electrically heated cyclones and consecutively to a candle filter. Thus, dragged particles like ashes, char and bed material are removed. After the candle filter, a part of the product gas is lead through a suction point to gas analysis. The main part of the product gas is lead

via stainless steel pipe heated to 350 °C to the FLOX®-Burner.

### 2.4. Fuel composition – experiments with synthetic gases

During typical air gasification the main combustible components in the product gas are carbon monoxide and hydrogen. The amount of methane and higher hydrocarbons is usually relatively small. However, the composition of the gasification product gas depends on the used solid fuel, gasifier operating parameters and gasifier type. During the experiments with synthetic gases the composition of the investigated fuels is similar to the product gases from gasification processes. In order to cover such big range of different gas compositions three synthetic gases with $CO/H_2$ ratios of 0.5, 0.7 and 1.5 were investigated. For each of the $CO/H_2$ ratio, methane content was varied between 0 and 10 vol-% to investigate the influence of hydrocarbons on the ammonia to $NO_x$ conversion during flameless combustion. The concentration of CO and $H_2$ was kept constant for each of $CO/H_2$ ratio. Therefore, increasing the methane content in the mixture the nitrogen ($N_2$) concentration was decreasing and the lower heating value of the fuel was increasing. The ammonia concentration of 700 ppmv was constant for all experiments. This concentration is related to the total mixture of fuel and combustion air to ensure the same ammonia partial pressure for each working point. All of mentioned experiments were carried out at the same power input of 18 kW. The compositions of the tested synthetic fuels are summarized in Table 1.

*Table 1. Composition and lower heating value (LHV) of the synthetic fuels.*

| | | Gas 1 | Gas 2 | Gas 3 |
|---|---|---|---|---|
| CO | (vol-%) | 18 | 18 | 27 |
| $H_2$ | (vol-%) | 16 | 25 | 18 |
| $CO_2$ | (vol-%) | 15 | 15 | 15 |
| $CH_4$ | (vol-%) | 0-10 | 0-10 | 0-10 |
| $CO/H_2$ | (-) | 0.5 | 0.7 | 1.5 |
| LHV | ($MJ/m^3_{stp}$) | 6.2-9.7 | 5.0-8.5 | 5.4-8.9 |
| $NH_3$ | (ppmv) | 700 | 700 | 700 |

### 2.5. Solid fuel composition and gasifier settings – experiments using BFB gasifier

In the second part of experiments wood pellets and rape cake pellets were used as a fuel for experiments in which the flameless burner was fired using product gas from the gasifier. During the experiments the air was used as a gasification agent. The characteristics of the solid fuels are given in Table 2.

*Table 2. Characteristics of the tested biomass*

| | | Wood pellets | Rape cake pellets |
|---|---|---|---|
| Moisture | (wt-% ar) | 7.36 | 8.10 |
| Ash | (wt-% ar) | 0.54 | 5.94 |
| C | (wt-% ar) | 46.43 | 45.00 |
| H | (wt-% ar) | 5.77 | 6.67 |
| N | (wt-% ar) | <0.3 | 4.98 |
| S | (wt-% ar) | <0.3 | 0.48 |
| LHV | (MJ/kg dm) | 20.20 | 17.76 |

Since rape cake pellets contain a high amount of nitrogen, high amounts of $NH_3$ and HCN and therefore high emissions of $NO_x$ are expected during the experiments. Both of the presented fuels were gasified under different temperatures and gasifier air ratios. All experimental conditions are presented in Table 3.

*Table 3. Gasifier operating parameters*

| Fuel | Gasification parameters | |
|---|---|---|
| | T (°C) | Air Ratio |
| Wood pellets | 750 | 0.15 |
| | | 0.22 |
| | 875 | 0.15 |
| | | 0.22 |
| Rape cake pellets | 750 | 0.22 |
| | 875 | 0.22 |

### 2.6. Analysis and measurement methods

In order to evaluate the conversion ratios of the fuel-N (injected $NH_3$ for experiments with synthetic gases or $NH_3$ and HCN in the product gas during experiments with gasifier) to $NO_x$ the following equation was applied

$$CR_{N\rightarrow NOx} = \frac{[NO_x]_{fluegas} \cdot \dot{V}_{fluegas}}{[N]_{fuel} \cdot \dot{V}_{fuel}}, \qquad (1)$$

where: $[NO_x]_{fluegas}$ - $NO_x$ concentration in the flue gas in $ppmv_{dry}$, $[N]_{fuel}$ - concentration of $NH_3$ and HCN in the fuel in $ppmv_{dry}$, $\dot{V}_{fluegas}$ - flue gas flow in $m^3_{stp}/h$, $\dot{V}_{fuel}$- fuel flow in $m^3_{stp}/h$. During all tests exhaust gas was continuously sampled and analysed at the combustion chamber exit with

respect to $O_2$, $CO_2$, CO, NO, $NO_2$ and $NO_x$. During the experiments in which the burner was coupled with the gasifier the product gas was analysed continuously with respect to CO, $CO_2$, $CH_4$, $H_2$ and $O_2$. Moreover, a gas chromatograph was used to determine the content of ethene ($C_2H_4$), ethane ($C_2H_6$) and propene ($C_3H_6$). The ammonia and hydrogen cyanide concentrations in the product gas were measured in order to investigate the dependences between gasifier operating parameters, product gas composition (combustibles, $NH_3$ and HCN concentration) and final $NO_x$ emission during flameless combustion of these gases. The product gas was sampled in the vicinity of the burner inlet. The gas sampling pipe was heated to 350 °C to avoid ammonia and tars condensation. The gas was flowing through heated filter and was lead to three impinger bottles placed in an ice bath. The ammonia was solved in a 0.01 M $H_2SO_4$ solution and hydrogen cyanide was solved in a 2 M NaOH solution. The gas flow, temperature, pressure and oxygen concentration in the sampling gas was measured to ensure high quality of the sampling. The content of $NH_3$ and HCN in the solutions was afterwards analysed in laboratory according to [8-9]. For each gasifier setting two gas samples were collected. The content of $NH_3$ and HCN is given as average value of the analysed samples.

## 3. Results

In this section the experimental results achieved using ammonia doped synthetic gases and product gases generated in the BFB gasifier are presented.

### 3.1. $NO_x$ emission during $NH_3$ doped synthetic gas combustion

In order to investigate the dependences between hydrocarbons concentration in the fuel and fuel nitrogen to $NO_x$ conversion experiments with varying methane content were conducted. The air ratio was set to 1.5. Since the high dilution of the reaction zone caused by the internal recirculation of the hot flue gases significantly decreases the temperature peaks in the chamber, the combustion of all tested fuel mixtures occurs at very similar temperature. When increasing the methane content the temperature was slightly changing in the range of 960 to 980 °C. However, such small temperature difference does not have any considerable influence on ammonia to $NO_x$ conversion ratios [10]. Fig. 3 shows the $NO_x$ concentration in the flue gas for three different $CO/H_2$ ratios as a function of methane concentration in the fuel. Increasing the methane content from 0 to ca. 6 vol-%, the concentration of $NO_x$ in the flue gas was rising rapidly. Further increase above 6 vol-% of methane content had only minor influence on the $NO_x$ emissions. At concentration of 10 vol-% the emissions reached the maximum observed values. Moreover, the emission of $NO_x$ increases with decreasing $CO/H_2$ ratio.

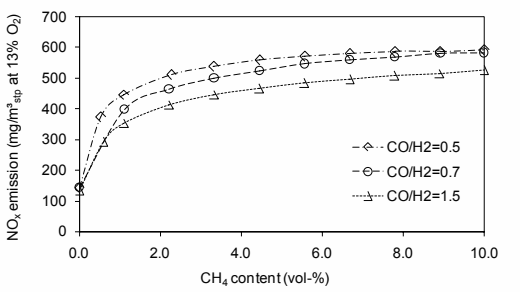


*Fig. 3. $NO_x$ concentration in the flue gas as a function of methane concentration in the fuel; ($t_{comb}$=970 °C, AR=1.5, P=18 kW)*

Fig. 4 presents the calculated ammonia to $NO_x$ conversion ratios. The results show that the investigated $CO/H_2$ ratios had no significant influence on the conversion ratios. Therefore, the higher $NO_x$ emissions by lower $CO/H_2$ ratios were observed due to the changing content of water vapour in the flue gas generated from the hydrogen oxidation. Varying the methane concentration, the conversion ratios increase from ca. 0.16 for methane-free mixtures to above 0.6, when 10 vol-% of methane was present in the fuel.

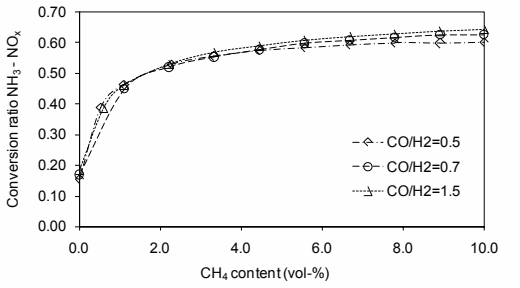


*Fig. 4. Ammonia to $NO_x$ conversion ratio as a function of methane concentration in the fuel; ($t_{comb}$=970 °C, AR=1.5, P=18 kW)*

In order to investigate the influence of the burner air ratio on the $NO_x$ emissions, ammonia doped

fuel with $CO/H_2$ ratio of 0.7 and varying methane concentration was burned with two different air to fuel ratios of 1.3 and 1.6. The methane content was varied between 0 and 4.5 vol-%. Figure 5 shows the $NO_x$ emissions obtained in these experiments. The tests were carried out at 970 °C and the power input of 18 kW. Similar to the previous experiments the $NO_x$ emissions were increasing with increasing methane content in the fuel for both investigated air ratios. However, for methane-free mixtures the air ratio had a minor influence on the $NO_x$ emissions. Increasing the methane content in the fuel, the influence of burner air ratio was slightly growing.

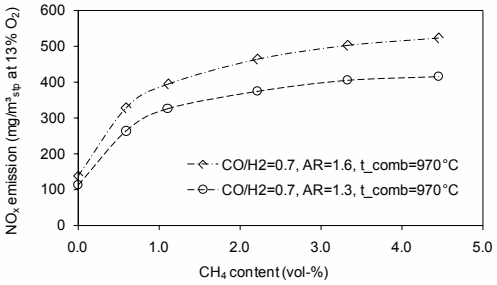


*Fig. 5. $NO_x$ concentration in the flue gas as a function of methane concentration in the fuel; ($t_{comb}$=970 °C, P=18 kW)*

## 3.2. $NO_x$ emission during flameless combustion of product gases generated in the BFB gasifier

In order to investigate if similar dependences described in Section 3.1 can also be observed using product gases generated from biomass gasification a series of experiments using wood pellets and rape cake pellets as a gasifier feedstock were conducted. The product gas generated in the gasifier was subsequently combusted using the flameless burner. During the experiments product gas composition, including $NH_3$ and HCN, and flue gas composition were measured simultaneously. The composition of product gas from gasification process can not be as precisely controlled as synthetic gas from mixing unit. Therefore, to influence the product gas composition the solid bio-fuels were gasified at 750 °C and 875 °C with the air ratio of 0.15 and 0.22 in case of wood pellets and 0.22 in case of rape cake pellets. Fig. 5 shows the measured hydrocarbons concentrations for both fuels for all tested operating gasifier parameters. With growing temperature and air ratio the total amount of hydrocarbons was slightly decreasing and was similar for both fuels. During gasification of rape cake pellets much higher amounts of $C_2H_4$ were present in the product gas in comparison to wood pellets product gas. Higher gaseous hydrocarbons than $C_3H_6$ and tars were not measured.

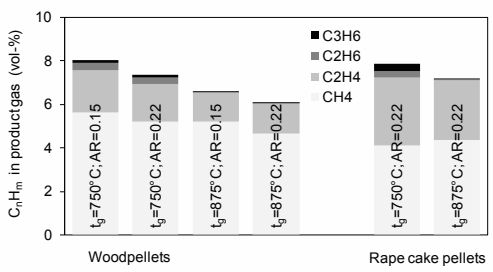


*Fig. 5. Hydrocarbons concentrations in the product gas during wood and rape cake pellets gasification*

### 3.2.1 Fuel-$NO_x$ precursors and $NO_x$ emission - wood pellets

The measurement results of fuel $NO_x$ precursors obtained during wood pellets gasification are presented in Fig. 6. Ammonia was the main nitrogen containing compound present in the gas. Its concentration was growing with the gasifier temperature. In quite opposite manner behaves the concentration of HCN which decreases with increasing temperature. The influence of gasifier air ratio was minor. However, the concentration of both of fuel-$NO_x$ precursors shows a tendency to increase with higher gasifier air ratio and temperature.

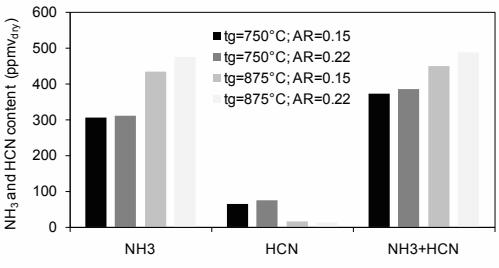


*Fig. 6. $NH_3$ and HCN concentrations in the wood pellets gasification product gas*

The product gases were combusted in the flameless burner at the average combustion chamber temperature of 1050 °C. Although the

quality and quantity of the product gas was changing due to gasification process instabilities the combustion process was very stable. The amount of combustion air was varied resulting in flue gas excess oxygen in the range between 1 to 8 vol-%. Complete combustion was observed already by 1.5 vol-% $O_2$ in the flue gas. By further decrease of excess oxygen, particularly below 1 vol-%, a rapid increase in CO emission was measured. Fig. 7a shows the $NO_x$ emission observed during the experiments. The black crosses represent $NO_x$ emission while burning product gas generated at gasifier temperature of 750 °C, whereas the grey crosses shows the emission achieved by gasifier temperature of 875 °C. The gasifier air ratio in both cases was 0.15. The $NO_x$ emissions are plotted against the excess oxygen in the flue gas.

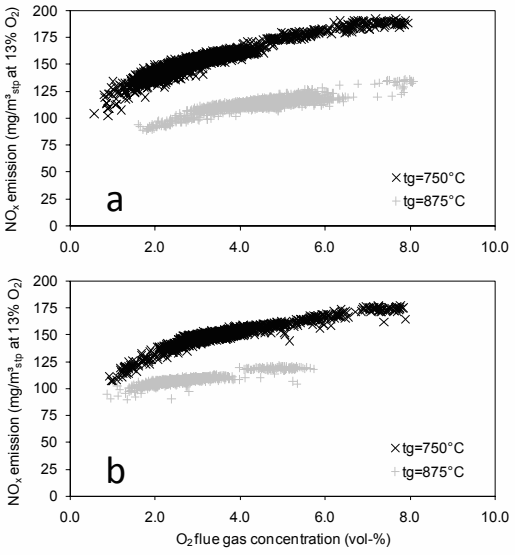


*Fig. 7. $NO_x$ emission during product gas combustion from wood pellets gasification; a – gasification air ratio 0.15, b – gasification air ratio 0.22*

Although, the $NH_3$ and HCN content in the product gas generated at 875 °C was higher the emissions of $NO_x$ are significantly lower. This fact confirms that also during combustion of gasifier product gases the content of the hydrocarbons is crucial for the ammonia and hydrogen cyanide conversion ratios. Due to lower hydrocarbons concentration much less of nitrogen containing compounds in the product gas are converted to $NO_x$ during flameless combustion. Very similar results were observed for higher gasifier air ratio. The results are presented in Fig. 7b. Also in this case higher $NO_x$ emission was measured during combustion of product gas generated at lower gasifier temperature, and thus containing less hydrocarbons. Higher excess oxygen by combustion slightly enhanced the $NO_x$ formation. The influence of the gasifier air ratio was minor. However by higher amount of gasification air the emissions were slightly lower.

### 3.2.2 Fuel-$NO_x$ precursors and $NO_x$ emission – rape cake pellets

In opposite to wood pellets the rape cake pellets contain a high amount of fuel bond nitrogen. Therefore, high concentrations of fuel-$NO_x$ precursors in the gasifier product gas and accordingly high $NO_x$ concentrations in the flue gas were expected.

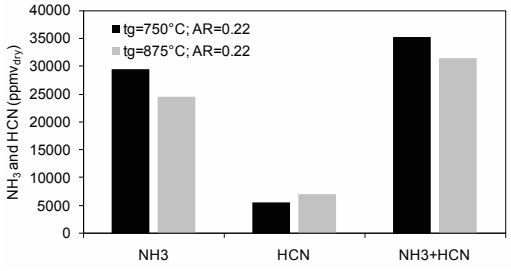


*Fig. 8. $NH_3$ and HCN concentrations in the rape cake pellets gasification product gas*

The concentrations of ammonia and hydrogen cyanide measured in the product gas were much higher than in the case of wood pellets gasification. The concentrations up to 35000 $ppmv_{dry}$ were observed. Contrary to results with wood pellets higher $NH_3$ concentration and lower HCN concentration were measured in the product gas generated at lower gasifier temperature. The total concentration of both fuel-$NO_x$ precursors was lower by higher gasifier temperature. The product gas was subsequently combusted using flameless burner. The average combustion chamber temperature of 1050 °C was the same as during combustion of wood pellets product gas. The amount of combustion air was varied in order to investigate the influence of burner air ratio on $NO_x$ emission. In the case of rape cake pellets product gas, complete combustion was possible beginning at excess oxygen level of 2 vol-%. The $NO_x$ emissions were

about 2 orders of magnitude higher in comparison to wood pellets product gas combustion. The results are presented in Fig. 9. Similarly to the wood pellets case higher $NO_x$ emission was measured by lower gasifier temperature. The difference was growing with the excess oxygen in the flue gas. Higher combustion air ratio significantly enhanced the $NO_x$ formation.

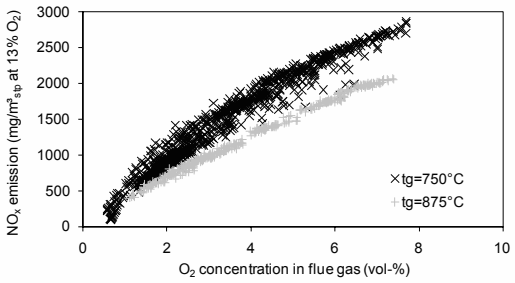


*Fig. 9. $NO_x$ emission during product gas combustion from rape cake pellets gasification (AR=0.22)*

The lower $NO_x$ emission by higher gasifier temperature was observed not only because of lower concentration of $NO_x$ precursors in the product gas. Similar to wood pellets experiments also in this case lower hydrocarbon concentration lead to lower conversion ratios of fuel-nitrogen. Fig. 10 shows the calculated conversion ratios for product gas from rape cake pellets gasification.

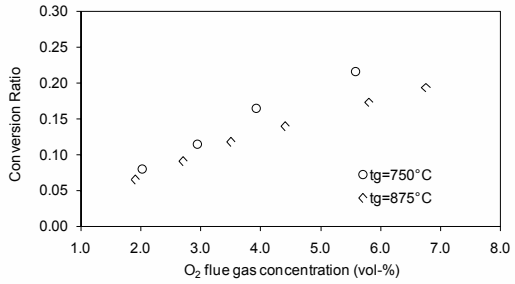


*Fig. 10. $NH_3$ and HCN to NOx conversion ratios during product gas combustion from rape cake pellets gasification (AR=0.22)*

The conversion ratios were calculated according to (1). The conversion ratios calculated for combustion pf product gases generated at the gasifier temperature of 875 °C are lower than by 750 °C in the whole investigated range of excess oxygen. The difference between them is increasing with increasing excess oxygen in the flue gas.

## 4. Discussion

During flameless combustion the fuel and preheated air are introduced with high velocity forming a jet. The high velocity causes strong internal recirculation of the flue gases. The mixing between the air, fuel and combustion products occurs continuously along the stream. Previous modelling studies [11] examined the ammonia chemistry in flameless jet during combustion of methane-free and methane-containing ammonia doped gases. It has been found that in the case of methane containing gas, the methane ignites with delay around the jet location where the air is already completely mixed with the fuel. Before the ignition occurs, the ammonia conversion is inhibited due to the absence of radicals. The radicals are consumed by methane decomposition. After methane ignition, ammonia oxidises mostly to NO. During combustion of methane-free gas, ignition occurs rapidly and ammonia decomposes in a substoichiometric region of the jet. In [12] investigation of combustion characteristics of hydrogen-hydrocarbon hybrid fuels is presented. This study confirms that the ignition delay can be significantly influenced by hydrocarbons. Moreover, [13] investigated the ammonia chemistry below 1400 K. They also reported that the methane in relatively low concentrations can strongly inhibits the ammonia conversion under fuel-rich conditions.

Increasing the methane or hydrocarbons content in the fuel, ammonia and hydrocarbons can start to compete for the same radicals occurring in the combustion process. Therefore, the composition of ammonia can be shifted toward the fuel lean side of the combustion, thus enhancing the conversion to $NO_x$.

## 5. Conclusions

The presented experimental studies show the fate of ammonia and hydrogen cyanide during flameless combustion of different low calorific value gases. The first series of experiments in which ammonia doped synthetic gases were burned under flameless conditions showed that depending on the gas composition, large difference in the conversion of $NH_3$ to $NO_x$ can occur. In particular, the methane in low concentrations influences the ammonia to $NO_x$ conversion. The lowest $NO_x$ emissions and therefore the lowest conversion ratios were measured while burning

methane-free gas. Increasing the methane content from 0 to ca. 6 vol-%, the concentration of $NO_x$ in the flue gas was rising rapidly. The tested $CO/H_2$ ratios in fuel had a minor influence on the conversion of ammonia to $NO_x$. During the second series of experiments product gases generated from two different solid bio-fuels in a BFB gasifier were burned in the flameless burner. The goal of these studies was to show the dependences between gasifier operating parameters and thus composition of the product gas and final $NO_x$ emissions during subsequent flameless combustion. The results shows the same tendencies observed during tests with ammonia doped synthetic gases. Also in this case the fuel nitrogen conversion was influenced by the product gas composition. According to investigated gasifier parameters the amount of hydrocarbons and fuel-$NO_x$ precursors was changing. In the case of wood pellets product gas combustion, much higher $NO_x$ emissions were observed with lower gasifier temperatures and thus by higher hydrocarbons concentrations in the product gas. This was observed even when the concentration of $NH_3$ and HCN was lower at lower gasifier temperature. In the case of nitrogen rich rape cake pellets much higher concentrations of $NH_3$ and HCN were measured in comparison to wood pellets. Here as well higher hydrocarbon concentrations lead to higher conversion rates of $NH_3$ and HCN to $NO_x$. In all cases higher combustion air ratio was enhancing the $NO_x$ emissions. This was observed particularly by combusting of nitrogen rich rape cake pellets product gas.

## References


[1] Wünning J.A. and Wünning J.G., 1997, Flameless oxidation to reduce thermal-NO formation, Prog. Energy Combust. Sci. 23, pp.81–94.

[2] Galletti C., Parente A., Tognotti L., 2007, Numerical and experimental investigation of a mild combustion burner, Combust. Flame 151, pp. 649-664.

[3] Cavaliere A., De Joannon M., 2004, Mild Combustion, Prog. Energy Combust. Sci. 30, pp. 329-366.

[4] Schuster A., Zieba M., Wünning J.G., Scheffknecht G., 2007, "Optimisation of conventional biomass combustion system by applying flameless oxidation", 15th IFRF Members' Conference, Pisa

[5] Schuster A., Zieba M., Scheffknecht G., Wünning J.G., 2007, "Application of FLOX® Technology for the utilisation of low-grade biofuels", Proceedings of 15th European Biomass Conference, Berlin, Germany, pp. 1703-1706.

[6] Leppälahti J., Koljonen T., 1995, Nitrogen evolution from coal, peat and wood during gasification: Literature review, Fuel Proc. Tech. 43, pp. 1-45.

[7] Becidan M., Skreiberg Ø., Hustad J.E., 2007, $NO_x$ and $N_2O$ Precursors ($NH_3$ and HCN) in Pyrolysis of Biomass Residues, Energy Fuels 21, p. 1173-1180, (2007)

[8] German Standard DIN 38406-E5, 1983, Methods for the examination of water, waste water and sludge; determination of ammonia-nitrogen (E5)

[9] German Standard DIN 38405-D13, 1981, Methods for the examination of water, waste water and sludge; determination of cyanides (D13)

[10] Zieba. M, Schuster A., Scheffknecht G., 2009, Influence of gas composition on ammonia to $NO_x$ conversion during flameless combustion of low calorific value gases, 16th IFRF Members' Conference, Boston

[11] Zieba. M. Brink. A., Schuster A., Hupa M., Scheffknecht G., 2009, Ammonia chemistry in a flameless jet, Combust. Flame 156, pp. 1950-1956.

[12] Choudhuri A.R., Gollahalli S.R., 2003, Characteristics of hydrogen-hydrocarbon composite fuel turbulent jet flames, Int. J. Hydrogen Energy 28, pp 445 – 454.

[13] Skreiberg Ø., Kilpinen P., Glarborg P., 2004, Ammonia chemistry below 1400 K, Combust. Flame 136 pp. 501-518.

# Modeling of a Solid Fuel Combustion in a Fixed Bed

*Rafał Buczyński*[a] *, Andrzej Szlęk*[a] *, Roman Weber*[b]

[a] *Institute of Thermal Technology, Silesian University of Technology, Gliwice, Poland*
[b] *Institute of Energy Process Engineering and Fuel Technology, Clausthal University of Technology, Clausthal-Zellerfeld, Germany*

**Abstract:** Coal is being used as a main type of fuel for small size boilers in Poland. Usually the design of mentioned boilers is not based on scientific knowledge but tradition and technical experience. In this paper a mathematical model of solid fuel combustion in a fixed bed is presented. Model may become a very useful optimization tool, which helps to construct boilers with low level of emission of harmful substances. Created model includes processes of moisture evaporation, pyrolysis of coal, combustion and gasification of char. The model takes into consideration a fixed- bed structure and solid fuel composition influence on thermal conductivity, specific heat and chemical reactivity of fuel. In this paper equations and boundary conditions as well as the model results are shown. In order to determine the main factors influencing the analyzed phenomenon a sensitivity analysis was applied. Parametric study shows that one of the most important factors are kinetic parameters of a char combustion reaction. The model has been validated against the experimental data. Gas species molar fractions and bed temperature were compared. Comparison shows that both experimental and calculated results are in good agreement.

**Keywords:** *Combustion, Fixed-bed, Numerical simulations*

## 1. Introduction

Through years Polish heat, power and energy systems were strictly determined by the prime role of a hard coal. This situation was caused by the two factors: numerous amount of this type of fuel, and by the relatively low price of hard coal on a Polish fuel market.

Also, there is a very similar situation on the domestic scale. Polish households were traditionally heat up by the usage of hard coal. This tendency has been developed long enough for changing hard coal into ultimately conceivable energy source, that outdistanced other possibilities.

Unfortunately, uncontrolled usage of a hard coal caused the series of a very significant issues and environmental problems. It is extremely hard to organize proper conditions, in which the process of hard coal combustion ensures not only high efficiency, but also can be characterized as a pollution free. It's worth of mentioning, that this task is also hampered by the neglecting attitude and insufficient knowledge of the maintaining stuff.

The countless number of small sized boilers, located on a relatively small territory, are the main reason for so called small emission problem.

The usage of an old conventional types of boilers, along with wrongly performed process of a hard coal combustion, are altogether the culprits responsible for the emission of a noxious combinations of: $NO_x$, CO, $SO_2$ and dust. In most of the cases, the smoke pollution make its way through the households chimneys, which are placed on a very small territory, causing at the same time a large impact on the health condition of inhabitants and animals. If one can also add: air, water and soil pollution, the scale of the damage will be fully realized.

That is why there are growing concerns about the dangerous side effects of expanding power industry. On the brim of the ecological catastrophe, the actions preventing further impact should be taken.

Since the last decade, on the domestic energy production market, the new type of small boilers appeared- retort boilers. This type of boiler is characterized by semi-automatic maintenance. Also, compared to the old types of systems the

efficiency rate of retort boiler is higher, and varies between 80 and 87% [1].

The introduction of the retort boiler into domestic appliance for heat production, has been a milestone for improvement and development of combustion devices, which effectively converts fuel into usable and applied form of energy. Retort boilers can be also used for the biomass (for example pellets) combustion.

In order to adjust and improve process of hard coal and biomass combustion, the air supply sections and combustion chamber were modified. Commonly recommended approach for searching for a new technical solutions, is to combine scientific knowledge with available and useful tools, in this particular case with numerical methods.

## 2. Mathematical model of solid fuel combustion

In this paper the model of fix-bed solid fuel combustion is presented. Model has been used for simulation of combustion process in the small sized retort boilers.

All important phenomena, connected with fix-bed combustion are presented. In a first order, during hard coal and biomass combustion, all moisture evaporates from hot fuel layer. Creating the model, author made an assumption, that all liquid water evaporates in the temperature of 100°C. Subsequently, fuel undergoes with the process of devolatilization. The process is described by the Arrhenius formula (1) [2, 3, 4]:

$$\dot{m} = A \cdot e^{-\frac{E}{RT}} (m_{\infty} - m) \tag{1}$$

During combustion, exothermic reactions are the main heat source. The most important exothermic reaction, is the heterogeneous reaction of char combustion (2):

$$C + O_2 \rightarrow CO_2 \tag{2}$$

During combustion, one of the conducive factors, is a high temperature of the heated fix-bed. It ensures the appearance of endothermic reactions. The most distinguished example of such reaction is (3):

$$C + CO_2 \rightarrow 2CO \tag{3}$$

The kinetic's of both reactions is also described by the Arrhenius formula (4) [2]:

$$k = B \cdot e^{-\frac{E}{RT}} \tag{4}$$

The values of kinetic parameters are given in Table 1:

*Table 1. The kinetic parameters of the most important phenomena during a solid fuel combustion [2].*

| KINETIC PARAMETERS | |
|---|---|
| COMBUSTION OF CHAR $C + O_2 \rightarrow CO_2$ | E = 96,4 kJ/mol, B = 4000 m/s. |
| GASIFICATION OF CHAR $C + CO_2 \rightarrow 2CO$ | E= 185,4 kJ/mol, B = 69400 m/s. |
| DEVOLATILIATION | E = 158 kJ/mol, A= $10^7$ 1/s. |

The contact surface S, between gaseous and solid phase, along with the substrates concentration, are the determinants that decide about the rapidity of heterogeneous reactions. It is proofed by the equation (5) [2, 3]:

$$\dot{m} = S \cdot k_{eff} \cdot C^n \tag{5}$$

All data, required for equations, were drawn from technical literature. Created model consider the process of diffusion between gaseous substrate and the surface of a fuel grain.

In order to considerate the influence of diffusion on the substitute, the rate of chemical reactions k has been introduced [2]:

$$\frac{1}{k_{eff}} = \frac{1}{k} + \frac{1}{\beta} \tag{6}$$

To determine the β coefficient, it is necessary to use nondimensional Sherwood number, which can be described as below [2, 3]:

$$Sh = \frac{\beta d}{D} \tag{7}$$

where:

$$Sh = 2 + 0{,}16\,\mathrm{Re}^{\frac{2}{3}} \tag{8}$$

$$D = D_o \left( \frac{T}{T_o} \right)^{1.75} \frac{p_o}{p} \quad (9)$$

Author took into account not only a series of heterogeneous reactions, but also the occurrence of two important reactions, which appear to take place only in the gaseous phase. The mentioned reactions are reaction of volatiles and carbon monoxide combustion (10 - 11):

$$vol. + 1.098 \cdot O_2 \rightarrow CO + 1.417 \cdot H_2O \quad (10)$$

$$CO + \frac{1}{2} O_2 \rightarrow CO_2 \quad (11)$$

The four main conservation equations were used for description of the change in the amount of the substance in the fix-bed, that appeared during solid fuel combustion, along with accompanying thermal effects:

$$\frac{\partial \rho g_i}{\partial t} + \nabla \cdot \left( \rho \vec{\upsilon} g_i \right) = S_i \quad (12)$$

where i- moisture, volatiles, char, ash.

All four balance equations are defining the basic content of the fuel, such as: ash, char, volatile and moisture. This work assumed that volatiles which have in real a complex chemical structure and consist of many species are described using only one equation and additional substance named volatile. in the model. For description of thermal effects, the solid fuel-energy balance was used:

$$\frac{\partial \rho c T}{\partial t} + \nabla \cdot \left( \rho \vec{\upsilon} c T - \lambda_{eff} \nabla T \right) = S_h \quad (13)$$

For obtaining the correctness of the created model, it was essential to define the value of the temperature, which appeared in the fix-bed during combustion. For this purpose the thermal properties with specific heat c and thermal conductivity $\lambda_{eff}$ must be known.

In the created model, author decided that the thermal capacity of fix-bed is determined by its composition and temperature [6]. This are main factors that decides about the thermal properties.

High temperature caused rapid increase of fuel specific heat value. After moisture evaporation and solid fuel devolatilization, its value drop sharply. This phenomena is caused by the fact, that the highest thermal capacity lies successively in the moisture and volatiles content [6]. The experimental relations used for setting the value of individual solid fuel components, are shown in the Table 2.

*Table 2. Specific heat of coal components [6].*

| SPECIFIC HEAT J/kgK | |
|---|---|
| ASH | $c_{pa} = 594 + 0,586T$ |
| VOLATILE -1 | $c_{v1} = 728 + 3,391T$ |
| VOLATILE -2 | $c_{v2} = 2273 + 2,554T$ |
| CHAR | $c_c = -218 + 3,807T + -1,758 \cdot 10^{-3} T^2$ |
| MOISTURE | $c_w = 4160$ |

The substitute of the specific heat value has been calculated form the equation (14):

$$c = \sum_{i=1}^{4} g_i c_i \quad (14)$$

The value of thermal conductivity has been calculated, by taking into the account the influence of the heat transfer through the fix-bed, which accrued mainly in form of heat radiation between fuel grains. Mentioned mechanism greatly develops in the higher ranges of temperatures, especially above 600°C [7]. In order to obtain real and trustworthy description of the heat transfer profile in created model, thermal conductivity coefficient has been depended on the structure of the bed itself. Author divided the fix-bed structure into two main zones: a particulate stage and coke stage. Both zones are characterized by the shapes and sizes of pores, which are responsible for the value of thermal conductivity [7].

The experimental relations used for setting the value of the thermal conductivity, are shown below.

The value of hard thermal conductivity has been calculated form the equation (15)[7]:

$$\lambda = \left( \frac{\rho}{4511} \right)^{3.5} T^{0.5} \quad (15)$$

In the particulate stage of the bed, the value of effective thermal conductivity has been calculated from the equation (16) [7]:

$$\lambda_{eff} = w_2\lambda_3 + \frac{(1-w_2)}{\frac{e'}{\lambda_1+\lambda_2} + \frac{(1-e')}{\lambda}} \quad (16)$$

where effective porosity is calculated from:

$$e' = 1-(1-e)^{0.33} \quad (17)$$

Thermal conductivity of gas between fuel particles is estimated using equation:

$$\lambda_1 = 7.45\cdot\left(10^{-5}\right)\cdot T\,. \quad (18)$$

Influence of radiative heat transfer between particles is calculated from:

$$\lambda_2 = 2.28\cdot\left(10^{-10}\right)\cdot T^3\,. \quad (19)$$

Thermal conductivity of moisture is assumed to be constant and equal:

$$\lambda_3 = 0.6\,. \quad (20)$$

Likewise, in the coke stage, the value of the thermal conductivity coefficient has been calculated from the equation (21) [7]:

$$\lambda_{eff} = (1-e)\lambda + e\lambda_1 + e_{in}\lambda_{2a} + e_{ex}\lambda_{2b} \quad (21)$$

where thermal conductivity of gas located inside pores is described by the equation:

$$\lambda_1 = 4.96\cdot\left(10^{-4}\right)\cdot T\,. \quad (22)$$

Heat transfer through thermal radiation is calculated using two following equations:

$$\lambda_{2a} = 3.42\cdot\left(10^{-11}\right)\cdot T^3\,, \quad (23)$$

$$\lambda_{2b} = 2.28\cdot\left(10^{-9}\right)\cdot T^3\,. \quad (24)$$

Furthermore, the heat amount between gaseous and solid phase has been estimated, by the knowledge of the effective heat transfer coefficient value. It includes two most important mechanisms in heat transfer: convection and radiation [8].

The intensity of heat transfer strongly relays on the temperature and size of solid fuel grains. In this work, effective heat transfer coefficient α has been calculated from the formula [8]:

$$Nu = \frac{\alpha\cdot d}{\lambda} \quad (25)$$

Equation (26) has been drawn from literature [8]:

$$Nu = f\left[\mathrm{Re},\mathrm{Pr}\right] \quad (26)$$

For the simulation of solid fuel commercial CFD package FLUENT has been used. Existing EDC model allowed for the simulation of the effects which appears in the gaseous phase of chemical reactions. Created model depend the reactions velocities on the substrates mixing rate and their kinetics.

Author also used the implemented Fluent model, which simulates the gas flow over porous volume. It was used in order to model air and exhaust flow through analyzed layer of solid fuel. Experimental dependency between gas velocity and pressure drop in the actual fuel bed was needed for mentioned model. Obtained dependence is presented by the equation (27):

$$\Delta p = 0{,}2615\upsilon^2 + 0{,}4881\upsilon \quad (27)$$

## 3. Validation of the model

Conscientious validation of all results from the model, has been obtained from comprehension between actual experimental results and numerical simulations.

All measurements were performed in specially prepared reactor, which is presented on the Fig. 1. During laboratory experiment, the hard coal was combusted. In the four, evenly displayed sections, the values of temperature have been measured. Also, outlet exhaust gas composition has been analyzed. All measurements have been conducted by Radvan Nosek and Jakub Rainczak. A detailed description of experimental technique and used instruments is included in [9].

All laboratory experiments were performed on the EKORET hard coal. This type of hard coal, is specially prepared fuel for small sized retort boilers. It is characterized by adequate rate of granulation, along with properly high calorific value. EKORET is chemically enriched, with lowered content of sulfur.

For model calculations, author assumed that the composition and calorific values of the simulated fuel, were identical with the values for the real EKORET fuel. The grain diameter has been set as a constant, d=0.02 m.

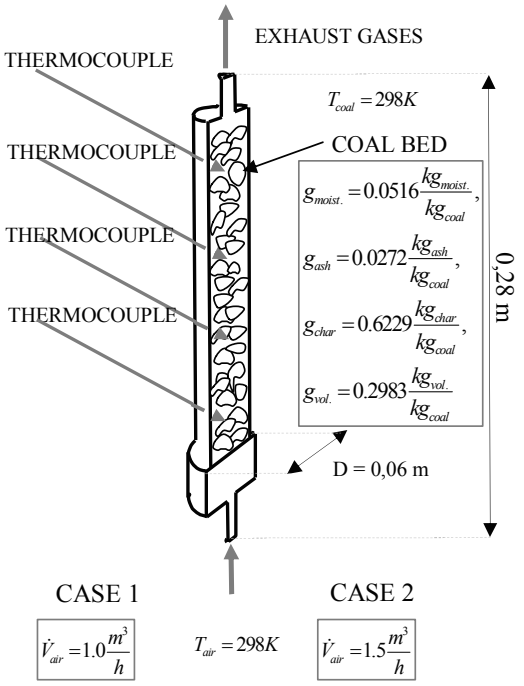


*Fig. 1. Geometry of the reactor.*

All experimental test were performed for two air flows rates: $V_a$=1.0 m$^3$/h and $V_a$=1.5 m$^3$/h.

Model validation has been carried, by using reliable comprehension between two factors: profile of the temperature and exhaust gases composition, which were obtained from theoretical calculations, and from laboratory scale experiments.

Obtained results (Fig. 2 and Fig. 3) suggested, that created model shows a good accordance with the real process of solid fuel combustion.

The correctness of above these is confirmed by the values of correlation coefficients (28), which were calculated for all measured quantities (Table 3- 4). Their values varies between 0.85 – 0.96.

$$\rho_{x,y} = \frac{cov(X,Y)}{\sigma_x \cdot \sigma_y} \tag{28}$$

Created model, accurately reflects all changes brought by the possible variations of air flows, and its consequences for the value of the temperatures and exhaust gases composition, in the real fix-bed reactor. The increase of air flow rate may cause rapid and fast fuel combustion, and after the end of the process, faster cooling of the fix-bed. (Fig. 3).

*Table 3. Correlation coefficient – fuel temperature.*

| TEMPERATURE | | |
|---|---|---|
| CHARACTEISTIC | CORRELATION COEFFICIENT (Va=1,0 m$^3$/h) | CORRELATION COEFFICIENT (Va=1,5 m$^3$/h) |
| THERMOCOUPLE 1 | 0,858 | 0,914 |
| THERMOCOUPLE 2 | 0,884 | 0,895 |
| THERMOCOUPLE 3 | 0,952 | 0,957 |
| THERMOCOUPLE 4 | 0,946 | 0,872 |

*Table 4 . Correlation coefficient – flue gas composition.*

| GAS COMPOSITION | | |
|---|---|---|
| CHARACTEISTIC | CORRELATION COEFFICIENT (Va=1,0 m$^3$/h) | CORRELATION COEFFICIENT (Va=1,5 m$^3$/h) |
| $O_2$ | 0,906 | 0,893 |
| $CO_2$ | 0,890 | 0,871 |
| CO | 0,650 | 0,589 |

Some discrepancy can be observed between real, experimental results and ones obtained form the model. It can be shown by the differences in the CO content in the exhaust gases (Fig. 2 and Fig. 3). In the first stage of combustion, CO concentration is relatively to high comparing it to the its real concentration in the combustion chamber. This situation is caused by chosen boundary conditions. To high temperature that was assumed during simulation as initial condition of the coal ignition zone, caused sudden rise of the CO concentration in the reactor's exhaust gases. The ignition zone is located in the upper part of reactor, near the flue gas outlet. High temperature applied in this area at the beginning of the calculations leads to production of CO by endothermic reactions. As the time went by, the bed temperature along with CO concentration reached the level of values, which were observed during all experimental tests.

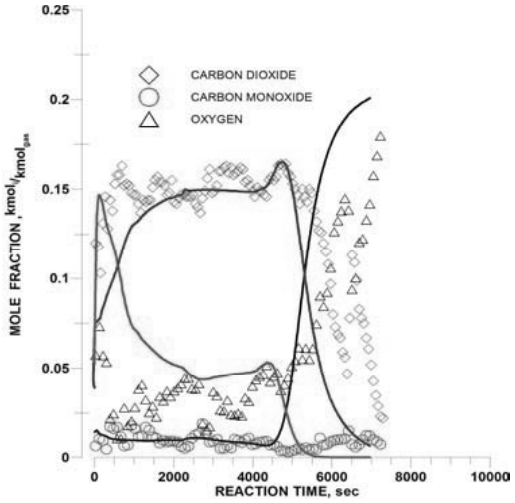


*Fig. 2. Flue gas composition. ($V_a$=1,0 $m^3$/h, $T_a$=298K, $p_a$=0,1MPa)*

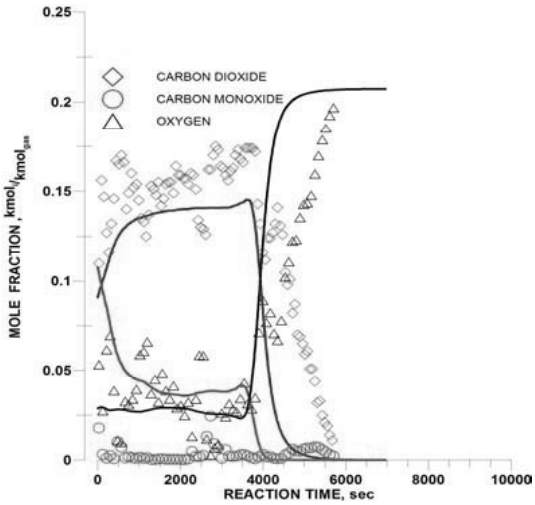


*Fig. 3. Flue gas composition. ($V_a$=1,5 $m^3$/h, $T_a$=298K, $p_a$=0,1MPa)*

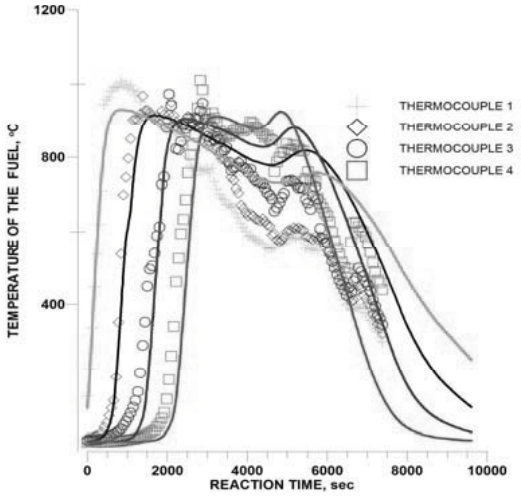


*Fig. 4. Coal bed temperature. ($V_a$=1,0 $m^3$/h, $T_a$=298K, $p_a$=0,1MPa)*

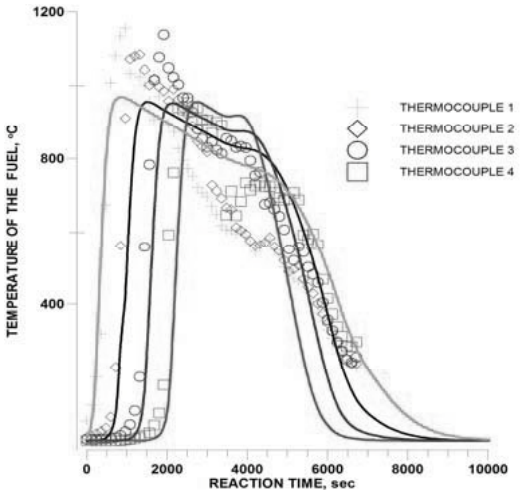


*Fig. 5. Coal bed temperature. ($V_a$=1,5 $m^3$/h, $T_a$=298K, $p_a$=0,1MPa)*

## 4. Sensitivity analysis

Created model of a fix-bed solid fuel combustion, requires plenty of data and results, that can be obtained only by the series of the experimental tests.

Basic quantities, that determines all phenomena connected with solid fuel combustion, are estimated with different accuracy margin. Presented analysis, proofs that there are valid values which need to be calculated with a great deal of precautions.

In the performed research, the influence of three important parameters, that has great impact on obtained results, were calculated. This parameters are:

- pre-exponential factor B of char combustion reaction,
- heat transfer coefficient α,
- energy activation of the devolatization process E.

Author for the evaluation of chosen P parameters on the y results (which were obtained from the created model of solid fuels combustion), assumed a logarithmic sensitivity factor LSF:

$$LSF = \frac{\partial \ln y}{\partial \ln P} = \frac{\partial y}{\partial P} \cdot \frac{P}{y} \tag{29}$$

For global, parametrical evaluation in the analyzed time range $t_1$ - $t_k$, the average logarithmic sensitivity factor ALSF was chosen:

$$ALSF = \frac{\sum_{i=1}^{k-1} \left| LSF(t_i) \cdot (t_{i+1} - t_i) \right|}{t_k - t_1} \tag{30}$$

The average logarithmic sensitivity factor ALSF (Table 5), that was calculated for four temperature measurement points, shows unanimously that the variation of exponential factor of char combustion, is very important for the model results.

Less importance on the actual value of temperature, is demonstrated by the effective heat transfer coefficient. Slight influence on the results can be assigned to the energy alteration in the process of coal devolatilization.

## 5. Conclusions

This paper is devoted to the research under solid fuels combustion. In order to develop the actual state of knowledge, the new model has been created. For all calculations, Fluent packet has been used.

In order to confirm the actual correctness of created model, all calculations were compared with real results, obtained from experimental performances.

The main, analyzed quantities were: temperature in the fix-bed and the composition of exhaust gases, which were created during the process of solid fuels combustion in the special reactor.

Obtained results proofed, that the created model shows a good accordance with the real process of solid fuel combustion. It was confirmed by the values of correlation coefficient. Their values varies between 0.85 – 0.96.

The lowest value of correlation coefficients were calculated for CO concentrations on the level of 0.6.

The sensitivity analysis confirmed, that most important factor, that decides about the chemical and physical course of solid fuels combustion, is the exponential factor of combustion reactions.

All results along with performed analysis shows, that created model is a correct and useful tool, that can be used not only for numerical simulations of solid fuel combustion, but also can be a valuable source of possible technical modifications, which can be successfully applied in the construction of small sized boilers.

*Table 5 . Average logarithmic sensitivity – fuel temperature.*

| TEMPERATURE | | |
|---|---|---|
| CHARACTEISTIC | PARAMETER | ALSF |
| THERMOCOUPLE 1 | B | 4.00 |
| | α | 1.82 |
| | E | 0.03 |
| THERMOCOUPLE 2 | B | 7.06 |
| | α | 3.04 |
| | E | 0.03 |
| THERMOCOUPLE 3 | B | 8.71 |
| | α | 3.70 |
| | E | 0.03 |
| THERMOCOUPLE 4 | B | 7.71 |
| | α | 3.32 |
| | E | 0.03 |

## Nomenclature

A pre-exponential factor of devolatilization process, m/s

B pre-exponential factor of a chemical reaction, m/s

C concentration of the species, kg/m$^3$

c specific heat, J/(kgK)

cov covariance

d grain diameter, m

D mass diffusivity, $m^2/s$
e porosity, $m^3/m^3$
$E$ activation energy, J/(kg K)
$g_i$ mass fraction of species i, $kg_i/kg$
R universal gas constant, J/(kmol/K)
Pr Prandtl number
Re Reynolds number
t time, s
T temperature, K
m mass of the product, kg
$\dot{m}$ devolatilization rate , kmol/s
Nu Nusselt number,
S contact surface area between phases
$S_i$ mass source term of species i, $kg/(m^3 s)$
$S_h$ energy source term, $W/m^3$
p pressure, Pa
k reaction rate coefficient, m/s
$m_\infty$ mass of the devolatilization products after $\tau \to \infty$, kg
$w_2$ mass fraction of the moisture, kg/kg
X,Y random variables

### Greek symbols

α heat transfer coefficient, $W/(m^2K)$
β mass transfer coefficient, m/s
λ thermal conductivity, W/(mK)
$\upsilon$ velocity of air, m/s
$\phi$ arbitrary scalar,
$\sigma$ standard deviation,
$\rho$ density of the fuel, $kg/m^3$
$\rho_{x,y}$ correlation coefficient.

### Subscripts and superscripts

a air
eff effective
in internal
ex external
i specific species
n reaction order
o arbitrary conditions

## References

[1] Kubica K., 2007, Efektywne i przyjazne środowisku źródła ciepła – ograniczenie niskiej emisji, Polski Klub Ekologiczny.
[2] Tomeczek J., 1992, *Spalanie węgla*, Wydawnictwo Politechniki Śląskiej, Gliwice, Poland.
[3] Tomeczek J., 1991, *Zgazowanie węgla*, Wydawnictwo Politechniki Śląskiej, Gliwice, Poland.
[4] Merrick D., 1982, Mathematical models of the thermal decomposition of coal 1. The evolution of volatile matter National Coal Board, Coal Research Establishment, Stoke Orchard, Cheltenham, Glos., GL52 4RZ, UK.
[5] Merrick D., 1982, Mathematical models of the thermal decomposition of coal 3. Density, porosity and contraction behaviour, National Coal Board, Coal Research Establishment, Stoke Orchard, Cheltenham, Glos., GL52 4RZ, UK.
[6] Merrick D., 1982, Mathematical models of the thermal decomposition of coal, 2. Specific heats and heats of reaction, National Coal Board, Coal Research Establishment, Stoke Orchard, Cheltenham, Glos., GL52 4RZ, UK.
[7] Atkinson B., and Merrick D., 1982, Mathematical models of the thermal decomposition of coal 4. Heat transfer and temperature profiles in a coke-oven charge, National Coal Board, Coal Research Establishment, Stoke Orchard, Cheltenham, Glos., GL52 4RZ, UK.
[8] Bes A., 2005, *Dynamic Process Simulation of Limestone Calcination in Normal Shaft Kiln*, Praca Doktorska, Magdeburg University, Germany.
[9] Nosek R., 2009, Simplified method of solid fuels characterization and its application for modelling of fixed bed combustion, Politechnika Śląska, Wydział Inżynierii Środowiska i Energetyki, Instytut Techniki Cieplnej , Zilina – Gliwice.

**Acknowledgments:** This work was supported by the financial assistance of the European Commission Marie Curie INSPIRE Network and Ministry of Science and Higher Education.

# Experimental investigation of strained, non-premixed butanol flames

*Maria S. Agathou and Dimitrios C. Kyritsis*

*Department of Mechanical Science and Engineering*
*University of Illinois at Urbana-Champaign*

**Abstract:** Pure butanol as well as methane assisted butanol non-premixed flames were studied in a counter-flow burner configuration in view of the emergence of butanol production from biological agricultural sources. Major combustion species were measured across the flame using line Raman imaging and temperature measurements were obtained with K-type thermocouples. Of particular importance was the comparison of flames of the same heating value and equivalence ratio, as well as flames of the same overall equivalence ratio but varying reactant flow rates. Extinction strain rates were measured for a wide range of conditions. It was shown that there was a decrease of extinction strain rate with increasing overall equivalence ratio for both constant fuel flow rates and constant heat release of combustion and that butanol flames were more vulnerable to extinction compared to methane. Species concentration measurements indicated that $N_2$ concentrations varied linearly with temperature across the non-premixed flame. Finally, the possibility of estimating the scalar dissipation rate at the stoichiometric surface $\chi_{stoich}$ was investigated through a measurement of the mixing layer thickness δ, acquired from the temperature distribution measurements as full width at half maximum. It was proven that this was not an appropriate method for the estimation of $\chi_{stoich}$. For certain cases, this was further investigated through an approximation of the gradient of the mixture fraction at the stoichiometric surface $\left|\nabla Z\right|_{stoich.}$.

**Keywords:** strained flames, bio-butanol, non-premixed flames

## 1. Introduction

The possibility of producing butanol efficiently from agricultural sources, with the use of *clostridia* through fermentation processes, has recently been demonstrated [1-4], thus highlighting the potential use of butanol as an alternative fuel. Bio-butanol fuel can be competitive to the widely used bio-ethanol, primarily due to its higher energy density. Specifically, the energy densities of butanol and ethanol are 36.4 and 24.8 MJ/kg respectively, whereas the energy content of gasoline is 44.9MJ/kg. The reason for the higher energy content of butanol lies behind the smaller oxygen content of the butanol molecule (22%) compared to the oxygen content of ethanol (35%)

Relatively few fundamental studies of butanol combustion have been reported, with their majority appearing within the last three years. Sarathy et al. [5] presented numerical and experimental results using a jet-stirred reactor, whereas Dagaut et al. [6-8] proposed modeling of butanol combustion kinetics based on results from a jet-stirred reactor. Premixed flames of all butanol isomers were studied in low pressure environments by Yang et al. [9]. Older studies involve fuel decomposition for kinetic modeling purposes in mixtures of $CH_4$ with the four butanol isomers [10], as well as internal combustion engine work by Alasfour [11,12] and Gautam et al. [13,14].

The current paper focuses on the counter-flow laminar flamelet, which constitutes the fundamental element of a turbulent flame [15-18]. Butanol flame structure and flame dynamics is probed. Specifically, a counter-flow burner was used that has

Corresponding Author: Dimitrios C. Kyritsis, Email: kyritsis@illinois.edu

been developed in previous work [19,20], and non-premixed flames of both pure butanol as well as of butanol-methane mixtures were established. The flames were studied for several different overall stoichiometry and total heat released. To our knowledge, we present the first spatially resolved temperature and species measurements in butanol methane-assisted laminar counter-flow flamelets, as well as measurements of extinction strain rates for both pure butanol and butanol-containing mixture flames. Scalar dissipation rate calculations are performed based on the measured temperature distributions and are compared to the respective calculations based on the gradient of the mixture fraction at the stoichiometric surface.

## 2. Experimental set-up

### 2.1 The counter-flow burner

An axisymmetric, laminar, methane assisted, butanol-oxygen flame was established in a counter-flow burner configuration, shown schematically in Fig. 1.

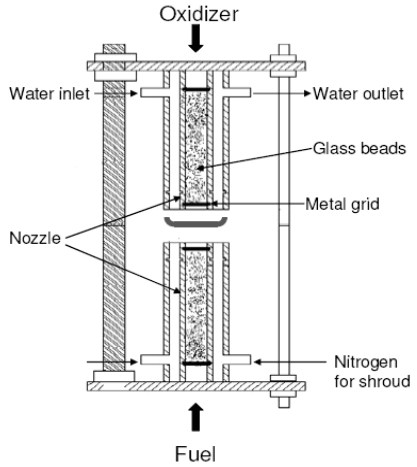


*Fig. 1. Cross-sectional area of the counter-flow burner.*

The oxygen stream was nitrogen-diluted and nitrogen was used as a shroud flowing from the outer annulus of the lower nozzle in order to isolate the flame from diffusion from ambient air as well as drafts in the laboratory. Fine grids and glass beads were used to achieve uniformity of the velocity profiles of the two reactants. The diameter of each of the nozzles was 12.5 mm, and the gap between them was 15 mm. Butanol flow rate was controlled by a syringe pump that fed a 4.5 mm diameter, 1m long, copper tube surrounded by heating tape. The tape was heated up to $170^0$C to assure butanol vaporization. Both methane and butanol streams were nitrogen-diluted before mixing at the inlet of the counter-flow burner. The outside surface of the burner lower section was also wrapped with heating tape and its temperature reached $220^o$C, so as to avoid butanol condensation.

### 2.2 Species concentration measurements

Major combustion species (C-H bond, $O_2$, $N_2$, $CO_2$ and $H_2O$) were measured using line Raman imaging. The experimental set-up applied, is shown in Fig. 2. A Quanta-Ray Pro-250 Nd-YAG laser delivering 300 mJ/pulse at 532 nm was used as an excitation source and the Stokes-shifted Raman signal was collected at the wavelengths shown in Table 1. It is noticeable that, for an incident laser beam wavelength of 532 nm, all three pure fuels have a detection wavelength around 629nm, thus this is the wavelength selected in order to detect the C-H bond in the fuel-mixture cases (Row 4 of Table 1). Separation of the several C-H lines corresponding to different organic molecules was not possible within the resolution of the spectrograph/camera couple that was used. The laser beam was focused to an approximately 500 μm thick and 60mm long horizontal line with a 1m plano-convex lens. An Acton Research 300 mm imaging spectrograph was used for the dispersion of Raman signals. Dispersion was achieved with a 68mm x 68mm ruled grating with 1200 grooves/mm and a 500 nm blaze wavelength.

*Table 1. Raman signal for the species under consideration.*

| Species | Wavelength [nm] |
|---|---|
| $C_4H_9OH$ | 628 |
| $CH_4$ | 629.7 |
| $C_2H_5OH$ | 630.2 |
| C-H bond | 629 |

| | |
|---|---|
| $O_2$ | 580 |
| $N_2$ | 607.3 |
| $CO_2$ | 571 |
| $H_2O$ | 660.3 |

The spectral images were captured using an Andor I-star ICCD which was coupled to the spectrograph. The horizontal images from the flame were rotated by 90° with a dove prism and were then focused onto the inlet mirror using a Nikon 50mm, f#1.8 lens. An OG550, 3mm thick glass filter was used to reject stray reflections from the burner hardware. The burner was mounted on a vertical translation stage so that the flame was scanned in the vertical direction. For each measurement, three sets of 300 Raman lines that were integrated on the chip were averaged, in order to achieve an acceptable signal-to-noise ratio (S/N > 10).

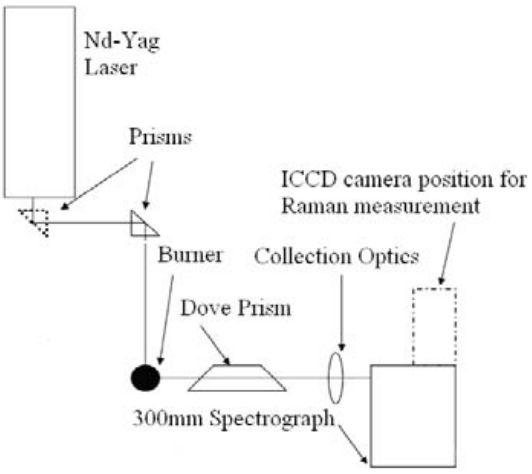


*Fig. 2. Experimental Set-up.*

### 2.3 Temperature & extinction measurements

Temperature measurements were obtained with a K-type thermocouple of 0.50 mm diameter, with an increment of 1mm. The thermocouple was positioned perpendicular to the burner axis, with its edge at the center of the inner annulus of the burner. The maximum temperature of the thermocouple was rated for 1473 K and the maximum flame temperature observed was 1382 K. Flame extinction was achieved by increasing the diluent mass flow rate while the ones of fuel and oxidizer were kept constant. In the particular measurements, no radiation correction was applied.

## 3. Results and discussion

### 3.1 Calculation of flame parameters

Six butanol-methane mixtures were considered. Their measured mass flow rates in [g/min], are presented in Table 2.

*Table 2. Mass flow rates for the butanol-methane flame configurations*

| Test Case | $C_4H_9OH$ | $N_2$ for $C_4H_9OH$ | $CH_4$ | $N_2$ for $CH_4$ | $O_2$ | $N_2$ for $O_2$ |
|---|---|---|---|---|---|---|
| | [g/min] | [g/min] | [g/min] | [g/min] | [g/min] | [g/min] |
| 1 | 0.067 | 1.121 | 0.133 | 1.162 | 1.465 | 0.388 |
| 2 | 0.135 | 0.697 | 0.052 | 1.093 | 1.151 | 0.769 |
| 3 | 0.202 | 0.565 | 0.065 | 1.207 | 1.623 | 0.769 |
| 4 | 0.296 | 0.565 | 0.051 | 1.093 | 1.544 | 0.769 |
| 5 | 0.270 | 1.056 | 0.042 | 0.999 | 1.544 | 1.074 |
| 6 | 0.337 | 1.056 | 0.011 | 1.139 | 1.937 | 0.388 |

The mixture of gases at the exit of the burner was assumed ideal and the density ρ was calculated through the equation:

$$\rho_i = \frac{\dot{m}_{tot}}{\dot{V}_{tot}} = \frac{P_{atm} MW_{mix\,i}}{\overline{R} T_i}, \qquad (1)$$

The subscript i denotes either the fuel or oxidizer nozzle exit location, $\dot{m}_{tot}$ and $\dot{V}_{tot}$ are the total mass and volumetric flow rates reaching the nozzle respectively, $\overline{R}$ is the ideal gas constant (8314 J/kmol K), T is the measured temperature and $P_{atm}$ is the atmospheric pressure. $MW_{mix}$ is the molecular weight of the mixture:

$$MW_{mix} = \frac{1}{\sum_{1}^{j} \frac{y_j}{MW_j}}, \qquad (2)$$

where $y_j$ and $MW_j$ are the mass fraction and molecular weight of species j. The speeds $U_i$ were calculated through:

$$U_i = \frac{\dot{m}_{tot,i}}{\rho_i A}, \quad (3)$$

where A is the nozzle cross-sectional area. The strain rate was then estimated, as suggested in [21]:

$$K = \frac{2U_{ox}}{d}\left[1 + \frac{U_{fuel}}{U_{ox}}\left(\frac{\rho_{fuel}}{\rho_{ox}}\right)^{\frac{1}{2}}\right], \quad (4)$$

where, *d* is the distance between the nozzles. The calculated densities and speeds for the six mixture flame configurations are presented in Table 3, both for the oxidizer and for the fuel nozzle exit location. In addition, strain rates at the stoichiometric surface are presented in the last column of Table 3, in [$s^{-1}$].

The fuel-to-air ratio (F/A), the stoichiometric fuel to air ratio $(F/A)_{stoich}$, as well as the overall equivalence ratio φ, are presented in Table 4. In order to calculate the overall equivalence ratio φ for the butanol-methane mixtures, both combustion reactions were taken under consideration:

$$C_4H_9OH + 6O_2 \rightarrow 4CO_2 + 5H_2O, \quad (5)$$

$$CH_4 + 2O_2 \rightarrow CO_2 + 2\,H_2O, \quad (6)$$

*Table 3. Densities and speeds at both nozzle exits and strain rates for all test cases.*

| Test Case | Oxidizer Density $\rho_{ox}$ | Fuel Density $\rho_{fuel}$ | Oxidizer Speed $u_{ox}$ | Fuel Speed $u_{fuel}$ | K |
|---|---|---|---|---|---|
| | [kg/m$^3$] | [kg/m$^3$] | [cm/s] | [cm/s] | [$s^{-1}$] |
| 1 | 0.379 | 0.744 | 66.32 | 45.29 | 173.02 |
| 2 | 0.388 | 0.797 | 67.16 | 33.68 | 153.88 |
| 3 | 0.404 | 0.792 | 80.40 | 34.97 | 172.48 |
| 4 | 0.373 | 0.802 | 84.21 | 33.94 | 178.63 |
| 5 | 0.496 | 0.817 | 71.72 | 39.32 | 162.93 |
| 6 | 0.480 | 0.844 | 65.80 | 40.93 | 160.12 |

Column $Q_{tot}$ of Table 4 presents the total heat released by the combustion of the mixtures under consideration, based on the lower heating values of the involved fuels. Notably, the LHV for butanol is 33.075 MJ/kg and for methane 50MJ/kg [22]. The last column of Table 4 presents the peak temperature measured at the flame region for each configuration. The Burke Schumann flame solution was not a realistic approximation for these flames, since they are highly non-adiabatic.

*Table 4. Overall equivalence ratios and total heat released for all flame configurations.*

| Test Case | FAR | FARst | Overall φ | $Q_{tot}$ | Tpeak |
|---|---|---|---|---|---|
| | | | | [W] | [K] |
| 1 | 0.14 | 0.28 | 0.5 | 148 | 1218 |
| 2 | 0.16 | 0.33 | 0.5 | 118 | 1231 |
| 3 | 0.16 | 0.34 | 0.5 | 165 | 1270 |
| 4 | 0.22 | 0.36 | 0.6 | 206 | 1329 |
| 5 | 0.20 | 0.36 | 0.6 | 183 | 1216 |
| 6 | 0.18 | 0.38 | 0.5 | 195 | 1382 |

### 3.2 Raman spectroscopy measurements

The raw data obtained during the Raman experiment correspond to curves that are in terms of arbitrary units of signal (number of counts) as a function of wavelength. In order to extract Raman signal intensity information out of these plots, the area under the curves was integrated. The result equaled the energy of the signal $E_s$:

$$E_s = E_o \cdot n \cdot \frac{\partial\sigma}{\partial\Omega} \cdot \Omega \cdot l \cdot \varepsilon, \quad (7)$$

In this last equation, $E_o$ is the energy of the incident light, l is the sampling length along the beam and n is the number density of scatterers, in our case the molecules of the gas under consideration. The collection efficiency is accounted by the term ε and $\frac{\partial\sigma}{\partial\Omega}$ constitutes the differential Raman cross-section. Recalling this equation, it is evident that if the number density $n_i$ of the species at a given location is known, then the number density of the species $n_s$ at other locations can be obtained in terms of this known value, the intensity of the Raman signals $E_i$, $E_s$ and the ratio of the differential Raman cross-section at the two locations, eq. 8:

$$n_s = n_i \cdot \frac{E_s}{E_i} \cdot \frac{\frac{\partial\sigma}{\partial\Omega_i}}{\frac{\partial\sigma}{\partial\Omega_s}}, \quad (8)$$

The rest of the terms of eq.7 are constant numbers and cancel out. As the known location for this study, the exit of the fuel nozzle was considered for $N_2$ and

C-H bond and the exit of the oxidizer nozzle for $O_2$. The number density of species j at the reference locations i, is calculated in [kmol/m$^3$] using eq. 9, where the total volumetric flow rate is calculated through eq. 1:

$$n_{i,j} = \frac{\frac{\dot{m}_j}{MW_j}}{\dot{V}_{tot}}, \quad (9)$$

The differential Raman cross-section is a temperature dependent term and for the temperature range of the current experiments its variation with temperature is plotted in Fig. 3 for the three major species under consideration. The polynomial expressions used for this calculation are found in [23].

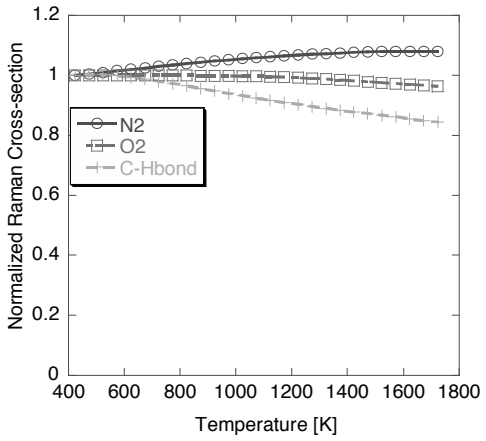


*Fig.3. Temperature Dependence of the Raman Cross-section*

Major species concentration measurements in kmol/m$^3$ for C-H bond, $O_2$, and $N_2$, as a function of the distance from the fuel nozzle exit in mm are shown in Fig. 4. Each figure corresponds to a different flame configuration from Table 2. In the figures, the measured temperature distribution is also presented on a separate y-axis. It should be noted, that the fuel concentrations are multiplied by a factor of 10 to achieve clearer illustration of the results.

The error of the Raman measurements deserves some discussion. The image intensifier is a noisy device, hence producing significant error, which translates to lower S/N ratios for weaker signals, i.e. in the flame region. The maximum error is observed in the flame region, where the S/N ratio for $N_2$ is around 4. The minimum error is observed at the nozzles, where for $N_2$, $O_2$ and C-H bond the S/N ratios are on the order of 10. S/N ratios are considered to represent the total uncertainty rising from the measurements of concentration, since their random and systematic components could not be further distinguished.

In all test cases, fuel concentration has its maximum at the location closest to the fuel nozzle and starts depleting as it approaches the flame zone. Similarly, oxidizer is maximum at the oxidizer nozzle and its destruction begins as it advances towards the flame. As far as nitrogen is concerned, its signal is highly affected by the high temperatures developed in the combustion region and this explains the drop-off observed in all configurations. The presence of the other two major species of Table 1, $H_2O$ and $CO_2$, was investigated both in the flame and in the product region, but their signal was not detected. Detection of combustion intermediates with this technique was infeasible, due to the low S/N ratios in the combustion region.

In cases with lower strain rates (5, 6), it is observed that oxidizer and fuel have vanished before the two curves interact. Fuel consumption has been initiated through pyrolysis, since the temperature is elevated and this is followed by combustion of the intermediate products with oxygen. In these cases, the reaction zone is broader and this is accompanied with broader temperature distribution curves, as well.

As the strain rate increases, the curves of the reactant concentration are brought closer (cases 3,4) or even vanish at the same location (case 1) This happens because with increasing strain, the residence time in the mixing layer is reduced, resulting to a thinner flame region. However, in case 2, even though it has the lowest strain rate, the above observations do not hold. An overlap of the reactant lines is observed indicating a fuel leakage in the oxidizer region. This phenomenon is observed in flames close to extinction and flame 2 has the lowest heat release and low peak temperature indicating a potential vicinity to extinction conditions.

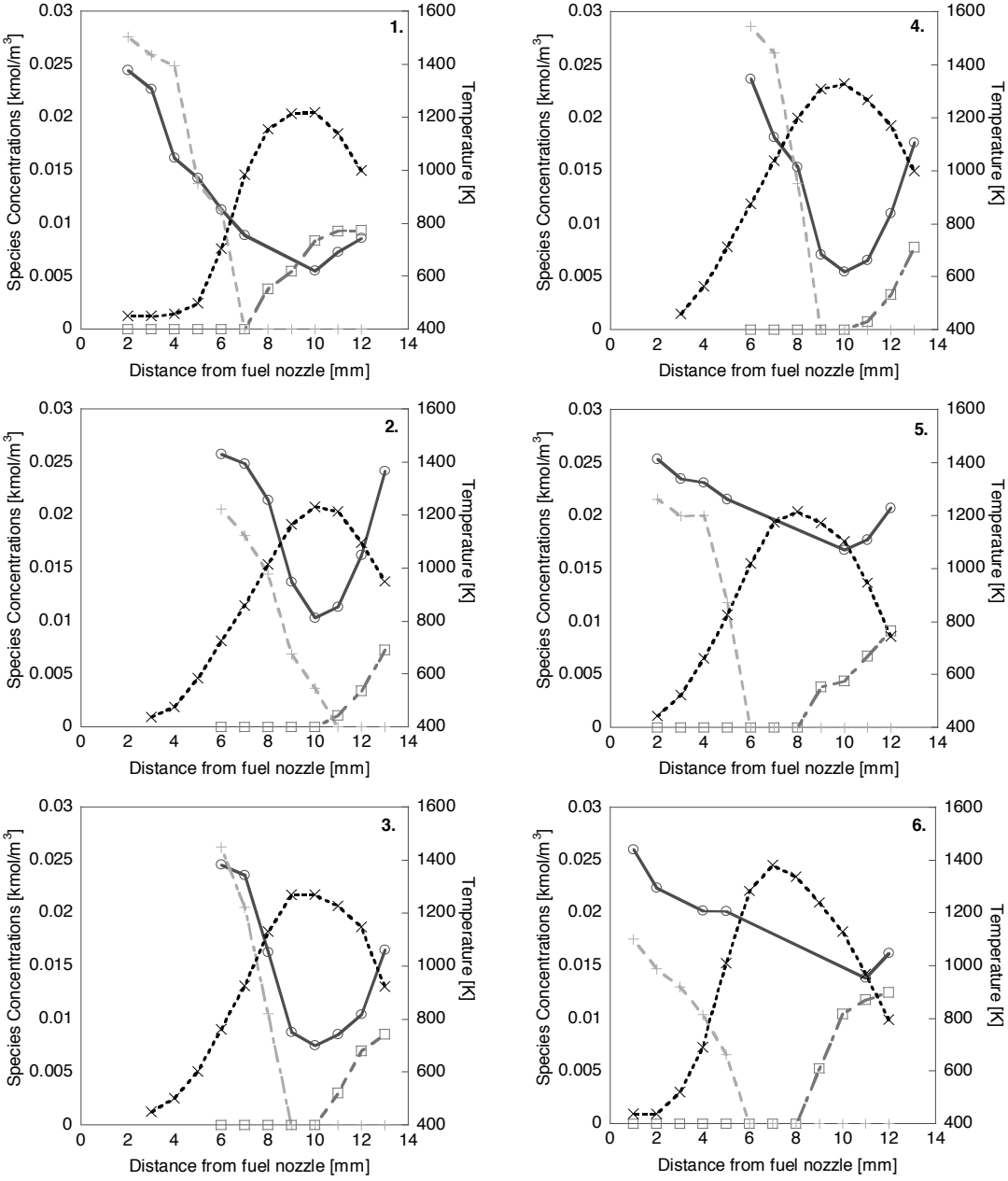


*Fig. 4. Species concentration measurements for $N_2$ (o), $O_2$ ( ) and C-H bond (+) and Temperature distribution curves (x). Flame configuration cases are in accordance to cases 1-6 in Table 2.*

Comparing cases with the same overall equivalence ratio (1, 2, 3 and 6), the combustion behavior of the involved species follows the pattern of steeper curves with increasing strain rate (except for case 2). Temperature distribution curves have their maximum value approximately at the center of the gap between the nozzles and this maximum increases with higher fuel energy release. The error in these measurements is to the order of 10% and is related to the slight instabilities of the reaction zone as it is being established in the real environment of the lab, as well as to the scatter in the seven measurements of temperature that corresponded to each data point.

It is reminded here that the flames are highly diluted ($N_2$ > 80% of the mixture) and as a result $N_2$ concentration can be seen as a measure of the total mixture density. Moreover, since $N_2$ is practically not reacting, its concentration can be seen as a conserved scalar. This leads to a fairly closely linear relation of nitrogen concentration with temperature across the flame that can be seen in Fig. 5. Regression coefficients $R^2$ vary between 0.88-0.97 for the various mixtures.

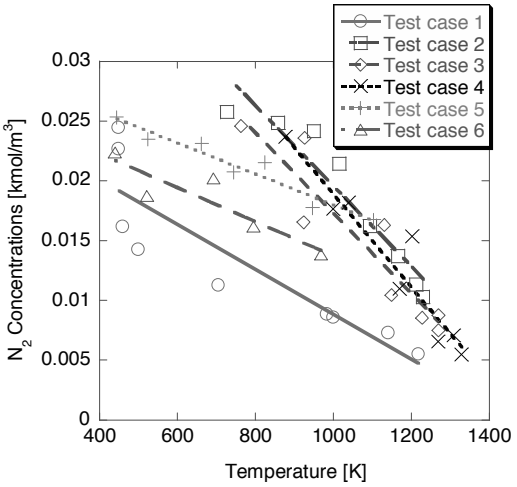


*Fig. 5. Nitrogen concentrations as a function of temperature for the six flame configurations.*

### 3.3 Extinction strain rate measurements

In order to study the extinction behavior of the butanol-methane mixture flames presented in the previous sections, the amount of fuel and oxidizer was kept constant and the concentration of diluent increased to achieve extinction. In this manner, the total heat released as well as the overall equivalence ratio of each flame case remained unaffected. The mixture cases are named M1-M6 and their flow rates at extinction are presented in Table 5. Notably, the fuel and oxidizer mass flow rates are identical to Table 2. $N_2$ flow rates increased to achieve extinction.

*Table 5. Mass flow rates for the butanol-methane flame configurations at extinction*

| Test Case | $C_4H_9OH$ | $N_2$ for $C_4H_9OH$ | $CH_4$ | $N_2$ for $CH_4$ | $O_2$ | $N_2$ for $O_2$ |
|---|---|---|---|---|---|---|
| | [g/min] | [g/min] | [g/min] | [g/min] | [g/min] | [g/min] |
| M1 | 0.067 | 0.729 | 0.133 | 2.752 | 1.465 | 0.407 |
| M2 | 0.135 | 0.729 | 0.052 | 1.641 | 1.151 | 0.799 |
| M3 | 0.202 | 0.729 | 0.065 | 2.319 | 1.623 | 0.799 |
| M4 | 0.296 | 0.729 | 0.051 | 2.706 | 1.544 | 0.799 |
| M5 | 0.270 | 0.893 | 0.042 | 2.167 | 1.544 | 1.190 |
| M6 | 0.337 | 0.893 | 0.011 | 2.659 | 1.937 | 0.407 |

In addition, six flames of pure butanol were established. The pure butanol flames (cases B1-B6) were selected such that they had the same overall equivalence ratio and total heat released with cases M1-M6 respectively. The related information is presented in Table 6.

*Table 6. Mass flow rates for the pure butanol flame configurations at extinction*

| Test Case | $C_4H_9OH$ | $N_2$ for $C_4H_9OH$ | $N_2$ for $CH_4$ | $O_2$ | $N_2$ for $O_2$ |
|---|---|---|---|---|---|
| | [g/min] | [g/min] | [g/min] | [g/min] | [g/min] |
| B1 | 0.270 | 0.729 | 1.944 | 1.465 | 0.407 |
| B2 | 0.216 | 0.729 | 1.620 | 1.151 | 0.407 |
| B3 | 0.301 | 0.729 | 1.963 | 1.623 | 0.407 |
| B4 | 0.377 | 0.729 | 2.544 | 1.544 | 0.407 |
| B5 | 0.333 | 0.729 | 2.283 | 1.543 | 0.407 |
| B6 | 0.354 | 0.729 | 2.191 | 1.941 | 0.407 |

Temperature measurements necessary for the calculation of strain rate at extinction were also obtained at both nozzle exits just before the flame extinguished. The calculated extinction strain rates for both M1-M6 and B1-B6, are presented in Table 7. It is reminded, that for each flame configuration the corresponding overall equivalence ratio and total heat release can be obtained from Table 4. In addition, Fig. 6 presents

the extinction strain rate values as a function of the total combustion heat release of each flame configuration.

*Table 7. Extinction strain rates for butanol-methane mixtures and for pure butanol flames.*

| Test Case | Kext | Test Case | Kext |
|---|---|---|---|
| | [$s^{-1}$] | | [$s^{-1}$] |
| M1 | 128.56 | B1 | 108.82 |
| M2 | 105.08 | B2 | 93.70 |
| M3 | 132.45 | B3 | 113.15 |
| M4 | 140.87 | B4 | 126.10 |
| M5 | 141.77 | B5 | 183.48 |
| M6 | 140.74 | B6 | 195.37 |

In all six cases, pure butanol flames are more vulnerable to extinction than butanol-methane mixture flames with the same overall equivalence ratio and total combustion heat release. Furthermore, an approximately monotonic behavior is observed with increasing heat release, which is evident both in pure butanol and in the mixture cases.

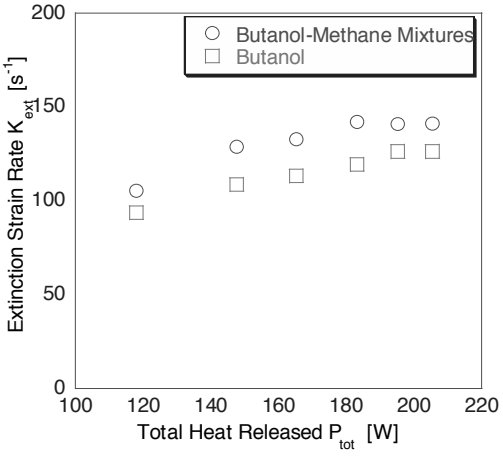


*Fig. 6. Calculations of extinction strain rate K as a function of the total heat released from combustion.*

### 3.4 Estimation of the scalar dissipation rate

The scalar dissipation rate, which represents the inverse of a characteristic diffusion/convection time is defined as:

$$\chi = 2D(\nabla Z)^2, \quad (10)$$

where D represents the diffusivity and Z is the mixture fraction. The importance of the scalar dissipation rate is highlighted when compared to strain rate, which represents the local velocity gradient. Unlike strain rate, it incorporates diffusion effects and therefore provides a better definition for the residence time. Moreover, for non-premixed and partially-premixed flames, it constitutes the determining parameter for the response of chemical reactions to sudden perturbations caused by variations of the turbulent flow field [24].

This definition points to the possibility of estimating the scalar dissipation rate at the stoichiometric surface $\chi_{stoich}$ either through the gradient of the mixture fraction at this location $|\nabla Z|_{stoich.}$, or through an approximation of the mixing layer thickness δ, since $\chi_{stoich}$ scales as:

$$\chi_{stoich} = 2D(\nabla Z)^2_{stoich} \propto D/\delta^2, \quad (11)$$

$$\delta \propto 1/|\nabla Z|_{stoich.}, \quad (12)$$

It is noted that for steady flames $\chi_{stoich}$ is proportional to the strain *K* [25]. The estimation of the thickness δ took place using the measured temperature distributions for the flame configurations of Table 2. In counter-flow diffusion flames, the temperature has a theoretically expected Gaussian distribution [26]. Thus, the experimentally obtained temperature curves were curve-fitted with a Gaussian distribution and the thickness was then approximated as the "full width at half maximum" (FWHM) of the curve. FWHM depends solely on the standard deviation σ of the Gaussian curve and was calculated through:

$$FWHM = 2\cdot\sqrt{2\cdot\ln 2}\cdot\sigma \approx 2.35482\cdot\sigma, \quad (13)$$

The calculated flame thicknesses δ are tabulated in Table 8.

*Table 8. Calculated mixing layer thickness δ as FWHM*

| **Test Case** | **1** | **2** | **3** | **4** | **5** | **6** |
|---|---|---|---|---|---|---|
| **δ [mm]** | 6.078 | 7.228 | 7.090 | 8.459 | 7.233 | 7.019 |

The inverse square root dependence of δ on strain rate that is implied by eq. (11) is investigated in Fig. 7. The experimental findings are plotted on a log-log

scale alongside with a curve depicting the theoretically expected behavior. Since only the slopes of the respective curves are significant for purposes of comparison, the theoretical curve is plotted such that the initial points of both curves coincide. The results of Fig. 7 show that there is a difference between the theoretically expected $1/K^{0.5}$ and the actually measured dependence of $\delta$ on strain rate which scales as $1/K^{0.90627}$. The exponent is far from the expected value and the regression constant is very poor R=0.61956.

The observed departure of the mixing layer thickness from the theoretically expected trend constitutes its calculation from the temperature distribution curves inappropriate for this study. For that reason, the scalar dissipation rate at the stoichiometric surface was approximated using the mixture fraction gradient $|\nabla Z|_{stoich.}$, as shown in eqs. (11) and (12).

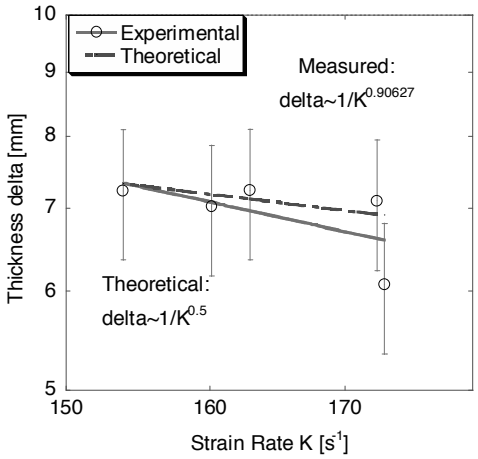


*Fig. 7. Mixing layer thickness δ vs. strain rate on a log-log scale.*

The definition of the mixture fraction is based on the mass fraction of major species and can be formulated in several ways, which were evaluated in [27]. A definition based on the mass fraction of $N_2$ can be followed, where:

$$Z = \frac{Y_{N_2} - Y_{N_2 Ox}}{Y_{N_2 Fuel} - Y_{N_2 Ox}}, \qquad (14)$$

In this last equation, $Y$ denotes mass fraction, $N_2$ subscript stands for nitrogen and $F$, $Ox$ for the fuel and oxidizer stream respectively. $Y_{N2}$ can be used as a conserved scalar since $N_2$ is non-reactive. However, in this study, due to the lack of information regarding the combustion products, $Y_{N2}$ was approximated through:

$$Y_{N_2} = \frac{C_{N_2} . MW_{N_2}}{C_{N_2} . MW_{N_2} + C_i \cdot MW_i}, \qquad (15)$$

In this equation, $C_{N2}$ and $MW_{N2}$ are the measured concentration and the molecular weight of nitrogen. Subscript i denotes either the fuel or oxidizer side outside the flame region and $C_i$ and $MW_i$ are the measured concentrations and molecular weights of either fuel or oxygen. Hence, in both sides, the values of $Ci$ were provided in [kmol/m$^3$] directly from the data of Fig.4. In the fuel side, the molecular weight was calculated as the weighted average, on a molar basis, of the mixture under consideration. This technique was applied in flame configurations 2, 3 and 4 of Fig 4, which had measured values of $N_2$ concentration in the flame region as well. Thus, for these three mixtures that had a butanol molar composition of 35.7%, 40.4% and 55.9%, $MWi$ was considered to be 36.7, 39.4 and 48.4 respectively.

The gap between the nozzles was assumed to consist of three regions: The reaction zone, located in the vicinity of the maximum temperature, and the fuel and oxidizer regions where no combustion products were present. After calculating the mixture fraction Z in all locations, an error function was curve-fitted to the $Z$ distribution, since this is the functional form expected from the theoretical analyses of [27,28]. The curve fit function is of the form:

$$Z = A * erfc(\frac{\mathbf{x} - B}{C}), \qquad (16)$$

where A, B and C are regression constants and x is the distance from the fuel nozzle. The stoichiometric surface was considered to be at the location of the maximum slope of the Z distribution and the corresponding plot for flame configuration 3 is shown in Fig. 8.

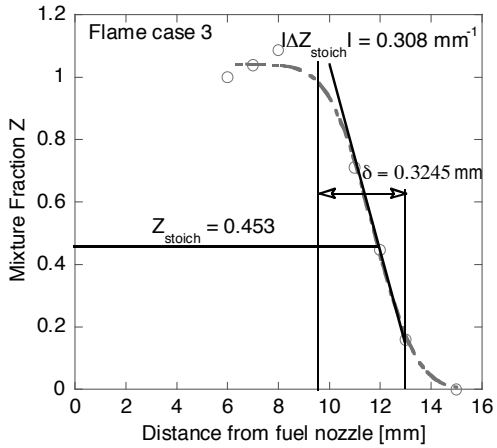


*Fig. 8. Mixture fraction distribution and curve-fitted error function for flame configuration 3.*

The calculated $|\nabla Z|_{stoich.}$ for each flame case was then used in order to determine the mixing layer thickness δ, which scales as the inverse $|\nabla Z|_{stoich.}$ and is shown in Fig.8. Table 9 contains these values and Fig. 9 presents the variation of δ with strain rate.

*Table 9. Calculated mixing layer thickness δ through* $|\nabla Z|_{stoich.}$

| **Test Case** | **2** | **3** | **4** |
|---|---|---|---|
| **δ [mm]** | 2.847 | 3.245 | 2.483 |

The investigation of the inverse square root dependence of δ on strain rate, is presented here similarly to Fig. 7 on a log-log scale and with the theoretical curve present. The results of Fig. 9 show that there is good agreement between the theoretically expected $1/K^{0.5}$ and the actually measured dependence of $\delta$ on strain rate which scales as $1/K^{0.42394}$.

In all three cases, the stoichiometric surface was found to be located approximately 2mm away from the location of maximum temperature in the oxidizer side. Specifically, it was 13.2 mm for cases 2 and 4 and 12 mm for case 3. This can be attributed to the significant experimental error rising from the Raman measurements. A more sensitive camera that would capture combustion products is necessary for a more accurate measurement of the mixture fraction.

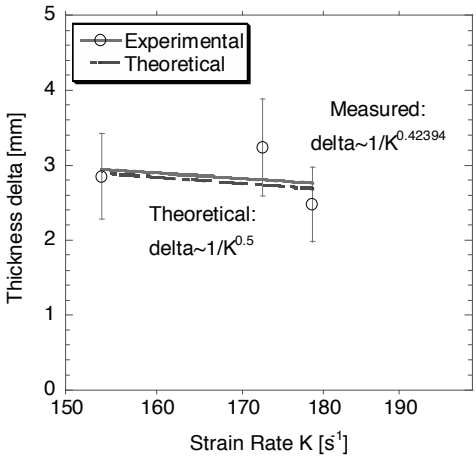


*Fig. 9. Mixing layer thickness δ vs. strain rate on a log-log scale.*

## Conclusions

Pure butanol flames were found to be more vulnerable to extinction than butanol-methane mixture flames with the same overall equivalence ratio and total combustion heat release. Furthermore, a monotonic behavior of the extinction strain rate was observed with increasing heat release, both in pure butanol and in the mixture cases.

The inverse square root dependence of the mixing layer thickness δ on strain and scalar dissipation rate was investigated, and δ was estimated using the temperature distribution across the flame. This was found to generate a departure of δ from the theoretically expected square-root behavior. For that reason, the scalar dissipation rate at the stoichiometric surface was approximated through the mixture fraction gradient $|\nabla Z|_{stoich.}$ for three flame cases. The results did show a better agreement with theoretical predictions.

## Nomenclature

$A$ Nozzle cross-sectional area ($m^2$)
$C$ Concentration of the measured species (kmol/$m^3$)
$D$ Diffusivity of the involved species ($m^2$/s)
$d$ Distance between the nozzles (m)
$K$ Strain rate ($s^{-1}$)
$\dot{m}$ Mass flow rate (kg/s)
$MW$ Molecular weight
$P$ Pressure (Pa)
$Q$ Heat released by fuel combustion (W)
$\overline{R}$ Ideal gas constant (8314 J/kmol K)
$T$ Measured temperature (K)
$U$ Speed of the counter-flowing streams (m/s)
$\dot{V}$ Volumetric flow rate ($m^3$/s)
$Y$ Mass fraction of involved species
Z Mixture fraction

### Greek Symbols

$\delta$ Mixing layer thickness (mm)
$\rho$ Density of a mixture (kg/$m^3$)
$\sigma$ Standard deviation
$\phi$ Overall equivalence ratio
$\chi$ Scalar dissipation rate ($s^{-1}$)

### Subscripts and superscripts

*atm* Atmospheric
*ext* Extinction conditions
*fuel* Fuel stream
*i* Fuel or oxidizer stream
*j* Species
*mix* Butanol-methane mixture
$N_2$ Nitrogen
ox Oxidizer stream
*stoich* Stoichiometric conditions
*tot* Total

## References

[1] Eseji, T., Qureshi N., and Blaschek H.P., 2007, Production of Acetone-Butanol-Ethanol in a continuous flow bioreactor using degermed corn and chlostridium beijernickii, *Process Biochemistry*, 42, pp. 34-39.

[2] Tashiro, Y., et al., 2007, Novel High-Efficient Butanol Production from Butyrate by Non-Growing Clostridium saccharoperbutyl-acetonicum N1-4 (ATCC 13564) with Methyl Viologen, *Biosci. Bioeng*, 104, pp. 238–240.

[3] Tashiro, Y., et al., 2005, High production of acetone–butanol–ethanol with high cell density culture by cell-recycling and bleeding, *Biotechnol,* 120, pp 197–206.

[4] Qureshi, N., and Maddox, I. S. J., 1995, Continuous production of acetone-butanol-ethanol using immobilized cells of Clostridium acetobutylicum and integration with product removal by liquid- liquid extraction, *Ferment. Bioeng,* 80, pp. 185–189.

[5] Sarathy, S. M., et al., 2009, An experimental and kinetic modeling study of *n*-butanol combustion, *Proceedings of the Combustion Institute*, 156, pp. 852-864.

[6] Dagaut, P., Sarathy S.M and Thomson M.J., 2009, A chemical kinetic study of n-butanol oxidation at elevated pressure in a jet stirred reactor, *Proc. Combust. Inst.*, 32, pp. 229–237.

[7] Dagaut, P., and Togbé, C., 2009, Experimental and modeling study of the kinetics of oxidation of butanol-n-heptane mixtures in a jet-stirred reactor, *Energy & Fuels,* 23, pp. 3527–3535

[8] Dagaut, P., and Togbé, C., 2008, Oxidation kinetics of butanol–gasoline surrogate mixtures in a jet-stirred reactor: Experimental and modeling study, *Fuel,* 87, pp. 3313–3321.

[9] Yang, B., et al., 2007, Identification of combustion intermediates in isomeric fuel-rich premixed butanol–oxygen flames at low pressure, *Combust. Flame*, 148, pp. 198–209.

[10] McEnally, C. S., et al., 2005, Fuel decomposition and hydrocarbon growth processes for oxygenated hydrocarbons: Butyl alcohols, *Proc. Combust. Inst.*, 30, pp. 1363–1370.

[11] Alasfour., F. N., 1997, Butanol - A single-cylinder engine study: Availability analysis, *App. Thermal Eng*., 17, pp. 537–549.

[12] Alasfour., F. N., 1997, Butanol - A single cylinder engine study: Engine performance, *Int. J. Energy Res.,* 21, pp. 21–30.

[13] Gautam, M. and Martin, D. W., 2000, Combustion Characteristics of Higher-alcohol/gasoline Blends, *Proc. Inst. Mech. Eng.. Part A,* 214, pp. 497–511.

[14] Gautam, M., et al., 2000, Emissions Characteristics of Higher Alcohol/gasoline Blends, *Proc. Inst. Mech. Eng. Part A*, 214, pp. 165–182.

[15] Peters, N., 1984, Laminar diffusion flamelet models in non-premixed turbulent combustion, *Prog. Energy Combust. Sci.,* 10, pp. 319–339.

[16] Peters, N., 1986, Laminar flamelet concepts in turbulent combustion, *Proc. Combust. Inst*., 21, pp. 1231–1250.

[17] Claramunt, K., et al., 2006, Analysis of the laminar flamelet concept for nonpremixed laminar flames, *Combustion and Flame*, 145, pp. 845–862.

[18] Karpetis, A. N. and Barlow, R. S., 2002, Measurements of scalar dissipation in a turbulent piloted methane/air jet flame, *Proceedings of the Combustion Institute*, 29, pp. 1929–1936.

[19] Bijjula, K. and Kyritsis, D. C., 2005, Experimental evaluation of flame observables for simplified scalar dissipation rate measurements in laminar diffusion flamelets, *Proceedings of the Combustion Institute*, 30, pp. 493-500.

[20] Bijjula, K. and Kyritsis, D. C., 2005, Comparative evaluation of flame observables for simplified scalar dissipation rate measurements, *43rd AIAA Aerospace Sciences Meeting and Exhibit*, Meeting Papers, pp. 2585-2591.

[21] Seshadri, K., and Williams, F.A., 1978, Laminar flow between parallel plates with injection of a reactant at high Reynolds number, *International Journal of Heat and Mass Transfer*, 21, pp. 251-253.

[22] Lide, D. R., 1994, *CRC Handbook of Chemistry and Physics*, 75th ed., CRC Press, London, UK.

[23] Wang G., Karpetis A. N. and Barlow R. S., 2007, Dissipation length scales in turbulent nonpremixed jet flames, *Proceedings of the Combustion Institute*, 148, pp. 62-75.

[24] Im, H. G., Chen J. H., and Chen, J.Y, 1999, Chemical Response of Methane/Air Diffusion Flames to Unsteady Strain Rate, *Combustion and Flame,* 118, pp. 204–212.

[25] Peters, N., 2002, *Turbulent combustion*, 2nd ed., Cambridge University Press, New York.

[26]Law, C. K., 2006, *Combustion Physics*, Cambridge University Press, New York.

[27] Santoro, V. S., Kyritsis, D. C. and Gomez A., 2003, Quantitative scalar dissipation rate measurements in vortex perturbed counter-flow diffusion flames, *Proceedings of the Combustion Institute*, 29, pp. 1679–1685.

[28] Santoro, V. S., et al., 2000, Vortex-induced extinction behavior in methane/gaseous flames: A comparison with quasi-steady extinction, *Proceedings of the Combustion Institute*, 28, pp. 2109–2116.

## Acknowledgements

The authors would like to acknowledge the support of the U.S. Department of Energy through the Graduate Automotive Technology Education (GATE) Center of Excellence at the University of Illinois.

# Decomposing Changes in the Energy Demand of UK Manufacturing

*G.P. Hammond*[a,b] *and J.B. Norman*[b]

[a] *Institute for Sustainable Energy & the Environment, Bath, UK*
[b] *Department of Mechanical Engineering, University of Bath, UK*

**Abstract:** Over the period 1990-2007 the energy demand of UK manufacturing has fallen. A decomposition analysis was conducted to identify the effects of changes in output, structure and energy intensity on the changing energy demand. It was found that a falling energy intensity (indicating improving energy efficiency) was the principle reason for the fall in energy demand. As the UK manufacturing sector is so broad in its uses of energy, it was split into an energy-intensive (EI) and a non-energy-intensive (NEI) sub-sector to better understand the improvement in energy efficiency. The NEI sub-sector made much greater relative reductions in energy intensity in comparison to the EI sub-sector. Previous studies indicate that the EI sector may have made larger improvements in energy intensity in the period between 1973 and 1990 and this may be the reason for the limited improvement seen here. Neither energy price nor production growth appears strongly correlated with the improving efficiency over the period 1990-2007.

**Keywords:** Decomposition, Efficiency, Energy, Intensity, Industry, Manufacturing.

## 1. Introduction

Reducing dependence on fossil fuels as an energy source protects against the dangers of both climate change and energy security. Decreasing energy demand through management and efficiency measures is often seen as the most technologically simple and economic option available, to achieve a reduction in fossil fuel use [1-3]. The UK manufacturing sector is a significant user of energy, accounting for approximately 20% of the UK's final user demand [4], reducing the energy use of manufacturing is important in reaching government targets. Industry is however difficult to analyse due to the large variability in the ways energy is used within the sector.

Past trends in energy use can help us better understand the current situation and influence future decisions aimed at reducing energy use. Changes in energy demand over time can be the result of a number of factors. Decomposition analysis methods can be used to analyse manufacturing, by examining the contribution of changes in industrial structure, output and energy intensity to changing energy demand [5]. The isolated effect of changing energy intensity is a useful measure of energy efficiency. It can therefore be used to examine improvements made and the success of energy policy.

A study of the Netherlands [6] examines the industrial sector over the years 1988-1999. Industry is split into an energy-intensive and a non-energy-intensive sub-sector. Decomposition analysis is performed on the non-energy-intensive sub-sector, which was found to have made no improvement in energy efficiency over the years studied. Decomposition studies of the UK industrial sector have been undertaken by previous studies [7-11] and cover the time period from the late 1960s, to the early 1990s.

The aim of the current work is to decompose changes seen in UK manufacturing energy demand over the recent time period. The manufacturing sector will be split, in common with the Dutch study above [6], into an energy-intensive (EI) and a non-energy-intensive (NEI) sub-sector, with a decomposition analysis undertaken of each. The EI sub-sector is expected to have stronger drivers for improving energy efficiency due to the greater possible financial gain for this sub-sector in reducing energy use and as the EI sub-sector is a target for energy policy in the UK. However previous studies have found that there is no simple link between energy price and efficiency improvements, indicating that financial gain is not the only motivation for increased efficiency [8, 9]. Other factors such as output growth and investment rate can have an important effect on

Corresponding Author: Jonathan Norman, Email: j.b.norman@bath.ac.uk

efficiency improvements. It will therefore be of interest to see how the EI and NEI sub-sectors differ in efficiency improvements made.

## 2. Methodology and datasources

### 2.1 Defining relevant measures

The manufacturing sector examined here is defined by SIC codes 15-37, excluding the sub-sector defined by SIC 23 (Manufacture of coke, refined petroleum products and nuclear fuel), full details of SIC classification are available in [12]. Energy demand is measured in terms of higher heating value (HHV) and primary energy. Data on final energy demand is obtained from the Digest of United Kingdom Energy Statistics (DUKES) [13] and Energy Consumption in the UK (ECUK) [13, 14]. Factors for the conversion to primary energy are those used in the Climate Change Agreements (CCAs) [15]. Electricity conversion factors are averaged over each studied period so improvements in the efficiency of electricity generation are not seen as improvements by the end user. There is no differentiation here between electricity supplied by combined heat and power plants and from the national grid. Value of production is used as the measure of manufacturing output as it better represents the true physical output of a sector than value added [16], being less likely to exaggerate changes in real output. The Index of Production (IoP) [17] is used with economic output data in current terms for 2005, taken from the Annual Business Inquiry (ABI) [18] to calculate value of production at constant 2005 prices. Aggregate energy intensity is defined as energy demand/output. Data on costs and number of enterprises in each sub-sector are taken from the ABI [18], energy price data are from the Quarterly Energy Prices publication [19].

### 2.2 Defining energy intensive industry

Various methods of defining an EI and NEI sub-sector within manufacturing are discussed by [6]. This paper follows the recommendation of [6] in defining a sub-sector as EI or NEI based on the values of a number of criteria, here these criteria and the values for the split between EI and NEI sub-sectors differ slightly to the previous study [6]. The criteria used are:

1. Aggregate energy intensity
2. Proportion of total costs represented by energy and water costs[1].
3. Energy demand per enterprise.

If a sub-sector had a sufficiently large value for any of the above criteria results it was defined as EI. Values should therefore represent a strong financial driver to explore and implement energy saving options in comparison to the remainder of the manufacturing sector. Values for the split between the EI and NEI sub-sectors are set as one and a half times the figure for the manufacturing sector for criteria 1 and 2. For criteria 3, due to a greater variation in values, and as it is seen as a weaker driver a limit of 100TJ/enterprise is used. The values used to define the sub-sectors as EI or NEI are the mean of the results for the years 2002-2006, after removing the highest and lowest values.

### 2.3 Decomposition analysis

There are a number of techniques available for decomposition analysis, a useful guide to the various options is given by [20]. The log mean Divisia index method I (LMDI I) is used here, it was first introduced by Ang, Zhang and Choi [21]. The method is perfect in decomposition, with no residual term, it is recommended for general use based on theoretical foundation, adaptability, ease of use and ease of result interpretation [20].

The methodology shown here is adapted from [22]. Additive decomposition analysis is used, where by the total change in energy demand ($\Delta E_{tot}$), over a time period (0 to T), is a sum of the changes due to changes in production volume[2] ($\Delta E_{pdn}$), changes in structure ($\Delta E_{str}$), and changes in intensity ($\Delta E_{int}$).

$$\Delta E_{tot} = E^T - E^0 = \Delta E_{pdn} + \Delta E_{str} + \Delta E_{\text{int}}, \qquad (1)$$

For i sub-sectors of industry, total energy demand can be given as,

$$E = \sum_i E_i = \sum_i Q \frac{Q_i}{Q} \frac{E_i}{Q_i} = \sum_i Q S_i I_i, \qquad (2)$$

[1] Ideally only energy costs would be used, however, due to restrictions in the data set used [18], energy and water costs were grouped.

[2] The term output is also used to refer to production volume.

where Q is output. $S_i$ (=$Q_i$/Q) and $I_i$ (=$E_i$/$Q_i$) are, respectively, the activity share and aggregate energy intensity of sector i. The components of change in (1) are calculated from,

$$\Delta E_{pdn} = \sum_i L\left(E_i^T, E_i^0\right) \ln \frac{Q^T}{Q^0}, \quad (3)$$

$$\Delta E_{str} = \sum_i L\left(E_i^T, E_i^0\right) \ln \frac{S_i^T}{S_i^0}, \quad (4)$$

$$\Delta E_{\text{int}} = \sum_i L\left(E_i^T, E_i^0\right) \ln \frac{I_i^T}{I_i^0}, \quad (5)$$

where,

$$L\left(E_i^T, E_i^0\right) = \frac{E_i^T - E_i^0}{\ln E_i^T - \ln E_i^0}. \quad (6)$$

The change due to intensity is a good measure of energy efficiency, such that as intensity drops, efficiency increases.

### 2.4 Timescale and disaggregation level of analysis

Some studies have found the level of disaggregation used in a decomposition analysis can significantly effect results [23], and structural change can be underestimated if analysis is not undertaken at a high enough level of disaggregation [9]. So initially the analysis was conducted at the highest disaggregation level possible, with the datasources utilised. This resulted in 70 sub-sectors of manufacturing (both for defining the EI/NEI split and the decomposition analysis). The time period that could be analysed at this level of disaggregation was however limited. An analysis was also carried out at the 2-digit SIC level (21 manufacturing sub-sectors). It was found that there were not significant differences between results using the different levels of disaggregation. The more aggregated results, at a 2-digit SIC level, were therefore used as a wider time period could be analysed.

The decomposition analysis covered the time period 1990-2007. Due to methodological changes in the collection of energy data [13], over the periods 1995-1996, 1998-1999 and 2000-2001, analysis could not span all years. Because of a lack of output data, the recycling sub-sector (SIC 37) could not be included in the decomposition analysis.

## 3. Results

### 3.1 Defining energy-intensive industry

There are nine sub-sectors classified as EI, these sub-sectors are labelled in Fig. 1. To be defined as EI a sub-sector requires an aggregate intensity greater than 6.46MJ/£, and/or energy and water costs greater than 3.3% of total costs, and/or energy demand per enterprise greater than 100TJ. Note the logarithmic scales on Fig. 1. There is an order of magnitude variation across the manufacturing sector for each of the three criteria plotted (the logarithmic scale does not apply to the area of the data points). The EI sub-sector is responsible for approximately 65% of energy demand, whereas the NEI sub-sector contributes approximately 65% of economic output. This leads to an aggregate intensity in the EI sub-sector of approximately four times that in the NEI sub-sector.

### 3.2 Decomposition analysis

Decomposition analysis for the manufacturing sector was undertaken at two levels of disaggregation: a 2-digit SIC level (21 sub-sectors), and by splitting into just the EI and NEI sub-sectors. The results are shown in Fig. 2. The results are indexed to the energy demand in 1990 and show cumulative additive change. The periods for which methodological change occurred in the data, preventing analysis, are indicated by dotted lines. As the results are stagnant during periods of methodological change the total changes over the period 1990-2007 may differ from than those presented here.

It can be seen in Fig. 2 that structural change has had little influence on energy demand. Manufacturing output has increased over the period studied, the reduction in output in the early 1990s was due to a recession in the UK. The reduction seen in energy demand, of 12% between 1990 and 2007 is driven principally by a decrease in intensity.

The total change in energy demand and change due to output are independent of disaggregation level and therefore equal in A and B of Fig. 2. The other results are also similar between the two disaggregation levels.

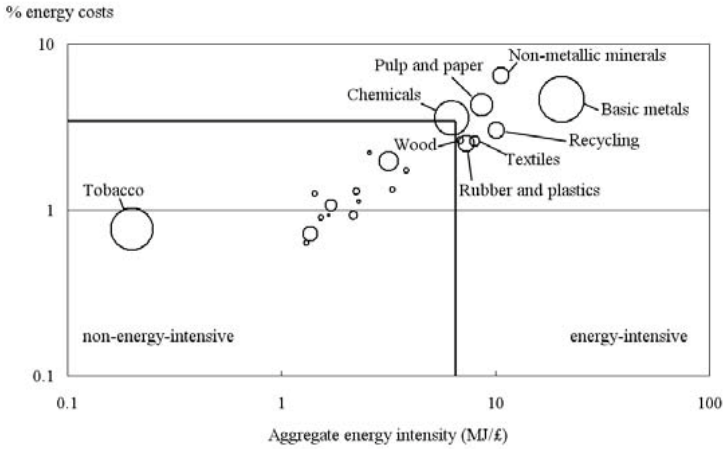


*Fig. 1 UK industrial aggregate energy intensity, and percentage of total costs: represented by energy and water, and energy use per enterprise (represented by area of data points). Manufacturing split at the 2-digit SIC level, 2002-2006.*

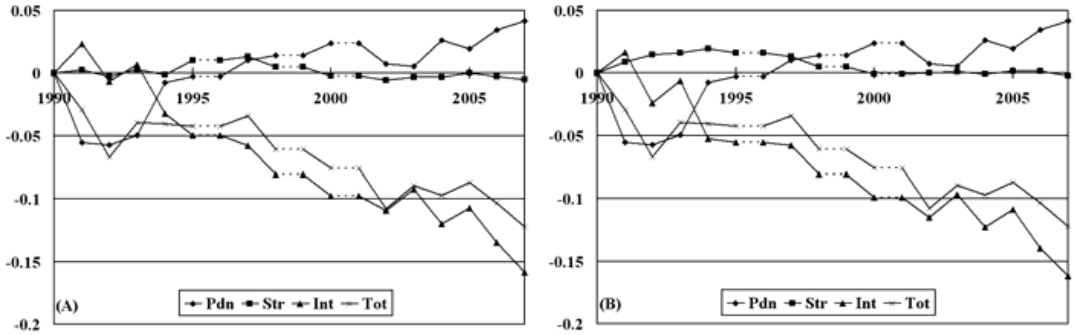


*Fig. 2 Decomposition of the UK manufacturing sector showing the change in energy demand (Tot) and the contributions due to changes in output (Pdn), structure of the sector (Str), and intensity (Int). (A) Disaggregation at the 2-digit SIC level. (B) Disaggregation into just two sub-sectors, EI and NEI.*

The EI and NEI sub-sectors are decomposed independently in Fig. 3. The changes are indexed to the energy demand in 1990, the baseline, for each sector. Much greater relative reductions in the energy demand of the NEI sub-sector have been made. This is predominantly due to the falling energy intensity in the NEI sub-sector. Over the period 1990-2007, if structure and output had been constant in each of the sub-sectors, then EI energy demand would have fallen just 7% due to the intensity effect. This contrasts with 32% in the NEI sub-sector.

The relationship between energy price for the manufacturing sector and falling intensity is shown in Fig. 4. Energy price does not appear to have an effect on the intensity. The intensity decreases at a fairly constant rate for manufacturing, (as it does in both the EI and NEI sub-sectors, when examined separately as shown in Fig. 3) and is unaffected by the fluctuations in energy price. Energy prices can also influence the structure of industry, causing a move to less energy-intensive industries, this was seen in the years following the first oil crisis [9]. However, for the present study, no significant structural change has been observed (Fig. 2 and Fig. 3). The most significant change in energy price occurred since 2004. It may take a few years of sustained high prices for companies to react, and the effect of increasing energy prices may therefore not yet have been seen.

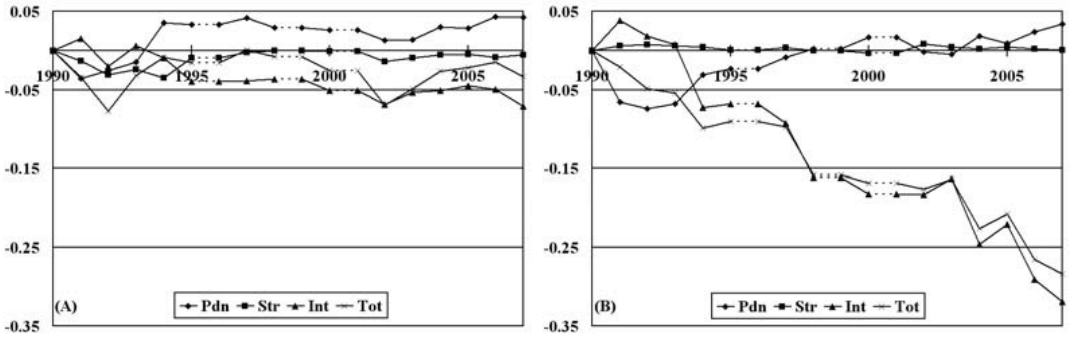


*Fig. 3 (A) Decomposition of the UK EI sub-sector. (B) Decomposition of the UK NEI sub-sector.*

If manufacturing output rises, investment in new technology usually rises as new plant and equipment are purchased, this tends to increase efficiency. Fig. 2 and 3 show some correlation in this regard. As production fell in the early 1990s, intensity was fairly stagnant; as output increased intensity fell. However, the NEI sub-sector shows less relative growth in output and yet the largest relative intensity improvements. If year-on-year changes in output and intensity are examined there is some correlation (see Fig. 5). Nevertheless, this correlation is much weaker when both the EI and NEI sub-sectors are examined independently. It cannot therefore be said that there is a good correlation between intensity drop and production increase.

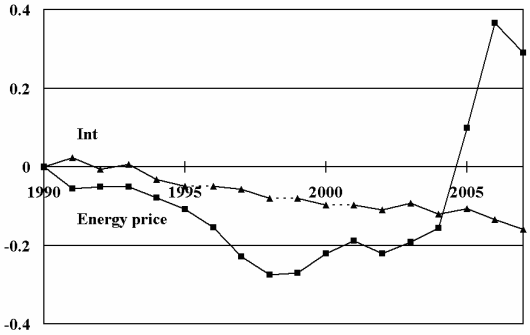


*Fig. 4 Total energy price for the UK industrial sector (in real terms, including the CCL) and change in energy demand due to intensity, from Fig. 2 (A). Both indexed to 0 in 1990.*

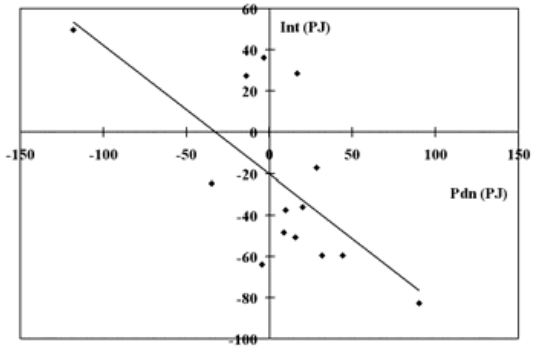


*Fig. 5 Correlation between increased production and falling intensity, for the UK manufacturing sector: 1990-2007.*

A changing fuel split could effect efficiency improvements. Electricity can generally be used more efficiently than other fuels in terms of final demand, due to the higher level of control possible. However electricity will lead to a higher primary energy demand than the fossil fuel alternatives, due to generation inefficiencies[3].

Fuel splits for the UK EI and NEI sub-sectors are shown in Fig. 6. The changing fuel splits in the EI and NEI sub-sectors are not vastly different and are unlikely to be a significant reason for the difference in changes of energy intensity observed.

[3] Electricity can be generated by low or zero carbon technologies, and so a higher proportion of electricity use could lead to future reductions in fossil fuel use and associated emissions.

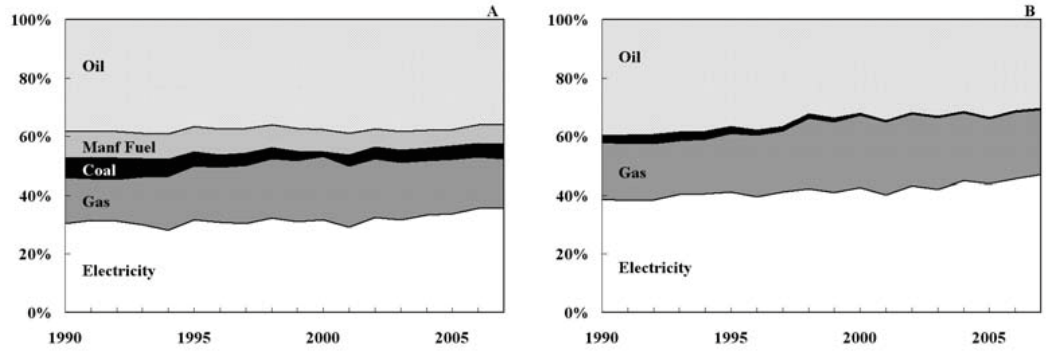


*Fig. 6 UK fuel split for the EI sub-sector (A) and the NEI sub-sector (B).*

## 4. Concluding remarks

The decomposition analysis undertaken with a disaggregation into only the EI and NEI sub-sectors yielded good agreement with those results using a higher level of disaggregation. This suggests that splitting UK manufacturing into just the EI and NEI sub-sectors characterises the sector well in this case.

It was found that the NEI sub-sector has made considerably greater reductions in energy demand due to improved efficiency (32%) relative the EI sub-sector (7%). Interestingly much larger improvements are seen in the UK than in the NEI sub-sector in the Netherlands [6][4]. No strong link was found in the present study between either energy price or manufacturing output and the improved efficiency. A previous study [8] examined the link between price and efficiency for eight OECD countries. Efficiency was not found to increase more rapidly when energy prices were high. Greater gains were sometimes observed when prices were low. These low prices were typically coupled with higher industrial growth, and hence investment in new technology. However, the same study [8], also displayed a decoupling of output and intensity improvements in the UK over the period 1973-87. Efficiency improvements are not insensitive to price, but the relationship is not a simple one and other factors can be important. Price can also influence structure, high energy prices encourage a move towards less energy-intensive manufacturing [9]. But there is very little influence on energy demand due to structural change from the UK results analysed here. It is only since 2004 that energy prices have increased in real terms from the 1990 baseline. The effect of this price increase may yet be seen, due to a lag in the response of manufacturing.

It is useful to put the results obtained here in a broader historical context. Whilst the various studies examined use different decomposition methods, disaggregation level, and have differing definitions of 'industry' or 'manufacturing', general trends may be extracted and will help to frame the present results. Since decomposition analyses were first conducted for UK manufacturing, in the late 1960s, intensity improvements have induced much greater reductions in energy demand than structural changes, [7, 8, 11]. The possible exception to this observation is during the period following the first oil crisis (1973-1978), when structural and intensity changes had similar effects on aggregate intensity [9]. All the previous studies [7-11] show continued improvements in efficiency over time, as would be expected. Nevertheless the sub-sectors in which these improvements were made is important. From 1968-1978 a previous study [9] found greater efficiency improvements generally occurred in those sub-sectors classed here as EI than in industry as a whole. A split into an energy-intensive and an "other" group of

[4] The NEI sector is defined slightly differently in the two studies, and therefore results are not directly comparable. However the difference is striking enough to still be indicative of a substantial difference in results.

industry was made by [10], in a broadly similar manner to that adopted here. Decomposition analysis was not undertaken, although the aggregate intensity was analysed. It was found that from 1973-1980 the energy-intensive group made relative year-on-year improvements in aggregate intensity three times those of the "other" group. From 1980-1988 the relative improvements seen in the two groups were almost equal.

Studies for the time period previous to that covered here indicate that the EI sub-sector may have made greater improvements in efficiency from the first oil crisis until the late 1980s. The greater relative improvements in efficiency by the NEI sub-sector, in the period 1990-2007, may therefore be as there were more "low hanging fruit" still available for the NEI sub-sector over this period. Larger improvements had perhaps already been made in the EI sub-sector, thereby making further improvements more difficult. Whether the improvements in energy efficiency seen in this study can be maintained or surpassed in the future is an important consideration and one that demands more attention than can be given here. However some sources indicate large improvements in the energy efficiency of manufacturing are still possible [24, 25].

Further analysis may investigate the effect sub-sectors at the 2-digit SIC level have on results to see if there are individual sub-sectors causing a substantial proportion of the changes in energy intensity observed here. This could indicate those sub-sectors to focus on in future. A decomposition analysis of carbon emissions would also be a useful exercise to compare savings delivered by improved industrial efficiency, to those achieved through fuel switching and improved efficiency of electricity generation.

Increasing energy prices through policy is a difficult balancing act. Price can act as a stimulus for increased efficiency but, if prices are too high, can lead to a lack of growth and stifle investment in efficient technology. High energy prices can also cause structural change and carbon leakage into areas of the world with lower prices. Price rises are also not the only way to stimulate efficiency improvements. Schemes that both supplement the cost, and encourage development of more efficient equipment can also be effective. Output growth can help this improvement in efficiency through the purchasing of new equipment, although output growth also increases energy demand. In order to reach future emission targets, consumerism and output growth may need to be curtailed and so cannot be relied upon to provide the required efficiency improvements.

## References

[1] House of Commons Environmental Audit Committee, 1999, Environmental Audit - Seventh Report: Energy Efficiency, TSO, London.

[2] The Institution of Engineering and Technology, 2007, The IET Energy Principles, IET, London.

[3] Expert Group on Energy Efficiency, 2007, Realizing the Potential of Energy Efficiency: Targets, Policies, and Measures for G8 Countries, U.N. Foundation, Washington, DC.

[4] DECC, 2009, DUKES: Table 1.1.5 Energy consumption by final user (energy supplied basis), 1970 to 2008, DECC, London. [Spreadsheet].

[5] Ang, B.W., and Zhang, F.Q., 2000, A survey of index decomposition analysis in energy and environmental studies, Energy, 25 (12), 1149-1176.

[6] Ramirez, C.A., Patel, M., and Blok, K., 2005, The Non-Energy Intensive Manufacturing Sector. An Energy Analysis Relating to the Netherlands, Energy, 30 (5), 749-767.

[7] Greening, L.A., et al., 1997, Comparison of Six Decomposition Methods: Application to Aggregate Energy Intensity for Manufacturing in 10 OECD Countries, Energy Economics, 19 (3), 375-390.

[8] Howarth, R.B., et al., 1991, Manufacturing Energy Use in Eight OECD Countries - Decomposing the Impacts of Changes in Output, Industry Structure and Energy Intensity, Energy Economics, 13 (2), 135-142.

[9] Jenne, C.A. and Cattell, R.K., 1983, Structural Change and Energy Efficiency in Industry, Energy Economics, 5 (2), 114-123.

[10] Park, S.H., Dissmann, B., and Nam, K.Y., 1993, A Cross-Country Decomposition

Analysis of Manufacturing Energy Consumption, Energy, 18 (8), 843-858.
[11] Unander, F., 2007, Decomposition of Manufacturing Energy-Use in IEA Countries. How do Recent Developments Compare with Historical Long-Term Trends?, Applied Energy, 84 (7), 771-780.
[12] Office of National Statistics, 2002, UK Standard Industrial Classification of Economic Activities 2003, TSO, London.
[13] Department of Energy and Climate Change, 2009, Digest of United Kingdom Energy Statistics (DUKES), TSO, London.
[14] Department of Energy and Climate Change, 2009, ECUK Table 4.6: Detailed Industrial Energy Consumption by Fuel 1990-2007, DECC, London. [Spreadsheet].
[15] Department of Energy and Climate Change, 2008, Climate Change Agreements: Conversion Factors and Procedures, DECC, London.
[16] Freeman, S.L., Niefer, M.J., and Roop, J.M., 1997, Measuring Industrial Energy Intensity: Practical Issues and Problems, Energy Policy, 25 (7-9), 703-714.
[17] Office of National Statistics, 2009, Index of Production: Time Series Data. [accessed 28th November 2009], Available from: http://www.statistics.gov.uk/statbase/tsdtables1.asp?vlnk=diop.
[18] Office of National Statistics, 2009, Annual Business Inquiry (ABI), ONS, Newport.
[19] Department of Energy and Climate Change, 2009, Table 3.3.1 Fuel Price Indices for the Industrial Sector from Quarterly Energy Prices Publication, DECC, London. [Spreadsheet].
[20] Ang, B.W., 2004, Decomposition Analysis for Policymaking in Energy: which is the Preferred Method?, Energy Policy, 32 (9), 1131-1139.
[21] Ang, B., Zhang, F., and Choi, K.H., 1998, Factorizing Changes in Energy and Environmental Indicators Through Decomposition, Energy, 23 (6), 489-495.
[22] Ang, B.W., 2005, The LMDI Approach to Decomposition Analysis: A Practical Guide, Energy Policy, 33 (7), 867-871.
[23] Ang, B.W. and Skea, J.F., 1994, Structural Change, Sector Disaggregation and Electricity Consumption in UK Industry, Energy & Environment, 5 (1), 1-16.
[24] De Beer, J., 1998, Long-Term Energy-Efficiency Improvements in the Paper and Board Industry, Energy, 23 (1), 21-42.
[25] Von Weizacker, E., Lovins, A.B., and Lovins, L.H., 1997, *Factor Four: Doubling Wealth, Halving Resource Use,* Earthscan, London.

**Acknowledgments:** The funded research of the first author (GPH) on industrial energy demand and carbon emissions reduction currently forms part of the research programme of the UK Energy Research Centre (UKERC); Phase II renewed in 2009. This national centre is funded by three of the UK Research Councils—the Economic and Social Research Council (ESRC), the EPSRC, and the Natural Environment Research Council (NERC). The second author (JBN) is supported by a research studentship co-funded by the Great Western Research (GWR) Alliance, EDF Energy and EDF R&D (Ecleer) (jointly supervised by Professor Hammond and Professor Catherine Mitchell of the University of Exeter's Cornwall Campus).

Authors' names appear alphabetically.

# Power station adapted for the production of heat feeding the district heating system

*Andrzej Ziębik, Professor Ph.D., D.Sc.*

*Institute of Thermal Technology, Silesian University of Technology*
*22 Konarskiego Str., 44-100 Gliwice, Poland*
*phone: (4832)237 1049; Fax: (4832)237 2872; e-mail: andrzej.ziebik@polsl.pl*

**Abstract:** The paper presents the algorithms and results of the energy, ecological and economical analysis of adapting a power station for the production of heat from the viewpoint of implementing the Directive 2004/8/EC on the promotion of high-efficiency cogeneration. Such an analysis is based on the duration curve of ambient temperature characterizing the distribution of ambient temperature treated as a random value. The distribution of heat loads between the heat exchangers (basic and peak load) determines the distribution of the PLC (Power Loss Coefficient) and thus also of the index PES (Primary Energy Saving) during the year. The resulting value of this analysis is the relative cost of heat (RCH) taking into account the benefits of certificates connected with the production of electricity in the mode of high-efficiency cogeneration. The developed algorithms maybe applied in the case of district heating/cooling systems. The exemplary results of this analysis concern a power station provided with power units of 360 $MW_{el}$ situated near the district heating system with a maximum demand of heat amounts 250$MW_{th}$, presently supplied with heat from the municipal heating plant.

**Keywords:** power station, high-efficiency cogeneration, PES (Primary Energy Saving), district heating system

## 1. Introduction

One of the ways of implementing the Directive 2004/8/EC on the promotion of high-efficiency cogeneration [2] is the adaptation of already existing power stations for the production of heat in order to feed a district heating system situated within the range of an economical distance of heat supply [4,5,6,8,9]. In some EU countries (e.g Poland) the potential of high-efficiency cogeneration in power stations adaptable for this purpose is considerable.

As has been stressed in the Directive, the promotion of cogeneration based on useful heat demand is a priority for EU. Besides primary energy saving, cogeneration leads to a reduction of emissions, particularly greenhouse gases if compared with the separate production of heat and electricity. The development of cogeneration influences also the security of primary energy supply and the depletion of the import of primary energy.

Cogeneration in a power station results in losses in the production of electricity due to the lack of reserves in the capacity of the boiler. This loss can be compensated by other power units of such a power station or by some other power stations within the national electro-energy system. The Power Loss Coefficient (PLC) of electricity production is the lower, the lower the pressure level at which steam is supplied to the heat exchangers. Therefore, steam ought to be mainly supplied from the regenerative bleeders of the low-pressure part of the turbine, although practically it is much easier to supply heating steam from the exhaust of the medium-pressure part of the turbine.

## 2. Power unit adapted for the heat production - Power Loss Coefficient

The adaptation of a power unit for the production of heat feeding the district heating system leads to cogeneration. The production of heat in a condensing power unit results in a decreased production of electricity if the consumption of chemical energy of fuels remains constant. This decrease must be compensated by additional production of electricity in the system power stations. The effect of electricity reduction is

determined by means of the Power Loss Coefficient PLC:

$$PLC = \frac{\left|-\Delta N_{el}\right|}{\dot{Q}_c}\eta_{th} \quad (1)$$

where:

$-\Delta N_{el}$ – power loss due to the adaptation of the power unit for heat production,

$\dot{Q}_c$ – heat flux from a power unit adapted for heat production,

$\eta_{th}$ – efficiency of the transport of heat from a power unit adapted for heat production.

The heat flux $\dot{Q}_c$ concerns the value loco consumer (at the point of net heat consumption).

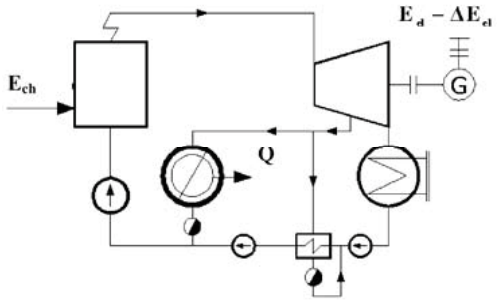


*Fig. 1. Power plant after its adaptation for heat production; $E_{ch}$ – chemical energy consumption, $E_{el}$ – electricity production before adaptation, $\Delta E_{el}$ – decrease of electricity production after adaptation assuming that $E_{ch}$=const.*

It has been assumed that the additional supply from the steam bleeder for heat production does not affect the distribution of pressure in the turbine and the temperature of the preheated condensate. Basing on the balances of the regenerative preheater (condensing power unit and power unit adapted for the production of heat - Fig. 1) the Power Loss Coefficient can be determined [8]:

$$PLC = \frac{\left(\dot{m}_h - \Delta\dot{m}\right)\cdot \Delta h_b \cdot \eta_{me}}{\dot{m}_h\left(h_b - h_c\right)} \quad (2)$$

and

$$\Delta\dot{m} = \dot{m}_h \frac{h_w - h_c}{h_w - h_b} \quad (3)$$

thus

$$PLC = \frac{\Delta h_b}{h_b - h_w}\eta_{em} \quad (4)$$

where:

$\dot{m}_h$ – steam flux supplying the heat exchanger,

$\Delta\dot{m}$ – decrease of the steam flux supplying the regenerative exchanger after the adaptation of the power unit for heat production,

$\Delta h_b$ – drop of specific enthalpy in the low-part of the turbine,

$h_c$ – specific enthalpy of the condensate,

$h_b$ – specific enthalpy of the bleed steam,

$h_w$ – specific enthalpy of feeding water before the regenerative exchanger,

$\eta_{em}$ – electro-mechanical efficiency of the turbogenerator.

If heat is supplied from several steam bleeders of the turbine, the averaged Power-Loss Coefficient must be used:

$$\overline{PLC} = \frac{1}{Q}\sum_{i=1}^{n} Q_i \cdot PLC_i \quad (5)$$

where $Q_i$ denotes the supply of heat from the i-th steam bleeder and $PLC_i$ is the Power Loss Coefficient for this bleed.

The method of PLC calculations by means of Eq. 4 is justified basing on the aforesaid assumptions. To some extend the accuracy of calculation can be improved by applying the approximated equation of Stodola-Flügel [7] concerning the steam flow capacity of the turbine. Practically, however, both these ways of calculations ought to be verified basing on measurements of the turbogenerator.

## 3. Energy analysis basing on PES (Primary Energy Saving)

The analysis of energy effects due to adapting the condensation power unit for heat supply presented in this paper is based on the index PES (Primary Energy Saving). This approach differs from traditionally algorithms applied so far.

PES (Primary Energy Saving) defined in the Directive 2004/8/EC is expressed by the relation [2]:

$$PES = 1 - \frac{1}{\frac{CHP\ H\eta}{Ref\ H\eta} + \frac{CHP\ E\eta}{Ref\ E\eta}} \quad (6)$$

where:

$CHP\,H\eta$, $CHP\,E\eta$ – the arithmetic partial efficiency of heat and electricity production in the cogeneration unit,

$Ref\,H\eta$, $Ref\,E\eta$ – the efficiency reference value for separate heat and electricity production.

This relation may be transformed to the equation:

$$PES = 1 - \frac{E_{ch\ COG}}{E_{ch\ SP}} \tag{7}$$

where:

$E_{ch\ COG}$ - consumption of chemical energy for the production of heat and electricity in cogeneration,

$E_{ch\ SP}$ - consumption of chemical energy for separate heat and electricity production.

The chemical energy of fuel $E_{ch\,COG}$ consumed in the cogeneration process of heat and electricity production is calculated from the equation:

$$E_{ch\,COG} = E_{ch} - E_{ch\,C} \tag{8}$$

and

$$E_{ch} = \frac{E_{el}}{\eta_{E\,PU}} \tag{9}$$

$$E_{ch\,C} = \frac{E_{el\,C}}{\eta_{E\,C}} \tag{10}$$

where:

$E_{el}$ – electricity production before adaptation,

$\eta_{E\,PU}$ – energy efficiency of the power unit,

$E_{el\,C}$ – electricity production in the condensation mode after adaptation,

$\eta_{E\,C}$ – energy efficiency of electricity production in the condensation mode.

The production of electricity in the condensation mode after the adaptation of the power unit for heat production is expressed by the relation:

$$E_{el\,C} = E_{el} - PLC \cdot Q - \sigma \cdot Q \tag{11}$$

where $\sigma$ denotes the coefficient of cogeneration.

Making use of the Eqs. (8), (9), (10) and assuming that $\eta_{E\,C} = \eta_{E\,PU}$ we get:

$$E_{ch\,COG} = \frac{PLC + \sigma}{\eta_{E\,PU}} Q \tag{12}$$

The chemical energy of fuel for the separate production of heat and electricity:

$$E_{ch\,SP} = Q\left(\frac{1}{Ref\ H\eta} + \frac{\sigma}{Ref\ E\eta}\right) \tag{13}$$

It has been assumed that the efficiency of heat transport from the power station after its adaptation and from the heat-generating plant is the same.

The relation concerning PES takes the following form:

$$PES = 1 - \frac{PLC + \sigma}{\eta_{E\,PU}\left(\frac{1}{Ref\ H\eta} + \frac{\sigma}{Ref\ E\eta}\right)} \tag{14}$$

In the considered case the reference values of energy efficiency may be assumed on the level Ref Hη=0,88 ; Ref Eη=0,405 [3] and the energy efficiency of power unit $\eta_{E\,PU}$=0,4.

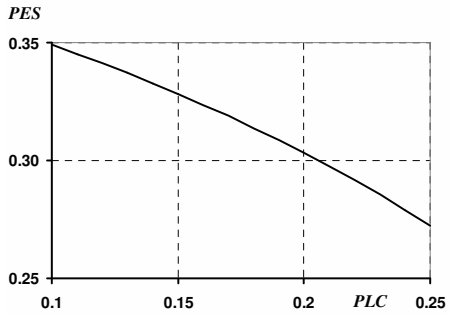


*Fig. 2. PES in the case of a power unit after its adaptation for heat production.*

Fig. 2. illustrates the changes of PES depending on the Power Loss Coefficient due to the adaptation of the power unit for the production of heat, as well as the energy efficiency of the power unit before adaptation. The lower values of the Power Loss Coefficient concern the supply of heating steam by the lowest steam bleeder of the low-pressure part of the turbine, whereas the upper range of these values concerns the supply of heating steam through the steam bleeders between the medium- and the low-pressure part of the turbine.

## 4. Relative reduction of noxious emissions, including $CO_2$

Similarly as PES, the index RER (Relative Emission Reduction) has been proposed in this paper, which can be defined as follows:

$$RER = 1 - \frac{S_{COG}}{S_{ref\ H} + S_{ref\ PU}} \quad (15)$$

where:

$S_{COG}$ – noxious emission in the cogeneration mode,

$S_{ref\ H}$ – noxious emission from the reference heating plant,

$S_{ref\ PU}$ – noxious emission from the reference power station.

The amount of noxious emissions from CHP and the separate production of heat and electricity is expressed by the following relations:

$$S_{COG} = \frac{(PLC + \sigma) \cdot Q}{\eta_{E\,PU} \cdot LHV_{PU}} e_{PU} \quad (16)$$

$$S_{ref\ H} = \frac{Q}{\mathrm{Re}\, f\ H\eta \cdot LHV_{HP}} e_{HP} \quad (17)$$

$$S_{ref\ EL} = \frac{\sigma \cdot Q}{\mathrm{Re}\, f\, E\eta \cdot LHV_{PU}} e_{PU} \quad (18)$$

The reference values of efficiency comprise also differences concerning the efficiency of transporting the heat and electricity, as well as the own needs of the CHP and separate production of these energy carriers.

In the case of a power unit adapted for the production of heat feeding the district heating system the relation concerning RER takes the following form:

$$RER = 1 - \frac{\frac{PLC + \sigma}{\eta_{E\,PU} \cdot LHV_{PU}} e_{PU}}{\frac{e_{HP}}{Re\, f\ H\eta \cdot LHV_{HP}} + \frac{\sigma \cdot e_{PU}}{Re\, f\ E\eta \cdot LHV_{PU}}} \quad (19)$$

If calculations of RER concern the emission of $CO_2$ and simultaneously in both energy installations (power unit and heat-generating plant) the same fuel is combusted (e.g. the same kind of hard coal), then:

$$RER = PES \quad (20)$$

Thus, all the conclusions concerning the saving of chemical energy of primary fuels hold true also in the case of the emission of $CO_2$.

## 5. Example of a power station adapted for heat production

The example concerns a system power station equipped with 360$MW_{el}$ power units situated 9 km from a large district heating system, up to now fed by a heat-generating plant equipped with hot water boilers fired with hard coal and operating at the following nominal temperatures of water: supplied hot water – 135°C, return water – 70°C. The steam is planned to be supplied from two power units making use mainly of steam bleeders of the low-pressure part of the turbine [1]. The peak exchanger will be fed with steam from the exhaust of the medium pressure of the turbine. Fig. 3 illustrates the calculation scheme of the power station system adapted for heat production.

The presented analysis is basing on the duration curve of ambient temperature characterizing the distribution of ambient temperature treated as a random value. The characteristic of the heat distribution network (Fig. 4) is also applied in this analysis. In the considered example the quality regulation of the district heating system has been assumed in the range (-20°C;+2,5°C).

The equation describing the lines concerning the temperature of supplied hot water and return water are as follows [9]:

$$t_{sw} = t_{en} + \frac{t_{sw\,max} - t_{en}}{t_{en} - t_{a\,min}} (t_{en} - t_a) \quad (21)$$

$$t_{rw} = t_{en} + \frac{t_{rw\,max} - t_{en}}{t_{en} - t_{a\,min}} (t_{en} - t_a) \quad (22)$$

Eqs. (21) and (22) hold true over the whole range of changes of the ambient temperature during the heating season ($t_{sb}$ = +12°C, $t_{a\,min}$ = -20°C) if there are only heating loads. The considered case comprises also the demand for warm water. Therefore the characteristics expressed by the Eqs. (21) and (22) are modified when the temperature of supplied hot water reaches 70°C, which is the minimum value of the temperature of supplied hot water to preheat the warm water. In the considered example this is the case then the ambient temperature amounts to +2,5°C. The further part of the characteristics consist of two parallel straights lines, and the regulation of the heating network is changed to a quantitative one. In the case of a mere heating load the further part of qualitative characteristics is denoted by broken lines. At the beginning of the heating season the ambient temperature has been assumed to amount to +12°C.

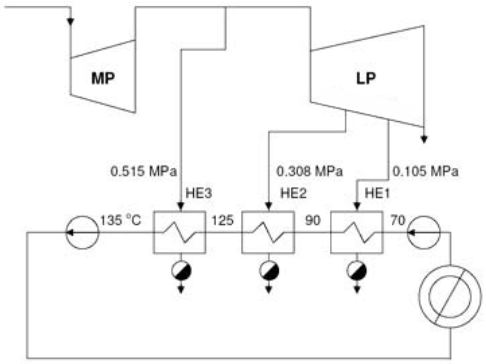


*Fig. 3. Flow sheet of the system of an adapted power station for heat supply; MP – medium-pressure part, LP – low-pressure part*

Data for the analysis:

- max heat flux for heating – $\dot{Q}_{H\max} = 220 MW_{th}$,
- demand for warm water – $\dot{Q}_{ww} = 30\, MW_{\text{th}}$
- duration of the heating season – $\tau_o = 4800$ hours per year,
- duration of warm water supply – $\tau_{ww}$=8000 hours per year,
- nominal temperature of water in the heat distribution network – $135/70^{\circ}C$,
- capital cost concerning the adaptation of power units for heat production – $I = 83.5$ mln PLN,
- annual cost of make-up water – $K_{MUW} = 0.5$ mln PLN per year,
- annual cost of maintenance connected with the adaptation – $K_M = 1$ mln PLN per year,
- unit cost of pumping the water into the heating network – $k_p = 0.28\ PLN/GJ$,
- annual rate of fixed costs – $\rho = 0.12,\ 1/a$,
- specific cost of electricity – $k_{el} = 150\ zł/MWh$,
- ratio of the price of the benefits of certificates due to high-efficiency cogeneration to the unit cost of electricity production in the condensing mode – β,
- minimum ambient temperature – $t_{a\min} = -20^{\circ}C$,
- temperature in heated enclosures – $t_{en} = +20^{\circ}C$,
- temperature at the beginning of the heating season – $t_{sb} = +12^{\circ}C$,
- index of $SO_2$ emission from the power station – $e_{PU} = 1.6\, g_{SO2}/kg$,
- index of $SO_2$ emission from heat-generating plant – $e_{HP} = 12.2 g_{SO2}/kg$,
- unit cost of heat from heat-generating plant – $k_{HP}$ = 18 PLN/GJ (without the part of the cost of the ordered thermal power),
- efficiency of heat transport – $\eta_{th}$=0.95.

Instantaneous demands for heat:

$$\dot{Q} = \dot{Q}_{ww} + \dot{Q}_{H\max}\frac{t_{en} - t_a}{t_{en} - t_{a\min}} \tag{23}$$

Duration curve of ambient temperature approximated by the Raiss equation [9]:

$$\frac{t_{sb} - t_a}{t_{sb} - t_{a\min}} = 1 - \sqrt[3]{\frac{\tau}{\tau_o}} + \left(\frac{\tau}{\tau_o}\right)^2\left(1 - \sqrt{\frac{\tau}{\tau_o}}\right) \tag{24}$$

Annual heat demand

$$Q_A = \dot{Q}_{ww}\cdot\tau_{ww} + \dot{Q}_{H\max}\int_o^{\tau_o}\left\{1 - 0{,}8\left[\sqrt[3]{\frac{\tau}{\tau_o}} - \left(\frac{\tau}{\tau_o}\right)^2\left(1 - \sqrt{\frac{\tau}{\tau_o}}\right)\right]\right\}d\tau \tag{25}$$

Fig. 4 presents the ranges of operation of the heat exchangers HE1, HE2, HE3. They are denoted by broken lines resulting from the constraints of saturation temperature of the heating steam. The distribution of loads over the particular heat exchangers permits to plot the curve of change of the Power Loss Coefficient.

The dependence of PES on the ambient temperature is to be seen in Fig. 5. Fig. 6 presents the duration curve of the demand for heat and the ranges of the operation of heat exchangers. The annual gross production of heat amounts to $Q_A$ = 2 529 TJ per year.

The average annual value of the Power Loss Coefficient, determined basing on the distribution of the PLC over the year, amounts to:

$$\overline{PLC} = 0{,}127$$

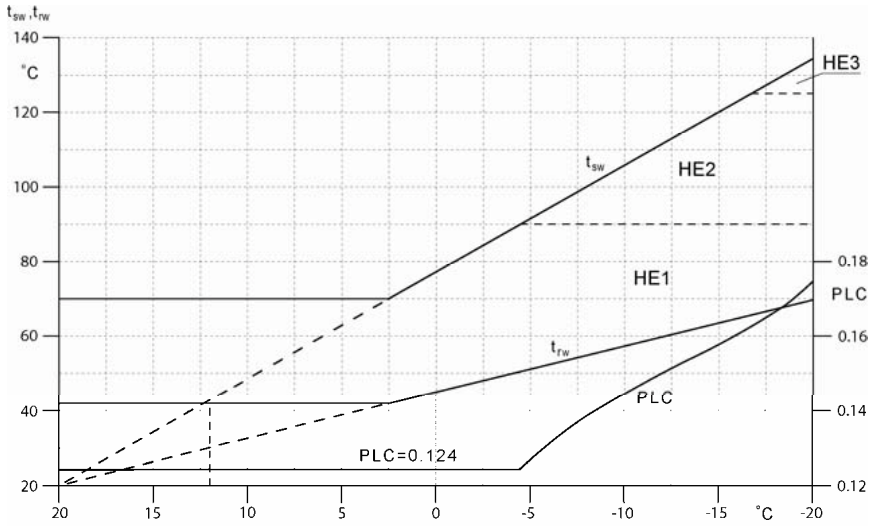


*Fig. 4. Ranges of the operation of heat exchangers and the dependence of the PLC on ambient temperature*

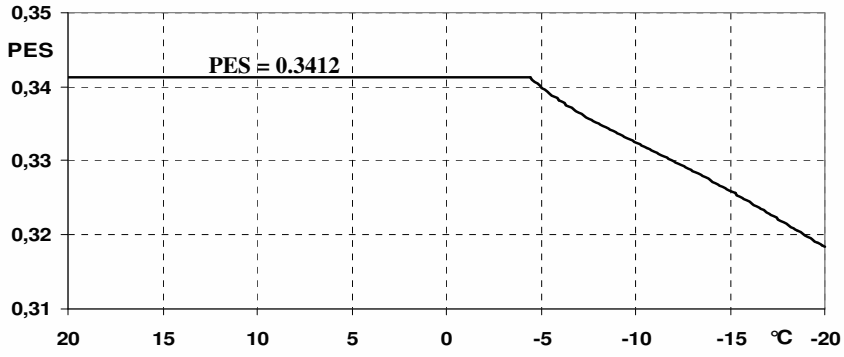


*Fig. 5. Dependence of the PES on ambient temperature*

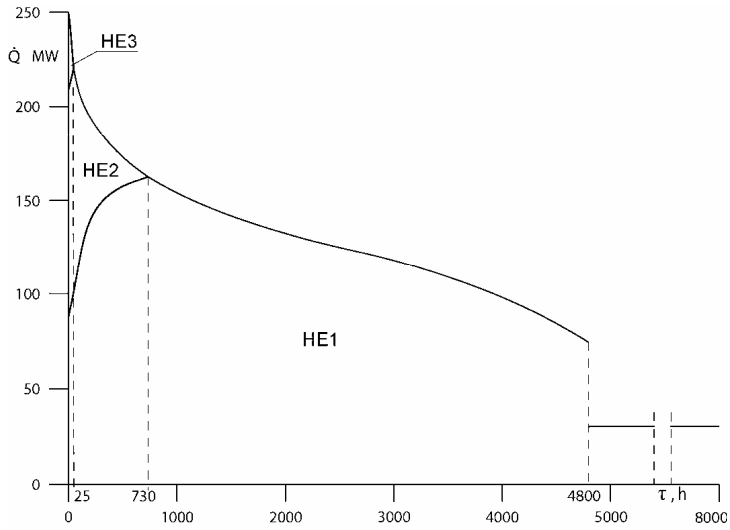


*Fig. 6. Duration curve of the demand of heat and the ranges of operation of the heat exchangers*

The value of the average annual coefficient of cogeneration corresponding to $\overline{PLC}$:

$\overline{\sigma} = 0{,}499$

The average value of $\overline{PES}$ over the year amounts to:

$\overline{PES}$ =0,338

The average value of $\overline{RER}$ concerning e.g. the emission of $SO_2$ amounts to:

$\overline{RER}$ =0,842

The relatively low value of the Power Loss Coefficient and the high value of cogeneration coefficient corresponding to $\overline{PLC}$ result from the supply of heating steam by the low-pressure part of the turbine. This influences on high value of $\overline{PES}$. The high value of $\overline{RER}$ is due to the lack of a desulphurization installation in the heat-generating plant.

Assuming that the amount of the chemical energy of primary fuel does not change after the adaptation of the power unit for heat production, the cost of heat comprises the following items:

- capital cost resulting from the investment outlay for the adaptation of the power units and the heat-pipeline,
- reduced income from the sale of electricity due to this adaptation (concerning the production of heat),
- income from the sale of certificates obtained due to high-efficiency cogeneration,
- cost of maintenance connected with the adaptation of the power station for heat production,
- cost of make-up water in the heating network,
- cost of pumping the water into the heating network.

The Relative Cost of Heat (RCH) calculated in relation to the unit cost of heat from the heat-generating plant at the same inlet of the district heating system taking into account the efficiency of transport, is:

$$RCH = \frac{\rho \cdot I + Q_A \cdot k_{el}(\overline{PLC} - \overline{\sigma} \cdot \beta)}{k_{HP} \cdot Q_A \cdot \eta_{th}} + \frac{K_M + K_{MUW} + Q_A \cdot k_p}{k_{HP} \cdot Q_A \cdot \eta_{th}} \quad (26)$$

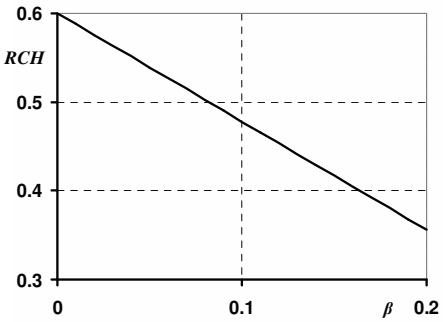


*Fig. 7. Relative Cost of Heat depending on the benefits of certifications*

Fig. 7 presents the changes of the Relative Cost of Heat in the power station adapted for the supply of heat depending on the ratio β of the price of the certificate to the unit cost of electricity production in the condensing mode. The index β has been treated as variable because the benefits of certificates due to high-efficiency cogeneration depend on regulations valid in the given country. It should be stressed that even if these in no income from certificates (β=0), the unit cost of heat from the power station adapted for heat supply is 0.6 unit cost from the separately operating heat-generating plant.

## 6. Conclusions

The adaptation of power units for district heat production is an effective way of realizing a high-efficiency cogeneration. In the case of the most frequently applied way of the adaptation of power units (supply of heat through steam bleeders between the medium- and low-pressure parts of the turbine) the PES factor amounts to 25%, which is higher than the classical CHP with a back-pressure turbine also fired with hard coal [9,10]. In the considered example the index PES is still more advantageous because heating steam is supplied from the low-pressure part of the turbine.

Besides the saving of primary fuels, the adaptation of power stations for heat supply provides ecological effects. E.g. in the case of $SO_2$ emission average annual RER amounts to 0.842. The coefficient characterizing the $CO_2$ emission equals PES=0.338.

The economical analysis devoted to the calculation of the unit cost of heat production confirms that adapting the coal-fired power station

for heat supply is a more effective way of high-efficiency cogeneration.

**Nomenclature**

$E$ – energy,
$e$ – index of noxious emissions,
$h$ – specific enthalpy,
$I$ – capital cost,
$K$ – cost of operation,
$k$ – unit cost,
LHV – Low Heating Value,
$\dot{m}$ – steam flux,
$N$ – power,
$PLN$ – Polish monetary unit,
$\dot{Q}$ – heat flux,
$S$ – emission.

Greek letters

$\beta$ – ratio of the price of the benefits of certificates to the unit cost of electricity production in the condensing mode,
$\Delta$ – decrease,
$\eta$ – efficiency,
$\rho$ – annual rate of fixed costs,
$\sigma$ – coefficient of cogeneration,
$\tau$ – time,
$\tau_o$ – duration of the heating season.

Subscripts

*A* – annual,
*a* – ambient,
*b* – bleeder,
*C* – condensing mode,
*c* – condensate,
*COG* – cogeneration,
*ch* – chemical energy,
*E* – energy,
*el* – electricity,
*em* – electro-mechanical,
*en* – heated enclosures,
*H* – heat,
*h* – heat exchanger,
*HP* – heat-generating plant,
*M* – maintenance,
*MUW* – make-up water,
*nom* – nominal,
*p* – pumping,
*PU* – power unit,
*rw* – return water,
*SP* – separate heat and electricity production,
*sb* – beginning of the heating season,
*sw* – supplied hot water,
*th* – transport of heat,
*w* – feeding water,
*ww* – warm water.

## Acknowledgments:

The paper was elaborated within the frame of the grant No N R06 0004 06/2009 "CHP STRATEG" supported by the Polish Ministry of Science and High Education.

## References

[1] ABB ALSTOM POWER: Adaptation of the turbines 18K360 for supply of heat. Report,1999.
[2] Directive 2004/8/EC of the European Parliament and of the Council of 11 February 2004 on the promotion of cogeneration based on a useful heat demand in the internal energy market and amending Directive 92/42/EEC.
[3] Guidelines for Implementation of the CHP Directive 2004/8/EC.European Commission DG TREN. November 2006.
[4] Horlock J. H: Cogeneration – Combined Heat and Power (CHP). Thermodynamics and Economics. Krieger Publishing Company, Malabar, Florida 1997.
[5] Marecki J.: Cogeneration of heat and electricity (in Polish). Technical Science Publishers, Warsaw 1991.
[6] Pawlik M.: Estimation of fuel economy in combined heat and power generation in condensing power plants supplying heat (in Polish). Archiwum Energetyki (1988) No 2, pp. 109-118.
[7] Perycz S.: Steam and gas turbine (in Polish). Ossolineum, Wrocław-Warszawa-Kraków, 1992.
[8] Szargut J.: Application of steam from regenerative bleeds for the production of network heat in large steam power plants. Archiwum Energetyki, XXVIII (1999), nr 1-2, 83-93.
[9] Szargut J., Ziębik A.: Cogeneration of heat and electricity – CHP (in Polish). Polish Academy of Sciences, Katowice-Gliwice, 2007.
[10] Ziębik A.: Combined heat and power in Poland according to the EU Directive on promotion of cogeneration. Archives of Thermodynamics, vol. 27 (2006), No 4, pp. 3-12.

# Life Cycle Assessment of Integrated Gasification Power Plants: Conceptual Design and Techno-Economic Evaluation

*A.D. Bojarski[a], M. Pérez-Fortes[a], E. Velo[a] and L. Puigjaner[a]*

[a] *Dept. of Chemical Engineering-CEPIMA, Universitat Politècnica de Catalunya, ETSEIB, Av. Diagonal 647, E08028, Barcelona, Spain*

**Abstract:** The objective of this work is to provide a useful approach for design purposes of combined cycle (CC) power plants. On the one hand, this work proposes a supporting tool for estimating Integrated Gasification Combined Cycle (IGCC) and Natural Gas Combined Cycle (NGCC) plants performance in terms of technical (power efficiency), environmental (based on life cycle assessment considerations) and economic metrics. A conceptual model has been built using commercial simulation (Aspen engineering suite) and validated with industrial data from ELCOGAS plant in Puertollano (Spain), of around 335 MW of gross power. On the other hand, this work considers and evaluates alternative ways of operation: addition of biomass to the traditional mixture of coal and petcoke in the IGCC model. Alternatives are evaluated through different key performance indicators (KPIs).

**Keywords:** IGCC Power Plants, NGCC Power Plants, Modeling, LCA.

## 1. Introduction

Although fossil fuels are and will be the main source of energy in a medium-term horizon, their scarce availability raises the question of the increasing need of renewable resources. Fossil fuels and its mid- and long-term supply uncertainty, as well as expanding economies and climate change are challenging issues which require cleaner and more efficient power plants. Integrated Gasification Combined Cycle (IGCC) power plants play a key role, since they allow obtaining electricity from coal and other solid fuels (coke, biomass) in a more efficient way, thus implying less costs and emissions per kWh than a conventional pulverized coal-fired power plant. In addition to that, the motivation of this work is the evaluation of alternate inputs and outputs that IGCC plants can afford; e.g., the use of alternate fuels such as petroleum coke and residual biomass, as well as the evaluation of the use of natural gas as fuel for the combined cycle (as in a Natural Gas Combined Cycle –NGCC power plant).

The flexibility of IGCC power plants has been already evaluated from different points of view simultaneously with several configurations of Carbon Capture and Storage (CCS) installations. In this sense we can mention its modeling including $CO_2$ removal and considering the improvement of the efficiency [1], or reduction of operating costs [2,3] and different types of coal as feedstock have also been evaluated [4]. NGCC power plants have been evaluated as well for a large amount of scenarios [5,6]. Life Cycle Assessment (LCA) has been already used as an environmental impact quantification tool for IGCC power plants [7,8]. We propose the analysis of different energy conversion performances from the point of view of operating cost, energy conversion efficiency and environmental impact, through a novel methodology for the assessment of fossil fuels energy conversion systems.

The paper is organized as follows: the next section describes the developed tool using a simulation environment and the included units in the root flowsheet, concluding with a description of the evaluated scenarios in this work. Section 3 deals with the methodology used to evaluate the installation cost and its efficiency, while section 4 describes the methodology used to evaluate the environmental impact. Finally, section 5 discusses the results for IGCC and NGCC power plants, and section 6 the future work, which is based on CCS techniques evaluation, through the methodology described in this paper.

## 2. The process layout and modeling

This section provides some general information about the developed tool for energy process design, and regarding the modeled flowsheet. Further information about both of them is provided in previous work [9].

Corresponding Author: Luis Puigjaner, Email: luis.puigjaner@upc.edu

### 2.1. The developed tool

AspenHysys and AspenPlus from the Aspen Engineering suite have been chosen as flowsheeting environments since they are flexible commercial environments for process simulation which provide thermodynamic and unit operation models. Models of two types have been implemented: reaction and unit operation models, both of them use the AspenHysys proprietary interface (see Fig 1). This approach increases the level of flexibility and the ability to re-use the existing predefined models in AspenHysys. Reaction and unit operation extensions are programmed in MS Visual Basic. AspenPlus is the selected software for modeling water and electrolytes systems, involving ionic species, the connection of both simulation environments has been done using artificial neural networks; further details are found in [9].

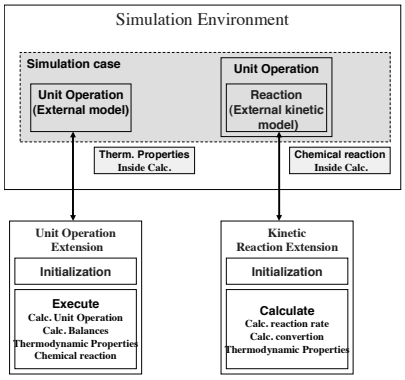


*Fig. 1. Use of user extensions characterizing some specific units and reactions in the flowsheet developed.*

### 2.2. Integrated Gasification Combined Cycle (IGCC) and Natural Gas Combined Cycle (NGCC)

In essence, the combined cycle (CC) for synthesis gas (syngas) production from solid fuel gasification or natural gas is the same (see Fig. 2, where a schematic NGCC power plant is represented). Main differences are found in terms of fluxes related to inlet air and fuel flows. For the last, the difference in mass flow of raw material remains three times higher for the IGCC mode. Natural gas is directly introduced into the gas turbine combustion chamber together with pressurized air, while gasification requires enriched oxygen (85%) that comes from an Air Separation Unit (ASU), which is fed from pressurized air from the gas turbine compressor. In IGCC, the Heat Recovery Steam Generator (HRSG) is enhanced with a Waste Heat Boiler which uses gasifier exhaust gases, taking profit of the raw syngas heat before entering the syngas cleaning units.

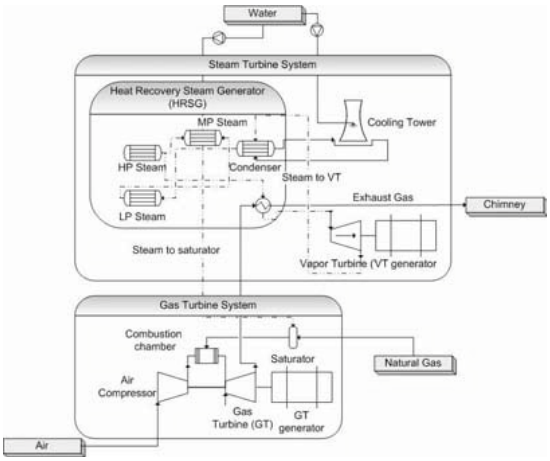


*Fig. 2. NGCC power plant diagram.*

The flowsheet of an IGCC power plant process includes a gasifier unit (in our case a pressurized entrained bed technology), and the subsequent syngas purification units. A ceramic filter removes the remaining solids and a venturi scrubber cleans the syngas with water from basic and acid pollutants. COS hydrolysis and MDEA absorber are the sulfur removal units, and a Claus plant provides a way for sulfur recovery. Polluted water is cleaned in a sour water stripper. Nevertheless, further treatment is required before the final disposal. Emissions are controlled before the combustion in the combustion chamber by: prior removal of sulfur in order to reduce $SO_2$, while $NO_x$ is reduced by injection of steam and waste $N_2$ from the ASU in the combustion chamber.

The model for NGCC and IGCC has been validated with data from the ELCOGAS power plant: inlet and outlet mass flows for each unit, and specific compositions for gas outlet streams from the purification units have been checked. Moreover, for the IGCC mode different feedstock compositions and their tendencies in terms of power and emissions have been analyzed (see [9] for more details).

IGCC and NGCC models are studied to assess process topologies prior to further process

optimization. These scenarios are summarized in Table 1. The selection of the combined cycle operating conditions for each mode of operation (IGCC or NGCC) uses general engineering guidelines and knowledge regarding air/fuel mass flow ratios, pressure in the steam turbine cycles and inter-stage compressor pressures. For air/fuel in the case of IGCC the ratio selected is 10 while in the case of NG is 50, in order to achieve the same flowrate, as well as the same Lower Heating Value (LHV) in the gas turbine inlet. In both cases the steam turbine cycle work at three pressures, namely: HP, 125 and 80 bar; IP, 30 and 15 bar and LP, 5 and 3 bar, for IGCC and NGCC configurations, respectively. Gas turbine compressor inter stage pressures have been selected at their thermodynamic optimal values, with PR as the Pressure Ratio, $PR_{stage}$ = PR^(i/n), where *i* is the specific stage, and *n* is the total number of stages, 4 in this specific case. Their selection has been done aiming at reproducing the current ELCOGAS operation while allowing for simulation flexibility.

*Table 1. Evaluated scenarios.*

| SC | Description |
|---|---|
| SC1 | IGCC plant with fixed coal & coke inlets (50% / 50%) |
| SC2 | IGCC plant with co-gasification of biomass (45% coal / 45% coke / 10% olive pomace) |
| SC3 | NGCC plant |

## 3. Techno-economic evaluation

Technical performance is assessed using conversion energy efficiency. Investment, operation, and maintenance costs are considered as economic indicators and an LCA derived metric is used for the environmental aspect.

### 3.1. Key Performance Indicators (KPI)

- Process efficiency is a key parameter to evaluate the final product to the market and the energy integration of the plant. The energy conversion efficiency is calculated using Eq. (1).

$$Efficiency(eff) = \frac{Power_{net}(MW)}{LHV_{raw}(MW)} \quad (1)$$

where, $Power_{net}$ is the final power to the grid (gross power minus plant electricity consumption), and $LHV_{raw}$ is the LHV of the fuel being considered, solid raw material mixture to the gasifier in the IGCC case or natural gas for the NGCC operation. The $LHV_{raw}$ values were obtained through Phyllis database and from ELCOGAS information. For each raw material mixture considering the following values: $LHV_{coal\&coke}$ 753 MW, $LHV_{coal\&coke\&olivepomace}$ 710 MW; and $LHV_{NG}$ 529 MW. Final powers optained for each case of study are 269.8 MW for SC1, 267.5 MW for SC2 and 209.3 MW for SC3.

- Cost of Energy (COE): The economic calculations in this work are based on [10,11]. The Total Capital Requirement (TCR) measuring the investment required and Total Operating Cost (TOC) are used here to calculate the COE. See in Tables 2 and 3 the included items in TCR and TOC.

*Table 2. Considered items in TCR*

| | |
|---|---|
| Total Direct Costs (TDC) | Equipment + General facilities |
| Total Indirect Costs (TIC) | Indirect construction costs |
| | Sales tax |
| | Engineering and home office overhead fees |
| | Environmental permits |
| Contingencies | Process contingency |
| | Project contingency |
| *TDC + TIC + Contingencies = Total Plant Cost (TPC)* | |
| Allowance for funds during construction (AFUDC) | |
| *TPC + AFUDC = Total Plant Investment (TPI)* | |
| Others | Prepaid royalties |
| | Spare parts inventory |
| | Startup or preproduction costs |
| | Inventory capital |
| | Initial chemicals and catalysts charges |
| | Land |
| *TPI + Others = TCR* | |

The levelized COE is a generating cost of energy for a determined power plant configuration. It is possible to assume that the COE is the energy price that should be used to pay back the power plant investment. In order to calculate it, cash flows have to be discounted appropriately as in Eq. (2).

$$COE = \frac{\sum_t (C_t + M_t + F_t)/(1+r)^t}{\sum_t E_t/(1+r)^t} \qquad (2)$$

where, $C_t$ is the investment or replacement cost for the year $t$, $M_t$ considers the operation and maintenance cost of for year $t$, $F_t$ is the cost of fuel for the year $t$, $E_t$ is net energy produced during the year $t$ and $r$ is a discount rate, which in this case we have assumed to be 5%. In the case of the energy produced ($E_t$) it was assumed that the early years of operation were done at: 75%, 85% of nominal plate capacity; consequently operating costs ($M_t$, $F_t$) were scaled down. An economic horizon of 30 years with an average of 7200 h/year of work was considered.

*Table 3. Considered items in TOC*

| | |
|---|---|
| Fixed Operating Costs (FOC) | Operating labor |
| | Maintenance labor |
| | Maintenance material |
| | Administrative and support labor |
| Variable operating Costs (VOC) | Total fuel cost |
| | Total consumable cost |
| | Ash disposal |
| | Byproduct credit (sulphur and slag) |
| *FOC + VOC = TOC* | |

For comparison purposes, Figures 3 and 4, show the breakdown of COE for IGCC and NGCC modes.

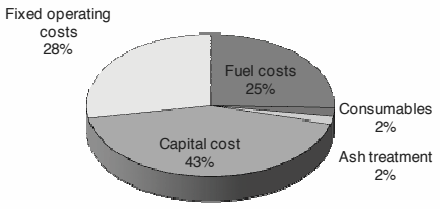


*Fig. 3. Breakdown of COE (cts€/kWh) for IGCC mode (SC1 and 2)*

For IGCC scenarios, the major contribution is due to investment costs; for NGCC scenario, the main contribution is on fixed operation costs. It is interesting to appreciate also the big difference in fuel costs.

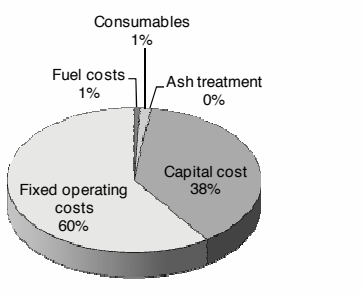


*Fig. 4. Breakdown of COE (cts€/kWh) for NGCC mode (SC3)*

## 4. KPI for environmental impact

Several different metrics can be calculated from the results of a LCA. In this work we followed the ISO14040 [12] guidelines requiring 4-steps as follows.

1. Goal definition and scope. This study is focused on the environmental contribution change attained by the different raw material composition feeds and associated topological flowsheet changes. The simulated co-gasification plant and natural gas power production considers extraction and processing of raw material, up to the power production to the grid, which constitutes a "*cradle to gate*" approach. Regarding system boundary, it is worth mentioning that emissions from waste water treatment plants and solid disposal are considered. Moreover, sulfur obtained from Claus plant is considered to be environmental credit, by reducing its production from virgin materials. All scenarios are compared based on a functional unit of 1MJ. Regarding total power plant production a similar time horizon was set and the same production hypothesis in the economic aspects were done.
2. The Life Cycle Inventory (LCI) is gathered for the different simulated flowsheets. Simulation results are used to estimate flue gas and plant wide emissions. The use of simulation software makes mass balances and energy balances to be met without requiring further data checks; making this approach a fairly robust one. This step constitutes a conservative approach (i.e. it overestimates emissions), given that the industry complies with all legal emission requirements, which in our analysis are disregarded. For all other echelons studied,

which are related to production/extraction of raw materials and transport, their corresponding LCIs are retrieved from the Ecoinvent database [13]. In the current case, production of: coal, petcoke, natural gas and other commodities (sulfuric acid, sodium hydroxide and others) are required given their consumption for plant operation, as shown in Table 4. Ecoinvent LCI information was gathered considering that the plant is located in Spain (ES), consequently geographical data for that region was considered when available, while the European average (RER) was selected otherwise.

*Table 4. Summary of different scenario LCI results, expressed in [kg/MJ].*

| Inputs | SC1 | SC2 | SC3 |
|---|---|---|---|
| HardCoal\ES | 0.0550 | 0.0499 | 0 |
| PetCoke\RER | 0.0550 | 0.0499 | 0 |
| Limestone milled\RER | 0.00382 | 0.00359 | 0 |
| Natural gas\RER | 0.00030 | 0.00030 | 0.05129 |
| $H_2O$ decarbonised\RER | 0.551 | 0.556 | 0.739 |
| Consumables (Inorganics\RER) | 0.000601 | 0.000606 | 0.000072 |
| Ouputs | | | |
| $CO_2$ | 0.2233 | 0.2119 | 0.1373 |
| $SO_2$ | 3.12E-05 | 2.55E-05 | 7.08E-06 |
| $NO_x$ | 9.99E-05 | 8.68E-05 | 1.77E-04 |
| Particles | 4.20E-07 | 4.23E-07 | 6.62E-07 |
| Solid Inert Waste | 0.02960 | 0.02960 | 0.00015 |
| Water to Waste treatment | 0.55978 | 0.55978 | 0.66555 |
| Sulfur produced | 0.00323 | 0.00321 | 0 |

Table 4 results shows that lower fuel consumption is done for the case of IGCC co-gasifying biomass. Solid wastes are considered to be inert and sent to a landfill, while water is sent to a waste water treatment plant. Consumables are considered to be inorganic chemicals and a proxy LCI is used considering the average production for first 20 most important inorganic compounds. Regarding sulfur by product, it is common practice to allocate emission and consequently impacts based on some criteria. However in this case we have decided to use a LCI of sulfur production and consider its production from virgin materials, consequently lowering the overall impact of IGCC operation.

3. Afterwards, the Life Cycle Impact Assessment (LCIA), based on the previously gathered LCI (see Table 4), is performed. Several environmental impact indicators are available, regarding different environmental issues, for the case of electricity generation, relevant environmental issues involve the estimation of impacts related to climate change using Global Warming Potentials (GWPs), regional acidification using Acidification Potentials (APs), and virgin resources consumption using Abiotic Depletion Potentials (ADPs). These metrics can be calculated using different ready to use LCIA methodologies such as the CML 2 [14] or the Impact 2002+ [15]. Other commonly used metrics are the ecological footprint (EF) [16] and the cumulative energy or exergy demand (CED or CExD) [17]. These metrics have an aggregating effect and serve in many cases of proxy of more complex environmental metrics. In the proposed methodology, the former metrics are calculated using Simapro [19], which allows gathering of LCI information from the Ecoinvent [13] database and its subsequent organization for LCIA calculation. Table 5, in results section, shows the LCIA results for CED, CExD, EF and $CO_2$-eq emission as well as the Impact2002+ overall environmental impact values.
4. Finally, the LCA results interpretation is done. It is found that operation using NG instead of solid fuels reduces the CED and CExD. In the first case the operation using IGCC requires approximately 60% more than the total amount of energy required in the NGCC. In the case of CExD, nearly three times more energy is required for IGCC than for NGCC; which clearly shows the low quality of energy produced from IGCC compared to NGCC. The differences found in the case of EF are not as great as in the CExD metric and the same happens for the $CO_2$-eq. Analyzing the Impact 2002+ results, it is found that the lowest impacts refer to the case of operation using NGCC followed by IGCC operation using olive pomace together with coal and coke as feedstock. Figure 5 shows the results of Impact 2002+ assessment methodology distributed along the different mid and end-point

categories of the LCIA methodology and along the different supply chain echelons. In the case of mid-point categories the largest impacts are associated to: non renewable energy and GWP, which are mimicked by the end-point categories: resources and climate change. Small differences are found for the end-point categories human health and ecosystem quality, which can not be traced directly to a single mid point impact as in the case of resources and climate change. Regarding end-point impacts, in the three electricity production cases, human health impact and ecosystem quality accounted for less than 13% of the total impact, while the remaining was almost evenly partitioned between resources and climate change impacts. In the case of IGCC operation the biggest overall impact is related to the plant operation itself. In second and third place, raw material production is found. Despite the fact that both IGCC scenarios use the same percentage of coal and coke, their associated impact is different. Coal production is found more environmentally friendly than coke production. In all the former environmental metrics, the life cycle stages associated to most impact are: raw materials production (coal, coke and NG respectively for each scenario), for the case for resources, while climate change is due to the IGCC/NGCC echelon. Sulphur recovery, which is studied in the case of IGCC operation, it is found that it allows for saving nearly 10% of the human health impact (see Figure 6), which only accounts for less than 12% of the total environmental impact; in the other categories the effect is not appreciable.

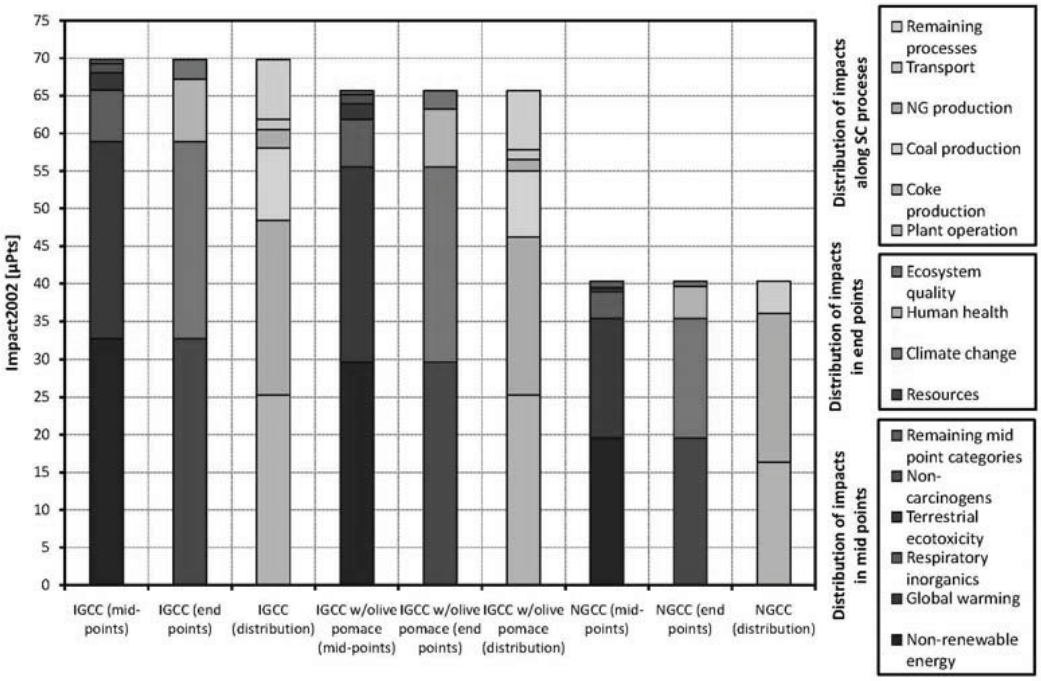


*Fig. 5. Results for Impact 2002+ assessment methodology distributed along mid and end point indicators as well as along different SC echelons.*

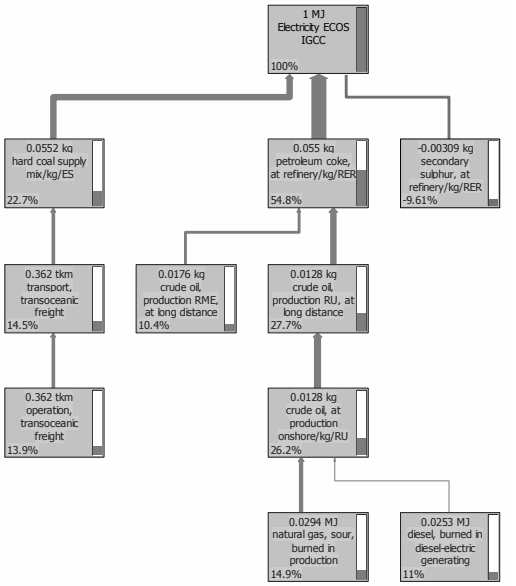


*Fig. 6. Distribution of the human health impact for the production using IGCC.*

### 4.2. Results

Table 5 presents the summary of all considered performance indicators. Economic values are referred to €$_{2007}$. The environmental metrics are related to environmental and raw material impacts; as described in the previous section. NGCC operation is found to have the lowest COE and the highest efficiency among the considered scenarios. This mode of operation has two values for the price of the energy; the larger one has been calculated with NG as a mode of an IGCC power plant. On the other hand, the lowest price only contemplates the usage of NG, so, only the investment associated to the CC is contemplated for the total plant investment. TCR and TOC values for NGCC mode consider this second configuration.

LCA results are in clear favor of the usage of NGCC instead of IGCC, and also show that the co-gasification of biomass also reduces the overall environmental impact. As expected, CED and EF are good proxy metrics for the case of electricity generation where raw material usage and climate change impacts are most important. Moreover for the case of these metrics which are mostly related to raw material origin, they heavily weight the use of non renewable fuels such as coal and coke. In this sense coke which is commonly considered a residue of refineries has been assigned 3% of emissions associated to overall refinery crude oil consumption [20,13], and consequently its energy and exergy demands are high. This fact is also found by using the Impact 2002 metric, where toxicological effects (human health or ecosystem quality) are small.

*Table 5. Key performance indicator results for the considered scenarios.*

| | SC1 | SC2 | SC3 |
|---|---|---|---|
| CED($MJ_{eq}$) | 5.0 | 4.5 | 2.8 |
| CExD($MJ_{eq}$) | 9.2 | 8.3 | 3.1 |
| EF ($m^2a$) | 0.70 | 0.69 | 0.41 |
| IPCC GWP ($kgCO_{2eq}$) | 0.27 | 0.27 | 0.16 |
| IMPACT 2002+ (μPts) | 69.8 | 65.7 | 40.3 |
| COE (€/kWh) | 0.0619 | 0.0593 | 0.0537<br>0.0249 |
| TCR (€/kW) | 3 119 | 2 987 | 1 026 |
| TOC (€/$kW_{year}$) | 273 | 261 | 108 |
| Eff (%) | 35.84 | 37.7 | 39.57 |

## 5. Conclusions

A novel methodology which joins the usage of commercial simulation and LCA commercial software has been presented. This tool allows for techno-economic assessment and LCA of different energy conversion processes. It allows finding and assessing explicit solutions for IGCC and NGCC power plants. Costs, efficiency and environmental impact have been considered as key parameters for selection criteria. In this way, a detailed calculation of these parameters has been developed here. The developed procedure and its implementation have been validated with data from the ELCOGAS power plant. The methods and tools developed constitute novel and powerful means for further implementation at a demonstration scale towards final plant design.

## 6. Future work

The consideration of CCS in pre- and post-combustion configurations under the described methodology is currently being developed.

Extended processes to capture $CO_2$ from fossil fuels (in this case, coal, petcoke and natural gas) are divided into post-combustion and pre-combustion capture (“combustion” is understood

as the energy conversion methodology, i.e. the CC). Two modes are envisaged:

- Post-combustion techniques are used after the power generation. Its main objective is to withdraw $CO_2$ from the flue gas to avoid its emission to the atmosphere. This separation can be done mainly by chemical absorption, where amines play an important role. $CO_2$ stream can be treated (compressed, so liquefied) to be prepared for transport to its final disposal [3]. After the IGCC and the NGCC the plant configuration to deal with flue gas can be similar [10].
- Pre-combustion techniques require the production of syngas. In the case of natural gas, syngas is obtained by steam reforming, while in the case of coal, petcoke and/or orujillo is the gasification process which provides the syngas. Then, both modes follow the same configuration. A water gas shift reactor (WGS) to produces $CO_2$ is used and downstream of it there is a set of unite operations for $CO_2$ capture, which separates $CO_2$ and $H_2$. The purified $H_2$ is then sent to a combined cycle to produce power. Analogously to the post-combustion scenario, $CO_2$ is sent to a compression system to be liquefied [18]. MDEA and MEA absorption and sorbent regeneration are the chosen amine systems. It has to be emphasized that in this case $CO_2$ is not completely removed, given that syngas leaving the WGS reactor still contains CO, and consequently chimney gas after combustion will contain $CO_2$.

## Nomenclature

| | |
|---|---|
| ADP | Abiotic Depletion Potentials |
| APs | Acidification Potentials |
| ASU | Air Separation Unit |
| CED | Cumulative energy demand |
| CExD | Cumulative exergy demand |
| CC | Combined cycle |
| CCS | $CO_2$ capture and storage |
| COE | Cost of Energy |
| EF | Ecological footprint |
| GWP | Global warming potential |
| HRSG | Heat Recovery Steam Generator |
| IGCC | Integrated Gasification Combined Cycle |
| IPCC | Intergovernmental panel on climate change |
| KPI | Key Performance Indicators |
| LCA | Life Cycle Assessment |
| LCIA | Life Cycle Impact Assessment |
| LCI | Life Cycle Inventory |
| LHV | Lower Heating Value |
| MEA | Monoethanolamine |
| MDEA | Methyl diethanolamine |
| NG | Natural Gas |
| NGCC | Natural Gas Combined Cycle |
| Pts | Points, of environmental impact in Impact 2002+ LCIA methodology |
| SC | Scenario |
| Syngas | Synthesis gas |
| TCR | Total Capital Requirement |
| TOC | Total Operating Cost |

## References

[1] Descamps, C. et al., 2008, Efficiency of an Integrated Gasification Combined Cycle (IGCC) power plant including $CO_2$ removal, Energy, 33, pp. 874-881.

[2] Kanniche, M. and Bouallob, C., 2007, $CO_2$ capture study in advanced integrated gasification combined cycle, Applied Thermal Engineering, 27, pp. 2693-2702.

[3] Desideri, U. and Paolucci, A., 1999, Performance modeling of a carbon dioxide removal system for power plants, Energy Conversion & Management, 40, pp. 1899-1915.

[4] Chen, C. and Rubin E. S., 2009, $CO_2$ control technology effects on IGCC plant performance and cost, Energy Policy, 37, pp. 915-924.

[5] Delattin, F. et al., 2009, Detailed study of the impact of co-utilization of biomass in a natural gas combined cycle power plant through perturbation analysis, Applied Energy, 86, pp. 622-629.

[6] Amann, J. M. et al., 2009, Natural gas combined cycle power plant modified into an $O_2/CO_2$ cycle for $CO_2$ capture, Energy Conversion and Management, 50, pp. 510-521.

[7] Corti, A. and Lombardi, L., 2004, Biomass integrated gasification combined cycle with reduced $CO_2$ emissions: Performance analysis

and life cycle assessment (LCA), Energy, 29, pp- 2109-2124.

[8] Fiaschi, D. and Lombardi, L., 2002, Integrated Gasifier Combined Cycle Plant with Integrated $CO_2$- $H_2S$ Removal: Performance Analysis, Life Cycle Assessment and Exergetic Life Cycle Assessment, International Journal of Applied Thermodynamics, 5 (1), pp. 13-24.

[9] Pérez-Fortes, M. et al. 2009, Conceptual model and evaluation of generated power and emissions in an IGCC plant, Energy, 34, pp. 1721-1732.

[10] Frey, H. C., 1991, Probabilistic modeling of innovative clean coal technologies: implications for technology evaluation and research planning, Ph.D. Dissertation, Carnegie-Mellon University for the US, Morgantown, WV.

[11] Frey, H. C. and Akunuri N., Probabilistic Modeling and Evaluation of the Performance, Emissions, and Cost of Texaco Gasifier-Based Integrated Gasification Combined Cycle Systems Using ASPEN, 2001, Technical Report, North Carolina State University, Raleigh, NC.

[12] ISO14040, 2006, Environmental management - Life cycle assessment - Principles and framework, Technical report, International Standards Organization (ISO).

[13] Swiss Centre for Life Cycle Inventories, 2006, *The Ecoinvent database*, URL: http://www.ecoinvent.ch/.

[14] Guinee, J. et al., 2001, Life cycle assessment. An operational guide to the ISO standards, Ministry of Housing, Spatial Planning and the Environment (VROM) and Centre of Environmental Science - Leiden University (CML).

[15] Humbert, S. et al., 2005, IMPACT 2002+: User Guide Draft for version 2.1., Technical report, Industrial Ecology & Life Cycle Systems Group, GECOS, Swiss Federal Institute of Technology Lausanne (EPFL), Lausanne, Switzerland.

[16] Huijbregts, M. A. et al., 2007, Ecological footprint accounting in the life cycle assessment of products, Ecological Economics, 64, pp. 798–807.

[17] Huijbregts, M. et al, 2006, Is Cumulative Fossil Energy Demand a Useful Indicator for the Environmental Performance of Products?, Environmental Science & Technology, 40, pp. 641–648.

[18] Damen, K. et al., 2006, A comparison of electricity and hydrogen production systems with $CO_2$ capture and storage. Part A: Review and selection of promising conversion and capture technologies, Progress in Energy and Combustion Science, 32, pp. 251-246.

[19] de Schryver, A. et al, 2006, Introduction to LCA with Simapro 7. Technical report, Pre-Product Ecology Consultants.

[20] Jungbluth, N. and Erdöl. In, 2007, Sachbilanzen von Energiesystemen: Grundlagen für den ökologischen Vergleich von Energiesystemen und den Einbezug von Energiesystemen in Ökobilanzen für die Schweiz (Ed. Dones R.). ecoinvent report No. 6-IV, Swiss Centre for Life Cycle Inventories, Duebendorf.

**Acknowledgments:** Data provided by ELCOGAS, AGAPUTE project (RFS-CR-04006,) and the support received from the European Commission are gratefully acknowledged. Financial support received from the "Generalitat de Catalunya" with the European Social Fund (FI grants) is fully appreciated.

# Irreversibility Parameter of a Combined Cycle Model for Power Generation

*L.A. Arias–Hernandez* [a], *J.J. Silva–Martinez* [b] *and F. Angulo–Brown* [a]

[a] *Escuela Superior de Física y Matemáticas del IPN, Ciudad de México, MÉXICO*
[b] *Escuela Superior de Cómputo del IPN, Ciudad de México, MÉXICO*

**Abstract:** In this paper we study the energetic performance of a series arrangement of totally irreversible heat engine models (combined cycle (CC) type). The origin of the irreversibilities is both of the external and internal types. The external irreversibilities are associated with the heat flows towards and from the temperature reservoirs, while the internal irreversibilities are associated to all those dissipative processes that occur within the working fluids. On the other hand, our model includes information provided by different optimization criteria that are commonly used in studies of irreversible heat engine models. This model, allow us to analyze two commercial CC–power plants which use fossil fuel and compare them with two commercial nuclear power plants, from the energetic point of view. Under this first approach to the comparison, we found that, despite of the high efficiency reported by CC manufacturers, the large temperature gradients required by these plants result in irreversibility parameters bigger than those for nuclear plants currently in operation.This so–called irreversibility parameter is defined as the quotient between the entropy produced by internal irreversibilities and the thermal conductances involved in the heat fluxes. By means of this energetic approach we find that CC plants have some economical disadvantages with respect to the nuclear power plants.

**Keywords:** Non-equilibrium and irreversible thermodynamics, Performance characteristics of energy conversion systems, figure of merit

## 1. Introduction

One of the most important topics in Thermodynamics is that related with the formulation of approaches to study the operation of real thermal engines. When two or more thermal engines are connected by means of flows of heat and energy, and all the group is working between two main energy reservoirs at fixed temperatures, we have an arrangement of thermal engines. In 1994 de Mey and de Vos [1] studied, the behavior of two arrangements of thermal engines with a linear heat transfer law operating between the temperatures $T_1$ and $T_2$ ($T_2 < T_1$), under the maximum power output ($MP$) working regime. In the present study we analyze the energetic behavior of the thermal engines in a series arrangement as that depicted in Fig. 1. For this study we use the following optimization criteria: Maximum Efficiency ($M\eta$), Maximum Power Output and Maximum Ecological Function ($ME$). The $MP$ criterion has been broadly used to study thermal engines made by men. However, the dissipation of thermal engines working under this $MP$–regime is very high (sometimes comparable or bigger than the power output) and the efficiency is not to high. This issue has motivated to think about other working regimes, among them the $M\eta$–regime and the $ME$–regime [2]. This last regime consisting in the maximization of the function,

$$E(\eta) = P(\eta) - \varepsilon(\tau) T_2 \sigma(\eta), \qquad (1)$$

where $\varepsilon(\tau) = \eta_{MP}/(\eta_C - \eta_{MP})$ [3, 4]. Equation 1, represents a measure of the commitment between the power output of a thermal cycle and their dissipation, in such a way that a thermal cycle working in the $ME$–regime represents a good trade–off among these two characteristic functions, which is simultaneously desirable from the energetic and ecological points of view. In fact, for a single thermal cycle, the power output under the $ME$–regime reaches around 75% of the power output in the $MP$–regime, but the dissipation considerably decreases (approximately 25% of the dissipation in the $MP$–regime)[3, 5]. For these reasons, the ecological function presents a very important characteristic: the efficiency of a thermal cycle working in this operation mode is bigger than the $MP$–regime efficiency. On the other

Corresponding author: L. A. Arias–Hernandez, Email: larias@esfm.ipn.mx, larias0570@gmail.com

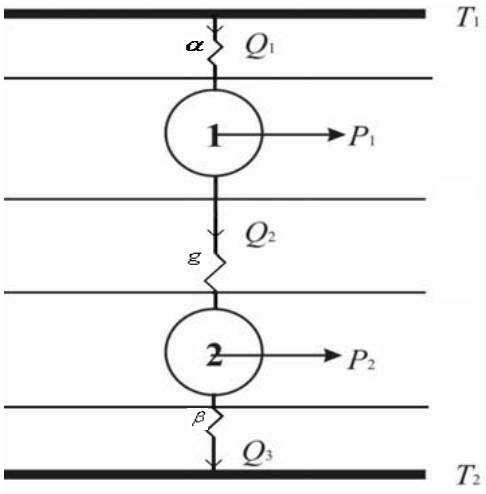


*Figure 1: Series array of two irreversible power cycles.*

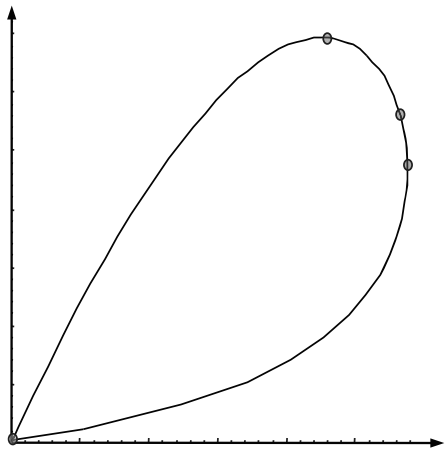

*Figure 2: Characteristic loop shaped curves of power output versus efficiency of the irreversible CC.*

hand, during the last years, the electric generation plants vendors have promoted the installation of CC plants or the transformation of plants of single thermal cycle to CC plants. The main motivation of the users to acquire these plants is the high efficiency that the vendors report. In these cycles, it is common to have a high temperature approximately of 1500 $K$ for the first working fluid. Then the working fluid goes through the first turbine where descends their temperature until 550 $K$. In this stage we obtain vapor of water, which goes across a second turbine, for finally to condense at 300 $K$. From the above description, we can model a combined cycle by means of a series arrangement of two thermal cycles. In this work we carry out the study of a model of this type which includes both external and internal irreversibilities; the external irreversibilities are associated to the flows of heat between reservoirs and the working fluids, and these heat transfers are modeled by means of a Newton's cooling law. The internal irreversibilities, are not modeled and they are only considered by means of a lumped quantity that is defined positive, as it demands the second law of thermodynamics. In this way we take into account all and each one of the contributions to the entropy production, of the irreversible processes that happen within the working fluids, with the help of the information that provides the different operation modes. In the first section we build the series arrangement model, and we establish their constitutive equations (first law, second law and laws of heat transfer). We also introduce the characteristic functions or process variables and the linear combinations of these, that will serve like objective functions for the thermodynamic optimization of the arrangement. The most important hypothesis used in the construction of the model, is that the working substances make irreversible cycles, and therefore their entropy change are null. We find that, contrary to other series arrangement models [6], the characteristic loop shaped curves of power output versus efficiency are obtained similar to those observed in real thermal engines [7]. In these loop shaped curves, it is possible to locate the points corresponding to different optimization criteria: Maximum Efficiency, Maximum Power Output and Maximum Ecological Function (see Fig. 2). In the second section, we compare the energetic performance of this series arrangement, under the mentioned different operation modes, for three characteristic functions: the irreversible efficiency of conversion, the irreversible power output and the dissipation of the process. Additionally, starting from the experimental reported data, we compare the energetic performance of two commercial CC plants, with some nuclear modern plants of single thermal cycle, and we find that the CC plants have a bigger irreversibility parameter than the nuclear ones. It means that CC plants are in economic disadvantage with respect the nuclear plants. This fact is not clearly observed if we only compare their reported efficiencies. Finally, we sketch some conclusions on this type of models

and their utility to qualitatively describe the energetic behavior of the real CC plants.

## 2. Series array model

The total entropy production of the irreversible thermal cycles arrangement, shown in Fig. 1, is given by,

$$\sigma_T = -\frac{Q_1}{T_1} + \frac{Q_1}{T_{1w}} - \frac{Q_2}{T_{2w}} + \frac{Q_2}{T_{3w}} - \frac{Q_3}{T_{4w}} + \frac{Q_3}{T_2} + \sigma_{i1} + \sigma_{i2} > 0, \quad (2)$$

where $Q_1$, $Q_2$ and $Q_3$; are the heat fluxes of the system. $T_1 > T_2$; are the reservoirs temperatures and $T_{1w} > T_{2w}$ and $T_{3w} > T_{4w}$ are the working fluid temperatures respectively. As the second law of the thermodynamics demands, the internal entropy production associated to irreversible internal processes, such as, chemical reactions of recombination, friction, viscosity, turbulence, etc., is a positive quantity, i.e., $\sigma_{i1} > 0$ and $\sigma_{i2} > 0$. Regrouping terms in 2 , we can write:

$$\sigma_T = \sigma_s + \sigma_{st}, \quad (3)$$

where each term is given by,

$$\sigma_s = \left[\frac{Q_3}{T_2} - \frac{Q_1}{T_1}\right] \quad (4)$$

and

$$\sigma_{st} = \left[\frac{Q_1}{T_{1w}} - \frac{Q_2}{T_{2w}} + \sigma_{i1}\right] + \left[\frac{Q_2}{T_{3w}} - \frac{Q_3}{T_{4w}} + \sigma_{i2}\right]. \quad (5)$$

The first term in 3, given by 4, corresponds to the entropy change of the energy reservoirs, while the second term given by 5, corresponds to entropy change of the working substances 1 and 2. The total entropy production equation 2, includes the supposition that in a thermal cycle the flows of heat can stay finite and the working substance returns to its initial state, that is the reservoirs entropy production is positive, while that of the working substances are null. Since the working fluids are operating in cycles, their changes of internal energy are,

$$\Delta U_{st1} = \Delta U_{st2} = 0. \quad (6)$$

The entropy is also a state function, then the entropy production of the working fluids satisfy

$$\Delta S_{st1} = \frac{Q_1}{T_{1w}} - \frac{Q_2}{T_{2w}} + \sigma_{i1} = 0, \quad (7)$$

and

$$\Delta S_{st2} = \frac{Q_2}{T_{3w}} - \frac{Q_3}{T_{4w}} + \sigma_{i2} = 0. \quad (8)$$

On the other hand, we can write the irreversible power output of each engine as:

$$P_1 = Q_1 - Q_2 \text{ and } P_2 = Q_2 - Q_3. \quad (9)$$

After the above equations the total power output is:

$$P = P_1 + P_2 = Q_1 - Q_3. \quad (10)$$

Finally, the thermal efficiency is given by

$$\eta = \frac{P}{Q_1} = 1 - \frac{Q_3}{Q_1}. \quad (11)$$

At this point we introduce the phenomenological heat transfer law as a Newton's cooling law,

$$Q_1 = \alpha\,(T_1 - T_{1w})\,, \quad (12)$$

$$Q_2 = g\,(T_{2w} - T_{3w})\,, \quad (13)$$

$$Q_3 = \beta\,(T_{4w} - T_2)\,, \quad (14)$$

where $\alpha$, $g$ and $\beta$ are the thermal conductances shown in Fig. 1. We also introduce the reduced temperatures,

$$a_h \equiv \frac{T_{1W}}{T_1},\ a_i \equiv \frac{T_{3w}}{T_{2w}},\ a_c \equiv \frac{T_2}{T_{4w}},\ \tau \equiv \frac{T_2}{T_1}, \quad (15)$$

therefore, $a_h$, $a_i$, $a_c$ *and* $\tau \in [0, 1]$. Using these definitions we can rewrite the constitutive equations. The efficiency is given by,

$$\eta = 1 - \frac{\frac{\alpha T_1 \tau}{\gamma_1 \gamma_2}\left[\frac{1}{1+\gamma_2 - \frac{\gamma_1\gamma_2\sigma_{i2}}{\alpha} - \frac{\gamma_2}{a_i}} - 1\right]}{\alpha T_1\left[1 - \frac{\alpha\gamma_1}{\alpha+\alpha\gamma_1-\gamma_1\sigma_{i1}-\alpha a_i}\right]}, \quad (16)$$

with $\gamma_1 = \alpha/g$ and $\gamma_2 = \beta/g$, and the total power output is,

$$P = \alpha T_1\left[1 - \frac{\alpha\gamma_1}{\alpha + \alpha\gamma_1 - \gamma_1\sigma_{i1} - \alpha a_i}\right] - \frac{\alpha T_1 \tau}{\gamma_1\gamma_2}\left[\frac{1}{1 + \gamma_2 - \frac{\gamma_1\gamma_2\sigma_{i2}}{\alpha} - \frac{\gamma_2}{a_i}} - 1\right]. \quad (17)$$

The parametric graph of the power output versus efficiency, shows the loop shaped curve behavior that characterizes the irreversible conversion of energy [7] (see Fig. 2). In this graph all the points on the loop are physically accessible. We mark only four which correspond to those working regimes that are of practical interest: the *MP*–regime, *ME*–regime,

the maximum efficiency regime, and the minimum entropy production regime (mep) (which is the origin of the graph where simultaneously the power and the efficiency are zero). Finally, the dissipation function can be written as,

$$T_2\sigma_S = \alpha T_1\tau\left[1-\frac{\alpha\gamma_1}{\alpha+\alpha\gamma_1-\gamma_1\sigma_{i1}-\alpha a_i}\right] -\frac{\alpha T_1\tau}{\gamma_1\gamma_2}\left[\frac{1}{1+\gamma_2-\frac{\gamma_1\gamma_2\sigma_{i2}}{\alpha}-\frac{\gamma_2}{a_i}}-1\right]. \quad (18)$$

Substituting 17 and 18 into 1, an expression is obtained for the ecological function, in terms of the reduced temperatures and the other physical parameters, this expression is not shown in explicit form because is very extensive.

### 2.1. $M\eta$, $ME$ and $MP$ working regimes for the series array

To establish each one of the optimal operation modes of the series arrangement, it is necessary to calculate the maxima of the power output, efficiency and ecological function, respect to the intermediate reduced temperature $a_i$,

$$\left(\frac{\partial\eta}{\partial a_i}\right)_{a_{i\eta}}=0,\ \left(\frac{\partial E}{\partial a_i}\right)_{a_{iE}}=0,\ and\ \left(\frac{\partial P}{\partial a_i}\right)_{a_{iMP}}=0. \quad (19)$$

From 19 we find that in the three cases this reduced temperature is of the form,

$$a_i = a_{i\phi}(\alpha, T_1, \gamma_1, \gamma_2, \sigma_{i1}, \sigma_{i2}, \tau), \quad (20)$$

where $\phi$ means $M\eta$, $ME$ or $MP$. When we evaluate the characteristic functions in each one of the three optimal reduced temperatures, we obtain the energetics of the CC in each working regime. In next section we use the reported data for a commercial unit by TOSHIBA (109FA-MS9001FA): $\alpha = 3.9\times10^6\ W/K$, $T_1 = 1573\ T$, $\gamma_1 = 1/2$, $\gamma_2 = 2$, $\sigma_{i1} = 5\sigma_{i2}/4$, $\sigma_{i2} = 0.155\times10^6\ W/K$ and $\tau\in[0,\ 0.75]$, to study the energetic performance of the array.

## 3. Energetic performance and irreversibility parameter

In the study of the energetic performance of the models of irreversible thermal cycles, the process variables: efficiency, power output and dissipation are the quantities that give us the estimated time recovery of the investment in the power plant construction. In Fig. 3a the efficiencies of each proposed operation mode are shown. As it was expected, the $M\eta$–efficiency is the biggest one, however, the efficiency that corresponds to the $ME$–regime is very near to the $M\eta$–efficiency but with a power output larger than the $M\eta$–power output. On the other hand, the $MP$–efficiency always goes under the efficiencies of the other two working regimes. Respect to the power output, when we observe Fig. 3b we see that the power output corresponding to the $ME$–regime always is above of the $M\eta$–power output and it is reasonably near to the power output of the $MP$–regime. Finally, in Fig. 3c we show the plots corresponding to the dissipation of the series array, here we observe that the dissipation in the $MP$–regime is bigger than both the $ME$–dissipation and the $M\eta$–dissipation within the

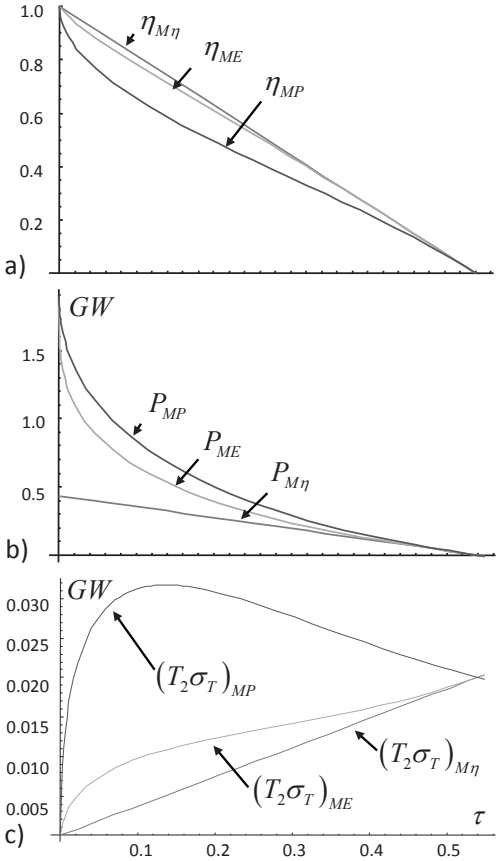


*Figure 3: a) Comparison between the efficiencies $\eta_{M\eta}$, $P_{ME}$ and $\eta_{MP}$ of the $M\eta$, $ME$ and $MP$ working regimes, respectively. b) Comparison between the power outputs: $P_{M\eta}$, $P_{ME}$ and $P_{MP}$. c) Dissipations ($T_2\sigma_{M\eta}$, $T_2\sigma_{ME}$ and $T_2\sigma_{MP}$ ) in each operation mode.*

typical operation temperatures interval of actual CC plants ($\tau \in [0.1,\ 0.3]$). On the contrary, the dissipations of these last two working regimes are very near to each other and they are smaller than the $MP$–dissipation in this interval. In summary, these results show that for a series array of two completely irreversible power cycles the ecological approach of optimization reaches a good trade–off between the power output and the efficiency of the arrangement.

### 3.1. Combined cycle power plants versus nuclear power plants

Now, we will use the model developed here to make a comparison between two commercial CC power plants and two modern nuclear power plants, this comparison is carried out by using the parameter,

$$f = \frac{\sigma_{i2}}{\alpha}, \tag{21}$$

called the irreversibility parameter. From the data of power output and efficiency, provided by the vendors of the power plants, and supposing that these power plants operate in some of the working regimes studied above, one can solve 16 and 17 for each working regime and obtain the two quantities involved in 21, i.e., starting from the experimental data and the information provided by the optimization process, one can quantitatively estimate the irreversibility parameter for each power plant. The results obtained by means of this procedure in the $M\eta$–regime are shown in Table 1, which is the regime recommend by the vendors for the the operation of the CC plants.

These results show that in spite of the high efficiencies of the CC–power plants, the relationship between their global conductance and the internal irreversibilities, in this case those associated to the vapor turbine, are two orders of magnitude bigger than the irreversibility factors of the nuclear power plants. This fact means, that the CC–power plants could have high operation costs rising the price of the kilowatt–hour.

## 4. Conclusions

In this work we have shown that the series array of completely irreversible power cycles, have the qualitative properties (loop shaped curves and operation modes) of the real energy converters. In particular it was shown that it is possible to operate the CC–power plants in a working regime representing a good trade–off between a high power output and low dissipation. Later on, with this model it was possible to make a comparison among power plants with different types of cycle. This result reissues one of the most appreciated characteristics of thermodynamic theory: with equivalent process variables (power output and efficiency) it is possible to study the energetic performance of two irreversible energy converters with different internal details. This previous result would justify an exhaustive revision of data of CC plants actually in operation, to calculate their irreversibility parameters and to estimate more accurately the real costs of operation and maintenance. However, we must take into account that our study has an important limitation, that is, our thermal engine models are very simplified versions of the real ones. Nevertheless, our models can be used to provide general guides to evaluate the thermodynamic performance of actual engines.

*Table 1: Irreversibility Parameter for some Power Plants actually in operation: a) Doel 4 (Belgium,1985), b) Cofrentes B (Spain, 1985), c) Toshiba (2004), d) Alstom (2004).*

| Plant | $\tau = T_2/T_1$ | $\eta_o$ | $P_o(GW)$ | $f$ |
|---|---|---|---|---|
| a | 0.500 | 0.35 | 0.985 | 0.009 |
| b | 0.514 | 0.34 | 0.991 | 0.008 |
| c | 0.193 | 0.48 | 0.342 | 0.0396 |
| d | 0.206 | 0.57 | 0.410 | 0.0227 |

## References

[1] de Mey G. and de Vos A. On the Optimum Efficiency of Edoreversible Thermodynamic Processes. *Journal of Physics D: Applied Physics*, 27(7):736–739, 1994.

[2] Angulo-Brown F. An Ecological Optimization Criterion. *Journal of Applied Physics*, 69(11):7465–7469, 1991.

[3] Angulo-Brown F. and Arias-Hernández L.A. Reply to "Comment on 'A General Property of Endoreversible Thermal Engines' " [J. Appl. Phys. 89, 1518 (2001)]. *Journal of Applied Physics*, 89(2):1520–1521, 2001.

[4] Arias-Hernandez L.A. et al. On Some Nonendoreversible Engine Models with Nonlinear Heat Transfer Laws. *Open systems & Information Dynamics*, 10(4):351–375, 2003.

[5] Arias-Hernández L.A. and Angulo-Brown F. A General Property of Endoreversible Thermal Engines. *Journal of Applied Physics*, 81(7):2973–2979, 1997.

[6] Rocha-Martínez J.A. et al. Optimization of Coupled Finite–Time Heat Engines. *Revista Mexicana de Física*, 42(4):588–597, 1996.

[7] Gordon J.M. and Ng K.C. *Cool Thermodynamics*. Cambridge International Publishing, Cambridge, UK, 2000.

**Acknowledgments:** SIP–COFAA–EDI–IPN–MÉXICO and CONACYT–SNI–MÉXICO.

# Sequential Rate-Based Model for $CO_2$ Absorber Column Using Monoethanolamine Solution

*Ali Haghtalab[a], Sana Jahanshahi Anbuhi[a]*

[a] *Department of Chemical Engineering, Tarbiat Modares University, P.O. Box 14115-143, Tehran, Iran*

**Abstract:** Presently $CO_2$, as the most important sources of green house gases, should be removed from gases exhausting power plants, refineries and sour natural gas. The management of $CO_2$ has been regarded as one of the basic concerns in field of environmental issues. Aligned with efforts and researches done in this regard, the present paper developed a sequential rate-based model to simulate the $CO_2$ absorption process in a contactor column using monoethanolamine (MEA) solution. In this model, each stage of the column consists of two virtual boxes, one for mass transfer and another as reaction part. The mass transfer box is based on two-film theory, and the reaction box is supposed as a batch reactor. After being ascertained of the method function, the effect of various parameters such as temperature, flow rate and solvent concentration on column efficiency have been studied.

Keywords: Absorber, Kinetic Modeling, Sequential Simulation, MEA, Carbon Dioxide.

## 1. Introduction

Presently, the exhaust gases of factories and petroleum refineries contain some amounts of air polluted gases such as $CO_2$ and also in natural gas treatment the carbon dioxide is a major contaminant that should be removed. $CO_2$ is a noninflammable compound that may cause suffocation in high concentration and in lower concentration it may cause headache in human and in natural gas reduces its heating value. On the other hand, $CO_2$ is the main consistent of greenhouse gases that leads to environmental pollution. According to the United Nations Framework Convention on Climate Change (UNFCCC) in Kyoto, a commitment to reduce $CO_2$ emissions by 6% below 1990 levels was made by several countries [1]. Industrialized countries should take the lead in combating climate change and its adverse effects. They were responsible for the majority of the historical cumulative emissions; thereby they were given quantified commitments to reduce emissions in the Kyoto Protocol [2]. $CO_2$ absorption or capturing is done by various methods that the most popular one is the chemical absorption in a contactor by a chemical solvent such as alkanolamines [3]. The most common alkanolamine solvents are MEA, MDEA, DEA, DGA, AMP etc. For years, both DEA and MEA have been used as chemical solvents, aqueous MEA solution is the most frequently used alkanolamines absorbent owing to its high reactivity with $CO_2$, low solvent cost, and can be regenerated easily [4]. However, the maximum $CO_2$ absorption capacity in MEA is limited by stoichiometry to 0.5 mol $CO_2$/mol amine [5].

The different contactor columns such as packing bed have been used for $CO_2$ removal [6] so that the various approaches such as equilibrium and rate-based non-equilibrium methods have been applied to design the contactor columns. In 1998, Cadours and Bouallou [7] used the film theory to study the simultaneous effect of mass transfer and chemical reaction in a contactor by writing a collection of complex partial differential equations. In 2000, Rinker et al. [8] studied $CO_2$ absorption in blends of MDEA and DEA. They simulated the absorption process by using the penetration theory together with a wide group of reversible chemical reactions so that Newton Homotopy sequence method was applied for solving the resulted equations. In 2001, Mandal et al. [9] modeled the contactor with mixed absorption of amines through equilibrium method so that the algebraic equations were simultaneously solved by applying the Newton Homotopy continuity method. In 2006, Van Loo et al. [10] simulated $CO_2$ absorption from natural gas by MDEA solution through non-equilibrium method in a tray column. They did not consider the non-ideality of phases and pressure drop in the column and considered

Corresponding Author: Ali Haghtalab, Tel:(09821)82883313, Email: haghtala@modares.ac.ir

the contactor as a series of ideally mixed reactors. They supposed the mass transfer based on a penetration theory and solved the non-linear differential equation by a numerical method. In 2007, Gabrielsen et al. [11] simulated the $CO_2$ absorption by AMP in a packing tower by considering a differential element along column and applying a sequential mass and energy balances. The enhancement factor was used for computation of mass transfer coefficient by combining the effects of mass transfer and chemical reaction.

In the present work, a contactor column is simulated by rate-based non-equilibrium approach. A sequential simulation method is applied for modeling of $CO_2$ adsorption column using alkanolamine.

The results of the simulation are compared with the experimental data which is gained from Ammonia Unit of Razi Petrochemical Company [12] which uses MEA solution to remove $CO_2$ from process stream so that the number of trays, temperature and pressure profiles are obtained.

## 2. Model framework

### 2.1. Analysis of chemical reaction

The chemical reactions between $CO_2$ and monoethanolamine can be considered as follows [13]:

$$CO_2 + 2H_2O \xleftrightarrow{k_1} H_3O^+ + HCO_3^- \quad (1)$$

$$H_2O + MEAH^+ \xleftrightarrow{k_2} H_3O^+ + MEA \quad (2)$$

$$H_2O + MEACOO^- \xleftrightarrow{k_3} MEA + HCO_3^- \quad (3)$$

So the overall reaction is written as [14]:

$$CO_2 + 2MEA \xleftrightarrow{k_1/k_2.k_3} MEACOO^- + MEAH^+ \quad (4)$$

The reaction between $CO_2$ and MEA is considered as a simple second order as bellow [14]:

$$r_{CO_2} = k_{am} C_{am} (P_{CO2} - P^*_{CO2}) \quad (5)$$

where according to the general mechanism the equilibrium partial pressure, $P^*_{CO_2}$, is obtained as bellow [14]:

$$P^*_{CO_2} = \frac{H}{K_c}\left(\frac{\alpha}{1-2\alpha}\right)^2 \quad (6)$$

Despite the fact that the chemical kinetics of $CO_2$ absorption in MEA solutions has been the subject of numerous studies, there is no universal agreement on the kinetic constant so it can be written as [6]:

$$k_{am} = 4.4\times10^8 \times \exp\left(\frac{-6863.8}{T}\right) \quad (7)$$

On the other hand, considering the high MEA concentration compared with $CO_2$, the conversion with respect to MEA can be regarded as pseudo-first-order as:

$$[CO_2] \xleftrightarrow{K_1/K_{-1}} [MEACOO^-] + [MEAH^+] \quad (8)$$

and the reaction rate can be expressed as:

$$r_{CO_2} = K_1 (P_{CO2} - P^*_{CO2}) \quad (9)$$

where $K_1 = k_{am}.C_{am}$ . Considering that the concentrations of the ionic complexes are equal, $[MEACOO^-] = [MEAH^+]$, so:

$$[MEACOO^-] + [MEAH^+] \cong 2[MEACOO^-] \quad (10)$$

By showing the sum of concentrations of ionic species as $C_{ion} = [MEACOO^-] + [MEAH^+]$, so the reaction rate is written as [15]:

$$r_{CO_2} = \frac{dC_{ion}}{dt} = -\frac{dC_{CO_2}}{dt} = C^o_{CO_2}\frac{dX_{CO_2}}{dt} = K_1 C_{CO_2} - K_{-1} C_{ion} \quad (11)$$

By considering $M = C^o_{ion} / C^o_{CO_2}$, one can write Eq. (11) as:

$$r_{CO_2} = K_1 (C^o_{CO_2} - C^o_{CO_2}.X_{CO_2}) - K_{-1}(M.C^o_{CO_2} + C^o_{CO_2}.X_{CO_2}) \quad (12)$$

Since in equilibrium the rate of the reaction assumed to be zero ( $dC_{CO_2}/dt = 0$ ), so using Eqs. (11) and (12) one can obtain:

$$\frac{K_1}{K_{-1}} = \frac{C^e_{ion}}{C^e_{CO_2}} = \frac{M + X^e_{CO_2}}{1 - X^e_{CO_2}} \quad (13)$$

By combining the above relations, the final reaction rate can be expressed as:

$$r_{CO_2} = C^o_{CO_2}\frac{dX_{CO_2}}{dt} = C^o_{CO_2}.\frac{K_1(M+1)}{M + X^e_{CO_2}}(X^e_{CO_2} - X_{CO_2}) \quad (14)$$

### 2.2. Analysis of mass transfer

The two-film theory has been used to describe mass transfer between vapor and liquid phases, so it is supposed that at the interface, the equilibrium concentrations of the $CO_2$ are the same in the both sides of the local phases. Thus, no mass accumulation exists in the interface so that the rate of the mass transfer shall be the same in the both phases. So based on the two-film theory, the mass transfer flux of $CO_2$ in gas phase can be expressed as [16]:

$$N_{CO_2} = K_{G,CO_2}(P_{CO_2} - P^*_{CO_2}) \quad (15)$$

where $P^*_{CO_2}$ and $P_{CO_2}$ are the equilibrium and the actual partial pressures of $CO_2$, respectively, that is easily computed by $P_{CO_2} = y_{CO_2} P_t$. The mass transfer coefficient, $K_{G,CO_2}$, is the general mass transfer coefficient of $CO_2$ that, based on two-film theory, is written as [16]:

$$\frac{1}{K_{G,CO_2}} = \frac{1}{k_{g,CO_2}} + \frac{H_{CO_2}}{k_{l,CO_2}} \quad (16)$$

Since the $CO_2$ solubility in solution is low, Henry's law is used here to present the partial pressure of $CO_2$ in liquid phase through its concentration. By substitution $K_{G,CO_2}$ into Eq. (15), one can obtain as:

$$N_{CO_2} = f\frac{k_{l,CO_2}.k_{g,CO_2}}{k_{l,CO_2} + H_{CO_2}.k_{g,CO_2}}(y_{CO_2}.P_t - P^*_{CO_2}) \quad (17)$$

where f is the correction factor given in Table 2.

### 2.3. Modeling of the contactor column

To describe gas absorption process, each stage or tray of the absorption contactor is considered as a series of compartments of a superficial box of mass transfer and a batch reactor as shown in Fig. 1. First, the streams of the liquid and gas enter the mass transfer box so that the $CO_2$ is transported physically across the interface of liquid and gas phases. Following mass transport of the gas across interface, liquid stream enters the batch reactor, so based on the described mechanism the complex reactions of MEA and $CO_2$ are taking placed. In this model, the non-ideality of gas phase and mass transfer of the other components except $CO_2$ are neglected. The physical, thermodynamic, transport and the other properties such as $\rho_l, \mu, k_c, K_{am}, a, \Delta H, C_{p_l}, H_{CO_2}, D$ are calculated tray by tray with considering temperature dependency or weight fractions of the components. The parameters $\rho_g, C_{p_g}, k_l, k_g$ are considered to be constant for all the trays. To simulate the contactor, the computations are performed sequentially downward from bottom tray and continue tray by tray up to top tray.

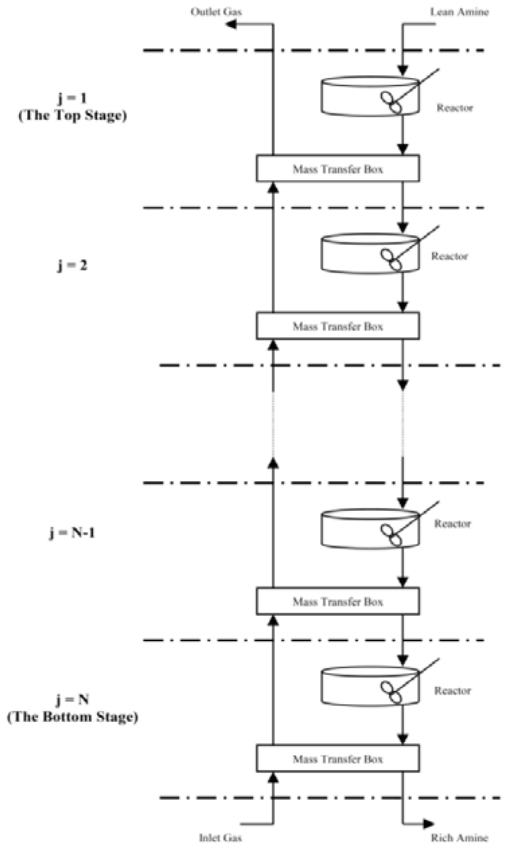


*Fig. 1. Schematic diagram of the $CO_2$ absorber column*

Since the stream gas phase loses $CO_2$ partially during passing each tray, so its flow rate and flux change continuously. In order to prevent this continuous change, the flux of the inert gas which includes the other components except $CO_2$ is used as [14]:

$$G_{inert} = G - y^{in}.G = G.(1 - y^{in}) \quad (18)$$

During absorption process, the total $CO_2$ separated from the gas phase shall be absorbed by liquid phase, so, writing a total mass balance for $CO_2$

component around the whole contactor, the total flux of absorbed $CO_2$ is resulted as follows:

$$N'^{(N)}_{total} = G_{inert}\left(\frac{y^{(N+1)}}{1-y^{(N+1)}} - \frac{y^{out}}{1-y^{out}}\right) \quad (19)$$

where the mole fraction of $CO_2$ in the gas outlet stream from top tray of the contactor will be the same as the specified composition in the sweet outlet gas( $y^{out} \equiv y_{spec}$).

## 2.4. Energy balance around the column

It is assumed that the temperature of the liquid stream at the first top tray is equal to the temperature of the lean solvent entering the contactor, so the overall energy balance over the contactor is used to calculate the temperature of the rich solvent which existing the column as [10]:

$$T_l^{out} = T_l^{in} + \frac{(T_g^{in} - T_g^{out}).\Phi_g^{in}.\rho_g.Cp_g}{\Phi_l.\rho_l.Cp_l} + \frac{\Delta H_{CO_2}.(N'^{(N)}_{total}.(\frac{A}{L}\times 1000))}{\rho_l.Cp_l} \quad (20)$$

where $\Delta H$ represents the sum of the heats of both reaction and absorption. Also one can assume as:

$$T_l^N = T_l^{out} \quad (21)$$

and $\Phi_g^{out}$ is the flow rate of the sweet gas exiting the column as:

$$\Phi_g^{out} = \frac{\Phi_g^{in}(1-y^{in})}{(1-y^{out})} \quad (22)$$

where the composition of $CO_2$ in the exiting gas stream from the contactor is known. In order to solve heat balance around the $N^{th}$ tray, thermal equilibrium is assumed between the gas and liquid streams leaving the tray [10], so $T_g^{(N)} = T_l^{(N)}$, where the subscripts $g$ and $l$ stand for gas and liquid phase, respectively.

## 2.5. The mass transfer and reactor boxes

A typical $N^{th}$ stage or a compartment consisting of a mass transfer box and a batch reactor box is shown in Fig. 2. The temperature, composition of $CO_2$ and concentration of the amine for the inlet and outlet gas and liquid streams of this stage are shown. The inlet gas temperature ($Tg^{(N+1)}$) and $CO_2$ mole fraction ($y^{(N+1)}$) in the inlet gas to the contactor are known, but the unknowns are as follows: the mole fraction of $CO_2$ in the outlet gas ($y^{(N)}$), amine concentration in the inlet liquid ($C_{am}^{(N-1)}$), amine concentration in the outlet liquid ($C_{am}^{(N)}$), temperature of outlet gas ($Tg^{(N)}$) and temperature of outlet liquid ($T_l^{(N)}$). First, when liquid and gas streams enter this mass transfer box, some of $CO_2$ is absorbed into liquid film so that the composition of acid gas is decreased from $y^{(N+1)}$ to $y^{(N)}$ in the outlet gas stream of the box.

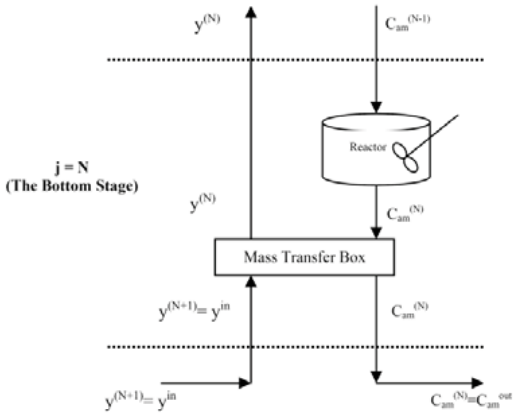


*Fig. 2. The $N^{th}$ stage of the column*

Thus, the change of the $CO_2$ flux is shown as below:

$$N'^{(N)}_{tray} = G_{inert}\left(\frac{y^{(N+1)}}{1-y^{(N+1)}} - \frac{y^{(N)}}{1-y^{(N)}}\right) \quad (23)$$

So by knowing that $N'^{(j)}_{tray} \times A = N^{(j)} \times V \times a$ , one can write as:

$$N^{(N)} = G_{inert}\left(\frac{y^{(N+1)}}{1-y^{(N+1)}} - \frac{y^{(N)}}{1-y^{(N)}}\right)/\left(\frac{V}{A}\times a\right) \quad (24)$$

On the other hand, based on mass transfer theory, the mass transfer flux of the acid gas is calculated by Eq. (15) where $y_{CO2} = y^{(N)}$, so equivalency of the two Eqs. (17) and (24) allows one to calculate the mole fraction of $CO_2$ in exiting gas stream phase ($y^{(N)}$) at the $N^{th}$ mass transfer box. As shown in Fig. 2, since the gas stream exiting the mass transfer box enters directly to the next tray, so in fact the composition of $CO_2$ at outlet of the $N^{th}$ tray has been gained. To calculate the changes in the next stage, the composition of the unreacted $CO_2$ entering to the $N^{th}$ tray should be calculated here. In the batch reactor of the $N^{th}$ stage, the reaction of the amine leads to protonation of amine, however some unreacted amount of $CO_2$ in the liquid phase is leaving the reactor box. So

using the total mass balance around the batch reactor [15]:

$$t = C^{o}_{CO_2} \int_0^X \frac{dX_{CO_2}}{-r_{CO_2}} \quad (25)$$

where t is the time of the reaction in each stage. Here, $C^{o}_{CO_2} \equiv C^{(N-1)}_{CO_2}$ is the total concentration of $CO_2$ in the liquid phase entering to the $N^{th}$ reactor. By combining Eqs (14) and (25) and following integration one can obtain as:

$$-\ln(1-\frac{X_{CO_2}}{X^{e}_{CO_2}}) = -\ln(\frac{C_{CO_2}-C^{e}_{CO_2}}{C^{o}_{CO_2}-C^{e}_{CO_2}}) = \frac{M+1}{M+X^{e}_{CO_2}}.k_1.t \quad (26)$$

Where $C_{CO2} \equiv C^{R}_{CO2}$ is the concentration of unreacted $CO_2$ exiting the $N^{th}$ reactor. Using Eq. (26), and calculating $t = V_{(cm^3)} / L_{(cm^3/s)}$, $C_{CO_2}$ is computed. Since the exit amine solution from the reactor is absorbing some $CO_2$ from the mass transfer box, so the concentration of unreacted $CO_2$ at $N^{th}$ tray is calculated as:

$$C^{unreacted(j)}_{CO_2} = C^{R\ (j)}_{CO_2} + N'^{(j)}_{tray}.\frac{A}{L}.1000 \quad (27)$$

On the other hand, the concentration of the amine exiting $N^{th}$ tray should be calculated using the mass balance that is based on stochiometry two mole amine is used per mole of $CO_2$, so one can obtain as:

$$C^{(j)}_{am} = C^{in}_{am} - [N'^{(j)}_{total}.(\frac{A}{L}\times 1000) - C^{unreacted(j)}_{CO_2}] \quad (28)$$

Where for j=N, $C^{(N)}_{am} \equiv C^{out}_{am}$. So, the computation of $N^{th}$ tray is complete here. Consequently, the calculation procedure should be continued for the upper tray ((N-1)$^{th}$ tray) so that tray by tray calculation is continued until the top tray of the contactor.

One should be noted that calculation of the kinetic constant of reaction, Henry's constant etc. depends on the temperature at each stage. Consequently, computation of the concentration of species in liquid and gases phases is dependent on temperature. So in the first iteration, the temperature profile along the contactor is assumed to be linear. However, for next calculating the temperature profile is modified as:

$$T^{(j)}_l = T^{in}_l + \frac{(T^{(j+1)}_g - T^{out}_g).\Phi^{(j+1)}_g.\rho_g.Cp_g}{\Phi_l.\rho^{(j)}_l.Cp^{(j)}_l} + \frac{\Delta H_{CO_2}.(N'^{(j)}_{total}.(\frac{A}{L}\times 1000))}{\rho^{(j)}_l.Cp^{(j)}_l} \quad (29)$$

and $T^{(j+1)}_g = T^{(j+1)}_l$. As one can see the temperature of outlet gas stream ($T^{out}_g$) and inlet lean amine ($T^{in}_l$) of the contactor are known.

## 3. Results and discussion

The model is developed for absorption of $CO_2$ in a contactor using MEA solution as a solvent. The mole percent of the $CO_2$ in the feed (sour) gas is 0.17529 and the rest are inert gas and water. The representative input conditions for an acid gas absorber are summarized in Table 1 [12].

*Table 1. The operation data and the known variables of the contactor [12]*

| retemaraP | lobmyS | eulaV | tinU |
|---|---|---|---|
| Gas inlet temperature | $T_g^{in}$ | 336.15 | K |
| Liquid inlet temperature | $T_l^{in}$ | 319.15 | K |
| Total Pressure | P | 27.34 | atm |
| $CO_2$ inlet mole fraction | $y^{in}$ | 0.17 | - |
| $CO_2$ outlet mole fraction (spec) | $y^{out}$ | $9\times10^{-5}$ | - |
| Total amine weight fraction | $W^{in}_{MEA}$ | 0.24 | - |
| Liquid inlet loading | $\alpha_{in}$ | 0.00027 | $\frac{moleCO_2}{moleAmine}$ |
| Liquid inlet molar flow | $\Phi_l$ | 41376.71 | $\frac{kmol}{hr}$ |
| Gas inlet flow | G | 6755.2 | $\frac{kmol}{hr}$ |

These known data were used in our modeling. The correlations and the equations used in the present modeling are given in Table 2. The algorithm which is used to simulation of the absorption column is given in Fig. 3. As one can observe, the physical and thermodynamic properties of the components are initially calculated. Then by

setting the stage number one, the calculation for absorption of $CO_2$ into amine are carried out through using a compartment of the mass transfer and the batch reactor boxes as explained in the theoretical part of this work.

*Table 2. The correlations and the equations used in the present modeling*

| Relation | Reference |
|---|---|
| $X_i = \frac{C_i^{in} - C_i^{out}}{C_i^{in}}$ | 14 |
| $H_{CO_2} = \exp\left(K_{10} + \frac{K_{11}}{T_l} + \frac{K_{12}}{T_l^2}\right)$ [lit.atm/gmole]<br>$K_{10} = 2.01874 - 2.37638\times10 W_{MEA} + 2.90092\times10^2 W_{MEA}^2 - 4.80196\times10^2 W_{MEA}^3$<br>$K_{11} = 3.13549\times10^3 + 1.54931\times10^4 W_{MEA} - 1.83987\times10^5 W_{MEA}^2 + 3.00562\times10\text{^}5 W_{MEA}^3$<br>$K_{12} = -8.13702\times10^5 - 2.48081\times10^6 W_{MEA} + 2.92013\times10^7 W_{MEA}^2 - 4.70852\times10\text{^}7 W_{MEA}^3$ | 17 |
| $\rho_l = 1000 + 31.7 W_{MEA} + 86.7 W_{MEA}^2 - 99.6 W_{MEA}^3$ | 18 |
| $K_C = \frac{k_1}{k_2 . k_3}$ | |
| $k_1 = \exp(231.465 - \frac{12092.1}{T} - 36.7816 \ln T)$ | |
| $k_2 = \exp(2.4211 - \frac{8189.38}{T} - 0.007484 \ln T)$ | |
| $k_3 = \exp(2.8898 - \frac{3635.09}{T})$ | 19 |
| $C_{pl} = (1 - W_{MEA}) C_{P_{H_2O}} + W_{MEA} C_{P_{MEA}} + W_{MEA}(1 - W_{MEA})(-0.9198 + 0.01369 T + 69.6243 \frac{W_{MEA}}{T^{1.5859}})$ (j/g.°c) | |
| $C_{R_{MEA}} = 2.5749 + 6.612\times10^{-3} T + 1.9\times10^{-5} T^2$ (j/g.°c) | |
| $C_{P_{H_2O}} = 4.1908 - 6.62\times10^{-4} T + 9.14\times10^{-6} T^2$ (j/g.°c) | |
| $\mu_l = \mu_{H_2O}^{(1-W_{MEA})} . \mu_{MEA}^{W_{MEA}} . \exp\left(\frac{12.70 (W_{MEA}^{2.650} \times (1 - W_{MEA}^{1.1812})}{T^{0.3314}}\right)$ (Pa.s) | |
| $\mu_{H_2O} = \exp\left(\frac{897.9879}{(T - 273.15)^{0.6542} + 78.1912} - \frac{17.6724}{(T - 273.15)^{0.004707}}\right)$ (Pa.s) | |
| $\mu_{MEA} = \exp\left(\frac{726.07334}{(T - 273.15)^{0.5297} + 22.0293} - \frac{35.3832}{(T - 273.15)^{0.0488}}\right)$ (Pa.s) | 21 |
| $f = 1 + 0.83(\ln P_{CO_2})^{0.8}$ for: $P_{CO_2} \geq 100 kpa$ | 22 |
| $\Delta H = -8500$ | 23 |

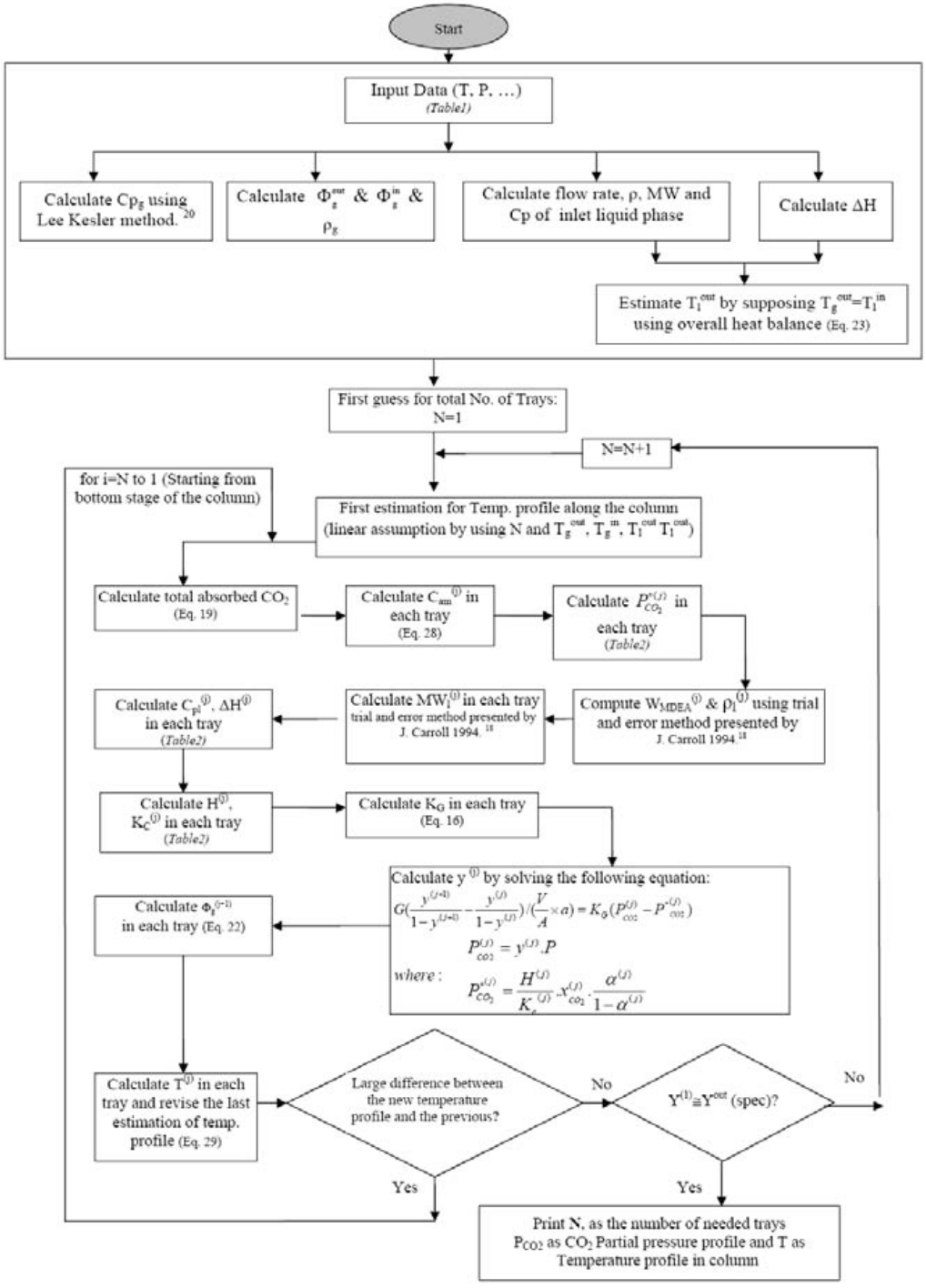


*Fig. 3. The algorithm of simulation of an absorption column using rate-based non-equilibrium model*

The simulation of the column is performed so that the partial pressure of $CO_2$ versus tray number, the total number of stages and temperature profile along the contactor are obtained. The results of the

simulation using the new model were compared with the experimental data gained from Ammonia Unit of Razi Petrochemical Company [12]. Fig. 4 presents the partial pressure of $CO_2$ versus stage number of the contactor. Also the results obtained by the equilibrium-method using the Electrolyte-NRTL activity coefficient equation and Kent-Eisenberg model are given in Figure 4.

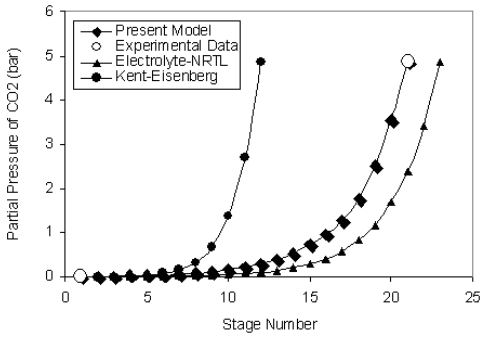


*Fig.4. $CO_2$ Partial pressure versus stage number in the column and comparing the results of new model with the experimental data of Ammonia Unit of Razi Petrochemical Company, Electrolyte-NTRL and Kent-Eisrenberg.*

Fig. 5 shows the temperature profile along the contactor that is obtained by the present model and compared with the experimental data of the Ammonia Unit of Razi Petrochemical Company and the equilibrium models

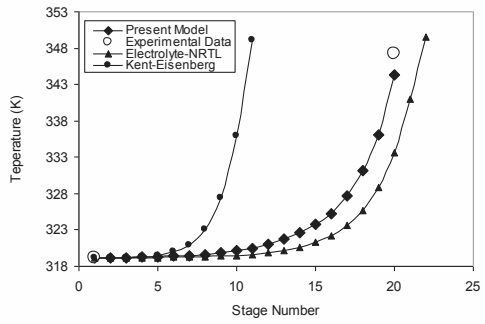


*Fig.5. Temperature profile in column and comparing the results of new model with Ammonia Unit of Razi Petrochemical Company experimental data, Electrolyte-NTRL and Kent-Eisenberg.*

As one can see the results of the present modeling of the absorber is very close to the experimental data. To show the deviation of the present model and the equilibrium models from experimental data of Razi Company, The Average Arithmetic Deviation (AAD) are used for partial pressure of $CO_2$ and temperature in terms of stage number, and also the total number of trays as following:

$$(AAD)_P\% = 100 \times \left| \frac{P_{CO_2}^{cal} - P_{CO_2}^{Exp}}{P_{CO_2}^{Exp}} \right| \quad (30)$$

$$(AAD)_T\% = 100 \times \left| \frac{T^{cal} - T^{Exp}}{T^{Exp}} \right| \quad (31)$$

$$(AAD)_N\% = 100 \times \left| \frac{N^{cal} - N^{Exp}}{N^{Exp}} \right| \quad (32)$$

Table 3 presents the AAD% of total number of the stages, partial pressure of CO2 and temperature of the top and bottom stages from Razi Company experimental data for the present work and the other two equilibrium-based models.

*Table 3. The results of the present model, Electrolyte-NTRL and Kent-Eisenberg in compared to the data of Ammonia Unit of Razi Petrochemical Company*

| | AAD% | | |
|---|---|---|---|
| | Present model | Electrolyte-NRT | Kent-Eisenberg |
| $y_{out}$ (spec) | 11.11 | 23.07 | 30.99 |
| T bottom | 0.82 | 0.70 | 0.58 |
| T top | 0.00 | 0.00 | 0.00 |
| Total Stages | 0.00 | 10.00 | 45.00 |

As one can observe the deviation of the present model is less than the equilibrium models. Moreover, a sensitivity analysis is carried out. So as Fig. 6 and 7 present the effect of changing in two parameters on the number of stages for achieving to the specific $CO_2$ concentration level in exhausting gas.

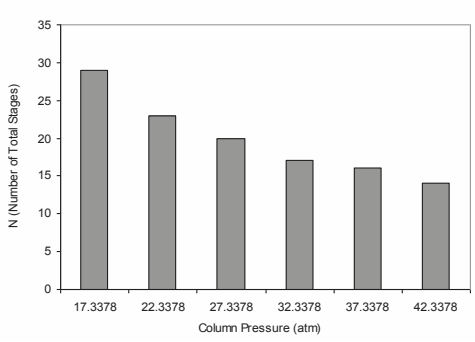


*Fig.6. the number of total stages versus change of the total column pressure for absorption of $CO_2$.*

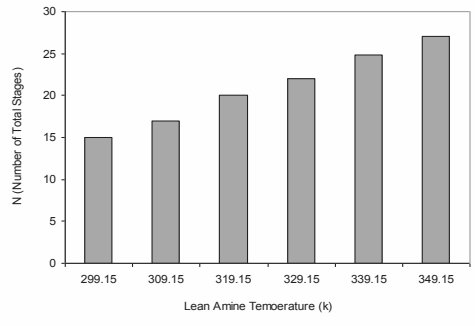


*Fig.7. The number of stages versus change of temperature of the lean amine for absorption of CO2.*

As one can see from Fig. 6, the number of trays required for $CO_2$ absorption decreases as the pressure of the column increases. On the other hand, as Fig. 7 shows the number of trays required for $CO_2$ absorption increases noticeably by increasing the temperature of the lean amine.

## 4. Conclusion

Using rate-based non-equilibrium approach, a new modeling of an absorption column was proposed. The absorber contactor was divided into the compartments so that each stage of the column is equivalent to a compartment which consisting of a mass transfer box and a bath reactor. The model provided in this work was applied to study $CO_2$ absorption in an alkanolamine solution so that the number of trays of the column and partial pressure of $CO_2$ in each stage were calculated by sequential simulation of the column through this new modeling. This new approach for modeling of an absorption contactor is simple so that no need to use the wide group of differential equations.

The results of the new model for absorption of $CO_2$ into MEA solution were obtained so that the number of stages, temperature profile of the contactor and the partial pressure of $CO_2$ are compared to Ammonia Unit of Razi Petrochemical Company experimental data. The results of the new model were compared with the two equilibrium models of Electrolyte-NTRL and Kent-Eisenberg models.

## Nomenclature

| | |
|---|---|
| $a$ | specific contact area ($cm^2/cm^3$) |
| $A$ | cross sectional area of the column ($cm^2$) |
| $C$ | concentration in the bulk of liquid (gmole/lit) |
| $C_p$ | heat capacity (J/kgK) |
| $C^{\circ}_{CO2}$ | concentration of $CO_2$ in the liquid phase entering reactor (gmole/lit) |
| $D$ | diameter of column (cm) |
| $G$ | molar flux of gas phase entering the column ($gmole/cm^2s$) |
| $G_{inert}$ | molar flux of inert gas entering the column (considering all components except $CO_2$) ($gmole/cm^2s$) |
| $H$ | Henry's constant (kg.atm/mol) |
| $j$ | tray number |
| $k_{am}$ | kinetic constant ($m^3$/mol.s) |
| $k_i$ | rate constant ($m^3$/mol.s) |
| $K_1$ | forward first-order rate constant (1/s) |
| $K_{-1}$ | backward first-order rate constant (1/s) |
| $K_{Gi}$ | overall mass transfer coefficient of component i (gmole/cm2satm) |
| $K_c$ | equilibrium constant |
| $k_g$ | local mass transfer coefficient of Gas phase ($gmole/cm^2satm$) |
| $k_l$ | local mass transfer coefficient Liquid phase (cm/s) |
| $L$ | volume flow rate of liquid phase ($cm^3/s$) |
| $MW_i$ | molecular weight of i component (g/gmole) |

| | |
|---|---|
| $N$ | total Number of column trays |
| $N$ | mass transfer flux of $CO_2$ based on mass transfer contact area (gmole/cm$^2$.s) |
| $N'^{(j)}_{total}$ | total amount of absorbed $CO_2$ from first tray to jth tray (gmole/cm$^2$.s) |
| $N'^{(j)}_{tray}$ | mass transfer of flux $CO_2$ between (j+1)$^{th}$ tray and j$^{th}$ tray based on cross sectional area (gmole/cm$^2$.s) |
| $P$ | column total pressure (atm) |
| $P_i$ | partial pressure of component i in the bulk gas phase (atm) |
| $P_i^*$ | equilibrium partial pressure of component i in gas phase (atm) |
| $r$ | reaction rate (gmole/lit.s) |
| $T_g$ | temperature of gas phase (K) |
| $T_l$ | temperature of liquid phase (K) |
| $V$ | volume of liquid on tray (cm$^3$) |
| $W_{MEA}$ | MEA mass fraction in the bulk of liquid phase |
| $x_{CO2}$ | mole fraction of $CO_2$ in the bulk of liquid phase (in both reacted and unreacted form) |
| $X_i$ | conversion of i component in reactor. |
| $y$ | $CO_2$ mole fraction in the bulk of gas phase |

Greek letters

| | |
|---|---|
| α | Liquid loading (mole $CO_2$/mole Amine) |
| $\rho$ | density (kg/m$^3$) |
| $\mu$ | viscosity (Pa.s) |
| $\Phi$ | amine molar flow rate (kg mole/hr) |
| $\Delta H$ | sum of the heats of both reaction and absorption (j/mole) |

Superscripts

| | |
|---|---|
| $e$ | equilibrium condition |
| $j$ | tray number |
| $R$ | reactor |
| $t$ | total |

Subscripts

| | |
|---|---|
| $am$ | amine |
| $g$ | gas phase |
| $i$ | species |
| $l$ | liquid phase |

## Literature Cited


[1] UNFCCC, 1997, Kyoto Protocol to the United Nations Framework Convention on Climate Change.

[2] Harald W., Randall S., Lwazikazi T., 2002. Comparing developing countries under potential carbon allocation schemes. Climate Policy, 2, 303–318.

[3] Rao A. B., Rubin E. S., 2002. A technical, economic, and environmental assessment of amine-based $CO_2$ capture technology for power plant greenhouse gas control. Environmental Science & Technology, 36, 4467–4475.

[4] Mandal B. P., Biswas A. K., Bandyopadhyay S. S., 2003. Absorption of carbon dioxide into aqueous blends of 2- amino-2-methyl-1-propanol and diethanolamine. Chemical Engineering Science, 58, 4137–4144.

[5] Choi W. J., Seo J. B., Jang S. Y., J. H., Oh K. J., 2009, Removal characteristics of $CO_2$ using aqueous MEA/AMP solutions in the absorption and regeneration process, Journal of Environmental Sciences, 21, 907–913

[6] Abu-Zahra M. R. M., Schneiders L. H. J., Niederer J. P .M., Feron P. H. M., Versteeg G, 2007, F.$CO_2$ capture from power plants Part I. A parametric study of technical performance based on monoethanolamine, INTERNATIONAL JORNAL OF GREENHOUSE GAS CONTROL I, 37-46.

[7] Cadours R., Bouallou C, 1998, Rigorous Simulation of Gas Absorption into Aqueous Solutions. Ind. Eng. Chem. Res., 37, 1063-1070.

[8] Rinker Edward B.; Ashour Sami S.; Sandall Orville C, 2000, Absorption of Carbon Dioxide into Aqueous Blend of Diethanolamine and Methyldiethanolamine, Ind. Eng. Chem. Res., 39, 4346-4356.

[9] Mandal L.De., 1986, Rigirous simulation and design of columns for absorption & chemical reaction. computers & chemical engineering, 10, 5-10.

[10] van Loo S., van Elk E.P., Versteeg G.F., 2007, The removal of carbon dioxide with activated solution of methyl-diethanol-amine, Jornal of Petroleum Science and Engineering, 135-145.

[11] Gabrielsen J., Svendsen H. F., Michelsen Michael L., Stenby Erling H., Stenby Erling H., Kontogeorgis Georgios M., 2007, Experimental validation of a rate-based model for $CO_2$ capture using an AMP solution. Chem. Eng. Sci., 62 , 2397-2413.

[12] Ammonia Unit of Razi Petrochemical Company, 2002. Specification of a practical case to be used for model simulation.

[13] Haghtalab A., Dehghani Tafti M., 2007, Electrolyte UNIQUAC-NRF Model to Study the Solubilityb of Acid Gases in Alkanolamines, Ind. Eng. Chem. Res., 46, 6053-6060.

[14] Dankwerts, P. V., 1970, *Gas-Liquid Reactions*, McGraw-Hill, New York.

[15] Levenspiel O., 1999, *Chemical Reaction Engineering*, 3rd ed., John Wiley & Sons, U.S.A.

[16] Traybal Robert E., Mass Transfer Operations, 3rd ed., McGraw Hill, New York.

[17] Al-Ghawas Hani A., Hagewiesche Daniel P., Gabriel Ruiz-Ibanez, Orville C. Sandall, 1989, Physicochemical Properties Important for Carbon Dioxide Absorption in Aqueous Methyldiethanolamine, J. Chem. Eng. Data, 34, 385-391.

[18] J.J. Carroll. Converting amine concentrations. Hydrocarbin Processing. 1994, 91-94.

[19] Huttenhuis P.J.G., Agrawal N.J., Solbraa E., Versteeg G.F., 1994, The solubility of carbon dioxide in aqueous N-methyldiethanolamine solution, Fluid Phase Equilibria, In Press.

[20] Reid Robert C., Prausnitz John M., Poling Bruce E., 1987, *The Properties of Gas & Liquids*, 4th ed., McGraw Hill, New York.

[21] Cheng S., Meisen A., 1996, Predict amine solution properties accurately, Hydrocarbon Processing, 81-83.

[22] Zhang X. Wang, J., Zang, C. F, Yang, Y. H., Xu, J. J., 2003, Absorption Rate into MDEA Aqueous Solution Blended Piperazine under High $CO_2$ Partial Pressure, Ind. Eng. Chem. Res., 42, 118-122.

[23] Kohl A.L., Nielsen R., 1974, *Gas Purification*, 5th edition; Gulf publication company, Gulf Publishing Company, Houston, U.S.A.

# Engineering Application of Exergy Analysis: Gas Recovery System in Steel Industry

*Sergio Usón[a], Javier Uche[a], Juan José Arribas[b], Rocío Llera[c] and Alicia Valero[a]*

[a] *CIRCE Institute Universidad de Zaragoza, Zaragoza, Spain*
[b] *Arcelor-Mittal España, Avilés, Spain*
[c] *Project Engineering Area of University of Oviedo, Oviedo, Spain*

**Abstract:** The Basic Oxygen Furnace (BOF) for steel making produces a stream of waste gas at high temperature which contains carbon monoxide. Accordingly, its proper recovery entails important energy savings in the steelmaking process. Exergy analysis is applied in this paper to analyze a system designed to use both thermal (in order to produce steam) and chemical energy of this gas. The system is characterized by transient operation and storing of both gas and steam. Actual plant data is used to calculate time evolution of exergy flows and irreversibilities. Besides, integral indicators are defined for characterizing the whole recovery cycle. The analysis provides important conclusions for improving plant operation, in order to maximize recovered exergy.

**Keywords:** exergy analysis, gas recovery, basic oxygen furnace

## 1. Introduction

According to the Best Available Techniques Reference Document (BREF) on Iron and Steel [1], 'Steel sector consume huge amounts of energy: specific consumption of 23 GJ/t of liquid steel in EU plants in 1980 has been reduced to 18 GJ/t in modern plants in 2004, but still strong reductions are required'. In this framework, steel companies are making a big effort to reduce energy consumption in order to decrease environmental impact and to improve their competitiveness.

Besides the development of innovative steelmaking processes and the improvement of existing ones, other ways of obtaining energy savings can be considered. Examples of them are the recovery of waste streams (both energy and materials) and the development and application of advanced analysis techniques, such as the concept of exergy [2, 3].

Exergy is a convenient magnitude for the analysis of systems and processes within steel industry for two main reasons. First, it is able to measure in homogeneous units not only different forms of energy but also different kinds of materials. Second, it takes into account not only losses through the system boundary but also irreversibilities within the processes. For this reasons, exergy analysis has been applied in steel industry for accounting energy and materials flows [4] and for improving energy efficiency [5]. This analysis has been applied not only to global analyses, but also to specific issues. For example, it has been used for analyzing an electric arc furnace [6], for proposing innovative methods for improving hot gas stoves efficiency in blast furnaces [7], or for analyzing methods for recover gas streams [8]. Not so related to steel works but also with steel is the application of exergy for the life cycle analysis of this material [9].

In this paper, exergy is applied to the analysis of the operation of a system for the recovery of gas from Basic Oxygen Furnace (BOF gas), in order to detect possibilities for improving its efficiency. The gas recovery system not only recovers the gas but also produces steam, which is used in steel treatments and can also be exported to the steelworks steam net [10]. Furthermore, both steam and gas can be stored.

Proper operation of such system is a complex issue, and the analysis developed here can shed light to improve it. The approach developed consists of two complimentary parts. First, actual operation data is used to obtain the time evolution of exergy-based parameters, which allows a detailed analysis of each recovery cycle. Second, integral cycle indicators are defined for characterizing the whole cycle, in order to compare it with other ones.

## 2. Development of the model.

### 2.1. Description of the system

A scheme of the gas recovery system is depicted in Fig. 1. Numbers 1 to 10 are used for gas flows, while numbers from 101 on refer to water or steam.

Corresponding Author: Sergio Usón, Email: suson@unizar.es

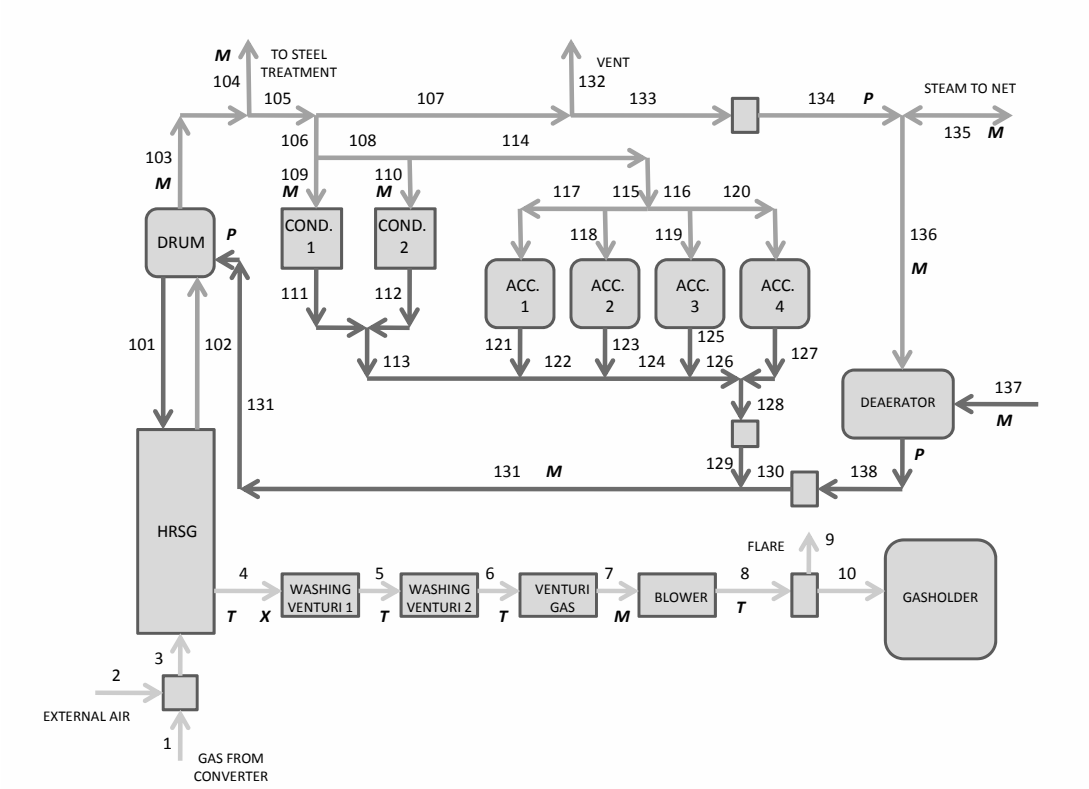


*Fig. 1. Flow scheme of the gas recovery system.*

Gas leaving the converter (flow 1) reacts with external air entering through the hole between the converter and the heat recovery generator (flow 2) to form flow 3, which is cooled in the heat recovery steam generator (HRSG) down to point 4. It should be noted that part of the burning reactions take place inside the HRSG, but here reaction and heat transfer have been separated for simplicity. Besides, the operator has two ways of controlling the amount of external air (under certain limits). First, the hood that directs gases towards the heat recovery steam generator can be moved upwards and downwards (and thus the gap between the converter and the hood can be modified). Second, position of venturi located downstream can also be modified.

Gas leaving the HRSG (flow 4) is washed and cooled in two washing venturi. Afterwards, a third venturi is present to measure the gas flow, and a blower establishes the draft needed to impulse the gases. Finally, a three-way valve is located in order to choose whether the gas is flared (flow 9) or stored in the gasholder (flow 10). In this choice, quality requirements to store gas are considered.

Heat released during gas cooling within the HRSG is used to transform saturated water from the drum (flow 101) into a mixture of liquid and steam going back to that component (flow 102). Part of the steam produced in the drum (flow 103) is used for steel treatments (flow 104). Another part flows through a pressure regulator and then can flow towards the general steam network of the steelworks (flow 135) or be used by the deaerator (flow 136). It should be noted that it is possible to import medium pressure from the steam network; accordingly, flow 135 can have two senses.

Steam generated in the drum can also be stored in four accumulators for later use (flows 114 to 120). Besides, if there is excess of steam, it is possible to condense part of it in two condensers (flows 109 and 110). For safety reasons, if pressure increases,

part of the steam can be vented (flow 132, normally closed).

Liquid water from condensers and accumulators (flows 111-113, 121-127) can be pumped and returned to the drum. Besides, the drum can be fed from external fresh water (flow 137), once the deaerator has passed.

## 2.2. Thermodynamic model.

Figure 1shows plant instrumentation used for the characterization of the thermodynamic state of the system: flow rates (*M*), pressures (*P*), temperatures (*T*) and gas composition (*X*). The latter refers to concentration of CO, $CO_2$ and $O_2$ in dry basis. Although they have not been represented in the figure, levels of the four accumulators and position of three-way valve are also available.

### 2.2.1. Gas flows

To characterize flows 3 to 10, measurements of flow rate and dry gas composition are available. In order to calculate the amount of water, it has been considered that gas is dry in flows 3 and 4 and that is water saturated in flows 5 and 6. In the other flows, temperature increases slightly and no water is added. Accordingly, it has been considered that the flow of water is kept constant. Nitrogen concentration is calculated by difference and, since it is no reaction, flow of CO, $CO_2$, $O_2$ and $N_2$ is maintained in flows 3 to 8. Depending on the position of the three way valve, flow 8 continues either in flow 9 or in flow 10.

In order to calculate flows 1 (converter output) and 2 (external air), a balance to carbon, nitrogen and oxygen is made. Besides, composition of 1 is known (air) and it has been considered that gas flow 2 does not contain significant amounts of $CO_2$ or $O_2$.

There are temperature measurements in flows 4 to 8 (except in point 7, which has been supposed to be equal to 6). Temperature of flow 2 is equal to the environment (considering that the control volume is far enough from the hot area around the converter), and temperature of flow 1 is calculated by energy balance of the HRSG.

### 2.2.2. Water/steam flows

First, there is no measurement of the flow of saturated liquid leaving the drum towards the HRSG (flow 101); accordingly, it is fixed by the design values. Since flows 131 and 103 are known, mass accumulated in the drum is calculated. Due to available measurements in flows 104 and 135 (and assuming that no steam is vented), it is possible to calculate flows 105, 106, 107, 133 and 134. Besides, flows entering the condensers are also measured.

In order to calculate flows corresponding to the accumulators, rate of level variation is used. This rate can be obtained because evolution of all signals is available. Besides, it has been supposed that the amount of water leaving all accumulators is the same. Finally, measurement in 137 allows one to calculate mass accumulation in the deaerator.

To calculate intensive properties, three pressure zones have been considered:

- Drum (high pressure): flows 103 to 133
- Steam network (medium pressure): flows 134 to 136
- Deaerator: flows 137 and 138

Besides, isentropic efficiency is imposed for pumps. Finally, an equation is introduced relating matter and energy accumulation in the drum in order to calculate the quality of flow 102 (which, in turn, allows one to calculate the temperature of gases leaving the converter by the energy balance of the HRSG).

## 2.3. Exergy analysis.

Once all flows defined in Fig. 1 have been characterized as described in the previous sections, exergy analysis can be performed [2,3]. Exergy of a flow *i* is composed of two parts: physical and chemical:

$$\dot{B}_i = \dot{B}_{ph,i} + \dot{B}_{ch,i}\,, \qquad (1)$$

Physical exergy appears because the flow has different conditions of temperature and/or pressure that the reference environment:

$$\dot{B}_{ph,i} = fm_i \cdot \left[ \left( h_i - h_{0,i} \right) - T_0 \cdot \left( s_i - s_{0,i} \right) \right], \qquad (2)$$

where *fm* is the molar rate, *h* is specific enthalpy and *s* is specific entropy. Properties are evaluated at the conditions of flow *i* and at reference conditions *0* (but for the same composition of flow *i*).

Chemical exergy is due to the composition of the flow (different than that of the environment):

$$\dot{B}_{ch,i} = fm_i \cdot \sum_{j=1}^{n} x_{i,j} \left( b_{ch,j} - R \cdot T_0 \cdot \ln x_{i,j} \right), \qquad (3)$$

where $x_{i,j}$ is the molar fraction of component $j$ in flow $i$, $b_{ch,j}$ is the specific exergy of component $j$ and $R$ is the constant of gases. The second part of the equation refers to the difference between the exergy of the different components of a mixture isolated, and the exergy of the components all mixed together. Szargut reference state [2] has been used for the calculation of chemical exergy.

After calculating the exergy of all flows, it is possible to obtain the irreversibility of each component ($I_k$). It should be noted that, in this paper, irreversibility will also include losses (external irreversibilities).

$$I_k = \sum_{inputs} \dot{B}_i - \sum_{outputs} \dot{B}_i \,, \tag{4}$$

In order to put in perspective the values of exergy and irreversibility obtained, two non-dimensional parameters have been defined. First, several efficiencies calculated by dividing the exergy of the outputs of the system into the main input (exergy of gases leaving the converter):

$$\eta_i = \frac{\dot{B}_i}{\dot{B}_1}, \tag{5}$$

Besides, irreversibility of components is made non-dimensional by dividing it also into the exergy of flow 1:

$$\varphi_k = \frac{I_k}{\dot{B}_1}, \tag{6}$$

### 2.4. Parameters for characterizing the whole cycle.

Exergy flows, irreversibility and non-dimensional parameters defined in the previous section vary with time, and thus they are suitable for a detailed study of a given recovery cycle. However, in order to summarize the results of a cycle and to compare it with others, integral indicators characterizing the whole cycle are needed.

Accordingly, the exergy of a flow $i$ over a cycle (kJ) is defined as:

$$B_{cycle,i} = \int_{cycle} \dot{B}_i(t) \cdot dt \,, \tag{7}$$

Besides, the irreversibility in a component $k$ over a cycle (kJ) is defined as:

$$I_{cycle,k} = \int_{cycle} I_k(t) \cdot dt \,, \tag{8}$$

Finally, the non-dimensional parameters $\eta$ and $\varphi$ can also be calculated for the whole cycle:

$$\eta_{cycle,i} = \frac{B_{cycle,i}}{B_{cycle,1}} = \frac{\int_{cycle} \dot{B}_i(t) \cdot dt}{\int_{cycle} \dot{B}_1(t) \cdot dt}, \tag{9}$$

$$\varphi_{cycle,k} = \frac{I_{cycle,k}}{B_{cycle,1}} = \frac{\int_{cycle} I_k(t) \cdot dt}{\int_{cycle} \dot{B}_1(t) \cdot dt}, \tag{10}$$

## 3. Results

The model described above is being applied for the study of the operation of the gas and steam recovery system by using information (detailed in Fig. 1 and at the beginning of section 2.2), which is stored by the plant information system every 16 seconds. In this section, the most important results corresponding to an example of a gas recovery cycle are presented. First, evolution of both exergy and irreversibility is presented, and then the cycle is summarized by the integral cycle indicators.

### 3.1. Exergy and irreversibility versus time.

Figure 2 shows the evolution of the exergy of flue gases leaving the BOF during a cycle. It can be seen how this amount increases during the first half of the cycle and decreases later, with smooth variations according to the blowing pattern of oxygen inside the converter.

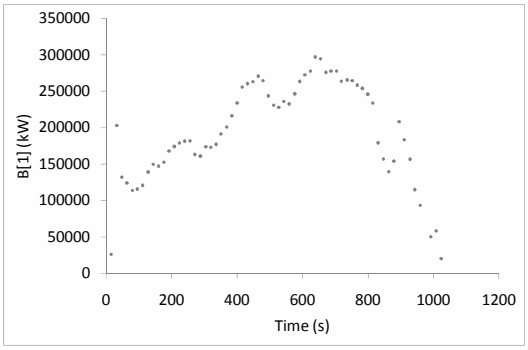


*Fig. 2. Exergy of gases leaving the converter.*

The exergy of gas which is recovered in the gasholder is shown in Fig. 3. In this figure and in the following ones, two families of points are plot: the absolute value (left axis) and the relative value (according to 5 or 6) in the right axis. Due to quality requirements of gas to be stored (e. g. minimum amount of CO), gas recovery only takes place during part of the cycle. It should be noted that the exergy of this gas represents between 50 and more than 80% of exergy of flow 1.

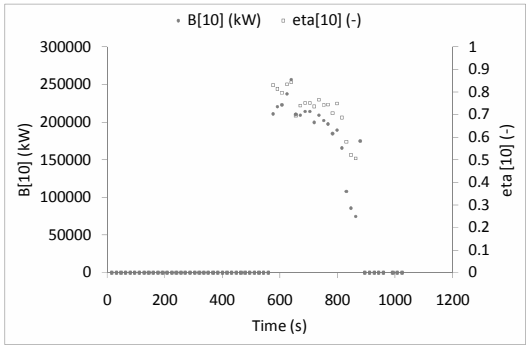


*Fig. 3. Exergy of recovered gas.*

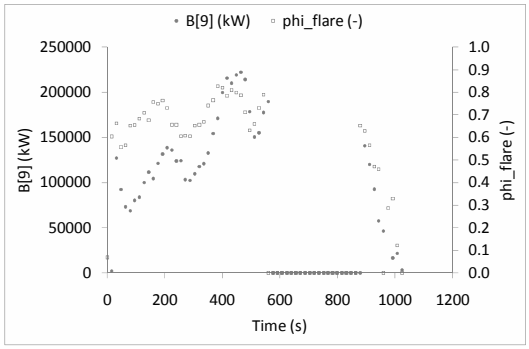


*Fig. 4. Exergy of flared gas.*

The part of the gas which is flared is represented in Fig. 4. This amount represents more than 50% of flow 1 before the recovery but falls at the end of the cycle. This result indicates that it is very interesting to extend the duration of the recovery as much as possible and to flare gas only when this is the only possibility.

As explained previously, the system not only recovers gas, but also produces steam. Figure 5 shows the evolution of exergy of steam used in several steel treatments (flow 104). This amounts around 12 MW, which corresponds to less than 10% of the exergy of converter gas.

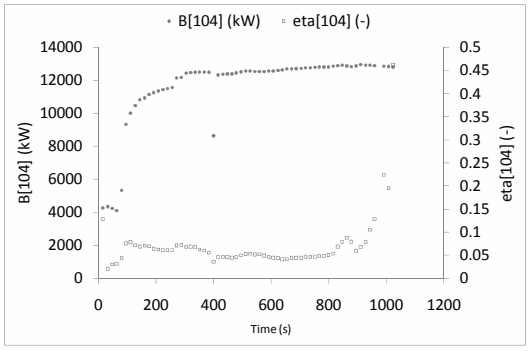


*Fig. 5. Exergy of steam to steel treatments.*

Exergy of steam exported to the steam net of steelworks is presented in Fig. 6. First, the system exports 1.5 MW of steam, which are progressively reduced and afterwards more than 2 MW are imported (negative value). These amounts are less than 2% of the exergy of flow 1.

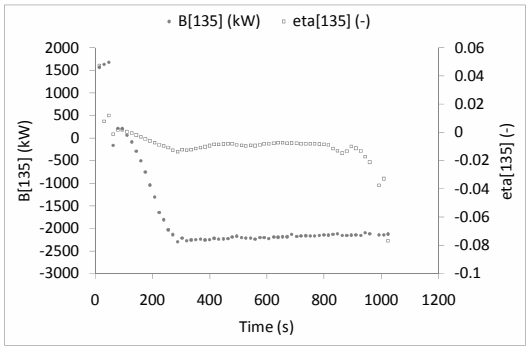


*Fig. 6. Exergy of steam exchanged with the net.*

Results presented above have shown the variation of the exergy of several flows leaving the system. However, a key advantage of the use of exergy is that it allows one to consider also losses of energy quality (irreversibilities) taking place inside the different component.

Figure 7 represents the exergy destroyed in the combustion process. The low value of this variable (around 2%) can be explained by considering two points. First, only a fraction of the CO contained in the gas is burned (the other part contributes strongly to the chemical exergy of gas which is either stored or flared, as it can be seen in Fig. 3

and 4). Second, due to the high temperature of flow 1, the combustion takes place at a high temperature (above 1400 ºC), which reduces substantially irreversibility due to heat transfer.

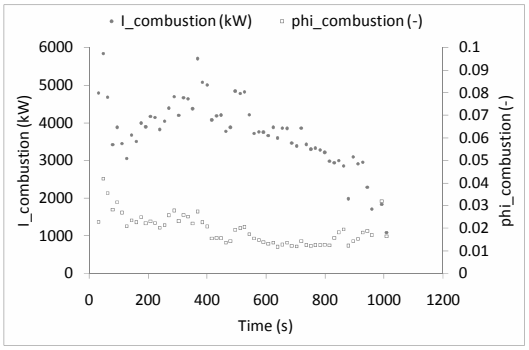


*Fig. 7. Irreversibility of combustion.*

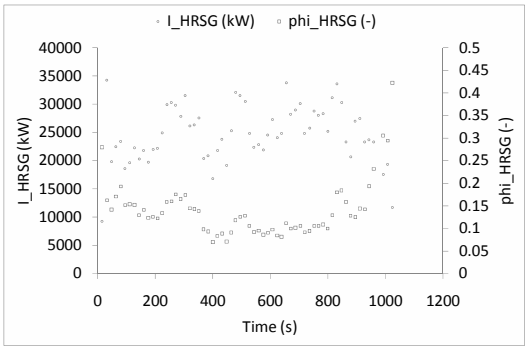


*Fig. 8. Irreversibility in the HRSG.*

Irreversibility in the heat recovery steam generator is plotted in Fig. 8. These losses can be as high as 30 MW, or more than 15%. They might be reduced by considering another design of the boiler, producing steam of different levels of pressure. It should be noted that the separation of combustion and heat transfer has been made to simplify the model. Accordingly, the actual distribution of losses between these two processes is not exactly the same as the values calculated here.

Figure 9 represents irreversibility produced in the first washing venturi, where gases are cooled from more than 700 ºC down to less than 100 ºC. This irreversibility is around 6% of the exergy of flow 1, and might be reduced by modifying the design of the HRSG in order to use a higher part of the thermal exergy of gases.

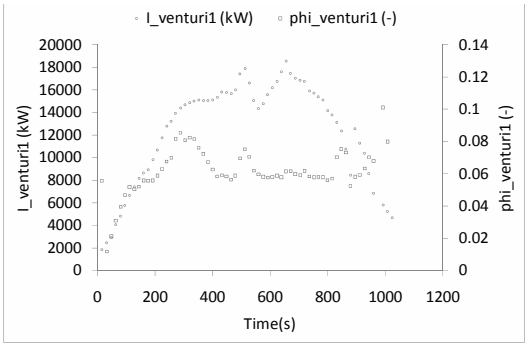


*Fig. 9. Irreversibility in the first washing venturi.*

Finally, Fig. 10 shows how 2.5 MW of exergy are destroyed without use in the steam condensers. This amount may seem not too high compared to flow 1 (between 1 and 2%), but represents around 20% of the exergy of steam used in steel treatments (flow 104). This value only depends on operation strategy and can be reduced substantially by a proper management of steam storage and steam export to plant net.

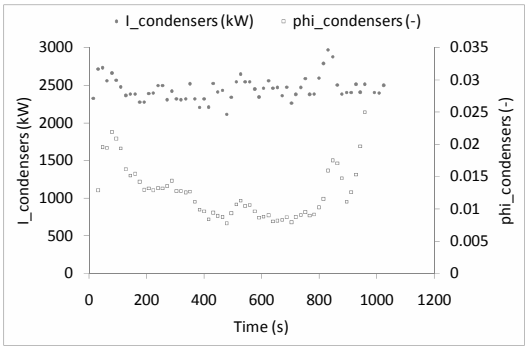


*Fig. 10. Irreversibility in the condensers.*

## 3.2. Integral cycle indicators.

In this section, parameters defined in (7-10) are used to summarize the performance of the whole recovery cycle. The main flows appear in Table 1, and the main components in Table 2.

*Table 1. Integral cycle indicators for the main flows*

| Flow | $B_{cycle}$ (GJ) | $\eta_{cycle}$(-) |
|---|---|---|
| 1, gases from converter | 193.31 | 1.0000 |
| 9, flared gas | 82.92 | 0.4290 |
| 10, recovered gas | 59.70 | 0.3089 |
| 104, steam to treatments | 11.55 | 0.0597 |
| 135, steam to net | -1.686 | -0.0087 |
| Accumulated steam | 8.438 | 0.0437 |

*Table 2. Integral cycle indicators for the components*

| Component | $I_{cycle}$ (GJ) | $\Phi_{cycle}$ (-) |
|---|---|---|
| HRSG | 24.58 | 0.1271 |
| Venturi 1 | 12.30 | 0.0636 |
| Combustion | 4.03 | 0.0209 |
| Condensers | 2.44 | 0.0126 |

The analysis of these indicators allows one to draw important conclusions regarding the efficiency of the system. First, the most important part of exergy (more than 70%) is available in gas flow which is stored in a gasholder (30.1%) or flared (42.9%). Accordingly, the minimization of gas flared is a key point in increasing efficiency of the system. The first action towards this goal is to avoid flaring when the gas quality is suitable for storing. The second step is to optimize the operation of the system in order to increase the time span when gas accomplishes the requirements for being recovered.

11.55 GJ of steam are consumed for steel treatments, while around 1.7 GJ are imported (this is the meaning of the minus sign) from the general steam net of the steelworks. In this context, the 2.44 GJ of exergy lost in the condenser represent a big potential of steam savings. Accordingly, operation of the steam part of the system should be improved to reduce this amount. Importance of these savings can be even larger, because if steam is properly used, operation can be more easily adapted for maximizing the gas recovered.

12.7% of exergy of entering gas is destroyed in the heat recovery steam generator and 6.4% in the first washing venturi. Accordingly, new developments of gas recovery systems may include more advanced HRSG producing steam at several pressures. Irreversibility in the combustion process is small (2.1%) because it takes place at high temperatures and only affects a part of the heating value of the gas. It should be noted that all these values correspond to a single cycle, and they vary according to the profile of gases leaving the BOF as well as the operation of the recovery system.

## 4. Conclusions

Exergy analysis has been applied to point out the energy savings potential of a system as complex as an installation for BOF gas recovery, which also produces steam and includes storage of both. The approach comprises two parts: a detailed analysis of the evolution of exergy and irreversibility, and the calculation of integral parameters for characterizing the whole recovery cycle. These integral parameters are the key point of the paper, because they allow to rigorously summarize the behavior of batch processes like the one studied here.

Results obtained in the analysis of a single cycle point out that there is strong potential for improvement, not only in the reduction of gas flared but also in the operation of the steam section (e.g. condensers). Due to the use of exergy, all these losses can be directly compared.

Although these results correspond to an example of converter cycle, the comparison of the integral parameters corresponding to the operation during several months (including different operation strategies) will provide useful information to improve the exergy efficiency of the system and thus the steam and gas recovered. This comparison may include the separation of exergy lost by flared gas into causes (due to gas low quality or to improper operation). Furthermore, the development of a thermoeconomic model based on exergy calculated here may highlight more clearly the potential points for improving.

## Nomenclature

| | |
|---|---|
| $\dot{B}$ | exergy, kW |
| $B_{cycle}$ | exergy in a cycle, kJ |
| *BOF* | basic oxygen furnace |
| *BREF* | Best Available Techniques Reference Document |
| *EU* | European Union |
| *fm* | molar rate, kmol/s |
| *h* | specific enthalpy, kJ/kmol |
| *HRSG* | heat recovery steam generator |
| *I* | irreversibility, kW |
| $I_{cycle}$ | irreversibility in a cycle, kJ |
| *M* | flow rate, kg/s |
| *n* | number of substances in a flow |
| *P* | pressure, Pa |
| *R* | constant of gases, kJ/(kmol·K) |
| *s* | specific entropy, kJ/(kmol·K) |
| *T* | temperature, K |
| *X,x* | composition |

Greek symbols

| | |
|---|---|
| $\eta$ | efficiency |

$\varphi$ non-dimensional irreversibility

Subscripts and superscripts

*ch* chemical

*i* flow

*j* *substance in a flow*

*k* component

*ph* physical

*0* reference conditions

## References

[1] European Commission, Join Research Centre, Institute for Prospective and Technological Studies, 2001, *Best Available Techniques Reference Document on Energy Efficiency*. http://eippcb.jrc.es/reference/i&s.html

[2] Szargut, J., 2005, *Exergy Method. Technical and Ecological Applications*, WIT Press, Southampton, UK.

[3] Kotas, T.J., 1985, *The exergy method of thermal plant analysis*, Butterworths, London.

[4] Costa, M. M. et. al., 2001, Exergy accounting of energy and materials flows in steel production systems, Energy, 26 (4), pp. 363-384.

[5] Bisio, G., 1993, Exergy method for efficient energy resource use in the steel industry, Energy, 18 (9), pp. 971-985.

[6] Çamdali, Ü., Tunç, M., 2003, Exergy analysis and efficiency in an industrial AC electric ARC furnace, Applied Thermal Engineering, 23(17), pp.2255-2267.

[7] Bisio, G., 1998, A second-law analysis of the "hot blast stove/gas turbine" combination by applying the parameter "usable exergy", Energy Conversion and Management, 39(3-4), pp. 217-227.

[8] Maruoka, N., Akiyama, T., 2006, Exergy recovery from steelmaking off-gas by latent heat storage for methanol production, Energy, 31(10-11), pp. 1632-1642.

[9] Michaelis, P., Jackson, T., Clift R., 1998, Exergy analysis of the life cycle of steel, Energy, 23(3), pp. 213-220.

[10] Nippon Steel Corporation, 2004, OG Specifications. Project ENSIDESA.

# Multistage Production Decision Model under the Deregulated Electricity Market (For CCGT)

*Samira Fazlollahi[a], Dr. Julián Barquín Gil[b],*

[a] *EPFL, Lausanne, Switzerland*

[b] *Universidad Pontificia Comillas, Madrid, Spain*

**Abstract:** In this paper, we propose a new methodology which is called multi stage production decision model that is suitable for companies with multi business line (gas distribution and Electricity generation) in the deregulated electricity market. We also consider computationally efficient procedures to solve it. Under these conditions, a company, who owns gas for selling in the gas market and also for producing electricity, is able to compare between these two markets in order to allocate the optimal quantity of gas for selling in the gas market and using it to produce electricity and sell it in the electricity market. We express the multi stage optimization problem in which the objective is to maximize expected profits and decisions are required to meet the standard operating constraints, under the assumption of competitive market and price taking. The volatility of the spot market price of electricity is represented by a stochastic model based on the pervious study and it is not in the scope of this paper. The mixed integer linear programming is used to solve the optimization problem.

**Keywords:** Electricity market, production decision model, MILP, UCP,

## 1. Introduction

In the electricity market, electricity price and the quantity of production are two main issues for utilities. In the regulated electricity market, Utilities are price taker which means they could not determined the electricity price with open competition and the price determined by central decision. In this case just quantity of production is the main issue for utilities and it is calculated by using the centralized Unit Commitment Method [1], in the short term based on the cost minimization.

Under the deregulation, the electricity price set by open competition so both electricity price and quantities of production are key issues for producers.

In this deregulated market the unit commitment method (UCP) for an electric power producer; will require a new formulation that includes the electricity market properties. As mentioned before the main difficulty here is that the spot price of electricity is no longer predetermined but set by open competition. Thus far, the hourly spot prices of electricity have shown evidence of being highly volatile. The unit commitment decisions are now more difficult and the modeling of spot price becomes very important in this new operating environment.

The problem is more complicated for companies with multi business line in gas and electricity, because these companies could switch between these two markets in order to maximize their benefits.

In this research new methodology, for solving this problem, is proposed, which we call it “multi stage production decision model for companies with multi business line - in a deregulated market”, and beside that the tools for implementing and using the mode are designed. This model implemented in the gas company in Spain but because of confidentially, in this paper we just present validation and verification results and not any other result.

Based on this short introduction the research motivation is:

To propose the suitable Model in deregulated electricity Market for the company with two businesses line in Gas and Electricity which covers the following conditions:

- The deregulated Market properties

Samira Fazlollahi, Email: samira.fazlollahi@epfl.ch

- The flexibility of these companies to switch from one market to another in regulatory framework
- The model in different time horizontal for a short and midterm planning.
- The flexible model which could run very fast with user friendly interface

These are the main motivation of this research.

The proposed model consists of three main stages:

- The electricity price forecasting
- The calculation of the marginal value of the gas
- The calculation of the optimal schedule of electricity production

In the first stage by using stochastic model, the hourly electricity price in the market for short term, midterm and long term is estimated. For this purpose, first we need to estimate the average electricity price. Then we could forecast hourly electricity price based on the estimation of average electricity price.

There are different methods in the literature for average electricity price forecasting [2], [3], [4], [5], [6], [7], [8], [9] and [10]. These methods could be categorized into three groups, a. Game theory models b. Simulation models c. Time series [11].

In this research we used MARAPE model. This model, referred to as the probabilistic production-costing model, incorporates the stochastic features of load and generator availabilities [12] The objective of this model is to allow the electricity company to evaluate the future evolution of the prices in the market in the midterm, i.e., ranging from one month to four or five years, both quantitatively and qualitatively.

In the proposed model the average electricity price for long term and mid term, like one month, is not useful and we need hourly electricity price estimation. We suggest using financial price approach [13], [14], [15] to estimate hourly electricity price by using historical data and average electricity price estimation as an input data. Finally the output of this step is hourly electricity price estimation (part 3.1).

The second step of the proposed model is the gas model for computing the gas marginal value and its optimum allocation for producing the electricity in the electricity market. We proposed the optimization approach to calculate the marginal value of gas.

The objective function of Gas model, therefore, is to obtain optimal allocation of gas for producing the electricity in thermal power plants so as to meet the system limits at a maximum benefit, maintaining a suitable level of reliability and guaranteeing compliance with system (technical, environmental and regulatory) constraints. The main idea is calculating the shadow price of Fuel balance equation, which is the marginal value of gas for producing the electricity. In other words how much the benefit will change by adding one extra unit of gas for producing the electricity? In this way the company could compare the gas price in the gas market with this marginal value and if this marginal value is higher than the gas price in the gas market then it is better to allocate more gas for producing electricity instead of selling the original gas (part 3.2).

The third step is the calculation of the optimal electricity production schedule. In this stage we propose the optimization mathematical model. The objective of this model, therefore, is to obtain an hourly schedule for each thermal power plant so as to meet the system limits at a maximum benefit, maintaining a suitable level of reliability and guaranteeing compliance with system (technical, environmental and regulatory) constraints.

Finally the optimization method with Mixed Integer Linear Programming (MILP) techniques for maximizing the Market revenue is proposed to calculate the third stage which is the hourly schedule of electricity production for each plant, taking in to account the technical characteristic of thermal plants and limited gas fuel (part3.3). In this part the electricity is an input data which is estimated in the first step so the model is represent the unit commitment method (UCP).

In order to implement the mathematical model we need to design a tool. GAMS is a good software for simulating and running the optimization model.

Excel is used for data structuring and also as an interface.

Each company with multi business lines in gas and electricity could use this model in order to:

- Calculate the optimal allocation of the Gas quantity for gas and electricity market by computing its marginal value
- Calculate the optimal production schedule of electricity for each plant
- Considering computationally efficient procedures to solve the model and use a user friendly tool for it, which is run very fast.

This paper is organized as follows: Section 2 explains the Methodology. Section 3 describes the proposed model, where as Section 4 focuses on model testing which is used to validate the model and, finally, Section 5 provides some conclusions.

## 2. Methodology overview

We use optimization method based on mixed integer linear programming (MILP) to solve the problem. In the following paragraph we will explained in details that why we used this method and what system optimization method is.

In mathematics, optimization or mathematical programming refers to choosing the best element from some set of available alternatives. It refers to where there are multiple options but optimization is all about choosing the best one, it is the search for optimum strategies.

In the simplest case, this means solving problems in which one seeks to minimize or maximize a real function by systematically choosing the values of real or integer variables from within an allowed set. This (a scalar real valued objective function) is actually a small subset of this field which comprises a large area of applied mathematics. More generally, it means finding "best available" values of some objective function given a defined domain, including a variety of different types of objective functions and different types of domains.

If the unknown variables are all required to be integers, then the problem is called an integer programming (IP) or integer linear programming (ILP) problem. In contrast to linear programming, which can be solved efficiently in the worst case, integer programming problems are in many practical situations (those with bounded variables) NP-hard. 0-1 integer programming or binary integer programming (BIP) is the special case of integer programming where variables are required to be 0 or 1 (rather than arbitrary integers). This problem is also classified as NP-hard, and in fact the decision version was one of Karp's 21 NP-complete problems.

If only some of the unknown variables are required to be integers, then the problem is called a mixed integer programming (MIP) problem. These are generally also NP-hard.

Advanced algorithms for solving integer linear programs include:

- cutting-plane method
- branch and bound
- branch and cut
- branch and price

Branch and bound (BB) is a general algorithm for finding optimal solutions of various optimization problems, especially in discrete and combinatorial optimization. The method was first proposed by A. H. Land and A. G. Doig in 1960 for linear programming[1]

### 2.1 General description

For definiteness, we assume that the goal is to find the minimum value of a function f(x) (e.g., the cost of manufacturing a certain product), where x ranges over some set S of admissible or candidate solutions (the search space or feasible region). Note that one can find the maximum value of f(x) by finding the minimum of g(x) = − f(x).

A branch-and-bound procedure requires two tools. The first one is a splitting procedure that, given a set S of candidates, returns two or more smaller sets $S_1, S_2, \ldots$ whose union covers S. Note that the minimum of f(x) over S is $\min\{v_1, v_2, \ldots\}$, where each $v_i$ is the minimum of f(x) within $S_i$. This step is called branching, since its recursive application defines a tree structure (the search tree) whose nodes are the subsets of S.

It was the short explanation about the methodology which is used for solving the problem.

### 2.2 Dynamic Hypothesis

[1] http://www.csulb.edu/~obenli/Research/IE-encyc/bb.html

The following assumptions are considered in the model:

- We just consider one firm in optimization model
- The transmission grid is not included in the model
- We Just consider the combined-cycle plants as a technology
- That is called the single node approach
- The chronological evolution of the system hour by hour must be modeled.
- The time wise representation of hourly period is used
- An uncertainty is not considered, a deterministic approach is used
- Increasing in the gas consumption in each step of running the model is small
- The Constance start up duration for startup ramp is considered
- The efficiency curve (input – output curve) for each thermal plant is considered as linear function

In the next part the model specification will explained.

## 3. Model specification

The purpose of this part is to explain the proposed multi stage production decision model in details

### 3.1 Multi stage production decision model

In the electricity market, electricity price and the quantity of production are two main issues for utilities and the unit commitment method (UCP) for an electric power producer will require a new formulation that includes the electricity market properties. As mentioned before the main difficulty here is that the spot price of electricity is no longer predetermined but set by open competition. The problem is more complicated for companies with multi business line in gas and electricity, because these companies could switch between these two markets in order to maximize their benefits, so they need flexible model to help them for making a decision.

For this purpose, we propose the new model which consist of three stages :1) electricity price forecasting for each hour during the time horizon, 2)calculation of gas margin for different available quantity of gas to produce electricity,3) optimum schedule of electricity production based on profit maximization, taking into account relevant technical and operational constraints of the generation system.

In the first stage the hourly electricity price in the market for short term, midterm and long term is estimated by using stochastic model. The optimal allocation of gas quantity for electricity power production is done in the second step. The outputs of the first and the second stage are inputs for the third stag which is the single firm commitment problem (figure 3).

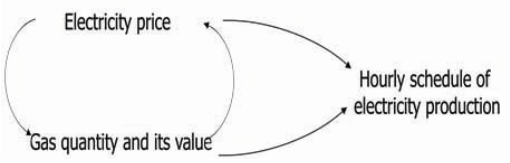


*Figure 1: multi stage production decision model*

We show that when the spot price of electricity is estimated in the first step, it is used in the second step as an input data. By using this input data in the second step, the marginal value of the gas can be calculated for different quantity of gas. The gas margin for each quantity should compare with gas price in the market. If the gas Margin is higher than the gas price then it is better to allocate more gas for electricity production instead of selling the gas. After fixing the available quantity of gas for electricity production, again we should run the first step model to update the electricity price estimation; because when the electricity production is increased by using more gas, then the electricity price in the market will change because of increase in the supply side. The stage one and two behave like one loop. This procedure could be continued up to the point where the electricity price doesn't change significantly from one run to another.

In the previous Market modeling with the price clearing process as exogenous to the firm's

optimization program, the influence of the firm's decisions on the market clearing price neglects but in the proposed model this influence considers by defining a loop between the first and second stage. As mentioned before, in the first stage the hourly electricity price in the market is estimated by using stochastic model and one of the input data for this step is the available quantity of gas for producing electricity. The optimal allocation of gas quantity for electricity power production is done in the second stage based on the output of the first stage and also comparing the marginal value of gas in electricity market and the gas price in the gas market. we should put again this new quantity of gas in the first step in order to update the electricity price, this loop will continue up to get the equilibrium point between electricity price and optimal quantity of gas. The outputs of the first stage, electricity price, and the second stage, available gas quantity, are inputs for the third stag which is the single firm commitment problem with the maximization objective function Figure 3 present the proposed procedure.

### 3.1 Step one: Electricity price forecasting

In liberalized electricity markets power producers face a wide range of decision problems that require modeling of electricity prices as a crucial input.

In the highly liquid and developed financial markets the literature on price modeling is extensive. To predict future price developments, analysts use both technical analysis based on patterns in historical market price movements and, fundamental analysis based on expectations about the development in the underlying market price drivers [7]. Electricity markets worldwide are still in the development phase and not surprisingly there exists conflicting views about the value of such modeling tools in electricity markets.

In this step, the main Idea is to estimate the Average of the electricity price for specific periods of time, for instance one month, and then estimate the electricity price for each hour by using one of the electricity price modeling methodologies.

#### 3.1.1 Price estimation for each hour

In this research we used financial price approach to estimate the hourly electricity price, based on the historical data and the estimation of average electricity price for each month. The average electricity price is estimated by using MARAPE model [12]. This model, which is referred to as the probabilistic production - costing model, incorporates the stochastic features of load and generator availabilities.

In financial price approach the time dynamics of market prices is driven by stochastic processes generally in the form of stochastic differential equations and parameters are estimated using market data such as historical spot and derivative prices.

As mentioned before, the out put of this step is the estimation of hourly electricity price and it is the input for the second and third steps.

### 3.2 Step two: Calculation of the gas marginal value

The second step of the proposed model is the gas model for calculation of its marginal value. The objective of Gas model, therefore, is to obtain optimal allocation of gas for producing the electricity in thermal power plants so as to meet the system limits at a maximum benefit, maintaining a suitable level of reliability and guaranteeing compliance with system (technical, environmental and regulatory) constraints. The main idea is calculating the shadow price of Fuel balance equation, which is the marginal value of gas for producing the electricity or in the other words how much the benefit will change by adding one extra unit of gas for producing the electricity. In this way the company could compare the gas price in the gas market with this marginal value and if this marginal value is higher than the gas price in the gas market then it is better to allocate more gas for producing electricity instead of selling the original gas.

The output of the first stage - electricity price – is an input data for this step and it is the most important model's characteristic, which means price is an exogenous variable for second stage so in order to solve the problem the levels of market modeling which represents the price clearing process as exogenous to the firm´s optimization program is needed.

Consequently, traditional Linear Programming (LP) and Mixed Integer Linear Programming (MILP) techniques can be employed

Gas model covers:

- Calculation of Marginal value of gas in electricity market
- optimal allocation of gas for producing the electricity

It is possible to run the model for more than one month in case of significant CPU time. When the model become bigger and bigger then it is not easy to solve it in a short CPU time.

### 3.2.1 Model formulation

In order to build the Mathematical model it is necessary to know: which kinds of constraints does the system have, what are the interested outputs and result and what are the objective function, decision and state variables inside the model. In the following paragraphs these items will be explained.

#### 3.2.1.1 Objective function

The objective function is the maximization of benefit in electricity market by considering the revenue and the operation cost, Eq. (1).

Maximize $\pi$ = Revenue [€]-cost [€] (1)

Revenue [€] itself is equal to Electricity price in each period ($EP_p$) multiplied by power production ($q_{gp}$) in each period (p) and in each thermal plant(g), Eq. (2).

Revenue [€] =$\sum_p \sum_g EP_p q_{gp}$ (2)

Total cost per unit of gas consist of the cost for getting access to the gas network for each plant (ATRg , [€/MWhpcs]) plus emission cost which is Factor emission (FEg , [ton/MWhpcs]) multiplied by Co2 cost (CO , [€/ton]) . The total amount of gas consumption is calculated by using the Input-Output (efficiency) curve of each unit. The characteristic input-output curve (efficiency of each thermal unit) that relate gross output to consumption in fuel vary depend on the plant technology (coal, fuel-oil, gas, CCGT). In short term operation model the fuel cost is generally expected as a quadratic function of output. We use the historical data of net power output and the corresponded gas consumption in the case company in order to draw this curve. The result shows the linear relation between gas consumption and power generation[2]. $\beta_g$ is the fix term of the input-output (efficiency) curve [MWhpcs] and $\alpha_g$ is the linear term of this curve [MWhpcs/ MWh].

The second part of the cost is equal to start up cost for each plant (γg) multiplied by start up decision in each period for each plant ($y_{pg}$) plus shutdown cost for each plant ($\theta_g$) multiplied by shutdown decision in each period for each plant ($Z_{gp}$) and plus operation cost for each plant ($O_g$) multiplied by working hour of each plant ($U_{gp}$) Eq. (3).

$$cost\ [€] = \sum_p \sum_g [(ATR_g + FE_g * CO) * (\beta_g U_{gp} + \alpha g q g p + \gamma g y g p + \theta g Z g p + O g U g p] \quad (3)$$

#### 3.2.1.1 Model constrains

In this optimization model, besides the objective function, there are some constraints which are related to limited resources and time like Fuel balance equation, Upper and lower output limits, Ramp constraints. This part describes these constraints.

Total amount of Gas which is available for consuming in thermal units (GAS) for producing electricity during the specific period is fixed and predetermined in step two, so the total amount of gas consumption, should be lower than total amount of available gas (GAS) during the given period Eq. (4).

$$\sum_p \sum_g (\beta_g U_{gp} + \alpha_g q_{gp}) \leq GAS \quad (4)$$

Where p is a period, g is a generator, $\beta_g$ and $\alpha_g$ are representing the efficiency curve, $q_{gp}$ is a Power produced by thermal plant g in period p, $U_{gp}$ is a binary Commitment decision variable (0, 1) and finally GAS is a available amount of gas for intra period.

Thermal set cannot produce power above their maximum capacity or below their minimum stable load. A binary variable, $U_{gp}$, is introduced the thermal unit connection or disconnection. When the thermal unit is connected (after the start up and before the shutdown ramp period) its output only adapts values within the minimum stable load ($qmin_g$) and its maximum capacity ($qmax_g$) Eq. (5,6).

[2] In fact it is not linear but we consider the linear approximation

$$q_{gp} \leq u_{gp}\, qmax_g \quad (5)$$

$$q_{gp} \geq u_{gp}\, qmin_g \quad (6)$$

In order to define the ramp constraint another variable could be defined to make the deference between the production in the ramp period and other period Eq. (7)

$$q'_{gp} = \text{Max}\{(q_{gp} - qmin_g),0\} \text{ Or}$$

$$\text{If } q_{gp} \geq qmin_g \text{ then } q'_{gp} = q_{gp} - qmin_g \quad (7)$$

$q'_{gp}$ is the power above the minimum stable load. This formulation is very useful to split the input-output curve or define the start up and shutdown ramp

These constraints, also known as load gradient constraints, limit the variations in power output in two consecutive periods. The ramping up and down constraints is formulated as bellow Eq. (8,9):

$$q'_{gp} - q'_{gp-1} \leq ru_g \quad (8)$$

$$q'_{gp-1} - q'_{gp} \leq rd_g \quad (9)$$

There is start up cost and production which are related to start up ramp. There is assumption of 3 hours start up ramp, and one hour for shutdown ramp. Based on expertise Idea this assumption doesn't have huge effect on the result Eq.(10, 11).

$$Rmax_{gp} = \left(\sum_{i=0}^{s} y_{p-i} * ou_{ig}\right) + \left(u_p - \sum_{p-s}^{p} y_p\right) * qmax_g + Z_{gp} * sr_g \quad \forall g,p \quad (10)$$

$$Rmin_{gp} = \left(\sum_{i=0}^{s} y_{p-i} * ou_{ig}\right) + \left(u_p - \sum_{p-s}^{p} y_p\right) * qmin_g + Z_{gp} * sr_g \quad \forall g,p \quad (11)$$

We define Rmaxgp and Rmingp for each plant in each period to show the maximum and minimum limit of power production considering the production during start up and shutdown ramp Eq. (12-13).

$$q_{gp} \leq \text{Rmax}_{gp} \quad \forall g,p \quad (12)$$

$$q_{gp} \geq \text{Rmin}_{gp} \quad \forall g,p \quad (13)$$

Where "s" is equal to 3 hours for startup ramp.

If we define Rmax and Rmin by using the above formula then it is not necessary to consider the equations 5 and 6. The Eq. (14) represents the relation between, start up ($y_{pg}$), shutdown ($Z_{pg}$) and unit commitment ($U_{pg}$) decision variables:

$$y_{gp} - z_{gp} = u_{gp} - u_{g(p-1)} \quad \forall g,p \quad (14)$$

Minimum shut down and operating time constraints requires for thermal units to remain on or off for certain number of hours after startup or shut down before being shut down or start up again. The aim is to prevent boiler wear and damage caused by changes in temperature. τg is defined as the minimum shut down time for set g and Ωg as minimum operating time Eq. (15,16):

$$u_{g(p+\tau)} + u_{g(p-1)} - u_{gp} \leq 1 \quad \forall g, \forall p = p_1, \dots, p_n, \forall \tau = 1, \dots, \min\{n-p, \tau_t - 1\} \quad (15)$$

$$u_{g(p+\Omega)} + u_{g(p-1)} - u_{gp} \geq 0 \quad \forall g, \forall p = p_1, \dots, p_n, \forall \Omega = 1, \dots, \min\{n-p, \Omega_t - 1\} \quad (16)$$

The limit number of start up could be presented by Eq. (17, 18)

$$st1_{gp'} = \sum_g \sum_{p''}^{p''+24} Y_{gp} \leq 2 \quad (17)$$

$$st2_{gp'} = \sum_g \sum_{p''+RI}^{p''+24} Y_{gp} \leq 0 \quad (18)$$

Where P' is the first period of each day, which means this constrain is define for each day. The first constrain shows that, the total number of starts per day should be lower than 3 times. And the second constrain shows there isn't any start up after specific hour of each day.

### 3.2.2 Expected out put

By running this part of model, we are interested to know a) the added Value of the gas by allocating one extra unit of gas for producing the electricity in order to do the tradeoff between producing the electricity and selling the gas in the gas market, b) The optimum quantity of gas for producing the electricity.

## 3.3 Step three: Optimal schedule of electricity production

The third step of the proposed model is the calculation of the optimal electricity production schedule.

In the short term, intervals ranging from one week to one month, decision makers are faced with the problem of optimal hourly scheduling for thermal plant. In the competitive market this problem is more complicated. Set start up and shutdown decisions are impact by the shape of the electricity demand curve over the time. In our model, the demand curve considered in the first step in order to estimate the electricity price so here we will consider the estimated electricity price during the specific period instead of demand curve to calculate the optimal schedule of electricity production. In other words, the output of the first stage - electricity price – and the optimal quantity of gas are input data for this step and it is the most important model's characteristic, which means price is an exogenous variable for second stage so in order to solve the problem, like the second step, the levels of market modeling which represents the price clearing process as exogenous to the firm´s optimization program is needed.

The objective of monthly model, therefore, is to obtain an hourly schedule for each thermal power plant so as to meet the system limits at a maximum benefit, maintaining a suitable level of reliability and guaranteeing compliance with system (technical, environmental and regulatory) constraints.

Monthly scheduling models cover:

- Generating set operation, including startup and shout down decisions and provisional hourly scheduling for all generator set.
- Economic considerations, with operating and marginal cost forecasting.

It is possible to run the model for more than one month in case of significant CPU time. When the model become bigger and bigger then it is not easy to solve it in the short CPU time.

### 3.3.1 Model formulation

The model of the third stage is more or less the same as the second step, It has the objective function of maximizing benefit and constrains of; Fuel balance equation, Upper and lower output limits, Ramp up and down constraint, Start up and shut down ramp constraint, Logic coherence start up, commitment and shut down constraint, Minimum shut dawn and operating time characteristic, limit in number of Start up (part 3.2.).

The decision variables are the generation power: $q_{pg}$ Power generated in period p with thermal plant g [MW]. Start up and shut down decision variables or unit commitment decision: $u_{pg}$ Commitment state of thermal plant t in period p (0, 1), $y_{pg}$ Startup decision in thermal plant g at the beginning of period p (0, 1), $z_{pg}$ Shutdown decision in thermal plant t at the beginning of period p.

In addition it is possible to consider the state variables like: $c_p$ Operational cost in period p [€] or fuel consumption $Q_g$.

By running this part of model, we are interested to know; a) the fuel of each plant for producing electricity in predetermined period b) the hourly schedule of each plant and start-up shutdown planning, for a given period of time, c) the estimated benefit and added value of each scenario based on gas price and available amount of fuel. The model could easily provide these results.

### 3.4 Size of the model

The proposed model is solved by using the mixed integer linear programming based on branch and bound algorithm. In this way of programming, the number of binary variables has a significant effect on running duration. In order to solve the model as fast as possible we should reduce the number of binary variables in the model by using the efficient formulas.
For presenting the minimum operation and shout down duration we could use formula with several binary variables based on literature, but we proposed to use following ones in order to reduce the number of binary variables. Consequently, the running duration decreased significantly Eg.(19-20).

$$u_{g(p+\tau)} + u_{g(p-1)} - u_{gp} \leq 1 \quad \forall g, \forall p = p_1, \dots, p_n, \forall \tau = 1, \dots, \min\{n-p, \tau_t - 1\} \qquad (19)$$

$$u_{g(p+\Omega)} + u_{g(p-1)} - u_{gp} \geq 0 \quad \forall g, \forall p = p_1, \dots, p_n, \forall \Omega = 1, \dots, \min\{n-p, \Omega_t - 1\} \qquad (20)$$

To determine the size of the model, the number of variables and constrains should be determined.

The Monthly model in the case of considering 9 thermal plant; has 28275 variables.
The model consist of several constrains, 6 constrains per period per thermal plants, 2 constrains per period and 4 free constrains, which means the total number of constrains are equal to 41668.

The monthly model runs in 45 second and it takes 65 second for reading the data from GAMS and importing them in excel. The model is quite fast.

The model for three months, consist of 84819 variables and the total number of constrains are equal to 124996.

This model runs in 12 minutes for running the model and reading the data from GAMS and importing them in excel.

The models are quite fast, especially for one month when the company is interested to running the model several times for checking different changes in parameters and input data.

## 4. Model testing

Investigating the suitability of a model for intended objective is very crucial part of our model study.

As mention before, this model implemented in the gas company in Spain but because of confidentially, in this paper we can not present any result but we did validation and verification test to make sure the model is correct and valid and the expertise in the company analyzed the result. The tests which are done are explained in this part.

For the first step of proposed model -electricity price forecasting- we used the available model and methodology - which is presented by other researcher [12], the evaluation of this model, had don by authors so it is not necessary to evaluate it again. We test other two steps of model by using two methodologies, verification and validation, in order to evaluate the suitability of the proposed model.

Several tests had performed on Gas model, e.g checking the code, dimension analysis, numerical error analysis, extreme analysis, expertise evaluation and Sensitivity analysis. The model has passed them all; and the results were valid and accurate enough from the expertise point of view. therefore it is suitable for its purpose.

The most sensitive factor is electricity price which depend on the quality of output in the First step of proposed model. With the better model for forecasting the electricity price the efficiency of gas model also will increase.

The same tests had performed on the third step of model. The model had passed them all; therefore it is suitable for its purpose. In this step the most sensitive factor was again the electricity price which depends on the quality of the output in the First step of proposed model.

If better model for forecasting the electricity price could be found then the efficiency of model will increase.

## 5. Conclusion

In this paper the proposed model, new multi stage production decision model for companies with multi business line, in a deregulated market, is explained.

The model consists of three stages:

1. The electricity price forecasting
2. The calculation of the marginal value of the gas
3. The optimal schedule of electricity production

In the first stage the hourly electricity price in the market for short term, midterm and long term is estimated based on the stochastic model. For this purpose, first we need to estimate the average electricity price and then forecast hourly electricity price by considering average electricity price estimation as an input.

There are different methods in the literature for average electricity price forecasting. We used MARAPE model in this research. This model, which is referred to as the probabilistic production-costing model, incorporates the stochastic features of load and generator availabilities [12]. The objective of this model is to allow the electricity company to evaluate the future evolution of the prices in the market in the

middle term, i.e., ranging from one month to four or five years, both quantitatively and qualitatively.

In the proposed model the average electricity price is not useful and we need hourly electricity price estimation. We suggest using financial price approach to estimate hourly electricity price by using historical data and average electricity price estimation as an input data. Finally the output of this step is hourly electricity price estimation (part 3.1).

The second step of the proposed model is the gas model to calculate the gas marginal value and its optimum allocation for producing the electricity in the electricity market. We proposed the optimization mathematical model to calculate this gas marginal value.

The objective of Gas model, therefore, is to obtain optimal allocation of gas for producing the electricity in thermal power plants so as to meet the system limits at a maximum benefit, maintaining a suitable level of reliability and guaranteeing compliance with system (technical, environmental and regulatory) constraints. The main idea is calculating the shadow price of Fuel balance equation, which is the marginal value of gas for producing the electricity or in the other words how much the benefit will change by adding one extra unit of gas for producing the electricity. In this way the company could compare the gas price in the gas market with this marginal value and if this marginal value is higher than the gas price in the gas market then it is better to allocate more gas for producing electricity instead of selling the original gas (part 3.2).

The third step of the proposed model is the calculation of the optimal electricity production schedule. In this stage we propose the optimization mathematical model. The objective of this model, therefore, is to obtain an hourly schedule for each thermal power plant so as to meet the system limits at a maximum benefit, maintaining a suitable level of reliability and guaranteeing compliance with system (technical, environmental and regulatory) constraints. The optimization method with Mixed Integer Linear Programming (MILP) techniques for maximizing the Market revenue is proposed to calculate the hourly schedule of electricity production for each plant, taking in to account the technical characteristic of thermal plants and limited gas fuel (part3.3).

In order to implement the mathematical model we need to design a tool. GAMS is a good software for simulating and running the optimization model but it doesn't have a good interface. It is possible to make a connection between GAMS and excel so excel could be used as an interface.
In this way we designed the tool to implement and use the mathematical model.

We did validation and verification test to evaluate the accuracy of model. It is done in the gas company in Spain and the expertise in the company analyzed the results of all validation and verification tests like dimension analysis, numerical error analysis, extreme analysis and Sensitivity analysis.

The model has passed them all; and the results were valid and accurate enough from the expertise point of view. Therefore it is suitable for its purpose

### 5.1 Future Research

In this research we consider several assumptions. For future work it will be interesting to work on these assumptions. For instance we considered the linear start up ramp but it is not the real case. The startup ramp depends on shutdown duration before start up but in the proposed model the start up ramp is defined linear in order to solve the model with mixed integer linear programming. For future work it is interesting to define it as a non linear function and try to solve the model with other methodology.

On the other hand, in the proposed model there are three steps and each of them solves one after another but the best case is to solve them at the same time. For this purpose we need a very complicated non linear model which could calculate the electricity price and production schedule simultaneously. It could be an interesting work for future research in order to get more realistic results.

## References

[1] Baillo, A., Ventosa, M., Ramos, A., Rivier, M., Canseco, A., 2001, Strategic unit commitment for generation companies in deregulated electricity markets, In: Hobbs, B., Rothkopf, M., O'Neil, R., Chao, H. (Eds.), The Next Generation of Unit Commitment

Models, Kluwer Academic Publishers, Boston,pp. 227–248.

[2] Clewlow, L. & Strickl and, C. (1999a), A multi- factor model for energy derivatives, Working paper, School of Finance and Economics Technical University of Sydney.

[3] Clewlow, L. & Strickland, C. (1999 b), Valuing energy options in a one factor model fitted to forward price s, Working paper, School of Finance and Economics, Technical University of Sydney.

[4] Clewlow, L. & Strickland, C. (2000), Energy Derivatives: Pricing and Risk Management, Lacima Publications, London.

[5] Deng, S. (2000), Stochastic models of energy commodities prices and their application: Mean reversion with jumps and spike snote , Working pap e r, POWER, University of California Energy Institute, Berkeley, California .

[6] DeJong, C. & Huisman, R. (2002) , Option formulas for mean-reverting power prices wit h spikes, Working paper, Rotterdam school of Management at Erasmus University Rotterdam, Netherlands.

[7] Jacob Lemming, 2007, Electricity Price Modelling For Profit at Risk Management, Systems Analysis Department Risø National Laboratory, DK-4000 ROSKILDE.

[8] Javier Garcia Gonzalez (2007), decision support model in electricity power system, Pontifical University of Comillas.

[9] Johnson, B. & Barz, G. (2000) , 'Selecting Stochastic Processes for Modelling Electricity Prices', Published in : Energy Modelling and the Management of Uncertainty , Risk Books, Lon don 2000 pp . 3–21

[10] Joy, C. (2000), 'Pricing Modelling and Managing Physical Power Derivatives', Published in: Energy Modelling and the Management of Uncertainty, Risk Books, London 2000 pp . 45– 58.

[11] Kellerhals, B.P. (2001), Pricing electricity forwards under stochastic volatility, Working paper, POWER, Department of Finance, College of Economics and Business Administration Eberhard -Karls-University Tubingen, Germany.

[12] C. Vázquez and C. Batlle , 2005, Strategic medium-term model for the Spanish electricity market, developed for: Gas Natural Electricidad,Madrid –spain.

[13] Knittel, C. R. & Roberts, M. (2000), financial models of deregulated electricity prices I: Discrete time models, Working paper, Department of Finance and Economics, Boston University.

[14] Lucia, J. J. & Schwartz, E. S. (2002), 'Electricity prices and power derivatives: Evidence from the Nordic power exchange', Review of Derivatives Research 5(1 ), 5– 50.

[15] Rudkevich,A.,Duckworth,M.,Rosen,R.,1998, Modelling electricity pricing in a deregulated generation industry: the potential for oligopoly pricing in a Poolco. Energy Journal 19 (3), 19–48.

# $CO_2$ Fixation Using Magnesium Silicate Minerals. Part 3: Integration with iron-and steelmaking

*Inês Romão [a,b], Experience Nduagu [a,c], Johan Fagerlund [a], Licínio M. Gando-Ferreira[b] and Ron Zevenhoven [a]*

[a] *Thermal and Flow Engineering Laboratory, Åbo Akademi University, Åbo/Turku, Finland*
[b] *Department of Chemical Engineering, University of Coimbra, Coimbra, Portugal*
[c] *Energy and environment System Group, Institute for Sustainable Energy Environment and Economy University of Calgary, Alberta, Canada*

**Abstract:** Mineral carbonation presents itself as the most promising method to sequester $CO_2$ in Finland. A staged process for $CO_2$ mineralisation, using magnesium silicates, is being intensively developed at Åbo Akademi. Aspen Plus ® software was used to model the process and a pinch and exergy analysis were performed to acquire information on process layout for optimal heat recovery and integration. The simulations allow for concluding that the fixation of 1kg of $CO_2$ requires 3.04MJ and 3.1kg of serpentinite mineral rock. Additionally, the process gives considerable amounts of goethite and $Ca(OH)_2$ as by-products making the integration of mineral carbonation with the steelmaking industry a very attractive opportunity to reduce $CO_2$ emissions and raw materials inputs.

**Keywords:** Mineral carbonation, exergy analysis, pinch analysis, steelmaking

## 1. Introduction

Carbon dioxide is the major greenhouse gas responsible for our planet's global warming and for that, its capture and storage is imperative. Unfortunately Finland lacks options for underground storage and $CO_2$ mineralization presents itself as a way to fix $CO_2$. A staged process for $CO_2$ mineralisation using magnesium silicates is being intensively studied at Åbo Akademi. It gives a significant amount of iron by-product from the mineral in the form of FeOOH. This may be used as an input stream for iron and steel making industry, providing for a secondary raw material [1]. Moreover, as the serpentinite minerals used in this study contain around 5-20 %-wt iron oxides the size of the iron oxides by-product stream is quite significant. In Finland the iron and steel sector is the largest point-source $CO_2$ producer, therefore, integrating steel industry's $CO_2$ emissions with mineralisation is crucial and would result in emissions reduction, valuable carbonates, and iron oxide by-products useful as a raw material for iron and steel industry. In this third paper of the short series the energy and chemicals integration of a magnesium silicate mineral carbonation process (as described in part 1 [2]) with a steelmaking plant is reported. It expands on a process where Mg extraction from silicate mineral is combined with $Mg(OH)_2$ carbonation in a stand-alone process (as described in part 2 [3]). Aspen Plus ® (version 7.0) is used for most of the calculations / simulations. The results give valuable information on process layout for optimal heat recovery and integration. The integrated system calculations show how $CO_2$ emissions from iron and steelmaking and input requirements for iron ore and lime could be reduced. A feature that is briefly addressed as well is that calcium-rich slag from steelmaking (more specifically steel converter slag) can be carbonated too, producing synthetic calcium carbonate that is of great interest to pulp and paper industry.

## 2. Serpentinite Carbonation

This section provides a description of the serpentinite carbonation process, and of the assumptions made in order to obtain a feasible process simulation using Aspen Plus ® software.

### 2.1. Process Description

The process system studied here is divided in six main steps, as shown in Fig. *1*:

Corresponding Author: Ron Zevenhoven, E-mail: ron.zevenhoven@abo.fi

1. Solid-solid extraction for reactive magnesium production from magnesium silicate mineral, using ammonium sulphate (AS)
2. Dissolution of reaction products
3. Precipitation of calcium and iron in the form of hydroxides
4. Precipitation of magnesium as $Mg(OH)_2$
5. Carbonation of $Mg(OH)_2$
6. Ammonium sulphate recovery

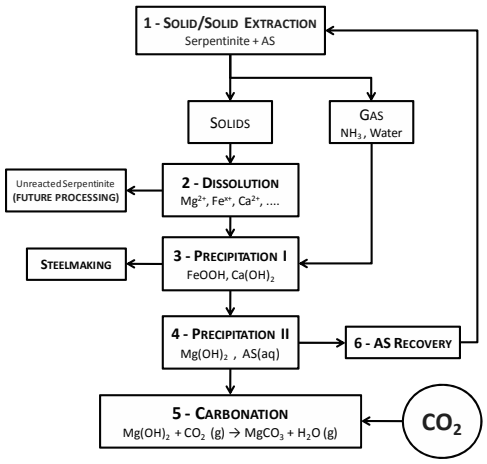


*Fig. 1. Scheme of the serpentine carbonation process*

Operating conditions and modeling of Steps 1 to 4 were based on experimental results obtained by Nduagu [4,5] whereas data for step 5 was based on Fagerlund's [2] experiments.

It is worth mentioning several problems which occurred along the simulation due to the lack of some components' properties in the Aspen's database. Therefore, in the simulation studies, data from HSC's database [6] was often used, particularly in stages 1 to 4.

### *Solid-solid (SS) Extraction*

In the Aspen model (represented in Figure A1-Appendix A) this step is simulated by a stochiometric reactor (presumably a kiln). It operates at 480ºC and atmospheric pressure. After being grinded, the serpentinite is mixed with AS and the following reactions occur:

$$Mg_3Si_2O_5(OH)_4 + 3(NH_4)_2SO_4 = 3MgSO_4 + 2SiO_2 + 6NH_3(g) + 5H_2O(g) \quad (1)$$

$$FeO + (NH_4)_2SO_4 = FeSO_4 + 2NH_3(g) + H_2O(g) \quad (2)$$

$$CaSiO_3 + (NH_4)_2SO_4 = CaSO_4 + SiO_2 + 2NH_3(g) + H_2O(g) \quad (3)$$

As shown by the above reactions, large amounts of $NH_3$ and water are released which are further used in the precipitation stages.

### *Solids Dissolution*

The solid compounds formed in the kiln must be dissolved and separated (by filtration) from the fractions of unreacted serpentine, iron oxide, wollastinite and freed silica.

The unreacted $(NH_4)_2SO_4$ will also dissolve releasing a considerable amount of heat. The rigorous control of this step is very important. Larger amounts of dissolved products result in larger amounts of recovered products in the two precipitation stages ahead. It is important to keep this dissolution tank at a temperature no higher than 35ºC, since $MgSO_4$ solubility decreases above this temperature. Water must be carefully added: in one hand increases the dissolution rate but later, during the AS recovery, its evaporation will require a considerable amount of energy.

This dissolution was difficult to simulate in Aspen and, once again, a stochiometric reactor was used and HSC data, for the heat of dissolution of the salts formed in stage 1, was introduced in the simulation.

### *Iron, calcium and magnesium precipitation*

At this point pH is the most important operation parameter. The solution must be rigorously kept at pH= 8~8.5 so that, in this first precipitation step, only iron and calcium are precipitated and, consequentially, reach a maximum magnesium recovery in the second precipitation stage at a pH of 9.0~11.0. The iron is precipitated in the form of goethite (FeOOH), calcium as $Ca(OH)_2$ and magnesium as $Mg(OH)_2$.

It is still not fully clear in which form the iron is present in the serpentinite ore. Probably it is a mixture of $Fe_2O_3$ and FeO partially combined as $Fe_3O_4$. However it is only possible to separate by precipitation the $Fe^{2+}$ because $Fe^{3+}$ has a much lower pH for precipitation and will thus remain in the solid residue. Therefore, for simulation purposes, it was considered that all the iron is FeO but it is not possible to extract more than 60% of it, as was found experimentally [4,5].

***$Mg(OH)_2$ Carbonation***

$Mg(OH)_2$ reacts with gaseous $CO_2$ to form $MgCO_3$ and water vapor in a pressurized fluidizing bed reactor, taken here to be 50 bar and 550ºC. This stage was simulated in Aspen with a Gibbs reactor.

The $CO_2$ flow going into this reactor was calculated assuming particles with a diameter $d_p$=100 $\mu$ m and a porosity $\varepsilon$ =0.6. The minimum fluidizing velocity ($u_{mf}$) was calculated using equation (4) [7]:

$$\frac{d_p u_{mf} \rho_g}{\mu} = \left[ (28.7)^2 + 0.0494 \left( \frac{d_p^3 \rho_g (\rho_s - \rho_g) g}{\mu^2} \right) \right]^{1/2} - 28.7 \quad (4)$$

and the fluidizing velocity ($u_f$) was estimated at 5 times $u_{mf}$ to assure a bubbling bed reactor.

Finally a 2000 $m^3CO_2$/hr (STP) flow was estimated and used in this simulation. It was decided to keep the fluidizing velocity ($u_f$), porosity, and $CO_2$ flow constant. The purpose of that is to maintain, for each simulation, all the carbonation conditions unchanged. The $MgCO_3/Mg(OH)_2$ solid product mix will be recirculated until the $Mg(OH)_2$ content becomes sufficiently low (few %).

***Use of the ammonia produced in the Solid/Solid Extraction reaction***

The ammonia gas produced during the extraction step is cooled and dissolved in water to form $NH_4OH$. A make-up of $NH_4OH$ is necessary to achieve the desirable pH of the precipitation stages. Since Aspen's database lacks data for $NH_4OH$, a make-up stream of ammonia (175 kg/hr) is used instead (see section 4.3). The appropriate temperature for this reactor was difficult to estimate. While modeling, and looking for conditions where the vapor fraction inside the reactor is negligible, the temperature calculated for this reactor was 146 ºC. This may be too high. It was decided to keep this absorber reactor at a temperature of 40ºC which is roughly the boiling temperature of an aqueous solution with 40% $NH_3$. The $NH_4OH$ produced in this tank is used to raise the pH in both precipitation steps.

***Ammonium Sulphate recovery***

It is very important to recover the AS present in the remaining solution after the $Mg(OH)_2$ precipitation not only for environmental reasons but also to make the process economically viable, although AS is a cheap chemical (cheaper than ammonia or sulphuric acid). The only way to achieve an AS recovery of 99% was modeled by two separators in series. This recovered AS is feed back to S/S extraction reactor. In order to keep a mass ratio of serpentinite/AS equal to 2/3, a make-up stream of 400 kg/hr of AS was added to the first reactor.

***Unreacted $CO_2$ recovery***

The stream leaving the carbonation reactor contains $MgCO_3$, $H_2O$ (g) and unreacted $Mg(OH)_2$ and $CO_2$ (g). The solid must be separated from the gas, most likely by a cyclone. The gaseous stream leaving the separation unit contains a 5-10% of water steam, generated in the carbonation reaction. Decompressing and cooling this stream allows the removal of water so that the unreacted $CO_2$ can be recovered, recompressed to 50 bar and then feed back to the carbonator.

## 3. Pinch and Exergy Analysis

In this section a pinch analysis was performed to obtain optimal heat recovery and integration of the process/model. Simulations were made for different levels of Mg, Ca and Fe (by-)product extraction and $Mg(OH)_2$ carbonation.

Although the S/S extraction, AS recovery, and recovered $CO_2$ recompressing are energy intensive stages of the process, it is possible to decrease the total energy demand by designing an efficient heat exchanger network, and recovering heat from the tank were the solids are dissolved and the reactor where $NH_4OH$ is produced. Also it is assumed that the $CO_2$ feed to process is delivered at 140 bar (transport pressure) and its decompression to 50 bar generates a considerable amount of energy.

### 3.1. Pinch Analysis

The application of this methodology [8] was not without difficulty. This design was optimized using data from the simulation relative to 90% of carbonation and an extraction of 80% of magnesium, 60% of iron and 100% of calcium, which is believed to be the real potential of this process. The numerical method given by Linnhoff and Flower was applied [8]. The composite curve of this problem was built using Aspen Energy Analyzer and it's shown in Figure 2. The grid with

the proposed (and applied) heat exchanger (HX) design is represented in Figure 2A-Appendix A.

The match between streams followed these main conditions:

- Above the pinch $CP_{hot}$[1] $\leq CP_{cold}$
- Below the pinch $CP_{hot} \geq CP_{cold}$.
- Solid streams must never be matched
- Temperature from stream 1 (mixture of unreacted $CO_2$ and water) must not go under the 120ºC to avoid condensation inside the turbine 2 (see Figure 1A -Appendix A).

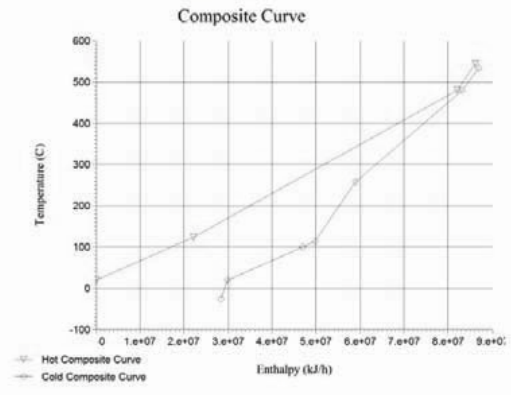


*Fig. 2. Cold and hot composite curves*

All these criteria could be satisfied except for the HX E (see Figure 2A-Appendix A). Stream 11 should have been split in two and then matched with two hot streams. However, for reasons unclear to us, by following this theory the simulation does not converge to a result in Aspen®.

Moreover, an additional HX–X (see Figure 2A-Appendix A) would be necessary to take stream 8 to the pinch point, but this does not follow the condition $CP_{hot} \geq CP_{cold}$. Stream 8 is no more than the mixture of streams 7 and 9. And when these two streams are heated up by heat exchangers F, G and H, stream 8 already reaches a temperature higher than the pinch, making HX-X unnecessary.

Finally the cooler from stream 2 was not included because below the 60% all the heat from this stream will go into stream 11.

[1] Stream heat capacity : $CP = \dot{m} C_p$ (W/K)
$CP_{hot}$: hot stream heat capacity
$CP_{cold}$: cold stream heat capacity

### 3.2. Simulation's Results

Simulations were made for different levels of Mg, Ca and Fe (by-)product extraction, and Mg carbonation. Fig. ***3*** and Fig. ***4*** summarize the results. It is important to stress that the simulations do not include grinding of the minerals but do include energy recovery from decompression the $CO_2$, which is expected to be delivered at 140 bar.

Intensive study on aqueous mineral carbonation using olivine, serpentine and wollastinite minerals was carried out at the Albany Research Center (ARC), in the US [9]. According to their results 3.4-6.3 kg of serpentinite (heat treated, 75 μm) may sequester 1 kg of $CO_2$ with an energy consumption of 3.7-7.6 MJ (mainly heat at 630ºC) and including grinding, at ~ 150 kJ/kg $CO_2$ fixed, approximately 3% of the energy needed.

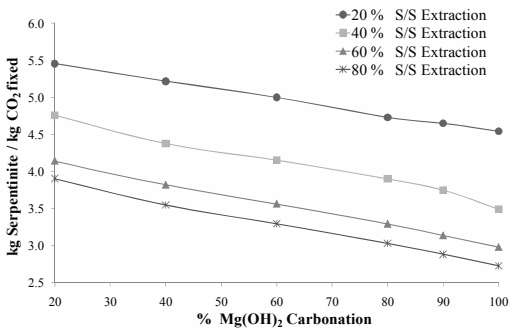


*Fig. 3. Serpeninite consumption per kg of $CO_2$ fixed*

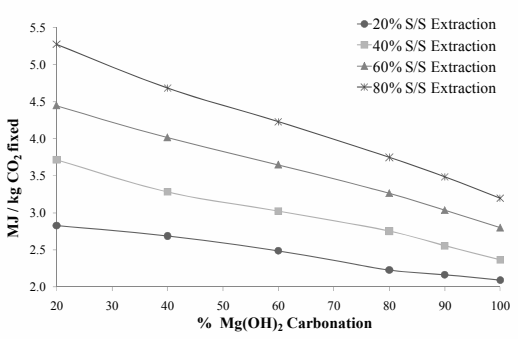


*Fig. 4. Energy consumption per kg of $CO_2$ fixed*

The modeling approach used in this study gives similar values. Experimental results [4,5] show that currently it is possible to extract 60% of magnesium and carbonate 90% of the $Mg(OH)_2$ [2], which requires 3.04 MJ (2.22 MJ as heat at 125ºC-550ºC + 0.82 MJ as power) and 3.1 kg of serpentinite to fix 1 kg of $CO_2$. However the

energy consumption is still too high. Note that, as also for the ARC work, the $CO_2$ production associated to the energy requirements is not taken into account. The use of the steam, at the right temperature, from a steam cycle of a power plant or other process comes across as good alternative to supply most of the energy needed for this process.

As shown in Fig. ***5***, the AS recovery presents a significant penalty in the process's total energy consumption and it is imperative to modify and improve this step in order to avoid this energy penalty.

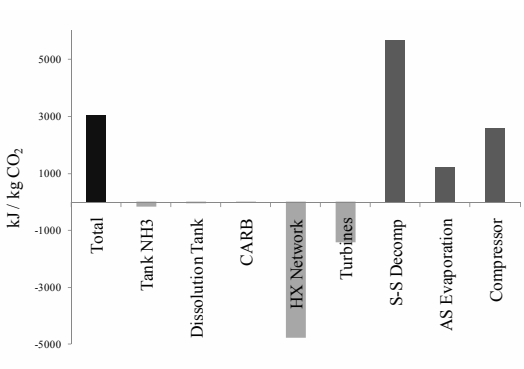


*Fig. 5. Comparison of the energy consumption /production in the different steps of the process.*

Considering the carbonation reactor, although the energy values given by the software implies an exothermic reaction, it was a goal that the released heat in this reactor would be enough to cover the energy input needed for the $Mg(OH)_2$ production [10], which clearly is not possible at this point. On the other hand, the values calculated by Aspen® for the enthalpy of carbonation reaction must be checked and compared to experimental results. These results may, in the future, be implemented into the simulation in order to obtain better results.

The HX network design appears to be efficient since the recovered energy covers 75 % of the process' energy requirements.

## 4. Process' by-products

In this section some potential applications of the by-products as well their contribution to minimize $CO_2$ emissions will be discussed. The results presented in this next section are based in data provided Raahe Works Ruukki (the biggest steelmaking company in Finland) for the year of 2006.

### 4.1. Goethite and Calcium Hydroxide

The iron and calcium based products can be supplied to the steelmaking industry, most likely to a sintering plant which is often integrated in a steel mill.

The sintering process is a pre-treatment stage of the raw materials to produce pig iron in a blast furnace (BF). The iron ore, limestone, small quantities of coke, and other fines are heated up to 1300-1400ºC to form a porous material suitable to be fed to the BF (see Fig. ***6***).

The main reactions of the process are:

$$C + O_2 = CO_2 \quad (5)$$

$$CaCO_3 = CaO + CO_2 \quad (6)$$

$$4Fe_3O_4 + O_2 = 6Fe_2O_3 \quad (7)$$

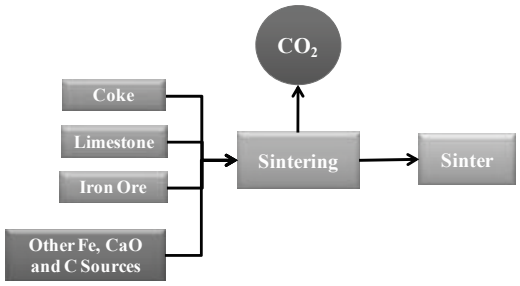


*Fig. 6. Main inputs and outputs of a sinter plant*

By supplying pure goethite and calcium hydroxide it is possible to decrease the $CO_2$ emissions of the sintering process because no $CO_2$ is released when they are oxidized as shown by equations (8) and (9):

$$2FeOOH = Fe_2O_3 + H_2O(g) \quad (8)$$

$$Ca(OH)_2 = CaO + H_2O(g) \quad (9)$$

A sintering plant producing 2.9 Mt of sinter per year requires 1800 kt iron ore, 165 kt of limestone, 118 kt of coke, 1080 kt of other products and emits 550 kt of $CO_2$. The calculation of how much $CO_2$ might be avoided by feeding the pure goethite and calcium hydroxide is then of very much interest.

Two case scenarios will be considered.

A. 60% Mg Extraction, 45% Fe Extraction, 75% extraction of Ca, 80% Carbonation

B. 80% Mg Extraction, 60% Fe Extraction, 100% extraction of Ca, 100% Carbonation

The Finnish steelmaking industry produces around 6.7 Mt of $CO_2$ per year from which 4.8 Mt are emitted by Ruukki (year 2006). The calculation of the quantities of goethite and $Ca(OH)_2$ produced is based on the assumption that all Ruukki's $CO_2$ emissions are fixed by this carbonation process.

The new sinter compositions were determined by mass balances as well the iron ore and limestone which may be replaceable. Finally the quantity of $CO_2$ avoided was calculated summing the $CO_2$ emissions prevented from iron ore and limestone[2] mining and from the sintering process itself. The results are presented in Table 1.

The results might look modest but is important to stress that this raw material replacement represents a reduction of ~5% emissions in a pre-treatment stage of the steelmaking process.

*Table 1. $CO_2$ emissions avoided by feeding iron and calcium by- products to a sinter plant.*

| | FeOOH kt/year | Iron ore replaced | $Ca(OH)_2$ kt/year | Limestone replaced | Total $CO_2$ kt/year |
|---|---|---|---|---|---|
| A | 331 | 17% | 33 | 37% | 28.4 |
| B | 365 | 18% | 36 | 41% | 31.2 |

### 4.2. Residue from mineral

The mineral residue after magnesium, iron and calcium extraction also has to be considered. Although it is logical that it should contain high amounts of valuable Si or $SiO_2$ more study and analyses are required to know its accurate composition and from there trace a plan for its processing and recovery of its constituents.

It's also important to note that the residue contains at least 40% of the iron existent in the serpentinite rock. So its future processing is not a preposterous possibility.

### 4.3. Contaminated water from AS recovery

In the second evaporation stage for the AS recovery water with 5% of $NH^{4+}$ is produced which implies a 0.7 % loss (i.e. ~30 kg/ton $CO_2$ fixed) of the incoming AS stream. This contaminated water might be corrosive and therefore its use for utility purposes should be avoided. One option would be its use for recovery of $SO_2$ from gaseous streams in the form of $(NH4)_2SO_4$ (Walther process) [14].

### 4.4. Magnesium carbonate

Significant amounts of this product will be produced and the question of what to do with such big amounts of it still remains. But it must be stressed that, depending on its purity, it finds applications in a wide range of industries such as chemical, pharmaceutical, cosmetic, food and construction (flooring and fireproofing). However, large-scale operation would naturally saturate any market as a product or by-product in the long run [15].

## 5. Steelmaking Slags Carbonation

Another interesting issue, briefly addressed, in this paper is the carbonation of slags produced by the steelmaking (SM) industry. In 2006 Raahe Works produced 0.2 Mt of steel converter slags. Said [16] describes a method to carbonate these slags and also models it using Aspen Plus ® Software. According to his results, with solvent recycling, 5.26 kg of steel slags sequester 1 kg of $CO_2$, producing 2.18 kg of $CaCO_3$ (PCC). PCC is a valuable product mainly consumed by the paper industry as filler and coating pigment for paper [15].

## 6. $CO_2$ NET emissions reduction and energy consumption

Equation (10) predicts the net reduction of $CO_2$ emissions when mineral carbonation is integrated with the SM industry. Table 2 Presents the values obtained when 4.8 Mt of $CO_2$ are mineralised and the subsequent products supplied to a SM plant for the two scenarios as in section 4.1.

$$CO_{2\ \text{net reduction}} = CO_{2\text{sequestred}} - CO_{2\text{Serpentine mining}} + CO_{2\ \text{Avoided Sintering}} + CO_{2\text{Avoided Steel slags}} \quad (10)$$

[2] Emissions from
- iron ore mining: 7.1 kg $CO_2$/t ore [11]
- limestone mining: 2.3 kg $CO_2$/t limestone [12]
- Serpentinite mining: 1.5 kg $CO_2$/t serpentinite [13]

*Table 2. Net $CO_2$ emissions, mineral and energy consumption for case scenarios A and B*

| | MINERAL CARBONATION (MODEL) | | |
|---|---|---|---|
| **Case** | $CO_2$ kt/year | SERPENTINITE Mt/year | ENERGY GJ/year |
| A | 4881 | 16.1 | 15.9 |
| B | 4881 | 13.3 | 15.6 |

| **Case** | SINTERING $CO_2$ kt/year | STEEL SLAGS $CO_2$ kt/year | NET REDUCTION $CO_2$ kt/year |
|---|---|---|---|
| A | 28.4 | 38 | 4923 |
| B | 31.2 | | 4930 |

In both cases A and B, the net reduction of $CO_2$ is higher than the $CO_2$ fixed by the mineralization process modeled, due to the emissions avoided when the goethite, and calcium hydroxide by-product are fed to the SM industry. Improvement of the S/AS extraction and of the carbonation percentages appears to have a greater impact on the amount of serpentinite consumed than on the final $CO_2$ emissions.

## 7. Conclusions and Future Work

The $CO_2$ mineralization process studied and simulated requires 3.04 MJ and 3.1 kg of serpentinite mineral rock to fix 1 kg of $CO_2$. This includes making use of the heat released by the carbonation reactor (~ 31 kJ/kg $CO_2$).

The mineralization of all the $CO_2$ emissions of a single steel company operating in Finland (Ruukki) is enough to reduce the Finnish $CO_2$ emissions by 10%.

The integration of mineral carbonation with the steel industry is of great interest since it permits a considerable reduction on raw materials inputs and a net $CO_2$ reduction superior to the initial $CO_2$ fixed, despite the faster rate of the carbonation reactor.

Nevertheless, this process is still very energy intensive and has to be optimized in order to make it energy-neutral. A less energy consuming alternative for the AS recovery must be found and the S/S extraction must be improved, not only for energetic reasons, but also to recover more by-products thereby reducing the amount of solid residue.

## References


[1] Zevenhoven, R., et al., 2009, *Mineralisation of $CO_2$ and recovery of iron using serpentinite rock*, R'09, Davos/Nagoya, Sept.14-17, Paper 149

[2] Fargerlund J., E. Nduagu, I. Romão and R. Zevenhoven, 2010, *$CO_2$ fixation using magnesium silicate minerals - Part 1: Process description and performance*. Submitted to ECOS 2010

[3] Zevenhoven R., I. Romão, J. Fagerlund and E. Nduagu, 2010, *CO2 fixation using magnesium silicate minerals - Part 2: Process energy efficiency*. Submitted to ECOS 2010

[4] Nduagu, E., et al., 2010, *Production of reactive magnesium from magnesium silicate for the purpose of $CO_2$ mineralization. Part 1. Application to Finnish serpentinite*, Int. J. Miner. Process. ([submitted])

[5] Nduagu, E., et al., 2010, *Production of reactive magnesium from magnesium silicate for the purpose of $CO_2$ mineralization. Part 2. Mg extraction modeling and application to different Mg silicate rocks*, Int. J. Miner. Process. ([submitted])

[6] HSC chemistry for Windows, version 5.11. Pori, Finland: Outokumpu Research Oy; 2002

[7] KL D Kunii, O Levenspiel, 1991, *Fluidisation Engineering*, 2nd ed, Butterworth-Heinemann

[8] Coulson & Richardson's, 1993 *Chemical Engineering Design*, 2nd ed. Pergamon Press, England, Chap. 3.17.

[9] Gerdemann S.J et al., 2007, *Ex Situ mineral carbonation*, Environ. Sci. Technol., 41, 2587-2593.

[10] Zevenhoven R, S. Teir and S. Eloneva, 2008, *Heat optimisation of a staged gas-solid mineral carbonation process for long-term $CO_2$ storage*. Energy 33: 362–370

[11] Rio Tinto, 2002, Social and environmental Report (http://www.riotinto.com/documents/ReportsPublications/2002_socEnv_Robe.pdf)

[12] Adachi T., Mogi G. and J Yamatomi, 2001, *Inventory Analysis for $CO_2$ Emission of Mining Process in Limestone Quarries*, Shigen-to-Sozai, Vol. 117(6) pp.520-526

[13] Hangx S.J.T., Spiers C.J., 2009, *Coastal spreading of olivine, to control atmospheric*

*$CO_2$ concentrations: a critical analysis of viability,* International Journal of Greenhouse Gas Control 3, pp.757-767.

[14] Scheuch, F., 2000, *Cost pressures drive flue gas treatment into new and fertile regions*, Modern Power Systems 20(11) pp. 31-32

[15] Lackner, K.S., D.P. Butt, C.H. Wendt, F. Goff, G. Guthrie. (1997), *Carbon dioxide disposal in mineral form - keeping coal competitive*, Report LA-UR-97-2094, LANL, Los Alamos (NM) U.S.

[16] Said A., et al., 2009, *Process simulation of utilization of $CO_2$ and Steelmaking slags to from precipitated calcium carbonate (PCC)*, ECOS 2009/Foz do Iguaçu, Paraná, Brazil, Aug. 31- Sept. 3, pp. 1261-1270

## Acknowledgments

This work was supported by the Academy of Finland program "Sustainable Energy" (2008-2011). I. Romão acknowledges the Leonardo da Vinci Project for financial support. Prof. Henrik Saxén and Dr. Mikko Helle are acknowledged for comments and help.

## Appendix A

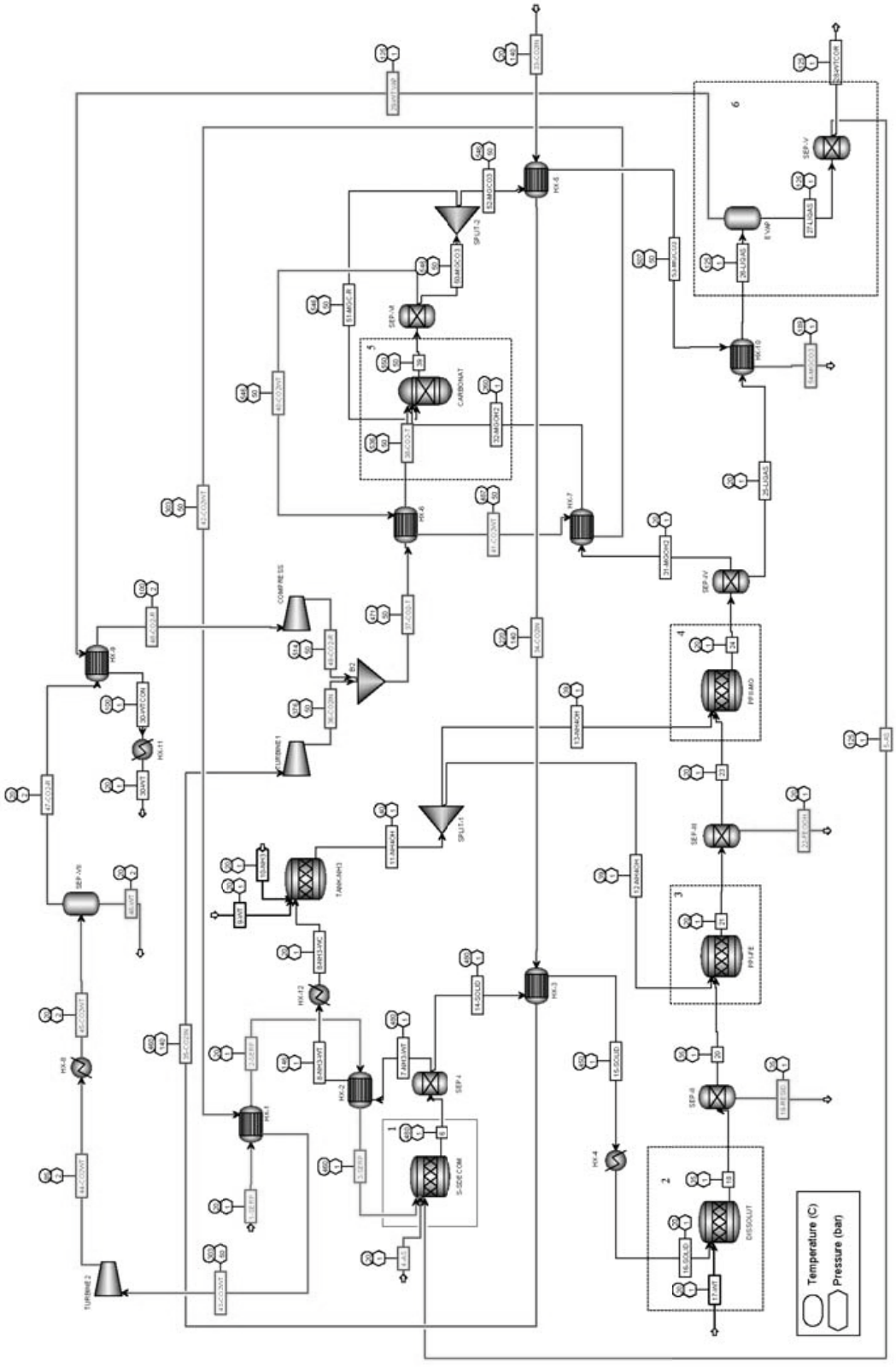


*Figure A1- Aspen Plus model: magnesium silicate carbonation via $Mg(OH)_2$ production.*

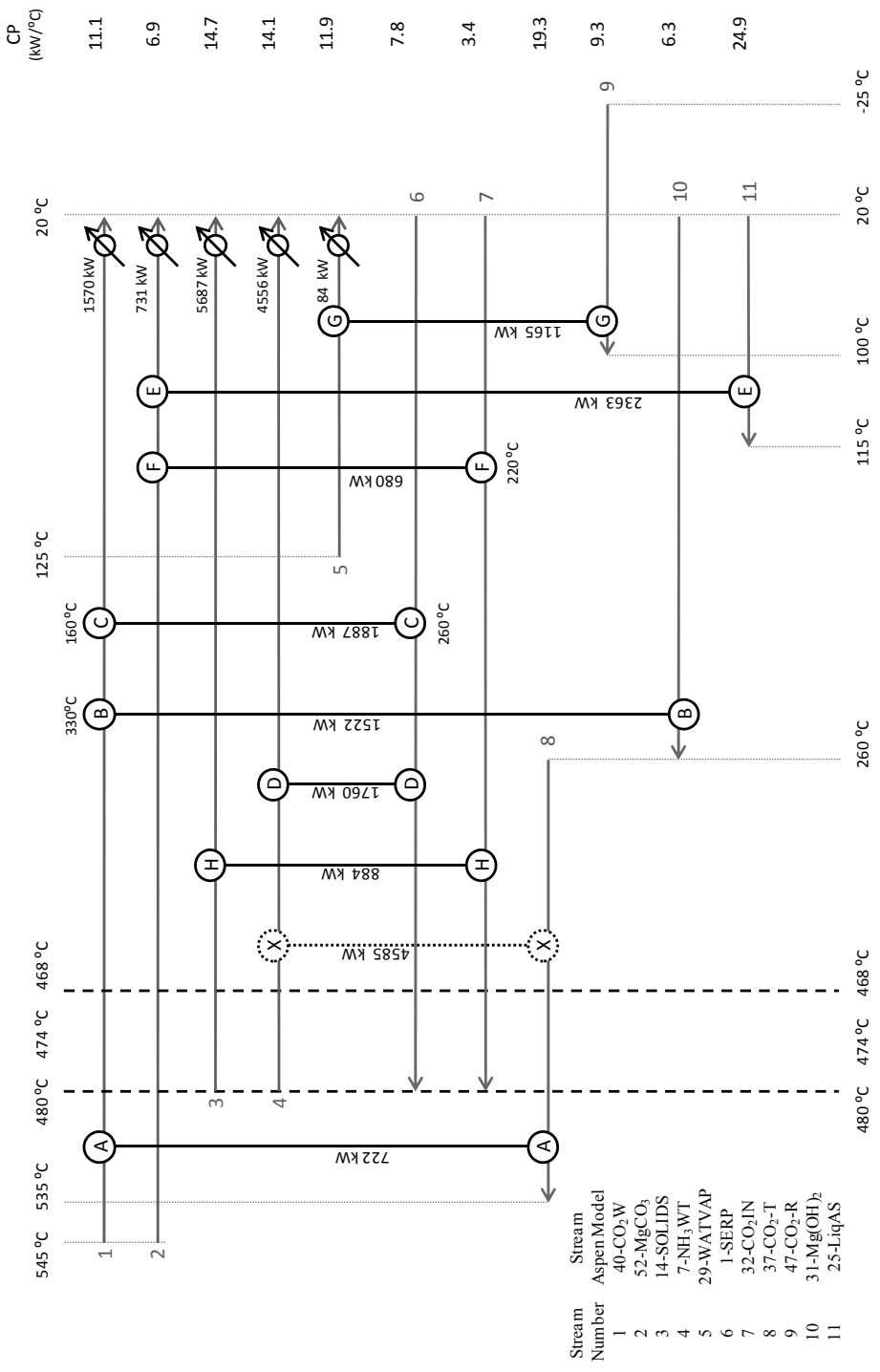


*Figure A2- Grid with the HX network proposed and applied.*

# Simulation and Optimization of Steam Network in LNG Plant

*Seyed Javad Motevallian[a], Majid Amidpour[b], M.H.Khoshgoftarmanesh[c]*

[a] *Energy and Enviroment Department*
*Science & Research Branch of Islamic Azad University,Tehran, Iran*
*Jmmechanics@yahoo.com*
[b] *Mechanical Faculty, Energy*
*Systems Department, K. N. Toosi University of Technology, Tehran, Iran*
*amidpour@kntu.ac.ir*
[c] *Oil and Gas Department*
*Iranian Power Projects Management Company (MAPNA), Tehran, Iran*
*mh.khoshgoftar@gmail.com*

**Abstract:** Steam has an impressive role in energy needs for industries because more than half of the fuel consumption is used in steam networks. Amount of fuel consumption in the network is varied due to boilers and other fuel components .In addition, overall operating costs increase sharply by processing and revamping costs and also maintenance costs. Thus the amount of energy save in fuel costs will dramatically reduce steam production costs if the optimization modeling is truly implemented in the plants. Central utility of IRANLNG Plant will be evaluated in this paper as a case study. The sour wet gas is supplied to IRANLNG by dedicated facilities, producing the raw gas from SOUTH PARS field. The main power generation facility in the plant is located in the utility area and consists of five gas turbine generators and HRSGs and two steam generators, which supply the required power for Liquefaction Units and other parts of two trains. Then, various scenarios could be proposed to modify the network. In this regard, computer code has been developed in GAMS environment for simulating steam network in different condition. Also, optimization has been performed in GAMS software through integration of simulation results. The objective of the optimization problem is minimum Total Annualized Cost (TAC).

**Keywords:** Steam Network, Simulation and Optimization, minimized total cost.

## 1. Introduction

Reduction in annual steam production cost is possible with the introduction of new scenarios that improve network performance due to extent problems solving, which used methods that are explained in brief. One of these methods is the thermodynamic analysis like pinch and exergy. Pinch technology is useful for heat recovery but main limitation is that only the thermal part could be evaluated not to optimize shaft work systems. Doll and Linhoff [1] introduced a method that allows analysis of the overall plant processes, including central utility systems. Exergy analysis provides clear understanding of energy levels and undesirable inefficiency according to the first and second law of thermodynamics. With the beginning of energy crisis in 70s, the exergy analysis gets into top thermodynamics. Nevertheless in the other hand exergy compares an existing system with an ideal system. Therefore, this method does not provide comprehensive system design. Other methods which are used are Heuristics. These methods presented in Nishio [2] work for process design and integration of gas turbine with steam cycle in Cho [3]. The Weakness is although desirable Thermodynamic targets could be obtained in the design process, costs of solutions probably will be very high because economic factors have not been considered in the model. Mathematical programming is another tool, which is used for constructing superstructures of utility systems. Brono [4] extended a method in a MINLP (Mixed Integer Non Linear Programming) model considering nonlinear cost functions with providing this possibility that temperature levels are considered as variables more degrees of freedom gained to revamping superstructures but the pressure levels are still preserved as

Corresponding Author: Majid Amidpour, Email: *amidpour@kntu.ac.ir*

parameters. Hence this approach can give us better results. To solve mathematical programming problems, special algorithms like LP, NLP, MILP and MINLP are created. The Solver for LP (Linear Programming) problems are effective as provided by ilog CPLEX to find the optimal global issues is the problem. Many of these algorithms can also be used to solve the MILP problem to find global optimal values. In NLP and MILP problems algorithms often require special mathematical tools to get global optimal value effectively and efficiently. (For example: Outer approximation method by Grossman [5]).

## 2. Problem Definition

Steam network design is a flowsheet synthesis problem, which includes location and size of boilers, heat recovery steam generators, steam and gas turbines. The candidate units can have many possible connections among them. The number of combinations can grow exponentially when a design problem becomes more complicated. As the tendency in a steam network when design moves towards more efficient and often more complex cycles, the combinatorial problem becomes more acute. However, the numbers of combinations increase for combined cycles. The design problem in this paper is stated as an objective function which gives the optimal network when generates a good conceptual design with minimizing the steam production cost. The main characteristics of the problem and the challenges for solving it are discussed in more detail as follows.

## 3. Overview of Methodology

The target of a comprehensive optimization sets to find a way that the operation of a network performs sufficiently in the best condition indeed needs tools, which are achieved by scientific progress. In this case, all interactions between industrial processes, steam systems such as steam turbines, gas turbines, boilers, heating and cooling equipment should be taken into account. As a result, investment planning can be defined in an effective manner by reducing energy cost. Despite traditional pinch technology that covers whole heating system but wasn't fully qualified for power systems because this method didn't apply pressure changes. On the other hand, exergy analysis compared system with the ideal conditions. Therefore, the single exergy analysis method did not provide comprehensive system design. To manage this restriction syntactical method was introduced and new Ω-H curve is illustrated by X.Feng and X.Zhu [6]. In this generic diagram Ω indicates the energy level and H states the amount of energy. Both energy and exergy balances for a whole system could therefore, be represented simultaneously on this diagram. In use of this diagram, the major advantages of both pinch and exergy analysis are combined, whereas the diagram enables one to view the performance of a system and sets targets for improvement. In This way quantity in system analysis decreases while promising modifications can be effectively determined and the designer doesn't face over large variability options that lead to dramatic changes in units that aren't desirable.

For modeling the problem, mathematical programming can be effective with the modeling systems like GAMS Brooke [7] and AMPL Fourer[8]. Although these systems need to be expressed in an algebraic form that explicates model, these modeling systems have the advantage that they automatically interface between different codes for solving problems. They also act automatically to decompose non linear problems in subcategories to be solved easier. By and large, the use of equations easily makes possible with significant index of large- scale models. It should be kept in mind that these modeling systems are running on most personal computers, and it makes them very popular.

The procedure starts with thermodynamic analysis of the reference model. In this level, the accuracy of the data is limited, but we are only interested in determining major heat destructions therefore promising modifications appear when evitable and inevitable exergies were determined by Ω-H curve. The change options proposed from thermodynamic analysis are added to the superstructure and the model modified. The reference model is used for the optimization of key variables and major structural features. All the process units are included in the reference model, but some of them are modeled at a low level of detail.

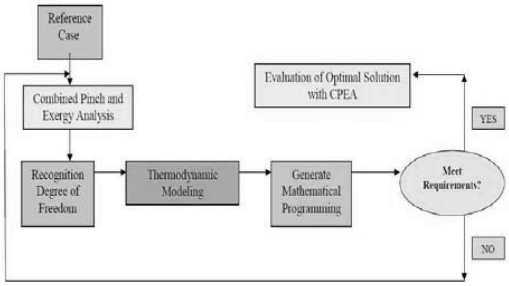


*Fig. 1. The Overall Methodology*

The modified model is built according to the equipment models and the energy and mass balance. The objective function is minimizing the steam production cost while satisfying given design constraints. The first step in making model is determining the units and specifying how are the communications between flowsheets. Then all these parameters should be valued. After these step equations should be written. In this case, there are only three types of equations; mass and energy balance equations and objective function. If additional units are considered, you must determine whether or not the units are installed and the cost functions which must be used. The model seems more real with considering the high and low levels for some variables. According to Fig 1 the above optimization and analysis procedure is repeated until no desirable improvement can be made. As a result, the reference model optimization determines the optimal flowsheet and parameters (e.g. Heat loads of various units) and these are used as requirements to design subsystems.

## 4. Mathematical Formulation of Optimization Model

If the steam network is removed from the synthesis stage, the problem is significantly simplified. Remember that a detached steam network is not essential in an LNG plant and is actually considered an option involving unnecessary high capital costs. Also, not including the supply of process heat in the preliminary power system design is a simplification that can be justified for LNG plants. The problem then canters entirely on satisfying mechanical and electrical power demands in the best possible way. (Nogel, Townsend, Perry [9]) It is imperative to account for the discrete nature of some equipment (e.g. Steam and gas turbines and related standard steam network). This is reflected in the form of a set of available sizes, performance and costs. Use continuous functions instead (e.g. from data regression) would lead to two possible situations once a solution is found. Firstly, if the equipment to be installed intends to feature exactly the same characteristics as in the optimization solution, then the high cost of custom components might cause the design to be uneconomical. Secondly, if standard models with higher capacities are adopted then the optimal conditions might be lost because the consequent of the higher costs have been neglected. Thus, it is critical that these discrete variables remain discrete in the formulation of the problem. It is also important to formulate the problem in a way that allows the solver enough flexibility in the arrangement of mechanical demands in order to consider the different alternatives [9].

The reference model is a mixed integer non-linear (MINLP) model. These terms come from heat recovery boilers, capital costs for different equipment and energy balance. The binary variables are used to consider the existence or non-existence of equipment and connections between equipment. Furthermore, binary variables are also used to select the optimal set of operating parameters. The nomenclature for the reference model is given at the end. It should be noted that for simplicity, not all equations are given here.

### 4.1. Objective Function

The objective function to be minimized is cost of energy. Costs are defined in the forms as following: The first part of the objective is the boiler's fuel consumption cost generated by calculating heat load. The second part is the operating cost of gas turbines and the third part represents the annualized capital expenditure of process units. The total fuel consumption of the system is the sum of the fuel used by all gas turbines and boileres and waste heat recovery systems and is calculated, in a discrete fashion, using equations 2 and 6.

$$\min C^{tot} = C^{B,f} + C^{GT,f} + C^{c,tot} \quad (1)$$

### 4.2. Parameters

A binary variable $\sum_{i\in I} y_I^e$ and $\sum_{i\in I} y_I^o$ are assigned for each parameter sets below. The following two equations are use to ensure that which equipments are selected and which one is operated.

1) Boiler and Heat Recovery System

$$Q_{ib,k}^{B,f} + Q_{ib,k}^{B,w} = (C_p \Delta T_k^{sat} + q)((1+b)M_{ib,k}^{B} + a y_{ib,k}^{B,o} M_{ib,k}^{B,\max}), ib \in IB, k \in K \quad (2)$$

2) Back Pressure Steam Turbine

$$W_{z,it,k}^{BT} = \frac{6}{5}\frac{1}{B_z}(\Delta h_z - \frac{A_z}{M_z^{BT,\max}})(M_{z,it,k}^{BT} - \frac{1}{6}M_{z,it}^{BT,\max} y_{z,it,k}^{BT,o}), z \in Z, it \in IT, k \in K \quad (3)$$

3) Condensate Steam Turbine

$$W_{ic,k}^{CT} = \frac{6}{5}\frac{1}{B_{ic}}(EIS_{ic} - \frac{A_{ic}}{M_{ic}^{CT,\max}})(M_{ic,k}^{CT} - \frac{1}{6}M_{ic}^{CT,\max} y_{it,k}^{CT,o}), ic \in IC, k \in K \quad (4)$$

4) Gas Turbine

$$W_{ig,k}^{GT} = \frac{1}{B^g}(\Delta H_f - \frac{A^g}{F_{ig}^{f,\max}}((1+n)F_{ig,k}^{f} - nF_{ig}^{f,\max} y_{ig,k}^{GT,o}), ig \in IG, k \in K \quad (5)$$

$$Q_{ig,k}^{GT,w} = \left[\frac{1}{f}C_p^a T^a + C_p^f T^f + \Delta H_f - (1+n)\frac{1}{B^g}(\Delta H_f - \frac{A^g}{F_{ig}^{f,\max}})\right] F_{ig}^{f}, ig \in IG, k \in K \quad (6)$$

5) Mass Balance

$$\sum_{it\in IT} M_{a,it,k}^{BT} + M_{z,k}^{t} = M_{z,k}^{c}, z \in Z, k \in K \quad (7)$$

6) Power Balance

$$\sum_{pg\in P} W_{pg,k} + W_k^{buy} = W_k^{dem}, k \in K \quad (8)$$

7) Boiler fuel cost

$$C^{B,f} = \sum_{\substack{k\in K \\ ib\in IB}} \left(U_k^f \, Q_{ib,k}^{B,f} \, T_k^s \, H\right) \quad (9)$$

8) Gas turbine fuel cost

$$C^{GT,f} = \sum_{\substack{k\in K \\ ig\in IG}} U_k^{GT,f} \, F_{ig,k}^{f} \, T_k^s \, H \quad (10)$$

9) Capital cost of equipments

$$C^{c,tot} = \sum_{i\in I} C_i^c \quad (11)$$

$\sum_{i\in I} C_i^c$ are calculated regarding to investment cost of equipments from Appendix A.

## 5. Combined Pinch and Exergy Analysis (CPEA)

Combined Pinch and Exergy Analysis (CPER) is a graphical representation of the heat transfer system in a steam network. It is based on the concepts of Exergy Composite Curves (ECC) and Exergy Grand Composite Curves (EGCC). The ECC and EGCC are obtained by replacing the temperature axis of the conventional Composite Curves and Grand Composite Curves with Carnot factor.

$$\eta_c = 1 - \frac{T_o}{T} \quad (12)$$

## 6. Case Study

The proposed optimization model is applied to a case study. The best resulting designs are compared against each other. The steam network of IRANLNG facility consists of 5 gas turbines (MW 160), 5 HRSG units and 2 Steam turbines (MW 100) which are illustrated in Fig 2. Two steam levels feed process units. The high pressure steam level feeds 60.3 t/hr HP steam for LNG units and the medium pressure steam level services near to 400 t/hr MP steams for other parts of LNG units. Fuel is Natural Gas and the low heating value is 46,272 kJ/kg. Data sheet of reference model is presented in Table 1.

## 7. Simulation and Optimization

The first step passes with CPEA and the combined pinch and exergy curve illustrated as Fig 4. Now after promising modification became clearer, the parameters set and variables determine for the reference model in GAMS environment and model running and the result is checked by simulation software.

Requirement inputs of Program included steam requirements, power demand and related temperature and pressure of each level and equipment. STAR as Computer aided software utility for simulating the network.

## 8. Result

Among the study of existing industrial units, it is essential to be aware of the framework of an industrial infrastructure system which affects the degree of freedom to gain economic results effectively and efficiently. These possibilities are provided by a combination of analysis that

designer doesn't waste his time for other design changes in the industry which may not be feasible or economical. Furthermore, the designer of this group doesn't face large variability options that lead to dramatic changes in industrial units that aren't desirable. This method results in a top level analysis with a specific strategy to save the steam inside the large unit. Prices used for fuel costs consist of the average price of natural gas in Iran equivalent to 98.2 Rials per square meter (13.7 dollars per ton) and the other is world average price in 2007 as the base year equivalent to 6.95 dollars per million Btu. The low heating value is 46,272 kJ/kg. STAR as Computer aided software utility for simulating the network and GAMS program used for modeling optimization. Inputs include steam and power requirements, corresponding temperature and pressure for each steam level and unit cost of fuel. Upside level of high pressure steam consumption equals 60.3 tons per hour and for medium pressure steam consumption equals 400 tons per hour.

Combined pinch and exergy analysis composite curve (CPEA) illustrated and for evaluation by steam network model has been studied. The main results by using the steam network model in LNG unit specify average fuel consumption reduction equals %17 for the base case and %18.4 for the reference case. According to Table 2 annual profit from total annual fuel consumption is equivalent to 6.102 million dollars per year, which includes reduction in the initial investment cost when 3 heat recovery steam generator recovery are unloaded and 2 other are replaced with one stage pressure level HRSG (Fig 2).

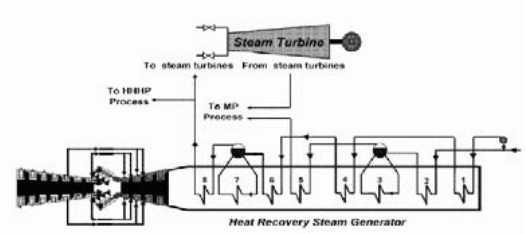


*Fig. 2. HRSG and Steam Turbine Connections*

*Table 1. Reference Case Data.*

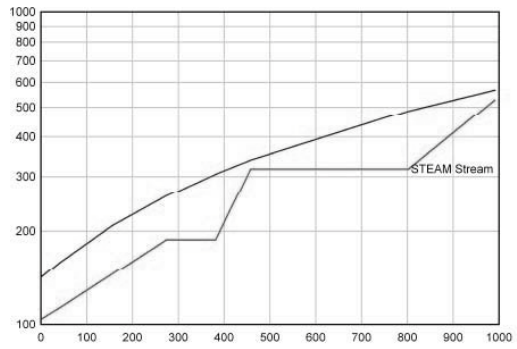


*Fig. 3. HRSG with 2 pressure stage which replaced with one stage*

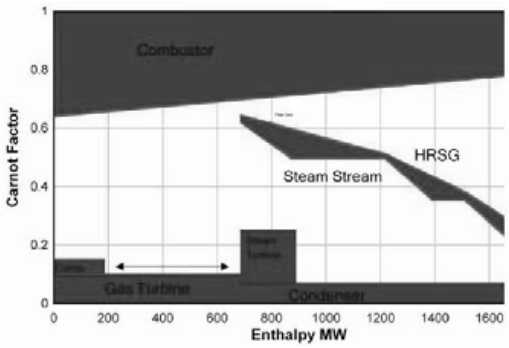


*Fig. 4. CPEA*

*Table 2. Reference Case Data*

| Case | Fuel Consumption t/hr | Steam Production Cost $/year | | Steam Production t/hr |
|---|---|---|---|---|
| | | Global | Iran | |
| Optimum | 114/9 | 342967000 | 59134100 | 1088/6 |

## Nomenclature

| | |
|---|---|
| Regression parameters of boiler model | a , b |
| Number of scenarios | K |
| Number of units | I |
| Number of zones | Z |
| Regression parameters of Steam Turbine model | $A_z$ , $B_z$ |
| Regression parameters of Gas Turbine model | $A_g$ , $B_g$ |
| Specific heat of saturation water between Tin and Tout | $C_p$ |
| Specific heat of flue gas | $C_{pg}$ |
| Specific heat of Air | $C_{pa}$ |

| | |
|---|---|
| Specific heat of fuel | $C_{pf}$ |
| Isentropic enthalpy change of steam turbine of expansion zone z | $EIS_z$ |
| Maximum fuel load of gas turbines | $F_f$ |
| Operating hours per year | H |
| Specific enthalpy of gas turbine fuel reaction | $\Delta H_f$ |
| Lower bound of boiler capacities | $L_b$ |
| Upper bound of boiler capacities | $U_b$ |
| Maximum steam load of boiler | $M_{ib}$ |
| Maximum steam load of steam turbine of expansion zone z | $M_{bt\,z}$ |
| Total steam load across each expansion zone z | $M_{c\,z}$ |
| Specific heat load of steam | q |
| Temperature of inlet air of gas turbines | $T_a$ |
| Temperature of gas turbine fuel | $T_f$ |
| Unit cost of fuel for Boiler under scenario | $U_{f\,k}$ |
| Unit cost of fuel for gas turbine under scenario | $U_{gt\,k}$ |
| Power demand of site processes under scenario | $W_{dem\,k}$ |
| Annual fuel cost of boilers | $C_{bf}$ |
| Annual fuel cost of gas turbine | $C_{gtf}$ |
| Total annual cost | $C_{tot}$ |

## Reference


[1] Dhole, V. R. & Linnhoff, B. Total site targets for fuel, cogeneration, emissions, and cooling *.European Symposium on Computer Aided Process Engineering-2.* Conference proceedings, Toulouse (1992), 101-109.

[2] Nishio, M., Itoh, J., Shioko, K. & Umeda, T., Thermodynamic Approach to Steam-Power System Design, *Ind. Eng. Chem. Process Des. Dev.,* 19, (1980), 306-312

[3] Chou, C-C & Shih, Y-S. A thermodynamic approach to the design and synthesis of plant utility systems, *Ind. Eng. Chem. Res.,* 26, (1987), 1100-1108

[4] Bruno, J.C., Fernandez, F., Castlles, F. & Grossmann I.E. A Rigorous MINLP Model for the Optimal Synthesis and Operation of Utility Plants. *Institution of Chemical Engineers, Trans IchemE,* Vol 76, Part a, March 1998, 246-258.

[5] Grossmann, I.E. (ed.), "Global Optimization in Engineering Design", Kluwer, Dordrecht (1996)

[6] X.Feng, X.X Zhu COMBINING PINCH AND EXERGY ANALYSIS FOR PROCESS MODIFICATIONS, Applied Thermal Engineering (1997)

[7] Brooke, A., Kendrick, D. and Meeraus, A., "GAMS – A User's Guide", Scientific Press, Palo Alto (1992)

[8] Fourer, R., D.M. Gay and B.W. Kereingham," AMPL: A Modelling Language for Mathematical Programming," Duxbury Press, Belomont, CA (1992)

[9] De. Nogal, F.L. Townsend, D.W. Perry, S.J - Synthesis of Power Systems for LNG Plants, GPA, Europe Spring Meeting 2003. Bournemouth, UK, May 2003

## Appendix A:
## Capital Cost calculassions
## (Bruno et al.) [4]

| Unit | Type of Cost Function | Investment Cost (S/year) |
|---|---|---|
| Large package boiler<br>F: steam flowrate (t/h)<br>P:Pressure (MPa) | Nonlinear<br><br>Linear (9Mpa) | $4954F^{0.77}fp_2$<br>$Fp_2=1.3794-0.5438P+0.1879P^2$<br>495384+13861F |
| Heat Recovery Boiler<br>Ffg:flue gas flowrate (t/h) | Nonlinear<br>Linear | $941Ffg^{0.75}$<br>6996+211.5Ffg |
| Steam turbine<br>Wst: power (kW) | Nonlinear | $2237\ Wst^{0.41}$ |
| Gas turbine<br>Wgt : power (kW) | Nonlinear | $952\ Wgt^{0.76}$ |
| Electric genetator<br>Weg : power (kW) | Nonlinear | $176\ Weg^{0.49}$ |
| Deaerator<br>$F_B$: BFW Flowrate (t/h) | Nonlinear | $904F_B^{0.62}$ |

# AUTHOR'S INDEX

## KEYWORD'S INDEX

# ecos 2010

## SPONSORS

ÉCOLE POLYTECHNIQUE FÉDÉRALE DE LAUSANNE

Schweizerische Eidgenossenschaft
Confédération suisse
Confederazione Svizzera
Confederaziun svizra

**Office fédéral de l'énergie OFEN**

## INSTITUTIONAL PARTNERS

Lausanne

canton de vaud
LIBERTÉ ET PATRIE

## TECHNICAL PARTNERS

ALPIQ

ecleer

HOLDI GAZ

BG
Ingénieurs Conseils
Ingenieure & Berater
Consulting Engineers

## SUPPORTING ORGANIZATION

ASME
SETTING THE STANDARD

International centre for applied thermodynamics
ICAT
1997